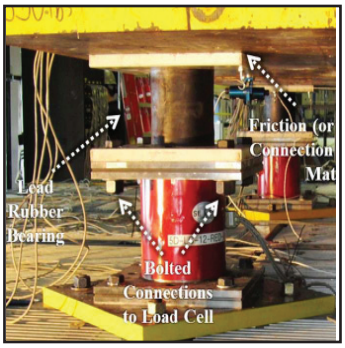
MCEER
EARTHQUAKE ENGINEERING TO EXTREME EVENTS

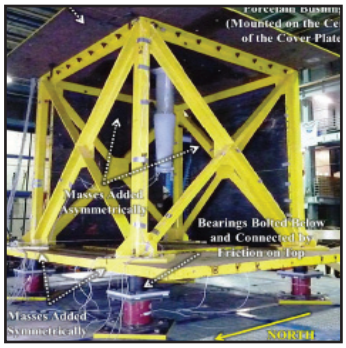
ISSN 1520-295X

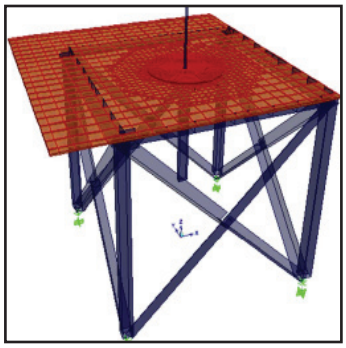
Seismic Isolation of High Voltage Electrical Power Transformers

by
Kostis Oikonomou, Michael C. Constantinou,
Andrei M. Reinhorn and Leon Kempner, Jr.









Technical Report MCEER-16-0006

November 2, 2016

This research was conducted at the University at Buffalo, State University of New York, and was supported primarily by MCEER Thrust Area 3: Innovative Technologies.

NOTICE

This report was prepared by the University at Buffalo, State University of New York, as a result of research sponsored by MCEER. Neither MCEER, associates of MCEER, its sponsors, University at Buffalo, State University of New York, nor any person acting on their behalf:

a. makes any warranty, express or implied, with respect to the use of any information, apparatus, method, or process disclosed in this report or that such use may not infringe upon privately owned rights; or

b. assumes any liabilities of whatsoever kind with respect to the use of, or the damage resulting from the use of, any information, apparatus, method, or process disclosed in this report.

Any opinions, findings, and conclusions or recommendations expressed in this publication are those of the author(s) and do not necessarily reflect the views of MCEER, the National Science Foundation or other sponsors.

Seismic Isolation of High Voltage Electrical Power Transformers

by

Kostis Oikonomou,[1] Michael C. Constantinou,[2] Andrei M. Reinhorn[3]
and Leon Kempner, Jr.[4]

Publication Date: November 2, 2016
Submittal Date: April 29, 2016

Technical Report MCEER-16-0006

MCEER Thrust Area 3: Innovative Technologies

1 Structural Engineer, Stevenson and Associates, Phoenix, AZ; former Graduate Student, Department of Civil, Structural and Environmental Engineering, University at Buffalo, State University of New York
2 Samuel P. Capen Professor and SUNY Distinguished Professor, Department of Civil, Structural and Environmental Engineering, University at Buffalo, State University of New York
3 Professor Emeritus, Department of Civil, Structural and Environmental Engineering, University at Buffalo, State University of New York
4 Principal Structural Engineer, Bonneville Power Administration

MCEER
University at Buffalo, State University of New York
212 Ketter Hall, Buffalo, NY 14260
E-mail: *mceer@buffalo.edu*; Website: *http://mceer.buffalo.edu*

Preface

MCEER is a national center of excellence dedicated to the discovery and development of new knowledge, tools and technologies that equip communities to become more disaster resilient in the face of earthquakes and other extreme events. MCEER accomplishes this through a system of multidisciplinary, multi-hazard research, in tandem with complimentary education and outreach initiatives.

Headquartered at the University at Buffalo, The State University of New York, MCEER was originally established by the National Science Foundation in 1986, as the first National Center for Earthquake Engineering Research (NCEER). In 1998, it became known as the Multidisciplinary Center for Earthquake Engineering Research (MCEER), from which the current name, MCEER, evolved.

Comprising a consortium of researchers and industry partners from numerous disciplines and institutions throughout the United States, MCEER's mission has expanded from its original focus on earthquake engineering to one which addresses the technical and socio-economic impacts of a variety of hazards, both natural and man-made, on critical infrastructure, facilities, and society.

The Center derives support from several Federal agencies, including the National Science Foundation, Federal Highway Administration, Department of Energy, Nuclear Regulatory Commission, and the State of New York, foreign governments and private industry.

This report investigates the feasibility of seismically isolating high voltage electrical power transformer structures and bushings in order to mitigate their vulnerability under strong seismic excitation. A methodical experimental and analytical study was performed and complemented by the development of design procedures applied to an actual transformer located in the West Coast of the United States. The report first describes a shake table experimental program performed at the University at Buffalo's Structural Engineering and Earthquake Simulation Laboratory (SEESL), which was developed to demonstrate the effectiveness of the selected isolation systems. The testing was performed on a simulated power transformer-bushing specimen that incorporated all of the important structural features of a typical power transformer tank. Several structural variations were tested, including isolated and non-isolated conditions, variation in the installation of the isolators, use of scaled and actual size isolators in testing, and different mounting configurations for the bushing. Furthermore, the development of numerical models of the tested frame-bushing model and the isolation systems in the commercial software SAP2000 are described, and comparisons between the numerical and experimental results are presented, to evaluate the capability of the models to predict the measured response. Finally, based on the findings of the experimental and analytical studies, design guidelines for the base isolation of electrical power transformers are developed and summarized in the form of suggested design steps. The design of base isolation for an actual electrical power transformer, which was constructed as part of this project, is presented to demonstrate these concepts.

ABSTRACT

High voltage power transformers are pieces of equipment essential for the operation of a power system. Together with high voltage bushings, which are critical components for their functionality, they have been shown to be particularly susceptible to damage during past strong earthquakes. In this work, base isolation is proposed and studied as a practical means of seismically protecting and retrofitting high voltage power transformers and their appendages.

Due to the differences between power transformers and conventional engineering structures, the design of seismic isolation systems for high voltage power transformers is controlled by specific parameters. Such parameters involve the requirement for small isolator displacements due to the limited slack of high voltage conductors connected to the power transformer and flexibility of connections to other ancillary equipment, limitations in the attachment method of the isolators to the power transformer to facilitate installation, highly asymmetric distribution of mass and stiffness of typical power transformer tanks, and the relatively light weight of power transformers. In light of these constraints, two systems are selected in this work as the best candidate systems for the seismic isolation of electrical power transformers: (a) stiff and highly damped Lead-Rubber Bearings (LRB), and (b) high friction Triple Friction Pendulum (Triple FP) bearings.

This report presents a shake table experimental program at the Structural Engineering and Earthquake Simulation Laboratory at the University at Buffalo, performed to demonstrate the effectiveness of the selected isolation systems. Testing was performed on a simulated power transformer-bushing specimen - which nonetheless incorporated all of the important structural features of a typical power transformer tank - and for several structural variations including isolated and non-isolated conditions, variation in the installation of the isolators, use of scaled and actual size isolators in testing, and different mounting configurations for the bushing. Furthermore, this report describes the development of numerical models of the tested frame-bushing model and the isolation systems in the commercial software SAP2000, and presents comparisons between the numerical and experimental results, to validate the capability of the models to predict the measured response. Finally, based on the findings of the experimental and the analytical studies, design guidelines for the base isolation of electrical power transformers are summarized in the form of suggested design steps, and the design of base isolation for an actual electrical power transformer is presented to demonstrate these concepts.

This Page is Intentionally Left Blank

ACKNOWLEDGEMENTS

This work is part of MCEER Thrust Area 1 (Infrastructure Systems and Public Policy) and is made possible with financial support from the Bonneville Power Administration with Dr. Leon Kempner, Jr. as the responsible technical officer, and the California Energy Commission. Their support is gratefully acknowledged.

This Page is Intentionally Left Blank

TABLE OF CONTENTS

SECTION 1 INTRODUCTION 1

1.1. POWER SYSTEMS AND ELECTRICAL SUBSTATION EQUIPMENT 1

1.2. CURRENT PRACTICE FOR THE SEISMIC QUALIFICATION OF BUSHINGS AND POWER TRANSFORMER DESIGN 6

1.3. PAST SEISMIC PERFORMANCE OF HIGH VOLTAGE POWER TRANSFORMERS AND BUSHINGS 8

1.4. DISCREPANCY BETWEEN THE CURRENT QUALIFICATION PRACTICE AND OBSERVED PERFORMANCE 10

1.5. MOTIVATION FOR CURRENT STUDY 13

1.6. OBJECTIVES AND SCOPE OF CURRENT STUDY 16

1.7. ORGANIZATION OF REPORT 19

SECTION 2 SEISMIC ISOLATION OF ELECTRICAL POWER TRANSFORMERS ... 21

2.1. OVERVIEW 21

2.2. PRINCIPLES OF OPERATION OF SEISMIC ISOLATION 21

2.3. SELECTION OF BASE ISOLATIONS FOR ELECTRICAL POWER TRANSFORMERS 24

2.4. MECHANICS OF LEAD-RUBBER BEARINGS 26

2.5. MECHANICS OF TRIPLE FRICTION PENDULUM BEARINGS 29

SECTION 3 EXPERIMENTAL PROGRAM 39

3.1. OVERVIEW – TEST OBJECTIVES 39

3.2. DESCRIPTION OF TEST SPECIMEN 39

3.3. DESCRIPTION OF INSTRUMENTATION 48

TABLE OF CONTENTS (CONT'D)

3.4. DESCRIPTION OF ISOLATION SYSTEMS USED IN TESTING 62

3.4.1. Isolation Systems for Length Scale 3 Tests 62

3.4.2. Isolation System for Full Length Scale Demonstration Tests 69

3.5. SIMILITUDE CONSIDERATIONS 74

3.6. SELECTION OF GROUND MOTIONS AND SCALING PROCEDURE 76

3.7. TESTING SCHEDULE 86

SECTION 4 SHAKE TABLE TESTING RESULTS AND EVALUATION 93

4.1. OVERVIEW 93

4.2. EXPERIMENTAL RESULTS FOR ISOLATED AND NON-ISOLATED STRUCTURE AT REDUCED LENGTH SCALE 93

4.3. EXPERIMENTAL RESULTS FOR ISOLATED STRUCTURE WITH FULL SCALE TRIPLE FP BEARINGS 105

4.4. COMMENTS – DISCUSSION ON RESULTS 108

4.4.1. Peak Resultant Displacements 108

4.4.2. Effect of Mass Asymmetry - Torsional Response 113

4.4.3. Tank Roof Motions - Response Spectra at the Base of the Bushing 119

4.4.4. Effect of Cover Plate Flexibility on the Bushing Response 126

4.4.5. Effect of Impact on the Results 134

SECTION 5 ANALYTICAL PREDICTION OF RESPONSE 139

5.1. OVERVIEW 139

5.2. DESCRIPTION OF FRAME AND BUSHING MODELING 139

5.3. MODELING OF ISOLATION SYSTEMS 145

TABLE OF CONTENTS (CONT'D)

5.4. NONLINEAR ANALYSIS PARAMETERS IN SAP2000 152

5.5. ANALYSIS RESULTS 154

5.6. COMMENTS AND DISCUSSION ON THE RESULTS 193

SECTION 6 AN EXAMPLE OF APPLICATION OF SEISMIC ISOLATION IN THE RETROFIT OF AN ELECTRICAL POWER TRANSFORMER 197

6.1. OVERVIEW 197

6.2. GENERAL SEISMIC DESIGN GUIDELINES 197

6.2.1. Geometric Properties of the Equipment 197

6.2.2. Seismic Site Response Spectrum 199

6.2.3. Vertical Effect of Earthquake 200

6.2.4. Selection of Isolation Systems and Properties 201

6.2.5. Simplified Method of Analysis 203

6.2.6. Dynamic Response History Analysis Method 207

6.2.6.1. Modeling of the Power Transformers and the Isolators 207

6.2.6.2. Selection and Scaling of Ground Motions 209

6.2.6.3. Analysis Procedure for Engineering Demand Parameter 210

6.2.7. Selection of Design Parameters 211

6.2.8. Construction Considerations 211

6.3. SUMMARY – DESIGN STEPS 214

6.4. EXAMPLE OF A FIELD POWER TRANSFORMER WITH SEISMIC ISOLATION 216

6.4.1. Power Transformer Characteristics 216

6.4.2. Maximum Considered Earthquake Spectrum 217

6.4.3. Seismic Isolation System 219

6.4.4. Foundation and Base-mat 223

TABLE OF CONTENTS (CONT'D)

6.4.5. Simplified Method of Analysis 224

6.4.6. Dynamic Response History Analysis 227

6.4.7. Testing of Isolators 243

SECTION 7 SUMMARY AND CONCLUDING REMARKS 247

SECTION 8 REFERENCES 255

APPENDIX A HISTORIES AND SPECTRA OF SHAKE TABLE MOTION 265

APPENDIX B SUMMARY OF EXPERIMENTAL DATA 301

APPENDIX C SUMMARY OF EXPERIMENTAL AND ANALYTICAL COMPARISONS FOR THE LEAD-RUBBER SYSTEM AND THE TRIPLE FRICTION PENDULUM SYSTEM MODELLED USING THE PARALLEL MODEL 411

APPENDIX D SUMMARY OF EXPERIMENTAL AND ANALYTICAL COMPARISONS FOR THE TRIPLE FRICTION PENDULUM SYSTEM MODELLED USING THE SERIES MODEL 541

APPENDIX E GROUND MOTION SCALING PROCEDURE 655

LIST OF ILLUSTRATIONS

FIGURE 1-1 SCHEMATIC OF THE ELECTRIC POWER SYSTEM (U.S.-CANADA POWER SYSTEM OUTAGE TASK FORCE, 2004) 1

FIGURE 1-2 TYPICAL HIGH VOLTAGE ELECTRICAL POWER TRANSFORMER 3

FIGURE 1-3 (A) 230KV BUSHING TESTED AT THE UB SEESL LAB AND (B) LONGITUDINAL SECTION OF A 550KV BUSHING (FROM GILANI ET AL, 1999) 4

FIGURE 1-4 HORIZONTAL HIGH REQUIRED RESPONSE SPECTRUM (IEEE 693, 2005) 6

FIGURE 2-1 EFFECT OF HORIZONTAL ISOLATION ON THE SPECTRAL ACCELERATION AND DISPLACEMENT DEMAND (IEEE 693 HIGH RRS SHOWN) 22

FIGURE 2-2 CUTOUT OF A LEAD-RUBBER BEARING (COURTESY OF DIS CORP.) 26

FIGURE 2-3 IDEALIZED FORCE-DISPLACEMENT RELATION OF A LEAD RUBBER BEARING 28

FIGURE 2-4 CUTOUT OF TRIPLE FRICTION PENDULUM BEARING 30

FIGURE 2-5 COMPONENTS OF TRIPLE FRICTION PENDULUM BEARING (COURTESY OF EPS) 30

FIGURE 2-6 CROSS SECTION OF THE TRIPLE FRICTION PENDULUM BEARING AND DEFINITION OF PARAMETERS (FROM FENZ AND CONSTANTINOU, 2008B) 32

FIGURE 2-7 FORCE-DISPLACEMENT RELATIONS OF TRIPLE FRICTION PENDULUM BEARING FOR EQUAL FRICTION ON SURFACES 2 AND 3 AND UNEQUAL FRICTION ON SURFACES 1 AND 4 ... 34

FIGURE 2-8 FORCE-DISPLACEMENT RELATIONS OF TRIPLE FRICTION PENDULUM BEARING FOR EQUAL FRICTION ON SURFACES 2 AND 3 AND EQUAL FRICTION ON SURFACES 1 AND 4 35

FIGURE 3-1 MODEL USED IN SHAKE TABLE TESTING WITH ADDED MASS IN SYMMETRIC BUSHING CONFIGURATION (MODEL SHOWN ISOLATED WITH LEAD RUBBER BEARINGS) 44

FIGURE 3-2 PLAN VIEW OF MODEL USED IN SHAKE TABLE TESTING WITH SYMMETRIC BUSHING INSTALLATION 45

LIST OF ILLUSTRATIONS (CONT'D)

FIGURE 3-3 ELEVATION VIEW OF MODEL USED IN SHAKE TABLE TESTING WITH SYMMETRIC BUSHING INSTALLATION (VIEW FORM WEST SIDE) 46

FIGURE 3-4 ELEVATION VIEW OF MODEL USED IN SHAKE TABLE TESTING WITH SYMMETRIC BUSHING INSTALLATION (VIEW FORM SOUTH SIDE)..... 47

FIGURE 3-5 INSTRUMENTATION USED TO MONITOR THE HIGH VOLTAGE BUSHING RESPONSE..... 52

FIGURE 3-6 INSTRUMENTATION USED TO MONITOR THE ADAPTOR PLATE RESPONSE 53

FIGURE 3-7 INSTRUMENTATION USED TO MONITOR THE FRAME STRUCTURE RESPONSE..... 54

FIGURE 3-8 INSTRUMENTATION USED TO MONITOR THE ISOLATION SYSTEM RESPONSE (MODEL SHOWN ISOLATED WITH SCALED TRIPLE FRICTION PENDULUM BEARINGS) 55

FIGURE 3-9 PLAN VIEW OF MODEL INSTRUMENTATION DIAGRAM..... 56

FIGURE 3-10 ELEVATION VIEW OF MODEL INSTRUMENTATION DIAGRAM (VIEW FORM EAST SIDE) 57

FIGURE 3-11 ELEVATION VIEW OF MODEL INSTRUMENTATION DIAGRAM (VIEW FORM NORTH SIDE)..... 58

FIGURE 3-12 VIEW OF A LEAD-RUBBER BEARING USED IN TESTING, AS-INSTALLED ON A LOAD CELL ON THE SHAKE TABLE 62

FIGURE 3-13 GEOMETRY OF SCALED LEAD-RUBBER BEARING (FROM WARN ET AL, 2006) 63

FIGURE 3-14 FORCE-DISPLACEMENT LOOPS OF SCALED LEAD-RUBBER BEARING 64

FIGURE 3-15 VIEW OF SCALED TRIPLE FRICTION PENDULUM BEARING USED IN TESTING..... 66

FIGURE 3-16 GEOMETRY OF SCALED TRIPLE FP BEARING 67

FIGURE 3-17 EXPERIMENTAL FORCE-DISPLACEMENT LOOP OF SCALED TRIPLE FRICTION PENDULUM BEARING AT LOAD OF 15KIP (RESULTS FROM TESTING OF THE BEARING WITH SINUSOIDAL MOTION OF FREQUENCY 0.2HZ PERFORMED BY SARLIS ET AL, 2013) 68

LIST OF ILLUSTRATIONS (CONT'D)

FIGURE 3-18 GEOMETRY OF FULL SIZE TRIPLE FP BEARING 72

FIGURE 3-19 BEHAVIOR OF FULL SIZE TRIPLE FP BEARING NO. 1 72

FIGURE 3-20 MODEL ISOLATED WITH FULL SIZE TRIPLE FRICTION PENDULUM BEARINGS 73

FIGURE 3-21 CLOSE UP VIEW OF FULL SIZE TRIPLE FRICTION PENDULUM BEARINGS ON SHAKE TABLE 74

FIGURE 3-22 HORIZONTAL 5% DAMPED RESPONSE SPECTRA OF REPRESENTATIVE EARTHQUAKE COMPONENTS USED IN TESTING OF THE ISOLATED MODEL AND COMPARISON TO THE IEEE 693 0.5G SPECTRUM 80

FIGURE 3-23 VERTICAL 5%-DAMPED RESPONSE SPECTRA OF REPRESENTATIVE EARTHQUAKE COMPONENTS USED IN TESTING OF THE ISOLATED MODEL AND COMPARISON TO THE IEEE 693 0.4G SPECTRUM 80

FIGURE 3-24 5%-DAMPED HORIZONTAL SITE-SPECIFIC AND IEEE 693 0.5G SPECTRA 82

FIGURE 3-25 COMPARISON OF THE SITE-SPECIFIC HORIZONTAL SPECTRUM TO THE AVERAGE OF THE GEOMETRIC MEAN SPECTRA OF THE 7 SCALED MOTIONS 83

FIGURE 3-26 V/H RATIO AND GENERATED SITE-SPECIFIC VERTICAL RESPONSE SPECTRUM 84

FIGURE 3-27 COMPARISON OF THE SITE-SPECIFIC VERTICAL SPECTRUM TO THE AVERAGE OF SPECTRA OF THE SIX SPECTRALLY MATCHED VERTICAL MOTIONS AND TO THE IEEE 693 0.4G SPECTRUM 85

FIGURE 4-1 COMPARISON OF PEAK ACCELERATION RESPONSES (NORMALIZED TO PGA) FOR ISOLATED (LRB, BOLTED-BOLTED CONFIGURATION) AND NON-ISOLATED MODELS IN THE EW AND NS DIRECTIONS (2D HORIZONTAL EXCITATION, BUSHING MOUNTED SYMMETRICALLY ON THE COVER, TESTING AT LENGTH SCALE OF 1:3, EXTRAPOLATED RESULTS FOR NON-ISOLATED MODEL) 98

LIST OF ILLUSTRATIONS (CONT'D)

FIGURE 4-2 COMPARISON OF PEAK ACCELERATION RESPONSES (NORMALIZED TO PGA) FOR ISOLATED (TRIPLE FP) AND NON-ISOLATED MODELS IN THE EW AND NS DIRECTIONS (2D HORIZONTAL EXCITATION, BUSHING MOUNTED SYMMETRICALLY ON THE COVER, TESTING AT LENGTH SCALE OF 1:3, EXTRAPOLATED RESULTS FOR NON-ISOLATED MODEL)..... 99

FIGURE 4-3 COMPARISON OF PEAK RESULTANT DISPLACEMENT RESPONSES FOR ISOLATED (LRB, BOLTED-BOLTED CONFIGURATION) AND NON-ISOLATED MODELS (2D HORIZONTAL EXCITATION, BUSHING MOUNTED SYMMETRICALLY ON THE COVER, TESTING AT LENGTH SCALE OF 1:3, EXTRAPOLATED RESULTS FOR NON-ISOLATED MODEL)..... 102

FIGURE 4-4 COMPARISON OF PEAK RESULTANT DISPLACEMENT RESPONSES FOR ISOLATED (TRIPLE FP) AND NON-ISOLATED MODELS (2D HORIZONTAL EXCITATION, BUSHING MOUNTED SYMMETRICALLY ON THE COVER, TESTING AT LENGTH SCALE OF 1:3, EXTRAPOLATED RESULTS FOR NON-ISOLATED MODEL)..... 102

FIGURE 4-5 PEAK RELATIVE RESULTANT DISPLACEMENTS AT THE TOP OF THE BUSHING FOR ISOLATED AND NON-ISOLATED CASES, TESTED WITH THE SPECTRALLY SCALED MOTIONS (TESTING PERFORMED AT REDUCED LENGTH SCALE, BUSHING MOUNTED AT THE CENTER OF THE PLATE)..... 109

FIGURE 4-6 PEAK RELATIVE RESULTANT DISPLACEMENTS AT THE TOP OF THE BUSHING FOR ISOLATED AND NON-ISOLATED CASES, TESTED WITH THE REPRESENTATIVE HISTORIC MOTIONS (TESTING PERFORMED AT REDUCED LENGTH SCALE, BUSHING MOUNTED ON THE SIDE OF THE PLATE)..... 111

FIGURE 4-7 PEAK RELATIVE RESULTANT DISPLACEMENTS AT THE TOP OF THE BUSHING FOR ISOLATED CASES, TESTED WITH THE REPRESENTATIVE HISTORIC MOTIONS (TESTING PERFORMED AT FULL LENGTH SCALE) 112

LIST OF ILLUSTRATIONS (CONT'D)

FIGURE 4-8 TA RATIOS FOR DIFFERENT SYSTEMS TESTED FOR THE SAME MOTION ENSEMBLE (REDUCED SCALE TESTING, 2D HORIZONTAL, BUSHING AT CENTER OF COVER PLATE) 115

FIGURE 4-9 TA RATIOS FOR THE SYSTEM WITH TRIPLE FP BEARINGS, TESTED FOR THE SAME MOTION ENSEMBLE AT INCREASING AMPLITUDES (REDUCED SCALE TESTING, 2D HORIZONTAL, BUSHING AT CENTER OF COVER PLATE) 116

FIGURE 4-10 CUMULATIVE SLIDING AT THE FRICTION CONNECTION OF LRB (NW CORNER OF THE ISOLATED MODEL) 118

FIGURE 4-11 COMPARISON OF FORCE-DISPLACEMENT LOOPS IN EW AND NS DIRECTIONS FOR THE NW LRB ISOLATOR BOLTED-BOLTED AND FRICTION-BOLTED CONFIGURATIONS (SARATOGA EXCITATION AT 157% OF ORIGINAL, BI-AXIAL HORIZONTAL EXCITATION) 119

FIGURE 4-12 RESPONSE SPECTRA RESULTS AT THE TABLE AND THE TOP OF THE ISOLATED FRAME FOR THE 137% KARAKYR EXCITATION (LRB ISOLATORS WITH FRICTION-BOLTED CONFIGURATION, BI-AXIAL HORIZONTAL EXCITATION, BUSHING MOUNTED SYMMETRICALLY ON THE COVER, TESTING AT LENGTH SCALE OF 1:3) 121

FIGURE 4-13 RESPONSE SPECTRA RESULTS AT THE TABLE AND THE TOP OF THE ISOLATED FRAME FOR THE 90% SYLMAR EXCITATION (LRB ISOLATORS WITH BOLTED-BOLTED CONFIGURATION, BI-AXIAL HORIZONTAL EXCITATION, BUSHING MOUNTED SYMMETRICALLY ON THE COVER, TESTING AT LENGTH SCALE OF 1:3) 122

FIGURE 4-14 RESPONSE SPECTRA RESULTS AT THE TABLE AND THE TOP OF THE ISOLATED FRAME FOR THE 94% LGPC EXCITATION (TRIPLE FP ISOLATORS, BI-AXIAL HORIZONTAL EXCITATION, BUSHING MOUNTED SYMMETRICALLY ON THE COVER, TESTING AT LENGTH SCALE OF 1:3) 123

LIST OF ILLUSTRATIONS (CONT'D)

FIGURE 4-15 RESPONSE SPECTRA RESULTS AT THE TABLE AND THE TOP OF THE ISOLATED FRAME FOR THE 300% EL-CENTRO EXCITATION (FULL SCALE TRIPLE FP ISOLATORS, BI-AXIAL HORIZONTAL EXCITATION, BUSHING MOUNTED SYMMETRICALLY ON THE COVER, TESTING AT FULL SCALE)..... 124

FIGURE 4-16 RESPONSE SPECTRA RESULTS AT THE TABLE AND THE TOP OF THE NON-ISOLATED FRAME FOR THE 97% JENSEN FILTER EXCITATION (BI-AXIAL HORIZONTAL EXCITATION, BUSHING MOUNTED SYMMETRICALLY ON THE COVER, TESTING AT LENGTH SCALE OF 1:3) 125

FIGURE 4-17 PEAK ACCELERATIONS (EW DIRECTION) FOR TRI-AXIAL TESTING, REDUCED SCALE TRIPLE FP BEARINGS AND NON-SYMMETRICAL INSTALLATION OF THE BUSHING 127

FIGURE 4-18 HORIZONTAL RESPONSE SPECTRA AT THE TANK ROOF FOR TRI-AXIAL TESTING, FULL SCALE TRIPLE FP BEARINGS AND NON-SYMMETRICAL INSTALLATION OF THE BUSHING (RESULTS FROM TESTING WITH ARBITRARILY SCALED HISTORIC MOTIONS – SEE SECTION 3.5) 131

FIGURE 4-19 HORIZONTAL RESPONSE SPECTRA AT THE TANK ROOF FOR BI-AXIAL HORIZONTAL TESTING, FULL SCALE TRIPLE FP BEARINGS AND NON-SYMMETRICAL INSTALLATION OF THE BUSHING (RESULTS FROM TESTING WITH ARBITRARILY SCALED HISTORIC MOTIONS – SEE SECTION 3.5)..... 132

FIGURE 4-20 VERTICAL RESPONSE SPECTRA AT THE TANK ROOF FOR TRI-AXIAL HORIZONTAL TESTING, FULL SCALE TRIPLE FP BEARINGS AND NON-SYMMETRICAL INSTALLATION OF THE BUSHING (RESULTS FROM TESTING WITH ARBITRARILY SCALED HISTORIC MOTIONS – SEE SECTION 3.5)..... 133

LIST OF ILLUSTRATIONS (CONT'D)

FIGURE 4-21 COMPARISON OF ACCELERATION RESPONSE HISTORIES AT THE TOP NE CORNER OF THE FRAME IN THE TWO HORIZONTAL DIRECTIONS, FROM TESTING WITH THE BI-AXIAL AND TRI-AXIAL 300% EL-CENTRO EXCITATION (FULL SCALE TRIPLE FP ISOLATORS, BUSHING MOUNTED SYMMETRICALLY ON THE COVER, TESTING AT FULL SCALE)..... 135

FIGURE 4-22 COMPARISON OF ACCELERATION RESPONSE SPECTRA AT THE TOP NE CORNER OF THE FRAME IN THE TWO HORIZONTAL DIRECTIONS, FROM TESTING WITH THE BI-AXIAL AND TRI-AXIAL 300% EL-CENTRO EXCITATION (FULL SCALE TRIPLE FP ISOLATORS, BUSHING MOUNTED SYMMETRICALLY ON THE COVER, TESTING AT FULL SCALE)..... 136

FIGURE 4-23 COMPARISON OF THE ACCELERATION RESPONSE SPECTRA AT THE TOP NE CORNER OF THE FRAME IN THE TWO HORIZONTAL DIRECTIONS, FROM TESTING WITH THE BI-AXIAL AND TRI-AXIAL 300% EL-CENTRO EXCITATION, WHERE THE EFFECT OF IMPACT IN THE TRI-AXIAL TEST HAS BEEN REMOVED (FULL SCALE TRIPLE FP ISOLATORS, BUSHING MOUNTED SYMMETRICALLY ON THE COVER, TESTING AT FULL SCALE) 138

FIGURE 5-1 FINITE ELEMENT MODEL OF ISOLATED FRAME STRUCTURE IN SAP2000..... 140

FIGURE 5-2: (A) CLOSE-UP OF BUSHING MODEL IN SAP2000 (EXTRUDED CROSS SECTIONS) AND (B) CLOSE-UP OF ADAPTER PLATE AND BUSHING FLANGE (NOT EXTRUDED) 142

FIGURE 5-3 COMPARISON OF ANALYTICAL AND EXPERIMENTAL RESULTS FOR ISOLATED FRAME FOR THE 97% JENSEN FILTER MOTION (LRB ISOLATORS WITH BOLTED-BOLTED CONFIGURATION, LENGTH SCALE OF 3, SYMMETRIC BUSHING CONFIGURATION AND 2D HORIZONTAL EXCITATION)..... 155

FIGURE 5-4 COMPARISON OF ANALYTICAL AND EXPERIMENTAL RESULTS FOR ISOLATED FRAME FOR THE 97% TAKARAZUKA MOTION (LRB ISOLATORS WITH BOLTED-BOLTED

LIST OF ILLUSTRATIONS (CONT'D)

CONFIGURATION, LENGTH SCALE OF 3, SYMMETRIC BUSHING CONFIGURATION AND 2D HORIZONTAL EXCITATION)..... 157

FIGURE 5-5 COMPARISON OF ANALYTICAL AND EXPERIMENTAL RESULTS FOR ISOLATED FRAME FOR THE 94% LGPC MOTION (TRIPLE FP ISOLATORS WITH FRICTION-BOLTED CONFIGURATION, LENGTH SCALE OF 3, SYMMETRIC BUSHING CONFIGURATION AND 2D HORIZONTAL EXCITATION)..... 159

FIGURE 5-6 COMPARISON OF ANALYTICAL AND EXPERIMENTAL RESULTS FOR ISOLATED FRAME FOR THE 90% SYLMAR MOTION (TRIPLE FP ISOLATORS WITH FRICTION-BOLTED CONFIGURATION, LENGTH SCALE OF 3, SYMMETRIC BUSHING CONFIGURATION AND 2D HORIZONTAL EXCITATION)..... 161

FIGURE 5-7 COMPARISON OF ANALYTICAL AND EXPERIMENTAL RESULTS FOR ISOLATED FRAME FOR THE 94% LGPC MOTION (TRIPLE FP ISOLATORS WITH FRICTION-BOLTED CONFIGURATION, LENGTH SCALE OF 3, SYMMETRIC BUSHING CONFIGURATION AND 3D EXCITATION)..... 163

FIGURE 5-8 COMPARISON OF ANALYTICAL AND EXPERIMENTAL RESULTS FOR ISOLATED FRAME FOR THE 90% SYLMAR MOTION (TRIPLE FP ISOLATORS WITH FRICTION-BOLTED CONFIGURATION, LENGTH SCALE OF 3, SYMMETRIC BUSHING CONFIGURATION AND 3D EXCITATION)..... 165

FIGURE 5-9 COMPARISON OF ANALYTICAL AND EXPERIMENTAL RESULTS FOR ISOLATED FRAME FOR THE 300% EL CENTRO MOTION (TRIPLE FP ISOLATORS WITH FRICTION-BOLTED CONFIGURATION, LENGTH SCALE OF 3, NON-SYMMETRIC BUSHING CONFIGURATION AND 2D HORIZONTAL EXCITATION)..... 167

LIST OF ILLUSTRATIONS (CONT'D)

FIGURE 5-10 COMPARISON OF ANALYTICAL AND EXPERIMENTAL RESULTS FOR ISOLATED FRAME FOR THE 300% EL CENTRO MOTION (TRIPLE FP ISOLATORS WITH FRICTION-BOLTED CONFIGURATION, LENGTH SCALE OF 3, NON-SYMMETRIC BUSHING CONFIGURATION AND 3D EXCITATION)..... 169

FIGURE 5-11 COMPARISON OF ANALYTICAL AND EXPERIMENTAL RESULTS FOR ISOLATED FRAME FOR THE 97% JENSEN FILTER MOTION (FULL SIZE TRIPLE FP ISOLATORS WITH FRICTION-BOLTED CONFIGURATION, NON-SYMMETRIC BUSHING CONFIGURATION AND 2D HORIZONTAL EXCITATION)..... 171

FIGURE 5-12 COMPARISON OF ANALYTICAL AND EXPERIMENTAL RESULTS FOR ISOLATED FRAME FOR THE 75% PACOIMA DAM MOTION (FULL SIZE TRIPLE FP ISOLATORS WITH FRICTION-BOLTED CONFIGURATION, NON-SYMMETRIC BUSHING CONFIGURATION AND 2D HORIZONTAL EXCITATION)..... 173

FIGURE 5-13 COMPARISON OF ANALYTICAL AND EXPERIMENTAL RESULTS FOR ISOLATED FRAME FOR THE 97% JENSEN FILTER MOTION (FULL SIZE TRIPLE FP ISOLATORS WITH FRICTION-BOLTED CONFIGURATION, NON-SYMMETRIC BUSHING CONFIGURATION AND 3D EXCITATION)..... 175

FIGURE 5-14 COMPARISON OF ANALYTICAL AND EXPERIMENTAL RESULTS FOR ISOLATED FRAME FOR THE 75% PACOIMA DAM MOTION (FULL SIZE TRIPLE FP ISOLATORS WITH FRICTION-BOLTED CONFIGURATION, NON-SYMMETRIC BUSHING CONFIGURATION AND 3D EXCITATION)..... 177

FIGURE 5-15 COMPARISON OF ANALYTICAL AND EXPERIMENTAL RESULTS FOR ISOLATED FRAME FOR THE 500% TAFT MOTION (FULL SIZE TRIPLE FP ISOLATORS WITH FRICTION-BOLTED

LIST OF ILLUSTRATIONS (CONT'D)

CONFIGURATION, SYMMETRIC BUSHING CONFIGURATION AND 2D HORIZONTAL EXCITATION) 179

FIGURE 5-16 COMPARISON OF ANALYTICAL AND EXPERIMENTAL RESULTS FOR ISOLATED FRAME FOR THE 100% CHILE MOTION (FULL SIZE TRIPLE FP ISOLATORS WITH FRICTION-BOLTED CONFIGURATION, SYMMETRIC BUSHING CONFIGURATION AND 3D EXCITATION) 181

FIGURE 5-17 COMPARISON OF ANALYTICAL AND EXPERIMENTAL RESULTS FOR ISOLATED FRAME FOR THE 70% MEXICO MOTION (FULL SIZE TRIPLE FP ISOLATORS WITH FRICTION-BOLTED CONFIGURATION, SYMMETRIC BUSHING CONFIGURATION AND 3D EXCITATION) 183

FIGURE 5-18 COMPARISON OF SERIES AND PARALLEL MODELS, AND EXPERIMENTAL RESULTS FOR ISOLATED FRAME FOR THE 137% KARAKYR MOTION (TRIPLE FP ISOLATORS WITH FRICTION-BOLTED CONFIGURATION, LENGTH SCALE OF 3, SYMMETRIC BUSHING CONFIGURATION AND 2D EXCITATION) 185

FIGURE 5-19 COMPARISON OF SERIES AND PARALLEL MODELS, AND EXPERIMENTAL RESULTS FOR ISOLATED FRAME FOR THE 104% BOLU MOTION (TRIPLE FP ISOLATORS WITH FRICTION-BOLTED CONFIGURATION, LENGTH SCALE OF 3, SYMMETRIC BUSHING CONFIGURATION AND 2D EXCITATION) 185

FIGURE 5-20 COMPARISON OF SERIES AND PARALLEL MODELS, AND EXPERIMENTAL RESULTS FOR ISOLATED FRAME FOR THE 137% KARAKYR MOTION (TRIPLE FP ISOLATORS WITH FRICTION-BOLTED CONFIGURATION, LENGTH SCALE OF 3, SYMMETRIC BUSHING CONFIGURATION AND 3D EXCITATION) 186

FIGURE 5-21 COMPARISON OF SERIES AND PARALLEL MODELS, AND EXPERIMENTAL RESULTS FOR ISOLATED FRAME FOR THE 104% BOLU MOTION (TRIPLE FP ISOLATORS WITH FRICTION-

LIST OF ILLUSTRATIONS (CONT'D)

Bolted Configuration, Length Scale of 3, Symmetric Bushing Configuration and 3D Excitation) 186

Figure 5-22 Comparison of Series and Parallel Models, and Experimental Results for Isolated Frame for the 97% Jensen Filter Motion (Full Size Triple FP Isolators with Friction-Bolted Configuration, Non-Symmetric Bushing Configuration and 2D Excitation) 187

Figure 5-23 Comparison of Series and Parallel Models, and Experimental Results for Isolated Frame for the 300% El Centro Motion (Full Size Triple FP Isolators with Friction-Bolted Configuration, Non-Symmetric Bushing Configuration and 2D Excitation) 187

Figure 5-24 Comparison of Series and Parallel Models, and Experimental Results for Isolated Frame for the 97% Jensen Filter Motion (Full Size Triple FP Isolators with Friction-Bolted Configuration, Non-Symmetric Bushing Configuration and 3D Excitation) 188

Figure 5-25 Comparison of Series and Parallel Models, and Experimental Results for Isolated Frame for the 300% El Centro Motion (Full Size Triple FP Isolators with Friction-Bolted Configuration, Non-Symmetric Bushing Configuration and 3D Excitation) 188

Figure 6-1 460 kV GE Power Transformer in Vancouver, WA 217

Figure 6-2 ASCE 7-2010 DE and MCE_R Spectra and Moderate/High RRS as per IEEE 693-2005 (5% Damped) 219

Figure 6-3 Lower Bound Conditions Force-Displacement Loop of Isolation System (M_1=M_4=0.12 and M_2=M_3=0.06) 221

LIST OF ILLUSTRATIONS (CONT'D)

FIGURE 6-4 UPPER BOUND CONDITIONS FORCE-DISPLACEMENT LOOP OF ISOLATION SYSTEM (M_1=M_4=0.18 AND M_2=M_3=0.09) 222

FIGURE 6-5 FORCE-DISPLACEMENT LOOP OF ISOLATION SYSTEM FOR CASE M_1=M_4=0.09 AND M_2=M_3=0.045 223

FIGURE 6-6 BILINEAR HYSTERETIC MODEL FOR ANALYSIS 224

FIGURE 6-7 POWER TRANSFORMER MODEL IN PROGRAM SAP2000 228

FIGURE 6-8 AVERAGE SRSS OF SCALED MOTIONS AND MCER SPECTRUM - PERIODS 0.6 TO 2.6 SEC 231

FIGURE 6-9 AVERAGE MAXIMUM DIRECTION SPECTRA OF SCALED MOTIONS AND MCER SPECTRUM 231

FIGURE 6-10 ACCELERATION RESPONSE SPECTRA AT BASE OF THE POWER TRANSFORMER (ON TOP OF ISOLATORS) FOR CASE M1=M4=0.09 AND M2=M3=0.045 238

FIGURE 6-11 ACCELERATION RESPONSE SPECTRA AT BASE OF THE POWER TRANSFORMER (ON TOP OF ISOLATORS) IN LOWER BOUND ANALYSIS (M_1=M_4=0.12 AND M_2=M_3=0.06) 239

FIGURE 6-12 ACCELERATION RESPONSE SPECTRA AT BASE OF THE POWER TRANSFORMER (ON TOP OF ISOLATORS) IN UPPER BOUND ANALYSIS (M_1=M_4=0.18 AND M_2=M_3=0.09) 240

FIGURE 6-13 ACCELERATION RESPONSE SPECTRA OF SCALED INPUT MOTIONS AT THE GROUND LEVEL (UNDER THE ISOLATORS) 241

FIGURE 6-14 460 KV POWER TRANSFORMER RETROFITTED WITH TRIPLE FP ISOLATORS (VANCOUVER, WA) 242

FIGURE 6-15 LATERAL FORCE/VERTICAL FORCE VS DISPLACEMENT LOOPS OF FULL SIZE TRIPLE FP BEARING NO. 3 UNDER SLOW (TOP) AND FAST (BOTTOM) MOTION 245

LIST OF TABLES

TABLE 2-1 SUMMARY OF TRIPLE FP BEARING BEHAVIOR (NOMENCLATURE REFERS TO FIGURE 2-6) 33

TABLE 2-2 SUMMARY OF BEHAVIOR OF SPECIAL CONFIGURATION OF THE TRIPLE FP BEARING (NOMENCLATURE REFERS TO FIGURE 2-6) 36

TABLE 3-1 COMPONENTS AND WEIGHTS OF TEST MODEL 42

TABLE 3-2 STRUCTURAL PROPERTIES OF THE ABB 196/230 KV PORCELAIN BUSHING (FAHAD, 2013) 43

TABLE 3-3 LIST OF INSTRUMENTATION USED AND RESPONSE QUANTITIES MEASURED 59

TABLE 3-4 PROPERTIES OF SCALED LEAD-RUBBER BEARINGS 64

TABLE 3-5 PROPERTIES OF SCALED TRIPLE FP BEARING 68

TABLE 3-6 PROPERTIES OF FULL SIZE TRIPLE FP BEARING 71

TABLE 3-7 CHARACTERISTICS OF EARTHQUAKE MOTIONS USED IN TESTING AT 100% LEVEL AND IN PROTOTYPE TIME SCALE 78

TABLE 3-8 SEED ACCELEROGRAMS AND SCALE FACTORS FOR HORIZONTAL MOTIONS 81

TABLE 3-9 TEST SCHEDULES AND CONFIGURATIONS 89

TABLE 4-1 PEAK ACCELERATION RESPONSE (VALUES IN UNITS OF G) AT SELECTED LOCATIONS ON THE MODEL FOR ISOLATED AND NON-ISOLATED CONDITIONS (BI-AXIAL HORIZONTAL EXCITATION, BUSHING MOUNTED SYMMETRICALLY ON THE COVER, TESTING AT LENGTH SCALE OF 1:3) 96

TABLE 4-2 PEAK ACCELERATION RESPONSE (VALUES IN UNITS OF G) AT SELECTED LOCATIONS FOR THE ISOLATED MODEL TESTED AT EXTREME CONDITIONS, AND FOR THE NON-ISOLATED MODEL (TRIPLE FP, BI-AXIAL HORIZONTAL EXCITATION, BUSHING MOUNTED SYMMETRICALLY ON THE COVER, TESTING AT LENGTH SCALE OF 1:3) 97

LIST OF TABLES (CONT'D)

TABLE 4-3 PEAK RESULTANT DISPLACEMENT RESPONSE (VALUES IN UNITS OF INCHES, RELATIVE TO THE SHAKE TABLE), AT SELECTED LOCATIONS ON THE MODEL FOR ISOLATED AND NON-ISOLATED CONDITIONS (BI-AXIAL HORIZONTAL EXCITATION, BUSHING MOUNTED SYMMETRICALLY ON THE COVER, TESTING AT LENGTH SCALE OF 1:3)..... 100

TABLE 4-4 PEAK RESULTANT DISPLACEMENT RESPONSE (VALUES IN UNITS OF INCHES, RELATIVE TO THE SHAKE TABLE), AT SELECTED LOCATIONS FOR THE ISOLATED MODEL TESTED AT EXTREME CONDITIONS, AND FOR THE NON-ISOLATED MODEL (TRIPLE FP, BI-AXIAL HORIZONTAL EXCITATION, BUSHING MOUNTED SYMMETRICALLY ON THE COVER, TESTING AT LENGTH SCALE OF 1:3) 101

TABLE 4-5 PEAK BASE SHEAR FORCES (VALUES IN UNITS OF KIP) FOR ISOLATED AND NON-ISOLATED CONDITIONS (BI-AXIAL HORIZONTAL EXCITATION, BUSHING MOUNTED SYMMETRICALLY ON THE COVER, TESTING AT LENGTH SCALE OF 1:3)..... 103

TABLE 4-6 PEAK BASE SHEAR FORCES (VALUES IN UNITS OF KIP) FOR THE ISOLATED MODEL TESTED AT EXTREME CONDITIONS, AND FOR THE NON-ISOLATED MODEL (TRIPLE FP, BI-AXIAL HORIZONTAL EXCITATION, BUSHING MOUNTED SYMMETRICALLY ON THE COVER, TESTING AT LENGTH SCALE OF 1:3) 104

TABLE 4-7 PEAK ACCELERATION RESPONSE (VALUES IN UNITS OF G) AT SELECTED LOCATIONS OF THE ISOLATED MODEL (FULL SCALE TRIPLE FP, BI-AXIAL HORIZONTAL OR TRI-AXIAL EXCITATION, BUSHING MOUNTED SYMMETRICALLY OR NON-SYMMETRICALLY ON THE COVER, TESTING AT FULL LENGTH SCALE) 106

TABLE 4-8 PEAK RESULTANT DISPLACEMENT RESPONSE (VALUES IN UNITS OF INCHES), RELATIVE TO THE SHAKE TABLE, AT SELECTED LOCATIONS OF THE ISOLATED MODEL (FULL SCALE TRIPLE FP, BI-AXIAL HORIZONTAL OR TRI-AXIAL EXCITATION, BUSHING MOUNTED

LIST OF TABLES (CONT'D)

SYMMETRICALLY OR NON-SYMMETRICALLY ON THE COVER, TESTING AT FULL LENGTH SCALE) 107

TABLE 4-9 PEAK BASE SHEAR FORCES (VALUES IN UNITS OF KIP) FOR THE ISOLATED MODEL (FULL SCALE TRIPLE FP, BI-AXIAL HORIZONTAL OR TRI-AXIAL EXCITATION, BUSHING MOUNTED SYMMETRICALLY OR NON-SYMMETRICALLY ON THE COVER, TESTING AT FULL LENGTH SCALE) 107

TABLE 4-10 HIGH VOLTAGE BUSHING FREQUENCIES (REINHORN ET AL, 2012) 126

TABLE 4-11 BI-AXIAL AND TRI-AXIAL TESTING RESULTS, FROM TESTING WITH FULL SCALE TRIPLE FP BEARINGS AND TWO DIFFERENT MOUNTING LOCATIONS OF THE BUSHING (75% PACOIMA DAM EXCITATION) 129

TABLE 5-1 VALUES OF PROPERTIES OF THE MODEL OF LEAD RUBBER BEARINGS AT LENGTH SCALE OF 3 IN SAP2000 FOR RESPONSE HISTORY ANALYSIS 147

TABLE 5-2 VALUES OF PROPERTIES OF THE PARALLEL MODELS OF TRIPLE FP BEARINGS AT LENGTH SCALE OF 3 IN SAP2000 FOR RESPONSE HISTORY ANALYSIS 148

TABLE 5-3 VALUES OF PROPERTIES OF THE PARALLEL MODELS OF FULL SIZE TRIPLE FP BEARINGS IN SAP2000 FOR RESPONSE HISTORY ANALYSIS 149

TABLE 5-4 VALUES OF PROPERTIES OF THE SERIES MODELS OF TRIPLE FP BEARINGS AT LENGTH SCALE OF 3 IN SAP2000 FOR RESPONSE HISTORY ANALYSIS 150

TABLE 5-5 VALUES OF PROPERTIES OF THE SERIES MODELS OF FULL SIZE TRIPLE FP BEARINGS IN SAP2000 FOR RESPONSE HISTORY ANALYSIS 151

TABLE 5-6 COMPARISON OF ANALYTICAL AND EXPERIMENTAL PEAK RESPONSES FOR SELECTED SETS OF TESTS AND ISOLATION WITH LEAD RUBBER BEARINGS IN BOLTED-BOLTED CONFIGURATION (LENGTH SCALE OF 3, SYMMETRIC BUSHING CONFIGURATION) 190

LIST OF TABLES (CONT'D)

TABLE 5-7 COMPARISON OF ANALYTICAL (PARALLEL MODEL) AND EXPERIMENTAL PEAK RESPONSES FOR SELECTED SETS OF TESTS AND ISOLATION WITH TRIPLE FRICTION PENDULUM BEARINGS IN FRICTION-BOLTED CONFIGURATION (LENGTH SCALE OF 3, SYMMETRIC BUSHING CONFIGURATION) 191

TABLE 5-8 COMPARISON OF ANALYTICAL (SERIES MODEL) AND EXPERIMENTAL PEAK RESPONSES FOR SELECTED SETS OF TESTS AND ISOLATION WITH TRIPLE FRICTION PENDULUM BEARINGS IN FRICTION-BOLTED CONFIGURATION (LENGTH SCALE OF 3, SYMMETRIC BUSHING CONFIGURATION)..... 192

TABLE 6-1 PROPERTIES OF TRIPLE FP PROPERTIES..... 220

TABLE 6-2 UPPER AND LOWER BOUND TRIPLE FP FRICTIONAL PROPERTIES 221

TABLE 6-3 RESULTS OF SIMPLIFIED ANALYSIS 225

TABLE 6-4 SEED ACCELEROGRAMS FOR USE IN RESPONSE HISTORY ANALYSIS 229

TABLE 6-5 SCALE FACTORS FOR GROUND MOTIONS 230

TABLE 6-6 PARAMETERS OF TRIPLE FP BEARINGS IN SAP2000 FOR RESPONSE HISTORY ANALYSIS (VALUE IN PARENTHESIS IS FOR CASE $M1=M4=0.09$ AND $M_2=M_3=0.045$)..... 233

TABLE 6-7 RESPONSE HISTORY ANALYSIS RESULTS FOR CASE $M1=M4=0.09$ AND $M_2=M_3=0.045$234

TABLE 6-8 RESPONSE HISTORY ANALYSIS RESULTS FOR LOWER BOUND PROPERTIES ($M_1=M_4=0.12$ AND $M_2=M_3=0.06$)..... 235

TABLE 6-9 RESPONSE HISTORY ANALYSIS RESULTS FOR UPPER BOUND PROPERTIES ($M_1=M_4=0.18$ AND $M_2=M_3=0.09$)..... 236

SECTION 1
INTRODUCTION

1.1. Power Systems and Electrical Substation Equipment

Modern-day societies rely on the consistent and uninterrupted supply of electrical power to maintain their welfare and development; the term supply encompasses the processes of production, transmission and distribution of electricity to the public and industrial customers, typically realized by means of the operation of critical lifelines, designated as electric power systems. Figure 1-1 provides a schematic of the elements of an electric power system.

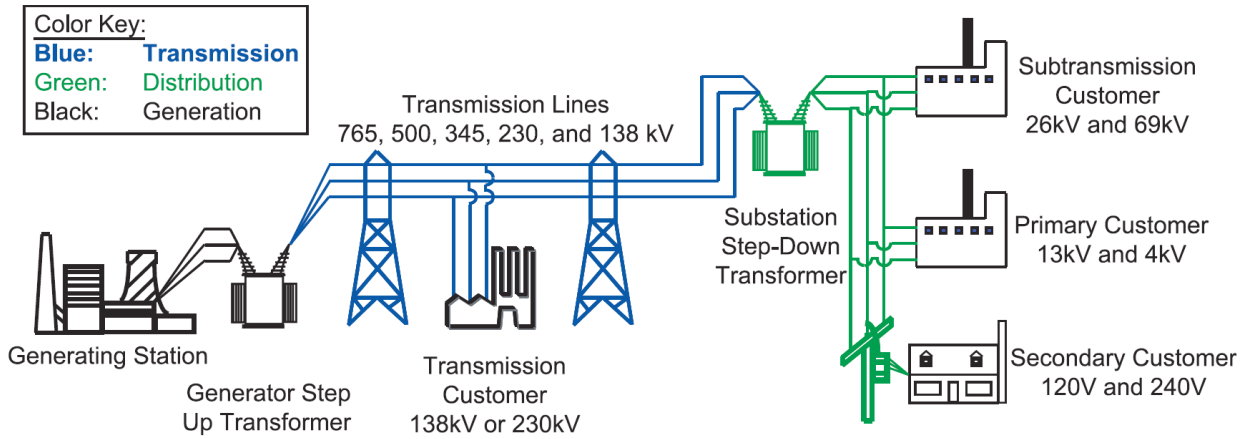


Figure 1-1 Schematic of the Electric Power System (U.S.-Canada Power System Outage Task Force, 2004)

The generating station of Figure 1-1 is generally a power plant which uses available energy sources to generate electricity. Power plants are often located at large distances from highly populated areas, located near the fuel sources, which can be combustible such as coal, oil and natural gas, or non-combustible such as solar, hydro and nuclear fuel. A transmission and distribution grid that comprises a large part of the power system, transports the produced electricity from the power plant to the industries and communities. In order to reduce heat losses in the conductors and enable economical shipment of power over the long distances required, a

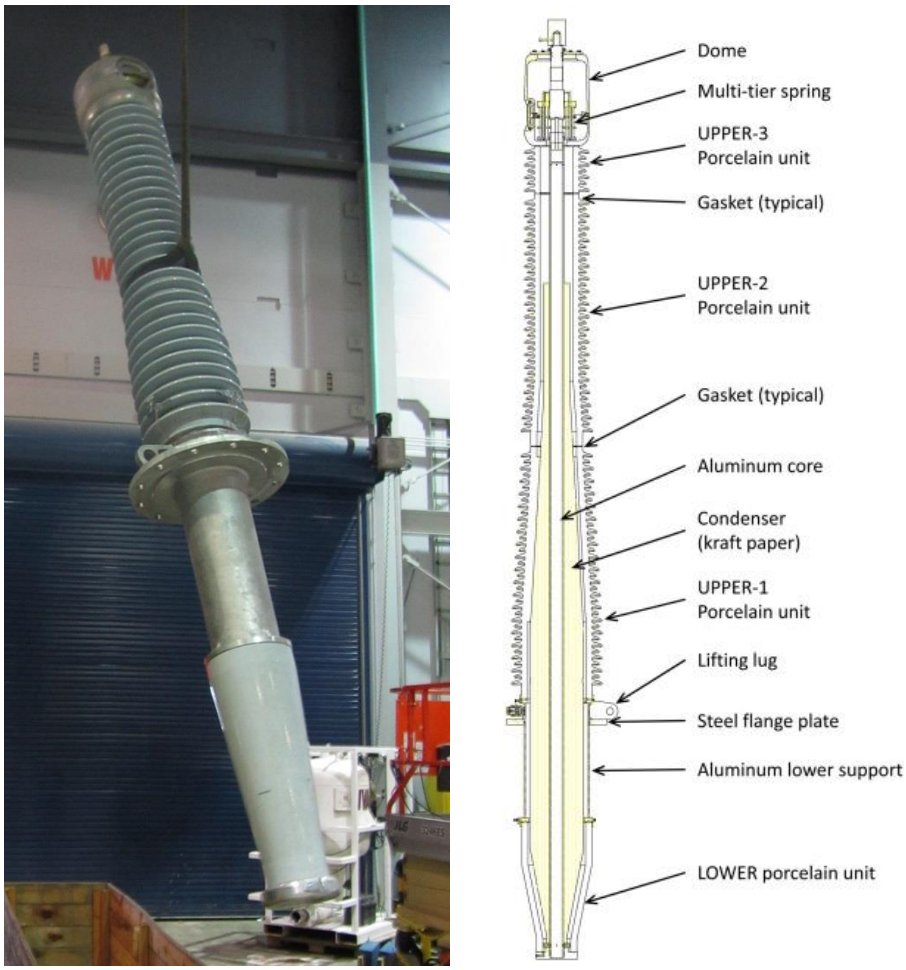
standard practice is to operate the transmission lines at voltages substantially higher than the typical 10kV-25kV of the generated electricity, and preferably in the range of 230kV to 765kV, and up to 1,100kV (particularly in P.R. China). At large load centers along the grid, the voltage is reduced and the electricity is either delivered to high demand transmission utilities and industrial customers, or enters the distribution grid. Thereafter, the voltage is further stepped down several times to reach smaller demand customers and, ultimately, residential customers.

The change of the voltage levels takes place within the electrical substations. The electrical substations are power plants located at various nodes of the power grid and contain equipment to change voltage of, regulate and distribute electricity. The central piece of equipment is the electrical power transformer which essentially transforms the voltage up and down.



Figure 1-2 Typical High Voltage Electrical Power Transformer

Figure 1-2 shows a typical high voltage electrical power transformer. The power transformer is a large and complex structure that consists of a massive tank with several appendages attached to it. The tank contains the core and coil assembly – the component that actually modifies the voltage – and oil for cooling the core and eliminating flashovers between the high voltage conductors and the surrounding internal equipment. Tank appendages include one or more external oil reservoir tanks which regulate the thermal expansion of the oil, radiators on the tank side walls to cool down the oil, lightning surge arresters, and one or more high and low voltage bushings to bring power in and out of the tank.



(a) (b)

Figure 1-3 (a) 230kV Bushing Tested at the UB SEESL Lab and (b) Longitudinal Section of a 550kV Bushing (from Gilani et al, 1999)

Amongst the various tank appendages, the high voltage bushings are arguably the most important ones because they facilitate the secure connection between the core-coil assembly and the electric grid. In particular, the role of a bushing is to provide sufficient insulation for the conductors in order to eliminate flashovers between the high voltage power lines and the power transformer tank, while simultaneously protecting the power transformer from leaking oil. A photo of a single 230kV bushing prior to its installation is shown in Figure 1-3a. Figure 1-3b presents a longitudinal section that reveals the parts composing a 550kV bushing (Gilani et al, 1999). The two high voltage bushings of Figure 1-3 differ in size and capacity, however their

structural configuration is very similar. The bushing core is a metal conductor (an aluminum core in Figure 1-3b) which transfers the electric power from the grid to the core assembly inside the power transformer. The conductor is typically encased in porcelain or composite units for insulation. Despite their excellent insulation properties, the insulating materials have limited thermal expansion capacity and cannot accommodate the high thermal expansion demands imposed by the metal conductor. To address this issue, bushings are manufactured in a segmental fashion, as an assembly of tapered units of varying thickness separated by rubber gasket rings, and prestressed together by the central conductor itself. Furthermore, and in order to prevent flashovers between the high voltage power lines (connected to the bushing top) and the tank, bushings are manufactured in the form of long cantilevers, similar to the ones installed on the roof of the power transformer of Figure 1-2. Hence, the need to satisfy the conflicting electric and structural requirements controls the bushing design, and its structural properties.

It should be emphasized that the bushings, typically projecting as cantilevers from the top of the power transformer's tank, are connected to the transmission line at their top. During earthquakes, while the tank is exciting these bushings at their mounting interface on the roof, the transmission line often moves in a different direction, thus further challenging the bushings in shear and flexure. When this additional input is coupled with the dynamics of the ceramic bushing and with the rigidity of the bushing construction, these sensitive insulators break leading to loss of power transformers and affecting entire grid operations. For this purpose, the bushings and the power transformers are challenged in qualification testing to insure their uninterrupted operation.

1.2. Current Practice for the Seismic Qualification of Bushings and Power Transformer Design

According to the IEEE 693 standard (IEEE, 2005), high voltage bushings of 161kV and above must be seismically qualified prior to their use in the field, through tri-directional shake table testing. Depending on the seismicity at the site of installation, IEEE 693 specifies three seismic levels for the qualification of electrical equipment located in substations: the high, moderate, and low seismic qualification levels, albeit the latter does not require testing. Each of the high and moderate seismic qualification levels are characterized by a corresponding Required Response Spectrum (RRS), which defines the input motion for testing or analysis when seeking a given seismic qualification. The horizontal high RRS, tied to a peak ground acceleration of 0.5g, is presented in Figure 1-4 for various damping levels. The vertical RRS of each seismic qualification level, is defined as 80% of the respective horizontal RRS.

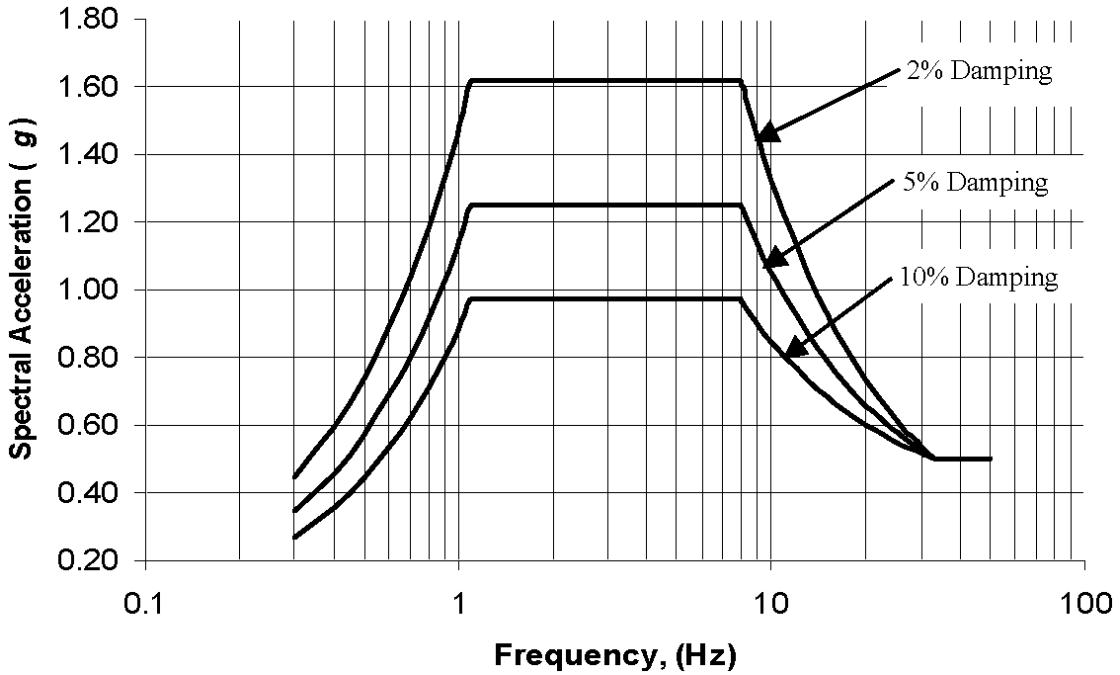


Figure 1-4 Horizontal High Required Response Spectrum (IEEE 693, 2005)

It should be noted that per IEEE 693, generic electrical equipment is expected to perform acceptably well at the performance level, which is in fact two times the corresponding seismic qualification level introduced above. Typically, actual testing of electrical equipment to the performance level is deemed impractical due to limitations in the seismic testing facilities, and the likelihood of damaging the equipment by testing it at such high levels; thus, IEEE 693 allows testing to be performed at the qualification level instead, and the monitored performance to be projected to the performance level. For high voltage bushings however, because of complexities in the flange connection and their criticality to the power transformer operation, projection of the performance is not permitted. Instead, bushings are required to be qualified directly to the performance level. Furthermore, because shake table testing of a bushing in its normal operating configuration, as-installed on a full scale power transformer, is costly and in most cases unfeasible, IEEE 693 allows testing to be performed with the bushing mounted inclined on a rigid stand, and at twice the performance level (two times RRS) to which the full power transformer-bushing system would have been theoretically qualified, in order to account for amplifications through the power transformer body. To summarize, bushings are qualified to four times the relevant RRS, arguably a significant level of shaking.

According to IEEE 693, power transformers are qualified by static analysis or load path calculations, depending on their capacity, and are designed to be field welded to embedded plates or beams of the foundation. In static analysis, the inertia forces of all components on the power transformer are obtained by applying both the vertical and horizontal seismic forces simultaneously in the direction that produces the most severe equipment stresses, in order to conservatively take into consideration the overturning moments of the tank. The forces are then combined using the SRSS method. When the high seismic level is specified, 0.5g is used in the

two horizontal directions and 0.4g is used in the vertical direction (zero period acceleration or ZPA of the horizontal and vertical high RRS). When the moderate seismic level is specified, 0.25g is used in the two horizontal directions and 0.2g is used in the vertical direction (ZPA of the horizontal and vertical moderate RRS).

1.3. **Past Seismic Performance of High Voltage Power Transformers and Bushings**

Power systems have been proven to be particularly susceptible to damage in recent major seismic events. The 1989 Loma Prieta earthquake, 1994 Northridge earthquake, 1995 Kobe earthquake, 1999 Izmit and Chi-Chi earthquakes (Schiff 1995, 1998, Schiff and Tang 2000, Tang 2000), 2010 Baja California earthquake (Schiff 2010) and 2010 Chile earthquake (Schiff, 2010) are some examples of strong earthquakes that caused considerable damage to electrical equipment. Despite the short duration of the power system disruption during these events, the estimated direct costs due to damaged equipment and rehabilitation costs amounted to hundreds of millions of dollars in each case. Furthermore, the loss of power due to the damaged network further prevented emergency response and recovery operations for the affected region and instigated significant collateral costs for the utilities, including revenue losses from blackouts. For instance, the Los Angeles Department of Water and Power (LADWP) reported that the net operational losses for LADWP's electrical system in a blackout condition following the 1994 Northridge earthquake averaged about $4.4 million per day (Shinozuka, 1998).

As discussed above, the power transformer is a vital component for the operation of a power system; it is also the single largest capital item in a substation, comprising almost 60% of the total investment (Woodcock, 2000). Depending on its capacity, the cost of a high voltage power transformer unit can range between $2M and $7M. Furthermore, the commercial power

transformers are not standardized and present high variability in their designs, with one manufacturer corresponding to roughly 1.3 high voltage electrical power transformer models in the field (NY Times, 2012). These factors, along with the typically massive dimensions of the power transformers, lead to extended transportation and replacement times that add to the challenge of substituting a failed power transformer. Loss of high voltage power transformers is thus highly undesirable. Nevertheless, seismic damage of power transformers is common and failure modes such as overturning of unrestrained power transformers, anchorage failure, and failure of power transformer attachments have often been reported in past strong events.

High voltage bushings mounted on power transformer tank roofs have also been shown to be particularly vulnerable to seismic damage. This vulnerability is primarily caused by the aforementioned structural irregularities in their design. The most commonly observed failures of bushings are oil leakage due to gasket slip and extrusion, and cracking of the porcelain units due to the inertia forces or stresses induced by insufficient slack in the high voltage cable connected to the top of the bushing. The failures of power transformer bushings are particularly harmful because once they occur, the electrical insulation is compromised and the entire power transformer has to be taken out of service.

In consideration of the above, it is of great interest to societies and power utilities to properly qualify power transformer bushings prior to their field installation, as well as to seismically protect high voltage power transformers and bushings in order to minimize earthquake damage and disruption to their systems.

1.4. **Discrepancy between the Current Qualification Practice and Observed Performance**

High voltage bushings are designed to fit power transformers from different manufacturers, and are rigorously qualified for such generic use in compliance with the requirements of IEEE 693 discussed above; the capacity of as-installed bushings (flexibly mounted condition), however, is typically only 1/3 to 3/4 of their seismic qualified shake-table capacity (stiff mounted condition) (Schiff, 2011).

Recent studies have indicated that the observed discrepancy between the tested and actual capacities can be attributed to, (i) the differences between the as-installed and tested bushing configurations, and (ii) to the potential for higher than anticipated amplification of the ground motion at the attachment of the bushing to the power transformer (bushing mounting interface or bushing flange-tank roof interface). More specifically, the natural frequency of a bushing qualified by testing in a fixed base configuration will be generally higher than the frequency of the same bushing as-installed on a flexible tank roof. The stiff-mounted frequency of a 230 kV porcelain bushing for instance, will be in the range between 14 Hz and 25 Hz; however, its as-installed frequency on a power transformer will typically be 1/4 to 1/2 of the stiff-mounted frequency (Schiff, 2011). With reference to the high RRS of Figure 1-4, it can be inferred that the actual demand on the 230 kV porcelain bushings will be higher than the demand for which they are normally qualified. On the other hand, it has been shown that the amplification at the bushing mounting interface can be larger than the factor of two recommended in IEEE 693. The amplification is more pronounced when the tank and bushing frequencies fall in the same frequency range, that is, when there is resonance between the two components.

The first of the research efforts that highlighted the above issues is the work of Bellorini et al (1997) who conducted in-situ testing on an actual power transformer, as well as numerical analyses using calibrated finite element models, and found that the amplification at the bushing flange level can exceed the value of 2 specified by the IEEE 693 standard. Villaverde et al (2001) also conducted field tests on high voltage power transformers and developed simplified analytical models calibrated to the experimental data to determine the amplification factor at the base of the bushing for different ground motion scenarios. A maximum amplification factor of 4 - twice the value specified by the IEEE 693 standard - was calculated at the bushing mounting interface or bushing flange-tank roof interface. Ersoy and Saadeghvaziri (2004) developed detailed finite element models of various power transformer-bushing systems to investigate their interactions. The amplification in the power transformer tank was found to be as high as 2.5. It was also shown that the flexibility of the tank roof affected the bushing dynamics significantly, reducing their fixed-base frequency from 14.4Hz to approximately 10Hz, when installed on the roof. Filiatrault and Matt (2005) performed shake table testing of an actual power transformer tank stripped of its appendages, oil and core, and with a mock bushing installed at its flexible cover. The spectral amplification on the tank roof, at the as-installed frequency of the bushing was found to be higher than 2, and as high as 3. Subsequently, the same authors performed numerical analyses of various power transformer-bushing systems (Filiatrault and Matt, 2006), and demonstrated that significant amplifications can occur in case of resonance between the tank and the bushings. In fact the input at the bushing mounting interface or bushing flange-tank roof interface was found to be amplified by as much as 17 times; this value is higher than the one proposed by IEEE 693 by as much as one order of magnitude. The effect of the tank roof flexibility on the dynamics of the as-installed bushing was also investigated.

Perhaps the most important discrepancy in determining the dynamic behavior of a bushing is the contribution of the roof of the tank on which the bushing is mounted. Reinhorn et al (2012) showed that the dynamic behavior of the roof-bushing assembly is completely different than fixed base bushings. Moreover, Koliou et al (2012, 2013a, 2013b) showed that structurally modifying the roof of the tank changes the behavior of the roof-bushing assembly, and further recommended remedies to improve the assembly dynamics and effectively minimize the damaging demands on the bushing construction.

The findings of the above studies suggest that the qualification of bushings needs to consider the as-installed conditions of the bushings. Furthermore, protective measures need to be taken to seismically strengthen the existing power transformers and bushings. On account of the aforementioned discrepancies in the boundary conditions used for the bushings in qualification testing, improved testing techniques and setups have already been proposed and utilized. For instance, Kong and Reinhorn (2010) developed a rigid frame with a flexible cover that simulates the flexible roof of the power transformer tank, and which can be appropriately relocated to qualify the bushing for various mounting configurations on the tank roof. As far as the seismic retrofit of electrical power transformers is concerned, several measures have been proposed, mostly towards stiffening the tank and its components. Filiatrault and Matt (2006) proposed stiffening the tank laterally in order to decouple the tank and bushing frequencies, and reduce the amplification of the bushing response. Seismic upgrading of existing power transformers - the great majority of which have been designed to meet much older seismic criteria - is also currently performed by utilities. For instance a seismic mitigation program initiated by the Bonneville Power Administration (BPA) in the aftermath of the 1994 Northridge earthquake included anchorage of power transformers (rail and pad mounted) and reactors, addition of

supplemental structural bracing for power transformer accessories (radiators, conservators, and surge arresters) and anchorage of station service power transformers (Knight, 2004). Protective measures specific to bushings have also been proposed, such as the use of ring configurations around the lower gasket for the prevention of slip and leakage (Gilani et al, 1999), and stiffening of the tank roof around the bushing mounting interface in order to reduce the seismic demand to the bushing by approaching a fixed-base configuration (Koliou, 2010).

1.5. **Motivation for Current Study**

Retrofitting of high voltage power transformers is complicated by the high variability in the commercial power transformer models, the various possible mounting configurations of the bushings, and the general high complexity in the power transformer's structural system. As an example, laterally stiffening of a power transformer tank may not always be a practical solution because of space constraints, limited capability for welding on the tank body and lack of extended foundation to support the lateral stiffeners. In addition to feasibility constraints, stiffening the power transformer as a retrofit measure does not necessarily guarantee improvement of its seismic behavior because the achieved frequency shift may ultimately increase its seismic demand. Furthermore, the local protection of selected attachments on the tank, such as the high voltage bushings, may shift the failure to other components which until then were not critical. Thus, there is a need to seek alternative protection measures which will generally protect the power transformer and its components.

Base isolation is a practical method of seismically protecting the electrical power transformers in a global fashion. The satisfactory performance of conventional base isolated structures, such as medium rise buildings and bridges, in recent earthquakes, as well as the extensive research on

the subject throughout the past 30 years, have increased the popularity of the technique. Base isolation is achieved by introducing flexible elements (isolators) between the structure and the foundation in order to decouple the structure from the damaging effects of the ground motion.

Analytical and experimental research efforts have demonstrated that seismic isolation can be very beneficial to electrical equipment. The first known application of base isolation in electrical equipment is found in the work of Kircher et al (1979) who isolated a 230 kV ATB 7 circuit breaker with asymmetric mass distribution, located in the A. D. Edmonston Pumping Plant on California Aqueduct, using low damping elastomeric seismic isolators. The isolated breaker subsequently survived a moderate earthquake that damaged and knocked off line about one-half of the breakers in the switchyard (Kircher, 2010). Suzuki et al (1987) developed a hybrid base isolation device for the retrofit of electrical power transformers, which combined a flat sliding surface with solid lubricator for energy dissipation, and a natural rubber ring for lateral restoring force. They performed unilateral shake table testing using three historic ground motions, on a 275kV power transformer-bushing-isolation model that was scaled in length by a factor of 4. While the properties of the bearing used were not provided, it was shown that the peak ground acceleration was reduced by as much as 75%. Furthermore, they retrofitted an actual 154kV, 216ton power transformer with the proposed isolation system and monitored it for two years; during that time, the base isolated power transformer survived two moderate earthquakes. Ersoy et al (2001) proposed the use of Single Friction Pendulum (FP) bearings for the base isolation of electrical power transformers and conducted experimental and analytical studies on an isolated power transformer model. The authors performed shake table testing using a model power transformer with a flexible roof, including a high voltage bushing. Testing was performed at fixed base conditions and the power transformer was isolated with FP bearings. Peak

acceleration reductions of 60% on average were achieved within the displacement limits of the FP bearings. Moreover, the numerical and experimental results were found to be in good agreement. Murota et al (2006) also performed shake table testing of seismically isolated power transformers. A model power transformer retrofitted with isolation systems consisting of multi-stage high damping elastomeric bearings or combined sliding-elastomeric bearings were tested. Isolator displacements of less than about 15 inches were recorded, and recorded accelerations in the isolated model were substantially less than those in the non-isolated model. Kong and Reinhorn (2009) performed testing of disconnect switches retrofitted with (i) Single FP bearings, and (ii) wire rope isolators. The FP bearings were found to perform remarkably well, reducing the stresses in the post insulators by 75%, and the maximum relative displacements (drift) to 40% of the ones of the non-isolated case.

The above studies considered systems with promising experimental and analytical results; however, several of the particular constraints of the isolation system design for electrical equipment, were not properly addressed. Electrical power transformers are often located in highly seismic regions; proposed isolation systems must be designed and tested for levels that address that level of seismicity, and the adequacy of their performance for such level needs to be properly investigated. Furthermore, the displacement response of the proposed systems will be within acceptable, bounded limits, so that the conductors connected to the top of the bushings should not endanger the bushing and connections to ancillary peripheral equipment. In the experimental studies presented above, the earthquake records used in testing (PGA of 0.5g or less) did not represent strong earthquakes consistent with the Maximum Earthquake in areas of strong seismicity (California, Chile, Turkey, New Zealand), and the short frequency spectral content of the records was substantially less than what industry standards require in the US (i.e.,

IEEE 693). Accordingly, the measured isolator displacements were relatively small and within the capacity of power transformers to properly function. By comparison, isolator displacement capacities in recent applications of seismic isolation to important structures in California and Turkey vary from 20 to over 40 inch depending on the proximity of the site to active faults.

1.6. **Objectives and Scope of Current Study**

This study deals with the design of isolation systems for electrical power transformers that comply with the aforementioned requirements. More specifically, the application of seismic isolation to power transformers is complicated by the constraints summarized below:

a. The supported weight is small so that isolation by significant shift of the effective period is not possible with elastomeric isolation systems. Rather, one has to rely on stiff elastomeric systems. This is desirable given that isolator displacements need to be relatively small for functionality of the power transformer but it leads to higher accelerations.

b. Sliding systems are ideal for low weight applications as the period can be independent of the supported weight but still the problem exists for the isolator displacements to be within prescribed tight limits.

c. Power transformers are prefabricated and are relatively vertically stiff structures that when isolated will be lifted and placed on the isolators (rather than built from the bottom up as in a building). This process results in uncertain distribution of weight on the isolators.

d. Power transformers are asymmetric structures, which coupled with the way they will be isolated (see item c above), will inevitably result in asymmetric distribution of load on the isolators and likely significant torsional response when elastomeric isolators are used.

e. Owners of power transformers require that installation and removal of the equipment from the isolation system during retrofit or maintenance of the power transformer is quick so that the transmission of power is not interrupted for long periods of time. This requires that the method of connection of the isolators to the equipment facilitates easy installation and removal. Isolators that are not bolted and only kept by friction at the isolator to equipment interface appear most desirable.

f. Earthquake excitation in areas of high seismicity is very strong. Added to this complexity are requirements imposed by the IEEE 693 standard for high spectral components in the low frequency range. The result is large isolator displacement demands.

g. The connections to ancillary equipment external to the power transformer will require special design to accommodate large isolator displacements.

The objectives and scope of the experimental study conducted was formed on the basis of the complexities identified above. Specifically, the study had the following objectives:

a. Develop seismic isolation system designs that are appropriate for low weight, highly asymmetric structures with weight in the range of about 100 to 500 kips. Isolator displacements should be small and ideally less than about 12 inches in strong seismic excitation.

b. Test these isolation systems in a simplified compact model structure on the shake table with appropriate asymmetry in mass distribution, symmetry and asymmetry in the location of bushings, appropriate flexibility of the bushing to structure connection and utilization of connection details that facilitate installation of the isolation system.

c. Test at reduced length scale and, if possible, at full length scale.

d. Demonstrate the effectiveness of isolation by comparison to the response of the same equipment without the isolation systems.

e. Develop analytical models of the tested specimen and compare results to experiments in order to establish the degree of accuracy of the analytical prediction.

The scope of this study is to develop practical seismic isolation for use in electrical power transformers using already established seismic isolation technologies and with due consideration for the complexities and requirements reported above. Based on the constraints identified above, two systems are selected as the best candidate systems for seismic isolation: (a) stiff and highly damped lead-rubber bearings, and (b) high friction Triple Friction Pendulum bearings. An experimental study is carried out using the selected systems and a mock power transformer model which nonetheless, incorporates all of the important structural features of the power transformer tank and the bushing dynamics. Analytical investigations are also performed to verify the predictability of the isolated system behavior. A design methodology follows which discusses effective installation measures for the isolators and the foundation, which eliminate the interruption of the power network operation. It is shown that both systems perform within the

said constraints under strong shaking and that their response is predictable and with sufficient accuracy.

1.7. **Organization of Report**

The report is organized as follows:

Section 2 presents the principles of operation of seismic isolation and the mechanics of isolation systems selected for the retrofit of electrical power transformers.

Section 3 presents the setup for an experimental program with the objective of investigating the performance of the selected base isolation systems for the retrofit of electrical power transformers.

Section 4 presents and discusses results obtained from shake table testing of a power transformer specimen tested under non-isolated and isolated conditions, with the selected base isolation systems.

Section 5 describes the development of analytical models of the frame-bushing specimen and the seismic isolation system selected and tested. Furthermore, it presents analysis results and comparisons with experimental measurements to assess the accuracy of the models.

Section 6 describes the design steps for the base isolation of electrical power transformers and presents an application example to demonstrate the methodology.

Finally, Section 7 presents the conclusions of this study.

This Page is Intentionally Left Blank

SECTION 2
SEISMIC ISOLATION OF ELECTRICAL POWER TRANSFORMERS

2.1. Overview

This section provides an overview of the seismic isolation systems selected in the present study as suitable for the seismic isolation of electrical power transformers. An introduction of the general principles of seismic isolation is first provided. The considerations behind the selection of seismic isolation systems to address the particular requirements of the electrical power transformers are also discussed. Two base isolation systems are considered fit for the seismic protection of electrical power transformers, highly damped lead rubber bearings and highly damped friction pendulum bearings. The mechanical properties and operation of these systems are presented.

2.2. Principles of Operation of Seismic Isolation

Seismic isolation is a design approach developed to mitigate the effects of earthquake shaking on structures. The technique has most commonly been applied to conventional civil engineering structures such as bridges and buildings; however, its principles of operation are not project specific and its applicability is not limited to these structures; non-conventional structures which have been seismically isolated in the past include oil platforms, liquefied natural gas (LNG) tanks, offshore oil and gas platforms, valuable museum artifacts such as statues, and electrical equipment. When the seismic isolation is applied at the base of a structure, it is typically referred to as base isolation. Since the most efficient way to isolate electrical power transformers is at their base, the latter term is conveniently adopted throughout this report.

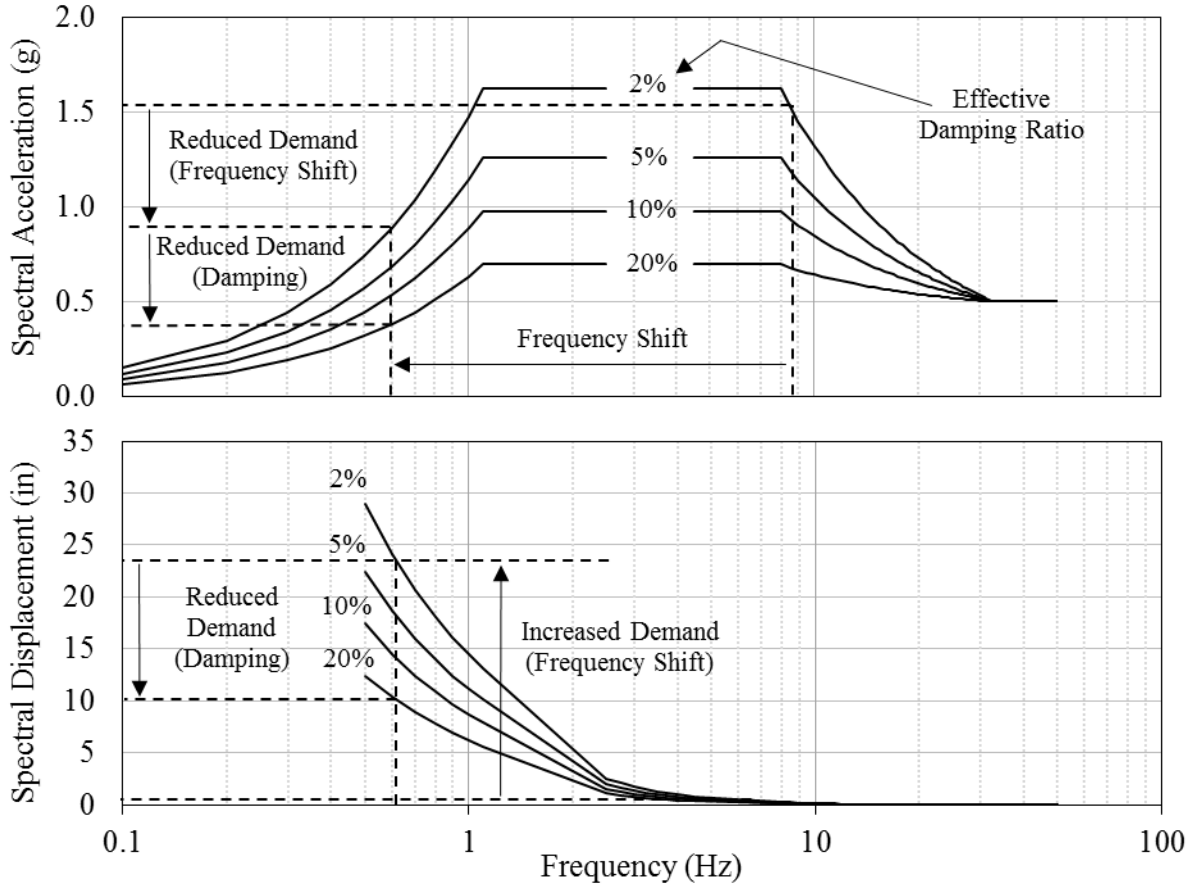


Figure 2-1 Effect of Horizontal Isolation on the Spectral Acceleration and Displacement Demand (IEEE 693 High RRS Shown)

Base isolation is achieved by introducing flexible elements, designated seismic isolators, between the structure and its foundation. The purpose of base isolation is to decouple the structure from the ground motion and ultimately reduce the forces transferred due to the earthquake shaking. Contemporary seismic isolation systems provide horizontal isolation; in the vertical direction they are designed considerably stiffer in order to safely transfer the static and seismic vertical loads to the foundation. In addition to their horizontal flexibility, seismic isolators typically possess an energy dissipation mechanism to reduce the system displacements, and, depending on the nature of damping, to further reduce the forces in the structure.

Based on the aforementioned properties it can be inferred that base isolation performs a dual task: it lowers the natural frequency of the structure as a result of the flexible action of the isolators, and dissipates energy by means of its inherent energy dissipating mechanism. The frequency reduction shifts the system in the spectral range where the earthquake demand is generally lower. The energy dissipation mechanism of seismic isolators is usually of hysteretic type, however for simplified analysis purposes it is commonly transformed into an equivalent or effective viscous damping on the basis of some rational procedure. Figure 2-1 demonstrates the combined effect of the frequency shift and energy dissipation (in the form of equivalent viscous damping) on both the acceleration and displacement demand. Note that the acceleration in Figure 2-1 is the pseudo-acceleration, or the acceleration at the instance of maximum displacement, which will be the maximum acceleration for a hysteretic system. For a truly viscous system the maximum acceleration is slightly larger than the pseudo-acceleration for the range of effective damping shown in the figure (Ramirez et al, 2001). The acceleration and displacement High RRS of the IEEE 693 have been selected for a range of damping ratios in the demonstration of Figure 2-1, as being pertinent to the seismic design and testing of electrical equipment. Consider an essentially elastic (low damping) and relatively stiff structure, which is the case of a high voltage power transformer. Figure 2-1 shows that for a typical effective frequency for the isolated system of less than 1Hz, the acceleration (inertial) demand is significantly reduced, and that the effect of the hysteretic energy dissipation mechanism (equivalent viscous damping) is to further reduce that demand. On the other hand, the frequency shift will increase the displacement demand of the system. Nevertheless, the hysteretic energy dissipation mechanism will compensate for that increase by operating to reduce the displacement demand.

2.3. **Selection of Base Isolations for Electrical Power Transformers**

The most popular contemporary base isolation systems are elastomeric and sliding isolation systems. A fundamental difference between the two systems is that the properties of elastomeric systems are practically independent of the structural weight, while the properties of sliding systems are proportional to the weight and its distribution within the structure.

Compared to conventional massive engineering structures such as bridges and buildings, electrical power transformers are relatively light structures. Furthermore, in designing seismic isolation systems for power transformers, for stability purposes as well as for simplicity in construction, it is preferable to use four bearings. This construction aspect combined with the inherently light weight of the power transformer result in small supported weights on the isolators.

The fundamental frequency of a non-isolated power transformer is usually larger than 10 Hz, that is, well beyond the effective frequency of a typical isolated system. Thus the power transformer can be treated as rigid and the effective frequency of the isolated system can be obtained from classical dynamics as:

$$f_{eff} = \frac{1}{2\pi}\sqrt{\frac{K_{eff}}{M}} \qquad (2\text{-}1)$$

where,

$K_{eff} = F_{\max}/D_{\max}$, is the effective stiffness of the isolation system at the maximum design displacement, D_{max}, and F_{max} is the force at maximum displacement.

When elastomeric isolators are used and in order to sufficiently reduce the effective frequency of the system and maximize the benefits from the reduction of acceleration demand, one would have to reduce the stiffness of the isolators, as dictated by Equation (2-1). Increasing the flexibility of elastomeric isolators requires the design of taller elements, which however would be susceptible to buckling. Consequently, significant frequency shift is difficult to achieve with elastomeric isolation systems. Rather, one can take advantage of the fact that electrical equipment has different performance criteria than conventional structures, in that equipment is a non-occupancy structure and the quality of user experience associated with the response of the structure is not relevant in the design. By doing so, the design requirement of maximizing the reduction of the accelerations in base isolated electrical power transformers can be relaxed. This is not a limitation given that isolator displacements will need to be relatively small so that the functionality of the power transformer is not at risk. Appropriately, stiff elastomeric systems are applicable.

Sliding isolators have stiffness and strength that are proportional to the weight. This is a very advantageous feature because one design can be used for a range of weights of supported structure. Additionally, the frictional properties can be appropriately designed to produce highly damped systems. Such systems are desirable for base isolating electrical power transformers to keep the seismic displacements acceptably low.

In the present study, two systems are selected as the best candidate systems for seismic isolation of electrical power transformers: (a) stiff and highly damped lead-rubber bearings, and (b) high friction Triple Friction Pendulum bearings. The mechanics of these two systems are discussed in the following sections.

2.4. **Mechanics of Lead-Rubber Bearings**

The lead-rubber bearing (LRB) is one of the most popular bearings currently used in seismic isolation design. Figure 2-2 provides a cutout of a LRB. The bearing consists of an array of steel reinforced rubber layers which provide stiffness and restoring force, and features a cylindrical lead core at its center for energy dissipation. The steel reinforcement provides very high vertical stiffness to the bearing while at the same time it allows the bearing to freely deform laterally. The lead core is typically manufactured with a diameter that matches the inner hole, but cut slightly longer in height. Subsequently, by bolting the top and bottom mounting plates to the internal end plates of the bearing the lead core is forced to fit tightly and become confined by the steel shims of the reinforcement. Under such configuration the lead core can dissipate energy effectively through plastic deformation when the isolator deforms laterally. An attractive feature of the LRB is the ability to provide large characteristic strength by selecting a large lead core diameter.

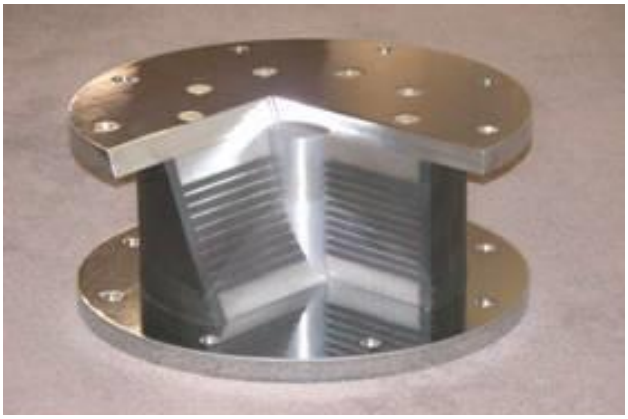


Figure 2-2 Cutout of a Lead-Rubber Bearing (Courtesy of DIS Corp.)

Figure 2-3 illustrates the idealized bilinear hysteretic behavior of a lead-rubber bearing. The mechanical behavior can be sufficiently described by three parameters: the characteristic strength

Q_d, the post-elastic stiffness K_d and the yield displacement Y. The force-displacement relationship for the lead-rubber bearing is expressed as:

$$F = K_d u + Q_d \tag{2-2}$$

The characteristic strength is related to the area of lead A_L and the effective yield stress of lead σ_L as follows:

$$Q_d = A_L \sigma_L \tag{2-3}$$

The post-elastic stiffness K_d is related to the shear modulus of rubber G, the bonded rubber area A_r, and the total rubber thickness T_r by:

$$K_d = \frac{GA_r}{T_r} \tag{2-4}$$

Lastly, the yield displacement Y is typically assumed to be in the range of 0.5 to 1.0 inch (12 to 25 mm) and useful in calculating the effective damping and in modeling the isolator for dynamic response history analysis.

It should be noted that the values of the yield stress of lead σ_L and the shear modulus of rubber G, used in Equations (2-3) and (2-4), respectively, are anticipated to be higher during the first cycle than the rest of the motion. That effect needs to be taken into account by performing analysis using upper and lower bound properties for the lead-rubber bearings. Guidelines for the selection of suitable LRB isolator properties in the design, as well as further details on the behavior of the LRB isolators may be found in Constantinou et al (2007). Formal procedures for

establishing the bounding values of properties for analysis are described in McVitty and Constantinou (2015).

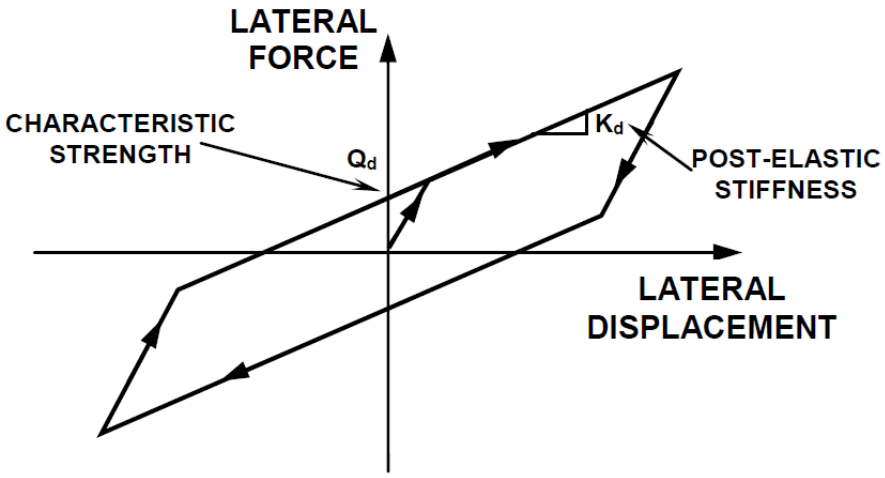


Figure 2-3 Idealized Force-Displacement Relation of a Lead Rubber Bearing

If the power transformer is idealized as a single degree of freedom system with weight W, the lateral force-displacement relation is as described in Figure 2-3 and the design displacement is D, the effective frequency (f_{eff}) and effective damping (β_{eff}) for use in design with the IEEE spectra shown in Figure 2-1, can be calculated as:

$$f_{eff} = \frac{1}{2\pi}\sqrt{\frac{K_{eff}\,g}{W}} = \frac{1}{2\pi}\sqrt{\frac{g}{W}\left(K_d + \frac{Q_d}{D}\right)} \qquad (2\text{-}5)$$

$$\beta_{eff} = \frac{1}{2\pi}\left[\frac{EDC}{K_{eff}D^2}\right] = \frac{1}{2\pi}\left[\frac{4Q_d\left(D-Y\right)}{K_dD^2 + Q_dD}\right] \qquad (2\text{-}6)$$

In the equations above, the effective stiffness K_{eff} at displacement D is:

$$K_{eff} = K_d + \frac{Q_d}{D} \qquad (2\text{-}7)$$

The energy dissipated per cycle, EDC, is:

$$EDC = 4Q_d\left(D - Y\right) \tag{2-8}$$

2.5. **Mechanics of Triple Friction Pendulum Bearings**

Friction pendulum bearings are isolators that rely on friction for energy dissipation, and on the geometry of the bearings for lateral resistance. The single Friction Pendulum bearing comprises a spherical stainless steel sliding surface and an articulated slider of equal curvature having a coating of low friction material. During earthquake shaking, the above configuration allows the two surfaces to slide relative to each other and dissipate energy through friction. When sliding occurs, the point of application of the axial force is displaced from the initial static equilibrium position, and shifted to a different location on the concave surface. At that displaced state, the component of the axial force, tangential to the concave surface, provides the lateral restoring force.

The Triple Friction Pendulum (Triple FP) bearing is an extension of the Single FP bearing which is based on the above described principles for its operation, but it is configured with four spherical sliding surfaces and accordingly has a large displacement capacity for its size. The existence of four sliding surfaces also partitions the top to bottom relative velocity, resulting thus in reduced heating effects for each surface. Furthermore, its special configuration allows the system to exhibit both adaptive stiffness and adaptive damping, which are intended to limit displacements during beyond-design basis earthquakes. To achieve that, the stiffness and effective friction are designed to change to predictable values at prescribed displacement amplitudes.

Figure 2-4 shows a cutout of a Triple FP bearing. The bearing comprises two sliding plates facing each other (top and bottom), each having a concave stainless steel surface, and a nested slider assembly. The slider assembly contains two facing slide plates, smaller in size, and a rigid slider. The inner side of each slide plate is configured as a concave stainless steel surface, while the outer side is coated with a low friction material and has the same curvature with the top and bottom concave sliding plates, to allow for sliding between the plates. Finally, both the top and bottom surfaces of the rigid slider are coated with a low friction material, typically lower than the slide plates, and has the same curvature with the slide plates to allow for sliding. Figure 2-5 provides an illustration of the components of the Triple FP bearing.

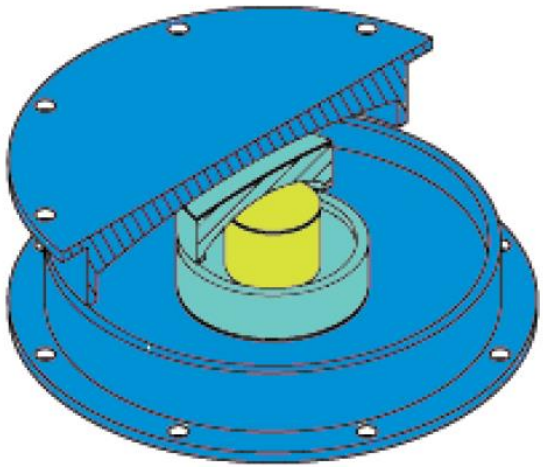


Figure 2-4 Cutout of Triple Friction Pendulum Bearing



Figure 2-5 Components of Triple Friction Pendulum Bearing (Courtesy of EPS)

The Triple FP isolator has a complex force-displacement behavior during its operation. During motion, only two of the four surfaces experience sliding while the rest remain inactive. Furthermore, throughout its motion, the bearing experiences multiple changes in the combination of the sliding surfaces, in a controlled manner, due to the adaptive nature of the system. In general, the force-displacement relationship of the bearing is dependent on the selection of geometric and frictional properties for the sliding surfaces, and varies in accordance to the bearing displacement as well as the history of motion.

Fenz and Constantinou (2008b) derive the force-displacement relationships of the triple FP bearing for the special and practical case for which $R_{eff\,2} = R_{eff\,3}$ $R_{eff\,1} = R_{eff\,4}$, $\mu_2 = \mu_3 < \mu_1 < \mu_4$, $d_2^* > (\mu_1 - \mu_2) R_{eff\,2}$ and $d_3^* > (\mu_4 - \mu_3) R_{eff\,3}$, with reference to the schematic of Figure 2-6 for definition of the relevant parameters. Note that $d_i^* > d_i \left(R_{effi} / R_i \right)$ is the actual displacement capacity on surface i. In this combination of parameters, it is obvious that besides the curvature and frictional properties of the sliding plates, it is also the displacement capacities designed for the slide plates and the rigid slider that influence the force-displacement behavior. It is shown that, with the above configuration, sliding will always take place on any two facing surfaces at any instant of motion. That is, sliding occurs simultaneously either on surfaces 2 and 3, or 1 and 3, or 2 and 4, with reference to the enumeration of Figure 2-6. The motion is organized into five sliding regimes, each corresponding to a distinct combination of surfaces upon which sliding occurs. A generic force-displacement relationship is provided for any regime as:

$$F = \frac{W}{R_{eff}} u + F_f \qquad (2\text{-}9)$$

Where,

$R_{eff} = R_{effi} + R_{effj}$, is the sum of the effective stiffnesses of the two surfaces i and j on which sliding occurs,

$R_{effi} = R_i + h_i$, is the effective stiffness of surface i, and,

F_f, is the threshold force that signifies the transition into the current sliding regime

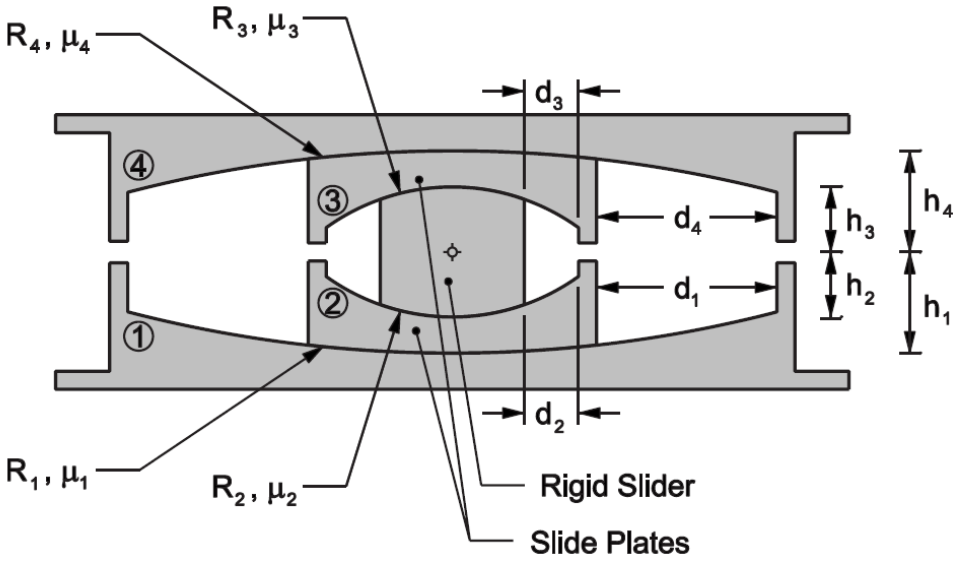


Figure 2-6 Cross Section of the Triple Friction Pendulum Bearing and Definition of Parameters (from Fenz and Constantinou, 2008b)

The force-displacement relationship for each regime of the Triple FP configuration is provided in Table 2-1 (Fenz and Constantinou, 2008b).

Table 2-1 Summary of Triple FP Bearing Behavior (Nomenclature Refers to Figure 2-6)

Regime	Description	Force-Displacement Relationship
I	Sliding on surfaces 2 and 3 only	$F = \frac{W}{R_{eff\,2} + R_{eff\,3}} u + \frac{F_{f\,2} R_{eff\,2} + F_{f\,3} R_{eff\,3}}{R_{eff\,2} + R_{eff\,3}}$ *Valid until:* $F = F_{f1}, \quad u = u^* = (\mu_1 - \mu_2) R_{eff\,2} + (\mu_1 - \mu_3) R_{eff\,3}$
II	Motion stops on surface 2; Sliding on surfaces 1 and 3	$F = \frac{W}{R_{eff\,1} + R_{eff\,3}} u + \frac{F_{f\,1}(R_{eff\,1} - R_{eff\,2}) + F_{f\,2} R_{eff\,2} + F_{f\,3} R_{eff\,3}}{R_{eff\,1} + R_{eff\,3}}$ *Valid until:* $F = F_{f\,4}, \quad u = u^{**} = u^* + (\mu_4 - \mu_1)(R_{eff\,1} + R_{eff\,3})$
III	Motion is stopped on surfaces 2 and 3; Sliding on surfaces 1 and 4	$F = \frac{W}{R_{eff\,1} + R_{eff\,4}} u + \frac{F_{f\,1}(R_{eff\,1} - R_{eff\,2}) + F_{f\,2} R_{eff\,2} + F_{f\,3} R_{eff\,3} + F_{f\,4}(R_{eff\,4} - R_{eff\,3})}{R_{eff\,1} + R_{eff\,4}}$ *Valid until:* $F = F_{dr1} = \frac{W}{R_{eff\,1}} d_1^* + F_{f\,1},$ $u = u_{dr1} = u^{**} + d_1^* \left(1 + \frac{R_{eff\,4}}{R_{eff\,1}}\right) - (\mu_4 - \mu_1)(R_{eff\,1} + R_{eff\,4})$
IV	Slider contacts restrainer on surface 1; Motion remains stopped on surface 3; Sliding on surface 2 and 4	$F = \frac{W}{R_{eff\,2} + R_{eff\,4}} (u - u_{dr1}) + \frac{W}{R_{eff\,1}} d_1^* + F_{f\,1}$ *Valid until:* $F = F_{dr4} = \frac{W}{R_{eff\,4}} d_4^* + F_{f\,4},$ $u = u_{dr4} = u_{dr1} + \left[\left(\frac{d_4^*}{R_{eff\,4}} + \mu_4\right) - \left(\frac{d_1^*}{R_{eff\,1}} + \mu_1\right)\right](R_{eff\,2} + R_{eff\,4})$
V	Slider bears on restrainer of surface 1 and 4; Sliding on surfaces 2 and 3	$F = \frac{W}{R_{eff\,2} + R_{eff\,3}} (u - u_{dr4}) + \frac{W}{R_{eff\,4}} d_4^* + F_{f\,4}$

Assumptions: (1) $R_{eff\,2} = R_{eff\,3}$ $R_{eff\,1} = R_{eff\,4}$, (2) $\mu_2 = \mu_3 < \mu_1 < \mu_4$, (3) $d_1^* > (\mu_4 - \mu_1) R_{eff\,1}$, (4) $d_2^* > (\mu_1 - \mu_2) R_{eff\,2}$, (5) $d_3^* > (\mu_4 - \mu_3) R_{eff\,3}$

In the above equations, $d_i^* > d_i\left(R_{effi}/R_i\right)$, is the actual displacement capacity of surface i, and $F_{fi} = \mu_i W$ is the force that signifies the initiation of sliding on surface i. Further details on the mechanical behavior of the Triple FP bearing may be found in Fenz and Constantinou (2008a, b, c and d). A more elaborate examination of the behavior of the Triple FP isolator without any constraints on its geometric and frictional properties may be found in Sarlis and Constantinou (2013). For demonstrative purposes, a qualitative summary of these regimes is given in Figure 2-7.

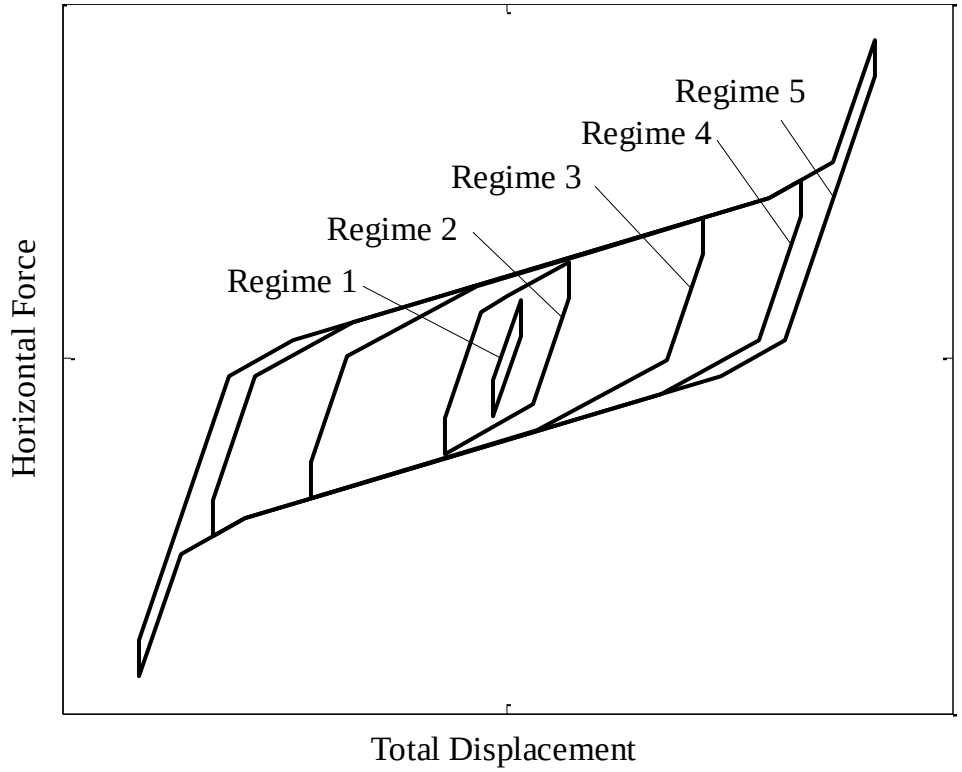


Figure 2-7 Force-Displacement Relations of Triple Friction Pendulum Bearing for Equal Friction on Surfaces 2 and 3 and Unequal Friction on Surfaces 1 and 4

A special case of a Triple FP bearing is a configuration with $R_{eff\,2} = R_{eff\,3}$ $R_{eff\,1} = R_{eff\,4}$ and $\mu_2 = \mu_3 < \mu_1 = \mu_4$ (Sarlis and Constantinou, 2010). In that configuration sliding occurs

simultaneously either on surfaces 2 and 3 or on surfaces 1 and 4 only. Consequently, the motion of the isolator is characterized by three sliding regimes. A qualitative summary of these regimes is given in Figure 2-8.

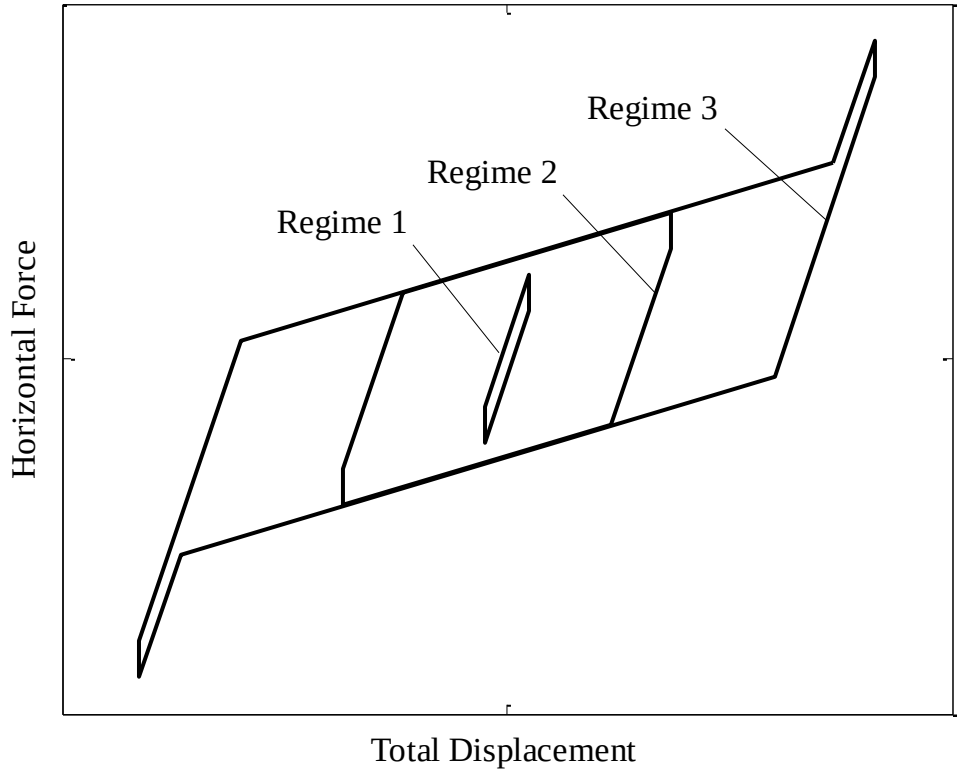


Figure 2-8 Force-Displacement Relations of Triple Friction Pendulum Bearing for Equal Friction on Surfaces 2 and 3 and Equal Friction on Surfaces 1 and 4

The latter configuration is a simpler version of the one studied by Fenz and Constantinou (2008b) and one often used in practice. In comparison to Figure 2-7, the force-displacement behavior of the second configuration presented in Figure 2-8 is missing regimes 2 and 4 of Figure 2-7, however it retains the desired adaptive behavior. The second configuration is adopted in the current study for facilitation of the design.

The force-displacement relationship for each regime of the simpler Triple FP configuration is provided in Table 2-2.

Table 2-2 Summary of Behavior of Special Configuration of the Triple FP Bearing (Nomenclature Refers to Figure 2-6)

Regime	Description		Force-Displacement Relationship
I	Sliding on surfaces 2 and 3 only		$F_1 = \frac{W}{2R_{eff\,2}}u + \mu_2 W$
		Valid until:	$F = F_{f1},\quad u = u^* = 2\left(\mu_1 - \mu_2\right)R_{eff\,2}$
II	Motion stops on surfaces 2 and 3; Sliding on surfaces 1 and 4		$F_2 = \frac{W}{2R_{eff\,1}}u + \left[\mu_1 - \left(\mu_1 - \mu_2\right)\frac{R_{eff\,2}}{R_{eff\,1}}\right]W$
		Valid until:	$F = F_{dr1} = \frac{W}{R_{eff\,1}}d_1^* + F_{f1},\ u = u^{**} = 2\left(\mu_1 - \mu_2\right)R_{eff\,2} + 2d_1^*$
III	Slider contacts restrainer on surfaces 1 and 4; Sliding on surfaces 2 and 3		$F_3 = \frac{W}{2R_{eff\,2}}\left(u - u^{**}\right) + \frac{W}{R_{eff\,1}}d_1^* + \mu_1 W$

Assumptions: (1) $R_{eff\,2} = R_{eff\,3}$ $R_{eff\,1} = R_{eff\,4}$, (2) $\mu_2 = \mu_3 < \mu_1 = \mu_4$, (3) $d_1^* = d_4^*$, (4) $d_2^* = d_3^*$

In the above equations, $d_1^* = d_4^* = d_1\left(R_{eff\,1}/R_1\right)$, is the actual displacement capacity of each of surfaces 1 and 4, and $F_{f1} = F_{f4} = \mu_1 W$ is the force that signifies the initiation of sliding on each of surfaces 1 and 4. Further details on the operation of this triple FP bearing configuration as well as the derivation of the above relationships can be found in the work of Sarlis and Constantinou (2010).

It is noted that, when designing a base isolation system using triple FP bearings, the nominal values of the coefficients of friction will generally be higher during the first cycle of motion. Similarly to the design of lead rubber bearings, the above effect should be accounted for by performing the analysis using upper and lower bound properties for the Triple FP bearings. A

contemporary example of derivation of the properties of Triple FP bearings for use in analysis and design is presented in McVitty and Constantinou (2015).

In seismic isolation design with the Triple FP system, the final regime is typically reserved for beyond design basis earthquakes. Specifically, the adaptive stiffening of that regime is employed as a final measure to prevent the exceedance of the displacement capacity of the bearing. Under normal conditions (design basis earthquake) the bearing will typically operate in the regime 2 as shown in Figure 2-8. If the power transformer is idealized as a single degree of freedom system with weight W, and designating D as the design displacement, the effective frequency f_{eff} and effective damping β_{eff} for use in design with the IEEE spectra shown in Figure 2-1, can be calculated as:

$$f_{eff} = \frac{1}{2\pi}\sqrt{\frac{K_{eff}\, g}{W}} = \frac{1}{2\pi}\sqrt{g\left(\frac{1}{2R_{eff\,1}} + \frac{\mu_1}{D}\right)} \tag{2-10}$$

$$\beta_{eff} = \frac{1}{2\pi}\left[\frac{EDC}{K_{eff} D^2}\right] = \frac{1}{2\pi}\left[\frac{EDC}{\frac{WD^2}{2R_{eff\,1}} + \mu_1 WD}\right] \tag{2-11}$$

In the above relationships the effective stiffness K_{eff} at displacement D is defined as:

$$K_{eff} = \frac{W}{2R_{eff\,1}} + \frac{\mu_1 W}{D} \tag{2-12}$$

It can also be easily shown that the energy dissipated per cycle is:

$$EDC = 4DW\left[\mu_1 - (\mu_1 - \mu_2)\frac{R_{eff\,2}}{R_{eff\,1}}\right] - 16WR_{eff\,2}(\mu_1 - \mu_2)^2\left(1 - \frac{R_{eff\,2}}{R_{eff\,1}}\right) \qquad (2\text{-}13)$$

Also, the force at zero displacement for the simpler version of the Triple FP bearing is given by:

$$\mu W = \left[\mu_1 - (\mu_1 - \mu_2)\frac{R_{eff\,2}}{R_{eff\,1}}\right]W \qquad (2\text{-}14)$$

SECTION 3
EXPERIMENTAL PROGRAM

3.1. Overview – Test Objectives

This section presents the setup for an experimental program that was carried out in the Structural Engineering and Earthquake Simulation Laboratory (SEESL) at the University at Buffalo (UB). The objective of the experimental program was to investigate the performance of selected base isolation designs, when applied to models that realistically simulate the structural characteristics and installation complexities encountered in the field for electrical equipment. Towards that, a mockup model representing an electrical power transformer with a high voltage bushing installed on its flexible roof was prepared in the lab. In order to directly compare the differences in the seismic response, a variety of configurations were tested, including different mounting locations for the bushing, different length scales for the model, and the structure supported on different base isolation systems as well as fixed to the shake table. Tests were performed with an ensemble of near fault ground motions scaled in amplitude systematically to represent the site conditions of a high seismicity region, and, additionally, with ground motions of historical significance scaled arbitrarily in amplitude in order to further challenge the model.

3.2. Description of Test Specimen

In consideration of the fact that high voltage power transformers are components of an electrical substation with weights in the range of 100 – 500 kips, mounting an actual power transformer on the shake table would be practically infeasible. In particular, if that was to be attempted, the load bearing and lateral force capacities of the shake table would be exceeded. In addition to the above, high voltage power transformers are not standardized structures; instead, they exhibit a

large variation in their structural properties, including their lateral flexibility and their mass distribution as described in Matt (2004) and Villaverde (1999), rendering difficult the selection of a representative model to use as a specimen for shake table testing.

On the other hand, considering that power transformer tanks are relatively stiff structures with frequencies in the order of 10 Hz and above (Matt, 2004), and that conventional base isolated structures are typically designed with effective fundamental frequencies below 1 Hz, a base isolated power transformer can be reasonably assumed to translate as a rigid body, with limited contribution of higher modes to its acceleration response. Therefore, for testing purposes it is judged sufficient to develop a stiff specimen to simulate a generic commercial power transformer model.

In the present experimental study, an existing support frame with a flexible roof is used to represent the power transformer tank. The support frame is envisioned to incorporate an actual high voltage bushing supported on its roof. The frame is designed to be laterally and vertically stiff (with frequencies higher than 33 Hz) to minimize the ground motion amplifications over the height of the frame (Kong, 2010). The roof is flexible in the vertical direction and in bending, in order to realistically simulate the mounting conditions of bushings in field power transformers (Kong, 2010). The rigid frame – flexible roof assembly has been extensively used in previous studies for the experimental and qualification testing of bushings (Kong, 2010; Koliou, 2010; Fahad, 2013).

The frame has dimensions of 8x8x8 feet (height x length x width) measured by the center to center distance of the members. It comprises of four steel square tube columns of TS5x5x½ connected by L5x5x¾ angles at the top and reinforced by cross-bracing of L5x5x¾ angles at the

sides. The flexible cover is a ¾ inch thick plate which is larger than the plan dimensions of the frame by approximately 2 feet in each direction; that is, its dimensions are 10'7"x10'7"x¾" (length x width x thickness). The plate contains a hole for mounting a bushing. The plate can be repositioned at the top of the frame, so that the bushing can either be mounted symmetrically (i.e., at the center of the frame in plan) or non-symmetrically (i.e., on the side, or the corner of the frame in plan). More information about the design and structural properties of the support frame can be found in the study of Kong (2010).

The specimen developed herein for use in testing, is a modification of the frame - flexible roof assembly described above. Specifically, the weight of the model was increased by supplementing it with four large steel plates, each having dimensions of 9'10"x6'7"x3½" (length x width x thickness) and weight of 8.6kip. Two of the plates were spliced together by two smaller steel plates with dimensions of 5'x5'x1½" (length x width x thickness) and weight of 1.4kip each, to compose a base mat slab. The base mat assembly is considered to represent the weight of internal components, symmetrically placed inside the power transformer tank, and primarily supported on the power transformer base. Subsequently, the frame pedestals were bolted to the base mat assembly. The remaining plates were connected on two adjacent sides of the frame, with two L8x6x¾ sections on each side to secure each plate to the base mat and to the frame top respectively. This configuration was intended to account for large mass eccentricities that can potentially be met in commercial power transformer models, so as to investigate its effect on the base isolation systems selected. The final assembly resulted in total weight of 47kip and eccentricity between the centers of mass and rigidity of the superstructure of about 10% of the frame plan dimensions in each direction. The achieved value of eccentricity is

expected to sufficiently represent the majority of commercial power transformers. A summary of the test model components and their respective weights is given in Table 3-1.

Table 3-1 Components and Weights of Test Model

Component	Weight (kip)
Frame Structure	
Top Plate	3.3
Top Angles	0.7
Columns	0.9
Diagonals	2.3
Footings	1.0
Bushing	
Adaptor Plate (Bushing Connection)	0.4
196/230 kV Bushing	0.8
Added Mass	
Large Plates	34.2
Small Plates (Base-mat Splicing)	2.8
L Sections (Side Plate Connections)	0.7
Total	**47.1**

The test specimen is shown in Figure 3-1, with the bushing in the symmetric configuration. It approximately simulates basic characteristics of a 500 kV power transformer at length scale S_L = 3, force scale $S_F = S_L^2 = 9$ and time scale $S_T = S_L^{1/2} = \sqrt{3}$. Specifically, for the model weight of 47 kip, the extrapolated weight of a prototype is 423 kip, which is typical of a power transformer in the 500 kV range. Schematics of the model used in the shake table testing with the bushing installed symmetrically are shown in Figure 3-2 through Figure 3-4.

A power transformer tank feature which is important for its dynamic response is the flexibility of the plate supporting the bushing. Data from testing a range of bushings at UB demonstrate that the as-installed frequency of 500/550 kV bushings - appropriate for use in power transformers of

the same capacity - is in the range of 2.6 to 7.7 Hz. Extrapolated in the prototype for a length scale of S_L=3, this frequency should be in the range of 4.5 to 13.3 Hz. In the present experimental study, an actual ABB 196/230kV high voltage porcelain bushing is selected for installation on the developed power transformer specimen. The bushing has been tested extensively at UB, and its fundamental frequency has been identified at about 25 Hz in both directions when installed on a fixed base, and at about 11 Hz in both directions when installed symmetrically on the flexible cover of the frame-roof assembly (Fahad, 2013; Koliou, 2010). The as-installed frequency of the bushing is suitable for either the length scale factor of S_L=3 or S_L=1 used in the testing. A summary of some relevant structural properties of the selected bushing is given in Table 3-2.

Table 3-2 Structural Properties of the ABB 196/230 kV Porcelain Bushing (Fahad, 2013)

Property	**Unit**	**Value**
Total Height	in	151.4
Length over Mounting Flange	in	91.4
Length below Mounting Flange	in	60.0
Location of Center of Gravity (CG) above Flange	in	14.0
Location of Upper Unit Center of Gravity	in	34.0
Location of Lower Unit Center of Gravity	in	28.0
Upper Unit Weight	lb	447
Lower Unit Weight	lb	293
Total Weight	lb	840

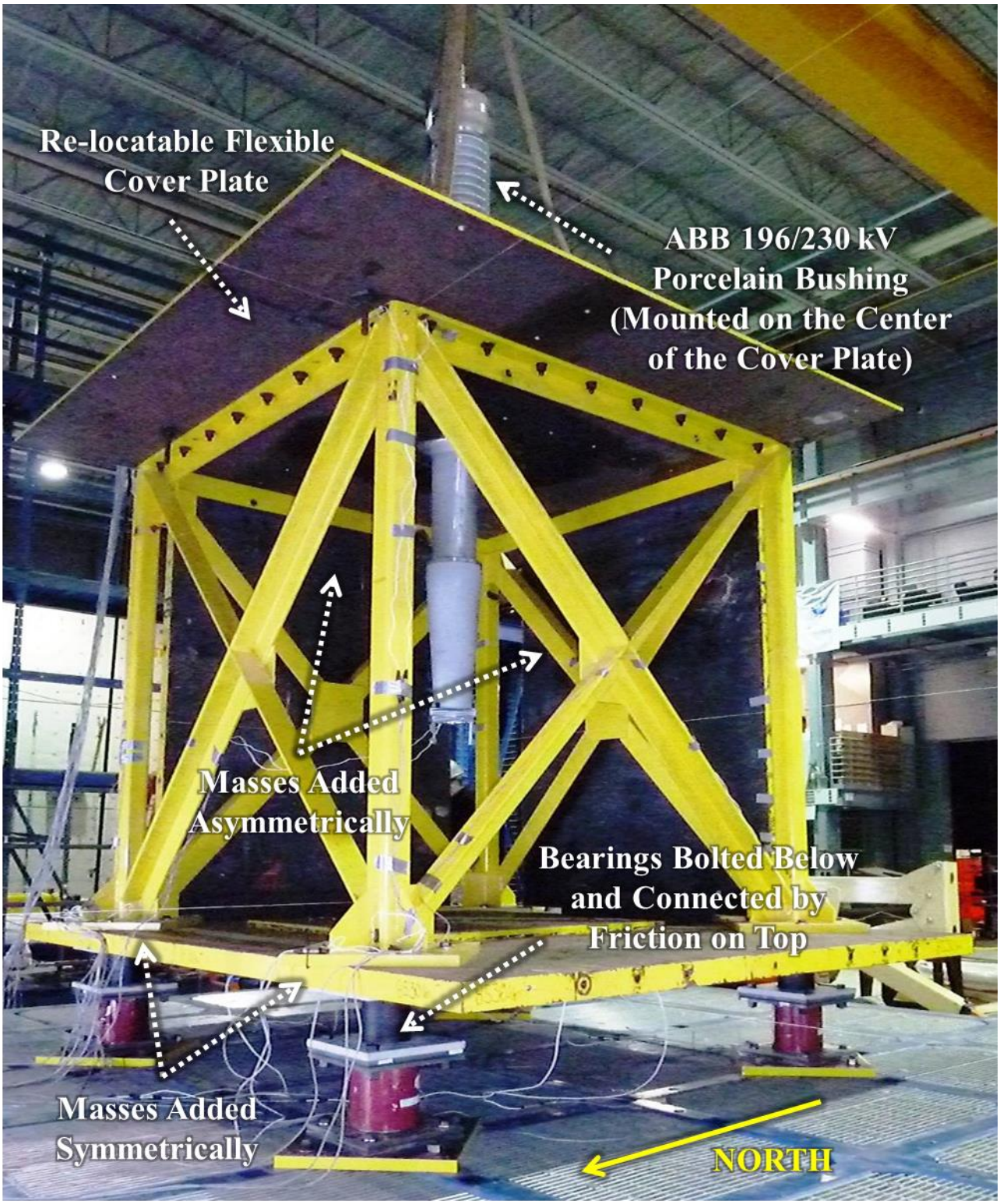


Figure 3-1 Model Used in Shake Table Testing with Added Mass in Symmetric Bushing Configuration (Model Shown Isolated with Lead Rubber Bearings)

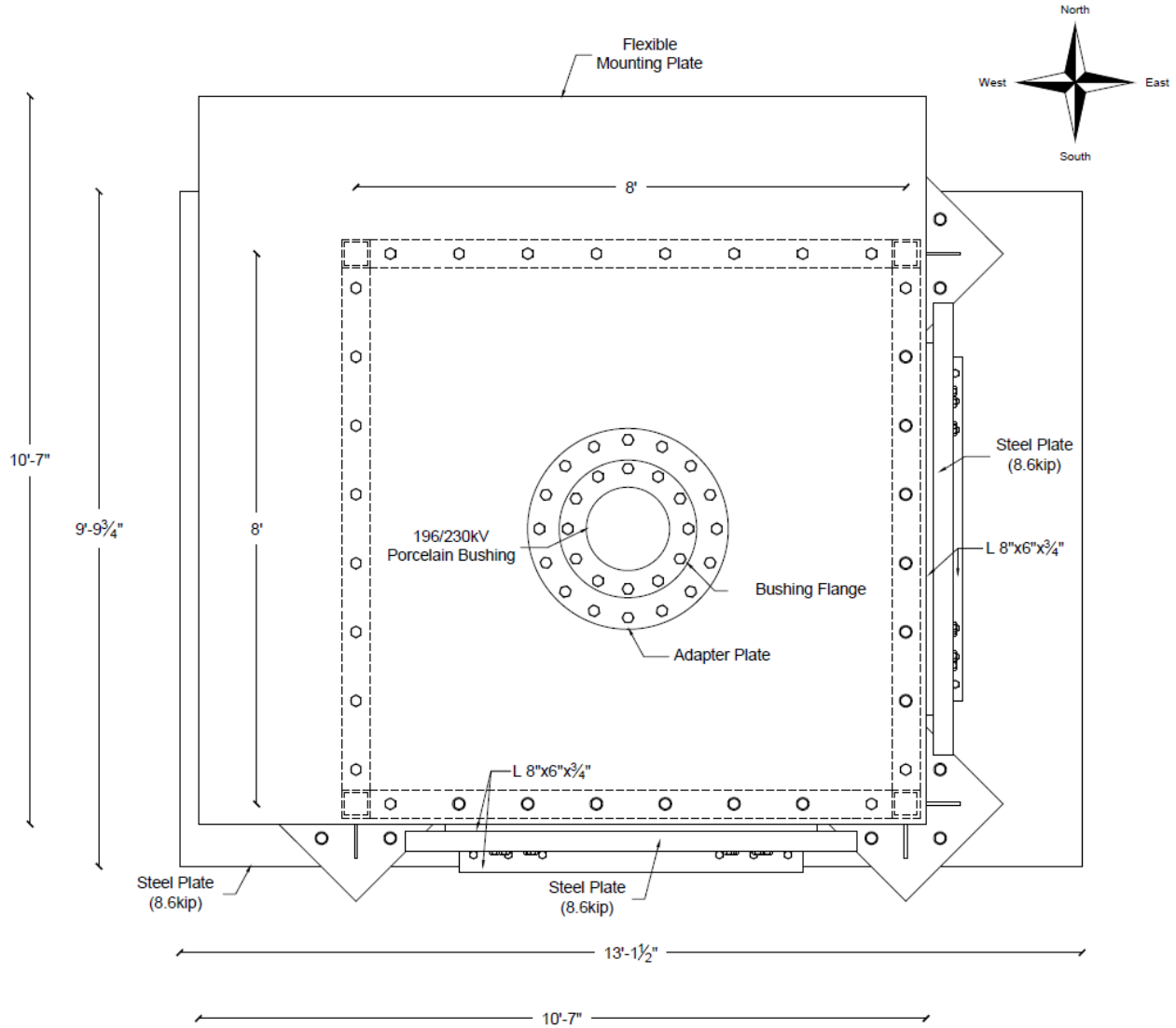


Figure 3-2 Plan View of Model Used in Shake Table Testing with Symmetric Bushing Installation

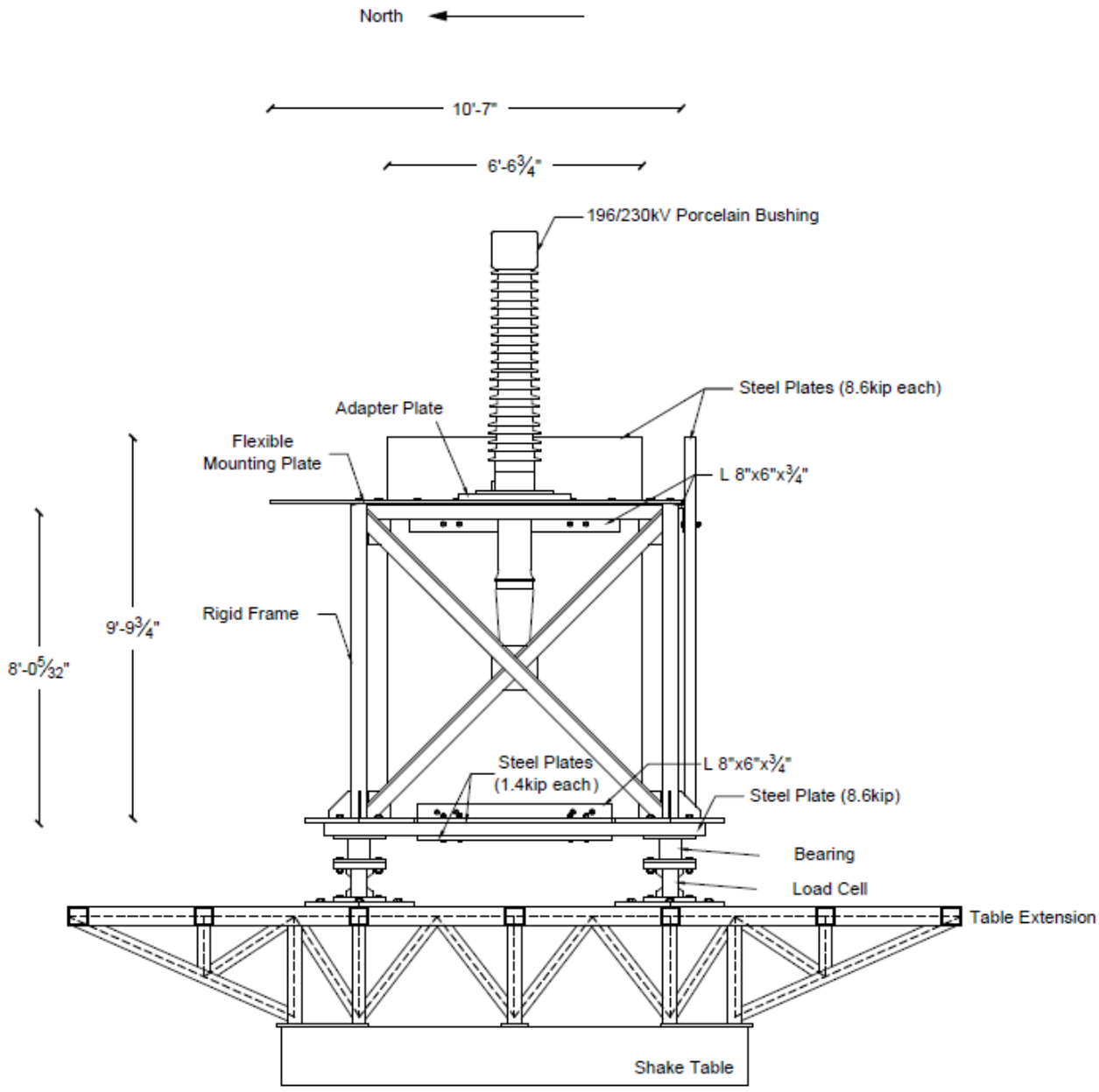


Figure 3-3 Elevation View of Model Used in Shake Table Testing with Symmetric Bushing Installation (View form West Side)

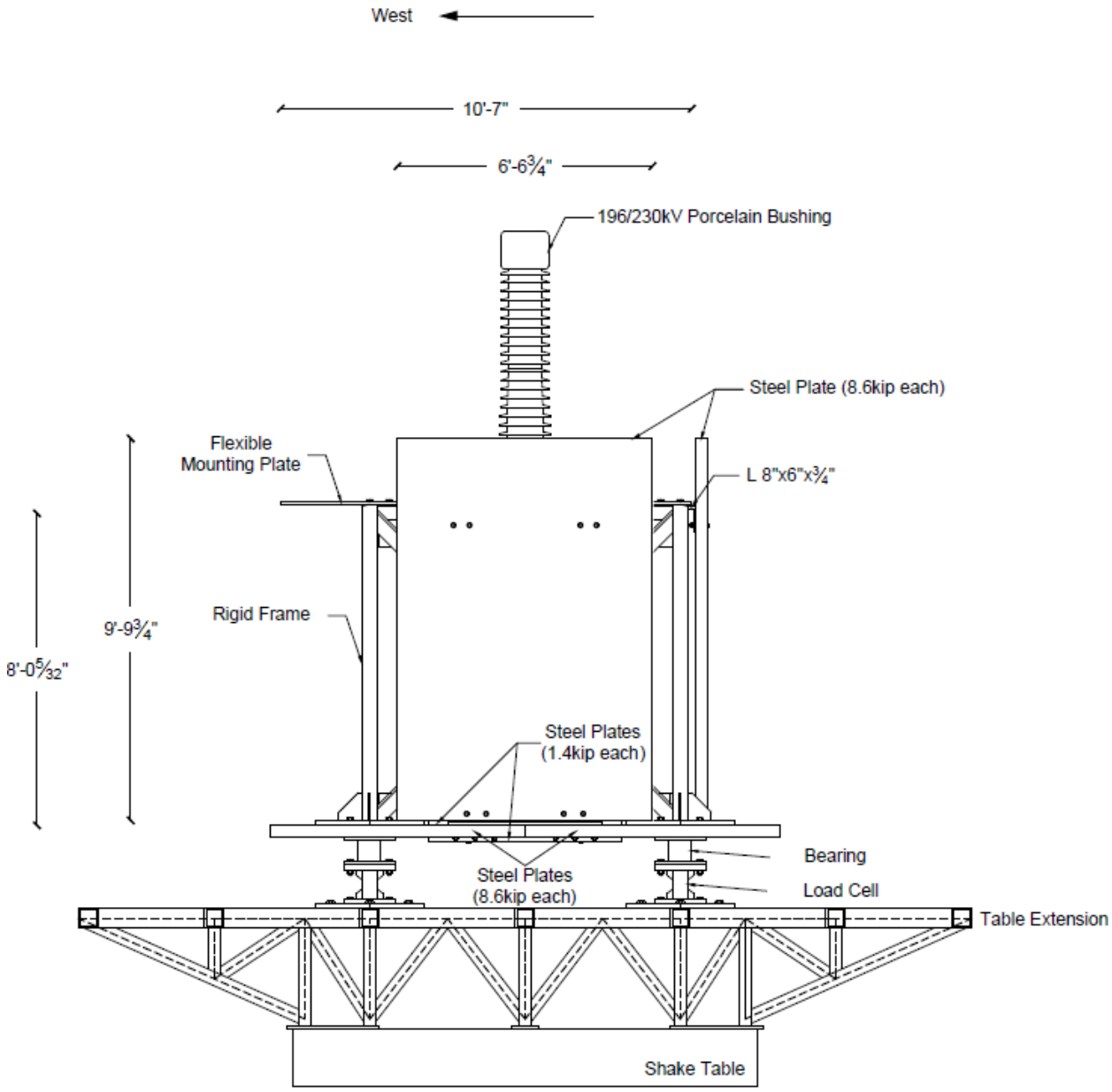


Figure 3-4 Elevation View of Model Used in Shake Table Testing with Symmetric Bushing Installation (View form South Side)

3.3. **Description of Instrumentation**

Instrumentation was used at several levels on the specimen in order to monitor the response of the shake table, the rigid frame, the bushing, and the bearings. Response quantities were measured in all principal directions, including the vertical and rotational response of the flexible cover at the mounting location of the bushing; the latter response quantities are expected to contribute significantly to the bushing response. The instrumentation consisted of accelerometers, displacement transducers, strain gages, load cells and Krypton LEDs used in monitoring motion with a video system. A total of 84 channels were monitored and are summarized in the instrumentation list of Table 3-3.

To monitor the response of the shake table, accelerometers and displacement transducers were installed at selected locations on both the main and the extension platforms. More specifically, the acceleration input on the main platform was monitored with three accelerometers which are installed on the shake table extension platform. The three accelerometers were installed at its center in plan, and close to the surface. For redundancy and in order to monitor potential rocking or twisting of the shake table, additional accelerometers were installed at the corners on the extension platform to measure the response in the longitudinal (NE corner), the transverse (NE and NW corners) and the vertical directions (NE, NW and SE corners). In addition, the corners of the extension platform were instrumented with displacement transducers measuring the longitudinal (at the NE corner) and the transverse (at the NE and NW corners) displacements with respect to a motionless reference frame. The vertical absolute displacement response of the platform was measured with a displacement transducer mounted at the bottom of the trough where the shake table is located.

The response of the isolation system was measured with load cells, displacement transducers and, in selected tests, with the Krypton video system. In particular, axial forces, shear forces and moments were measured with five component load cells (designated as 5D-LC-12-RED), installed underneath each bearing. Because in many tests the bearings were kept by friction to the base mat of the superstructure and there was potential for sliding, the relative displacements between each bearing and the base mat were monitored in both horizontal directions using a total of eight displacement transducers. The relative displacements were obtained by securely installing the displacement transducers on the bottom side of the base mat and connecting them to the top plates of the bearings. Additionally, for a limited number of tests of the reduced scale model when base isolated with the Triple FP system, Krypton LEDs were installed on one of the Triple FP bearings to monitor the response of its internal components. It is noted that during testing of the non-isolated model, some of the aforementioned instruments were inactive or removed. In that case, the frame assembly was bolted directly to the load cells, the latter located underneath the base of each pedestal.

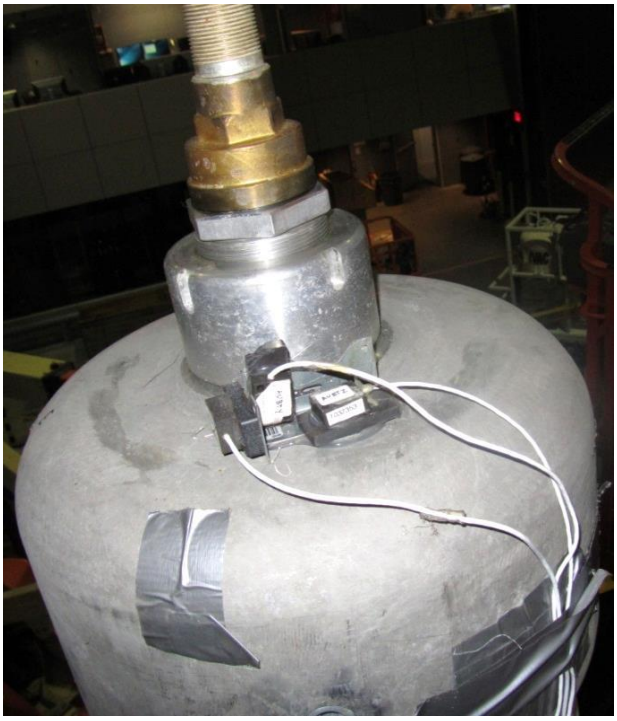
With regard to the frame structure, it was desirable to monitor its global response in order to capture potential amplifications over its height. Thus, the frame was equipped with instrumentation at its bottom as well as the top at the same locations. In particular, accelerometers were installed both at the pedestals and at the top of selected columns to measure the response in the longitudinal (NE column), the transverse (NE and NW columns) and the vertical directions (NE, NW and SE columns). An additional accelerometer was installed vertically at the bottom of the SW column for redundancy and to capture potential local effects such as uplift and pounding of the SW bearing. Displacement transducers were connected to the

same locations to measure absolute longitudinal (NE corner) and transverse (NE and NW corners) displacements.

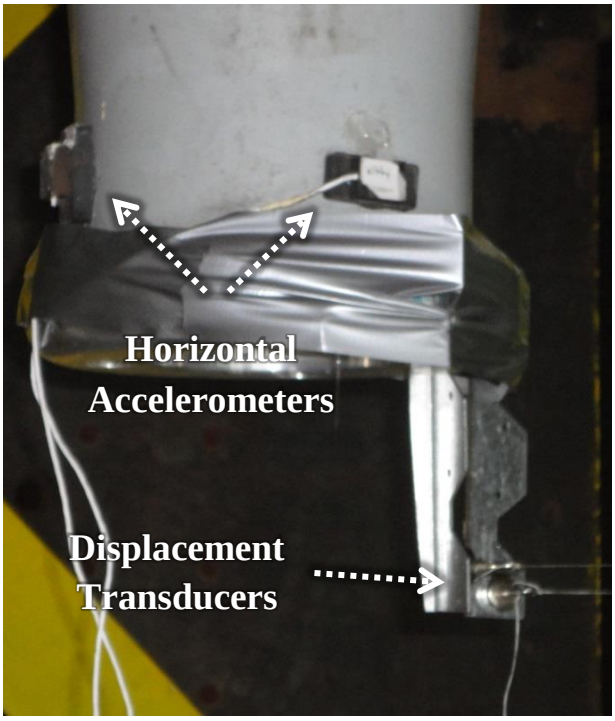
The flexible cover plate was instrumented with accelerometers only, which were installed at the base of the bushing to measure the linear (and, by calculation, the rotational) responses at that location. Two accelerometers were installed horizontally on the east and north sides of the adaptor plate, to measure accelerations in the longitudinal and transverse directions, respectively. Additionally, four accelerometers were installed vertically on the adaptor plate in a crosswise configuration (i.e., on the N, E, S and W sides of the adaptor plate) to record the vertical (and, by calculation, the rotational) responses.

The response of the high voltage bushing was of the major importance in the experimental study, and therefore it was appropriately instrumented in order to acquire sufficient measurements. The absolute acceleration response was measured with accelerometers installed horizontally at the top, center of gravity and bottom of the bushing in the longitudinal and transverse directions, as well as vertically at the top of the bushing. Absolute displacements were measured with displacement transducers connected at the top and bottom of the bushing. Forces and moments at the base of the bushing were measured through strain rosettes installed on each face of the base of the bushing (on the north, south, east and west faces). Individual strain gauge measurements were not obtained, but instead the strain rosettes were calibrated with pull tests in the lab in order to measure forces and moments directly. Photographs of instrumentation used can be found in Figure 3-5 through Figure 3-8. Schematics of the instrumentation diagram are shown in Figure 3-9 through Figure 3-11.

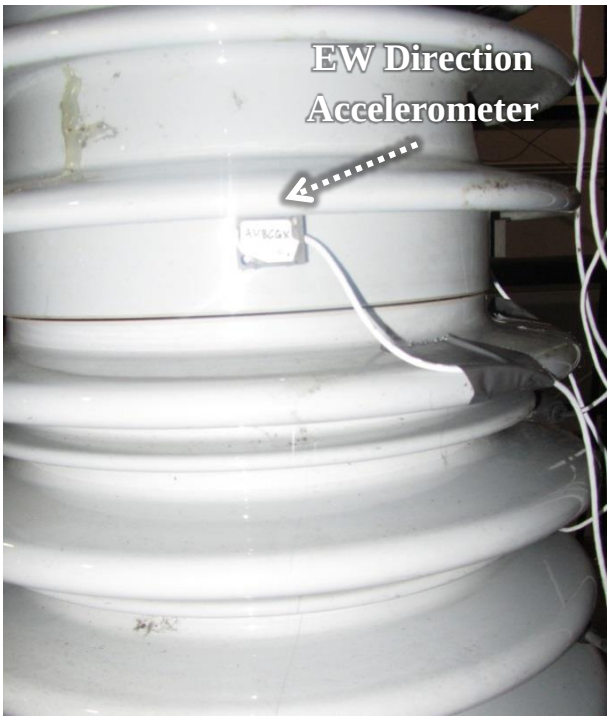
It is noted that, except for the special case of the relative sliding of the bearings, only absolute displacements were measured during testing of the power transformer specimen. The relative displacements at various points on the superstructure were post-calculated by subtracting from the absolute displacement response at the location of interest, the absolute displacement of the shake table interpolated to that particular location using the absolute displacements at the corners of the extension platform. The redundancy in the instrumentation was also useful to check the validity of displacement measurements by doubly integrating the measured accelerations from accelerometers installed at the same points as the displacement transducers.



(a) Top



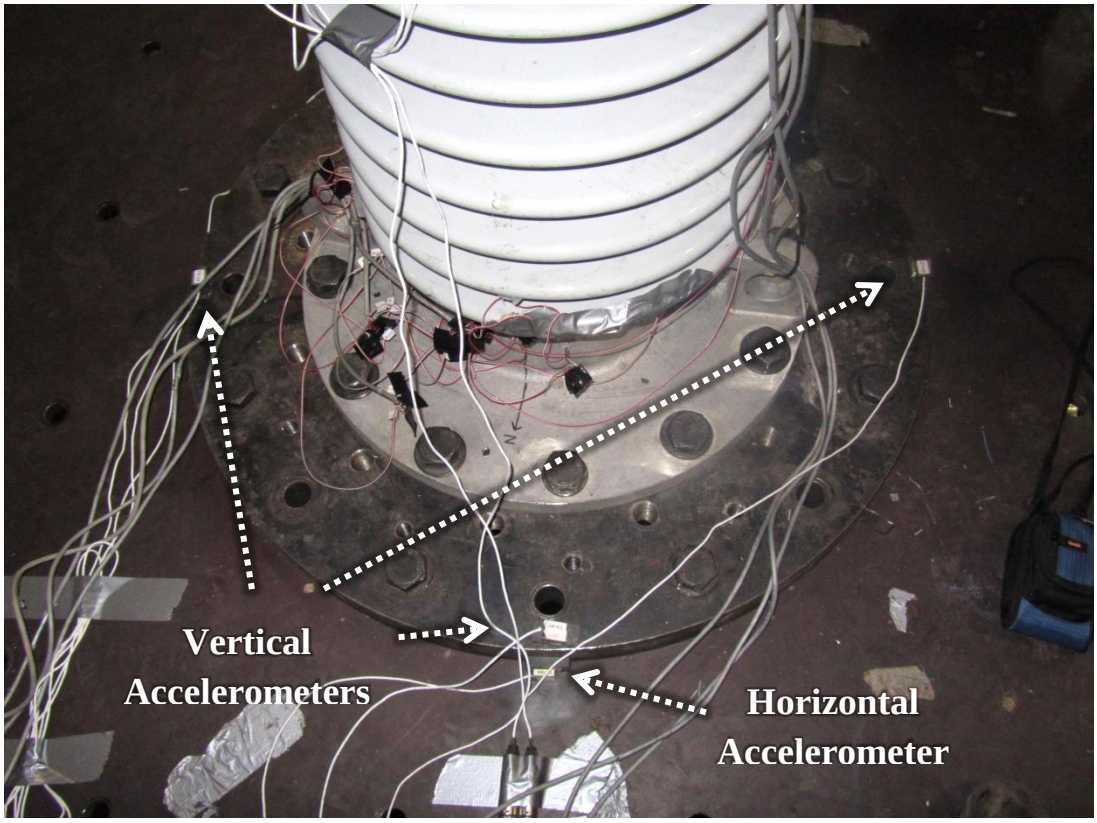
(b) Bottom



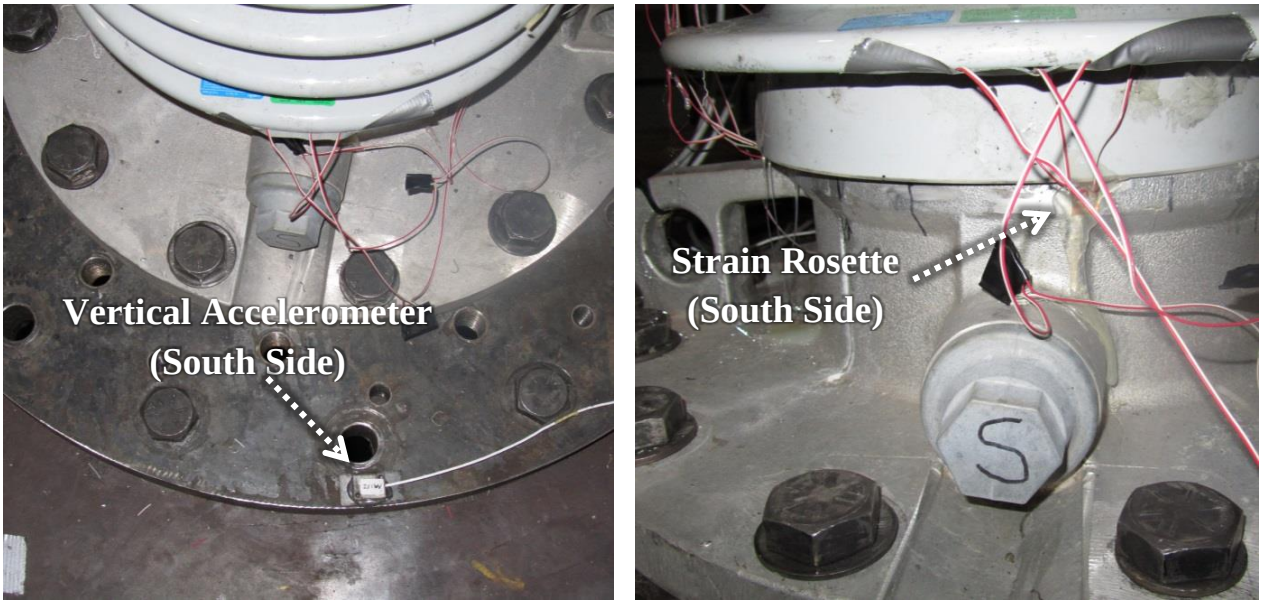


(c) Center of Gravity

Figure 3-5 Instrumentation used to Monitor the High Voltage Bushing Response

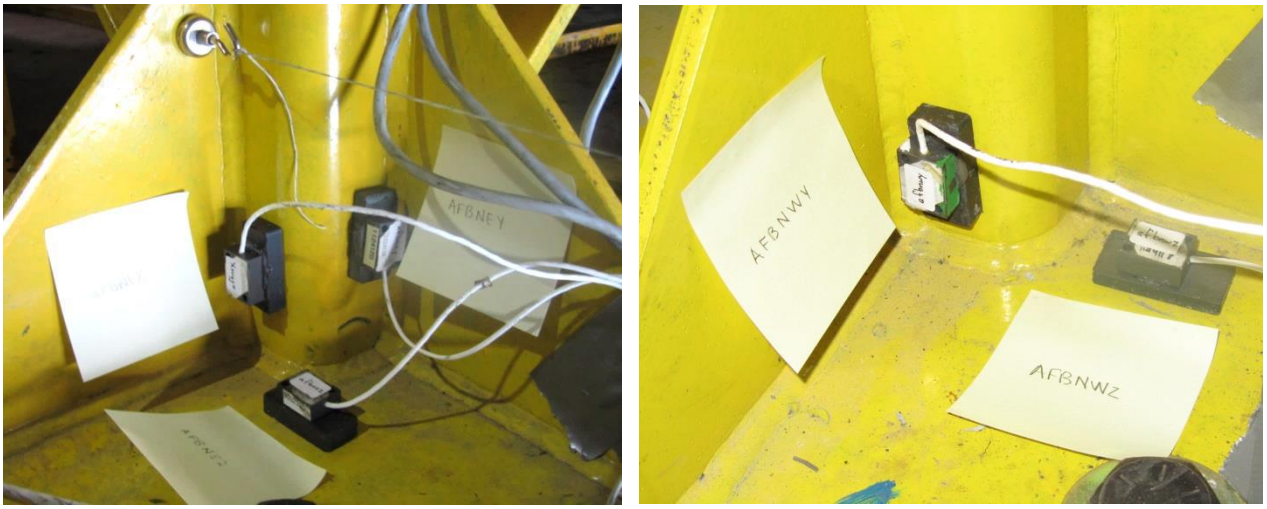


(a) View from North Side

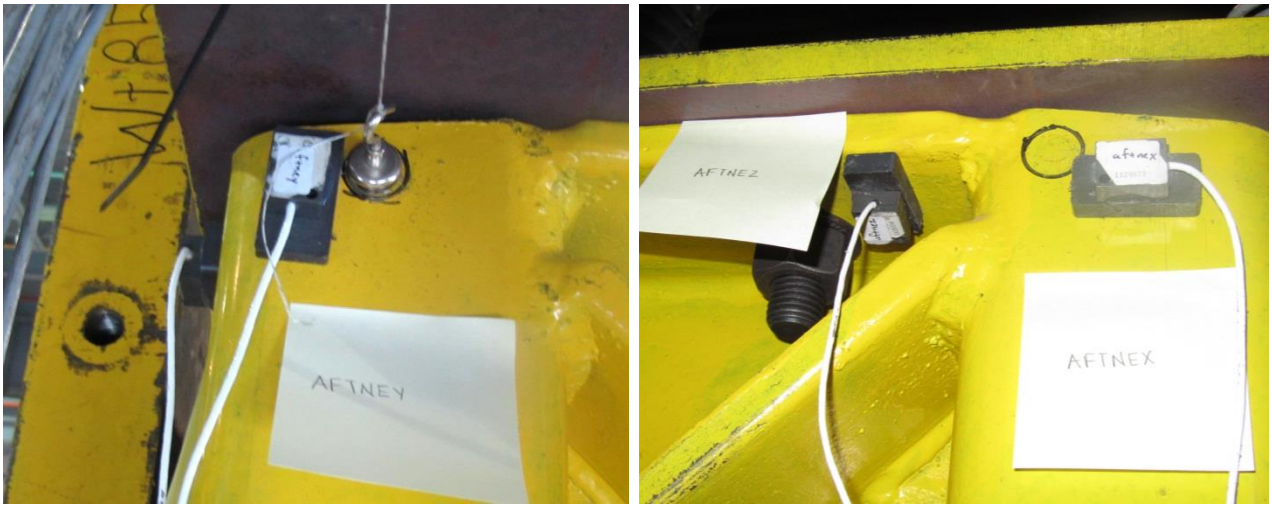


(b) South Side

Figure 3-6 Instrumentation used to Monitor the Adaptor Plate Response



(a) Frame Bottom NE and NW Corners



(b) Frame Top NE Corner



(c) Frame Top NW Corner

Figure 3-7 Instrumentation used to Monitor the Frame Structure Response

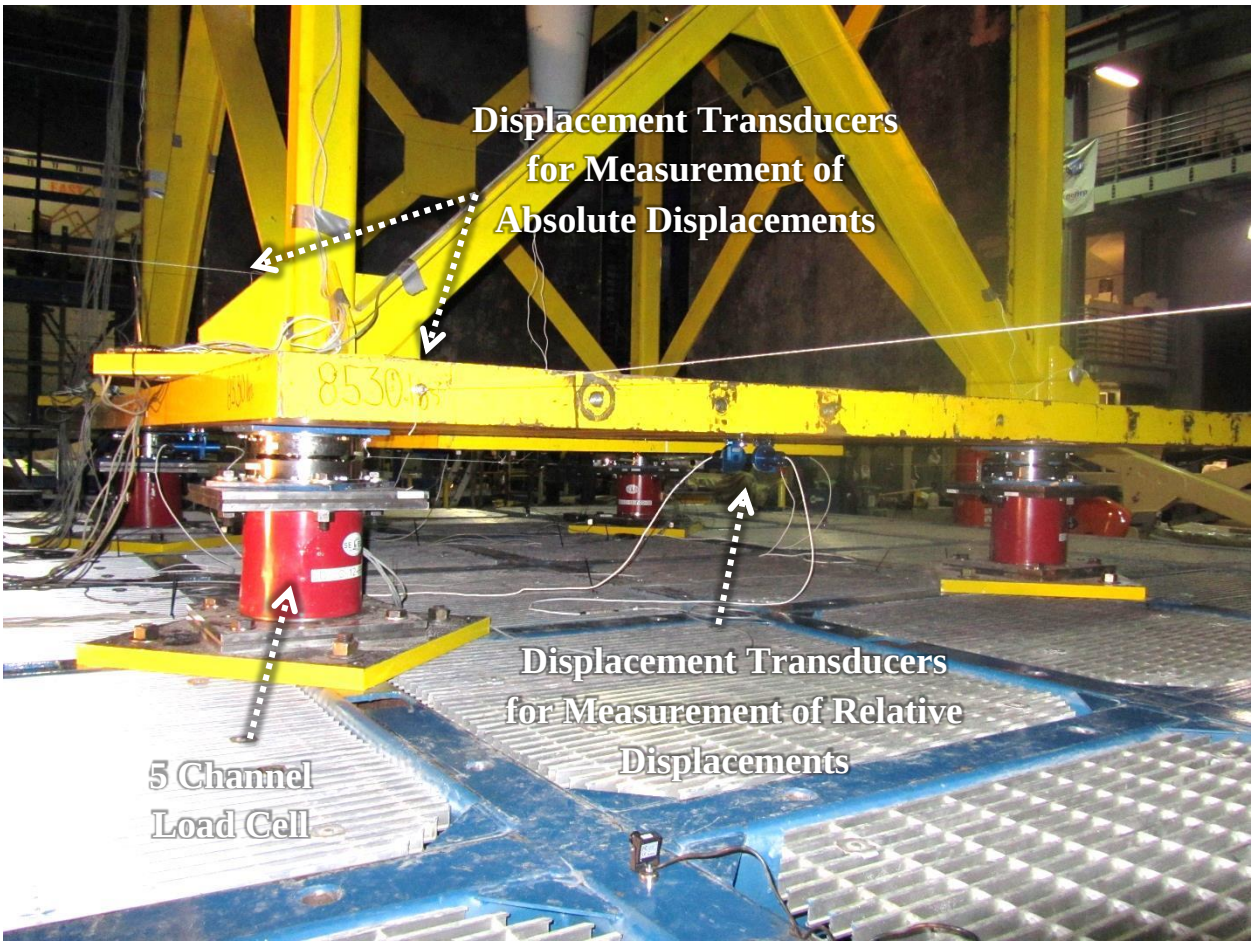


Figure 3-8 Instrumentation used to Monitor the Isolation System Response (Model Shown Isolated with Scaled Triple Friction Pendulum Bearings)

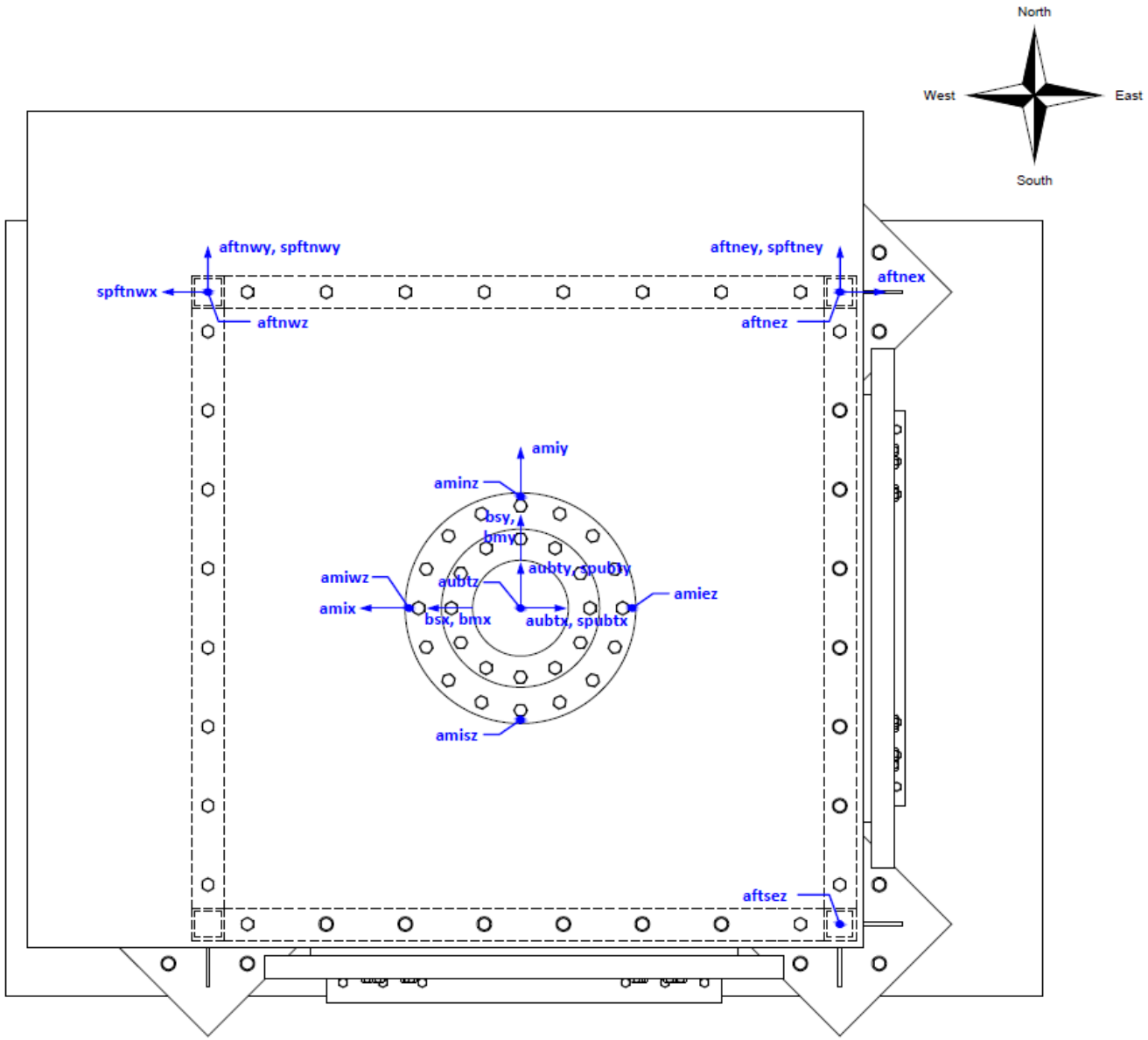


Figure 3-9 Plan View of Model Instrumentation Diagram

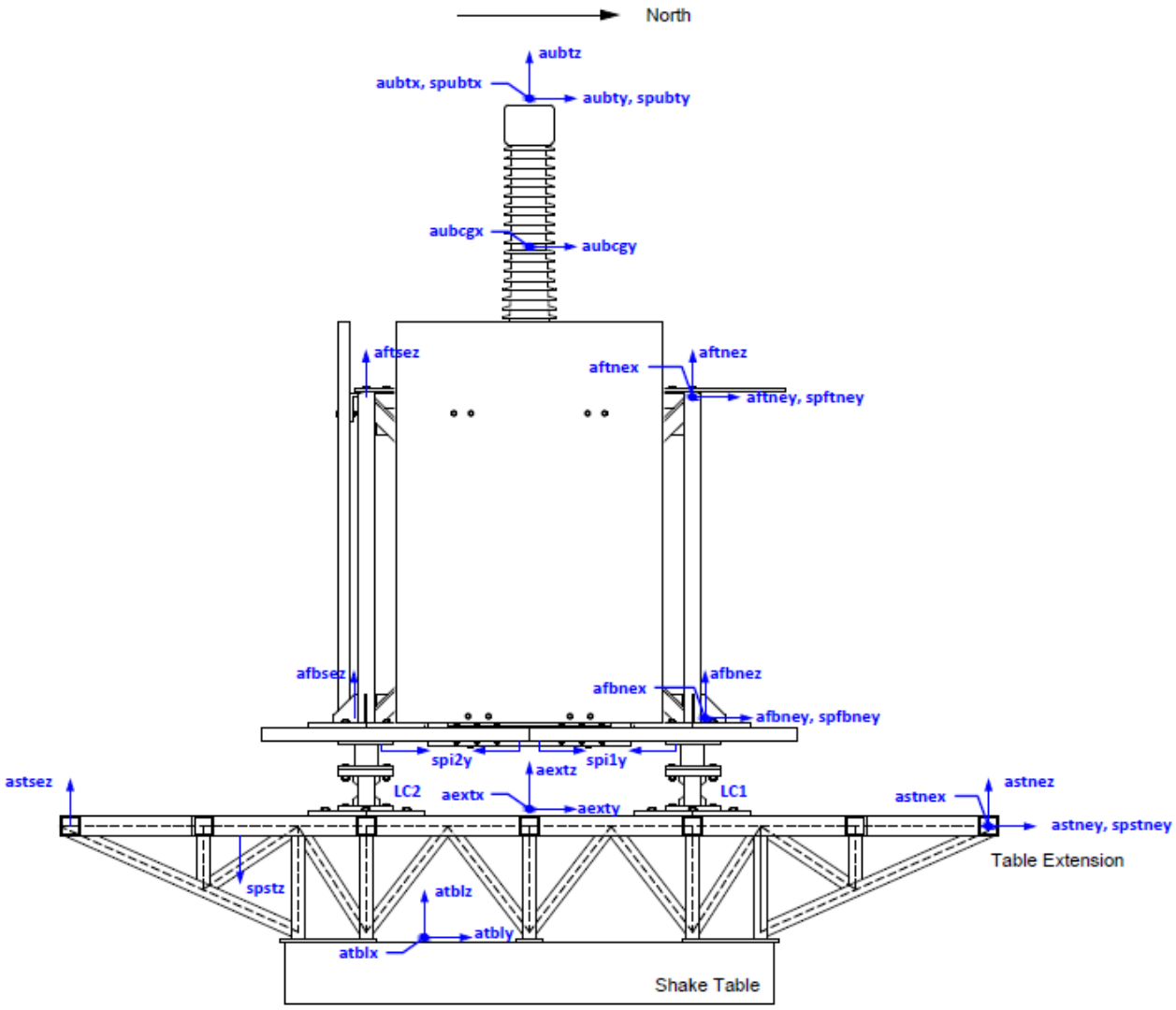


Figure 3-10 Elevation View of Model Instrumentation Diagram (View form East Side)

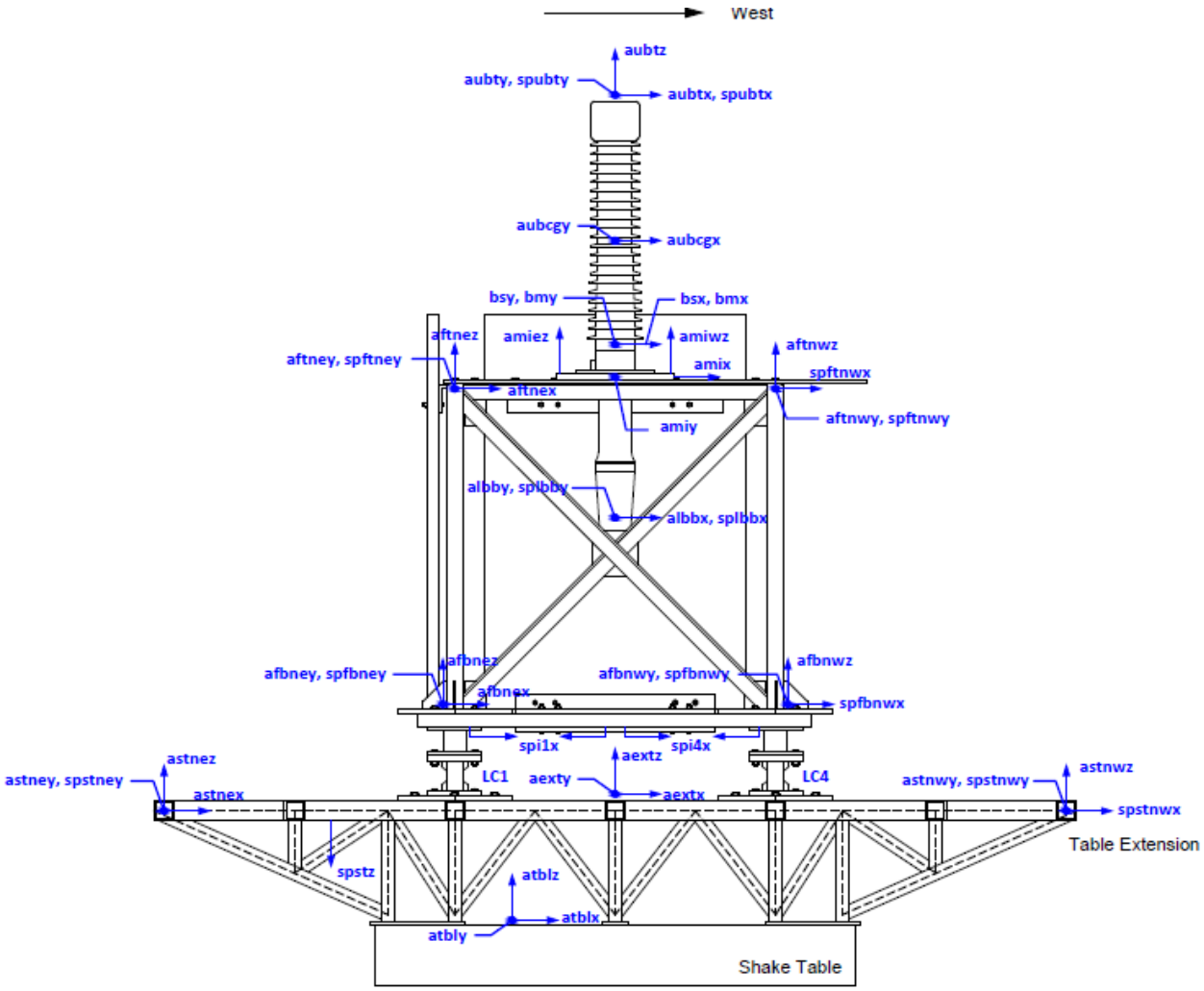


Figure 3-11 Elevation View of Model Instrumentation Diagram (View form North Side)

Table 3-3 List of Instrumentation Used and Response Quantities Measured

Channel	Notation	Instrument	Location	Measured Quantity	Direction
1	Time	clock	-	time	-
2	aubtx	accelerometer	Bushing top	abs acceleration	EW
3	aubty	accelerometer	Bushing top	abs acceleration	NS
4	aubtz	accelerometer	Bushing top	abs acceleration	V
5	aubcgx	accelerometer	Bushing CG	abs acceleration	EW
6	aubcgy	accelerometer	Bushing CG	abs acceleration	NS
7	amix	accelerometer	Adaptor plate	abs acceleration	EW
8	amiy	accelerometer	Adaptor plate	abs acceleration	NS
9	aminz	accelerometer	Adaptor plate (north)	abs acceleration	V
10	amisz	accelerometer	Adaptor plate (south)	abs acceleration	V
11	amiez	accelerometer	Adaptor plate (east)	abs acceleration	V
12	amiwz	accelerometer	Adaptor plate (west)	abs acceleration	V
13	albbx	accelerometer	Lower bushing bottom	abs acceleration	EW
14	albby	accelerometer	Lower bushing bottom	abs acceleration	NS
15	aftnwy	accelerometer	Frame top (NW)	abs acceleration	NS
16	aftnwz	accelerometer	Frame top (NW)	abs acceleration	V
17	aftnex	accelerometer	Frame top (NE)	abs acceleration	EW
18	aftney	accelerometer	Frame top (NE)	abs acceleration	NS
19	aftnez	accelerometer	Frame top (NE)	abs acceleration	V
20	aftsez	accelerometer	Frame top (SE)	abs acceleration	V
21	afbswz	accelerometer	Frame bottom (SW)	abs acceleration	V
22	afbnwy	accelerometer	Frame bottom (NW)	abs acceleration	NS
23	afbnwz	accelerometer	Frame bottom (NW)	abs acceleration	V
24	afbnex	accelerometer	Frame bottom (NE)	abs acceleration	EW
25	afbney	accelerometer	Frame bottom (NE)	abs acceleration	NS
26	afbnez	accelerometer	Frame bottom (NE)	abs acceleration	V
27	afbsez	accelerometer	Frame bottom (SE)	abs acceleration	V
28	astnwy	accelerometer	Shake table extension (NW)	abs acceleration	NS

Table 3-3 (cont'd) List of Instrumentation Used and Response Quantities Measured

Channel	Notation	Instrument	Location	Measured Quantity	Direction
29	astnwz	accelerometer	Shake table extension (NW)	abs acceleration	V
30	astnex	accelerometer	Shake table extension (NE)	abs acceleration	EW
31	astney	accelerometer	Shake table extension (NE)	abs acceleration	NS
32	astnez	accelerometer	Shake table extension (NE)	abs acceleration	V
33	astsez	accelerometer	Shake table extension (SE)	abs acceleration	V
34	aextx	accelerometer	Shake table extension	abs acceleration	EW
35	aexty	accelerometer	Shake table extension	abs acceleration	NS
36	aextz	accelerometer	Shake table extension	abs acceleration	V
37	atblx	accelerometer	Shake table	abs acceleration	EW
38	atbly	accelerometer	Shake table	abs acceleration	NS
39	atblz	accelerometer	Shake table	abs acceleration	V
40	spubtx	string pot	Bushing top	abs displacement	EW
41	spubty	string pot	Bushing top	abs displacement	NS
42	splbbx	string pot	Lower bushing bottom	abs displacement	EW
43	splbby	string pot	Lower bushing bottom	abs displacement	NS
44	spftnwx	string pot	Frame top (NW)	abs displacement	EW
45	spftnwy	string pot	Frame top (NW)	abs displacement	NS
46	spftney	string pot	Frame top (NE)	abs displacement	NS
47	spfbnwx	string pot	Frame bottom (NW)	abs displacement	EW
48	spfbnwy	string pot	Frame bottom (NW)	abs displacement	NS
49	spfbney	string pot	Frame bottom (NE)	abs displacement	NS
50	spbi1x	string pot	Isolator top plate (SW)	rel displacement	EW
51	spbi1y	string pot	Isolator top plate (SW)	rel displacement	NS
52	spbi2x	string pot	Isolator top plate (NW)	rel displacement	EW
53	spbi2y	string pot	Isolator top plate (NW)	rel displacement	NS
54	spbi3x	string pot	Isolator top plate (NE)	rel displacement	EW
55	spbi3y	string pot	Isolator top plate (NE)	rel displacement	NS
56	spbi4x	string pot	Isolator top plate (SE)	rel displacement	EW

Table 3-3 (cont'd) List of Instrumentation Used and Response Quantities Measured

Channel	Notation	Instrument	Location	Measured Quantity	Direction
57	spbi4y	string pot	Isolator top plate (SE)	rel displacement	NS
58	spstnwx	string pot	Shake table (NW)	abs displacement	EW
59	spstnwy	string pot	Shake table (NW)	abs displacement	NS
60	spstney	string pot	Shake table (NE)	abs displacement	NS
61	spstz	string pot	Shake table	abs displacement	V
62	bsx	load cell	Adaptor plate (north)	shear force	EW
63	bsy	load cell	Adaptor plate (south)	shear force	NS
64	bmy	load cell	Adaptor plate (east)	moment	EW
65	bmx	load cell	Adaptor plate (west)	moment	NS
66	lc1n	load cell	Load cell (NE)	axial force	V
67	lc1sx	load cell	Load cell (NE)	shear force	EW
68	lc1sy	load cell	Load cell (NE)	shear force	NS
69	lc1my	load cell	Load cell (NE)	moment	NS
70	lc2n	load cell	Load cell (SE)	axial force	V
71	lc2sx	load cell	Load cell (SE)	shear force	EW
72	lc2sy	load cell	Load cell (SE)	shear force	NS
73	lc2mx	load cell	Load cell (SE)	moment	EW
74	lc2my	load cell	Load cell (SE)	moment	NS
75	lc3n	load cell	Load cell (SW)	axial force	V
76	lc3sx	load cell	Load cell (SW)	shear force	EW
77	lc3sy	load cell	Load cell (SW)	shear force	NS
78	lc3mx	load cell	Load cell (SW)	moment	EW
79	lc3my	load cell	Load cell (SW)	moment	NS
80	lc4n	load cell	Load cell (NW)	axial force	V
81	lc4sx	load cell	Load cell (NW)	shear force	EW
82	lc4sy	load cell	Load cell (NW)	shear force	NS
83	lc4mx	load cell	Load cell (NW)	moment	EW
84	lc4my	load cell	Load cell (NW)	moment	NS

3.4. **Description of Isolation Systems Used in Testing**

3.4.1. Isolation Systems for Length Scale 3 Tests

The isolation systems tested are:

1) Scaled Lead-rubber bearings for use in the length scale 3 tests, designed with large characteristic strength and stiffness in order to reduce displacement demands. Figure 3-13 below is a cut out view of the lead-rubber bearing used that shows the internal construction. The mechanical behavior of the LRB is discussed in section 2.4. The bearing was installed bolted down to a load cell (representing the foundation). At the top to the power transformer, the bearing was either bolted or connected only through friction. The latter modifies the behavior of the bearing by allowing for sliding at lateral forces that exceed the friction force at the interface of the bearing to the isolated structure. This friction force was not known.

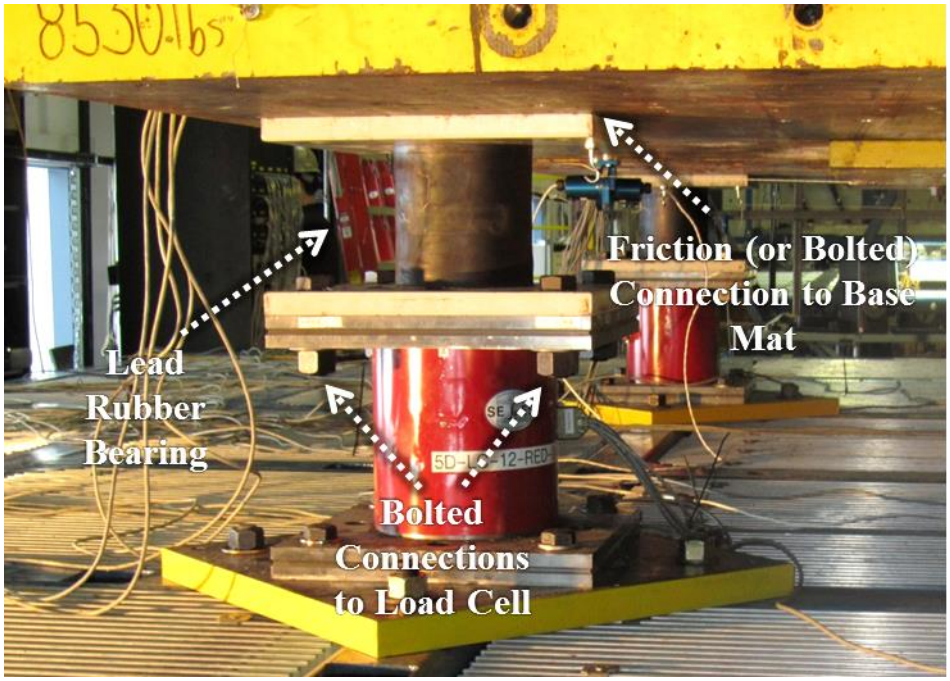


Figure 3-12 View of a Lead-Rubber Bearing used in Testing, As-Installed on a Load Cell on the Shake Table

The lead rubber bearings used in the testing have the geometry shown in Figure 3-13 and the behavior characterized by the representative force-displacement loop shown in Figure 3-14 (for bolted connections up and down). The properties of this bearing are listed in Table 3-4. Further information on these bearings is available in Warn and Whittaker (2006) from where the geometric and mechanical properties were obtained.

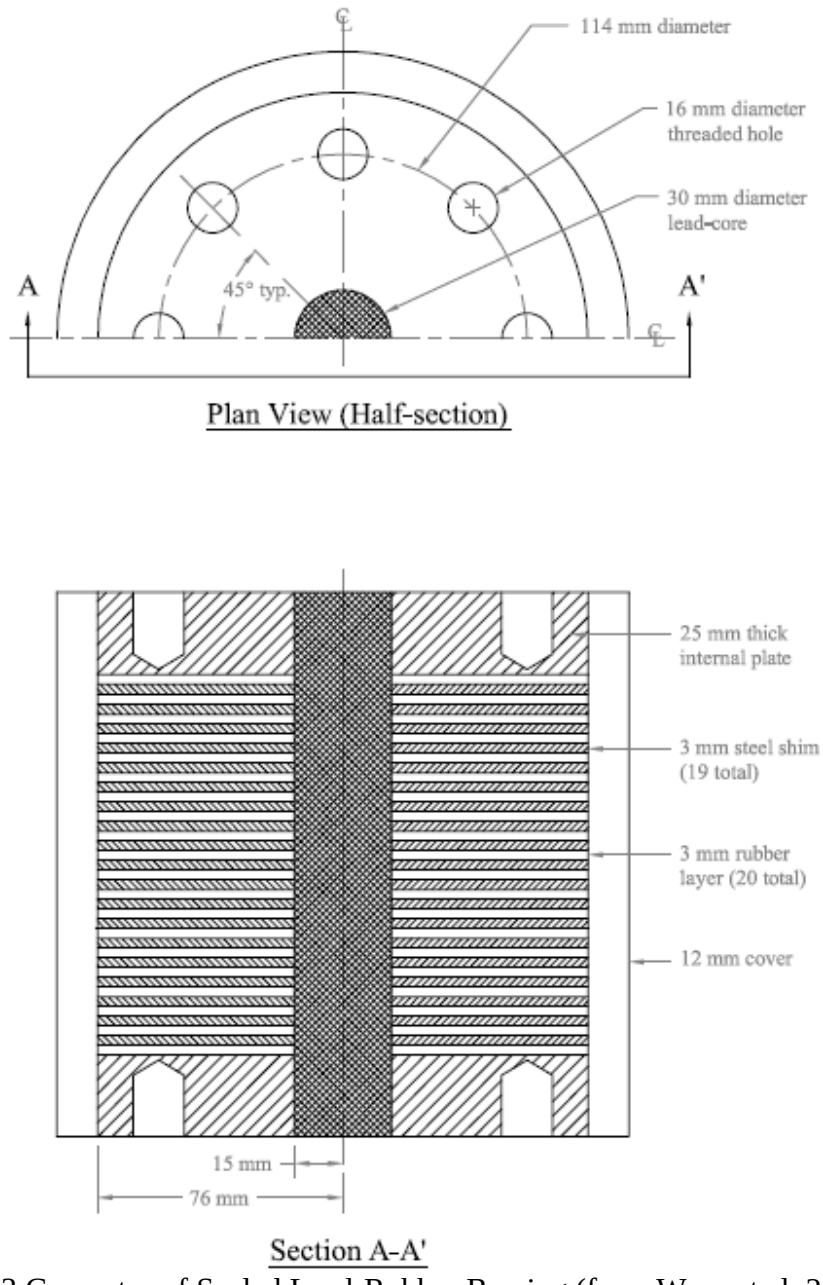


Figure 3-13 Geometry of Scaled Lead-Rubber Bearing (from Warn et al, 2006)

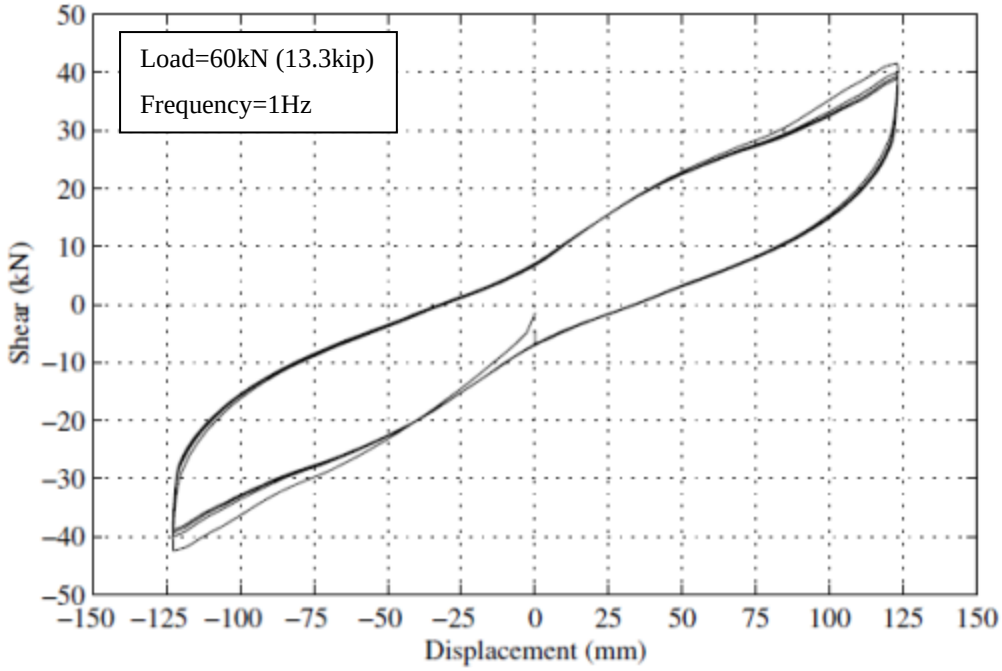


Figure 3-14 Force-displacement Loops of Scaled Lead-Rubber Bearing (from Warn et al, 2006 - 1kip=4.45kN, 1in=25.4mm)

Table 3-4 Properties of Scaled Lead-Rubber Bearings

Property	Notation	Unit	Value
Characteristic Strength	Q	kip	1.6
Post Elastic Stiffness	K_d	kip/in	1.7
Elastic Stiffness	K_{el}	kip/in	28

Use of four lead rubber bearings results in a characteristic strength of 0.14W (for W=47kip) and a frequency based on the post-elastic stiffness equal to 1.19Hz ($f = (1/2\pi)\sqrt{4gK_d/W}$) as tested for length scale factor S_L=3 or 0.69Hz in prototype scale. This is a stiff and highly damped isolation system.

2) Scaled Triple Friction Pendulum (Triple FP) bearings for use in the length scale 3 tests, were designed with high strength (friction) and geometric characteristics to allow for stiffening

that will limit displacements in strong earthquakes. The mechanical behavior of the Triple FP bearing is discussed in section 2.5. Figure 3-15 illustrates the Triple FP bearing used in testing. Table 3-5 presents values of the parameters of one of the bearings. Figure 3-16 presents drawings of the bearing with geometrical details. Figure 3-17 shows force-displacement relations of the bearing. Note that the bearings were installed unbolted at the interface to the power transformer structure above so that the lateral force is limited by the friction at the bearing to power transformer interface. Therefore, the loops shown should be capped at the friction force of the interface which is not known.

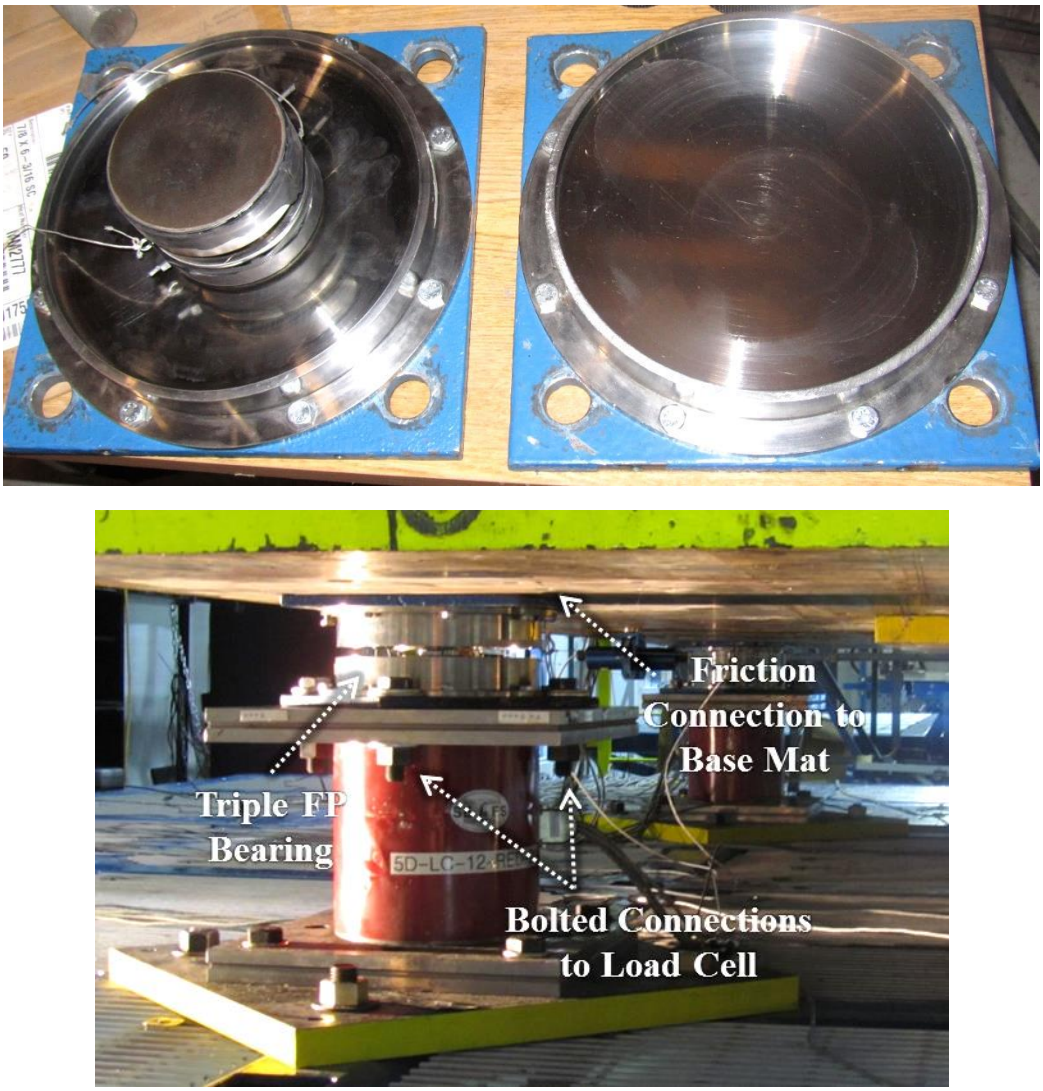


Figure 3-15 View of Scaled Triple Friction Pendulum Bearing used in Testing

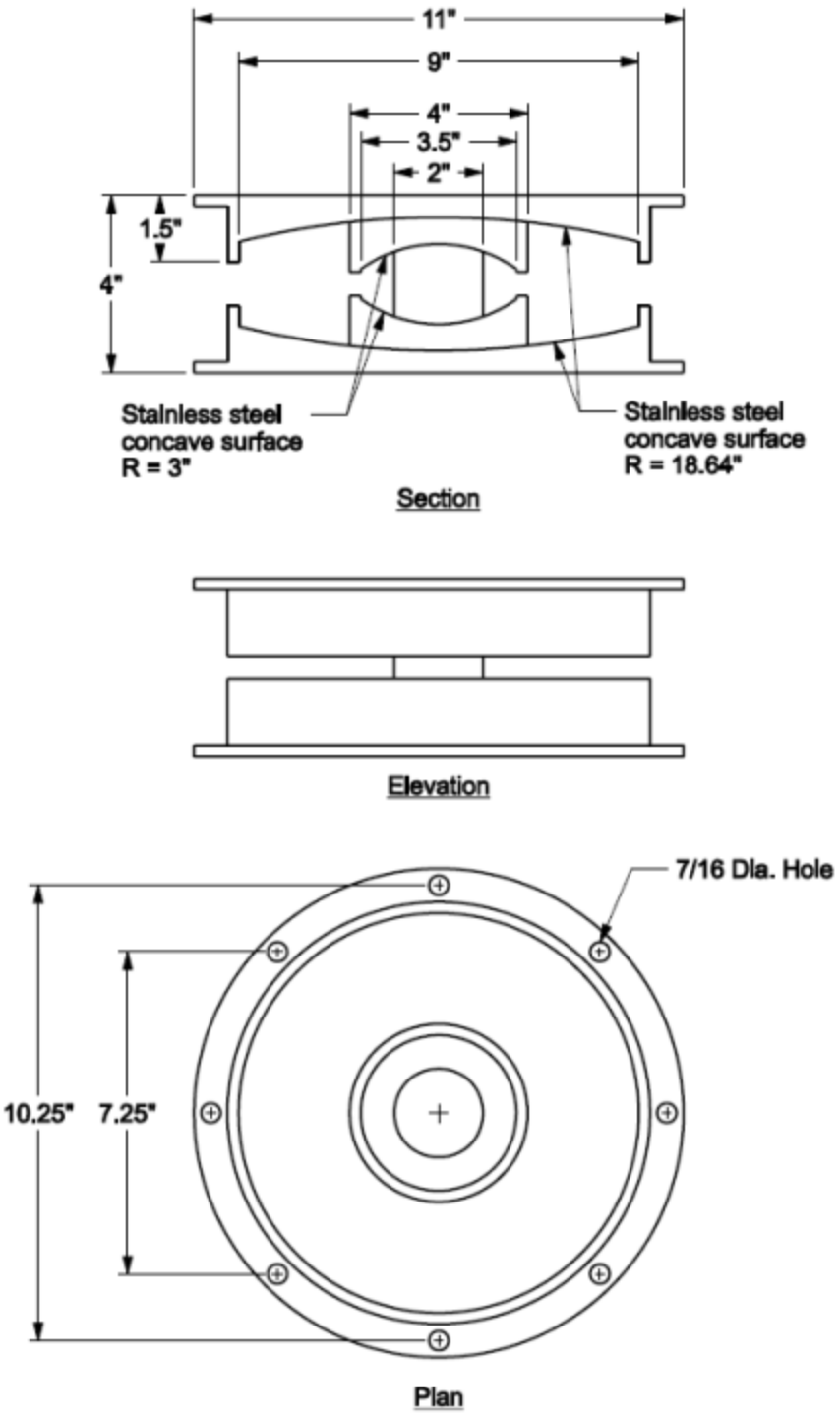


Figure 3-16 Geometry of Scaled Triple FP Bearing

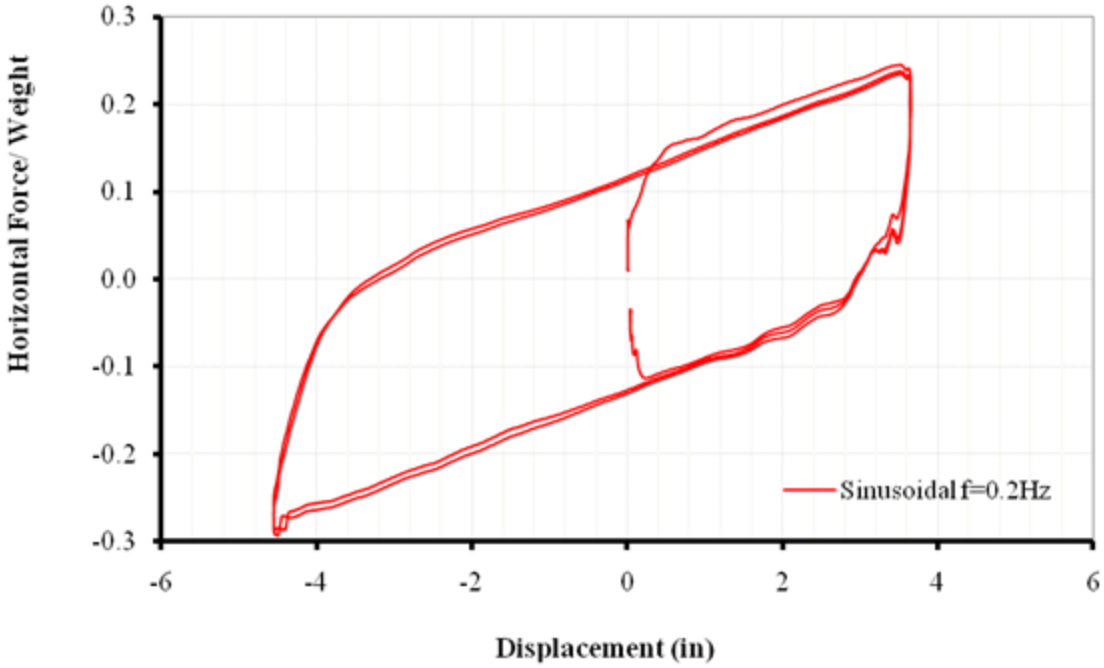


Figure 3-17 Experimental Force-Displacement Loop of Scaled Triple Friction Pendulum Bearing at Load of 15kip (Results from Testing of the Bearing with Sinusoidal Motion of Frequency 0.2Hz performed by Sarlis et al, 2013)

Table 3-5 Properties of Scaled Triple FP Bearing

Parameter	Notation	Unit	Value
Axial Load	W	kip	15.00
Outer Surface Effective Radius	$R_{eff\,1} = R_{eff\,4}$	in	17.12
Inner Surface Effective Radius	$R_{eff\,2} = R_{eff\,3}$	in	2.09
Outer Surface Displacement Capacity	$d_1^* = d_4^*$	in	2.32
Inner Surface Displacement Capacity	$d_2^* = d_3^*$	in	0.52
Outer Surface Coefficient of Friction	$\mu_1 = \mu_4$	-	0.13
Inner Surface Coefficient of Friction	$\mu_2 = \mu_3$	-	0.04

Four of these bearings were used in testing. When experiments were conducted with length scale S_L=3, the prototype bearings corresponded to an effective radius ($R_{eff} = 2R_{eff\,1}$) equal to 102.7in and a frequency based on the post-elastic stiffness ($f = (1/2\pi)\sqrt{g/R_{eff}}$) equal to 0.31Hz. The

characteristic strength is equal to 0.12W (this is the force at zero displacement given by equation (2-14)). This is a flexible and highly damped isolation system.

3.4.2. Isolation System for Full Length Scale Demonstration Tests

A demonstration test was designed using the power transformer specimen of Figure 3-1 and full size Triple FP bearings, to perform testing at full length scale, S_L=1. A demonstration test at full scale is challenged however by the following:

a) The weight of the model is unrealistically light (weighing only 47kip) so that only an isolation system for which the stiffness is proportional to the weight supported can be utilized. Accordingly, only Triple FP bearings could be used.
b) The frictional properties of the Triple FP bearings need to be sufficiently low (friction coefficient larger than 0.10 and preferably about 0.15) under the loading conditions in the test which are about 5 to 10 times lower that in actual equipment. This requires modification of the bearings to ensure proper frictional properties under the loads of 8 to 15 kips per bearing expected in the demonstration test. This can be accomplished by the introduction of lubrication and then by running-in the bearings until stable frictional properties were achieved.
c) Actual strong earthquake motions at full length scale cannot be exactly reproduced due to limitations in the displacement and velocity capacities of the shake table.

The demonstration test allows however a viewer to observe the actual bearings in realistic seismic motion and better appreciate the implications of this motion on the performance of the equipment. Moreover, data on full scale response may be recorded so that comparisons to

analytical predictions can be made. The experiments are essentially performed to collect data that can be used to verify the ability to make analytical predictions, which subsequently can be used for other equipment, isolation system configurations and seismic excitation.

A schematic of the full size Triple FP bearing selected is shown in Figure 3-18. The effective radius of this bearing is ($R_{eff} = 2R_{eff\,1} = 2R - h$) equal to 73 in. The displacement capacity of the bearing in the least friction condition (see Section SECTION 6, Figure 6-5) is 13.7 in with an additional 1.0 in of high stiffness portion. The force-displacement relation of one of the four bearings is shown in Figure 3-19 in a test under load of 108 kips for three cycles at amplitude of 10 inch and peak velocity of 27.9 in/sec. Note that the bilinear representation shown in color red in this figure is based on a lateral force to vertical force ratio (strength to weight ratio) of 0.13 and stiffness normalized by weight equal to 1/73 $inch^{-1}$. The actual strength to weight ratio varies during the three cycles from 0.13 to 0.15. These properties apply for the bearing when tested at the load of 108 kips prior to modification of its frictional properties for use in the shake table testing at much lower load. The behavior of the tested bearings differed as they were modified in terms of friction properties with the addition of lubricant in order to operate at a much smaller load. The geometric properties of the bearings and their actual frictional values as they were observed in the shake table testing are shown in Table 3-6.

Table 3-6 Properties of Full Size Triple FP Bearing

Parameter	Notation	Unit	Value
Average Axial Load on each Bearing	W	kip	11.80
Outer Surface Effective Radius	$R_{eff\,1} = R_{eff\,4}$	in	36.50
Inner Surface Effective Radius	$R_{eff\,2} = R_{eff\,3}$	in	6.50
Outer Surface Displacement Capacity	$d_1^* = d_4^*$	in	6.55
Inner Surface Displacement Capacity	$d_2^* = d_3^*$	in	0.81
Outer Surface Coefficient of Friction	$\mu_1 = \mu_4$	-	0.090
Inner Surface Coefficient of Friction	$\mu_2 = \mu_3$	-	0.045

Figure 3-20 shows a view of the isolated model with the full size FP bearings on the shake table and Figure 3-21 shows a close view of the bearing as installed with only frictional contact supporting the power transformer (unbolted at the interface to the power transformer model).

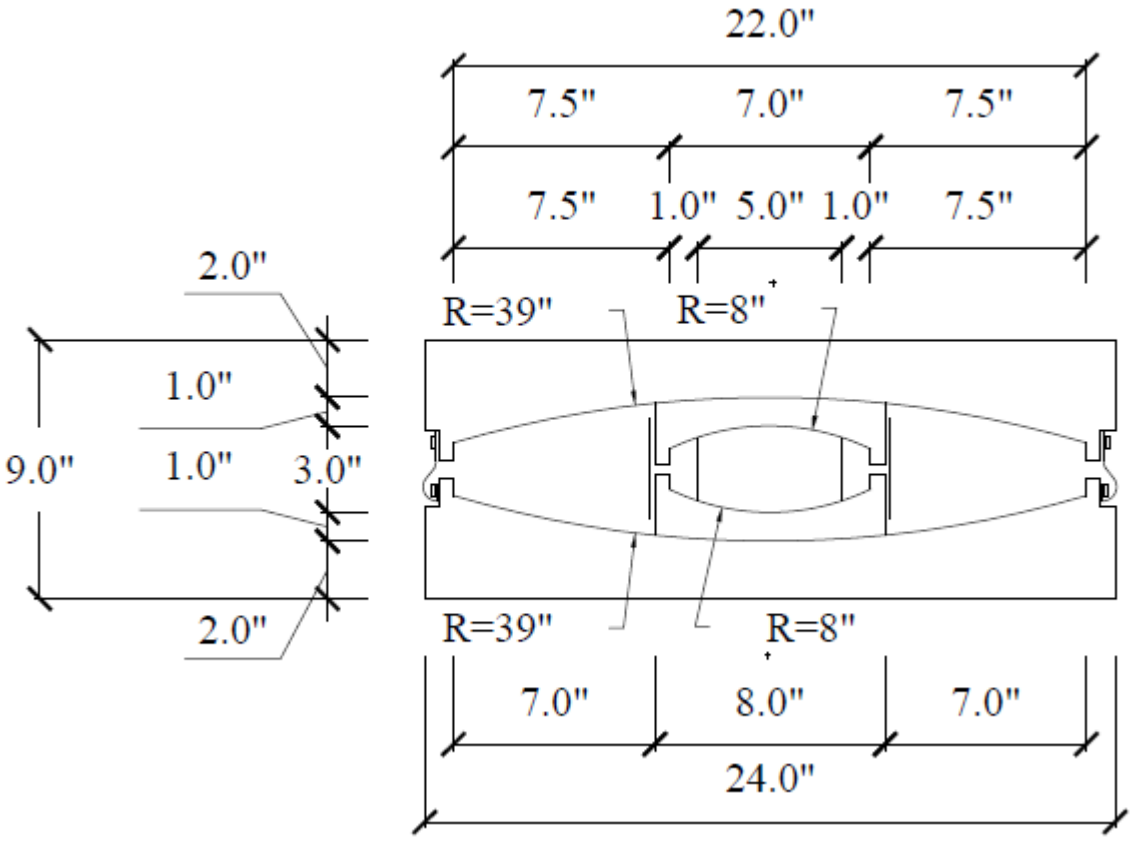


Figure 3-18 Geometry of Full Size Triple FP Bearing

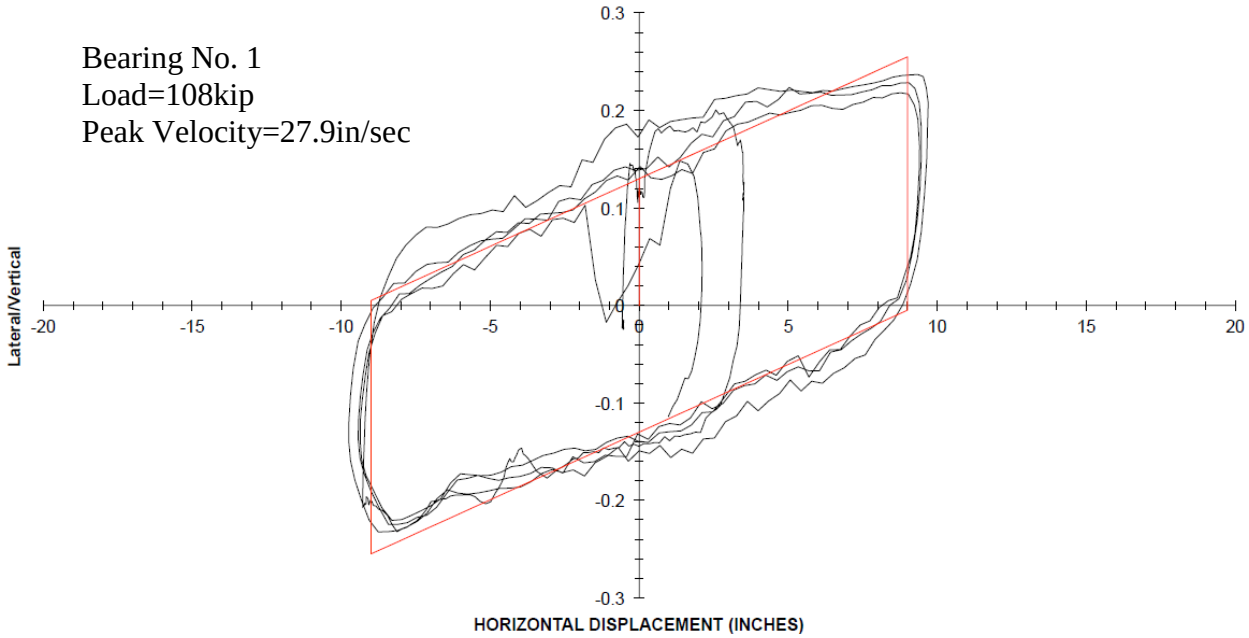


Figure 3-19 Behavior of Full Size Triple FP Bearing No. 1



Figure 3-20 Model Isolated with Full Size Triple Friction Pendulum Bearings

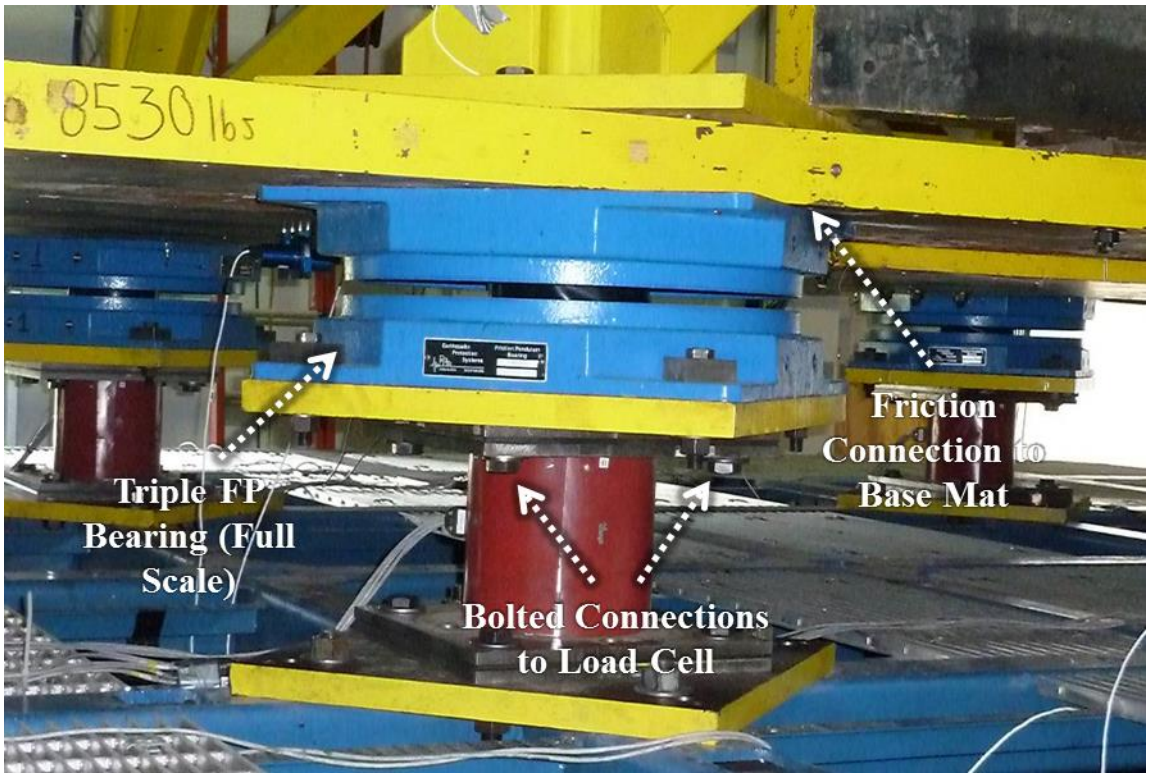


Figure 3-21 Close Up View of Full Size Triple Friction Pendulum Bearings on Shake Table

3.5. **Similitude Considerations**

In constructing the scaled power transformer specimen and in selecting the base isolation systems for shake table testing at reduced length scale as was discussed above, it should be emphasized that the similitude requirements for the scaled specimen were achieved in an approximate sense only (incomplete similitude). It may be observed that the test specimen in the laboratory is not an exact representation of the tank and, in extension, the structural system of an actual field power transformer. Furthermore, the isolators and the bushing used in the reduced length scale testing will not generally correspond to the actual dimensions of the isolators and bushings when extrapolated to the prototype scale.

Nevertheless, the achieved similitude is sufficient to capture the dynamic properties of the power transformer and bushing assembly, which are important for this study. Specifically, the built

specimen captures the mass asymmetry in a commercial high voltage power transformer, it achieves meaningful scaling in the bushing dynamics on the basis of the selected length scale, and approximates well the effect of the power transformer roof on the bushing dynamics. Moreover, realistic weight distribution and pressures are achieved on the isolators and the interface between the isolation system and the superstructure, which will result in realistic performance of the isolation system.

In the case of testing with the full size Triple FP isolators, the weight of the specimen was not increased accordingly to match the weight of the prototype. However, the particular isolation system is friction based and, consequently, independent of the mass and weight distribution on the isolators. Furthermore, any potential effects on the frictional values of the Triple FP isolators due to the low weight are bypassed due to the small friction achieved through the introduction of lubricant in the isolators.

Other phenomena that cannot be captured perfectly with the achieved similitude include temperature effects on the strength of the lead core for the LRB isolators, and temperature and velocity effects on the frictional properties of the Triple FP isolators. In extrapolating the results obtained from testing of the reduced scale specimen to the prototype scale, the contribution of the above effects is considered to be small, and disregarded in this study.

3.6. **Selection of Ground Motions and Scaling Procedure**

Testing was conducted for isolated and non-isolated support conditions (bearings removed and the frame was bolted to the shake table) and for bi-directional horizontal and tri-axial excitation. A portion of the ground motions used throughout testing were an ensemble of 7 recorded earthquakes and were scaled to represent a particular seismic hazard. The rest of the ground motions used were historic earthquakes scaled arbitrarily in amplitude with the purpose of challenging the test specimen but without the objective of representing a specific seismic hazard. Motions were scaled down in amplitude for testing the non-isolated model in order to protect the load cells from excessive shear forces and to avoid inducing large overturning moments in the superstructure and subsequent rocking of the shake table which could affect the quality of the measurements. For the isolated specimen with the scaled Triple FP bearings and for selected tests, the motions were scaled up in amplitude, consistently to the shake table capacity, often until the bearing displacements reached the bearing limits. The time of the original records was either compressed by $\sqrt{3}$ for the scaled tests or was not modified for the full size tests.

Table 3-7 presents characteristics of the historic earthquake records used in the testing. The data are presented for the as recorded amplitude of the motions and in the prototype time scale. Figure 3-22 and Figure 3-23 present the 5%-damped spectra of selected horizontal and vertical components of these motions, respectively, as they were used in testing of the isolated model (however, shown in prototype time scale in the figures) and compared to the IEEE 693 0.5g RRS for the horizontal motions (Figure 3-22) and to the IEEE 693 0.4g RRS for the vertical motions (Figure 3-23). Evidently, most of the horizontal and vertical components of the motions used in testing far exceed the IEEE 693 spectrum in the high frequency range, and on average the

horizontal components approximate well the low frequency tail of the IEEE 693 spectrum down to frequencies of about 0.33Hz. Most of the motions were used in testing with the stronger of the two horizontal components (in terms of PGA) applied in the EW direction of the shake table. Some of the motions recorded close to known active faults were first rotated along the fault-normal (FN) and the fault-parallel (FP) directions and then used in testing with the fault-normal component applied along the shake table EW direction.

Table 3-7 Characteristics of Earthquake Motions Used in Testing at 100% Level and in Prototype Time Scale

Designation	Earthquake	Recording Station	Moment Magnitude	Distance (km)	Component	Peak Ground Motion		
						Accel. (g)	Vel. (in/sec)	Displ. (in)
El Centro	1940 Imperial Valley	El Centro	7.0	6.09	S00E	0.31	11.7	5.1
					N90W	0.21	11.7	8.7
					V	0.21	4.2	3.3
Taft	1952 Kern County	Taft Lincoln School	7.4	38.89	N21E	0.16	6.0	3.6
					S69E	0.18	6.9	3.5
					V	0.11	2.6	1.8
Pacoima	1971 San Fernando	Pacoima Dam	6.6	1.81	S16E	1.23	44.3	13.9
					S74W	1.16	21.3	4.6
					V	0.70	22.2	7.2
Karakyr	1976 Gazli, USSR	Karakyr	6.8	5.46	FN	0.60	25.6	9.5
					FP	0.71	28.0	9.7
					V	1.26	25.3	11.8
Mexico	1985 Mexico City	SCT Building	8.1	400.00	N90W	0.17	23.8	8.6
					S00E	0.10	15.3	7.5
					V	0.04	3.5	3.0
LGPC	1989 Loma Prieta	LGPC	6.9	3.88	FN	0.94	38.2	24.6
					FP	0.54	28.4	12.0
					V	0.89	27.1	25.6

Table 3-7 (cont'd) Characteristics of Earthquake Motions Used in Testing at 100% Level and in Prototype Time Scale

Designation	Earthquake	Recording Station	Moment Magnitude	Distance (km)	Component	Peak Ground Motion		
						Accel. (g)	Vel. (in/sec)	Displ. (in)
Saratoga	1989 Loma Prieta	Saratoga, W. Valley Coll.	6.9	9.31	FN	0.40	28.1	8.2
					FP	0.26	23.6	11.7
					V	N/A	N/A	N/A
Jensen	1994 Northridge	Jensen Filter Plant	6.7	5.43	FN	0.52	26.5	16.8
					FP	1.07	25.7	9.2
					V	0.82	12.5	5.8
Sylmar	1994 Northridge	Sylmar, Coverter Sta. East	6.7	5.19	FN	0.84	45.9	15.5
					FP	0.50	30.8	11.5
					V	0.38	9.6	2.9
Kobe	1995 Kobe, Japan	Takarazuka	6.9	3.00	FN	0.65	28.6	8.2
					FP	0.70	32.7	10.5
					V	0.43	13.7	4.9
Bolu	1999 Duzce, Turkey	Bolu	7.1	12.41	FN	0.79	21.6	8.9
					FP	0.78	24.6	5.3
					V	0.20	6.8	5.6
Chile	2010 Chile	Concepcion	8.8	105.00	EW	0.61	17.0	5.1
					NS	0.65	14.6	3.6
					V	0.58	8.6	2.5

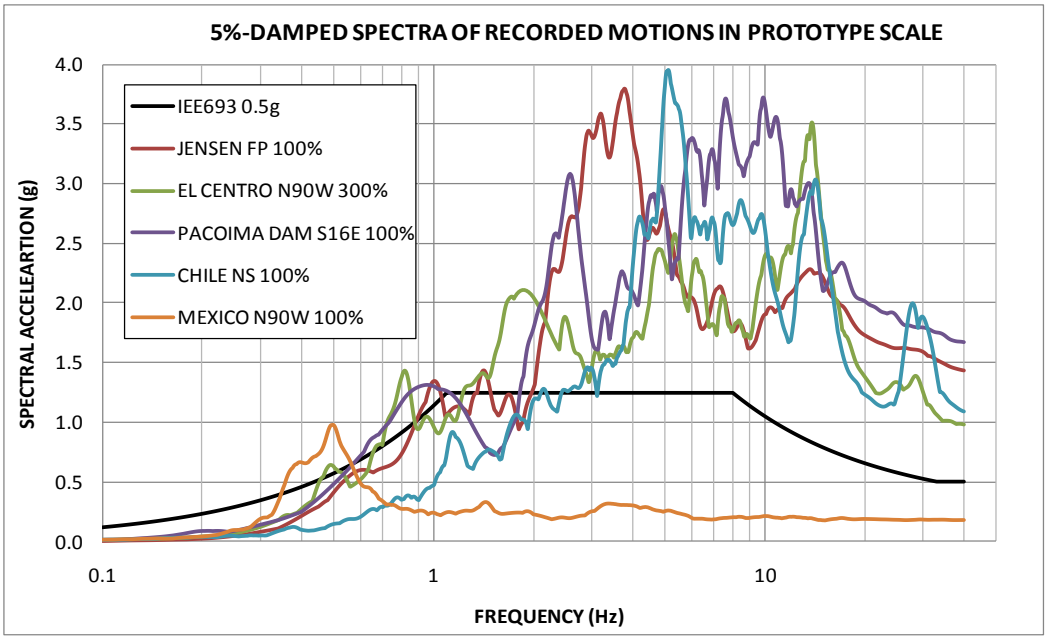


Figure 3-22 Horizontal 5% Damped Response Spectra of Representative Earthquake Components Used in Testing of the Isolated Model and Comparison to the IEEE 693 0.5g Spectrum

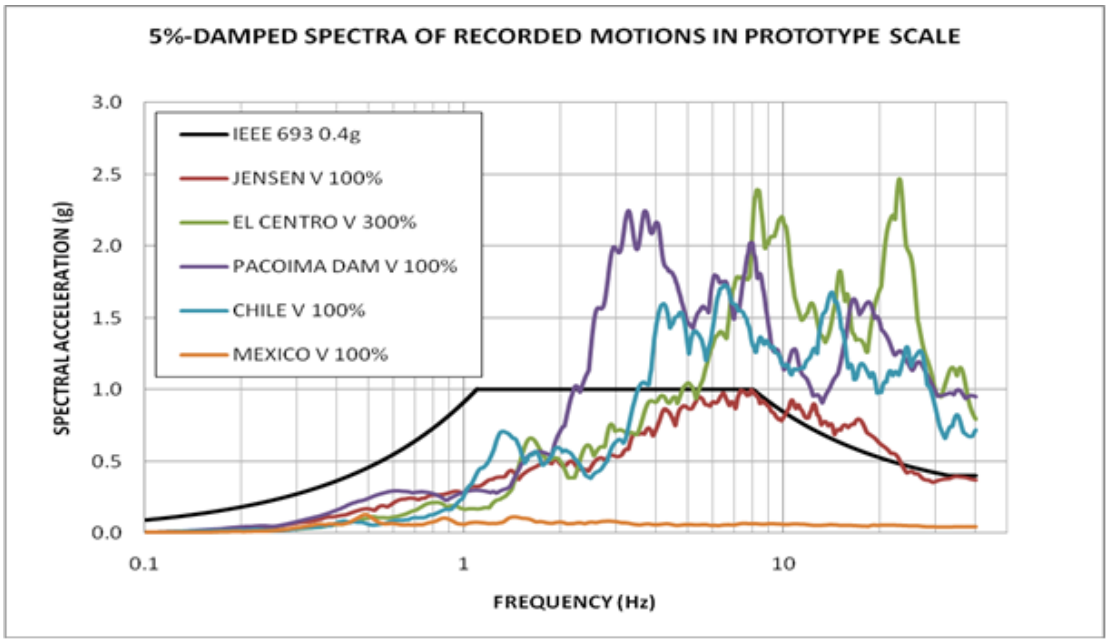


Figure 3-23 Vertical 5%-Damped Response Spectra of Representative Earthquake Components Used in Testing of the Isolated Model and Comparison to the IEEE 693 0.4g Spectrum

Table 3-8 presents 7 pairs of ground motions which were selected for scaling to match a horizontal site-specific spectrum in an average sense. The motions were selected to have near-

fault characteristics. Each pair of the selected ground motions has been rotated to fault-normal and fault-parallel directions. The moment magnitudes for the selected motions are between 6.7 and 7.1, the site-to-source distances (Campbell R distance) are between 3 and 12 km, and all the records are from Site Classes C and D per the ASCE 7-2010 (American, 2010). The ground-motion pair No.1 is from a backward-directivity region and all other motions are from forward-directivity regions (PEER-NGA database, http://peer.berkeley.edu/nga/). The scale factors calculated for each motion are also shown. It is noted that the motions are identical to those used in the examples in Constantinou et al (2011) where the scaling process is described.

Table 3-8 Seed Accelerograms and Scale Factors for Horizontal Motions

No	Earthquake Name	Recording Station	M_W[1]	r[2] (km)	Site[3]	Scale Factor
1	1976 Gazli, USSR	Karakyr	6.8	5.46	C	1.37
2	1989 Loma Prieta	LGPC	6.9	3.88	C	0.94
3	1989 Loma Prieta	Saratoga, W. Valley Coll.	6.9	9.31	C	1.57
4	1994 Northridge	Jensen Filter Plant	6.7	5.43	C	0.97
5	1994 Northridge	Sylmar, Coverter Sta. East	6.7	5.19	C	0.90
6	1995 Kobe, Japan	Takarazuka	6.9	3.00	D	0.97
7	1999 Duzce, Turkey	Bolu	7.1	12.41	D	1.04

1. Moment magnitude, 2. Campbell R distance, 3. Site class classification per 2010 ASCE 7

Scaling of the selected motions was performed for a horizontal site-specific spectrum which was obtained based on the procedures of the California Department of Transportation (Caltrans) from the Caltrans ARS website (http://dap3.dot.ca.gov/ARS_Online/index.php). The site-specific spectrum corresponds to a location in California with latitude 38.079857^o, longitude -122.232513^o (location just North of the Carquinez Bridge in Vallejo, CA) and shear wave velocity (V_{S30}) equal to 400 m/sec. The response spectrum for the site is the greatest among the

spectra calculated for the site, which for this location was one of the 2008 USGS National Hazard Map for a 5% probability of being exceeded in 50 years (1000 year return period) with adjustments for near-fault effects. Figure 3-24 presents the 5%-damped horizontal acceleration response spectrum of the site, and the IEEE 693 0.5g spectrum for comparison. It may be seen that the site-specific spectrum follows well the IEEE 693 spectrum in the high frequency range but falls below the IEEE 693 spectrum for frequencies less than 3Hz.

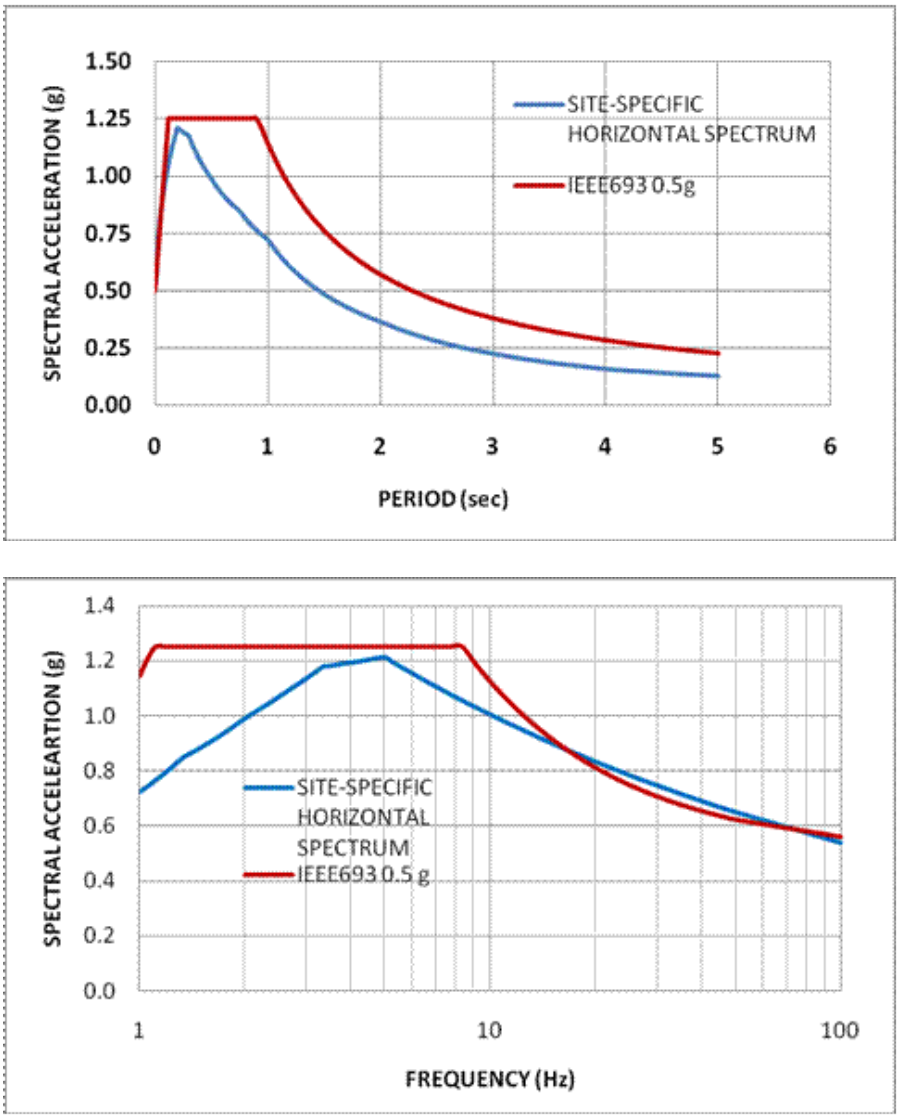


Figure 3-24 5%-Damped Horizontal Site-Specific and IEEE 693 0.5g Spectra

Figure 3-25 shows a comparison between the horizontal site-specific spectrum and the average geometric mean spectrum of the scaled motion ensemble, scaled by the factors presented in Table 3-8. The spectra compare very well, particularly in the period range of 1 to 4 sec that bounds the effective period of the tested isolated structures.

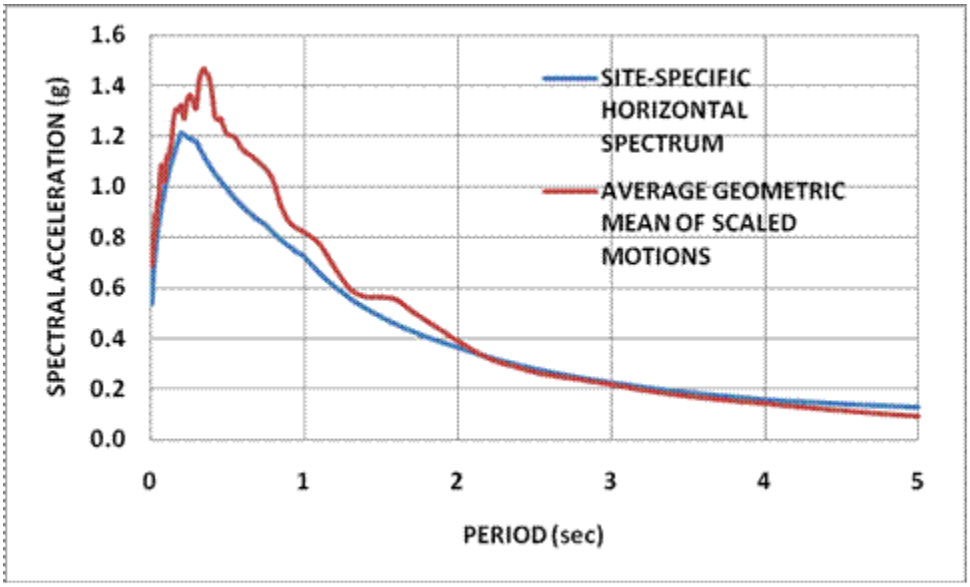


Figure 3-25 Comparison of the Site-Specific Horizontal Spectrum to the Average of the Geometric Mean Spectra of the 7 Scaled Motions

The vertical earthquake component, which was used in three-directional testing, was generated separately from the horizontal components with spectral matching procedures. The actual vertical ground motion of each of the earthquakes shown in Table 3-8 was used, with the exception of motion No. 3 (Saratoga) for which the vertical component was not available. Each of the remaining 6 motions was matched to a site-specific vertical response spectrum, generated by the method of Bozorgnia and Campbell (2004). In this method, the site-specific vertical spectrum is related to the site-specific horizontal spectrum through a vertical-to-horizontal spectral ratio (V/H ratio). The V/H ratio was found by the above authors to be a strong function of the period, soil type and distance to the fault. Based on the soil class and fault distance

characteristics of the ground motions selected (see Table 3-8), the V/H ratio of Figure 3-26 was considered appropriate for use in the present study. The generated vertical response spectrum is also shown in comparison to the horizontal site-specific response spectrum.

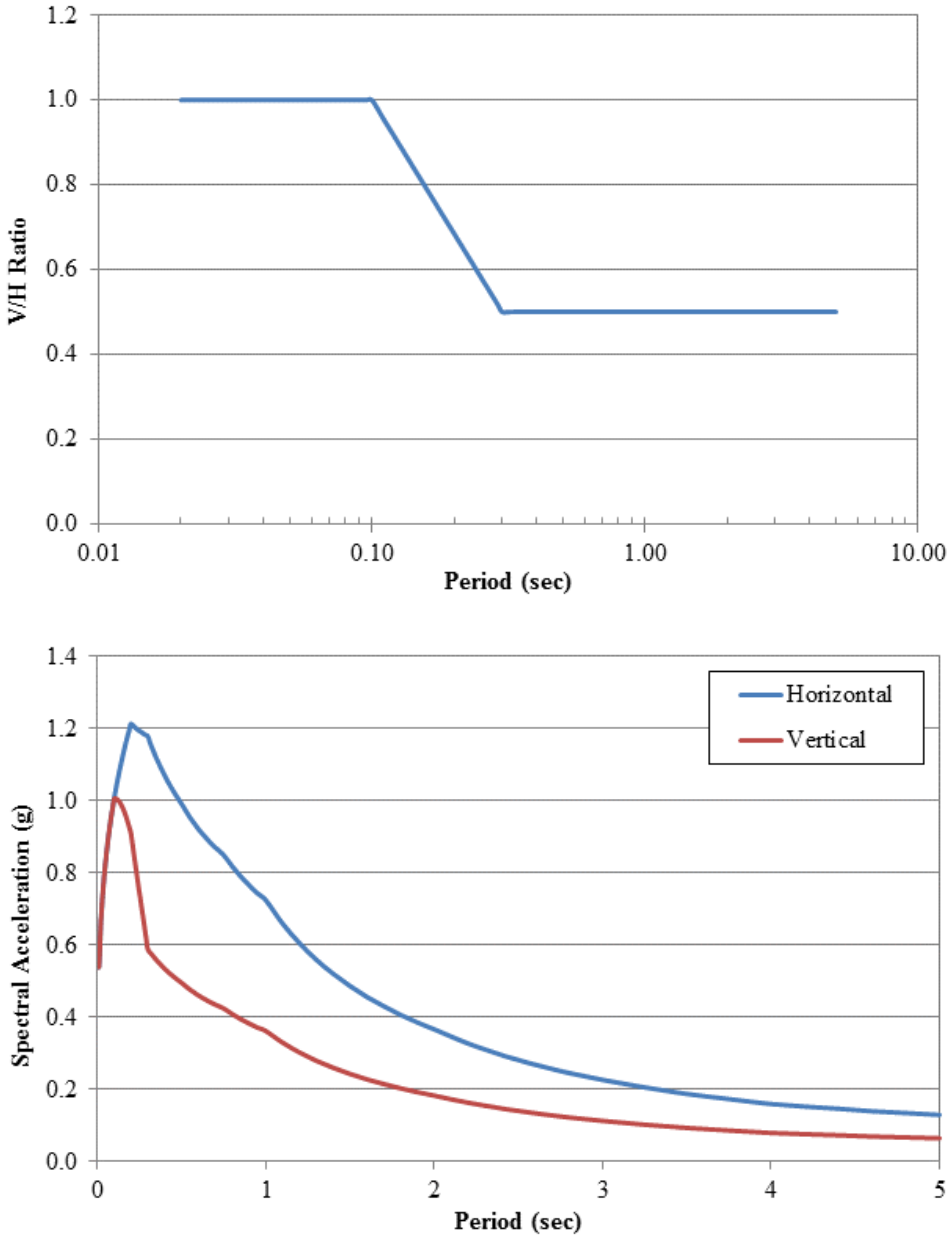


Figure 3-26 V/H Ratio and Generated Site-Specific Vertical Response Spectrum

Figure 3-27 presents the vertical site-specific response spectrum and the average of the spectrally matched vertical components of the motions of Table 3-8. Also, the IEEE 693 0.4g vertical RRS is included in Figure 3-27 for comparison.

Further details on the scaled motions are provided in Appendix A including the time histories of the motions as recorded on the shake table, and achieved versus target spectral accelerations.

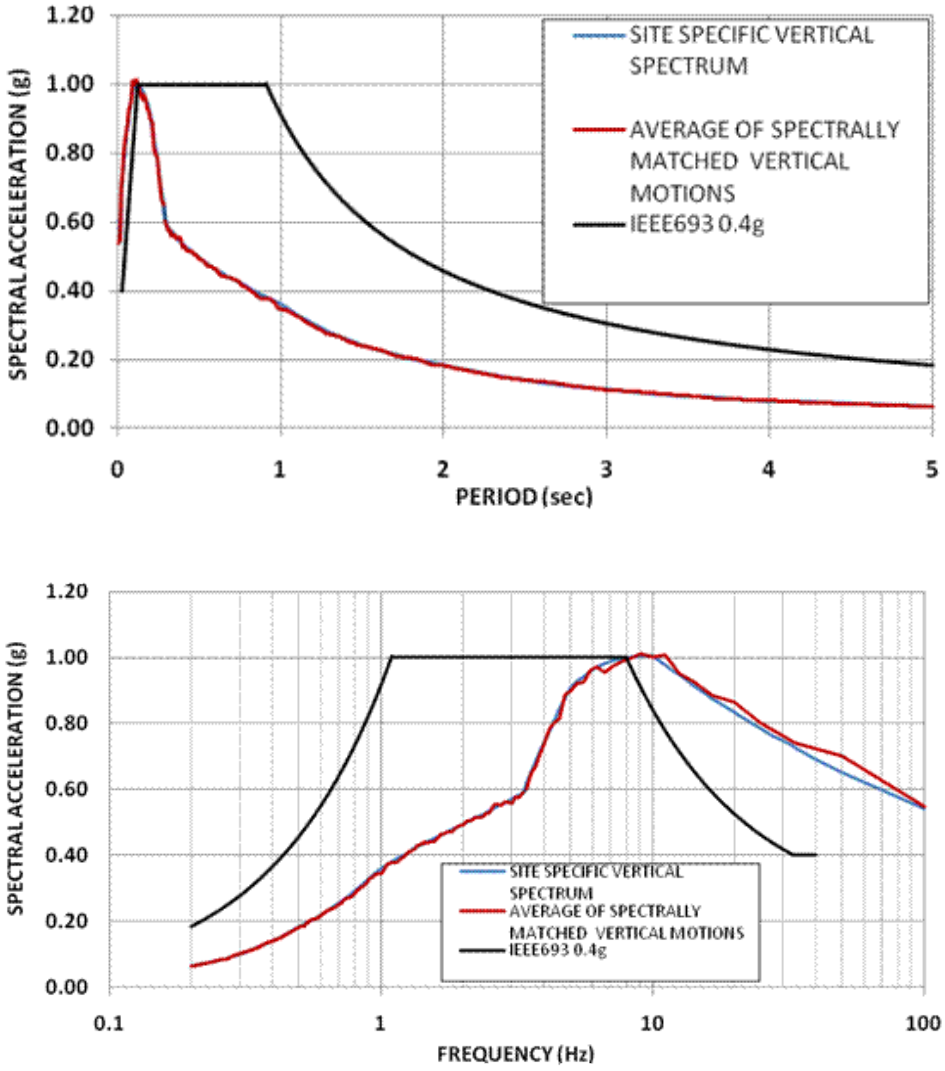


Figure 3-27 Comparison of the Site-Specific Vertical Spectrum to the Average of Spectra of the Six Spectrally Matched Vertical Motions and to the IEEE 693 0.4g Spectrum

3.7. **Testing Schedule**

The power transformer model was tested for a total of 17 variations and configurations. The test configurations used include:

a. Use of different base isolation systems. Three distinct systems were used, scaled Lead Rubber Bearings, scaled Triple Friction Pendulum bearings and full size Triple Friction Pendulum bearings. The properties of these systems have been discussed above.

b. Testing under different sets of ground motions. Two distinct sets of ground motions were used, with a different scaling approach for each, as discussed above.

c. Testing at various seismic levels. Specifically, testing of the scaled Triple FP bearings was performed with increased magnitude of the ground motions in order to challenge the isolation system. For the testing of the full size Triple FP bearings (length scale factor of 1) some of the motions were decreased in magnitude due to shake table capacity limitations.

d. Variation in the connection between the base isolation and the superstructure. Testing with the Triple FP bearings was carried out with the power transformer model simply mounted on the bearings (kept by friction). The Lead Rubber bearings were tested under the same configuration, as well as directly bolted to the bottom (base mat plate) of the power transformer specimen, in order to prevent sliding on the model-isolation system interface. In all cases, the bearings were bolted to the load cells located underneath them.

e. Testing under non-isolated conditions. It is noted that in order to eliminate rocking of the shake table, the fixed base tests were conducted at a lower level as compared to the isolated structure (25%-50% of the full amplitude).

f. Bi-axial horizontal and tri-axial testing with the aforementioned ground motion sets.

g. Variation in the bushing mounting position on the flexible roof of the power transformer model. Two different configurations were tested for which the bushing was mounted (i) at the center and (ii) at the side of the plate.

Table 3-9 presents a summary of the configurations presented. For each set the numbers and the ground motion names for the individual tests are provided as well as the attributes of the respective configuration are shown.

Table 3-9 Test Schedules and Configurations

Test Set #	Test #	Motion	Magnitude Scale Factor[1]	Isolation System				Length Scale		Test Type		Bushing Location	
				LRB (FB[2])	LRB (BB[3])	Triple FP	Non-Isolated[4]	1	3	2D (Horizontal)	3D	Center	Side
	42	Karakyr	137%	X					X	X		X	
	43	LGPC	94%	X					X	X		X	
	44	Saratoga	157%	X					X	X		X	
1	45	Jensen Filter	97%	X					X	X		X	
	48	Sylmar	90%	X					X	X		X	
	49	Takarazuka	97%	X					X	X		X	
	50	Bolu	104%	X					X	X		X	
	65	Karakyr	137%		X				X	X		X	
	66	LGPC	94%		X				X	X		X	
	67	Saratoga	157%		X				X	X		X	
2	68	Jensen Filter	97%		X				X	X		X	
	69	Sylmar	90%		X				X	X		X	
	70	Takarazuka	97%		X				X	X		X	
	71	Bolu	104%		X				X	X		X	
	76	Karakyr	69%				X		X	X		X	
	77	LGPC	47%				X		X	X		X	
	78	Saratoga	79%				X		X	X		X	
3	79	Jensen Filter	49%				X		X	X		X	
	80	Sylmar	45%				X		X	X		X	
	81	Takarazuka	49%				X		X	X		X	
	82	Bolu	52%				X		X	X		X	
	157	Karakyr	137%			X			X	X		X	
	158	LGPC	94%			X			X	X		X	
	159	Saratoga	157%			X			X	X		X	
4	160	Jensen Filter	97%			X			X	X		X	
	161	Sylmar	90%			X			X	X		X	
	162	Takarazuka	97%			X			X	X		X	
	163	Bolu	104%			X			X	X		X	

1. For the 7 motion ensemble (Karakyr, LGPC, Saratoga, Jensen Filter, Sylmar, Takarazuka, Bolu) this factor was applied to the horizontal components only. For the remaining motions (El Centro, Pacoima Dam, Taft, Chile, Mexico) this factor was applied to all components
2. FB: Friction-Bolted - Top plate of lead rubber bearing connected to the base mat by friction, bottom plate bolted to the load cells
3. BB: Bolted-Bolted - Top and bottom plates of lead rubber bearing bolted
4. Testing for the Non-Isolated model was performed at half of the scaled motions magnitude

Table 3-9 Test Schedules and Configurations (continued)

Test Set #	Test #	Motion	Magnitude Scale Factor[1]	Isolation System				Length Scale		Test Type		Bushing Location	
				LRB (FB[2])	LRB (BB[3])	Triple FP	Non-Isolated[4]	1	3	2D (Horizontal)	3D	Center	Side
5	165	Karakyr	171%			X			X	X		X	
	166	LGPC	118%			X			X	X		X	
	167	Saratoga	196%			X			X	X		X	
	168	Jensen Filter	121%			X			X	X		X	
	169	Sylmar	113%			X			X	X		X	
	170	Takarazuka	121%			X			X	X		X	
	171	Bolu	130%			X			X	X		X	
6	173	Karakyr	206%			X			X	X		X	
	175	Saratoga	236%			X			X	X		X	
	176	Jensen Filter	146%			X			X	X		X	
	177	Sylmar	135%			X			X	X		X	
	178	Takarazuka	146%			X			X	X		X	
	179	Bolu	156%			X			X	X		X	
7	189	Karakyr	137%			X			X		X	X	
	190	LGPC	94%			X			X		X	X	
	191	Jensen Filter	97%			X			X		X	X	
	192	Sylmar	90%			X			X		X	X	
	193	Takarazuka	97%			X			X		X	X	
	194	Bolu	104%			X			X		X	X	
8	214	El Centro	300%			X			X		X	X	
	208	Pacoima Dam	100%			X			X		X	X	
	217	Chile	100%			X			X		X	X	
	219	Mexico	100%			X			X		X	X	
9	221a	Jensen Filter	24%				X		X		X	X	
	222	El Centro	50%				X		X		X	X	
	224	Pacoima Dam	25%				X		X		X	X	
	228	Chile	50%				X		X		X	X	
	230	Mexico	100%				X		X		X	X	

1. For the 7 motion ensemble (Karakyr, LGPC, Saratoga, Jensen Filter, Sylmar, Takarazuka, Bolu) this factor was applied to the horizontal components only. For the remaining motions (El Centro, Pacoima Dam, Taft, Chile, Mexico) this factor was applied to all components
2. FB: Friction-Bolted - Top plate of lead rubber bearing connected to the base mat by friction, bottom plate bolted to the load cells
3. BB: Bolted-Bolted - Top and bottom plates of lead rubber bearing bolted
4. Testing for the Non-Isolated model was performed at half of the scaled motions magnitude

Table 3-9 Test Schedules and Configurations (continued)

Test Set #	Test #	Motion	Magnitude Scale Factor[1]	Isolation System				Length Scale		Test Type		Bushing Location	
				LRB (FB[2])	LRB (BB[3])	Triple FP	Non-Isolated[4]	1	3	2D (Horizontal)	3D	Center	Side
10	223	El Centro	50%				X		X	X		X	
	225	Pacoima Dam	25%				X		X	X		X	
	229	Chile	50%				X		X	X		X	
	231	Mexico	100%				X		X	X		X	
11	232	Jensen Filter	24%				X		X		X		X
	233	El Centro	50%				X		X		X		X
	235	Pacoima Dam	25%				X		X		X		X
	237	Taft	100%				X		X		X		X
	239	Chile	50%				X		X		X		X
	241	Mexico	100%				X		X		X		X
12	234	El Centro	50%				X		X	X			X
	236	Pacoima Dam	25%				X		X	X			X
	238	Taft	100%				X		X	X			X
	240	Chile	50%				X		X	X			X
	242	Mexico	100%				X		X	X			X
13	251	Jensen Filter	97%			X			X		X		X
	245	El Centro	300%			X			X		X		X
	246	Pacoima Dam	100%			X			X		X		X
	247	Taft	500%			X			X		X		X
	248	Chile	100%			X			X		X		X
	249a	Mexico	100%			X			X		X		X
14	253	El Centro	300%			X			X	X			X
	255	Pacoima Dam	100%			X			X	X			X
	257	Taft	500%			X			X	X			X
	258	Chile	100%			X			X	X			X

1. For the 7 motion ensemble (Karakyr, LGPC, Saratoga, Jensen Filter, Sylmar, Takarazuka, Bolu) this factor was applied to the horizontal components only. For the remaining motions (El Centro, Pacoima Dam, Taft, Chile, Mexico) this factor was applied to all components
2. FB: Friction-Bolted - Top plate of lead rubber bearing connected to the base mat by friction, bottom plate bolted to the load cells
3. BB: Bolted-Bolted - Top and bottom plates of lead rubber bearing bolted
4. Testing for the Non-Isolated model was performed at half of the scaled motions magnitude

Table 3-9 Test Schedules and Configurations (continued)

Test Set #	Test #	Motion	Magnitude Scale Factor[1]	Isolation System				Length Scale		Test Type		Bushing Location	
				LRB (FB[2])	LRB (BB[3])	Triple FP	Non-Isolated[4]	1	3	2D (Horizontal)	3D	Center	Side
15	259a	Jensen Filter	97%			X		X			X		X
	268a	El Centro	300%			X		X			X		X
	261	Pacoima Dam	75%			X		X			X		X
	263a	Taft	500%			X		X			X		X
	264	Chile	100%			X		X			X		X
	270	Mexico	70%			X		X			X		X
16	271	Jensen Filter	97%			X		X		X			X
	272	El Centro	300%			X		X		X			X
	273	Pacoima Dam	75%			X		X		X			X
	275	Chile	100%			X		X		X			X
	276	Mexico	70%			X		X		X			X
17	283	Jensen Filter	97%			X		X			X	X	
	284	El Centro	300%			X		X			X	X	
	285	Pacoima Dam	75%			X		X			X	X	
	286	Taft	500%			X		X			X	X	
	287	Chile	100%			X		X			X	X	
	288	Mexico	70%			X		X			X	X	
18	283a	Jensen Filter	97%			X		X		X		X	
	284a	El Centro	300%			X		X		X		X	
	285a	Pacoima Dam	75%			X		X		X		X	
	286a	Taft	500%			X		X		X		X	
	287a	Chile	100%			X		X		X		X	
	288a	Mexico	70%			X		X		X		X	

1. For the 7 motion ensemble (Karakyr, LGPC, Saratoga, Jensen Filter, Sylmar, Takarazuka, Bolu) this factor was applied to the horizontal components only. For the remaining motions (El Centro, Pacoima Dam, Taft, Chile, Mexico) this factor was applied to all components
2. FB: Friction-Bolted - Top plate of lead rubber bearing connected to the base mat by friction, bottom plate bolted to the load cells
3. BB: Bolted-Bolted - Top and bottom plates of lead rubber bearing bolted
4. Testing for the Non-Isolated model was performed at half of the scaled motions magnitude

SECTION 4
SHAKE TABLE TESTING RESULTS AND EVALUATION

4.1. Overview

This section presents experimental results obtained from shake table testing of the isolated and non-isolated power transformer specimen, for the configurations described in Section SECTION 3. Comprehensive summaries of test data for each conducted test are presented in Appendix B.

4.2. Experimental Results for Isolated and Non-Isolated Structure at Reduced Length Scale

This section presents comparisons between selected experimental results obtained from shake table testing of the isolated and non-isolated power transformer models. The results are presented in raw form (unfiltered) in order to eliminate potential bias in the interpretation of the results. Moreover, for each test the displacements have been post-processed by removing the initial offset so that any permanent offset from the previous test is not being reported. That was preferred for consistency because in some tests the displacement measurements were physically re-set to zero at the start of the test, while in several other tests sliding occurred on the isolation interface and the system was subsequently manually re-centered. Thus the measured initial offsets at the start of a test did not always match the actual permanent offsets at the end of the previous test. To better illustrate the effect of base isolation on the bushing response, the peak acceleration responses obtained at the bottom of the frame (at a location above the isolators on the base mat) and at the bushing center of gravity (CG) are presented in Table 4-1 and Table 4-2. The response at the bushing CG is used herein as a sufficiently acceptable measure of the global performance of the bushing, as it has also been used in past studies (Kong, 2010, Koliou, 2010, Fahad, 2013).

Table 4-1 presents comparisons between peak acceleration results obtained from bi-axial excitation of the scaled specimen when isolated with LRB (connected either by friction or bolted to the base mat), when isolated with Triple FP bearings (connected only by friction to the base mat), and when non-isolated (base mat fixed directly to the load cells). Table 4-2 presents similar comparisons, however only for the case when Triple FP bearings were used, and with testing performed at increasing earthquake intensities, by up to 50% higher than the earthquake intensity of the Table 4-1 results (Design Earthquake vs Maximum Considered Earthquake). In this case, during some of the tests the Triple FP bearings reached their displacement capacities, and some sliding of the specimen on top of the isolators occurred. Both tables present results from bi-axial horizontal excitation with the bushing mounted symmetrically on the cover plate. Furthermore, average results are included in the tables to better represent the response for the particular hazard to which the motions have been scaled to represent in an average sense. Figure 4-1 and Figure 4-2 present additional comparisons of peak acceleration responses, over the height of the model, between the non-isolated and the models isolated with the LRB in a bolted-bolted configuration and with the scaled Triple FP bearings respectively. In both figures the peak accelerations have been normalized by the peak table acceleration (PGA) for ease in the presentation.

Comparisons of peak relative resultant displacement results between the isolated and non-isolated cases are shown in Table 4-3 and Table 4-4, at the bushing mounting interface and at the top of the bushing. The relative displacements were calculated by subtracting the absolute displacement of the shake table from the absolute displacement measured at the point of interest. Subsequently, the peak resultant horizontal relative displacement was obtained through the vectorial addition of the individual horizontal relative displacement components. Figure 4-3 and

Figure 4-4 present additional comparisons of peak resultant displacement responses, over the height of the model, between the non-isolated and the models isolated with the LRB in a bolted-bolted configuration and with the scaled Triple FP bearings respectively. In both figures the peak resultant displacement responses are presented relative to the shake table.

Finally, comparisons of peak base shear force results between the isolated and non-isolated cases are shown in Table 4-5 and Table 4-6. The base shear force for each test and in each direction was calculated by obtaining the total shear force history adding up all the individual shear force histories from each of the four load cells in the direction of interest (eliminating the initial offsets).

In the above comparisons it should be noted that the non-isolated model was actually tested at 50% of the scaled motions. However, for comparative purposes, the non-isolated model results were linearly extrapolated to match the level at which the isolated models were tested, assuming that the non-isolated model would have remained elastic under such increased demand.

Table 4-1 Peak Acceleration Response (Values in Units of g) at Selected Locations on the Model for Isolated and Non-Isolated Conditions (Bi-axial Horizontal Excitation, Bushing Mounted Symmetrically on the Cover, Testing at Length Scale of 1:3)

Motion	Direction	Acceleration Response (g)				Response Reduction (% with Respect to Non-Isolated)		
		LRB (FB[1])	LRB (BB[2])	Triple FP	Non-Isolated[3]	LRB (FB)	LRB (BB)	Triple FP
Frame Bottom								
Karakyr	**EW**	0.39	0.56	0.39	1.67	77%	67%	77%
	NS	0.38	0.44	0.39	1.54	75%	71%	75%
LGPC	**EW**	0.41	0.53	0.28	1.06	61%	50%	73%
	NS	0.31	0.32	0.23	0.85	63%	62%	72%
Saratoga	**EW**	0.44	0.54	0.23	1.12	61%	51%	80%
	NS	0.33	0.31	0.18	0.82	59%	63%	78%
Jensen	**EW**	0.35	0.37	0.24	0.99	65%	62%	75%
	NS	0.46	0.48	0.27	2.40	81%	80%	89%
Sylmar	**EW**	0.48	0.41	0.22	1.51	68%	73%	85%
	NS	0.47	0.54	0.22	0.83	44%	35%	74%
Takarazuka	**EW**	0.35	0.50	0.21	1.11	69%	55%	81%
	NS	0.37	0.55	0.20	1.17	68%	53%	83%
Bolu	**EW**	0.41	0.34	0.24	1.60	74%	79%	85%
	NS	0.39	0.46	0.26	1.17	67%	61%	78%
Average	***EW***	***0.40***	***0.46***	***0.26***	***1.29***	***68%***	***62%***	***79%***
	NS	***0.39***	***0.44***	***0.25***	***1.25***	***65%***	***61%***	***78%***
Bushing CG								
Karakyr	**EW**	0.57	0.65	0.90	3.19	82%	80%	72%
	NS	0.76	0.57	0.79	4.21	82%	86%	81%
LGPC	**EW**	0.65	0.63	0.54	2.46	74%	74%	78%
	NS	0.39	0.35	0.32	1.38	72%	75%	77%
Saratoga	**EW**	0.96	0.64	0.36	1.67	42%	62%	78%
	NS	0.55	0.51	0.34	2.08	74%	76%	84%
Jensen	**EW**	0.48	0.42	0.39	1.89	75%	78%	79%
	NS	0.51	0.51	0.49	3.49	85%	85%	86%
Sylmar	**EW**	0.56	0.64	0.42	2.50	78%	74%	83%
	NS	0.62	0.60	0.44	1.50	58%	60%	71%
Takarazuka	**EW**	0.52	0.49	0.37	2.90	82%	83%	87%
	NS	0.94	0.70	0.36	2.34	60%	70%	85%
Bolu	**EW**	0.40	0.37	0.42	2.21	82%	83%	81%
	NS	0.51	0.61	0.35	2.27	78%	73%	85%
Average	***EW***	***0.59***	***0.55***	***0.49***	***2.40***	***73%***	***76%***	***80%***
	NS	***0.61***	***0.55***	***0.44***	***2.47***	***73%***	***75%***	***81%***

1. FB: Friction-Bolted - Top plate connected by friction to the base mat, bottom plate bolted to the load cells
2. BB: Bolted-Bolted - Top and bottom plates bolted
3. The Non-Isolated model was actually tested at 50% of the scaled motions but for comparative purposes the results were linearly extrapolated, assuming that the structure would remain elastic

Table 4-2 Peak Acceleration Response (Values in Units of g) at Selected Locations for the Isolated Model Tested at Extreme Conditions, and for the Non-Isolated Model (Triple FP, Bi-axial Horizontal Excitation, Bushing Mounted Symmetrically on the Cover, Testing at Length Scale of 1:3)

Motion	Direction	Acceleration Response (g)				Response Reduction (% with Respect to Non-Isolated, Extrapolated to the Same Level)		
		Triple FP (DE[1])	Triple FP (1.25DE)	Triple FP (MCE[2])	Non-Isolated[3] (DE)	Triple FP (DE)	Triple FP (1.25DE)	Triple FP (MCE)
Frame Bottom								
Karakyr	**EW**	0.39	0.47	1.13	1.67	77%	77%	55%
	NS	0.39	0.52	0.82	1.54	75%	73%	64%
LGPC	**EW**	0.28	0.63	N/A	1.06	73%	53%	N/A
	NS	0.23	0.75	N/A	0.85	72%	30%	N/A
Saratoga	**EW**	0.23	0.24	0.59	1.12	80%	83%	65%
	NS	0.18	0.21	0.54	0.82	78%	80%	56%
Jensen	**EW**	0.24	0.24	1.95	0.99	75%	80%	-31%
	NS	0.27	0.30	0.77	2.40	89%	90%	79%
Sylmar	**EW**	0.22	0.26	0.41	1.51	85%	86%	82%
	NS	0.22	0.27	0.44	0.83	74%	74%	65%
Takarazuka	**EW**	0.21	0.22	0.24	1.11	81%	84%	86%
	NS	0.20	0.22	0.23	1.17	83%	85%	87%
Bolu	**EW**	0.24	0.22	0.23	1.60	85%	89%	90%
	NS	0.26	0.24	0.29	1.17	78%	83%	84%
Average	***EW***	***0.26***	***0.33***	***0.76***	***1.29***	***79%***	***79%***	***58%***
	NS	***0.25***	***0.36***	***0.51***	***1.25***	***78%***	***74%***	***72%***
Bushing CG								
Karakyr	**EW**	0.90	0.82	2.24	3.19	72%	79%	53%
	NS	0.79	0.78	1.67	4.21	81%	85%	73%
LGPC	**EW**	0.54	1.09	N/A	2.46	78%	65%	N/A
	NS	0.32	1.84	N/A	1.38	77%	-7%	N/A
Saratoga	**EW**	0.36	0.40	1.10	1.67	78%	81%	56%
	NS	0.34	0.39	1.34	2.08	84%	85%	57%
Jensen	**EW**	0.39	0.43	2.69	1.89	79%	82%	5%
	NS	0.49	0.55	1.45	3.49	86%	87%	72%
Sylmar	**EW**	0.42	0.49	0.97	2.50	83%	84%	74%
	NS	0.44	0.51	1.03	1.50	71%	73%	54%
Takarazuka	**EW**	0.37	0.54	0.49	2.90	87%	85%	89%
	NS	0.36	0.45	0.44	2.34	85%	85%	88%
Bolu	**EW**	0.42	0.42	0.41	2.21	81%	85%	88%
	NS	0.35	0.33	0.33	2.27	85%	88%	90%
Average	***EW***	***0.49***	***0.60***	***1.32***	***2.40***	***80%***	***80%***	***61%***
	NS	***0.44***	***0.69***	***1.04***	***2.47***	***81%***	***71%***	***72%***

1. DE: Design Earthquake (Level of Testing)
2. MCE: Maximum Considered Earthquake (Level of Testing)
3. The Non-Isolated model was actually tested at 50% of the scaled motions but for comparative purposes the results were linearly extrapolated, assuming that the structure would remain elastic

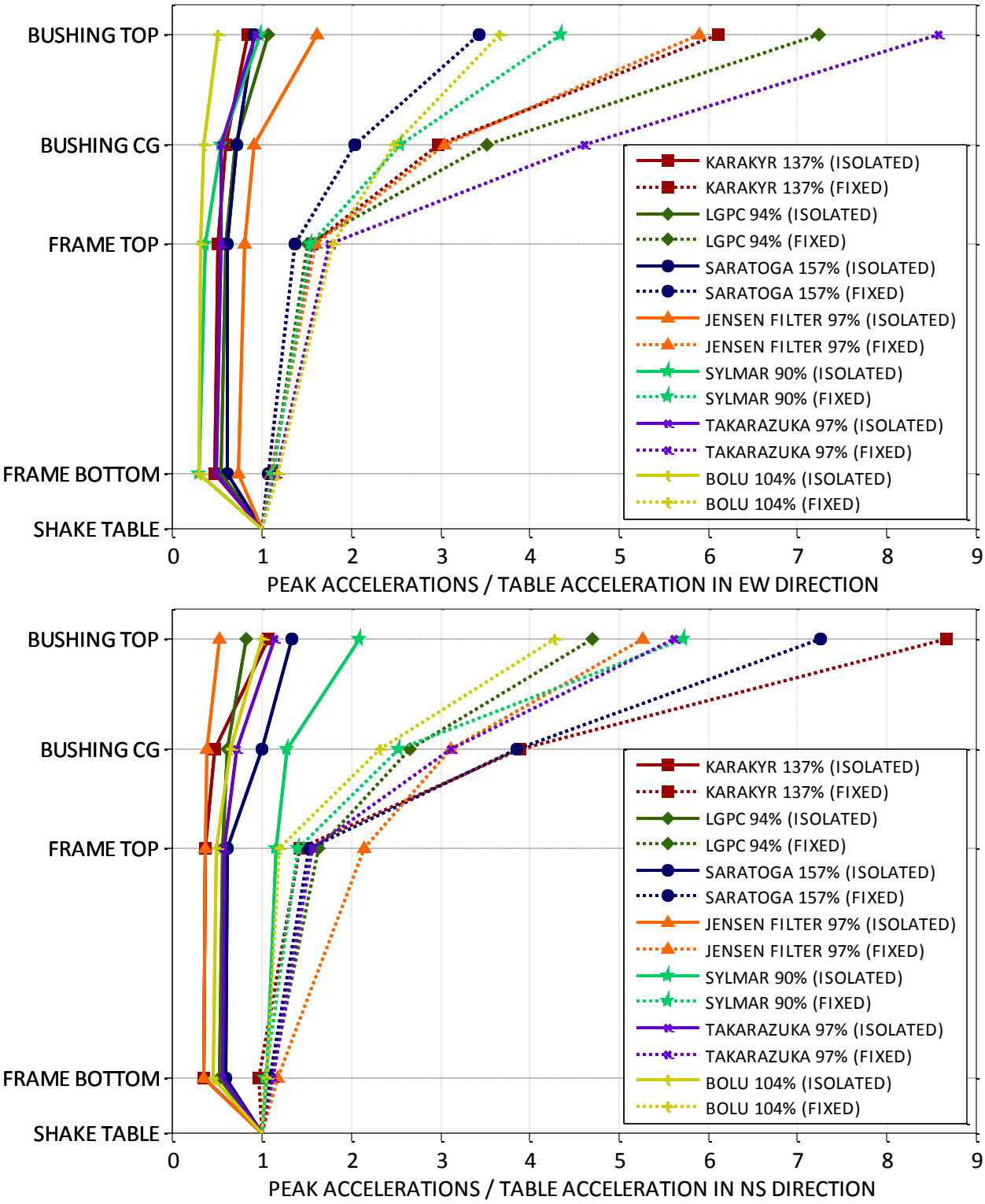


Figure 4-1 Comparison of Peak Acceleration Responses (Normalized to PGA) for Isolated (LRB, Bolted-Bolted Configuration) and Non-Isolated Models in the EW and NS Directions (2D Horizontal Excitation, Bushing Mounted Symmetrically on the Cover, Testing at Length Scale of 1:3, Extrapolated Results for Non-Isolated Model)

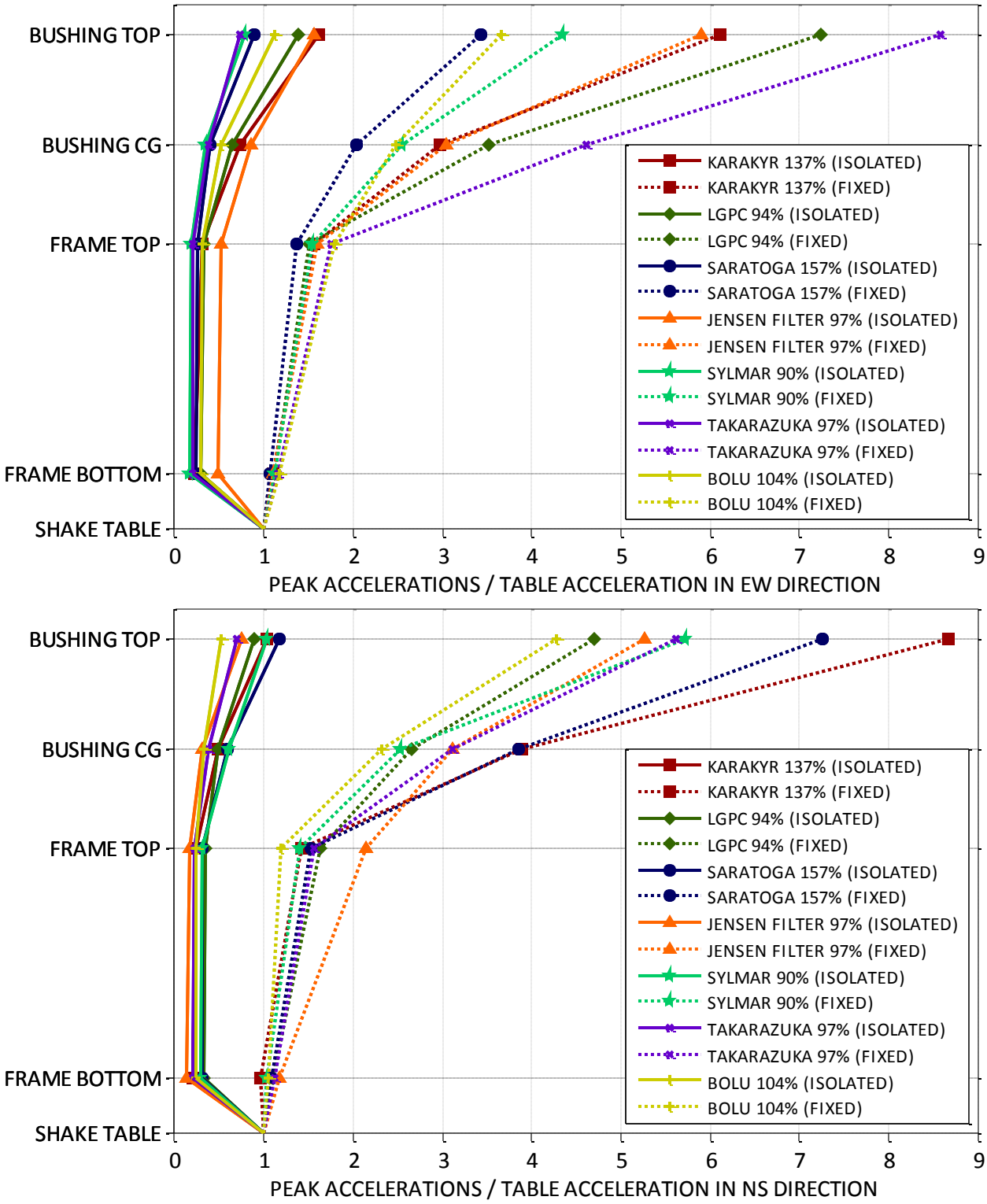


Figure 4-2 Comparison of Peak Acceleration Responses (Normalized to PGA) for Isolated (Triple FP) and Non-Isolated Models in the EW and NS Directions (2D Horizontal Excitation, Bushing Mounted Symmetrically on the Cover, Testing at Length Scale of 1:3, Extrapolated Results for Non-Isolated Model)

Table 4-3 Peak Resultant Displacement Response (Values in Units of inches, Relative to the Shake Table), at Selected Locations on the Model for Isolated and Non-Isolated Conditions (Bi-axial Horizontal Excitation, Bushing Mounted Symmetrically on the Cover, Testing at Length Scale of 1:3)

Motion	Resultant Displacement Response (in)								Response Amplification at Bushing Top (% with Respect to Cover Plate)			
	Frame Top (Bushing - Plate Interface)				Bushing Top							
	LRB (FB[1])	LRB (BB[2])	Triple FP	Non-Isolated[3]	LRB (FB)	LRB (BB)	Triple FP	Non-Isolated	LRB (FB)	LRB (BB)	Triple FP	Non-Isolated
Karakyr	3.9	3.7	3.5	0.4	3.9	3.9	3.6	1.2	1%	4%	3%	69%
LGPC	5.0	3.3	3.7	0.2	5.0	3.4	3.7	0.8	0%	3%	1%	69%
Saratoga	5.2	3.7	3.8	0.3	5.1	3.7	3.8	0.6	-2%	1%	0%	54%
Jensen	3.0	2.9	2.7	0.4	3.0	3.0	2.8	1.2	1%	4%	4%	68%
Sylmar	4.4	3.8	3.5	0.2	4.5	3.9	3.6	0.9	2%	3%	2%	74%
Takarazuka	2.9	3.4	2.8	0.3	3.0	3.5	2.9	1.0	4%	3%	3%	73%
Bolu	2.4	2.5	2.1	0.3	2.4	2.6	2.2	0.9	3%	4%	1%	68%
Average	***3.8***	***3.3***	***3.2***	***0.3***	***3.8***	***3.4***	***3.2***	***0.9***	***1%***	***3%***	***2%***	***68%***

1. FB: Friction-Bolted - Top plate connected by friction to the base mat, bottom plate bolted to the load cells
2. BB: Bolted-Bolted - Top and bottom plates bolted
3. The Non-Isolated model was actually tested at 50% of the scaled motions but for comparative purposes the results were linearly extrapolated, assuming that the structure would remain elastic

Table 4-4 Peak Resultant Displacement Response (Values in Units of inches, Relative to the Shake Table), at Selected Locations for the Isolated Model Tested at Extreme Conditions, and for the Non-Isolated Model (Triple FP, Bi-axial Horizontal Excitation, Bushing Mounted Symmetrically on the Cover, Testing at Length Scale of 1:3)

Motion	Resultant Displacement Response (in)								Response Amplification at Bushing Top (% with Respect to Cover Plate)			
	Frame Top (Bushing - Plate Interface)				Bushing Top							
	Triple FP (DE[1])	Triple FP (1.25DE)	Triple FP (MCE[2])	Non-Isolated[3] (DE)	Triple FP (DE)	Triple FP (1.25DE)	Triple FP (MCE)	Non-Isolated (DE)	Triple FP (DE)	Triple FP (1.25DE)	Triple FP (MCE)	Non-Isolated (DE)
Karakyr	3.5	4.8	6.6	0.4	3.6	5.0	6.6	1.2	3%	3%	-1%	69%
LGPC	3.7	6.8	N/A	0.2	3.7	7.0	N/A	0.8	1%	2%	N/A	69%
Saratoga	3.8	4.8	4.7	0.3	3.8	4.8	5.0	0.6	0%	0%	6%	54%
Jensen	2.7	3.1	6.8	0.4	2.8	3.2	7.4	1.2	4%	3%	9%	68%
Sylmar	3.5	4.3	5.2	0.2	3.6	4.4	5.7	0.9	2%	2%	9%	74%
Takarazuka	2.8	3.4	3.9	0.3	2.9	3.5	4.0	1.0	3%	3%	1%	73%
Bolu	2.1	2.8	3.5	0.3	2.2	2.9	3.5	0.9	1%	2%	2%	68%
Average	***3.2***	***4.3***	***5.1***	***0.3***	***3.2***	***4.4***	***5.4***	***0.9***	***2%***	***2%***	***5%***	***68%***

1. DE: Design Earthquake (Level of Testing)
2. MCE: Maximum Considered Earthquake (Level of Testing)
3. The Non-Isolated model was actually tested at 50% of the scaled motions but for comparative purposes the results were linearly extrapolated, assuming that the structure would remain elastic

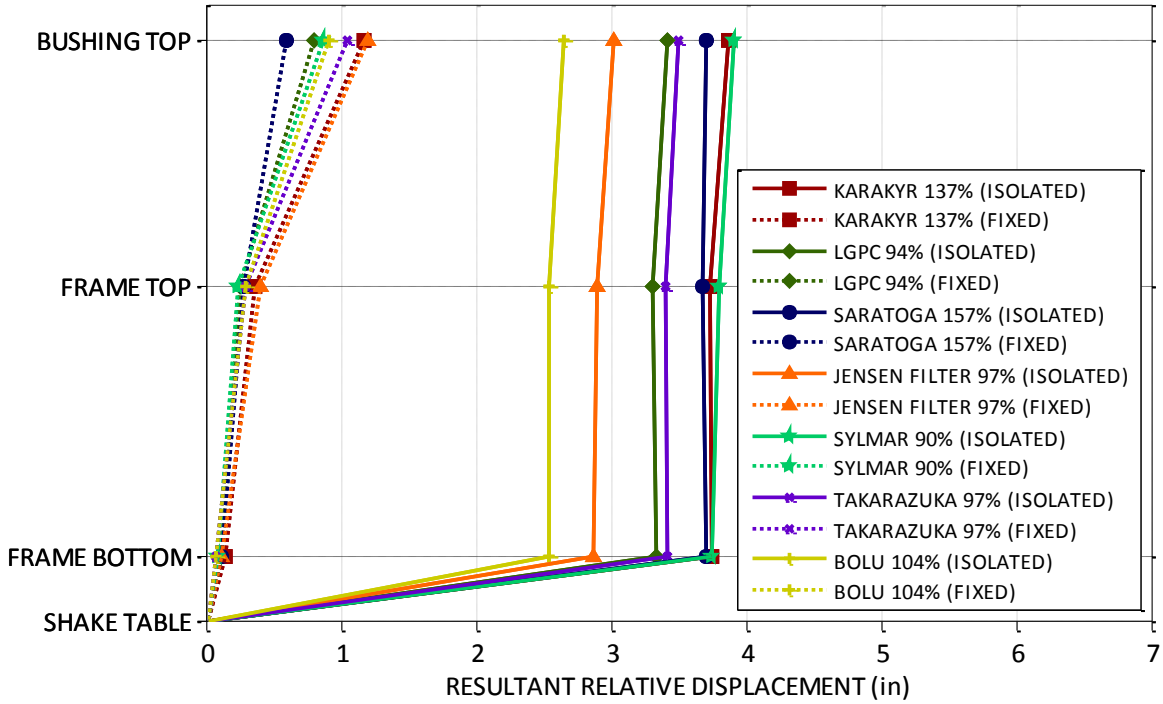


Figure 4-3 Comparison of Peak Resultant Displacement Responses for Isolated (LRB, Bolted-Bolted Configuration) and Non-Isolated Models (2D Horizontal Excitation, Bushing Mounted Symmetrically on the Cover, Testing at Length Scale of 1:3, Extrapolated Results for Non-Isolated Model)

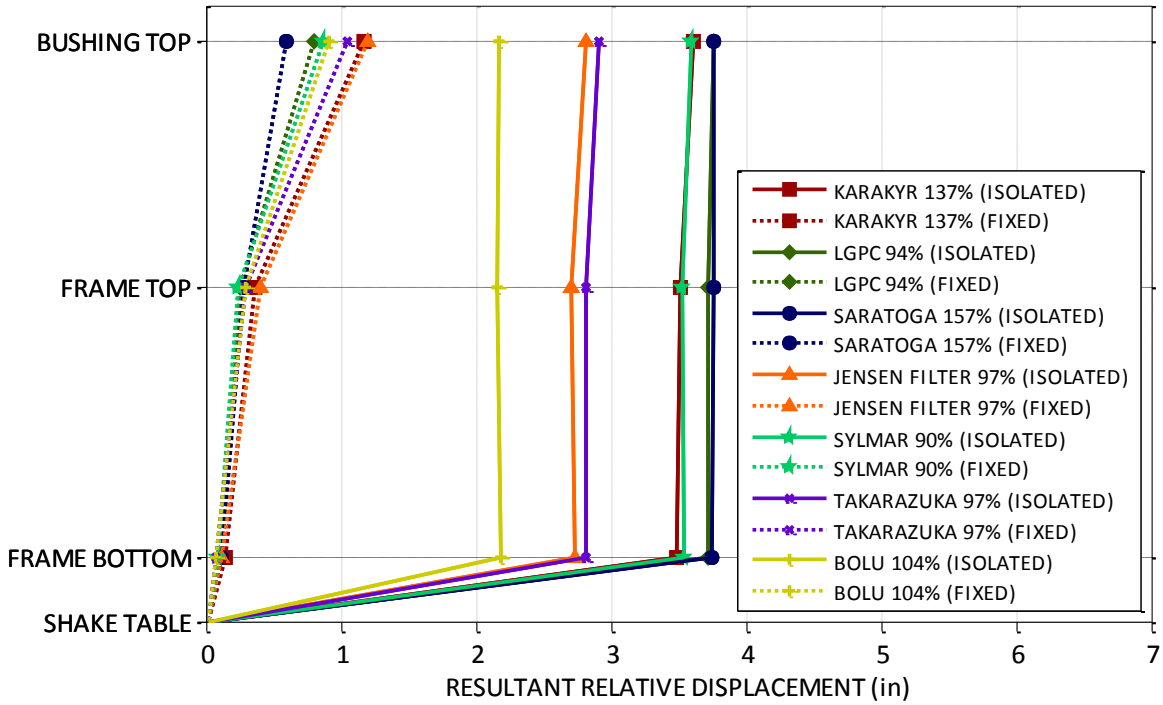


Figure 4-4 Comparison of Peak Resultant Displacement Responses for Isolated (Triple FP) and Non-Isolated Models (2D Horizontal Excitation, Bushing Mounted Symmetrically on the Cover, Testing at Length Scale of 1:3, Extrapolated Results for Non-Isolated Model)

Table 4-5 Peak Base Shear Forces (Values in Units of kip) for Isolated and Non-Isolated Conditions (Bi-axial Horizontal Excitation, Bushing Mounted Symmetrically on the Cover, Testing at Length Scale of 1:3)

Motion	Direction	Peak Base Shear Force (kip)				Response Reduction (% with Respect to Non-Isolated)		
		LRB (FB[1])	LRB (BB[2])	Triple FP	Non-Isolated[3]	LRB (FB)	LRB (BB)	Triple FP
Karakyr	**EW**	15.9	24.7	9.7	56.6	72%	56%	83%
	NS	15.9	19.7	9.5	53.9	71%	63%	82%
LGPC	**EW**	16.8	24.3	10.9	44.2	70%	57%	81%
	NS	13.3	14.6	8.5	33.2	75%	73%	84%
Saratoga	**EW**	16.2	26.2	10.4	49.7	71%	54%	82%
	NS	17.3	19.5	8.4	34.4	68%	64%	84%
Jensen	**EW**	14.4	17.3	8.7	40.6	74%	69%	85%
	NS	17.6	21.4	9.5	78.4	67%	60%	82%
Sylmar	**EW**	17.0	17.5	9.8	61.2	70%	69%	83%
	NS	17.1	25.5	9.9	33.2	68%	53%	82%
Takarazuka	**EW**	13.7	18.4	9.5	45.9	76%	67%	83%
	NS	16.5	23.9	8.9	47.3	69%	56%	84%
Bolu	**EW**	15.1	15.5	9.2	62.8	73%	73%	84%
	NS	18.3	20.1	9.3	50.7	66%	63%	83%
Average	***EW***	***15.6***	***20.6***	***9.7***	***51.6***	***72%***	***64%***	***83%***
	NS	***16.6***	***20.7***	***9.1***	***47.3***	***69%***	***62%***	***83%***

1. FB: Friction-Bolted - Top plate connected by friction to the base mat, bottom plate bolted to the load cells
2. BB: Bolted-Bolted - Top and bottom plates bolted
3. The Non-Isolated model was actually tested at 50% of the scaled motions but for comparative purposes the results were linearly extrapolated, assuming that the structure would remain elastic

Table 4-6 Peak Base Shear Forces (Values in Units of kip) for the Isolated Model Tested at Extreme Conditions, and for the Non-Isolated Model (Triple FP, Bi-axial Horizontal Excitation, Bushing Mounted Symmetrically on the Cover, Testing at Length Scale of 1:3)

Motion	Direction	Peak Base Shear Force (kip)				Response Reduction (% with Respect to Non-Isolated, Extrapolated to the Same Level)		
		Triple FP (DE[1])	Triple FP (1.25DE)	Triple FP (MCE[2])	Non-Isolated[3] (DE)	Triple FP (DE)	Triple FP (1.25DE)	Triple FP (MCE)
Karakyr	**EW**	9.7	12.3	13.3	56.6	83%	83%	84%
	NS	9.5	10.8	15.6	53.9	83%	85%	82%
LGPC	**EW**	10.9	20.7	N/A	44.2	75%	62%	N/A
	NS	8.5	10.8	N/A	33.2	81%	80%	N/A
Saratoga	**EW**	10.4	11.5	12.6	49.7	79%	81%	83%
	NS	8.4	9.6	10.2	34.4	83%	84%	86%
Jensen	**EW**	8.7	10.1	12.7	40.6	79%	80%	79%
	NS	9.5	9.6	9.9	78.4	77%	81%	84%
Sylmar	**EW**	9.8	10.7	11.9	61.2	84%	86%	87%
	NS	9.9	10.6	11.5	33.2	84%	86%	87%
Takarazuka	**EW**	9.5	9.9	10.3	45.9	79%	83%	85%
	NS	8.9	9.5	13.2	47.3	81%	83%	81%
Bolu	**EW**	9.2	10.0	10.7	62.8	85%	87%	89%
	NS	9.3	9.6	10.7	50.7	85%	88%	89%
Average	***EW***	***9.7***	***12.2***	***11.9***	***51.6***	***81%***	***80%***	***85%***
	NS	***9.1***	***10.1***	***11.8***	***47.3***	***82%***	***84%***	***85%***

1. DE: Design Earthquake (Level of Testing)
2. MCE: Maximum Considered Earthquake (Level of Testing)
3. The Non-Isolated model was actually tested at 50% of the scaled motions but for comparative purposes the results were linearly extrapolated, assuming that the structure would remain elastic

4.3. **Experimental Results for Isolated Structure with Full Scale Triple FP Bearings**

This section presents selected peak response results obtained from shake table testing of the power transformer model when isolated with full scale Triple FP bearings. Note that the set of ground motions presented herein is different than the ensemble upon which the results of the previous section were based. Testing of the non-isolated model with this ground motion set was not performed and therefore, similar comparisons to the ones of section 4.2 are not possible. Nevertheless, various comparisons are performed to investigate the effect of different testing conditions on the response of the system, such as the inclusion of the vertical component of the ground motion in testing and the bushing mounting location on the flexible roof.

Table 4-7 presents peak acceleration responses obtained at the top of the frame and at the CG of the bushing. For comparative purposes, results from testing using bi-axial (horizontal) and tri-axial excitations, as well as from testing with the bushing mounted either symmetrically or non-symmetrically on the cover, are presented. Note that the factor used to scale the motions is included in the tables (100% implies that the motion is as recorded; 300% implies that it was scaled in amplitude by a factor of 3). In a similar fashion, Table 4-8 and Table 4-9 present peak resultant displacement and peak base shear force responses for the same testing configurations and number of ground motion components used in testing.

Table 4-7 Peak Acceleration Response (Values in Units of g) at Selected Locations of the Isolated Model (Full Scale Triple FP, Bi-axial Horizontal or Tri-axial Excitation, Bushing Mounted Symmetrically or Non-Symmetrically on the Cover, Testing at Full Length Scale)

Motion	Direction	Bushing at Center of Cover Plate		Bushing at Side of Cover Plate	
		2D	3D	2D	3D
Frame Top					
Jensen 97%	**EW**	0.24	0.25	0.16	0.23
	NS	0.18	0.28	0.16	0.19
El Centro 300%	**EW**	0.24	0.44	0.23	0.49
	NS	0.22	0.38	0.21	0.32
Pacoima 75%	**EW**	0.16	0.22	0.16	0.23
	NS	0.13	0.17	0.12	0.18
Taft 500%	**EW**	0.17	0.23	N/A	0.25
	NS	0.19	0.17	N/A	0.19
Chile 100%	**EW**	0.15	0.19	0.13	0.21
	NS	0.16	0.19	0.15	0.22
Mexico 70%	**EW**	0.18	0.17	0.20	0.18
	NS	0.07	0.07	0.10	0.10
Bushing CG					
Jensen 97%	**EW**	0.31	0.69	0.32	0.81
	NS	0.55	0.74	0.45	0.82
El Centro 300%	**EW**	0.30	1.22	0.41	2.76
	NS	0.57	1.42	0.50	1.24
Pacoima 75%	**EW**	0.29	0.43	0.36	0.81
	NS	0.40	0.51	0.50	0.60
Taft 500%	**EW**	0.50	0.57	N/A	0.81
	NS	0.42	0.43	N/A	0.48
Chile 100%	**EW**	0.37	0.69	0.48	1.42
	NS	0.38	0.65	0.40	0.79
Mexico 70%	**EW**	0.19	0.17	0.21	0.21
	NS	0.11	0.11	0.16	0.14

Table 4-8 Peak Resultant Displacement Response (Values in Units of inches), Relative to the Shake Table, at Selected Locations of the Isolated Model (Full Scale Triple FP, Bi-axial Horizontal or Tri-axial Excitation, Bushing Mounted Symmetrically or Non-Symmetrically on the Cover, Testing at Full Length Scale)

Motion	Frame Top (Bushing - Plate Interface)				Bushing Top			
	Bushing at Center of Cover Plate		Bushing at Side of Cover Plate		Bushing at Center of Cover Plate		Bushing at Side of Cover Plate	
	2D	3D	2D	3D	2D	3D	2D	3D
Jensen 97%	7.2	6.9	6.9	8.3	7.2	6.9	6.9	8.4
El Centro 300%	10.8	11.1	10.9	10.6	10.9	11.1	11.1	10.8
Pacoima 75%	7.8	7.7	7.4	7.2	7.9	7.8	7.4	7.2
Taft 500%	7.5	7.4	0.0	7.4	7.7	7.6	0.0	7.7
Chile 100%	5.3	5.1	5.0	4.9	5.3	5.1	5.0	4.9
Mexico 70%	9.8	9.1	10.9	10.5	9.9	9.2	11.0	10.6

Table 4-9 Peak Base Shear Forces (Values in Units of kip) for the Isolated Model (Full Scale Triple FP, Bi-axial Horizontal or Tri-axial Excitation, Bushing Mounted Symmetrically or Non-Symmetrically on the Cover, Testing at Full Length Scale)

Motion	Direction	Bushing at Center of Cover Plate		Bushing at Side of Cover Plate	
		2D	3D	2D	3D
Jensen 97%	**EW**	6.4	7.6	5.9	7.2
	NS	7.3	9.4	6.4	7.5
El Centro 300%	**EW**	9.1	10.6	8.6	9.7
	NS	9.8	10.4	9.4	9.8
Pacoima 75%	**EW**	8.1	9.3	7.3	8.1
	NS	4.8	4.7	4.6	4.6
Taft 500%	**EW**	9.4	9.9	N/A	8.9
	NS	8.7	8.1	N/A	7.9
Chile 100%	**EW**	6.8	7.8	6.4	7.0
	NS	6.0	6.5	5.4	5.9

4.4. **Comments – Discussion on Results**

4.4.1. Peak Resultant Displacements

Figure 4-5 through Figure 4-7 show peak resultant horizontal displacements (relative to the shake table) as a function of the peak horizontal resultant velocity of the shake table. Figure 4-5 presents results from tests in which the spectrally scaled ground motion ensemble was used, while Figure 4-6 and Figure 4-7 present results from testing with arbitrarily scaled historic motions. The displacements shown were measured at the top of the bushing, for two different mounting locations, two different isolation system configurations, at reduced and full scale testing, and for two dimensional horizontal and three dimensional testing of the specimen. The peak resultant table velocity was selected as a representative measure of the seismic intensity, considered appropriate for highly flexible systems, as are the isolated systems in this study.

Figure 4-5 presents results from tests in which the spectrally scaled ground motion ensemble was used. It can be observed that the peak relative displacements of all isolation systems tested are between 3 and 4 inches, approximately. The actual calculated average displacement responses were found to lie in that range of values and present minor differences among the systems tested. Namely, that range is bound by a minimum average of 3.2 inches, calculated for the Triple FP system (two-dimensional testing), and a maximum average of 3.8 inches, calculated for the LRB Friction-Bolted system. The median responses were found to follow closely the respective averages. When projected to the prototype length scale, the above values are in the order of 9 to 12 inches, less than the upper bound set in this study for the conductor slack.

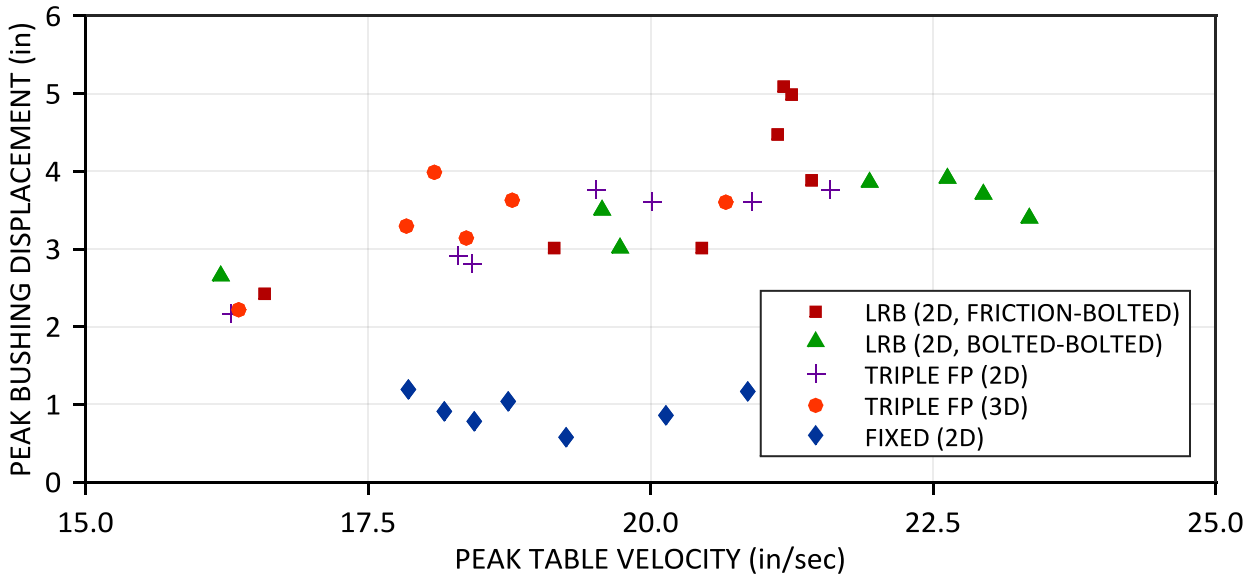


Figure 4-5 Peak Relative Resultant Displacements at the Top of the Bushing for Isolated and Non-isolated Cases, Tested with the Spectrally Scaled Motions (Testing Performed at Reduced Length Scale, Bushing Mounted at the Center of the Plate)

The aforementioned values correspond to peak resultant bushing displacements which were measured relative to the shake table and with reference to the equilibrium position of the structure at the beginning of each test, and therefore, cumulative effects are not included. These effects are particularly important for the LRB, Friction-Bolted configuration, because this configuration was found to suffer from excess sliding and permanent displacement offsets in the experiments. For example, from Figure 4-5 the maximum response of the LRB, Friction-Bolted configuration, is found to be approximately 5 inches (15 inches when extrapolated to the prototype scale) which could be acceptable as per the IEEE standard (allowing deflections greater than 16 inches). However, when the cumulative permanent displacements of the specimen are accounted for, and the peak relative displacement of the bushing is measured with respect to the equilibrium position at the onset of testing (the geometric center of the system), the actual maximum response is 7.3 inches (22 inches when extrapolated to the prototype scale). In the unfavorable case that this value is used in design and if the conductor at the top of the

bushing has not been provided with additional slack, this displacement could be detrimental for the bushing. With regard to the excess permanent offsets observed during testing of the LRB in the Friction-Bolted configuration, it was observed that the displacements did not increase for all tests and that during the last tests the structure had the tendency to re-center.

Testing the system with the selected representative historic motions was performed for the Triple FP system only. Figure 4-6 presents results from two-dimensional (horizontal) and three-dimensional testing, with the bushing installed on the side of the cover plate. It can be seen that the response is comparable to the one observed in testing using the spectrally scaled motion ensemble, with calculated average displacement response of 3.2 inches (9.5 inches when extrapolated to the prototype scale). This average is the same for both the two- and the three-dimensional cases, indicating that the inclusion of the vertical component of motion in testing did not have an effect on the observed displacement response of the system.

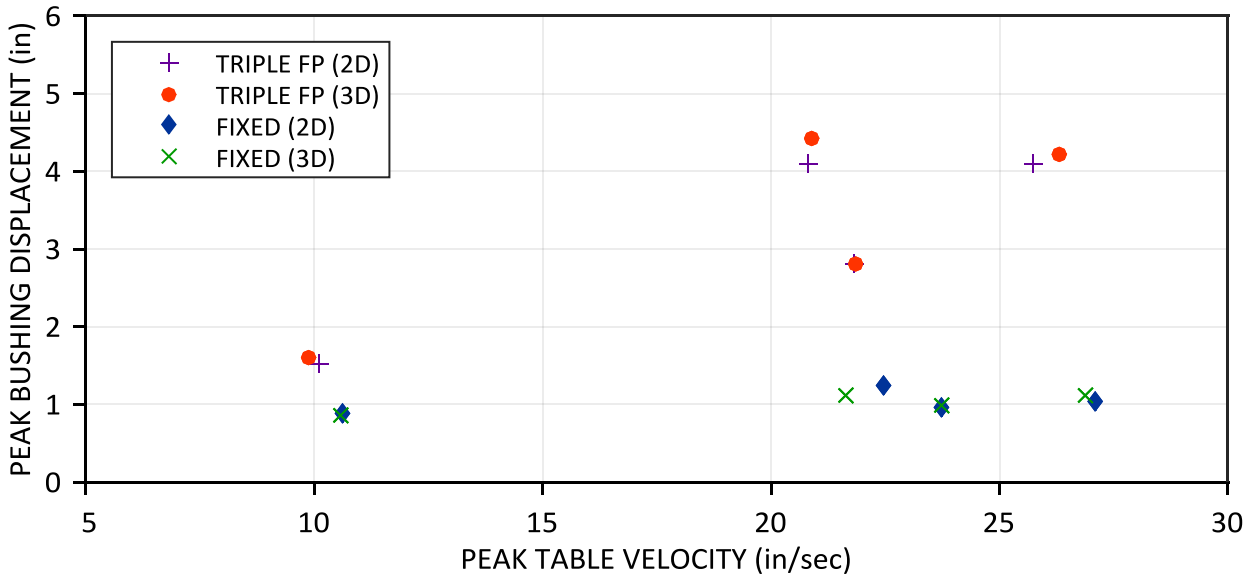


Figure 4-6 Peak Relative Resultant Displacements at the Top of the Bushing for Isolated and Non-isolated Cases, Tested with the Representative Historic Motions (Testing Performed at Reduced Length Scale, Bushing Mounted on the Side of the Plate)

Figure 4-7 presents results from two-dimensional (horizontal) and three-dimensional testing, with the bushing installed on the side and the center of the cover plate. Testing was performed at full length scale, using the same frame and bushing but full scale Triple FP bearings. The calculated average displacements were found to be close to 8 inches for all cases tested, which is a value well within the displacement limits set in the study. The average response of 8 inches is less than average response of 9.5 inches predicted from testing with the reduced scale Triple FP bearings after extrapolation to the prototype scale. It is thus clearly seen that neither the location of the bushing installation on the cover nor the inclusion of the vertical ground motion component in testing had any significant effect on the bushing displacement response.

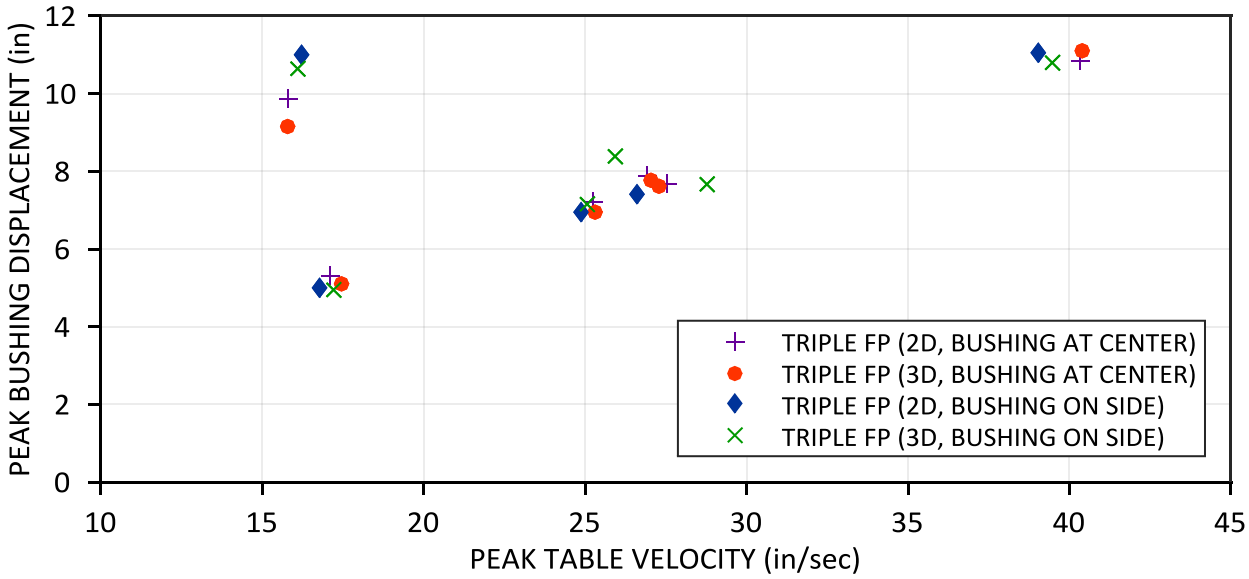


Figure 4-7 Peak Relative Resultant Displacements at the Top of the Bushing for Isolated Cases, Tested with the Representative Historic Motions (Testing Performed at Full Length Scale)

As shown in Figure 4-5 and Figure 4-6, the peak relative bushing displacement when the specimen was fixed, was close to 1 inch (3 inches in prototype scale), that is, the use of isolation systems in the experiments led to an approximate fourfold increase in displacements. The bushing used in the current study is relatively stiff with a frequency of around 11 Hz when installed on the flexible cover plate of the frame. However, as-installed bushings frequencies as low as 3 to 4 Hz are common in practice (Filiatrault et al. 2006, Kong 2010, Fahad 2013). A component in that frequency range, typical of tall high voltage bushings (e.g. 500kV) installed on fixed-base equipment, could have a higher displacement response depending on the ground motion characteristics. For example, Kong (2010) has reported peak relative displacements as high as 7 inches, from shake table testing of a 550kV bushing with as installed frequency of 4 Hz at the 0.5g RRS. If the bushing was to be qualified to, say, the moderate performance level (corresponding to 1.0g RRS), the design displacement could be expected to be as high as 14 inches, assuming that the bushing would remain elastic and functional at that level. Fahad (2013) also carried out shake table tests on a 500kV composite bushing with as installed

frequency of 3.5 Hz and reported peak relative displacements of 8 and 14 inches for testing at 1.5g RRS and 2.25g RRS respectively (it is noted that bushings are qualified to the high performance level, mounted on a rigid base and tested at 2g RRS as per the IEEE 693-2005 standard). Furthermore, the same researcher tested the bushing at 3g RRS, with the intention of determining its capacity, however, the bushing was not damaged and a peak relative displacement of 22 inches was reported. Therefore, recognizing that in an isolated power transformer the displacement response will be mostly the result of the rigid body motion and based on the observed average experimental values discussed earlier, the use of base isolation in a power transformer can be expected to lead to acceptable and, potentially, improved displacement response depending on the bushing flexibility.

4.4.2. Effect of Mass Asymmetry - Torsional Response

An important feature in the experiments conducted is the simulation of highly asymmetric mass distribution which is typical of commercial power transformers. As discussed in section 3.2, asymmetry in the experimental model was achieved through the addition of two massive vertical plates on two adjacent sides of the rigid frame. That resulted in an eccentricity between the center of mass and the center of rigidity of the superstructure of about 10% in each horizontal direction.

The isolation systems tested exhibited torsional response. The torsional response was quantified herein with the Torsional Amplification (TA) ratio. The TA ratio is defined as the ratio between the maximum resultant displacement of the bottom corners of the frame (pedestals), and the maximum resultant displacement at the center of the horizontal steel plate assembly representing the base mat. Both of these displacements were measured relative to the shake table.

Furthermore, for the calculation of the TA in each test the initial offsets of the relative displacements were removed, so that the TA ratio was directly related to the particular test. Thus the TA did not include cumulative sliding effects of the superstructure, in case that had occurred prior to the test of interest. A similar measure of the torsional amplification can be found in the work of Wolff et al (2004), where the quantities used for the calculation of the relevant ratio were the average and peak displacements of the isolation bearings. In the present study, such an approach would be inaccurate due to sliding of the superstructure on the connection interface, particularly for the LRB, Friction-Bolted configuration. Therefore, instead of the bearing displacements, the displacements of the base mat were selected for the calculations of the TA ratio. Note that the measured rotations were small so that the measurement of displacement using string pots of sufficient string length was not affected and is considered accurate.

Shown in Figure 4-8 is a comparison of the TA ratios of three isolation configurations tested, as a function of the peak horizontal resultant velocity of the shake table. The results of Figure 4-8 were obtained for 2D horizontal testing with the ground motions ensemble that was scaled to the site specific spectrum, at reduced length scale (length scale factor of 3) and with the bushing mounted at the center of the cover plate. The shake table velocities were not directly measured in the tests. Instead, they were post-calculated by numerically differentiating the measured shake table displacements.

It can be seen that the LRB system had significant torsional response for both tested connection details. More specifically, the configuration permitting sliding of the superstructure at the connection (LRB Bolted-Friction) exhibited the largest amplification. In contrast, the Triple FP system was practically insensitive to torsion with measured TA ratios ranging from 1.00 to 1.05.

This, of course, was expected as the source of the eccentricity was a shift in the center of mass, for which the FP system is insensitive. In order to better understand the differences between the isolation systems tested in terms of their torsional response, it is useful to review their characteristics as well as examine to what extend each system is affected by a superstructure with asymmetric mass distribution. Isolation systems based on friction (i.e. the Triple FP bearings), have the natural property of adapting their behavior in accordance to the distribution of the axial force. Namely, any asymmetric distribution of vertical load on the isolators due to mass eccentricity in the superstructure will result in the Triple FP bearings adjusting their stiffness and friction force characteristics. Provided that the coefficients of friction are similar for all the isolators used (as is the case for the present study), the center of rigidity and the center of mass of the isolated structure tend to coincide, thus eliminating irregularities in mass distribution. Lead Rubber bearings have properties that are weight-independent and maintain a fixed center of rigidity. In such systems, high mass asymmetry is expected to inevitably result in torsional response.

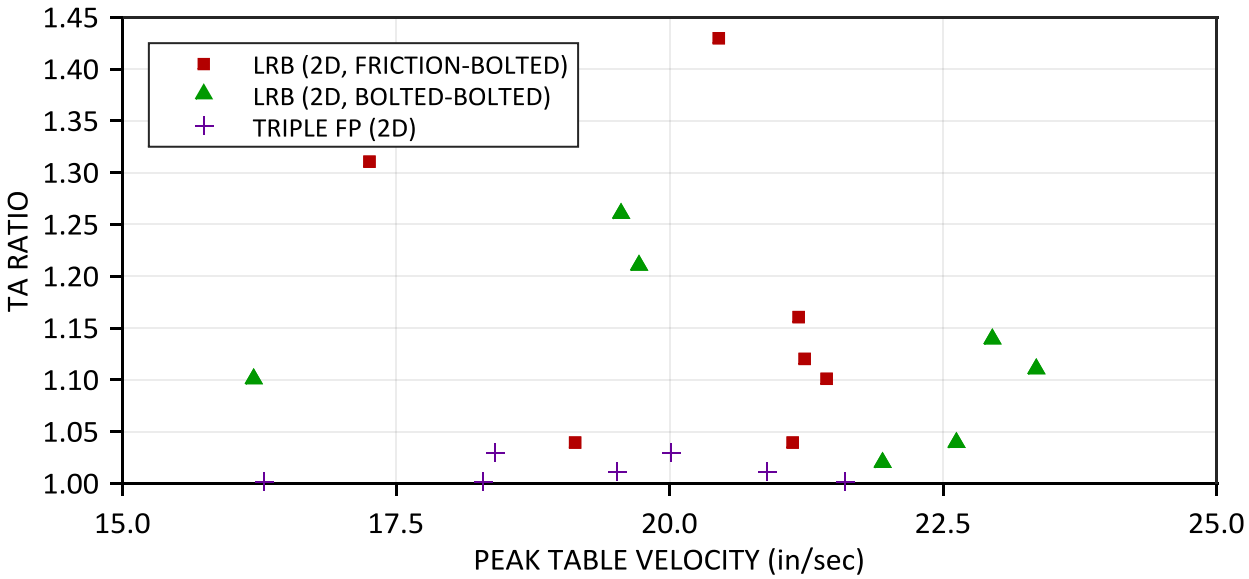


Figure 4-8 TA Ratios for Different Systems Tested for the Same Motion Ensemble (Reduced Scale Testing, 2D Horizontal, Bushing at Center of Cover Plate)

Figure 4-9 presents results for the configuration with the Triple FP system and tested under the same ground motion ensemble, but at increased amplitudes of 125% and 150% with respect to the original scaling of the ground motions (original scaling to the design earthquake). During some of the tests shown in Figure 4-9 at such increased amplitudes, some of the bearings reached their displacement capacity and sliding occurred at the interface of the bearings to the superstructure where the connection was only by friction. Subsequently to these extreme events the Triple FP isolators were approximately re-centered by lifting each corner of the superstructure with jacks and manually restoring the isolator components to the apparent central position. In consideration of the fact that both the shifting of the center of mass due to extensive sliding, as well as the re-centering procedure adopted during testing, introduce further asymmetry in the system, it can be concluded that the torsional response of the Triple FP system was very satisfactory.

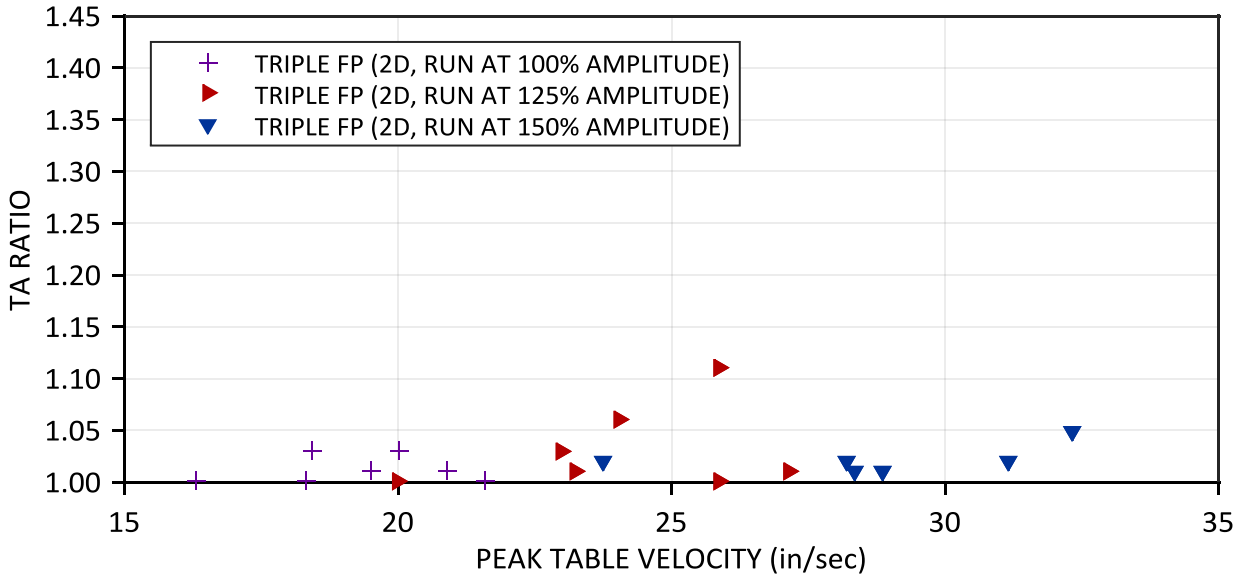


Figure 4-9 TA Ratios for the System with Triple FP Bearings, Tested for the Same Motion Ensemble at Increasing Amplitudes (Reduced Scale Testing, 2D Horizontal, Bushing at Center of Cover Plate)

Considering the two LRB configurations tested, Figure 4-8 shows that, excluding the two last tests during which the Friction-Bolted configuration exhibited large torsion (TA of 1.45), both have comparable torsional responses. Nevertheless, the global structural behavior relies heavily on the installation method used in each configuration. For the LRB Bolted-Bolted configuration, resistance to torsion is provided by the lateral deformation of all bearings, while at the end of shaking, the structure returns to its original equilibrium position. For the LRB Friction-Bolted configuration, torsion is resisted by the lateral deformation of the bearings but only during some instances of the motion. In fact, in that case the lateral resistance of each bearing is bounded by the friction at the sliding interface of the connection. Specifically, the LRB provides lateral resistance through lateral deformation up to the point that the axial load reduction, occurring due to the overturning moments, is such that the lateral restoring force overcomes the static friction on the isolation interface.

An important characteristic of the LRB is that they are laterally stiff bearings with significant self-centering capability. Therefore, when the static friction is exceeded at a bearing friction connection, sliding is initiated on that interface, but additionally, the bearing will partially re-center as the kinetic friction drops to a value less than the static friction. This is a complex phenomenon which can occur at different bearings at various instances, and further affects the torsional response of the system. When the LRB were connected to the superstructure through friction (Friction-Bolted configuration), all of the isolators experienced snap-back during testing and sliding of up to 4.5inch was recorded at the friction connection interface. When the Triple FP system is subjected to the same conditions, self-centering at small vertical loads is not possible since the lateral restoring force of the bearing is proportional to the vertical load.

Sliding leads to bounding of the lateral forces transmitted by the LRB which has a positive effect on their stability. However, it became problematic after consecutive tests as permanent displacements accumulated and re-centering of the superstructure was eventually needed. Figure 4-10 demonstrates the effect of cumulative sliding where the bearing is seen in a different position after repeated events of sliding and permanent distortion followed by manual repositioning.

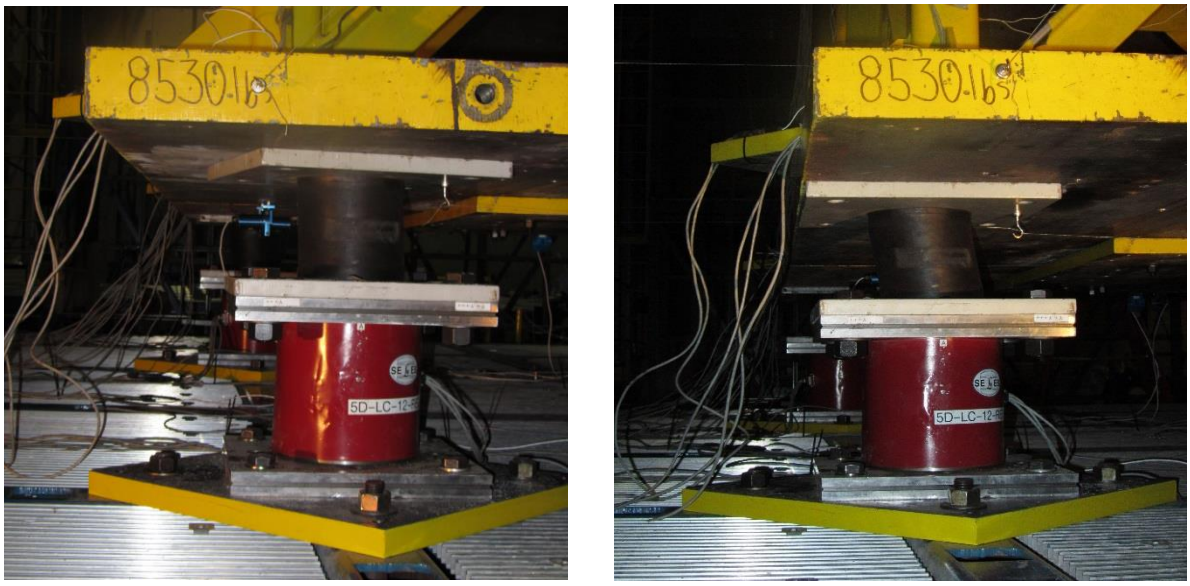


Figure 4-10 Cumulative Sliding at the Friction Connection of LRB (NW Corner of the Isolated Model)

A comparison between the force-displacement loops obtained for the Bolted-Bolted LRB and the Friction-Bolted LRB (the latter shown in Figure 4-10), is provided in Figure 4-11. It is noted that the displacements of Figure 4-11 are the displacements of the top bearing plate relative to the shake table (that is, the displacements represent the bearing deformation). It can be seen that the responses of the two configurations partially overlap, with the Friction-Bolted LRB configuration experiencing less deformation of the isolator that the bolted-bolted configuration.

However, this seemingly desirable behavior came at the expense of additional displacement (sliding) at the sliding connection with the implications depicted in Figure 4-10.

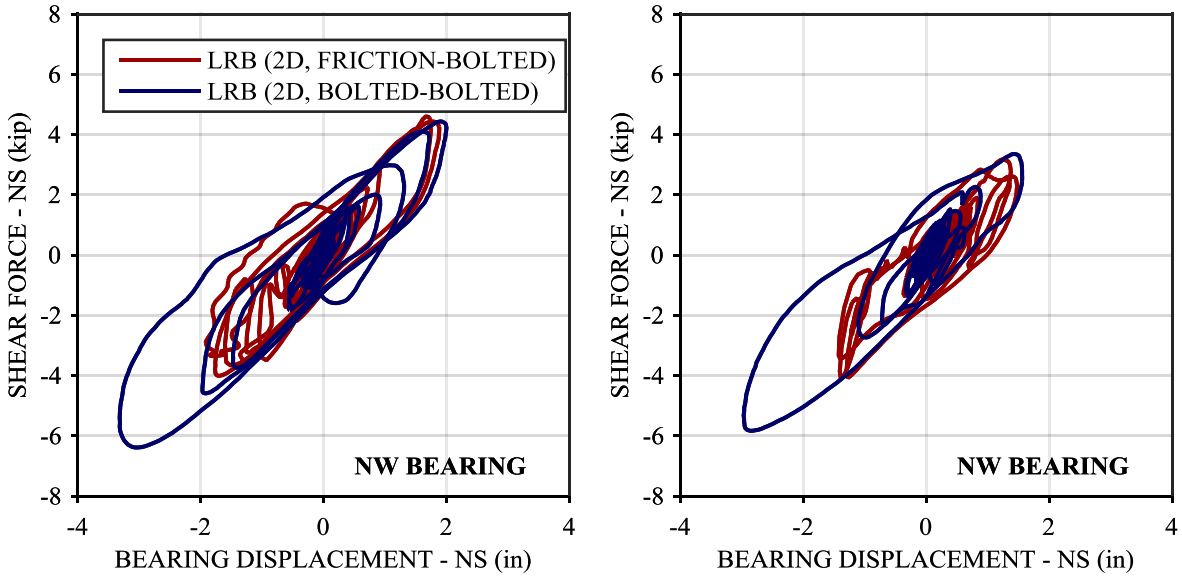


Figure 4-11 Comparison of Force-Displacement Loops in EW and NS Directions for the NW LRB Isolator Bolted-Bolted and Friction-Bolted Configurations (Saratoga Excitation at 157% of Original, Bi-axial Horizontal Excitation)

4.4.3. Tank Roof Motions - Response Spectra at the Base of the Bushing

The effectiveness of base isolation in reducing the seismic demand on the roof of the power transformer model can be readily observed from direct comparison between the responses of the isolated and non-isolated cases tested. Figure 4-12 through Figure 4-16 present response spectra at the shake table and at the roof of the power transformer in the proximity of the bushing mounting location. The spectra are presented in the prototype scale, and are obtained from acceleration response histories on the rigid frame and the shake table from testing under reduced length scale (and then extrapolated) and actual length scale conditions, and for non-isolated and isolated configurations. For comparison with the current seismic qualification recommendations, the IEEE 693 High RRS at the ground level (i.e. shake table level herein) as well as the High

RRS at the roof level, equal to twice the High RRS per the IEEE 693 recommendations for the qualification of high voltage bushings mounted on power transformer covers, are shown.

It may be seen that base isolation effectively acts as a filter for the input horizontal accelerations and significantly reduces the demand on the power transformer for a wide range of frequencies approximately above 1.0 Hz for the LRB isolation system and 0.3 Hz for the Triple FP system. These frequencies are close to the post yielding response frequencies of the isolation systems selected as discussed in section 3.4. The frequency range of the demand reduction encompasses the frequencies of commercial high voltage power transformers when fixed to the foundation, and the frequencies of their attachments including the high voltage bushings. Therefore it is expected that base isolation will protect a power transformer globally including its external and internal components, such as the core and coil assembly, that otherwise would not be possible to seismically retrofit.

It is noted that for some cases, local phenomena such as sliding and impact in the power transformer model were observed during testing. While the exact origin of these phenomena has not been identified, their effects on the response are reflected in some of the spectra presented below. For example, the effect of impact is shown in Figure 4-12 in the form of spectral amplification at a frequency close to 15 Hz at the power transformer cover plate (control point). More spectral comparisons can be found in the results of Appendix B.

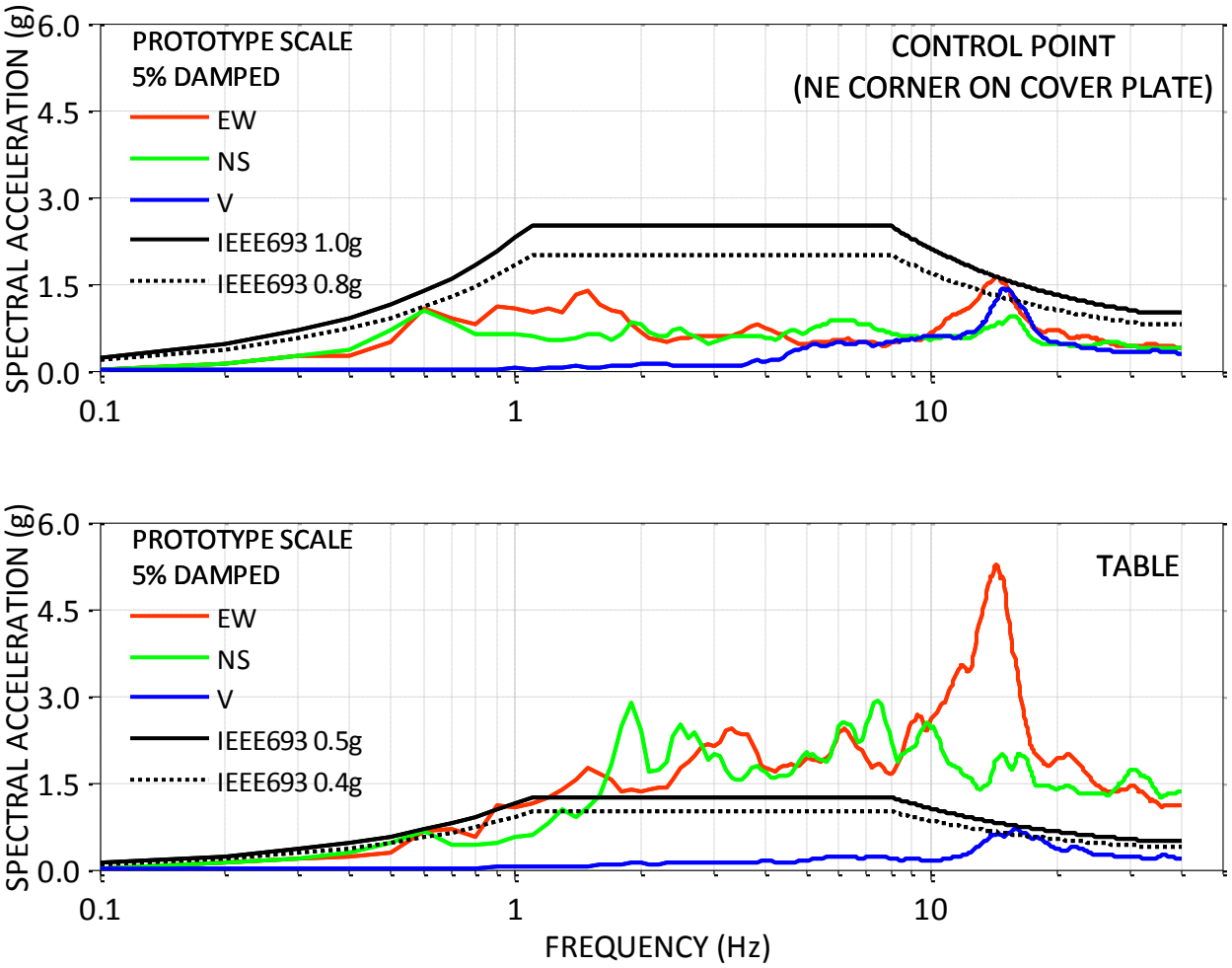


Figure 4-12 Response Spectra Results at the Table and the Top of the Isolated Frame for the 137% Karakyr Excitation (LRB Isolators with Friction-Bolted Configuration, Bi-axial Horizontal Excitation, Bushing Mounted Symmetrically on the Cover, Testing at Length Scale of 1:3)

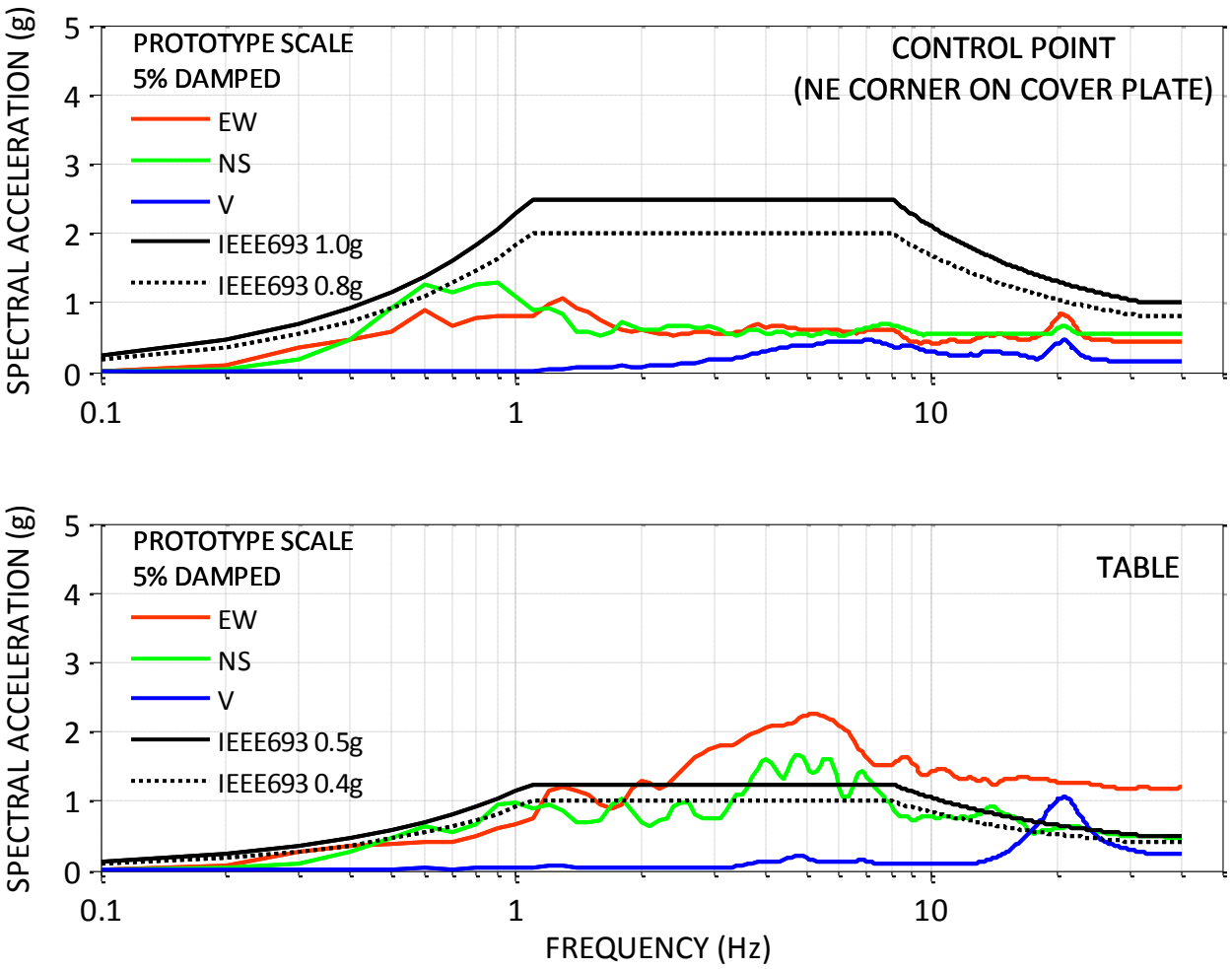


Figure 4-13 Response Spectra Results at the Table and the Top of the Isolated Frame for the 90% Sylmar Excitation (LRB Isolators with Bolted-Bolted Configuration, Bi-axial Horizontal Excitation, Bushing Mounted Symmetrically on the Cover, Testing at Length Scale of 1:3)

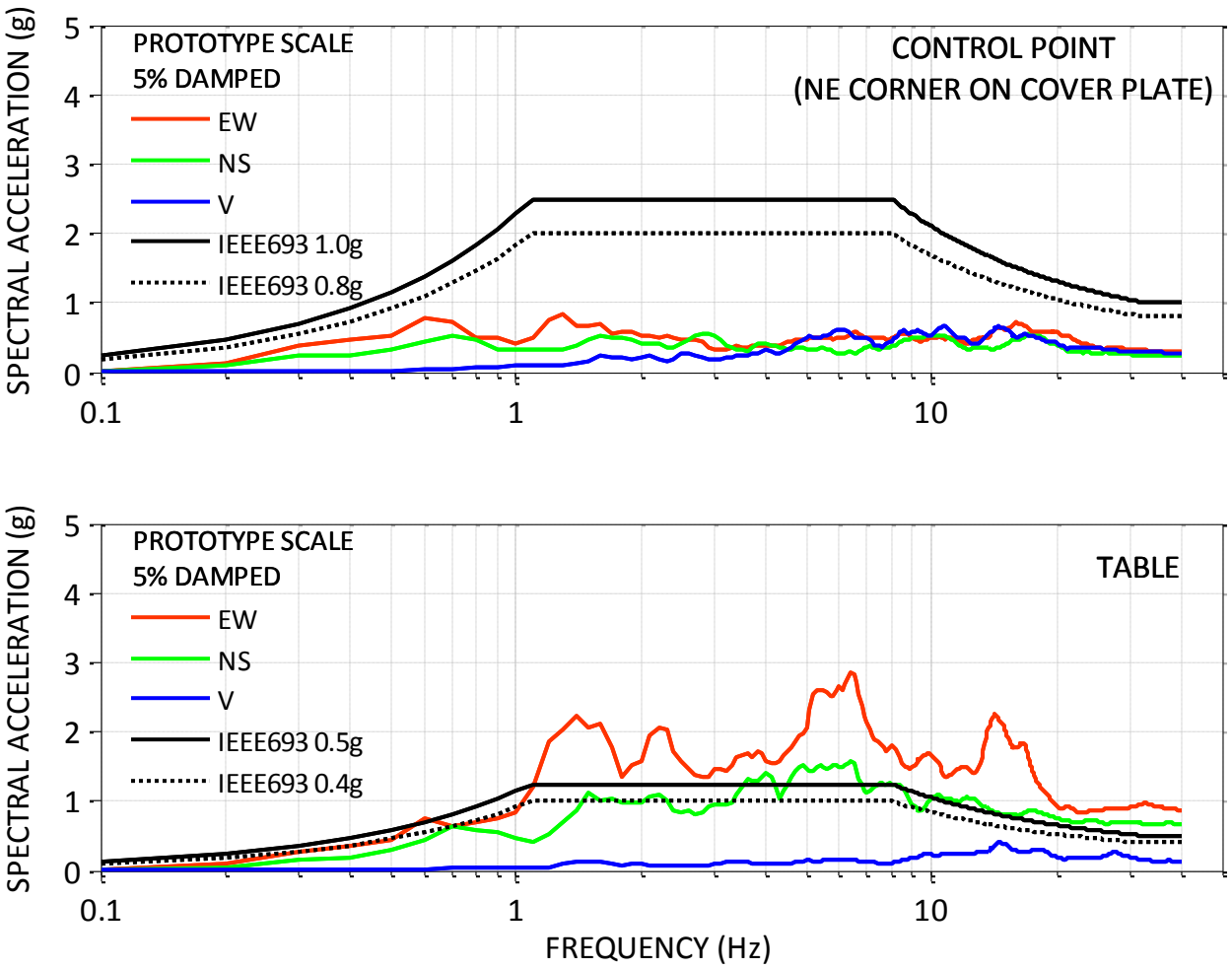


Figure 4-14 Response Spectra Results at the Table and the Top of the Isolated Frame for the 94% LGPC Excitation (Triple FP Isolators, Bi-axial Horizontal Excitation, Bushing Mounted Symmetrically on the Cover, Testing at Length Scale of 1:3)

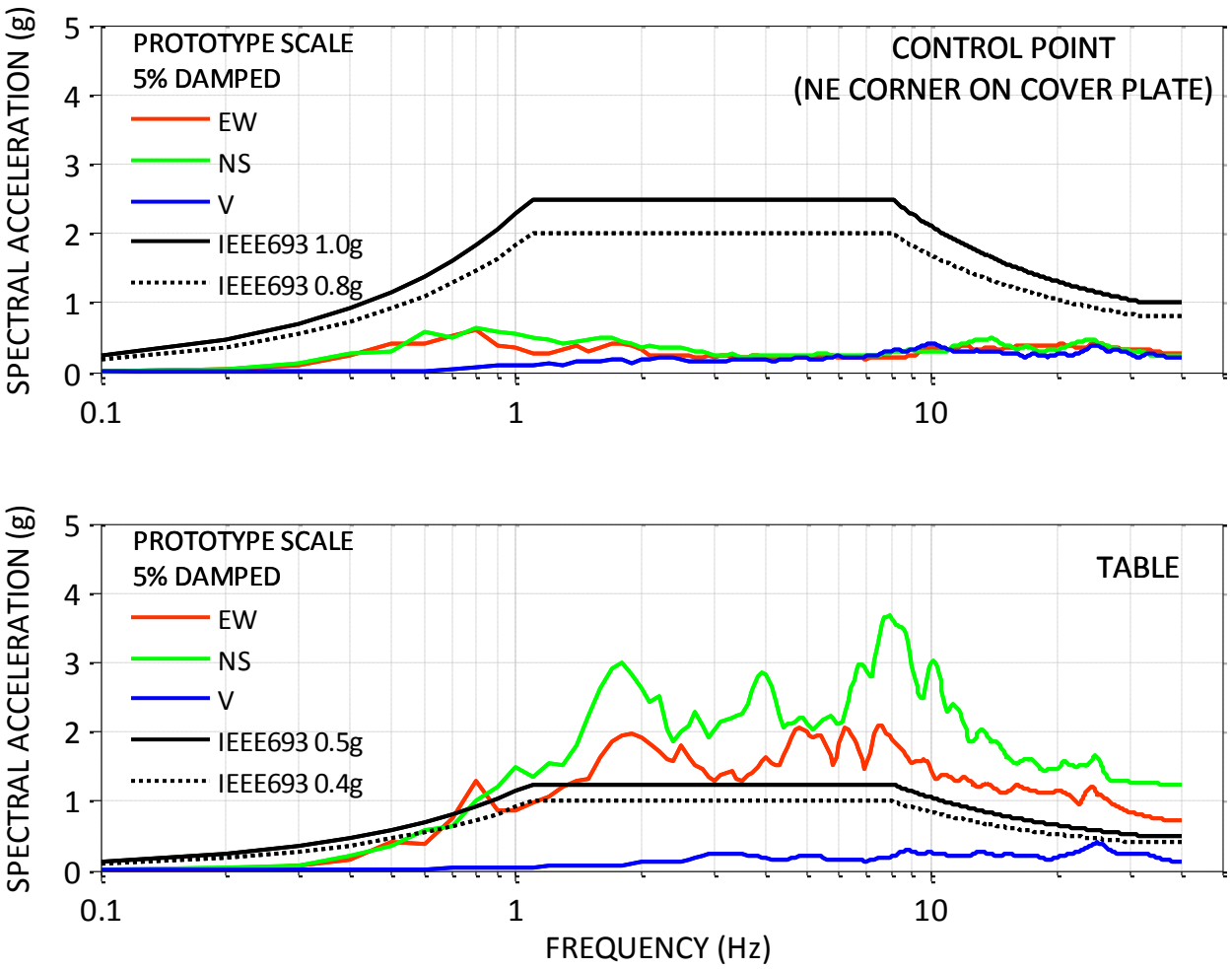


Figure 4-15 Response Spectra Results at the Table and the Top of the Isolated Frame for the 300% El-Centro Excitation (Full Scale Triple FP Isolators, Bi-axial Horizontal Excitation, Bushing Mounted Symmetrically on the Cover, Testing at Full Scale)

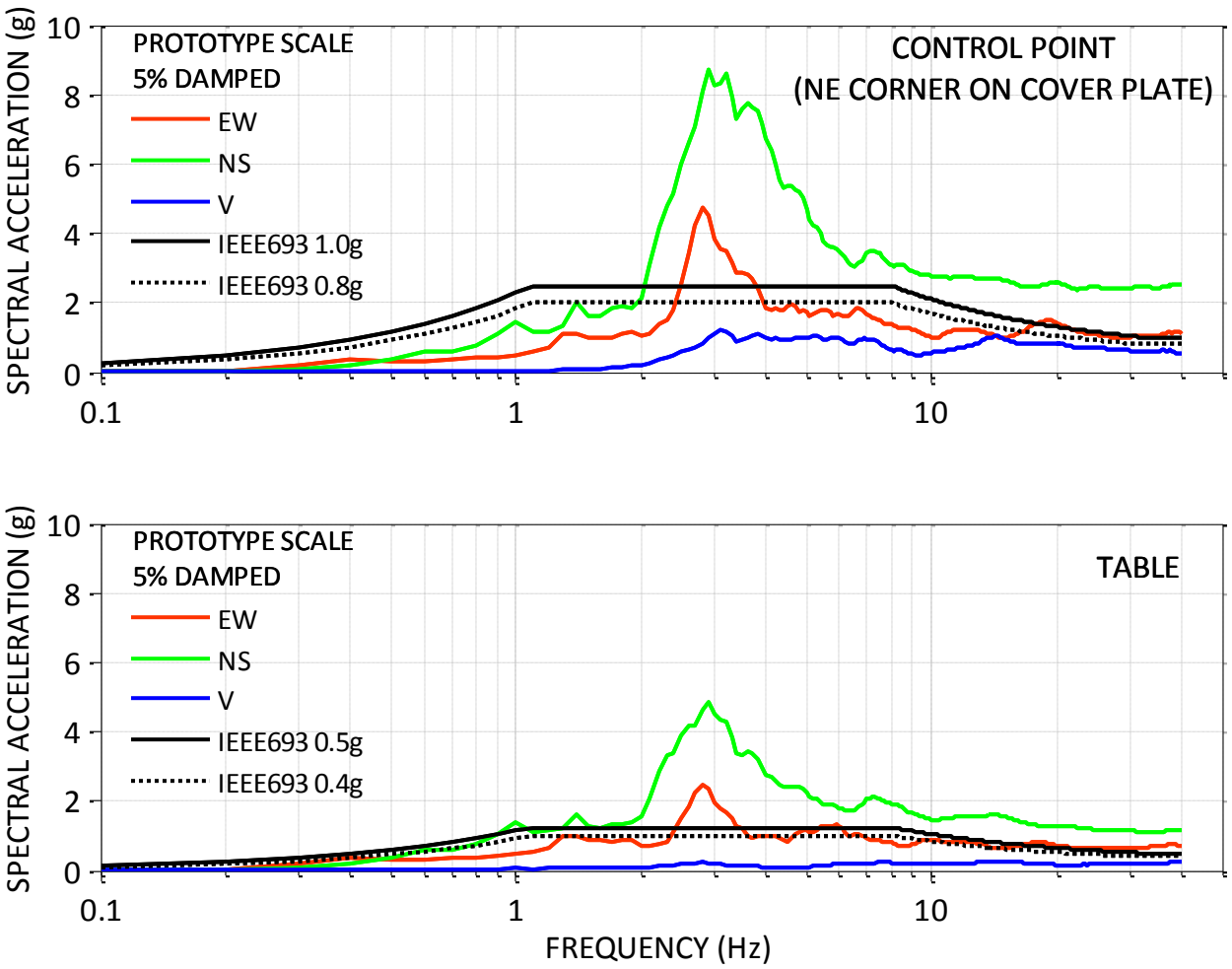


Figure 4-16 Response Spectra Results at the Table and the Top of the Non-Isolated Frame for the 97% Jensen Filter Excitation (Bi-axial Horizontal Excitation, Bushing Mounted Symmetrically on the Cover, Testing at Length Scale of 1:3)

4.4.4. Effect of Cover Plate Flexibility on the Bushing Response

The effect of the flexible power transformer cover on the dynamic response of the bushing has been indicated by several analytical and experimental studies in the past. In particular, it has been shown (Reinhorn et al, 2012) that the apparent frequency of the bushing when installed on the tank roof is predominantly controlled by the local flexibility of the roof. The resulting frequency of the roof-bushing assembly is significantly reduced as compared to the corresponding fixed base frequency of the bushing alone. The frequency reduction is a function of the plate flexibility and the location of installation of the bushing on the plate. Table 4-10 presents the as-installed natural frequencies identified for the two different bushing mounting locations tested, as well as the fixed base frequency of the bushing as measured in previous experimental studies (Reinhorn et al, 2012).

Table 4-10 High Voltage Bushing Frequencies (Reinhorn et al, 2012)

Boundary Conditions	Frequency (Hz)	
	North-South	East-West
Fixed	25.0	25.0
As-installed (Center of Cover)	10.5	10.9
As-installed (Side of Cover)	12.5	9.6

The comparison in Figure 4-17 between the responses of the non-isolated model and the model isolated with Triple FP at reduced length scale, non-symmetrical installation of the bushing on the cover plate and tri-axial testing conditions, demonstrates the enhanced structural performance of the isolated power transformer for all ground motions tested (fixed model results shown extrapolated from testing at reduced amplitude). It is noted that in some tests, the isolated model experienced uplift and impact which further amplified the bushing response in addition to the

amplification due to the vertical component of testing. That also affected the measured peak shake table accelerations. For the same motions and due to uplift and impact, the peak shake table accelerations are higher in the isolated model tests than in the non-isolated model tests. The non-isolated model did not experience impacts possibly because it was tested at much lower levels of motion and then extrapolated for the sake of comparisons with the isolated model.

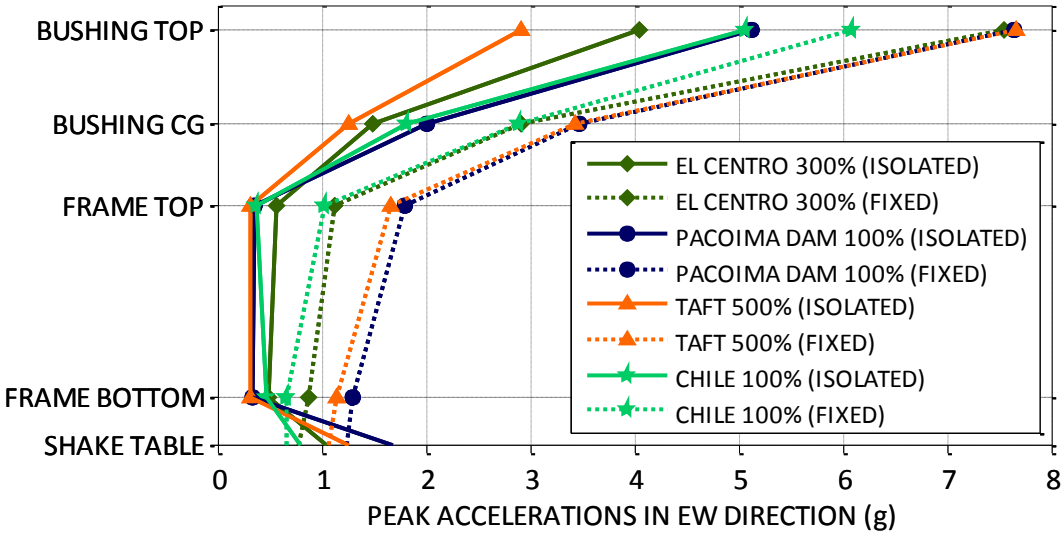


Figure 4-17 Peak Accelerations (EW Direction) for Tri-axial Testing, Reduced Scale Triple FP Bearings and Non-symmetrical Installation of the Bushing

The effect of the cover plate on the bushing response is better illustrated in the results of Table 4-11, obtained from bi-axial and tri-axial testing of the full scale power transformer model in the cases of mounting the bushing at the center and at the side of the cover. In the results presented in Table 4-11, no uplift or sliding between the bearing and the structure was monitored during testing. As can be directly inferred from the data presented, the response of the bushing when mounted on the side is larger than that of the case when the bushing is symmetrically installed on the cover. Furthermore, when the bushing is installed on the side of the cover and subjected to

tri-axial excitation, the response is amplified, especially in the East-West direction which is the direction in which the bushing was installed eccentrically from the center of the plate.

Past experimental studies have shown that eccentricity in the as-installed location of bushings on flexible plates generates coupling in their vertical and rotational dynamic properties (Kong, 2010). In the present study, coupling occurs in the direction of eccentricity (EW) and the acceleration response is amplified due to the effect of the vertical input to the bushing response. Some amplification also occurred for the tri-axial excitation of the structure with the bushing installed symmetrically, though this should be attributed to accidental eccentricities in the plate-bushing system.

Table 4-11 Bi-axial and Tri-axial Testing Results, from Testing with Full Scale Triple FP Bearings and Two Different Mounting Locations of the Bushing (75% Pacoima Dam Excitation)

Excitation	As-Installed Location	Directions of Motion		Peak Table Response		Peak Structural Response		
				Accel.	Vel.	Frame Top Accel.	Bushing Bottom Accel.	Bushing CG Accel.
				(g)	(in/sec)	(g)	(g)	(g)
Pacoima Dam	Side	3D	EW	1.29	22.52	0.23	0.23	0.81
			NS	0.84	18.93	0.18	0.21	0.60
			V	0.63	11.00	0.65	0.77	-
		2D	EW	1.30	23.47	0.16	0.18	0.36
			NS	0.93	17.80	0.12	0.13	0.50
			V	0.07	1.16	0.09	0.25	-
	Center	3D	EW	1.25	23.80	0.22	0.20	0.43
			NS	0.91	18.22	0.17	0.25	0.51
			V	0.62	11.67	0.70	1.17	-
		2D	EW	1.26	23.83	0.16	0.16	0.29
			NS	0.92	17.99	0.13	0.14	0.40
			V	0.07	1.15	0.14	0.30	-

Figure 4-18 through Figure 4-20 show horizontal and vertical response spectra at the mounting interface of the bushing when installed at the side of the cover. These spectra specify the seismic demand on the bushing. A comparison between Figure 4-18 (tri-axial testing) and Figure 4-19 (bi-axial testing) reveal that the horizontal response spectra are amplified in the frequency range of 10Hz and above in the case of tri-axial testing. Nevertheless, regardless of whether the vertical component of the ground motion was used in testing, the horizontal response spectra are significantly reduced in the isolated configuration compared to the non-isolated configuration, in the frequency range of interest (3-25Hz). The horizontal response spectra of the isolated configuration are also below the IEEE 693 recommended high RRS at the top of the tank. The vertical response spectra for both the isolated and the non-isolated configurations are of

comparable magnitudes, which is the result of the inability of the isolation systems to provide vertical isolation.

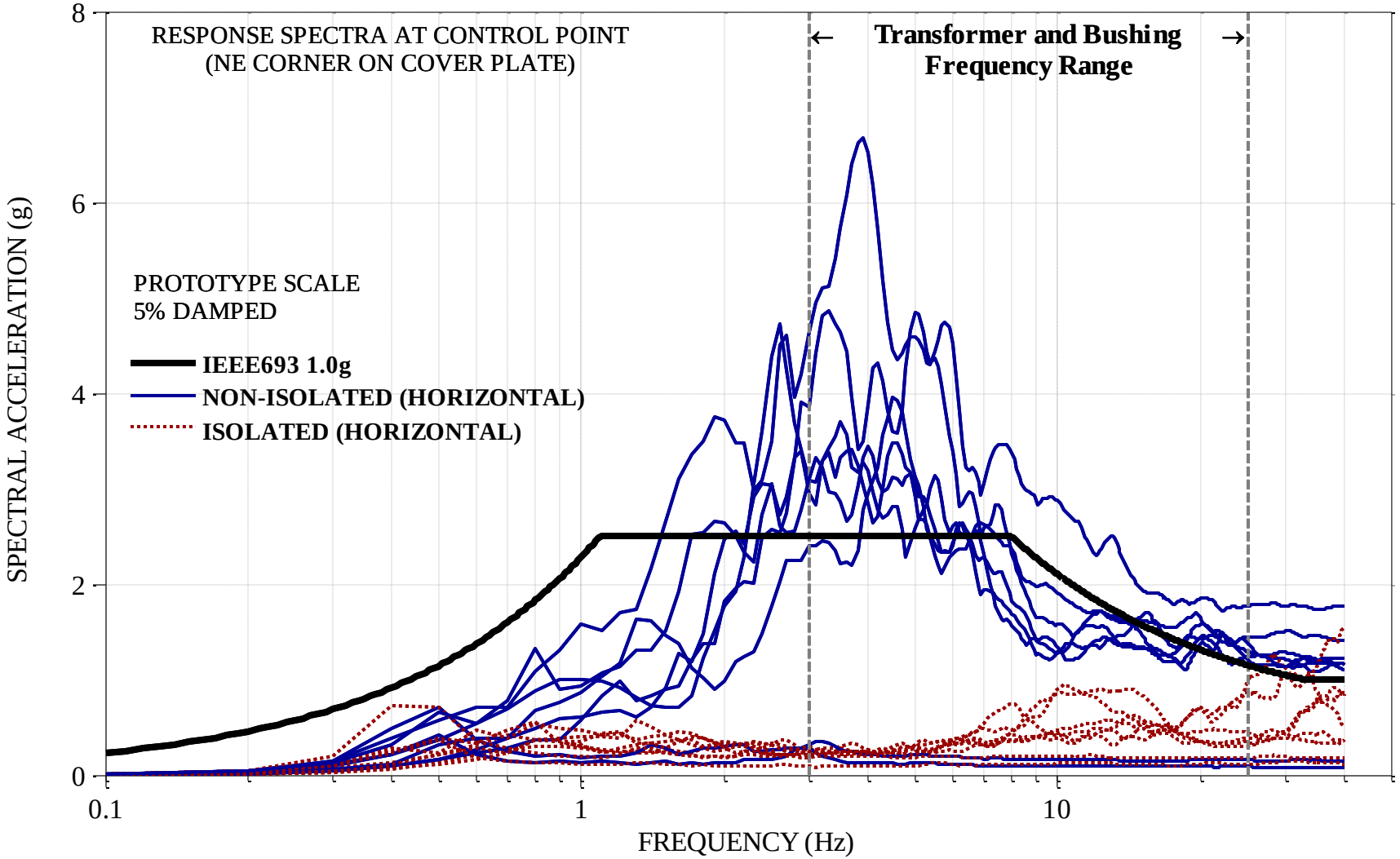


Figure 4-18 Horizontal Response Spectra at the Tank Roof for Tri-axial Testing, Full Scale Triple FP Bearings and Non-symmetrical Installation of the Bushing (Results from Testing with Arbitrarily Scaled Historic Motions – see section 3.5)

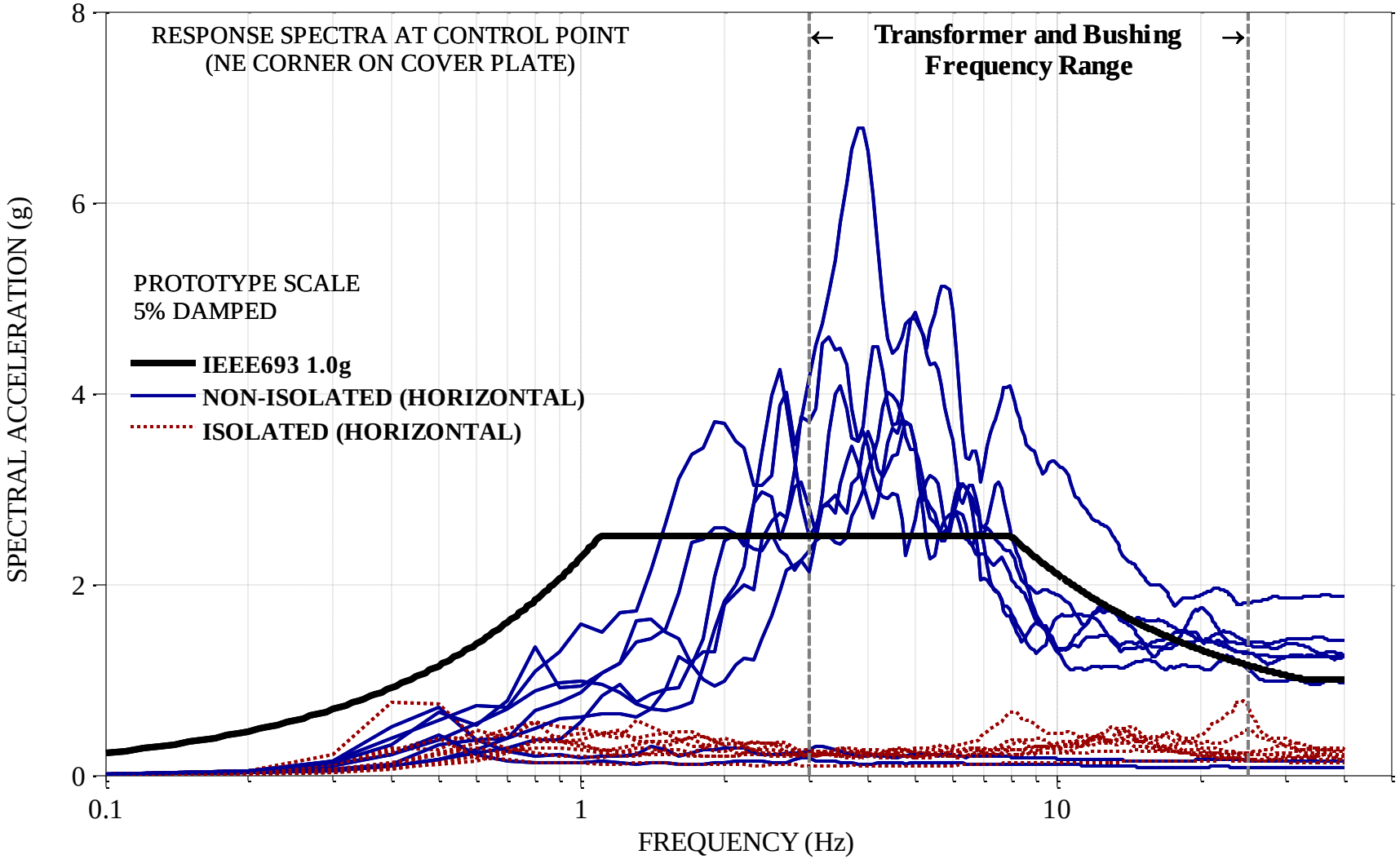


Figure 4-19 Horizontal Response Spectra at the Tank Roof for Bi-axial Horizontal Testing, Full Scale Triple FP Bearings and Non-symmetrical Installation of the Bushing (Results from Testing with Arbitrarily Scaled Historic Motions – see section 3.5)

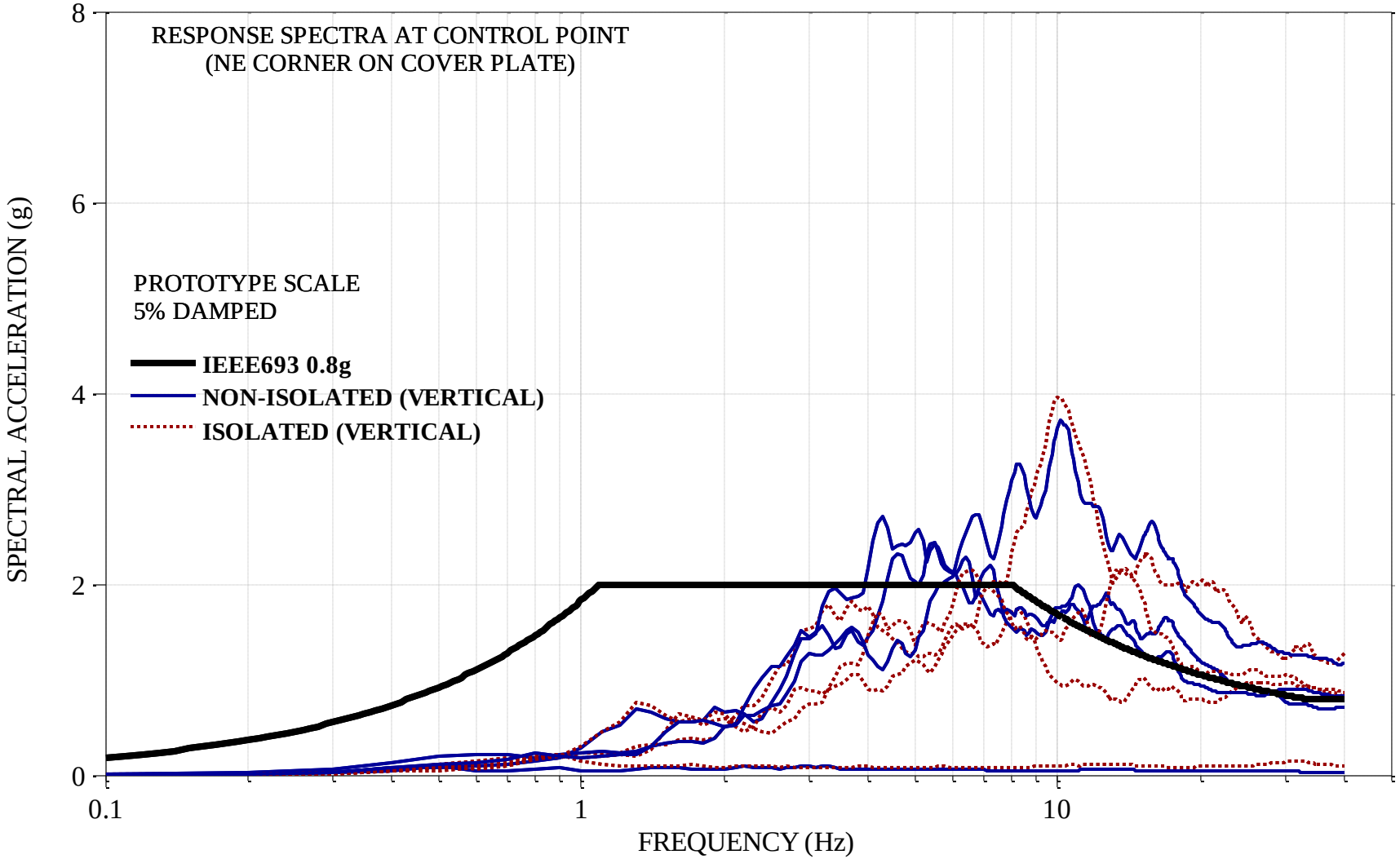


Figure 4-20 Vertical Response Spectra at the Tank Roof for Tri-axial Horizontal Testing, Full Scale Triple FP Bearings and Non-symmetrical Installation of the Bushing (Results from Testing with Arbitrarily Scaled Historic Motions – see section 3.5)

4.4.5. Effect of Impact on the Results

As discussed in the experimental results presented earlier in this section, it was shown that for some cases, local phenomena, for instance impact in the power transformer model, were observed during testing. These phenomena were accompanied by audible rattling sounds from the structure, and although they could not be identified visually or through instrumentation measurements, they can be reasonably attributed to local effects, such as sliding and pounding of the side plates due to loose connections.

Regardless of their origin, these phenomena were found to have an effect on the experimental measurements and particularly on some acceleration measurements, which were significantly amplified in the presence of impact. For demonstration of these effects, the results of two tests have been selected and compared in which the effect of impact is prominent. Specifically, the results selected are taken from bi-axial and tri-axial testing of the power transformer specimen with the 300% El-Centro excitation, isolated with the full size Triple FP isolators and with the high voltage bushing installed symmetrically.

Figure 4-21 and Figure 4-22 present comparisons of the recorded acceleration histories and their respective 5%-damped response spectra at the top NE corner of the frame in the two horizontal directions, for the aforementioned tests. It may be readily seen that the acceleration histories differ between the two cases in that the accelerations obtained from the tri-axial test are significantly amplified as compared to the accelerations obtained from the bi-axial test particularly in the time range of 10 to 15 sec. Indeed, at approximately 11 sec into the tri-axial test, a loud pounding sound was identified in the test videos. Such a sound was however not heard during the bi-axial test. The amplification in the acceleration responses is also evident in

the spectra of Figure 4-22 in which it can be seen that the spectra obtained from the two tests deviate significantly for frequencies beyond 10 Hz.

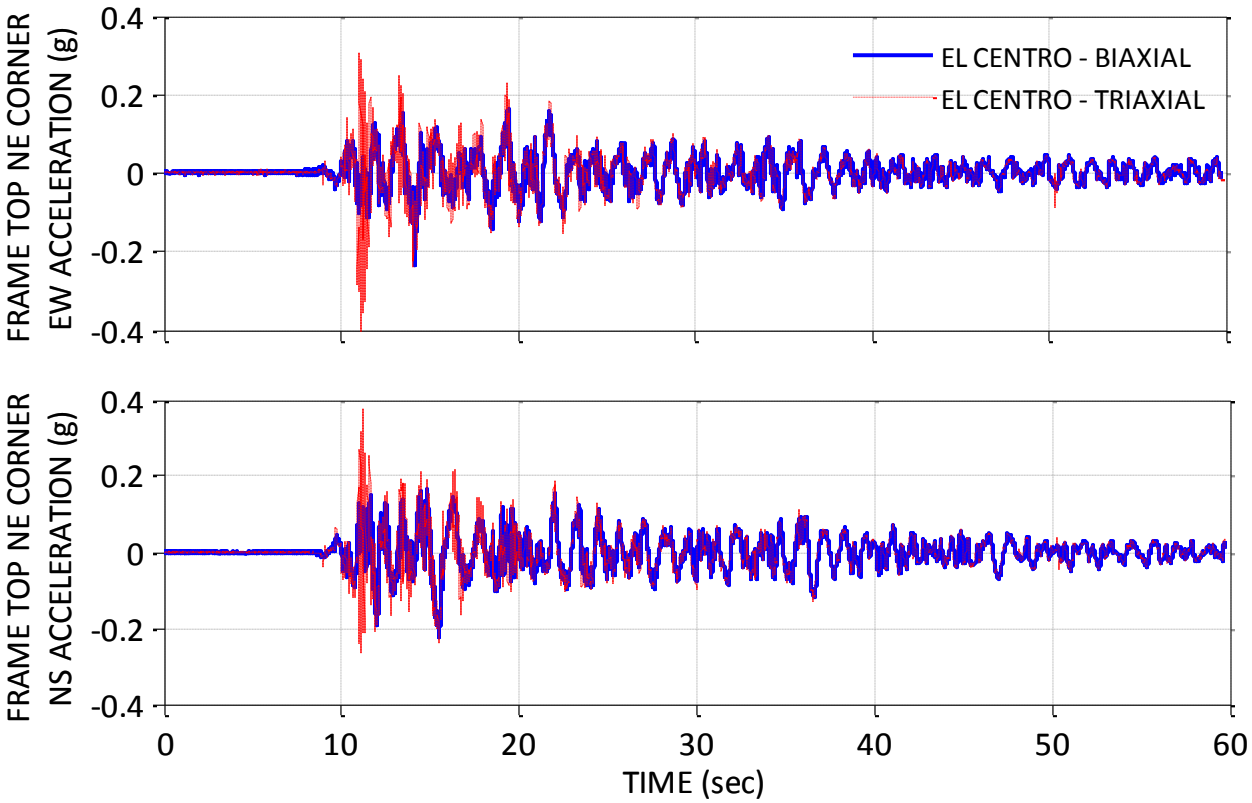


Figure 4-21 Comparison of Acceleration Response Histories at the Top NE Corner of the Frame in the two Horizontal Directions, from Testing with the Bi-axial and Tri-axial 300% El-Centro Excitation (Full Scale Triple FP Isolators, Bushing Mounted Symmetrically on the Cover, Testing at Full Scale)

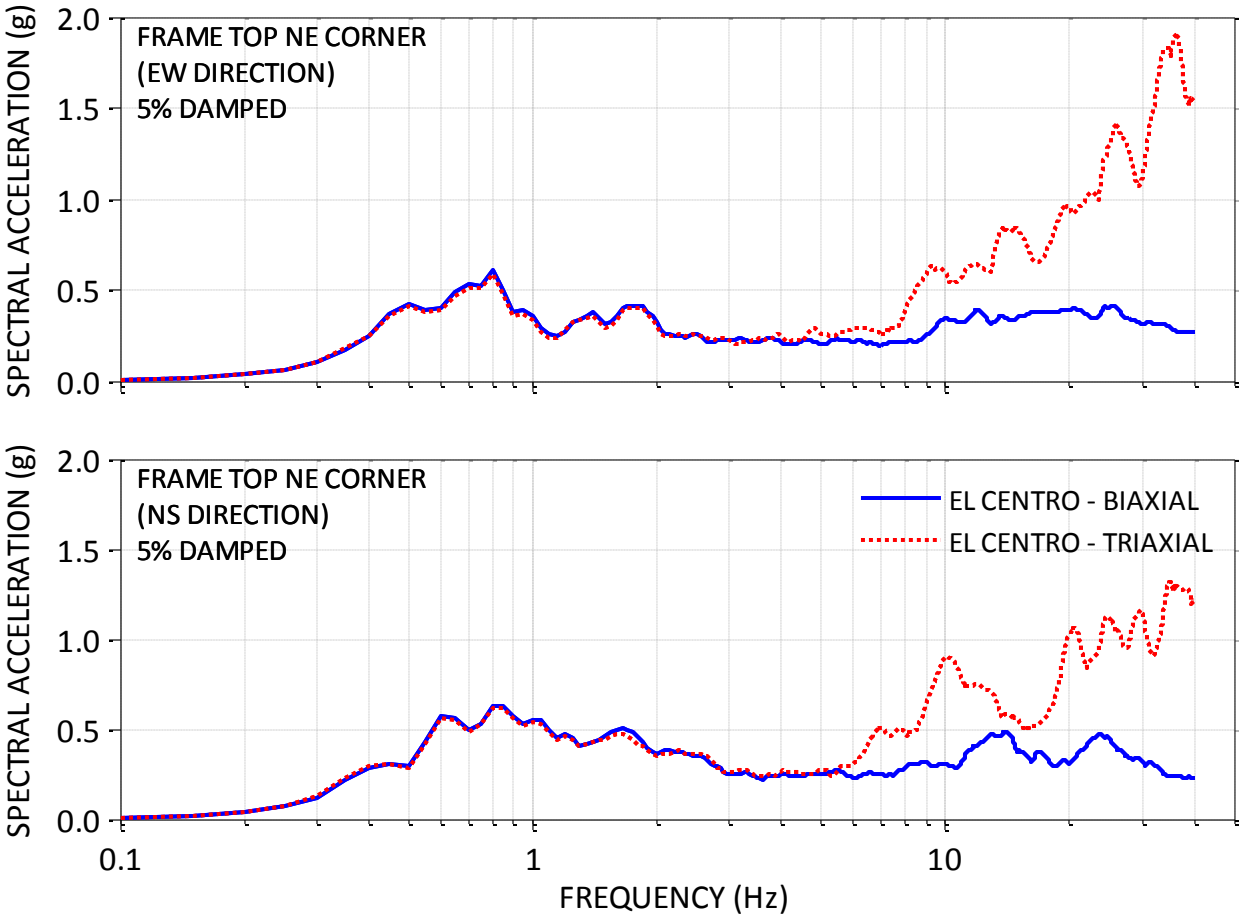


Figure 4-22 Comparison of Acceleration Response Spectra at the Top NE Corner of the Frame in the two Horizontal Directions, from Testing with the Bi-axial and Tri-axial 300% El-Centro Excitation (Full Scale Triple FP Isolators, Bushing Mounted Symmetrically on the Cover, Testing at Full Scale)

A typical approach when attempting to remove high frequency noise from experimental results is to filter the results using a low pass filter. However, by filtering unsystematically, one might remove actual high frequency information from the results. In this example, since the time occurrence of the impact was identified using the technique discussed above, its effect could be eliminated by discarding the portion of the acceleration history during which impact occurred from the calculation of the response spectra. Comparisons between the acceleration response spectra from bi-axial testing and from tri-axial testing, the latter "filtered" by removing the impulsive component of impact from the acceleration response histories of Figure 4-21 between

11 and 11.5 sec, are provided in Figure 4-23. As can be seen, the spectra compare very well once the impulsive component of impact is eliminated.

It is noted that the above example is provided only for demonstration of the effect of impact on the response of the system. Impact that occurred during the testing could not always be identified, and its effect could not be easily removed from the measured response. The results presented in this section and in the appendices are unfiltered and in some cases include amplification due to impact that are not the result of real isolated power transformer behavior but rather the result of testing of a model with occasionally having loose parts impacting.

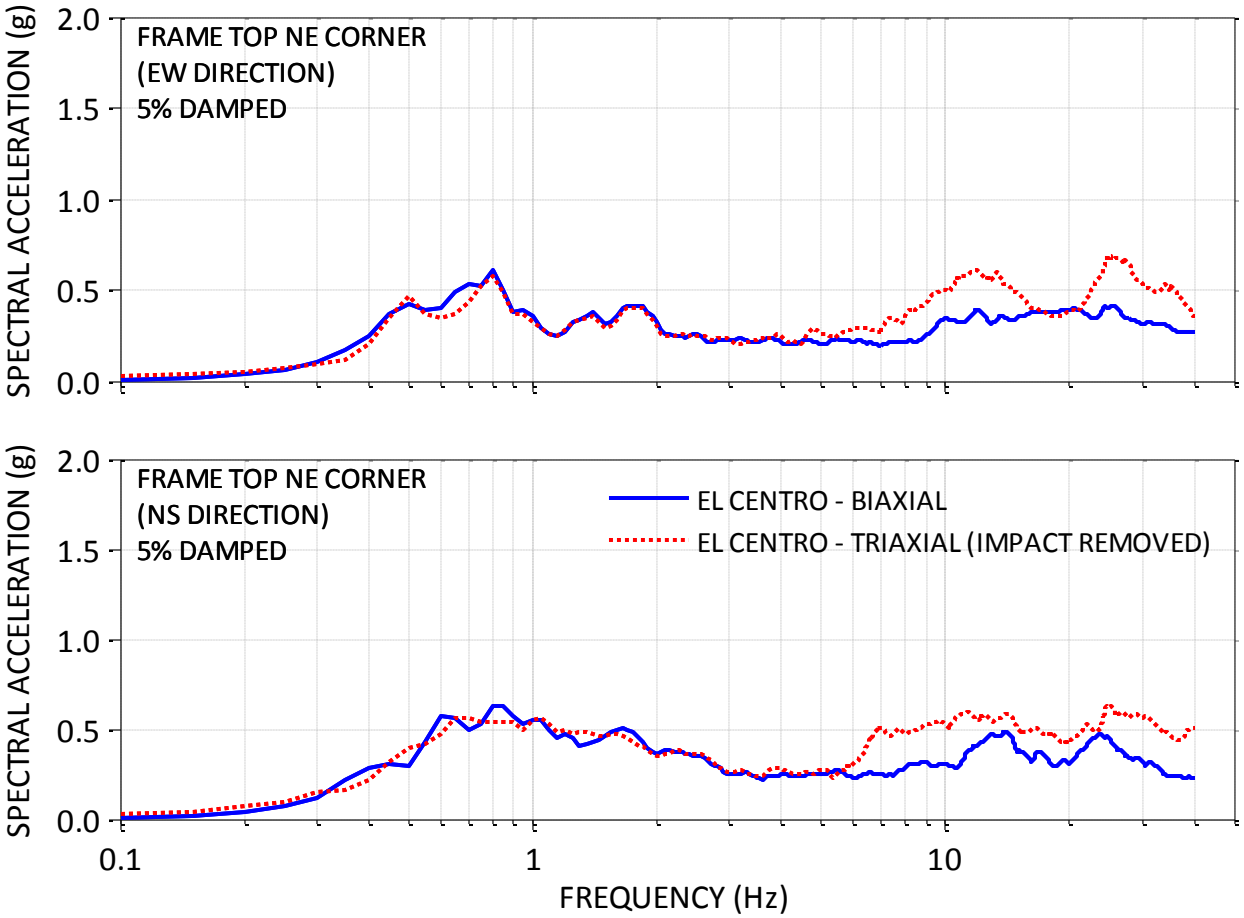


Figure 4-23 Comparison of the Acceleration Response Spectra at the Top NE Corner of the Frame in the two Horizontal Directions, from Testing with the Bi-axial and Tri-axial 300% El-Centro Excitation, where the Effect of Impact in the Tri-Axial Test has been Removed (Full Scale Triple FP Isolators, Bushing Mounted Symmetrically on the Cover, Testing at Full Scale)

SECTION 5
ANALYTICAL PREDICTION OF RESPONSE

5.1. Overview

This section describes the development of analytical models of the tested frame-bushing model and the isolation systems in the commercial software SAP2000, and presents comparisons of experimental and analytical results.

5.2. Description of Frame and Bushing Modeling

Figure 5-1 illustrates a finite element model of the frame and bushing assembly, prepared in program SAP2000 (CSI, 2002) and used in response history analysis of the tested systems. The model of Figure 5-1 corresponds to the symmetric bushing configuration and is similar to the one developed by Kong et al (2010) and used to simulate the response of the bushing under fixed boundary conditions (Kong, 2010; Fahad, 2012; Koliou, 2012). In the current study, the same model is utilized, with minor structural modifications so that the flexibility of the bushing, the mass of the large plates on the sides and bottom of the frame, and the isolators are properly accounted for. More specifically, the frame has been modeled in SAP2000 as follows:

a. The sections used for the columns and beams of the frame were modeled explicitly as described in Kong (2010). The roof plate was also modeled in accordance to the actual geometry and material. Its connection to the top beams of the frame was realized through beam elements representing the bolts used in the specimen, which are interposed between the roof plate and the top beams at appropriate locations on the perimeter of the frame. The numerical model of the roof plate features a hole to which an annular adapter plate - modeled with shell elements - is connected using beam elements representing bolts. Finally, a model

of the high voltage bushing is connected to the top of the adapter plate also using beam elements that represent bolts. The main body of the adapter plate is represented by beam elements and its mounting flange is modeled as a disk of shell elements. Further details on the modeling of the high voltage bushing are provided later in the section.

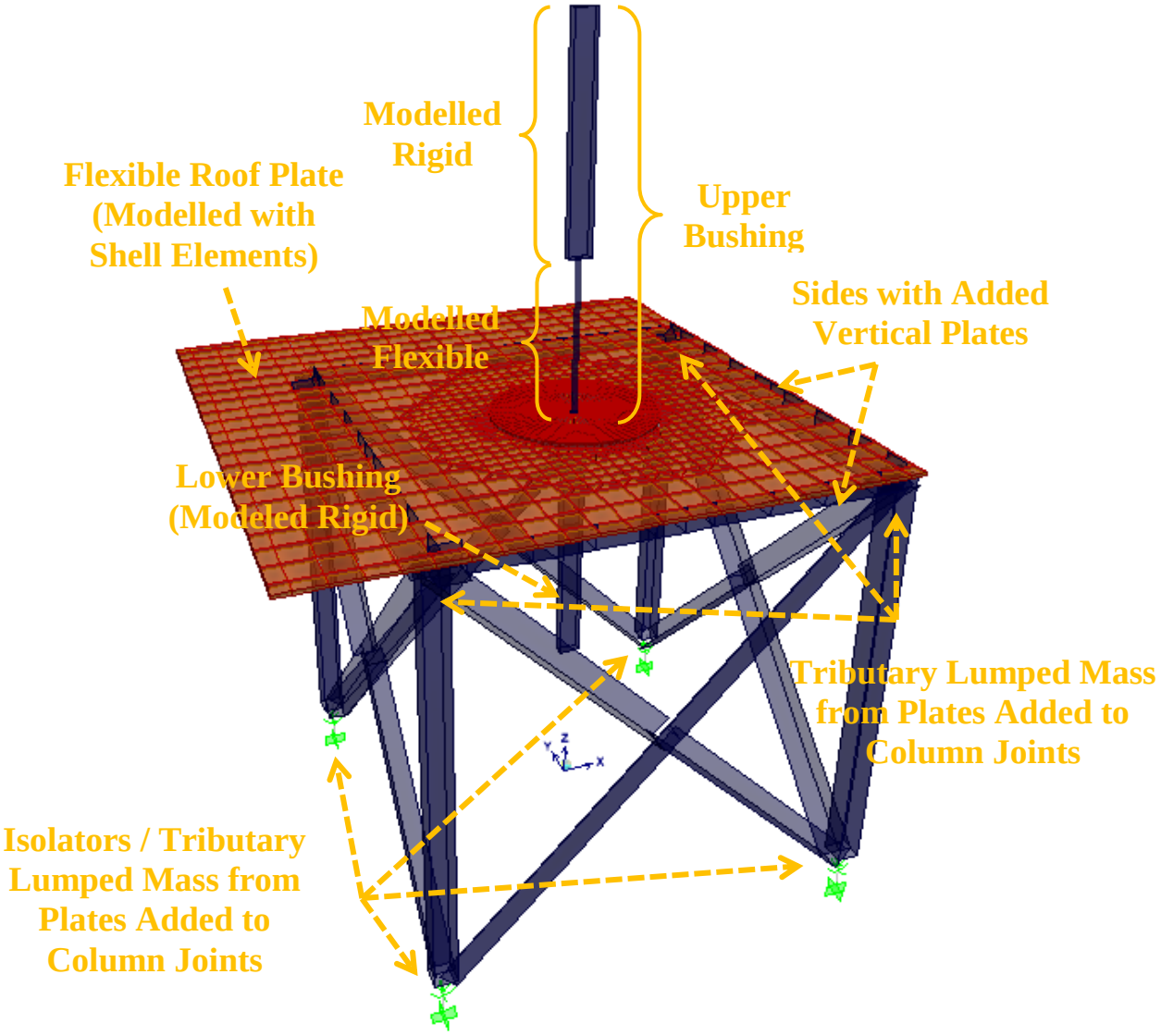


Figure 5-1 Finite Element Model of Isolated Frame Structure in SAP2000

b. The base mat at the bottom of the frame, the two large vertical plates at the two adjacent sides of the frame and the angle sections utilized for the connection of the side plates to the

frame and the base mat were not explicitly modeled in SAP2000. Instead, the weight of each plate and beam was equally distributed to its tributary nodes as lumped masses. The weights of the frame pedestals were also included in the model as lumped masses at the bottom of the each frame column.

c. The base mat at the bottom of the frame provides significant axial stiffness and that effect was incorporated in the SAP2000 model by imposing diaphragmatic constraints at the bottom joints of the columns. The contribution of the side vertical plates to the lateral stiffness of the frame was disregarded in the model.

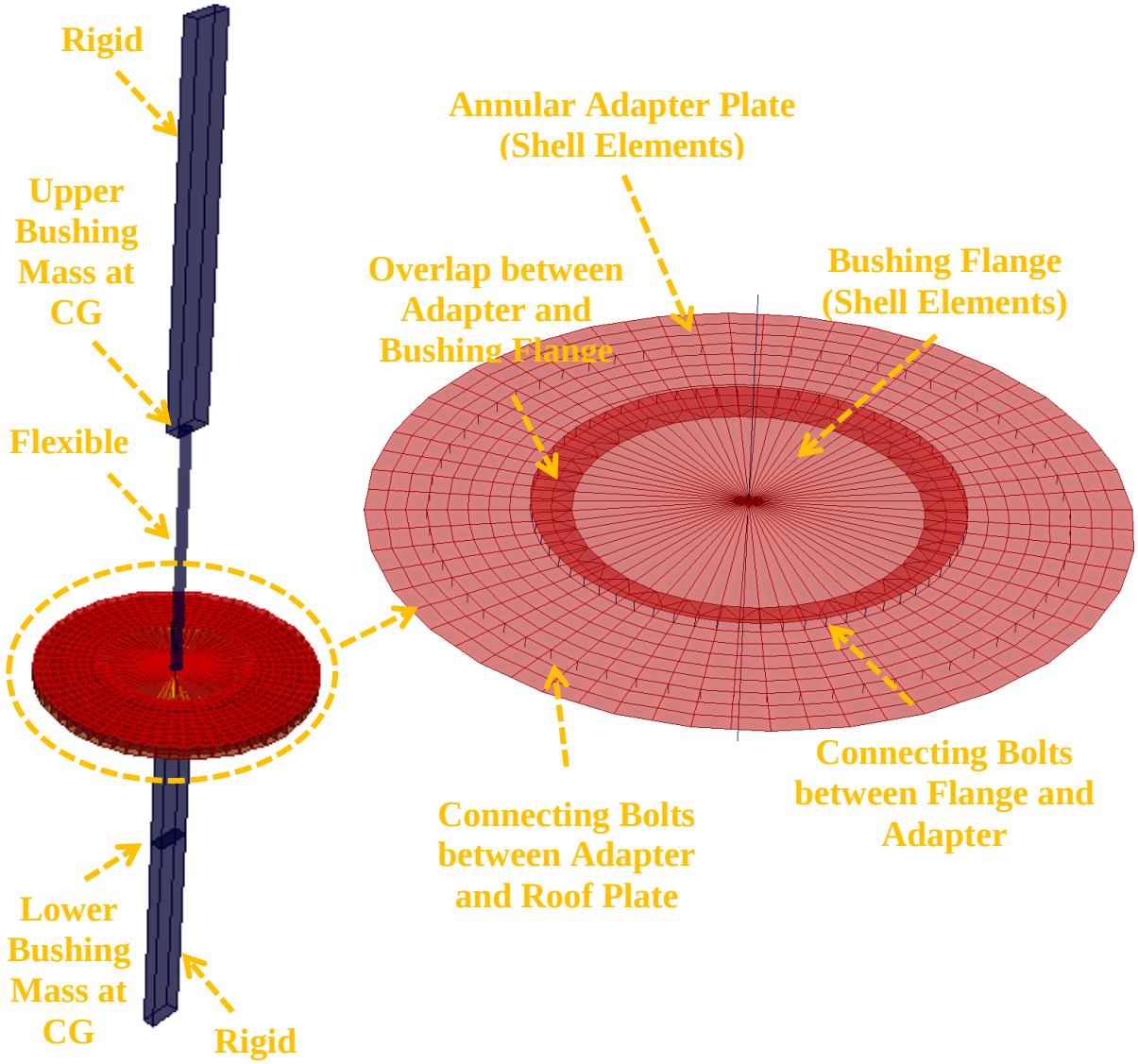


Figure 5-2: (a) Close-up of Bushing Model in SAP2000 (Extruded Cross Sections) and (b) Close-up of Adapter Plate and Bushing Flange (Not Extruded)

In order to capture the bushing dynamic behavior as accurately as possible, attention was given to the modeling of the bushing in SAP2000. Figure 5-2 illustrates the bushing model used in SAP2000 in close-up view. The modeling approach was as follows:

a. The upper part of the bushing was modeled as a flexible beam up to the center of gravity of the upper part, where the mass of the upper part was lumped. The stiffness of the beam was calibrated such that the fixed base frequency of the upper part of the bushing equaled 25Hz, obtained from previous identification testing at the UB SEESL with the bushing bolted at its flange on a quasi-rigid concrete block (Fahad, 2012, Koliou, 2010).

b. The top part of the upper bushing was modeled as a rigid, mass-less beam. At this point, it should be noted that the bushing is a fairly complicated structure comprised of alternating porcelain units and flexible rubber gasket rings, which are held together by the pre-stressing force of a central metal conductor. The flexibility and nonlinearity of the rubber gaskets and their significant effect on the bushing dynamics have been demonstrated in a number of previous studies. Several complex models have been developed to include the gaskets and/or the central conductor in the bushing model (Gilani et al, 1999; Matt and Filiatrault, 2005; Ersoy et al, 2004; Fahad, 2012). Due to lack of detailed information on the geometric and material properties of the bushing components, the development of an exact model was not attempted. Instead, a simplified model was used. The simplified approach is based on experimental calibration of the upper bushing rather than explicitly modeling the individual components. This approach has been employed in earlier studies and shown to yield good agreement between the experimental results and numerical predictions of the response at the top of the bushing for fixed base conditions of the frame (Kong, 2010). It is considered sufficiently accurate for the requirements of the current study.

c. The lower part of the bushing was modeled as a rigid, mass-less beam with its mass lumped at the center of gravity of the lower part.

d. The adapter plate, used to connect the bushing to the flexible roof, was explicitly modeled in SAP2000 as an annulus with shell elements having the same geometric properties (i.e. radius and thickness) and material properties (steel) as the actual plate. Careful modeling of the adapter plate is important in capturing the bushing dynamic behavior since its connection to the roof determines the bushing boundary conditions and its rotational flexibility at the mounting location. Moreover, the plate itself adds flexibility at the bushing flange level. While it is recognized that the contact between the adapter plate and the roof plate introduces some nonlinearity during the dynamic response of the bushing, this nonlinearity was disregarded in the model, and the connection to the roof was achieved simply through bolts at the circumference of the adapter plate. The bolts were modeled as beam elements in SAP2000, having the same properties as the ones used in the test specimen, and were interposed between the adapter plate and the roof plate at all points on a circumference with a radius that matches the actual location of the bolts used in the test specimen.

e. Likewise, the bushing flange was modeled as a circular structure, with shell elements having the same geometric and material properties as the actual flange. Bolts with the same properties as the ones used in the test specimen for the connection of the bushing to the adapter plate, were used in a radial configuration. A larger number of bolts than the actual system have been used in the model in an effort to approximately capture the contact forces between the bushing flange, the adapter plate and the roof plate. These contact forces are of highly non-linear nature and their exact modeling is out of the scope of this study. In both the adapter plate and flange configurations, parametric analyses were performed and it was verified that the number of the bolts did not actually have a significant effect on the as-

installed bushing frequencies. On the other hand, the radius of the bolt location was found to have a more significant effect on the bushing frequencies.

5.3. **Modeling of Isolation Systems**

The isolators were modeled as follows:

a. The scaled lead-rubber bearings were modeled as smooth bilinear hysteretic elements with properties as presented in Table 3-4. The bearings were modeled as fixed at both ends (Bolted-Bolted configuration). Due to incomplete information on the axial load distribution on the bearings and the friction coefficient at the friction interface, the behavior at the friction connection could not be reliably predicted and modeled. Furthermore, when tests were conducted with the Friction-Bolted configuration, significant torsion and sliding occurred that made prediction of the response practically impossible. Therefore, the modeling of the lead rubber bearings described above is valid only for the tests conducted with the Bolted-Bolted configuration.

b. The scaled Triple FP bearings were modeled with properties as presented in Table 3-5. The full size Triple FP bearings were modeled using frictional properties identified from shake table testing, as presented in Table 3-6. Two modeling approaches were attempted for the bearings. Specifically, the bearings were modeled once using the parallel model described in Sarlis and Constantinou (2009, 2010), and once using the series model described by Fenz and Constantinou (2008d), in order to assess and compare the accuracy of the models with respect to the experimental results. The parallel model features two overlapped smooth bilinear hysteretic elements and is valid for displacements prior to initiation of stiffening,

which was satisfactory for most tests. The series model features three smooth bilinear hysteretic elements connected vertically in series, and, optionally, nonlinear gap elements connected to the intermediate joints of the smooth hysteretic elements, to model stiffening of the bearing at large displacements. The gap elements must be placed radially to approximately capture stiffening in multiple directions as described in Fenz and Constantinou (2008d). In the current study, gap elements were used to model the stiffening behavior of the bearings. In order to keep the computational time low, a small number of gap elements was utilized. Namely, gap elements were introduced at 45° increments, amounting to a total of 16 gap elements for each bearing. This arrangement effectively models contact with a horizontal octagonal boundary rather than the true circular boundary.

c. The exact vertical load distribution on the bearings was not known but was calculated on the basis of the analytical model shown in Figure 5-1. This assumption was not found to have any significant effect on the quality of the analytical predictions, despite the unpredictable distribution of load. For the Triple FP bearings, the performance can be attributed to the property of the bearings to adjust the lateral force proportionally to the axial load.

The properties of the bearings used in SAP2000 are shown in Table 5-1 through Table 5-5. Specifically for the Triple FP bearings, Table 5-2 and Table 5-3 show the properties used in the parallel model, and Table 5-4 through Table 5-5 show the properties used in the series model.

Table 5-1 Values of Properties of the Model of Lead Rubber Bearings at Length Scale of 3 in SAP2000 for Response History Analysis

Parameter		Value
Supported Weight	**kip**	11.81 (NE Bearing) 15.84 (SE Bearing) 11.82 (SW Bearing) 7.80 (NW Bearing)
Dynamic Mass[1]	**kips-s^2/in**	1.29e-04
Rotational Inertia[1]	**kips-s^2-in**	1.35e-03
Height[2]	**in**	8.75
Vertical Stiffness	**kip/in**	5867
Yield Displacement	**in**	0.061
Yield Strength	**kip**	1.70
Post Yield Stiffness Ratio	**-**	0.0571
Elastic Stiffness	**kip/in**	28.00
Effective Stiffness[3]	**kip/in**	1.60
Torsional Stiffness	**kip-in/rad**	0.00
Rotational Stiffness	**kip-in/rad**	0.00

1 Value of 0.05kip used in the calculation.
2 Shear deformation location is at mid-height of the element.
3 Effective stiffness specified as the post-elastic stiffness in order to minimize parasitic damping effects.

Table 5-2 Values of Properties of the Parallel Models of Triple FP Bearings at Length Scale of 3 in SAP2000 for Response History Analysis

Parameter		NE Bearing	SE Bearing	SW Bearing	NW Bearing
Supported Weight	**kip**	11.81	15.84	11.82	7.80
Dynamic Mass[1]	**kips-s^2/in**	1.29e-04	1.29e-04	1.29e-04	1.29e-04
Rotational Inertia[1] (FP1)	**kips-s^2-in**	2.16e-04	2.16e-04	2.16e-04	2.16e-04
Height[2] (FP1 and FP2)	**in**	4.00	4.00	4.00	4.00
Vertical Stiffness[3]	**kip/in**	5694.14	5694.14	5694.14	5694.14
Friction Fast (FP1)	-	0.080	0.080	0.080	0.080
Friction Fast (FP2)	-	0.1580	0.1580	0.1580	0.1580
Friction Slow (FP1)	-	0.040	0.040	0.040	0.040
Friction Slow (FP2)	-	0.1106	0.1106	0.1106	0.1106
Yield Displacement	**in**	0.01	0.01	0.01	0.01
Elastic Stiffness[4] (FP1)	**kip/in**	20.62	27.71	20.63	13.56
Elastic Stiffness[4] (FP2)	**kip/in**	2.46	3.31	2.46	1.62
Effective Stiffness[5] (FP1)	**kip/in**	0.00	0.00	0.00	0.00
Effective Stiffness[5] (FP2)	**kip/in**	0.34	0.46	0.34	0.22
Effective Radius (FP1)	**in**	0.00	0.00	0.00	0.00
Effective Radius (FP2)	**in**	17.12	17.12	17.12	17.12
Rate Parameter	**sec/in**	1.27	1.27	1.27	1.27
Torsional Stiffness	**kip-in/rad**	0.00	0.00	0.00	0.00
Rotational Stiffness	**kip-in/rad**	0.00	0.00	0.00	0.00

1 Value of 0.1kip used in the calculation.
2 Shear deformation location is at mid-height of the element.
3 Elements have same axial stiffness. Calculated for E=14500ksi, height 4inch, diameter 2inch and divided by 2.
4 Calculated as $W/2R_{eff\,2} - W/2R_{eff\,1}$ in order to account for the way SAP2000 calculates the elastic stiffness (specified elastic stiffness plus post elastic stiffness).
5 Effective stiffness specified as the post-elastic stiffness ($W/2R_{eff\,1}$) in order to minimize parasitic damping effects.

Table 5-3 Values of Properties of the Parallel Models of Full Size Triple FP Bearings in SAP2000 for Response History Analysis

Parameter		NE Bearing	SE Bearing	SW Bearing	NW Bearing
Supported Weight	**kip**	11.81	15.84	11.82	7.80
Dynamic Mass[1]	**kips-s^2/in**	6.47e-04	6.47e-04	6.47e-04	6.47e-04
Rotational Inertia[1] (FP1)	**kips-s^2-in**	5.72e-03	5.72e-03	5.72e-03	5.72e-03
Height[2]	**in**	9.00	9.00	9.00	9.00
Vertical Stiffness[3]	**kip/in**	15817.05	15817.05	15817.05	15817.05
Friction Fast (FP1)	-	0.090	0.090	0.090	0.090
Friction Fast (FP2)	-	0.074	0.074	0.074	0.074
Friction Slow (FP1)	-	0.045	0.045	0.045	0.045
Friction Slow (FP2)	-	0.037	0.037	0.037	0.037
Yield Displacement	**in**	0.01	0.01	0.01	0.01
Elastic Stiffness[4] (FP1)	**kip/in**	24.58	33.33	24.60	15.87
Elastic Stiffness[4] (FP2)	**kip/in**	0.72	0.97	0.72	0.46
Effective Stiffness[5] (FP1)	**kip/in**	0.00	0.00	0.00	0.00
Effective Stiffness[5] (FP2)	**kip/in**	0.15	0.21	0.16	0.10
Effective Radius (FP1)	**in**	0.00	0.00	0.00	0.00
Effective Radius (FP2)	**in**	36.50	36.50	36.50	36.50
Rate Parameter	**sec/in**	1.27	1.27	1.27	1.27
Torsional Stiffness	**kip-in/rad**	0.00	0.00	0.00	0.00
Rotational Stiffness	**kip-in/rad**	0.00	0.00	0.00	0.00

1 Value of 0.5kip used in the calculation.
2 Shear deformation location is at mid-height of the element.
3 Elements have same axial stiffness. Calculated for E=14500ksi, height 9inch, diameter 5inch and divided by 2.
4 Calculated as $W/2R_{eff\,2} - W/2R_{eff\,1}$ in order to account for the way SAP2000 calculates the elastic stiffness (specified elastic stiffness plus post elastic stiffness).
5 Effective stiffness specified as the post-elastic stiffness ($W/2R_{eff\,1}$) in order to minimize parasitic damping effects.

Table 5-4 Values of Properties of the Series Models of Triple FP Bearings at Length Scale of 3 in SAP2000 for Response History Analysis

Parameter		NE Bearing	SE Bearing	SW Bearing	NW Bearing
Supported Weight	**kip**	11.81	15.84	11.82	7.80
Dynamic Mass[1]	**kips-s^2/in**	8.63e-05	8.63e-05	8.63e-05	8.63e-05
Rotational Inertia[1] (FP1)	**kips-s^2-in**	1.44e-04	1.44e-04	1.44e-04	1.44e-04
Height[2] (FP1 and FP3)	**in**	1.095	1.095	1.095	1.095
Height[2] (FP2)	**in**	1.810	1.810	1.810	1.810
Vertical Stiffness[3]	**kip/in**	34164.82	34164.82	34164.82	34164.82
Friction Fast (FP1)	-	0.040	0.040	0.040	0.040
Friction Fast (FP2 and FP3)	-	0.130	0.130	0.130	0.130
Friction Slow (FP1)	-	0.020	0.020	0.020	0.020
Friction Slow (FP2 and FP3)	-	0.083	0.083	0.083	0.083
Yield Displacement	**in**	0.0062	0.0062	0.0062	0.0062
Elastic Stiffness (FP1)	**kip/in**	37.83	50.85	37.86	24.88
Elastic Stiffness[4] (FP2 and FP3)	**kip/in**	122.94	165.25	123.05	80.86
Effective Stiffness[5] (FP1)	**kip/in**	2.80	3.77	2.80	1.84
Effective Stiffness[5] (FP2 and FP3)	**kip/in**	0.78	1.05	0.78	0.51
Effective Radius (FP1)	**in**	4.18	4.18	4.18	4.18
Effective Radius (FP2 and FP3)	**in**	15.03	15.03	15.03	15.03
Rate Parameter (FP1)	**sec/in**	1.27	1.27	1.27	1.27
Rate Parameter (FP2 and FP3)	**sec/in**	2.89	2.89	2.89	2.89
Torsional Stiffness	**kip-in/rad**	0.00	0.00	0.00	0.00
Rotational Stiffness	**kip-in/rad**	0.00	0.00	0.00	0.00
Number of Gap Elements	**-**	8	8	8	8
Gap Element Opening	**in**	2.04	2.04	2.04	2.04
Gap Element Closing Stiffness	**kip/in**	165.25	165.25	165.25	165.25

1 Value of 0.1kip used in the calculation.
2 Shear deformation location is at mid-height of the element.
3 Elements have same axial stiffness. Calculated for E=14500ksi, height 4inch, diameter 2inch and multiplied by 3.
4 Calculated as $W/2R_{eff\,2} - W/2R_{eff\,1}$ in order to account for the way SAP2000 calculates the elastic stiffness (specified elastic stiffness plus post elastic stiffness).
5 Effective stiffness specified as the post-elastic stiffness ($W/2R_{eff\,1}$) in order to minimize parasitic damping effects.

Table 5-5 Values of Properties of the Series Models of Full Size Triple FP Bearings in SAP2000 for Response History Analysis

Parameter		NE Bearing	SE Bearing	SW Bearing	NW Bearing
Supported Weight	**kip**	11.81	15.84	11.82	7.80
Dynamic Mass[1]	**kips-s^2/in**	4.31e-04	4.31e-04	4.31e-04	4.31e-04
Rotational Inertia[1] (FP1)	**kips-s^2-in**	3.81e-03	3.81e-03	3.81e-03	3.81e-03
Height[2] (FP1 and FP3)	**in**	2.5	2.5	2.5	2.5
Height[2] (FP2)	**in**	4	4	4	4
Vertical Stiffness[3]	**kip/in**	94902.28	94902.28	94902.28	94902.28
Friction Fast (FP1)	-	0.045	0.045	0.045	0.045
Friction Fast (FP2 and FP3)	-	0.090	0.090	0.090	0.090
Friction Slow (FP1)	-	0.0225	0.0225	0.0225	0.0225
Friction Slow (FP2 and FP3)	-	0.045	0.045	0.045	0.045
Yield Displacement	**in**	0.005	0.005	0.005	0.005
Elastic Stiffness (FP1)	**kip/in**	50.89	69.02	50.94	32.85
Elastic Stiffness[4] (FP2 and FP3)	**kip/in**	101.78	138.04	101.87	65.71
Effective Stiffness[5] (FP1)	**kip/in**	0.87	1.18	0.87	0.56
Effective Stiffness[5] (FP2 and FP3)	**kip/in**	0.38	0.51	0.38	0.24
Effective Radius (FP1)	**in**	13.00	13.00	13.00	13.00
Effective Radius (FP2 and FP3)	**in**	30.00	30.00	30.00	30.00
Rate Parameter (FP1)	**sec/in**	1.27	1.27	1.27	1.27
Rate Parameter (FP2 and FP3)	**sec/in**	3.09	3.09	3.09	3.09
Torsional Stiffness	**kip-in/rad**	0.00	0.00	0.00	0.00
Rotational Stiffness	**kip-in/rad**	0.00	0.00	0.00	0.00
Number of Gap Elements	**-**	8	8	8	8
Gap Element Opening	**in**	5.38	5.38	5.38	5.38
Gap Element Closing Stiffness	**kip/in**	138.04	138.04	138.04	138.04

1 Value of 0.5kip used in the calculation.
2 Shear deformation location is at mid-height of the element.
3 Elements have same axial stiffness. Calculated for E=14500ksi, height 9inch, diameter 5inch and multiplied by 3.
4 Calculated as $W/2R_{eff\,2} - W/2R_{eff\,1}$ in order to account for the way SAP2000 calculates the elastic stiffness (specified elastic stiffness plus post elastic stiffness).
5 Effective stiffness specified as the post-elastic stiffness ($W/2R_{eff\,1}$) in order to minimize parasitic damping effects.

5.4. **Nonlinear Analysis Parameters in SAP2000**

The procedure selected for the analysis of the isolated frame model was the Nonlinear Modal Time History Analysis method, also known as Fast Nonlinear Analysis (FNA) method (Wilson, 1998), which has the advantage of much faster computational times as compared with the much slower Nonlinear Direct Integration Time History Analysis (NLDI) method. Another advantage of the FNA method that makes it more appealing for analysis over the NLDI method, is the ability to control the phenomenon of damping leakage in SAP2000, which has been identified and documented by Sarlis and Constantinou (2010). Damping leakage describes the undesirable scenario where the user-assigned modal damping in an isolated model in SAP2000 is effectual for the modes corresponding to the isolation system, thus "leaking" into the isolation system and ultimately resulting in underestimation of the actual response. This phenomenon can be easily controlled in the FNA because the method gives the capability to the user to assign global values of damping for all the modes (e.g. by Rayleigh, constant and linear damping) while at the same time damping values can be manually overridden for a number of modes, a feature that is not available in the NLDI method. In the analyses presented herein, a constant damping of 2% of critical was assigned to all structural modes and zero damping overrides were assigned to the first six modes (two in each direction), which had previously been identified through modal analysis to be the isolation modes of vibration. The damping of 2% of critical for the superstructure was not identified from experiments, but was instead selected as the typical value of a regular steel structure, on the assumption that the latter remained elastic during testing.

The analysis in SAP2000 with seismic ground motion is typically preceded by a slow time history analysis (so inertia effects are negligible) which serves to slowly impose the vertical

loads on the isolators, by applying the gravitational acceleration with a ramp function. The results of the vertical loading time history analysis are used as the initial conditions for the subsequent FNA ground motion analysis. Both of the vertical load application and ground motion FNA utilize the results of a modal analysis of the isolated model, also performed in SAP2000. As per the recommendation of Sarlis and Constantinou (2010), the appropriate number of modes in the FNA method should be selected iteratively, such that at the end of the vertical loading time history analysis, the weight of the structure has been fully applied to the isolators. A numerical investigation performed for the requirements of the current study revealed that a relatively small number of modes would be sufficient to successfully apply the vertical loads. However, other quantities of interest such as accelerations and base shear forces could not be properly captured with the assessed modes and finally a total of 200 modes were found to be adequate for all the configurations used in analysis. The Ritz vectors were used as the method for the calculation of the modes, as recommended by Wilson (1998). The ground motions used in analysis were the ones recorded in the experiments at the top of the shake table extension. During horizontal biaxial testing, some small vertical motion was also recorded at the shake table. These components were included in the analyses.

Finally, similarly to the procedure described earlier for the vertical loading time history analysis, SAP2000 offers the option to sequentially run FNA. Namely, the final conditions of one FNA can be used as the initial conditions of another, thus allowing for the simulation of successive tests. In this study, this feature was not utilized and all analyses were performed with the same initial conditions, specifically, the ones obtained from the results of the vertical loading time history analysis.

5.5. **Analysis Results**

Figure 5-3 to Figure 5-17 present comparisons between experimental results and analysis results obtained with SAP2000 for various specimen configurations, isolation systems, ground motions and directions of testing. More specifically:

a. Figure 5-3 and Figure 5-4 present comparisons from biaxial horizontal excitation of the LRB system in Bolted-Bolted configuration and symmetric bushing configuration.

b. Figure 5-5 to Figure 5-10 present comparisons from biaxial and triaxial horizontal excitation of the scaled Triple FP system for symmetric and non-symmetric bushing configurations.

c. Figure 5-11 to Figure 5-17 present comparisons from biaxial and triaxial horizontal excitation of the full size Triple FP system for symmetric and non-symmetric bushing configurations.

For the Triple Friction Pendulum bearings (b and c above) it was found that similar results were obtained by using either the parallel or the series model, although the computational time required for the series model was approximately an order of magnitude higher than the computational time required for the parallel model. For reasons of simplicity only results from analysis using the parallel model are shown in this section. For illustrative purposes, Figure 5-18 to Figure 5-25 present comparisons between the two models in terms of acceleration response spectra and normalized base shear – displacement loops. Additional results are presented in Appendices C and D for the parallel and the series models, respectively.

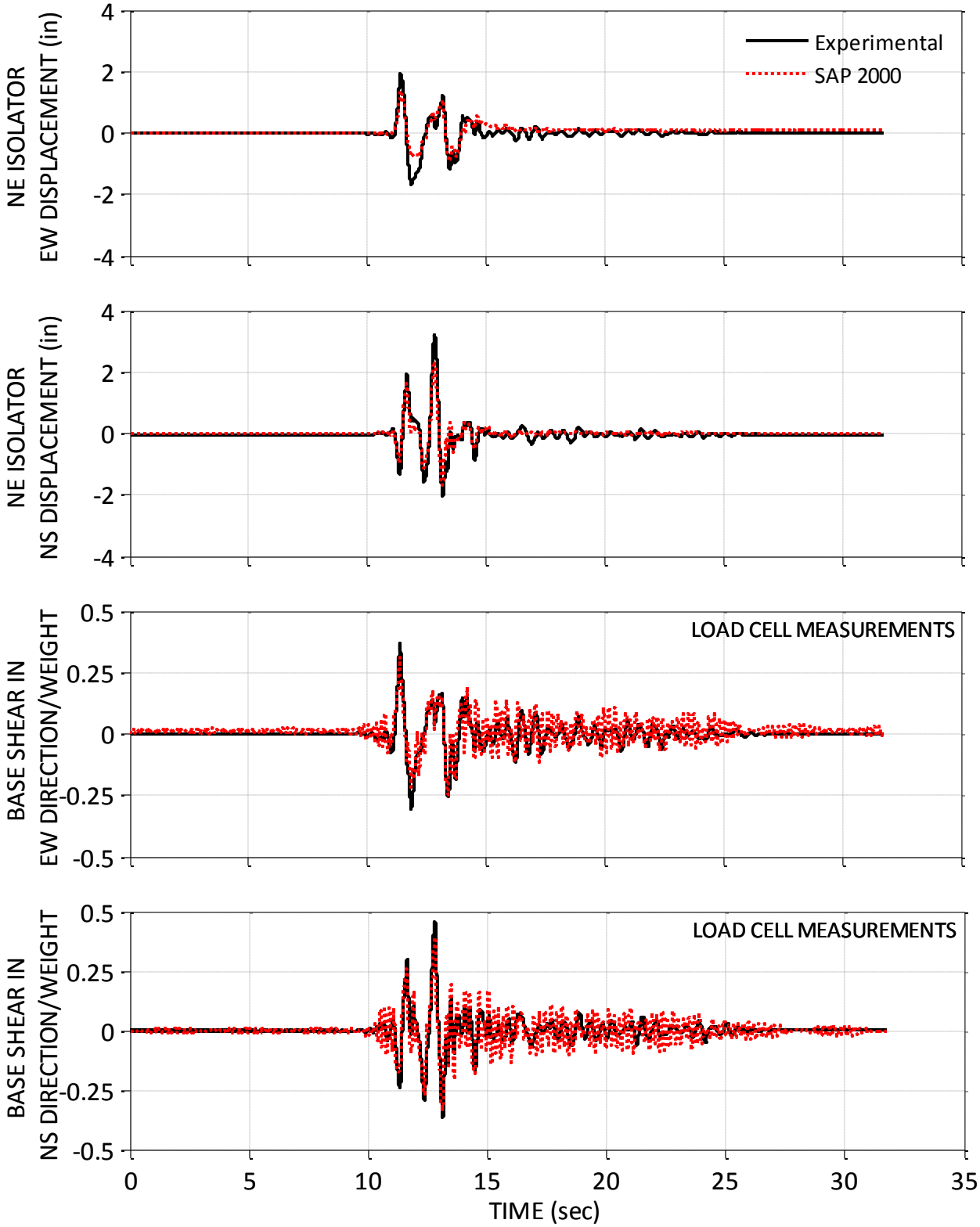


Figure 5-3 Comparison of Analytical and Experimental Results for Isolated Frame for the 97% Jensen Filter Motion (LRB Isolators with Bolted-Bolted Configuration, Length Scale of 3, Symmetric Bushing Configuration and 2D Horizontal Excitation)

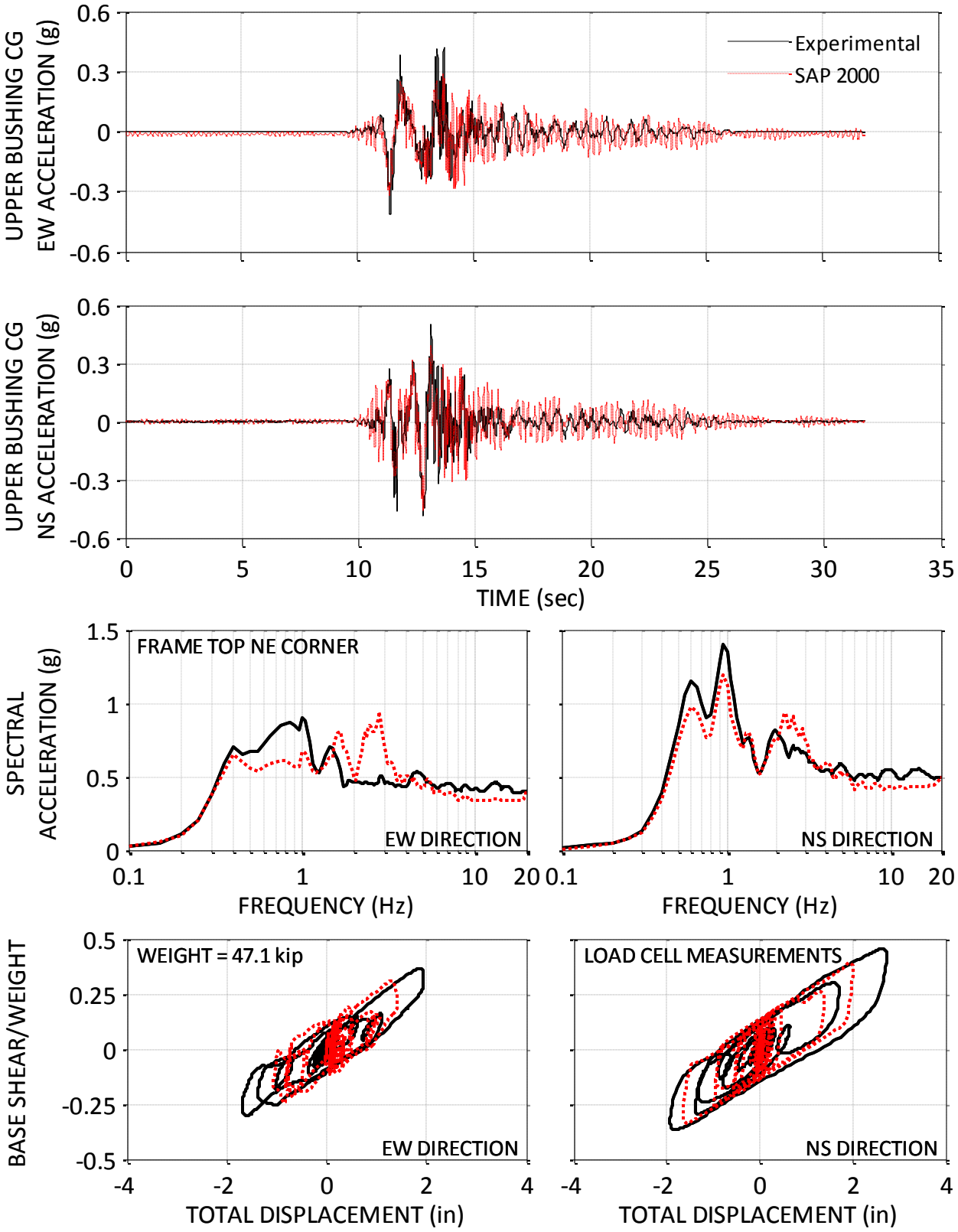


Figure 5-3 (cont'd) Comparison of Analytical and Experimental Results for Isolated Frame for the 97% Jensen Filter Motion (LRB Isolators with Bolted-Bolted Configuration, Tested at Length Scale of 3, Symmetric Bushing Configuration and 2D Horizontal Excitation)

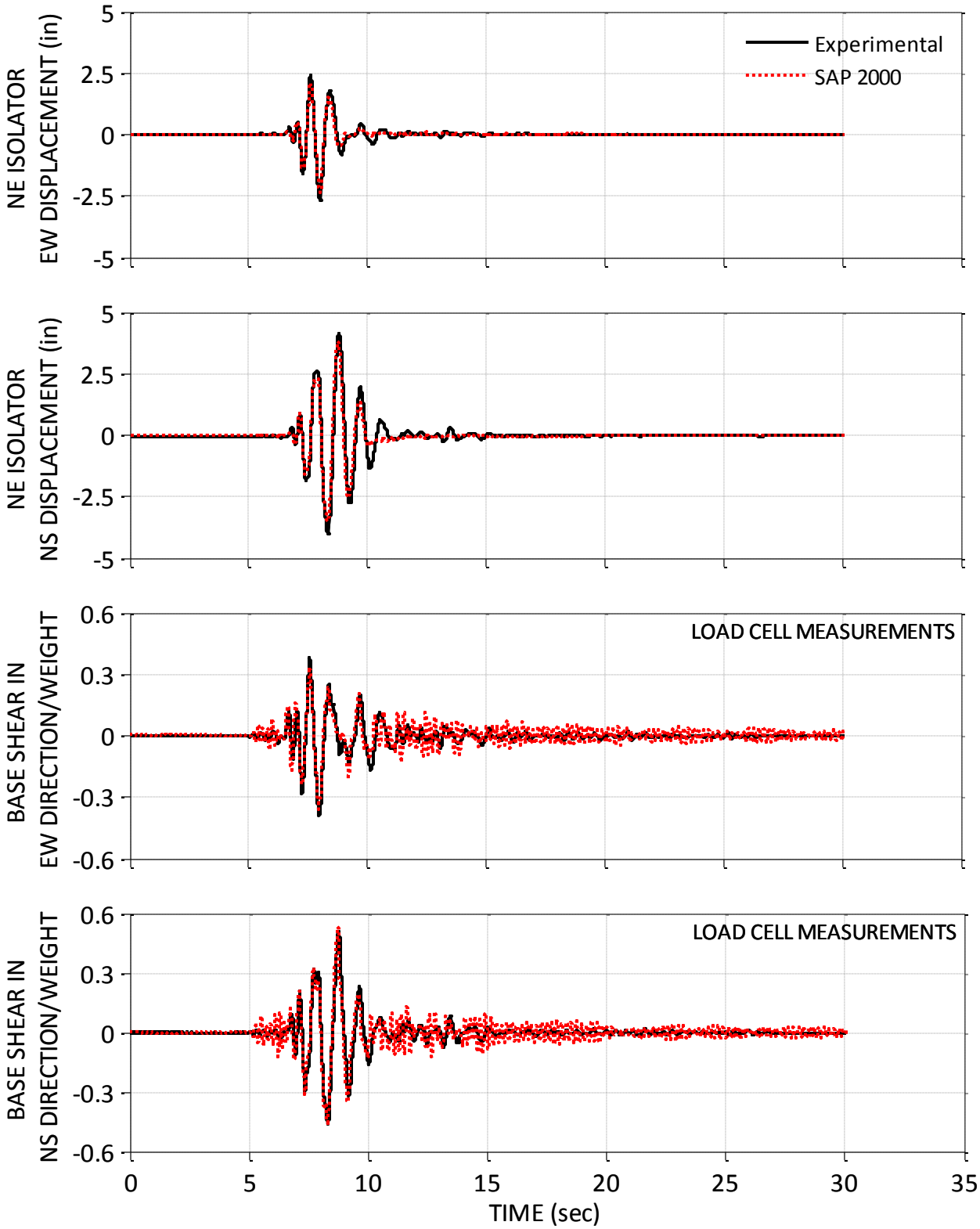


Figure 5-4 Comparison of Analytical and Experimental Results for Isolated Frame for the 97% Takarazuka Motion (LRB Isolators with Bolted-Bolted Configuration, Length Scale of 3, Symmetric Bushing Configuration and 2D Horizontal Excitation)

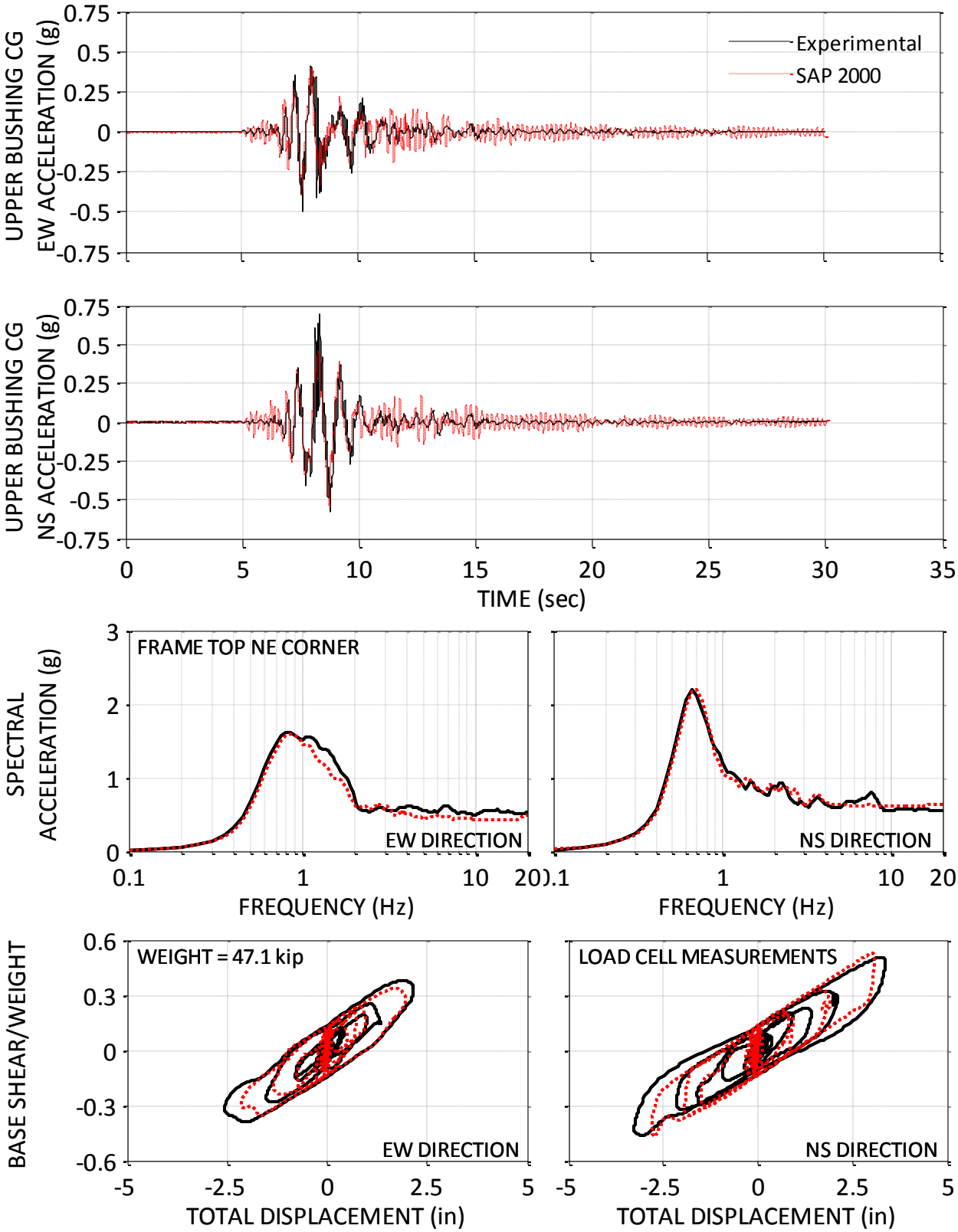


Figure 5-4 (cont'd) Comparison of Analytical and Experimental Results for Isolated Frame for the 97% Takarazuka Motion (LRB Isolators with Bolted-Bolted Configuration, Length Scale of 3, Symmetric Bushing Configuration and 2D Horizontal Excitation)

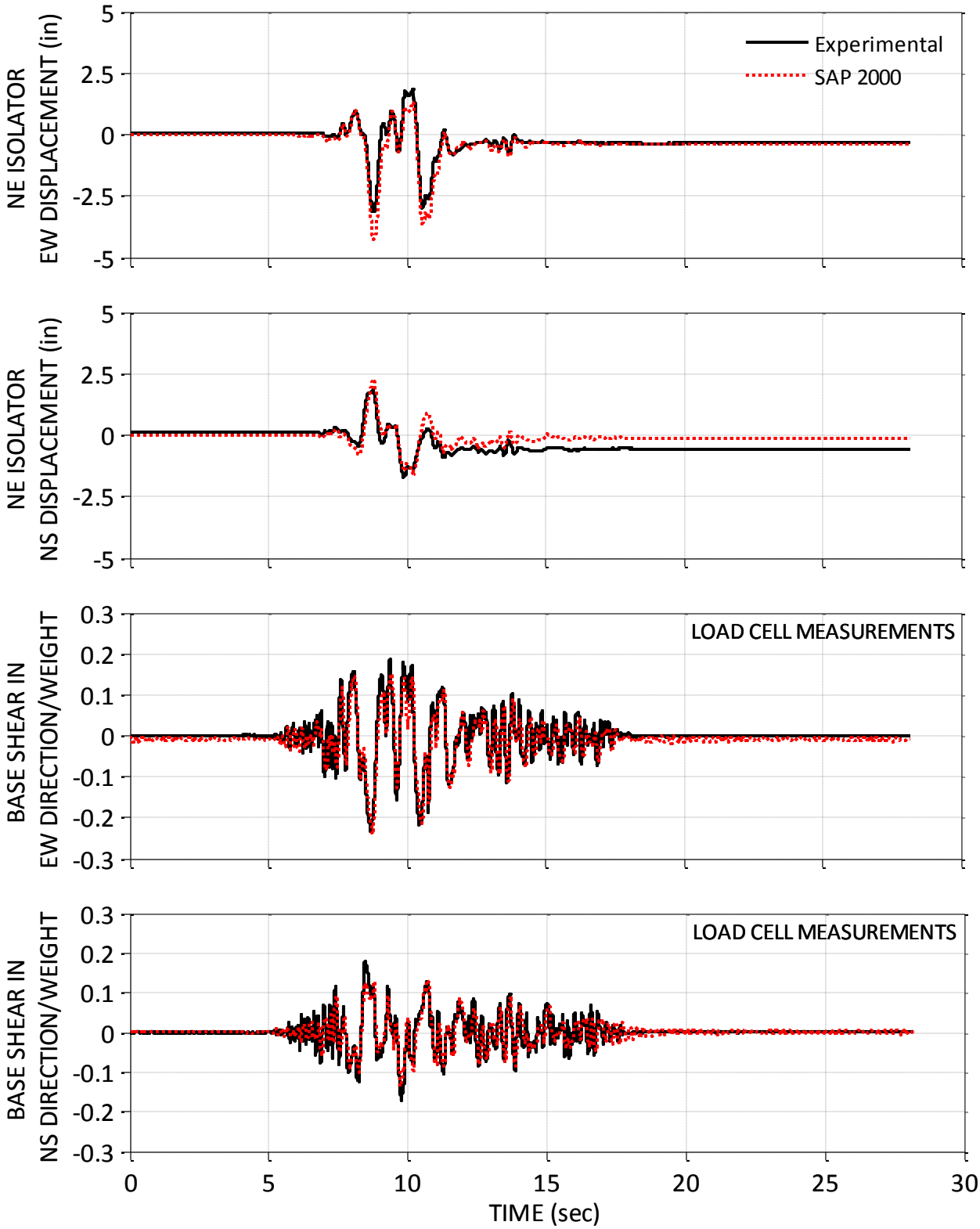


Figure 5-5 Comparison of Analytical and Experimental Results for Isolated Frame for the 94% LGPC Motion (Triple FP Isolators with Friction-Bolted Configuration, Length Scale of 3, Symmetric Bushing Configuration and 2D Horizontal Excitation)

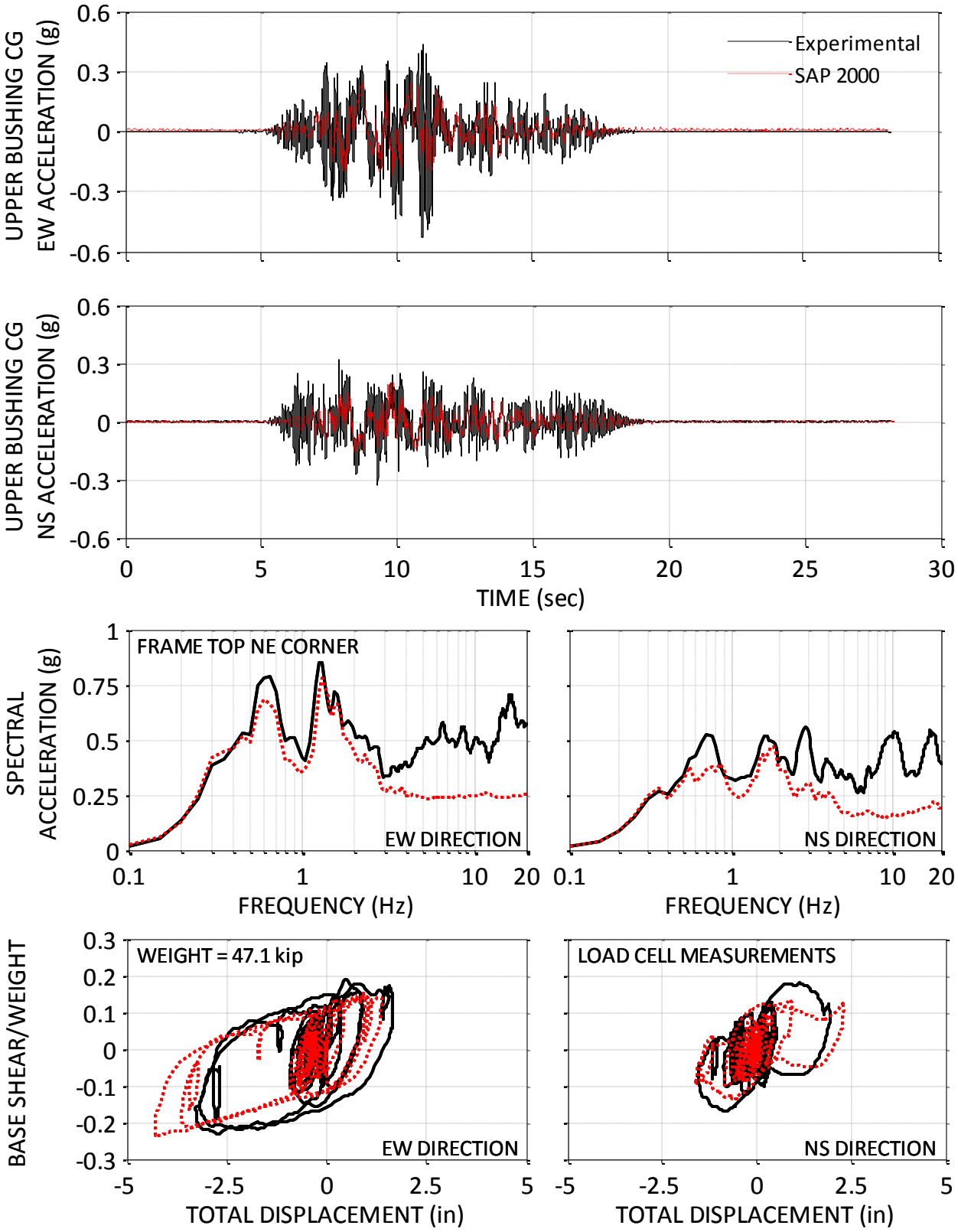


Figure 5-5 (cont'd) Comparison of Analytical and Experimental Results for Isolated Frame for the 94% LGPC Motion (Triple FP Isolators with Friction-Bolted Configuration, Length Scale of 3, Symmetric Bushing Configuration and 2D Horizontal Excitation)

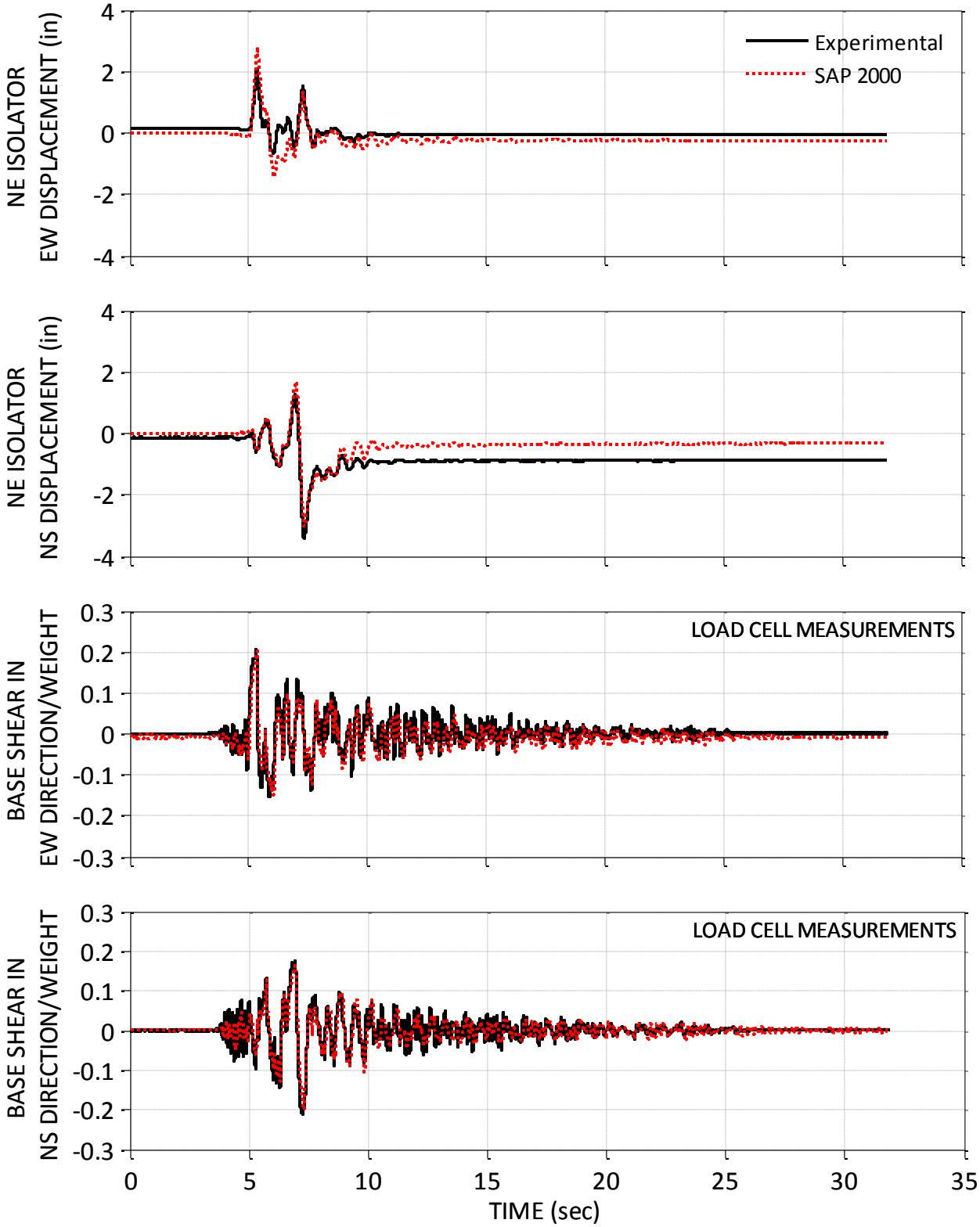


Figure 5-6 Comparison of Analytical and Experimental Results for Isolated Frame for the 90% Sylmar Motion (Triple FP Isolators with Friction-Bolted Configuration, Length Scale of 3, Symmetric Bushing Configuration and 2D Horizontal Excitation)

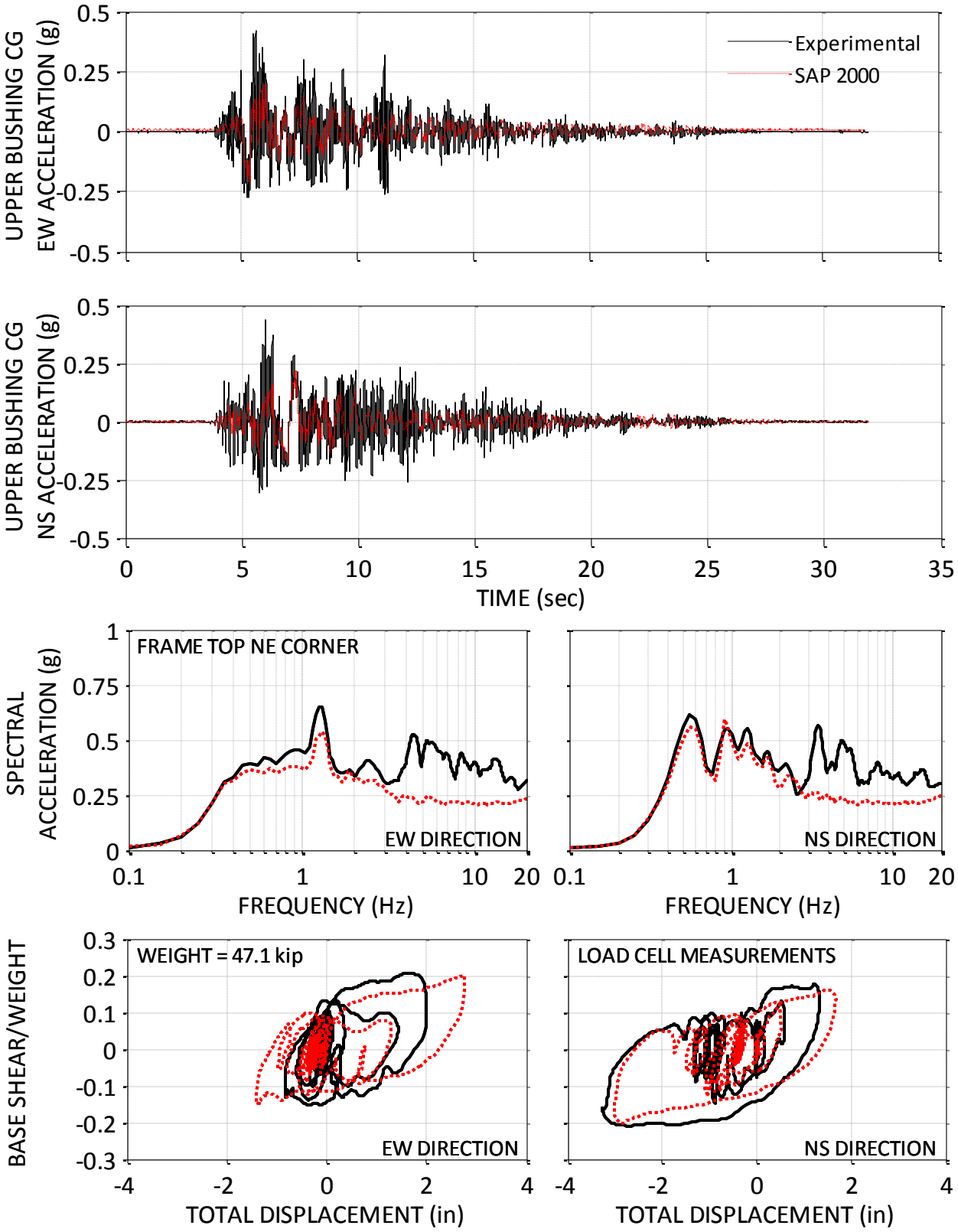


Figure 5-6 (cont'd) Comparison of Analytical and Experimental Results for Isolated Frame for the 90% Sylmar Motion (Triple FP Isolators with Friction-Bolted Configuration, Length Scale of 3, Symmetric Bushing Configuration and 2D Horizontal Excitation)

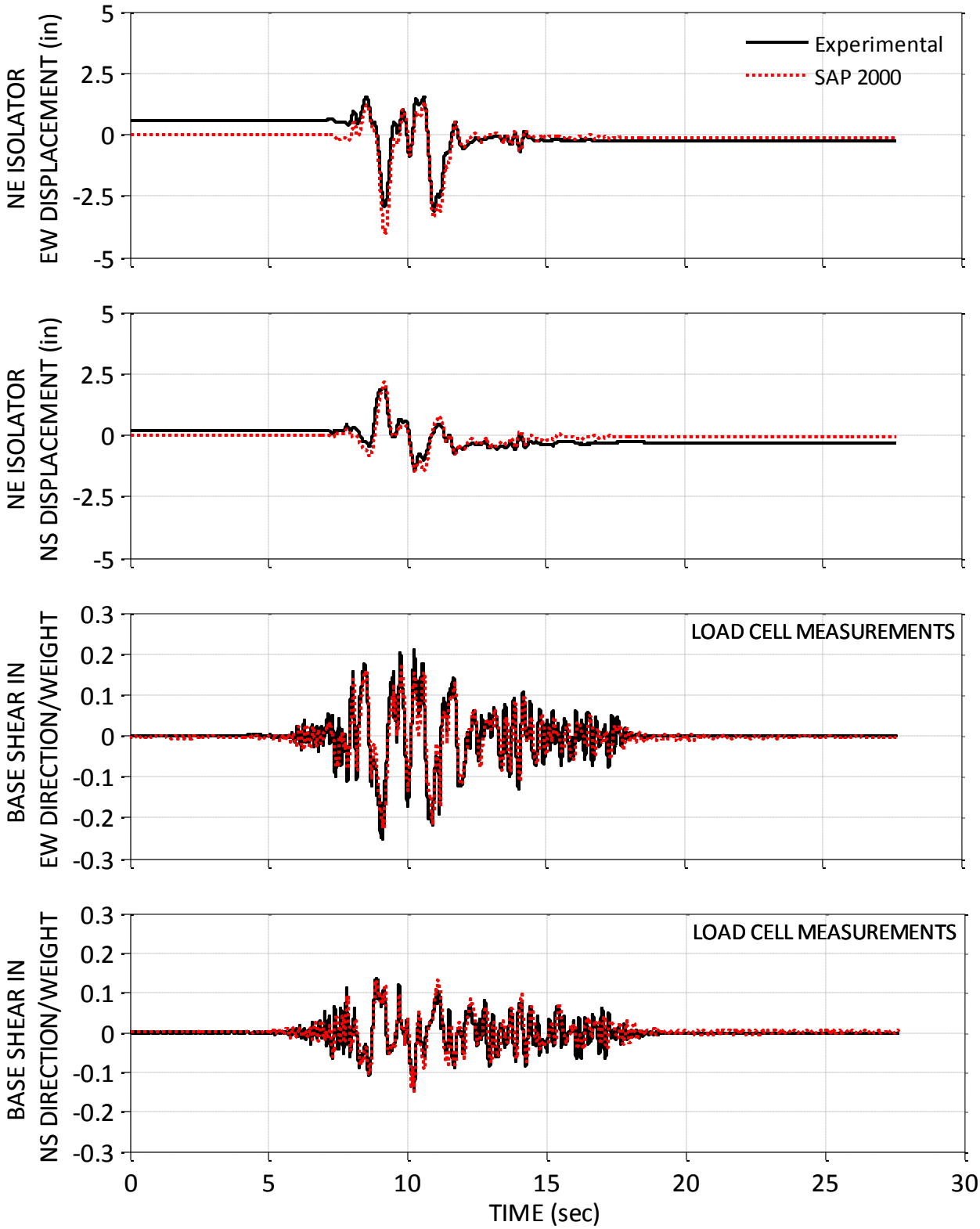


Figure 5-7 Comparison of Analytical and Experimental Results for Isolated Frame for the 94% LGPC Motion (Triple FP Isolators with Friction-Bolted Configuration, Length Scale of 3, Symmetric Bushing Configuration and 3D Excitation)

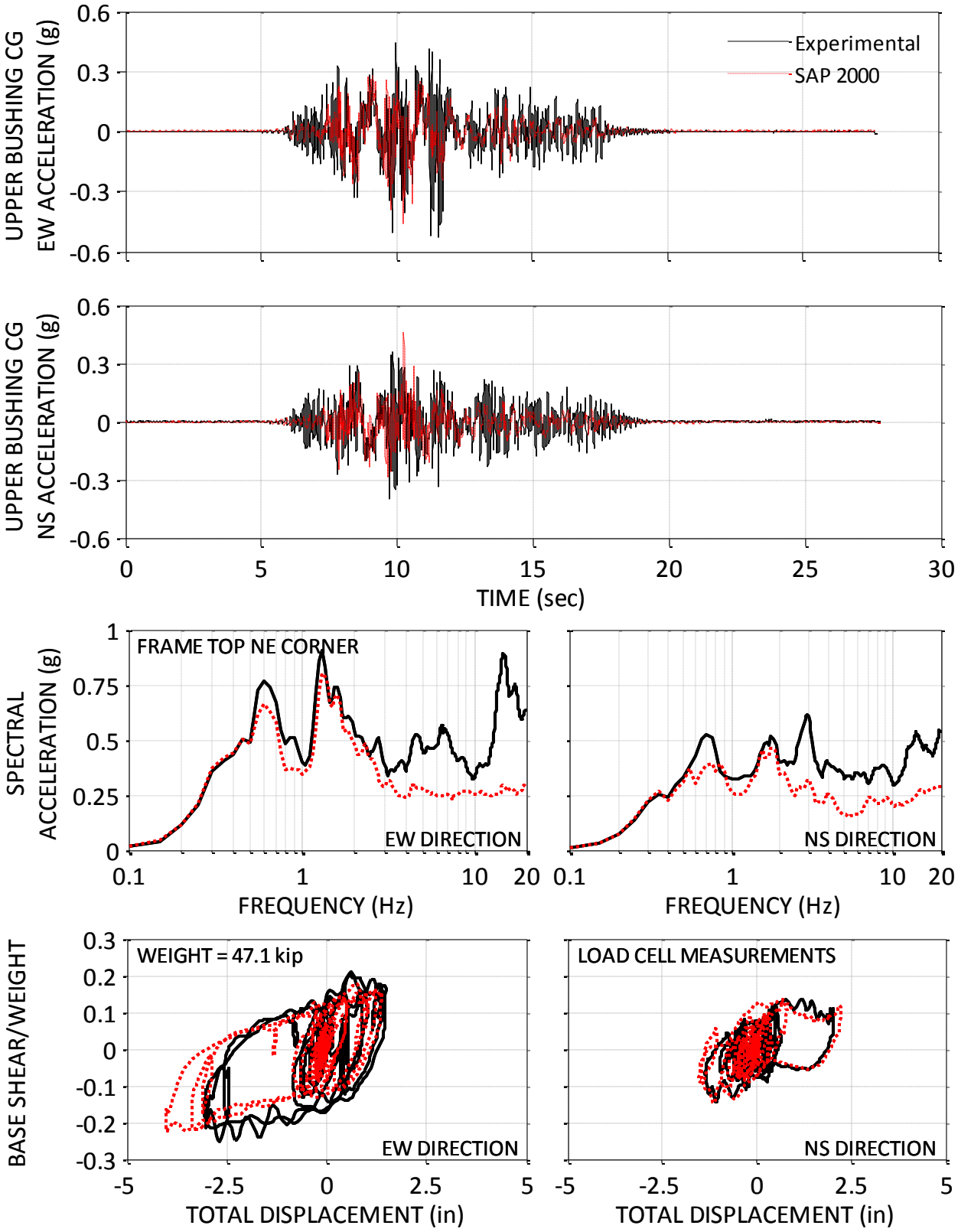


Figure 5-7 (cont'd) Comparison of Analytical and Experimental Results for Isolated Frame for the 94% LGPC Motion (Triple FP Isolators with Friction-Bolted Configuration, Length Scale of 3, Symmetric Bushing Configuration and 3D Excitation)

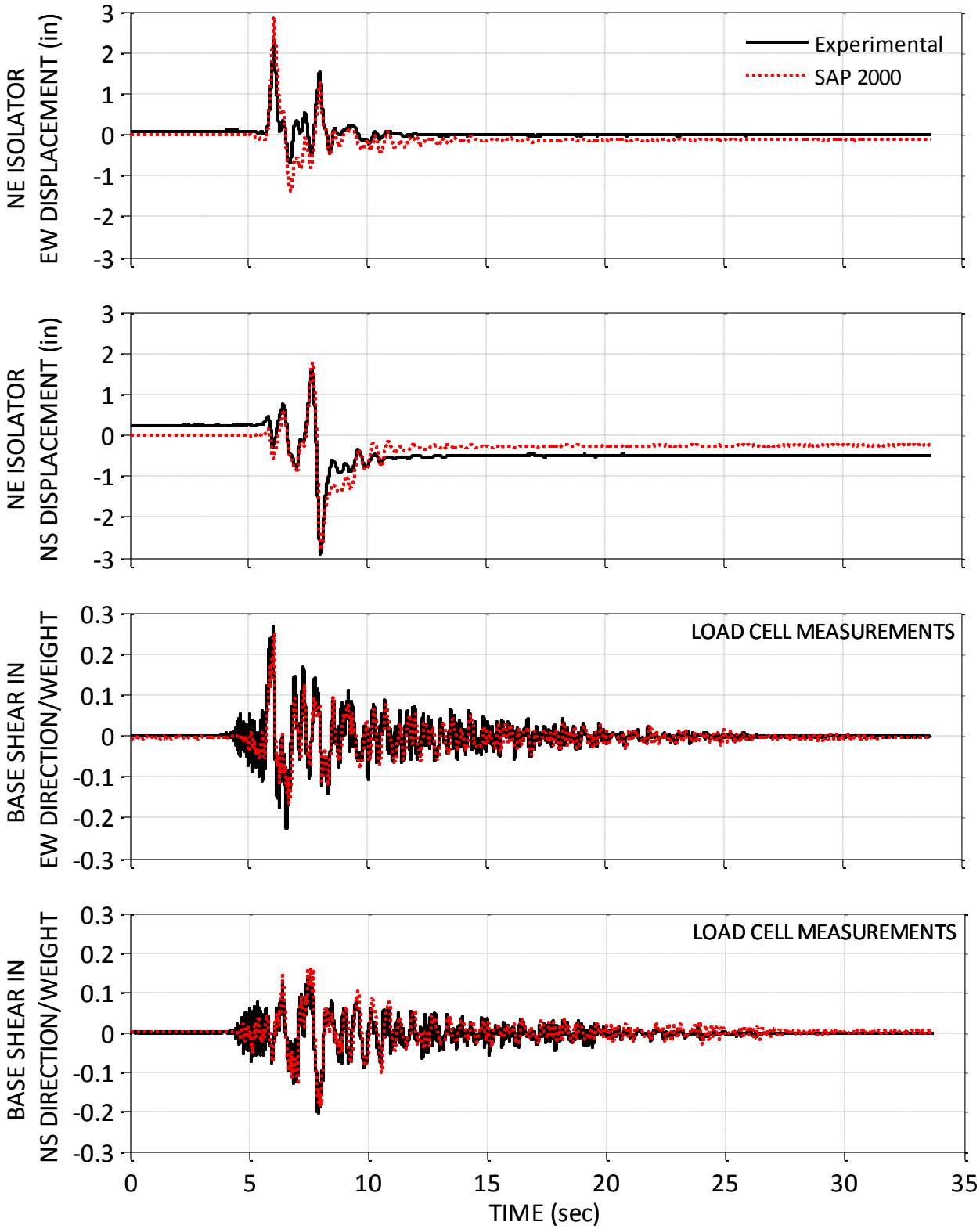


Figure 5-8 Comparison of Analytical and Experimental Results for Isolated Frame for the 90% Sylmar Motion (Triple FP Isolators with Friction-Bolted Configuration, Length Scale of 3, Symmetric Bushing Configuration and 3D Excitation)

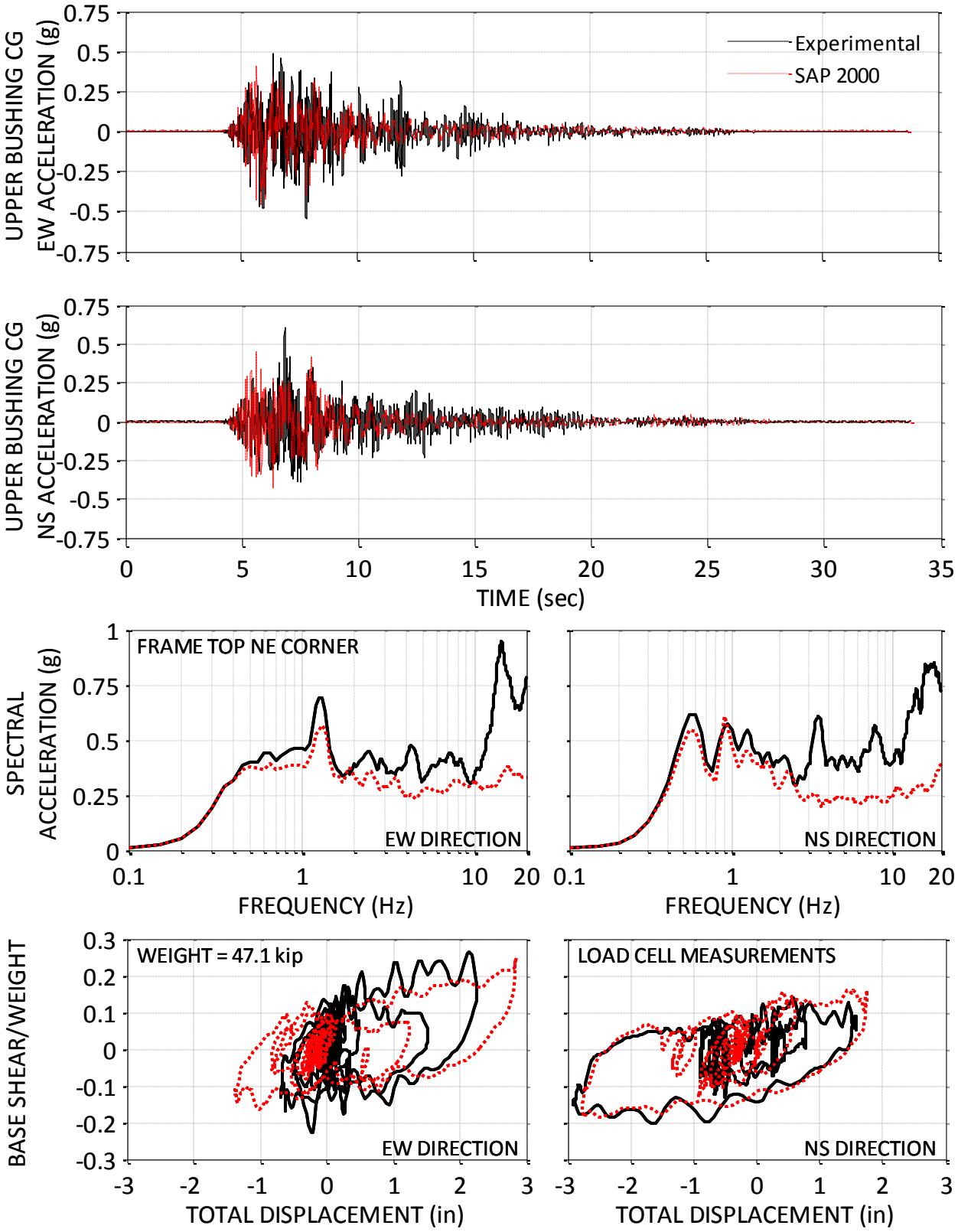


Figure 5-8 (cont'd) Comparison of Analytical and Experimental Results for Isolated Frame for the 90% Sylmar Motion (Triple FP Isolators with Friction-Bolted Configuration, Length Scale of 3, Symmetric Bushing Configuration and 3D Excitation)

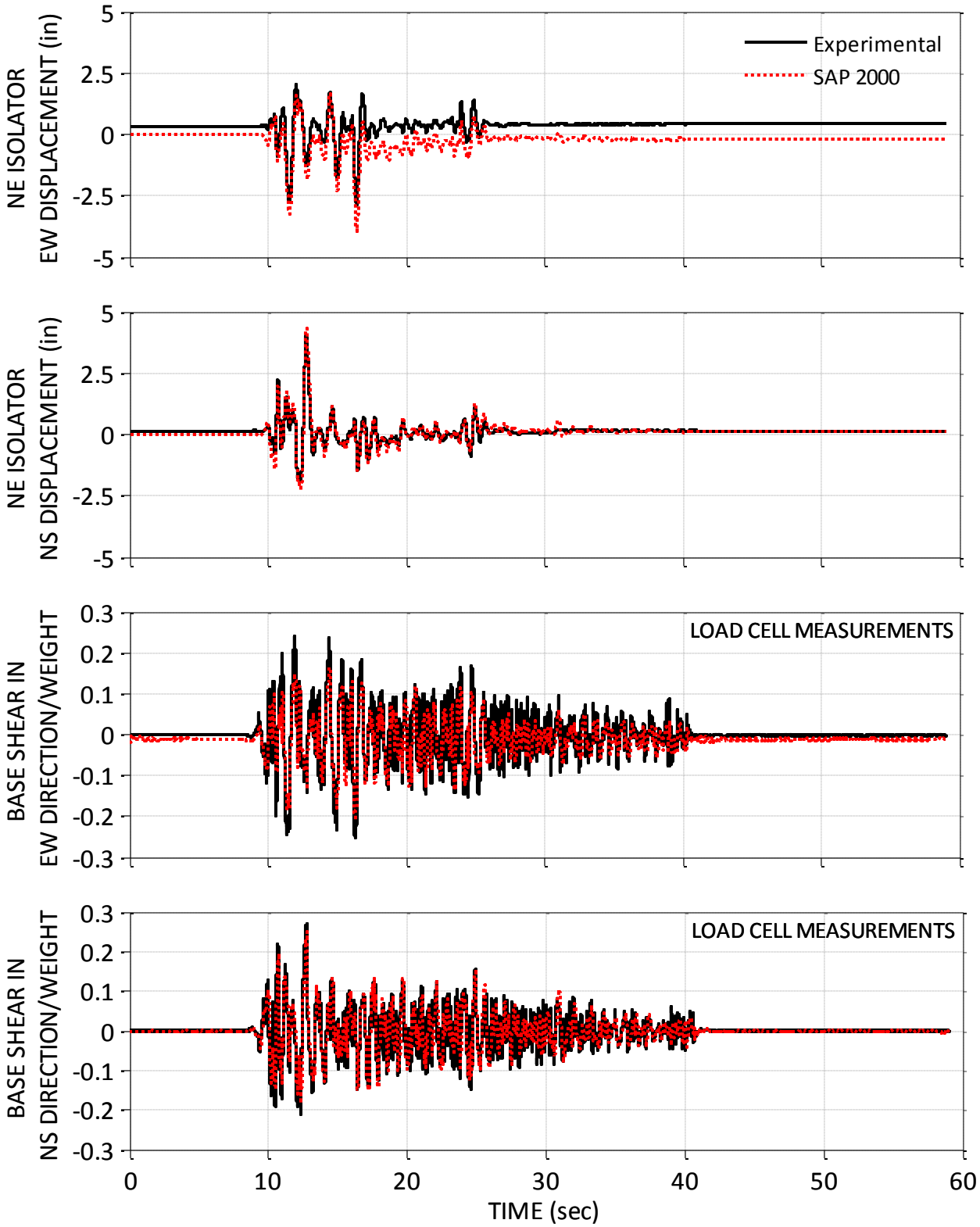


Figure 5-9 Comparison of Analytical and Experimental Results for Isolated Frame for the 300% El Centro Motion (Triple FP Isolators with Friction-Bolted Configuration, Length Scale of 3, Non-Symmetric Bushing Configuration and 2D Horizontal Excitation)

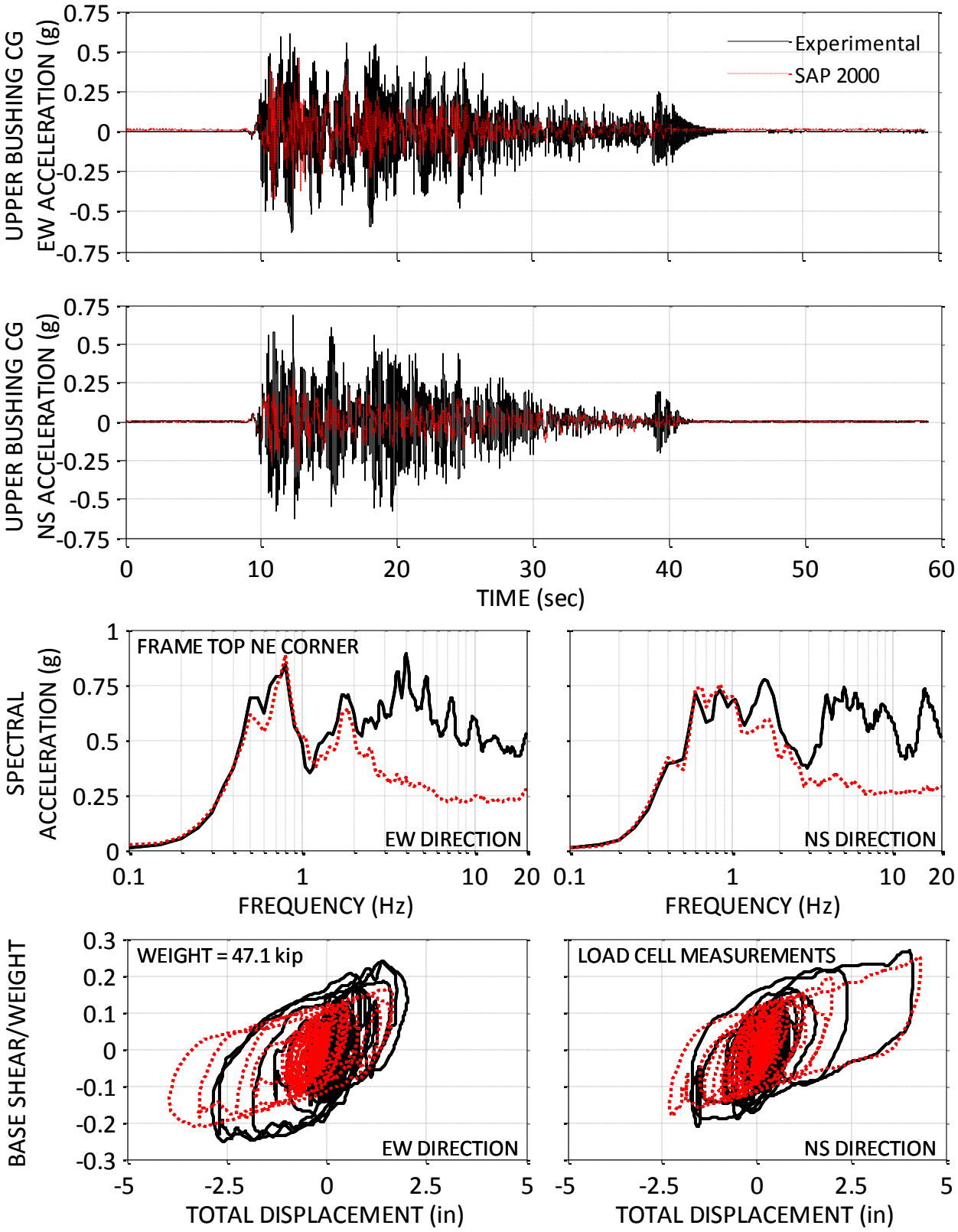


Figure 5-9 (cont'd) Comparison of Analytical and Experimental Results for Isolated Frame for the 300% El Centro Motion (Triple FP Isolators with Friction-Bolted Configuration, Length Scale of 3, Non-Symmetric Bushing Configuration and 2D Horizontal Excitation)

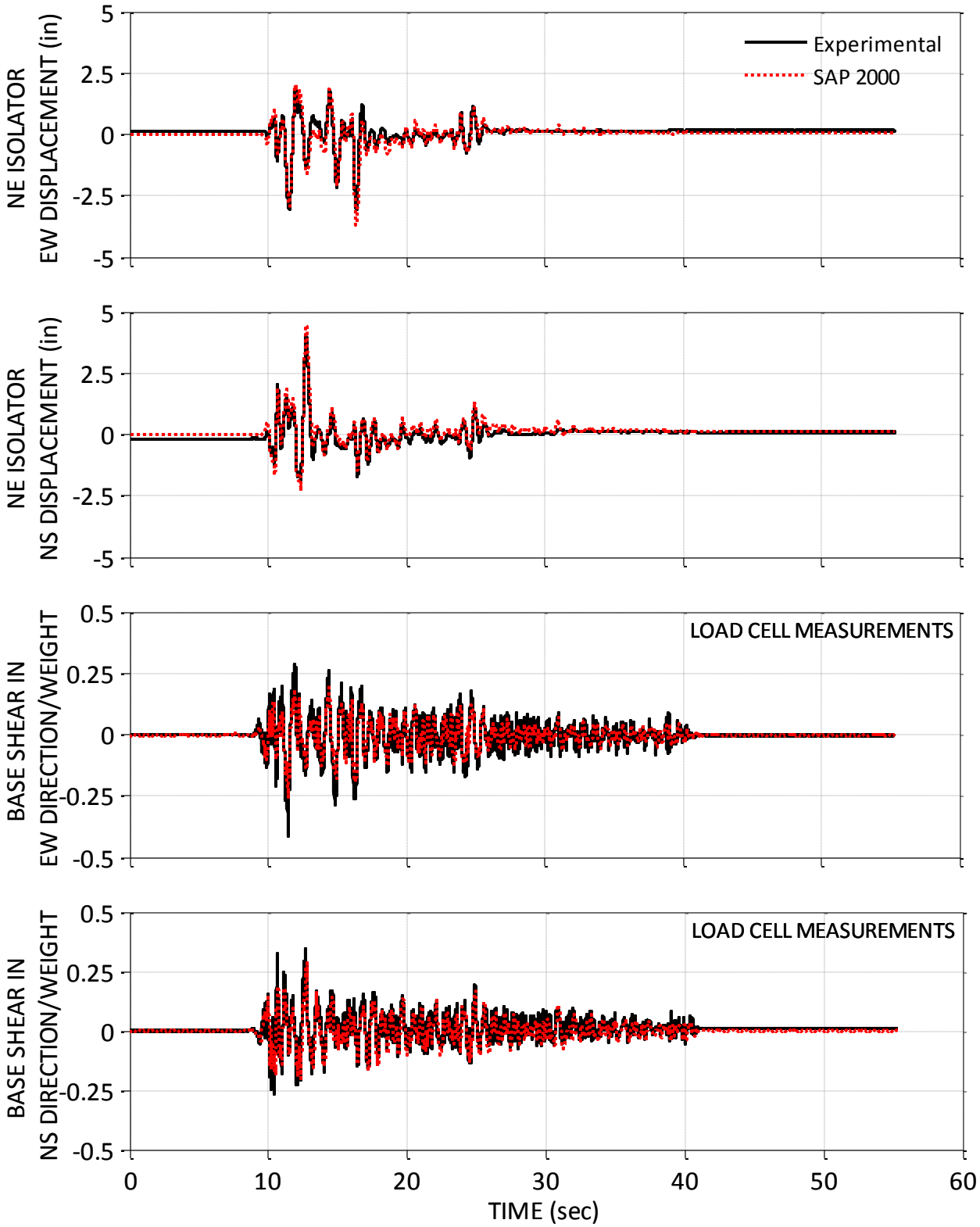


Figure 5-10 Comparison of Analytical and Experimental Results for Isolated Frame for the 300% El Centro Motion (Triple FP Isolators with Friction-Bolted Configuration, Length Scale of 3, Non-Symmetric Bushing Configuration and 3D Excitation)

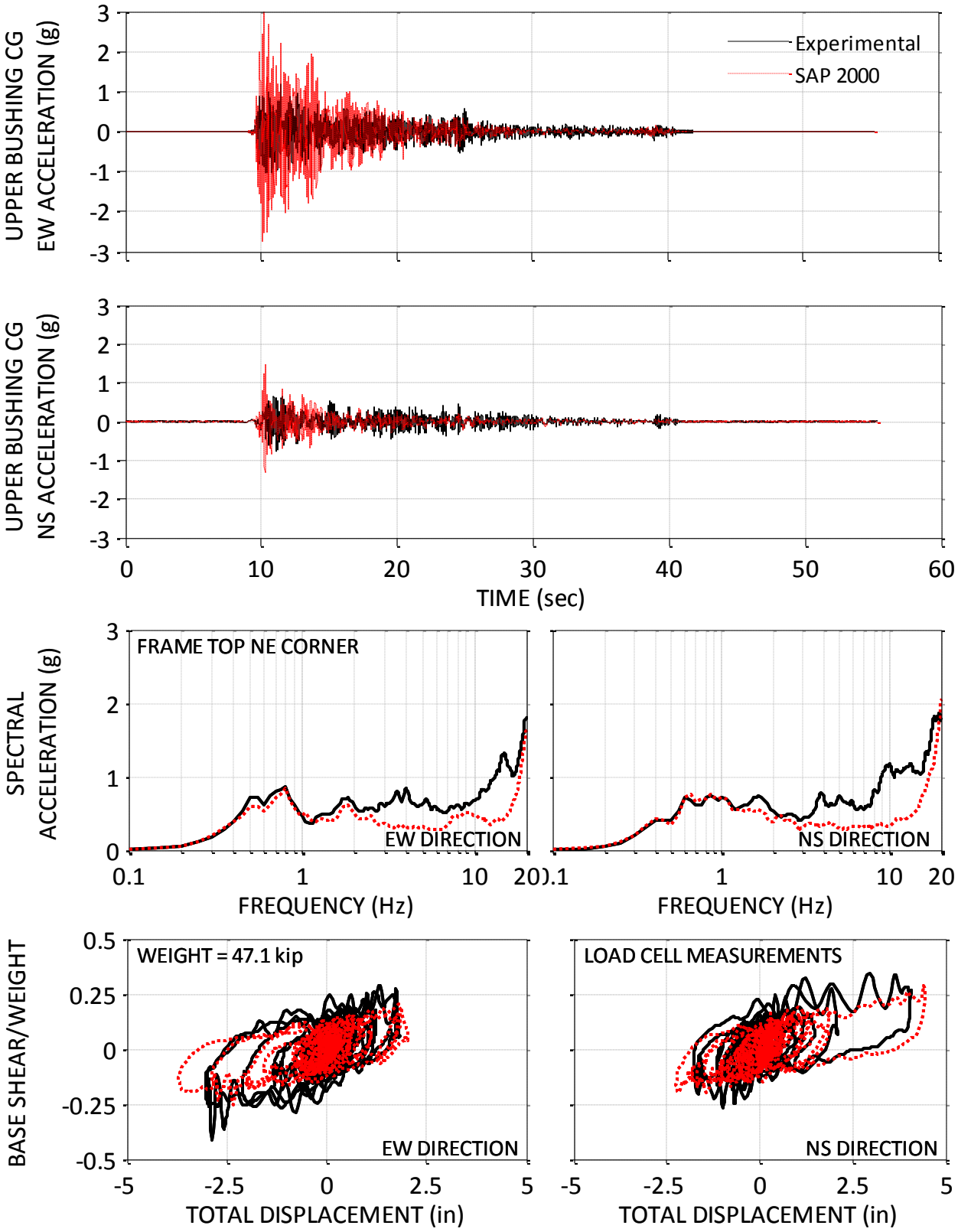


Figure 5-10 (cont'd) Comparison of Analytical and Experimental Results for Isolated Frame for the 300% El Centro Motion (Triple FP Isolators with Friction-Bolted Configuration, Length Scale of 3, Non-Symmetric Bushing Configuration and 3D Excitation)

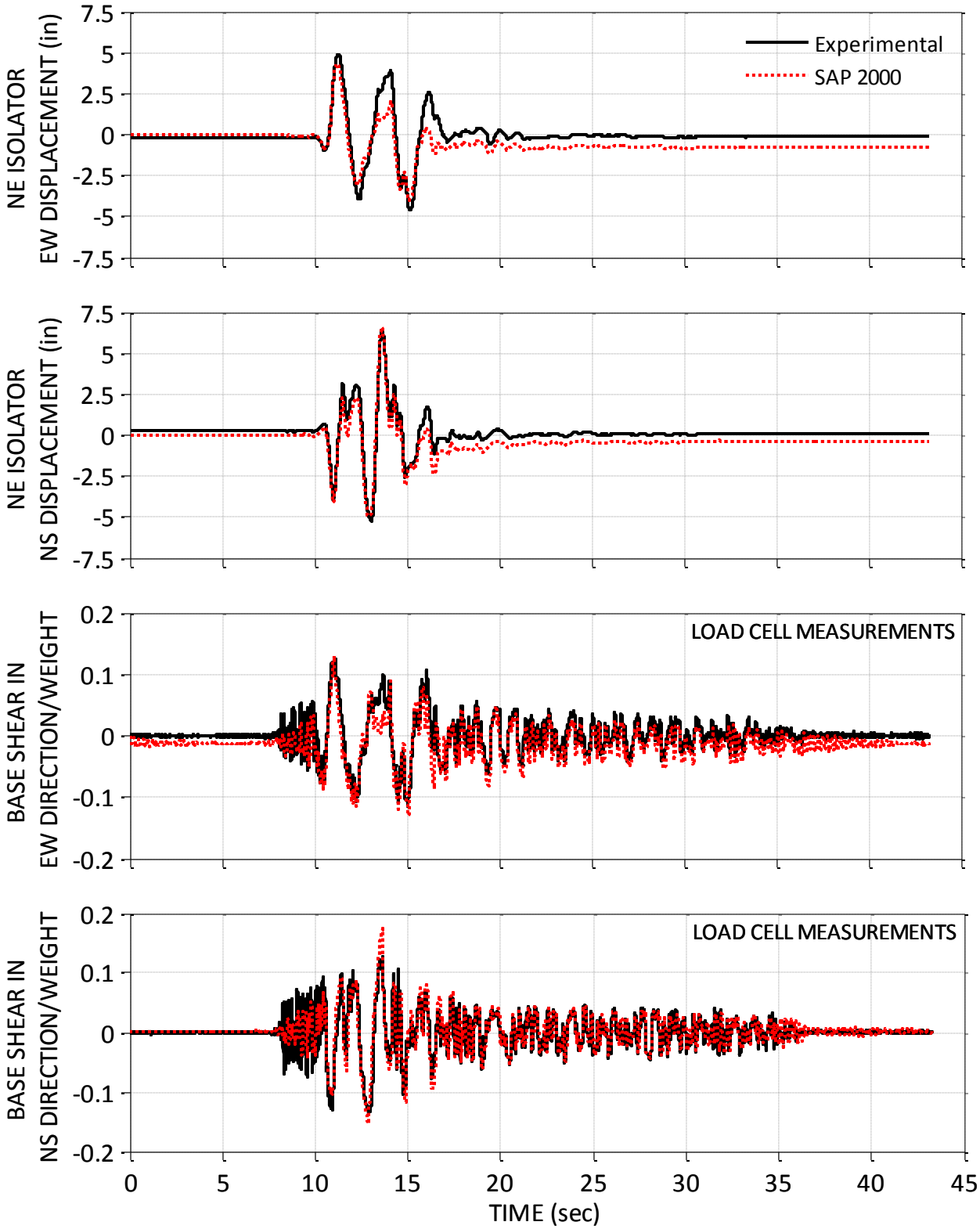


Figure 5-11 Comparison of Analytical and Experimental Results for Isolated Frame for the 97% Jensen Filter Motion (Full Size Triple FP Isolators with Friction-Bolted Configuration, Non-Symmetric Bushing Configuration and 2D Horizontal Excitation)

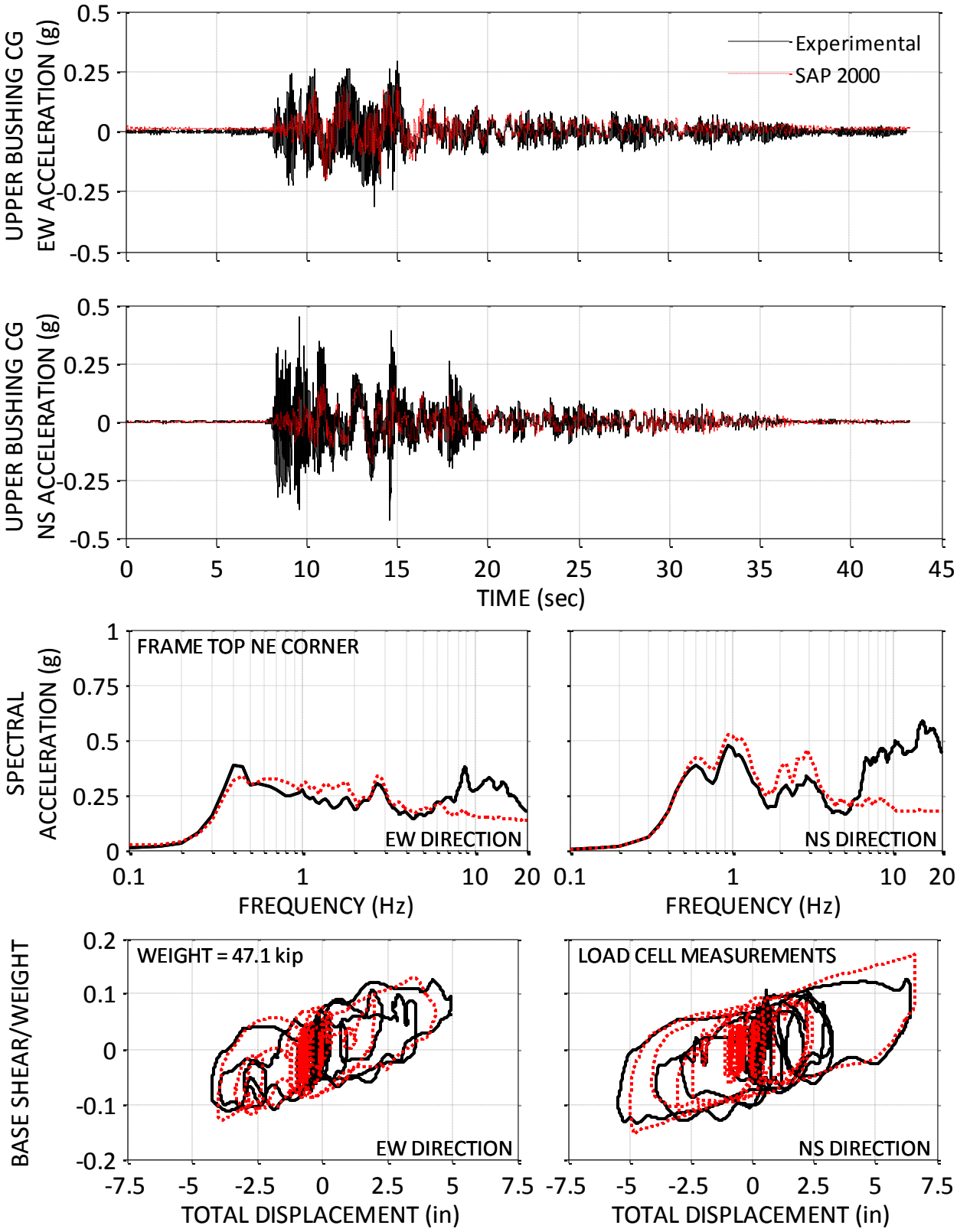


Figure 5-11 (cont'd) Comparison of Analytical and Experimental Results for Isolated Frame for the 97% Jensen Filter Motion (Full Size Triple FP Isolators with Friction-Bolted Configuration, Non-Symmetric Bushing Configuration and 2D Horizontal Excitation)

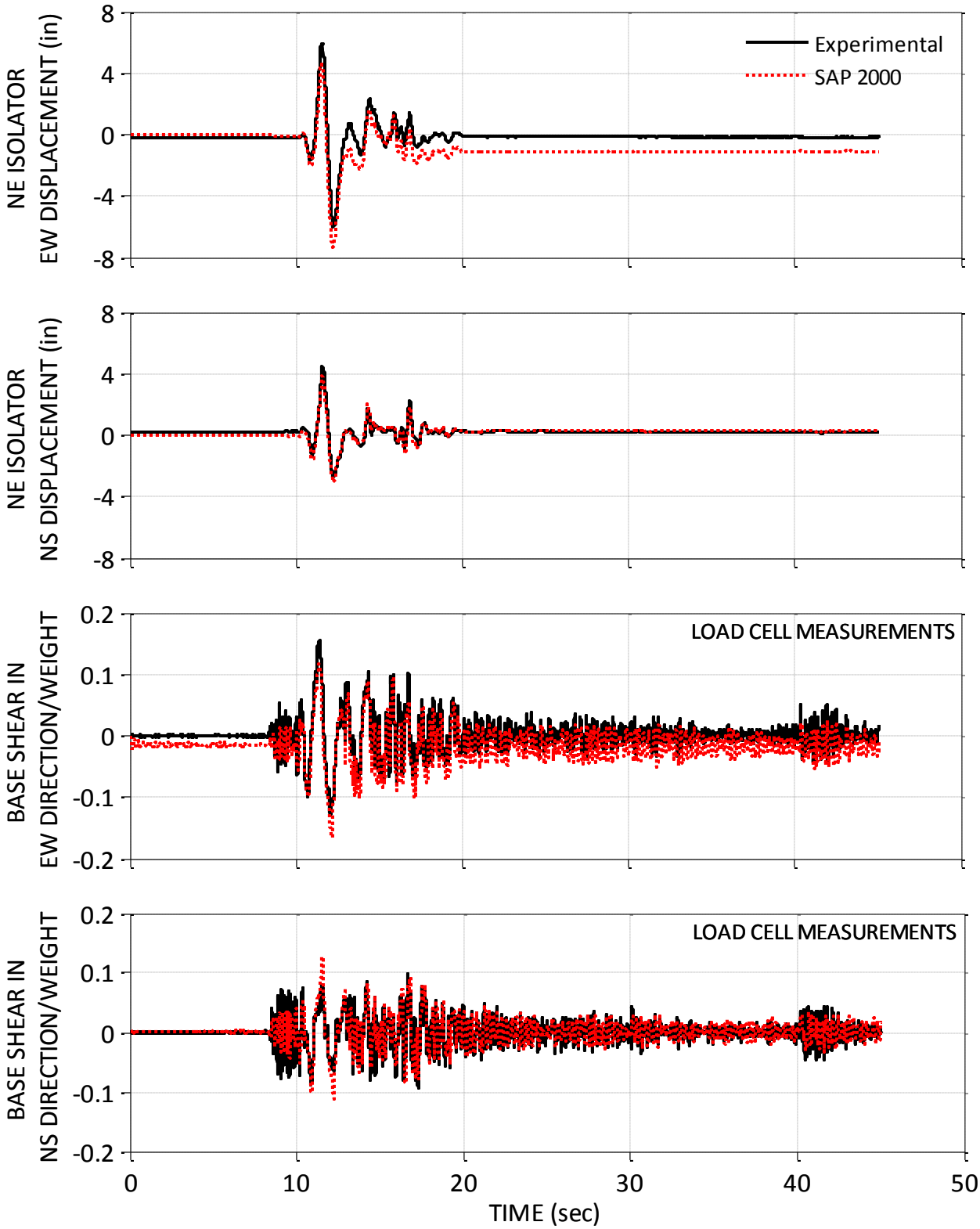


Figure 5-12 Comparison of Analytical and Experimental Results for Isolated Frame for the 75% Pacoima Dam Motion (Full Size Triple FP Isolators with Friction-Bolted Configuration, Non-Symmetric Bushing Configuration and 2D Horizontal Excitation)

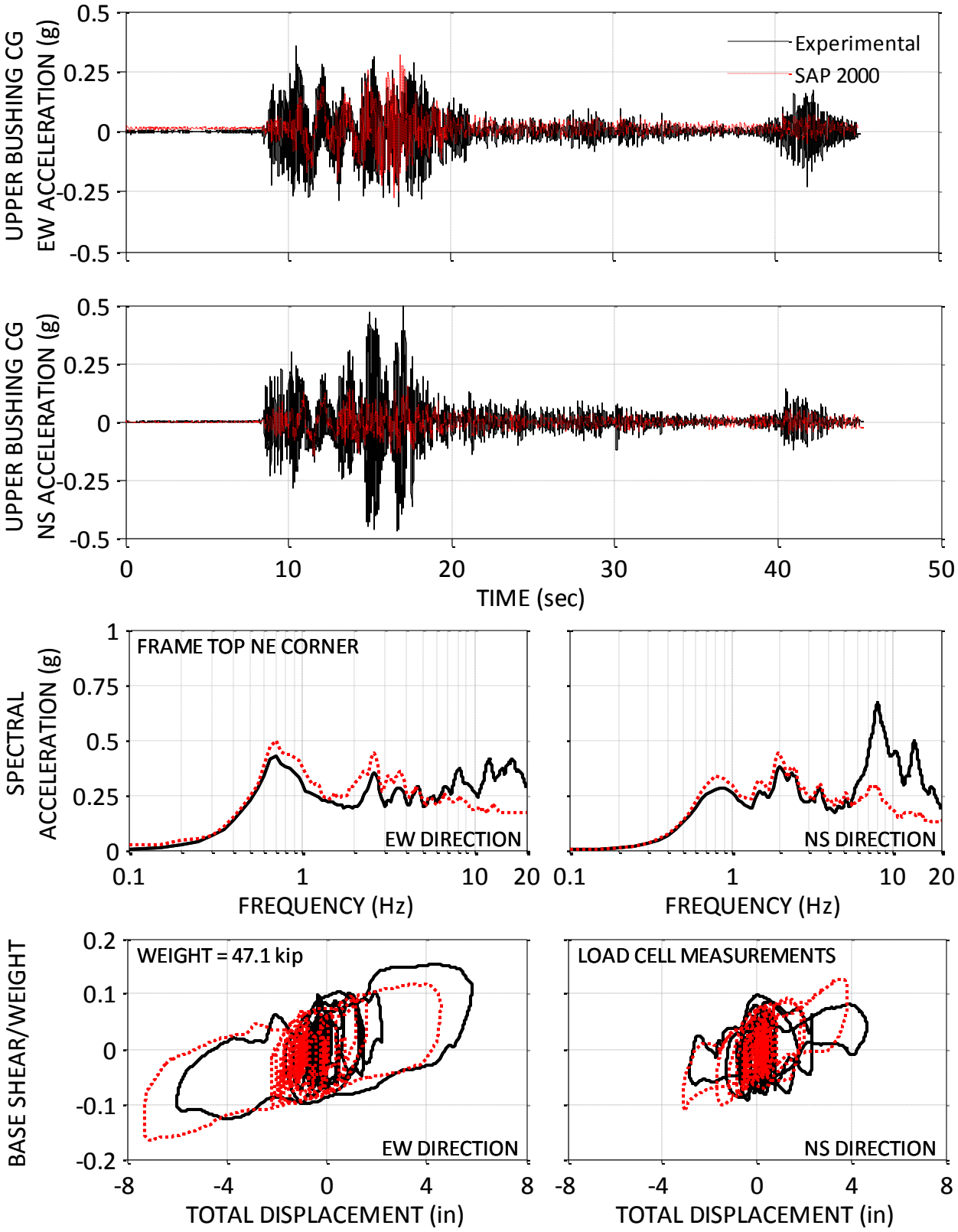


Figure 5-12 (cont'd) Comparison of Analytical and Experimental Results for Isolated Frame for the 75% Pacoima Dam Motion (Full Size Triple FP Isolators with Friction-Bolted Configuration, Non-Symmetric Bushing Configuration and 2D Horizontal Excitation)

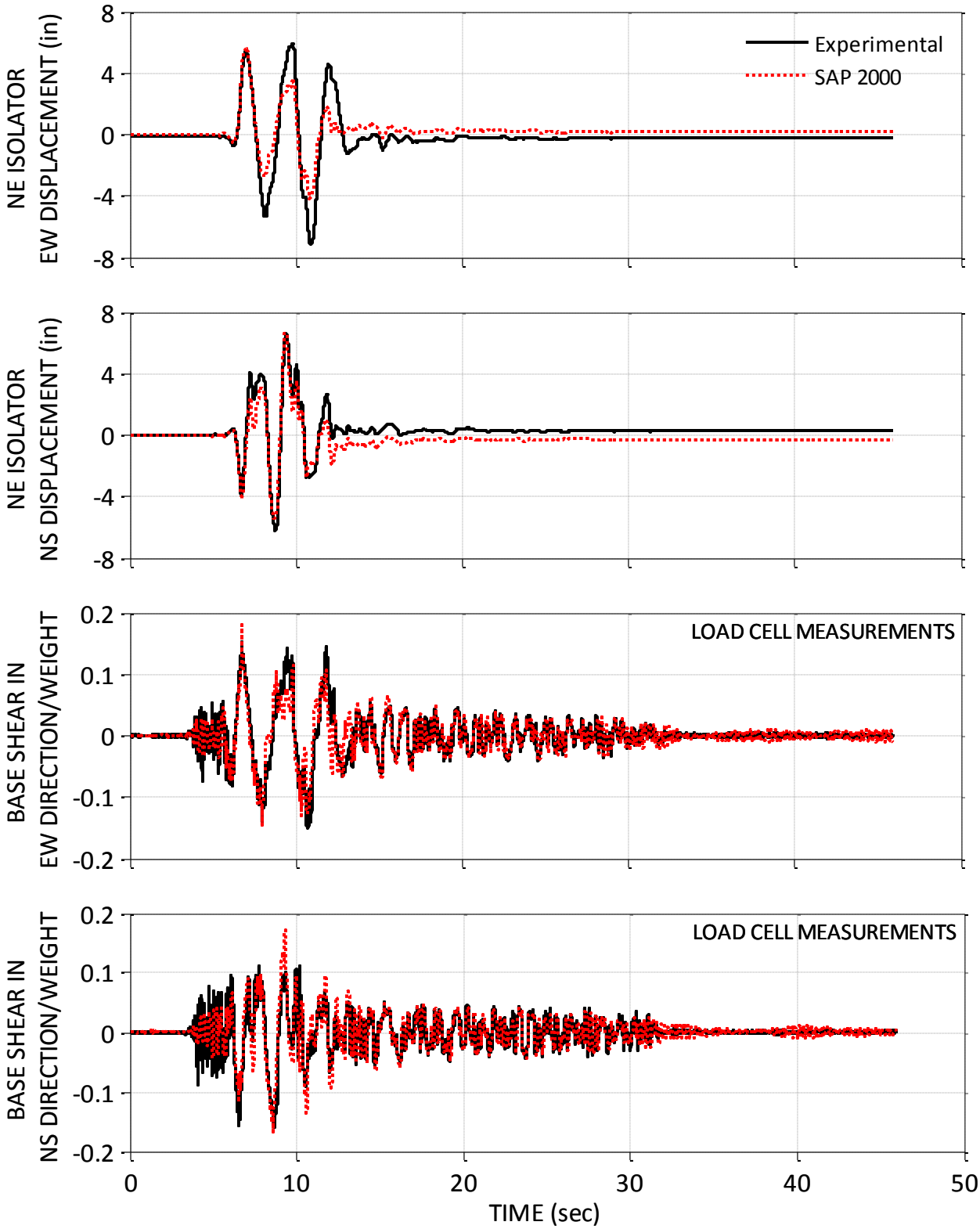


Figure 5-13 Comparison of Analytical and Experimental Results for Isolated Frame for the 97% Jensen Filter Motion (Full Size Triple FP Isolators with Friction-Bolted Configuration, Non-Symmetric Bushing Configuration and 3D Excitation)

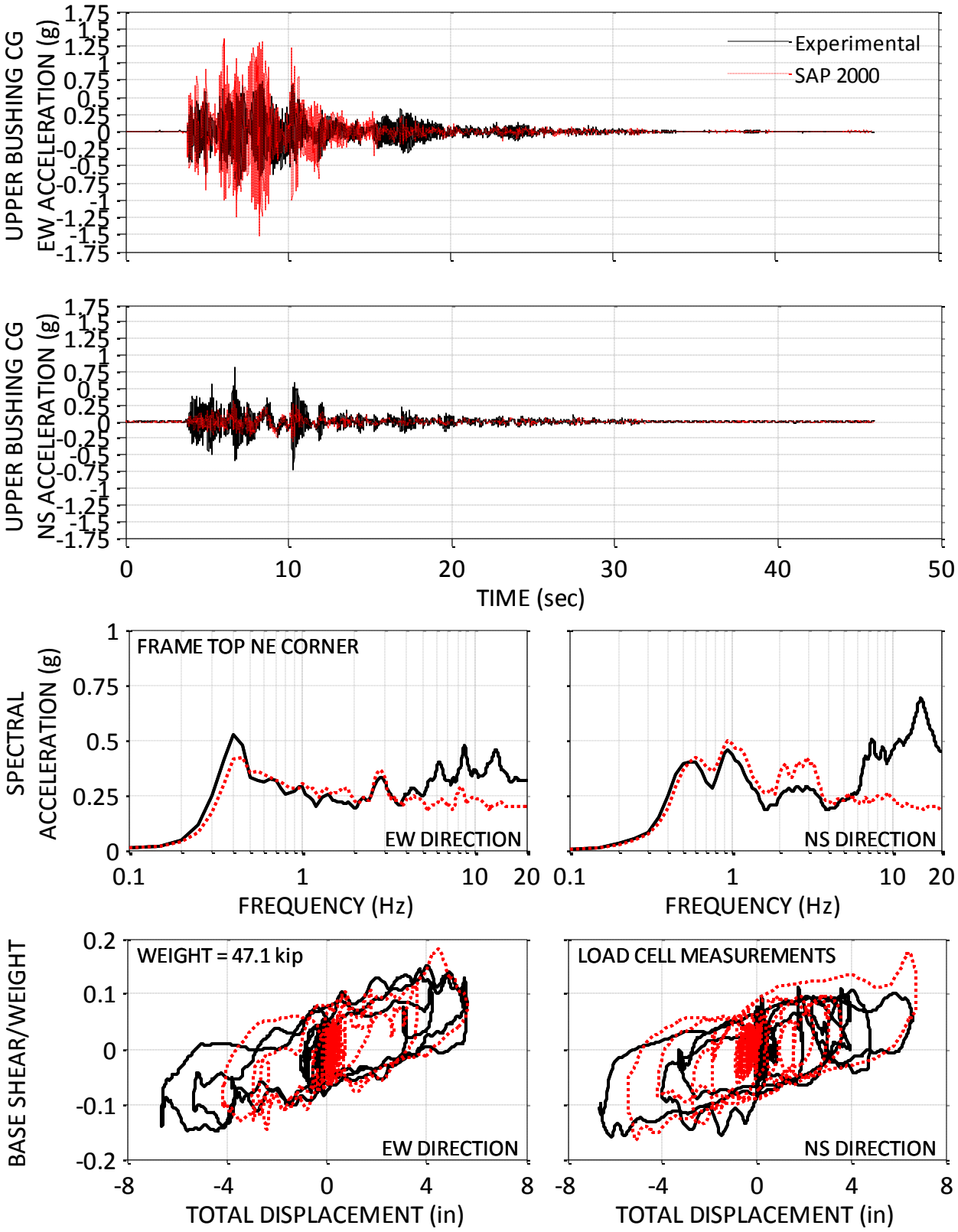


Figure 5-13 (cont'd) Comparison of Analytical and Experimental Results for Isolated Frame for the 97% Jensen Filter Motion (Full Size Triple FP Isolators with Friction-Bolted Configuration, Non-Symmetric Bushing Configuration and 3D Excitation)

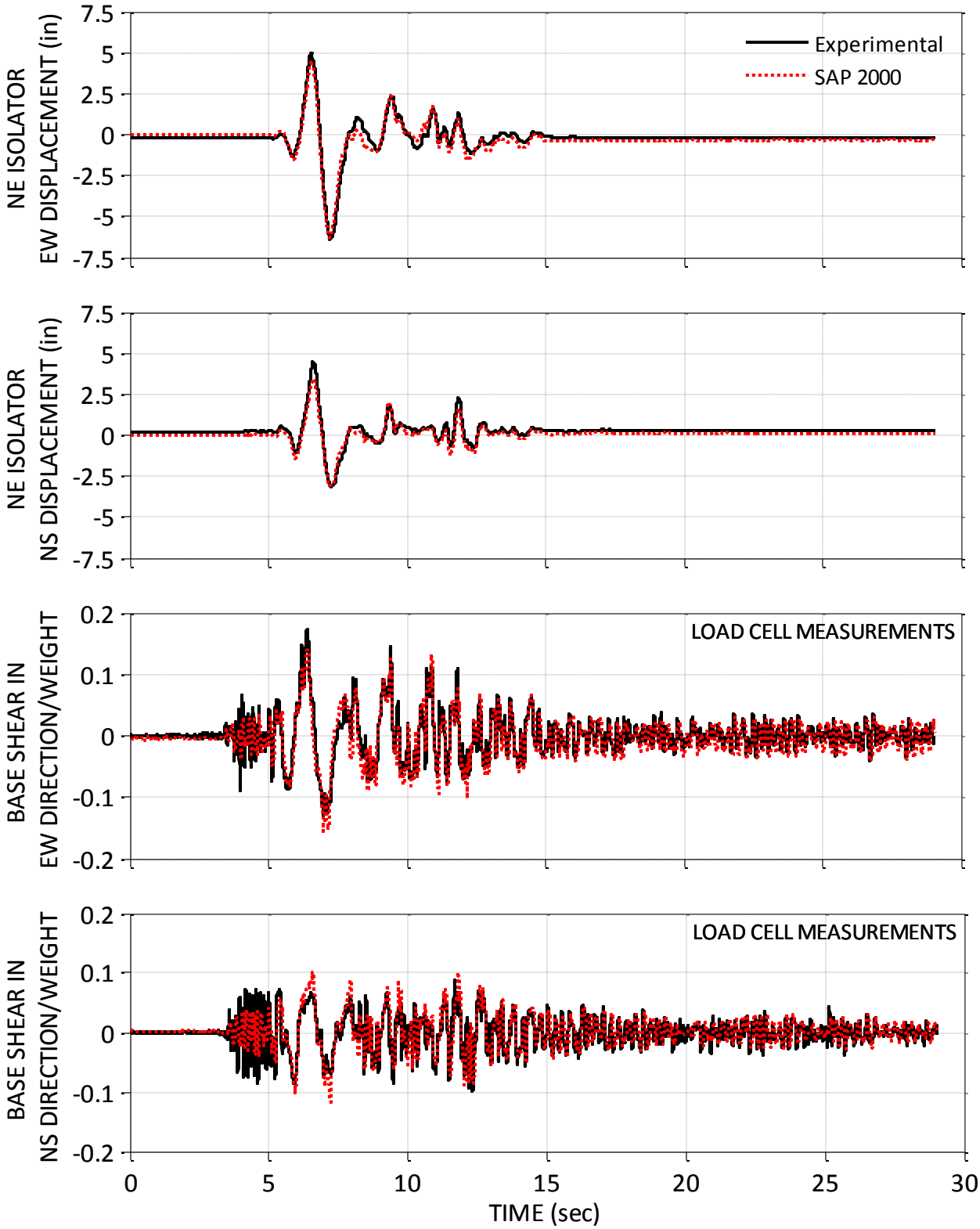


Figure 5-14 Comparison of Analytical and Experimental Results for Isolated Frame for the 75% Pacoima Dam Motion (Full Size Triple FP Isolators with Friction-Bolted Configuration, Non-Symmetric Bushing Configuration and 3D Excitation)

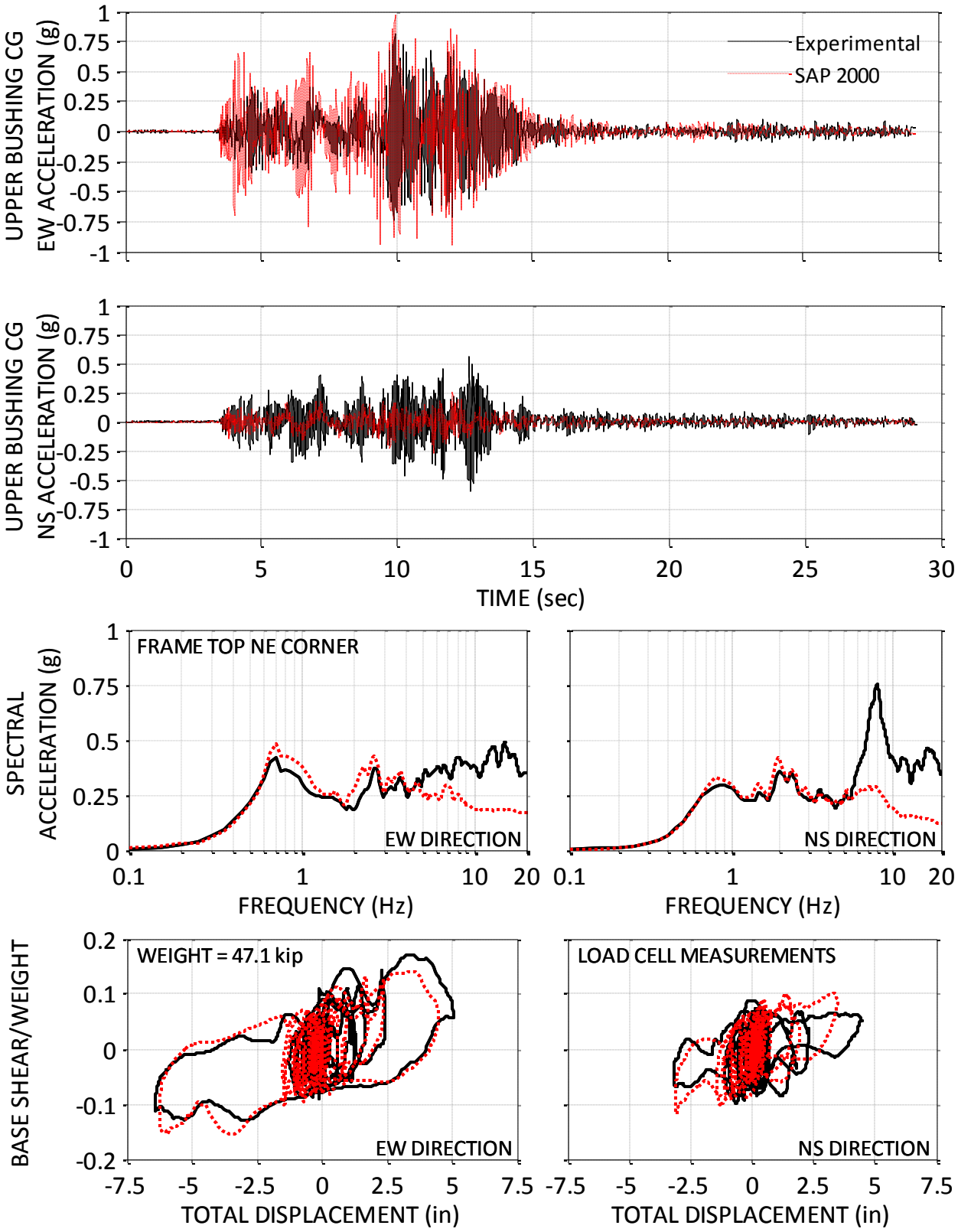


Figure 5-14 (cont'd) Comparison of Analytical and Experimental Results for Isolated Frame for the 75% Pacoima Dam Motion (Full Size Triple FP Isolators with Friction-Bolted Configuration, Non-Symmetric Bushing Configuration and 3D Excitation)

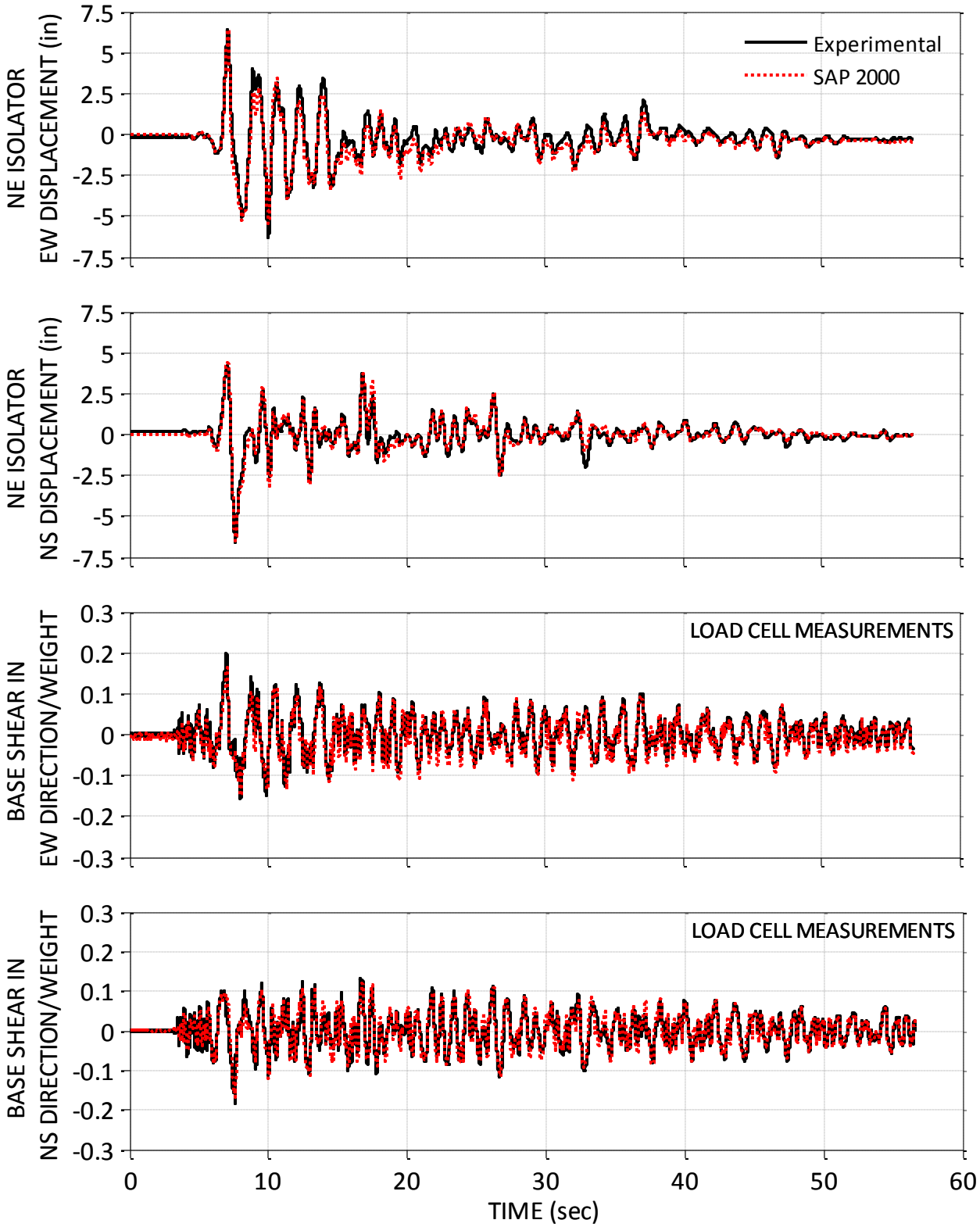


Figure 5-15 Comparison of Analytical and Experimental Results for Isolated Frame for the 500% Taft Motion (Full Size Triple FP Isolators with Friction-Bolted Configuration, Symmetric Bushing Configuration and 2D Horizontal Excitation)

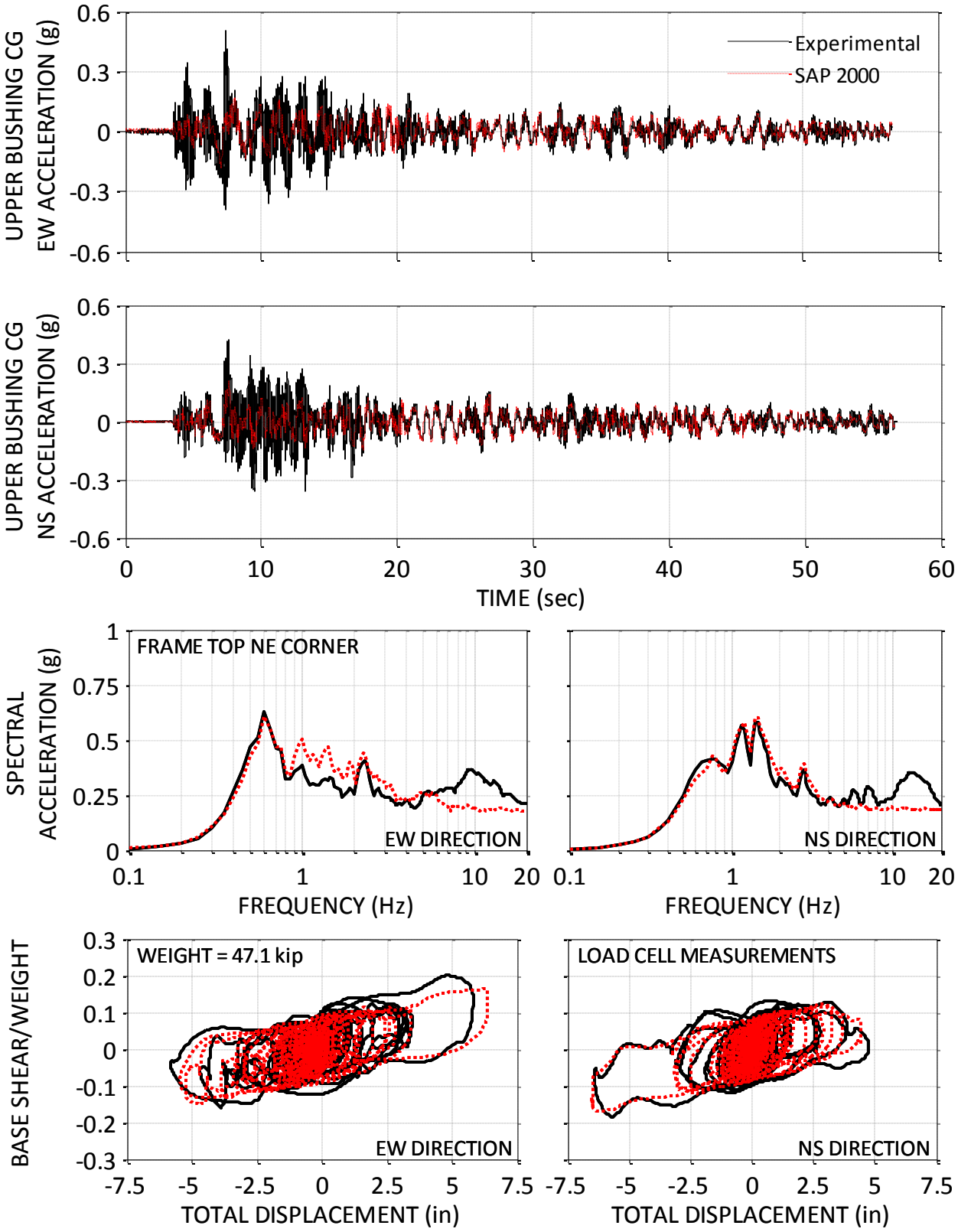


Figure 5-15 (cont'd) Comparison of Analytical and Experimental Results for Isolated Frame for the 500% Taft Motion (Full Size Triple FP Isolators with Friction-Bolted Configuration, Symmetric Bushing Configuration and 2D Horizontal Excitation)

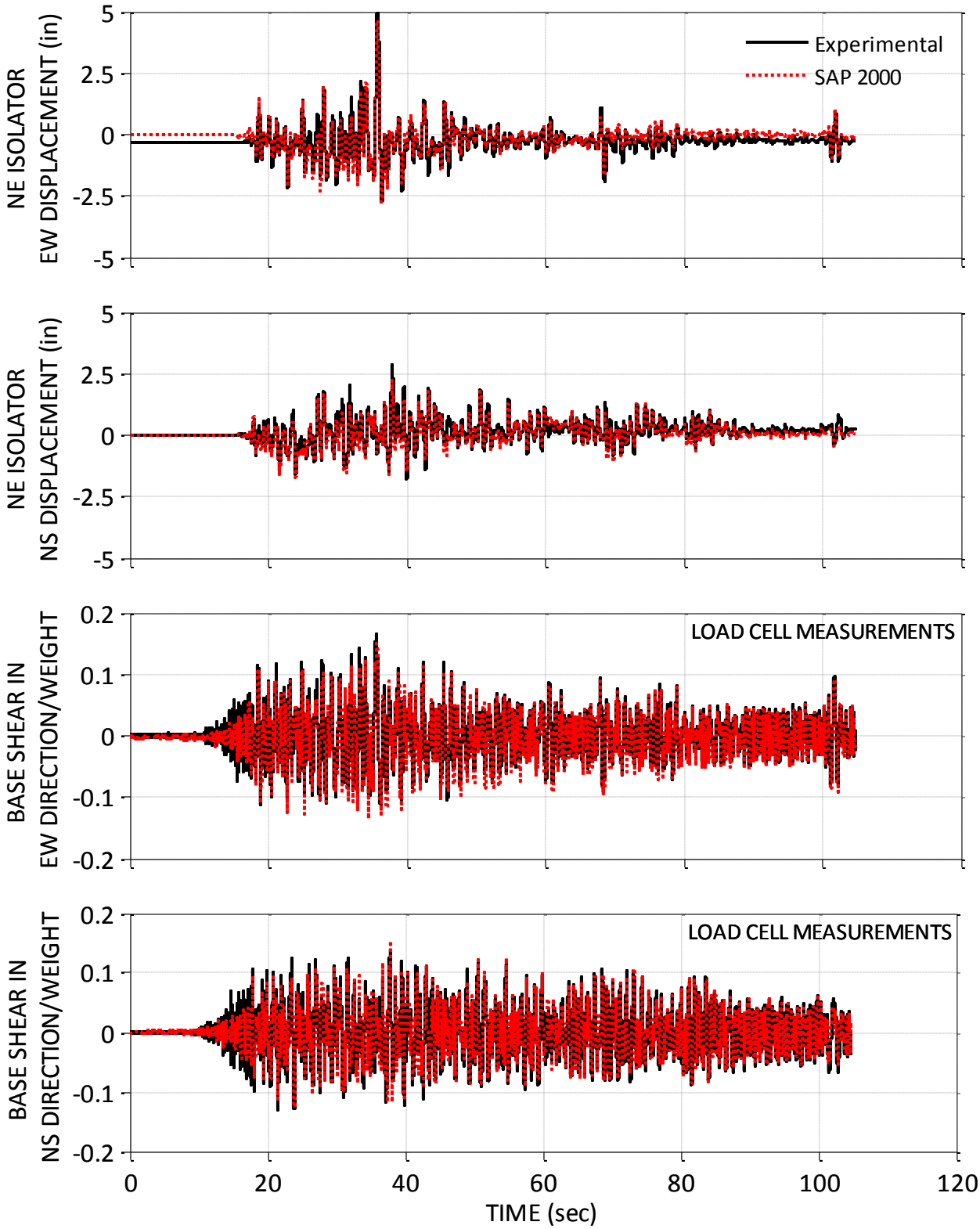


Figure 5-16 Comparison of Analytical and Experimental Results for Isolated Frame for the 100% Chile Motion (Full Size Triple FP Isolators with Friction-Bolted Configuration, Symmetric Bushing Configuration and 3D Excitation)

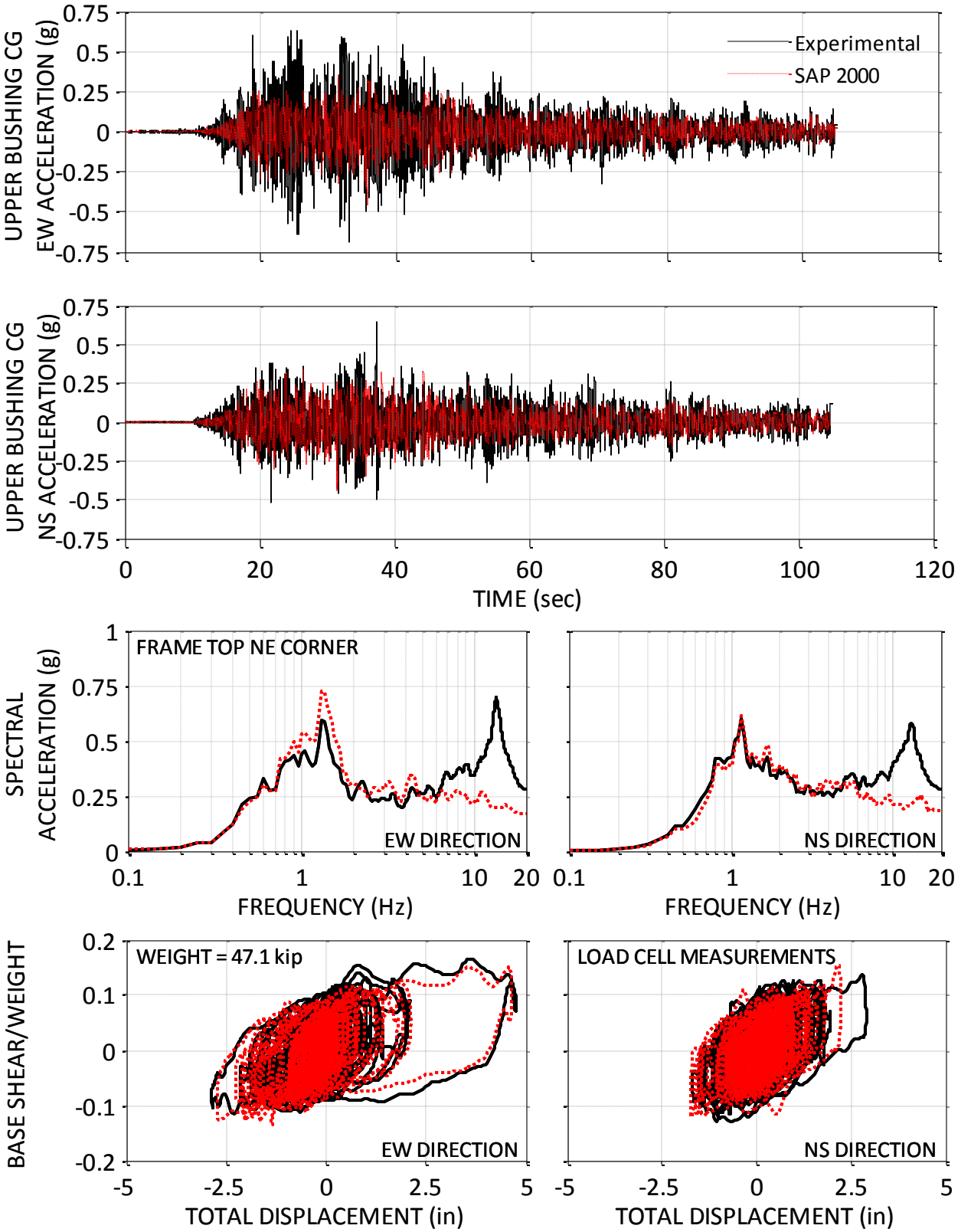


Figure 5-16 (cont'd) Comparison of Analytical and Experimental Results for Isolated Frame for the 100% Chile Motion (Full Size Triple FP Isolators with Friction-Bolted Configuration, Symmetric Bushing Configuration and 3D Excitation)

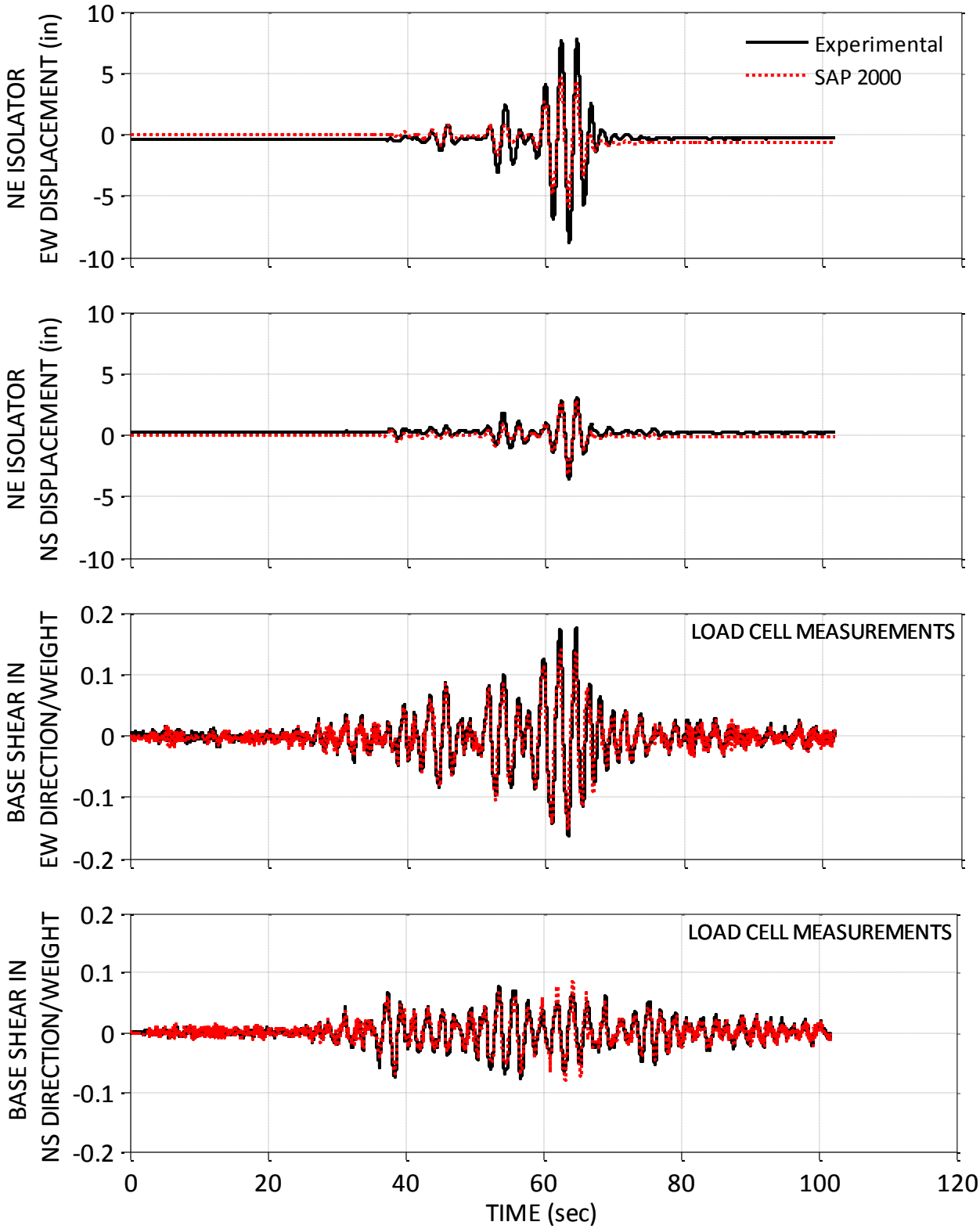


Figure 5-17 Comparison of Analytical and Experimental Results for Isolated Frame for the 70% Mexico Motion (Full Size Triple FP Isolators with Friction-Bolted Configuration, Symmetric Bushing Configuration and 3D Excitation)

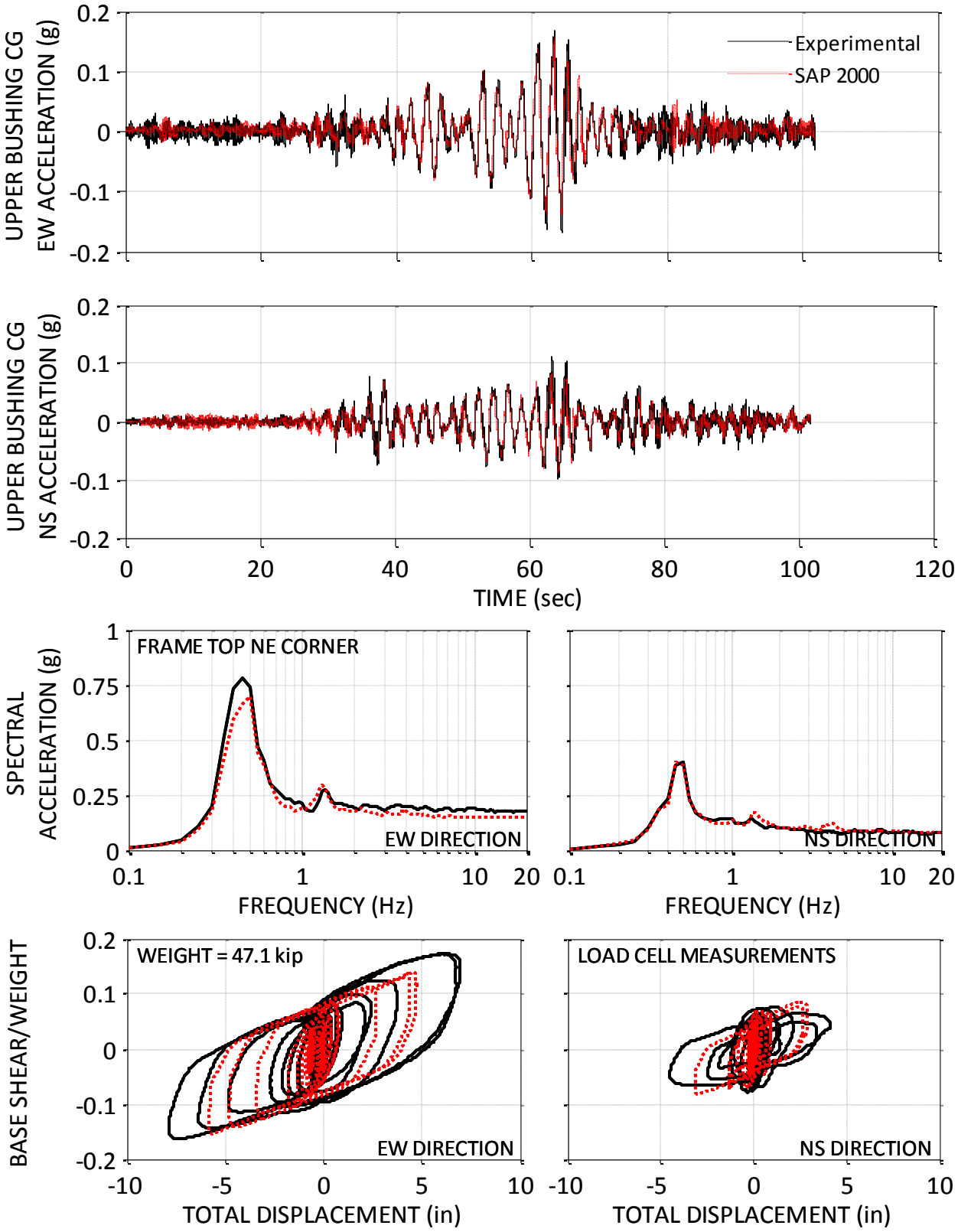


Figure 5-17 (cont'd) Comparison of Analytical and Experimental Results for Isolated Frame for the 70% Mexico Motion (Full Size Triple FP Isolators with Friction-Bolted Configuration, Symmetric Bushing Configuration and 3D Excitation)

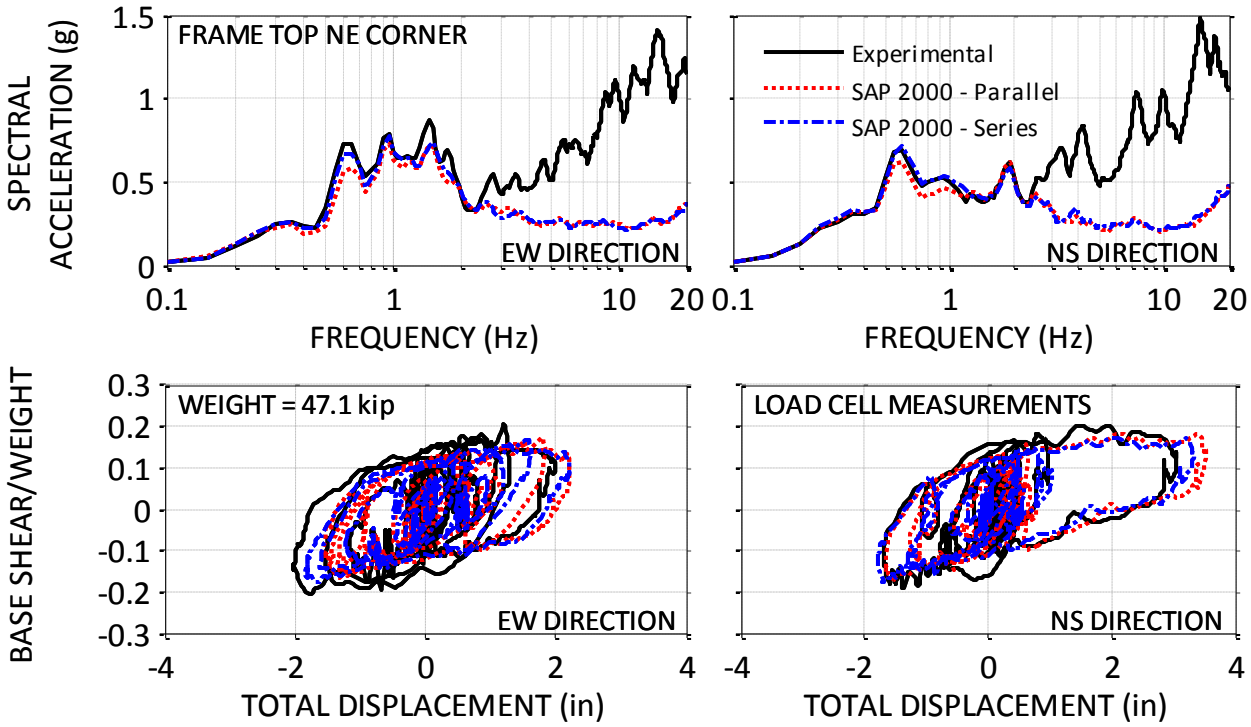


Figure 5-18 Comparison of Series and Parallel Models, and Experimental Results for Isolated Frame for the 137% Karakyr Motion (Triple FP Isolators with Friction-Bolted Configuration, Length Scale of 3, Symmetric Bushing Configuration and 2D Excitation)

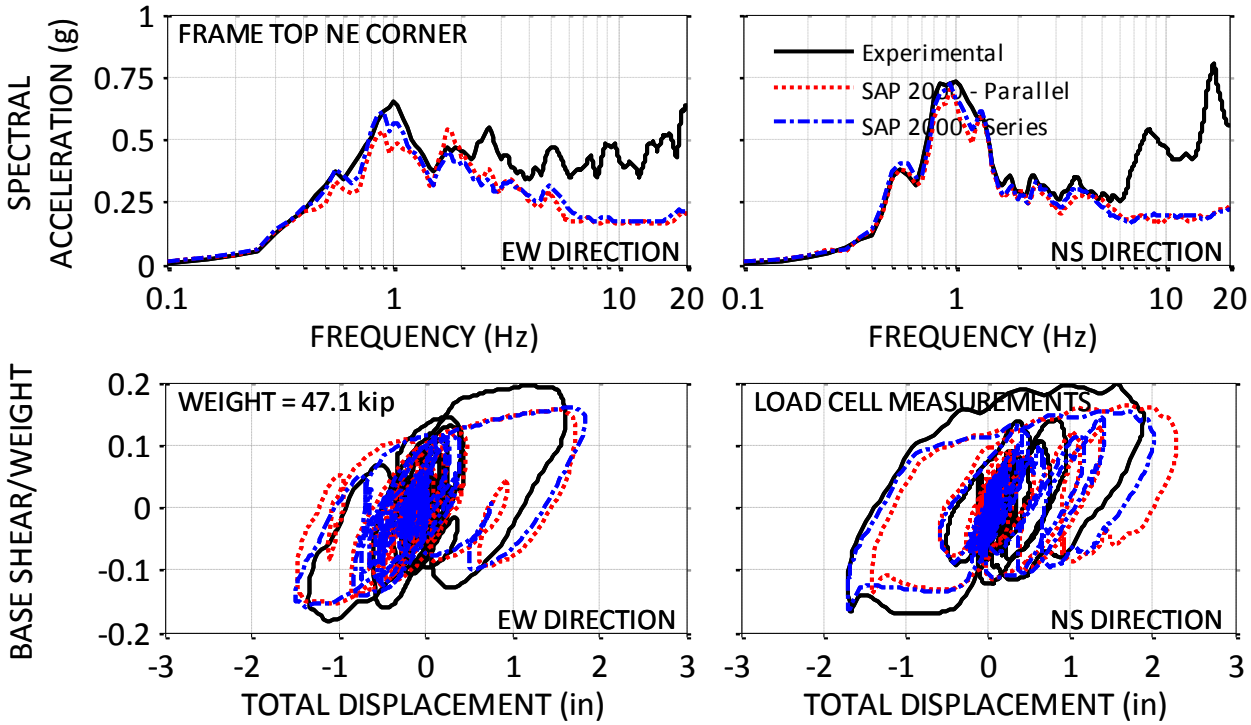


Figure 5-19 Comparison of Series and Parallel Models, and Experimental Results for Isolated Frame for the 104% Bolu Motion (Triple FP Isolators with Friction-Bolted Configuration, Length Scale of 3, Symmetric Bushing Configuration and 2D Excitation)

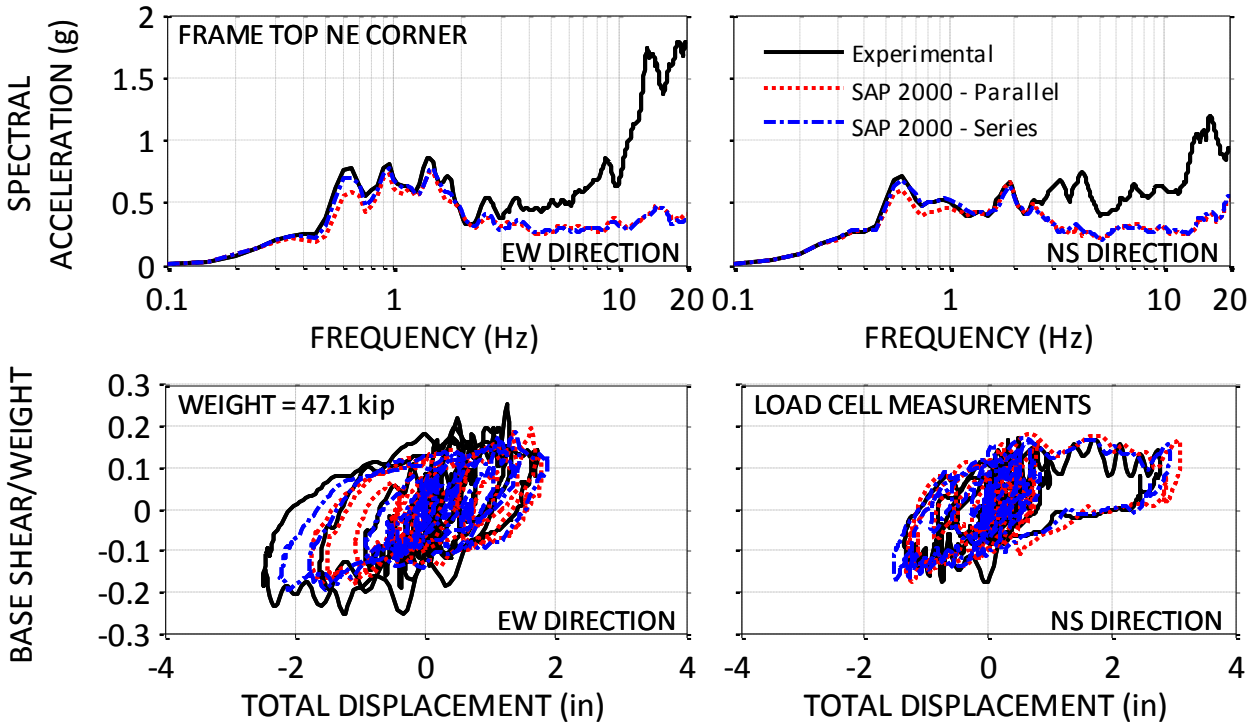


Figure 5-20 Comparison of Series and Parallel Models, and Experimental Results for Isolated Frame for the 137% Karakyr Motion (Triple FP Isolators with Friction-Bolted Configuration, Length Scale of 3, Symmetric Bushing Configuration and 3D Excitation)

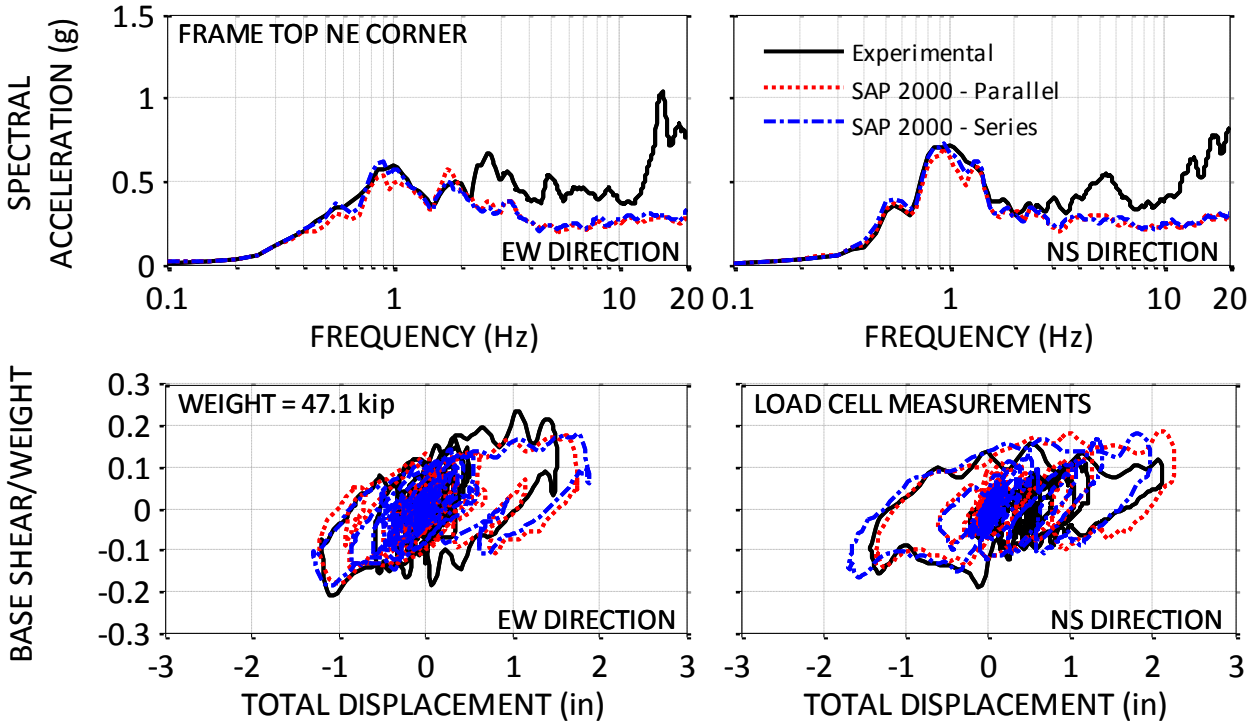


Figure 5-21 Comparison of Series and Parallel Models, and Experimental Results for Isolated Frame for the 104% Bolu Motion (Triple FP Isolators with Friction-Bolted Configuration, Length Scale of 3, Symmetric Bushing Configuration and 3D Excitation)

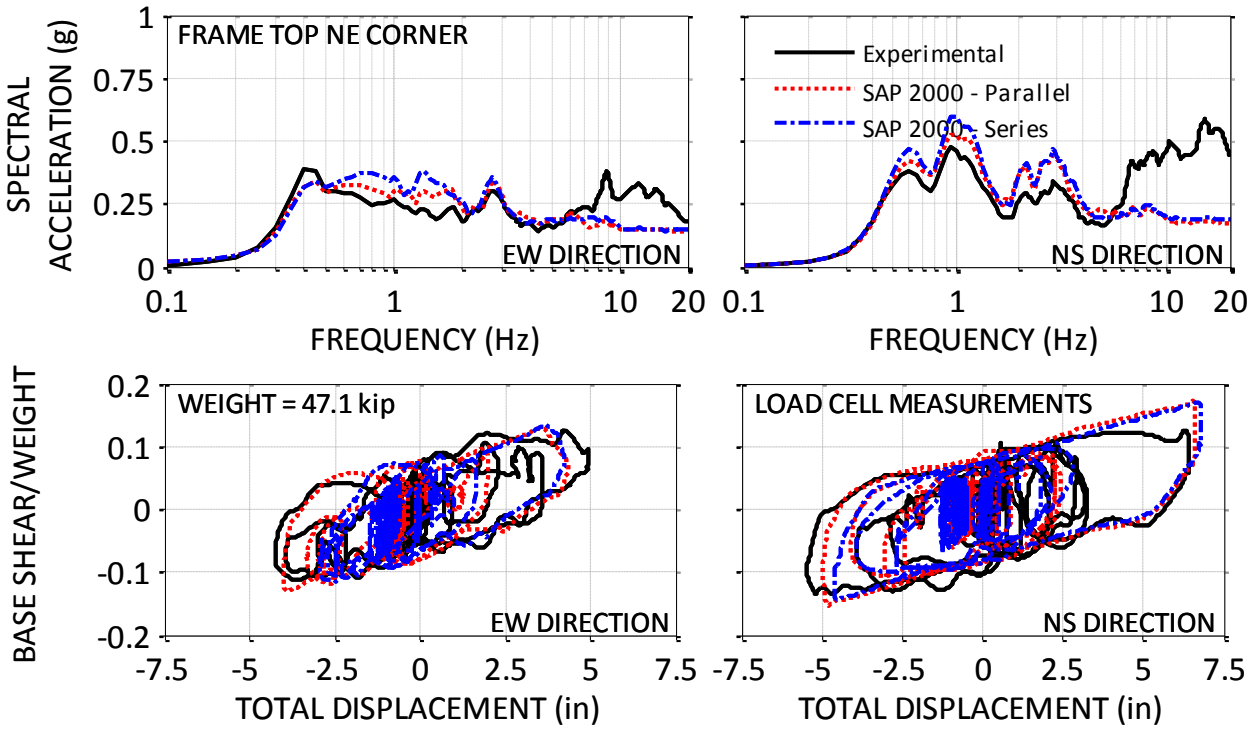


Figure 5-22 Comparison of Series and Parallel Models, and Experimental Results for Isolated Frame for the 97% Jensen Filter Motion (Full Size Triple FP Isolators with Friction-Bolted Configuration, Non-Symmetric Bushing Configuration and 2D Excitation)

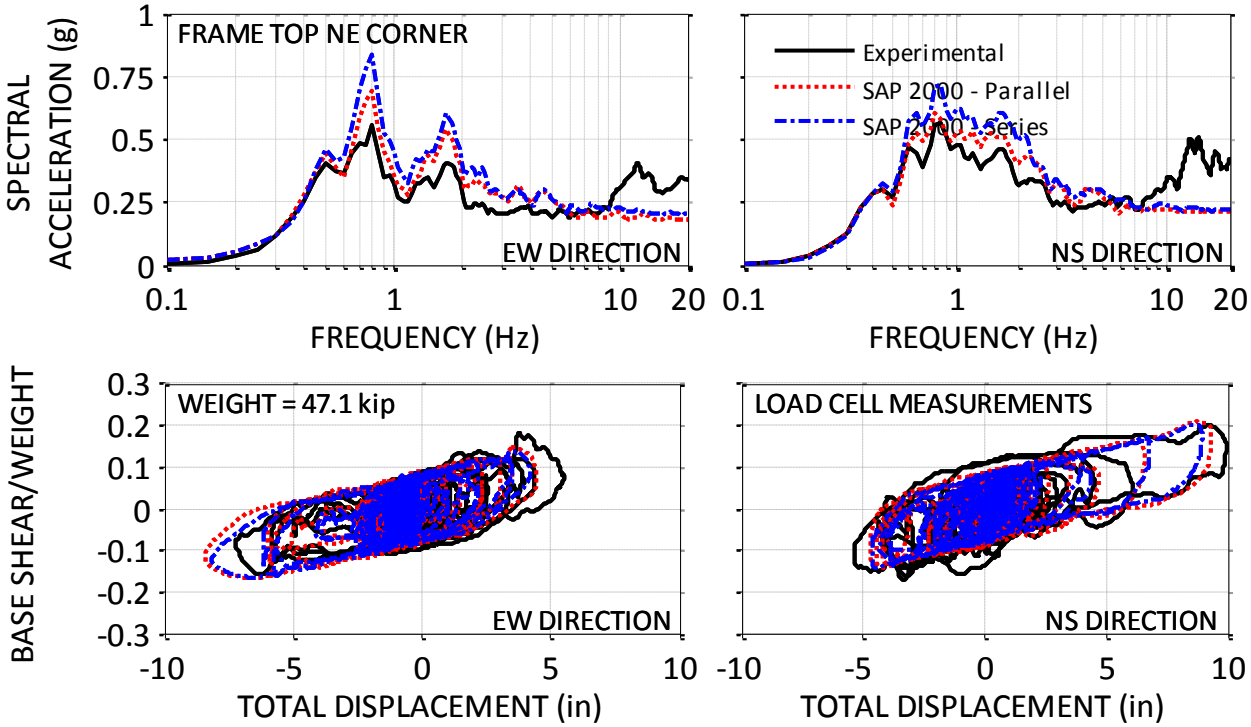


Figure 5-23 Comparison of Series and Parallel Models, and Experimental Results for Isolated Frame for the 300% El Centro Motion (Full Size Triple FP Isolators with Friction-Bolted Configuration, Non-Symmetric Bushing Configuration and 2D Excitation)

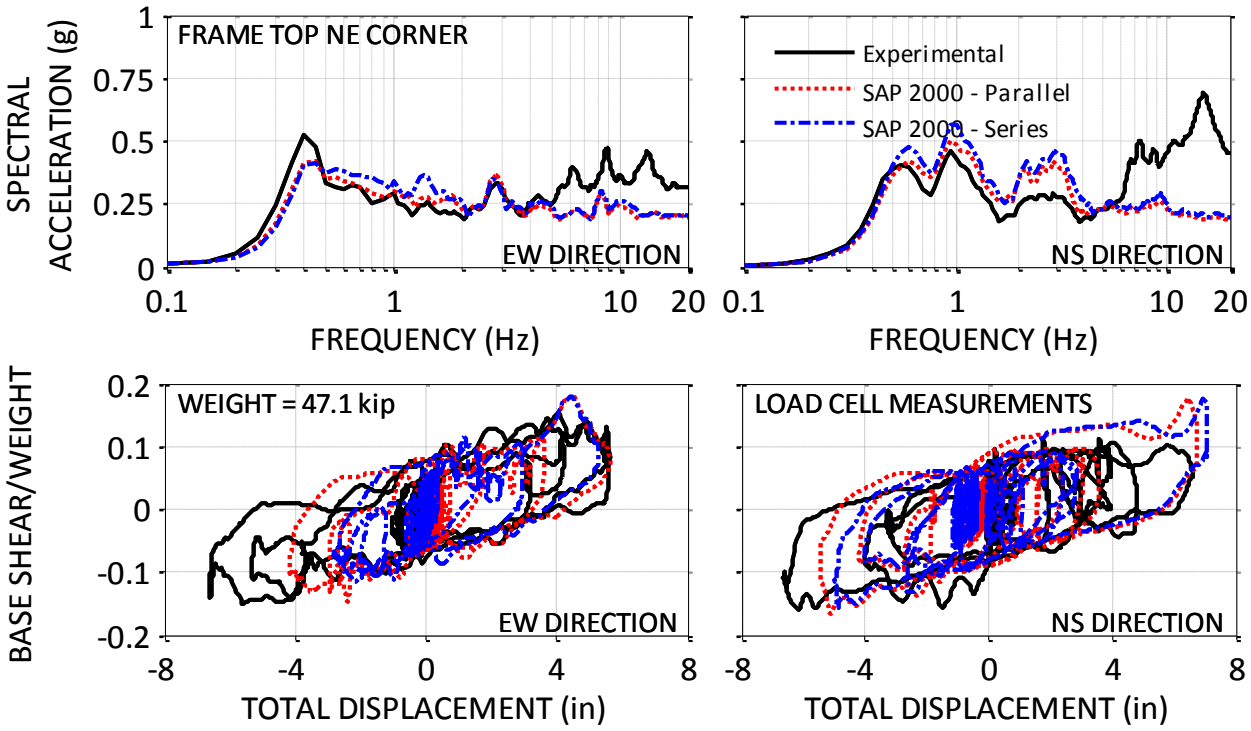


Figure 5-24 Comparison of Series and Parallel Models, and Experimental Results for Isolated Frame for the 97% Jensen Filter Motion (Full Size Triple FP Isolators with Friction-Bolted Configuration, Non-Symmetric Bushing Configuration and 3D Excitation)

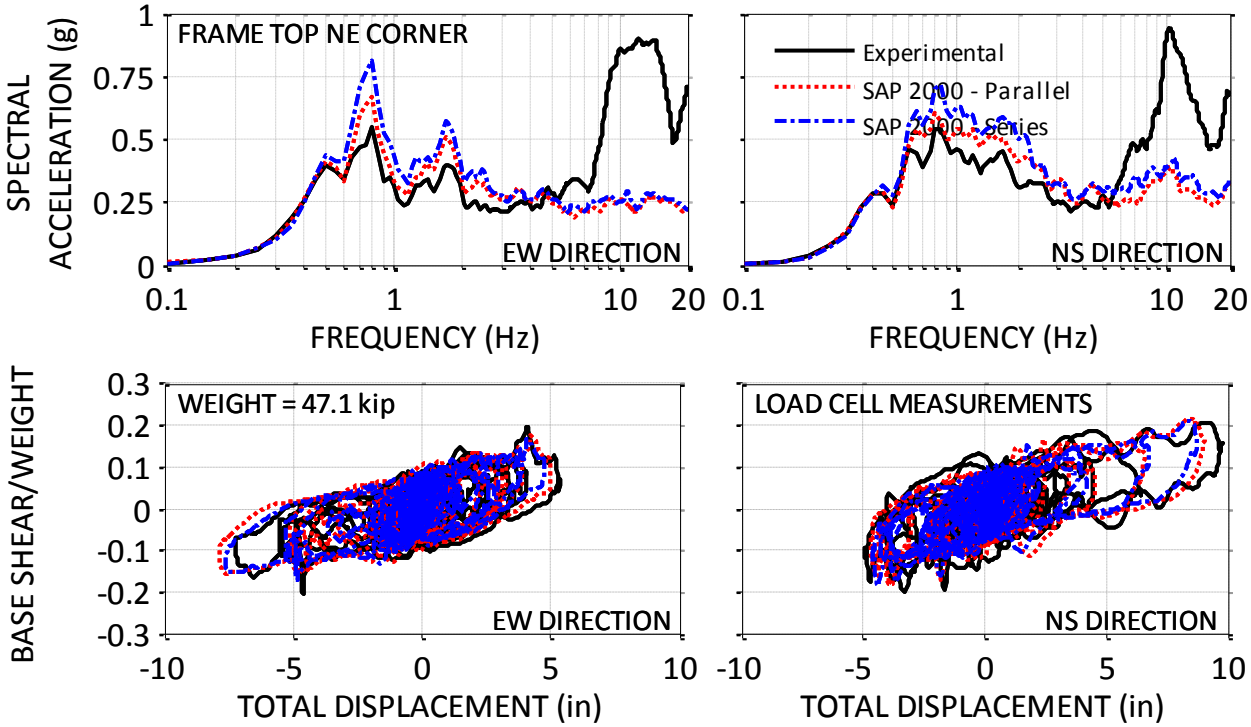


Figure 5-25 Comparison of Series and Parallel Models, and Experimental Results for Isolated Frame for the 300% El Centro Motion (Full Size Triple FP Isolators with Friction-Bolted Configuration, Non-Symmetric Bushing Configuration and 3D Excitation)

Furthermore, Table 5-6 to Table 5-8 provide comparisons between peak values of selected experimental and analytical response quantities, for the configurations with Lead Rubber and Triple Friction Pendulum isolators (parallel and series models). Average values for these quantities and percentile differences between the averages are also provided. At this point, it should be noted that a typical design of a seismic isolation system, involves the selection of a ground motion ensemble with at least 7 components, scaling of the motions to a site specific spectrum, modeling the isolated structure in structural analysis software and obtaining average values of selected response quantities-the average values to be used as design parameters. In view of the fact that the tabular results have been drawn from analysis and testing with an ensemble of 7 scaled ground motions, as would be the case for an actual design scenario, arguably the results presented herein allow for realistic evaluations of the predicted and actual responses of the isolation systems.

Table 5-6 Comparison of Analytical and Experimental Peak Responses for Selected Sets of Tests and Isolation with Lead Rubber Bearings in Bolted-Bolted Configuration (Length Scale of 3, Symmetric Bushing Configuration)

Motion		**Resultant Corner Displ.**	**Frame Top Corner Accel.**		**Upper Bushing CG Accel.**		**Base Shear**	
			EW	**NS**	**EW**	**NS**	**EW**	**NS**
		(in)	**(g)**	**(g)**	**(g)**	**(g)**	**(kip)**	**(kip)**
Lead Rubber Bearings (Bolted-Bolted Configuration, 2D Testing)								
Karakyr	Test	3.81	0.48	0.35	0.58	0.57	24.74	19.67
	SAP	3.72	0.48	0.40	0.45	0.42	24.48	18.06
LGPC	Test	3.76	0.48	0.32	0.56	0.35	23.04	14.55
	SAP	2.95	0.48	0.32	0.53	0.35	21.86	12.25
Saratoga	Test	4.22	0.54	0.31	0.64	0.51	17.52	10.41
	SAP	3.72	0.54	0.28	0.56	0.41	17.33	10.47
Jensen Filter	Test	3.42	0.34	0.39	0.42	0.51	17.29	21.43
	SAP	2.61	0.27	0.37	0.29	0.39	14.57	18.43
Sylmar	Test	3.92	0.41	0.54	0.64	0.56	17.55	17.25
	SAP	3.08	0.44	0.52	0.42	0.53	15.65	18.08
Takarazuka	Test	4.35	0.43	0.54	0.41	0.70	17.93	23.93
	SAP	3.99	0.43	0.54	0.40	0.46	15.88	25.05
Bolu	Test	2.77	0.31	0.36	0.37	0.35	15.50	20.11
	SAP	2.55	0.25	0.37	0.29	0.36	12.67	20.45
Average	***Test***	***3.75***	***0.43***	***0.40***	***0.52***	***0.51***	***19.08***	***18.19***
	SAP	***3.23***	***0.41***	***0.40***	***0.42***	***0.42***	***17.49***	***17.54***
% Difference		***-13.8%***	***-3.1%***	***-0.7%***	***-18.7%***	***-17.9%***	***-8.3%***	***-3.6%***

Table 5-7 Comparison of Analytical (Parallel Model) and Experimental Peak Responses for Selected Sets of Tests and Isolation with Triple Friction Pendulum Bearings in Friction-Bolted Configuration (Length Scale of 3, Symmetric Bushing Configuration)

Motion		Resultant Corner Displ.	Frame Top Corner Accel.		Upper Bushing CG Accel.		Base Shear	
			EW	NS	EW	NS	EW	NS
		(in)	(g)	(g)	(g)	(g)	(kip)	(kip)
Triple Friction Pendulum Bearings (2D Testing, Analysis with the Parallel Model)								
Karakyr	Test	3.60	0.39	0.29	0.82	0.79	9.64	9.54
	SAP	3.77	0.20	0.27	0.31	0.38	8.18	8.59
LGPC	Test	3.94	0.28	0.20	0.44	0.32	8.90	8.47
	SAP	4.92	0.24	0.16	0.25	0.21	7.13	6.31
Saratoga	Test	3.30	0.21	0.18	0.36	0.31	10.35	6.67
	SAP	3.02	0.18	0.20	0.22	0.23	9.72	5.27
Jensen Filter	Test	2.76	0.20	0.19	0.39	0.49	8.73	9.50
	SAP	2.73	0.18	0.17	0.22	0.19	8.18	9.02
Sylmar	Test	3.67	0.20	0.22	0.42	0.44	9.77	8.36
	SAP	3.25	0.15	0.22	0.20	0.22	9.46	7.63
Takarazuka	Test	2.68	0.21	0.20	0.37	0.36	7.98	8.17
	SAP	2.41	0.15	0.18	0.18	0.23	5.96	7.18
Bolu	Test	2.17	0.24	0.21	0.42	0.27	9.22	9.30
	SAP	2.53	0.16	0.14	0.19	0.15	7.40	7.75
Average	***Test***	***3.16***	***0.25***	***0.21***	***0.46***	***0.43***	***9.23***	***8.57***
	SAP	***3.23***	***0.18***	***0.19***	***0.22***	***0.23***	***8.00***	***7.39***
% Difference		***2.2%***	***-27.9%***	***-9.4%***	***-51.8%***	***-46.6%***	***-13.3%***	***-13.8%***
Triple Friction Pendulum Bearings (3D Testing, Analysis with the Parallel Model)								
Karakyr	Test	3.81	0.42	0.33	0.61	0.63	11.89	8.12
	SAP	3.47	0.21	0.30	0.43	0.50	9.19	8.55
LGPC	Test	3.77	0.25	0.25	0.45	0.36	9.82	6.45
	SAP	4.64	0.23	0.17	0.28	0.46	8.30	6.29
Jensen Filter	Test	2.79	0.21	0.23	0.39	0.46	10.07	6.36
	SAP	2.84	0.18	0.21	0.37	0.40	9.73	9.09
Sylmar	Test	3.26	0.28	0.30	0.49	0.59	12.54	6.54
	SAP	3.01	0.19	0.25	0.41	0.45	11.69	7.62
Takarazuka	Test	2.72	0.22	0.23	0.65	0.50	8.93	5.39
	SAP	2.44	0.15	0.25	0.20	0.43	6.48	8.68
Bolu	Test	2.21	0.25	0.27	0.69	0.43	11.00	7.37
	SAP	2.37	0.20	0.20	0.35	0.32	8.29	8.88
Average	***Test***	***3.09***	***0.27***	***0.27***	***0.55***	***0.49***	***10.71***	***6.70***
	SAP	***3.13***	***0.19***	***0.23***	***0.34***	***0.43***	***8.95***	***8.18***
% Difference		***1.1%***	***-30.3%***	***-15.5%***	***-37.6%***	***-13.9%***	***-16.4%***	***22.1%***

Table 5-8 Comparison of Analytical (Series Model) and Experimental Peak Responses for Selected Sets of Tests and Isolation with Triple Friction Pendulum Bearings in Friction-Bolted Configuration (Length Scale of 3, Symmetric Bushing Configuration)

Motion		Resultant Corner Displ.	Frame Top Corner Accel.		Upper Bushing CG Accel.		Base Shear	
			EW	NS	EW	NS	EW	NS
		(in)	(g)	(g)	(g)	(g)	(kip)	(kip)
Triple Friction Pendulum Bearings (2D Testing, Analysis with the Series Model)								
Karakyr	Test	3.60	0.39	0.29	0.82	0.79	9.64	9.54
	SAP	3.76	0.20	0.28	0.32	0.38	7.90	8.17
LGPC	Test	3.94	0.28	0.20	0.44	0.32	8.90	8.47
	SAP	4.96	0.24	0.17	0.28	0.23	7.02	6.43
Saratoga	Test	3.30	0.21	0.18	0.36	0.31	10.35	6.67
	SAP	3.18	0.19	0.21	0.22	0.23	9.52	5.96
Jensen Filter	Test	2.76	0.20	0.19	0.39	0.49	8.73	9.50
	SAP	2.92	0.16	0.17	0.19	0.20	8.15	9.30
Sylmar	Test	3.67	0.20	0.22	0.42	0.44	9.77	8.36
	SAP	3.57	0.15	0.23	0.18	0.26	9.28	7.47
Takarazuka	Test	2.68	0.21	0.20	0.37	0.36	7.98	8.17
	SAP	2.39	0.16	0.18	0.19	0.23	5.96	7.47
Bolu	Test	2.17	0.24	0.21	0.42	0.27	9.22	9.30
	SAP	2.27	0.17	0.17	0.20	0.16	7.54	7.25
Average	***Test***	***3.16***	***0.25***	***0.21***	***0.46***	***0.43***	***9.23***	***8.57***
	SAP	***3.29***	***0.18***	***0.20***	***0.23***	***0.24***	***7.91***	***7.44***
% Difference		***4.2%***	***-27.2%***	***-3.9%***	***-50.7%***	***-43.5%***	***-14.3%***	***-13.3%***
Triple Friction Pendulum Bearings (3D Testing, Analysis with the Series Model)								
Karakyr	Test	3.81	0.42	0.33	0.61	0.63	11.89	8.12
	SAP	3.57	0.22	0.30	0.42	0.50	8.89	8.20
LGPC	Test	3.77	0.25	0.25	0.45	0.36	9.82	6.45
	SAP	4.62	0.25	0.19	0.30	0.50	8.42	6.73
Jensen Filter	Test	2.79	0.21	0.23	0.39	0.46	10.07	6.36
	SAP	2.97	0.17	0.21	0.36	0.41	9.56	9.35
Sylmar	Test	3.26	0.28	0.30	0.49	0.59	12.54	6.54
	SAP	3.37	0.18	0.27	0.40	0.45	11.31	7.40
Takarazuka	Test	2.72	0.22	0.23	0.65	0.50	8.93	5.39
	SAP	2.55	0.17	0.25	0.20	0.43	6.50	8.71
Bolu	Test	2.21	0.25	0.27	0.69	0.43	11.00	7.37
	SAP	2.12	0.21	0.22	0.39	0.36	8.49	8.55
Average	***Test***	***3.09***	***0.27***	***0.27***	***0.55***	***0.49***	***10.71***	***6.70***
	SAP	***3.20***	***0.20***	***0.24***	***0.34***	***0.44***	***8.86***	***8.16***
% Difference		***3.5%***	***-27.3%***	***-10.3%***	***-36.9%***	***-10.3%***	***-17.3%***	***21.7%***

5.6. **Comments and Discussion on the Results**

The analytical investigations performed in SAP2000 and presented herein investigated the capability of the models to predict the isolation system response with acceptable accuracy.

Of the response quantities examined, the isolation system displacements were found to be the ones most accurately predicted for all the isolation system configurations examined. Between elastomeric and friction-based systems used in this study, the models for the Triple FP system were found to be more accurate in the prediction of the displacements, likely due to the inherent insensitivity of the isolators to the mass distribution in the superstructure. This can be further verified by the results of Table 5-7 where it is seen that the parallel model predicted the average displacement response at the NE bottom corner of the frame with an error of only 2%. Table 5-6 on the other hand, shows that for the LRB system the model underestimated the average displacements by about 15%.

The base shear was also captured with acceptable accuracy for all systems studied. In this case the discrepancies between the peak experimental and analytical values were found to be more pronounced for the Triple FP system than the LRB system. With reference again to Table 5-6 and Table 5-7, the LRB system was found to underestimate the maximum average base shear by less than 10%, while for the Triple FP system the analysis underestimated the maximum average base shear by about 15% in biaxial testing. In the tri-axial testing of the Triple FP system the analysis underestimated the average base shear by 15% in one direction, and gave conservative results in the other by about 20%.

Regarding the acceleration predictions, it can be seen in the graphs presented above that the time history trends of the experimental response were captured with good accuracy by the SAP2000 analysis. For the LRB system the analysis was found to underestimate the average accelerations at the top corner of the frame and the center of gravity of the bushing by less than 5% and 20%, respectively, as can be seen in Table 5-6. For the triple FP system the analysis was found to underestimate the average accelerations by about 30% at the top corner of the frame and about 50% at the center of gravity of the bushing as seen in Table 5-7.

In conclusion, the numerical models in SAP2000 were found to have acceptable accuracy in predicting global response quantities but the predictions of acceleration of attachments was less accurate and differences of as much as 50% were observed. Discrepancies between the analytical and experimental results can be attributed to the various assumptions adopted in the modeling of the superstructure and isolation systems, and in the parameters used for the SAP2000 analysis, as well as in potential uncontrolled errors in experimental measurements. More specifically:

1. In all cases, the isolation systems were modeled in SAP2000 using properties that were obtained by averaging the results of testing individual isolator units on the bearing testing machine in SEESL, which preceded shake table testing. The behavior of the isolators when installed in the model and tested on the shake table is generally different than when installed and tested uniaxially on the bearing testing machine, due to differences in the boundary conditions, the multidirectional coupling of the isolator properties and the wide frequency range of the shake table excitation. For example, Sarlis et al (2013) reported differences in the values of the mechanical properties of triple FP isolators, when those were identified

from shake table tests as opposed to identification testing using the bearing testing machine. Such differences in properties among the isolators were not accounted for in the numerical models.

2. Due to time constraints in the laboratory, many tests had to be performed sequentially and in a limited time frame, and therefore both the LRB and the Triple FP systems were subjected to prolonged shake table excitation. That has cumulative effects on the isolators such as heating, traveling and wear of the materials, and in the connections of the isolators and other attachments to the structure, which aggravated the actual system response and could not be accounted for in the numerical models. The above differences as well as potential inaccuracies in the modeling of the mass distribution in the numerical model likely have contributed to the discrepancies in the prediction of the displacement response of the LRB configurations.

3. The weights on the isolators were applied in an approximate sense only. Additionally, the P-Δ effects on the isolators, whose inclusion in the analysis has been shown to potentially improve the numerical predictions (Sarlis and Constantinou, 2010), were not accounted for in the current study.

4. The large discrepancies in the prediction of the accelerations, as compared to the better accuracy in the prediction of the displacements and base shears, are mostly due to artificially high values of acceleration obtained from testing. More specifically, during testing, and particularly for the configurations with the Triple FP systems, it was identified that the bushing responded frequently with unusually high accelerations, which were not however coupled with increased displacements. This response was also accompanied by audible

rattling sounds from the structure, which although were not located, they can be reasonably attributed to local effects, such as sliding and pounding of the side plates due to loose connections, and some small rocking of the internal components of the Triple FP isolators. Regarding the latter issue, Sarlis et al (2013) have demonstrated that the natural variability in the frictional properties among isolators in the same isolation system can cause small differential vertical motions among the isolators, redistribution of the axial loads and misalignments of the isolators during the course of testing. These misalignments are likely to have resulted in rocking in the isolators which, combined with the lack of damping mechanisms, the unusually high stiffness of the superstructure and the relatively small mass of the high voltage bushing, generated high frequency response on the frame and the bushing. The high frequency response of the specimen is evident in many of the response acceleration spectra presented in Figure 5-5 to Figure 5-17 for the Triple FP configurations tested. These effects could not be captured in the SAP2000 models.

5. More importantly, the contribution of the experimental errors in the discrepancies discussed above has not been accounted for. Such errors may originate directly from the environmental setting of the specimen (such as elevated temperatures in the laboratory, and extraneous noise due to other labor in the laboratory that could likely affect the instrumentation measurements), as well as from limitations in the capabilities of the measuring instruments (such as inherent randomness and uncertainty in the measurements of the instruments). In consideration of the fact that such experimental errors can be within 10% to 20% of the actual response, and that the errors in the analytical results can be within the same order of magnitude due to the reasons discussed above, the analytical predictions of this study are judged to be sufficiently accurate.

SECTION 6
AN EXAMPLE OF APPLICATION OF SEISMIC ISOLATION IN THE RETROFIT OF AN ELECTRICAL POWER TRANSFORMER

6.1. Overview

The design of an isolation system for electrical power transformers differs from the design of conventional structures, in that the former is constrained by special characteristics and requirements for functionality of the equipment which are not generally required in conventional structures. The focus in this section is to identify, clarify and categorize these constraints and describe important design parameters, with a view to laying out a straightforward procedure for the design of isolation systems for the seismic retrofit of electrical equipment. Some of the design components discussed deal with the identification of the important structural characteristics of the power transformers, the assessment of the seismic demand for the site location, the selection of design properties for the isolation system, the description of modeling issues and standard analysis procedures, foundation construction issues and the installation of the isolation system. Furthermore, design guidelines are summarized in the form of suggested design steps. The design of base isolation for an actual electrical power transformer is presented for demonstration of these concepts.

6.2. General Seismic Design Guidelines

6.2.1. Geometric Properties of the Equipment

High voltage power transformers are complex structures with non-uniformity in their commercial models. Some of the structural variations encountered in the field and pertinent to the design are the oil tank shape, the total power transformer weight, the mounting position of

attached components and the location of external connections to the tank. While these details are generally available by the manufacturers or can be measured in situ, there are several other components the details of which are proprietary and might not be easily shared with the structural engineers. Such are, for instance, structural details of the core-and-coil assembly and the high voltage bushings. It is then necessary that the design of the isolation system for a power transformer will be a relatively simple procedure, which at the same time addresses the constraints that the structural characteristics of the power transformer and the site conditions entail. Fortunately, the application of base isolation itself will essentially cause the power transformer to move as a rigid body during shaking, because the fundamental frequencies of a fixed power transformer – typically having values above 10 Hz – are well beyond the effective frequencies of the isolation system, which can be designed in the range of 0.2-1.0 Hz. Therefore, the issues discussed above can be bypassed by opting to model the power transformer as a rigid body for the purposes of the design, in which the geometry of the tank, the power transformer total weight and its distribution (i.e. location of center of gravity) will only be required. This information can be easily obtained from power transformer outline drawings provided by the power transformer manufacturers.

For design purposes, it is also necessary to obtain information on the slack availability of the high voltage conductors connected to the tips of the high voltage bushings - usually mounted vertically on the tank roof - and the flexibility of the conductors connecting the power transformer tank with external secondary equipment. Aside from the displacement capacity of the isolation system, which is constrained by the selected geometry of the isolators, the displacement capacity of the conductors can also impose limitations on the design of the system. Specifically, excessive motion of the conductors can affect the electrical loads and consequently,

the performance of the electrical equipment. These issues can be addressed by consulting with the electrical engineers regularly along the design procedure.

6.2.2. Seismic Site Response Spectrum

The design procedures require information on the expected spectral demand during the lifecycle of the electrical system. The Design Earthquake (DE) is defined per ASCE 7-2010 to have a spectrum equal to 2/3 of the Maximum Considered Earthquake, maximum direction (MCE_R) spectrum. The MCE_R spectrum is a risk-targeted spectrum and is defined in the direction of maximum horizontal response for 5% damping. The DE spectrum is used in ASCE 7-2010 for the design of isolated building structures, whereas the MCE_R spectrum is used for establishing the capacity of the isolators. In the base isolation retrofit design presented herein, the power transformer will not be modified and thus, only the MCE_R spectrum will be used in the design. More specifically, the MCE_R spectrum will be used directly in the simplified method of analysis for the assessment of the displacement demand of the isolation system and the design forces for the foundation, and indirectly in the response history method for scaling the ground motions that will be used in the dynamic analyses. In order to determine the spectral parameters required to define the spectrum, information on the location of the equipment and the site soil classification will be utilized. Once this information is known, the spectral parameters can be calculated using the USGS application:

https://geohazards.usgs.gov/secure/designmaps/dev-us/application.php

The capacity of the equipment to withstand (without isolation) seismic demands is determined based on the spectrum used for seismic qualification. Unless information on the qualification of

the equipment is provided for the design process, the power transformer and its components will be assumed to have been qualified on the basis of the Required Response Spectra (RRS) defined in the IEEE 693-2005 Recommendations for Seismic Design of Substations, for a seismic input at the base of the tank comparable to the one represented by the MCE_R spectrum.

The corresponding seismic level for the seismic qualification of the equipment can be assessed with the seismic exposure map method described in IEEE 693-2005, in which the PGA is calculated from the site specific S_{MS} value at 0.2 sec, as determined as per ASCE 7-2010, divided by 2.5. The input seismic level is represented by the High RRS or the Moderate RRS if the calculated PGA is greater than 0.5g, or in case it lies in the range of 0.25g and 0.5g, respectively. When dynamic response history analysis is used, the 5% damped response spectra, obtained and calculated from the dynamic response history analysis just above the isolators, should accordingly fall below the 5% damped IEEE 693-2005 High or Moderate RRS. It is emphasized that the High and Moderate RRS, represent only the input seismic motion at the ground level, and not necessarily the seismic level for which the equipment and its appendages have been qualified. For instance, a high voltage bushing intended for installation on a power transformer located at a site with seismicity represented by the High RRS, is required to be qualified at much higher seismic input, equal to four times the High RRS, which accounts for power transformer amplification and for conservative bushing response.

6.2.3. Vertical Effect of Earthquake

Regarding the influence of the vertical effect of the earthquake in the design, currently there isn't a generally accepted way to generate scaled vertical ground motion components and use them in analysis. As per ASCE 7-2010 the effect of the vertical component of the earthquake shall be

accounted for in the design of members by applying a constant vertical force equal to $\pm 0.2S_{MS}$ times the dead load, where S_{MS} is the MCE_R, 5 percent damped, spectral response acceleration parameter at short periods adjusted for site class effects. Herein, this approach is extended to apply an effective constant vertical acceleration of $\pm 0.2gS_{MS}$ in the simplified analysis and also applied throughout each dynamic response history analysis. Specifically, a constant negative (downward) vertical acceleration will be applied to calculate the maximum isolator displacement demand in the lower bound analysis and a constant positive (upward) vertical acceleration will be applied to calculate the maximum structural acceleration in the upper bound analysis. This is known to produce conservative results for the displacement demand and the peak inertia force.

6.2.4. Selection of Isolation Systems and Properties

The mechanical behavior of a lead rubber bearing is characterized by its characteristic strength Q_d, post-elastic stiffness K_d and yield displacement Y. These properties depend on the area of the lead core, the bonded area of rubber, the yield stress of the lead core and the thickness and shear modulus of the rubber. The mechanical behavior of a Triple FP bearing is characterized by the radii R_1, R_2, R_3 and R_4, heights h_1, h_2, h_3 and h_4, displacement capacities d_1, d_2, d_3 and d_4 and the friction coefficients μ_1, μ_2, μ_3 and μ_4. These parameters are shown in the schematic of Figure 2-6. A typical design will have radii $R_1 = R_4 > R_2 = R_3$, heights $h_1 = h_4$ and $h_2 = h_3$, and displacement capacities $d_1 = d_4 > d_2 = d_3$. The friction coefficients in the standard Triple FP configuration presented by Fenz and Constantinou (2007) are $\mu_1 \neq \mu_4 > \mu_2 = \mu_3$, however, the simpler configuration with $\mu_1 = \mu_4 > \mu_2 = \mu_3$ has been often used. Additional parameters

relevant to the design of the isolator are the diameters of the outer plates, the slide plates and the rigid slider.

In selecting the bearing properties and in order to bypass the complexity involved in optimizing for a large number of parameters, the engineer should contact the selected bearing manufacturer to obtain relevant information on isolator designs that may be classified as similar to those to be used in the application. This approach may require some iteration but is highly desirable as it results in isolator designs with good understanding of the mechanical properties prior to testing the prototype or production specimens. The reader is referred to McVitty and Constantinou (2015) for examples of obtaining the bounding values of mechanical properties from similar specimens.

Following the selection of the isolation system, the number and distribution of the bearings should be such that the power transformer stability is not compromised, while the total cost of the isolation system is kept low. The use of four bearings is considered sufficient to seismically isolate and support the power transformer. A larger number of bearings will have undesirable effects on the design, regardless of the system selected. More specifically, the lead rubber bearing properties are generally independent of the weight of the superstructure and therefore a larger number of isolators will produce an isolation system with higher than desired frequency. In such case and in view of reducing the frequency of the system, the engineer may reasonably attempt to design more slender and flexible lead rubber isolators, with the caveat that the system will be rendered unstable in buckling for the required seismic displacements, or will have unpredictable lifetime behavior if very soft (low modulus) rubbers are used. The properties of the Triple FP bearings are linearly dependent on weight so that a larger number of bearings is, in

principle, possible without any effect on the isolation system frequency and friction. However, use of a larger number of isolators will affect costs.

Important for the design is the selection of the characteristic strength of the isolation system which is typically expressed as a portion of the total weight of the structure. To achieve the dual objective in the retrofit design of a power transformer with base isolation, to reduce the seismic forces on the power transformer while retaining the bushing displacements at acceptably low levels, the isolation systems should be designed to be flexible and highly damped. In order to obtain a highly damped isolation system, its characteristic strength must be higher than what is generally used in typical structures, and preferably more than 10% of the total weight of the power transformer. The characteristic strengths of the isolation systems utilized in the present experimental study ranged between 7.5% (for the full scale Triple FP bearings) and 20% (for the lead rubber bearings) of the total weight, and the reduction of the input motion to the power transformer and the bushing was found to be satisfactory with acceptable displacement responses in all cases. For the Triple FP bearing design presented in the application of this section, the bounds of friction were determined to be in the range of 0.12 to 0.18. Testing of the bearings determined the lower bound friction to be 0.12.

6.2.5. Simplified Method of Analysis

The simplified method of analysis presented herein is the equivalent lateral force procedure described in ASCE 7-2010. The simplified method is easy to apply, and produces a good estimation of the displacement demands as compared to the more complicated response history method of analysis (Pant et al, 2013). ASCE 7-2010 imposes limitations in its application, but regardless, its results are used to gage the validity of the results of response history analysis.

In this method, the isolated structure is treated as a linear elastic and linear viscous single degree of freedom system, and an iterative procedure is used to calculate the effective properties and the response for a seismic hazard described by a response spectrum. The iterative procedure is performed as follows:

1. A maximum displacement *D* is first assumed

2. The effective stiffness is calculated as:

$$K_{eff} = \frac{F_{\max}}{D}$$

where F_{max} is the force corresponding to displacement *D*.

3. The effective period is calculated as:

$$T_{eff} = 2\pi\sqrt{\frac{W}{gK_{eff}}}$$

4. The effective damping is calculated as:

$$\beta_{eff} = \frac{EDC}{2\pi K_{eff} D^2}$$

where *EDC* is the energy dissipated per cycle of harmonic motion at displacement. The EDC is equal to the area enclosed by the force-displacement loop constructed for displacement D.

5. The damping reduction factor is calculated as:

$$B = \left(\frac{\beta_{eff}}{0.05} \right)^{0.3}$$

6. The displacement demand is calculated as the spectral displacement after adjustment for increased damping and the base shear force normalized by the weight is calculated as the corresponding spectral acceleration value normalized by the acceleration of gravity:

$$D = \frac{gS_{M1}T_{eff}}{4\pi^2 B} \quad \text{and} \quad \frac{V_b}{W} = \frac{4\pi^2 D}{gT_{eff}^2}$$

   The calculated displacement is compared to the initial assumption from step 1. Note that V_b must be equal to $K_{eff} D$.

7. Steps 1 to 6 are repeated until convergence.

In the procedure above, it is presumed that the earthquake occurs along one of the two principal directions. Therefore, once the design parameters have been determined, the lateral earthquake effect may be calculated by means of the 100%-30% combination rule as:

$$D_M = \sqrt{(0.3xD)^2 + D^2}$$

Furthermore, the ASCE 7-2010 specifies that the total displacement shall also account for the effects of accidental and actual torsion which results from variations in the spatial distribution of the lateral stiffness of the isolators and the mass eccentricity in the superstructure, which cannot be explicitly captured in the simplified analysis. The effect of torsion may be accounted for

using the ASCE 7-2010 approach but modified to account for the effect of the distribution of isolators:

$$D_{TM} = D_M \left[1 + \frac{12ey}{A^2(b^2 + d^2)} \right]$$

where b and d are the plan dimensions of the power transformer, e is the actual eccentricity between the center of mass and the center of rigidity plus accidental eccentricity assumed equal to 5%, both measured perpendicular to the direction under consideration, and y is the distance of the corner bearing to the center of rigidity measured perpendicular to the direction under consideration. Parameter A is the ratio of the lateral period to torsional period of the isolated structure, which for structures with a large number of bearings (buildings) is about equal to unity. Parameter A may be calculated as (Winters and Constantinou, 1993; Wolff et al, 2014):

$$A = \frac{1}{r} \sqrt{\frac{\sum_i^N (x_i^2 + y_i^2)}{N}}$$

where x_i and y_i are the coordinates of the bearings with respect to the center of mass, N is the number of bearings of identical stiffness (N=4 for electrical power transformers) and r is the radius of gyration of the electrical power transformer equal to $\sqrt{(b^2 + d^2)/12}$ (disregarding mass eccentricity for simplicity). Note that for a configuration with 4 isolators, parameter A^2=3 so that torsion is significantly inhibited (system is torsionally very stiff). It is noted that, per ASCE 7-2010, D_{TM} is not permitted to be taken less than 1.1 times the D_M.

6.2.6. Dynamic Response History Analysis Method

6.2.6.1. Modeling of the Power Transformers and the Isolators

The dynamic response history analysis is considered the most accurate method of analysis because it allows for a detailed representation of the power transformer and modeling of the nonlinear characteristics of the isolators. In accordance with the ASCE 7-2010, the method is permitted to be used for the design of any seismically isolated structure, and is mandatory for the design of structures that do not satisfy the necessary criteria in order to be designed with the simplified method of analysis. In the design procedure presented herein, it is recommended that both the simplified analysis method and the dynamic response history analysis method be used in a complemental manner to select the final design parameters.

The power transformer and isolation system assembly should be modeled in such way that the translational horizontal and the torsional behavior of the power transformer are properly captured, as well as the overturning and uplift forces on the isolators. The power transformer can be effectively represented as a rigid structure with its mass appropriately distributed so that the actual eccentricity between the instantaneous center of rigidity of the isolation system and the center of mass of the superstructure is accounted for.

The isolators should be modeled below the corners of the rigid power transformer model in their actual spatial distribution and using hysteretic elements that can appropriately capture their nonlinear force-deformation properties. The isolation systems studied herein have been shown to produce reliable predictions when modeled with bilinear hysteretic elements typically available in commercial structural analysis software. For instance, in SAP2000 there is a

dedicated element for the modeling of the lead rubber isolator, termed Rubber Isolator element, which is a smooth bilinear hysteretic model without capability to model deterioration of strength due to heating effects and without capability to describe the behavior in tension. Another element in SAP2000, termed Friction Isolator element, can be used for the modeling of frictional isolators. The Friction Isolator element can also capture the biaxial interaction of the frictional forces in the isolator, and is also capable of updating the model at each time step to account for the effect of axial force variation and the effect of velocity on the coefficient of friction. Furthermore, it can predict the occurrence of uplift by behaving as a gap element in the vertical direction. The Triple friction pendulum isolator can be modeled as a combination of such elements. In particular, the most general or fully adaptive configuration of the Triple FP, that is the one with $R_{eff\,2} = R_{eff\,3}$ $R_{eff\,1} = R_{eff\,4}$ and $\mu_2 = \mu_3 < \mu_1 < \mu_4$ with reference to the geometry shown in Figure 2-6, can be modeled in SAP2000 with the so-called "series model" developed by Fenz and Constantinou (2008), which is an arrangement of three Friction Isolator elements in series together with gap elements. The series model is an exact representation of the Triple FP isolator - although unable of capturing the motion of the internal components - however it is complicated by the use of a large number of degrees of freedom and the several parameters per element, a fact that makes its implementation cumbersome. A configuration of the Triple FP isolator frequently encountered in practice, is the one with $R_{eff\,2} = R_{eff\,3}$ $R_{eff\,1} = R_{eff\,4}$ and $\mu_2 = \mu_3 < \mu_1 = \mu_4$, which can be represented with a much simpler model to implement in analysis, the so called "parallel model" developed by Sarlis and Constantinou (2009, 2010). The parallel model can be constructed by overlapping two bilinear hysteretic models to produce the trilinear force-displacement loop of the aforementioned configuration, and can essentially capture the behavior of the isolator up to the initiation of the final stiffening regime. The models

described above have been already incorporated in the 3D-BASIS program (Sarlis et al, 2009, Ray et al, 2014), as well as in the commercial structural analysis software SAP2000 (CSI, 2002). Other computer programs capable of analysis of isolated structures are ABAQUS and ANSYS, and some examples of such analyses can be found in the work of Rousis et al (2003), Clarke et al (2005), Tsopelas et al (2005).

6.2.6.2. Selection and Scaling of Ground Motions

As per the requirements of the ASCE 7-2010, the dynamic non-linear analysis shall be performed using an ensemble of at least three horizontal pairs of appropriate ground motion records. In that context, appropriate ground motions are considered ones that have been selected from events with magnitudes, fault distances, and source mechanisms that are consistent with the conditions of the site where the equipment is located. For the case that an ensemble of less than seven ground motions is selected, the maximum values of force and displacement obtained from the non-linear analyses must be used in the design, whereas for the case that seven or more ground motions are selected, the average of the force and displacement values obtained from the non-linear analyses is permitted to be used in the design. Furthermore, the standard allows for the generation of synthetic motion horizontal pairs to make up the total number required for the analysis when the required number of recorded ground motion pairs is not available. In the base retrofit design presented herein, the use of seven ground motion pairs is recommended.

Subsequently, the horizontal pairs of the selected ground motions shall be scaled accordingly so as to closely represent the MCE_R spectrum for a certain range of frequencies. As per ASCE 7-2010, the scaling procedure will depend on the distance of the site to the fault. The reader is

referred to Pant et al (2013) for examples of scaling procedures and their effect on the displacement demand calculation.

6.2.6.3. Analysis Procedure for Engineering Demand Parameter

Once the numerical model has been put together and the ground motions have been selected and scaled, dynamic analysis should be performed as per ASCE 7-2010 with the pairs of the ground motions applied simultaneously to the model in such way that the most disadvantageous mass eccentricity is accounted for. To address that requirement, two sets of analysis should be carried out: one with the scaled ground motion components oriented in the transverse and longitudinal directions and one with the components rotated. Furthermore, upper and lower bound analyses should be performed for each set using the corresponding upper and lower bound isolator properties, in order to determine the maximum forces and displacements. The effect of the vertical earthquake may be included in the above analyses by applying an additional positive (upward) vertical acceleration throughout the upper bound analyses and an additional negative (downward) throughout the lower bound analyses.

The response parameters of interest are the peak resultant displacement of the most critical isolator, the peak absolute base shear forces in the transverse and longitudinal directions, the peak absolute accelerations in the transverse and longitudinal directions, and the maximum and minimum axial forces on the most critical isolator (to assess uplift or tension). The peak resultant displacement in particular, should be calculated as the peak value of the vectorial sum of the two horizontal displacement components at each time step. In case that seven or more ground motion pairs are used in the analysis, the average value of the calculated response parameters of interest should be used in the design otherwise, the maximum value of the

response parameters should be used. Conservatively, the most adverse average (or maximum) parameter value of the four ensembles should be chosen for the design.

In the dynamic analysis procedure described above, accidental eccentricity in the system (i.e. one occurring from uncertainty in the isolators' properties) is not accounted for. To correct for the effect of accidental mass eccentricity, the peak resultant displacement obtained for the most critical isolator will be amplified using the factor calculated as described in section 6.2.5.

6.2.7. Selection of Design Parameters

The average design parameters calculated by the dynamic response history analysis are expected to be generally lower than the parameters calculated by the simplified procedure. In accordance to the requirements of ASCE 7-2010, the results of the dynamic analysis are allowed to be used in the design with the condition that:

a. The isolation system design displacement should not be taken as less than 80% of the displacement determined by the simplified procedure, and

b. The design base shear forces for the isolation system and the foundation should not be taken less than 90% of the base shear forces determined by the simplified procedure.

6.2.8. Construction Considerations

As suggested by the findings of the current study, the Triple FP bearings may be installed underneath the power transformer tank without fixing them to the tank base plate, but instead relying only on the friction between the top plate of the isolator and the tank to hold them in

place. This is possible due to the inherent ability of the Triple FP bearings to adjust their lateral force properties proportionally to the axial forces they carry. On the contrary, lead rubber bearings should always be fixed to both the foundation and the tank, because they tend to slide during shaking when the axial force on them is varied, since their properties are independent of the weight carried. In any case and for installation purposes, it is recommended that a concrete slab will be constructed and interposed between the tank and the isolation interface, which will serve as a base-mat for the power transformer, on which the top plates of the isolators will be bolted or kept by friction. Furthermore, a concrete foundation slab needs to be constructed for supporting the isolation system, on which the bottom plates of the isolators will be connected.

The procedure for the construction of the foundation system is envisioned as follows: initially, the power transformer will be moved sideways, to rest temporarily next to its current position so that its functionality remains unobstructed. Subsequently, the foundation and base-mat slabs will be built stacked on top of each other at the original position of the power transformer, in such way that the top of the base-mat is leveled with the bottom of the tank. Once the concrete slabs have been constructed, the power transformer will be repositioned back to its original location to rest on top of the base-mat. Finally, the power transformer and base-mat assembly will be lifted up with bottle jacks on four sides of the base-mat slab, and the isolators will be inserted between the two slabs. Alternatively, the bottom slab may be constructed first and allowed to cure, then the isolators are installed on top, and then the second slab is cast on top of the isolators and allowed to cure. The power transformer is then placed on top of the isolation system.

In consideration of the requirements of the main construction procedure presented above, the base-mat slab will be equipped with four lifting lugs (two on each side of the power transformer)

to serve as supports for the bottle jacks. One option is to construct each lifting lug as a custom-made steel block which will protrude outwards and consist of an L-shaped steel section with triangular steel plate reinforcements on each side of the section, and will extend at some distance inside the base-mat slab via steel plates connected to the top and bottom of the block. The internal part of the assembly will be connected to the slab reinforcement. In the vicinity of the lifting lugs, the slab will be specially reinforced to withstand the high punching shear and bending loads imposed by the bottle jacks. For the calculation of the reinforcement it can be conservatively presumed that the power transformer and base-mat assembly is supported diagonally on two bottle jacks only (i.e. the assembly is wobbling on the bottle jacks).

For the installation of the isolators, the base-mat and the foundation slabs should each be provided with four holes at the installation locations of the isolators, for bolting the isolators. In case the isolators are placed relative to the sides of the slabs in such way that not all of the holes are manually accessible, then fewer than four bolts may be permitted to be installed per each bearing plate, but at a minimum of two bolts per plate.

Regarding the base-mat slab, it should be born in mind that power transformers are normally connected to the substation control house through various cables that end up in cable conduit runs, and that the construction of the base-mat should not hinder their operation. Therefore, in the design of the base-mat slab, the locations of these cables should be identified by visual inspection or communication with the manufacturers and the electrical engineers in charge of the equipment, and accounted for by providing holes on the slab at appropriate locations, as well as by providing enough slack for the cables to supply them with displacement capacity during shaking.

Finally, the foundation slab should be constructed to protrude from the ground at sufficient height so that the bearings are protected from flooding. The foundation slab should lay shallow enough into the ground so that its bottom lies at or above the frost line.

6.3. **Summary – Design Steps**

The design procedure for the seismic retrofit of electrical power transformers with base isolation and described in the previous section, can be summarized in the following steps:

1. Obtain the power transformer geometric characteristics and weight (including the location of the center of mass), the high voltage cable slacks and flexibility of conductors to external electrical equipment, the site coordinates (latitude and longitude) and the site soil classification.

2. Construct the 5% damped MCE_R spectrum as per ASCE 7-2010 using the site coordinates and soil class.

3. Select the desired type of the isolation system for the application and calculate the upper and lower bound properties for the isolators based on rational procedures and assumptions.

4. Perform lower and upper bound simplified analyses to calculate the maximum isolator displacement demand and the maximum structural acceleration demand respectively, and modify the displacements to account for accidental eccentricity and torsion. Check for tension or uplift forces on the isolators and adjust their distance if such potential exists.

5. In case the displacement capacity of the bearings is insufficient, or the bearings are likely to be rendered unstable, or the conductors and cables cannot be operational under the calculated displacement demand, the isolation system shall be redesigned (step 3) so that the displacement demand is within capacity.

6. Select an ensemble of 7 or more ground motion pairs having characteristics consistent with the site where the equipment is located, and scale them appropriately to represent the site-specific 5% damped MCE_R spectrum in the period range of interest.

7. Develop a numerical model in which the power transformer is represented as a rigid structure with its mass distribution realistically modeled, and the isolators modeled in their actual spatial distribution and using hysteretic elements that can appropriately capture their nonlinear force-deformation properties.

8. Perform lower and upper bound dynamic response history analysis with the scaled ground motion pairs oriented in the longitudinal and transverse directions and reversed (four sets of analysis overall). Report the following response parameters of interest: (a) the most critical isolator peak vectorial resultant displacement, (b) peak base shear forces, (c) peak accelerations, and (d) the most critical isolator maximum and minimum axial forces. Modify the displacements to account for accidental eccentricity and torsion. The average value of the calculated response parameters is allowed to be used in the design.

9. In case the displacement capacity of the bearings is insufficient, or the bearings are likely to be rendered unstable, or the conductors and cables cannot be operational under the

calculated displacement demand, the isolation system shall be redesigned (step 3) so that the displacement demand is within capacity.

10. The design displacement and base shear forces obtained from the dynamic analysis are allowed to be used in the design however they should be taken as not less than 80% and 90%, respectively, of the values determined by the simplified procedure.

11. Design a concrete base-mat slab and a concrete foundation slab, the former with the provision of four lifting lugs for supporting bottle jacks.

12. Test all isolators.

6.4. Example of a Field Power Transformer with Seismic Isolation

6.4.1. Power Transformer Characteristics

This section presents a design example for the seismic retrofit of an actual power transformer with base isolation. The power transformer is a 460 kV GE model (Figure 6-1) located in Vancouver, Washington. The orientation of the power transformer in Figure 6-1 has been chosen arbitrarily for the sake of this example.

The power transformer has a total weight of 380 kip. The tank base has plan dimensions of 227 inches in the E-W direction and 110 inches in the S-N direction. For simplicity in the design, the total mass was assumed to be lumped at the Center of Gravity (CG) of the power transformer, which is found at a height of 81 inches from the base of the tank and a distance of 4 inches west

from the geometric center of the tank base. In the S-N direction, the CG coincides with the geometric center.

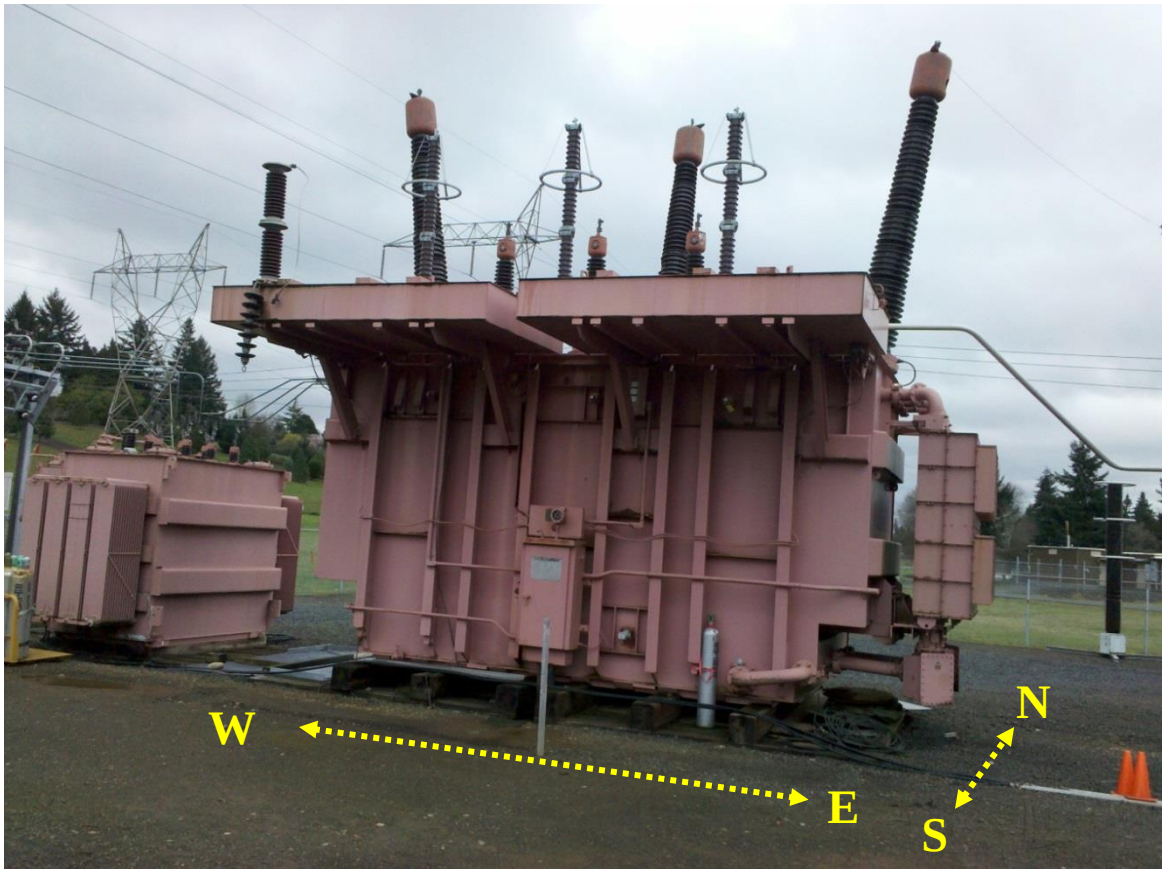


Figure 6-1 460 kV GE Power Transformer in Vancouver, WA

6.4.2. Maximum Considered Earthquake Spectrum

The maximum considered earthquake, maximum direction spectrum (MCE_R) for the site was developed in accordance with ASCE 7-2010 (American, 2010). This spectrum is defined in the direction of maximum horizontal response for 5% damping. The spectrum was determined for the power transformer site in Vancouver, WA with latitude of 45.6582^o N and longitude of 122.6578^o W. The specific spectral parameters were determined for a Site Class D to be S_{MS}=1.039g and S_{M1}=0.64g. These two parameters define the peak plateau of the spectrum and

the spectral value at period of 1sec, respectively. These quantities were found for the above site coordinates and using the USGS application:

https://geohazards.usgs.gov/secure/designmaps/dev-us/application.php.

The Design Earthquake (DE) is defined per ASCE 7-2010 to have a spectrum equal to 2/3 of the MCE_R spectrum. The DE spectrum is used in ASCE 7-2010 for the design of isolated building structures whereas the MCE_R spectrum is used for establishing the capacity of the isolators. Herein only the MCE_R spectrum was used to assess the performance of the isolated power transformer. Figure 6-2 presents graphs of the DE and MCE_R 5%-damped spectra for the Vancouver site. Also shown are the High and Moderate Required Response Spectra (RRS) of the IEEE 693-2005 Recommendations for Seismic Design of Substations. In order to assess the appropriate PGA for the seismic qualification level, the site specific S_{MS} value determined as per ASCE 7-2010 was divided by 2.5. For the Vancouver, WA site the PGA for the qualification level was calculated as 0.42g. Accordingly, the response spectra calculated above the isolators for the isolated equipment (that is, at the base of the power transformer) through dynamic response history analysis should, on an average sense, fall below the IEEE 693-2005 High RRS.

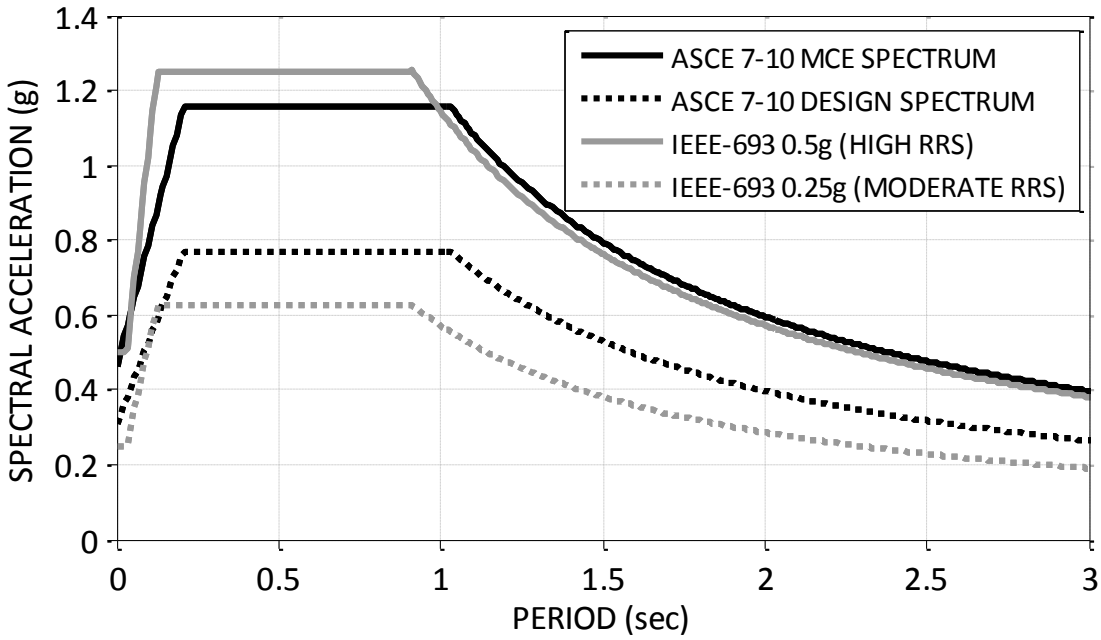


Figure 6-2 ASCE 7-2010 DE and MCE_R Spectra and Moderate/High RRS as per IEEE 693-2005 (5% Damped)

6.4.3. Seismic Isolation System

The seismic isolation system selected consists of four Triple Friction pendulum bearings having the nominal properties shown in Table 6-1 and with reference to Figure 2-6 for definition of the geometric and frictional properties. The friction coefficients for the four sliding interfaces of the bearings are expected to be $\mu_1=\mu_4=0.12$ and $\mu_2=\mu_3=0.06$ for axial load of about 100 kip (provided by the manufacturer). The weight of the isolated power transformer is expected to be about 425 kip when including the weight of the base mat. Therefore, each bearing will carry axial load of about 106kip, although the actual values will depend on the weight distribution of the power transformer. Uncertainty in values of friction (analysis and design were preformed prior to testing the isolators) required the assumption of a range of values. Herein, this range was assumed to be 0.12 to 0.15 for μ_1 and 0.06 to 0.07 for μ_2.

Table 6-1 Properties of Triple FP Properties

$R_1=R_4$	in	39.00
$R_2=R_3$	in	8.00
$d_1=d_4$	in	7.00
$d_2=d_3$	in	1.00
$h_1=h_4$	in	2.50
$h_2=h_3$	in	1.50
$\mu_1=\mu_4$	-	0.12 to 0.15
$\mu_2=\mu_3$	-	0.06 to 0.07
$R_{eff1}=R_{eff4}=R_1-h_1$	in	36.50
$R_{eff2}=R_{eff3}=R_2-h_2$	in	6.50
$d_1^*=d_4^*=d_1R_{eff1}/R_1$	in	6.55
$d_2^*=d_3^*=d_2R_{eff2}/R_2$	in	0.81

The frictional properties in Table 6-1 represent the range of nominal values which only account for uncertainty but does not account for the effects of aging, contamination or low temperature. Accordingly, the lower bound values were defined to be: $\mu_1=\mu_4=0.12$ and $\mu_2=\mu_3=0.06$. The upper bound values were obtained by multiplying $\mu_1=\mu_4=0.15$ and $\mu_2=\mu_3=0.07$ by factor 1.1 for aging and again by factor 1.05 for contamination and then rounded up for possible effects of low ambient temperature. The resultant upper bound values for use in analysis and design are then: $\mu_1=\mu_4=0.18$ and $\mu_2=\mu_3=0.09$. A summary of lower and upper bound values are shown in Table 6-2. Force-displacement loops of the isolation system in the lower and upper bound stages are presented in Figure 6-3 and Figure 6-4.

Table 6-2 Upper and Lower Bound Triple FP Frictional Properties

Lower Bound $\mu_1 = \mu_4$	0.12
Lower Bound $\mu_2 = \mu_3$	0.06
Upper Bound $\mu_1 = \mu_4$	0.18
Upper Bound $\mu_2 = \mu_3$	0.09

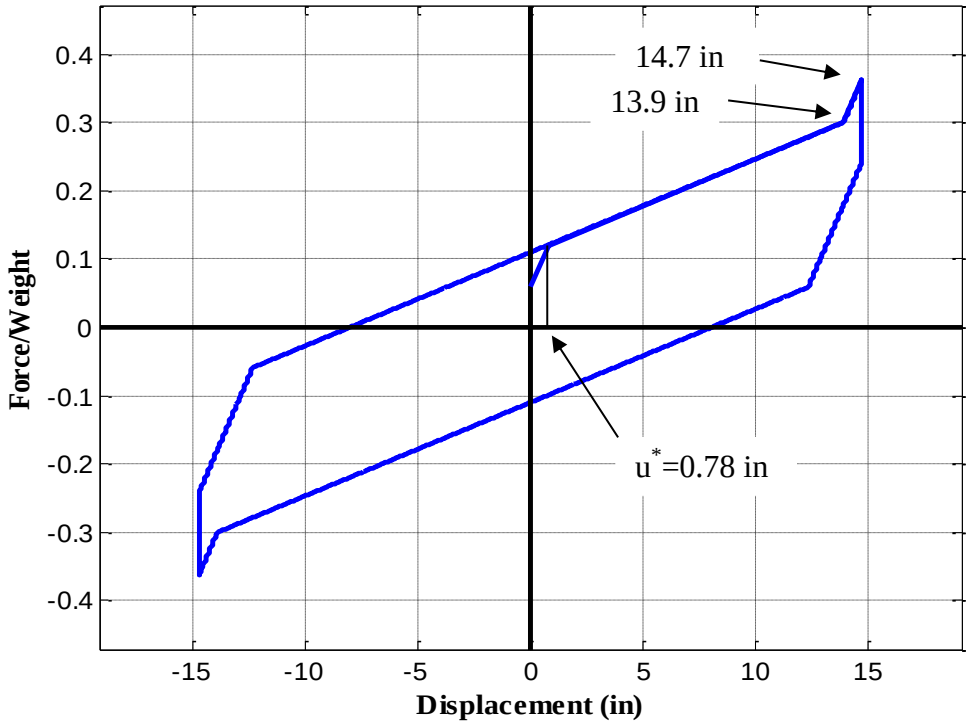


Figure 6-3 Lower Bound Conditions Force-Displacement Loop of Isolation System ($\mu_1=\mu_4=0.12$ and $\mu_2=\mu_3=0.06$)

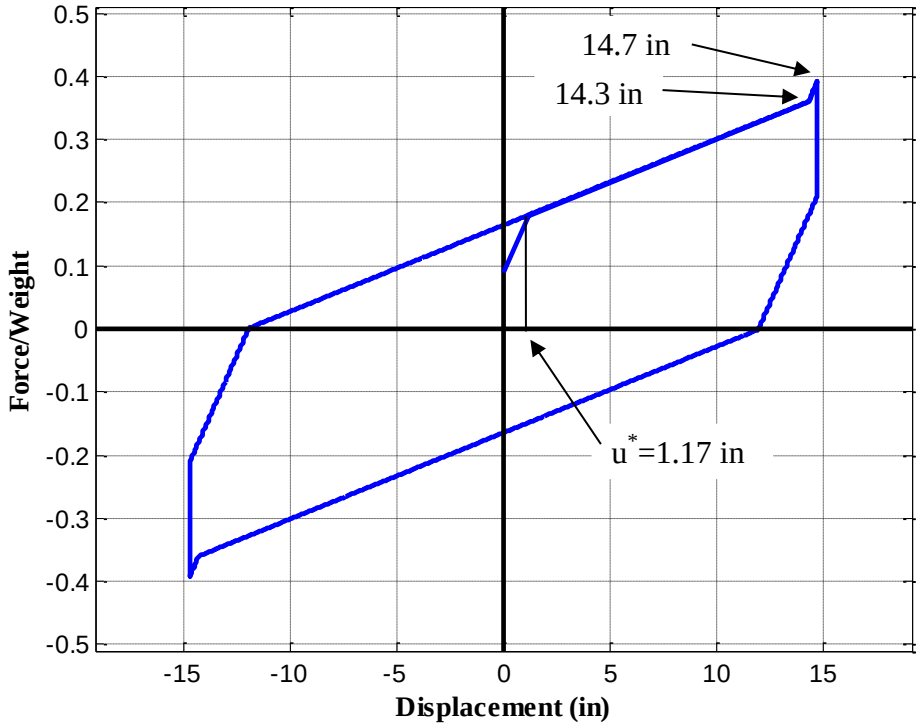


Figure 6-4 Upper Bound Conditions Force-Displacement Loop of Isolation System ($\mu_1=\mu_4=0.18$ and $\mu_2=\mu_3=0.09$)

Owing to uncertainties in the frictional properties of the bearings for the light load of about 100 kip, and in order to avoid modifications to the bearings for achieving the desired nominal friction values of $\mu_1=\mu_4=0.12$ and $\mu_2=\mu_3=0.06$, a worst case scenario was considered, in which the lower bound friction coefficients were further reduced to $\mu_1=\mu_4=0.09$ and $\mu_2=\mu_3=0.045$. Analysis was performed for this case also in order to establish that the bearing displacement capacity is sufficient. Figure 6-5 shows the force-displacement loop of the bearings for the case of $\mu_1=\mu_4=0.09$ and $\mu_2=\mu_3=0.045$.

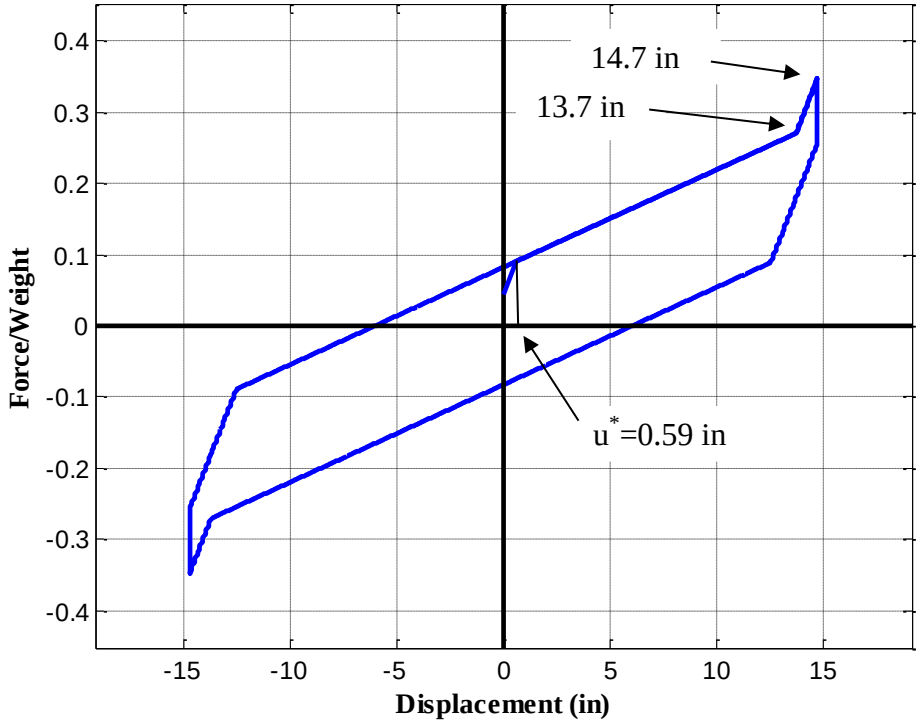


Figure 6-5 Force-Displacement Loop of Isolation System for Case $\mu_1=\mu_4=0.09$ and $\mu_2=\mu_3=0.045$

6.4.4. Foundation and Base-mat

For installation purposes, a concrete base-mat slab and a concrete foundation slab were planned to be constructed: the base-mat slab to be introduced between the tank and the isolation system, and the foundation slab to be positioned underneath the isolation system in order to support it. The base-mat slab was designed to extend an extra 2 feet on each side of the power transformer (275 inches in the E-W direction and 160 inches in the S-N direction) and to have a thickness of 12 inches. The total weight of the base-mat plate was then estimated not to exceed 45 kip. It is noted that initially the base-mat slab was intended to have a thickness of 10 inches instead of the 12 inches in the final design, and the weight was then estimated at 38 kip which is what was used in the analyses. The small difference in weight (7kip) is insignificant in the response of the system. The foundation slab was designed to extend an extra 1 foot on each side of the base-mat

slab (300 inches in the E-W direction and 185 inches in the S-N direction) and to have a thickness of 18 inches.

The design and construction of the foundation system was carried out based on the method presented in section 6.2.8.

6.4.5. Simplified Method of Analysis

For reasons of simplicity in the calculations, simplified analysis was carried out using the bilinear hysteretic model shown in Figure 6-6, instead of the tri-linear force-displacement loops presented above. The yield displacement Y equals u*/2 where u* is defined in Figure 6-3 through Figure 6-5.

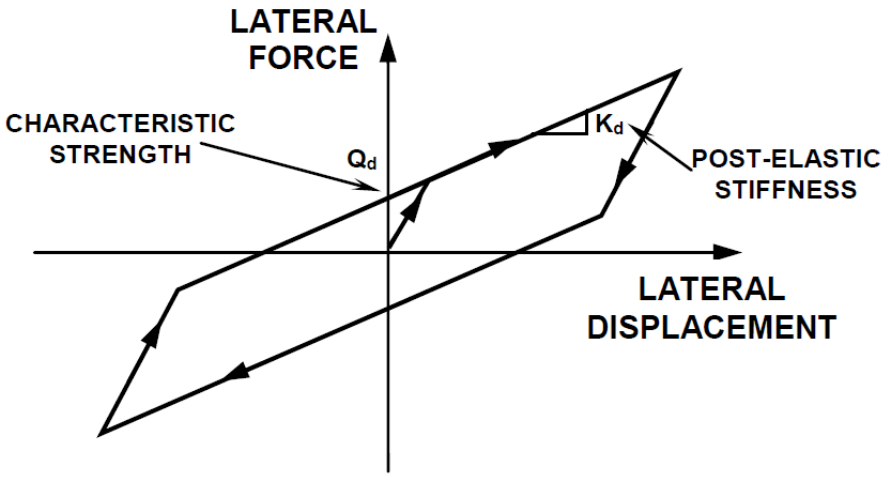


Figure 6-6 Bilinear Hysteretic Model for Analysis

The iterative method that was presented in detail in section 6.2.5 was used, in which the effective stiffness was calculated based on the above idealization as:

$$K_{eff} = \frac{\alpha W}{2\mathrm{R}_{eff\,1}} + \frac{\mu\alpha W}{D}$$

and the effective damping was calculated as:

$$\beta_{eff} = \frac{4\mu a W\left(D - Y\right)}{2\pi K_{eff} D^2}$$

Note that α is a parameter (less or more than unity) to adjust the weight for the effect of the vertical ground acceleration. It is the acceleration of gravity in units of g minus or plus a portion of the acceleration of gravity that is assumed to constantly act in the vertical direction (either up or down) during the entire episode of the horizontal excitation.

Table 6-3 presents the results of simplified analysis for the MCE_R spectrum, where the weight W was assumed to be 418 kip. To account for vertical earthquake effects, a constant vertical acceleration of either $-0.2S_{MS}$=-0.21g (in lower bound analysis with the factor α=0.79) or $+0.2S_{MS}$=+0.21g (in upper bound analysis with the factor α=1.21) was used.

Table 6-3 Results of Simplified Analysis

Quantity	**Unit**	**Lower Bound Case with α=0.79**	**Upper Bound Case with α=1.21**	**Friction $\mu_1=\mu_4=0.09$ Case with α=0.79**
μ	-	0.12	0.18	0.09
T_{eff}	sec	2.09	1.22	2.33
K_{eff}	kip/in	9.81	29.22	7.86
β_{eff}	-	0.325	0.414	0.261
B	-	1.75	1.88	1.64
D	in	7.5	4.2	8.9
V/W	kip/kip	0.18	0.29	0.17
Base Shear V	kip	72.2	120.4	70.0

Adding the lateral earthquake effect using the 100%-30% rule, the maximum resultant displacement for the lower bound case was calculated at $D_M = \sqrt{(0.3x7.5)^2 + 7.5^2} = 7.8in$. For the case of μ_1=μ_4=0.09, the resultant displacement is $D_M = \sqrt{(0.3x8.9)^2 + 8.9^2} = 9.3in$.

The effect of torsion is accounted for using the ASCE 7-2010 approach but modified to account for the effect of the spatial distribution of the isolators:

$$D_{TM} = D_M \left[1 + \frac{12ey}{A^2(b^2 + d^2)} \right]$$

where *b* and *d* are the dimensions of the base-mat equal to 110 inches and 227 inches, respectively, *e* is the accidental eccentricity between the center of mass and the center of rigidity assumed to be equal to 5% of dimension e=0.05x227=11.35 inches and *y* is the distance between the corner bearing and the center of resistance which is equal to 106 inches. Parameter A^2=3, so that for the case of friction μ_1=μ_4=0.09:

$$D_{TM} = D_M \left[1 + \frac{12ey}{A^2(b^2 + d^2)} \right] = 9.3 \left[1 + \frac{12x11.35x106}{3x(110^2 + 227^2)} \right] = 9.3x1.08 \geq 9.3x1.1 = 10.2in$$

The value of 10.2 inches is well within the displacement capacity of the bearings of 14.7 inches (as shown in Figure 6-3 to Figure 6-5).

Given that the center of gravity of the power transformer is at a height of about 100 inches from the center of the bearings, and the minimum distance between bearings in the transverse

direction is 86 inches, bearing uplift can occur when the acceleration exceeds 86α/(2x100) or 0.34g when α=0.79 and 0.52g when α=1.21. The acceleration calculated through the simplified analysis is represented in Table 6-3 by the ratio V/W, which corresponds to the calculated base shear V normalized by the weight W of the power transformer. The calculated V/W values of 0.18 and 0.29 of the Lower Bound and Upper Bound cases respectively are less than the above limits so that uplift will not occur.

6.4.6. Dynamic Response History Analysis

Dynamic response history analysis was performed in SAP2000 (CSI, 2002) using a rigid model of a power transformer, with its mass appropriately distributed so that the actual eccentricity was incorporated in the model. The model used for dynamic response history analysis in SAP2000 is shown in Figure 6-7. The stiffness of the members used was set sufficiently high so that the frame was practically rigid. The model height is 100 inches, including the height of the isolators (9 inches) and the height of the concrete base-mat (assumed 10 inches). The weight of the power transformer (380 kip) was distributed among the top nodes so that asymmetric initial loading conditions were achieved in the isolators as depicted in the drawings (so that total CG of the structure was 4 inches west from the geometric center). The weight of the concrete slab between the power transformer and the isolation system (estimated at 38 kip; later revised to 45kip), was equally distributed among the bottom nodes.

The Triple FP bearings were modeled in SAP2000 using the parallel model described in Sarlis et al (2009, 2010). The model is valid for displacements less than 13.9 inches, that is, it cannot capture the behavior of the bearing in the final, stiffening regime. Table 6-6 presents the parameters of the Triple FP bearings used in program SAP2000 for nonlinear dynamic analysis.

It is noted that the weight on the bearings was specified different than the average (=418/4=104.5 kip) because of the asymmetric distribution of the weight of the power transformer.

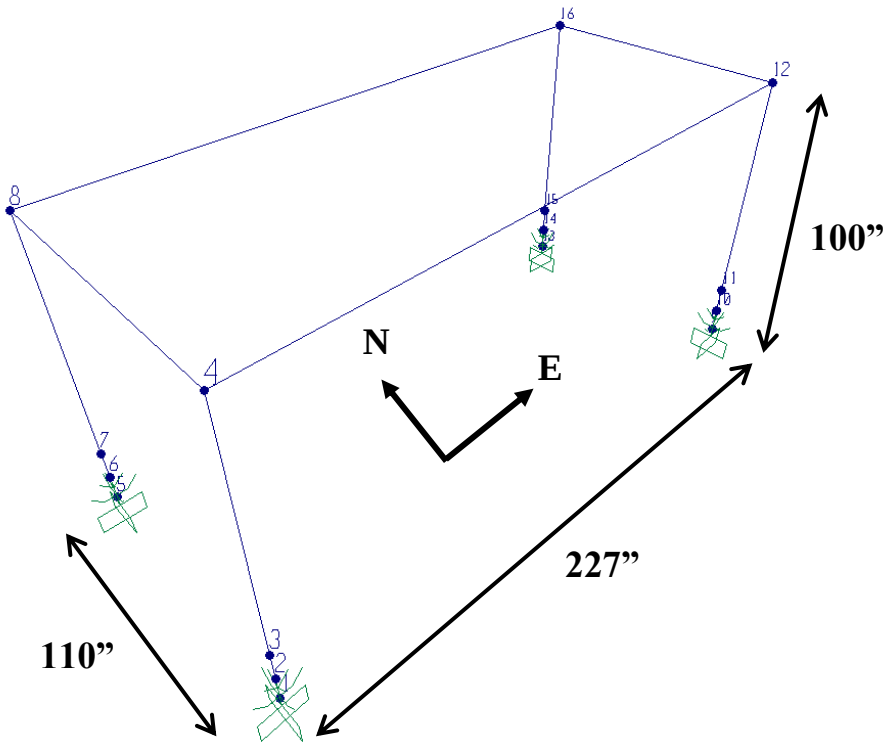


Figure 6-7 Power Transformer Model in Program SAP2000

Seven pairs of ground motions with near-fault characteristics were selected to be used in the dynamic analyses and are shown in Table 6-4. Each pair of the seed ground motions has been rotated to fault-normal and fault-parallel directions. The moment magnitudes for the seed motions are between 6.7 and 7.1; the site-to-source distances (Campbell R distance) are between 3 and 12 km and all records are from Site Classes C and D per the ASCE 7-2010. The motions are identical to those used in the examples in Constantinou et al (2011).

Table 6-4 Seed Accelerograms for Use in Response History Analysis

No.	Earthquake Name	Recording Station	M_W [1]	r [2]	Site [3]	PGV
			(n/d)	(km)		(cm/s)
1	1976 Gazli, USSR	Karakyr	6.80	5.46	C	61.50
2	1989 Loma Prieta	LGPC	6.93	3.88	C	77.15
3	1989 Loma Prieta	Saratoga – W. Valley Coll.	6.93	9.31	C	57.09
4	1994 Northridge	Jensen Filter Plant	6.69	5.43	C	73.99
5	1994 Northridge	Sylmar – Coverter Sta. East	6.69	5.19	C	95.07
6	1995 Kobe, Japan	Takarazuka	6.90	3.00	D	75.88
7	1999 Duzce, Turkey	Bolu	7.14	12.41	D	59.68
1. Moment magnitude, 2. Campbell R distance, 3. Site class classification per ASCE 7-10						

The ground motion pairs were selected and scaled as per ASCE 7-2010. Scaling of the seed motions was performed as per the requirements of ASCE 7-2010 (Section 16.1.3.2) for a site at a distance greater than 5 km from active faults. The motions were only scaled in amplitude using the weighted scaling procedures described in Pant et al (2013). The scale factors obtained are presented in Table 6-5. More details on the procedure used for the scaling of the ground motions can be found in Appendix E.

Table 6-5 Scale Factors for Ground Motions

No.	Earthquake Name	Recording Station	Factor F_J	Factor F_1	Final Scale Factor
1	1976 Gazli, USSR	Karakyr	0.731	1.2	0.877
2	1989 Loma Prieta	LGPC	0.508	1.2	0.610
3	1989 Loma Prieta	Saratoga – W. Valley Coll.	0.840	1.2	1.008
4	1994 Northridge	Jensen Filter Plant	0.478	1.2	0.574
5	1994 Northridge	Sylmar – Coverter Sta. East	0.487	1.2	0.584
6	1995 Kobe, Japan	Takarazuka	0.546	1.2	0.655
7	1999 Duzce, Turkey	Bolu	0.564	1.2	0.677

A comparison of the average SRSS spectra of the scaled motions to the target MCE_R spectrum is shown in Figure 6-8 in the period range between 0.6 and 2.6 sec, where it can be seen that the average SRSS spectrum of the scaled motions envelope the target spectrum per the criteria of ASCE 7-2010.

Figure 6-9 presents a comparison between the average of the geometric mean spectra of the scaled motions multiplied by 1.3 (to obtain the maximum direction spectrum) and the target MCE_R spectrum in the period range between 0.6 and 2.6 sec. Evidently the scaled motions sufficiently represent the target maximum direction spectrum.

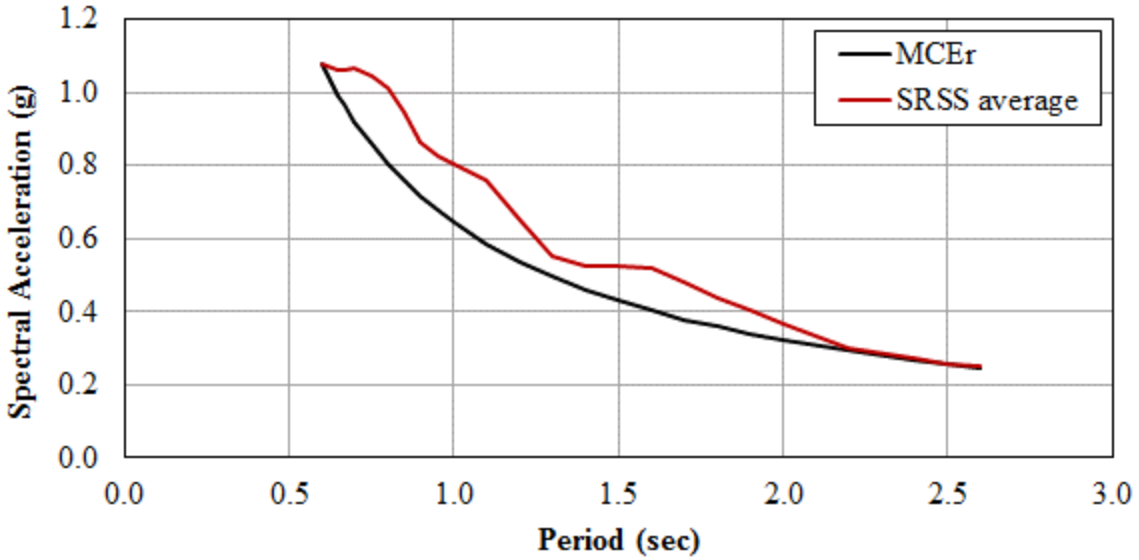


Figure 6-8 Average SRSS of Scaled Motions and MCER Spectrum - Periods 0.6 to 2.6 sec

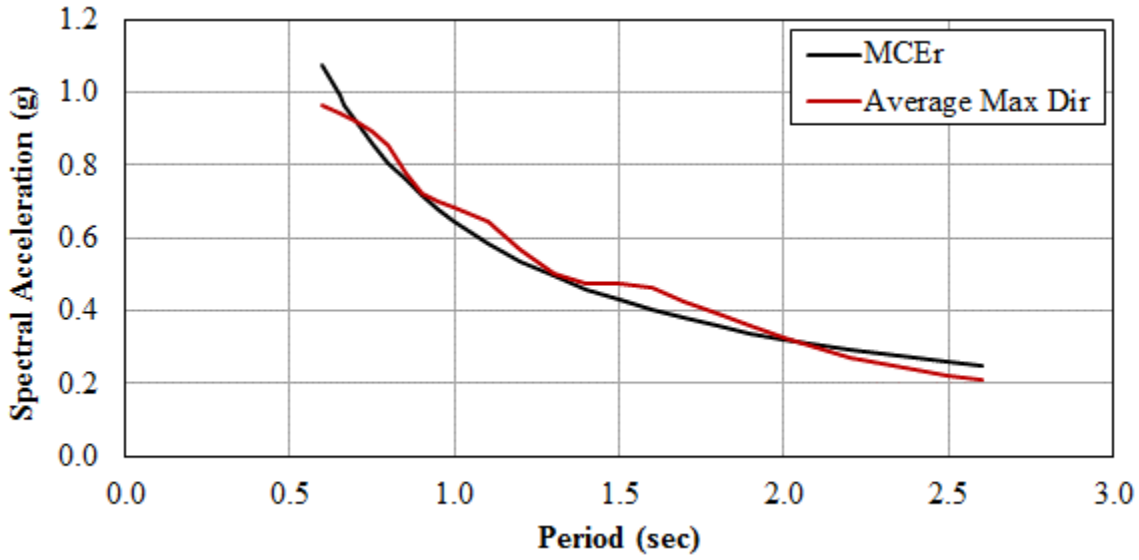


Figure 6-9 Average Maximum Direction Spectra of Scaled Motions and MCER Spectrum

Subsequently, response history analysis was performed for the ensemble of the seven scaled ground motions, with their FN and FP components along the EW and NS directions, and then again having the two components applied in NS and EW directions, respectively. Analysis was performed for the upper bound and for the lower bound frictional properties of the isolators shown in Table 6-2, and constant vertical acceleration equal to $0.2S_{MS}$=0.21g throughout each

analysis in addition to the gravitational acceleration, applied as follows: for upper bound analysis applied upwards, or +0.21g, and for lower bound analysis applied downwards, or -0.21g. Moreover, analysis was performed in the case of assumed friction $\mu_1=\mu_4=0.09$ and $\mu_2=\mu_3=0.045$ and with a constant vertical acceleration of -0.21g (downward). Note that the motions for the latter analysis were further scaled up by factor of 1.05 to meet the ASCE 7-2010 criteria for the period range of $0.5T_{eff}$ to $1.25T_{eff}$, now equal to 0.6 sec to 1.25x2.33=2.9 sec. Consistent with the definition of the seismic hazard in ASCE 7-2010 and the method of scaling of the ground motions, the average results of the dynamic response history analysis are used in design. Results of individual analyses are presented so that the reader obtains some information on the range of possible responses. However, the sample of motions used is not sufficient in number to obtain information on statistical response quantities other than the average.

Table 6-6 Parameters of Triple FP Bearings in SAP2000 for Response History Analysis (Value in Parenthesis is for Case $\mu 1=\mu 4=0.09$ and $\mu_2=\mu_3=0.045$)

Parameter		**Upper Bound Analysis Vertical Acceleration =+0.21g**		**Lower Bound Analysis (and for $\mu_1=\mu_4=0.09$ when different) Vertical Acceleration =-0.21g**	
		West Bearings	**East Bearings**	**West Bearings**	**East Bearings**
Supported Weight	**kip**	140.75	111.50	92.32	73.13
Dynamic Mass[1]	**kips-s^2/in**	2.588E-04	2.588E-04	2.588E-04	2.588E-04
Height[2] **Link Element FP1 and FP2**	**in**	9.0	9.0	9.0	9.0
Vertical Stiffness[3] **Link Element FP1 and FP2**	**kip/in**	15817.05	15817.05	15817.05	15817.05
Friction Fast (fmax) Link Element FP1	-	0.180	0.180	0.120 (0.09)	0.120 (0.09)
Friction Fast (fmax) Link Element FP2	-	0.1479	0.1479	0.0986 (0.074)	0.0986 (0.074)
Friction Slow (fmin) Link Element FP1	-	0.090	0.090	0.060 (0.045)	0.060 (0.045)
Friction Slow (fmin) Link Element FP2	-	0.0740	0.0740	0.0493 (0.037)	0.0493 (0.037)
Horizontal Elastic Stiffness Link Element FP1	**kip/in**	622.56	493.15	269.86 (200.62)	213.77 (158.92)
Horizontal Elastic Stiffness[4] **Link Element FP2**	**kip/in**	8.90	7.05	5.84	4.62
Horizontal Effective Stiffness[5] **Link Element FP1**	**kip/in**	0.00	0.00	0.00	0.00
Horizontal Effective Stiffness[5] **Link Element FP2**	**kip/in**	1.93	1.53	1.26	1.00
Effective Radius Link Element FP1	**in**	0	0	0	0
Effective Radius Link Element FP2	**in**	36.5	36.5	36.5	36.5
Rate Parameter Link Element FP1 and FP2	**sec/in**	1.27	1.27	1.27	1.27
Torsional Stiffness Link Element FP1 and FP2	**kip-in/rad**	0.00	0.00	0.00	0.00
Rotational Stiffness Link Element FP1 and FP2	**kip-in/rad**	0.00	0.00	0.00	0.00

1 Value of 0.2 kip used in the calculation.
2 Shear deformation location is at mid-height of the element.
3 Elements have same axial stiffness. Calculated for E=14500ksi, height 9inch, diameter 5inch and divided by 2.
4 Calculated as $W/2R_{eff2}$- $W/2R_{eff1}$ in order to account for the way SAP2000 calculates the elastic stiffness (specified elastic stiffness plus post elastic stiffness).
5 Effective stiffness specified as the post-elastic stiffness ($W/2R_{eff1}$) in order to minimize parasitic damping effects.

Table 6-7 Response History Analysis Results for Case $\mu 1=\mu 4=0.09$ and $\mu_2=\mu_3=0.045$

Earthq.	Resultant Displ.	Long. Accel.	Trans. Accel.	Long. Base Shear	Trans. Base Shear	Max Axial Force	Min Axial Force
	(in)	(g)	(g)	(kip)	(kip)	(kip)	(kip)
Direction FN-FP (EW-NS)							
01 NP	8.5	0.12	0.15	48.3	60.2	128.1	39.0
02 NP	14.2	0.20	0.10	83.0	41.7	130.5	36.2
03 NP	8.2	0.14	0.14	59.4	58.3	119.9	46.6
04 NP	6.9	0.13	0.10	54.1	40.6	110.8	55.8
05 NP	6.9	0.14	0.12	57.0	49.4	117.7	49.1
06 NP	7.1	0.08	0.13	35.5	52.2	118.0	48.5
07 NP	5.4	0.10	0.09	41.7	39.1	117.1	49.5
Average	**8.2**	**0.13**	**0.12**	**54.1**	**48.8**	**120.3**	**46.4**
Direction FP-FN (EW-NS)							
01 PN	8.5	0.14	0.11	60.3	48.3	115.5	51.4
02 PN	14.2	0.10	0.20	41.7	83.0	130.5	36.5
03 PN	8.2	0.14	0.14	58.2	59.4	122.7	44.2
04 PN	6.9	0.10	0.13	40.7	54.0	120.0	46.7
05 PN	6.9	0.12	0.14	49.4	57.0	122.7	44.2
06 PN	7.1	0.13	0.08	52.2	35.5	111.9	54.6
07 PN	5.4	0.09	0.10	39.1	41.7	113.4	53.2
Average	**8.2**	**0.12**	**0.13**	**48.8**	**54.1**	**119.5**	**47.3**
The peak displacement response is the maximum of all 4 isolators used. The maximum axial force occurs in the NW isolator and the minimum axial force occurs in the SE isolator							

The results are presented in Table 6-7 for the case of $\mu_1=\mu_4=0.09$ and $\mu_2=\mu_3=0.045$, in Table 6-8 for the Lower Bound case and in Table 6-9 for the Upper Bound case.

The displacements calculated in the dynamic analysis are generally less than the values calculated by the simplified procedure. Concentrating on the case of $\mu_1=\mu_4=0.09$ and applying the factor of 1.1 for torsion on the calculated displacement of 8.2 inches in the dynamic analysis, results in a value $D_{TM}=9.0$ inches. By comparison, the simplified procedure resulted in $D_{TM}=10.2$ inches. The least value of displacement allowed by ASCE 7-2010 is the largest of a) $0.8D_{TM}$ as calculated by the simplified procedure, or 0.8x10.2=8.2 inches, and b) D_{TM} calculated

in the dynamic analysis, or 9.0 inches. Therefore, the results of the dynamic analysis control the design. The isolator resultant displacement in the MCE in the conservatively low friction case of $\mu_1=\mu_4=0.09$ is expected to be 9.0 inches, that is, well within the capacity of the bearings. It may also be observed that the displacement capacity of the bearings is larger than the largest displacement calculated in one of the seven motions used in the analysis for the case $\mu_1=\mu_4=0.09$.

Table 6-8 Response History Analysis Results for Lower Bound Properties ($\mu_1=\mu_4=0.12$ and $\mu_2=\mu_3=0.06$)

Earthq.	**Resultant Displ.**	**Long. Accel.**	**Trans. Accel.**	**Long. Base Shear**	**Trans. Base Shear**	**Max Axial Force**	**Min Axial Force**
	(in)	(g)	(g)	(kip)	(kip)	(kip)	(kip)
Direction FN-FP (EW-NS)							
01 NP	6.8	0.12	0.13	51.8	53.9	127.0	41.6
02 NP	10.7	0.19	0.09	77.4	38.4	128.6	39.4
03 NP	6.8	0.15	0.15	61.7	62.4	123.7	44.5
04 NP	4.7	0.12	0.13	51.0	53.4	118.6	50.2
05 NP	6.3	0.14	0.14	59.0	59.3	121.3	47.4
06 NP	5.7	0.10	0.13	40.4	55.6	121.8	46.3
07 NP	4.8	0.12	0.12	48.1	48.9	122.7	45.8
Average	**6.5**	**0.13**	**0.13**	**55.6**	**53.1**	**123.4**	**45.0**
Direction FP-FN (EW-NS)							
01 PN	6.7	0.13	0.12	54.0	51.9	120.2	48.4
02 PN	10.7	0.09	0.19	38.4	77.5	129.6	39.6
03 PN	6.8	0.15	0.15	62.4	61.7	125.9	43.3
04 PN	4.7	0.13	0.12	53.4	51.0	123.3	45.3
05 PN	6.3	0.14	0.14	59.4	59.0	125.3	43.8
06 PN	5.7	0.13	0.10	55.6	40.3	116.5	51.9
07 PN	4.8	0.12	0.12	48.9	48.1	117.9	50.4
Average	**6.5**	**0.13**	**0.13**	**53.2**	**55.6**	**122.7**	**46.1**
The peak displacement response is the maximum of all 4 isolators used. The maximum axial force occurs in the NW isolator and the minimum axial force occurs in the SE isolator							

Spectra for each of the scaled motions in the two orthogonal directions are presented together with the average geometric mean spectrum in the cases (a) $\mu_1=\mu_4=0.09$ (Figure 6-10), (b) lower bound (Figure 6-11) and (c) upper bound (Figure 6-12). More specifically, first the 5%-damped

geometric mean spectrum above the isolators was calculated for each motion and then the seven spectra were averaged. In each case, the IEEE 693-2005 High RRS (0.5g PGA) and the IEEE 693-2005 Moderate RRS (0.25g) spectra for 5% damping are also included in order to demonstrate the achieved filtering of the input motions at the base of the equipment, due to the use of the Triple FP isolation system. Furthermore, Figure 6-13 presents the 5%-damped acceleration response spectra at the ground level for the non-isolated power transformer. These spectra were calculated from the scaled ground motions used in the dynamic analysis (presented in Table 6-5).

Table 6-9 Response History Analysis Results for Upper Bound Properties ($\mu_1=\mu_4=0.18$ and $\mu_2=\mu_3=0.09$)

Earthq.	**Resultant Displ.**	**Long. Accel.**	**Trans. Accel.**	**Long. Base Shear**	**Trans. Base Shear**	**Max Axial Force**	**Min Axial Force**
	(in)	(g)	(g)	(kip)	(kip)	(kip)	(kip)
Direction FN-FP (EW-NS)							
01 NP	4.4	0.24	0.20	99.5	85.9	198.2	59.5
02 NP	3.7	0.25	0.17	105.9	70.1	187.3	69.3
03 NP	4.2	0.25	0.20	103.6	82.8	185.6	70.2
04 NP	2.2	0.19	0.21	80.3	86.0	185.6	72.0
05 NP	3.3	0.20	0.24	85.6	99.4	192.8	64.7
06 NP	3.5	0.20	0.24	84.3	100.5	192.0	64.3
07 NP	4.0	0.18	0.25	73.2	106.1	201.4	58.0
Average	**3.6**	**0.22**	**0.21**	**90.4**	**90.1**	**191.8**	**65.4**
Direction FP-FN (EW-NS)							
01 PN	4.3	0.21	0.23	86.6	98.4	194.8	63.7
02 PN	3.8	0.17	0.25	70.8	106.1	198.5	59.8
03 PN	4.2	0.20	0.25	83.2	103.4	190.0	67.9
04 PN	2.0	0.21	0.19	86.1	79.8	188.4	68.9
05 PN	3.2	0.24	0.20	99.6	85.0	191.3	66.6
06 PN	3.5	0.24	0.20	100.4	83.3	187.6	68.7
07 PN	3.9	0.25	0.17	106.2	71.9	185.2	71.6
Average	**3.6**	**0.22**	**0.21**	**90.4**	**89.7**	**190.8**	**66.7**
The peak displacement response is the maximum of all 4 isolators used. The maximum axial force occurs in the NW isolator and the minimum axial force occurs in the SE isolator							

Evidently, the isolation system is sufficiently effective to reduce the average geometric mean spectral acceleration so that the equipment qualifies for the IEEE 693-2005 Moderate RRS. Interestingly, every single response spectrum calculated is below the IEEE 693-2005 High RRS for the cases of lower and upper bound analysis. Furthermore, comparing the spectra of the input motions at the base of the isolated power transformer (Figure 6-10 to Figure 6-12) and non-isolated (Figure 6-13), one can observe that base isolation is reducing substantially the demands in the range of the fundamental frequencies of the bushings and of other components.

Figure 6-14 presents a view of the power transformer retrofitted with the isolation system that was designed as discussed above.

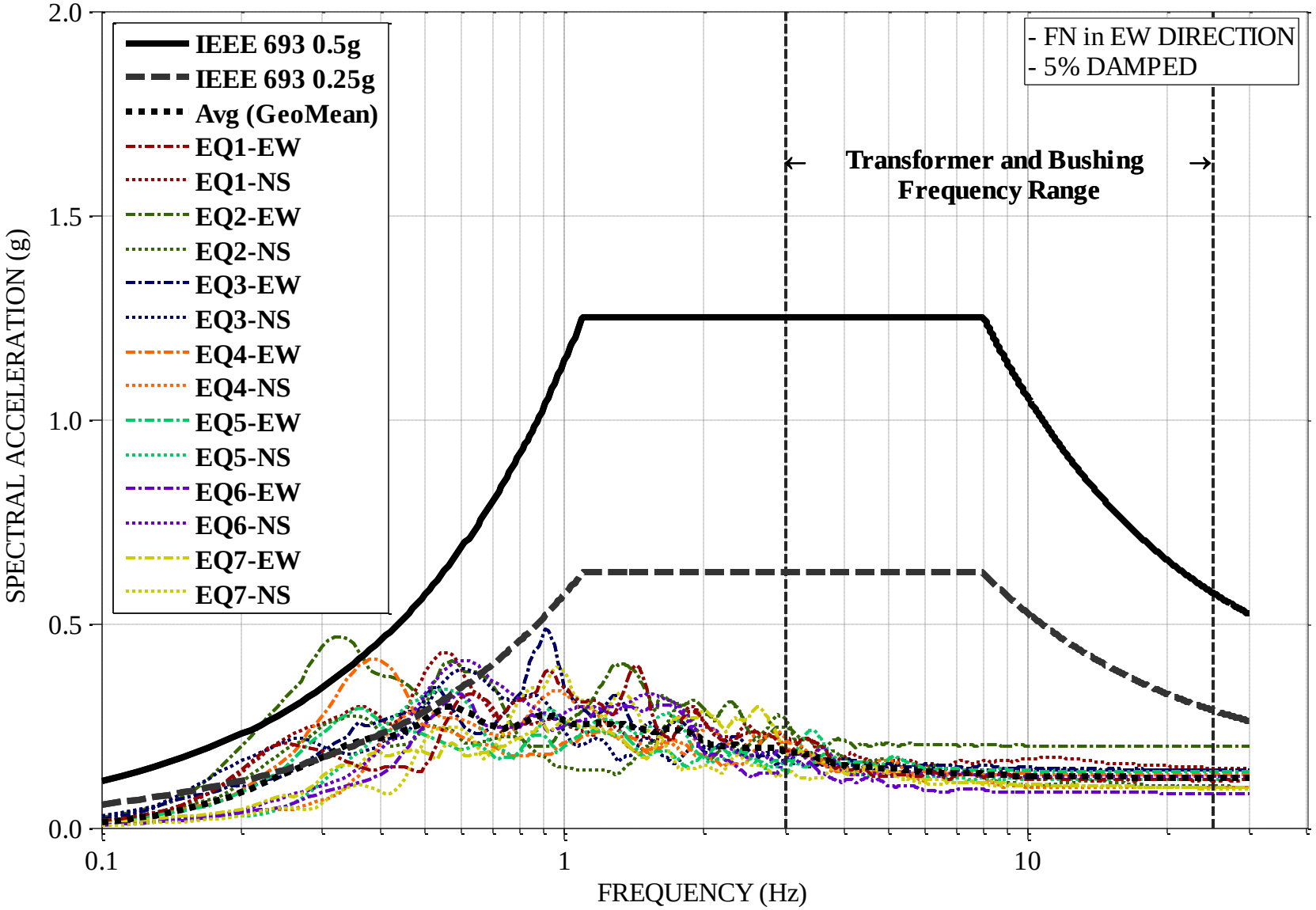


Figure 6-10 Acceleration Response Spectra at Base of the Power Transformer (on Top of Isolators) for Case μ1=μ4=0.09 and μ2=μ3=0.045

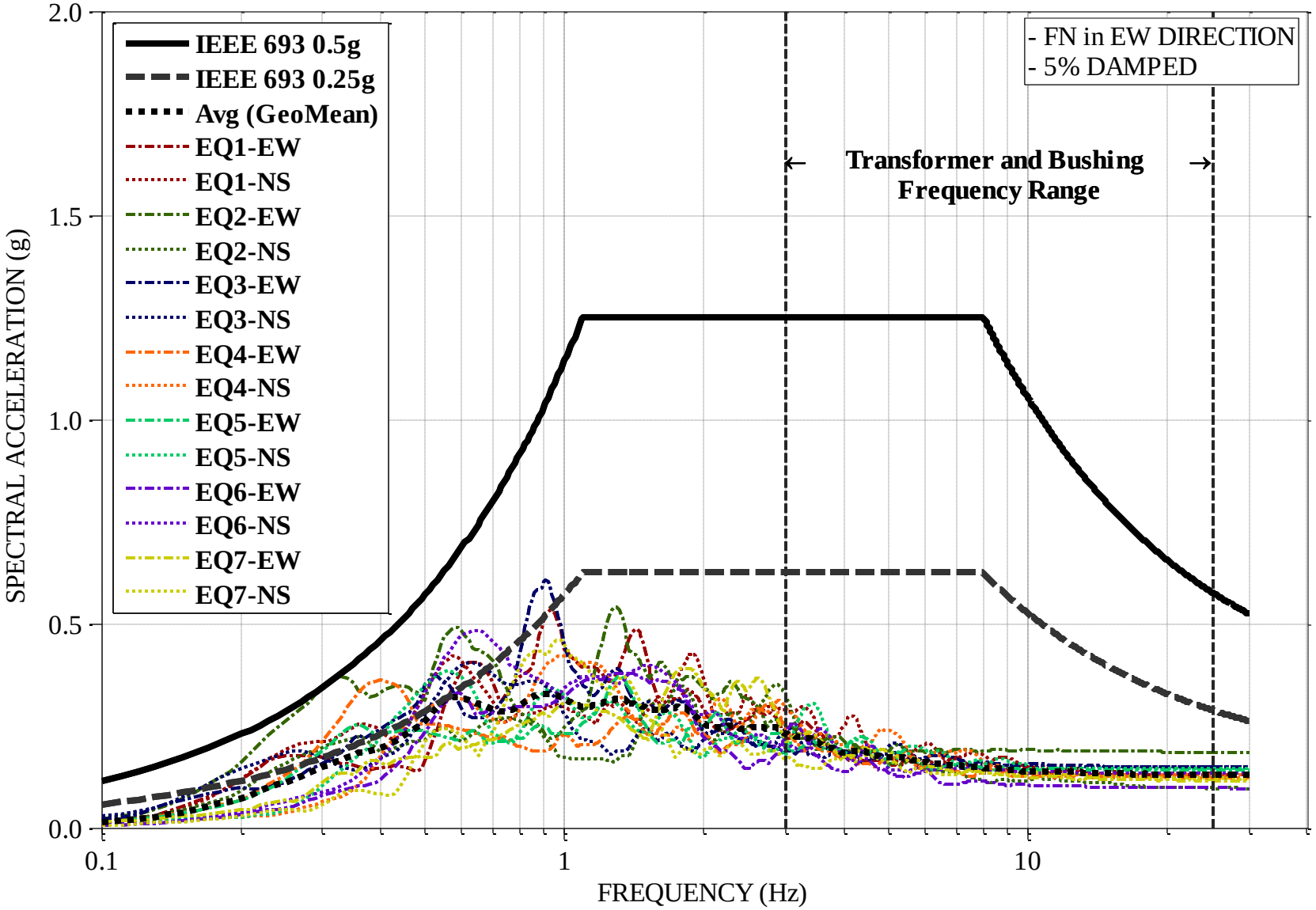


Figure 6-11 Acceleration Response Spectra at Base of the Power Transformer (on Top of Isolators) in Lower Bound Analysis ($\mu_1=\mu_4=0.12$ and $\mu_2=\mu_3=0.06$)

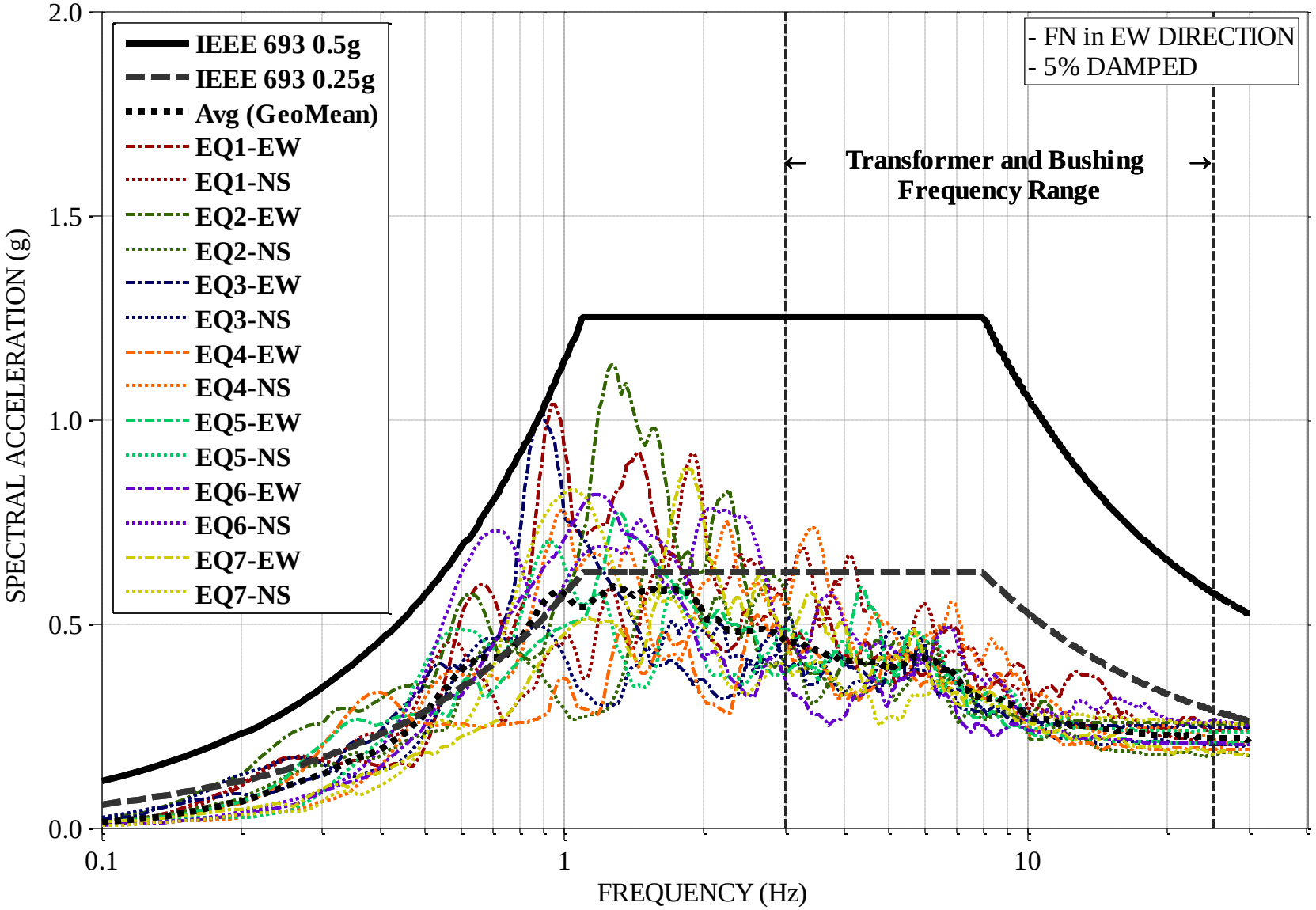


Figure 6-12 Acceleration Response Spectra at Base of the Power Transformer (on Top of Isolators) in Upper Bound Analysis ($\mu_1=\mu_4=0.18$ and $\mu_2=\mu_3=0.09$)

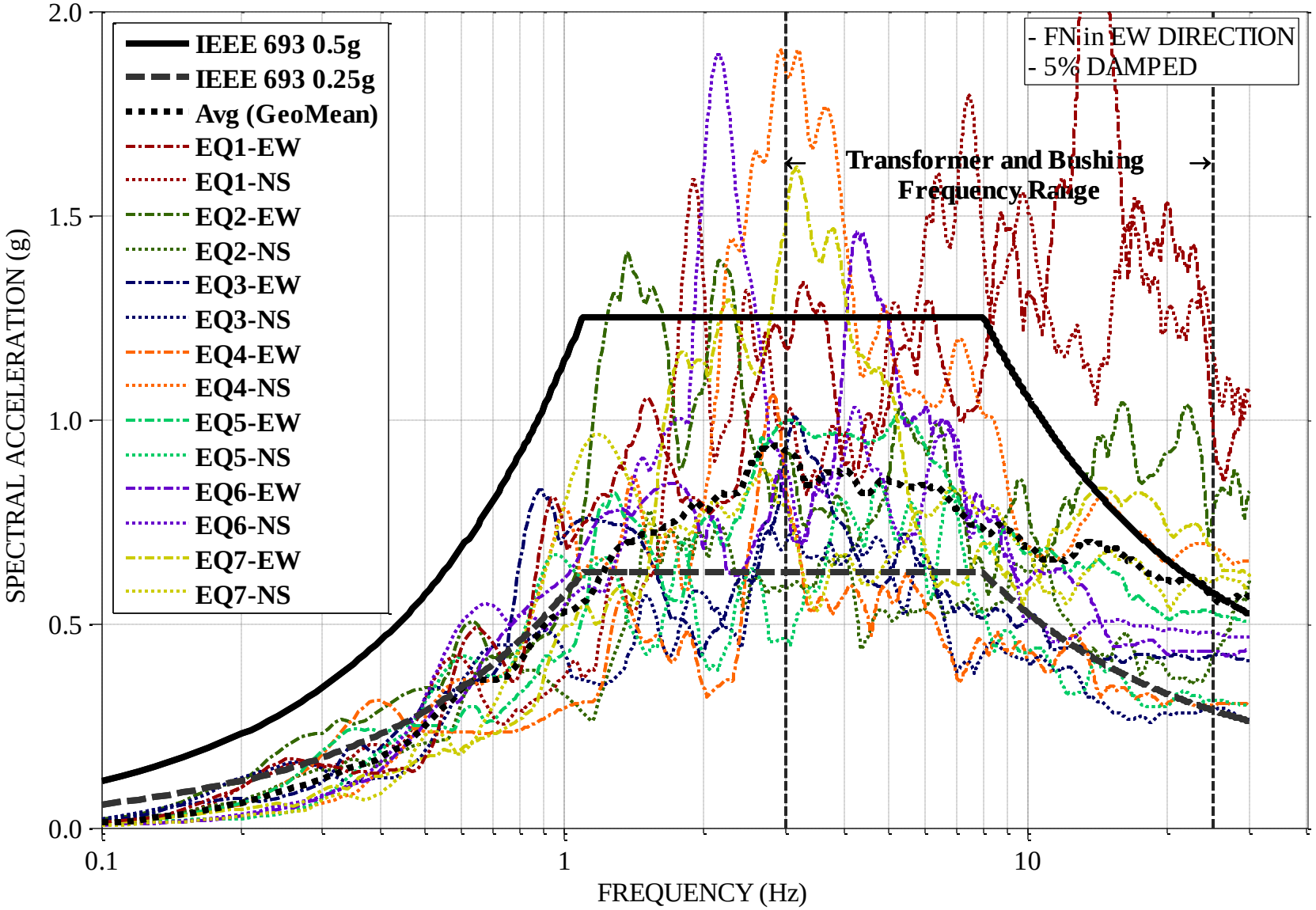


Figure 6-13 Acceleration Response Spectra of Scaled Input Motions at the Ground Level (Under the Isolators)

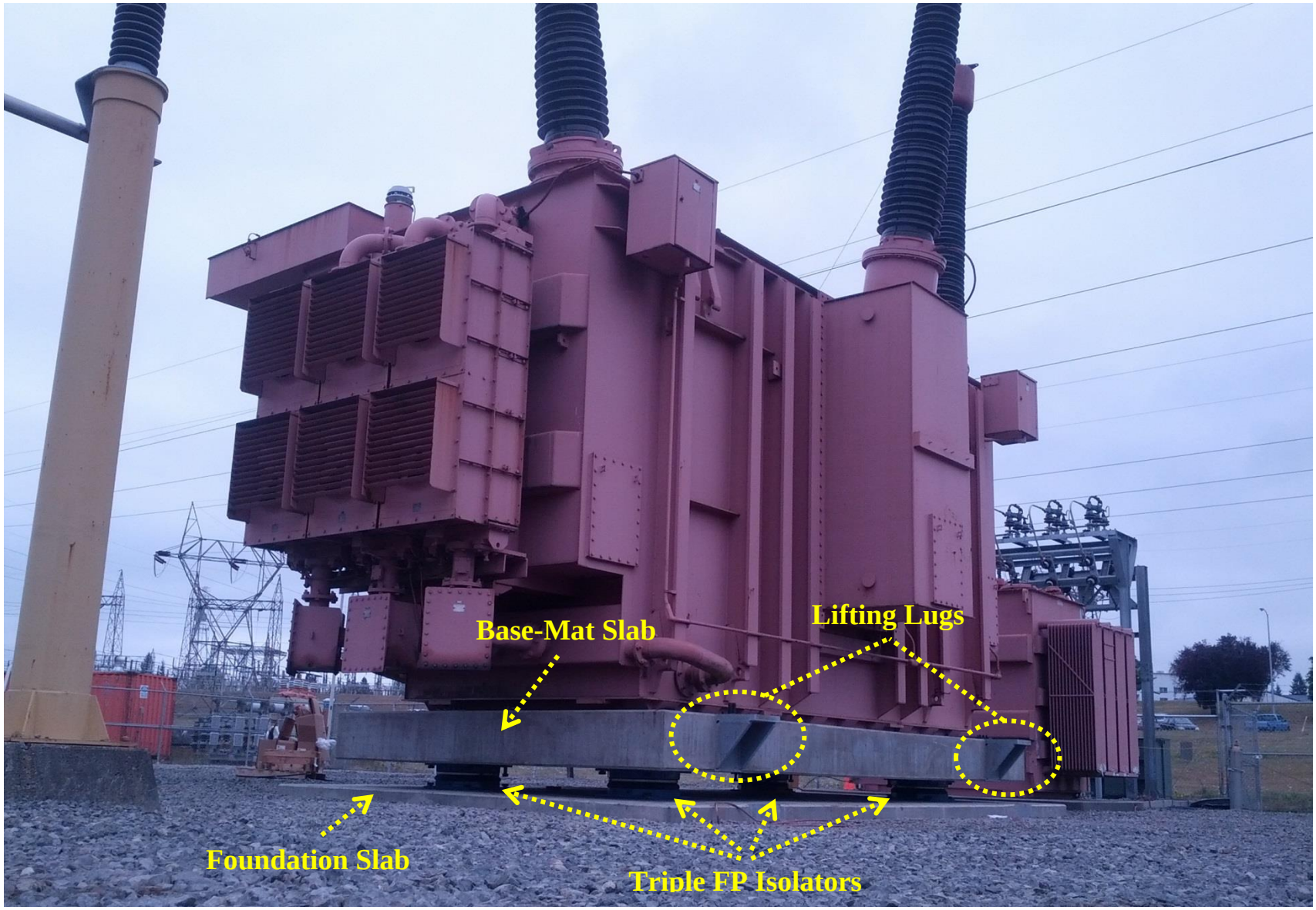


Figure 6-14 460 kV Power Transformer Retrofitted with Triple FP Isolators (Vancouver, WA)

6.4.7. Testing of Isolators

The isolators used in the design example presented herein, are identical in geometry to those used in the full-scale shake table testing of the isolated power transformer model as discussed in previous sections. These isolators were returned to the manufacturer after testing, where they were refurbished, tested and shipped for installation to the Vancouver power transformer.

During testing, each bearing was subjected to compressive load of about 110 kips (average temporal load with fluctuations of up to ±15%) and three (3) cycles of lateral harmonic motion at amplitude of 9 inch (±0.5 inch). Slow and fast tests were performed, in order to obtain the frictional properties of the isolators. For each bearing, the coefficient of friction was measured as the average of the three cycles of motion using the following procedure:

- The instantaneous lateral force was divided by the instantaneous vertical force to obtain the history of normalized lateral force. The normalized lateral force was plotted against the imposed lateral displacement for all three cycles.

- The coefficient of friction was calculated as:

$$\mu_i = \frac{E_i}{\Delta_i}$$

where E_i is the total area (normalized energy) enclosed by the hysteresis loops in the three cycles and Δ_i is the total travel in the three cycles (equal to 4x3=12 times the displacement amplitude).

Results from slow and fast testing are shown in Figure 6-15 for one of the four bearings tested. The red line in these graphs shows the theoretical loop for perfect rigid-linear behavior (normalized stiffness equal to $1/2R_{eff1}=1/72$ inch^{-1}) and friction coefficient of 0.12. Note that the fluctuating loops in the dynamic test are due to fluctuations in the axial force and in the velocity during testing.

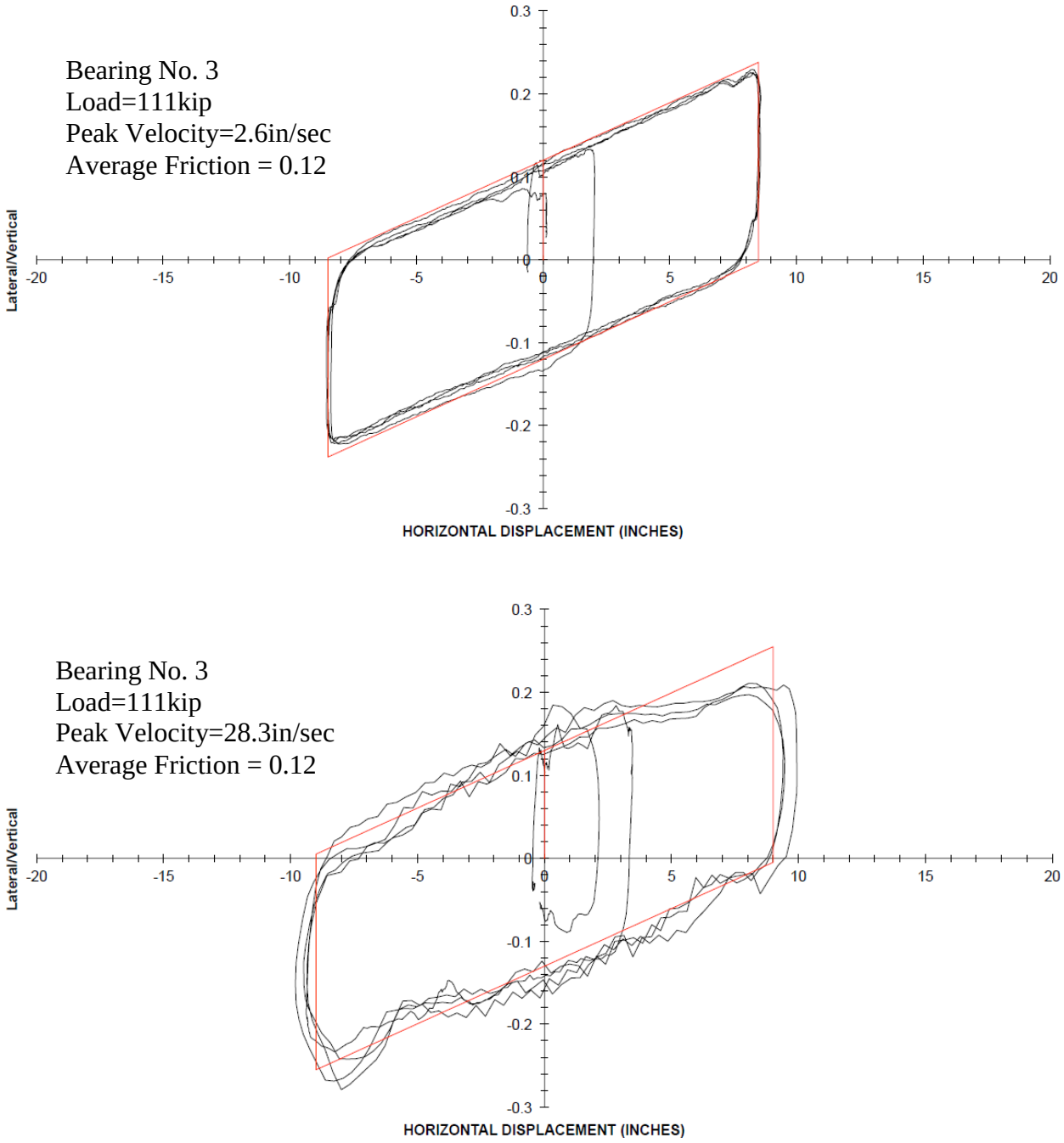


Figure 6-15 Lateral Force/Vertical Force vs Displacement Loops of Full Size Triple FP Bearing No. 3 under Slow (Top) and Fast (Bottom) Motion

This Page is Intentionally Left Blank

SECTION 7
SUMMARY AND CONCLUDING REMARKS

A high voltage power transformer is an important piece of electrical substation equipment for the operation of a power system. High voltage power transformers together with high voltage bushings, which are critical components for the functionality of power transformers, have been shown to be particularly susceptible to damage during past strong earthquakes. Base isolation is studied in this work as a practical means of seismically protecting and retrofitting high voltage power transformers and their appendages.

In order to effectively base isolate high voltage power transformers, isolation systems that appropriately account for the special structural characteristics of electrical power transformers are selected, recognizing that the differences between the electrical power transformers and conventional engineering structures will impose certain constraints in the use of base isolation. For instance, in base isolated power transformers, the isolation system displacements are limited by the slack of the connections of power transformers to high voltage conductors and ancillary equipment. Also, the highly asymmetric mass distribution typically featured in commercial power transformers can potentially generate significant torsion in the isolation system. Furthermore, power transformers have small weight which encumbers the lengthening of the effective period when certain isolation systems are used. In addition to the above, the connection of the isolators to the equipment needs to be achieved in such way that retrofit or maintenance of the power transformer will not cause lengthy interruptions in power transmission. In light of such constraints, two systems have been selected in the present study as the best candidate

systems for seismic isolation of electrical power transformers: (a) stiff and highly damped lead-rubber bearings, and (b) high friction Triple Friction Pendulum bearings.

The effectiveness of the selected isolation systems was investigated through an experimental program in the Structural Engineering and Earthquake Simulation Laboratory at the University at Buffalo. The design details of this experimental program are discussed in Section 3. Specifically, shake table tests were carried out on an isolated simulated power transformer specimen which nonetheless incorporated all of the important structural features of a typical power transformer tank, such as high asymmetry in mass, roof flexibility and realistic bushing dynamics by simulating the mounting conditions of the bushing as it is installed in the field. In order to evaluate the effectiveness of base isolation, testing under non-isolated conditions was also carried out using the same power transformer specimen configurations. Testing of the base isolated specimen was performed with the bearings bolted at the bottom, but only connected through friction at the top to the power transformer base mat (Friction-Bolted configuration), with the exception of the lead rubber bearings, which were additionally tested bolted both at the bottom and at the top to the power transformer base mat (Bolted-Bolted configuration). The sensitivity in the seismic response of the isolated power transformer and bushing model assembly was investigated by performing bi-axial horizontal and tri-axial testing at various seismic levels, and testing with the bushing mounted symmetrically or asymmetrically on the roof. Additionally, tests were carried out for the configurations described above but with full size Triple Friction Pendulum bearings connected by friction at the top and bolted at the bottom (Friction-Bolted configuration) and tested in actual time scale. The results obtained from the shake table testing, and the evaluation of the testing results, are presented in Section 4. The key findings from this experimental program are summarized below:

a. The isolation systems tested (the Lead Rubber Bearings and Triple FP bearings in the Friction-Bolted configuration, and the Lead Rubber Bearings in the Bolted-Bolted configuration) resulted in similar reductions in the seismic demand on the bushing, in comparison to the non-isolated specimen. For symmetric installation of the bushing on the cover, the achieved reduction in the average acceleration response at the roof of the power transformer specimen and at the center of gravity of the bushing (an acceptable measure of the global performance of the bushing), was found to be on the order of 70%-80%. Similar reductions in the seismic demand on the power transformer specimen were also achieved, as reflected in the measured base shear forces.

b. The isolation displacements were within the limits prescribed to avoid compromising the peripheral connections to the power transformer in an actual application. Specifically, from reduced scale testing of the isolated model, the peak relative resultant displacements at the top of the bushing were found to be between 3 and 4 inches for all isolation systems, which are on the order of 9 to 12 inches when extrapolated to the prototype length scale. These displacements are smaller than the typical slack of conductors installed in the field. Testing with the full scale Triple FP bearings yielded similar relative displacements (on the order of 5 to 11 inches), regardless of the mounting configuration of the bushing. The reported displacements are attributed to the rigid body motion of the base isolated power transformer specimen. Note that the observed displacements measured at the top of bushings in the base-isolated system are comparable to the flexural deformations of the bushings mounted on the flexible rooftop cover for the case when the power transformer is not isolated.

c. Of the configurations tested, the one featuring the LRB in the Friction-Bolted configuration resulted in significant sliding at the friction connection interface, whereas the Triple FP system did not experience sliding at this interface except in extreme earthquake motions when the displacement capacity of the isolators was consumed. Sliding was found to be beneficial for the stability of the LRB by acting to reduce the forces and deformations obtained when the bearings were bolted to the base mat. However, this seemingly desirable behavior comes at the expense of additional displacements (sliding) which may accumulate to large enough values to compromise the global stability of the system. Bolting the LRB to the base mat eliminated the problem, leaving the global performance of the system unaffected.

d. The torsional response of both tested connection details of the LRB system was significantly higher than that of the Triple FP system. Specifically, torsion amplified the displacements of the LRB by as much as 45%, while the corresponding amplification for the Triple FP isolators was less than 5%, even when the Triple FP isolators reached their displacement capacity in the event of extreme shaking. In the case of high mass asymmetry in the tested system, the resulting eccentricity between the center of mass of the superstructure and the center of stiffness of the isolators generated torsional response. The above discrepancy is explained by the relation of the center of mass of the superstructure and center of rigidity in the two systems. Since the LRB have fixed strength and stiffness properties, the center of rigidity is only dependent on the location of the bearings and seldom coincides with the center of mass, which is calculated from the generally asymmetrical distribution of weight in the power transformer. Thus, for the LRB system, there usually exists some eccentricity between the centers of mass and rigidity which leads to torsion. On the contrary, provided

that the coefficients of friction are the same for all isolators, the Triple FP have strength and stiffness properties that are dependent on the (mass) weight tributary to each bearing, with the center of rigidity always coinciding with the center of mass (weights), thus eliminating eccentricity and consequently torsion. Since there is some variation in friction coefficient between the bearings due to large differences in the load they carry, some small torsional response is generated and it has been observed in the tests.

e. Base isolation filtered the input horizontal accelerations and reduced the demand at the base of the power transformer and at the bushing mounting interface for a wide range of frequencies. Specifically, the demand was significantly reduced for frequencies beyond the post yielding response frequencies of the tested isolation systems (above 1Hz for the LRB isolation system and 0.3Hz for the Triple FP system). Since this frequency range encompasses the frequencies of commercial high voltage power transformers when fixed to the foundation, and the frequencies of their attachments, it is expected that base isolation will protect a power transformer globally including external and internal components, such as the core and coil assembly, that otherwise would not be possible to seismically retrofit. Due to the fact that several other components of an electrical substation have frequencies similar to high voltage power transformers and bushings, the broad frequency range for which seismic demand reduction was achieved suggests the potential for application of base isolation in the seismic protection of a wide variety of substation equipment.

f. The bushing acceleration response was found to be amplified due to the combination of the rooftop cover flexibility and the vertical input at the mounting interface of the bushing. The effect of the rooftop cover flexibility in particular is to significantly reduce the frequency of

the roof-bushing assembly in comparison to the corresponding fixed base frequency of the bushing alone. The acceleration response amplification was found to be more pronounced when the bushing was mounted on the side of the roof, due to coupling between the vertical and rotational dynamic properties of the bushing-rooftop cover system, and when tri-axial testing was performed. Nevertheless, regardless of the bushing mounting configuration and whether the vertical component of the ground motion was used in testing, the base isolation achieved considerable reduction in the bushing horizontal response in comparison to the non-isolated case. There was no reduction in the acceleration response in the vertical direction as the isolation systems were essentially vertically rigid.

g. Local phenomena such as small uplift and impact were witnessed during testing. The exact origin of these phenomena could not be identified, and they are attributed to imperfections in the construction of the test specimen. Their effect on the response of the system is exaggerated due to the small mass of the components used in the assembly, as well as the unrealistically high stiffness of the power transformer specimen itself. These phenomena, however likely to occur, are not expected to have prominent effects in full size isolated power transformers. The major effect of uplift and impact during testing was to amplify the system response and the spectral demands in the high frequency range, however not importantly in the frequency range of interest (frequencies higher than 20Hz were markedly affected). Even when these amplifications were accounted for in the calculation of the response spectra at the mounting interface of the bushing (obtained from testing of the isolated models), the spectral demand was significantly lower than the one of the required response spectra for the corresponding seismic level and location recommended by the IEEE 693 standard for the seismic qualification of high voltage bushings.

Section 5 presents the development of analytical models of the tested frame-bushing model and the isolation systems in the commercial software SAP2000, and analytical investigations performed to assess the capability of the models to predict the observed response. Modeling of the isolation systems utilized in testing of the reduced length scale configurations was performed using properties obtained from testing of the individual isolator units in the bearing testing machine in SEESL. The properties used in the modeling of the full size Triple FP isolators were not known a priori but were identified in shake table testing. Other parameters that likely affected the properties of the isolators, including cumulative effects on the isolators due to prolonged and sequential testing (heating, traveling and wear of the materials), differences between the isolator units, and uplift and sliding at the isolator connection interface, were disregarded in the analysis. Additionally, the vertical loads on the isolators in SAP2000 were taken as the resulting loads from static analysis of the SAP2000 model with the defined mass distribution; the actual vertical loads on the bearings could not be accurately measured by the load cells. In light of these simplifications, the analytical models were found to provide sufficiently accurate predictions of the response. For instance, the average isolation system displacements were predicted within 2% of the average experimental values obtained for the Triple FP system, and about 15% of the average experimental values obtained for the LRB system. In the prediction of the base shear, the average peak analytical values were found to be within 20% of the average experimental values obtained for the Triple FP system and about 10% of the average experimental values obtained for the LRB system. The average accelerations at the center of gravity of the bushing were predicted with a discrepancy of about 20% for the LRB system but by as much 50% for the Triple FP system. This large discrepancy for the Triple FP system is attributed primarily to artificially high values of acceleration generated by sliding and

pounding of the vertical side plates of the superstructure due to loose connections, and some misalignment of the internal components of the Triple FP isolators. These effects could not be captured in the SAP2000 model. Secondarily, the above discrepancy is attributed to the simplified modeling of the high voltage bushing in SAP2000, particularly the mass distribution, which could not capture higher mode effects caused by impact. Moreover all the differences stated above do not represent the errors of experimentation, the errors of analytical calculations and the modeling errors. When those are considered, the agreements can be considered suitable for all practical purposes.

Section 6 presents an example of analysis and design of a base isolation system for the seismic retrofit of an electrical power transformer in Washington. Some of the design components discussed deal with the identification of the important structural characteristics of the power transformers, the assessment of the seismic demand for the site location, the selection of design properties for the isolation system, the description of modeling issues and standard analysis procedures, foundation construction issues and the installation of the isolation system. Furthermore, design guidelines are summarized in the form of suggested design steps.

The retrofit described in Section 6 was implemented in the field and future observations in actual earthquakes could add to the confidence of using the methodology developed herein.

SECTION 8
REFERENCES

American Society of Civil Engineers, "Minimum Design Loads for Buildings and Other Structures", ASCE Standard ASCE 7-10, 2010.

Bellorini, S., Bettinali, F., Salvetti, M., and Zafferani, G. (1998), "Seismic Qualification of Transformer High Voltage Bushings," IEEE Transactions on Power Delivery, 13 (4), pp. 1208–1213.

Bozorgnia, Y. and Campbell, K.W. (2004), "The Vertical-to-Horizontal Response Spectral Ratio and Tentative Procedures for Developing Simplified V/H and Vertical Design Spectra," Journal of Earthquake Engineering, Vol. 8, No.2, 175-207.

Clarke, C.S.J., Buchanan, R., Efthymiou, M., and Shaw, C. (2005), "Structural Platform Solution for Seismic Arctic Environments–Sakhalin II Offshore Facilities," Paper OTC- 17378-PP, Offshore Technology Conference, Houston, Texas.

Constantinou, M.C., Kalpakidis, I., Filiatrault, A. and Ecker Lay, R.A. (2011), "LRFD-based Analysis and Design Procedures for Bridge Bearings and Seismic Isolators", PEER and MCEER Report, University of California and University at Buffalo.

Constantinou, M.C., Whittaker, A.S., Kalpakidis, Y., Fenz, D.M. and Warn, G.P. (2007), "Performance of Seismic Isolation Hardware under Service and Seismic Loading," Report No. MCEER-07-0012, Multidisciplinary Center for Earthquake Engineering Research, Buffalo, NY.

CSI (2002), “SAP2000 Analysis Reference Manual,” Computers and Structures Inc., Berkeley, CA.

Ersoy, S., Saadeghvaziri, M.A., Liu, G., and Mau, S.T. (2001), “Analytical and Experimental Seismic Studies of Transformers Isolated with Friction Pendulum System and Design Aspects,” Earthquake Spectra, 17(4), pp. 569–595.

Ersoy, S., and Saadeghvaziri, M.A. (2004), “Seismic Response of Transformer-Bushing Systems,” IEEE Transactions on Power Delivery, 19 (1), pp. 131-137.

Fadi, F. and Constantinou, M.C. (2010), “Evaluation of Simplified Methods of Analysis for Structures with Triple Friction Pendulum Isolators,” Earthquake Engineering & Structural Dynamics, Vol. 39, No. 1, 5-22.

Fahad, M. (2013), “Seismic Evaluation and Qualification of Transformer Bushings,” Doctor of Philosophy in Civil Engineering Dissertation, University at Buffalo, The State University of New York, Buffalo, U.S.A.

Fenz, D. and Constantinou, M.C. (2008a), “Spherical Sliding Isolation Bearings with Adaptive Behavior: Experimental Verification,” Earthquake Engineering and Structural Dynamics, Vol. 37, No. 2, 185-205.

Fenz, D.M. and Constantinou, M.C. (2008b),”Mechanical Behavior of Multi-spherical Sliding Bearings,” Report No. MCEER-08-0007, Multidisciplinary Center for Earthquake Engineering Research, Buffalo, NY.

Fenz, D.M. and Constantinou, M.C. (2008c),"Development, Implementation and Verification of Dynamic Analysis Models for Multi-spherical Sliding Bearings," Report No. MCEER-08-0018, Multidisciplinary Center for Earthquake Engineering Research, Buffalo, NY.

Fenz, D. and Constantinou, M.C. (2008d), "Modeling Triple Friction Pendulum Bearings for Response-history Analysis," Earthquake Spectra, Vol. 24, No. 4, 1011-1028.

Filiatrault, A. and Matt, H. (2005), "Experimental Seismic Response of High-Voltage Transformer-Bushing Systems," Earthquake Spectra, 21 (4), pp.1009–1025.

Filiatrault, A. and Matt, H. (2006), "Seismic Response of High Voltage Transformer-Bushing Systems," ASCE Journal of Structural Engineering, 132(2), pp. 287-295.

Gilani, A.S.J., Whittaker, A.S., Fenves, G. L., and Fujisaki, E. (1999). "Seismic Evaluation of 550-kV Porcelain Transformer Bushings," Report No. PEER 99/05, Pacific Earthquake Engineering Research Center, University of California at Berkeley.

Huang Y.N., Whittaker, A.S., Luco, N., (2008), "Maximum Spectral Demands in the Near-Fault Region", Earthquake Spectra, Vol. 24, No. 1, 319-341.

IEEE (2005), "IEEE Recommended Practice for Seismic Design of Substations," IEEE-SA Standards Board, NY.

Kircher, C.A., Delfosse, G.C., Schoof, C.C., Khemici, O., Shah, H.C. (1979), "Performance of a 230 KV ATB 7 Power Circuit Breaker Mounted on GAPEC Seismic Isolators," Report No 40, John A. Blume Earthquake Engineering Center, Stanford University, CA, U.S.A.

Kircher, C.A. (2010). Personal communication with M.C. Constantinou.

Knight, B.T., Kempner, L. Jr (2004), "A Utility's Approach to Seismically Hardening Existing High-Voltage Electrical Transmission Substation Equipment," Proceedings of 13th WCEE, August 1-6, 2004, Vancouver, B.C., Canada.

Koliou, M. (2010), "Seismic Protection of Electrical Transformer Bushing Systems by Stiffening Techniques," Master of Science in Civil Engineering Thesis, University at Buffalo, The State University of New York, Buffalo, U.S.A.

Koliou, M., Filiatrault, A., Reinhorn, A.M. and Oliveto, N. (2012), "Seismic Protection of Electrical Transformer Bushing Systems by Stiffening Techniques," Report No. MCEER-12-0002, Multidisciplinary Center for Earthquake Engineering Research, Buffalo, NY.

Koliou, M., Filiatrault, A., Reinhorn, A.M. (2013a), "Seismic Response of High-Voltage Transformer-Bushing Systems Incorporating Flexural Stiffeners I: Numerical Study," Earthquake Spectra, 29 (4), pp.1335–1352.

Koliou, M., Filiatrault, A., Reinhorn, A.M. (2013b), "Seismic Response of High-Voltage Transformer-Bushing Systems Incorporating Flexural Stiffeners II: Experimental Study," Earthquake Spectra, 29 (4), pp.1353–1367.

Kong, D. (2010), "Protection of High Voltage Electrical Equipment Against Severe Shock and Vibration," Doctor of Philosophy in Civil Engineering Dissertation, University at Buffalo, The State University of New York, Buffalo, U.S.A.

Kong, D. and Reinhorn, A.M. (2009), “Seismic Evaluation and Protection of High Voltage Disconnect Switches,” TCLEE Lifeline Earthquake Engineering in a Multihazard Environment, ASCE, 221-231.

McVitty, W.J., Constantinou, M.C. (2015), “Property Modification Factors for Seismic Isolators: Design Guidance for Buildings,” Report No. MCEER-XX-XXXX (under Preparation), Multidisciplinary Center for Earthquake Engineering Research, Buffalo, NY.

Murota, N., Feng, M.Q. and Liu, G.Y. (2006), “Earthquake Simulator Testing of Base-Isolated Power Transformers,” IEEE Transactions of Power Delivery, Vol. 21, No. 3, July, 1291-1299.

Pant, D.R., Constantinou, M.C., Wijeyewickrema, A.C. (2013), “Re-evaluation of Equivalent Lateral Force Procedure for Prediction of Displacement Demand in Seismically Isolated Structures,” Engineering Structures, Vol. 52, pp. 455-465.

Park, Y.J., Wen, Y.K. and Ang, A.H.S. (1986), "Random vibration of hysteretic systems under bi-directional ground motions," Earthquake Engineering & Structural Dynamics, Vol. 14, No. 4, 543-557.

Prevost T., Woodcock D.J. and Krause C. “The Effect on Winding Clamping Pressure Due to Changes in Moisture, Temperature and Insulation Age”, WEIDMANN Electrical Technology

Ramirez, O.M., Constantinou, M.C., Gomez, J.D., Whittaker, A.S., Chrysostomou, C.Z. (2002), “Evaluation of Simplified Methods of Analysis of Yielding Structures with Damping Systems”, Earthquake Spectra, Vol. 18, No. 3, 501-530.

Ray, T., Sarlis, A.A., Reinhorn A.M., Constantinou M.C. (2013), "Hysteretic Models for Sliding Bearings with Varying Frictional Force," Earthquake Engineering & Structural Dynamics, Vol. 42, No. 15, 2341–2360.

Reinhorn, A.M.; Filiatrault, A., Fahad, M., Kong, D., Koliou, M., Oikonomou, K., Oliveto, N. and Schiff A. (2012). Evaluation of the Seismic Performance of High-voltage Transformer Bushings. California Energy Commission. Publication number: CEC-XXX-2012.

Roussis, P. C. and Constantinou, M. C. (2005), "Experimental and Analytical Studies of 89 Structures Seismically Isolated with an Uplift-Restraint Isolation System," Technical Report MCEER-05-0001, Multidisciplinary Center for Earthquake Engineering Research, State University of New York, Buffalo, NY.

Sarlis, A.A., Tsopelas, P.C., Constantinou, M.C. and Reinhorn, A.M. (2009), "3D-BASIS-ME-MB: Computer Program for Nonlinear Dynamic Analysis of Seismically Isolated Structures, Element for Triple Pendulum Isolator and Verification Examples", supplement to MCEER Report 05-009, document distributed to the engineering community together with executable version of program and example files, University at Buffalo.

Sarlis, A.A. and Constantinou, M.C. (2010), "Modeling Triple Friction Pendulum Isolators in SAP2000," document distributed to the engineering community together with example files, University at Buffalo, June.

Sarlis, A.A., Constantinou, M.C. and Reinhorn, A.M. (2013), "Shake Table Testing of Triple Friction Pendulum Isolators under Extreme Conditions," Report No. MCEER-13-0011, Multidisciplinary Center for Earthquake Engineering Research, Buffalo, NY.

Schiff, A.J. (1998), "Hyogoken Nabu (Kobe) Earthquake of January 17, 1995 Lifeline Performance," Technical Council on Lifeline Earthquake Engineering (TCLEE), Monograph No. 14, ASCE.

Schiff, A.J. and Tang, A.K. (2000), "Chi Chi, Taiwan Earthquake of September 21, 1999 Lifeline Performance," Technical Council on Lifeline Earthquake Engineering (TCLEE), Monograph No. 18, ASCE.

Schiff, A. (2011), "Ready or Not… Lessons from the 1994 Northridge Earthquake in California," IEEE Power and Energy Magazine.

Shinozuka, M., Rose, A., and Eguchi, R.T., (1998), "Engineering and Socioeconomic Impacts of Earthquakes," Monograph Series 2, Multidisciplinary Center for Earthquake Engineering Research, State University of New York at Buffalo

Suzuki, H., Sugi, T., Kuwahara, H., Kaizu, N. (1987), "Studies on Aseismic Isolation Device for Electric Substation Equipment," Developments in Geotechnical Engineering, 43, pp.347-357.

Tang, A.K. (2000), "Izmit (Kocaeli), Turkey, Earthquake August 17, 1999 - Including Duzce Earthquake of November 12, 1999 - Lifeline Performance," Technical Council on Lifeline Earthquake Engineering (TCLEE), Monograph No.17, ASCE.

The New York Times, “A Drill to Replace Crucial Transformers (Not the Hollywood Kind)”, from http://www.nytimes.com/2012/03/15/business/energy-environment/electric-industry-runs-transformer-replacement-test.html?_r=0, March 14, 2012

The Power System Seismic Program Management Committee of the City of Los Angeles Department of Water and Power, (1995), “Intermediate Term Plan for Seismically Hardening the Los Angeles Transmission-Level Power Facilities,” Power Syst. Seismic Program Manage. Comm. City of Los Angeles Dept. Water and Power.

Tsopelas, P.C., Constantinou, M.C., Kircher C.A. and Whittaker, A.S. (1997), “Evaluation of simplified methods of analysis for yielding structures,” Report No. NCEER-97-0012, National Center for Earthquake Engineering Research, Buffalo, N.Y.

Tsopelas P.C., Roussis, P. C., Constantinou, M. C., Buchanan, R. and Efthymiou, M. (2005), “3D-BASIS-ME-MB: Computer Program for Nonlinear Dynamic Analysis of Seismically Isolated Structures,” Technical Report MCEER-05-0009, Multidisciplinary Center for Earthquake Engineering Research, State University of New York, Buffalo, NY.

U.S.-Canada Power System Outage Task Force. “Final Report on the August 14, 2003 Blackout in the United States and Canada: Causes and Recommendations,” April 2004.

Villaverde, R., Pardoen, G.C. and Carnalla, S. (2001), “Ground Motion Amplification at Flange Level of Bushings Mounted on Electric Substation Transformers,” Earthquake Engineering and Structural Dynamics, 30, pp. 621-632.

Warn, P.G. and Whittaker, A.S. (2006), "A Study of the Coupled Horizontal-Vertical Behavior of Elastomeric and Lead-Rubber Seismic Isolation Bearings," Report No. MCEER-06-0011, Multidisciplinary Center for Earthquake Engineering Research, Buffalo, NY.

Wilson, E.L. (1998), "Three-Dimensional Static and Dynamic Analysis of Structures: A Physical Approach with Emphasis on Earthquake Engineering", Computers and Structures Inc.; 2nd edition.

Winters, C.W. and Constantinou, M.C. (1993), "Evaluation of Static and Response Spectrum Analysis Procedures of SEAOC/UBC for Seismic Isolated Structures" Report No. NCEER 93-0004, National Center for Earthquake Engineering Research, Buffalo, NY.

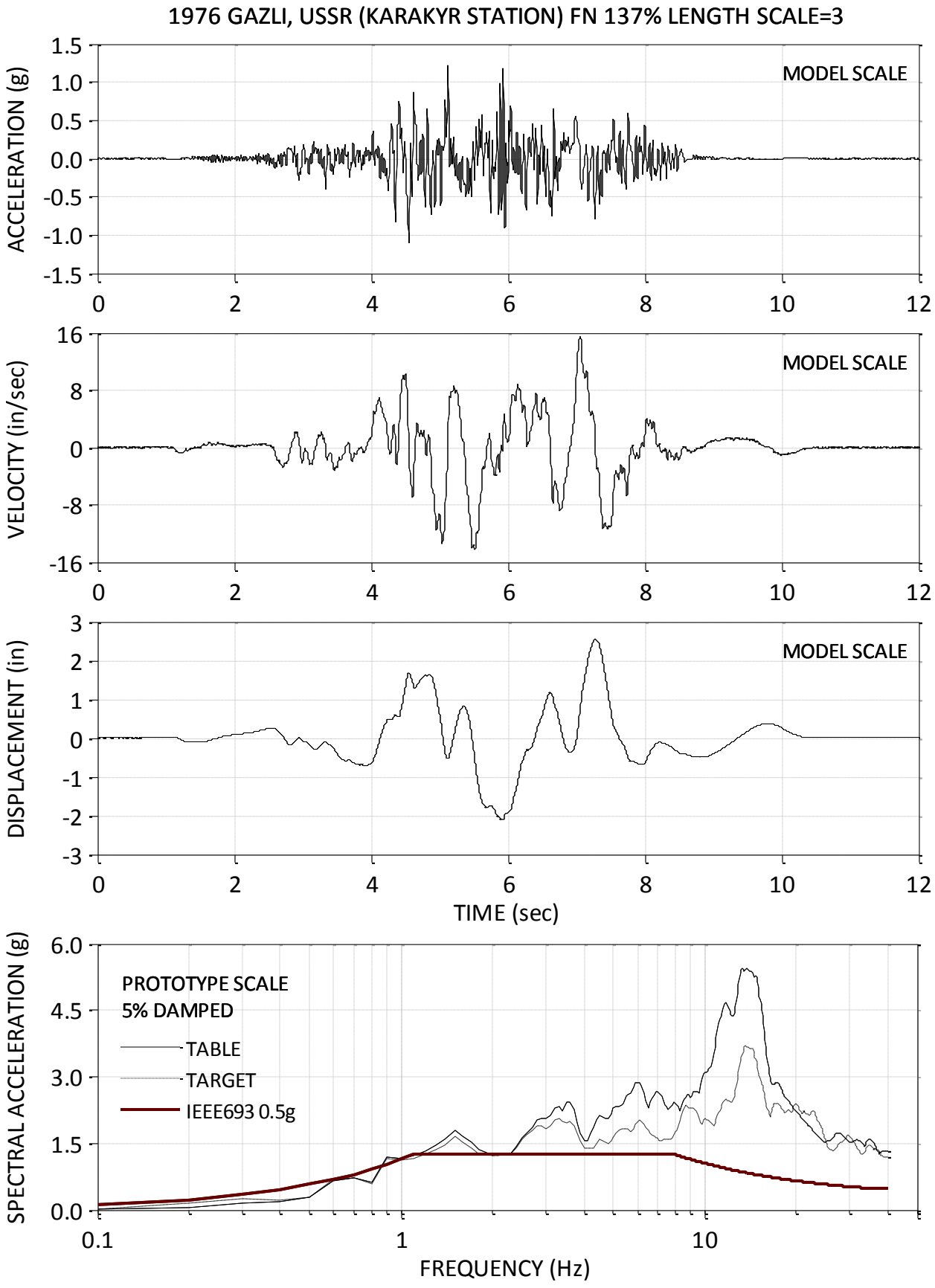
Wolff, E.D. and Constantinou, M.C. (2004), "Experimental Study of Seismic Isolation Systems with Emphasis on Secondary System Response and Verification of Accuracy of Dynamic Response History Analysis Methods," Report No. MCEER-04-0001, Multidisciplinary Center for Earthquake Engineering Research, Buffalo, NY.

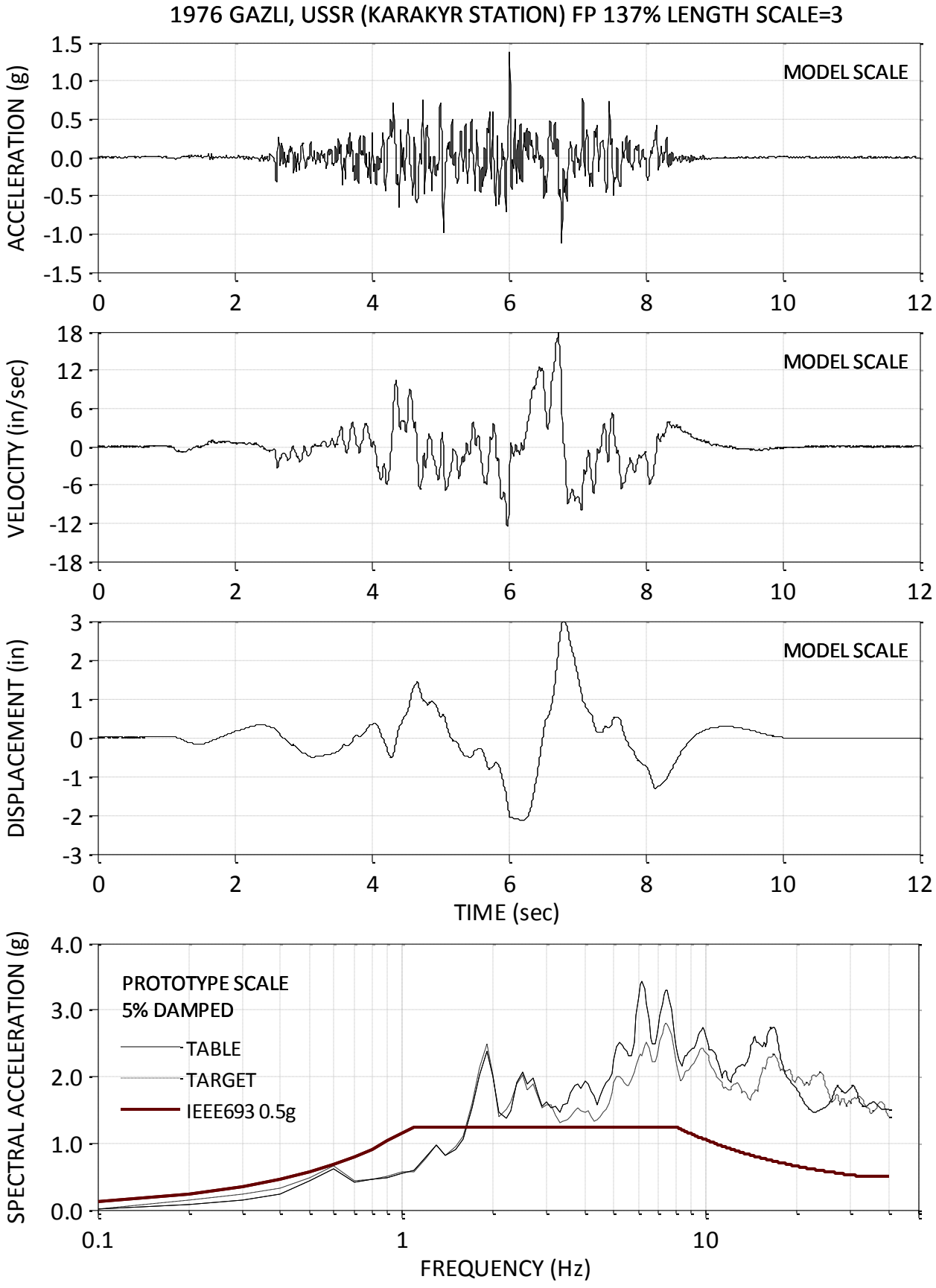
Wolff, E.D., Ipek, C., Constantinou, M.C., Morillas, L. (2014), "Torsional Response of Seismically Isolated Structures Revisited," Engineering Structures, Vol. 59, pp. 462-468.

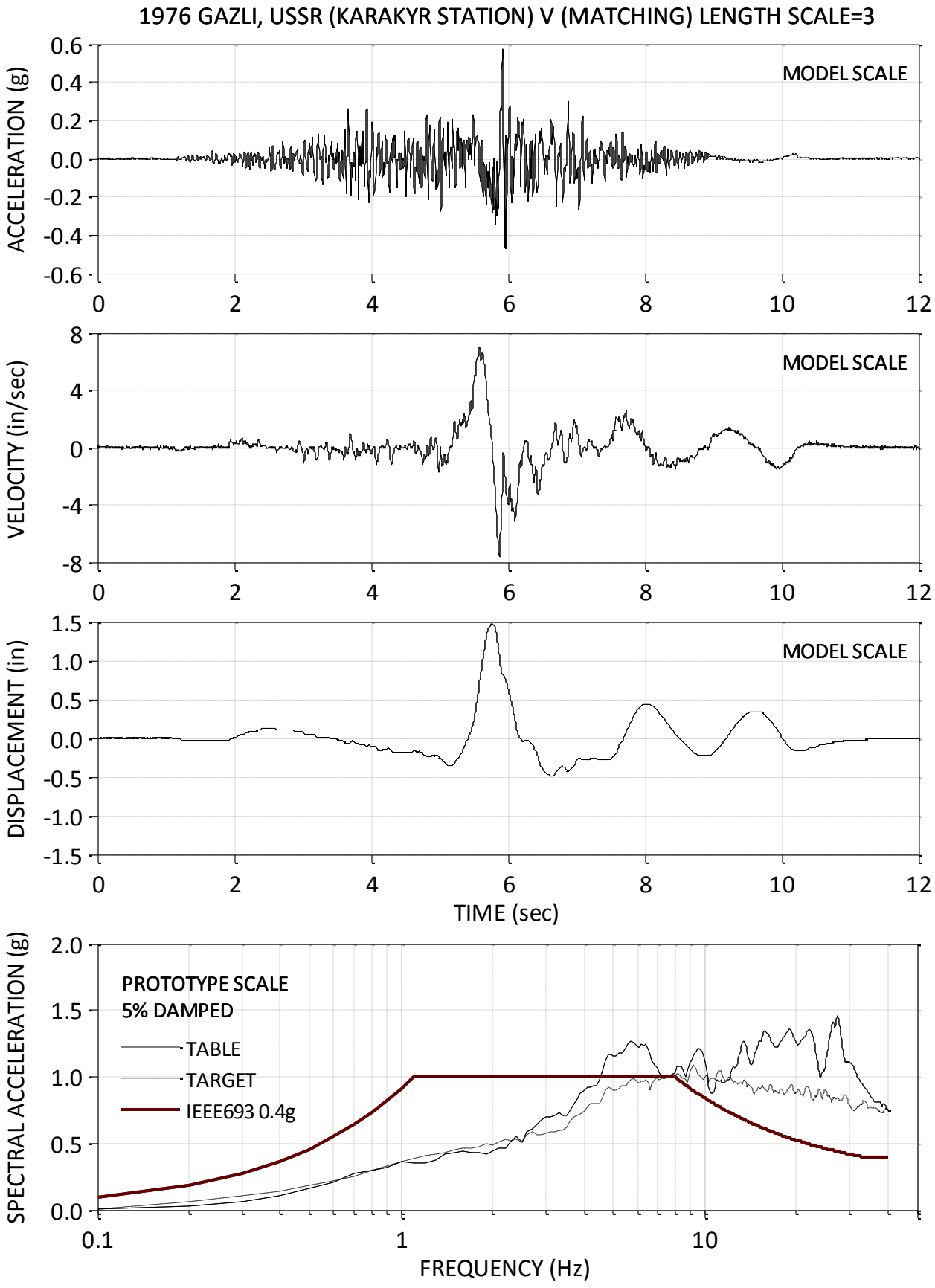
This Page is Intentionally Left Blank

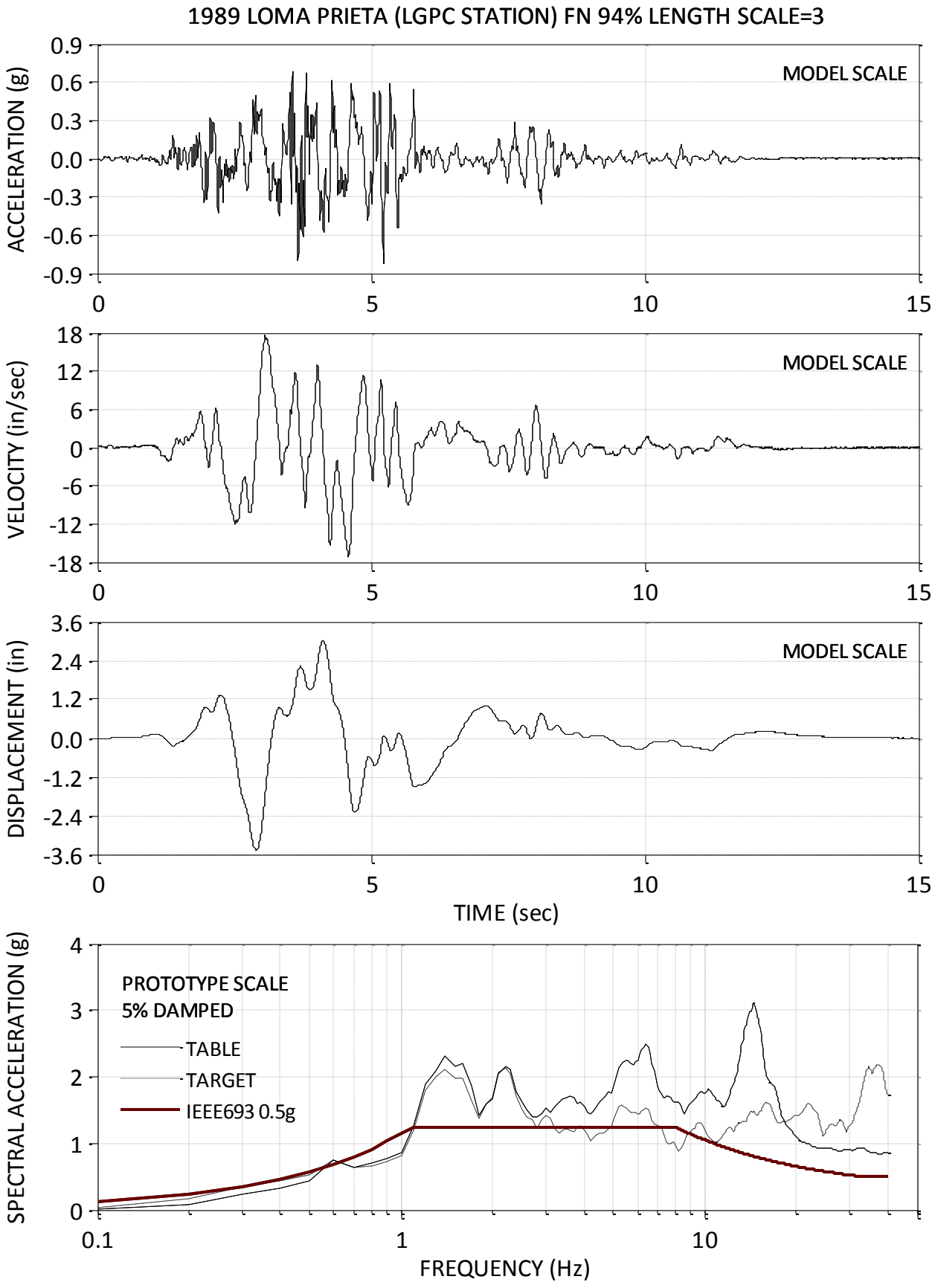
APPENDIX A
HISTORIES AND SPECTRA OF SHAKE TABLE MOTION

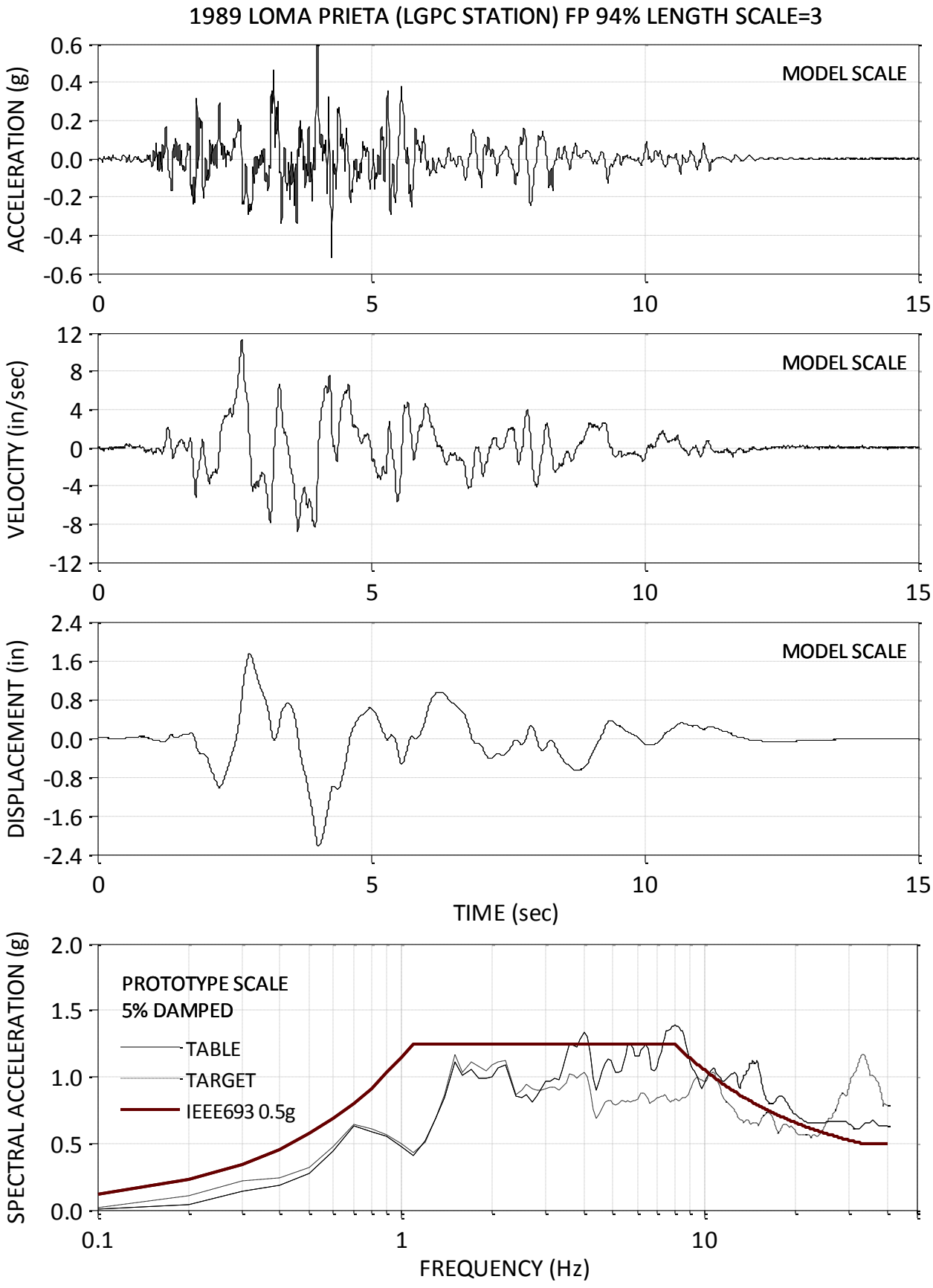
(PERCENTAGE AMOUNT IS SCALE FACTOR APPLIED TO ACCELERATION OF ACTUAL MOTION. FOR EXAMPLE, 100% DENOTES MOTION AS RECORDED, 200% DENOTES THAT ACCELERATION WAS SCALED UP BY FACTOR OF 2)

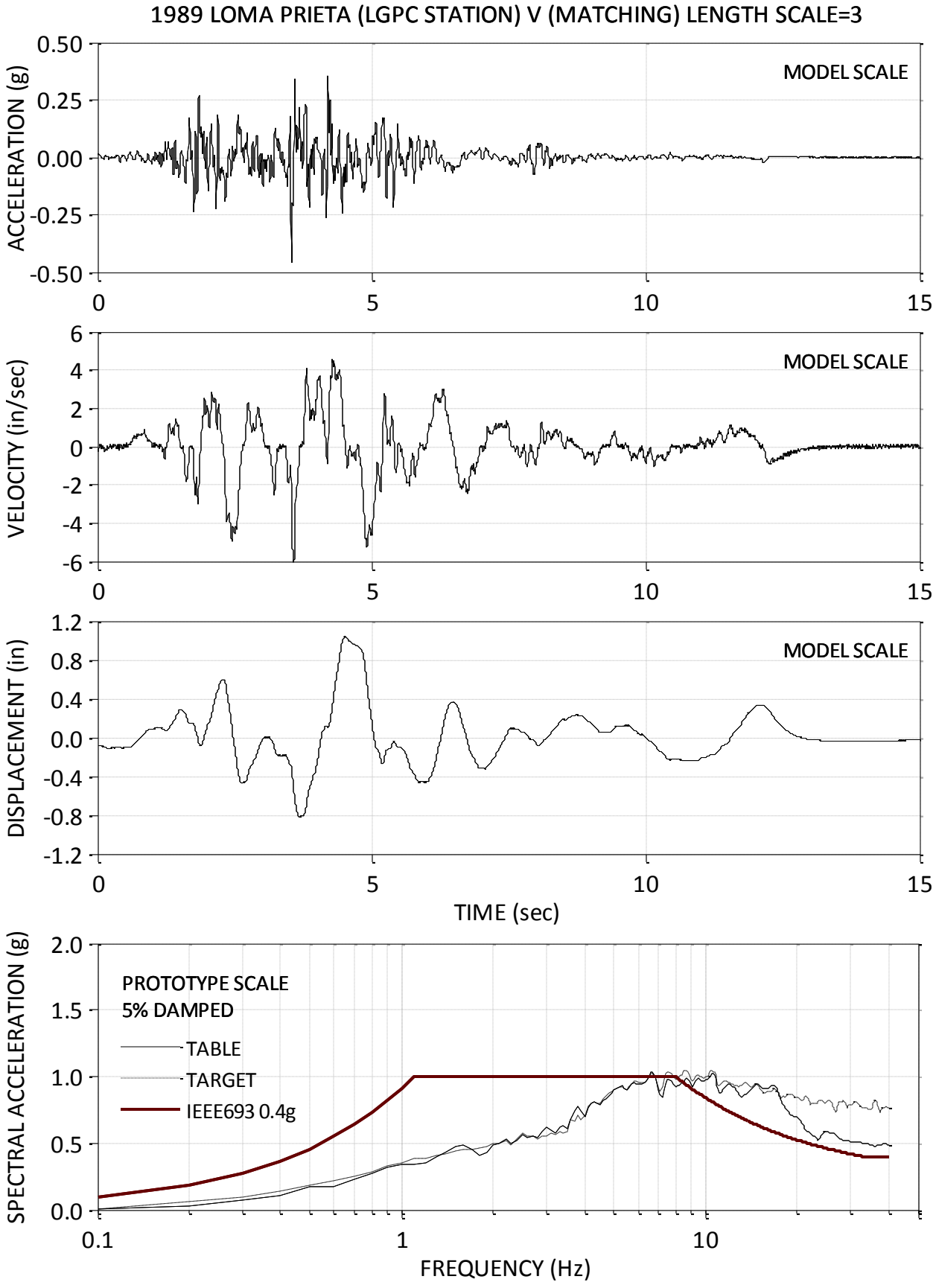

1976 GAZLI, USSR (KARAKYR STATION) FN 137% LENGTH SCALE=3
ACCELERATION (g)
MODEL SCALE
VELOCITY (in/sec)
MODEL SCALE
DISPLACEMENT (in)
MODEL SCALE
TIME (sec)
SPECTRAL ACCELERATION (g)
PROTOTYPE SCALE
5% DAMPED
TABLE
TARGET
IEEE693 0.5g
FREQUENCY (Hz)

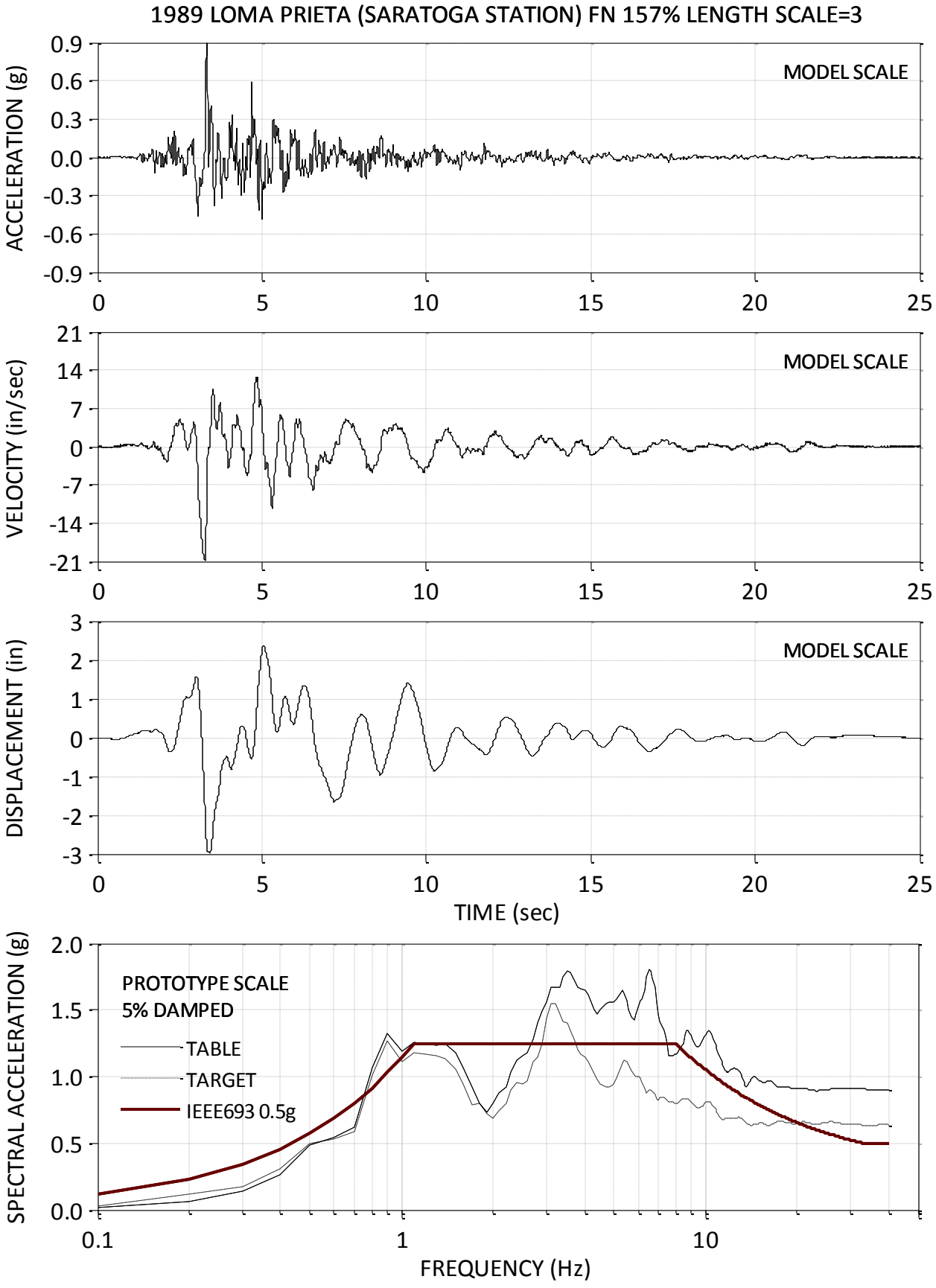

1976 GAZLI, USSR (KARAKYR STATION) FP 137% LENGTH SCALE=3
ACCELERATION (g)
MODEL SCALE
VELOCITY (in/sec)
MODEL SCALE
DISPLACEMENT (in)
MODEL SCALE
TIME (sec)
SPECTRAL ACCELERATION (g)
PROTOTYPE SCALE
5% DAMPED
TABLE
TARGET
IEEE693 0.5g
FREQUENCY (Hz)

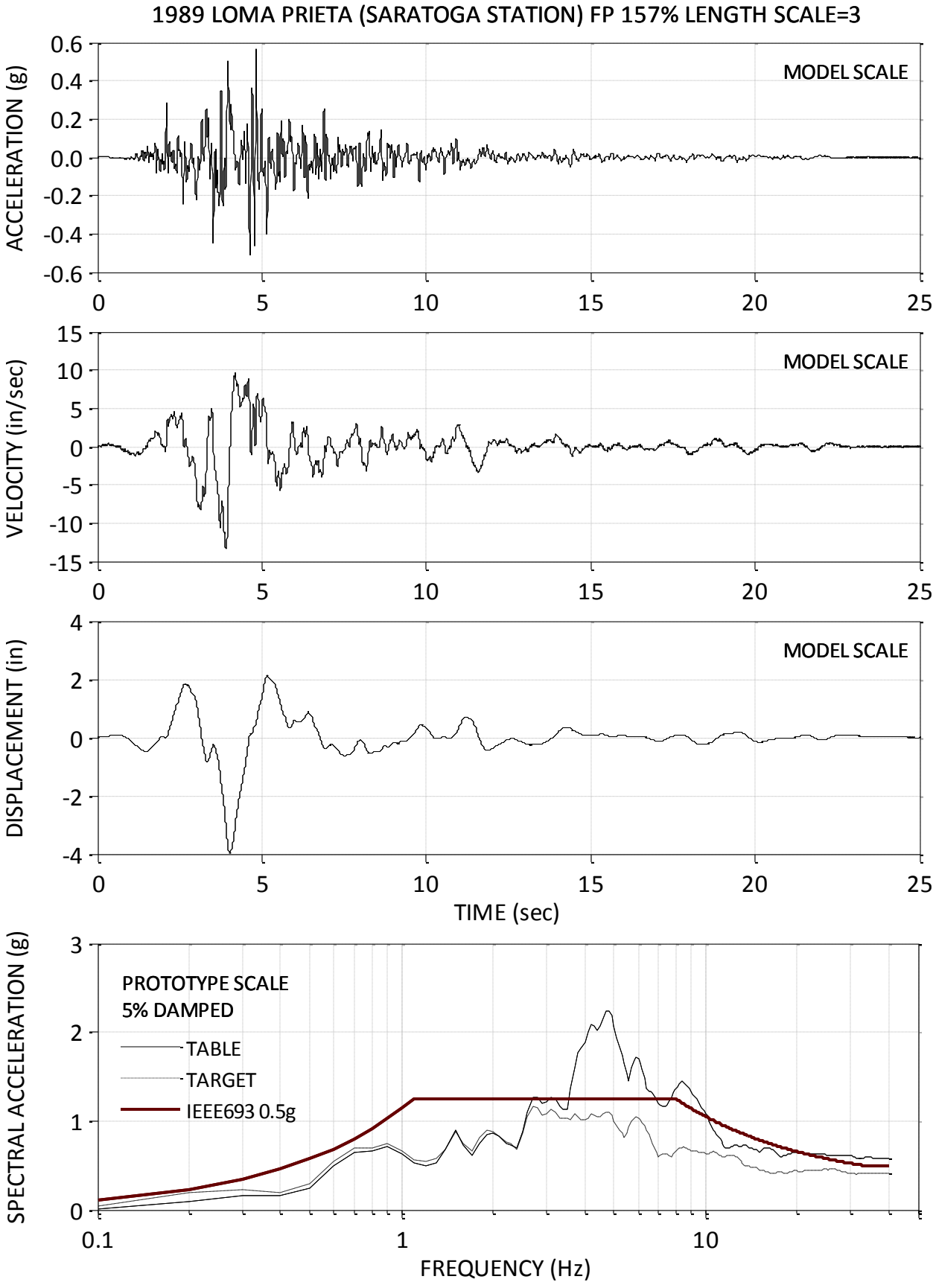

1976 GAZLI, USSR (KARAKYR STATION) V (MATCHING) LENGTH SCALE=3
ACCELERATION (g)
MODEL SCALE
VELOCITY (in/sec)
MODEL SCALE
DISPLACEMENT (in)
MODEL SCALE
TIME (sec)
SPECTRAL ACCELERATION (g)
PROTOTYPE SCALE
5% DAMPED
TABLE
TARGET
IEEE693 0.4g
FREQUENCY (Hz)

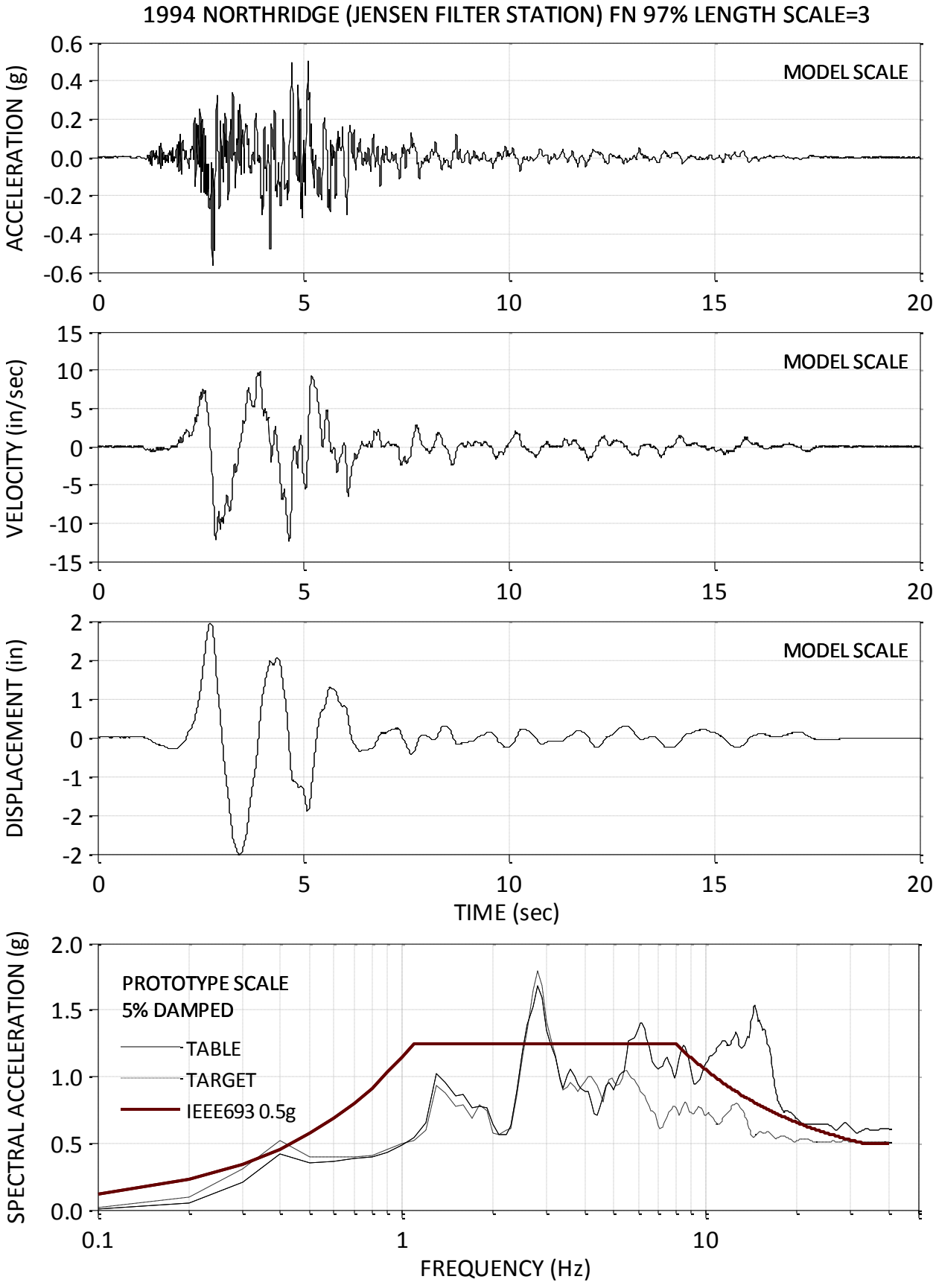

1989 LOMA PRIETA (LGPC STATION) FN 94% LENGTH SCALE=3
ACCELERATION (g)
MODEL SCALE
VELOCITY (in/sec)
MODEL SCALE
DISPLACEMENT (in)
MODEL SCALE
TIME (sec)
SPECTRAL ACCELERATION (g)
PROTOTYPE SCALE
5% DAMPED
TABLE
TARGET
IEEE693 0.5g
FREQUENCY (Hz)

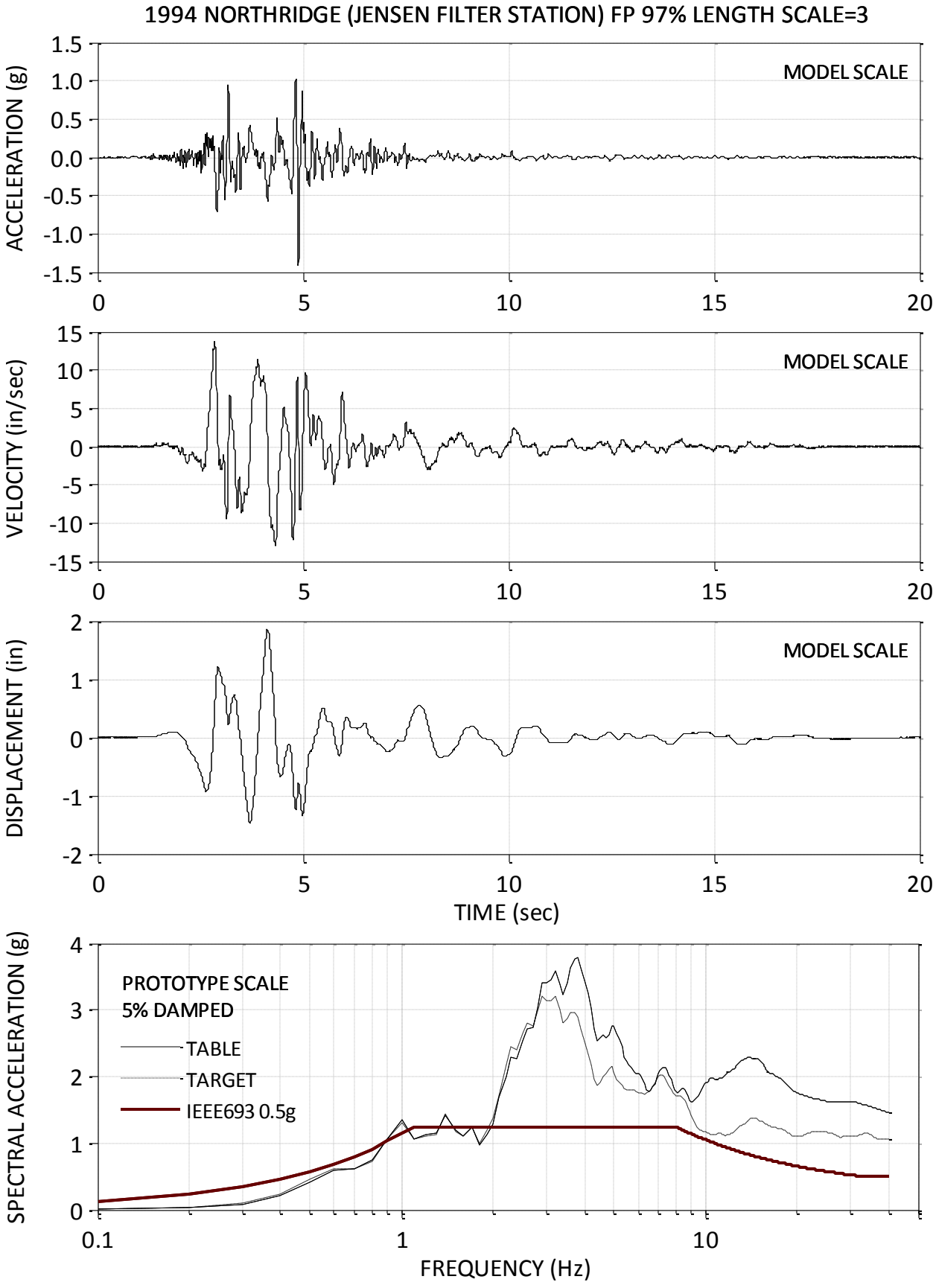

1989 LOMA PRIETA (LGPC STATION) FP 94% LENGTH SCALE=3
ACCELERATION (g)
MODEL SCALE
VELOCITY (in/sec)
MODEL SCALE
DISPLACEMENT (in)
MODEL SCALE
TIME (sec)
SPECTRAL ACCELERATION (g)
PROTOTYPE SCALE
5% DAMPED
TABLE
TARGET
IEEE693 0.5g
FREQUENCY (Hz)

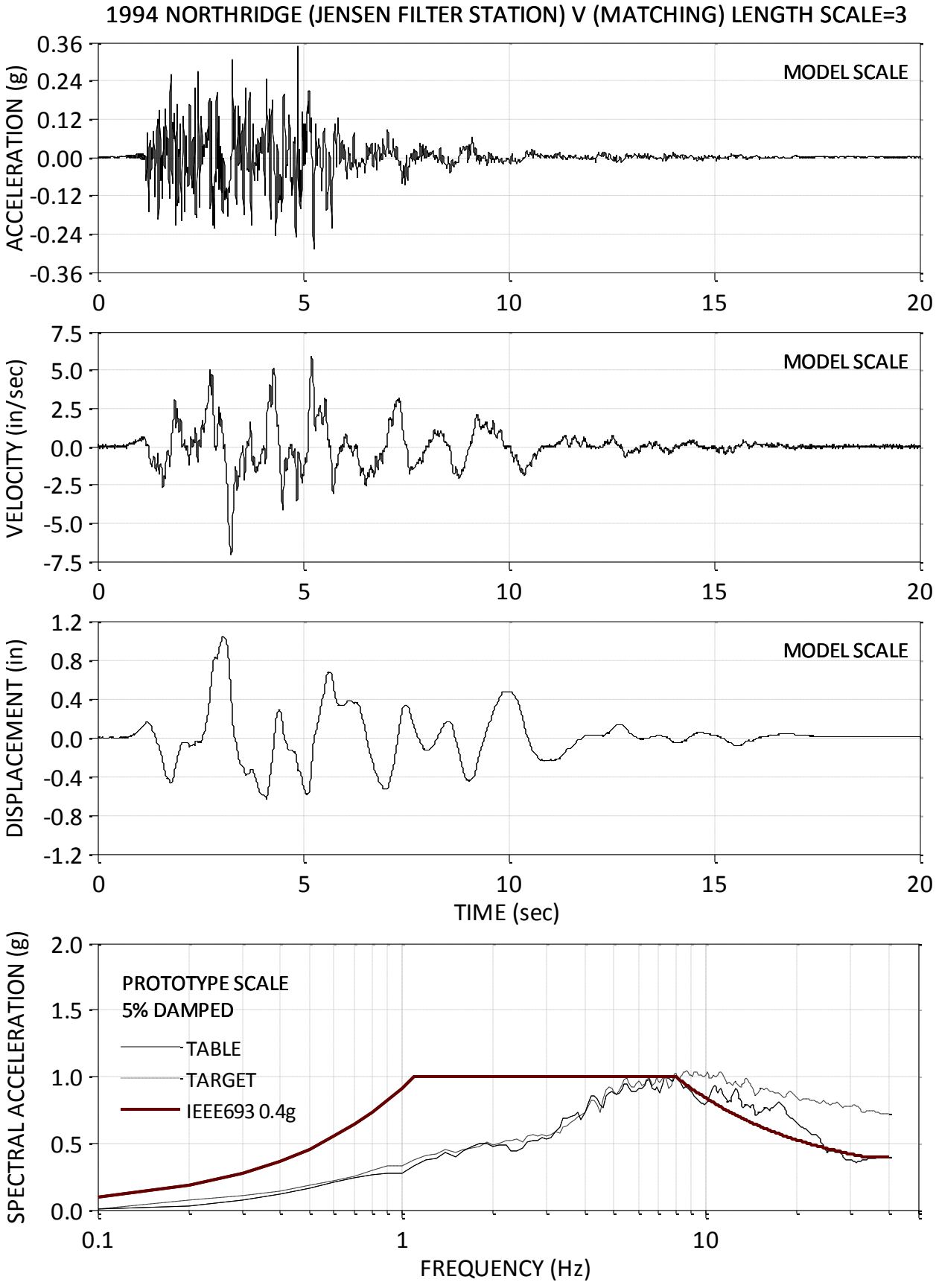

1989 LOMA PRIETA (LGPC STATION) V (MATCHING) LENGTH SCALE=3
ACCELERATION (g)
0.50
0.25
0.00
-0.25
-0.50
MODEL SCALE
0
5
10
15
VELOCITY (in/sec)
6
4
2
0
-2
-4
-6
MODEL SCALE
DISPLACEMENT (in)
1.2
0.8
0.4
0.0
-0.4
-0.8
-1.2
MODEL SCALE
TIME (sec)
SPECTRAL ACCELERATION (g)
2.0
1.5
1.0
0.5
0.0
PROTOTYPE SCALE
5% DAMPED
TABLE
TARGET
IEEE693 0.4g
0.1
1
10
FREQUENCY (Hz)

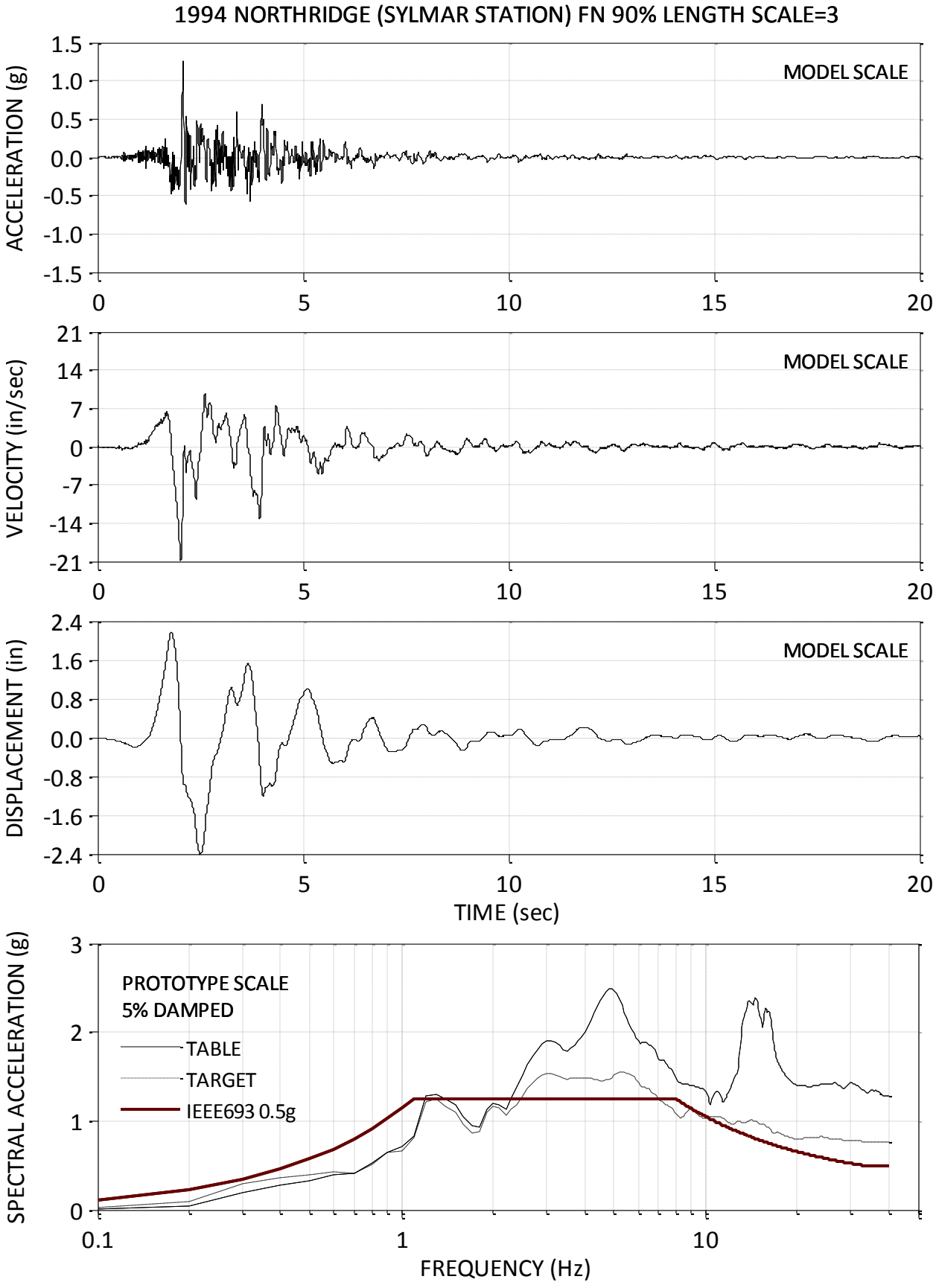

1989 LOMA PRIETA (SARATOGA STATION) FN 157% LENGTH SCALE=3
ACCELERATION (g)
MODEL SCALE
VELOCITY (in/sec)
MODEL SCALE
DISPLACEMENT (in)
MODEL SCALE
TIME (sec)
SPECTRAL ACCELERATION (g)
PROTOTYPE SCALE
5% DAMPED
TABLE
TARGET
IEEE693 0.5g
FREQUENCY (Hz)

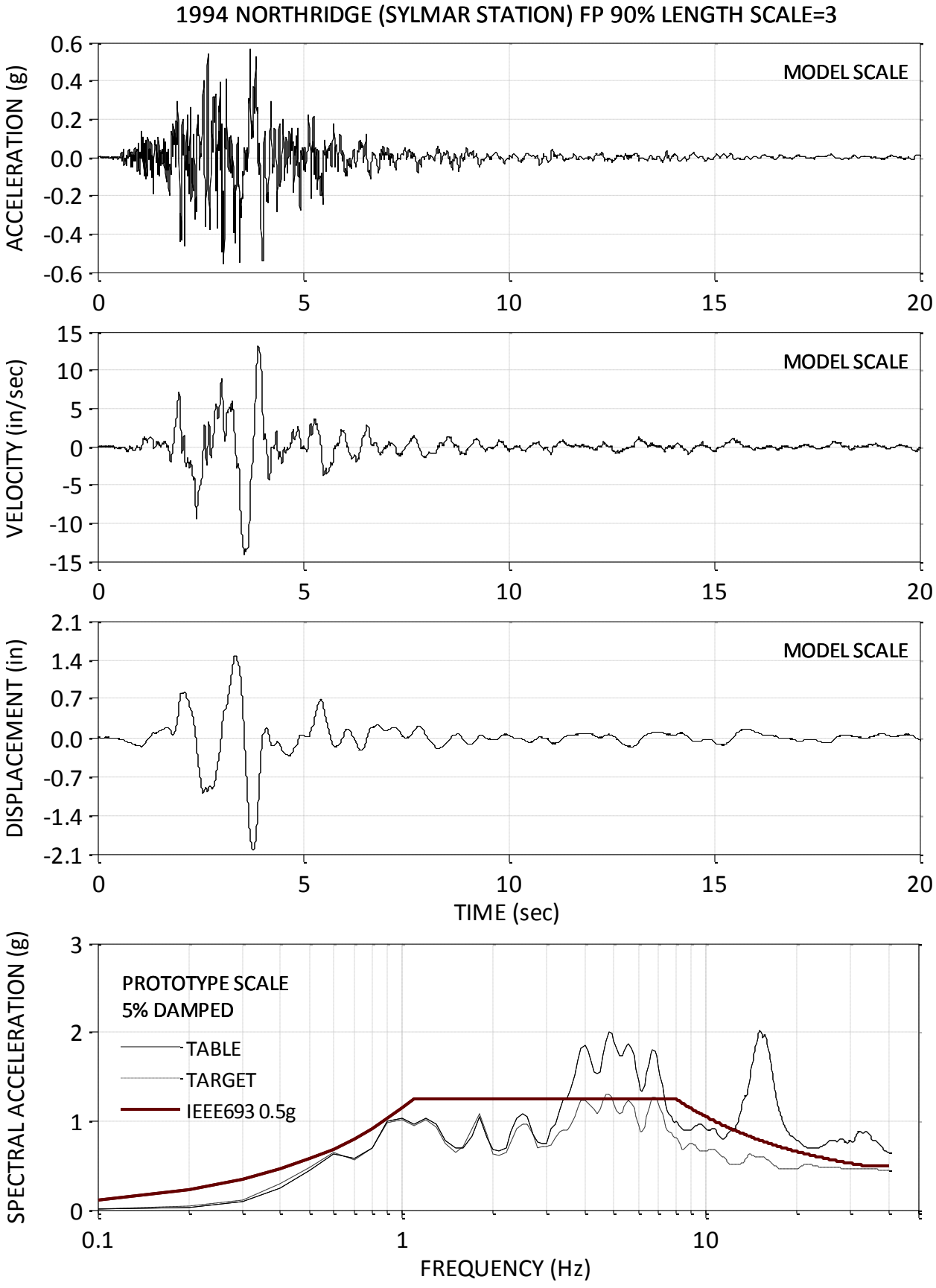

1989 LOMA PRIETA (SARATOGA STATION) FP 157% LENGTH SCALE=3
ACCELERATION (g)
MODEL SCALE
VELOCITY (in/sec)
MODEL SCALE
DISPLACEMENT (in)
MODEL SCALE
TIME (sec)
SPECTRAL ACCELERATION (g)
PROTOTYPE SCALE
5% DAMPED
TABLE
TARGET
IEEE693 0.5g
FREQUENCY (Hz)

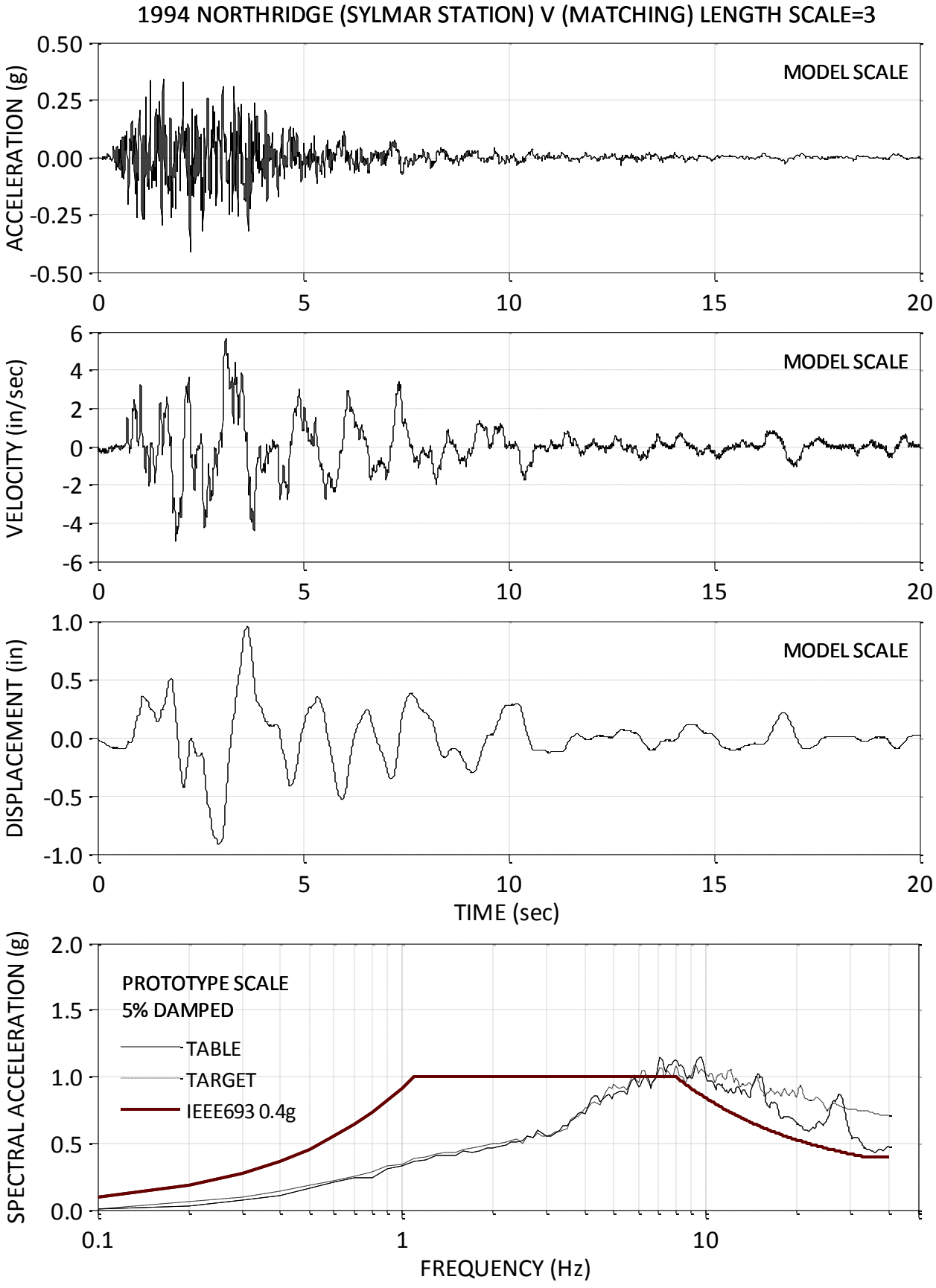

1994 NORTHRIDGE (JENSEN FILTER STATION) FN 97% LENGTH SCALE=3
ACCELERATION (g)
MODEL SCALE
VELOCITY (in/sec)
MODEL SCALE
DISPLACEMENT (in)
MODEL SCALE
TIME (sec)
SPECTRAL ACCELERATION (g)
PROTOTYPE SCALE
5% DAMPED
TABLE
TARGET
IEEE693 0.5g
FREQUENCY (Hz)

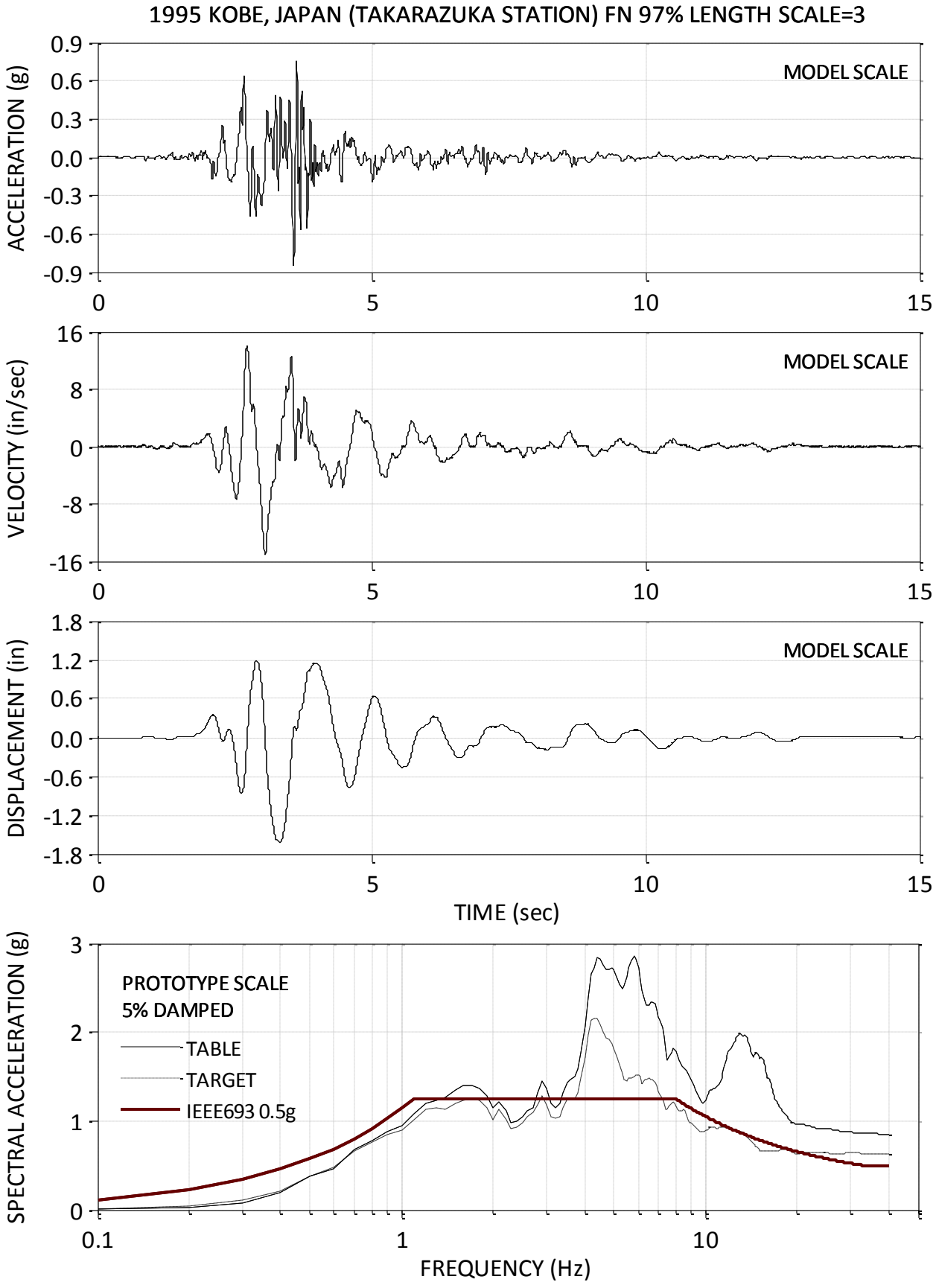

1994 NORTHRIDGE (JENSEN FILTER STATION) FP 97% LENGTH SCALE=3
ACCELERATION (g)
MODEL SCALE
VELOCITY (in/sec)
MODEL SCALE
DISPLACEMENT (in)
MODEL SCALE
TIME (sec)
SPECTRAL ACCELERATION (g)
PROTOTYPE SCALE
5% DAMPED
TABLE
TARGET
IEEE693 0.5g
FREQUENCY (Hz)

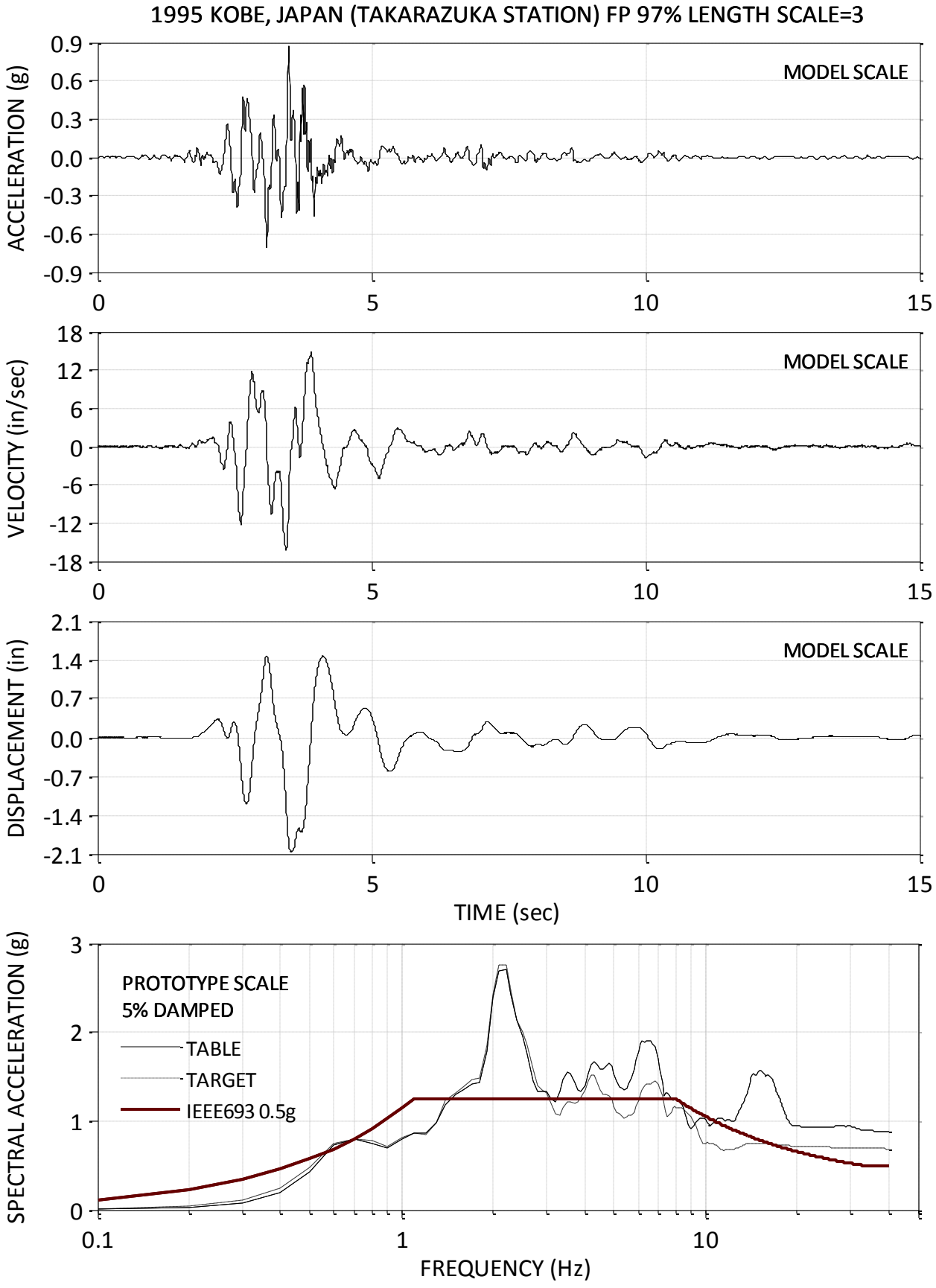

1994 NORTHRIDGE (JENSEN FILTER STATION) V (MATCHING) LENGTH SCALE=3
ACCELERATION (g)
0.36
0.24
0.12
0.00
-0.12
-0.24
-0.36
MODEL SCALE
0
5
10
15
20
VELOCITY (in/sec)
7.5
5.0
2.5
0.0
-2.5
-5.0
-7.5
MODEL SCALE
DISPLACEMENT (in)
1.2
0.8
0.4
0.0
-0.4
-0.8
-1.2
MODEL SCALE
TIME (sec)
SPECTRAL ACCELERATION (g)
2.0
1.5
1.0
0.5
0.0
PROTOTYPE SCALE
5% DAMPED
TABLE
TARGET
IEEE693 0.4g
0.1
1
10
FREQUENCY (Hz)

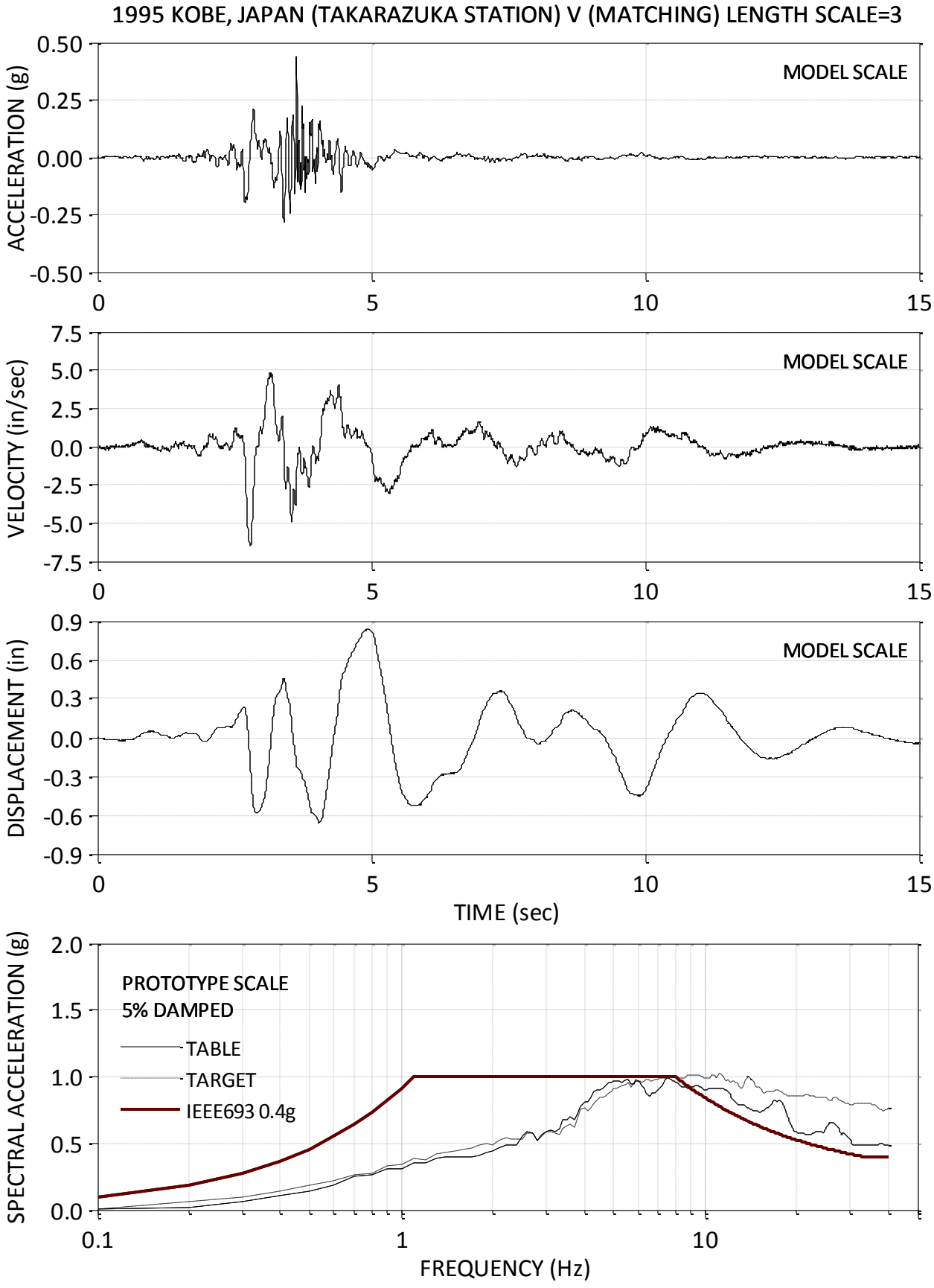

1994 NORTHRIDGE (SYLMAR STATION) FN 90% LENGTH SCALE=3
ACCELERATION (g)
MODEL SCALE
VELOCITY (in/sec)
MODEL SCALE
DISPLACEMENT (in)
MODEL SCALE
TIME (sec)
SPECTRAL ACCELERATION (g)
PROTOTYPE SCALE
5% DAMPED
TABLE
TARGET
IEEE693 0.5g
FREQUENCY (Hz)

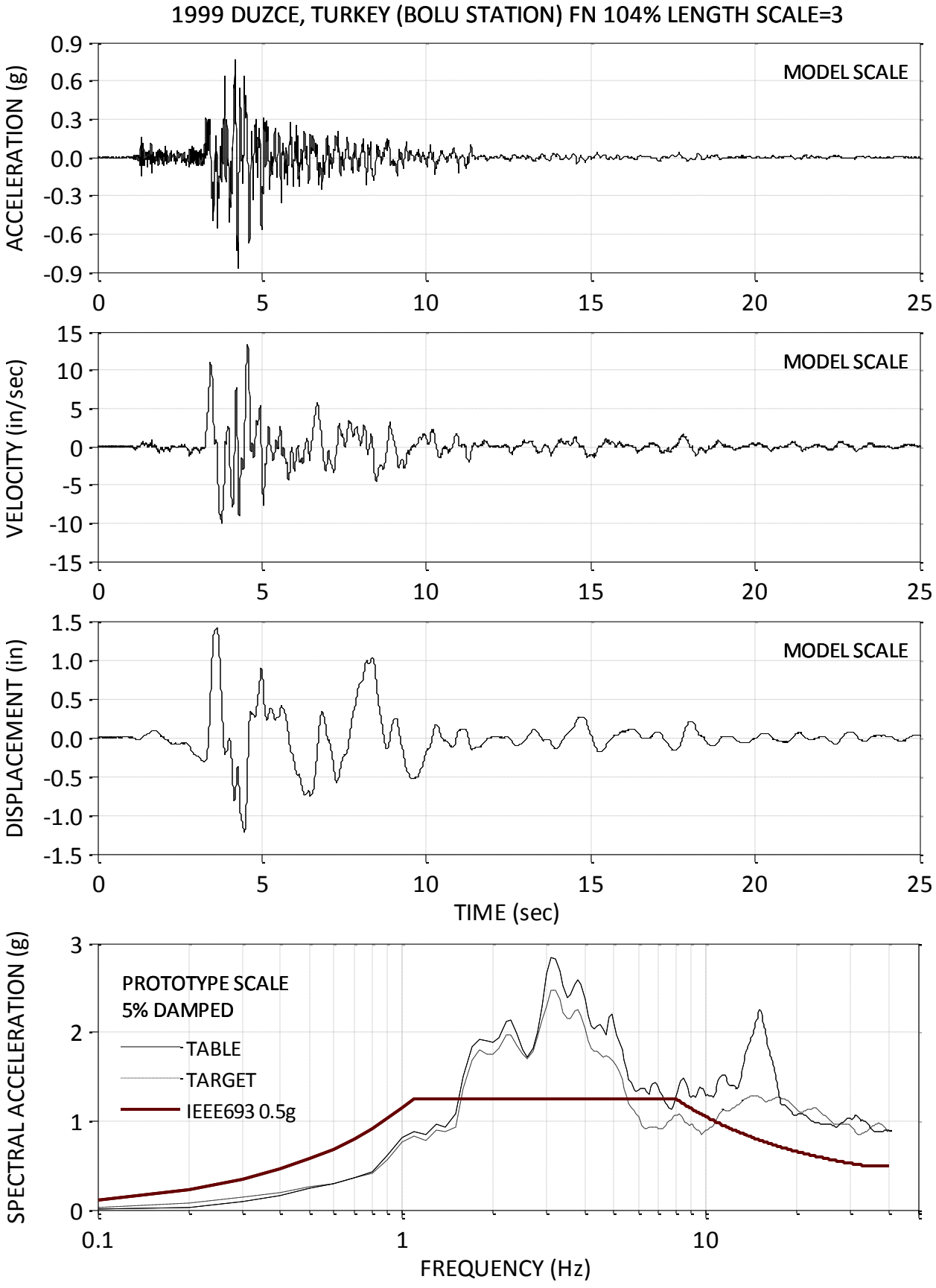

1994 NORTHRIDGE (SYLMAR STATION) FP 90% LENGTH SCALE=3
ACCELERATION (g)
MODEL SCALE
VELOCITY (in/sec)
MODEL SCALE
DISPLACEMENT (in)
MODEL SCALE
TIME (sec)
SPECTRAL ACCELERATION (g)
PROTOTYPE SCALE
5% DAMPED
TABLE
TARGET
IEEE693 0.5g
FREQUENCY (Hz)

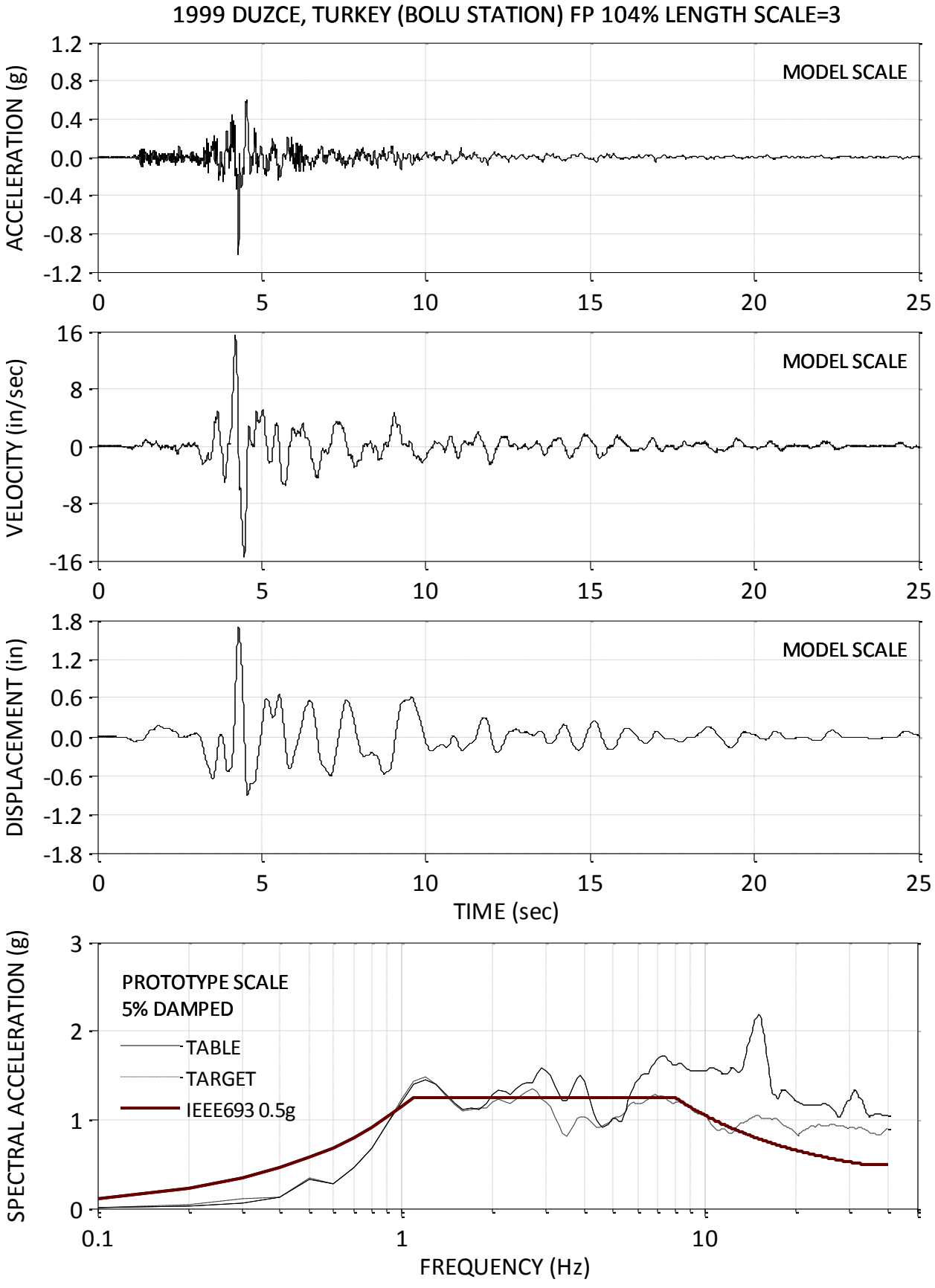

1994 NORTHRIDGE (SYLMAR STATION) V (MATCHING) LENGTH SCALE=3
ACCELERATION (g)
0.50
0.25
0.00
-0.25
-0.50
MODEL SCALE
0
5
10
15
20
VELOCITY (in/sec)
6
4
2
0
-2
-4
-6
MODEL SCALE
DISPLACEMENT (in)
1.0
0.5
0.0
-0.5
-1.0
MODEL SCALE
TIME (sec)
SPECTRAL ACCELERATION (g)
2.0
1.5
1.0
0.5
0.0
PROTOTYPE SCALE
5% DAMPED
TABLE
TARGET
IEEE693 0.4g
0.1
1
10
FREQUENCY (Hz)

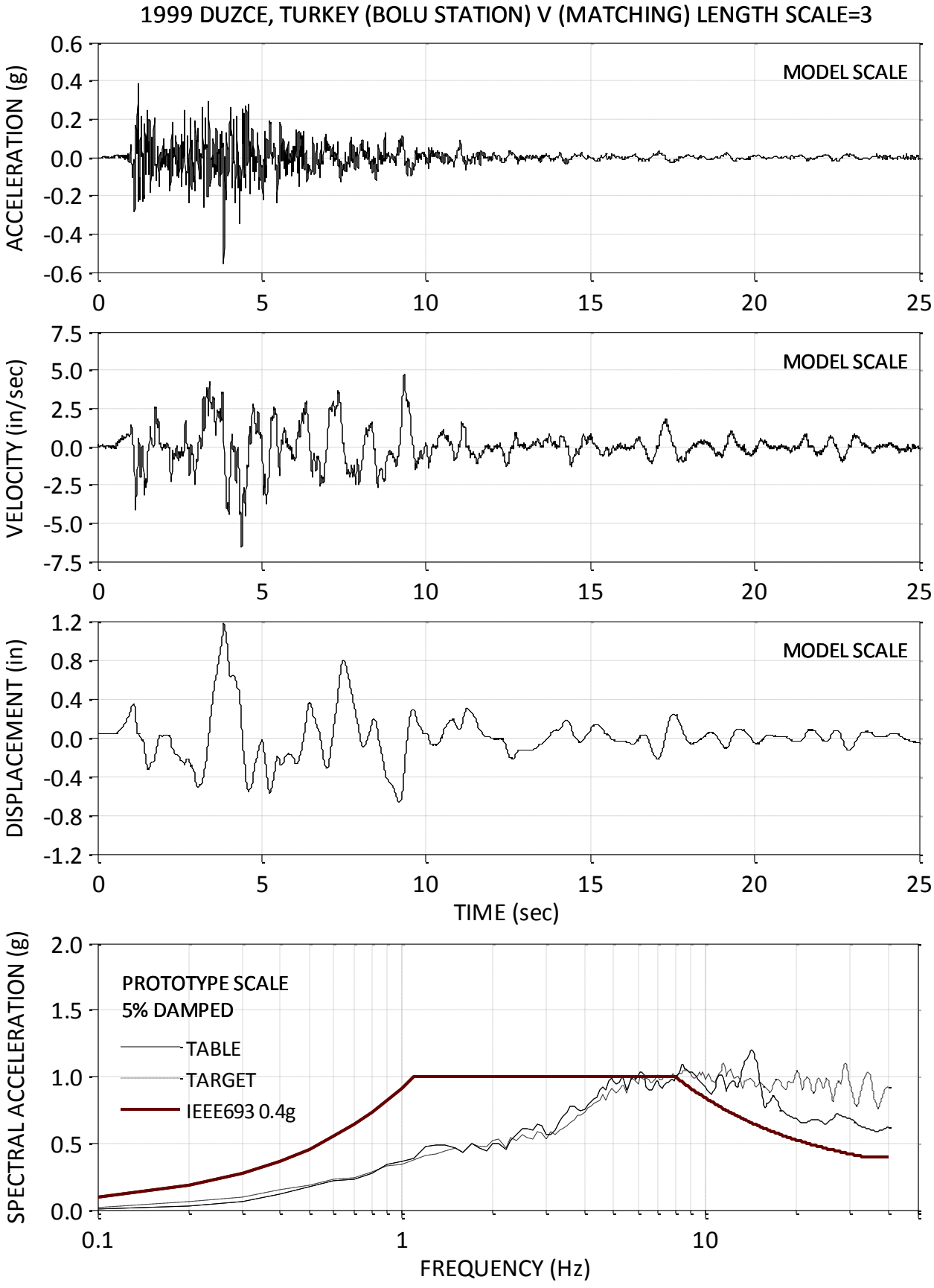

1995 KOBE, JAPAN (TAKARAZUKA STATION) FN 97% LENGTH SCALE=3
ACCELERATION (g)
0.9
0.6
0.3
0.0
-0.3
-0.6
-0.9
MODEL SCALE
0
5
10
15
VELOCITY (in/sec)
16
8
0
-8
-16
MODEL SCALE
DISPLACEMENT (in)
1.8
1.2
0.6
0.0
-0.6
-1.2
-1.8
MODEL SCALE
TIME (sec)
SPECTRAL ACCELERATION (g)
3
2
1
0
PROTOTYPE SCALE
5% DAMPED
TABLE
TARGET
IEEE693 0.5g
0.1
1
10
FREQUENCY (Hz)

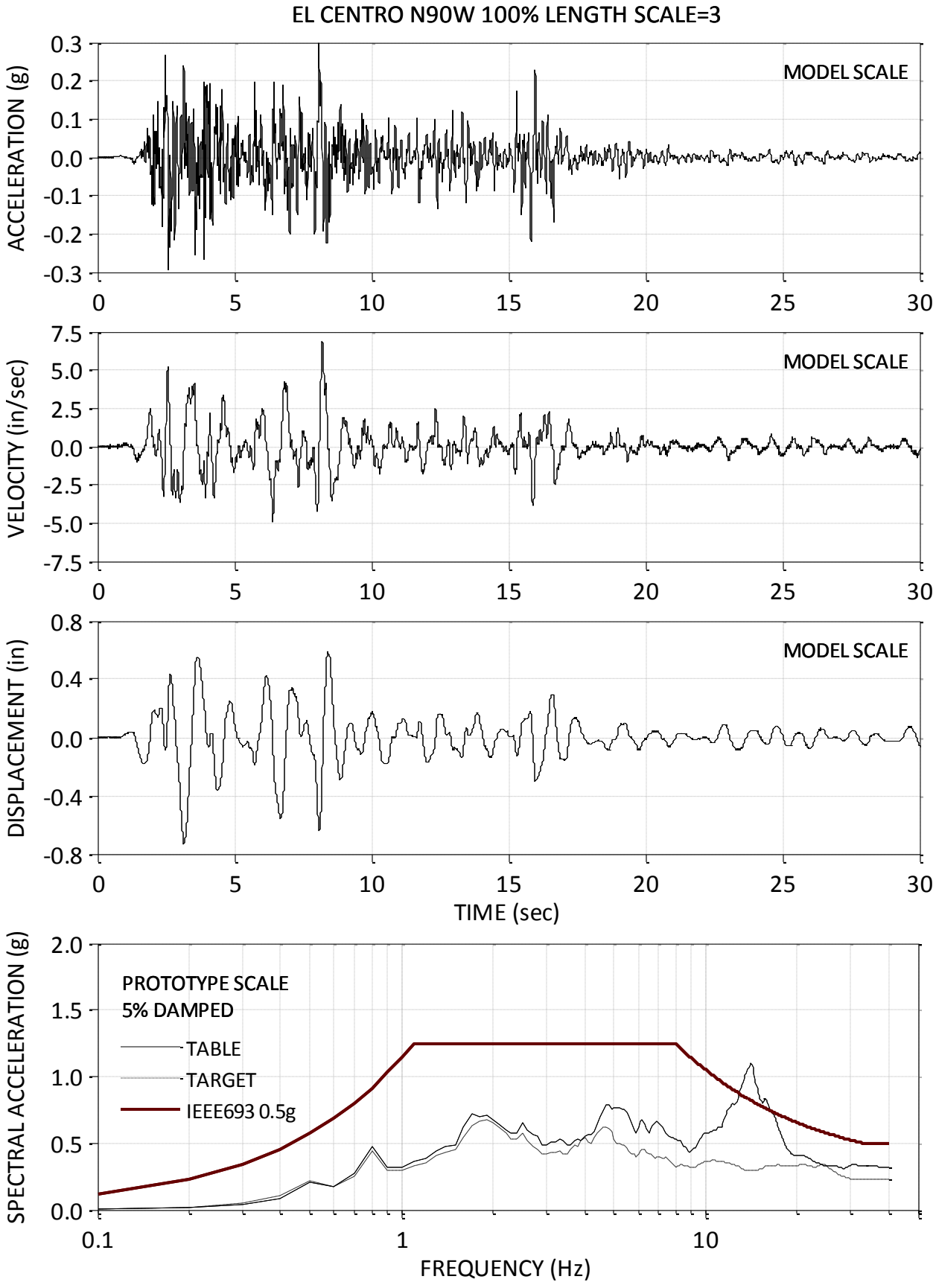

1995 KOBE, JAPAN (TAKARAZUKA STATION) FP 97% LENGTH SCALE=3
ACCELERATION (g)
0.9
0.6
0.3
0.0
-0.3
-0.6
-0.9
MODEL SCALE
0
5
10
15
VELOCITY (in/sec)
18
12
6
0
-6
-12
-18
MODEL SCALE
DISPLACEMENT (in)
2.1
1.4
0.7
0.0
-0.7
-1.4
-2.1
MODEL SCALE
TIME (sec)
SPECTRAL ACCELERATION (g)
3
2
1
0
PROTOTYPE SCALE
5% DAMPED
TABLE
TARGET
IEEE693 0.5g
0.1
1
10
FREQUENCY (Hz)

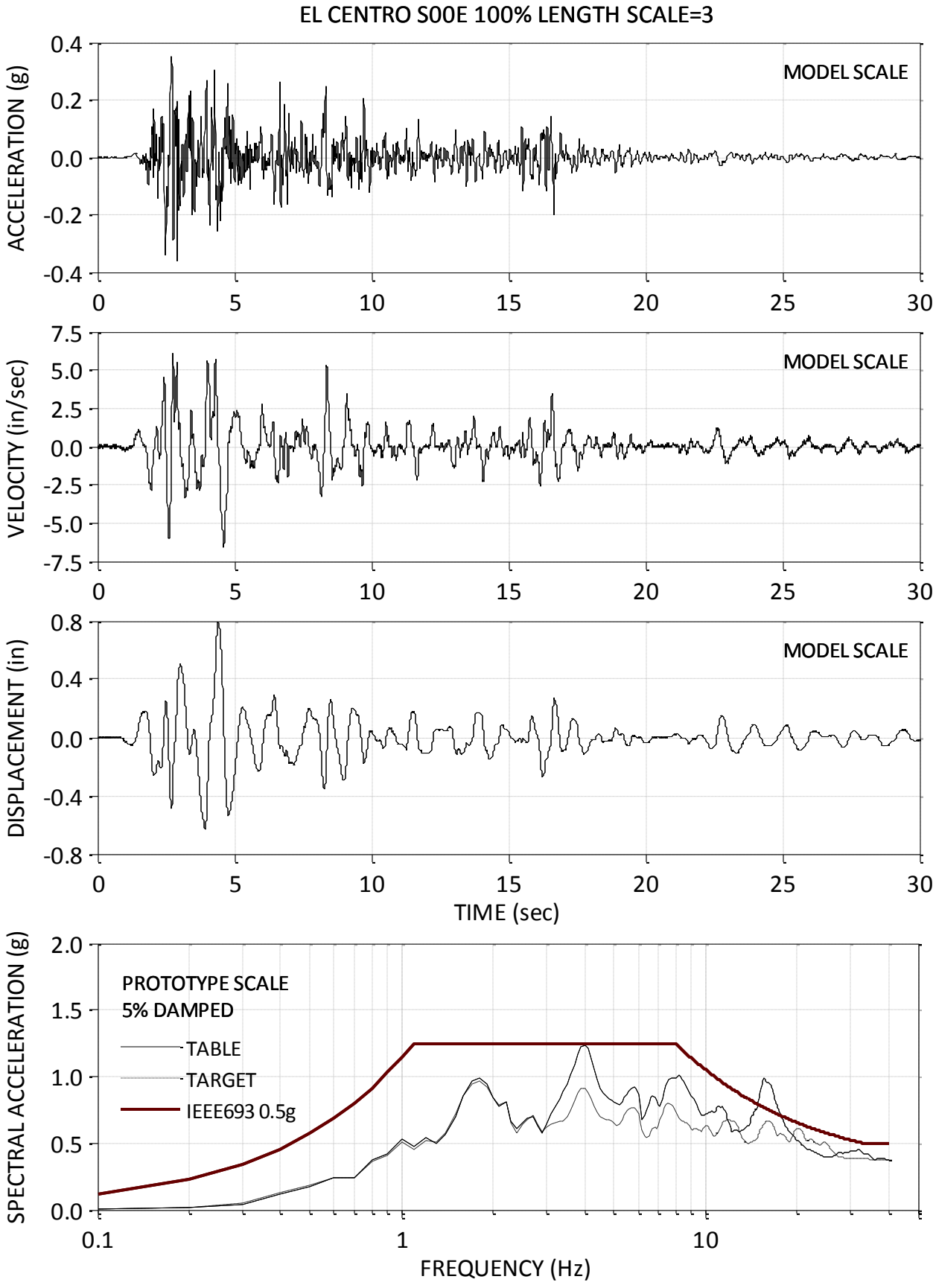

1995 KOBE, JAPAN (TAKARAZUKA STATION) V (MATCHING) LENGTH SCALE=3
ACCELERATION (g)
0.50
0.25
0.00
-0.25
-0.50
MODEL SCALE
0
5
10
15
VELOCITY (in/sec)
7.5
5.0
2.5
0.0
-2.5
-5.0
-7.5
MODEL SCALE
DISPLACEMENT (in)
0.9
0.6
0.3
0.0
-0.3
-0.6
-0.9
MODEL SCALE
TIME (sec)
SPECTRAL ACCELERATION (g)
2.0
1.5
1.0
0.5
0.0
PROTOTYPE SCALE
5% DAMPED
TABLE
TARGET
IEEE693 0.4g
0.1
1
10
FREQUENCY (Hz)

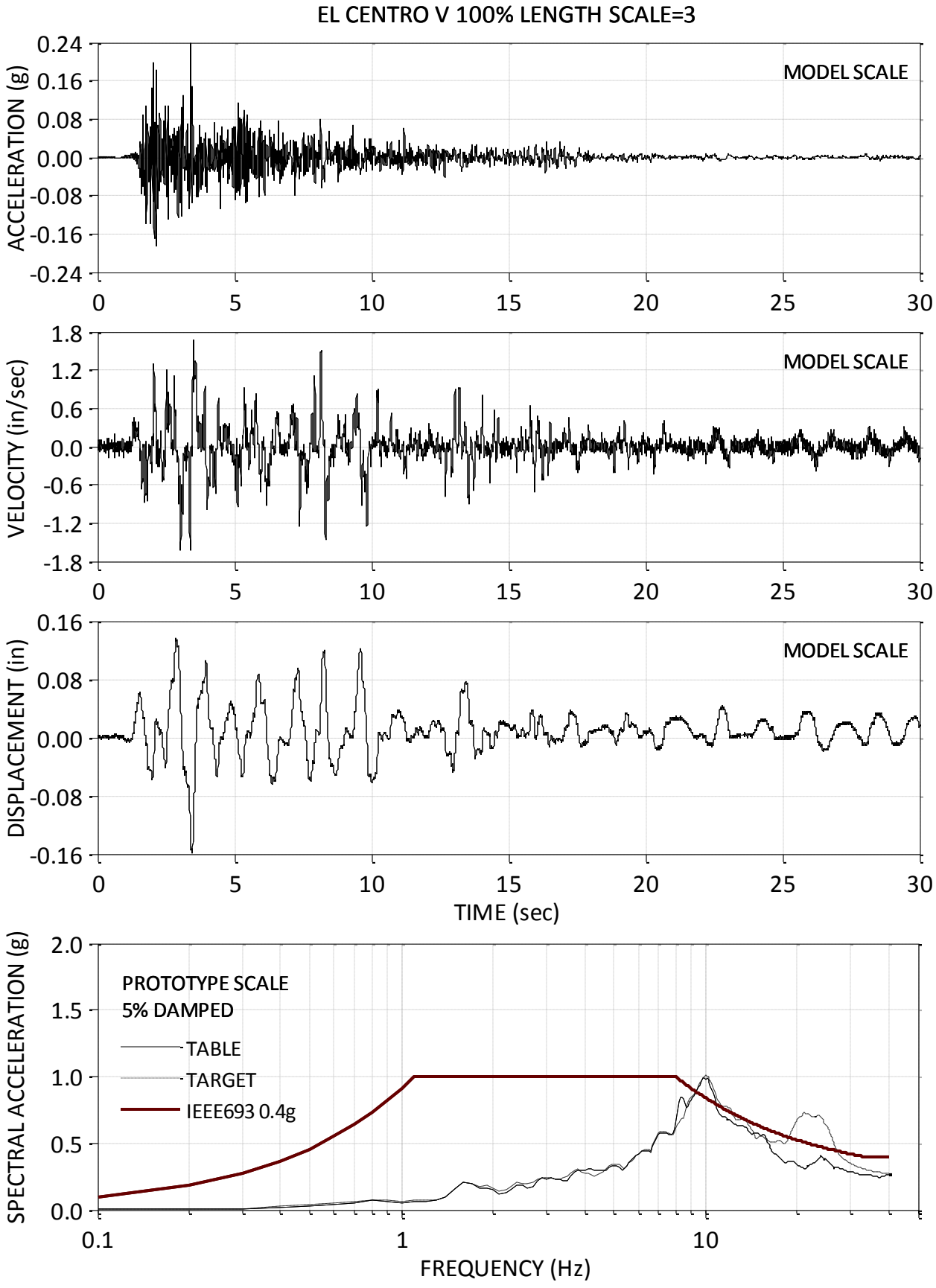

1999 DUZCE, TURKEY (BOLU STATION) FN 104% LENGTH SCALE=3
ACCELERATION (g)
MODEL SCALE
VELOCITY (in/sec)
MODEL SCALE
DISPLACEMENT (in)
MODEL SCALE
TIME (sec)
SPECTRAL ACCELERATION (g)
PROTOTYPE SCALE
5% DAMPED
TABLE
TARGET
IEEE693 0.5g
FREQUENCY (Hz)

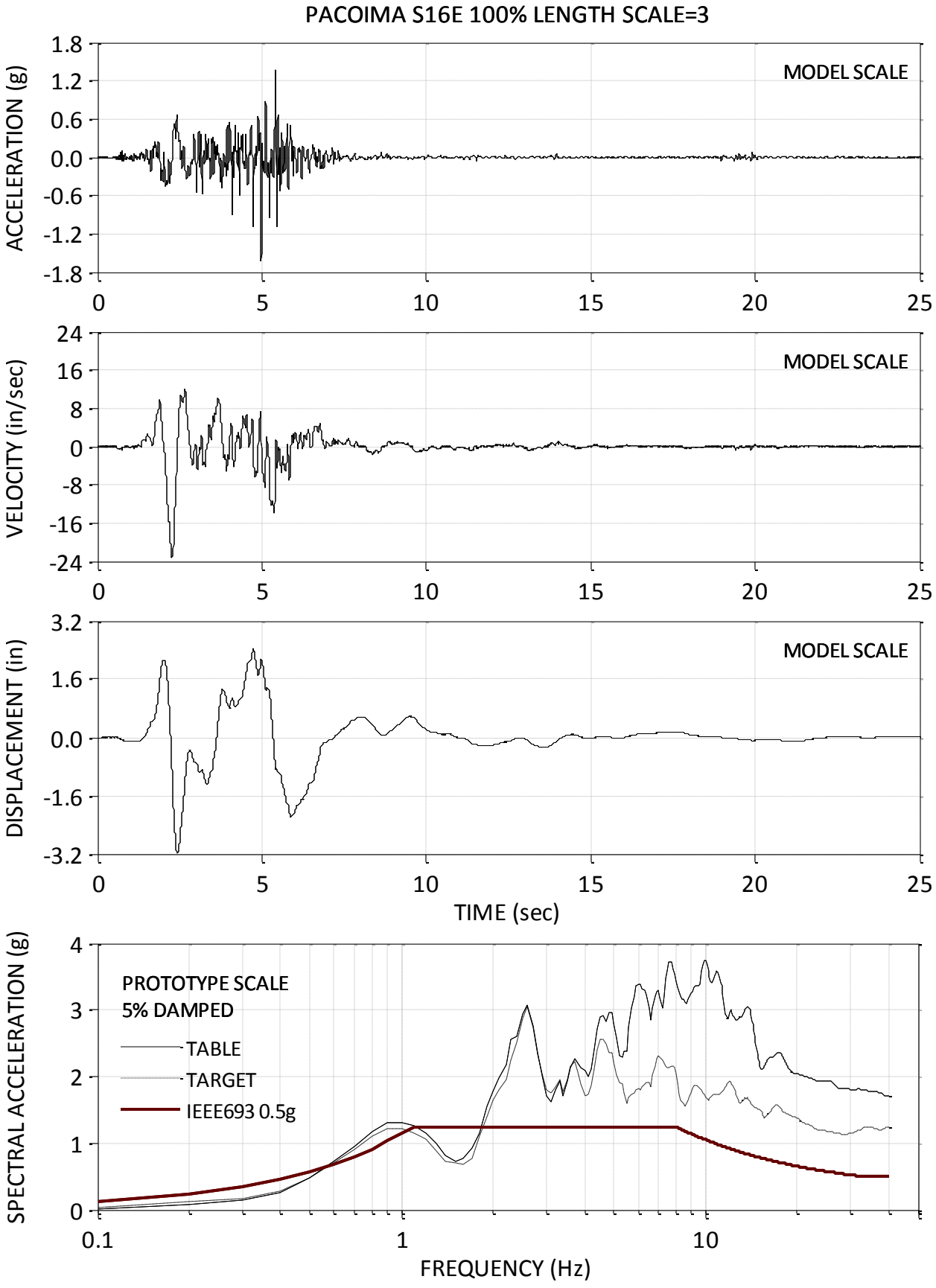

1999 DUZCE, TURKEY (BOLU STATION) FP 104% LENGTH SCALE=3
ACCELERATION (g)
MODEL SCALE
VELOCITY (in/sec)
MODEL SCALE
DISPLACEMENT (in)
MODEL SCALE
TIME (sec)
SPECTRAL ACCELERATION (g)
PROTOTYPE SCALE
5% DAMPED
TABLE
TARGET
IEEE693 0.5g
FREQUENCY (Hz)

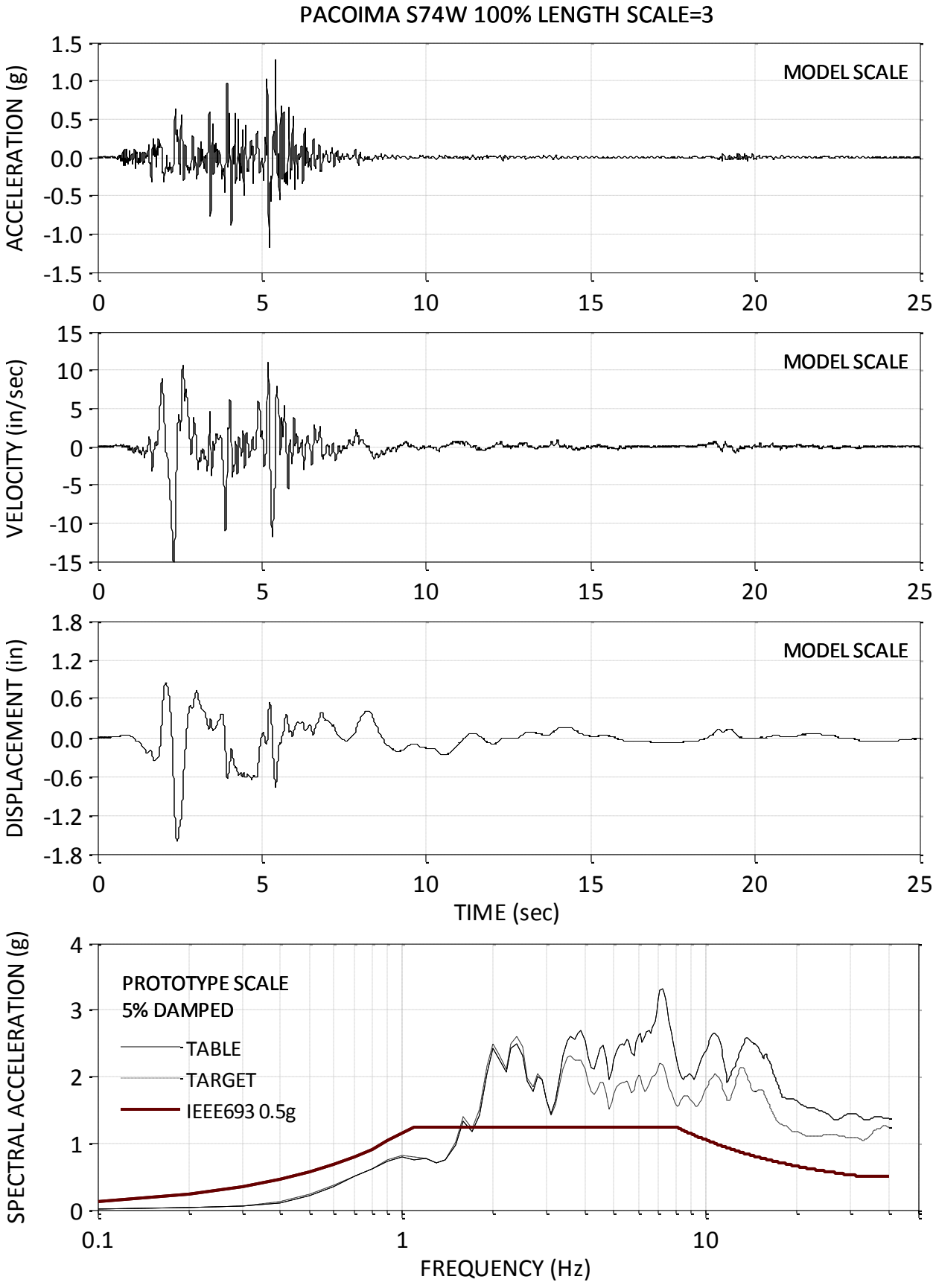

1999 DUZCE, TURKEY (BOLU STATION) V (MATCHING) LENGTH SCALE=3
ACCELERATION (g)
MODEL SCALE
VELOCITY (in/sec)
MODEL SCALE
DISPLACEMENT (in)
MODEL SCALE
TIME (sec)
SPECTRAL ACCELERATION (g)
PROTOTYPE SCALE
5% DAMPED
TABLE
TARGET
IEEE693 0.4g
FREQUENCY (Hz)

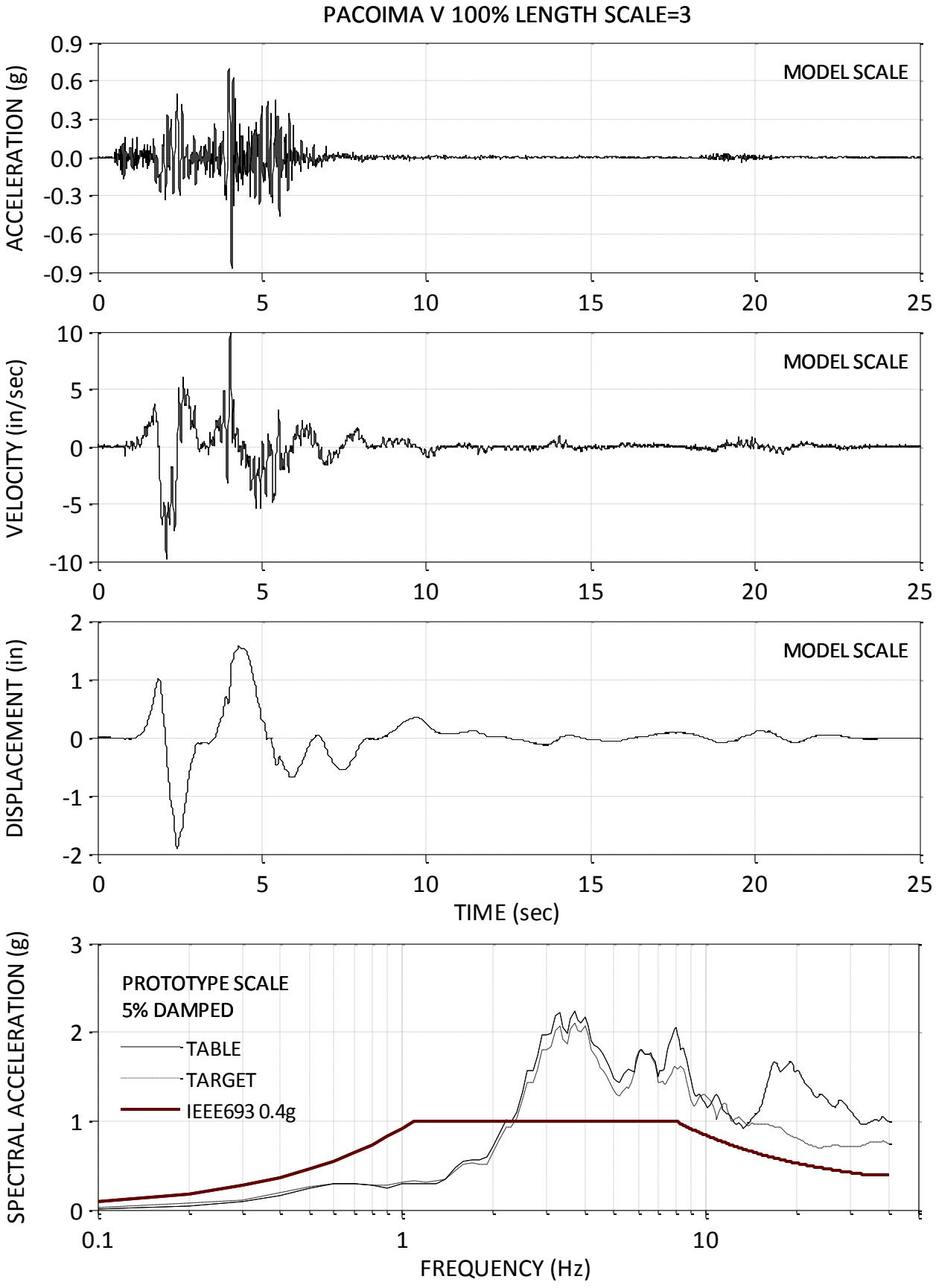

EL CENTRO N90W 100% LENGTH SCALE=3
ACCELERATION (g)
MODEL SCALE
VELOCITY (in/sec)
MODEL SCALE
DISPLACEMENT (in)
MODEL SCALE
TIME (sec)
SPECTRAL ACCELERATION (g)
PROTOTYPE SCALE
5% DAMPED
TABLE
TARGET
IEEE693 0.5g
FREQUENCY (Hz)

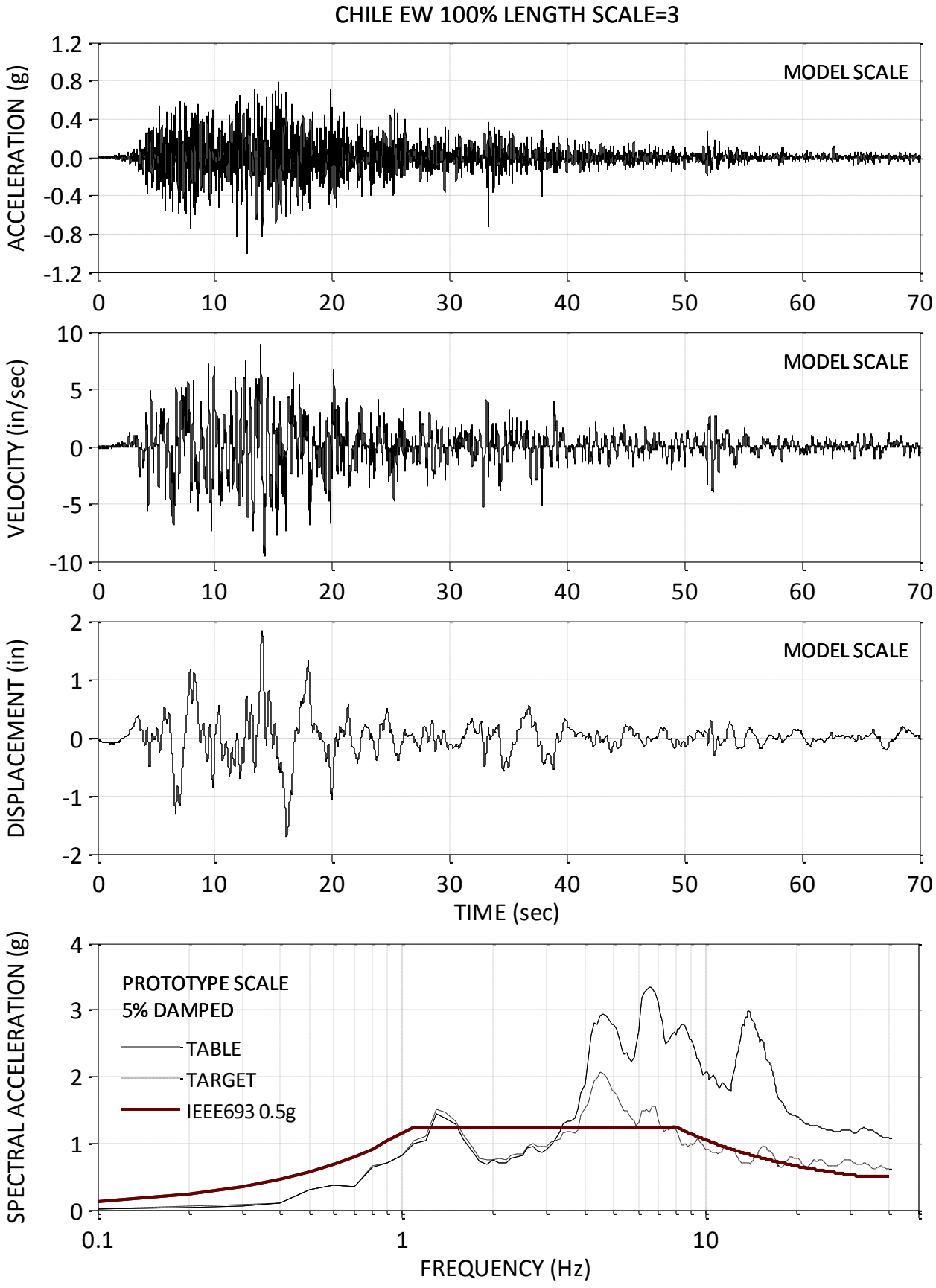

EL CENTRO S00E 100% LENGTH SCALE=3
ACCELERATION (g)
MODEL SCALE
VELOCITY (in/sec)
MODEL SCALE
DISPLACEMENT (in)
MODEL SCALE
TIME (sec)
SPECTRAL ACCELERATION (g)
PROTOTYPE SCALE
5% DAMPED
TABLE
TARGET
IEEE693 0.5g
FREQUENCY (Hz)

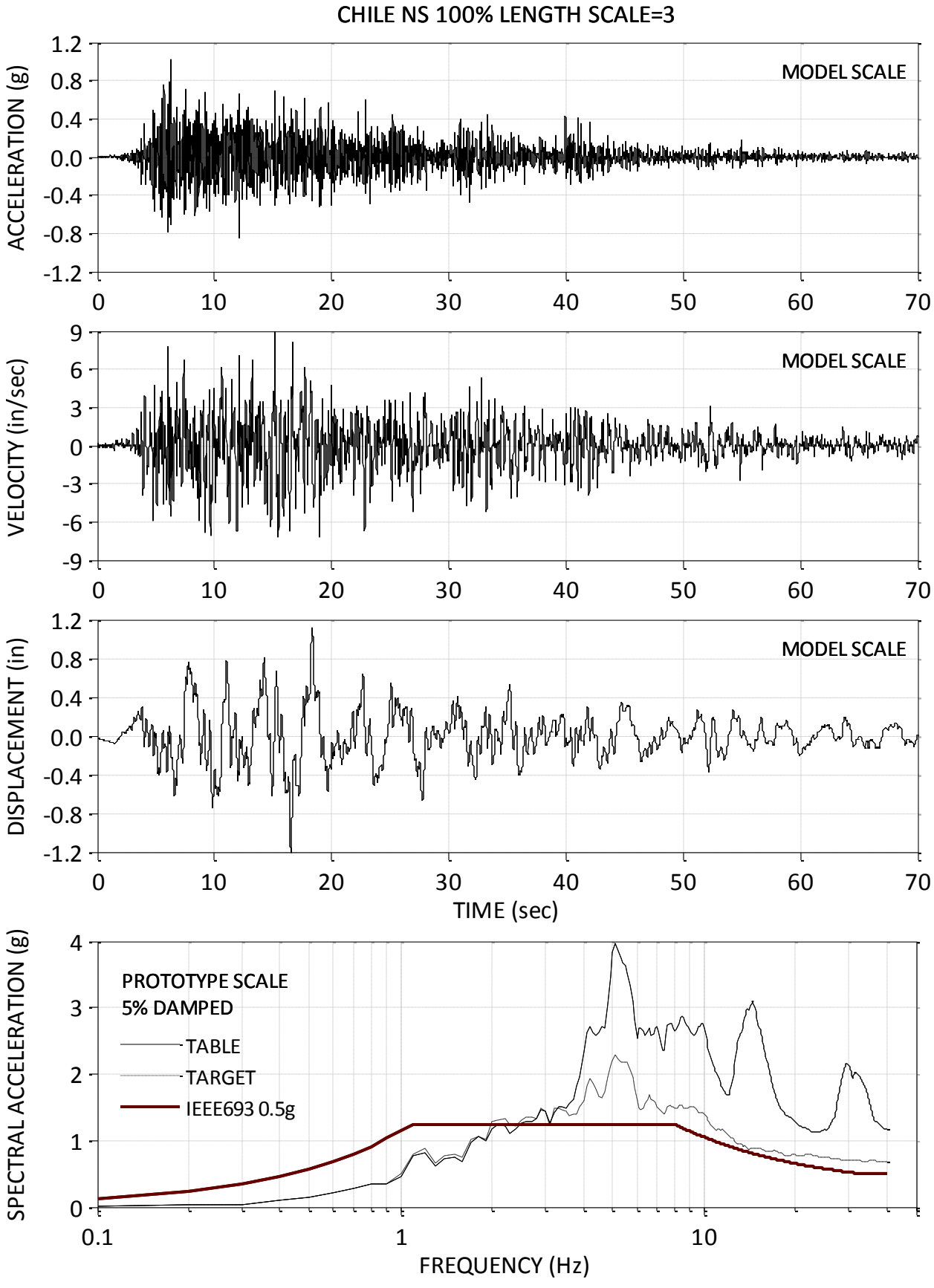

EL CENTRO V 100% LENGTH SCALE=3
ACCELERATION (g)
0.24
0.16
0.08
0.00
-0.08
-0.16
-0.24
MODEL SCALE
0
5
10
15
20
25
30
VELOCITY (in/sec)
1.8
1.2
0.6
0.0
-0.6
-1.2
-1.8
MODEL SCALE
DISPLACEMENT (in)
0.16
0.08
0.00
-0.08
-0.16
MODEL SCALE
TIME (sec)
SPECTRAL ACCELERATION (g)
2.0
1.5
1.0
0.5
0.0
PROTOTYPE SCALE
5% DAMPED
TABLE
TARGET
IEEE693 0.4g
0.1
1
10
FREQUENCY (Hz)

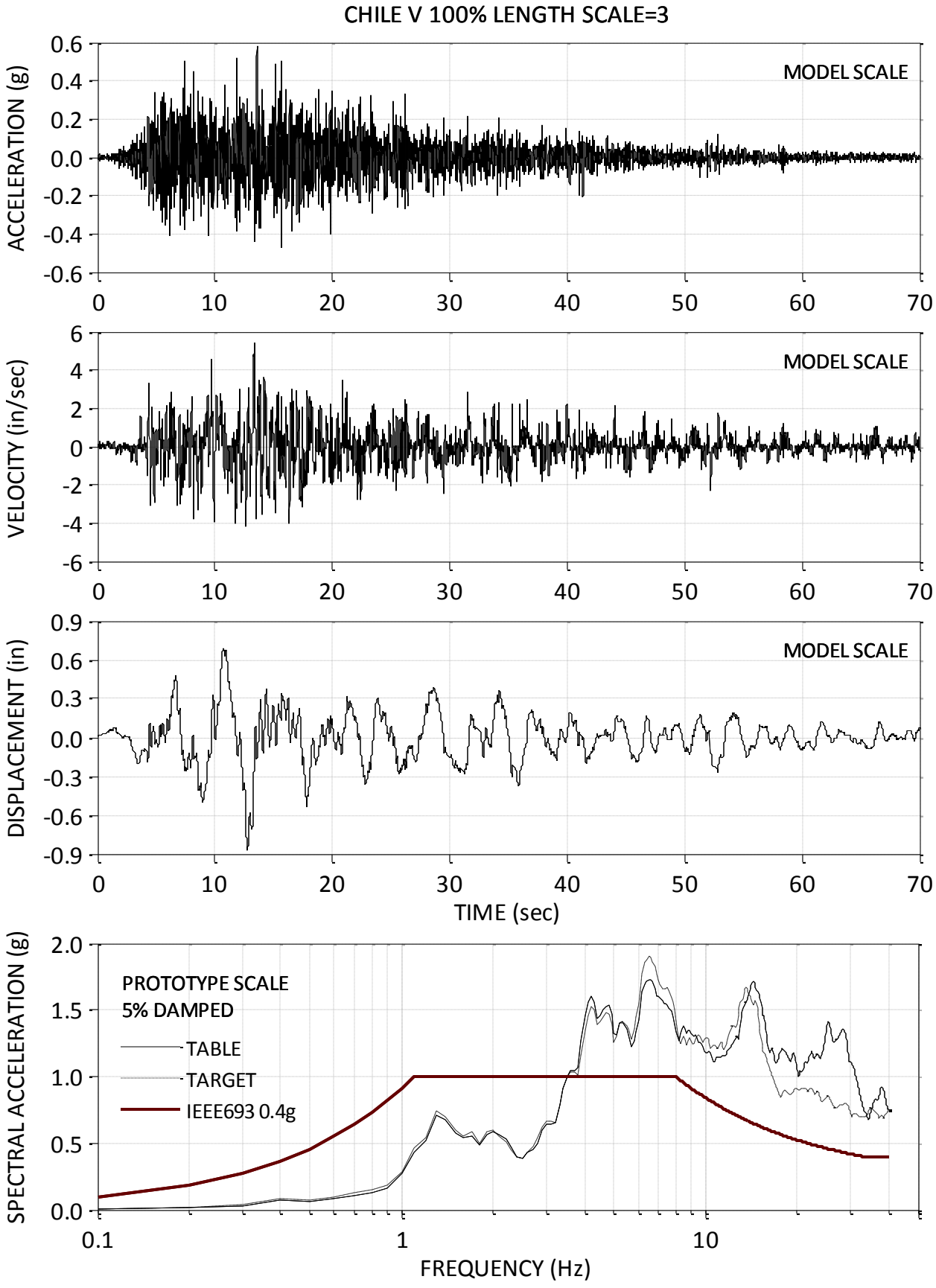

PACOIMA S16E 100% LENGTH SCALE=3
ACCELERATION (g)
MODEL SCALE
VELOCITY (in/sec)
MODEL SCALE
DISPLACEMENT (in)
MODEL SCALE
TIME (sec)
SPECTRAL ACCELERATION (g)
PROTOTYPE SCALE
5% DAMPED
TABLE
TARGET
IEEE693 0.5g
FREQUENCY (Hz)

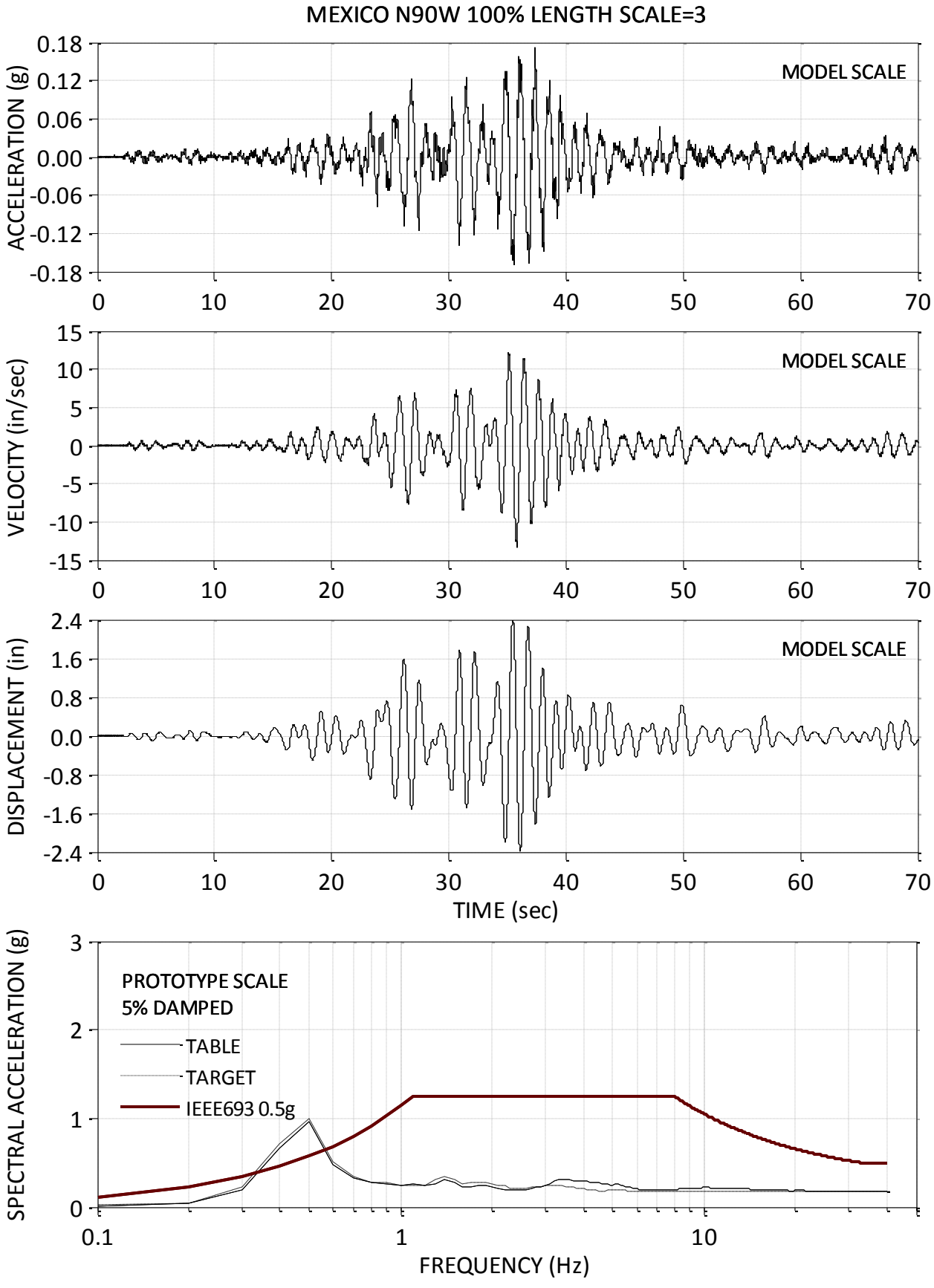

PACOIMA S74W 100% LENGTH SCALE=3
ACCELERATION (g)
MODEL SCALE
VELOCITY (in/sec)
MODEL SCALE
DISPLACEMENT (in)
MODEL SCALE
TIME (sec)
SPECTRAL ACCELERATION (g)
PROTOTYPE SCALE
5% DAMPED
TABLE
TARGET
IEEE693 0.5g
FREQUENCY (Hz)

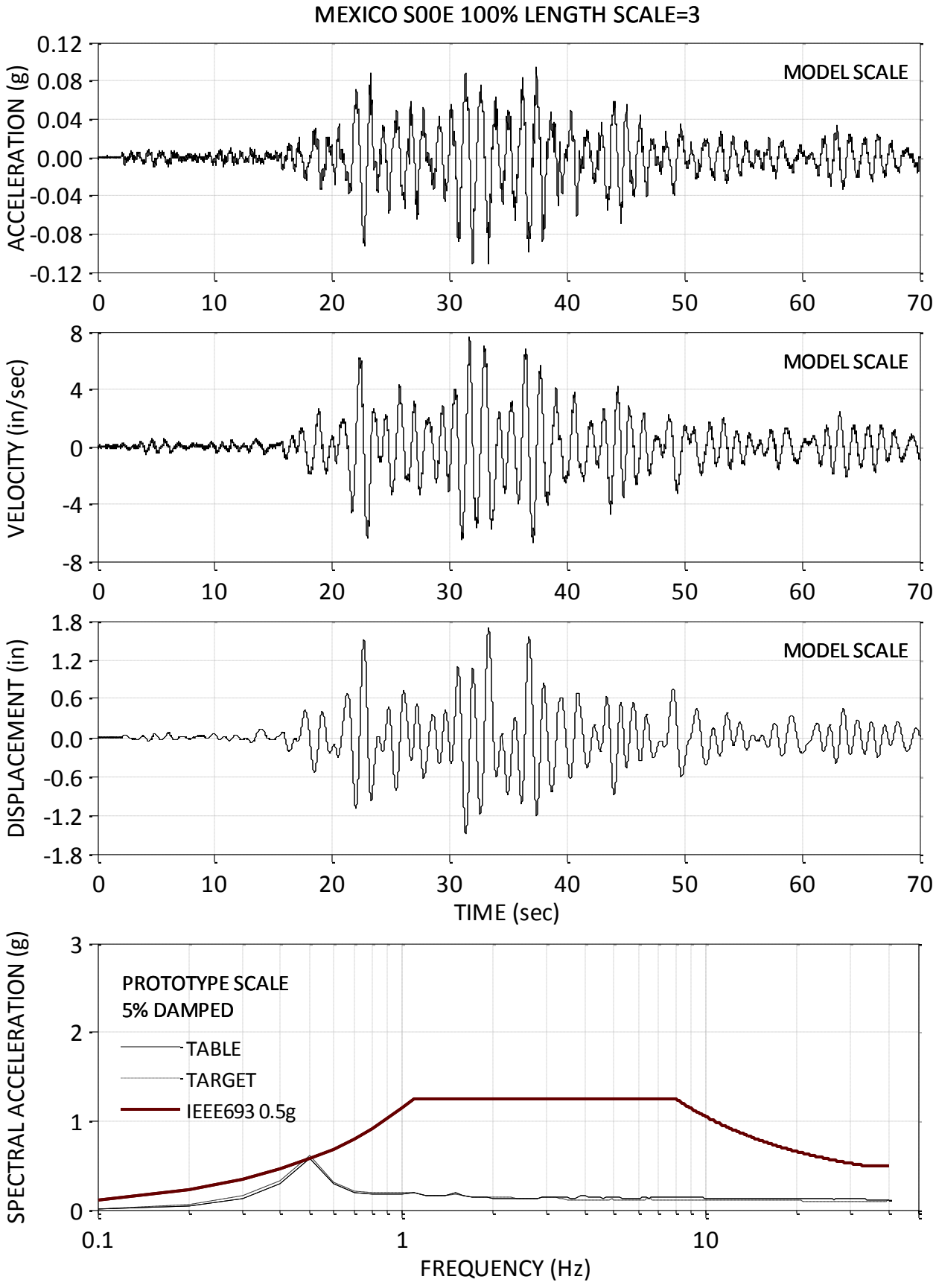

PACOIMA V 100% LENGTH SCALE=3
ACCELERATION (g)
MODEL SCALE
VELOCITY (in/sec)
MODEL SCALE
DISPLACEMENT (in)
MODEL SCALE
TIME (sec)
SPECTRAL ACCELERATION (g)
PROTOTYPE SCALE
5% DAMPED
TABLE
TARGET
IEEE693 0.4g
FREQUENCY (Hz)

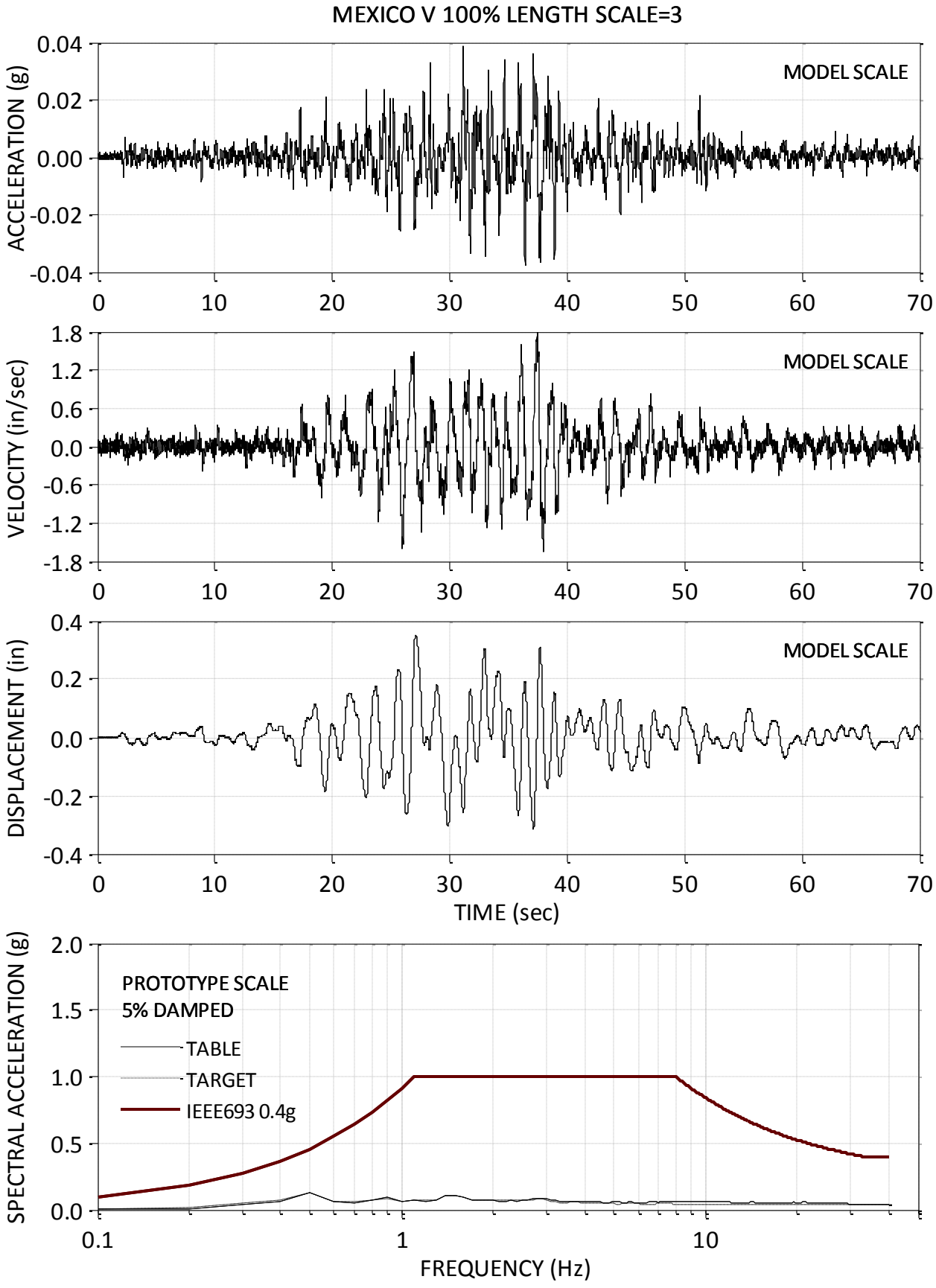

CHILE EW 100% LENGTH SCALE=3
ACCELERATION (g)
MODEL SCALE
VELOCITY (in/sec)
MODEL SCALE
DISPLACEMENT (in)
MODEL SCALE
TIME (sec)
SPECTRAL ACCELERATION (g)
PROTOTYPE SCALE
5% DAMPED
TABLE
TARGET
IEEE693 0.5g
FREQUENCY (Hz)

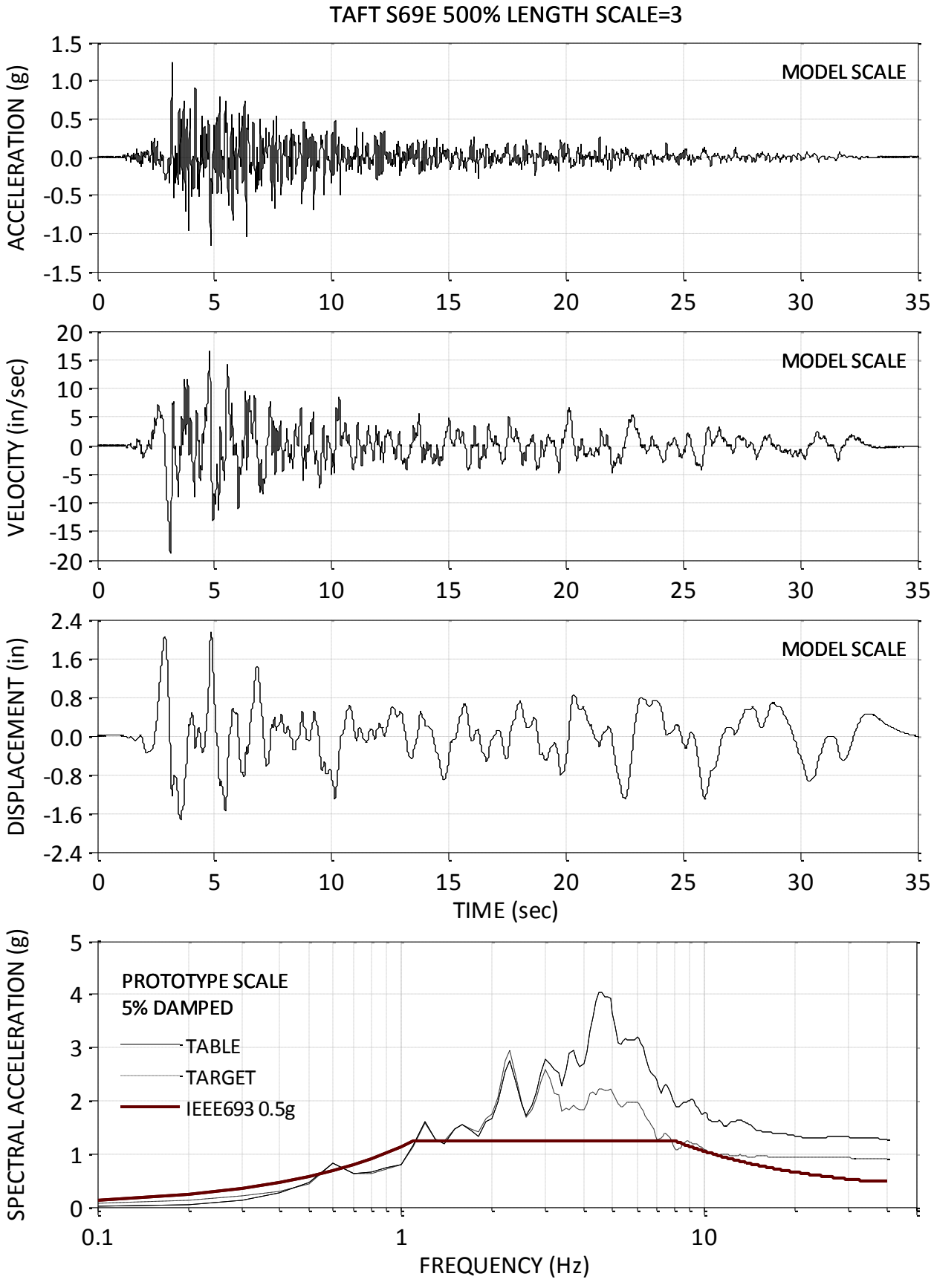

CHILE NS 100% LENGTH SCALE=3
ACCELERATION (g)
MODEL SCALE
VELOCITY (in/sec)
MODEL SCALE
DISPLACEMENT (in)
MODEL SCALE
TIME (sec)
SPECTRAL ACCELERATION (g)
PROTOTYPE SCALE
5% DAMPED
TABLE
TARGET
IEEE693 0.5g
FREQUENCY (Hz)

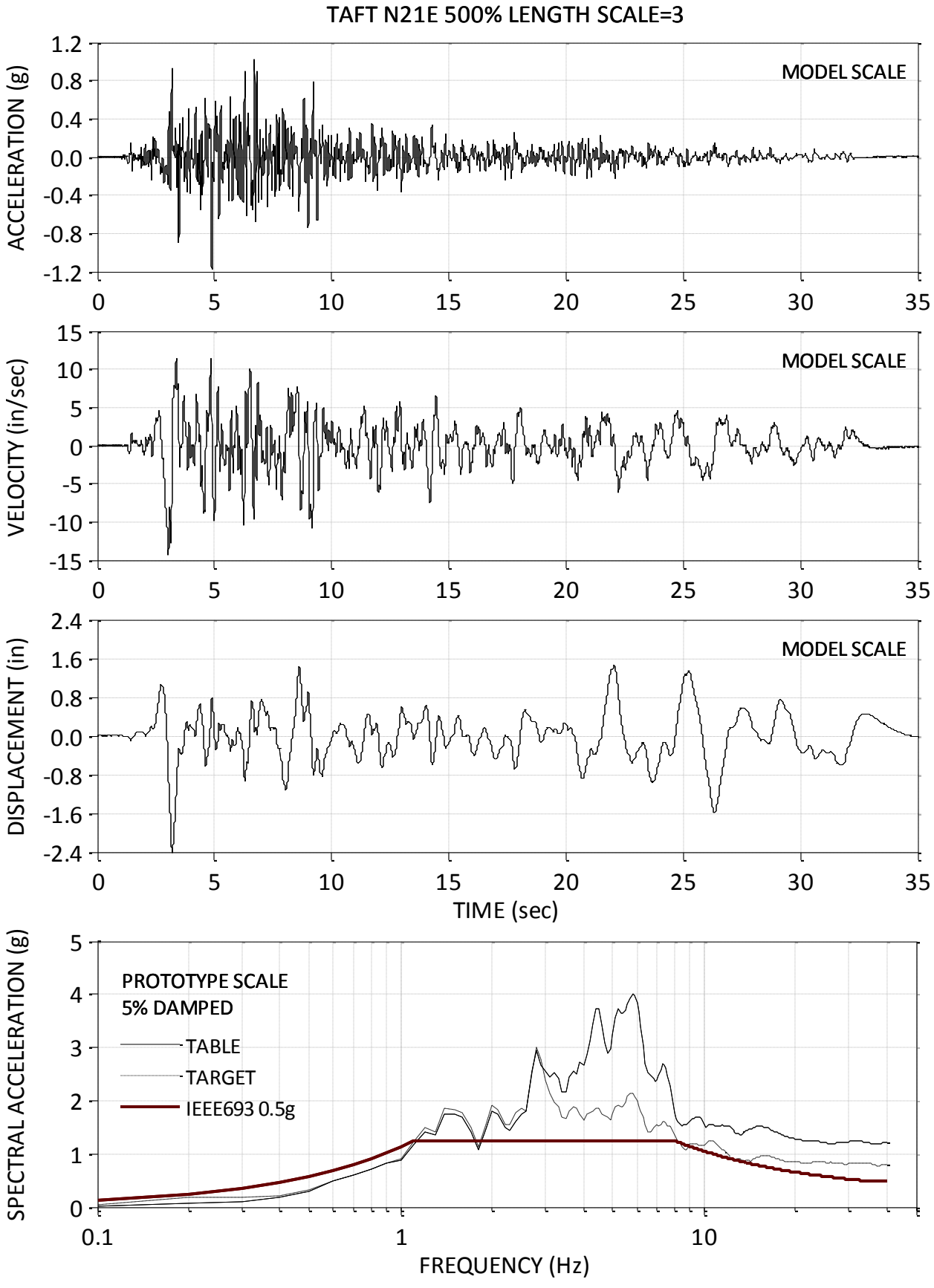

CHILE V 100% LENGTH SCALE=3
ACCELERATION (g)
MODEL SCALE
VELOCITY (in/sec)
MODEL SCALE
DISPLACEMENT (in)
MODEL SCALE
TIME (sec)
SPECTRAL ACCELERATION (g)
PROTOTYPE SCALE
5% DAMPED
TABLE
TARGET
IEEE693 0.4g
FREQUENCY (Hz)

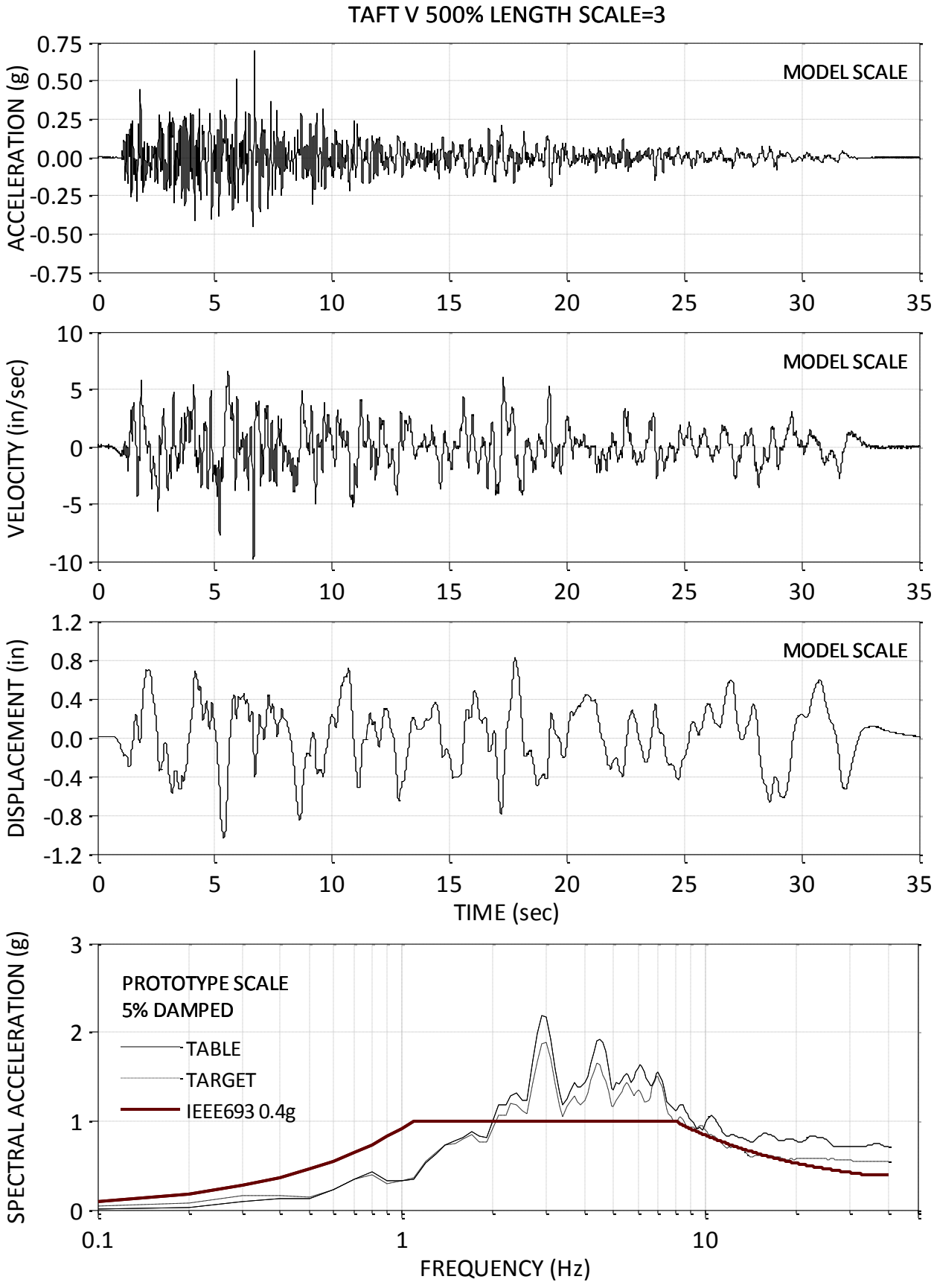

MEXICO N90W 100% LENGTH SCALE=3
ACCELERATION (g)
0.18
0.12
0.06
0.00
-0.06
-0.12
-0.18
MODEL SCALE
0
10
20
30
40
50
60
70
VELOCITY (in/sec)
15
10
5
0
-5
-10
-15
MODEL SCALE
DISPLACEMENT (in)
2.4
1.6
0.8
0.0
-0.8
-1.6
-2.4
MODEL SCALE
TIME (sec)
SPECTRAL ACCELERATION (g)
3
2
1
0
PROTOTYPE SCALE
5% DAMPED
TABLE
TARGET
IEEE693 0.5g
0.1
1
10
FREQUENCY (Hz)


MEXICO S00E 100% LENGTH SCALE=3
ACCELERATION (g)
MODEL SCALE
VELOCITY (in/sec)
MODEL SCALE
DISPLACEMENT (in)
MODEL SCALE
TIME (sec)
SPECTRAL ACCELERATION (g)
PROTOTYPE SCALE
5% DAMPED
TABLE
TARGET
IEEE693 0.5g
FREQUENCY (Hz)


MEXICO V 100% LENGTH SCALE=3
ACCELERATION (g)
MODEL SCALE
VELOCITY (in/sec)
MODEL SCALE
DISPLACEMENT (in)
MODEL SCALE
TIME (sec)
SPECTRAL ACCELERATION (g)
PROTOTYPE SCALE
5% DAMPED
TABLE
TARGET
IEEE693 0.4g
FREQUENCY (Hz)


TAFT S69E 500% LENGTH SCALE=3
ACCELERATION (g)
MODEL SCALE
VELOCITY (in/sec)
MODEL SCALE
DISPLACEMENT (in)
MODEL SCALE
TIME (sec)
SPECTRAL ACCELERATION (g)
PROTOTYPE SCALE
5% DAMPED
TABLE
TARGET
IEEE693 0.5g
FREQUENCY (Hz)


TAFT N21E 500% LENGTH SCALE=3
ACCELERATION (g)
MODEL SCALE
VELOCITY (in/sec)
MODEL SCALE
DISPLACEMENT (in)
MODEL SCALE
TIME (sec)
SPECTRAL ACCELERATION (g)
PROTOTYPE SCALE
5% DAMPED
TABLE
TARGET
IEEE693 0.5g
FREQUENCY (Hz)


TAFT V 500% LENGTH SCALE=3
ACCELERATION (g)
MODEL SCALE
VELOCITY (in/sec)
MODEL SCALE
DISPLACEMENT (in)
MODEL SCALE
TIME (sec)
SPECTRAL ACCELERATION (g)
PROTOTYPE SCALE
5% DAMPED
TABLE
TARGET
IEEE693 0.4g
FREQUENCY (Hz)

APPENDIX B
SUMMARY OF EXPERIMENTAL DATA

PART B-1
SUMMARY OF EXPERIMENTAL DATA FOR LEAD-RUBBER SYSTEM AT LENGTH SCALE OF 3

(PERCENTAGE AMOUNT IS SCALE FACTOR APPLIED TO ACCELERATION OF ACTUAL MOTION. FOR EXAMPLE, 100% DENOTES MOTION AS RECORDED, 200% DENOTES THAT ACCELERATION WAS SCALED UP BY FACTOR OF 2)

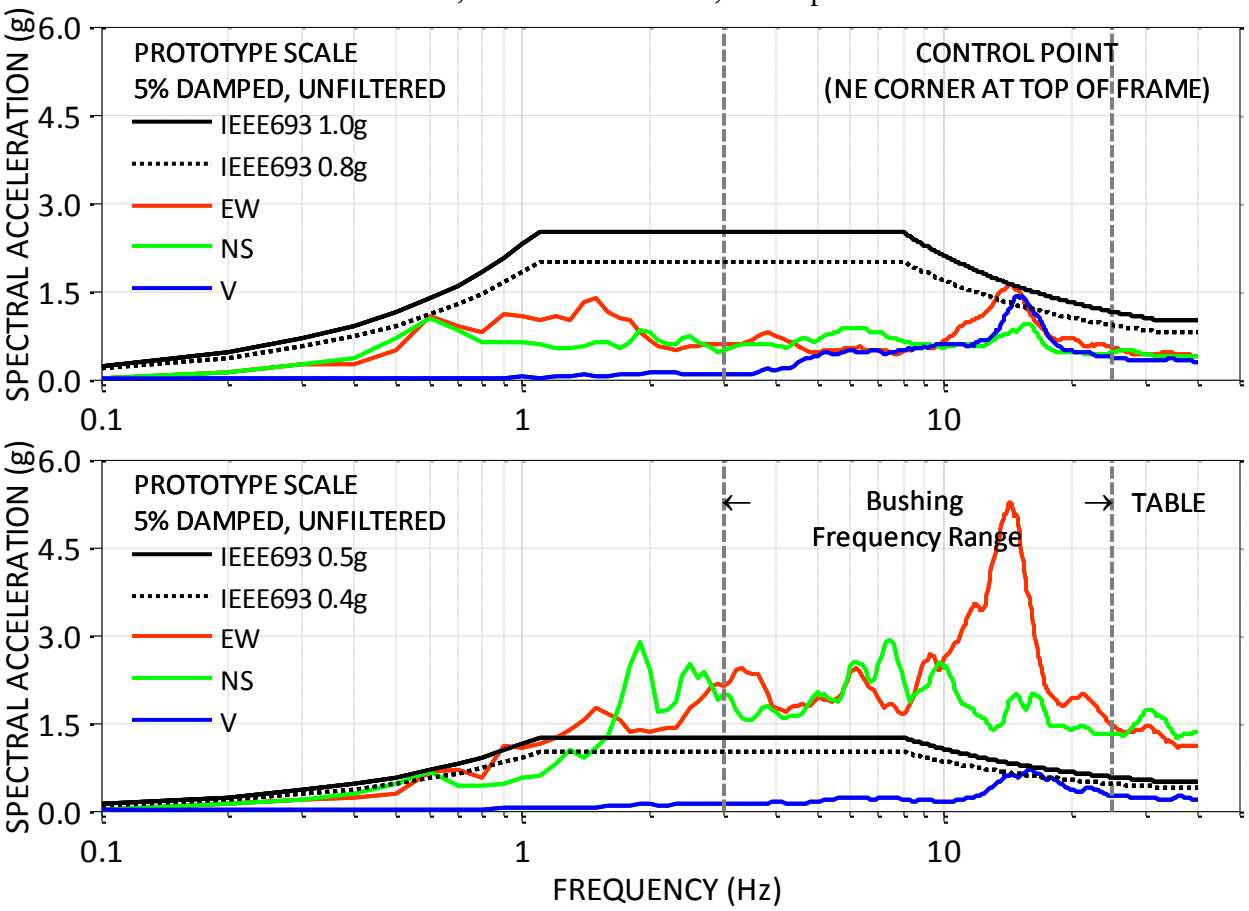
LRB SYSTEM (Friction-Bolted Configuration)
KARAKYR 137% BI-AXIAL (FN in EW direction)
LENGTH SCALE=3 SYMMETRIC BUSHING CONFIGURATION

Peak Table Motion								
Acceleration (g)			Velocity (in/sec)			Displacement (in)		
EW	NS	V	EW	NS	V	EW	NS	V
1.08	1.20	0.15	15.66	21.03	0.91	3.44	3.85	0.07

OBSERVATIONS
Sliding at friction connection of about 2.3 inches (NE), 1.4 inches (SE), 1.1 inches (SW) and 1.4 inches (NW)

Peak Resultant Displacement (in)				Peak Acceleration (g)							
Bushing Top		Isolator	Torsional Ampl[3] Ratio (TA)	Bushing Top			Bushing Bottom		Control Point		
Abs[1]	Rel[2]			EW	NS	V	EW	NS	EW	NS	V
5.15	3.89	4.24	1.10	1.21	1.54	0.34	0.38	0.36	0.39	0.38	0.26

1. Absolute, 2. Relative to table, 3. Amplification



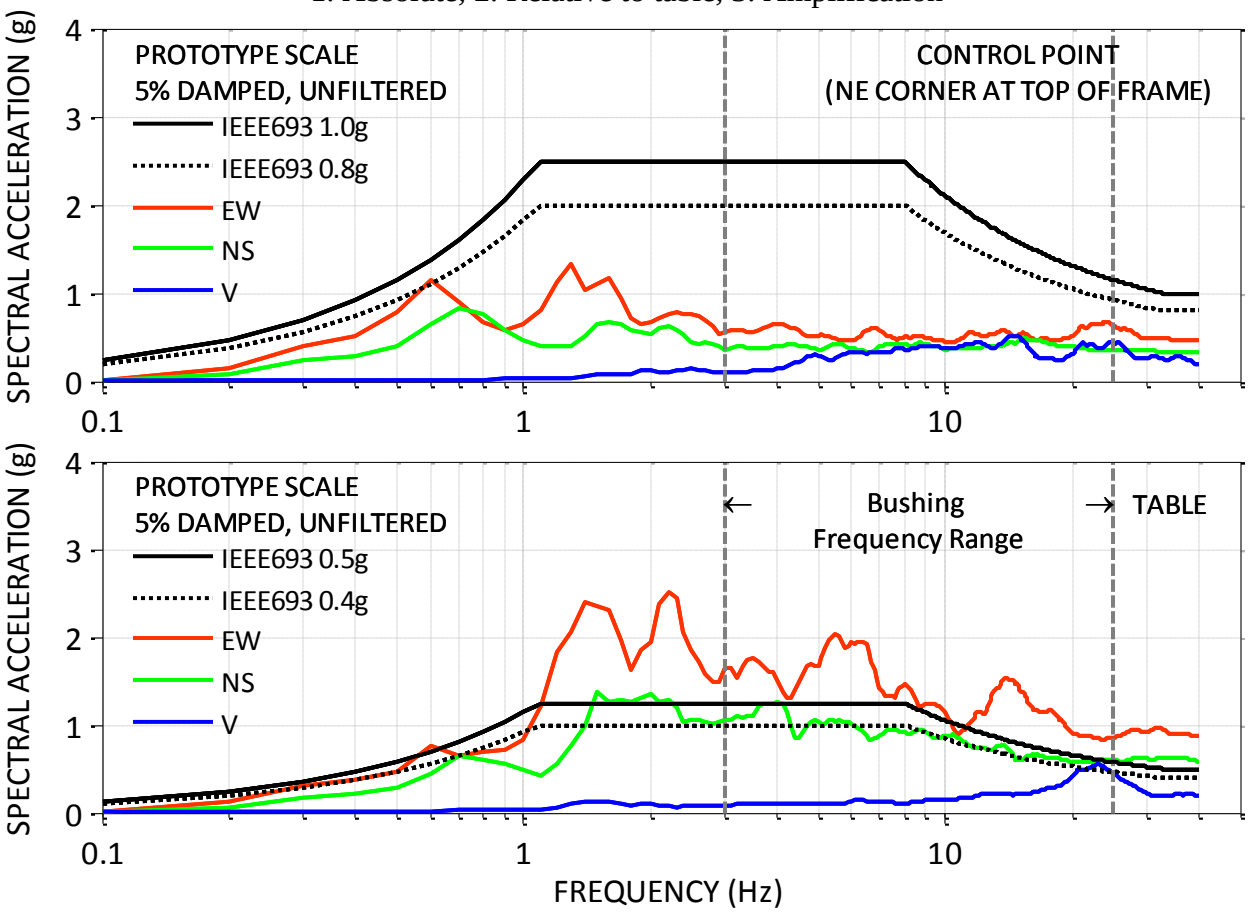
LRB SYSTEM (Friction-Bolted Configuration)
LGPC 94% BI-AXIAL (FN in EW direction)
LENGTH SCALE=3 SYMMETRIC BUSHING CONFIGURATION

Peak Table Motion								
Acceleration (g)			Velocity (in/sec)			Displacement (in)		
EW	NS	V	EW	NS	V	EW	NS	V
0.82	0.58	0.11	19.67	11.75	1.15	3.97	3.22	0.12

OBSERVATIONS
Sliding at friction connection of about 2.8 inches (NE), 3.6 inches (SE), 4.3 inches (SW) and 2.9 inches (NW)

Peak Resultant Displacement (in)				Peak Acceleration (g)							
Bushing Top		Isolator	Torsional Ampl[3] Ratio (TA)	Bushing Top			Bushing Bottom		Control Point		
Abs[1]	Rel[2]			EW	NS	V	EW	NS	EW	NS	V
6.83	4.98	5.61	1.12	1.26	0.70	0.30	0.35	0.28	0.41	0.31	0.13

1. Absolute, 2. Relative to table, 3. Amplification



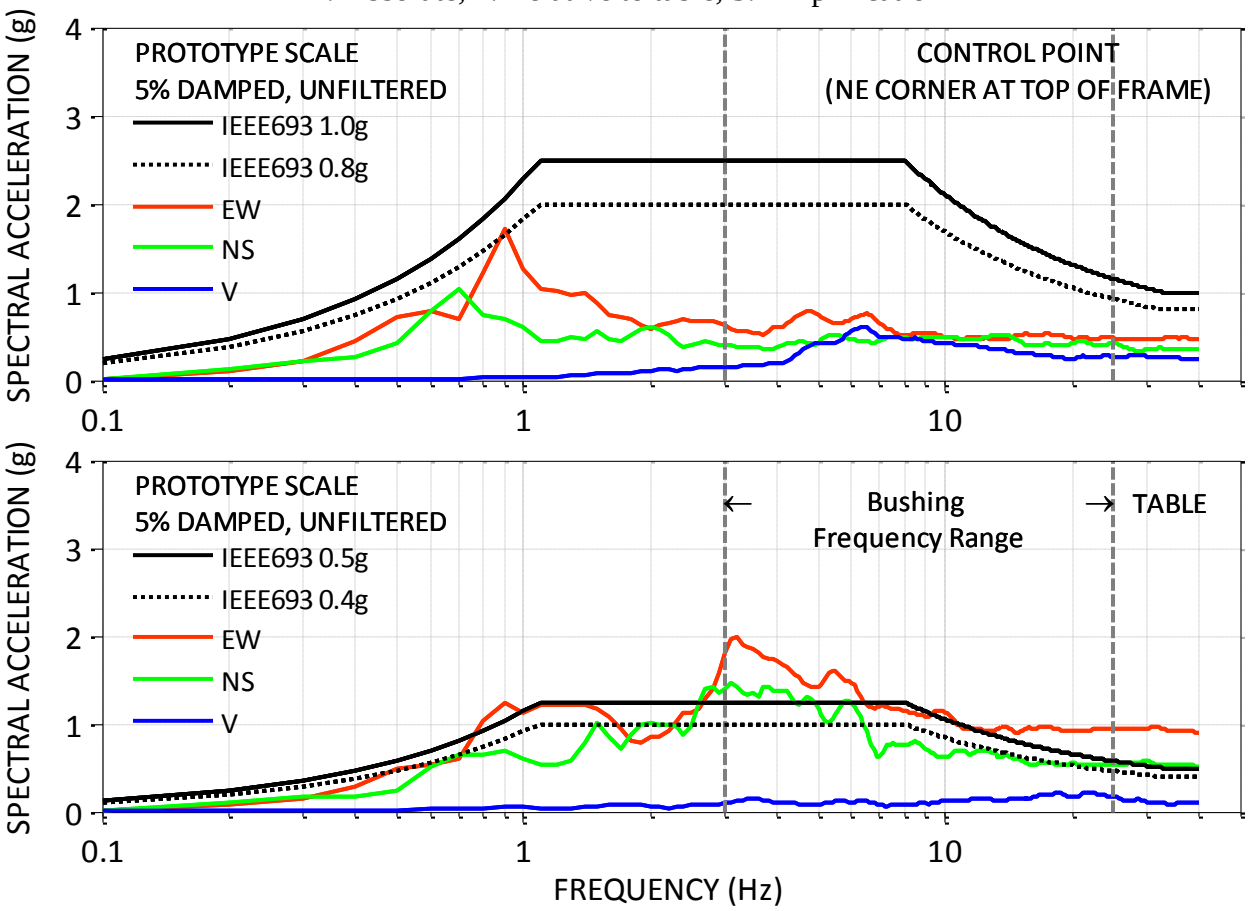
LRB SYSTEM (Friction-Bolted Configuration)
SARATOGA 157% BI-AXIAL (FN in EW direction)
LENGTH SCALE=3 SYMMETRIC BUSHING CONFIGURATION

Peak Table Motion								
Acceleration (g)			Velocity (in/sec)			Displacement (in)		
EW	NS	V	EW	NS	V	EW	NS	V
0.90	0.52	0.06	20.30	13.93	0.92	3.15	4.59	0.10

OBSERVATIONS
Sliding at friction connection of about 4.0 inches (NE), 1.8 inches (SE), 2.2 inches (SW) and 4.7 inches (NW)

Peak Resultant Displacement (in)				Peak Acceleration (g)							
Bushing Top		Isolator	Torsional Ampl[3] Ratio (TA)	Bushing Top			Bushing Bottom		Control Point		
Abs[1]	Rel[2]			EW	NS	V	EW	NS	EW	NS	V
7.27	5.08	6.04	1.16	1.98	1.02	0.34	0.38	0.39	0.44	0.33	0.17

1. Absolute, 2. Relative to table, 3. Amplification



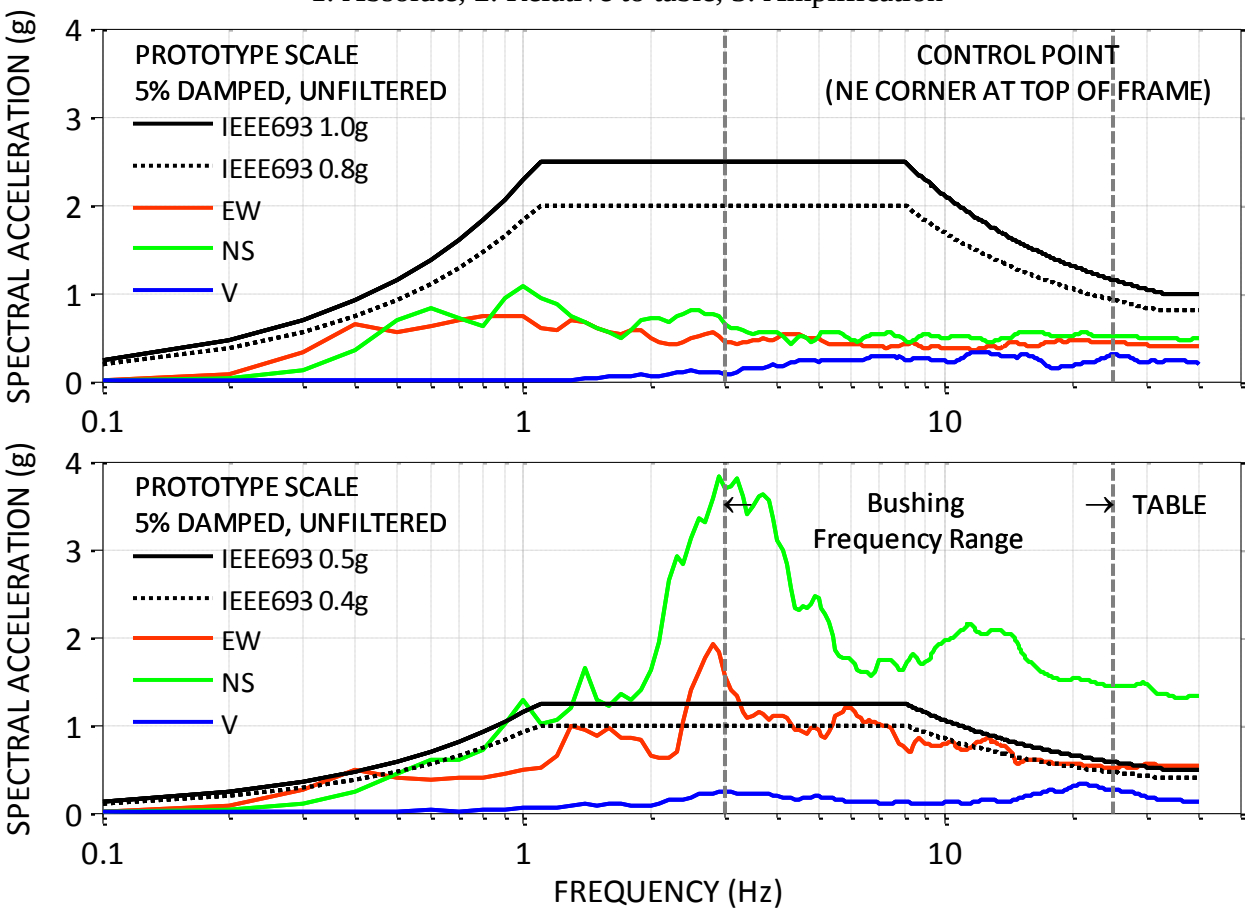
LRB SYSTEM (Friction-Bolted Configuration)
JENSEN FILTER 97% BI-AXIAL (FN in EW direction)
LENGTH SCALE=3 SYMMETRIC BUSHING CONFIGURATION

Peak Table Motion								
Acceleration (g)			Velocity (in/sec)			Displacement (in)		
EW	NS	V	EW	NS	V	EW	NS	V
0.51	1.29	0.10	14.07	14.45	0.60	3.23	1.83	0.05

OBSERVATIONS
Sliding at friction connection of about 0.9 inches (NE), 1.1 inches (SW) and 1.0 inches (NW)

Peak Resultant Displacement (in)				Peak Acceleration (g)							
Bushing Top		Isolator	Torsional Ampl[3] Ratio (TA)	Bushing Top			Bushing Bottom		Control Point		
Abs[1]	Rel[2]			EW	NS	V	EW	NS	EW	NS	V
4.14	3.00	3.11	1.04	0.90	0.68	0.18	0.32	0.40	0.35	0.46	0.14

1. Absolute, 2. Relative to table, 3. Amplification



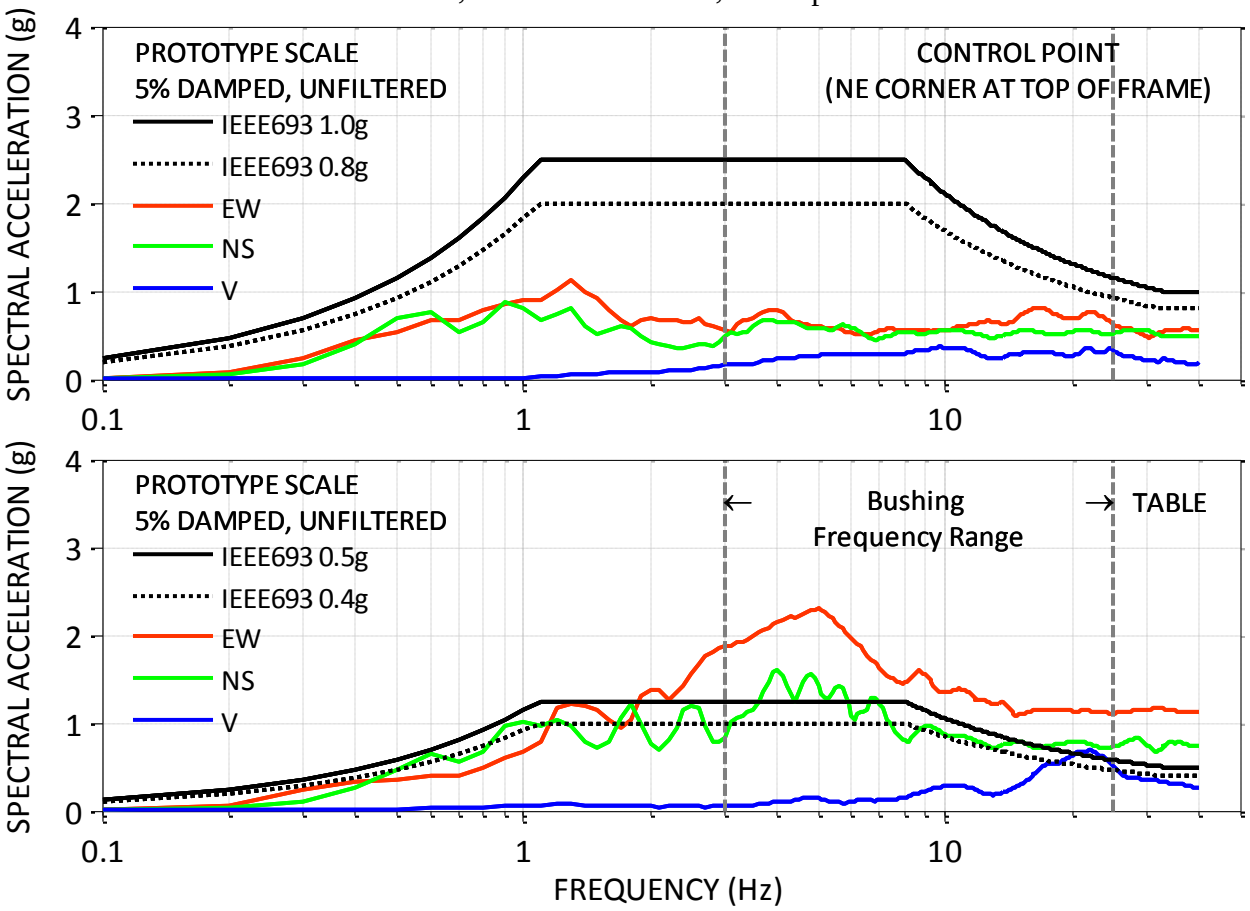
LRB SYSTEM (Friction-Bolted Configuration)
SYLMAR 90% BI-AXIAL (FN in EW direction)
LENGTH SCALE=3 SYMMETRIC BUSHING CONFIGURATION

Peak Table Motion								
Acceleration (g)			Velocity (in/sec)			Displacement (in)		
EW	NS	V	EW	NS	V	EW	NS	V
1.09	0.65	0.18	21.03	14.51	1.00	3.17	2.34	0.05

OBSERVATIONS
Sliding at friction connection of about 3.1 inches (NE), 1.5 inches (SE) and 2.5 inches (NW)

Peak Resultant Displacement (in)				Peak Acceleration (g)							
Bushing Top		Isolator	Torsional Ampl[3] Ratio (TA)	Bushing Top			Bushing Bottom		Control Point		
Abs[1]	Rel[2]			EW	NS	V	EW	NS	EW	NS	V
4.76	4.47	4.58	1.04	1.18	1.43	0.43	0.40	0.43	0.48	0.47	0.17

1. Absolute, 2. Relative to table, 3. Amplification



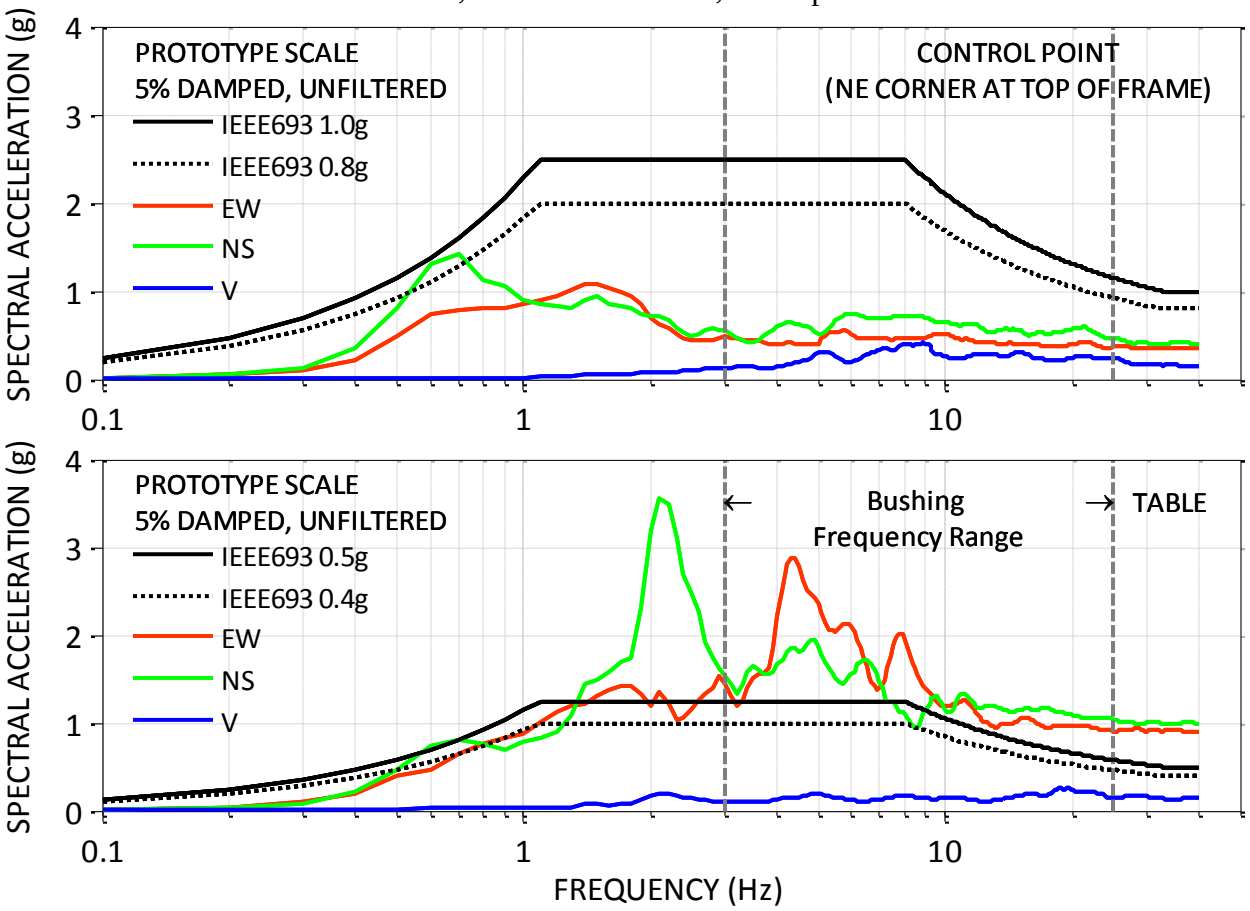
LRB SYSTEM (Friction-Bolted Configuration)
TAKARAZUKA 97% BI-AXIAL (FN in EW direction)
LENGTH SCALE=3 SYMMETRIC BUSHING CONFIGURATION

Peak Table Motion								
Acceleration (g)			Velocity (in/sec)			Displacement (in)		
EW	NS	V	EW	NS	V	EW	NS	V
0.89	0.99	0.11	14.77	18.81	0.44	1.78	2.41	0.02

OBSERVATIONS
Sliding at friction connection of about 2.4 inches (NE), 1.0 inches (SE), 2.2 inches (SW) and 2.3 inches (NW)

Peak Resultant Displacement (in)				Peak Acceleration (g)							
Bushing Top		Isolator	Torsional Ampl[3] Ratio (TA)	Bushing Top			Bushing Bottom		Control Point		
Abs[1]	Rel[2]			EW	NS	V	EW	NS	EW	NS	V
4.00	3.01	4.12	1.43	0.94	1.92	0.32	0.30	0.38	0.35	0.37	0.11

1. Absolute, 2. Relative to table, 3. Amplification



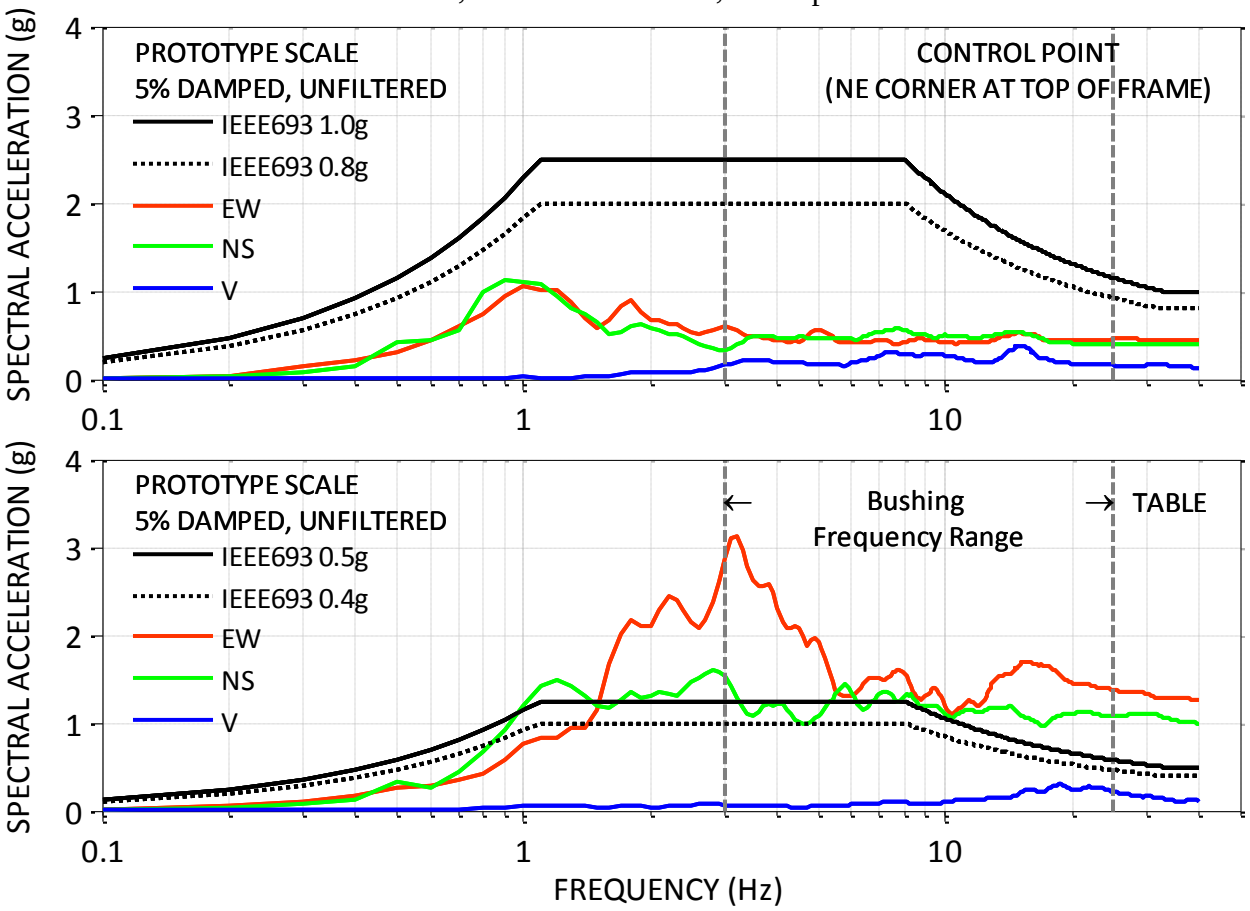
LRB SYSTEM (Friction-Bolted Configuration)
BOLU 104% BI-AXIAL (FN in EW direction)
LENGTH SCALE=3 SYMMETRIC BUSHING CONFIGURATION

Peak Table Motion								
Acceleration (g)			Velocity (in/sec)			Displacement (in)		
EW	NS	V	EW	NS	V	EW	NS	V
1.19	0.97	0.08	13.91	14.96	0.60	1.65	1.82	0.03

OBSERVATIONS
Sliding at friction connection of about 2.5 inches (NE), 0.6 inches (SE), 1.2 inches (SW) and 1.4 inches (NW)

Peak Resultant Displacement (in)				Peak Acceleration (g)							
Bushing Top		Isolator	Torsional Ampl[3] Ratio (TA)	Bushing Top			Bushing Bottom		Control Point		
Abs[1]	Rel[2]			EW	NS	V	EW	NS	EW	NS	V
2.67	2.43	3.11	1.31	0.64	0.97	0.23	0.31	0.45	0.41	0.39	0.12

1. Absolute, 2. Relative to table, 3. Amplification



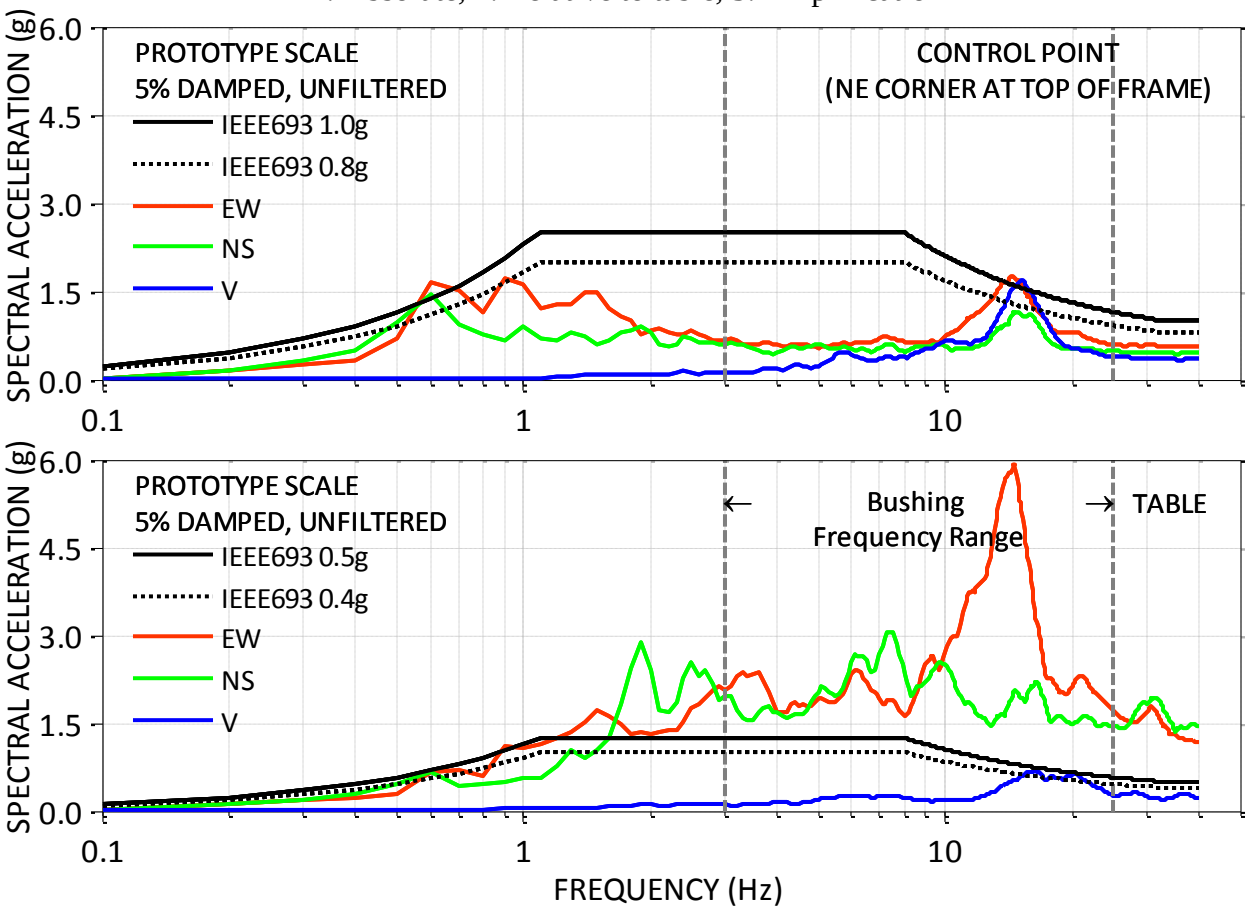
LRB SYSTEM (Bolted-Bolted Configuration)
KARAKYR 137% BI-AXIAL (FN in EW direction)
LENGTH SCALE=3 SYMMETRIC BUSHING CONFIGURATION

Peak Table Motion								
Acceleration (g)			Velocity (in/sec)			Displacement (in)		
EW	NS	V	EW	NS	V	EW	NS	V
1.11	1.24	0.16	15.76	21.78	1.02	3.77	4.02	0.10

OBSERVATIONS

Peak Resultant Displacement (in)				Peak Acceleration (g)							
Bushing Top		Isolator	Torsional Ampl[3] Ratio (TA)	Bushing Top			Bushing Bottom		Control Point		
Abs[1]	Rel[2]			EW	NS	V	EW	NS	EW	NS	V
5.69	3.87	3.80	1.02	0.93	1.32	0.50	0.51	0.46	0.56	0.44	0.31

1. Absolute, 2. Relative to table, 3. Amplification



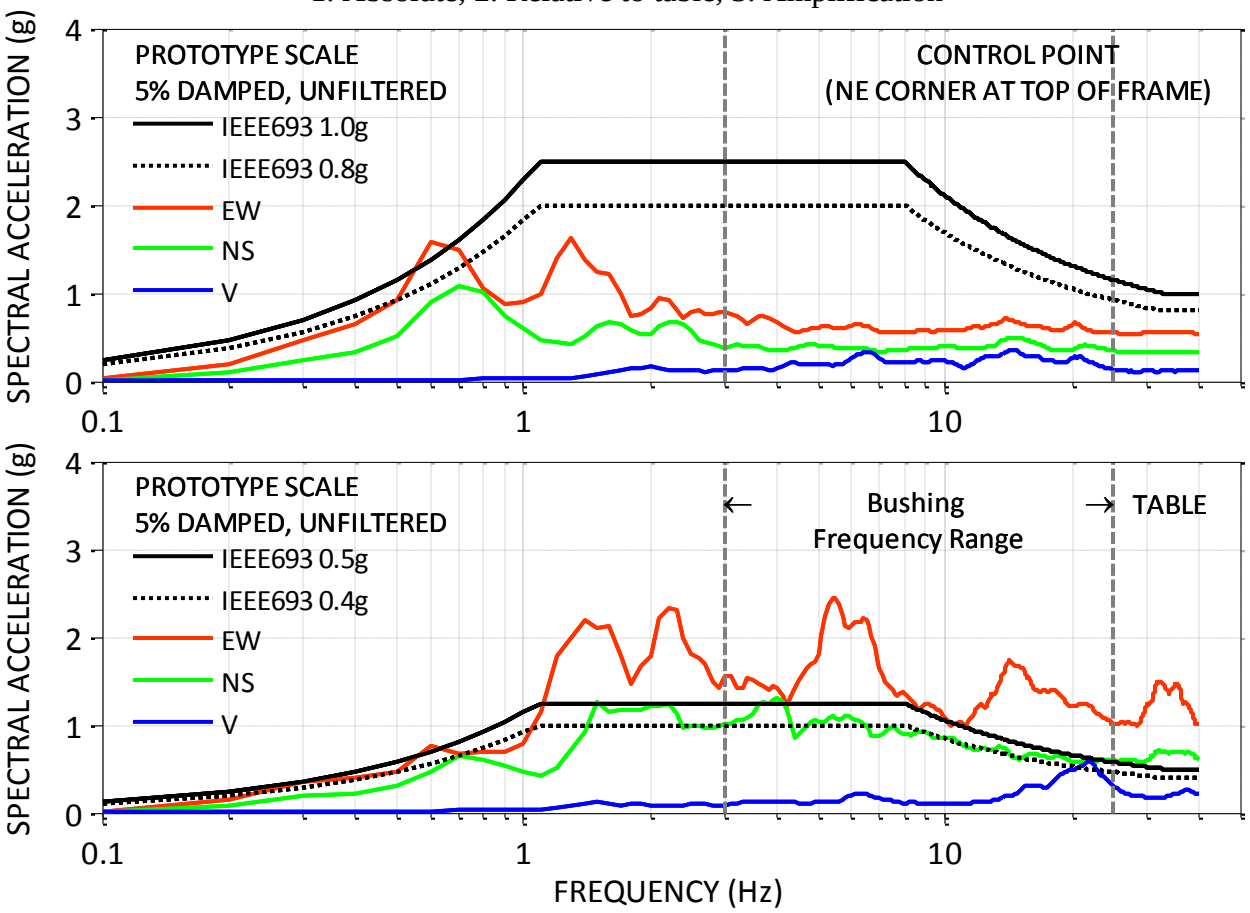
LRB SYSTEM (Bolted-Bolted Configuration)
LGPC 94% BI-AXIAL (FN in EW direction)
LENGTH SCALE=3 SYMMETRIC BUSHING CONFIGURATION

Peak Table Motion								
Acceleration (g)			Velocity (in/sec)			Displacement (in)		
EW	NS	V	EW	NS	V	EW	NS	V
0.89	0.59	0.10	21.75	12.29	1.01	4.94	4.03	0.16

OBSERVATIONS

Peak Resultant Displacement (in)				Peak Acceleration (g)							
Bushing Top		Isolator	Torsional Ampl[3] Ratio (TA)	Bushing Top			Bushing Bottom		Control Point		
Abs[1]	Rel[2]			EW	NS	V	EW	NS	EW	NS	V
6.81	3.41	3.70	1.11	0.95	0.49	0.27	0.48	0.33	0.53	0.32	0.10

1. Absolute, 2. Relative to table, 3. Amplification



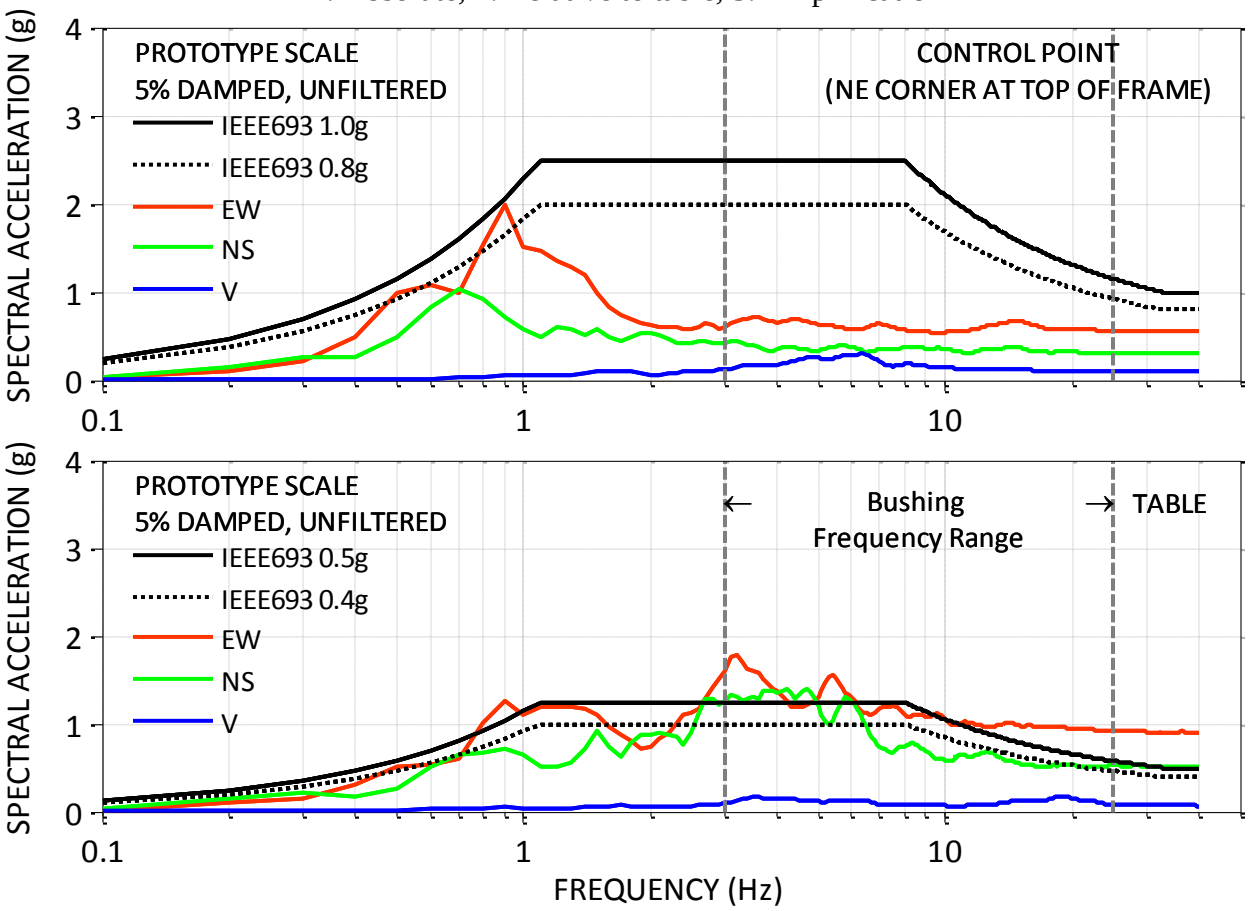
LRB SYSTEM (Bolted-Bolted Configuration)
SARATOGA 157% BI-AXIAL (FN in EW direction)
LENGTH SCALE=3 SYMMETRIC BUSHING CONFIGURATION

Peak Table Motion								
Acceleration (g)			Velocity (in/sec)			Displacement (in)		
EW	NS	V	EW	NS	V	EW	NS	V
0.89	0.50	0.05	21.21	14.05	0.88	3.77	5.91	0.16

OBSERVATIONS

Peak Resultant Displacement (in)				Peak Acceleration (g)							
Bushing Top		Isolator	Torsional Ampl[3] Ratio (TA)	Bushing Top			Bushing Bottom		Control Point		
Abs[1]	Rel[2]			EW	NS	V	EW	NS	EW	NS	V
7.39	3.70	4.21	1.14	0.81	0.67	0.23	0.53	0.44	0.54	0.31	0.10

1. Absolute, 2. Relative to table, 3. Amplification



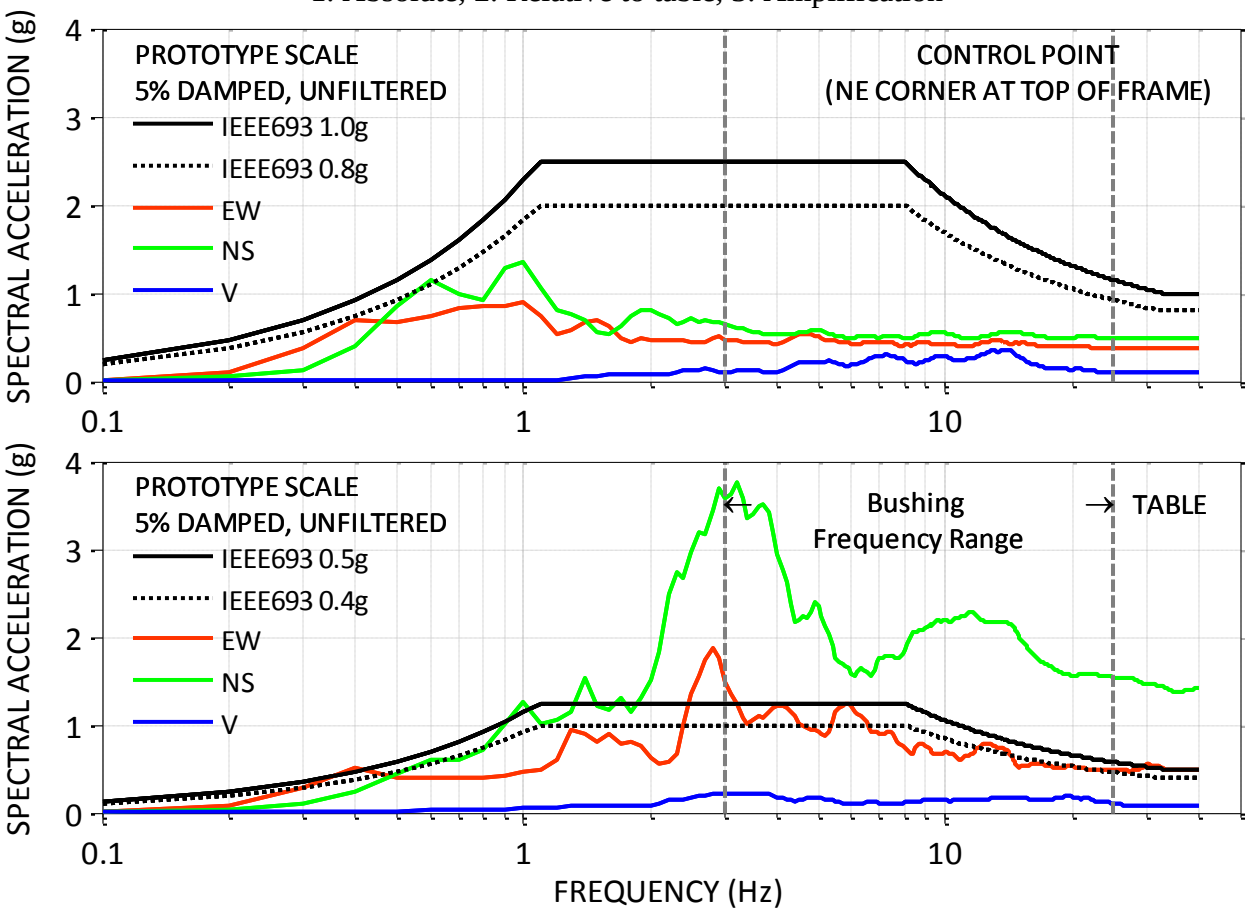
LRB SYSTEM (Bolted-Bolted Configuration)
JENSEN FILTER 97% BI-AXIAL (FN in EW direction)
LENGTH SCALE=3 SYMMETRIC BUSHING CONFIGURATION

Peak Table Motion								
Acceleration (g)			Velocity (in/sec)			Displacement (in)		
EW	NS	V	EW	NS	V	EW	NS	V
0.47	1.36	0.08	14.65	14.50	0.47	3.86	1.90	0.05

OBSERVATIONS

Peak Resultant Displacement (in)				Peak Acceleration (g)							
Bushing Top		Isolator	Torsional Ampl[3] Ratio (TA)	Bushing Top			Bushing Bottom		Control Point		
Abs[1]	Rel[2]			EW	NS	V	EW	NS	EW	NS	V
5.41	3.02	3.46	1.21	0.75	0.70	0.22	0.35	0.46	0.37	0.48	0.09

1. Absolute, 2. Relative to table, 3. Amplification



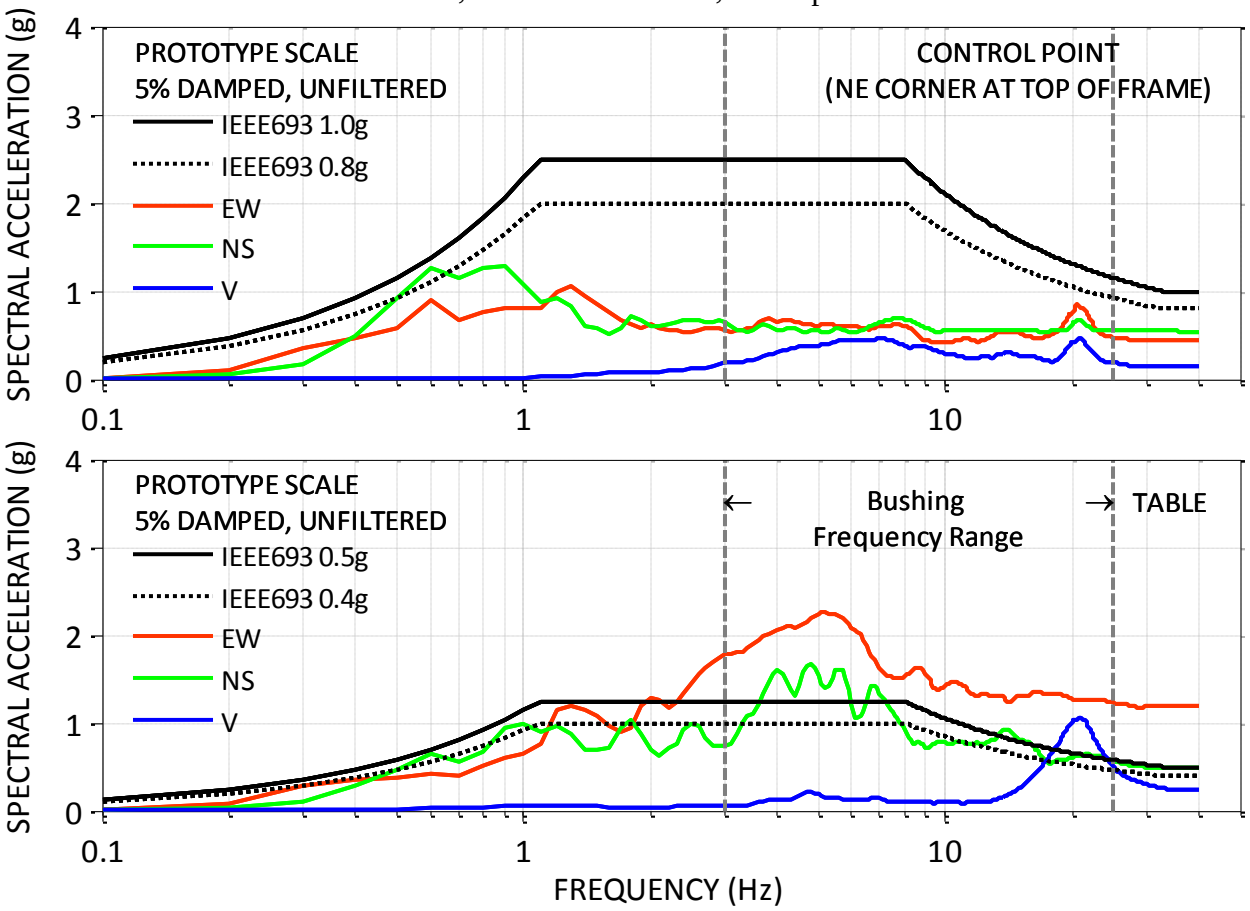
LRB SYSTEM (Bolted-Bolted Configuration)
SYLMAR 90% BI-AXIAL (FN in EW direction)
LENGTH SCALE=3 SYMMETRIC BUSHING CONFIGURATION

Peak Table Motion								
Acceleration (g)			Velocity (in/sec)			Displacement (in)		
EW	NS	V	EW	NS	V	EW	NS	V
1.16	0.47	0.16	22.58	14.94	0.87	4.06	2.94	0.08

OBSERVATIONS

Peak Resultant Displacement (in)				Peak Acceleration (g)							
Bushing Top		Isolator	Torsional Ampl[3] Ratio (TA)	Bushing Top			Bushing Bottom		Control Point		
Abs[1]	Rel[2]			EW	NS	V	EW	NS	EW	NS	V
5.30	3.90	3.88	1.04	1.15	0.97	0.21	0.38	0.56	0.41	0.54	0.15

1. Absolute, 2. Relative to table, 3. Amplification



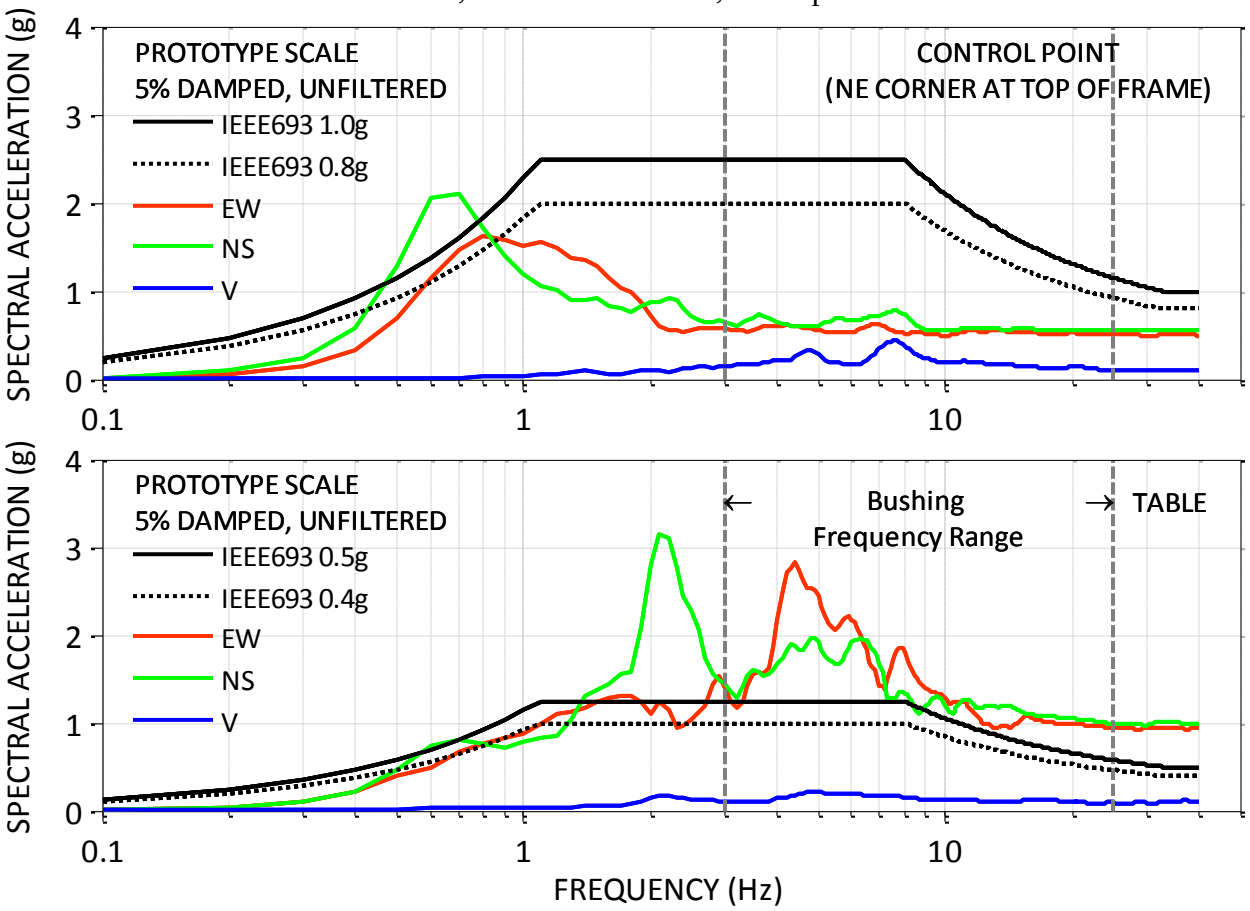
LRB SYSTEM (Bolted-Bolted Configuration)
TAKARAZUKA 97% BI-AXIAL (FN in EW direction)
LENGTH SCALE=3 SYMMETRIC BUSHING CONFIGURATION

Peak Table Motion								
Acceleration (g)			Velocity (in/sec)			Displacement (in)		
EW	NS	V	EW	NS	V	EW	NS	V
0.91	0.97	0.09	14.51	17.92	0.46	1.93	2.50	0.02

OBSERVATIONS

Peak Resultant Displacement (in)				Peak Acceleration (g)							
Bushing Top		Isolator	Torsional Ampl[3] Ratio (TA)	Bushing Top			Bushing Bottom		Control Point		
Abs[1]	Rel[2]			EW	NS	V	EW	NS	EW	NS	V
5.12	3.49	4.30	1.26	0.84	1.10	0.17	0.40	0.49	0.50	0.55	0.10

1. Absolute, 2. Relative to table, 3. Amplification



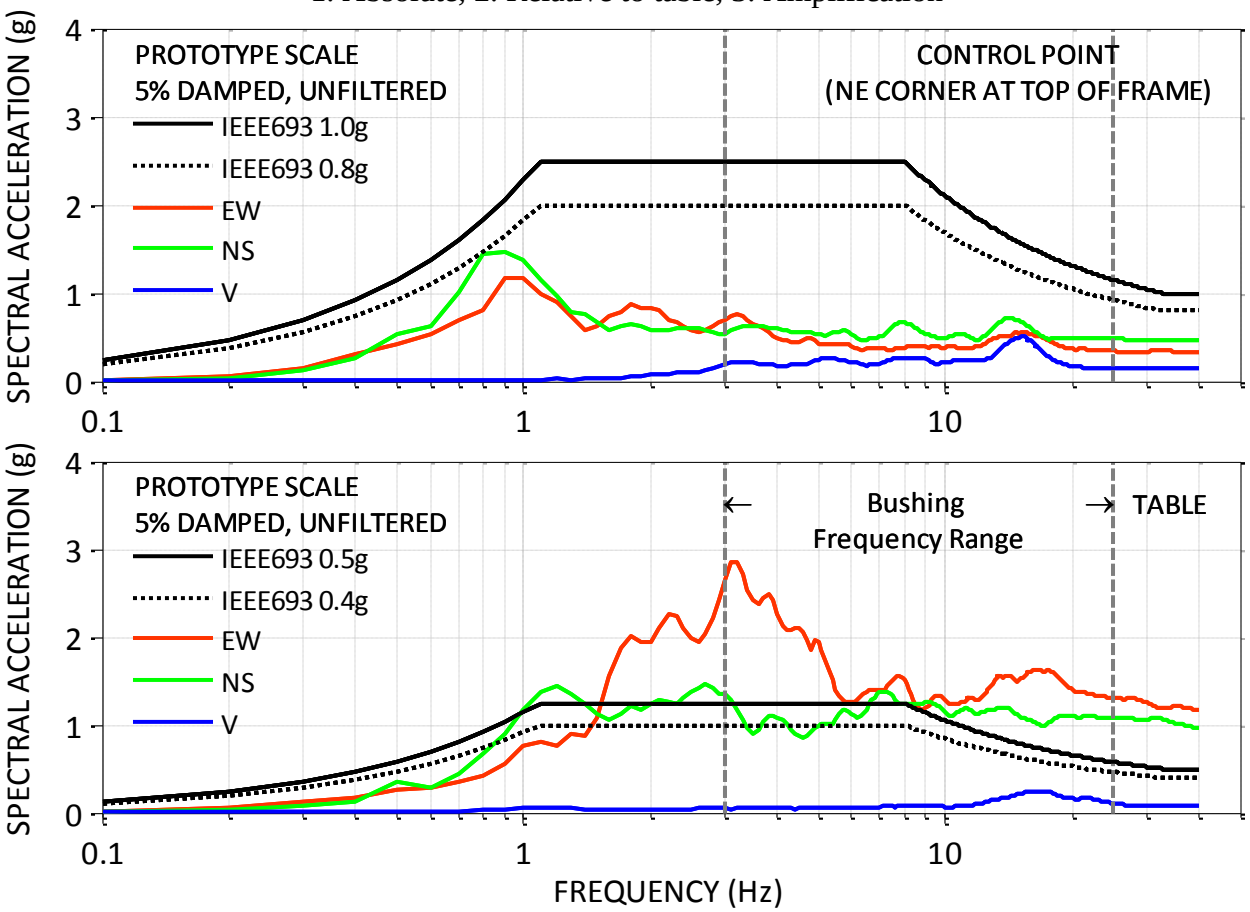
LRB SYSTEM (Bolted-Bolted Configuration)
BOLU 104% BI-AXIAL (FN in EW direction)
LENGTH SCALE=3 SYMMETRIC BUSHING CONFIGURATION

Peak Table Motion								
Acceleration (g)			Velocity (in/sec)			Displacement (in)		
EW	NS	V	EW	NS	V	EW	NS	V
1.10	0.94	0.06	13.41	15.04	0.90	2.31	1.82	0.03

OBSERVATIONS

Peak Resultant Displacement (in)				Peak Acceleration (g)							
Bushing Top		Isolator	Torsional Ampl[3] Ratio (TA)	Bushing Top			Bushing Bottom		Control Point		
Abs[1]	Rel[2]			EW	NS	V	EW	NS	EW	NS	V
2.58	2.65	2.80	1.10	0.55	0.93	0.18	0.32	0.45	0.34	0.46	0.12

1. Absolute, 2. Relative to table, 3. Amplification



PART B-2
SUMMARY OF EXPERIMENTAL DATA FOR TRIPLE FP SYSTEM
AT LENGTH SCALE OF 3

(PERCENTAGE AMOUNT IS SCALE FACTOR APPLIED TO ACCELERATION OF ACTUAL MOTION. FOR EXAMPLE, 100% DENOTES MOTION AS RECORDED, 200% DENOTES THAT ACCELERATION WAS SCALED UP BY FACTOR OF 2)

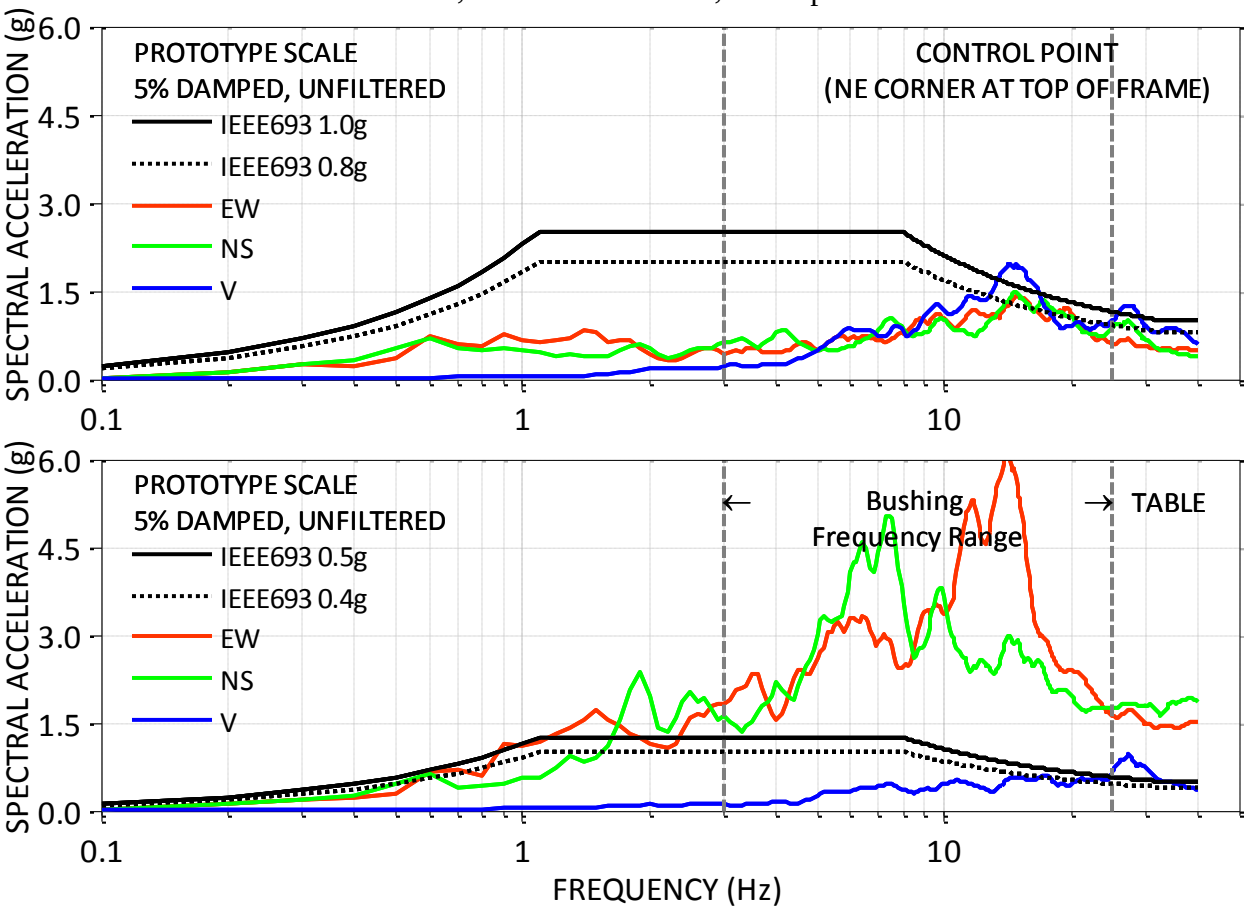
TRIPLE FP SYSTEM (Friction-Bolted Configuration)
KARAKYR 137% BI-AXIAL (FN in EW direction)
LENGTH SCALE=3 SYMMETRIC BUSHING CONFIGURATION

Peak Table Motion								
Acceleration (g)			Velocity (in/sec)			Displacement (in)		
EW	NS	V	EW	NS	V	EW	NS	V
1.24	1.65	0.23	15.48	19.18	0.94	3.37	3.65	0.07

OBSERVATIONS

Peak Resultant Displacement (in)				Peak Acceleration (g)							
Bushing Top		Isolator	Torsional Ampl[3] Ratio (TA)	Bushing Top			Bushing Bottom		Control Point		
Abs[1]	Rel[2]			EW	NS	V	EW	NS	EW	NS	V
4.59	3.61	3.59	1.03	2.01	1.71	0.68	0.43	0.43	0.39	0.39	0.45

1. Absolute, 2. Relative to table, 3. Amplification



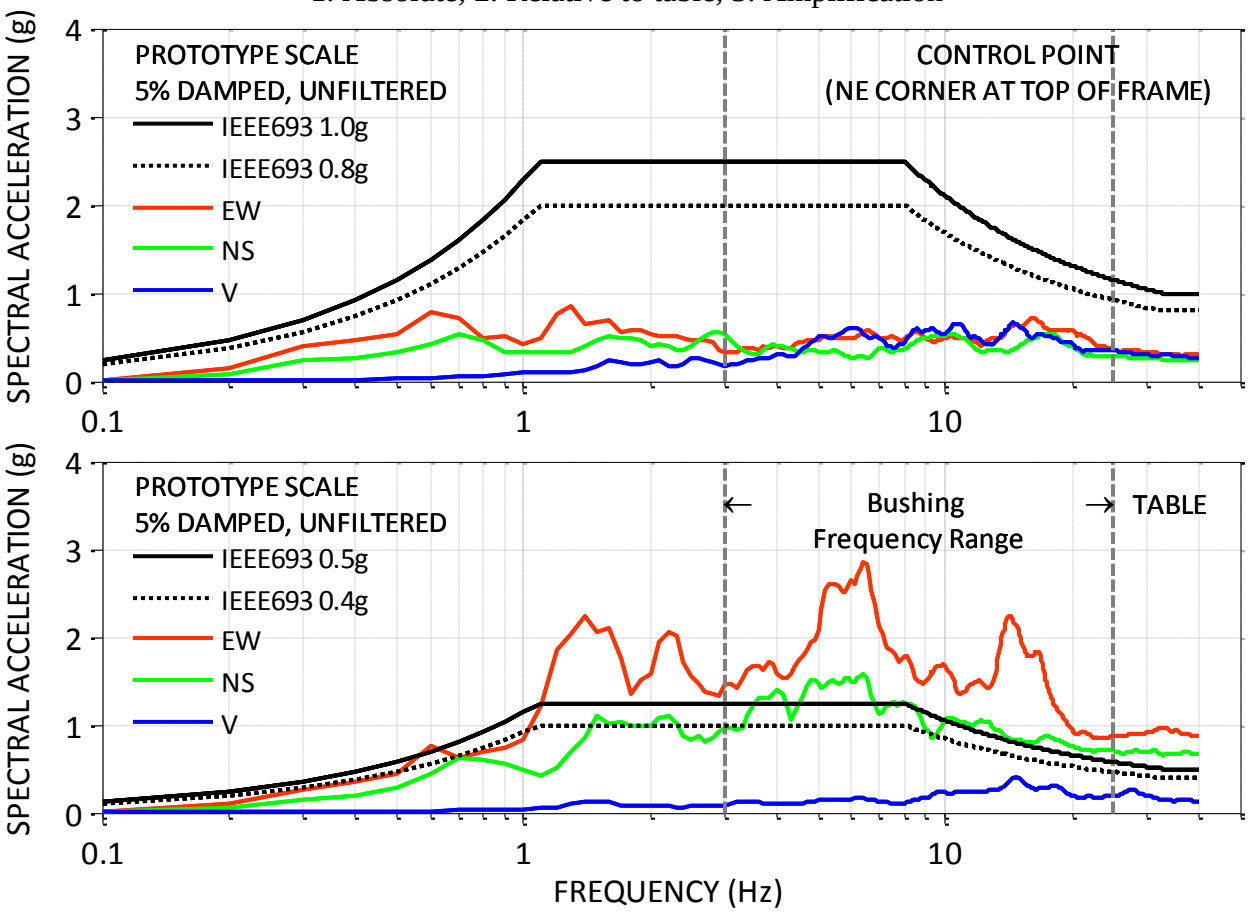
TRIPLE FP SYSTEM (Friction-Bolted Configuration)
LGPC 94% BI-AXIAL (FN in EW direction)
LENGTH SCALE=3 SYMMETRIC BUSHING CONFIGURATION

Peak Table Motion								
Acceleration (g)			Velocity (in/sec)			Displacement (in)		
EW	NS	V	EW	NS	V	EW	NS	V
0.84	0.66	0.12	18.20	11.18	0.88	3.67	2.74	0.10

OBSERVATIONS

Peak Resultant Displacement (in)				Peak Acceleration (g)							
Bushing Top		Isolator	Torsional Ampl[3] Ratio (TA)	Bushing Top			Bushing Bottom		Control Point		
Abs[1]	Rel[2]			EW	NS	V	EW	NS	EW	NS	V
5.12	3.75	3.77	1.01	1.17	0.59	0.57	0.27	0.24	0.28	0.23	0.25

1. Absolute, 2. Relative to table, 3. Amplification



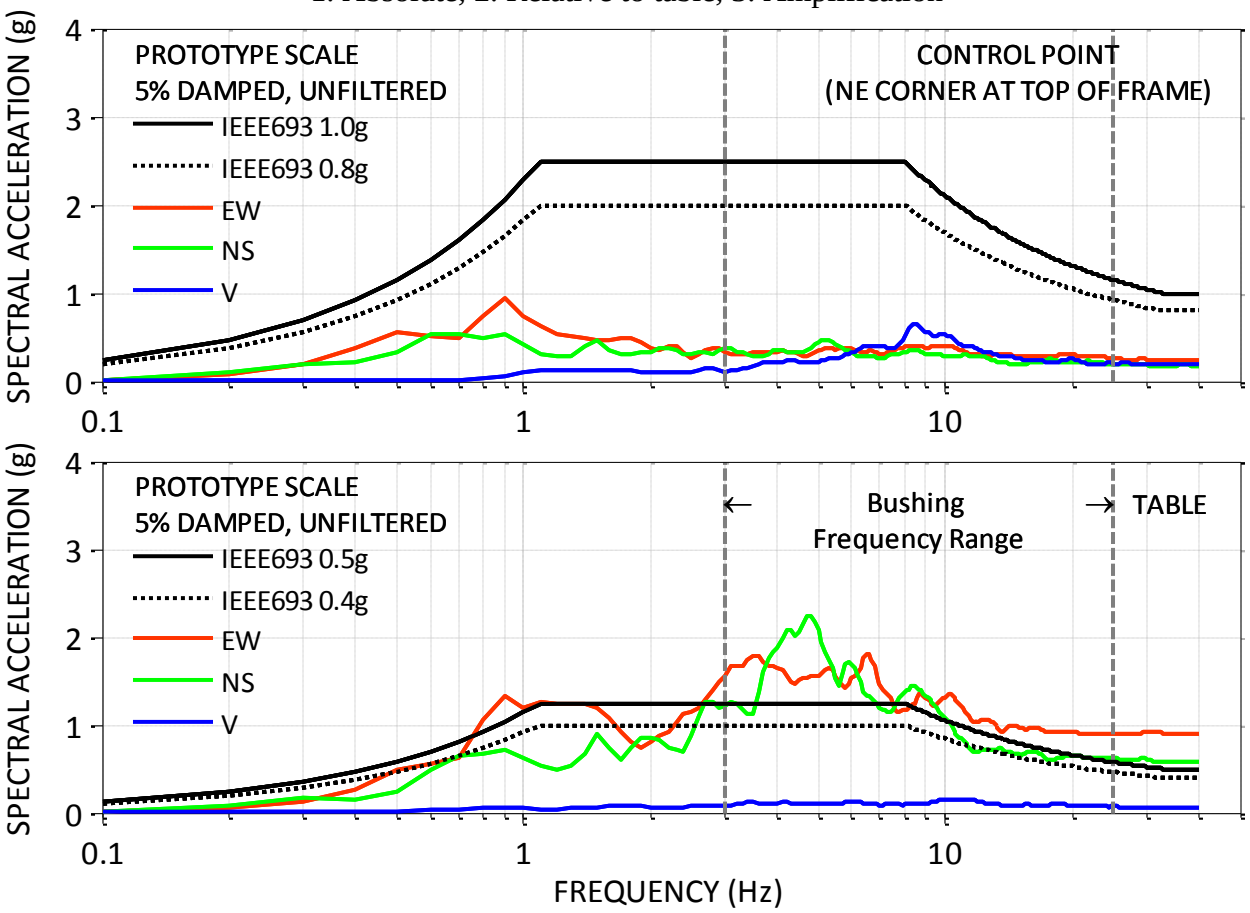
TRIPLE FP SYSTEM (Friction-Bolted Configuration)
SARATOGA 157% BI-AXIAL (FN in EW direction)
LENGTH SCALE=3 SYMMETRIC BUSHING CONFIGURATION

Peak Table Motion								
Acceleration (g)			Velocity (in/sec)			Displacement (in)		
EW	NS	V	EW	NS	V	EW	NS	V
0.90	0.57	0.05	20.70	13.32	0.44	2.95	3.97	0.09

OBSERVATIONS

Peak Resultant Displacement (in)				Peak Acceleration (g)							
Bushing Top		Isolator	Torsional Ampl[3] Ratio (TA)	Bushing Top			Bushing Bottom		Control Point		
Abs[1]	Rel[2]			EW	NS	V	EW	NS	EW	NS	V
5.73	3.75	3.75	1.00	0.80	0.67	0.41	0.24	0.20	0.23	0.18	0.17

1. Absolute, 2. Relative to table, 3. Amplification



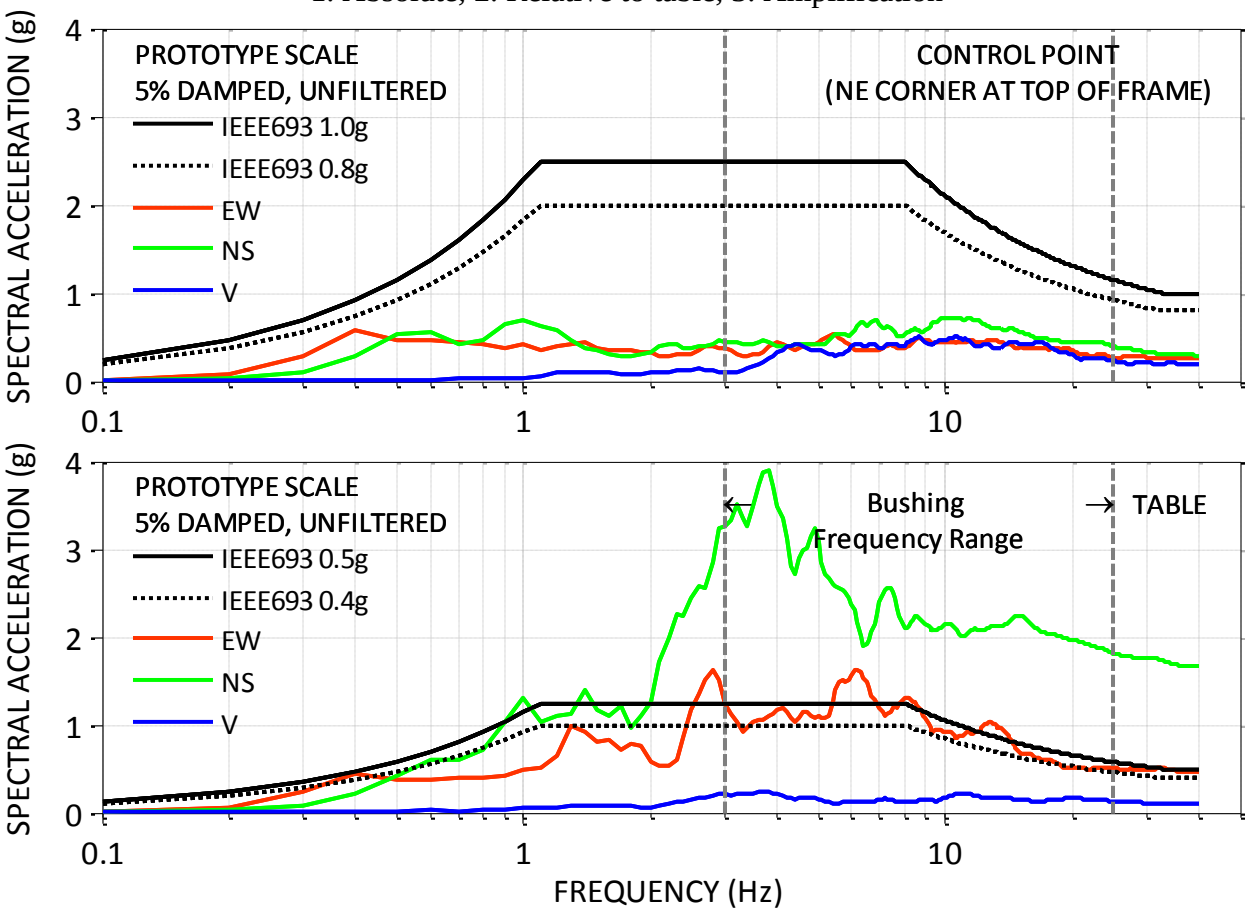
TRIPLE FP SYSTEM (Friction-Bolted Configuration)
JENSEN FILTER 97% BI-AXIAL (FN in EW direction)
LENGTH SCALE=3 SYMMETRIC BUSHING CONFIGURATION

Peak Table Motion								
Acceleration (g)			Velocity (in/sec)			Displacement (in)		
EW	NS	V	EW	NS	V	EW	NS	V
0.46	1.60	0.09	13.50	13.93	0.38	2.82	1.77	0.03

OBSERVATIONS

Peak Resultant Displacement (in)				Peak Acceleration (g)							
Bushing Top		Isolator	Torsional Ampl[3] Ratio (TA)	Bushing Top			Bushing Bottom		Control Point		
Abs[1]	Rel[2]			EW	NS	V	EW	NS	EW	NS	V
3.25	2.81	2.79	1.03	0.72	1.21	0.34	0.22	0.26	0.24	0.27	0.18

1. Absolute, 2. Relative to table, 3. Amplification



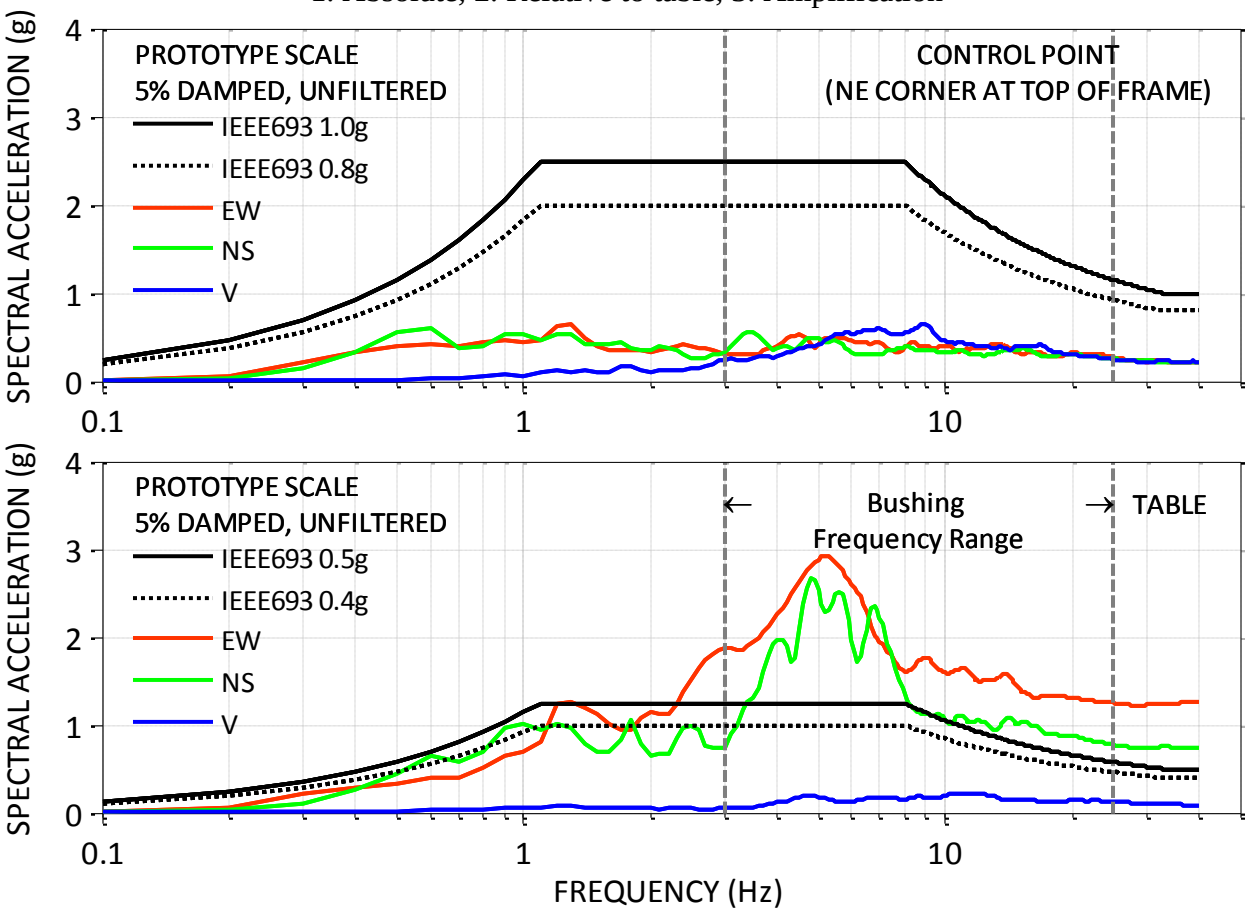
TRIPLE FP SYSTEM (Friction-Bolted Configuration)
SYLMAR 90% BI-AXIAL (FN in EW direction)
LENGTH SCALE=3 SYMMETRIC BUSHING CONFIGURATION

Peak Table Motion								
Acceleration (g)			Velocity (in/sec)			Displacement (in)		
EW	NS	V	EW	NS	V	EW	NS	V
1.22	0.71	0.07	20.85	13.93	0.52	2.79	2.24	0.04

OBSERVATIONS

Peak Resultant Displacement (in)				Peak Acceleration (g)							
Bushing Top		Isolator	Torsional Ampl[3] Ratio (TA)	Bushing Top			Bushing Bottom		Control Point		
Abs[1]	Rel[2]			EW	NS	V	EW	NS	EW	NS	V
3.56	3.59	3.57	1.01	0.96	0.73	0.49	0.22	0.24	0.22	0.22	0.22

1. Absolute, 2. Relative to table, 3. Amplification



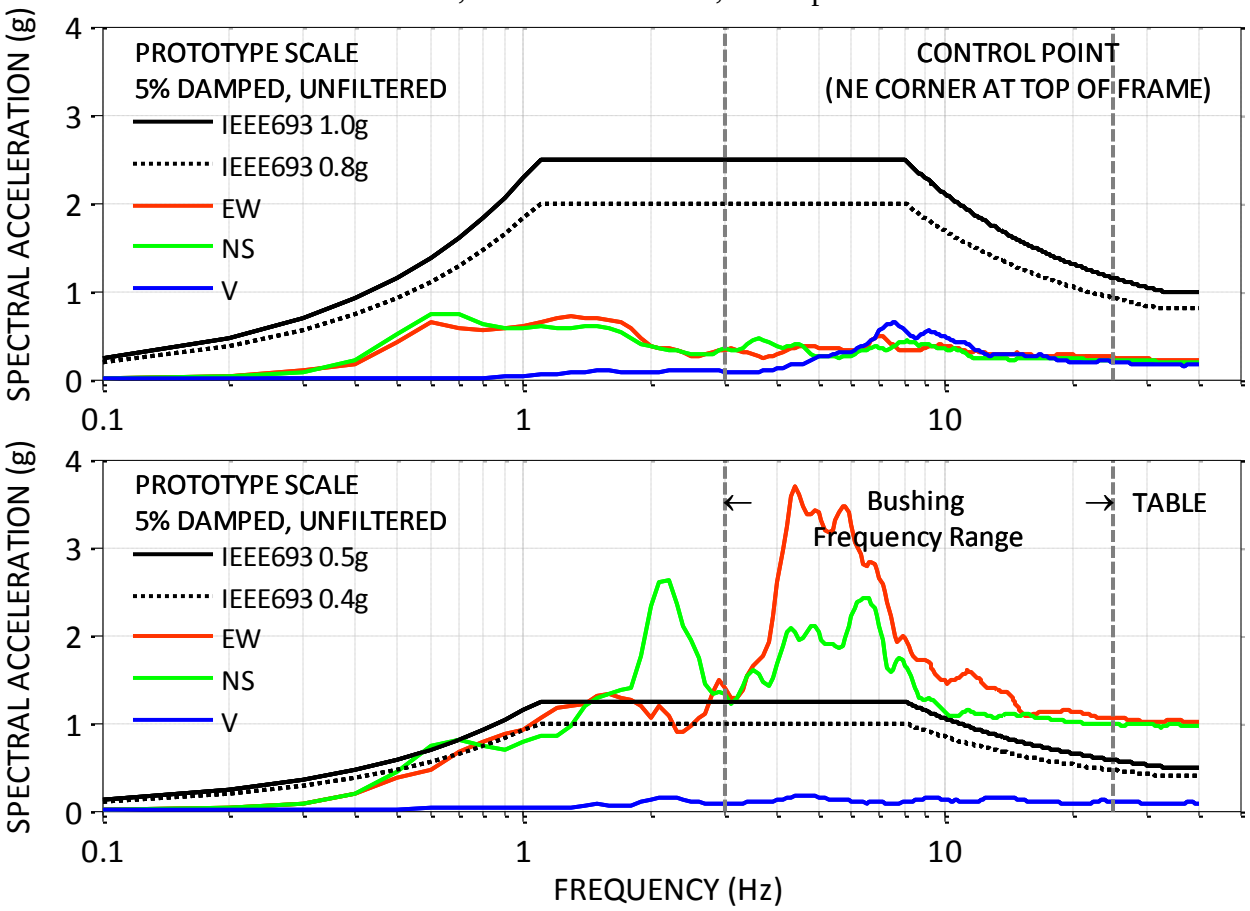
TRIPLE FP SYSTEM (Friction-Bolted Configuration)
TAKARAZUKA 97% BI-AXIAL (FN in EW direction)
LENGTH SCALE=3 SYMMETRIC BUSHING CONFIGURATION

Peak Table Motion								
Acceleration (g)			Velocity (in/sec)			Displacement (in)		
EW	NS	V	EW	NS	V	EW	NS	V
1.00	0.94	0.06	15.17	16.30	0.49	1.71	2.16	0.03

OBSERVATIONS

Peak Resultant Displacement (in)				Peak Acceleration (g)							
Bushing Top		Isolator	Torsional Ampl[3] Ratio (TA)	Bushing Top			Bushing Bottom		Control Point		
Abs[1]	Rel[2]			EW	NS	V	EW	NS	EW	NS	V
2.88	2.90	2.81	1.00	0.73	0.66	0.23	0.21	0.21	0.21	0.20	0.15

1. Absolute, 2. Relative to table, 3. Amplification



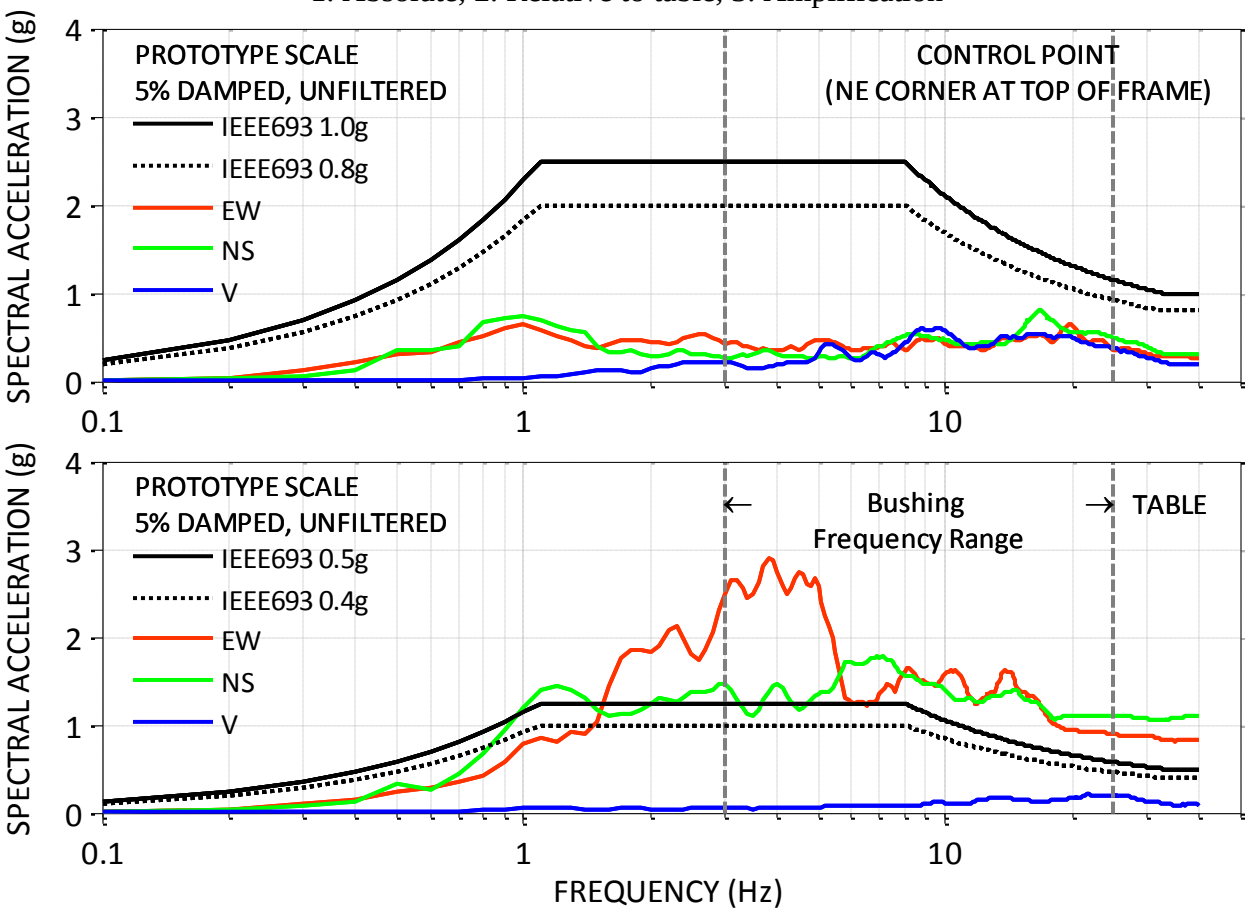
TRIPLE FP SYSTEM (Friction-Bolted Configuration)
BOLU 104% BI-AXIAL (FN in EW direction)
LENGTH SCALE=3 SYMMETRIC BUSHING CONFIGURATION

Peak Table Motion								
Acceleration (g)			Velocity (in/sec)			Displacement (in)		
EW	NS	V	EW	NS	V	EW	NS	V
0.79	1.06	0.06	12.55	15.30	0.44	1.44	1.74	0.02

OBSERVATIONS

Peak Resultant Displacement (in)				Peak Acceleration (g)							
Bushing Top		Isolator	Torsional Ampl[3] Ratio (TA)	Bushing Top			Bushing Bottom		Control Point		
Abs[1]	Rel[2]			EW	NS	V	EW	NS	EW	NS	V
2.09	2.16	2.18	1.00	0.88	0.55	0.44	0.21	0.28	0.24	0.26	0.17

1. Absolute, 2. Relative to table, 3. Amplification



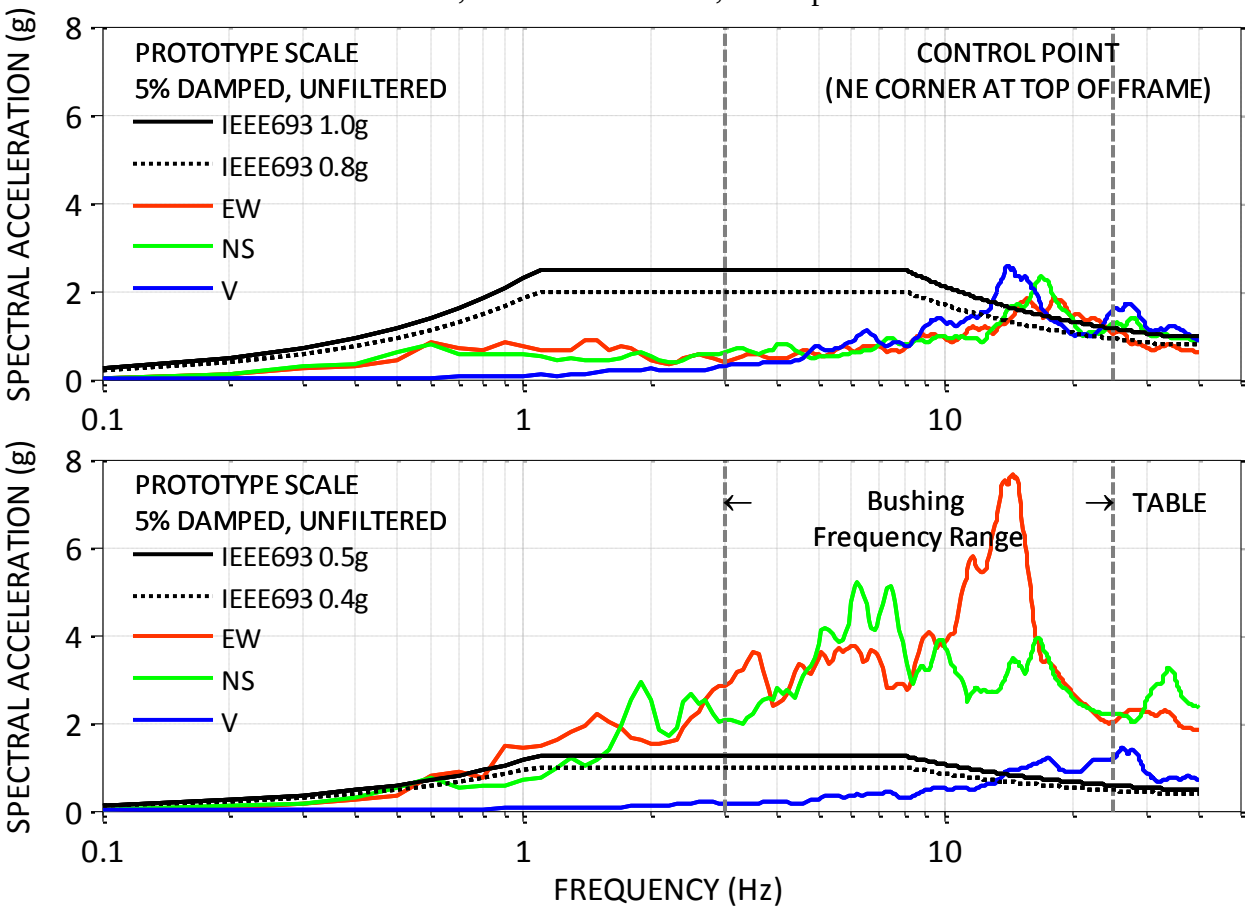
TRIPLE FP SYSTEM (Friction-Bolted Configuration)
KARAKYR 171% BI-AXIAL (FN in EW direction)
LENGTH SCALE=3 SYMMETRIC BUSHING CONFIGURATION

Peak Table Motion								
Acceleration (g)			Velocity (in/sec)			Displacement (in)		
EW	NS	V	EW	NS	V	EW	NS	V
1.48	2.07	0.30	19.76	21.54	1.36	3.21	3.67	0.06

OBSERVATIONS

Peak Resultant Displacement (in)				Peak Acceleration (g)							
Bushing Top		Isolator	Torsional Ampl[3] Ratio (TA)	Bushing Top			Bushing Bottom		Control Point		
Abs[1]	Rel[2]			EW	NS	V	EW	NS	EW	NS	V
5.44	5.00	4.94	1.03	1.91	1.97	1.02	0.52	0.55	0.47	0.52	0.59

1. Absolute, 2. Relative to table, 3. Amplification



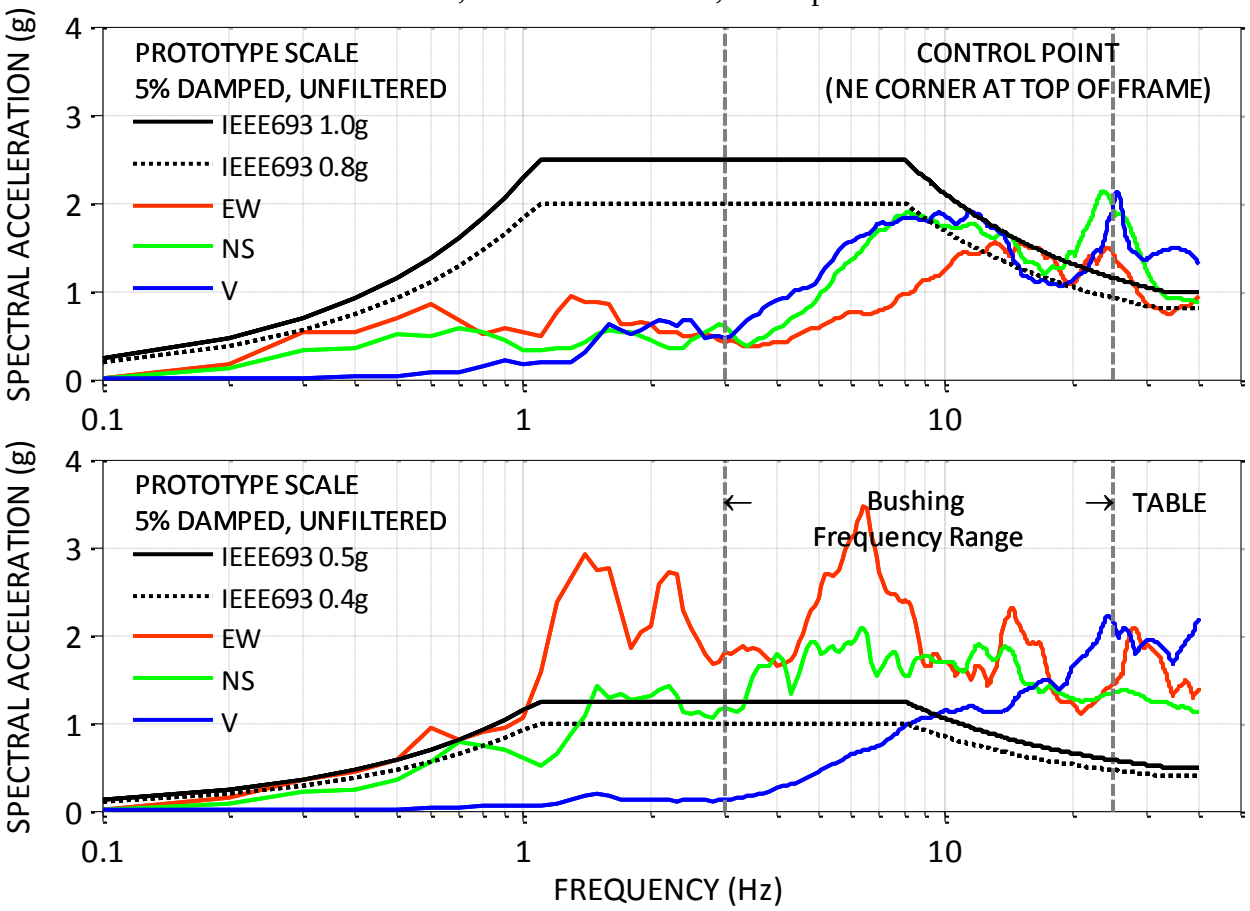
TRIPLE FP SYSTEM (Friction-Bolted Configuration)
LGPC 118% BI-AXIAL (FN in EW direction)
LENGTH SCALE=3 SYMMETRIC BUSHING CONFIGURATION

Peak Table Motion								
Acceleration (g)			Velocity (in/sec)			Displacement (in)		
EW	NS	V	EW	NS	V	EW	NS	V
1.03	0.85	0.62	23.99	13.57	4.70	4.76	3.77	0.16

OBSERVATIONS
Displacement limit reached for isolators Uplift at NE and NW isolators Sliding at friction connection of about 4.1 inches (NE), 1.4 inches (SE), 1.8 inches (SW) and 3.3 inches (NW)

Peak Resultant Displacement (in)				Peak Acceleration (g)							
Bushing Top		Isolator	Torsional Ampl[3] Ratio (TA)	Bushing Top			Bushing Bottom		Control Point		
Abs[1]	Rel[2]			EW	NS	V	EW	NS	EW	NS	V
8.90	6.96	7.53	1.11	2.88	5.28	2.14	0.77	0.73	0.63	0.75	0.77

1. Absolute, 2. Relative to table, 3. Amplification



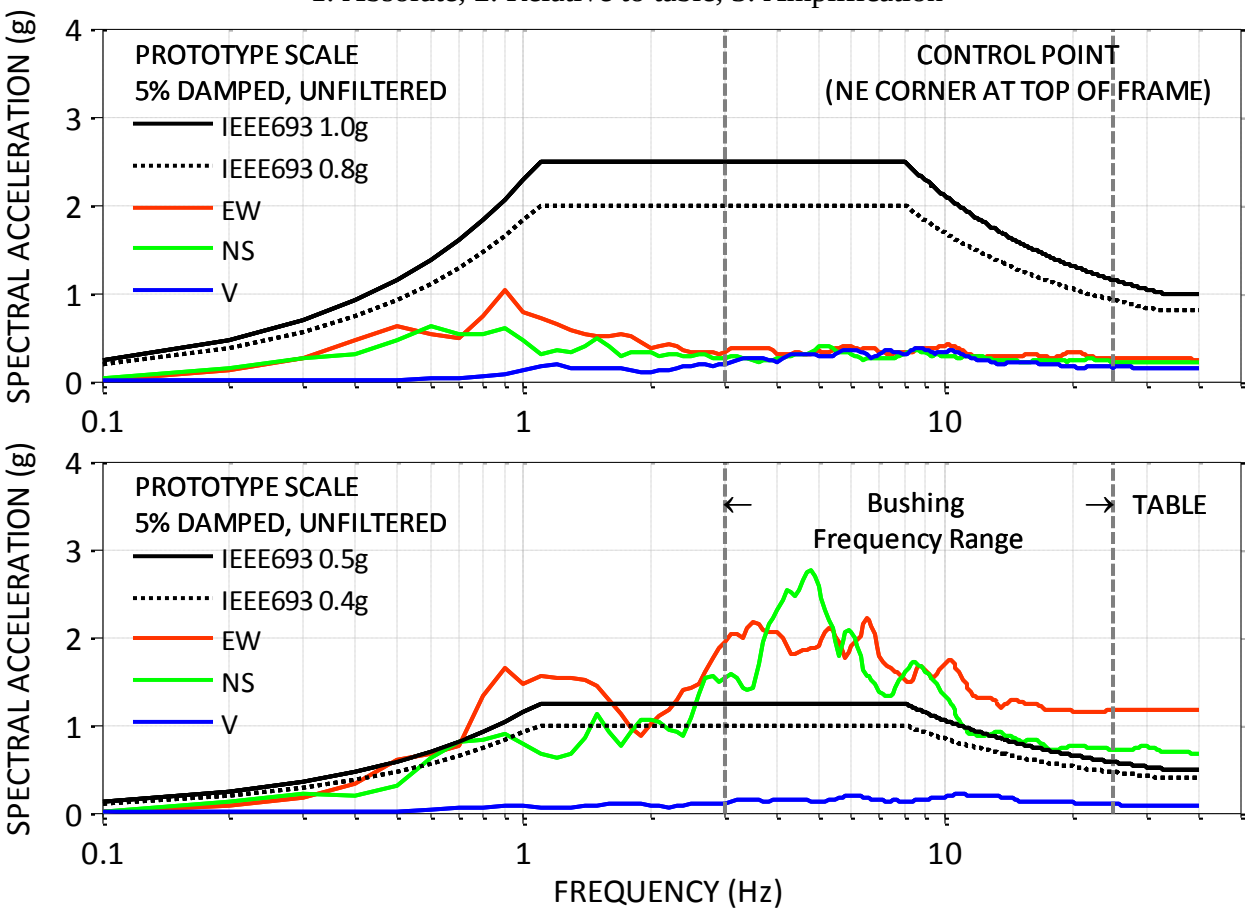
TRIPLE FP SYSTEM (Friction-Bolted Configuration)
SARATOGA 196% BI-AXIAL (FN in EW direction)
LENGTH SCALE=3 SYMMETRIC BUSHING CONFIGURATION

Peak Table Motion								
Acceleration (g)			Velocity (in/sec)			Displacement (in)		
EW	NS	V	EW	NS	V	EW	NS	V
1.15	0.67	0.07	25.77	16.43	0.79	3.89	5.41	0.15

OBSERVATIONS

Peak Resultant Displacement (in)				Peak Acceleration (g)							
Bushing Top		Isolator	Torsional Ampl[3] Ratio (TA)	Bushing Top			Bushing Bottom		Control Point		
Abs[1]	Rel[2]			EW	NS	V	EW	NS	EW	NS	V
7.39	4.81	4.86	1.01	0.74	0.74	0.37	0.23	0.24	0.24	0.21	0.14

1. Absolute, 2. Relative to table, 3. Amplification



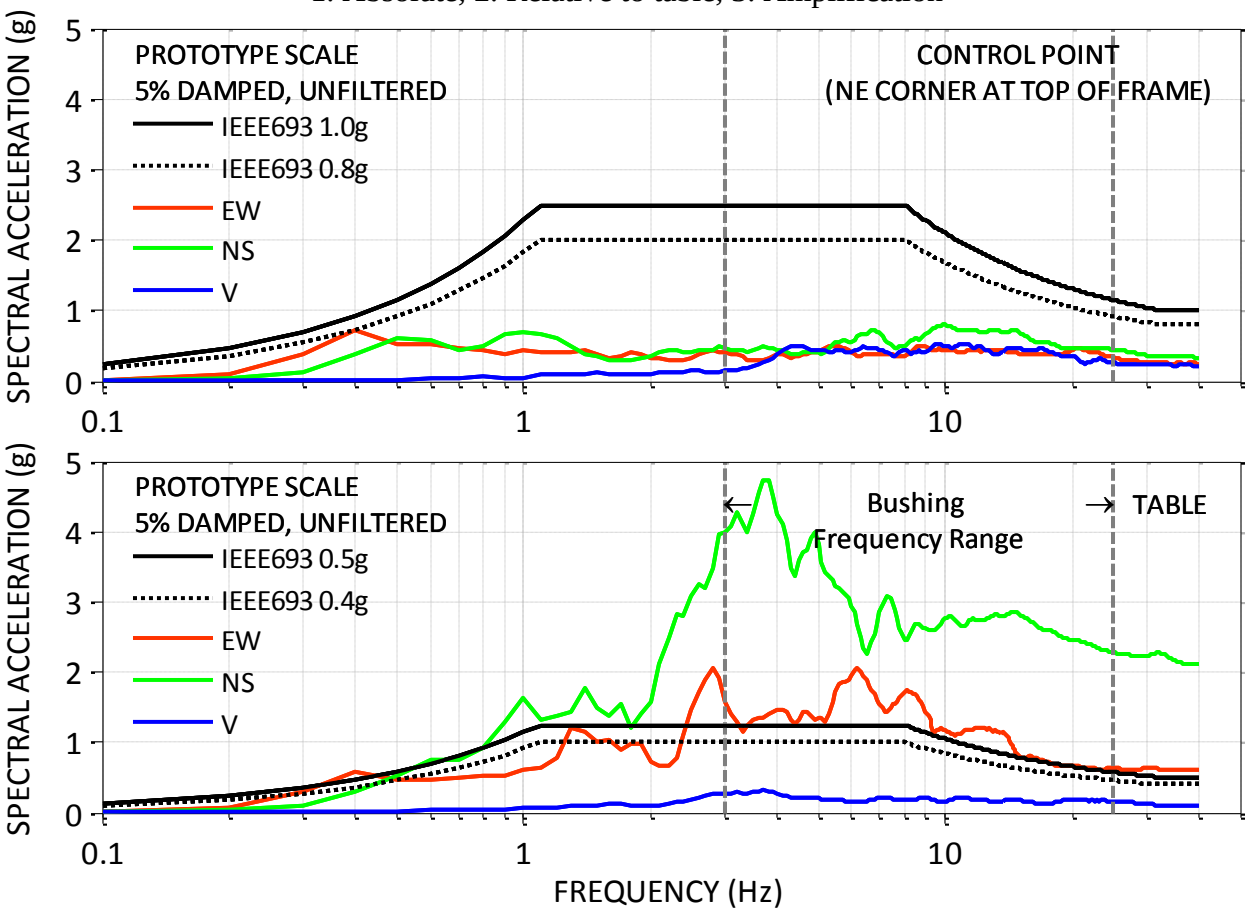
TRIPLE FP SYSTEM (Friction-Bolted Configuration)
JENSEN FILTER 121% BI-AXIAL (FN in EW direction)
LENGTH SCALE=3 SYMMETRIC BUSHING CONFIGURATION

Peak Table Motion								
Acceleration (g)			Velocity (in/sec)			Displacement (in)		
EW	NS	V	EW	NS	V	EW	NS	V
0.59	2.01	0.10	16.80	18.01	0.56	3.77	2.20	0.04

OBSERVATIONS

Peak Resultant Displacement (in)				Peak Acceleration (g)							
Bushing Top		Isolator	Torsional Ampl[3] Ratio (TA)	Bushing Top			Bushing Bottom		Control Point		
Abs[1]	Rel[2]			EW	NS	V	EW	NS	EW	NS	V
4.45	3.19	3.25	1.06	0.83	1.21	0.41	0.23	0.29	0.24	0.30	0.20

1. Absolute, 2. Relative to table, 3. Amplification



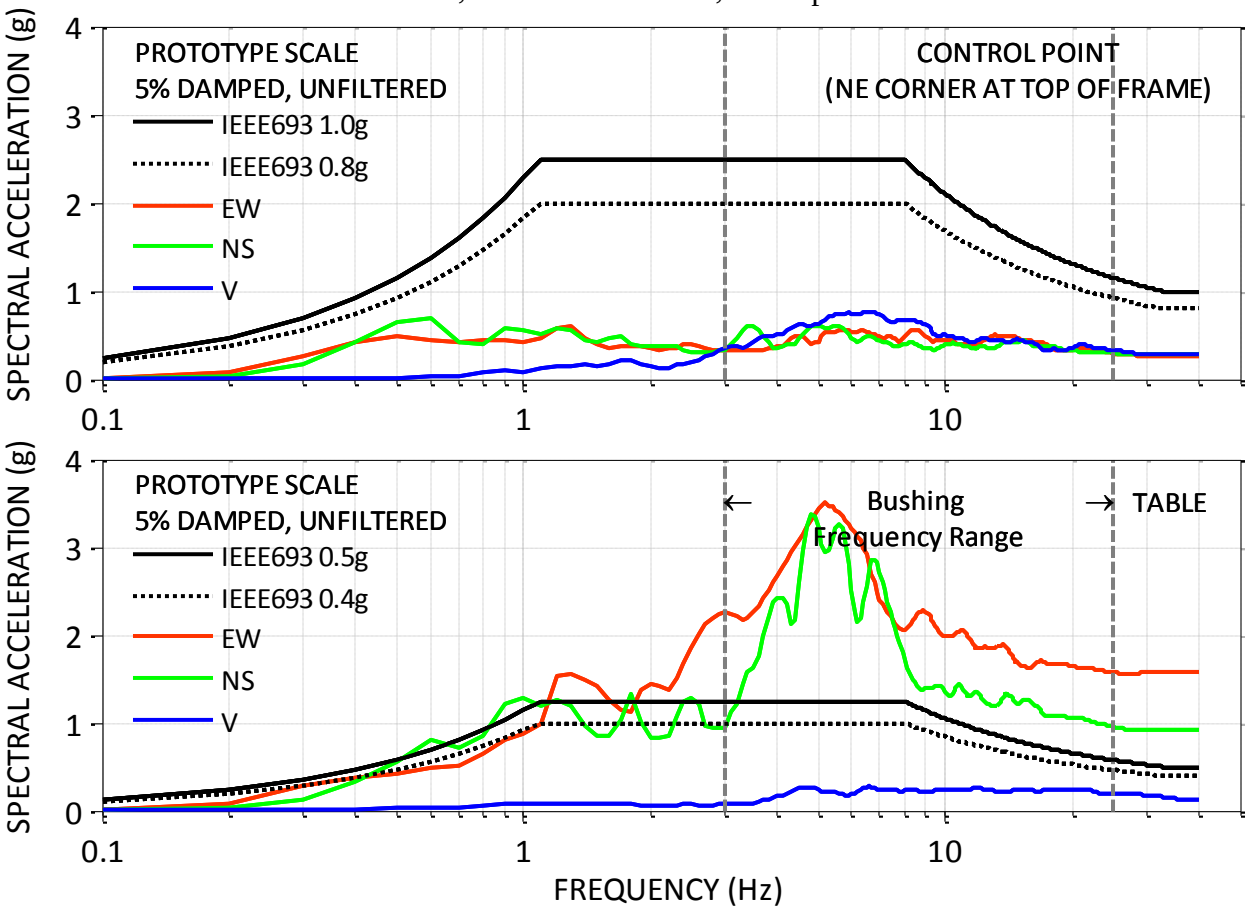
TRIPLE FP SYSTEM (Friction-Bolted Configuration)
SYLMAR 113% BI-AXIAL (FN in EW direction)
LENGTH SCALE=3 SYMMETRIC BUSHING CONFIGURATION

Peak Table Motion								
Acceleration (g)			Velocity (in/sec)			Displacement (in)		
EW	NS	V	EW	NS	V	EW	NS	V
1.54	0.88	0.11	25.81	17.53	0.68	3.71	2.93	0.06

OBSERVATIONS

Peak Resultant Displacement (in)				Peak Acceleration (g)							
Bushing Top		Isolator	Torsional Ampl[3] Ratio (TA)	Bushing Top			Bushing Bottom		Control Point		
Abs[1]	Rel[2]			EW	NS	V	EW	NS	EW	NS	V
4.30	4.36	4.29	1.00	1.10	0.97	0.61	0.25	0.29	0.26	0.27	0.26

1. Absolute, 2. Relative to table, 3. Amplification



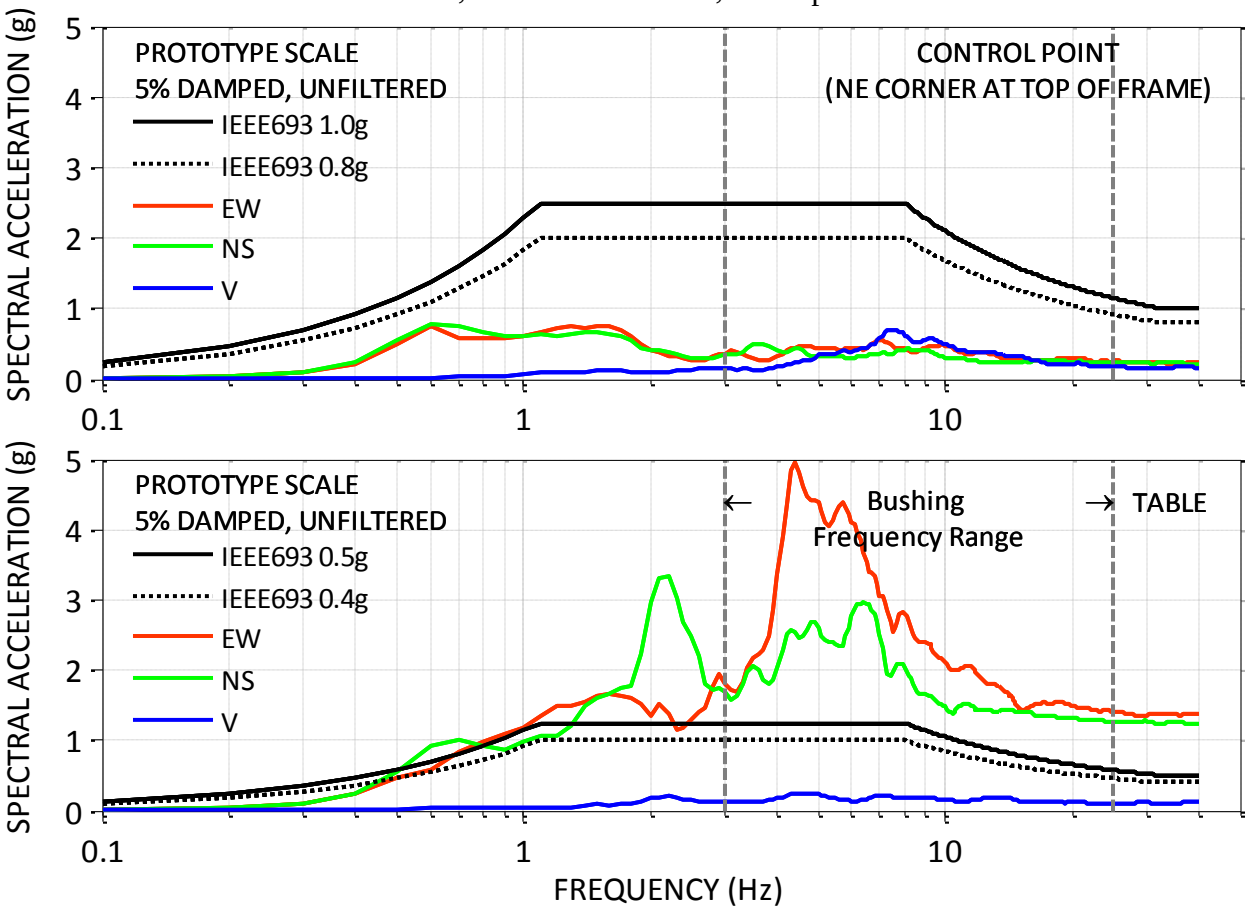
TRIPLE FP SYSTEM (Friction-Bolted Configuration)
TAKARAZUKA 121% BI-AXIAL (FN in EW direction)
LENGTH SCALE=3 SYMMETRIC BUSHING CONFIGURATION

Peak Table Motion								
Acceleration (g)			Velocity (in/sec)			Displacement (in)		
EW	NS	V	EW	NS	V	EW	NS	V
1.34	1.22	0.10	19.46	20.89	0.75	2.16	2.71	0.05

OBSERVATIONS

Peak Resultant Displacement (in)				Peak Acceleration (g)							
Bushing Top		Isolator	Torsional Ampl[3] Ratio (TA)	Bushing Top			Bushing Bottom		Control Point		
Abs[1]	Rel[2]			EW	NS	V	EW	NS	EW	NS	V
3.08	3.47	3.39	1.01	1.10	0.84	0.28	0.22	0.24	0.22	0.22	0.16

1. Absolute, 2. Relative to table, 3. Amplification



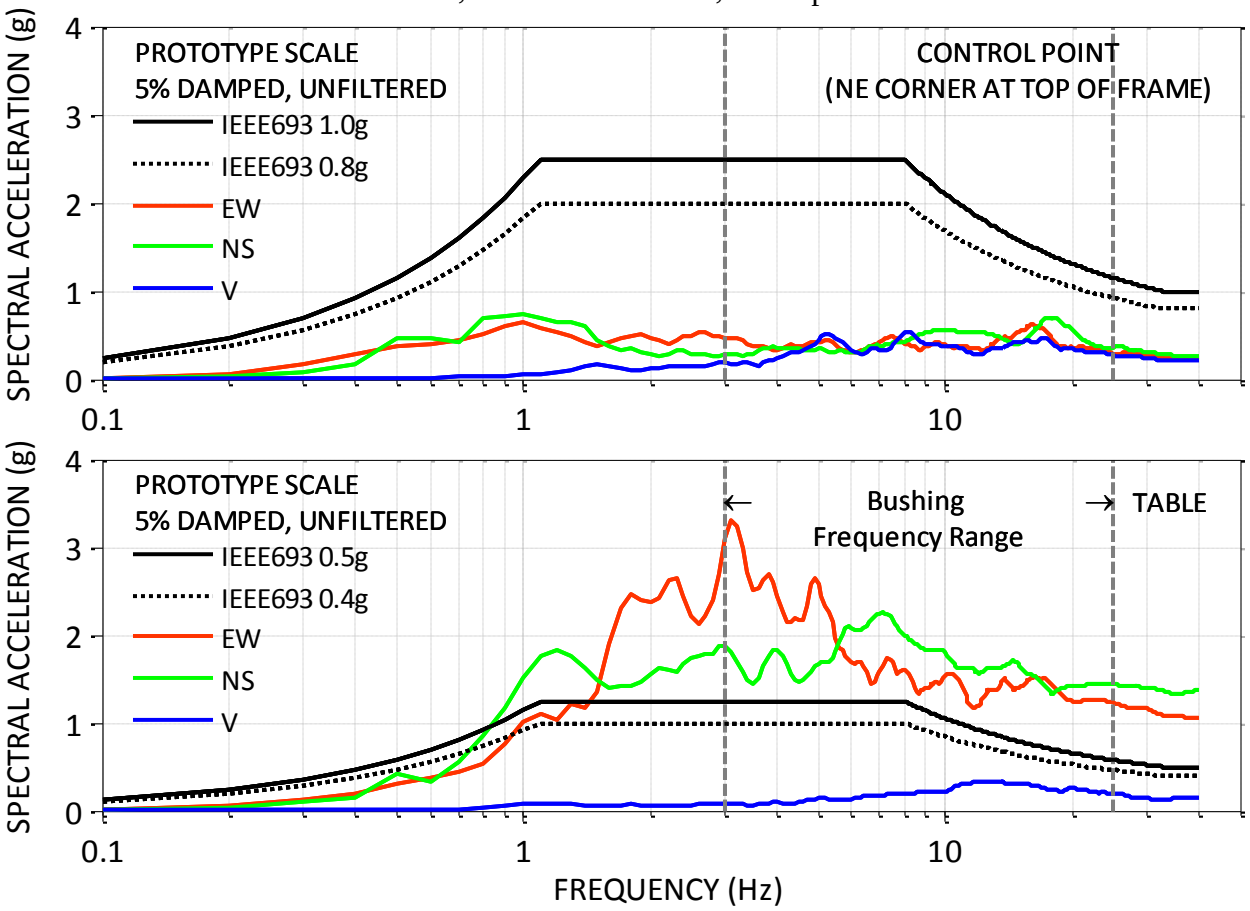
TRIPLE FP SYSTEM (Friction-Bolted Configuration)
BOLU 130% BI-AXIAL (FN in EW direction)
LENGTH SCALE=3 SYMMETRIC BUSHING CONFIGURATION

Peak Table Motion								
Acceleration (g)			Velocity (in/sec)			Displacement (in)		
EW	NS	V	EW	NS	V	EW	NS	V
1.02	1.34	0.13	16.44	19.22	0.55	1.92	2.20	0.03

OBSERVATIONS

Peak Resultant Displacement (in)				Peak Acceleration (g)							
Bushing Top		Isolator	Torsional Ampl[3] Ratio (TA)	Bushing Top			Bushing Bottom		Control Point		
Abs[1]	Rel[2]			EW	NS	V	EW	NS	EW	NS	V
2.62	2.87	2.82	1.00	0.86	0.56	0.68	0.21	0.26	0.22	0.24	0.20

1. Absolute, 2. Relative to table, 3. Amplification



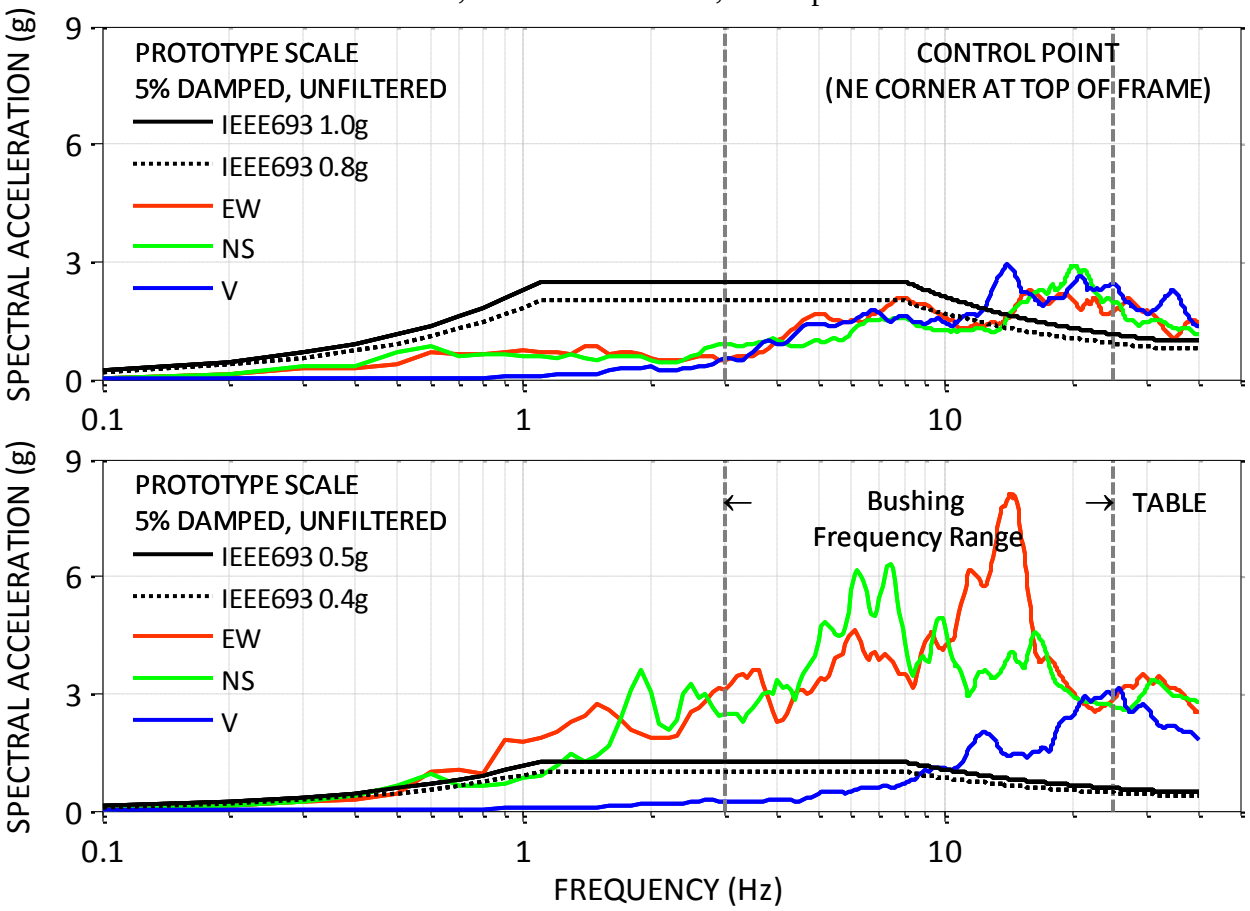
TRIPLE FP SYSTEM (Friction-Bolted Configuration)
KARAKYR 206% BI-AXIAL (FN in EW direction)
LENGTH SCALE=3 SYMMETRIC BUSHING CONFIGURATION

Peak Table Motion								
Acceleration (g)			Velocity (in/sec)			Displacement (in)		
EW	NS	V	EW	NS	V	EW	NS	V
1.85	2.46	0.88	22.72	26.75	3.87	4.20	4.69	0.13

OBSERVATIONS
Displacement limit reached for isolators Uplift at NE, SW and NW isolators Sliding at friction connection of about 0.7 inches (NE), 3.8 inches (SE), 2.8 inches (SW) and 1.5 inches (NW)

Peak Resultant Displacement (in)				Peak Acceleration (g)							
Bushing Top		Isolator	Torsional Ampl[3] Ratio (TA)	Bushing Top			Bushing Bottom		Control Point		
Abs[1]	Rel[2]			EW	NS	V	EW	NS	EW	NS	V
7.60	6.60	6.82	1.01	6.83	5.31	1.64	0.99	0.91	1.13	0.82	0.85

1. Absolute, 2. Relative to table, 3. Amplification



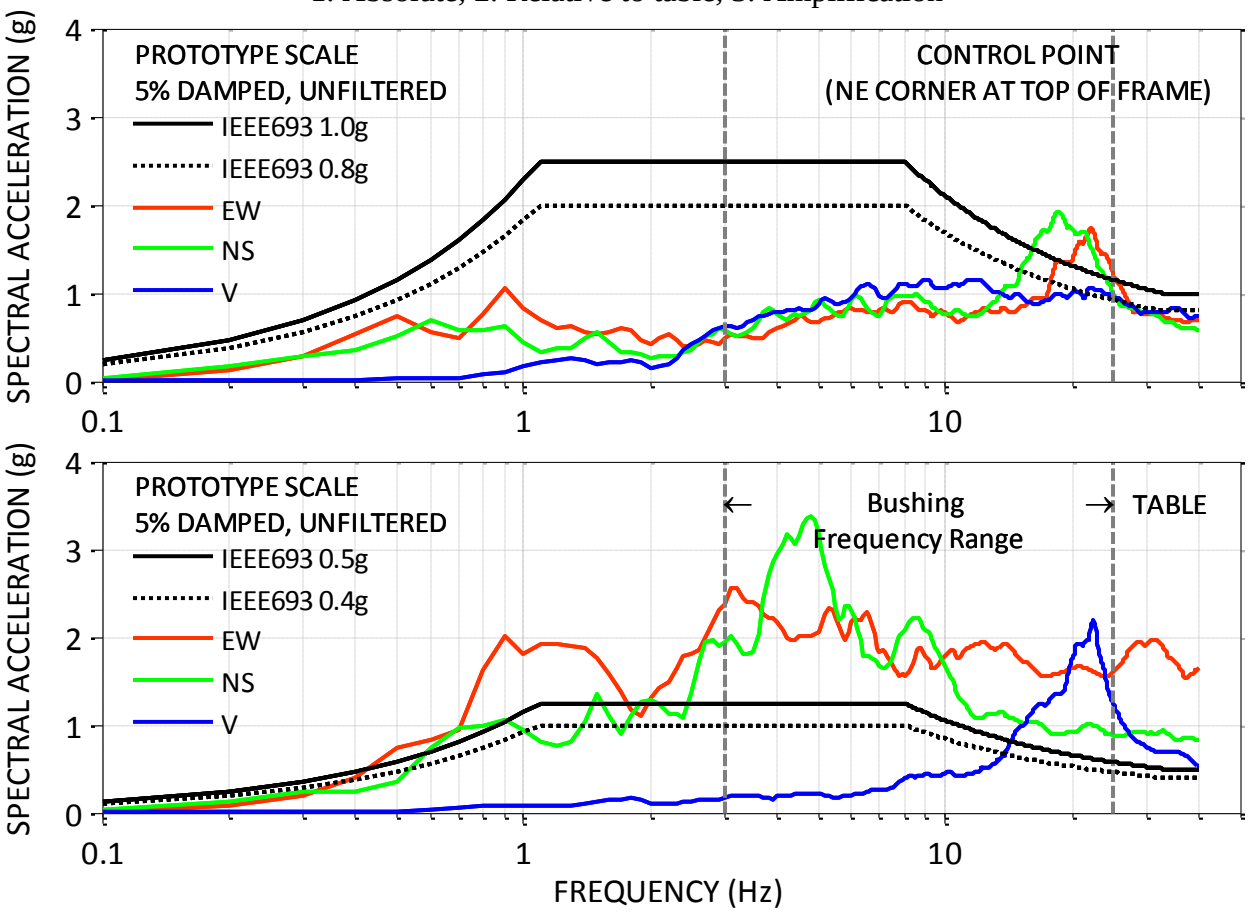
TRIPLE FP SYSTEM (Friction-Bolted Configuration)
SARATOGA 236% BI-AXIAL (FN in EW direction)
LENGTH SCALE=3 SYMMETRIC BUSHING CONFIGURATION

Peak Table Motion								
Acceleration (g)			Velocity (in/sec)			Displacement (in)		
EW	NS	V	EW	NS	V	EW	NS	V
1.53	0.82	0.36	30.92	19.84	1.34	4.48	5.93	0.20

OBSERVATIONS
Displacement limit reached for isolators Uplift at NE, SW and NW isolators Sliding at friction connection of about 0.4 inches (NE), 1.9 inches (SE), 0.3 inches (SW) and 0.8 inches (NW)

Peak Resultant Displacement (in)				Peak Acceleration (g)							
Bushing Top		Isolator	Torsional Ampl[3] Ratio (TA)	Bushing Top			Bushing Bottom		Control Point		
Abs[1]	Rel[2]			EW	NS	V	EW	NS	EW	NS	V
7.51	4.98	4.68	1.05	2.12	2.89	1.06	0.55	0.51	0.59	0.54	0.60

1. Absolute, 2. Relative to table, 3. Amplification



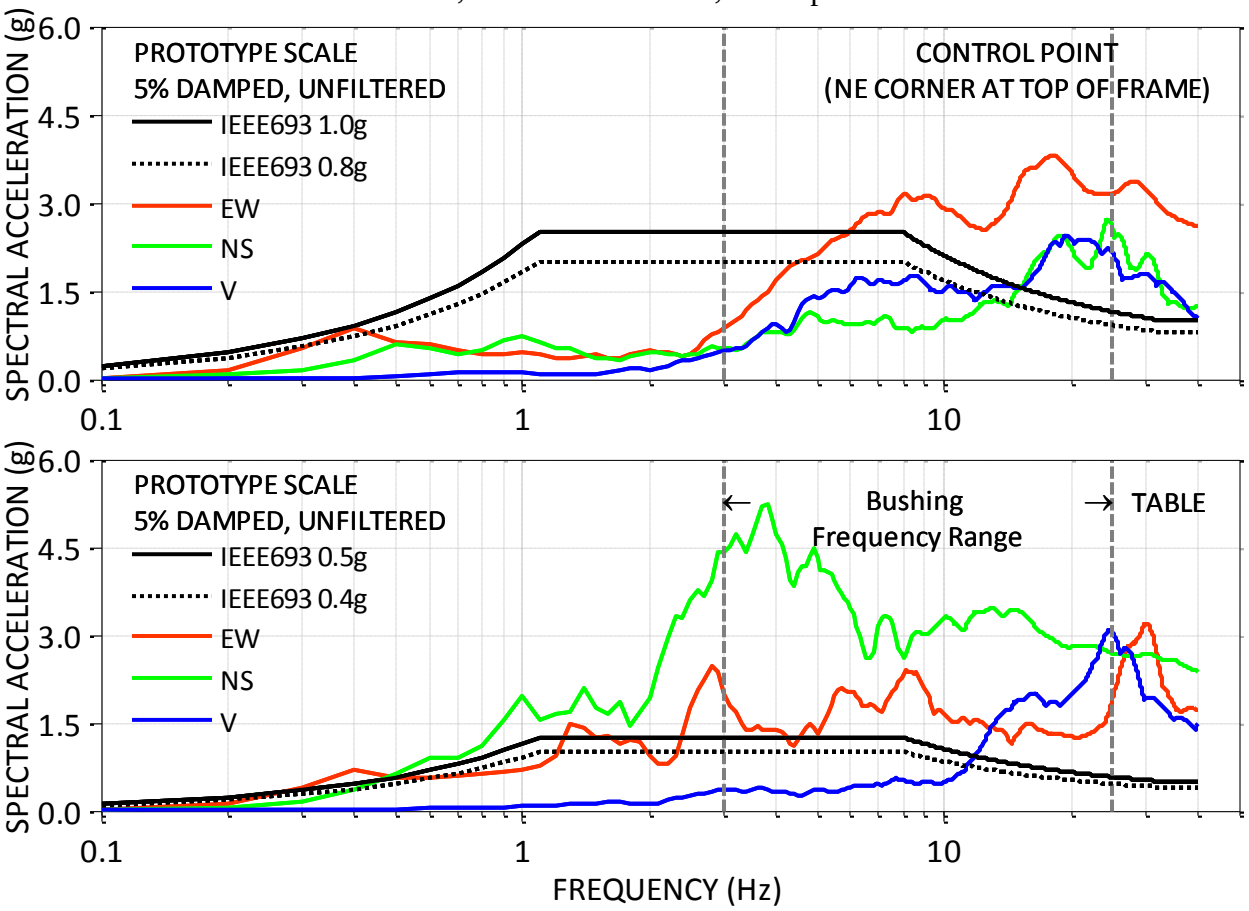
TRIPLE FP SYSTEM (Friction-Bolted Configuration)
JENSEN FILTER 146% BI-AXIAL (FN in EW direction)
LENGTH SCALE=3 SYMMETRIC BUSHING CONFIGURATION

Peak Table Motion								
Acceleration (g)			Velocity (in/sec)			Displacement (in)		
EW	NS	V	EW	NS	V	EW	NS	V
0.96	2.27	0.70	21.30	21.72	6.89	5.11	2.62	0.14

OBSERVATIONS
Displacement limit reached for isolators Uplift at NE, SW and NW isolators Sliding at friction connection of about 1.2 inches (NE), 3.6 inches (SE), 2.7 inches (SW) and 2.4 inches (NW)

Peak Resultant Displacement (in)				Peak Acceleration (g)							
Bushing Top		Isolator	Torsional Ampl[3] Ratio (TA)	Bushing Top			Bushing Bottom		Control Point		
Abs[1]	Rel[2]			EW	NS	V	EW	NS	EW	NS	V
7.49	7.43	6.68	1.01	6.42	3.87	1.68	1.72	0.80	1.95	0.77	0.82

1. Absolute, 2. Relative to table, 3. Amplification



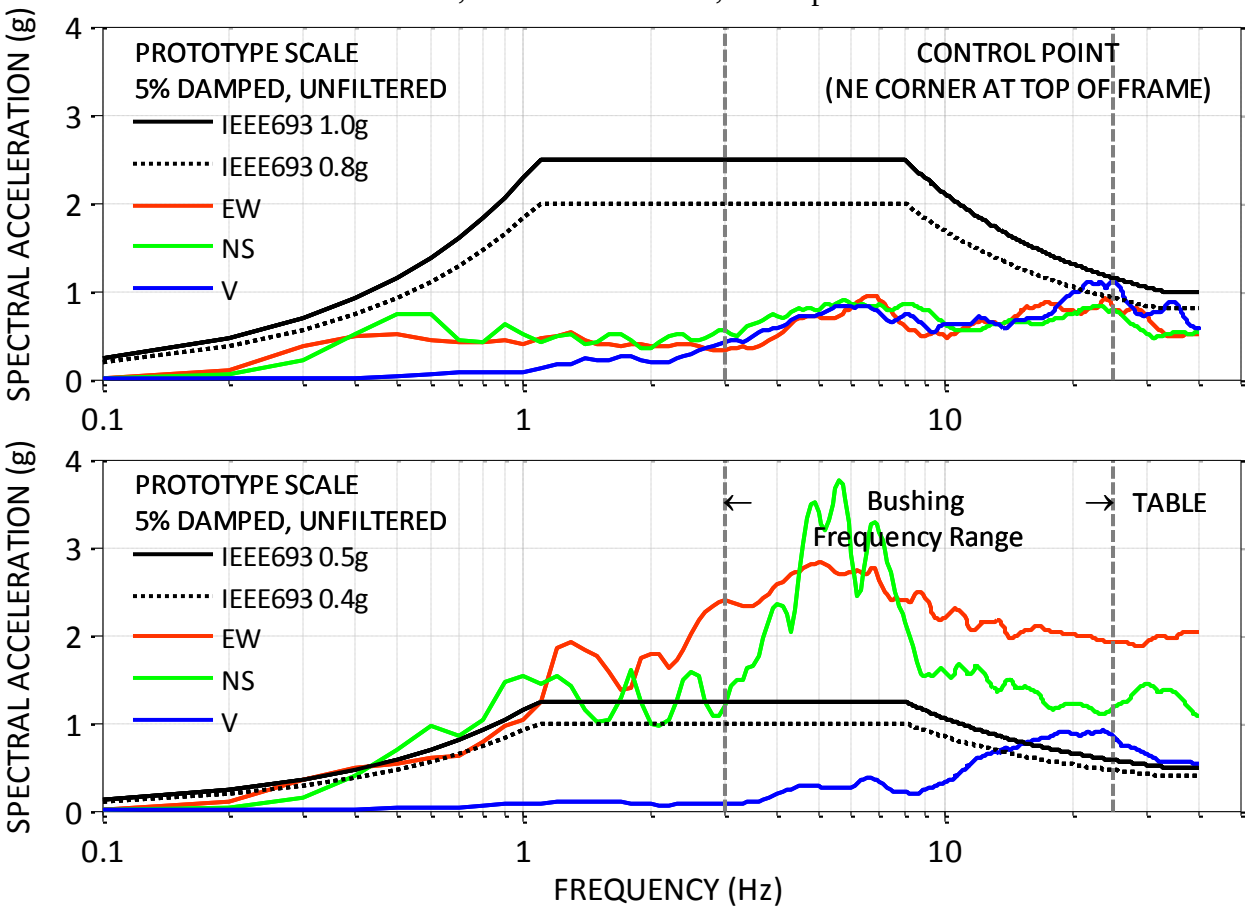
TRIPLE FP SYSTEM (Friction-Bolted Configuration)
SYLMAR 135% BI-AXIAL (FN in EW direction)
LENGTH SCALE=3 SYMMETRIC BUSHING CONFIGURATION

Peak Table Motion								
Acceleration (g)			Velocity (in/sec)			Displacement (in)		
EW	NS	V	EW	NS	V	EW	NS	V
1.76	0.95	0.31	31.07	21.65	1.63	5.01	3.82	0.11

OBSERVATIONS
Displacement limit reached for isolators Uplift at NW isolator Sliding at friction connection of about 2.6 inches (SE) and 0.9 inches (NW)

Peak Resultant Displacement (in)				Peak Acceleration (g)							
Bushing Top		Isolator	Torsional Ampl[3] Ratio (TA)	Bushing Top			Bushing Bottom		Control Point		
Abs[1]	Rel[2]			EW	NS	V	EW	NS	EW	NS	V
5.61	5.70	4.97	1.02	2.55	2.08	0.52	0.31	0.46	0.41	0.44	0.41

1. Absolute, 2. Relative to table, 3. Amplification



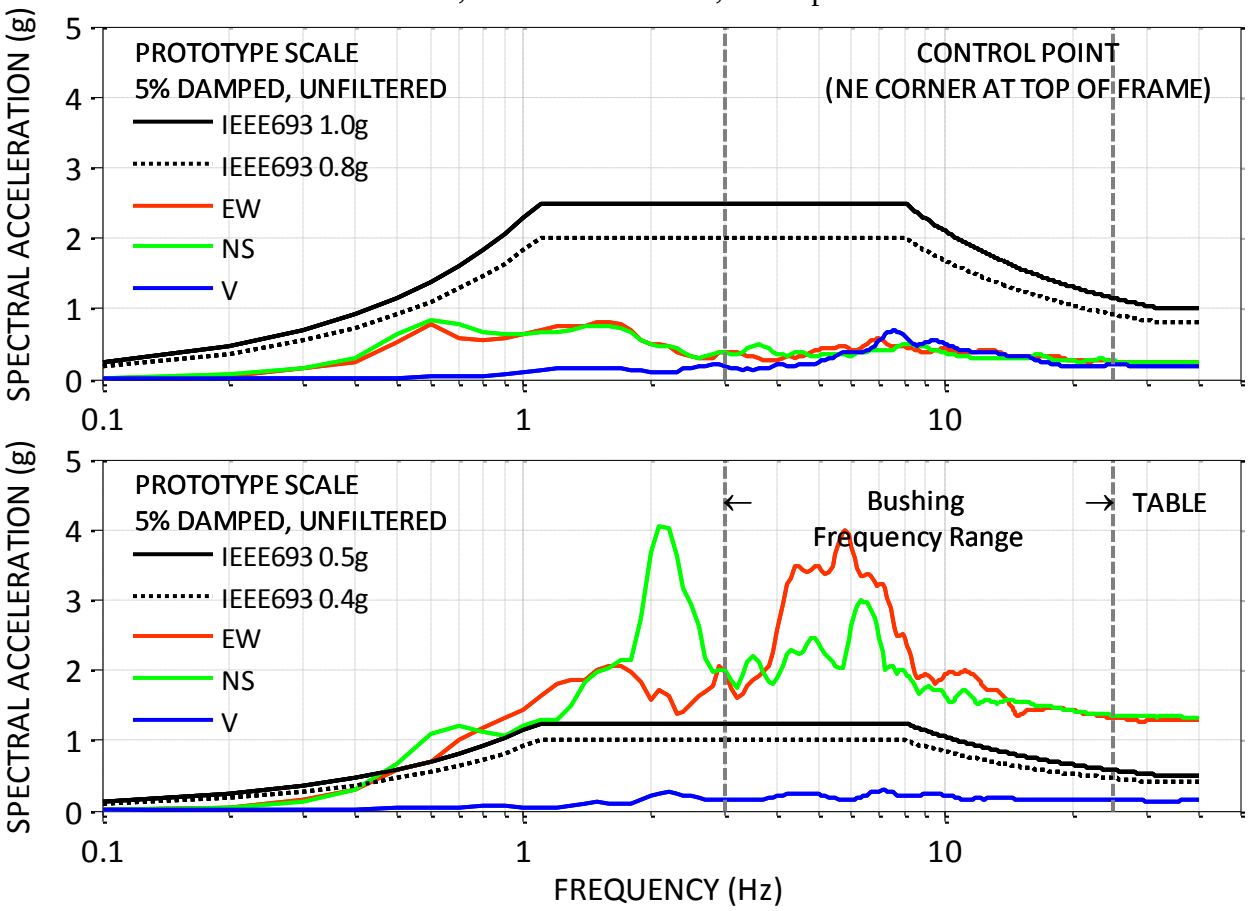
TRIPLE FP SYSTEM (Friction-Bolted Configuration)
TAKARAZUKA 146% BI-AXIAL (FN in EW direction)
LENGTH SCALE=3 SYMMETRIC BUSHING CONFIGURATION

Peak Table Motion								
Acceleration (g)			Velocity (in/sec)			Displacement (in)		
EW	NS	V	EW	NS	V	EW	NS	V
1.27	1.30	0.13	22.06	24.44	0.82	2.71	3.48	0.07

OBSERVATIONS

Peak Resultant Displacement (in)				Peak Acceleration (g)							
Bushing Top		Isolator	Torsional Ampl[3] Ratio (TA)	Bushing Top			Bushing Bottom		Control Point		
Abs[1]	Rel[2]			EW	NS	V	EW	NS	EW	NS	V
3.34	3.96	3.95	1.02	0.98	0.86	0.31	0.24	0.25	0.24	0.23	0.17

1. Absolute, 2. Relative to table, 3. Amplification



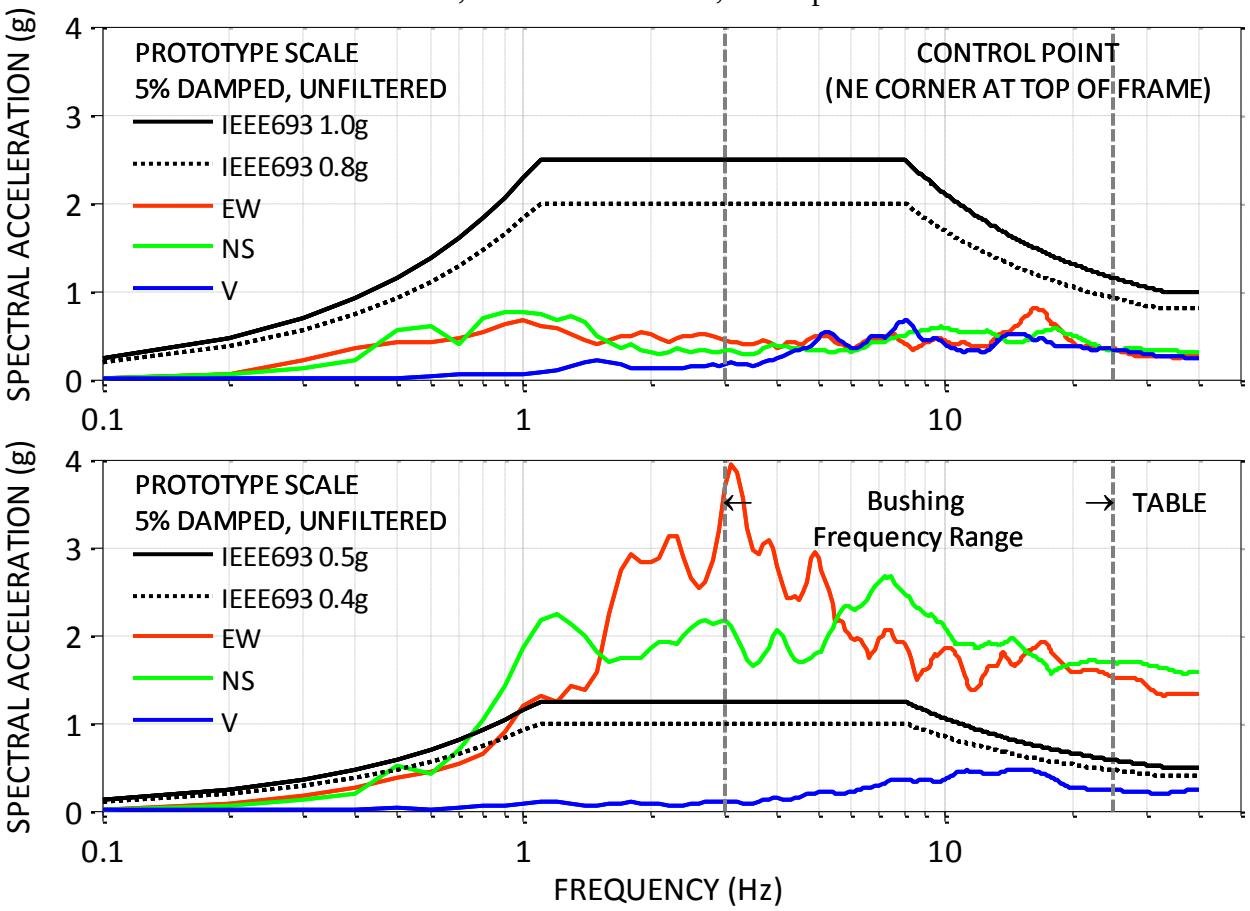
TRIPLE FP SYSTEM (Friction-Bolted Configuration)
BOLU 156% BI-AXIAL (FN in EW direction)
LENGTH SCALE=3 SYMMETRIC BUSHING CONFIGURATION

Peak Table Motion								
Acceleration (g)			Velocity (in/sec)			Displacement (in)		
EW	NS	V	EW	NS	V	EW	NS	V
1.26	1.57	0.19	19.75	22.84	0.77	2.84	2.69	0.05

OBSERVATIONS

Peak Resultant Displacement (in)				Peak Acceleration (g)							
Bushing Top		Isolator	Torsional Ampl[3] Ratio (TA)	Bushing Top			Bushing Bottom		Control Point		
Abs[1]	Rel[2]			EW	NS	V	EW	NS	EW	NS	V
3.19	3.55	3.50	1.02	0.88	0.59	0.88	0.23	0.28	0.23	0.29	0.23

1. Absolute, 2. Relative to table, 3. Amplification



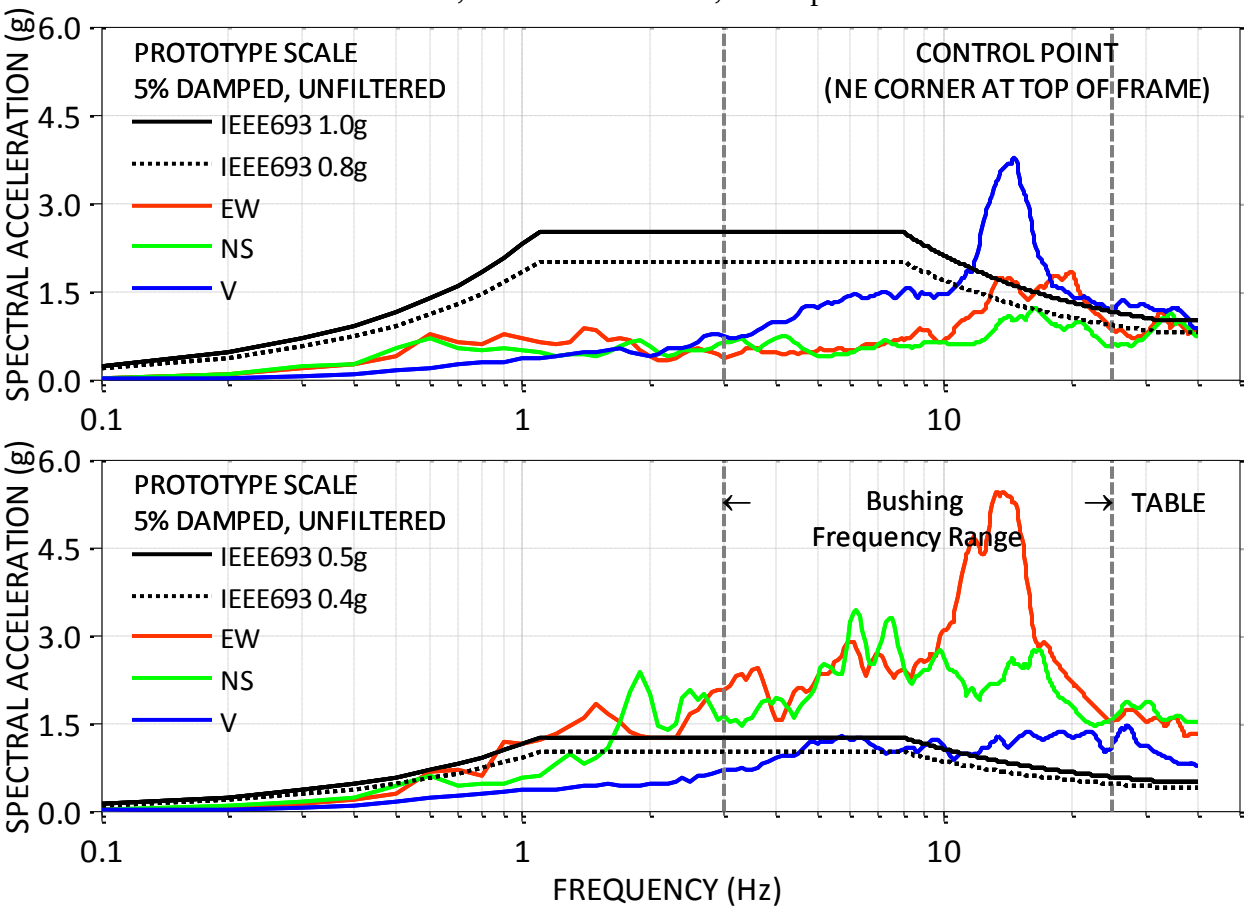
TRIPLE FP SYSTEM (Friction-Bolted Configuration)
KARAKYR 137% TRI-AXIAL (FN in EW direction)
LENGTH SCALE=3 SYMMETRIC BUSHING CONFIGURATION

Peak Table Motion								
Acceleration (g)			Velocity (in/sec)			Displacement (in)		
EW	NS	V	EW	NS	V	EW	NS	V
1.22	1.38	0.58	15.39	17.32	7.67	2.56	2.97	1.48

OBSERVATIONS

Peak Resultant Displacement (in)				Peak Acceleration (g)							
Bushing Top		Isolator	Torsional Ampl[3] Ratio (TA)	Bushing Top			Bushing Bottom		Control Point		
Abs[1]	Rel[2]			EW	NS	V	EW	NS	EW	NS	V
3.77	3.63	3.85	1.06	1.49	1.49	1.72	0.48	0.36	0.42	0.33	0.84

1. Absolute, 2. Relative to table, 3. Amplification



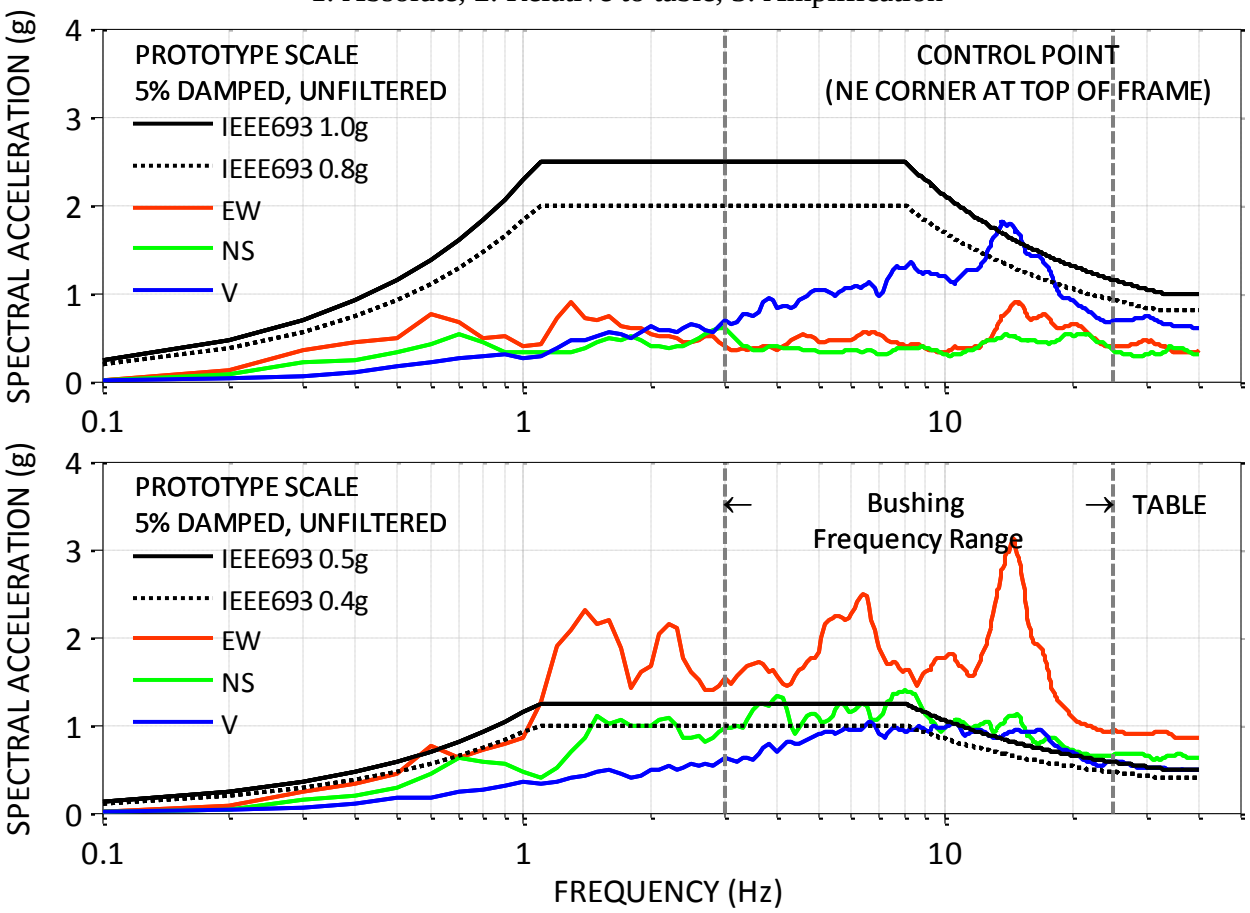
TRIPLE FP SYSTEM (Friction-Bolted Configuration)
LGPC 94% TRI-AXIAL (FN in EW direction)
LENGTH SCALE=3 SYMMETRIC BUSHING CONFIGURATION

Peak Table Motion								
Acceleration (g)			Velocity (in/sec)			Displacement (in)		
EW	NS	V	EW	NS	V	EW	NS	V
0.83	0.61	0.46	17.29	11.25	6.02	3.43	2.26	1.04

OBSERVATIONS

Peak Resultant Displacement (in)				Peak Acceleration (g)							
Bushing Top		Isolator	Torsional Ampl[3] Ratio (TA)	Bushing Top			Bushing Bottom		Control Point		
Abs[1]	Rel[2]			EW	NS	V	EW	NS	EW	NS	V
4.99	3.99	3.97	1.00	1.20	0.98	1.22	0.33	0.25	0.33	0.25	0.57

1. Absolute, 2. Relative to table, 3. Amplification



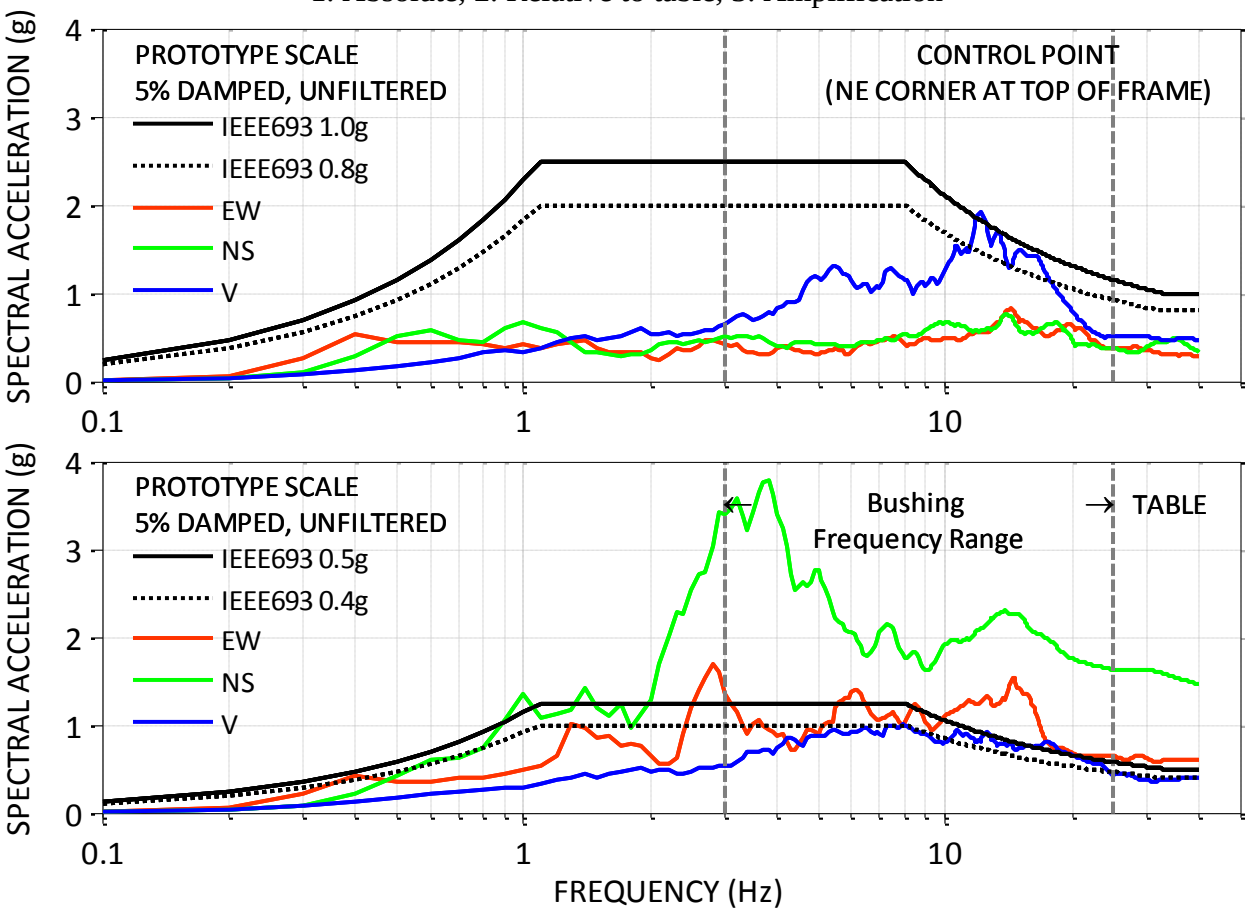
TRIPLE FP SYSTEM (Friction-Bolted Configuration)
JENSEN FILTER 97% TRI-AXIAL (FN in EW direction)
LENGTH SCALE=3 SYMMETRIC BUSHING CONFIGURATION

Peak Table Motion								
Acceleration (g)			Velocity (in/sec)			Displacement (in)		
EW	NS	V	EW	NS	V	EW	NS	V
0.57	1.41	0.35	12.35	13.82	7.06	2.39	1.84	1.04

OBSERVATIONS
Uplift at NW isolator Sliding at friction connection of about 0.5 inches

Peak Resultant Displacement (in)				Peak Acceleration (g)							
Bushing Top		Isolator	Torsional Ampl[3] Ratio (TA)	Bushing Top			Bushing Bottom		Control Point		
Abs[1]	Rel[2]			EW	NS	V	EW	NS	EW	NS	V
3.79	3.29	3.21	1.01	1.14	0.96	2.18	0.25	0.27	0.27	0.24	0.44

1. Absolute, 2. Relative to table, 3. Amplification



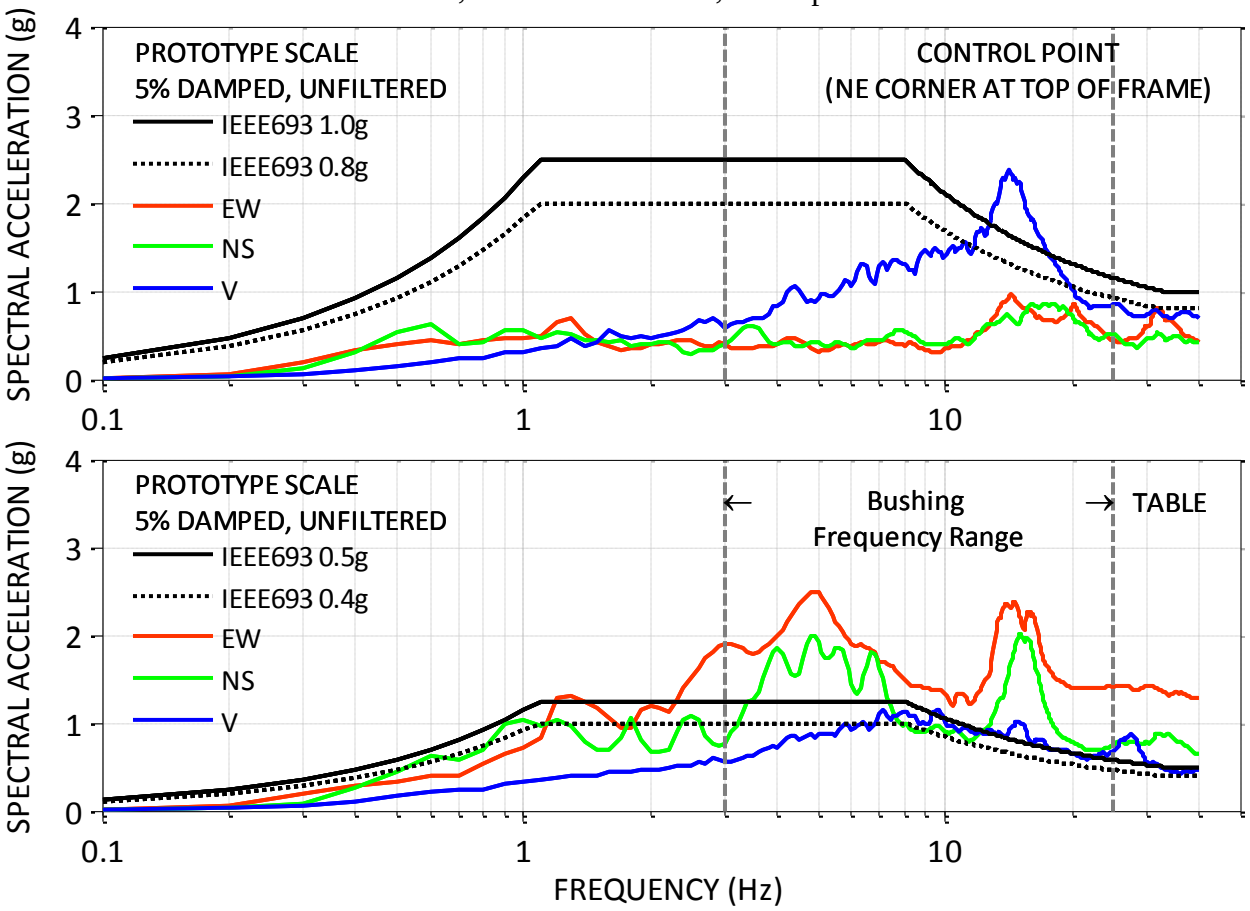
TRIPLE FP SYSTEM (Friction-Bolted Configuration)
SYLMAR 90% TRI-AXIAL (FN in EW direction)
LENGTH SCALE=3 SYMMETRIC BUSHING CONFIGURATION

Peak Table Motion								
Acceleration (g)			Velocity (in/sec)			Displacement (in)		
EW	NS	V	EW	NS	V	EW	NS	V
1.25	0.57	0.41	20.48	14.21	5.69	2.39	2.04	0.95

OBSERVATIONS
Uplift at NW isolator

Peak Resultant Displacement (in)				Peak Acceleration (g)							
Bushing Top		Isolator	Torsional Ampl[3] Ratio (TA)	Bushing Top			Bushing Bottom		Control Point		
Abs[1]	Rel[2]			EW	NS	V	EW	NS	EW	NS	V
3.31	3.61	3.51	1.01	1.34	1.21	1.82	0.28	0.32	0.30	0.30	0.59

1. Absolute, 2. Relative to table, 3. Amplification



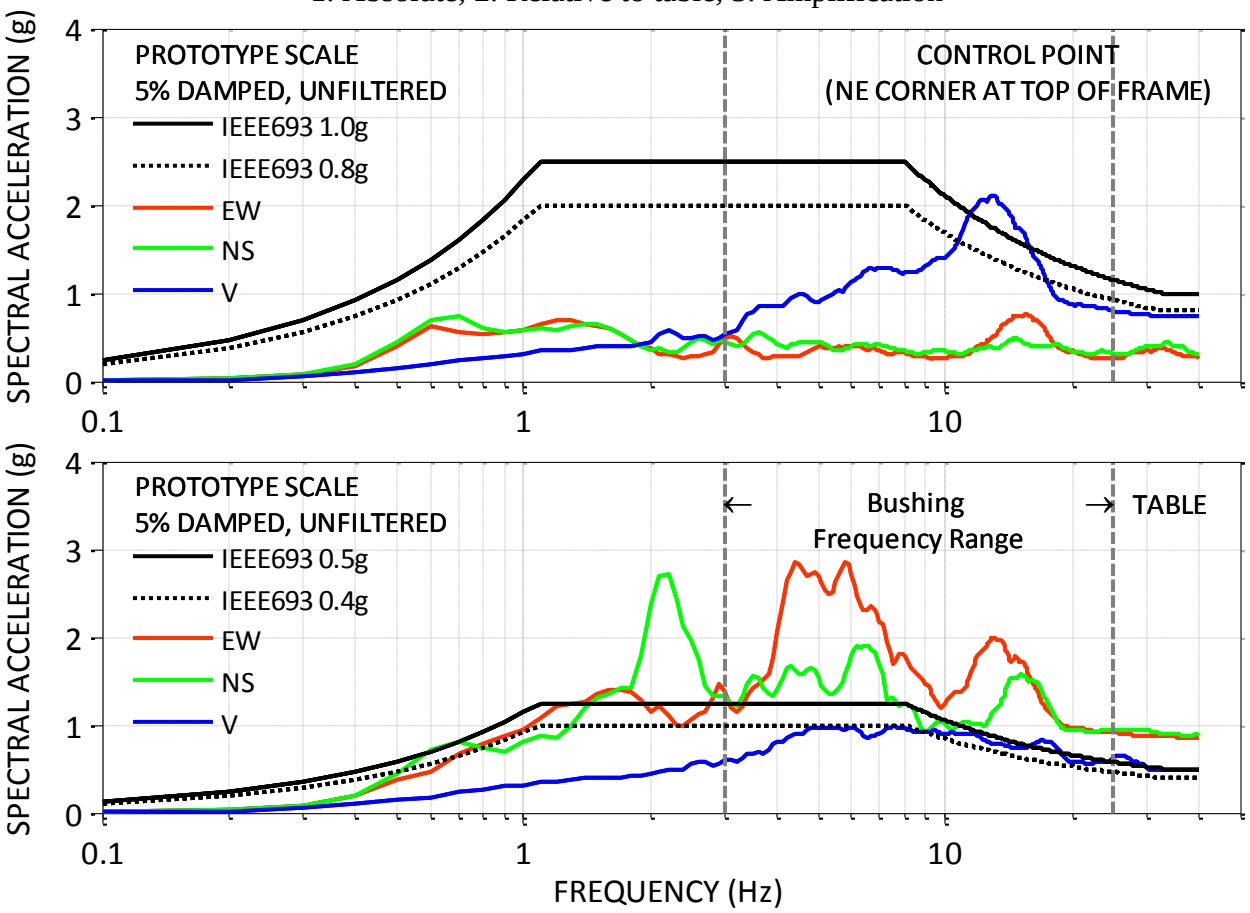
TRIPLE FP SYSTEM (Friction-Bolted Configuration)
TAKARAZUKA 97% TRI-AXIAL (FN in EW direction)
LENGTH SCALE=3 SYMMETRIC BUSHING CONFIGURATION

Peak Table Motion								
Acceleration (g)			Velocity (in/sec)			Displacement (in)		
EW	NS	V	EW	NS	V	EW	NS	V
0.85	0.87	0.44	14.98	16.46	6.46	1.61	2.08	0.84

OBSERVATIONS

Peak Resultant Displacement (in)				Peak Acceleration (g)							
Bushing Top		Isolator	Torsional Ampl[3] Ratio (TA)	Bushing Top			Bushing Bottom		Control Point		
Abs[1]	Rel[2]			EW	NS	V	EW	NS	EW	NS	V
2.38	3.13	3.18	1.06	1.72	0.94	1.17	0.23	0.27	0.22	0.23	0.67

1. Absolute, 2. Relative to table, 3. Amplification



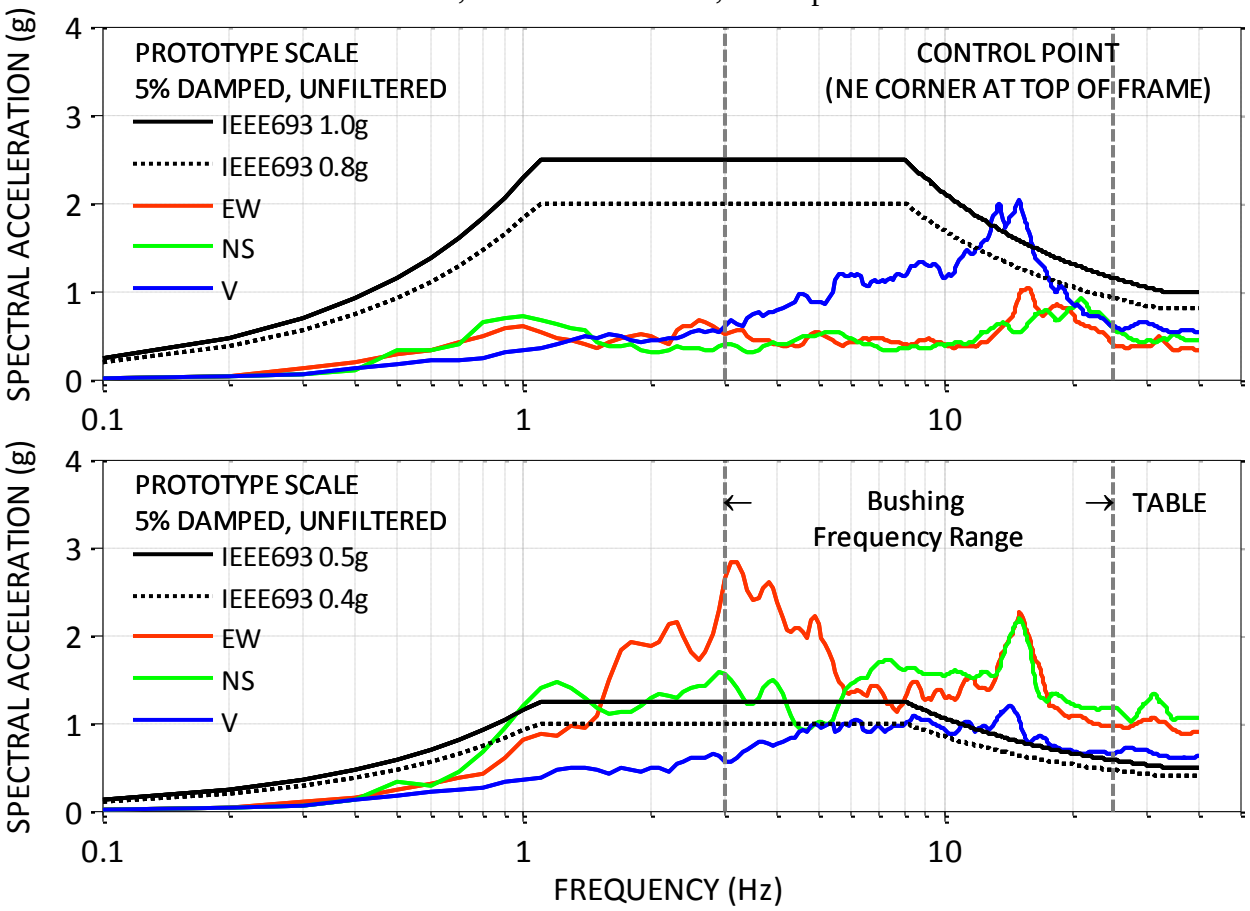
TRIPLE FP SYSTEM (Friction-Bolted Configuration)
BOLU 104% TRI-AXIAL (FN in EW direction)
LENGTH SCALE=3 SYMMETRIC BUSHING CONFIGURATION

Peak Table Motion								
Acceleration (g)			Velocity (in/sec)			Displacement (in)		
EW	NS	V	EW	NS	V	EW	NS	V
0.87	1.02	0.56	13.49	15.53	6.59	1.42	1.71	1.18

OBSERVATIONS
Uplift at NW isolator Sliding at friction connection of about 0.1 inches

Peak Resultant Displacement (in)				Peak Acceleration (g)							
Bushing Top		Isolator	Torsional Ampl[3] Ratio (TA)	Bushing Top			Bushing Bottom		Control Point		
Abs[1]	Rel[2]			EW	NS	V	EW	NS	EW	NS	V
2.04	2.21	2.08	1.01	1.55	1.04	1.79	0.26	0.34	0.25	0.32	0.52

1. Absolute, 2. Relative to table, 3. Amplification



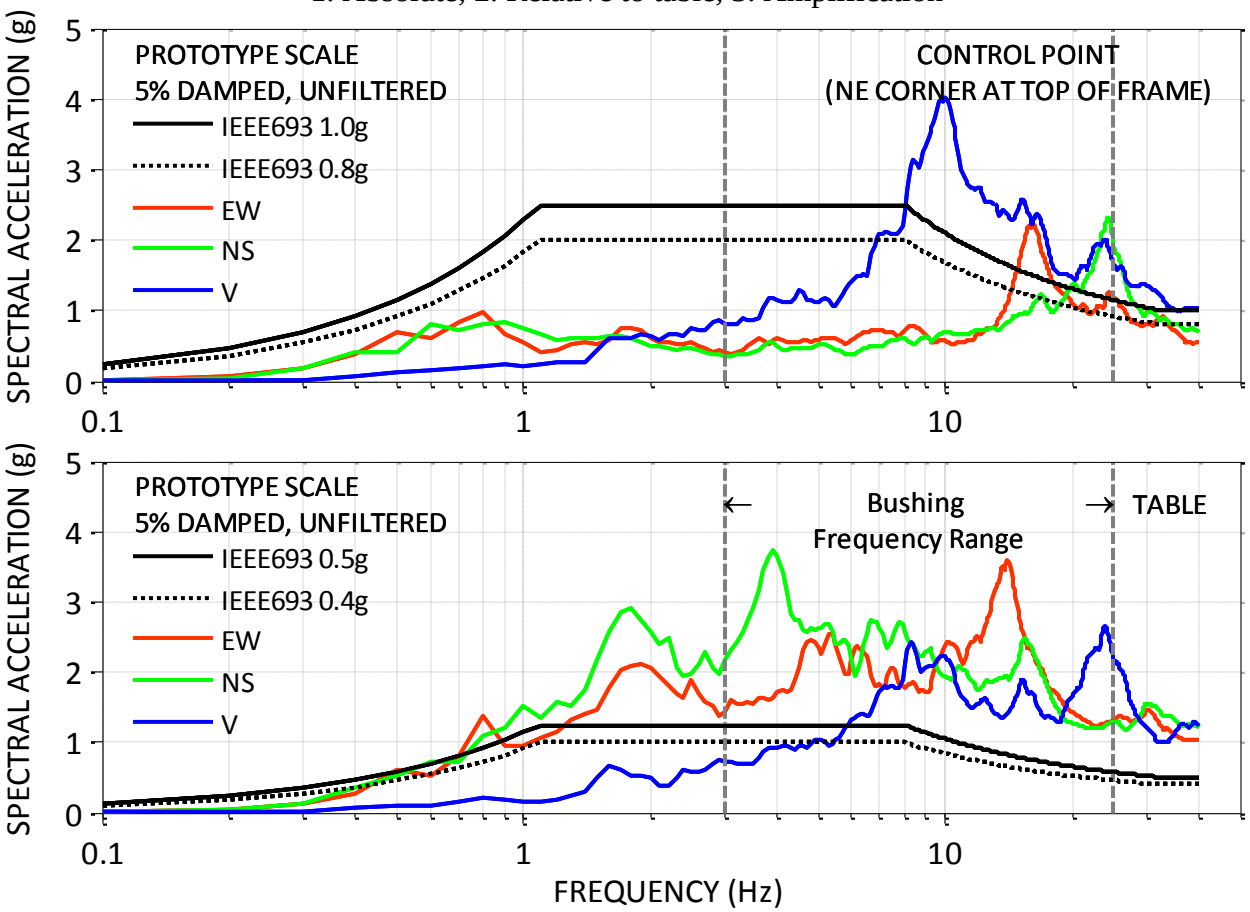
TRIPLE FP SYSTEM (Friction-Bolted Configuration)
EL CENTRO 300% TRI-AXIAL (FN in EW direction)
LENGTH SCALE=3 SYMMETRIC BUSHING CONFIGURATION

Peak Table Motion								
Acceleration (g)			Velocity (in/sec)			Displacement (in)		
EW	NS	V	EW	NS	V	EW	NS	V
0.90	1.11	0.76	21.42	19.44	5.34	2.23	2.44	0.58

OBSERVATIONS
Uplift at the NE and SW isolators Sliding at friction connection of about 0.1 inches (NE) and 0.1 inches (SW)

Peak Resultant Displacement (in)				Peak Acceleration (g)							
Bushing Top		Isolator	Torsional Ampl[3] Ratio (TA)	Bushing Top			Bushing Bottom		Control Point		
Abs[1]	Rel[2]			EW	NS	V	EW	NS	EW	NS	V
3.55	4.17	4.33	1.03	1.87	1.81	2.70	0.54	0.61	0.46	0.50	0.90

1. Absolute, 2. Relative to table, 3. Amplification



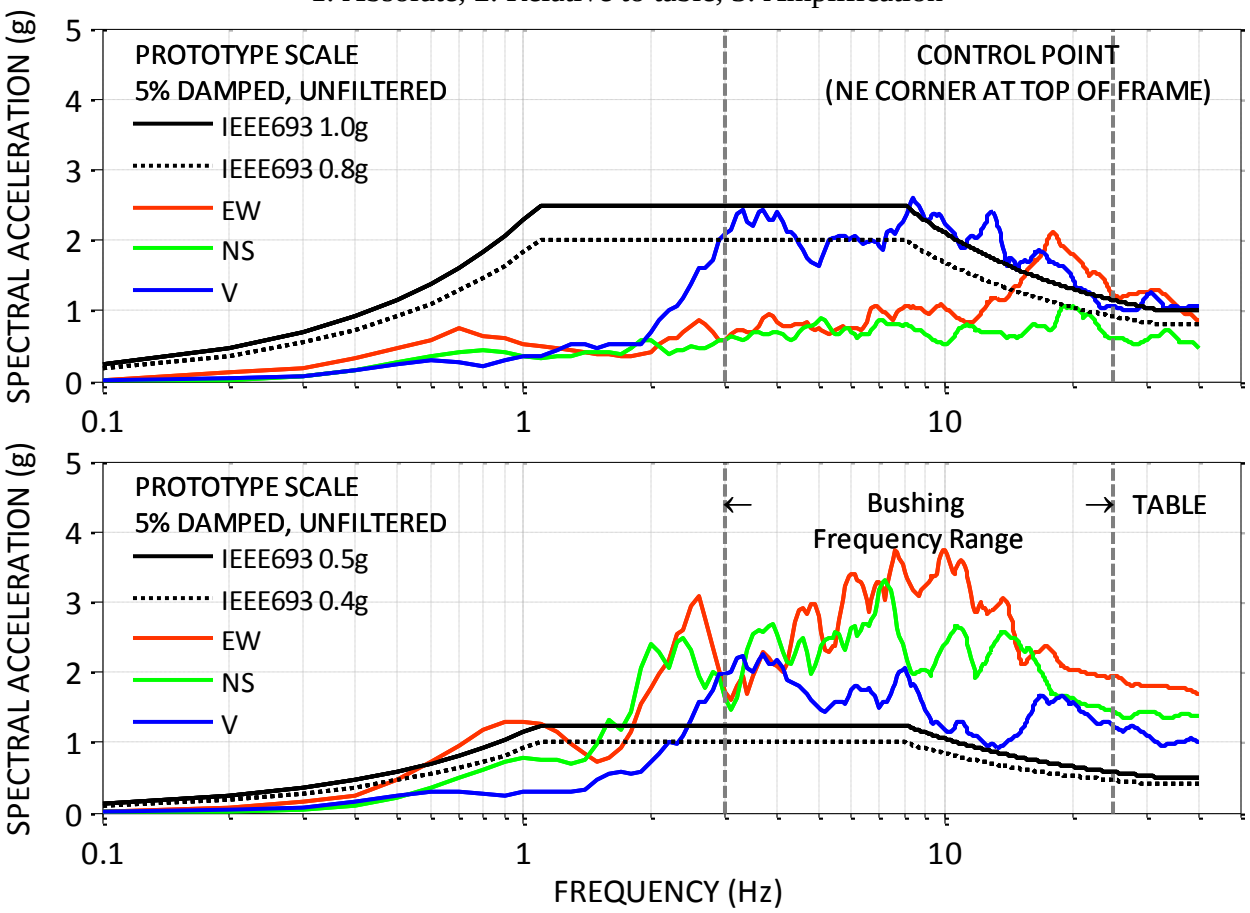
TRIPLE FP SYSTEM (Friction-Bolted Configuration)
PACOIMA DAM 100% TRI-AXIAL (FN in EW direction)
LENGTH SCALE=3 SYMMETRIC BUSHING CONFIGURATION

Peak Table Motion								
Acceleration (g)			Velocity (in/sec)			Displacement (in)		
EW	NS	V	EW	NS	V	EW	NS	V
1.61	1.27	0.87	22.98	14.94	9.97	3.14	1.58	1.90

OBSERVATIONS
Uplift at NE and SW isolators Sliding at friction connection of about 0.1 inches

Peak Resultant Displacement (in)				Peak Acceleration (g)							
Bushing Top		Isolator	Torsional Ampl[3] Ratio (TA)	Bushing Top			Bushing Bottom		Control Point		
Abs[1]	Rel[2]			EW	NS	V	EW	NS	EW	NS	V
3.97	4.28	4.27	1.03	2.24	2.19	3.07	0.50	0.38	0.60	0.32	0.98

1. Absolute, 2. Relative to table, 3. Amplification



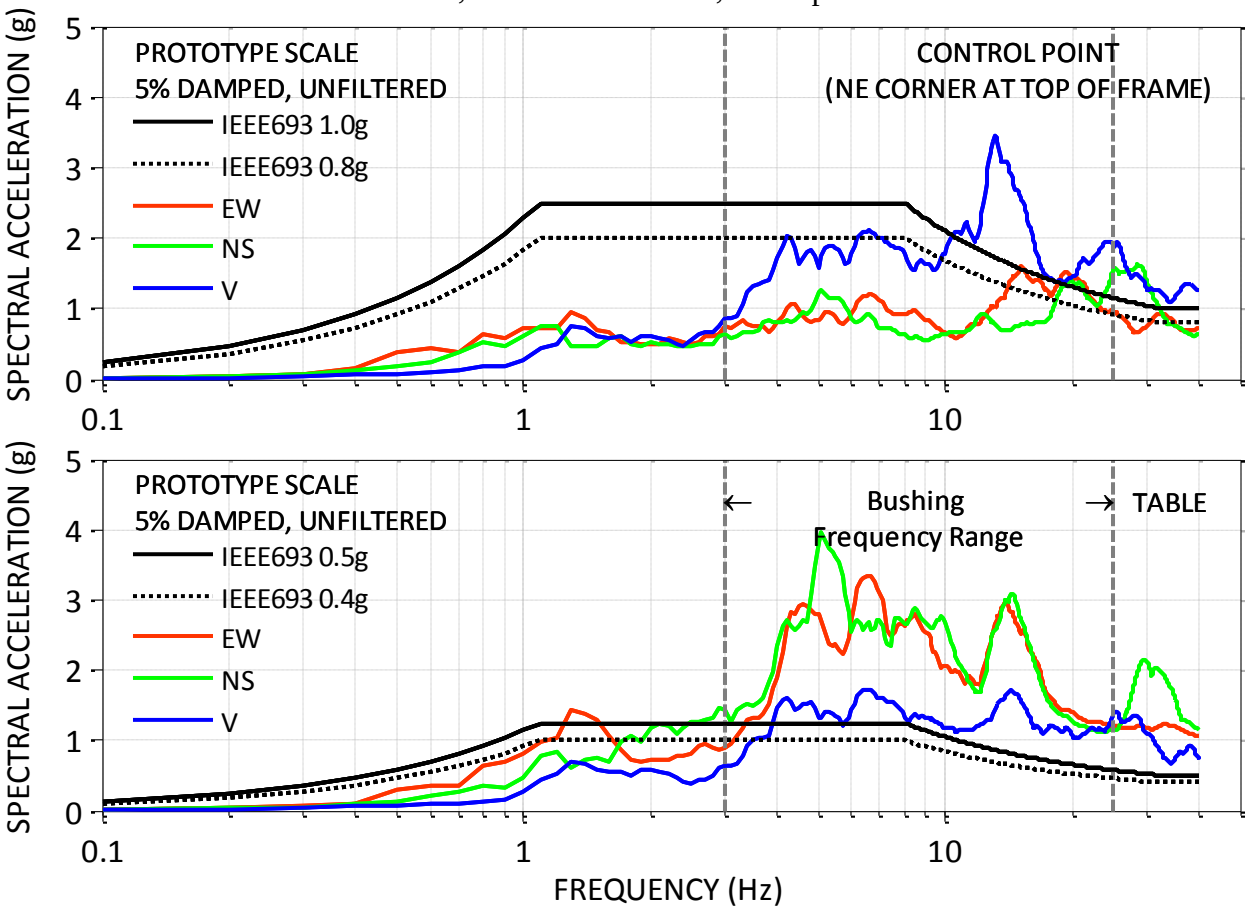
TRIPLE FP SYSTEM (Friction-Bolted Configuration)
CHILE 100% TRI-AXIAL (FN in EW direction)
LENGTH SCALE=3 SYMMETRIC BUSHING CONFIGURATION

Peak Table Motion								
Acceleration (g)			Velocity (in/sec)			Displacement (in)		
EW	NS	V	EW	NS	V	EW	NS	V
1.01	1.02	0.58	9.52	8.83	5.40	1.84	1.21	0.88

OBSERVATIONS
Uplift at NE and SW isolators Sliding at friction connection of about 0.3 inches

Peak Resultant Displacement (in)				Peak Acceleration (g)							
Bushing Top		Isolator	Torsional Ampl[3] Ratio (TA)	Bushing Top			Bushing Bottom		Control Point		
Abs[1]	Rel[2]			EW	NS	V	EW	NS	EW	NS	V
2.36	1.56	1.47	1.02	2.93	3.40	3.04	0.46	0.60	0.46	0.53	0.81

1. Absolute, 2. Relative to table, 3. Amplification



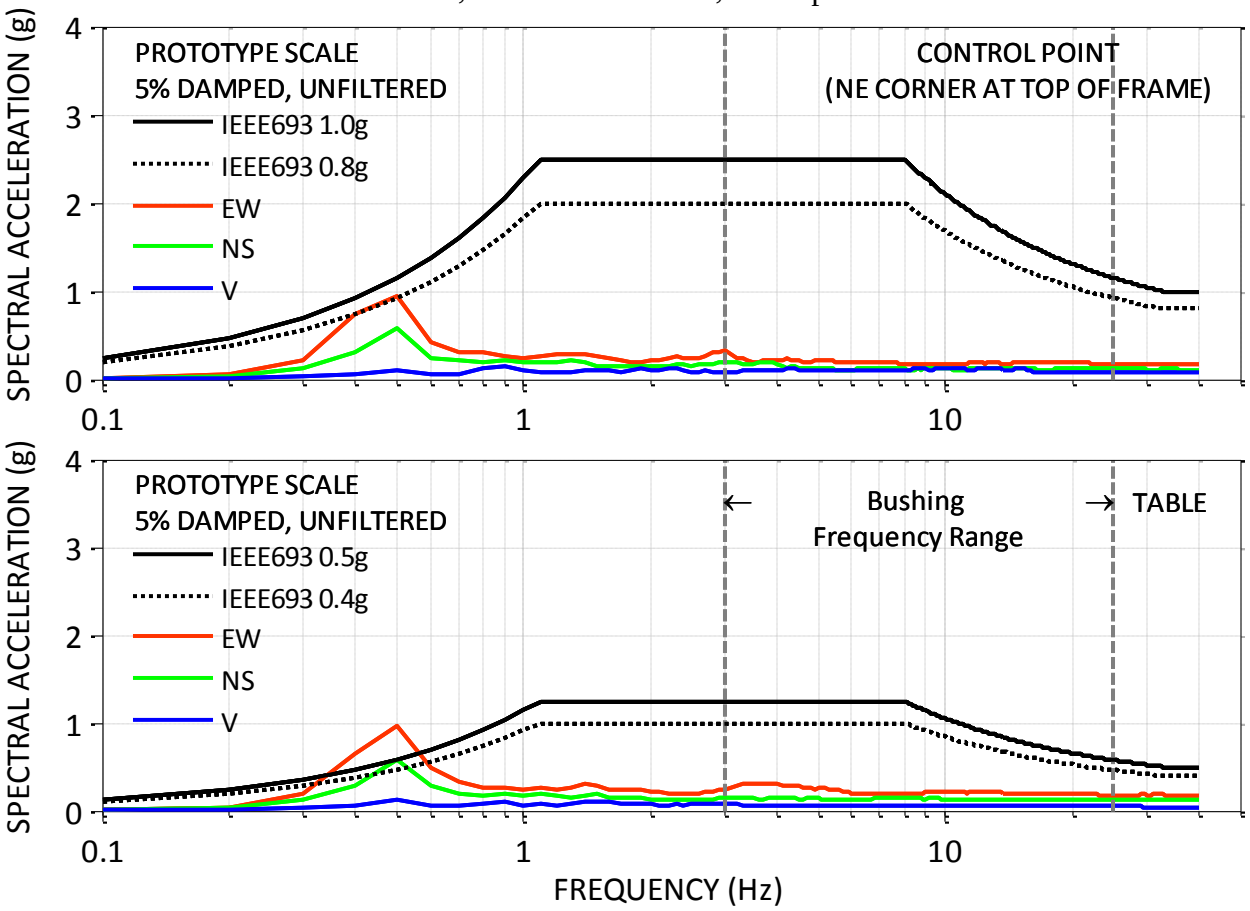
TRIPLE FP SYSTEM (Friction-Bolted Configuration)
MEXICO CITY 100% TRI-AXIAL (FN in EW direction)
LENGTH SCALE=3 SYMMETRIC BUSHING CONFIGURATION

Peak Table Motion								
Acceleration (g)			Velocity (in/sec)			Displacement (in)		
EW	NS	V	EW	NS	V	EW	NS	V
0.17	0.11	0.04	13.11	7.50	1.80	2.40	1.69	0.35

OBSERVATIONS

Peak Resultant Displacement (in)				Peak Acceleration (g)							
Bushing Top		Isolator	Torsional Ampl[3] Ratio (TA)	Bushing Top			Bushing Bottom		Control Point		
Abs[1]	Rel[2]			EW	NS	V	EW	NS	EW	NS	V
3.42	1.92	2.03	1.05	0.27	0.18	0.10	0.19	0.11	0.17	0.11	0.07

1. Absolute, 2. Relative to table, 3. Amplification



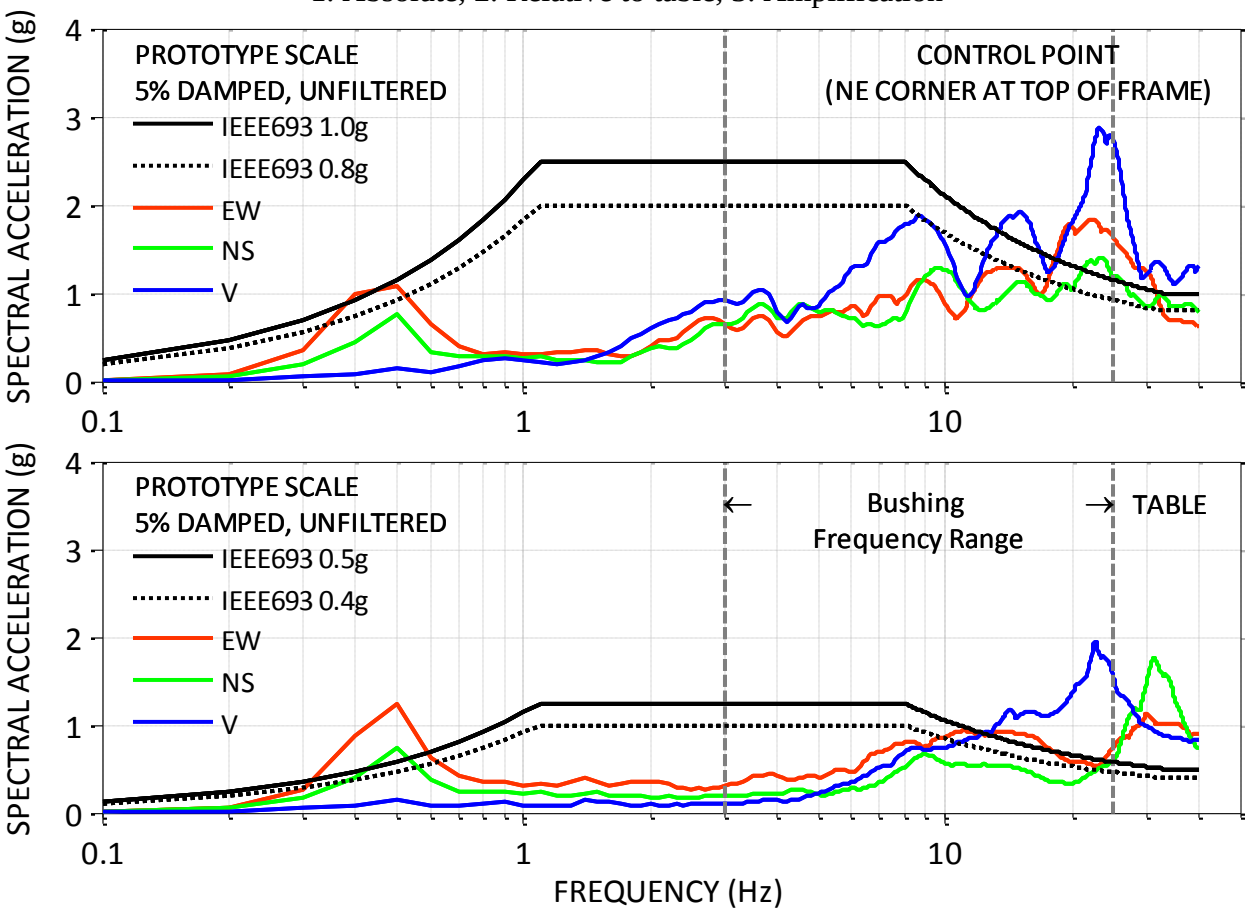
TRIPLE FP SYSTEM (Friction-Bolted Configuration)
MEXICO CITY 125% TRI-AXIAL (FN in EW direction)
LENGTH SCALE=3 SYMMETRIC BUSHING CONFIGURATION

Peak Table Motion								
Acceleration (g)			Velocity (in/sec)			Displacement (in)		
EW	NS	V	EW	NS	V	EW	NS	V
0.58	0.35	0.55	16.83	9.59	2.93	3.13	2.46	0.58

OBSERVATIONS
Displacement limit reached for isolators Uplift for all isolators Sliding at friction connection of about 2.3 inches (NE), 1.0 inches (SE), 1.1 inches (SW) and 0.6 inches (NW)

Peak Resultant Displacement (in)				Peak Acceleration (g)							
Bushing Top		Isolator	Torsional Ampl[3] Ratio (TA)	Bushing Top			Bushing Bottom		Control Point		
Abs[1]	Rel[2]			EW	NS	V	EW	NS	EW	NS	V
5.18	6.59	5.86	1.05	3.83	3.19	1.76	0.68	0.76	0.59	0.60	0.84

1. Absolute, 2. Relative to table, 3. Amplification



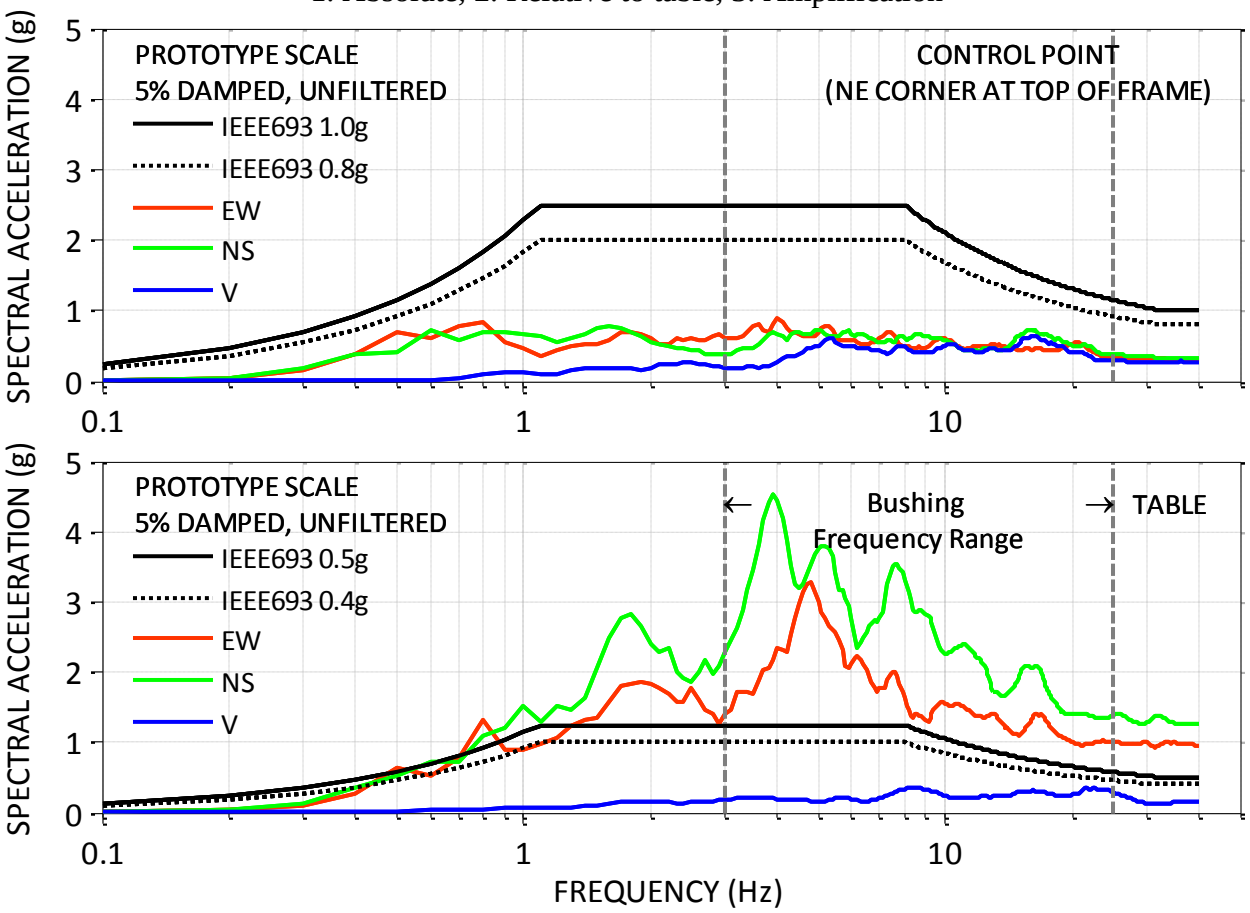
TRIPLE FP SYSTEM (Friction-Bolted Configuration)
EL CENTRO 300% BI-AXIAL (N90W in EW direction)
LENGTH SCALE=3 NON-SYMMETRIC BUSHING CONFIGURATION

Peak Table Motion								
Acceleration (g)			Velocity (in/sec)			Displacement (in)		
EW	NS	V	EW	NS	V	EW	NS	V
0.93	1.21	0.11	19.47	19.29	0.89	2.23	2.44	0.04

OBSERVATIONS
Uplift at the NW isolator Sliding at friction connection of about 1.3 inches (NW)

Peak Resultant Displacement (in)				Peak Acceleration (g)							
Bushing Top		Isolator	Torsional Ampl[3] Ratio (TA)	Bushing Top			Bushing Bottom		Control Point		
Abs[1]	Rel[2]			EW	NS	V	EW	NS	EW	NS	V
3.23	4.09	4.18	1.01	1.61	1.42	0.64	0.30	0.32	0.27	0.31	0.25

1. Absolute, 2. Relative to table, 3. Amplification



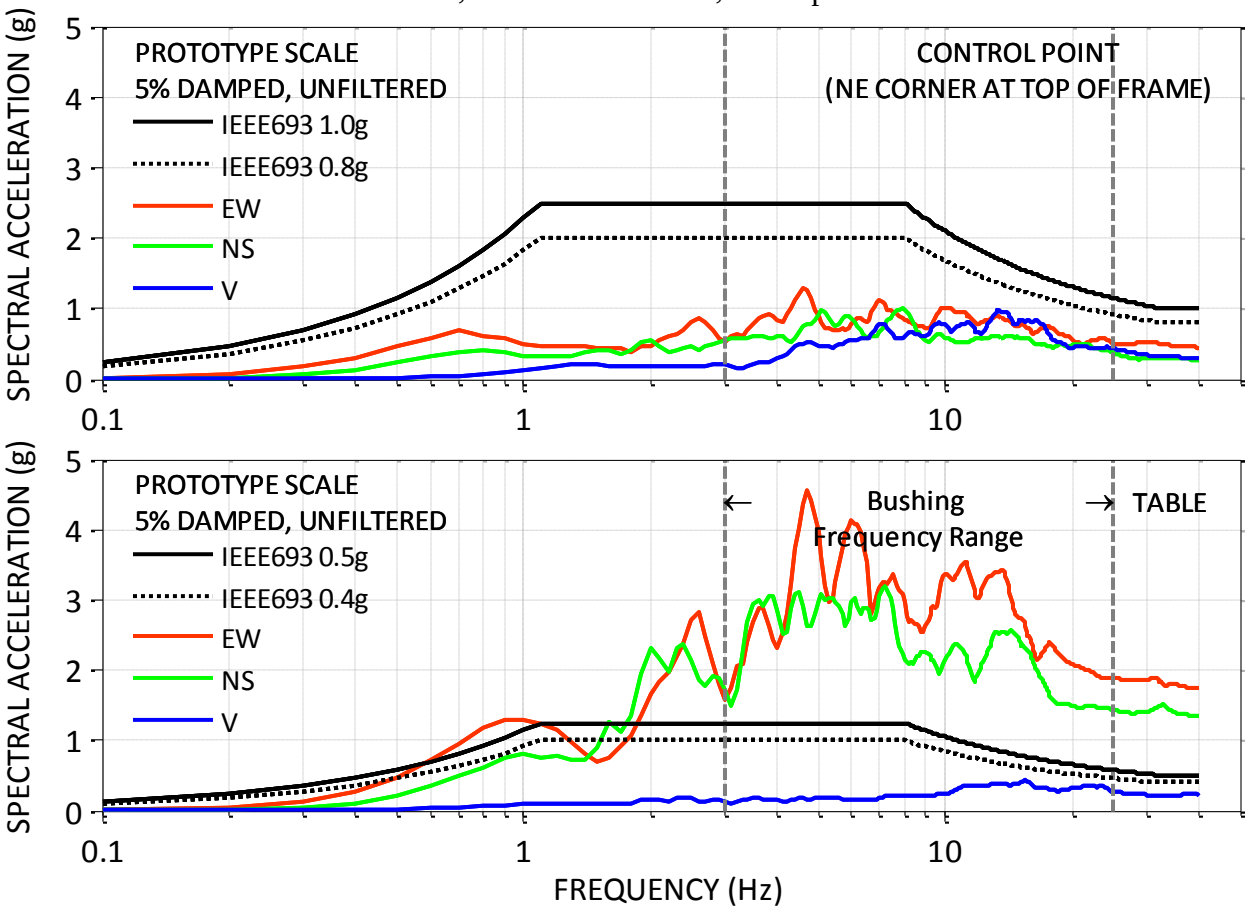
TRIPLE FP SYSTEM (Friction-Bolted Configuration)
PACOIMA DAM 100% BI-AXIAL (S16E in EW direction)
LENGTH SCALE=3 NON-SYMMETRIC BUSHING CONFIGURATION

Peak Table Motion								
Acceleration (g)			Velocity (in/sec)			Displacement (in)		
EW	NS	V	EW	NS	V	EW	NS	V
1.65	1.31	0.17	23.43	14.78	1.25	2.63	1.51	0.04

OBSERVATIONS
Uplift at NW isolator Sliding at friction connection of about 0.3 inches (NW)

Peak Resultant Displacement (in)				Peak Acceleration (g)							
Bushing Top		Isolator	Torsional Ampl[3] Ratio (TA)	Bushing Top			Bushing Bottom		Control Point		
Abs[1]	Rel[2]			EW	NS	V	EW	NS	EW	NS	V
3.15	4.08	4.21	1.02	2.26	1.99	0.71	0.40	0.29	0.39	0.27	0.27

1. Absolute, 2. Relative to table, 3. Amplification



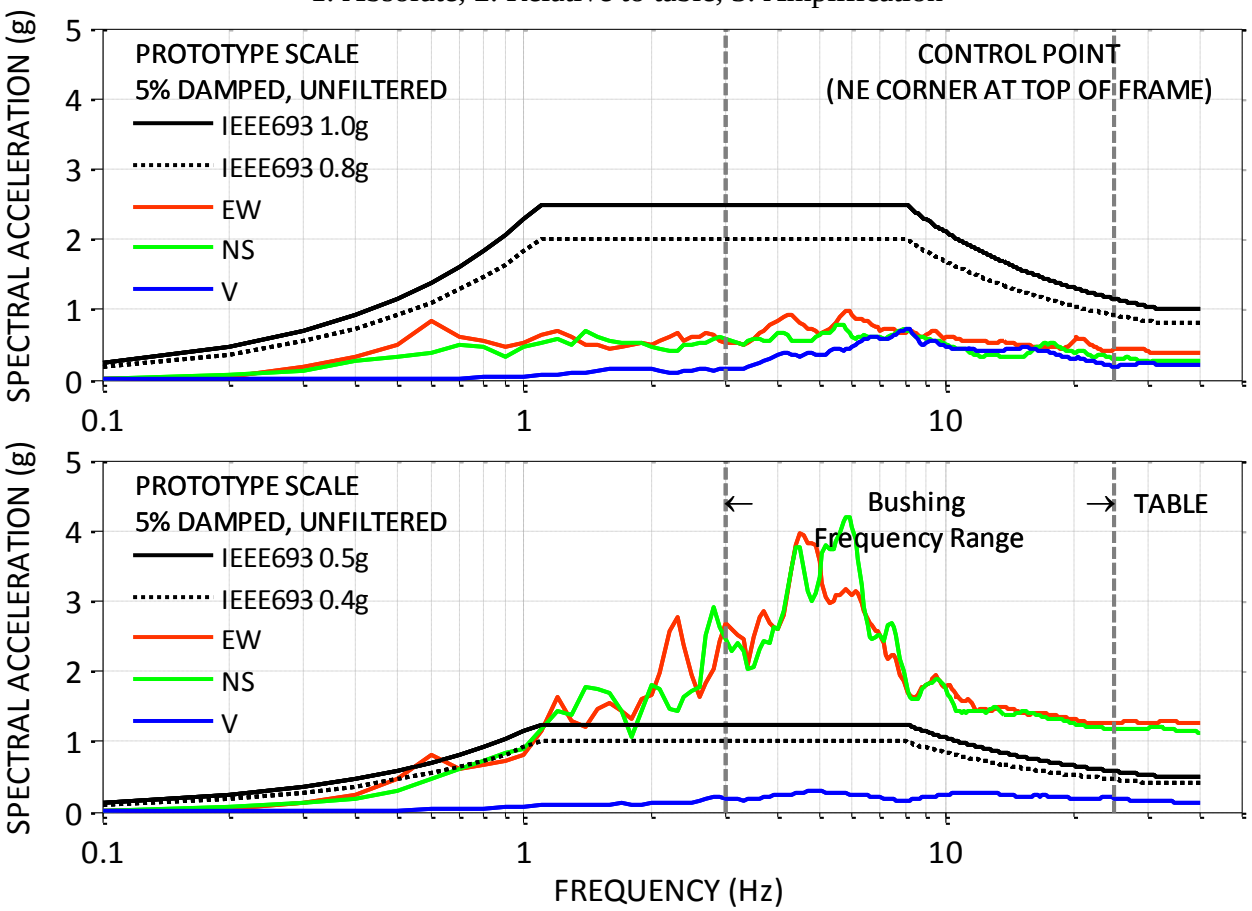
TRIPLE FP SYSTEM (Friction-Bolted Configuration)
TAFT 500% BI-AXIAL (S69E in EW direction)
LENGTH SCALE=3 NON-SYMMETRIC BUSHING CONFIGURATION

Peak Table Motion								
Acceleration (g)			Velocity (in/sec)			Displacement (in)		
EW	NS	V	EW	NS	V	EW	NS	V
1.23	1.11	0.13	18.72	14.76	1.15	2.16	2.61	0.05

OBSERVATIONS
Uplift at NW isolator Sliding at friction connection of about 0.3 inches (NW)

Peak Resultant Displacement (in)				Peak Acceleration (g)							
Bushing Top		Isolator	Torsional Ampl[3] Ratio (TA)	Bushing Top			Bushing Bottom		Control Point		
Abs[1]	Rel[2]			EW	NS	V	EW	NS	EW	NS	V
4.02	2.82	2.84	1.03	1.80	1.64	0.48	0.35	0.26	0.36	0.26	0.18

1. Absolute, 2. Relative to table, 3. Amplification



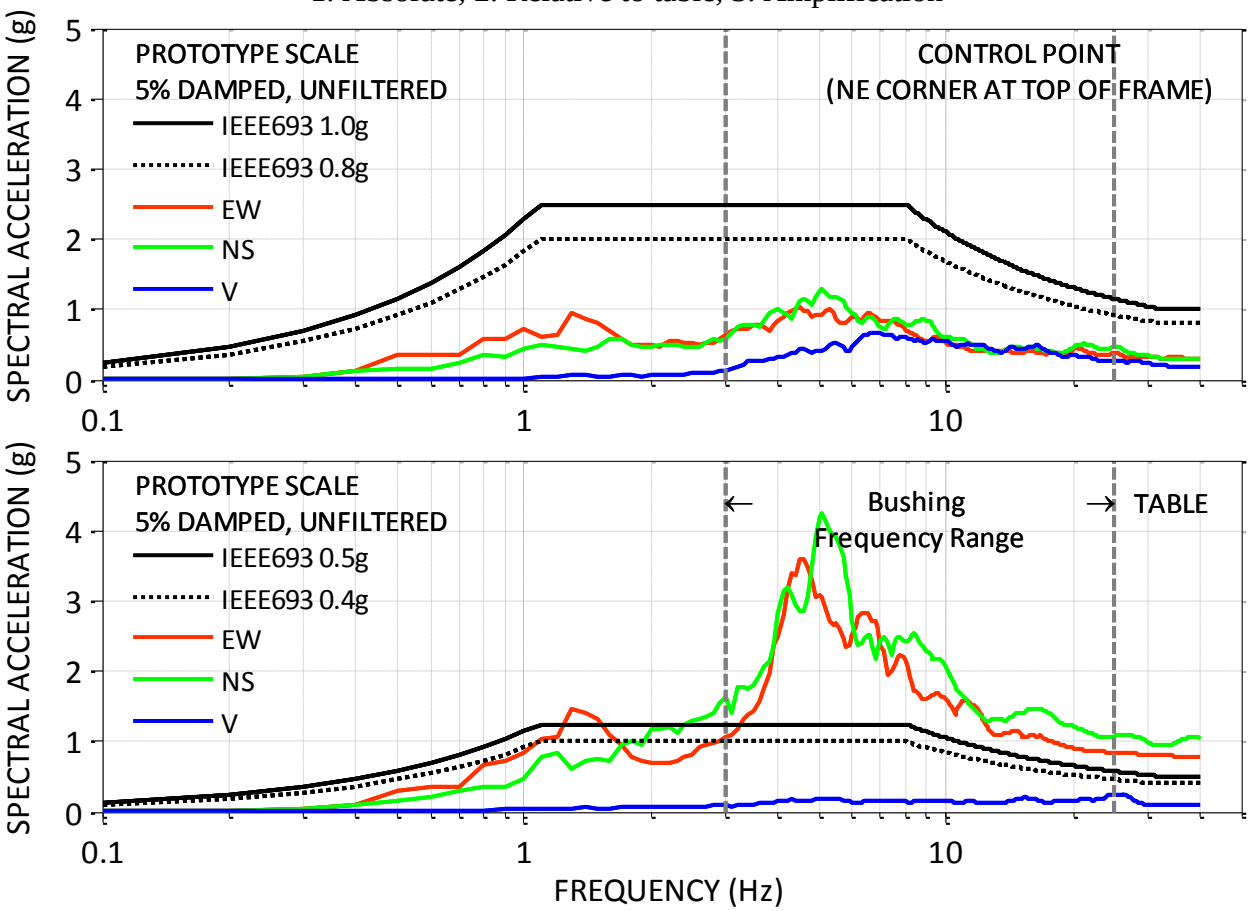
TRIPLE FP SYSTEM (Friction-Bolted Configuration)
CHILE 100% BI-AXIAL (EW in EW direction)
LENGTH SCALE=3 NON-SYMMETRIC BUSHING CONFIGURATION

Peak Table Motion								
Acceleration (g)			Velocity (in/sec)			Displacement (in)		
EW	NS	V	EW	NS	V	EW	NS	V
0.76	0.96	0.07	9.61	8.92	0.94	1.30	0.73	0.02

OBSERVATIONS

Peak Resultant Displacement (in)				Peak Acceleration (g)							
Bushing Top		Isolator	Torsional Ampl[3] Ratio (TA)	Bushing Top			Bushing Bottom		Control Point		
Abs[1]	Rel[2]			EW	NS	V	EW	NS	EW	NS	V
1.66	1.52	1.67	1.18	1.96	2.08	0.53	0.26	0.33	0.26	0.27	0.18

1. Absolute, 2. Relative to table, 3. Amplification



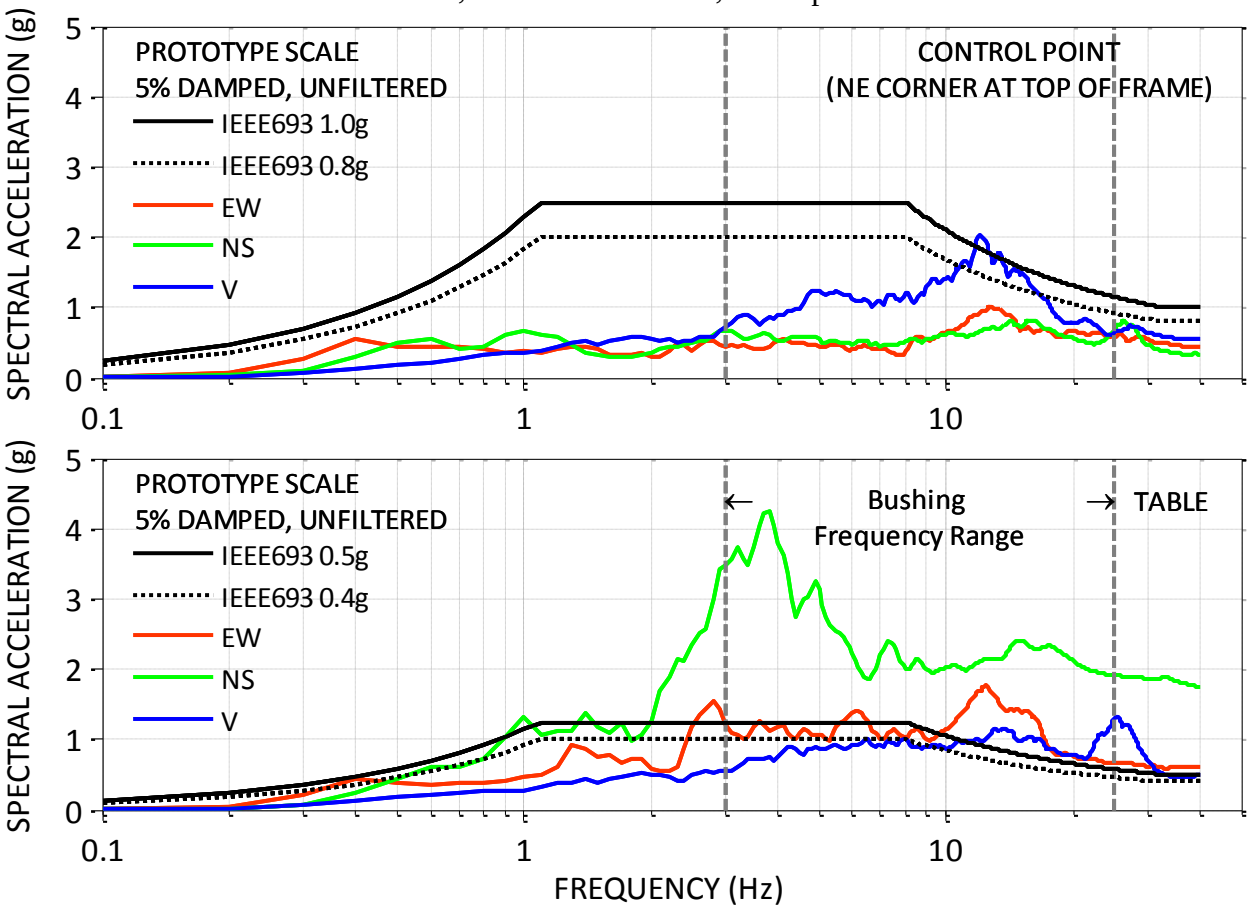
TRIPLE FP SYSTEM (Friction-Bolted Configuration)
JENSEN FILTER 97% TRI-AXIAL (FN in EW direction)
LENGTH SCALE=3 NON-SYMMETRIC BUSHING CONFIGURATION

Peak Table Motion								
Acceleration (g)			Velocity (in/sec)			Displacement (in)		
EW	NS	V	EW	NS	V	EW	NS	V
0.57	1.63	0.34	13.03	14.28	7.36	2.44	1.86	1.06

OBSERVATIONS
Uplift at NW isolator Sliding at friction connection of about 0.1 inches (NW)

Peak Resultant Displacement (in)				Peak Acceleration (g)							
Bushing Top		Isolator	Torsional Ampl[3] Ratio (TA)	Bushing Top			Bushing Bottom		Control Point		
Abs[1]	Rel[2]			EW	NS	V	EW	NS	EW	NS	V
3.31	2.32	2.37	1.01	3.82	1.36	2.18	0.41	0.30	0.38	0.28	0.42

1. Absolute, 2. Relative to table, 3. Amplification



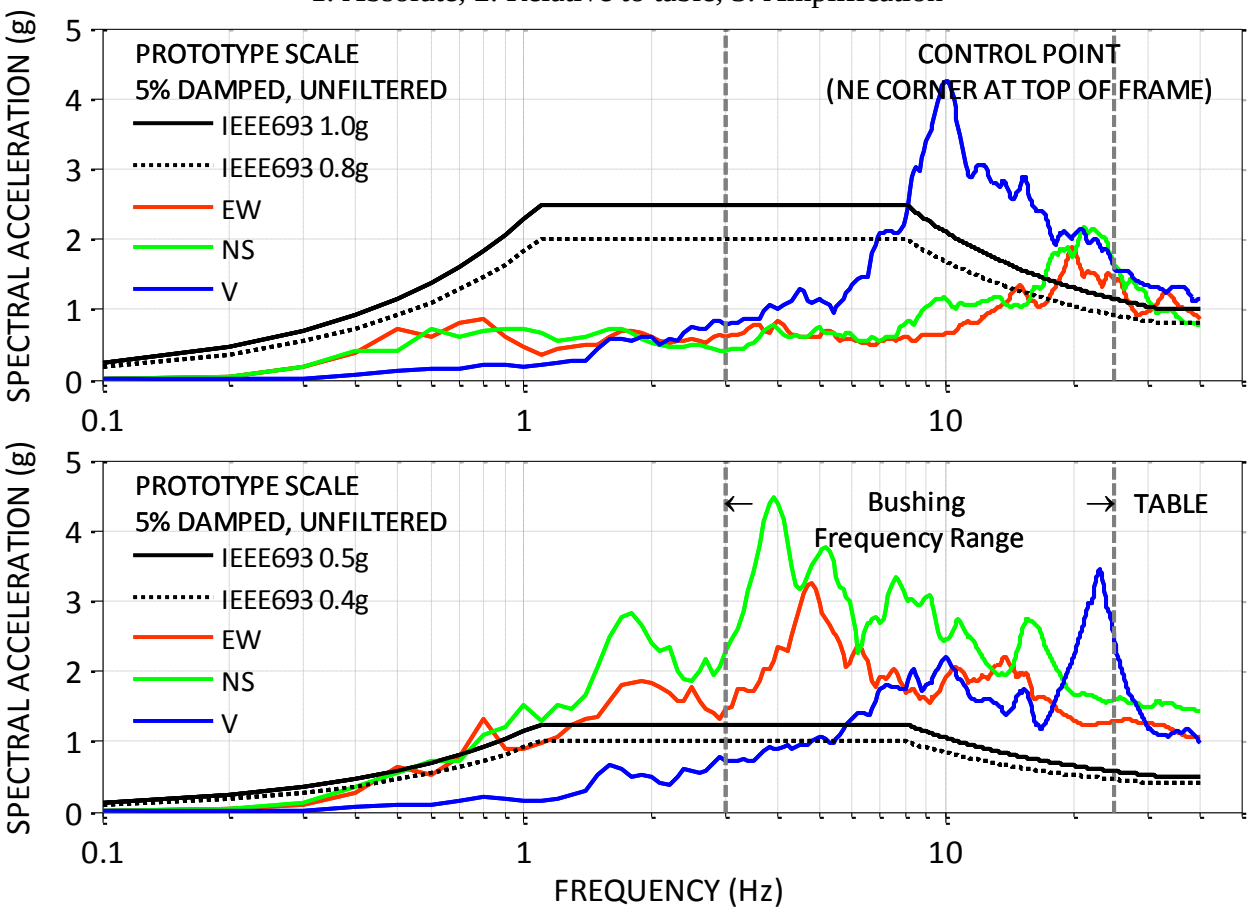
TRIPLE FP SYSTEM (Friction-Bolted Configuration)
EL CENTRO 300% TRI-AXIAL (N90W in EW direction)
LENGTH SCALE=3 NON-SYMMETRIC BUSHING CONFIGURATION

Peak Table Motion								
Acceleration (g)			Velocity (in/sec)			Displacement (in)		
EW	NS	V	EW	NS	V	EW	NS	V
1.03	1.37	0.74	19.96	19.22	5.15	2.22	2.44	0.59

OBSERVATIONS
Uplift at the NW isolator Sliding at friction connection of about 0.5 inches (NW)

Peak Resultant Displacement (in)				Peak Acceleration (g)							
Bushing Top		Isolator	Torsional Ampl[3] Ratio (TA)	Bushing Top			Bushing Bottom		Control Point		
Abs[1]	Rel[2]			EW	NS	V	EW	NS	EW	NS	V
3.61	4.42	4.40	1.00	4.03	2.16	2.21	0.55	0.47	0.55	0.46	0.91

1. Absolute, 2. Relative to table, 3. Amplification



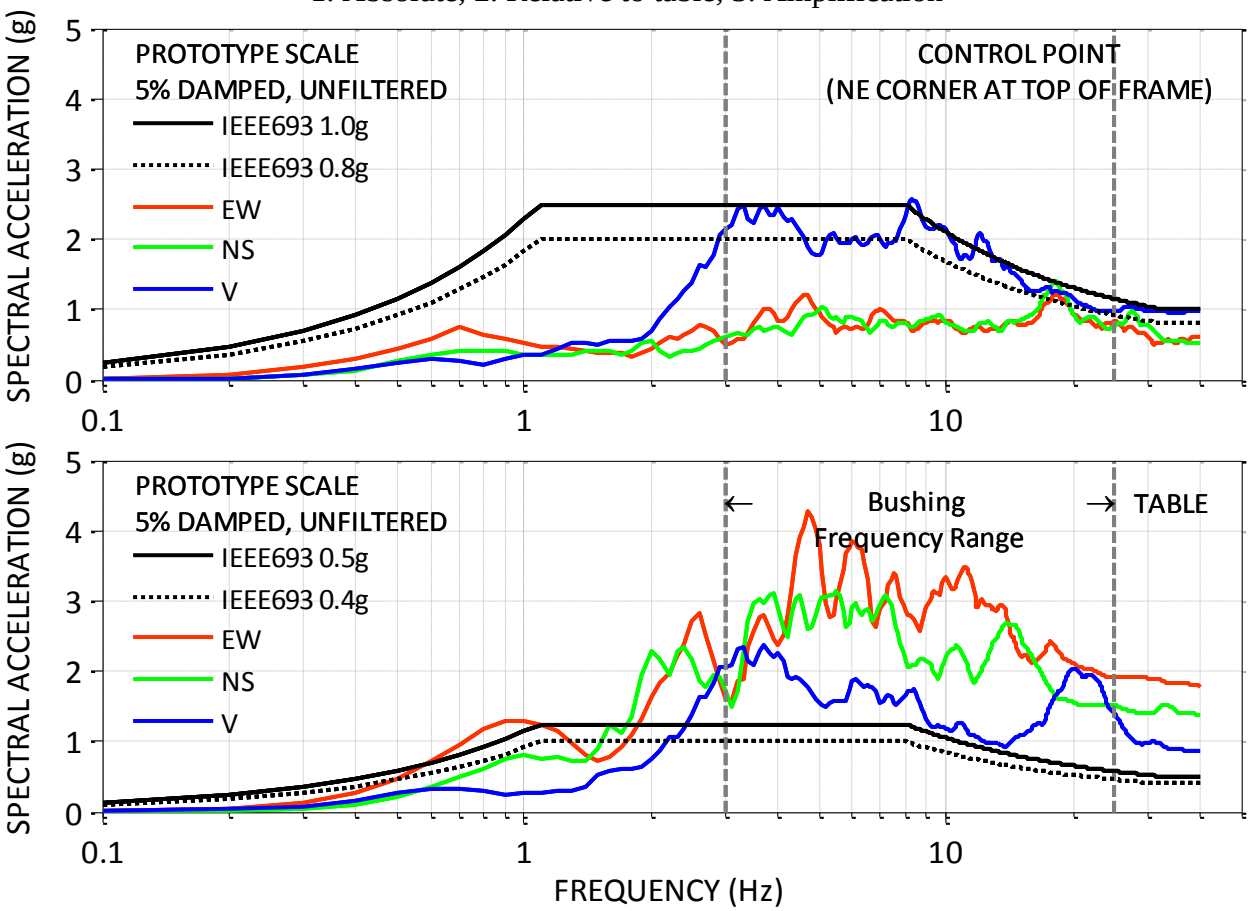
TRIPLE FP SYSTEM (Friction-Bolted Configuration)
PACOIMA DAM 100% TRI-AXIAL (S16E in EW direction)
LENGTH SCALE=3 NON-SYMMETRIC BUSHING CONFIGURATION

Peak Table Motion								
Acceleration (g)			Velocity (in/sec)			Displacement (in)		
EW	NS	V	EW	NS	V	EW	NS	V
1.67	1.33	0.85	23.21	15.34	9.95	2.63	1.49	1.43

OBSERVATIONS
Uplift at NW isolator Sliding at friction connection of about 0.1 inches (NW)

Peak Resultant Displacement (in)				Peak Acceleration (g)							
Bushing Top		Isolator	Torsional Ampl[3] Ratio (TA)	Bushing Top			Bushing Bottom		Control Point		
Abs[1]	Rel[2]			EW	NS	V	EW	NS	EW	NS	V
3.34	4.22	4.09	1.01	5.13	2.82	1.57	0.41	0.60	0.34	0.46	0.95

1. Absolute, 2. Relative to table, 3. Amplification



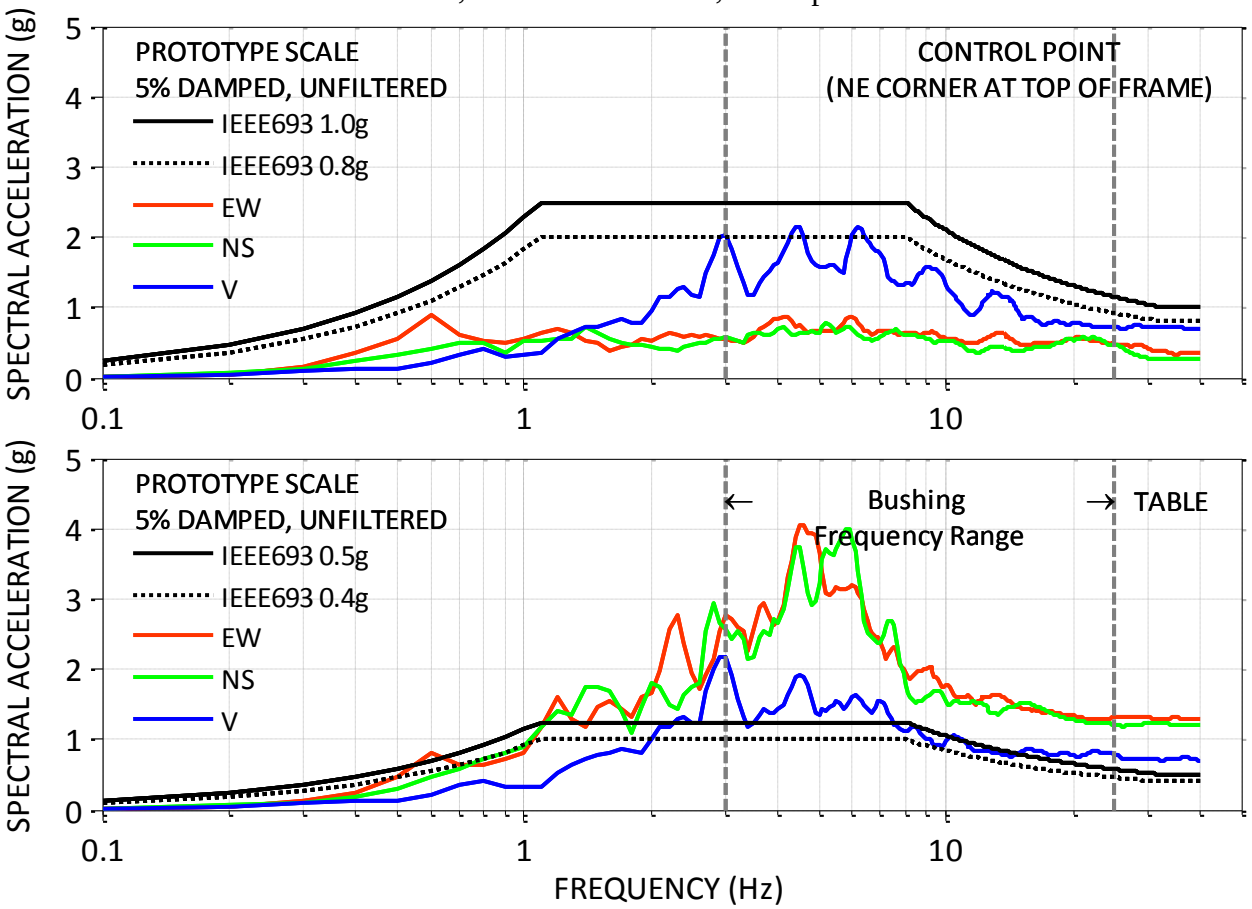
TRIPLE FP SYSTEM (Friction-Bolted Configuration)
TAFT 500% TRI-AXIAL (S69E in EW direction)
LENGTH SCALE=3 NON-SYMMETRIC BUSHING CONFIGURATION

Peak Table Motion								
Acceleration (g)			Velocity (in/sec)			Displacement (in)		
EW	NS	V	EW	NS	V	EW	NS	V
1.25	1.17	0.69	18.74	14.52	9.80	2.14	2.43	1.04

OBSERVATIONS
Uplift at NW isolator Sliding at friction connection of about 0.1 inches (NW)

Peak Resultant Displacement (in)				Peak Acceleration (g)							
Bushing Top		Isolator	Torsional Ampl[3] Ratio (TA)	Bushing Top			Bushing Bottom		Control Point		
Abs[1]	Rel[2]			EW	NS	V	EW	NS	EW	NS	V
3.87	2.82	2.82	1.02	2.91	1.79	1.28	0.33	0.24	0.31	0.23	0.69

1. Absolute, 2. Relative to table, 3. Amplification



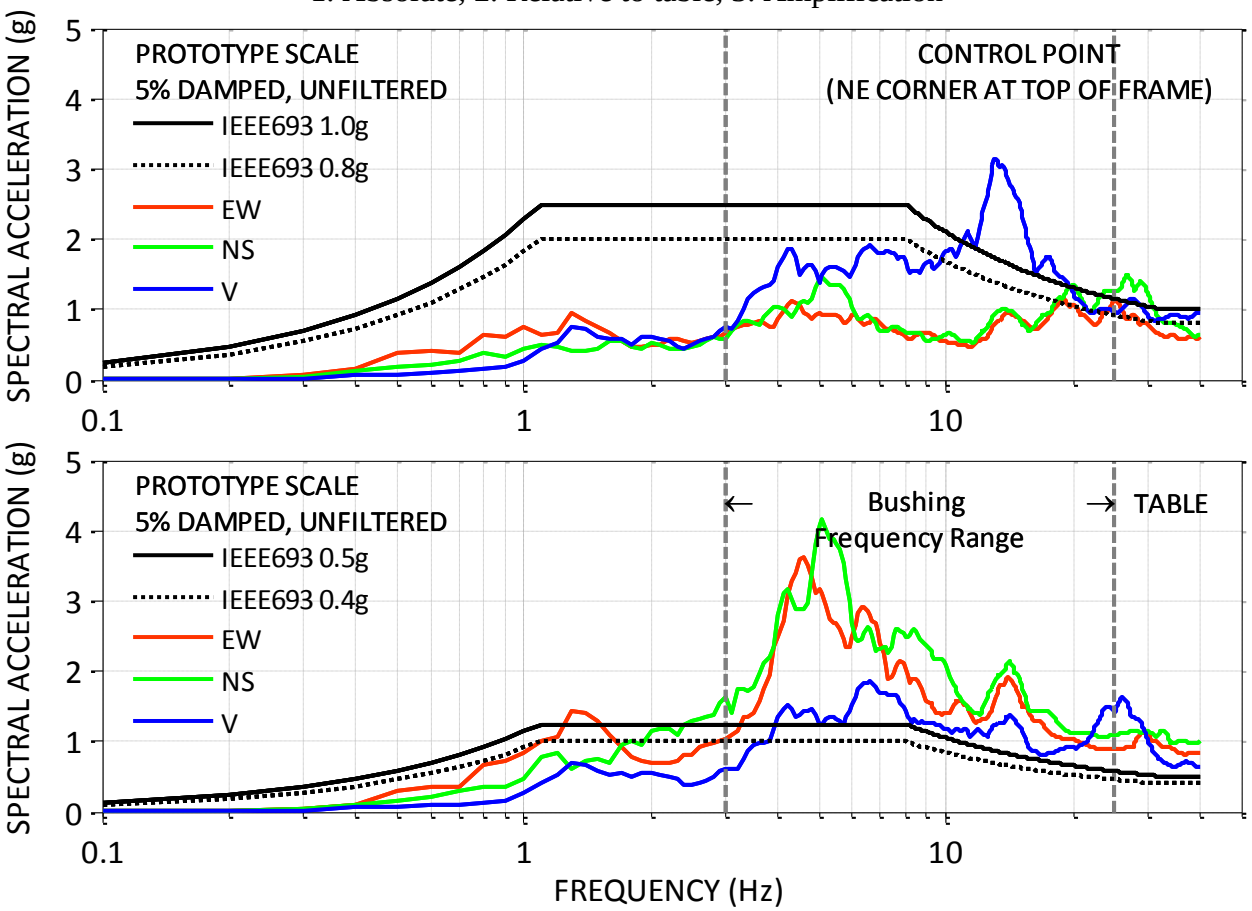
TRIPLE FP SYSTEM (Friction-Bolted Configuration)
CHILE 100% TRI-AXIAL (EW in EW direction)
LENGTH SCALE=3 NON-SYMMETRIC BUSHING CONFIGURATION

Peak Table Motion								
Acceleration (g)			Velocity (in/sec)			Displacement (in)		
EW	NS	V	EW	NS	V	EW	NS	V
0.79	0.93	0.54	9.37	9.35	4.85	1.30	0.73	0.44

OBSERVATIONS
Uplift at NW isolator

Peak Resultant Displacement (in)				Peak Acceleration (g)							
Bushing Top		Isolator	Torsional Ampl[3] Ratio (TA)	Bushing Top			Bushing Bottom		Control Point		
Abs[1]	Rel[2]			EW	NS	V	EW	NS	EW	NS	V
1.82	1.59	1.49	1.11	5.07	2.33	2.52	0.38	0.50	0.36	0.50	0.66

1. Absolute, 2. Relative to table, 3. Amplification



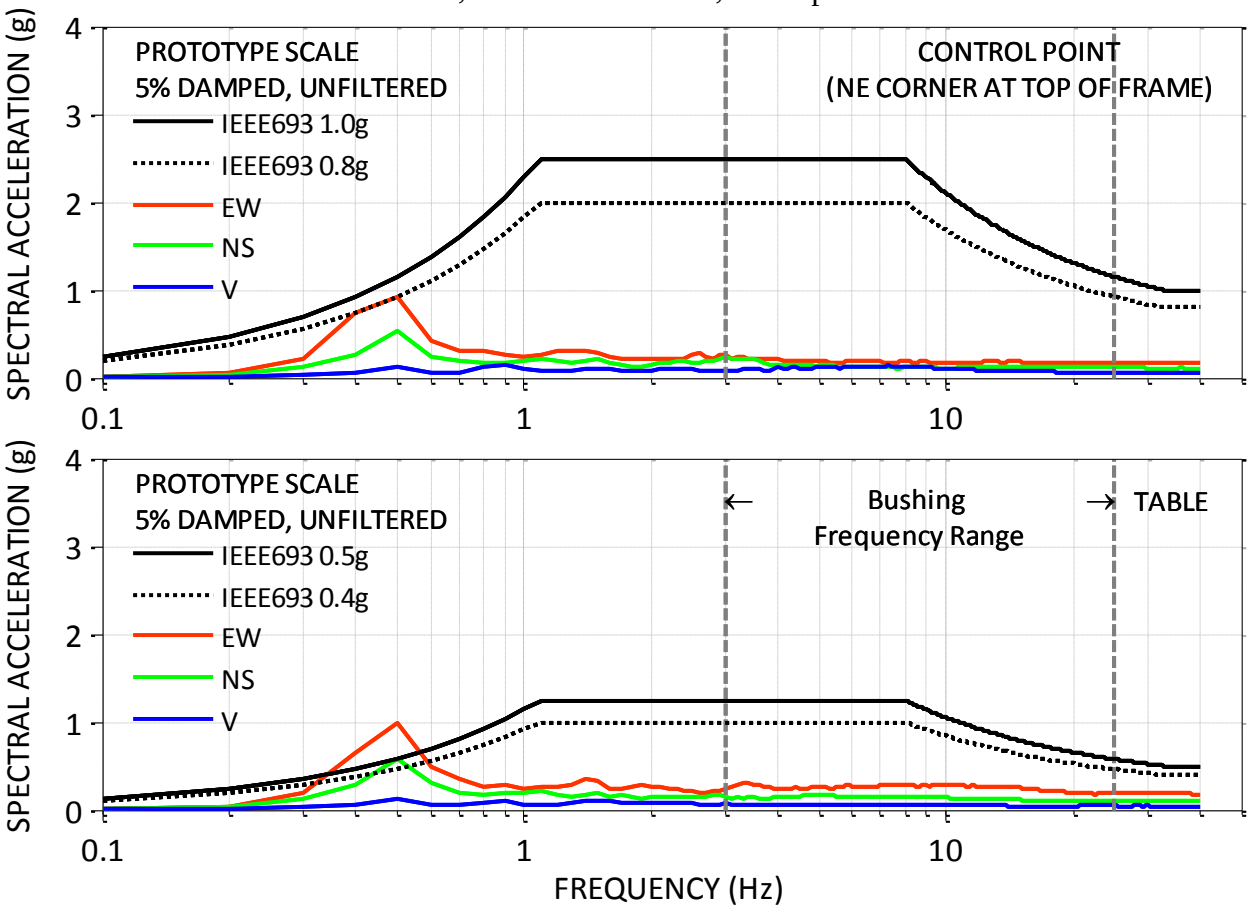
TRIPLE FP SYSTEM (Friction-Bolted Configuration)
MEXICO CITY 100% TRI-AXIAL (N90W in EW direction)
LENGTH SCALE=3 NON-SYMMETRIC BUSHING CONFIGURATION

Peak Table Motion								
Acceleration (g)			Velocity (in/sec)			Displacement (in)		
EW	NS	V	EW	NS	V	EW	NS	V
0.18	0.10	0.04	13.69	7.53	1.88	2.45	1.45	0.32

OBSERVATIONS
Uplift at NW isolator

Peak Resultant Displacement (in)				Peak Acceleration (g)							
Bushing Top		Isolator	Torsional Ampl[3] Ratio (TA)	Bushing Top			Bushing Bottom		Control Point		
Abs[1]	Rel[2]			EW	NS	V	EW	NS	EW	NS	V
3.15	1.93	2.11	1.09	0.31	0.20	0.09	0.17	0.10	0.16	0.11	0.06

1. Absolute, 2. Relative to table, 3. Amplification



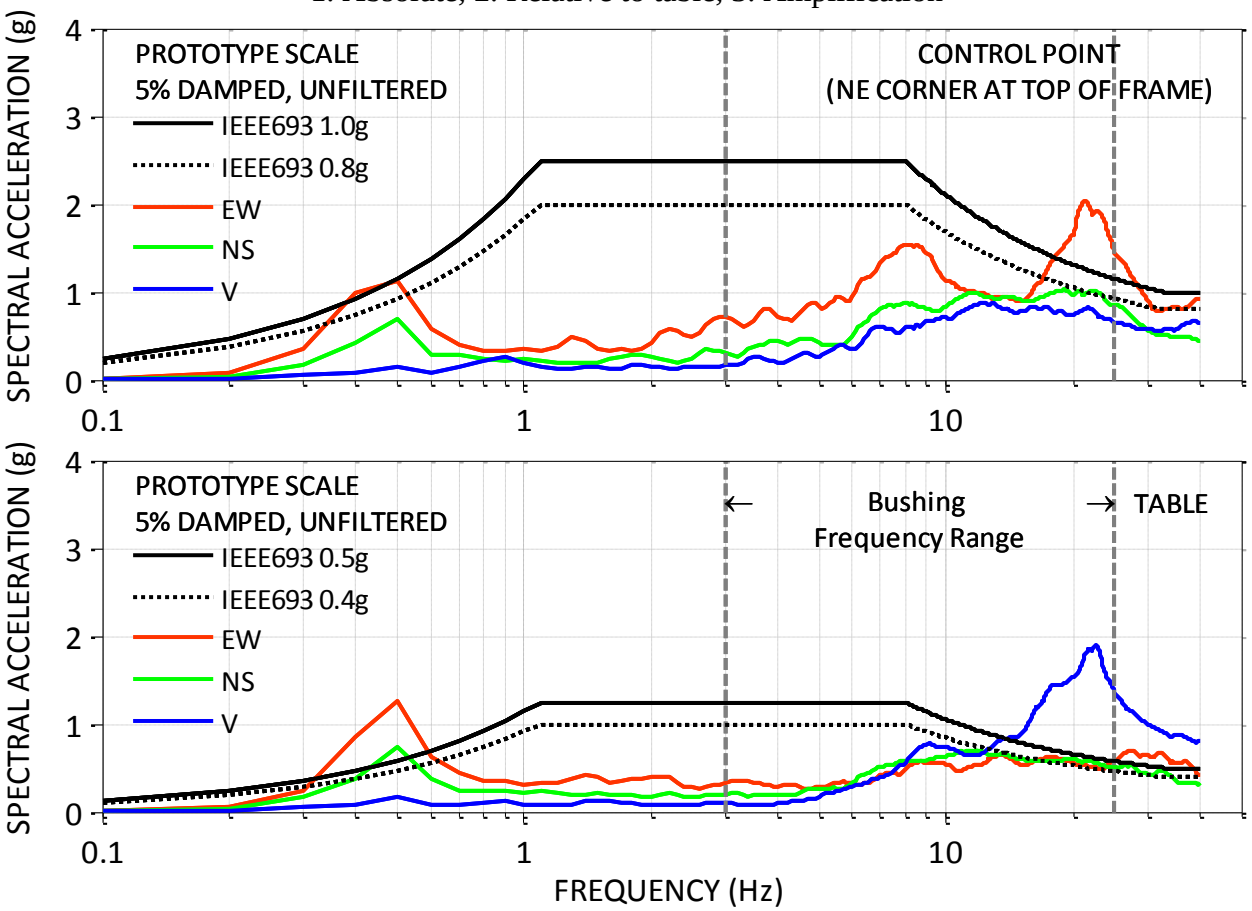
TRIPLE FP SYSTEM (Friction-Bolted Configuration)
MEXICO CITY 125% TRI-AXIAL (N90W in EW direction)
LENGTH SCALE=3 NON-SYMMETRIC BUSHING CONFIGURATION

Peak Table Motion								
Acceleration (g)			Velocity (in/sec)			Displacement (in)		
EW	NS	V	EW	NS	V	EW	NS	V
0.27	0.26	0.46	16.78	9.92	2.96	3.21	2.21	0.50

OBSERVATIONS
Displacement limit reached for isolators Uplift for NW isolator Sliding at friction connection of about 0.2 inches (NE), 0.8 inches (SE), 1.1 inches (SW) and 1.3 inches (NW)

Peak Resultant Displacement (in)				Peak Acceleration (g)							
Bushing Top		Isolator	Torsional Ampl[3] Ratio (TA)	Bushing Top			Bushing Bottom		Control Point		
Abs[1]	Rel[2]			EW	NS	V	EW	NS	EW	NS	V
5.12	5.75	6.26	1.07	2.23	3.35	1.37	0.62	0.59	0.62	0.40	0.40

1. Absolute, 2. Relative to table, 3. Amplification



PART B-3
SUMMARY OF EXPERIMENTAL DATA FOR TRIPLE FP SYSTEM
AT LENGTH SCALE OF 1

(PERCENTAGE AMOUNT IS SCALE FACTOR APPLIED TO ACCELERATION OF ACTUAL MOTION. FOR EXAMPLE, 100% DENOTES MOTION AS RECORDED, 200% DENOTES THAT ACCELERATION WAS SCALED UP BY FACTOR OF 2)

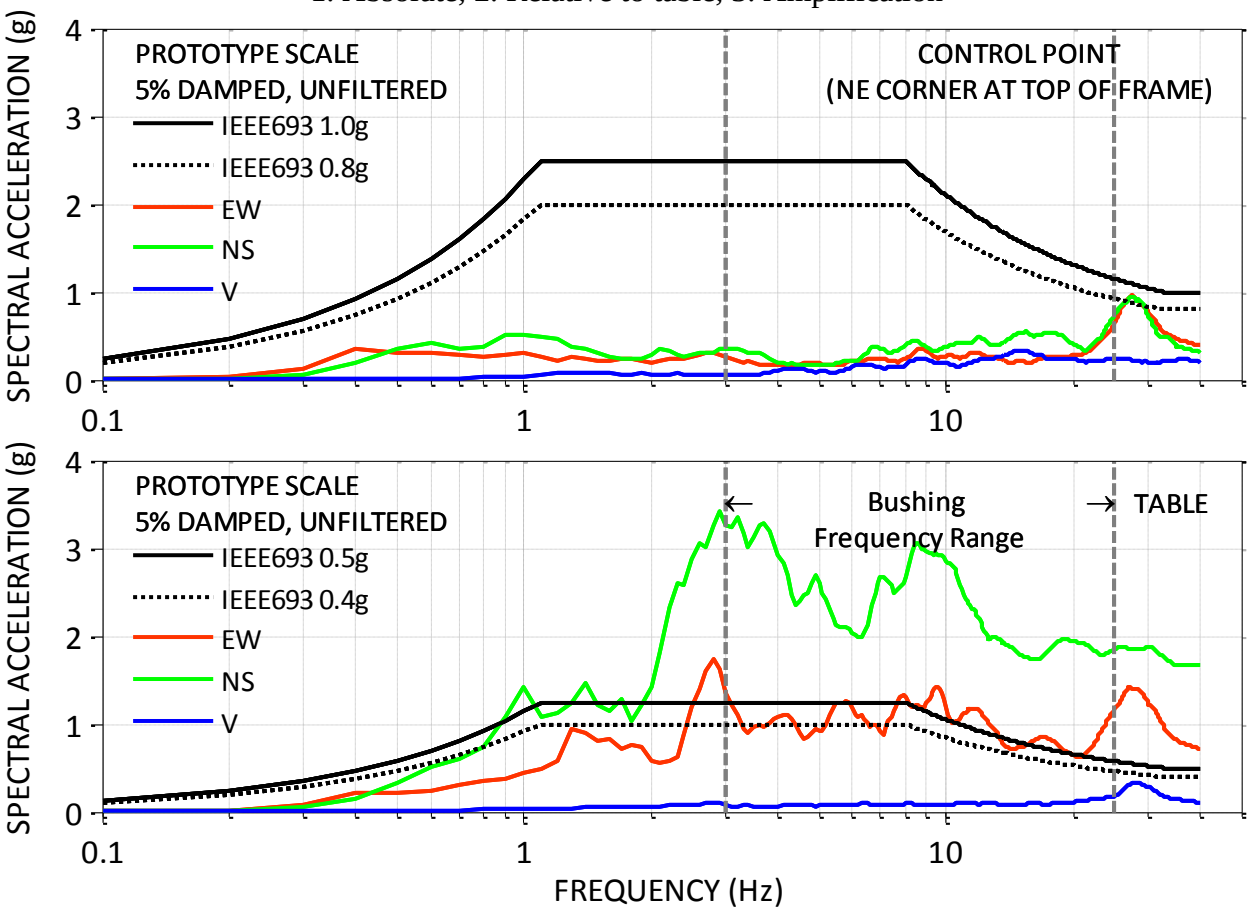
TRIPLE FP SYSTEM (Friction-Bolted Configuration)
JENSEN FILTER 97% BI-AXIAL (FN in EW direction)
LENGTH SCALE=1 SYMMETRIC BUSHING CONFIGURATION

Peak Table Motion								
Acceleration (g)			Velocity (in/sec)			Displacement (in)		
EW	NS	V	EW	NS	V	EW	NS	V
0.62	1.58	0.07	15.26	21.03	1.00	3.43	4.45	0.20

OBSERVATIONS

Peak Resultant Displacement (in)				Peak Acceleration (g)							
Bushing Top		Isolator	Torsional Ampl[3] Ratio (TA)	Bushing Top			Bushing Bottom		Control Point		
Abs[1]	Rel[2]			EW	NS	V	EW	NS	EW	NS	V
5.97	7.20	7.56	1.05	0.63	1.26	0.29	0.22	0.20	0.24	0.18	0.09

1. Absolute, 2. Relative to table, 3. Amplification



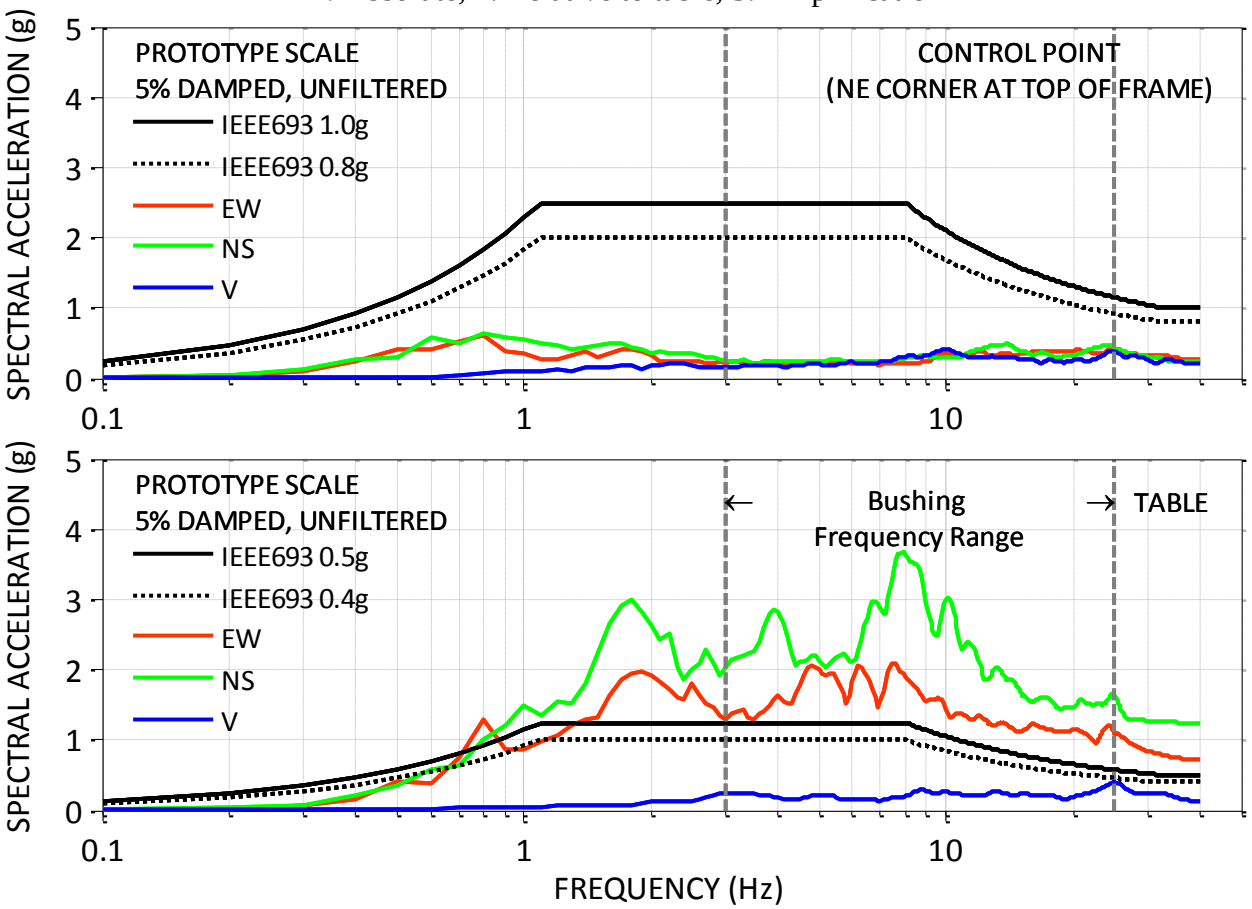
TRIPLE FP SYSTEM (Friction-Bolted Configuration)
EL CENTRO 300% BI-AXIAL (N90W in EW direction)
LENGTH SCALE=1 SYMMETRIC BUSHING CONFIGURATION

Peak Table Motion								
Acceleration (g)			Velocity (in/sec)			Displacement (in)		
EW	NS	V	EW	NS	V	EW	NS	V
0.69	1.20	0.12	30.88	34.07	1.60	4.56	5.49	0.25

OBSERVATIONS

Peak Resultant Displacement (in)				Peak Acceleration (g)							
Bushing Top		Isolator	Torsional Ampl[3] Ratio (TA)	Bushing Top			Bushing Bottom		Control Point		
Abs[1]	Rel[2]			EW	NS	V	EW	NS	EW	NS	V
6.95	10.85	10.99	1.02	0.65	1.29	0.41	0.23	0.22	0.24	0.22	0.19

1. Absolute, 2. Relative to table, 3. Amplification



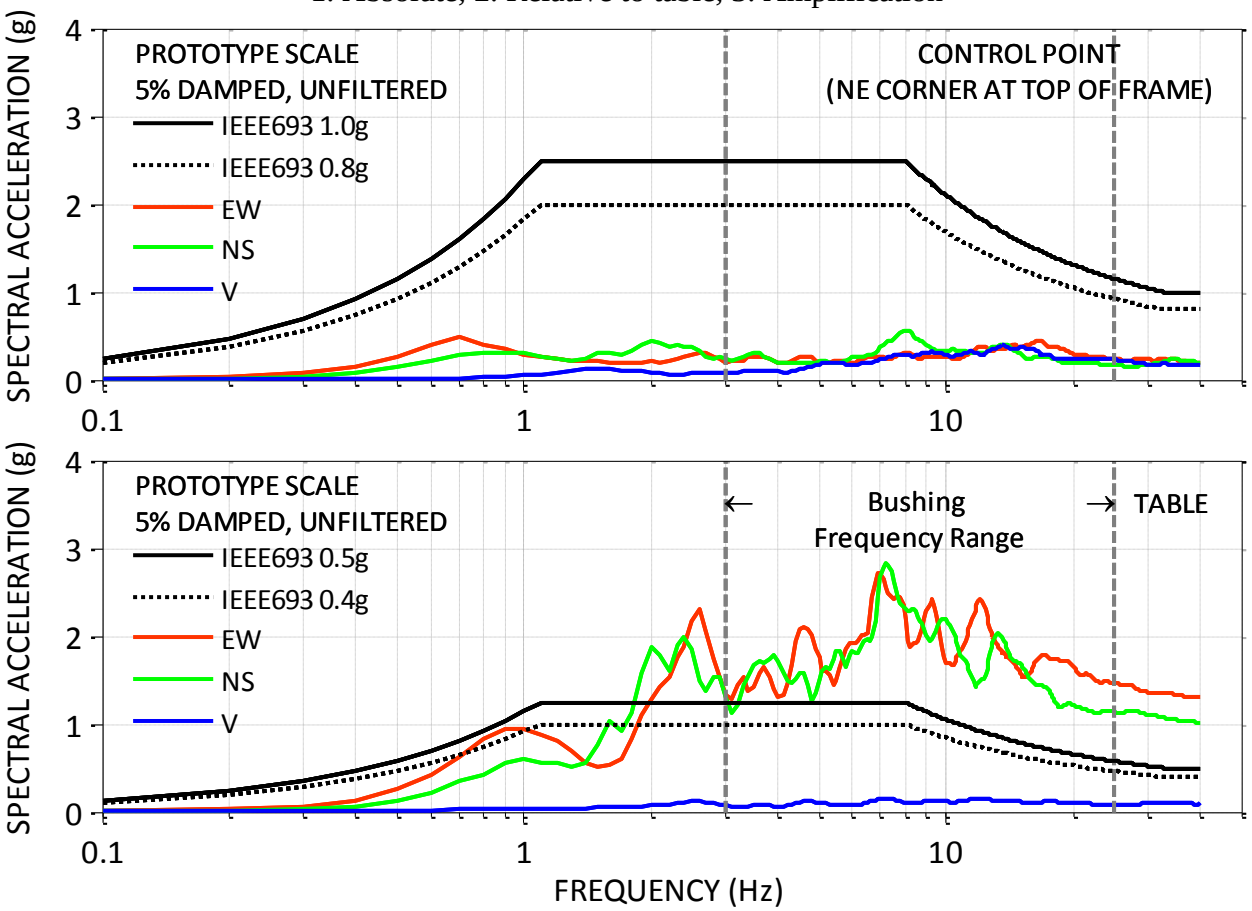
TRIPLE FP SYSTEM (Friction-Bolted Configuration)
PACOIMA DAM 75% BI-AXIAL (S16E in EW direction)
LENGTH SCALE=1 SYMMETRIC BUSHING CONFIGURATION

Peak Table Motion								
Acceleration (g)			Velocity (in/sec)			Displacement (in)		
EW	NS	V	EW	NS	V	EW	NS	V
1.26	0.92	0.07	23.82	17.94	1.15	4.54	2.93	0.17

OBSERVATIONS

Peak Resultant Displacement (in)				Peak Acceleration (g)							
Bushing Top		Isolator	Torsional Ampl[3] Ratio (TA)	Bushing Top			Bushing Bottom		Control Point		
Abs[1]	Rel[2]			EW	NS	V	EW	NS	EW	NS	V
4.79	7.88	8.30	1.06	0.59	0.87	0.30	0.16	0.14	0.16	0.13	0.14

1. Absolute, 2. Relative to table, 3. Amplification



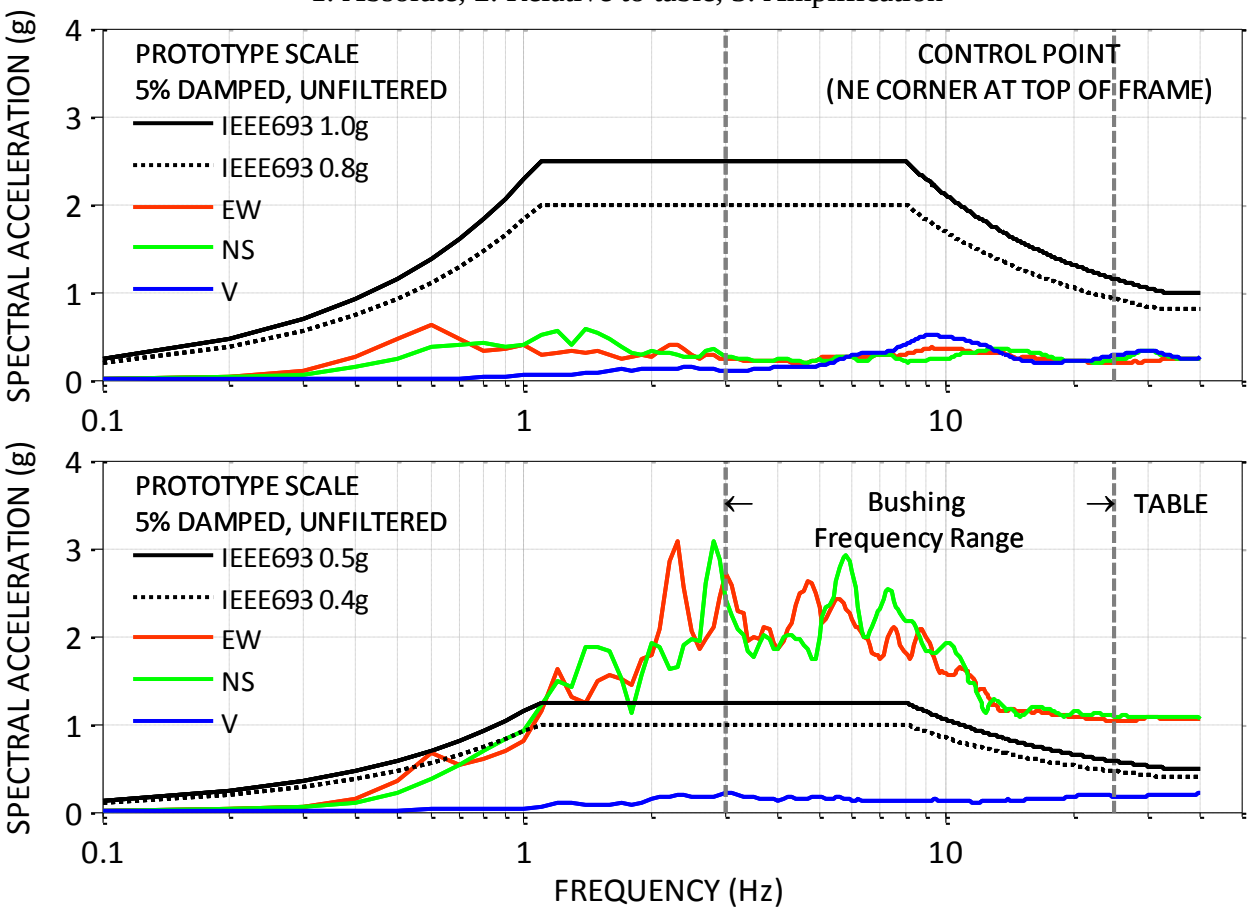
TRIPLE FP SYSTEM (Friction-Bolted Configuration)
TAFT 500% BI-AXIAL (S69E in EW direction)
LENGTH SCALE=1 SYMMETRIC BUSHING CONFIGURATION

Peak Table Motion								
Acceleration (g)			Velocity (in/sec)			Displacement (in)		
EW	NS	V	EW	NS	V	EW	NS	V
1.01	1.02	0.12	26.06	21.54	1.44	4.64	5.01	0.25

OBSERVATIONS

Peak Resultant Displacement (in)				Peak Acceleration (g)							
Bushing Top		Isolator	Torsional Ampl[3] Ratio (TA)	Bushing Top			Bushing Bottom		Control Point		
Abs[1]	Rel[2]			EW	NS	V	EW	NS	EW	NS	V
6.10	7.65	8.35	1.11	1.10	0.93	0.30	0.17	0.19	0.17	0.19	0.20

1. Absolute, 2. Relative to table, 3. Amplification



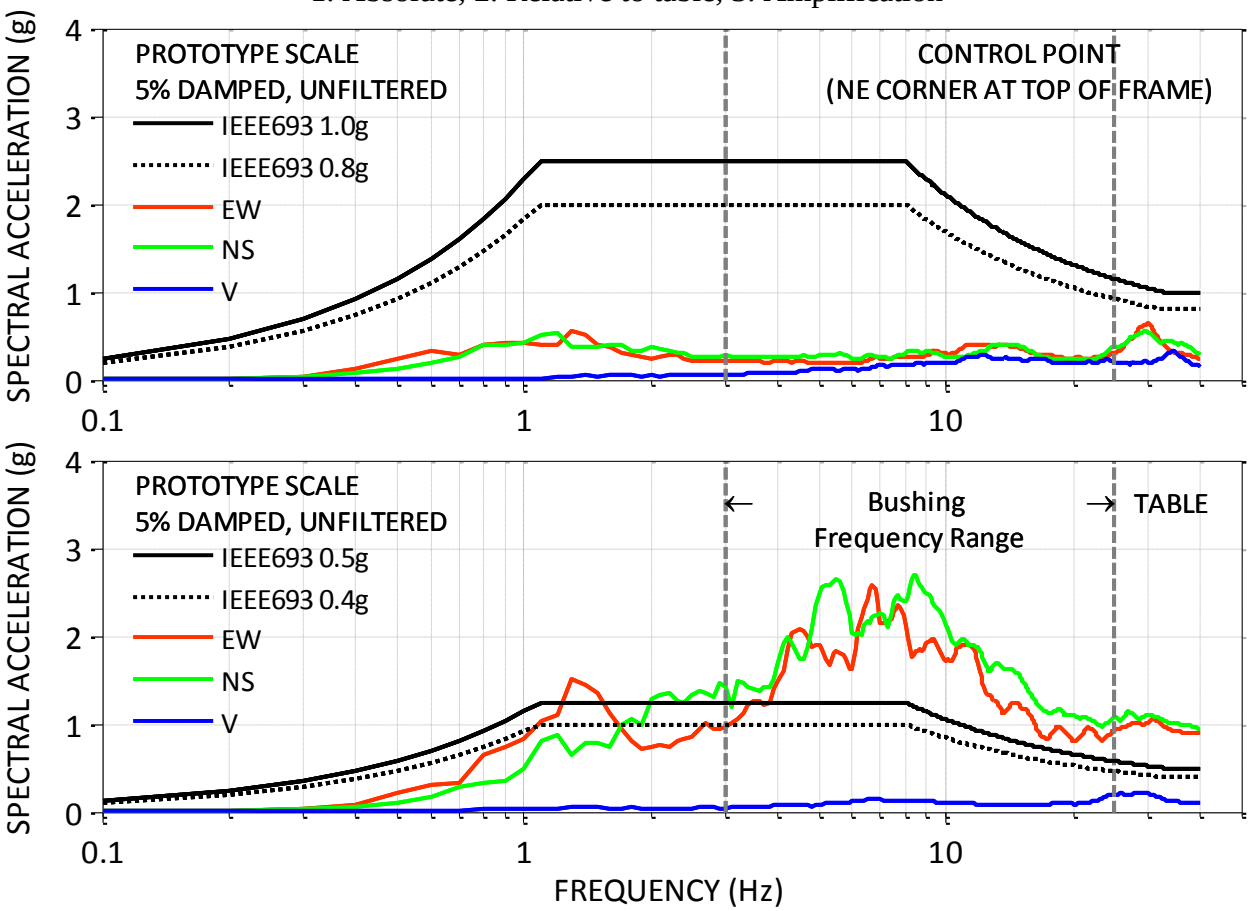
TRIPLE FP SYSTEM (Friction-Bolted Configuration)
CHILE 100% BI-AXIAL (EW in EW direction)
LENGTH SCALE=1 SYMMETRIC BUSHING CONFIGURATION

Peak Table Motion								
Acceleration (g)			Velocity (in/sec)			Displacement (in)		
EW	NS	V	EW	NS	V	EW	NS	V
0.80	0.81	0.06	15.98	13.11	0.76	2.92	1.83	0.10

OBSERVATIONS

Peak Resultant Displacement (in)				Peak Acceleration (g)							
Bushing Top		Isolator	Torsional Ampl[3] Ratio (TA)	Bushing Top			Bushing Bottom		Control Point		
Abs[1]	Rel[2]			EW	NS	V	EW	NS	EW	NS	V
3.96	5.32	5.56	1.04	0.75	0.83	0.28	0.15	0.18	0.16	0.16	0.10

1. Absolute, 2. Relative to table, 3. Amplification



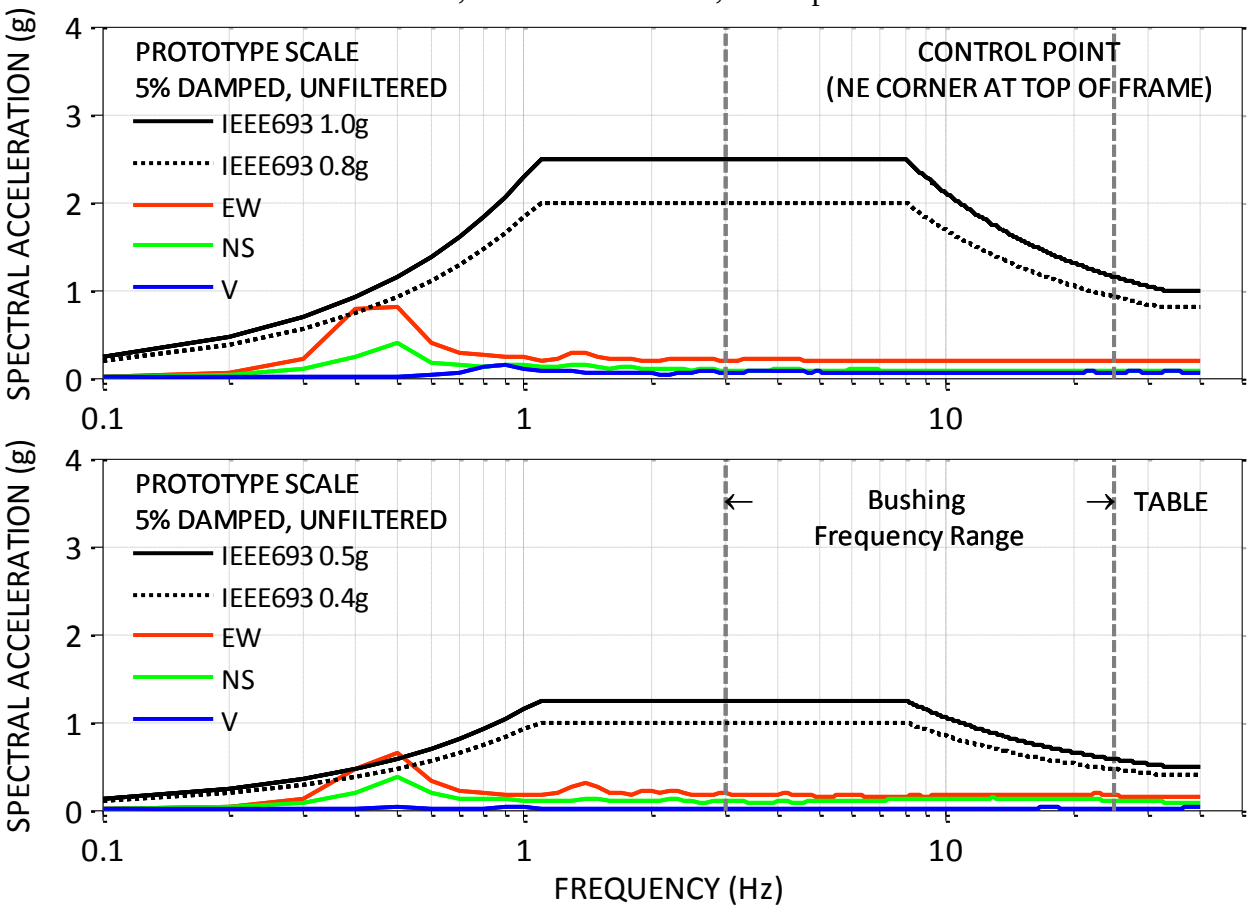
TRIPLE FP SYSTEM (Friction-Bolted Configuration)
MEXICO 70% BI-AXIAL (N90W in EW direction)
LENGTH SCALE=1 SYMMETRIC BUSHING CONFIGURATION

Peak Table Motion								
Acceleration (g)			Velocity (in/sec)			Displacement (in)		
EW	NS	V	EW	NS	V	EW	NS	V
0.13	0.08	0.01	15.01	8.68	0.91	5.06	3.45	0.29

OBSERVATIONS

Peak Resultant Displacement (in)				Peak Acceleration (g)							
Bushing Top		Isolator	Torsional Ampl[3] Ratio (TA)	Bushing Top			Bushing Bottom		Control Point		
Abs[1]	Rel[2]			EW	NS	V	EW	NS	EW	NS	V
10.00	9.86	11.10	1.16	0.22	0.16	0.06	0.17	0.11	0.19	0.07	0.04

1. Absolute, 2. Relative to table, 3. Amplification



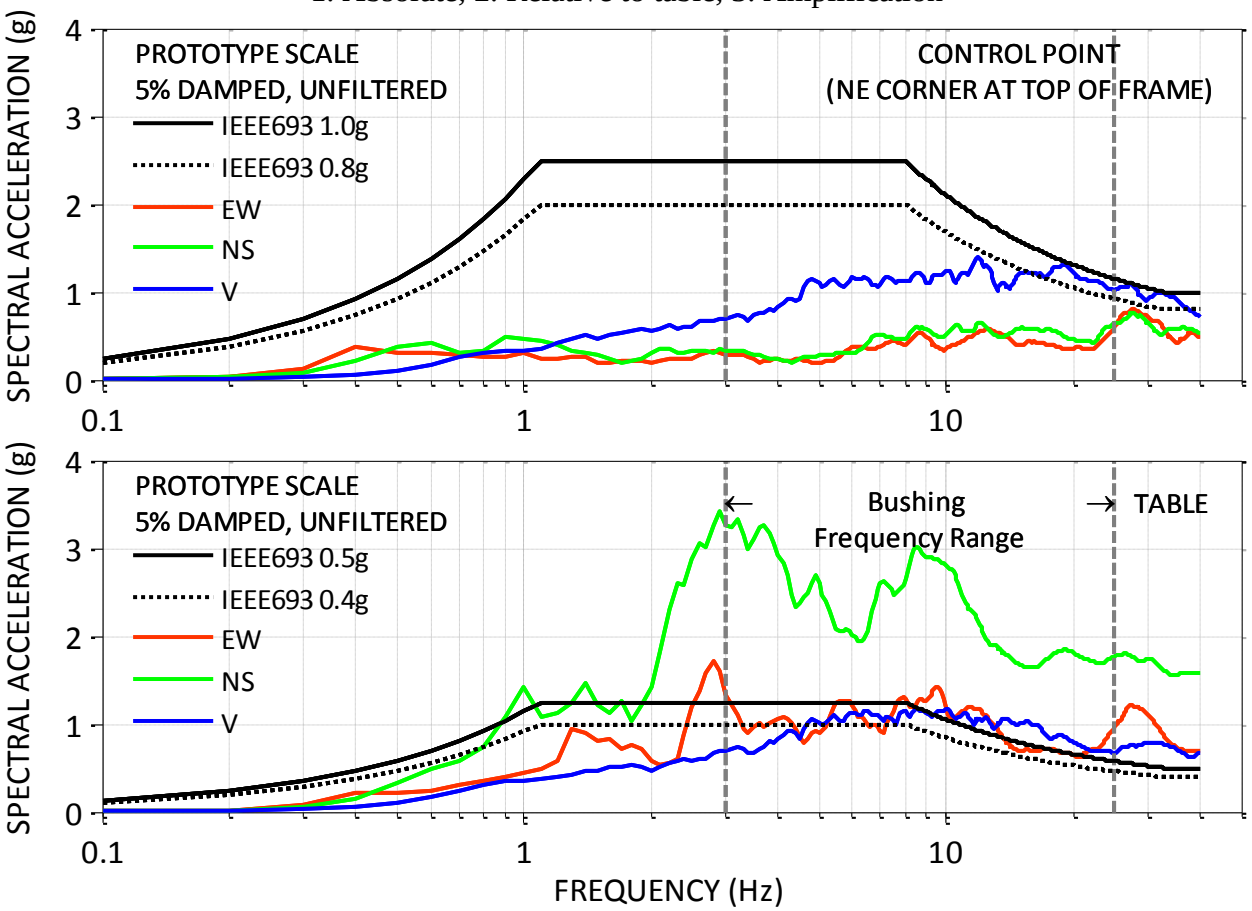
TRIPLE FP SYSTEM (Friction-Bolted Configuration)
JENSEN FILTER 97% TRI-AXIAL (FN in EW direction)
LENGTH SCALE=1 SYMMETRIC BUSHING CONFIGURATION

Peak Table Motion								
Acceleration (g)			Velocity (in/sec)			Displacement (in)		
EW	NS	V	EW	NS	V	EW	NS	V
0.58	1.53	0.55	15.20	21.12	9.29	3.41	4.41	1.44

OBSERVATIONS

Peak Resultant Displacement (in)				Peak Acceleration (g)							
Bushing Top		Isolator	Torsional Ampl[3] Ratio (TA)	Bushing Top			Bushing Bottom		Control Point		
Abs[1]	Rel[2]			EW	NS	V	EW	NS	EW	NS	V
5.78	6.93	7.17	1.03	1.43	1.56	2.10	0.26	0.33	0.24	0.28	0.62

1. Absolute, 2. Relative to table, 3. Amplification



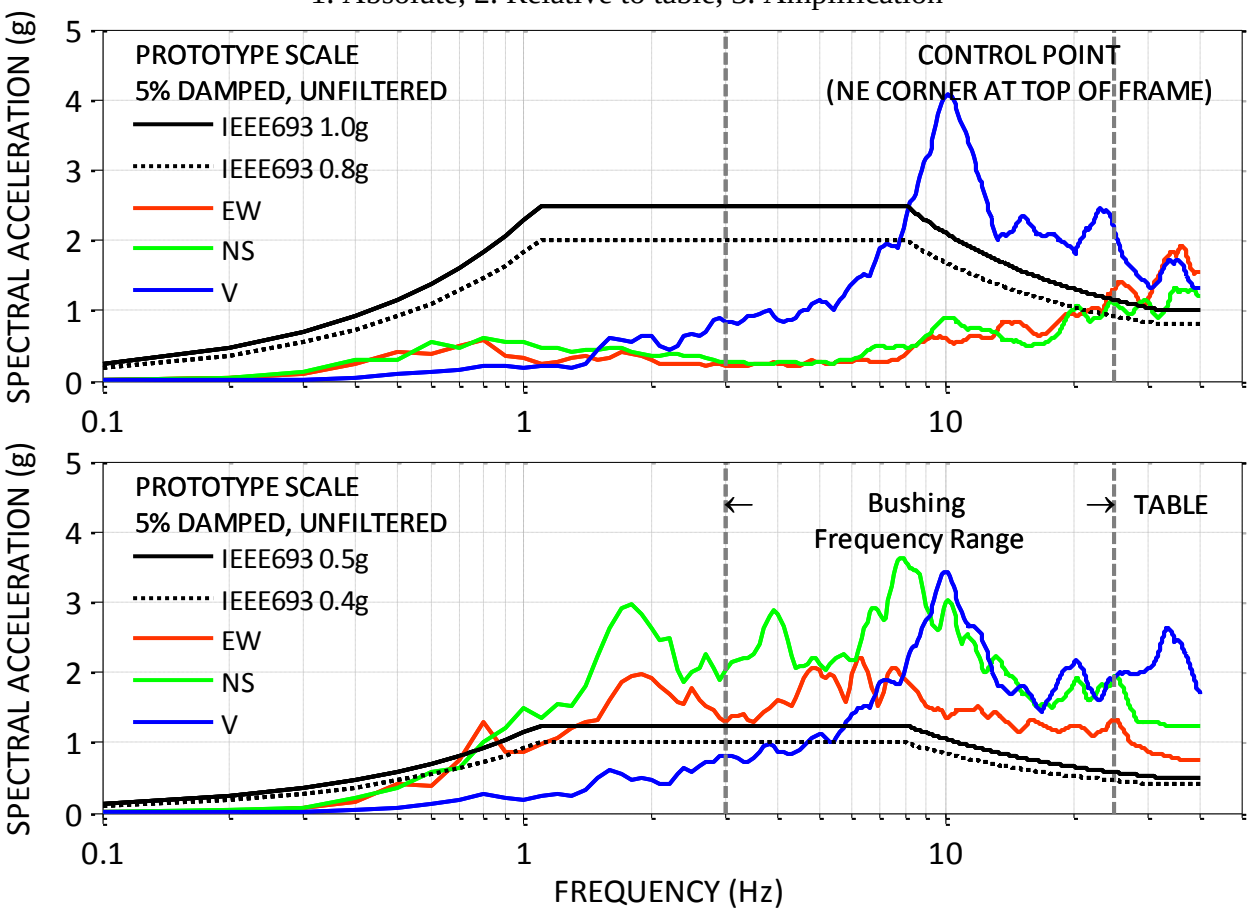
TRIPLE FP SYSTEM (Friction-Bolted Configuration)
EL CENTRO 300% TRI-AXIAL (N90W in EW direction)
LENGTH SCALE=1 SYMMETRIC BUSHING CONFIGURATION

Peak Table Motion								
Acceleration (g)			Velocity (in/sec)			Displacement (in)		
EW	NS	V	EW	NS	V	EW	NS	V
0.70	1.20	0.84	31.02	34.06	9.26	4.56	5.46	1.24

OBSERVATIONS

Peak Resultant Displacement (in)				Peak Acceleration (g)							
Bushing Top		Isolator	Torsional Ampl[3] Ratio (TA)	Bushing Top			Bushing Bottom		Control Point		
Abs[1]	Rel[2]			EW	NS	V	EW	NS	EW	NS	V
7.13	11.08	11.15	1.01	3.01	3.33	2.72	0.37	0.44	0.44	0.38	0.91

1. Absolute, 2. Relative to table, 3. Amplification



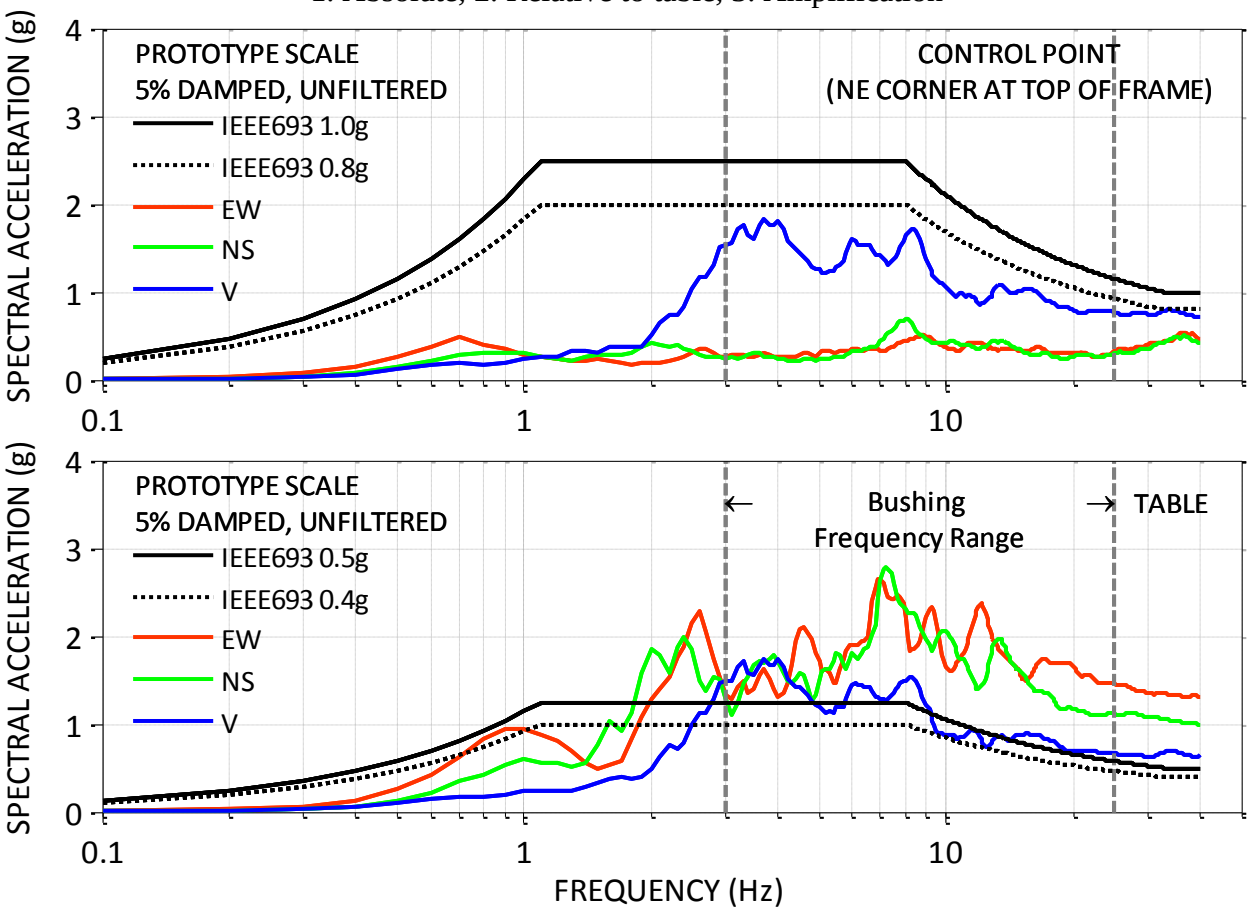
TRIPLE FP SYSTEM (Friction-Bolted Configuration)
PACOIMA DAM 75% TRI-AXIAL (S16E in EW direction)
LENGTH SCALE=1 SYMMETRIC BUSHING CONFIGURATION

Peak Table Motion								
Acceleration (g)			Velocity (in/sec)			Displacement (in)		
EW	NS	V	EW	NS	V	EW	NS	V
1.25	0.91	0.62	23.78	18.22	11.67	4.36	3.01	1.76

OBSERVATIONS
Uplift at NW isolator

Peak Resultant Displacement (in)				Peak Acceleration (g)							
Bushing Top		Isolator	Torsional Ampl[3] Ratio (TA)	Bushing Top			Bushing Bottom		Control Point		
Abs[1]	Rel[2]			EW	NS	V	EW	NS	EW	NS	V
5.00	7.76	8.05	1.06	0.99	1.09	1.20	0.20	0.25	0.22	0.17	0.70

1. Absolute, 2. Relative to table, 3. Amplification



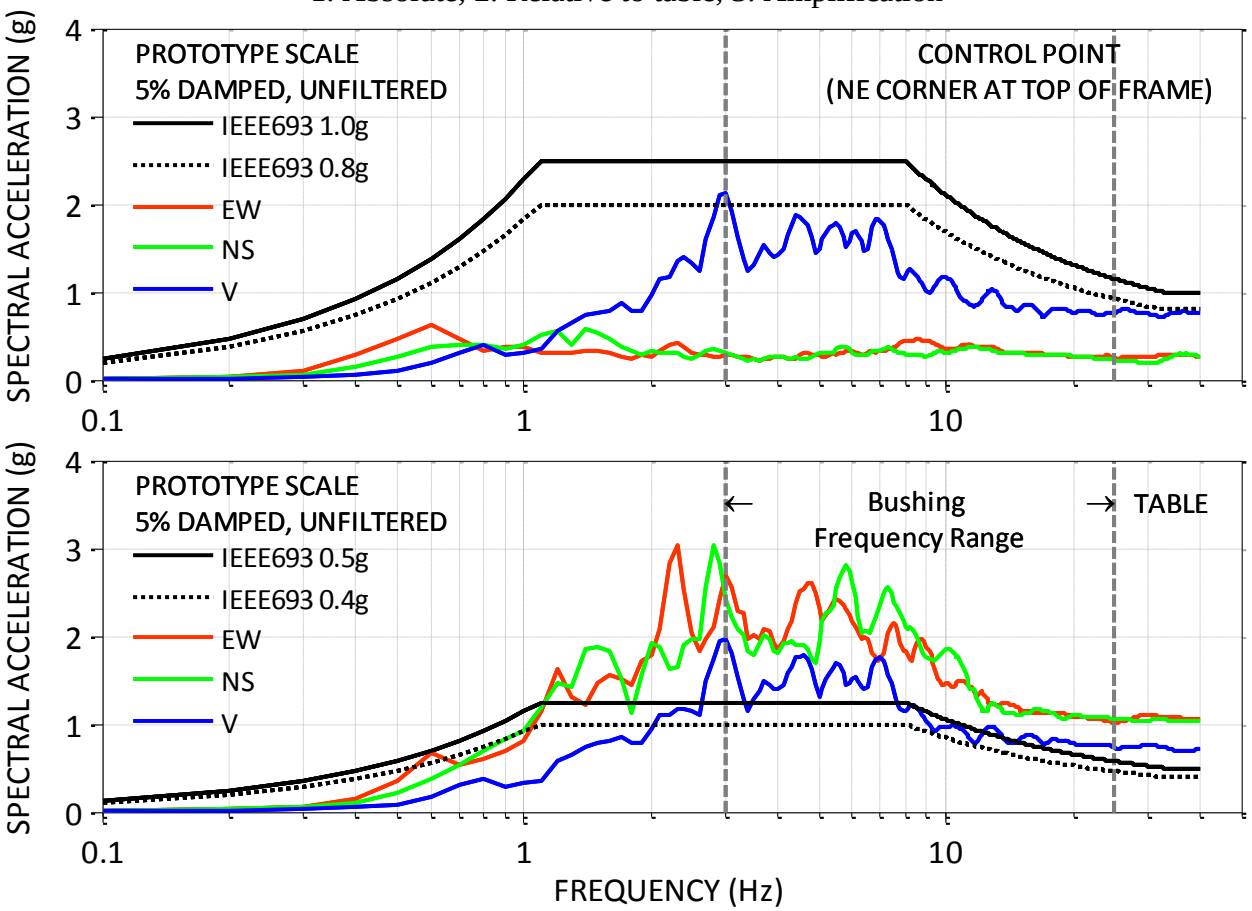
TRIPLE FP SYSTEM (Friction-Bolted Configuration)
TAFT 500% TRI-AXIAL (S69E in EW direction)
LENGTH SCALE=1 SYMMETRIC BUSHING CONFIGURATION

Peak Table Motion								
Acceleration (g)			Velocity (in/sec)			Displacement (in)		
EW	NS	V	EW	NS	V	EW	NS	V
1.02	0.99	0.70	25.67	21.90	16.01	4.62	5.01	1.80

OBSERVATIONS
Sliding of about 0.1 inches (NW)

Peak Resultant Displacement (in)				Peak Acceleration (g)							
Bushing Top		Isolator	Torsional Ampl[3] Ratio (TA)	Bushing Top			Bushing Bottom		Control Point		
Abs[1]	Rel[2]			EW	NS	V	EW	NS	EW	NS	V
6.55	7.58	8.15	1.10	1.19	0.92	1.07	0.22	0.18	0.23	0.17	0.71

1. Absolute, 2. Relative to table, 3. Amplification



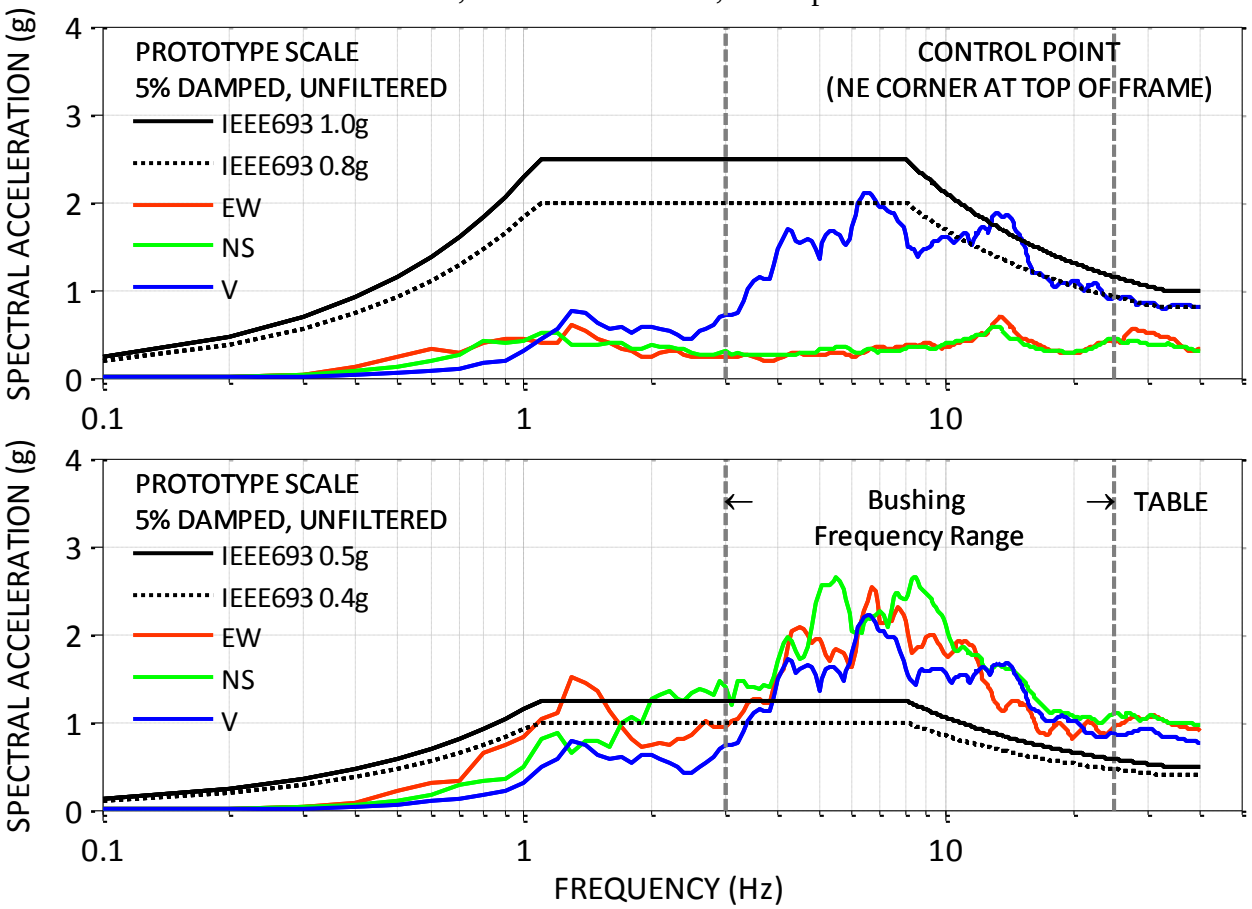
TRIPLE FP SYSTEM (Friction-Bolted Configuration)
CHILE 100% TRI-AXIAL (EW in EW direction)
LENGTH SCALE=1 SYMMETRIC BUSHING CONFIGURATION

Peak Table Motion								
Acceleration (g)			Velocity (in/sec)			Displacement (in)		
EW	NS	V	EW	NS	V	EW	NS	V
0.81	0.81	0.69	16.14	12.96	9.06	2.92	1.82	0.95

OBSERVATIONS

Peak Resultant Displacement (in)				Peak Acceleration (g)							
Bushing Top		Isolator	Torsional Ampl[3] Ratio (TA)	Bushing Top			Bushing Bottom		Control Point		
Abs[1]	Rel[2]			EW	NS	V	EW	NS	EW	NS	V
3.89	5.08	5.31	1.04	1.51	1.29	2.68	0.20	0.23	0.19	0.19	0.68

1. Absolute, 2. Relative to table, 3. Amplification



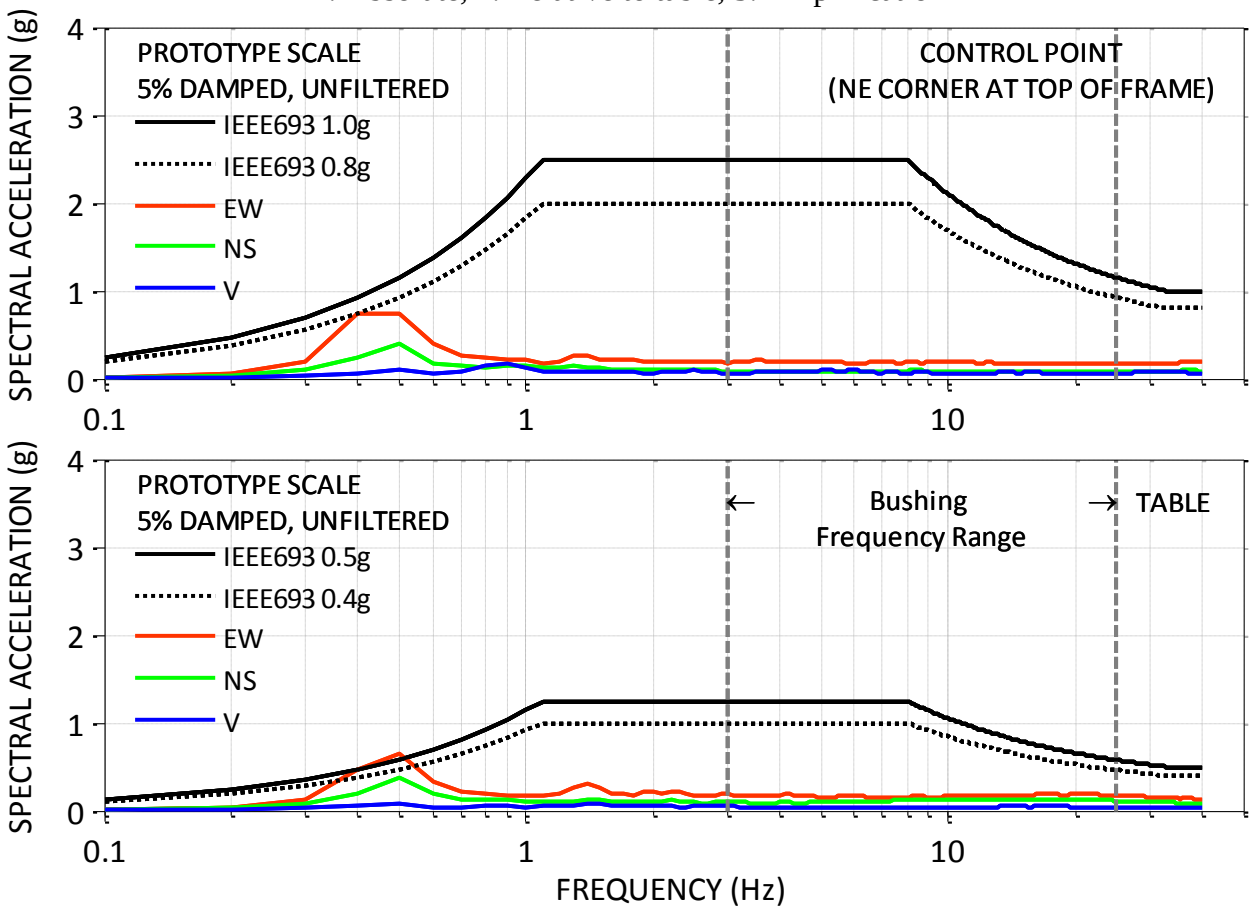
TRIPLE FP SYSTEM (Friction-Bolted Configuration)
MEXICO 70% TRI-AXIAL (N90W in EW direction)
LENGTH SCALE=1 SYMMETRIC BUSHING CONFIGURATION

Peak Table Motion								
Acceleration (g)			Velocity (in/sec)			Displacement (in)		
EW	NS	V	EW	NS	V	EW	NS	V
0.13	0.08	0.03	15.00	8.69	2.11	5.05	3.45	0.74

OBSERVATIONS
Uplift at NW isolator

Peak Resultant Displacement (in)				Peak Acceleration (g)							
Bushing Top		Isolator	Torsional Ampl[3] Ratio (TA)	Bushing Top			Bushing Bottom		Control Point		
Abs[1]	Rel[2]			EW	NS	V	EW	NS	EW	NS	V
9.50	9.16	10.14	1.14	0.21	0.16	0.07	0.16	0.11	0.17	0.07	0.06

1. Absolute, 2. Relative to table, 3. Amplification



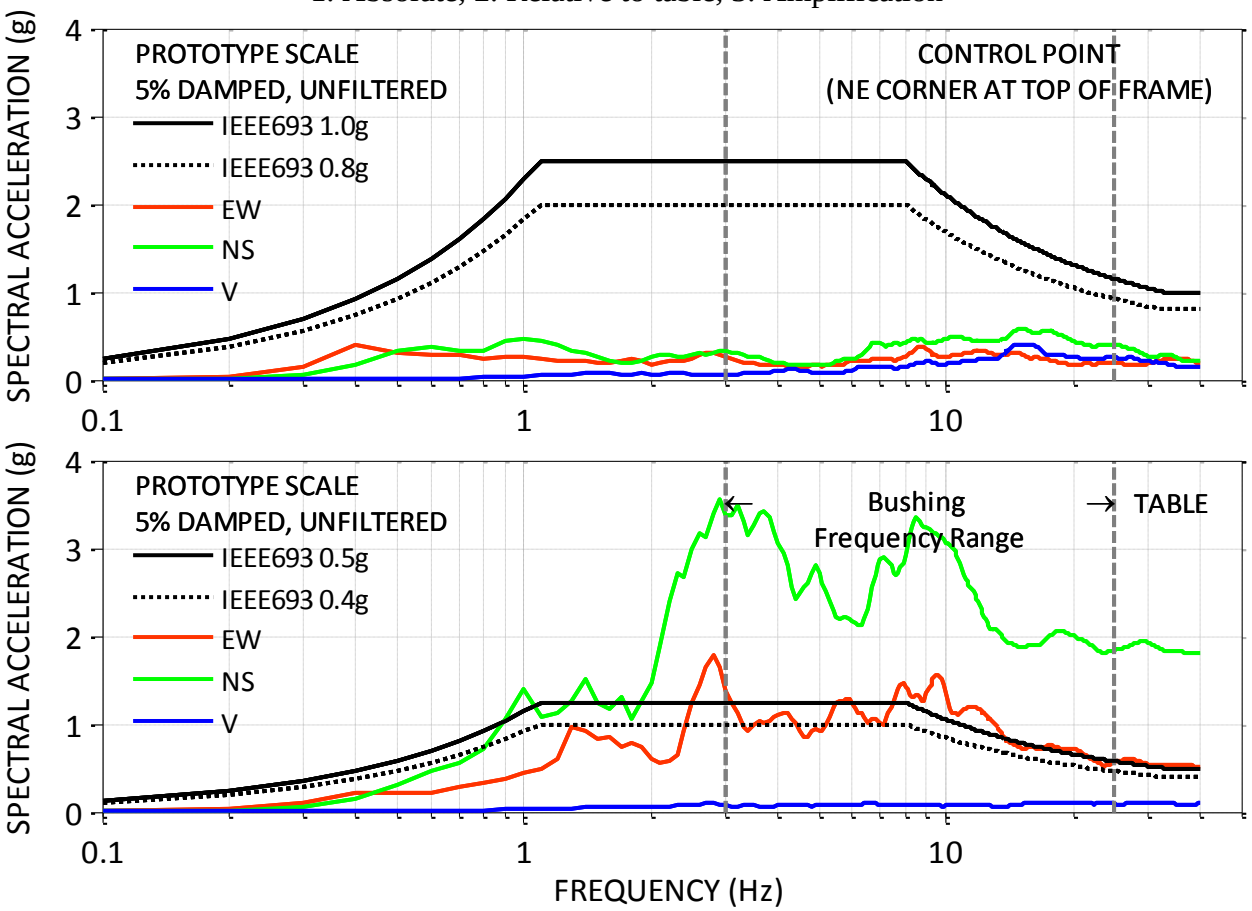
TRIPLE FP SYSTEM (Friction-Bolted Configuration)
JENSEN FILTER 97% BI-AXIAL (FN in EW direction)
LENGTH SCALE=1 NON-SYMMETRIC BUSHING CONFIGURATION

Peak Table Motion								
Acceleration (g)			Velocity (in/sec)			Displacement (in)		
EW	NS	V	EW	NS	V	EW	NS	V
0.49	1.72	0.03	16.14	20.87	0.91	3.27	4.25	0.16

OBSERVATIONS

Peak Resultant Displacement (in)				Peak Acceleration (g)							
Bushing Top		Isolator	Torsional Ampl[3] Ratio (TA)	Bushing Top			Bushing Bottom		Control Point		
Abs[1]	Rel[2]			EW	NS	V	EW	NS	EW	NS	V
6.24	6.92	6.99	1.02	0.62	0.98	0.26	0.15	0.16	0.16	0.16	0.10

1. Absolute, 2. Relative to table, 3. Amplification



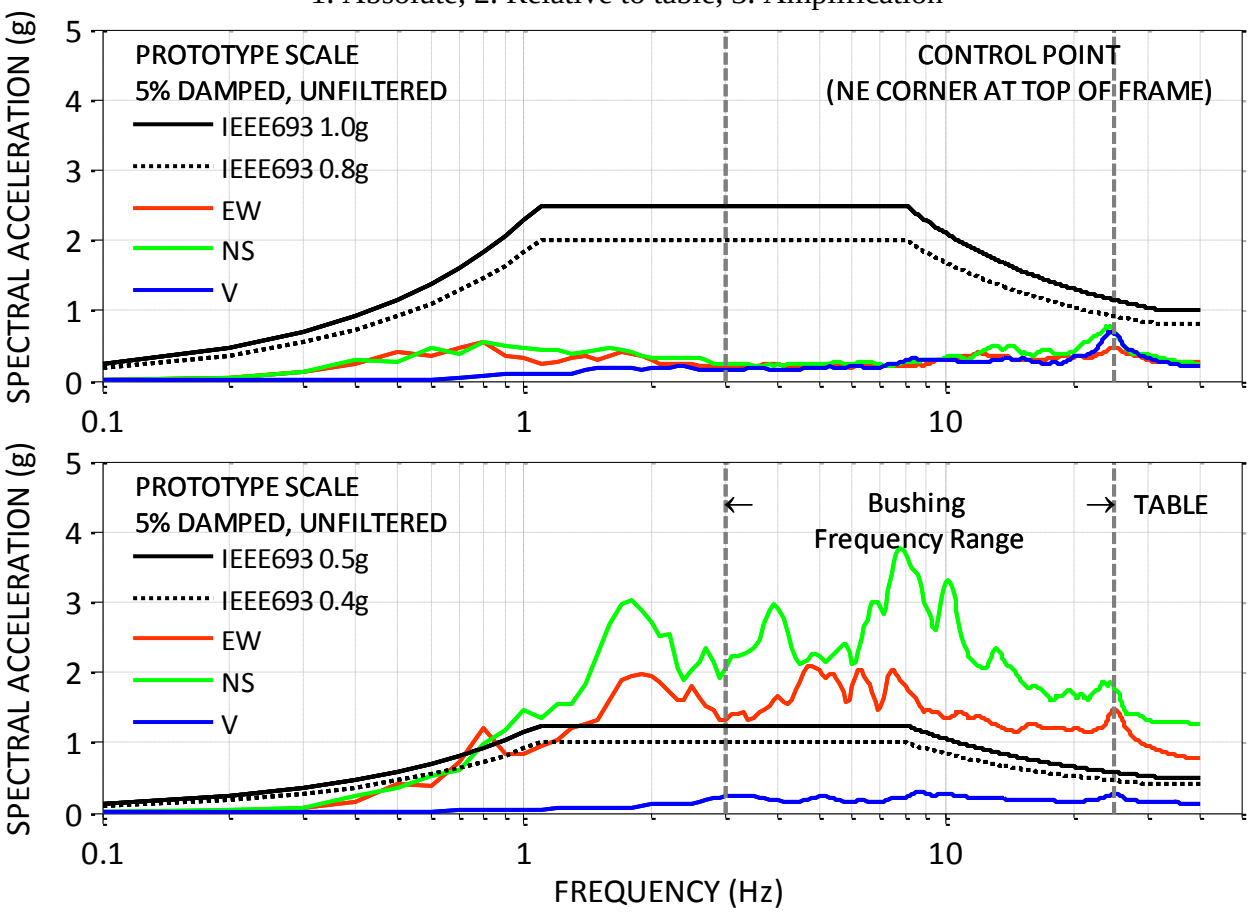
TRIPLE FP SYSTEM (Friction-Bolted Configuration)
EL CENTRO 300% BI-AXIAL (N90W in EW direction)
LENGTH SCALE=1 NON-SYMMETRIC BUSHING CONFIGURATION

Peak Table Motion								
Acceleration (g)			Velocity (in/sec)			Displacement (in)		
EW	NS	V	EW	NS	V	EW	NS	V
0.74	1.20	0.11	30.83	33.14	1.78	4.51	5.27	0.24

OBSERVATIONS

Peak Resultant Displacement (in)				Peak Acceleration (g)							
Bushing Top		Isolator	Torsional Ampl[3] Ratio (TA)	Bushing Top			Bushing Bottom		Control Point		
Abs[1]	Rel[2]			EW	NS	V	EW	NS	EW	NS	V
6.93	11.04	11.06	1.01	0.97	1.21	0.32	0.24	0.20	0.23	0.21	0.16

1. Absolute, 2. Relative to table, 3. Amplification



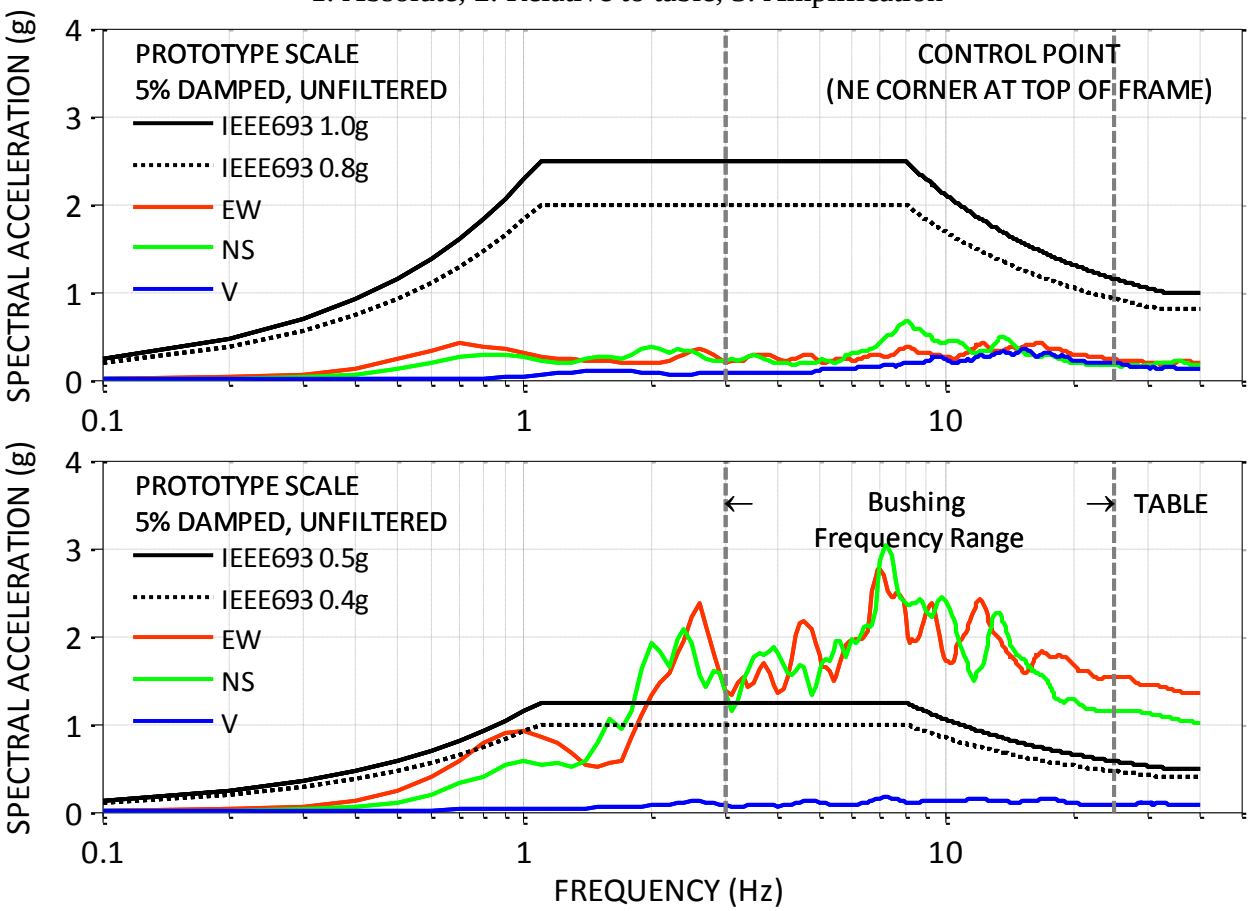
TRIPLE FP SYSTEM (Friction-Bolted Configuration)
PACOIMA DAM 75% BI-AXIAL (S16E in EW direction)
LENGTH SCALE=1 NON-SYMMETRIC BUSHING CONFIGURATION

Peak Table Motion								
Acceleration (g)			Velocity (in/sec)			Displacement (in)		
EW	NS	V	EW	NS	V	EW	NS	V
1.30	0.93	0.07	23.34	17.81	1.17	4.59	2.97	0.22

OBSERVATIONS

Peak Resultant Displacement (in)				Peak Acceleration (g)							
Bushing Top		Isolator	Torsional Ampl[3] Ratio (TA)	Bushing Top			Bushing Bottom		Control Point		
Abs[1]	Rel[2]			EW	NS	V	EW	NS	EW	NS	V
4.50	7.40	7.54	1.02	0.81	1.09	0.25	0.18	0.13	0.16	0.12	0.09

1. Absolute, 2. Relative to table, 3. Amplification



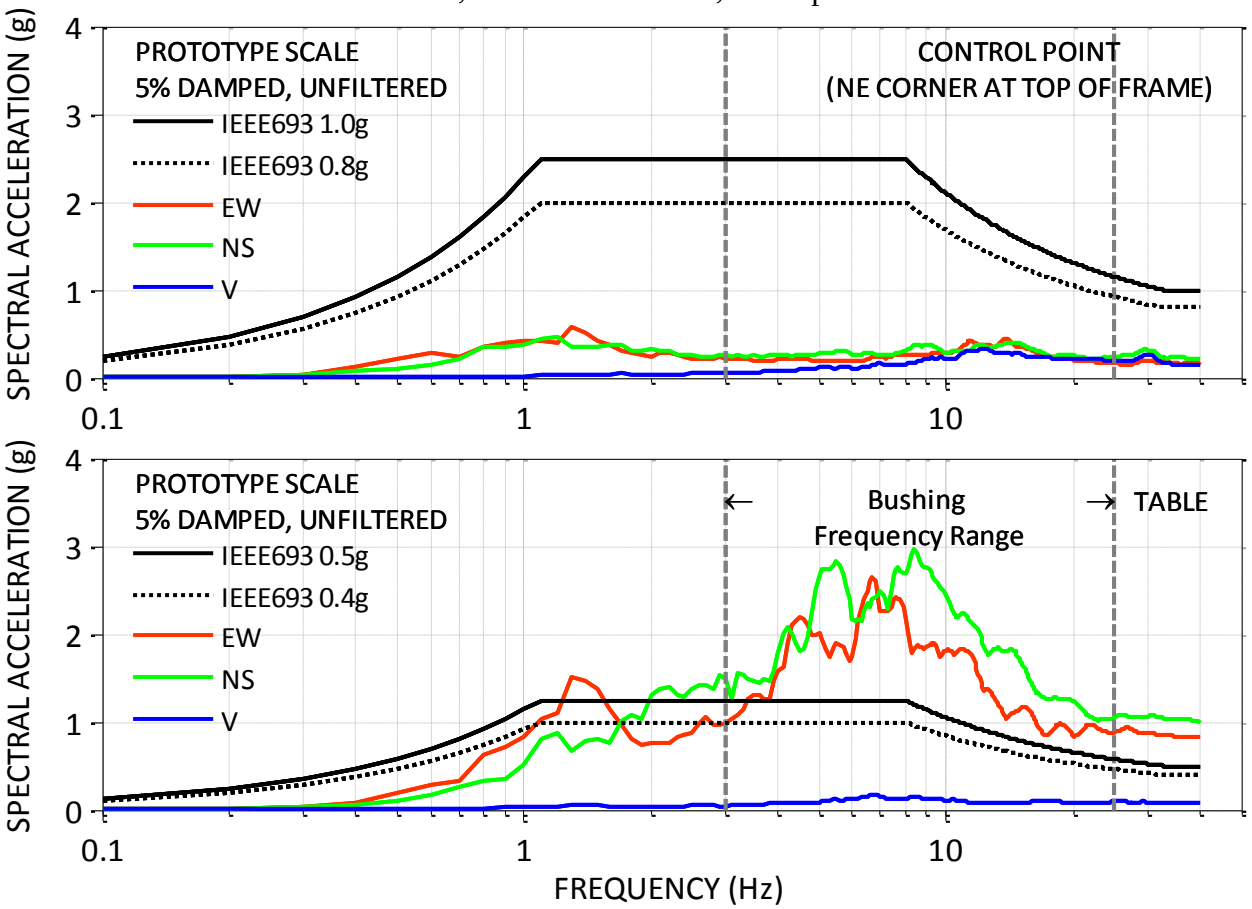
TRIPLE FP SYSTEM (Friction-Bolted Configuration)
CHILE 100% BI-AXIAL (EW in EW direction)
LENGTH SCALE=1 NON-SYMMETRIC BUSHING CONFIGURATION

Peak Table Motion								
Acceleration (g)			Velocity (in/sec)			Displacement (in)		
EW	NS	V	EW	NS	V	EW	NS	V
0.78	0.87	0.06	15.77	13.47	0.69	2.94	1.80	0.08

OBSERVATIONS

Peak Resultant Displacement (in)				Peak Acceleration (g)							
Bushing Top		Isolator	Torsional Ampl[3] Ratio (TA)	Bushing Top			Bushing Bottom		Control Point		
Abs[1]	Rel[2]			EW	NS	V	EW	NS	EW	NS	V
3.66	5.01	5.16	1.03	1.20	0.89	0.32	0.13	0.16	0.13	0.15	0.10

1. Absolute, 2. Relative to table, 3. Amplification



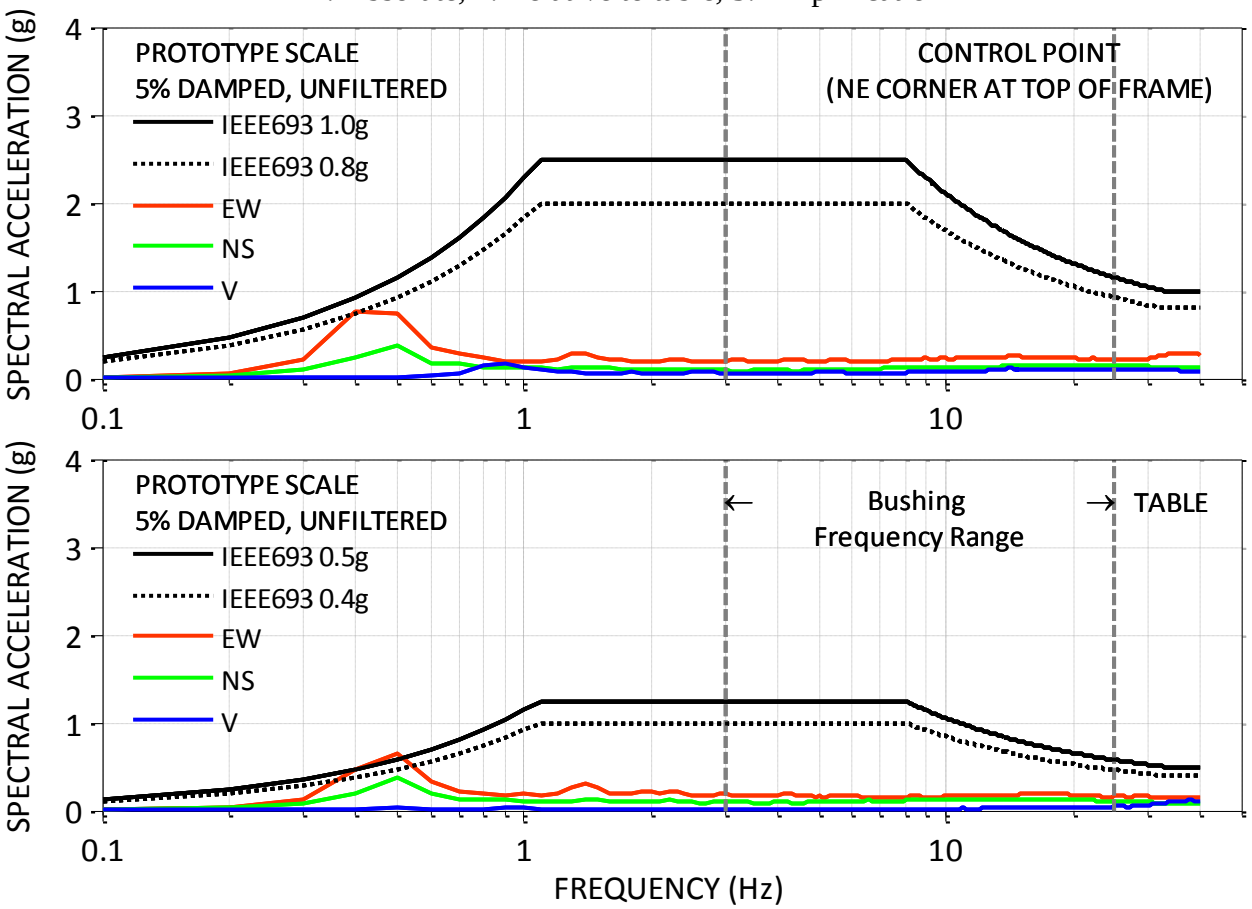
TRIPLE FP SYSTEM (Friction-Bolted Configuration)
MEXICO 70% BI-AXIAL (N90W in EW direction)
LENGTH SCALE=1 NON-SYMMETRIC BUSHING CONFIGURATION

Peak Table Motion								
Acceleration (g)			Velocity (in/sec)			Displacement (in)		
EW	NS	V	EW	NS	V	EW	NS	V
0.13	0.08	0.03	15.34	9.03	0.84	5.15	3.55	0.26

OBSERVATIONS

Peak Resultant Displacement (in)				Peak Acceleration (g)							
Bushing Top		Isolator	Torsional Ampl[3] Ratio (TA)	Bushing Top			Bushing Bottom		Control Point		
Abs[1]	Rel[2]			EW	NS	V	EW	NS	EW	NS	V
10.34	10.99	11.36	1.07	0.30	0.27	0.09	0.20	0.11	0.21	0.10	0.05

1. Absolute, 2. Relative to table, 3. Amplification



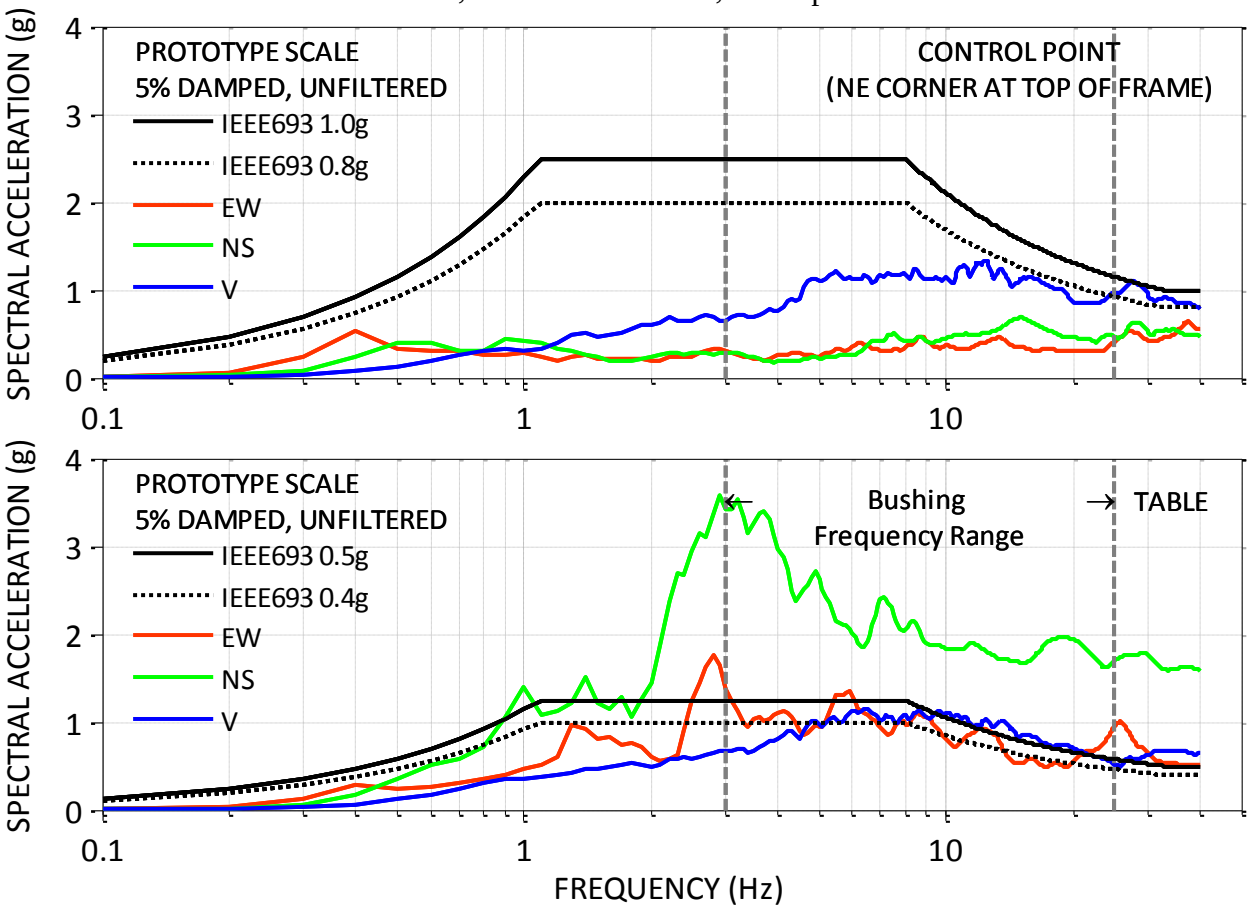
TRIPLE FP SYSTEM (Friction-Bolted Configuration)
JENSEN FILTER 97% TRI-AXIAL (FN in EW direction)
LENGTH SCALE=1 NON-SYMMETRIC BUSHING CONFIGURATION

Peak Table Motion								
Acceleration (g)			Velocity (in/sec)			Displacement (in)		
EW	NS	V	EW	NS	V	EW	NS	V
0.48	1.50	0.43	17.86	21.63	9.77	4.05	4.40	1.60

OBSERVATIONS

Peak Resultant Displacement (in)				Peak Acceleration (g)							
Bushing Top		Isolator	Torsional Ampl[3] Ratio (TA)	Bushing Top			Bushing Bottom		Control Point		
Abs[1]	Rel[2]			EW	NS	V	EW	NS	EW	NS	V
8.41	8.36	8.31	1.00	1.82	1.72	0.90	0.23	0.25	0.23	0.19	0.54

1. Absolute, 2. Relative to table, 3. Amplification



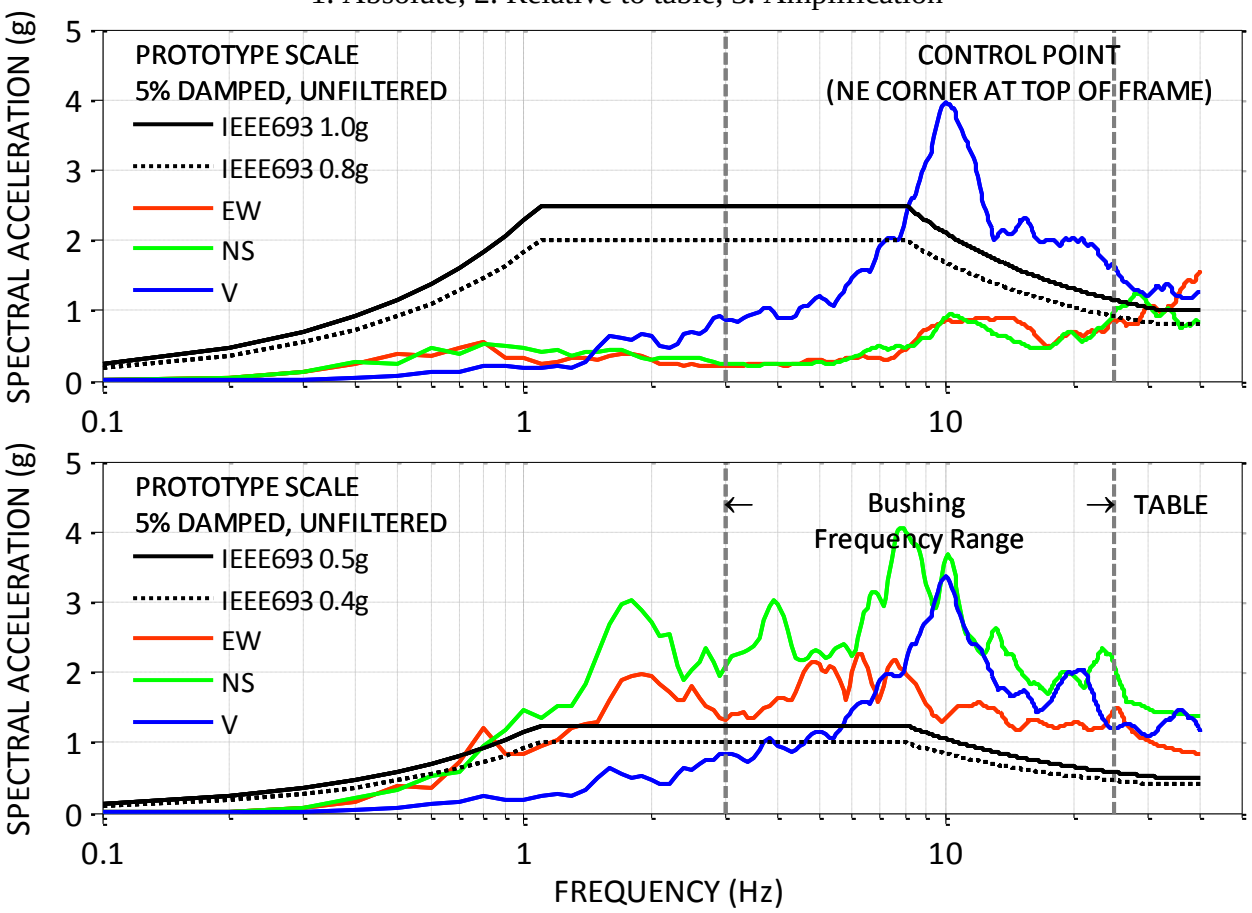
TRIPLE FP SYSTEM (Friction-Bolted Configuration)
EL CENTRO 300% TRI-AXIAL (N90W in EW direction)
LENGTH SCALE=1 NON-SYMMETRIC BUSHING CONFIGURATION

Peak Table Motion								
Acceleration (g)			Velocity (in/sec)			Displacement (in)		
EW	NS	V	EW	NS	V	EW	NS	V
0.76	1.30	0.86	30.86	33.40	9.20	4.44	5.12	1.20

OBSERVATIONS
Sliding at friction connection of about 0.1 inches (NW)

Peak Resultant Displacement (in)				Peak Acceleration (g)							
Bushing Top		Isolator	Torsional Ampl[3] Ratio (TA)	Bushing Top			Bushing Bottom		Control Point		
Abs[1]	Rel[2]			EW	NS	V	EW	NS	EW	NS	V
6.71	10.81	10.77	1.01	6.39	2.71	1.60	0.46	0.34	0.49	0.32	0.91

1. Absolute, 2. Relative to table, 3. Amplification



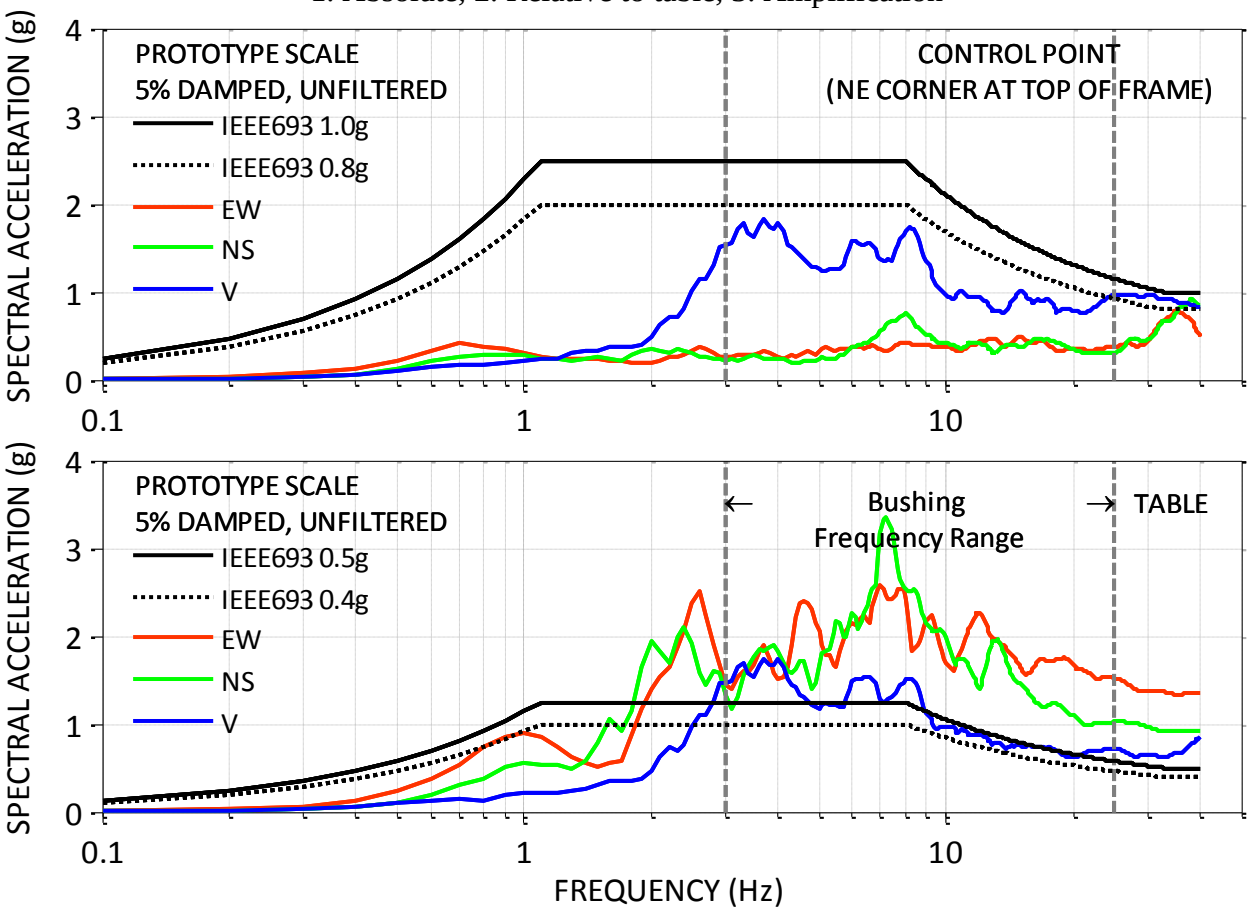
TRIPLE FP SYSTEM (Friction-Bolted Configuration)
PACOIMA DAM 75% TRI-AXIAL (S16E in EW direction)
LENGTH SCALE=1 NON-SYMMETRIC BUSHING CONFIGURATION

Peak Table Motion								
Acceleration (g)			Velocity (in/sec)			Displacement (in)		
EW	NS	V	EW	NS	V	EW	NS	V
1.30	0.84	0.63	22.47	18.93	11.01	4.41	2.99	1.59

OBSERVATIONS

Peak Resultant Displacement (in)				Peak Acceleration (g)							
Bushing Top		Isolator	Torsional Ampl[3] Ratio (TA)	Bushing Top			Bushing Bottom		Control Point		
Abs[1]	Rel[2]			EW	NS	V	EW	NS	EW	NS	V
4.98	7.17	7.22	1.02	1.98	1.33	0.79	0.23	0.21	0.23	0.18	0.65

1. Absolute, 2. Relative to table, 3. Amplification



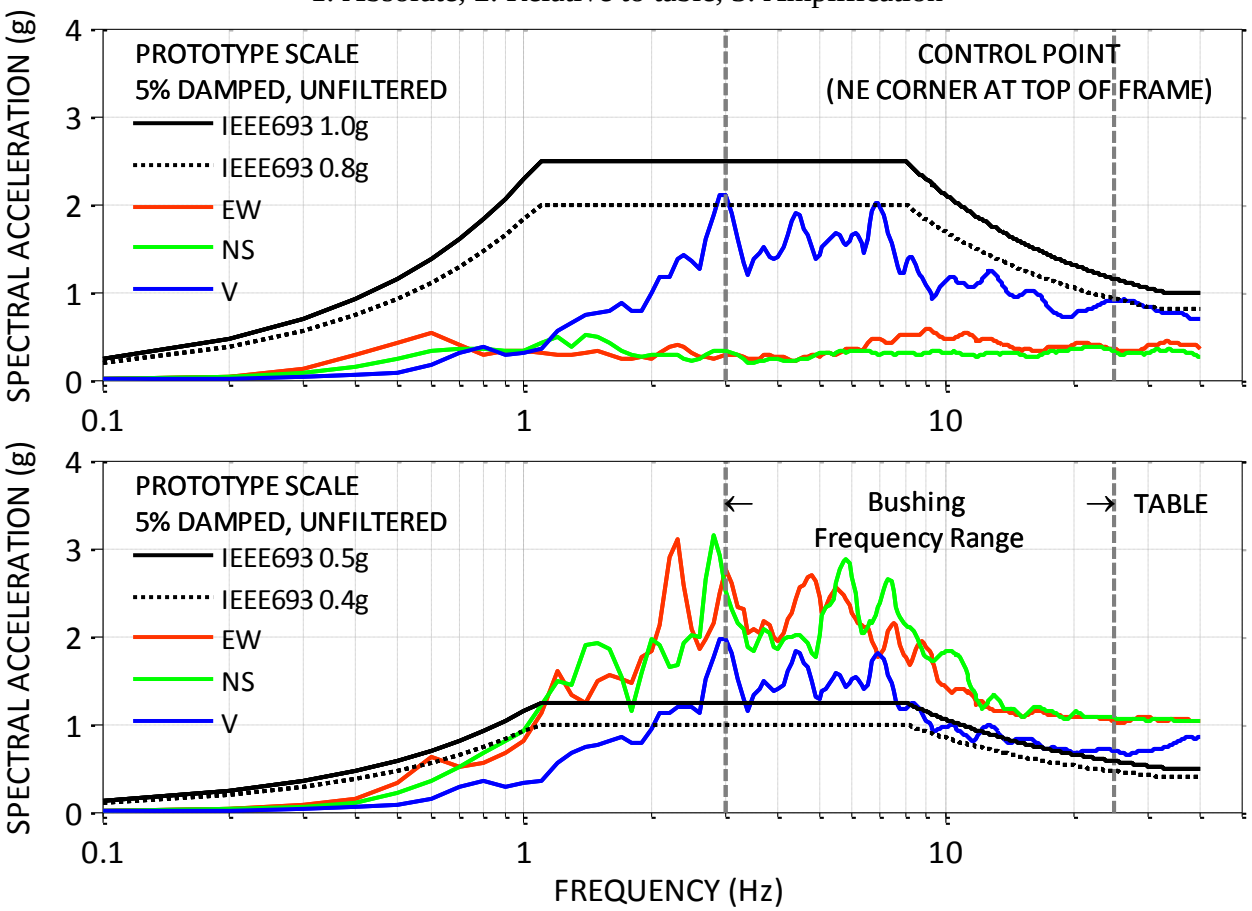
TRIPLE FP SYSTEM (Friction-Bolted Configuration)
TAFT 500% TRI-AXIAL (S69E in EW direction)
LENGTH SCALE=1 NON-SYMMETRIC BUSHING CONFIGURATION

Peak Table Motion								
Acceleration (g)			Velocity (in/sec)			Displacement (in)		
EW	NS	V	EW	NS	V	EW	NS	V
1.00	0.99	0.67	25.64	22.00	15.46	4.63	5.31	1.81

OBSERVATIONS

Peak Resultant Displacement (in)				Peak Acceleration (g)							
Bushing Top		Isolator	Torsional Ampl[3] Ratio (TA)	Bushing Top			Bushing Bottom		Control Point		
Abs[1]	Rel[2]			EW	NS	V	EW	NS	EW	NS	V
6.64	7.68	7.80	1.05	1.90	1.02	0.80	0.26	0.19	0.25	0.19	0.69

1. Absolute, 2. Relative to table, 3. Amplification



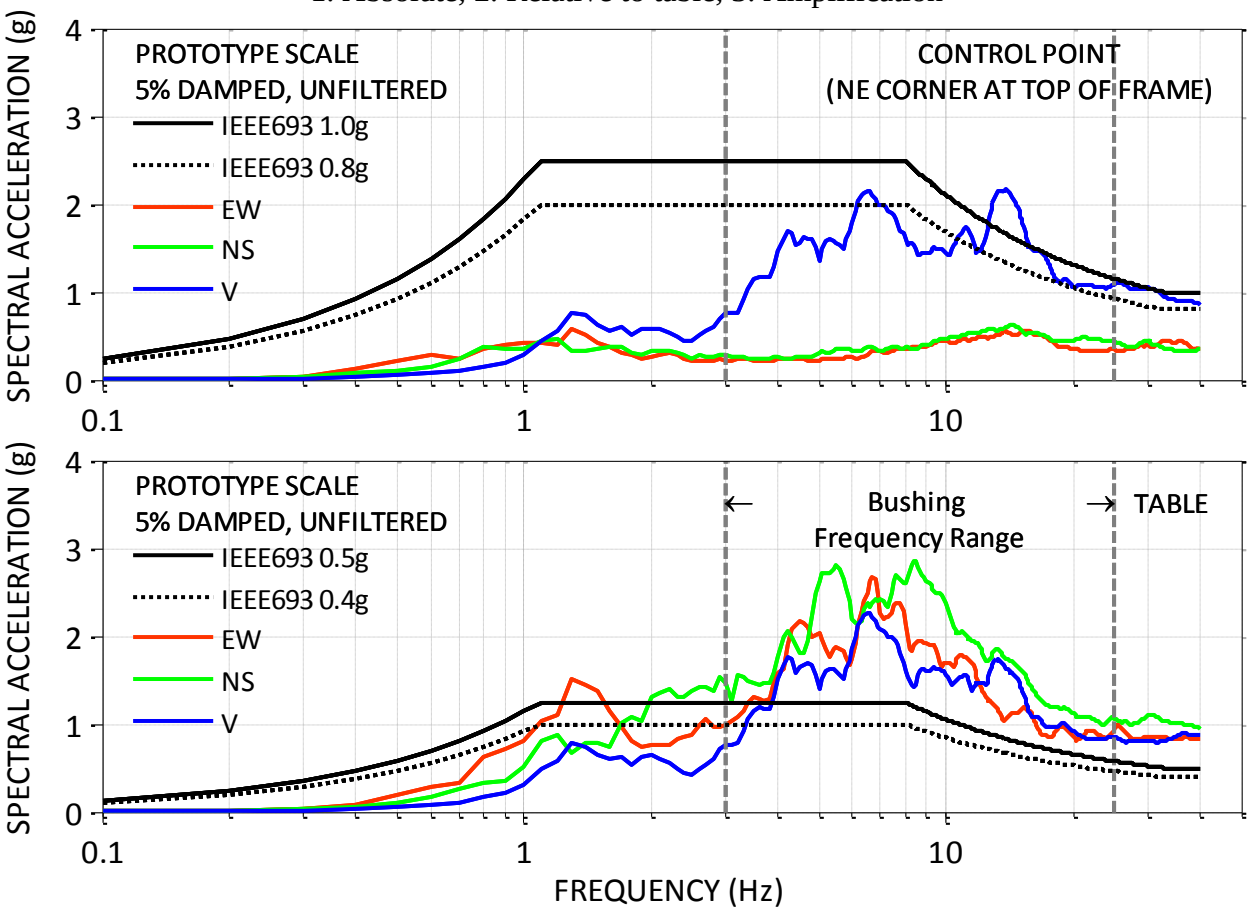
TRIPLE FP SYSTEM (Friction-Bolted Configuration)
CHILE 100% TRI-AXIAL (EW in EW direction)
LENGTH SCALE=1 NON-SYMMETRIC BUSHING CONFIGURATION

Peak Table Motion								
Acceleration (g)			Velocity (in/sec)			Displacement (in)		
EW	NS	V	EW	NS	V	EW	NS	V
0.74	0.83	0.66	16.22	13.24	9.16	2.94	1.80	1.02

OBSERVATIONS

Peak Resultant Displacement (in)				Peak Acceleration (g)							
Bushing Top		Isolator	Torsional Ampl[3] Ratio (TA)	Bushing Top			Bushing Bottom		Control Point		
Abs[1]	Rel[2]			EW	NS	V	EW	NS	EW	NS	V
3.57	4.92	4.98	1.02	3.37	1.77	1.06	0.22	0.24	0.22	0.22	0.75

1. Absolute, 2. Relative to table, 3. Amplification



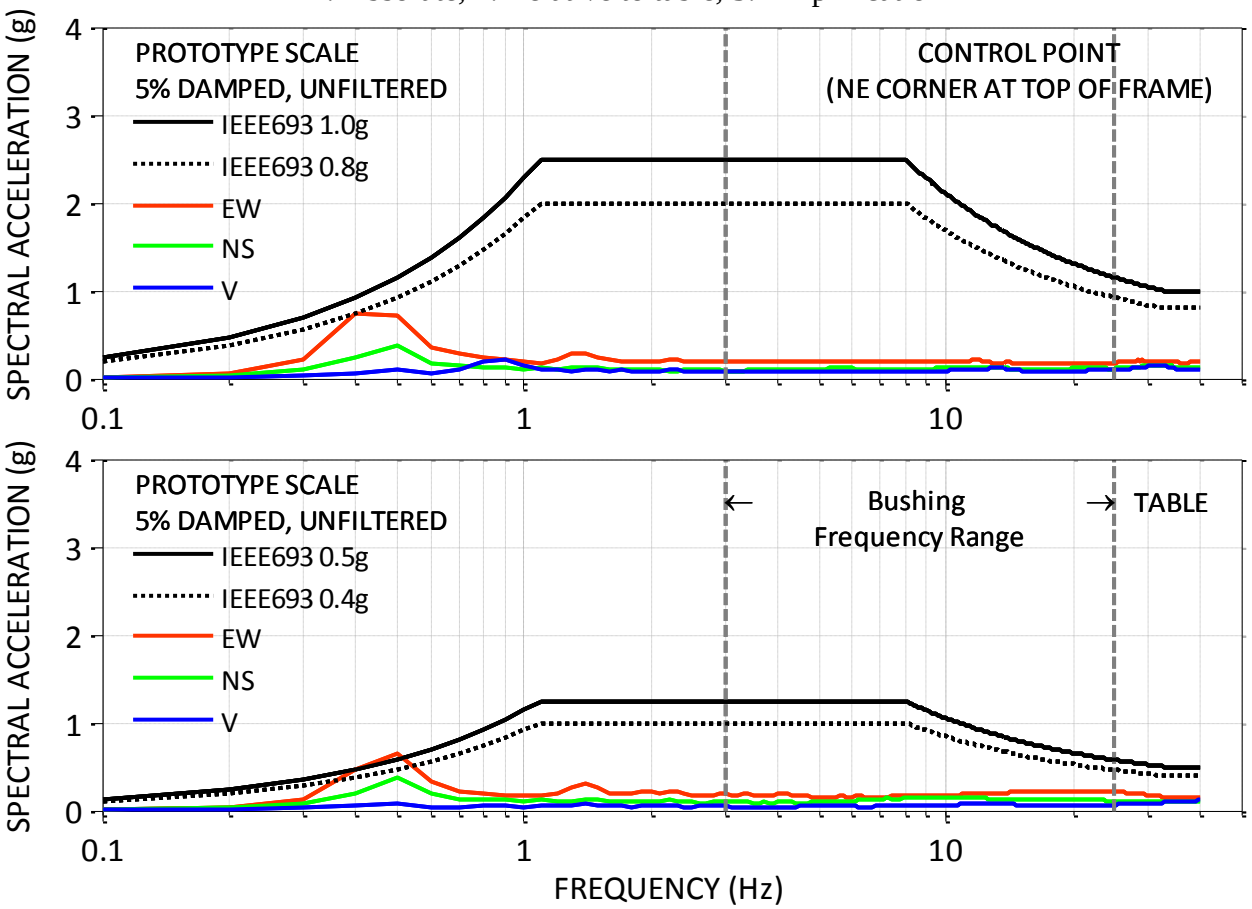
TRIPLE FP SYSTEM (Friction-Bolted Configuration)
MEXICO 70% TRI-AXIAL (N90W in EW direction)
LENGTH SCALE=1 NON-SYMMETRIC BUSHING CONFIGURATION

Peak Table Motion								
Acceleration (g)			Velocity (in/sec)			Displacement (in)		
EW	NS	V	EW	NS	V	EW	NS	V
0.14	0.09	0.05	15.22	8.96	2.23	5.15	3.55	0.77

OBSERVATIONS

Peak Resultant Displacement (in)				Peak Acceleration (g)							
Bushing Top		Isolator	Torsional Ampl[3] Ratio (TA)	Bushing Top			Bushing Bottom		Control Point		
Abs[1]	Rel[2]			EW	NS	V	EW	NS	EW	NS	V
10.02	10.62	10.91	1.06	0.32	0.31	0.15	0.17	0.10	0.18	0.10	0.07

1. Absolute, 2. Relative to table, 3. Amplification



PART B-4
SUMMARY OF EXPERIMENTAL DATA FOR NON-ISOLATED MODEL AT LENGTH SCALE OF 3

(ACTUAL TESTS HAVE BEEN CONDUCTED AT A FRACTION OF THE LEVEL OF EXCITATION USED IN THE ISOLATED MODEL TESTS AND THE RESULTS HAVE BEEN EXTRAPOLATED TO THE ISOLATED MODEL FOR EASE IN COMPARISON)

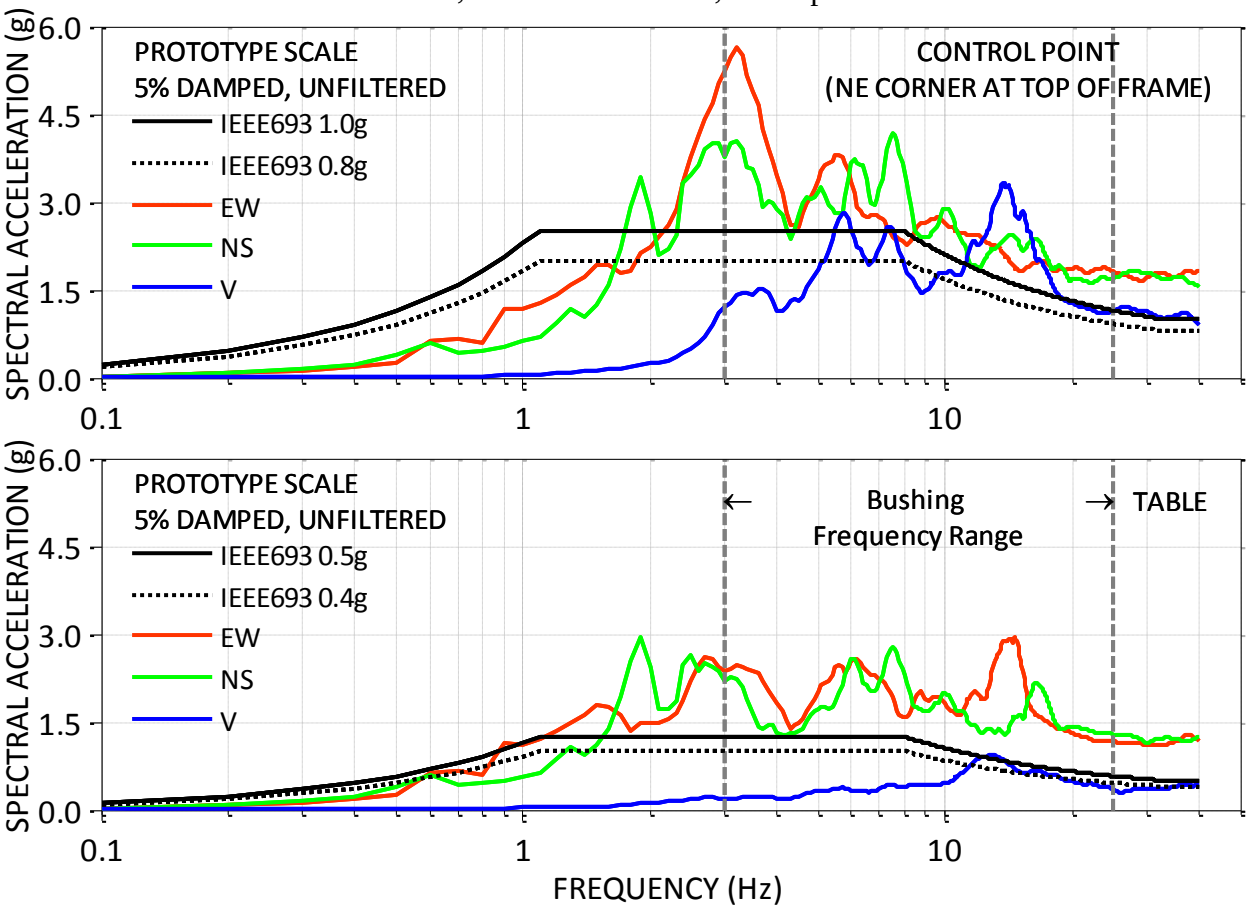
NON-ISOLATED SYSTEM (FIXED)
KARAKYR 137% BI-AXIAL (FN in EW direction) (ACTUAL TEST AT 69%)
LENGTH SCALE=3 SYMMETRIC BUSHING CONFIGURATION

Peak Table Motion								
Acceleration (g)			Velocity (in/sec)			Displacement (in)		
EW	NS	V	EW	NS	V	EW	NS	V
1.07	1.08	0.26	15.08	18.90	8.18	2.49	3.02	0.25

OBSERVATIONS

Peak Resultant Displacement (in)				Peak Acceleration (g)							
Bushing Top		Isolator	Torsional Ampl[3] Ratio (TA)	Bushing Top			Bushing Bottom		Control Point		
Abs[1]	Rel[2]			EW	NS	V	EW	NS	EW	NS	V
3.75	1.16	N/A	N/A	6.55	9.36	1.05	1.70	1.66	1.67	1.54	0.76

1. Absolute, 2. Relative to table, 3. Amplification



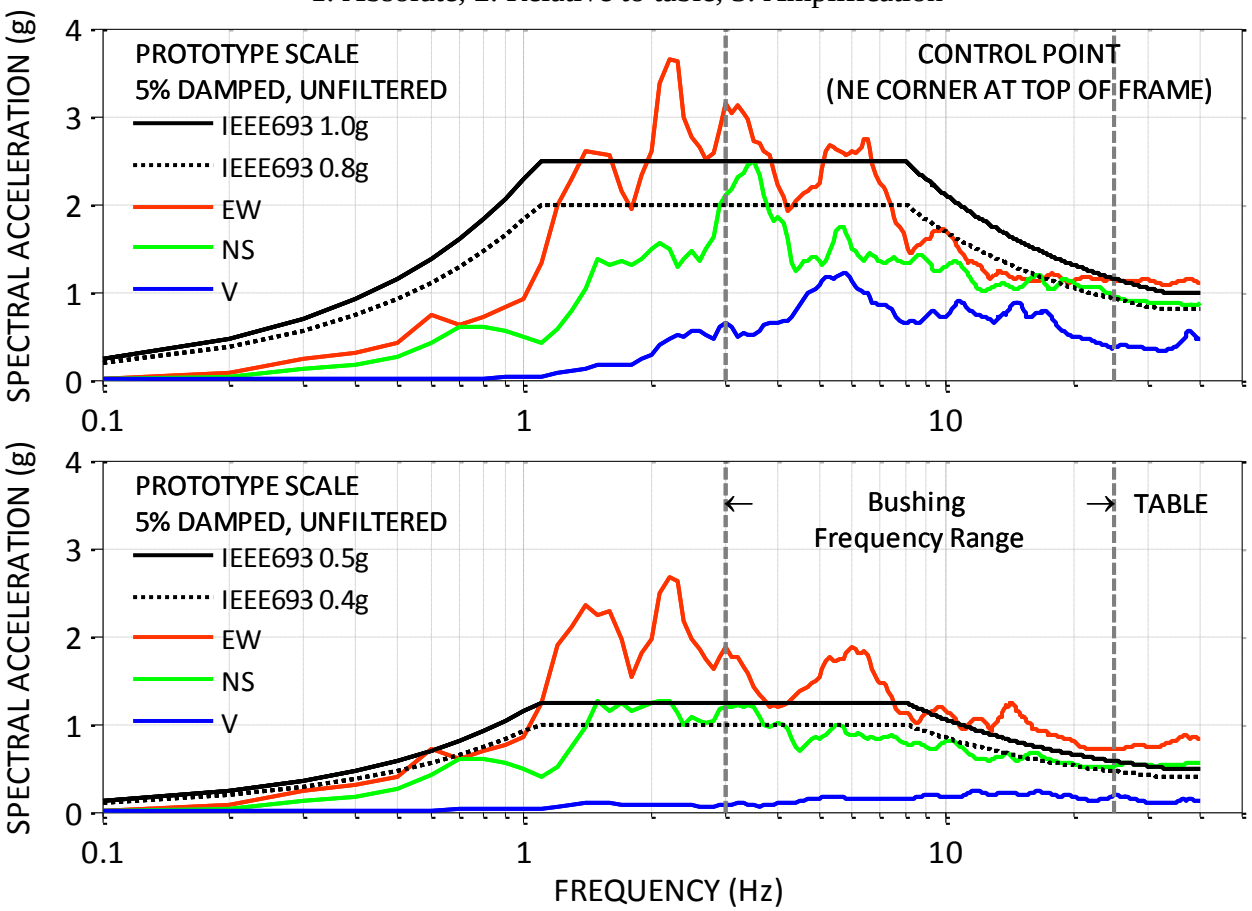
NON-ISOLATED SYSTEM (FIXED)
LGPC 94% BI-AXIAL (FN in EW direction) (ACTUAL TEST AT 47%)
LENGTH SCALE=3 SYMMETRIC BUSHING CONFIGURATION

Peak Table Motion								
Acceleration (g)			Velocity (in/sec)			Displacement (in)		
EW	NS	V	EW	NS	V	EW	NS	V
0.70	0.52	0.08	17.35	11.50	4.10	3.30	2.25	0.11

OBSERVATIONS

Peak Resultant Displacement (in)				Peak Acceleration (g)							
Bushing Top		Isolator	Torsional Ampl[3] Ratio (TA)	Bushing Top			Bushing Bottom		Control Point		
Abs[1]	Rel[2]			EW	NS	V	EW	NS	EW	NS	V
4.04	0.79	N/A	N/A	5.07	2.45	0.57	1.10	0.87	1.06	0.85	0.33

1. Absolute, 2. Relative to table, 3. Amplification



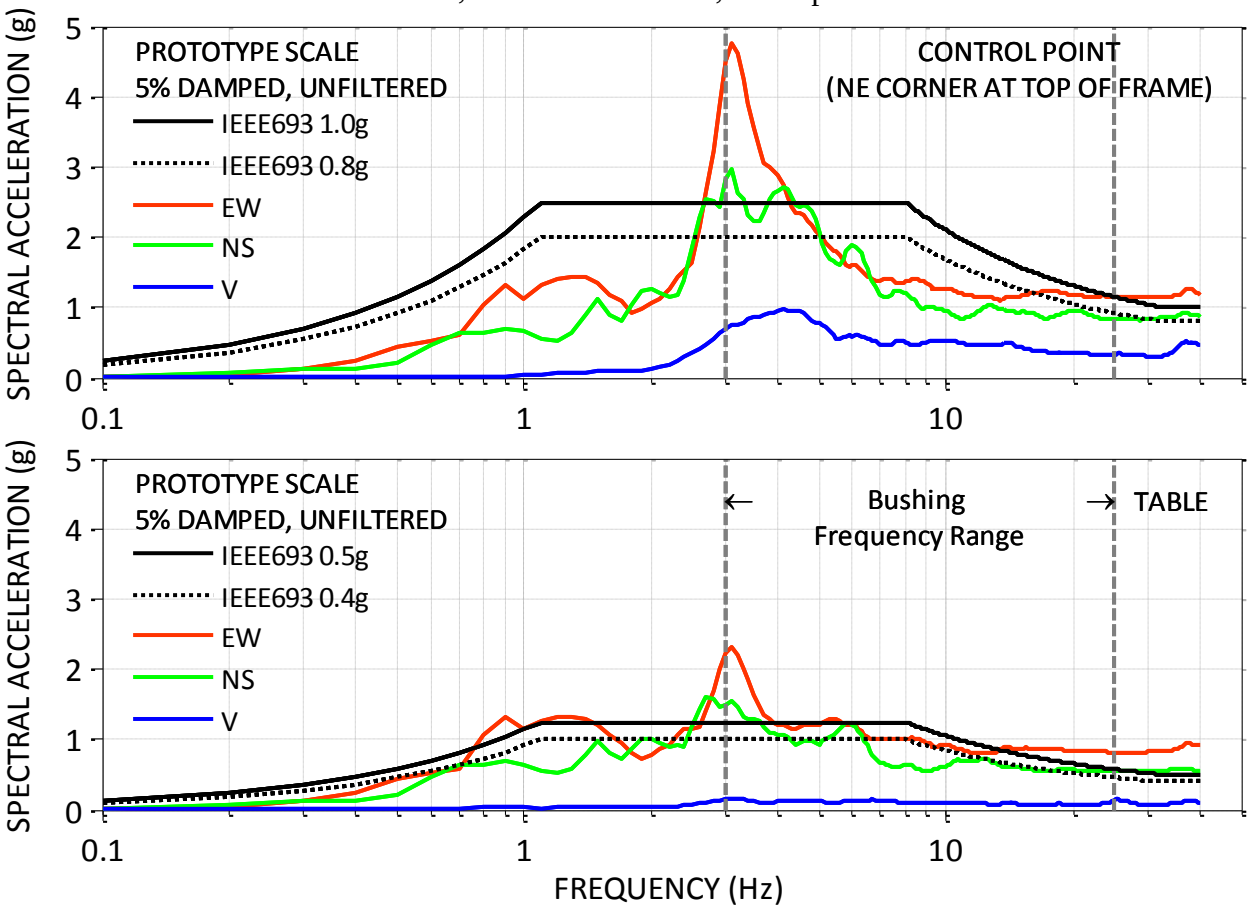
NON-ISOLATED SYSTEM (FIXED)
SARATOGA 157% BI-AXIAL (FN in EW direction) (ACTUAL TEST AT 79%)
LENGTH SCALE=3 SYMMETRIC BUSHING CONFIGURATION

Peak Table Motion								
Acceleration (g)			Velocity (in/sec)			Displacement (in)		
EW	NS	V	EW	NS	V	EW	NS	V
0.82	0.54	0.05	18.96	13.09	4.50	2.65	3.33	0.13

OBSERVATIONS

Peak Resultant Displacement (in)				Peak Acceleration (g)							
Bushing Top		Isolator	Torsional Ampl[3] Ratio (TA)	Bushing Top			Bushing Bottom		Control Point		
Abs[1]	Rel[2]			EW	NS	V	EW	NS	EW	NS	V
3.83	0.58	N/A	N/A	2.81	3.92	0.51	1.13	0.87	1.12	0.82	0.30

1. Absolute, 2. Relative to table, 3. Amplification



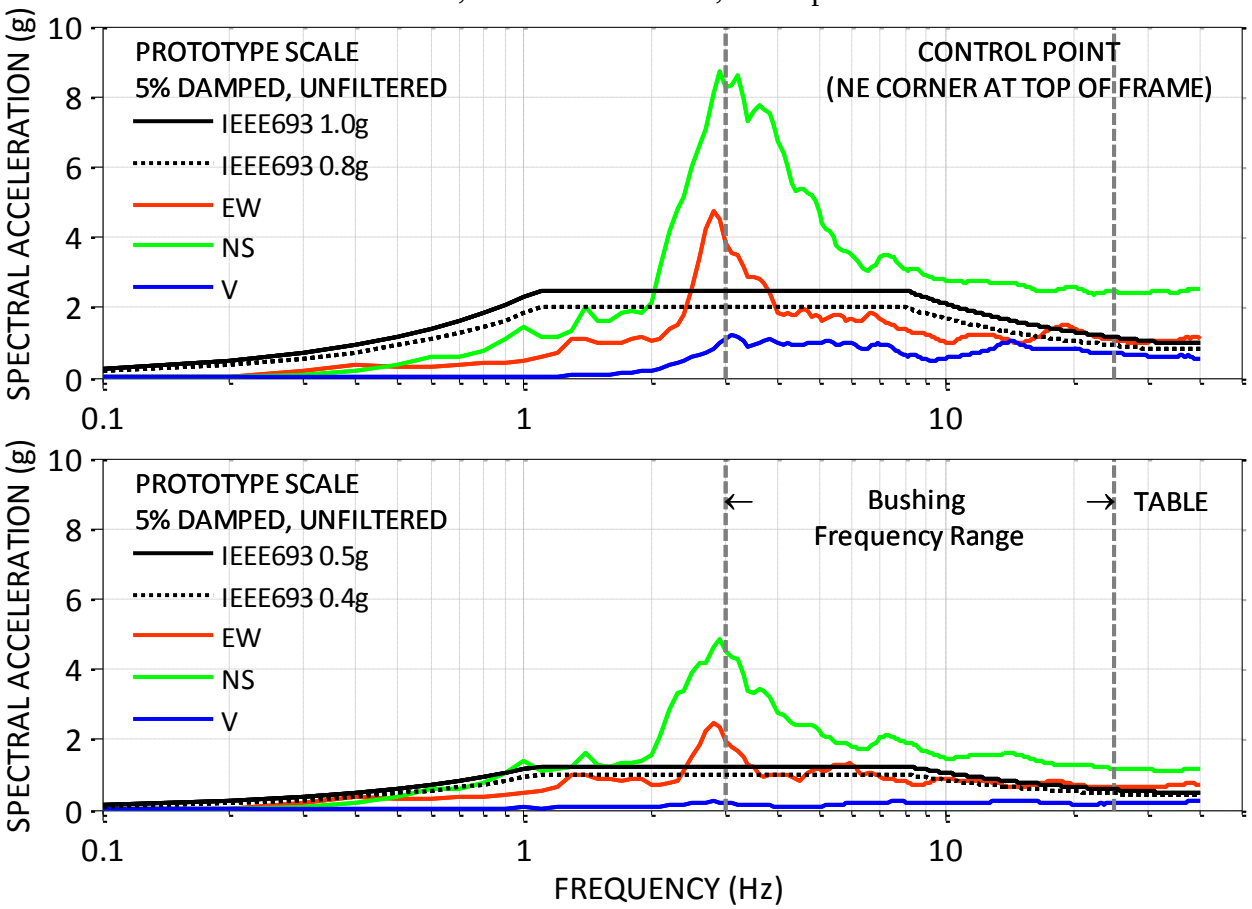
NON-ISOLATED SYSTEM (FIXED)
JENSEN FILTER 97% BI-AXIAL (FN in EW direction) (ACTUAL TEST AT 49%)
LENGTH SCALE=3 SYMMETRIC BUSHING CONFIGURATION

Peak Table Motion								
Acceleration (g)			Velocity (in/sec)			Displacement (in)		
EW	NS	V	EW	NS	V	EW	NS	V
0.62	1.12	0.12	12.65	16.48	4.57	2.31	1.76	0.12

OBSERVATIONS

Peak Resultant Displacement (in)				Peak Acceleration (g)							
Bushing Top		Isolator	Torsional Ampl[3] Ratio (TA)	Bushing Top			Bushing Bottom		Control Point		
Abs[1]	Rel[2]			EW	NS	V	EW	NS	EW	NS	V
2.58	1.18	N/A	N/A	3.66	5.89	0.47	0.94	2.44	0.99	2.40	0.47

1. Absolute, 2. Relative to table, 3. Amplification



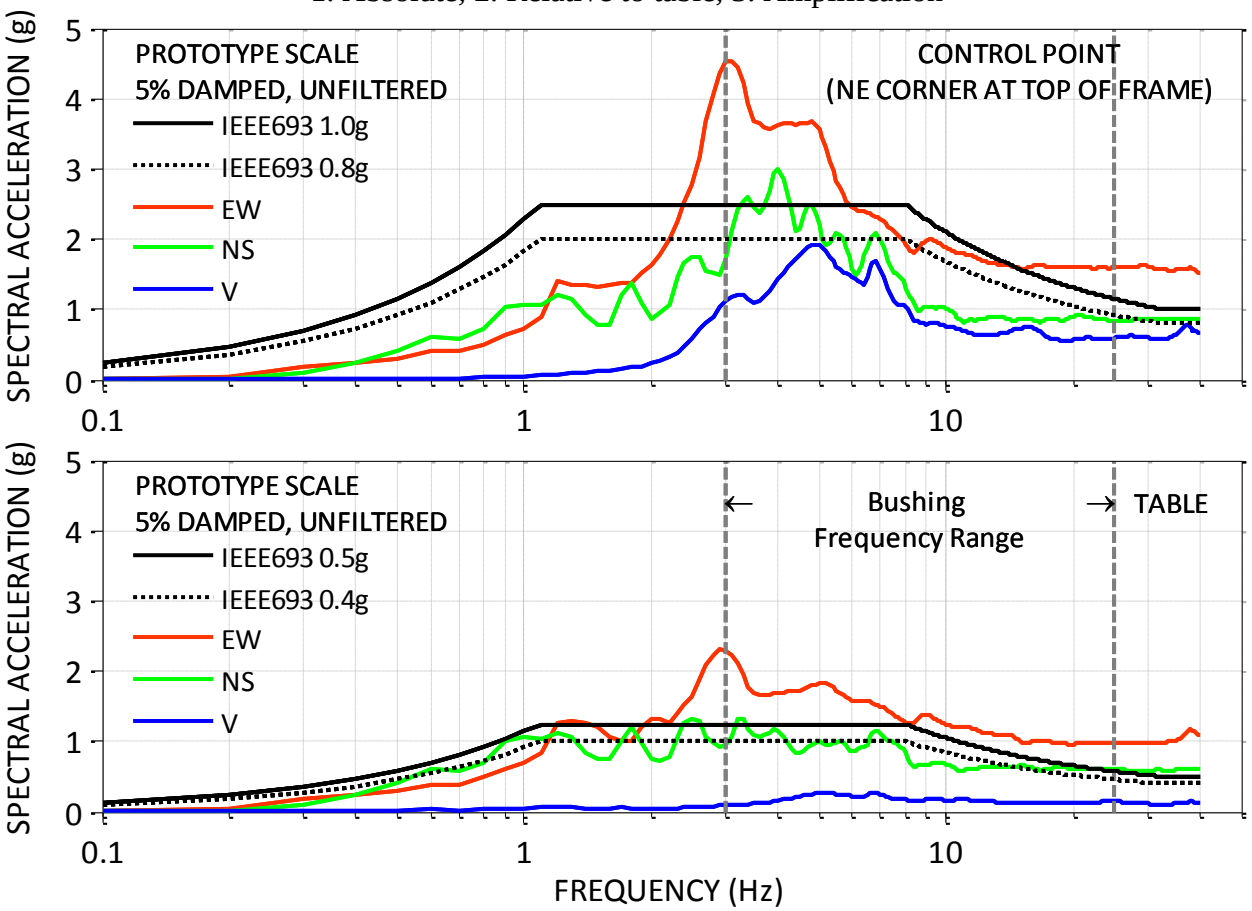
NON-ISOLATED SYSTEM (FIXED)
SYLMAR 90% BI-AXIAL (FN in EW direction) (ACTUAL TEST AT 45%)
LENGTH SCALE=3 SYMMETRIC BUSHING CONFIGURATION

Peak Table Motion								
Acceleration (g)			Velocity (in/sec)			Displacement (in)		
EW	NS	V	EW	NS	V	EW	NS	V
0.98	0.59	0.09	19.94	14.99	7.54	2.39	2.02	0.19

OBSERVATIONS

Peak Resultant Displacement (in)				Peak Acceleration (g)							
Bushing Top		Isolator	Torsional Ampl[3] Ratio (TA)	Bushing Top			Bushing Bottom		Control Point		
Abs[1]	Rel[2]			EW	NS	V	EW	NS	EW	NS	V
3.00	0.86	N/A	N/A	4.26	3.38	0.40	1.54	0.86	1.51	0.83	0.53

1. Absolute, 2. Relative to table, 3. Amplification



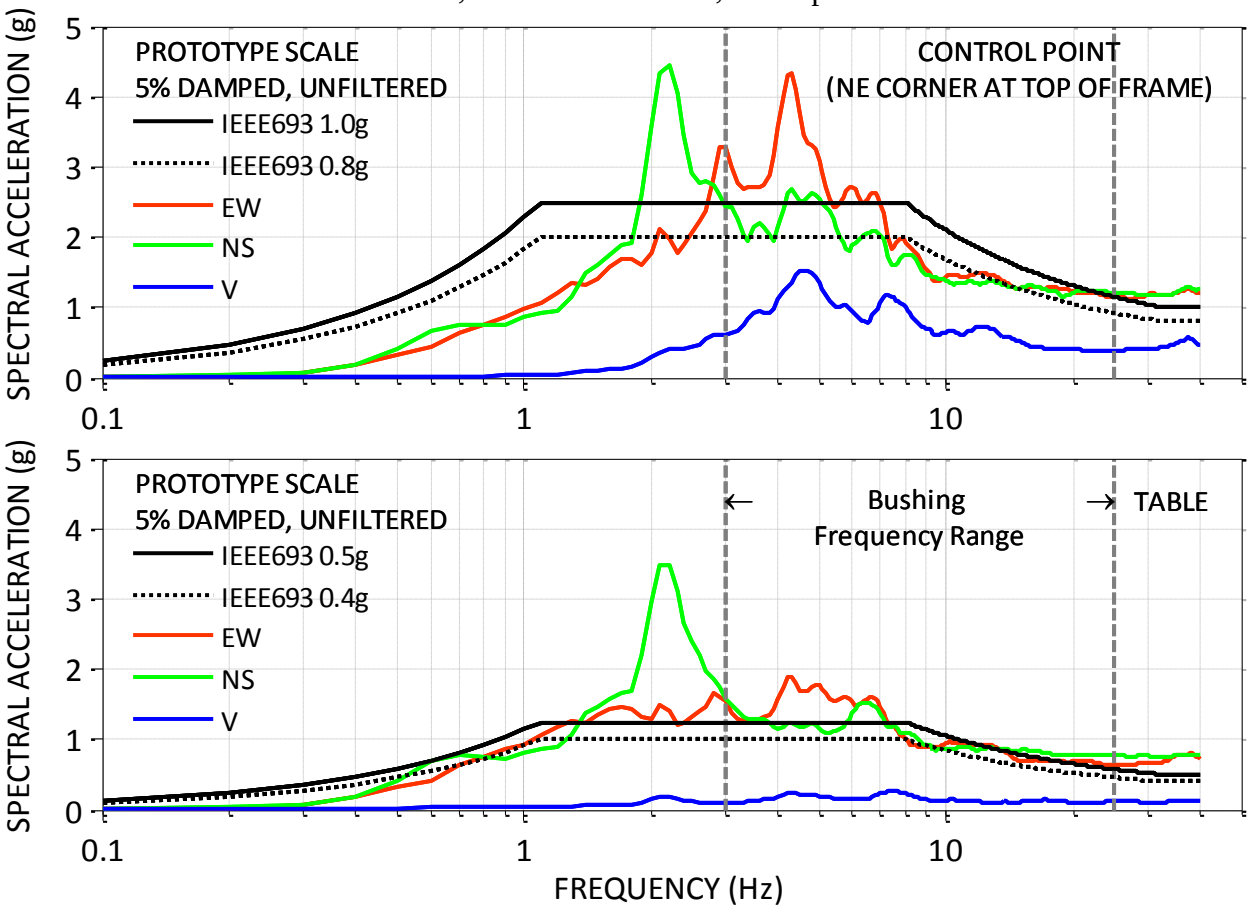
NON-ISOLATED SYSTEM (FIXED)
TAKARAZUKA 97% BI-AXIAL (FN in EW direction) (ACTUAL TEST AT 49%)
LENGTH SCALE=3 SYMMETRIC BUSHING CONFIGURATION

Peak Table Motion								
Acceleration (g)			Velocity (in/sec)			Displacement (in)		
EW	NS	V	EW	NS	V	EW	NS	V
0.63	0.75	0.08	15.89	17.18	6.43	1.54	2.11	0.14

OBSERVATIONS

Peak Resultant Displacement (in)				Peak Acceleration (g)							
Bushing Top		Isolator	Torsional Ampl[3] Ratio (TA)	Bushing Top			Bushing Bottom		Control Point		
Abs[1]	Rel[2]			EW	NS	V	EW	NS	EW	NS	V
2.50	1.03	N/A	N/A	5.41	4.21	0.58	1.14	1.24	1.11	1.17	0.35

1. Absolute, 2. Relative to table, 3. Amplification



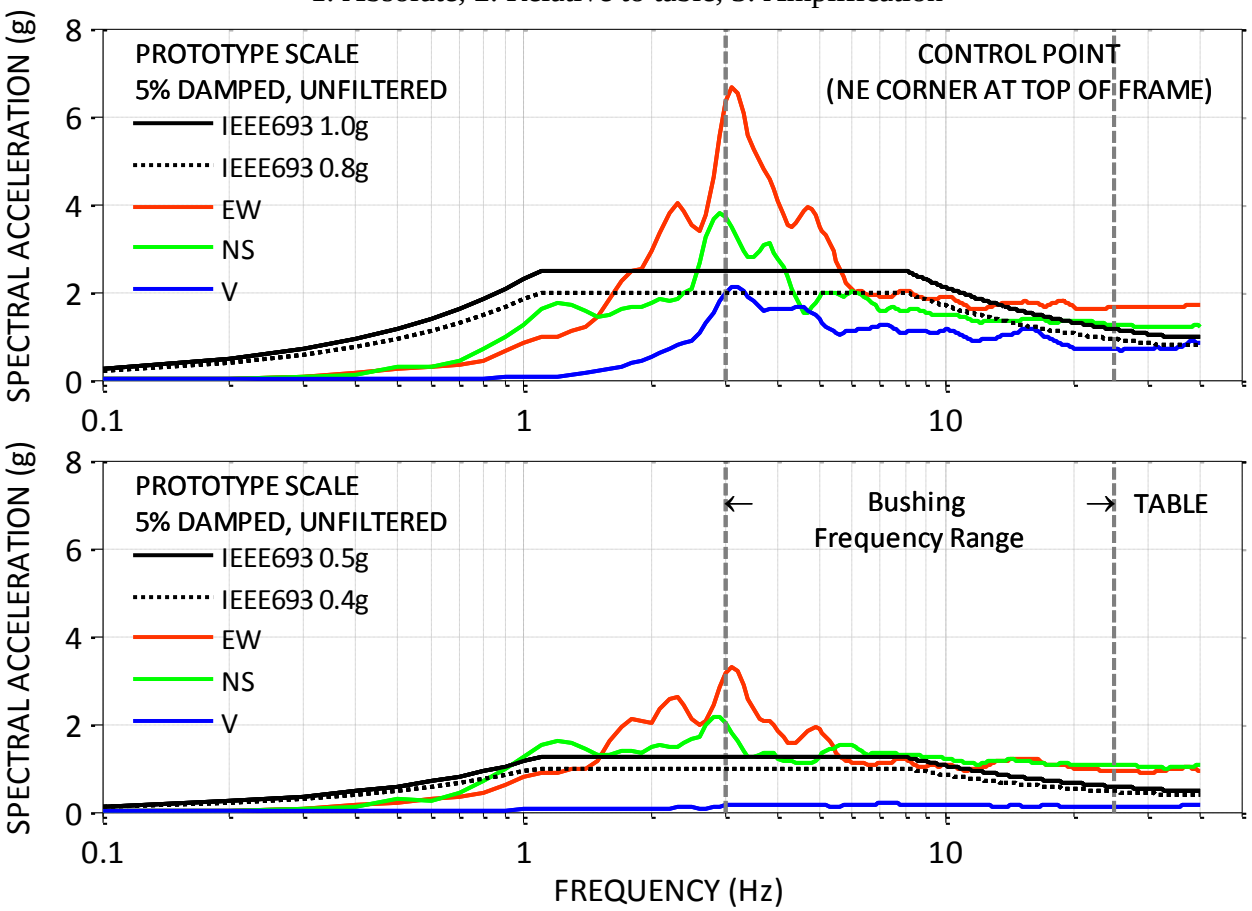
NON-ISOLATED SYSTEM (FIXED)
BOLU 104% BI-AXIAL (FN in EW direction) (ACTUAL TEST AT 52%)
LENGTH SCALE=3 SYMMETRIC BUSHING CONFIGURATION

Peak Table Motion								
Acceleration (g)			Velocity (in/sec)			Displacement (in)		
EW	NS	V	EW	NS	V	EW	NS	V
0.89	0.98	0.09	13.55	16.07	7.53	1.29	1.79	0.23

OBSERVATIONS

Peak Resultant Displacement (in)				Peak Acceleration (g)							
Bushing Top		Isolator	Torsional Ampl[3] Ratio (TA)	Bushing Top			Bushing Bottom		Control Point		
Abs[1]	Rel[2]			EW	NS	V	EW	NS	EW	NS	V
2.24	0.90	N/A	N/A	3.26	4.19	0.42	1.65	1.24	1.60	1.17	0.67

1. Absolute, 2. Relative to table, 3. Amplification



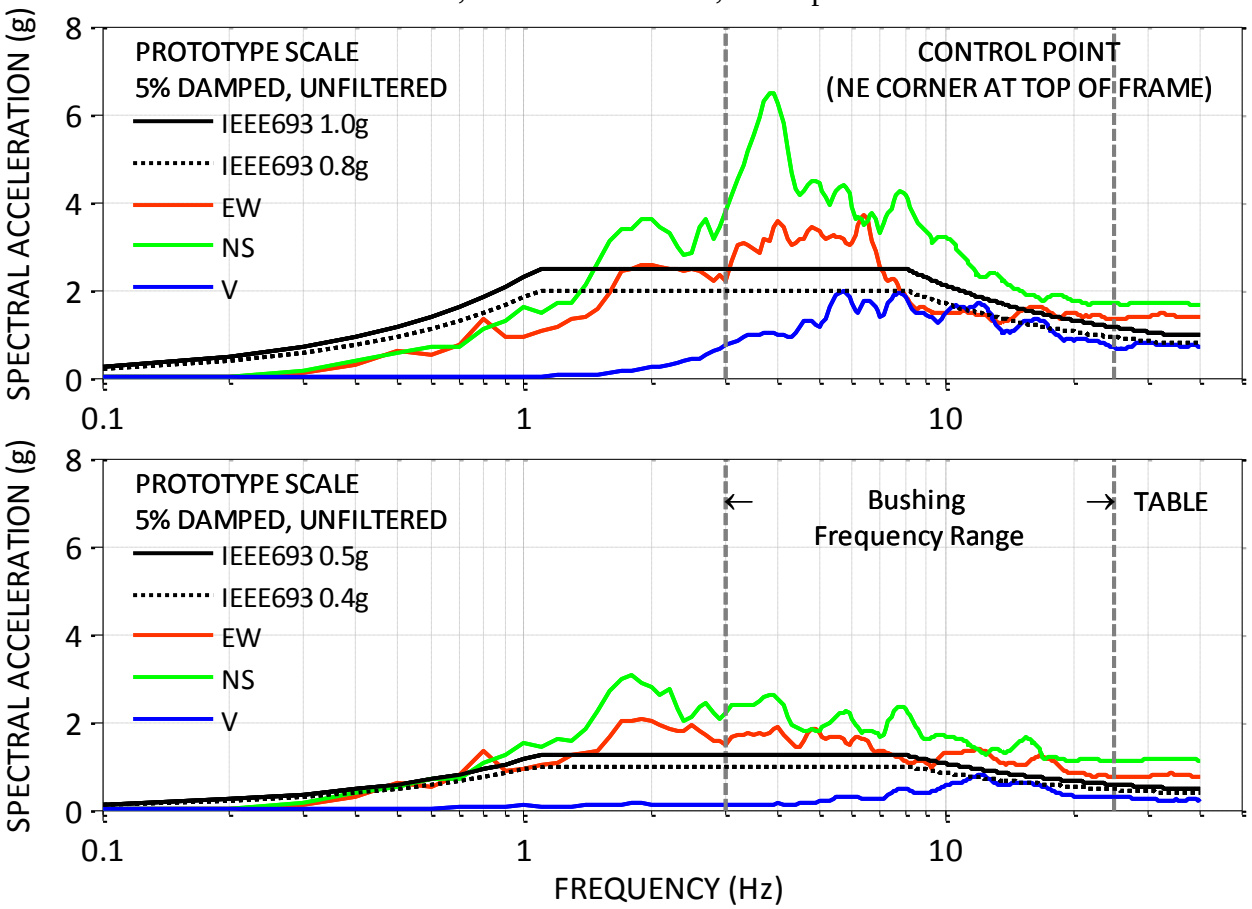
NON-ISOLATED SYSTEM (FIXED)
EL CENTRO 300% BI-AXIAL (N90W in EW direction) (ACTUAL TEST AT 50%)
LENGTH SCALE=3 SYMMETRIC BUSHING CONFIGURATION

Peak Table Motion								
Acceleration (g)			Velocity (in/sec)			Displacement (in)		
EW	NS	V	EW	NS	V	EW	NS	V
0.72	1.10	0.17	20.85	20.48	3.07	2.42	2.58	0.13

OBSERVATIONS

Peak Resultant Displacement (in)				Peak Acceleration (g)							
Bushing Top		Isolator	Torsional Ampl[3] Ratio (TA)	Bushing Top			Bushing Bottom		Control Point		
Abs[1]	Rel[2]			EW	NS	V	EW	NS	EW	NS	V
3.72	1.41	N/A	N/A	8.07	10.30	1.20	1.13	1.84	1.22	1.67	0.60

1. Absolute, 2. Relative to table, 3. Amplification



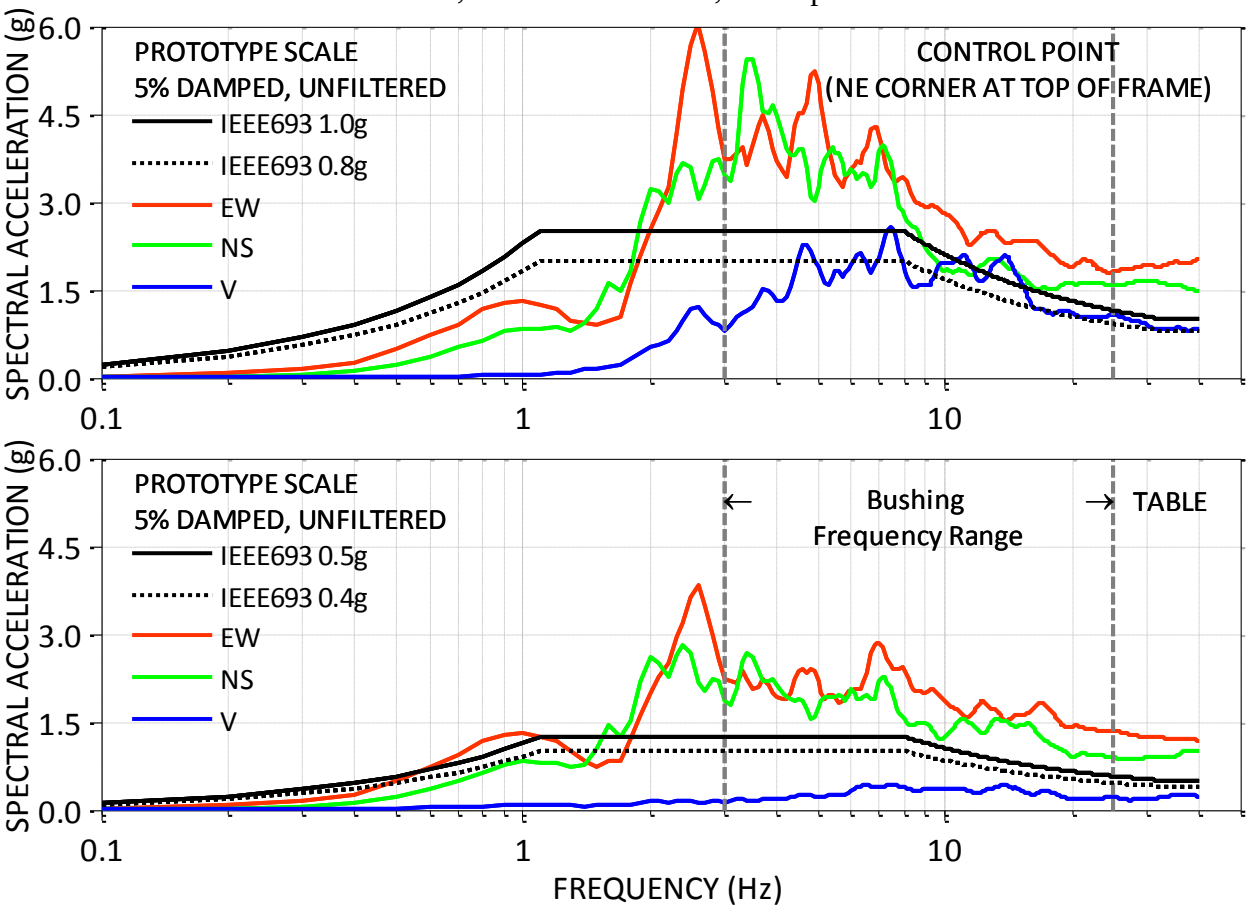
NON-ISOLATED SYSTEM (FIXED)
PACOIMA DAM 100% BI-AXIAL (S16E in EW direction) (ACTUAL TEST AT 25%)
LENGTH SCALE=3 SYMMETRIC BUSHING CONFIGURATION

Peak Table Motion								
Acceleration (g)			Velocity (in/sec)			Displacement (in)		
EW	NS	V	EW	NS	V	EW	NS	V
1.17	0.85	0.15	24.51	15.33	7.72	3.21	1.51	0.22

OBSERVATIONS

Peak Resultant Displacement (in)				Peak Acceleration (g)							
Bushing Top		Isolator	Torsional Ampl[3] Ratio (TA)	Bushing Top			Bushing Bottom		Control Point		
Abs[1]	Rel[2]			EW	NS	V	EW	NS	EW	NS	V
3.86	1.13	N/A	N/A	7.80	8.18	1.12	1.79	1.56	1.81	1.47	0.82

1. Absolute, 2. Relative to table, 3. Amplification



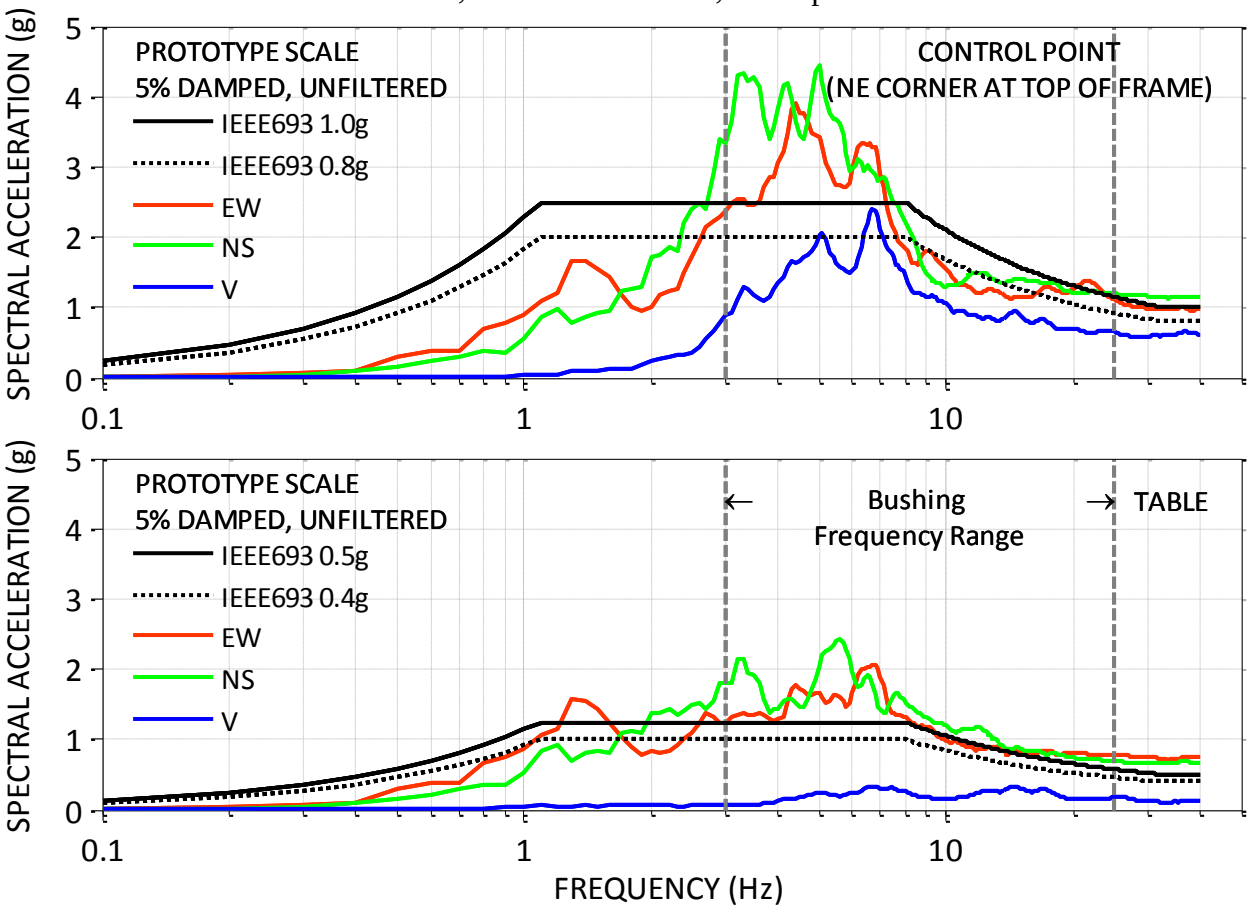
NON-ISOLATED SYSTEM (FIXED)
CHILE 100% BI-AXIAL (EW in EW direction) (ACTUAL TEST AT 50%)
LENGTH SCALE=3 SYMMETRIC BUSHING CONFIGURATION

Peak Table Motion								
Acceleration (g)			Velocity (in/sec)			Displacement (in)		
EW	NS	V	EW	NS	V	EW	NS	V
0.71	0.65	0.09	9.84	8.57	5.02	1.51	0.92	0.10

OBSERVATIONS

Peak Resultant Displacement (in)				Peak Acceleration (g)							
Bushing Top		Isolator	Torsional Ampl[3] Ratio (TA)	Bushing Top			Bushing Bottom		Control Point		
Abs[1]	Rel[2]			EW	NS	V	EW	NS	EW	NS	V
2.13	1.04	N/A	N/A	6.47	7.27	0.84	0.99	1.18	0.95	1.14	0.60

1. Absolute, 2. Relative to table, 3. Amplification



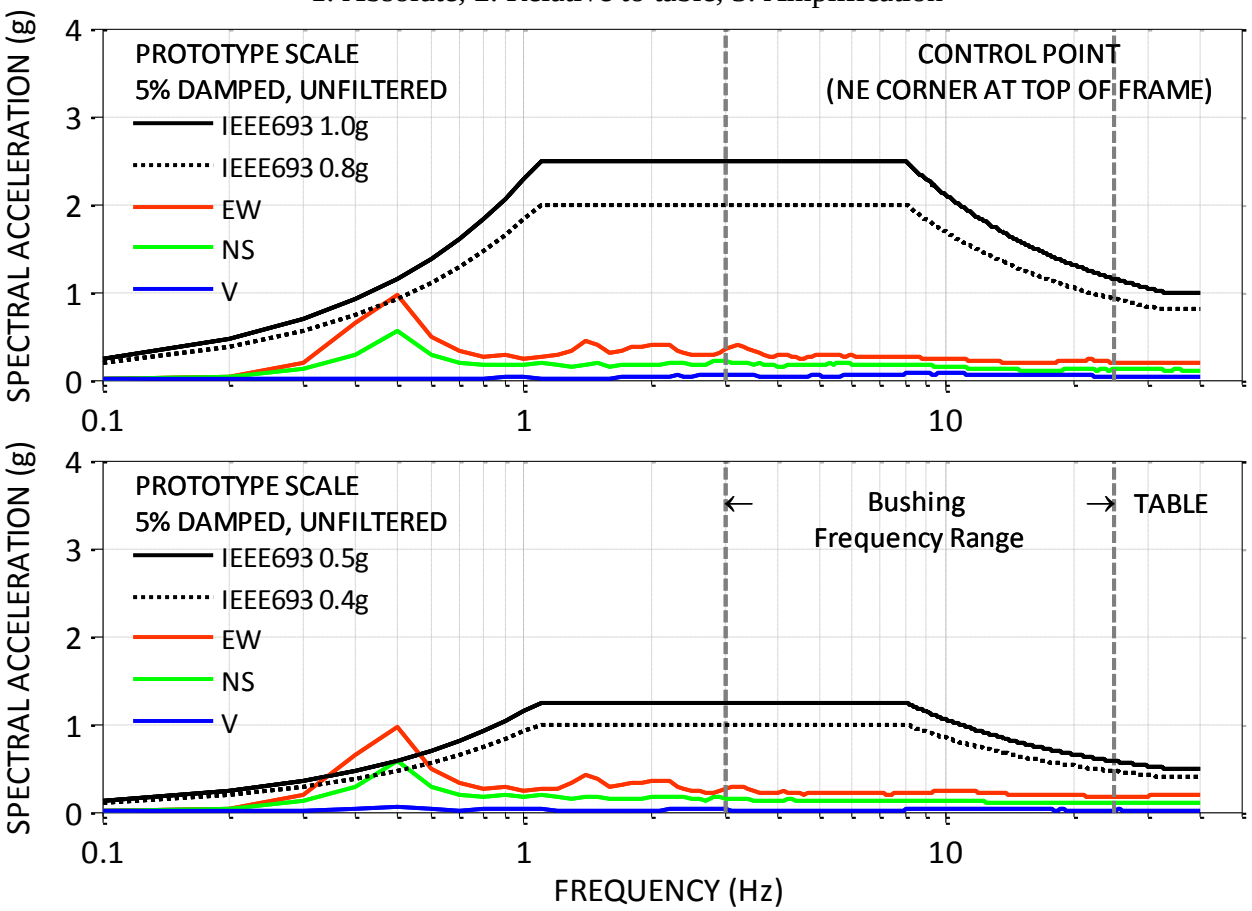
NON-ISOLATED SYSTEM (FIXED)
MEXICO CITY 100% BI-AXIAL (N90W in EW direction) (ACTUAL TEST AT 100%)
LENGTH SCALE=3 SYMMETRIC BUSHING CONFIGURATION

Peak Table Motion								
Acceleration (g)			Velocity (in/sec)			Displacement (in)		
EW	NS	V	EW	NS	V	EW	NS	V
0.18	0.10	0.02	13.05	7.52	0.47	2.39	1.61	0.04

OBSERVATIONS

Peak Resultant Displacement (in)				Peak Acceleration (g)							
Bushing Top		Isolator	Torsional Ampl[3] Ratio (TA)	Bushing Top			Bushing Bottom		Control Point		
Abs[1]	Rel[2]			EW	NS	V	EW	NS	EW	NS	V
2.80	0.18	N/A	N/A	0.46	0.32	0.07	0.19	0.12	0.18	0.11	0.03

1. Absolute, 2. Relative to table, 3. Amplification



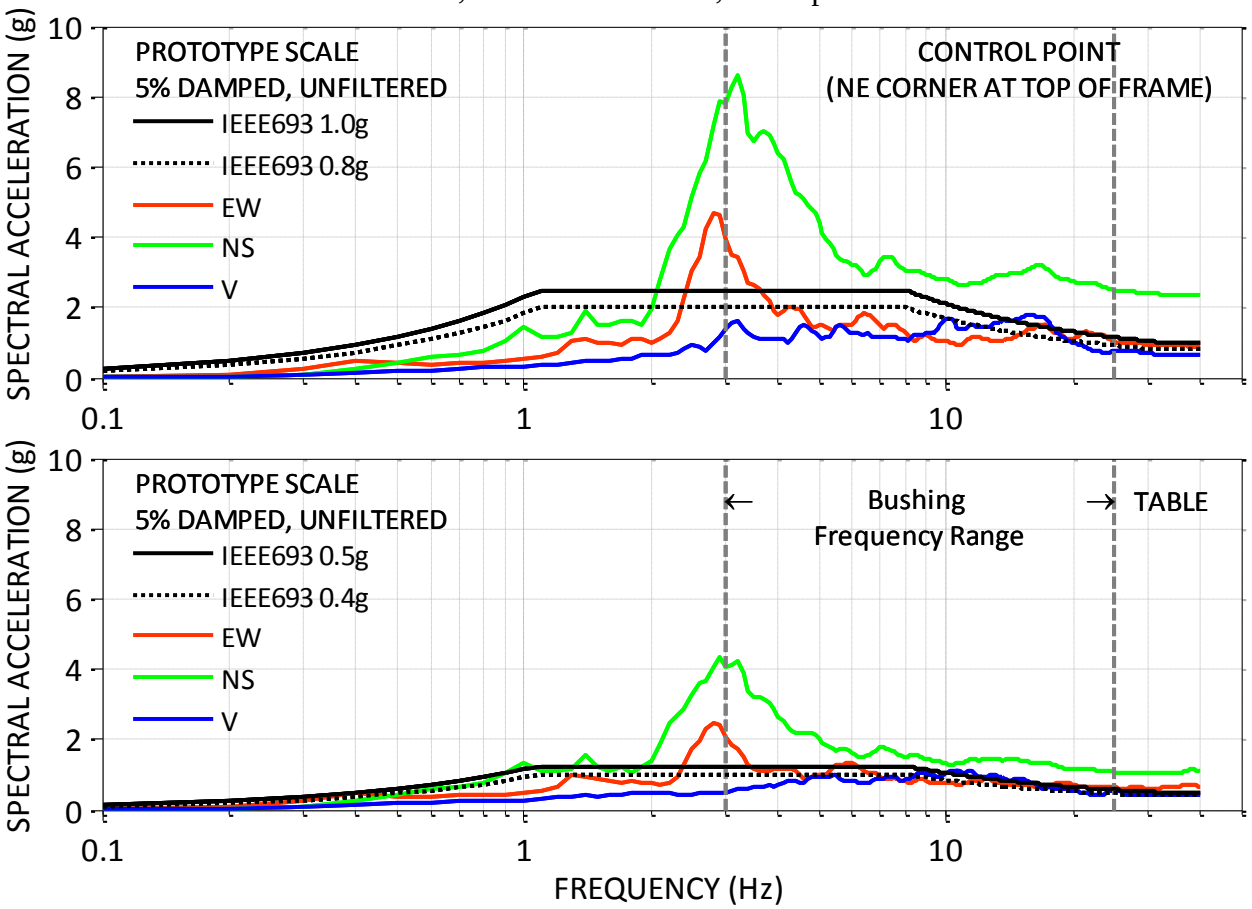
NON-ISOLATED SYSTEM (FIXED)
JENSEN FILTER 97% TRI-AXIAL (FN in EW direction) (ACTUAL TEST AT 24%)
LENGTH SCALE=3 SYMMETRIC BUSHING CONFIGURATION

Peak Table Motion								
Acceleration (g)			Velocity (in/sec)			Displacement (in)		
EW	NS	V	EW	NS	V	EW	NS	V
0.60	1.00	0.35	15.37	14.46	10.48	3.28	1.83	1.29

OBSERVATIONS

Peak Resultant Displacement (in)				Peak Acceleration (g)							
Bushing Top		Isolator	Torsional Ampl[3] Ratio (TA)	Bushing Top			Bushing Bottom		Control Point		
Abs[1]	Rel[2]			EW	NS	V	EW	NS	EW	NS	V
3.51	1.07	N/A	N/A	4.96	6.04	2.23	0.82	2.32	0.88	2.29	0.59

1. Absolute, 2. Relative to table, 3. Amplification



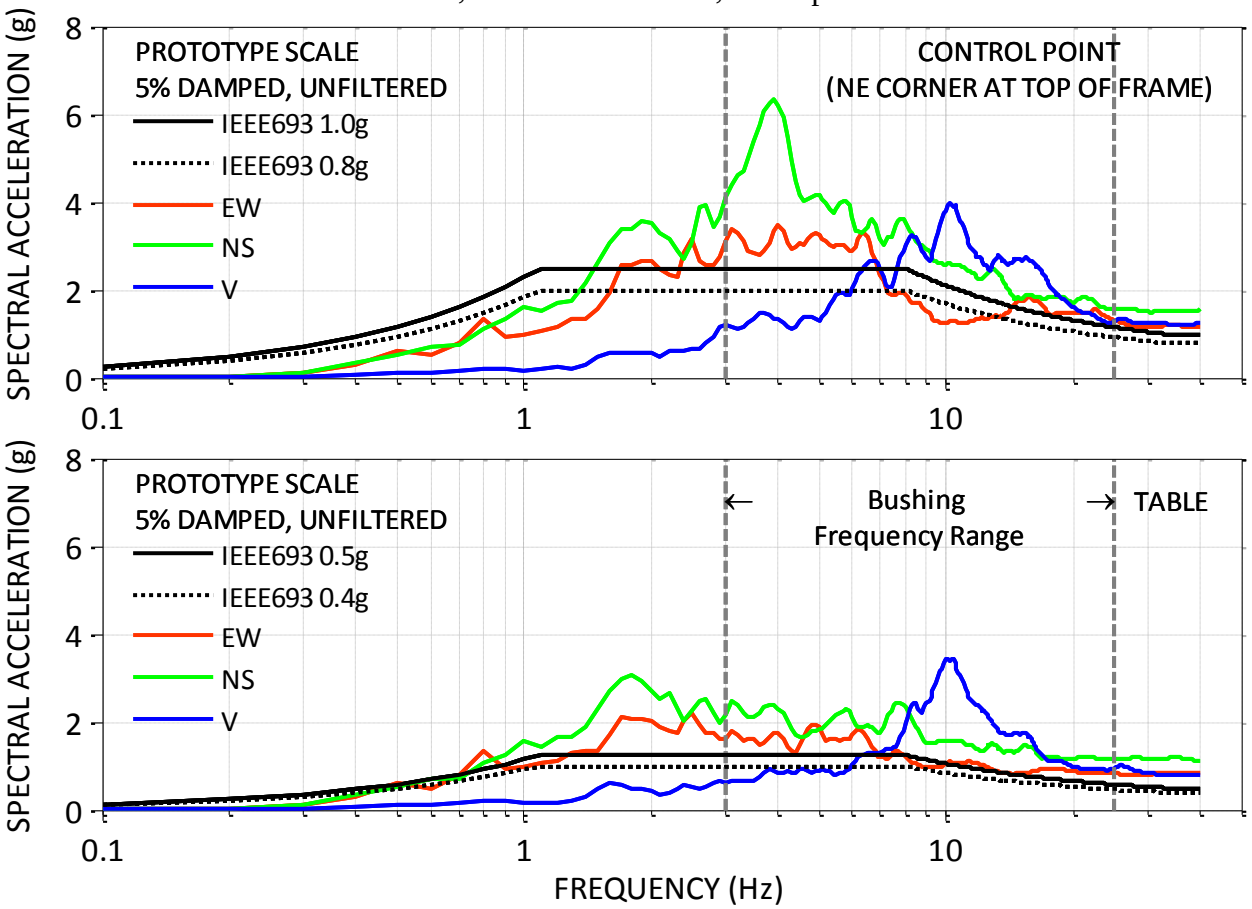
NON-ISOLATED SYSTEM (FIXED)
EL CENTRO 300% TRI-AXIAL (N90W in EW direction) (ACTUAL TEST AT 50%)
LENGTH SCALE=3 SYMMETRIC BUSHING CONFIGURATION

Peak Table Motion								
Acceleration (g)			Velocity (in/sec)			Displacement (in)		
EW	NS	V	EW	NS	V	EW	NS	V
0.80	1.11	0.74	20.82	20.48	8.37	2.30	2.50	0.53

OBSERVATIONS

Peak Resultant Displacement (in)				Peak Acceleration (g)							
Bushing Top		Isolator	Torsional Ampl[3] Ratio (TA)	Bushing Top			Bushing Bottom		Control Point		
Abs[1]	Rel[2]			EW	NS	V	EW	NS	EW	NS	V
3.67	1.36	N/A	N/A	7.37	10.08	2.51	1.05	1.55	1.12	1.49	1.09

1. Absolute, 2. Relative to table, 3. Amplification



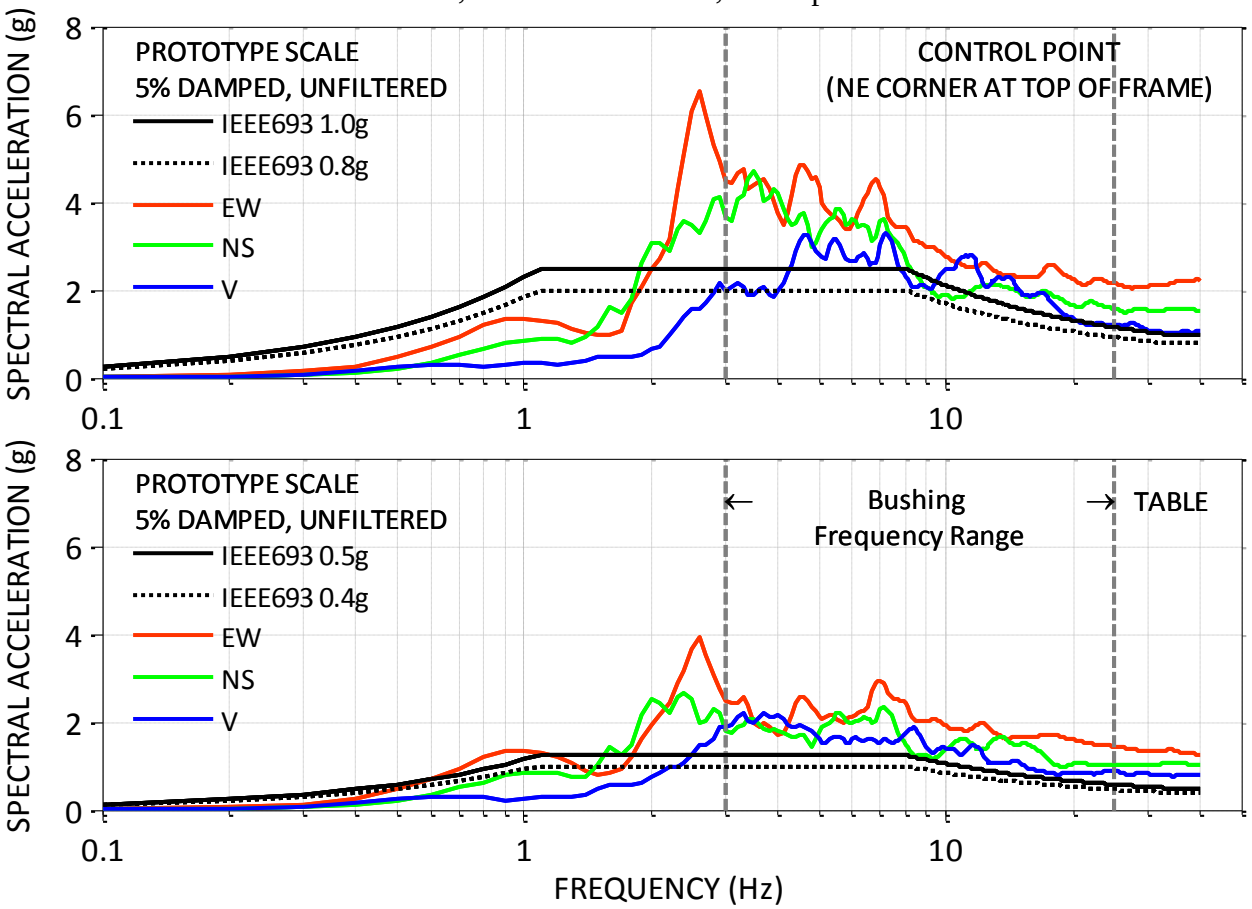
NON-ISOLATED SYSTEM (FIXED)
PACOIMA DAM 100% TRI-AXIAL (S16E in EW direction) (ACTUAL TEST AT 25%)
LENGTH SCALE=3 SYMMETRIC BUSHING CONFIGURATION

Peak Table Motion								
Acceleration (g)			Velocity (in/sec)			Displacement (in)		
EW	NS	V	EW	NS	V	EW	NS	V
1.26	0.92	0.77	23.87	14.31	10.50	2.76	1.42	1.44

OBSERVATIONS

Peak Resultant Displacement (in)				Peak Acceleration (g)							
Bushing Top		Isolator	Torsional Ampl[3] Ratio (TA)	Bushing Top			Bushing Bottom		Control Point		
Abs[1]	Rel[2]			EW	NS	V	EW	NS	EW	NS	V
3.60	1.09	N/A	N/A	8.62	7.79	3.01	1.87	1.50	1.99	1.48	0.99

1. Absolute, 2. Relative to table, 3. Amplification



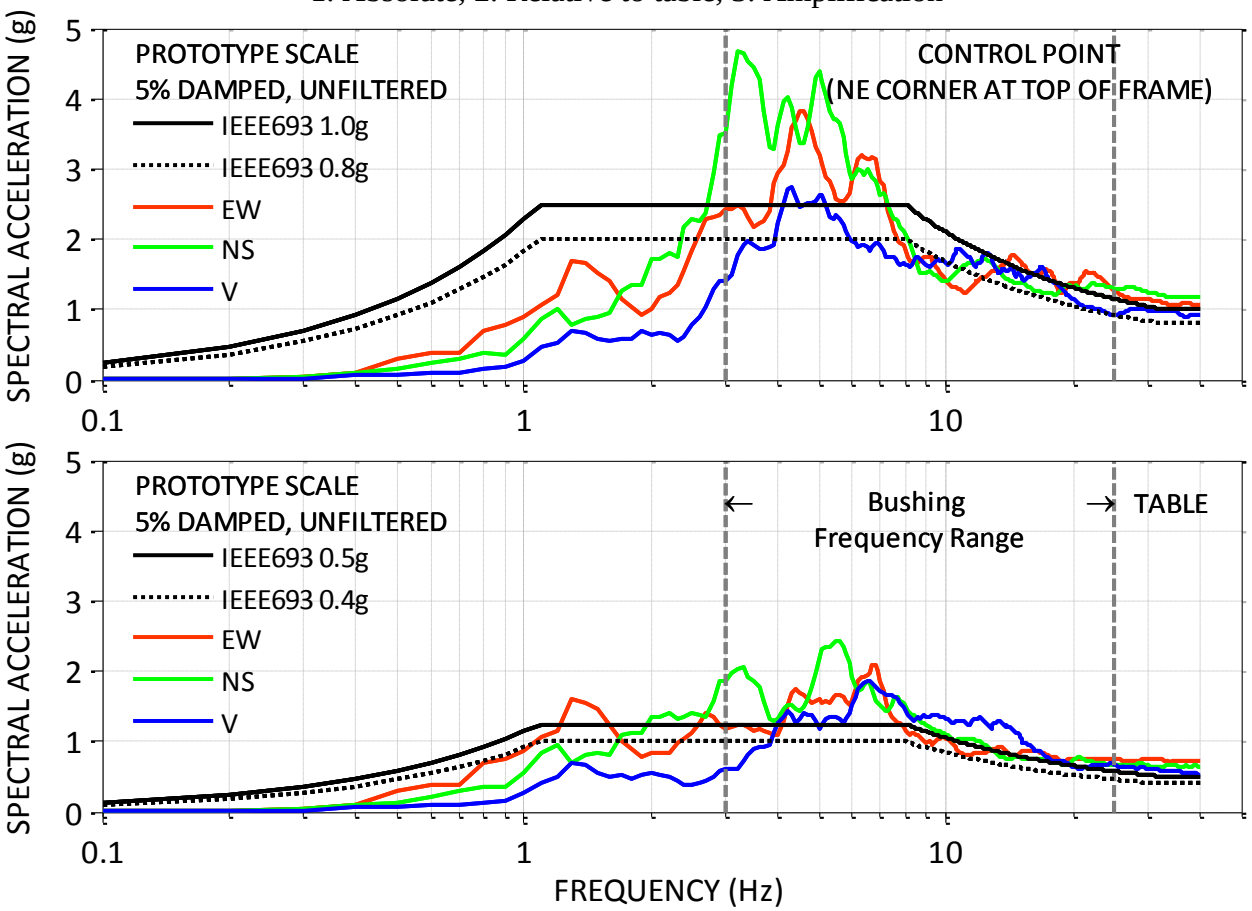
NON-ISOLATED SYSTEM (FIXED)
CHILE 100% TRI-AXIAL (EW in EW direction) (ACTUAL TEST AT 50%)
LENGTH SCALE=3 SYMMETRIC BUSHING CONFIGURATION

Peak Table Motion								
Acceleration (g)			Velocity (in/sec)			Displacement (in)		
EW	NS	V	EW	NS	V	EW	NS	V
0.69	0.63	0.51	10.01	8.27	6.96	1.37	0.83	0.51

OBSERVATIONS

Peak Resultant Displacement (in)				Peak Acceleration (g)							
Bushing Top		Isolator	Torsional Ampl[3] Ratio (TA)	Bushing Top			Bushing Bottom		Control Point		
Abs[1]	Rel[2]			EW	NS	V	EW	NS	EW	NS	V
1.90	1.02	N/A	N/A	7.12	7.43	3.26	0.99	1.31	1.04	1.17	0.90

1. Absolute, 2. Relative to table, 3. Amplification



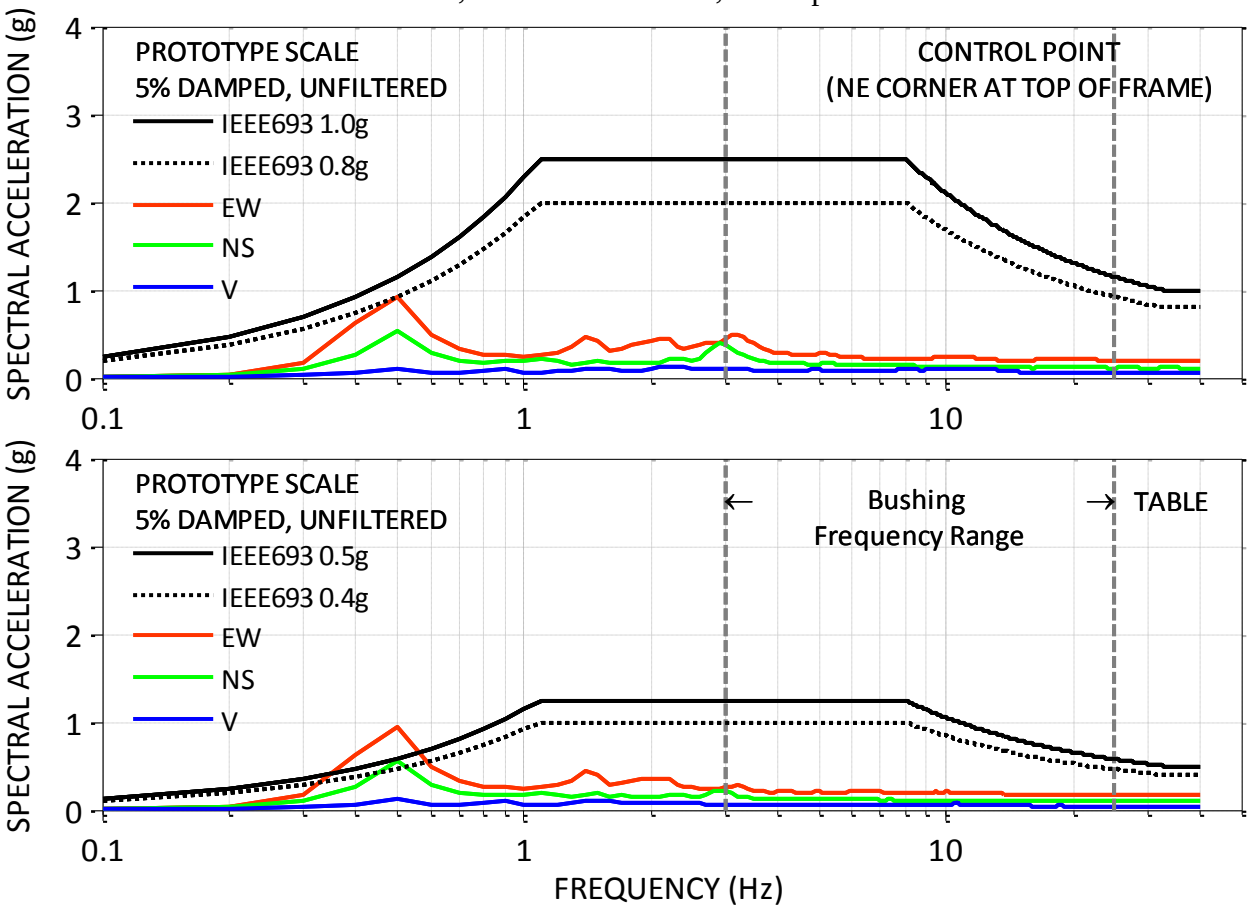
NON-ISOLATED SYSTEM (FIXED)
MEXICO CITY 100% TRI-AXIAL (N90W in EW direction) (ACTUAL TEST AT 100%)
LENGTH SCALE=3 SYMMETRIC BUSHING CONFIGURATION

Peak Table Motion								
Acceleration (g)			Velocity (in/sec)			Displacement (in)		
EW	NS	V	EW	NS	V	EW	NS	V
0.16	0.09	0.04	12.98	7.26	1.99	2.33	1.44	0.32

OBSERVATIONS

Peak Resultant Displacement (in)				Peak Acceleration (g)							
Bushing Top		Isolator	Torsional Ampl[3] Ratio (TA)	Bushing Top			Bushing Bottom		Control Point		
Abs[1]	Rel[2]			EW	NS	V	EW	NS	EW	NS	V
2.62	0.17	N/A	N/A	0.37	0.28	0.07	0.19	0.12	0.19	0.11	0.04

1. Absolute, 2. Relative to table, 3. Amplification



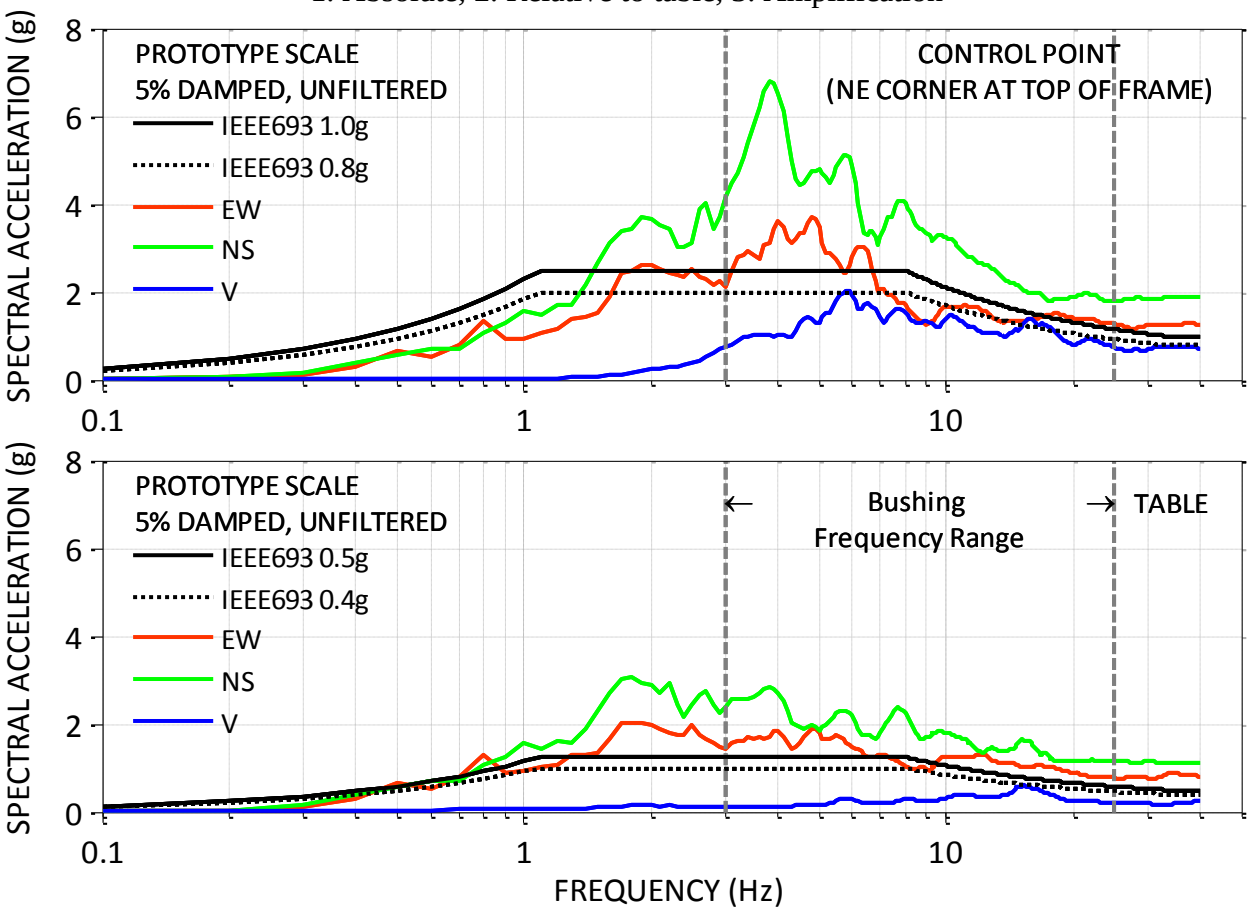
NON-ISOLATED SYSTEM (FIXED)
EL CENTRO 300% BI-AXIAL (N90W in EW direction) (ACTUAL TEST AT 50%)
LENGTH SCALE=3 NON-SYMMETRIC BUSHING CONFIGURATION

Peak Table Motion								
Acceleration (g)			Velocity (in/sec)			Displacement (in)		
EW	NS	V	EW	NS	V	EW	NS	V
0.71	1.11	0.13	21.50	21.99	2.97	2.50	2.62	0.15

OBSERVATIONS

Peak Resultant Displacement (in)				Peak Acceleration (g)							
Bushing Top		Isolator	Torsional Ampl[3] Ratio (TA)	Bushing Top			Bushing Bottom		Control Point		
Abs[1]	Rel[2]			EW	NS	V	EW	NS	EW	NS	V
3.20	0.96	N/A	N/A	5.53	7.81	1.56	1.18	1.86	1.17	1.79	0.61

1. Absolute, 2. Relative to table, 3. Amplification



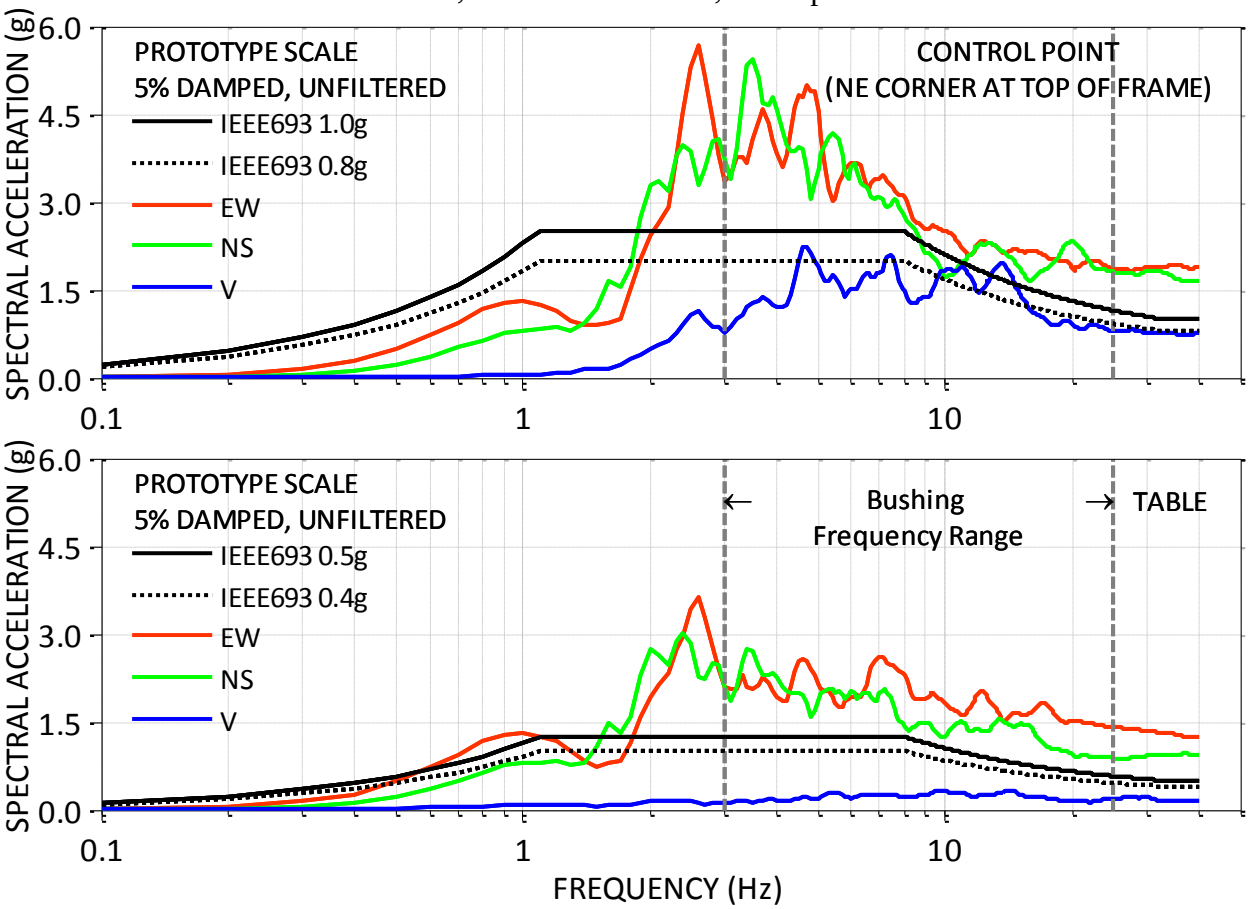
NON-ISOLATED SYSTEM (FIXED)
PACOIMA DAM 100% BI-AXIAL (S16E in EW direction) (ACTUAL TEST AT 25%)
LENGTH SCALE=3 NON-SYMMETRIC BUSHING CONFIGURATION

Peak Table Motion								
Acceleration (g)			Velocity (in/sec)			Displacement (in)		
EW	NS	V	EW	NS	V	EW	NS	V
1.21	0.85	0.13	23.89	15.70	7.82	2.82	1.52	0.21

OBSERVATIONS

Peak Resultant Displacement (in)				Peak Acceleration (g)							
Bushing Top		Isolator	Torsional Ampl[3] Ratio (TA)	Bushing Top			Bushing Bottom		Control Point		
Abs[1]	Rel[2]			EW	NS	V	EW	NS	EW	NS	V
3.53	1.05	N/A	N/A	7.20	8.31	1.40	1.85	1.61	1.76	1.62	0.71

1. Absolute, 2. Relative to table, 3. Amplification



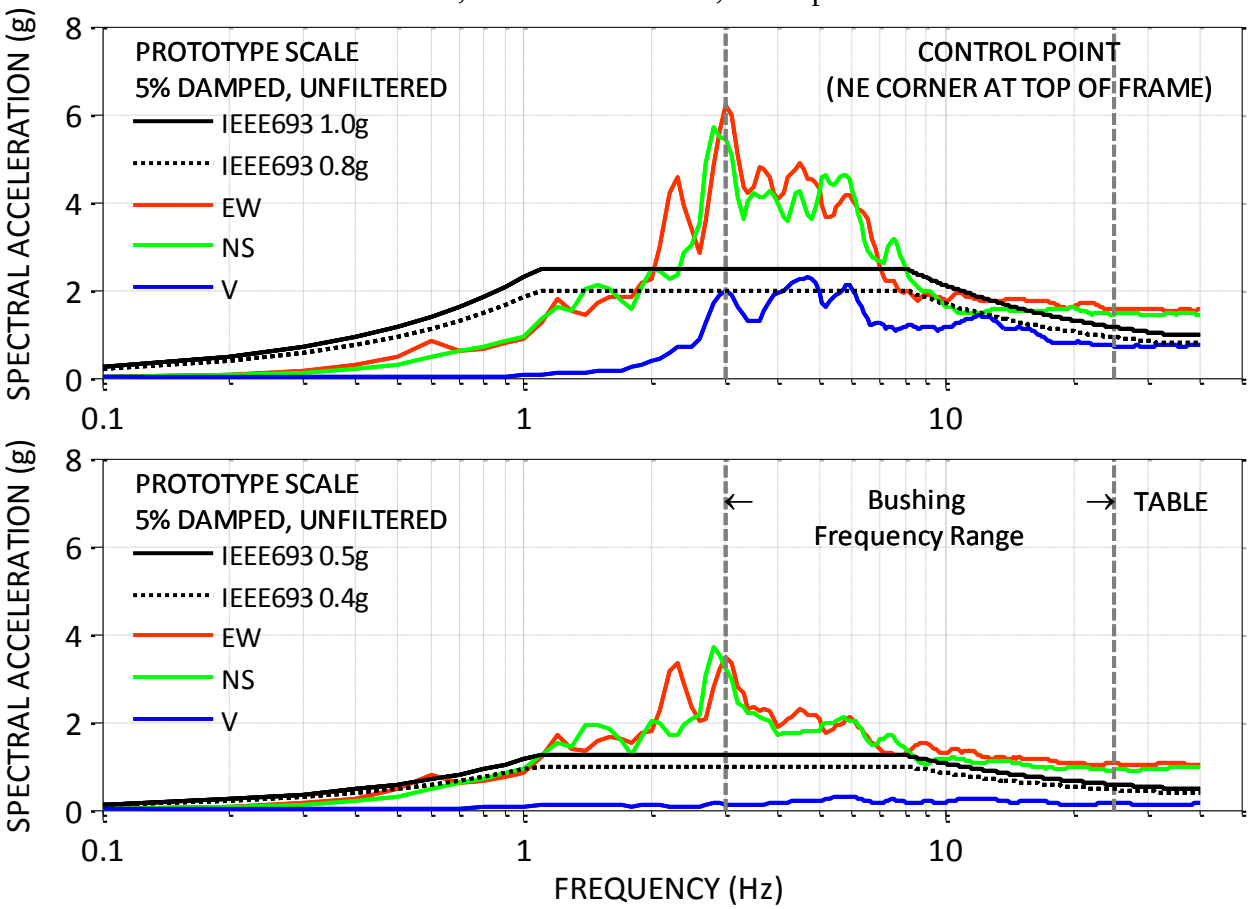
NON-ISOLATED SYSTEM (FIXED)
TAFT 500% BI-AXIAL (S69E in EW direction) (ACTUAL TEST AT 100%)
LENGTH SCALE=3 NON-SYMMETRIC BUSHING CONFIGURATION

Peak Table Motion								
Acceleration (g)			Velocity (in/sec)			Displacement (in)		
EW	NS	V	EW	NS	V	EW	NS	V
1.00	0.89	0.08	18.82	16.33	5.83	2.29	2.66	0.17

OBSERVATIONS

Peak Resultant Displacement (in)				Peak Acceleration (g)							
Bushing Top		Isolator	Torsional Ampl[3] Ratio (TA)	Bushing Top			Bushing Bottom		Control Point		
Abs[1]	Rel[2]			EW	NS	V	EW	NS	EW	NS	V
3.45	1.24	N/A	N/A	7.76	6.14	1.46	1.57	1.39	1.51	1.38	0.68

1. Absolute, 2. Relative to table, 3. Amplification



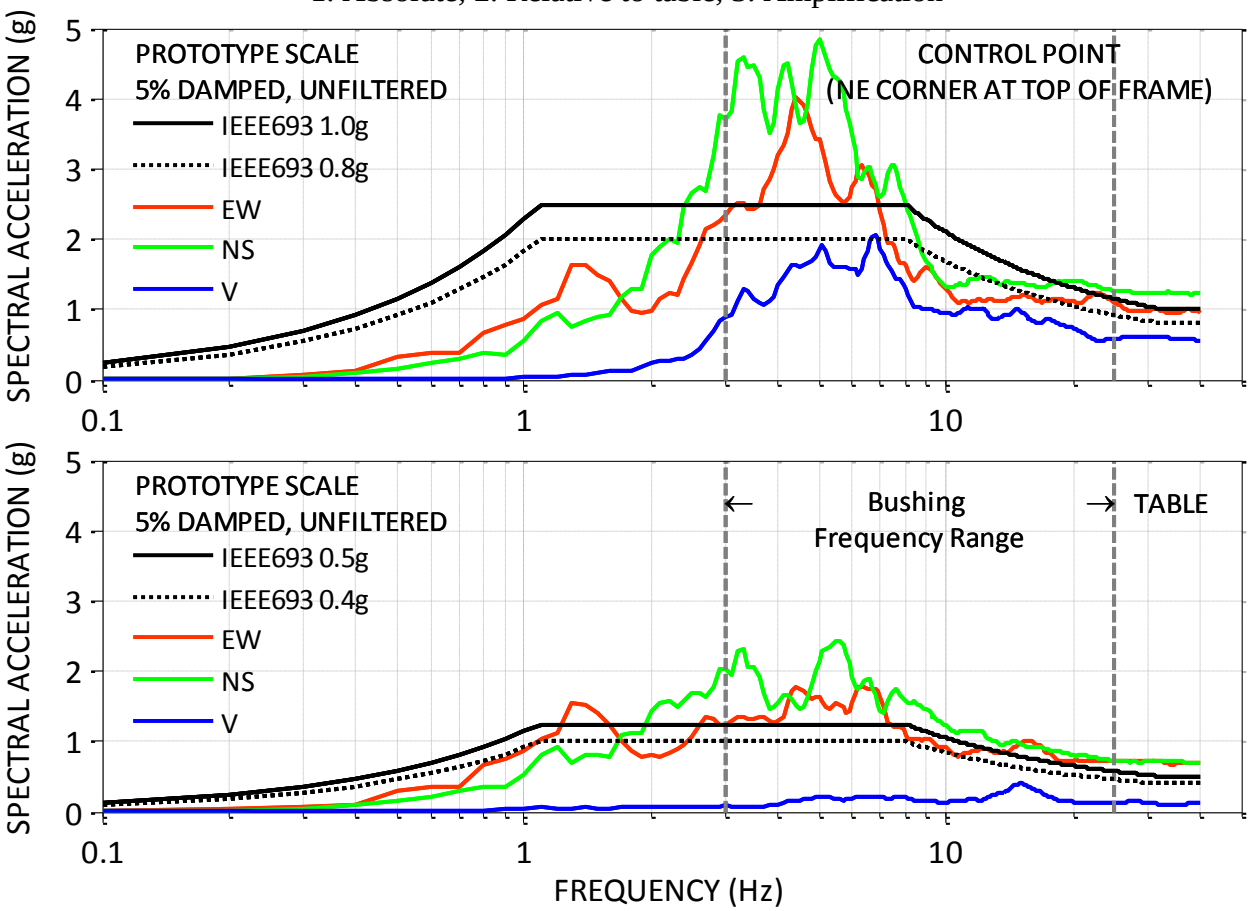
NON-ISOLATED SYSTEM (FIXED)
CHILE 100% BI-AXIAL (EW in EW direction) (ACTUAL TEST AT 50%)
LENGTH SCALE=3 NON-SYMMETRIC BUSHING CONFIGURATION

Peak Table Motion								
Acceleration (g)			Velocity (in/sec)			Displacement (in)		
EW	NS	V	EW	NS	V	EW	NS	V
0.68	0.70	0.08	9.87	8.73	5.15	1.42	0.85	0.10

OBSERVATIONS

Peak Resultant Displacement (in)				Peak Acceleration (g)							
Bushing Top		Isolator	Torsional Ampl[3] Ratio (TA)	Bushing Top			Bushing Bottom		Control Point		
Abs[1]	Rel[2]			EW	NS	V	EW	NS	EW	NS	V
1.74	0.88	N/A	N/A	5.59	5.99	1.24	1.00	1.20	0.92	1.20	0.55

1. Absolute, 2. Relative to table, 3. Amplification



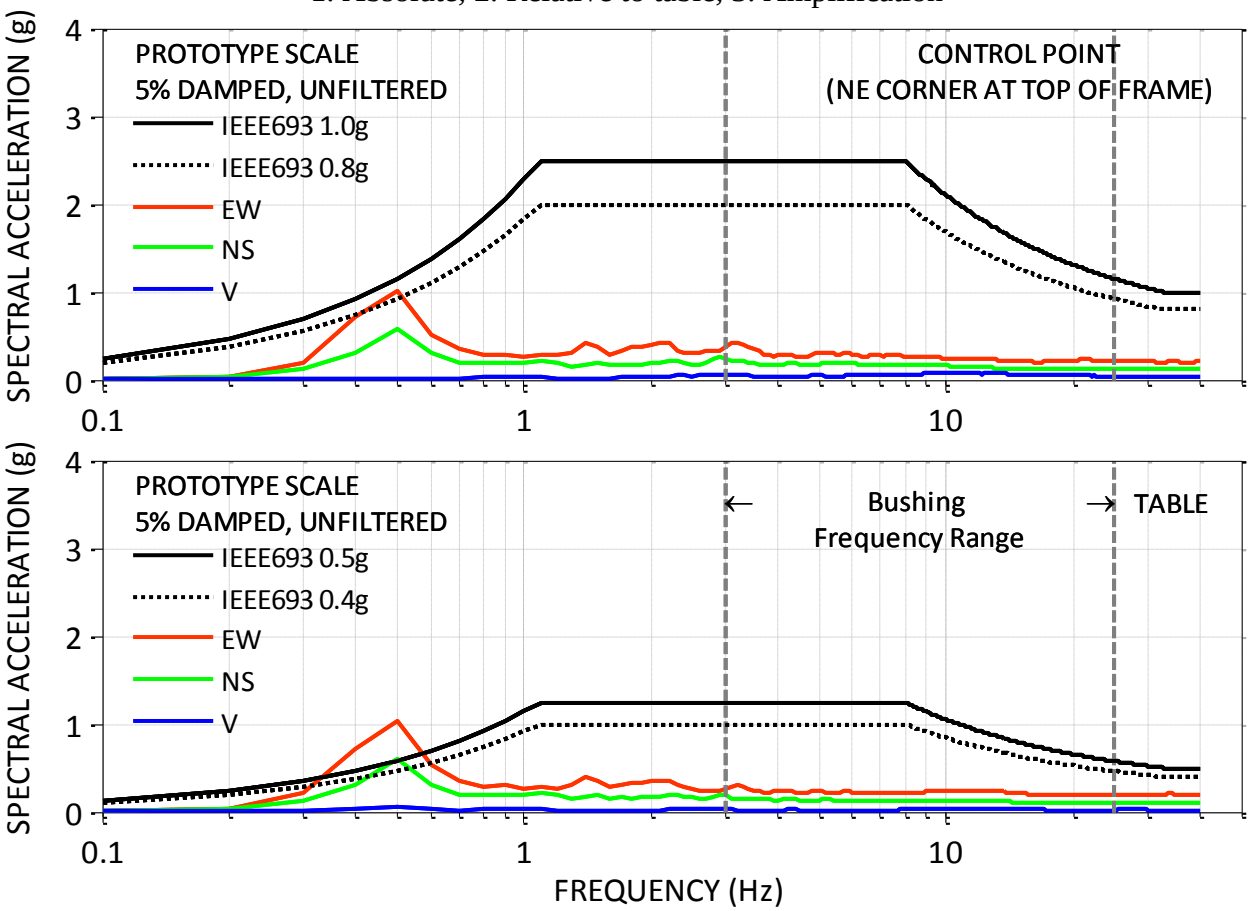
NON-ISOLATED SYSTEM (FIXED)
MEXICO CITY 100% BI-AXIAL (N90W in EW direction) (ACTUAL TEST AT 100%)
LENGTH SCALE=3 NON-SYMMETRIC BUSHING CONFIGURATION

Peak Table Motion								
Acceleration (g)			Velocity (in/sec)			Displacement (in)		
EW	NS	V	EW	NS	V	EW	NS	V
0.19	0.10	0.02	14.51	8.27	0.46	2.71	1.58	0.04

OBSERVATIONS

Peak Resultant Displacement (in)				Peak Acceleration (g)							
Bushing Top		Isolator	Torsional Ampl[3] Ratio (TA)	Bushing Top			Bushing Bottom		Control Point		
Abs[1]	Rel[2]			EW	NS	V	EW	NS	EW	NS	V
2.96	0.17	N/A	N/A	0.39	0.31	0.08	0.21	0.11	0.20	0.11	0.03

1. Absolute, 2. Relative to table, 3. Amplification



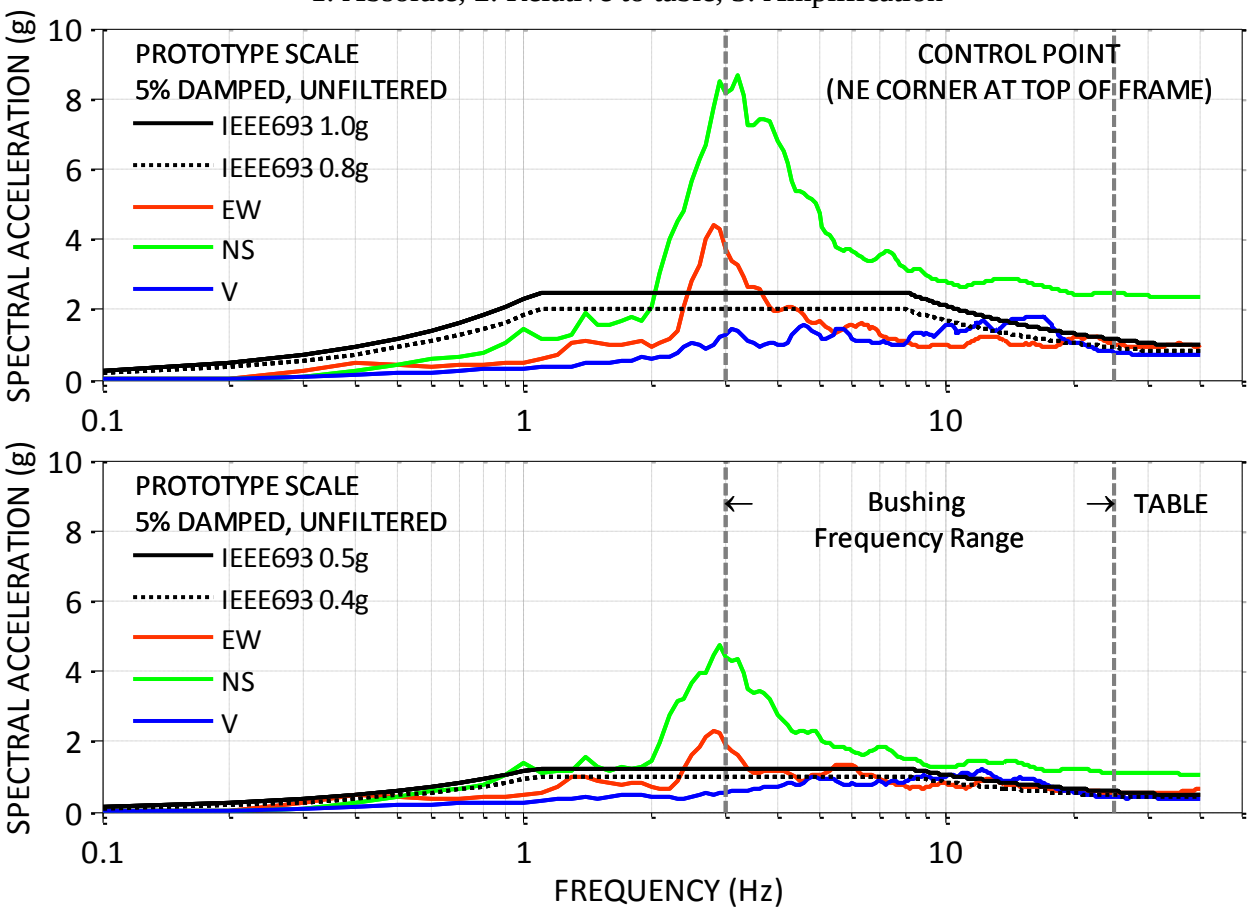
NON-ISOLATED SYSTEM (FIXED)
JENSEN FILTER 97% TRI-AXIAL (FN in EW direction) (ACTUAL TEST AT 24%)
LENGTH SCALE=3 NON-SYMMETRIC BUSHING CONFIGURATION

Peak Table Motion								
Acceleration (g)			Velocity (in/sec)			Displacement (in)		
EW	NS	V	EW	NS	V	EW	NS	V
0.56	1.04	0.36	15.52	16.54	9.64	2.63	1.94	1.04

OBSERVATIONS

Peak Resultant Displacement (in)				Peak Acceleration (g)							
Bushing Top		Isolator	Torsional Ampl[3] Ratio (TA)	Bushing Top			Bushing Bottom		Control Point		
Abs[1]	Rel[2]			EW	NS	V	EW	NS	EW	NS	V
3.00	1.13	N/A	N/A	4.63	6.77	1.53	0.89	2.44	0.87	2.36	0.66

1. Absolute, 2. Relative to table, 3. Amplification



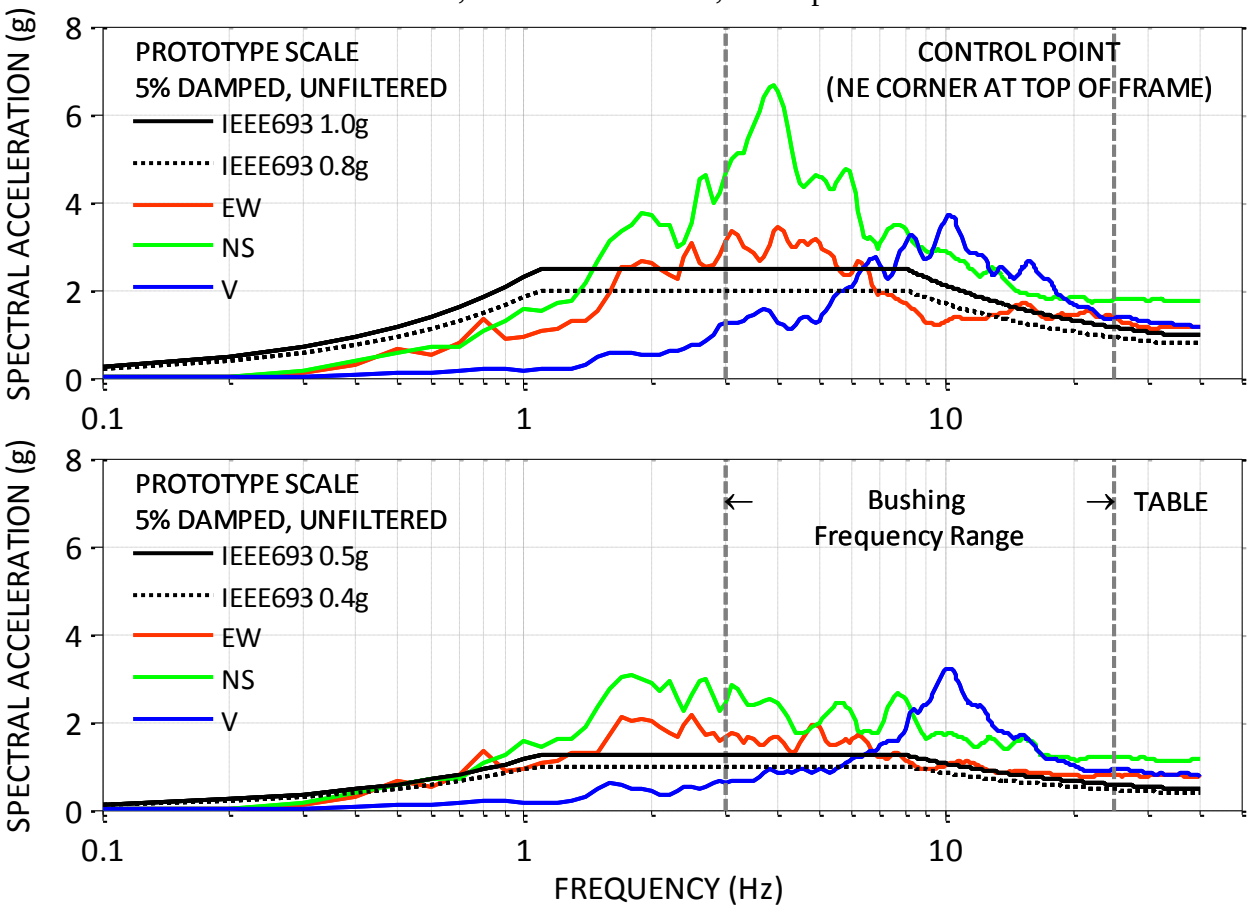
NON-ISOLATED SYSTEM (FIXED)
EL CENTRO 300% TRI-AXIAL (N90W in EW direction) (ACTUAL TEST AT 50%)
LENGTH SCALE=3 NON-SYMMETRIC BUSHING CONFIGURATION

Peak Table Motion								
Acceleration (g)			Velocity (in/sec)			Displacement (in)		
EW	NS	V	EW	NS	V	EW	NS	V
0.77	1.12	0.73	21.24	22.33	8.71	2.40	2.61	0.61

OBSERVATIONS

Peak Resultant Displacement (in)				Peak Acceleration (g)							
Bushing Top		Isolator	Torsional Ampl[3] Ratio (TA)	Bushing Top			Bushing Bottom		Control Point		
Abs[1]	Rel[2]			EW	NS	V	EW	NS	EW	NS	V
3.14	0.99	N/A	N/A	7.55	7.04	2.26	1.18	1.74	1.10	1.68	1.11

1. Absolute, 2. Relative to table, 3. Amplification



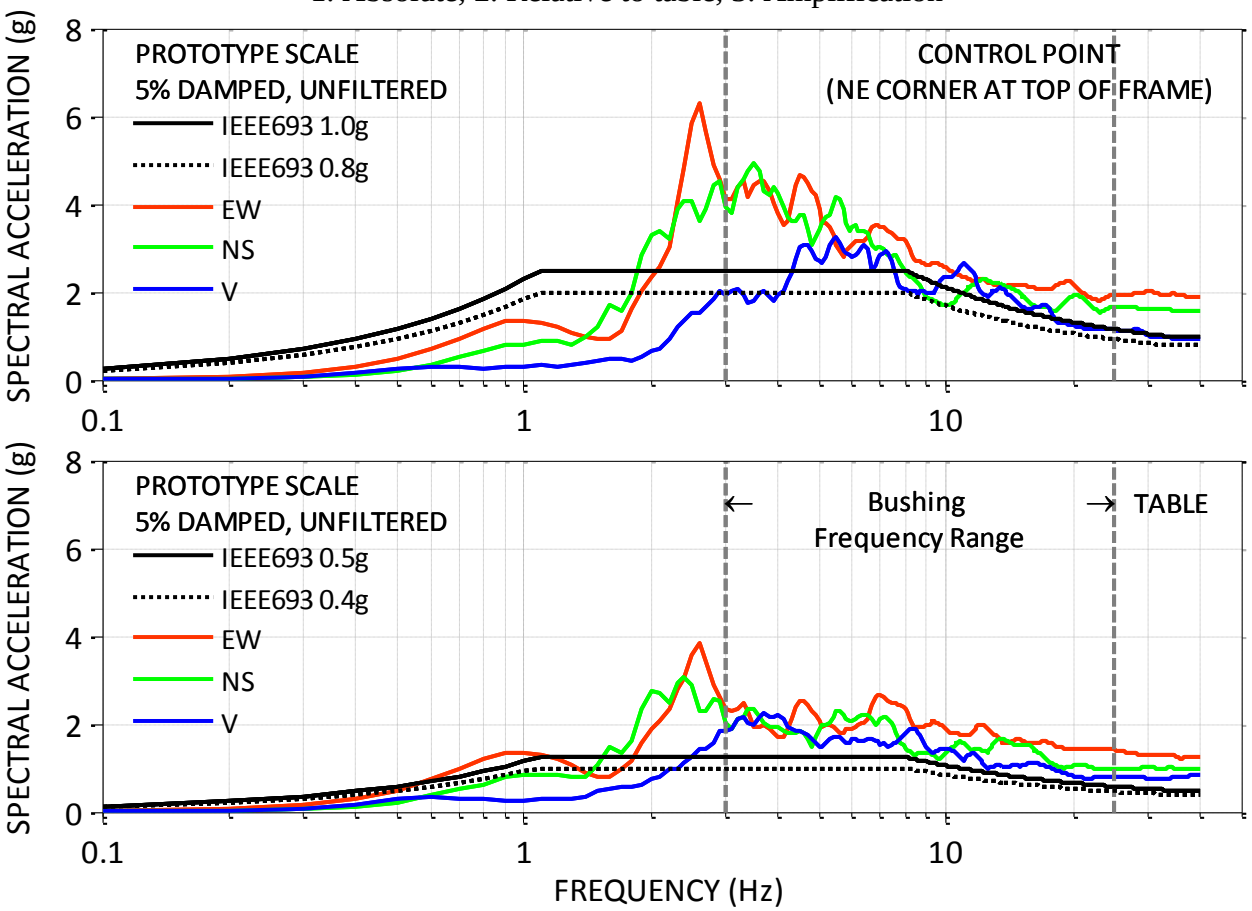
NON-ISOLATED SYSTEM (FIXED)
PACOIMA DAM 100% TRI-AXIAL (S16E in EW direction) (ACTUAL TEST AT 25%)
LENGTH SCALE=3 NON-SYMMETRIC BUSHING CONFIGURATION

Peak Table Motion								
Acceleration (g)			Velocity (in/sec)			Displacement (in)		
EW	NS	V	EW	NS	V	EW	NS	V
1.23	0.92	0.76	24.36	15.44	10.36	2.62	1.49	1.37

OBSERVATIONS

Peak Resultant Displacement (in)				Peak Acceleration (g)							
Bushing Top		Isolator	Torsional Ampl[3] Ratio (TA)	Bushing Top			Bushing Bottom		Control Point		
Abs[1]	Rel[2]			EW	NS	V	EW	NS	EW	NS	V
3.36	1.11	N/A	N/A	7.64	7.91	2.16	1.85	1.53	1.78	1.54	0.91

1. Absolute, 2. Relative to table, 3. Amplification



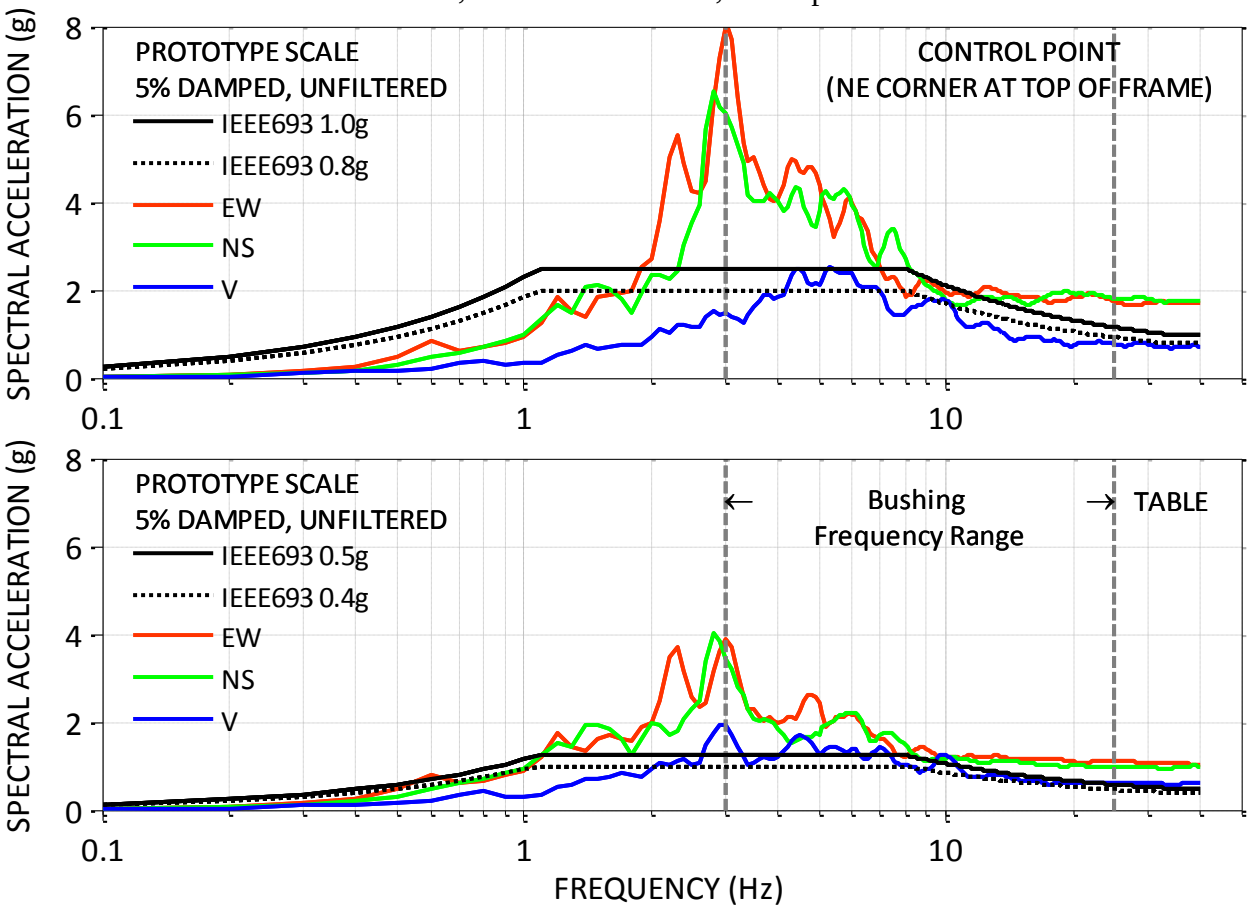
NON-ISOLATED SYSTEM (FIXED)
TAFT 500% TRI-AXIAL (S69E in EW direction) (ACTUAL TEST AT 100%)
LENGTH SCALE=3 NON-SYMMETRIC BUSHING CONFIGURATION

Peak Table Motion								
Acceleration (g)			Velocity (in/sec)			Displacement (in)		
EW	NS	V	EW	NS	V	EW	NS	V
1.04	0.91	0.59	19.45	15.34	14.33	2.27	2.31	1.14

OBSERVATIONS

Peak Resultant Displacement (in)				Peak Acceleration (g)							
Bushing Top		Isolator	Torsional Ampl[3] Ratio (TA)	Bushing Top			Bushing Bottom		Control Point		
Abs[1]	Rel[2]			EW	NS	V	EW	NS	EW	NS	V
3.16	1.11	N/A	N/A	7.66	6.26	1.38	1.74	1.62	1.65	1.68	0.63

1. Absolute, 2. Relative to table, 3. Amplification



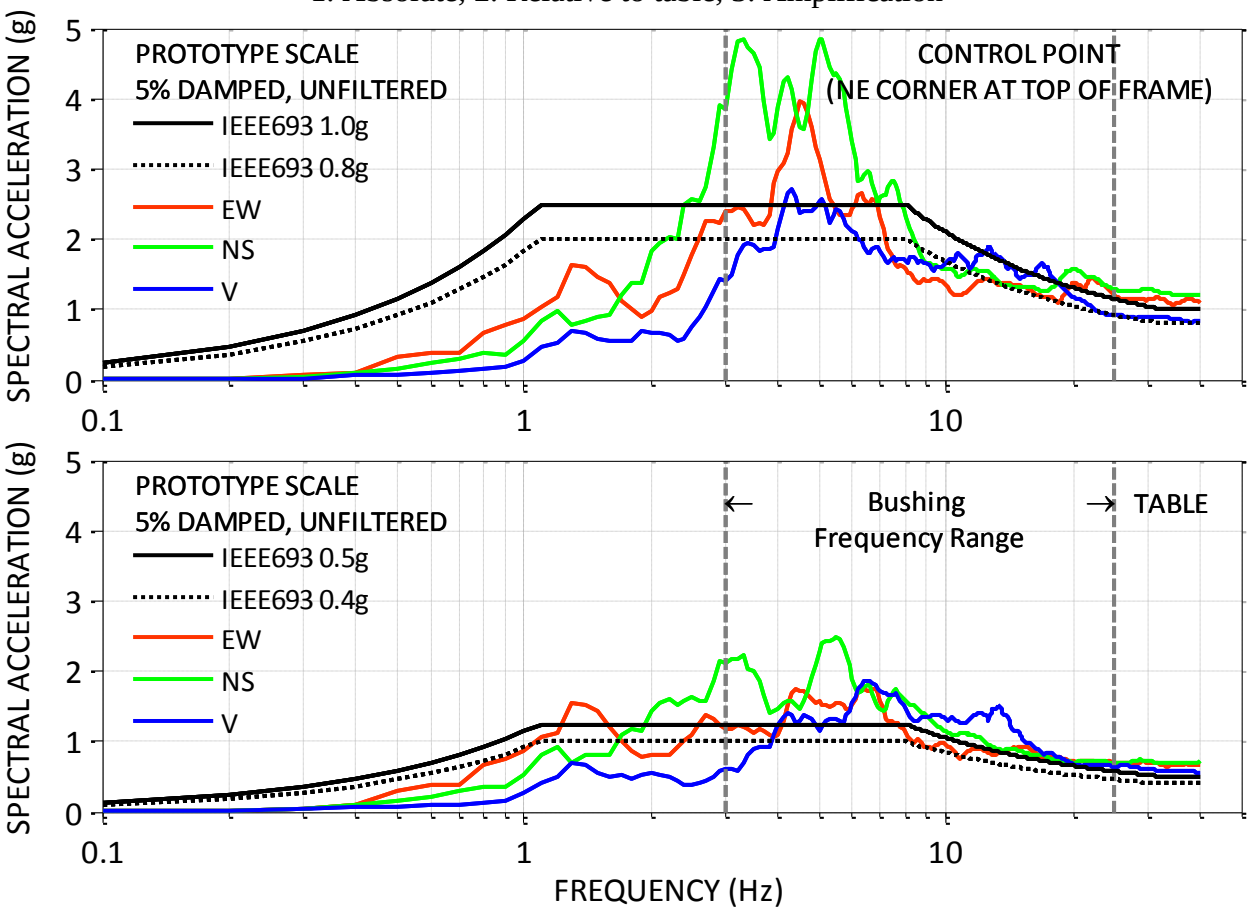
NON-ISOLATED SYSTEM (FIXED)
CHILE 100% TRI-AXIAL (EW in EW direction) (ACTUAL TEST AT 50%)
LENGTH SCALE=3 NON-SYMMETRIC BUSHING CONFIGURATION

Peak Table Motion								
Acceleration (g)			Velocity (in/sec)			Displacement (in)		
EW	NS	V	EW	NS	V	EW	NS	V
0.65	0.68	0.53	10.28	8.58	6.74	1.28	0.87	0.45

OBSERVATIONS

Peak Resultant Displacement (in)				Peak Acceleration (g)							
Bushing Top		Isolator	Torsional Ampl[3] Ratio (TA)	Bushing Top			Bushing Bottom		Control Point		
Abs[1]	Rel[2]			EW	NS	V	EW	NS	EW	NS	V
1.74	0.85	N/A	N/A	6.09	6.25	2.45	1.04	1.21	1.01	1.20	0.83

1. Absolute, 2. Relative to table, 3. Amplification



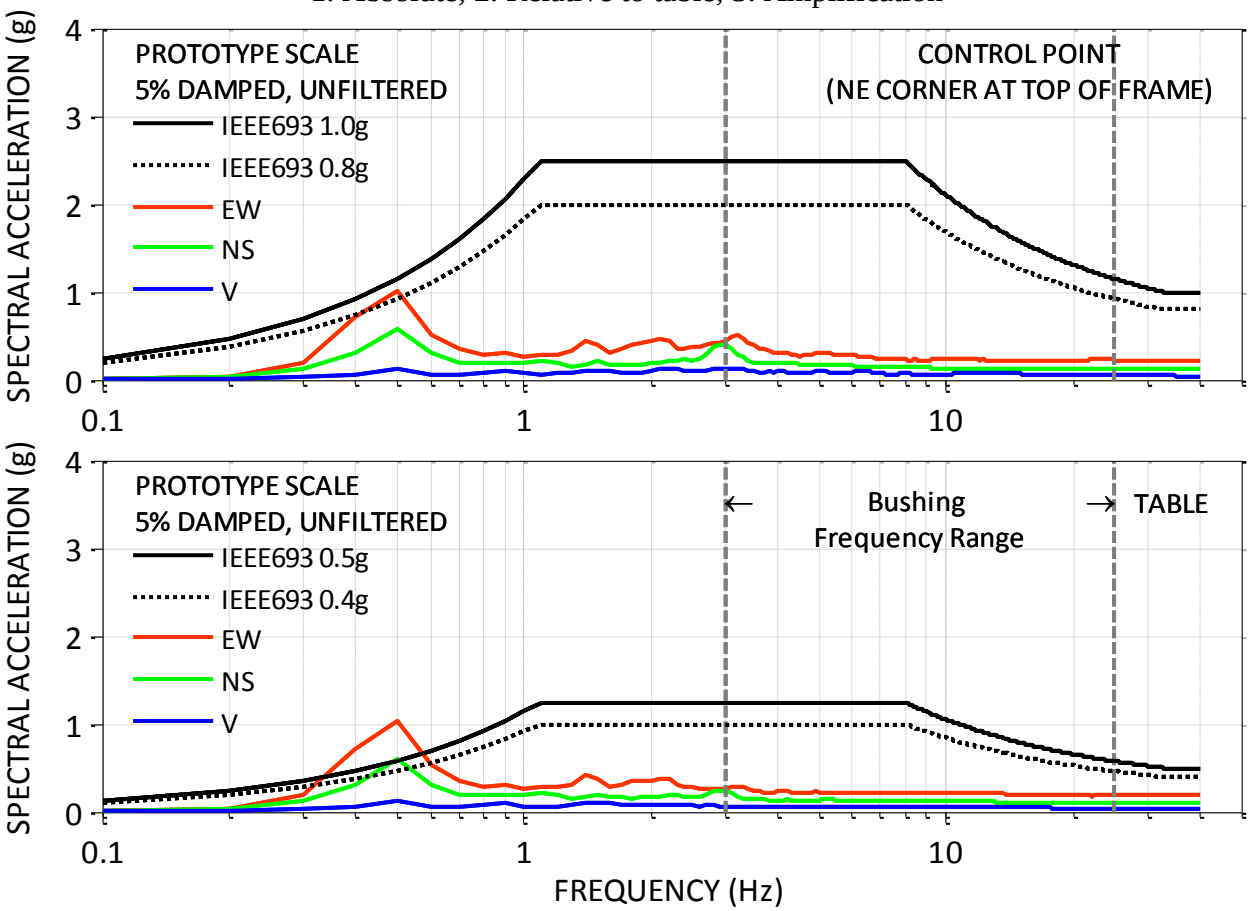
NON-ISOLATED SYSTEM (FIXED)
MEXICO CITY 100% TRI-AXIAL (N90W in EW direction) (ACTUAL TEST AT 100%)
LENGTH SCALE=3 NON-SYMMETRIC BUSHING CONFIGURATION

Peak Table Motion								
Acceleration (g)			Velocity (in/sec)			Displacement (in)		
EW	NS	V	EW	NS	V	EW	NS	V
0.18	0.10	0.04	14.67	8.06	2.11	2.69	1.49	0.35

OBSERVATIONS

Peak Resultant Displacement (in)				Peak Acceleration (g)							
Bushing Top		Isolator	Torsional Ampl[3] Ratio (TA)	Bushing Top			Bushing Bottom		Control Point		
Abs[1]	Rel[2]			EW	NS	V	EW	NS	EW	NS	V
2.86	0.17	N/A	N/A	0.36	0.24	0.08	0.21	0.12	0.21	0.12	0.04

1. Absolute, 2. Relative to table, 3. Amplification

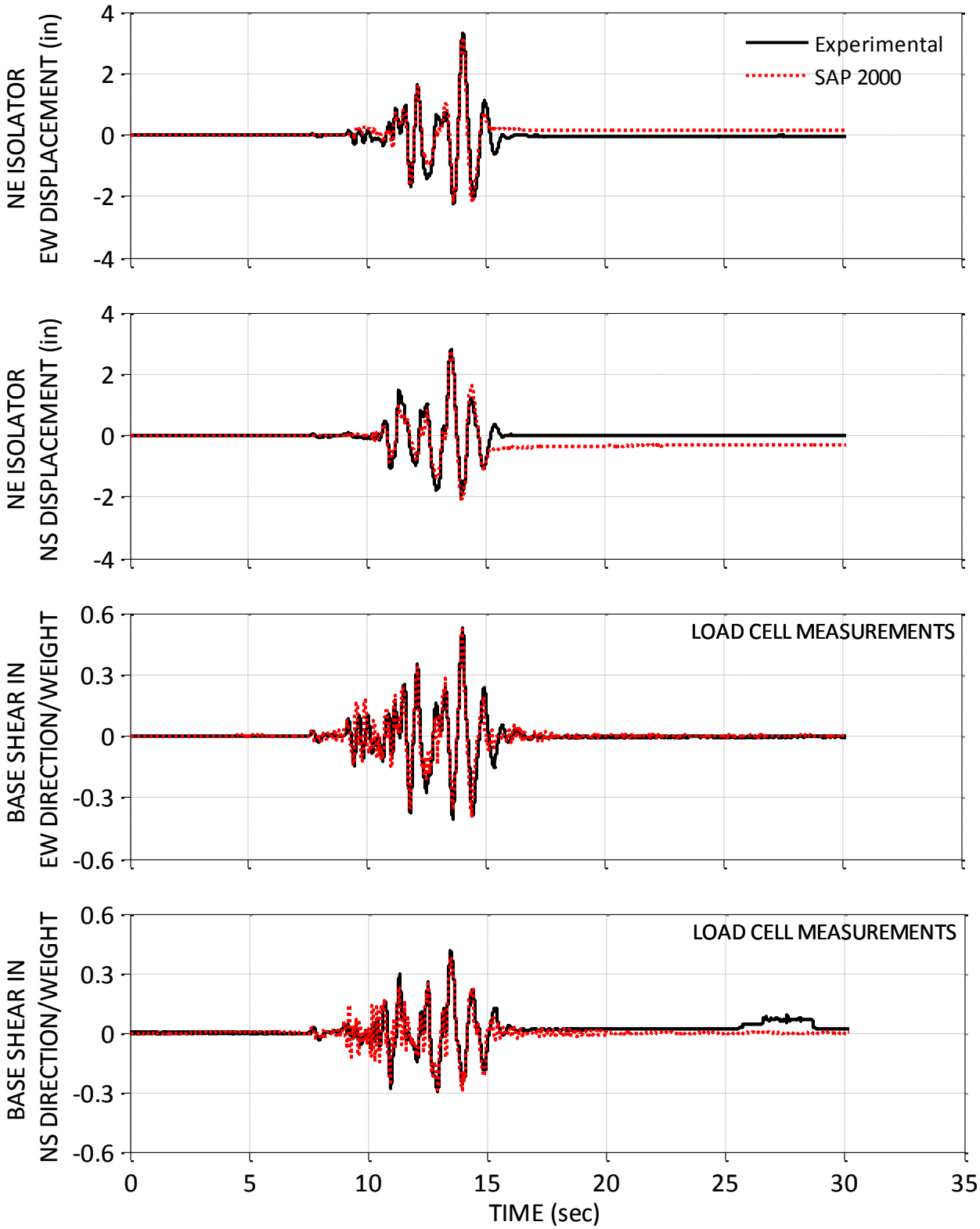


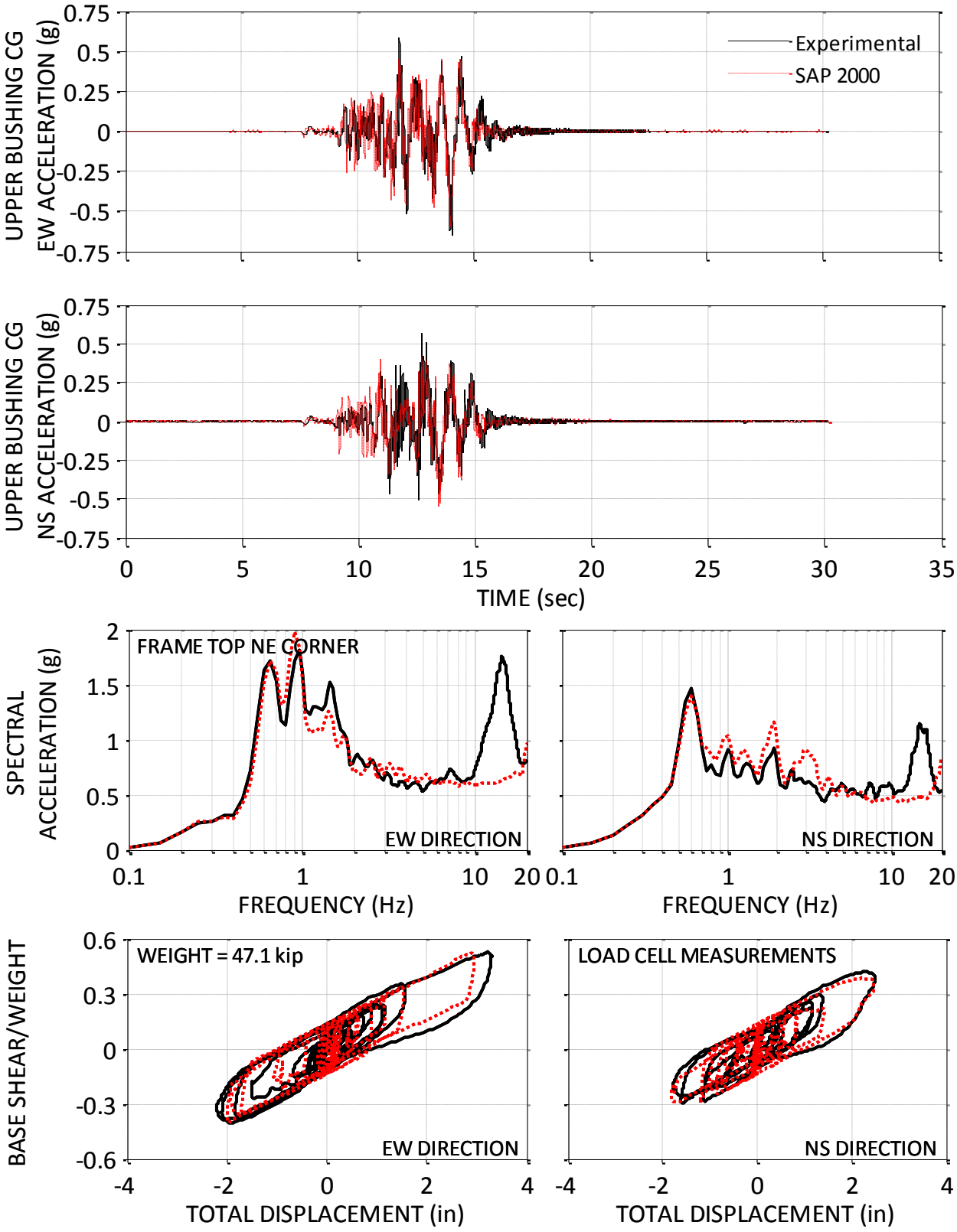
APPENDIX C
SUMMARY OF EXPERIMENTAL AND ANALYTICAL COMPARISONS FOR THE LEAD-RUBBER SYSTEM AND THE TRIPLE FRICTION PENDULUM SYSTEM MODELLED USING THE PARALLEL MODEL

PART C-1
SUMMARY OF EXPERIMENTAL AND ANALYTICAL COMPARISONS FOR LEAD-RUBBER SYSTEM AT LENGTH SCALE OF 3

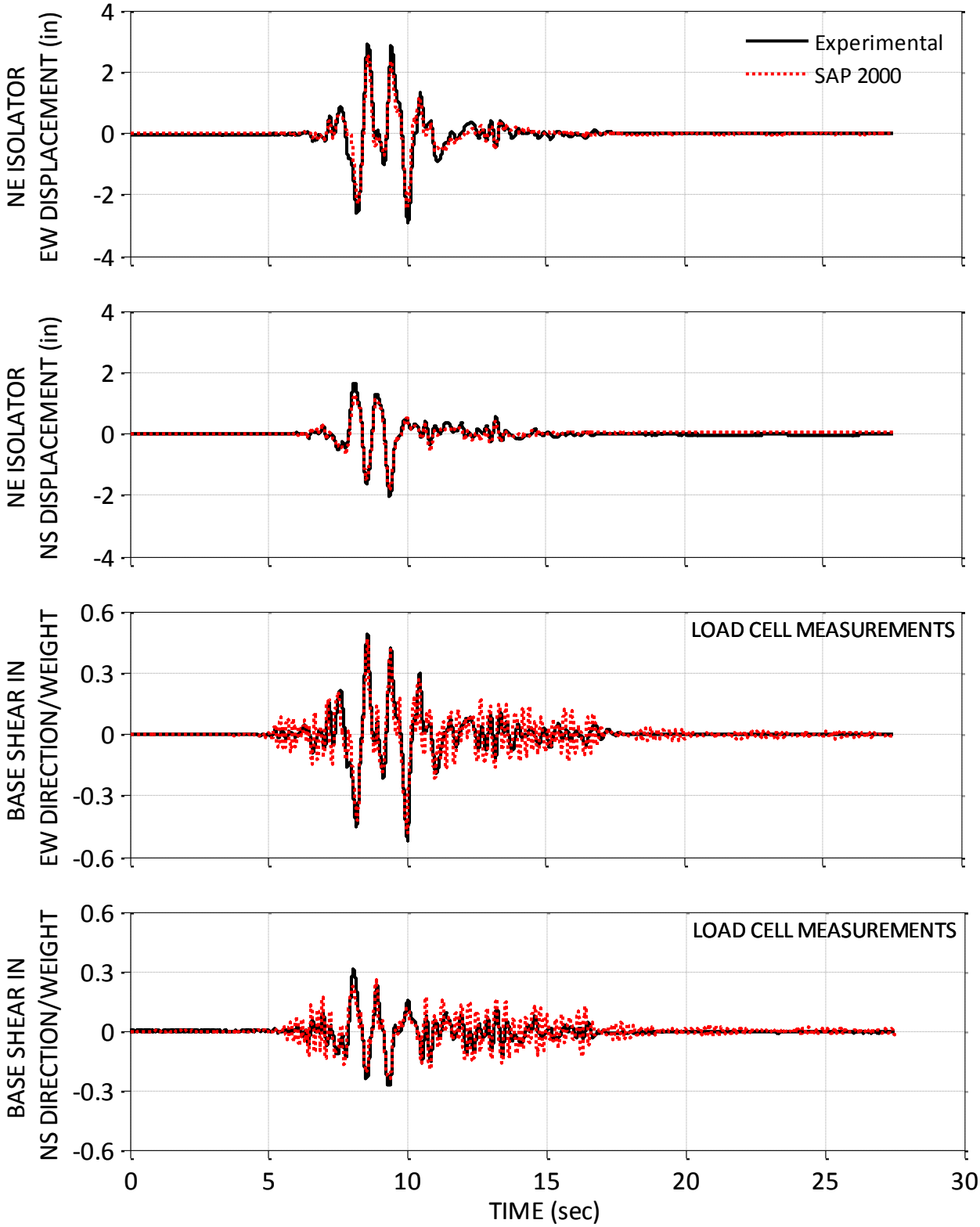
(PERCENTAGE AMOUNT IS SCALE FACTOR APPLIED TO ACCELERATION OF ACTUAL MOTION. FOR EXAMPLE, 100% DENOTES MOTION AS RECORDED, 200% DENOTES THAT ACCELERATION WAS SCALED UP BY FACTOR OF 2)

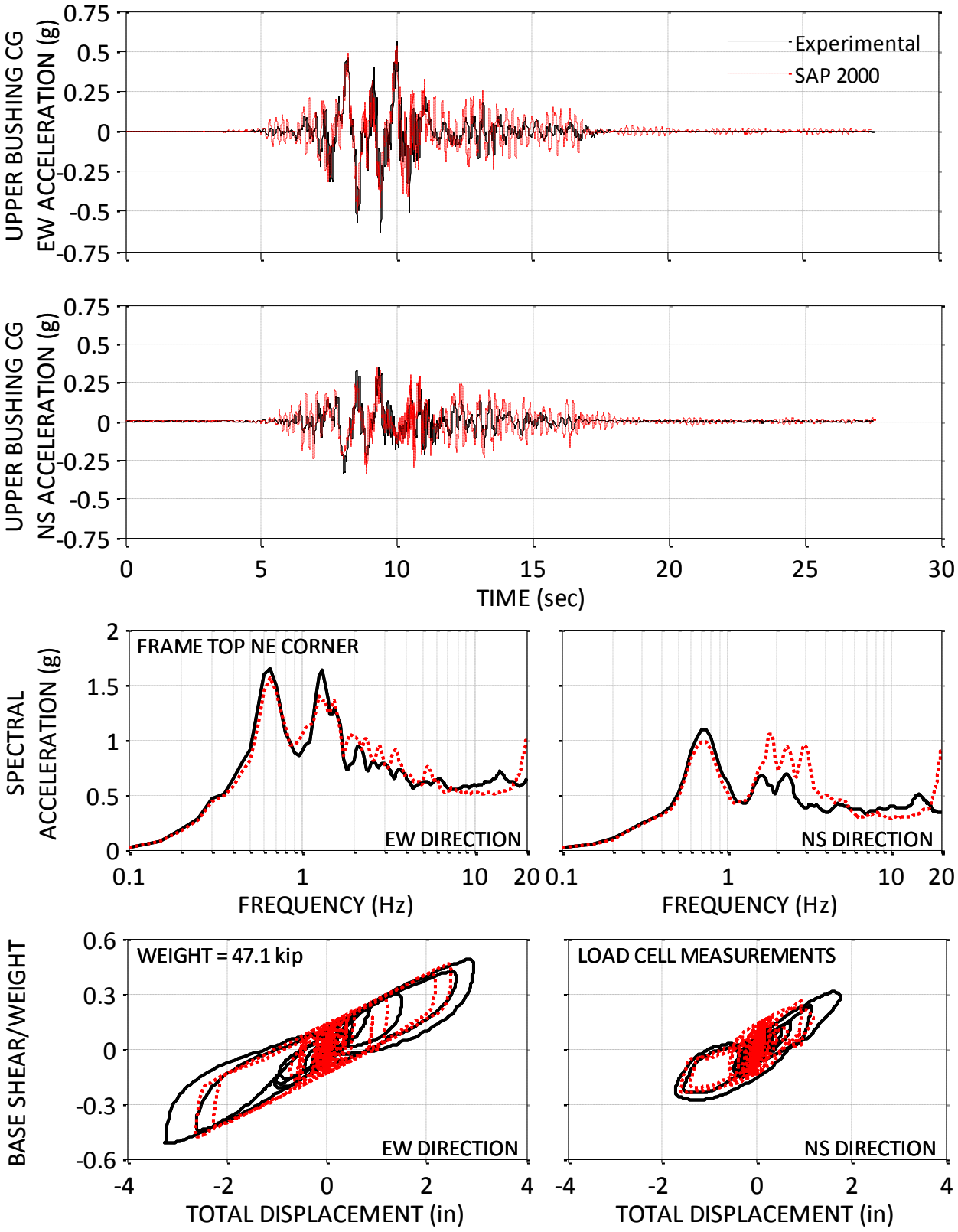
LRB SYSTEM (Bolted-Bolted Configuration)
KARAKYR 137% BI-AXIAL (FN in EW direction)
LENGTH SCALE=3 SYMMETRIC BUSHING CONFIGURATION

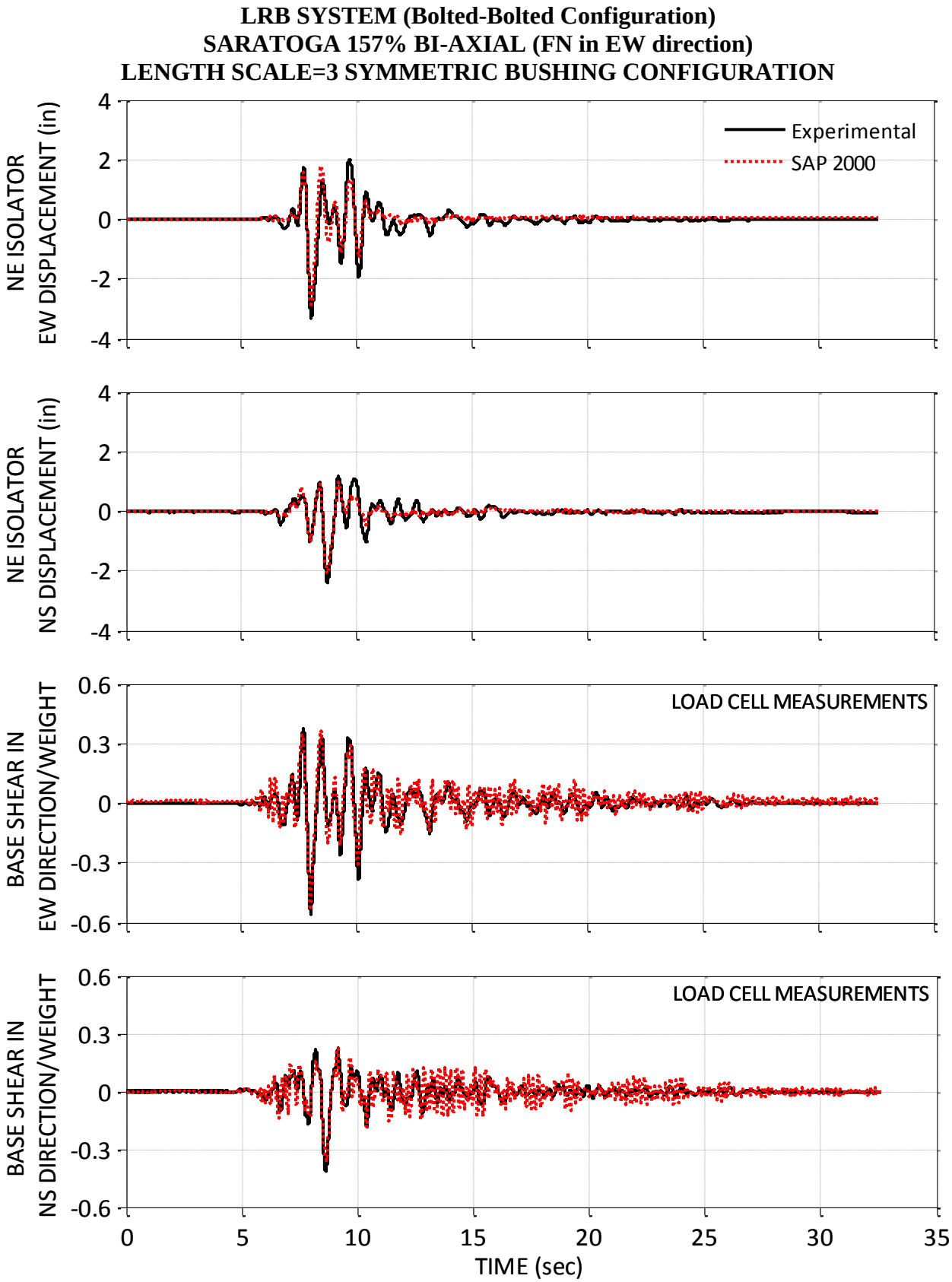


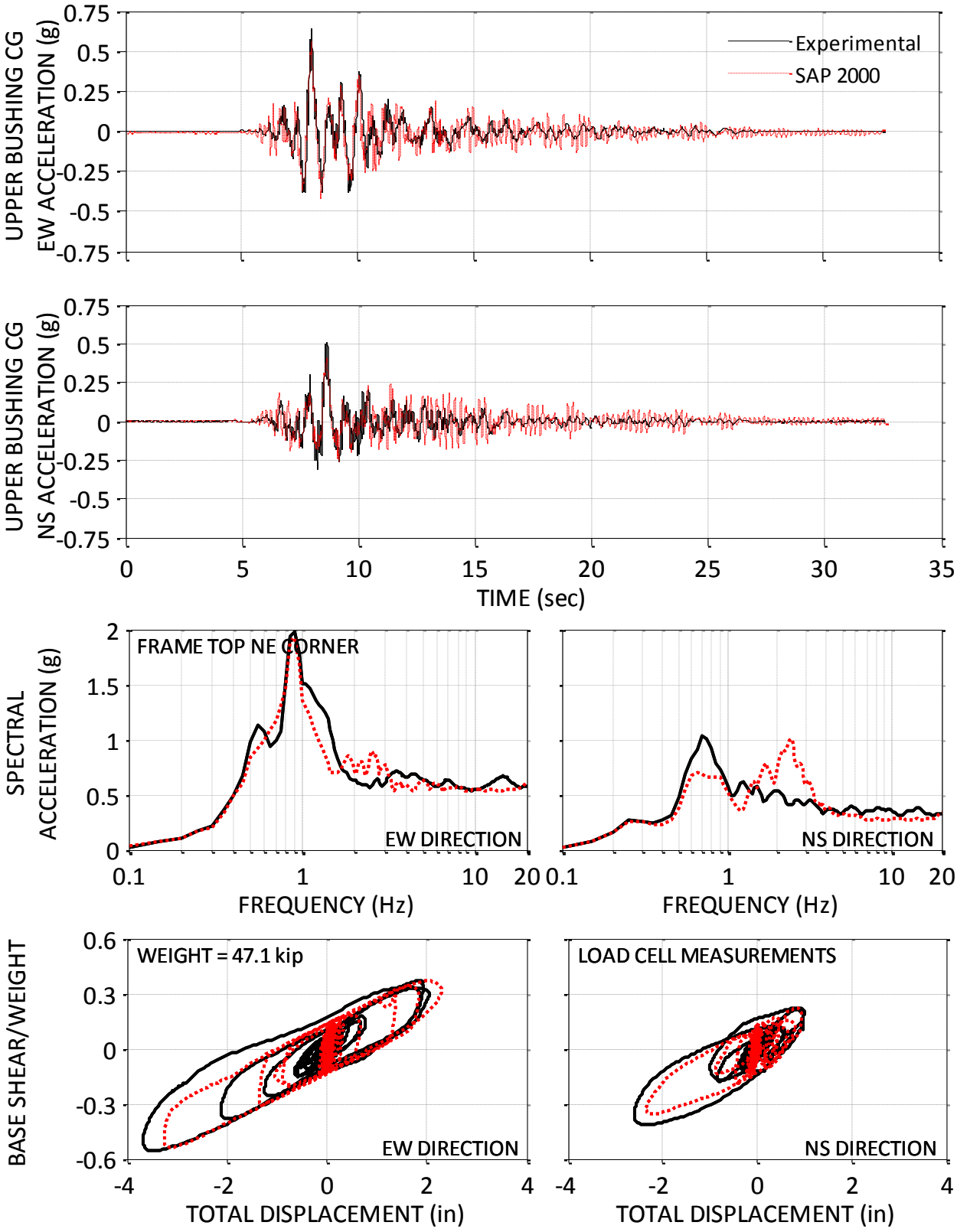

UPPER BUSHING CG
EW ACCELERATION (g)
0.75
0.5
0.25
0
-0.25
-0.5
-0.75
Experimental
SAP 2000
UPPER BUSHING CG
NS ACCELERATION (g)
0
5
10
15
20
25
30
35
TIME (sec)
SPECTRAL
ACCELERATION (g)
FRAME TOP NE CORNER
EW DIRECTION
NS DIRECTION
2
1.5
1
0.5
0
0.1
1
10
20
FREQUENCY (Hz)
BASE SHEAR/WEIGHT
WEIGHT = 47.1 kip
LOAD CELL MEASUREMENTS
0.6
0.3
0
-0.3
-0.6
-4
-2
0
2
4
TOTAL DISPLACEMENT (in)

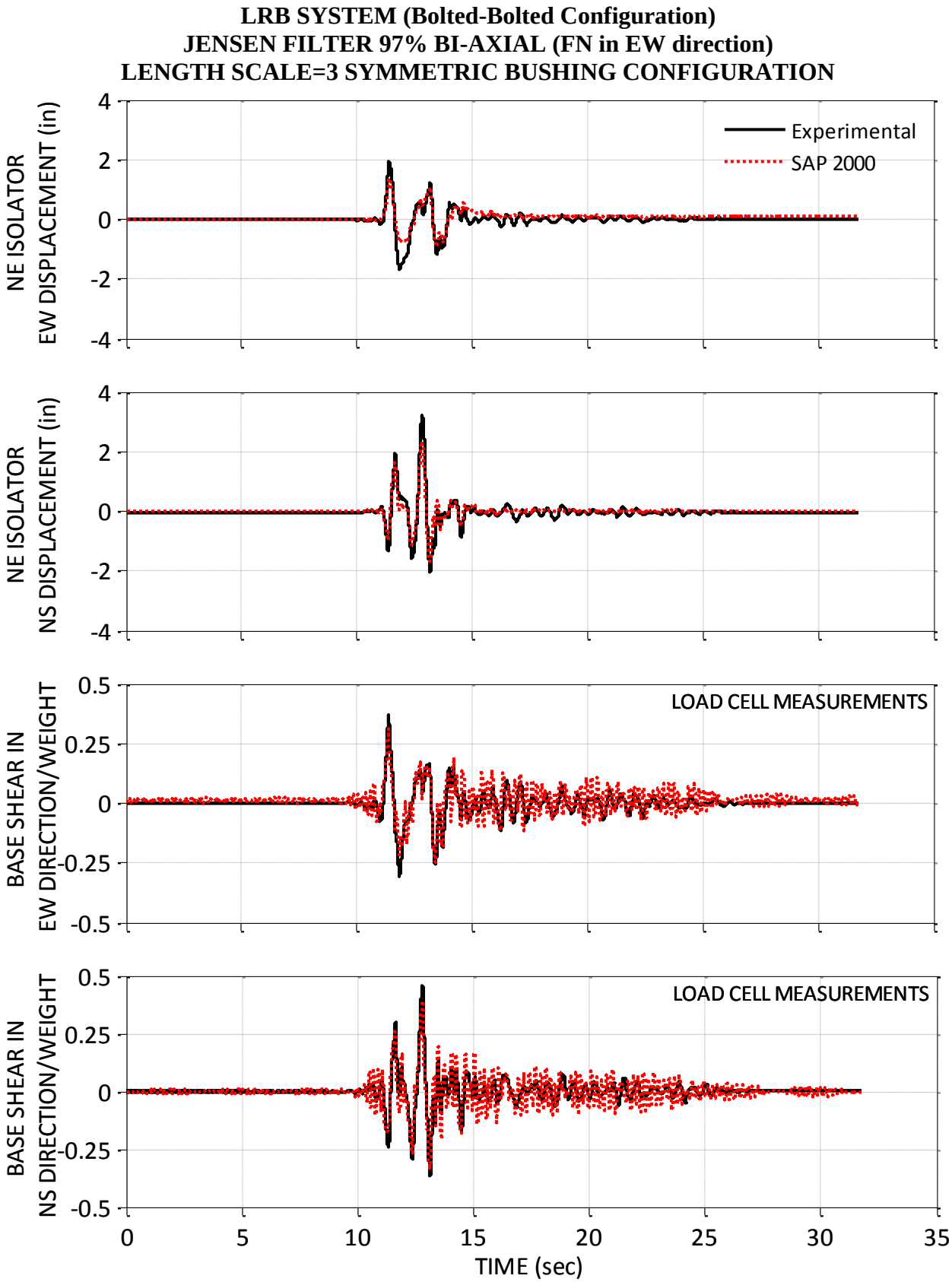
LRB SYSTEM (Bolted-Bolted Configuration)
LGPC 94% BI-AXIAL (FN in EW direction)
LENGTH SCALE=3 SYMMETRIC BUSHING CONFIGURATION

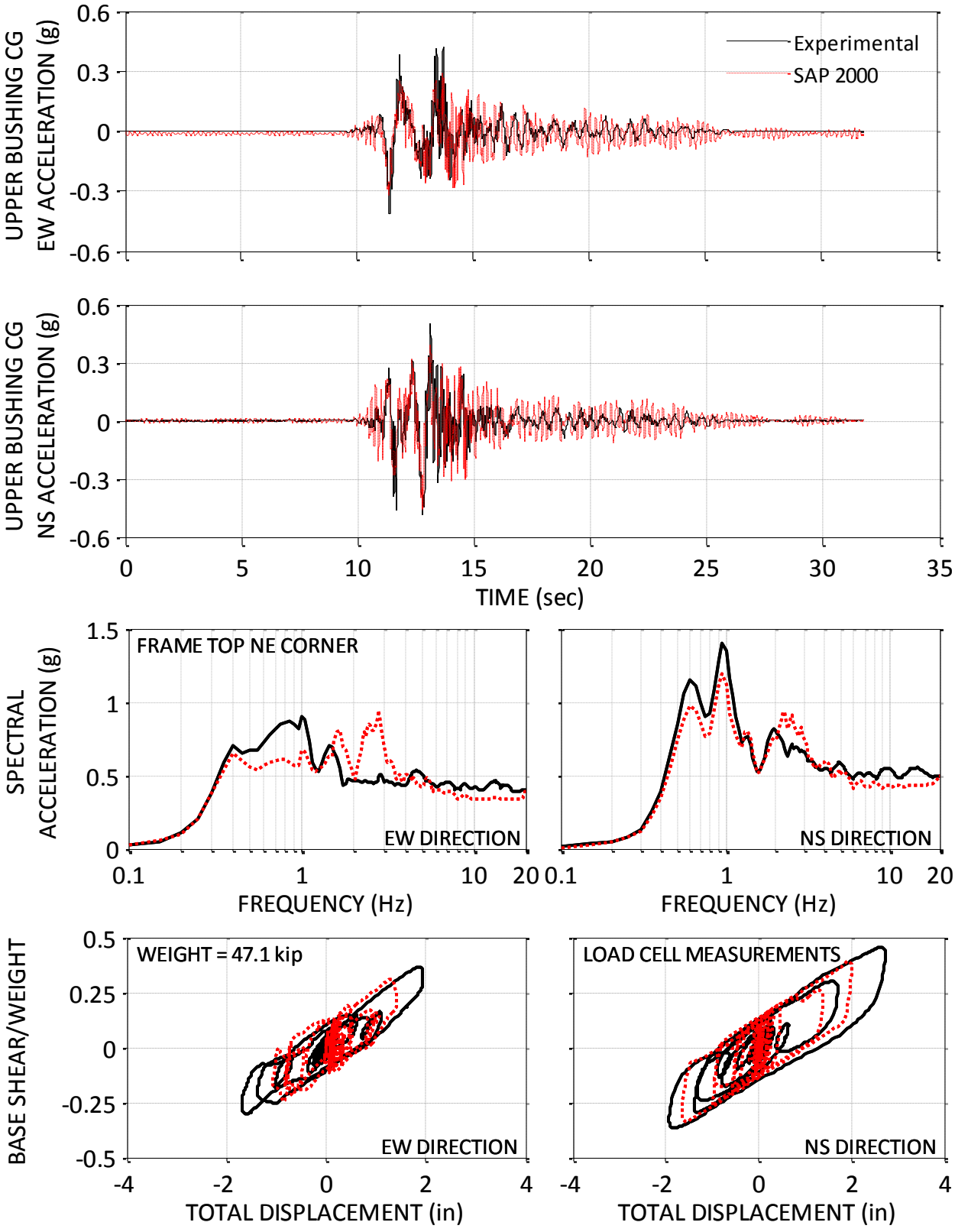



UPPER BUSHING CG
EW ACCELERATION (g)
0.75
0.5
0.25
0
-0.25
-0.5
-0.75
Experimental
SAP 2000
UPPER BUSHING CG
NS ACCELERATION (g)
0
5
10
15
20
25
30
TIME (sec)
SPECTRAL
ACCELERATION (g)
FRAME TOP NE CORNER
EW DIRECTION
NS DIRECTION
2
1.5
1
0.5
0
0.1
1
10
20
FREQUENCY (Hz)
BASE SHEAR/WEIGHT
WEIGHT = 47.1 kip
LOAD CELL MEASUREMENTS
0.6
0.3
-0.3
-0.6
-4
-2
2
4
TOTAL DISPLACEMENT (in)

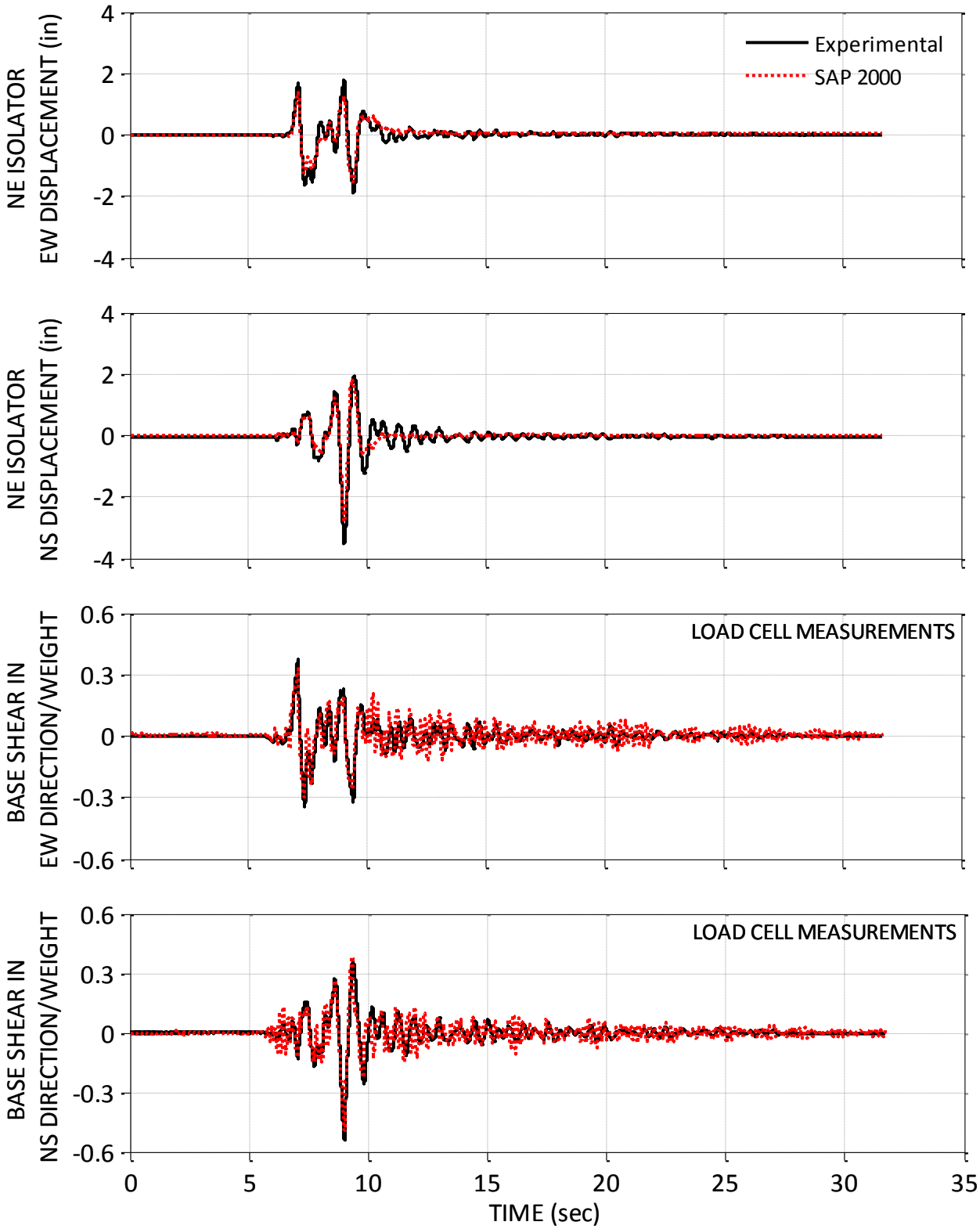

LRB SYSTEM (Bolted-Bolted Configuration)
SARATOGA 157% BI-AXIAL (FN in EW direction)
LENGTH SCALE=3 SYMMETRIC BUSHING CONFIGURATION
NE ISOLATOR
EW DISPLACEMENT (in)
Experimental
SAP 2000
NE ISOLATOR
NS DISPLACEMENT (in)
BASE SHEAR IN
EW DIRECTION/WEIGHT
LOAD CELL MEASUREMENTS
BASE SHEAR IN
NS DIRECTION/WEIGHT
LOAD CELL MEASUREMENTS
TIME (sec)

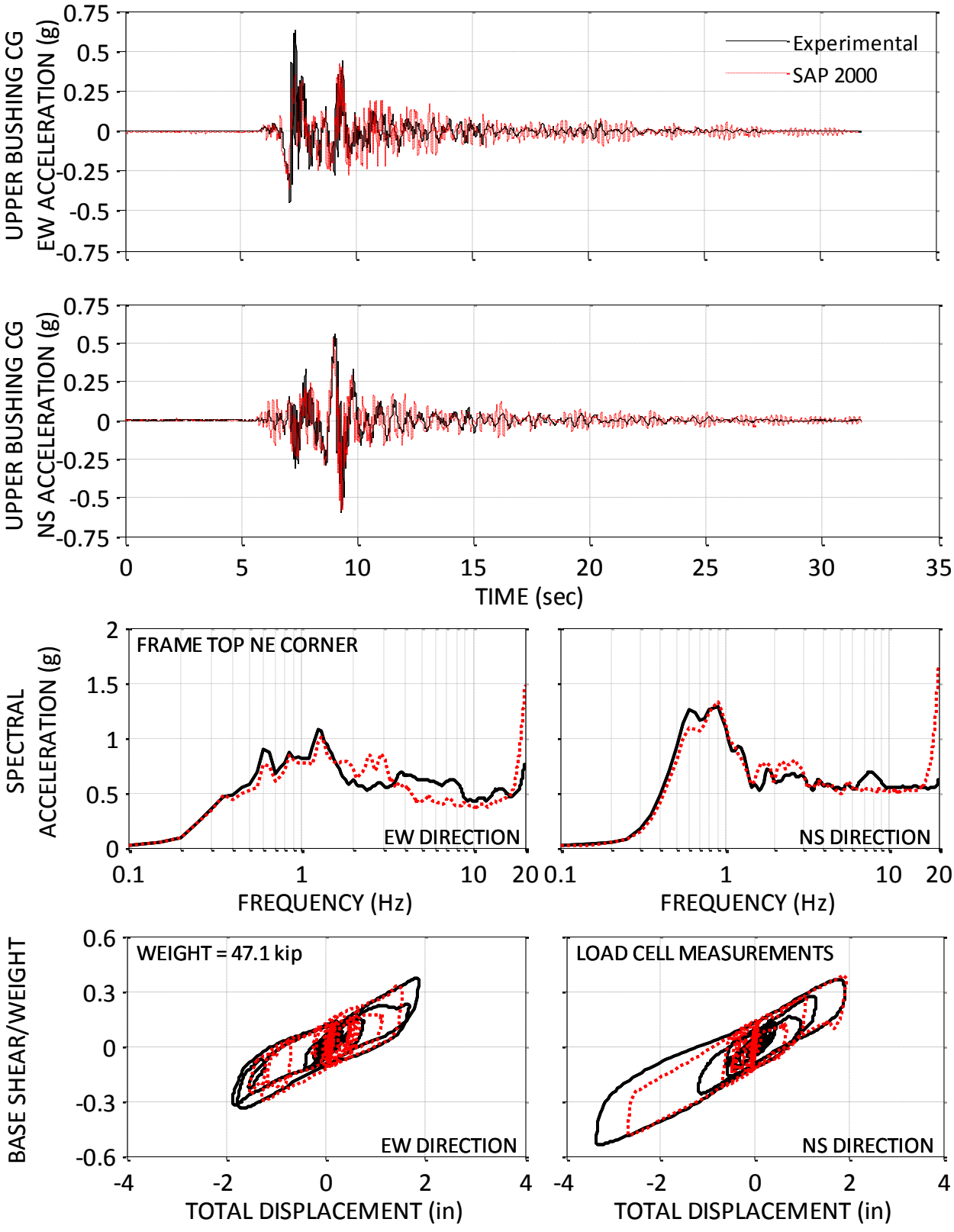

UPPER BUSHING CG
EW ACCELERATION (g)
0.75
0.5
0.25
0
-0.25
-0.5
-0.75
Experimental
SAP 2000
UPPER BUSHING CG
NS ACCELERATION (g)
0
5
10
15
20
25
30
35
TIME (sec)
SPECTRAL
ACCELERATION (g)
FRAME TOP NE CORNER
EW DIRECTION
NS DIRECTION
2
1.5
1
0.5
0
0.1
1
10
20
FREQUENCY (Hz)
BASE SHEAR/WEIGHT
WEIGHT = 47.1 kip
LOAD CELL MEASUREMENTS
0.6
0.3
0
-0.3
-0.6
-4
-2
0
2
4
TOTAL DISPLACEMENT (in)


LRB SYSTEM (Bolted-Bolted Configuration)
JENSEN FILTER 97% BI-AXIAL (FN in EW direction)
LENGTH SCALE=3 SYMMETRIC BUSHING CONFIGURATION
NE ISOLATOR EW DISPLACEMENT (in)
Experimental
SAP 2000
NE ISOLATOR NS DISPLACEMENT (in)
BASE SHEAR IN EW DIRECTION/WEIGHT
LOAD CELL MEASUREMENTS
BASE SHEAR IN NS DIRECTION/WEIGHT
LOAD CELL MEASUREMENTS
TIME (sec)

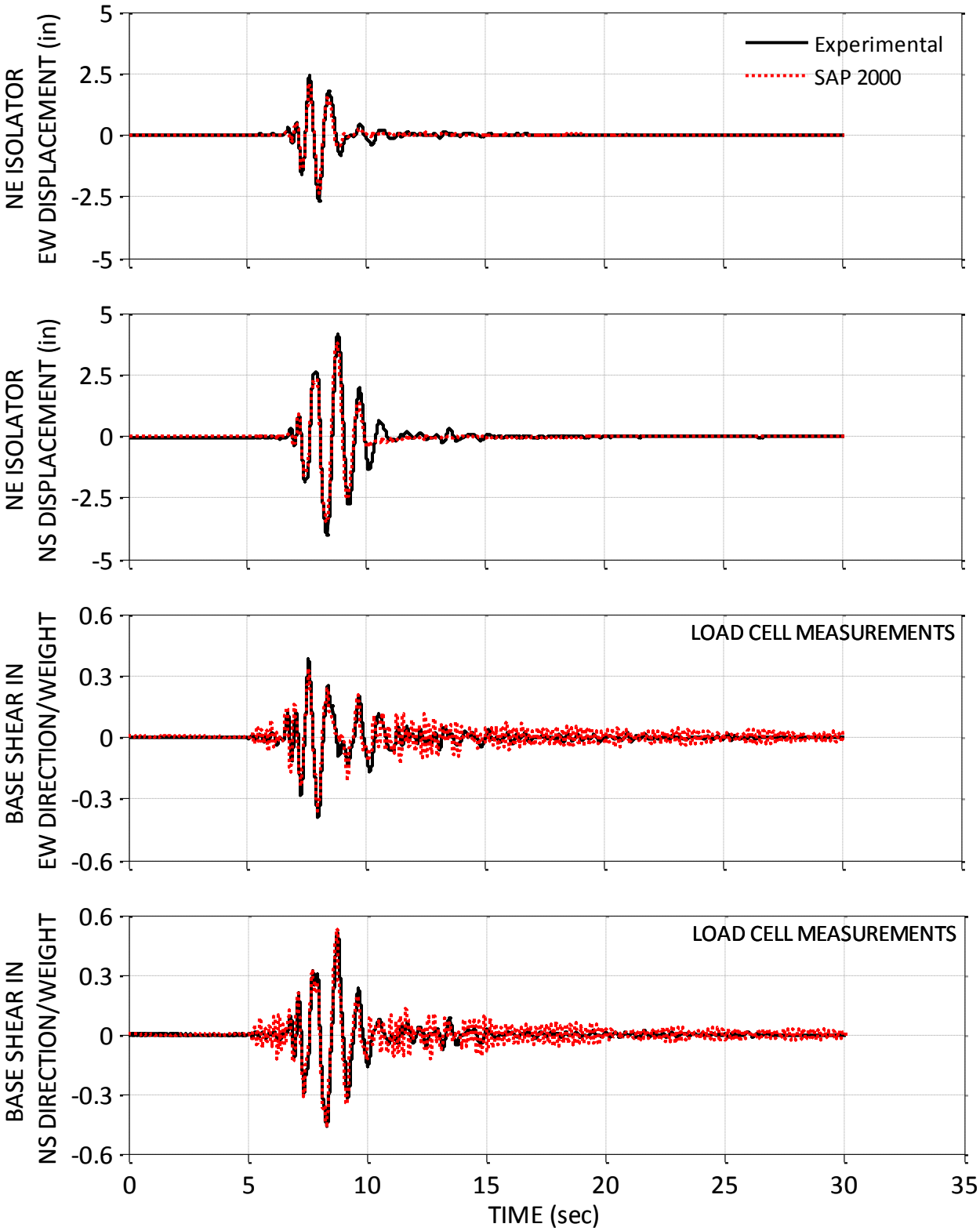

UPPER BUSHING CG
EW ACCELERATION (g)
0.6
0.3
0
-0.3
-0.6
Experimental
SAP 2000
UPPER BUSHING CG
NS ACCELERATION (g)
0
5
10
15
20
25
30
35
TIME (sec)
SPECTRAL
ACCELERATION (g)
1.5
1
0.5
FRAME TOP NE CORNER
EW DIRECTION
NS DIRECTION
0.1
1
10
20
FREQUENCY (Hz)
BASE SHEAR/WEIGHT
0.25
-0.25
WEIGHT = 47.1 kip
LOAD CELL MEASUREMENTS
-4
-2
2
4
TOTAL DISPLACEMENT (in)

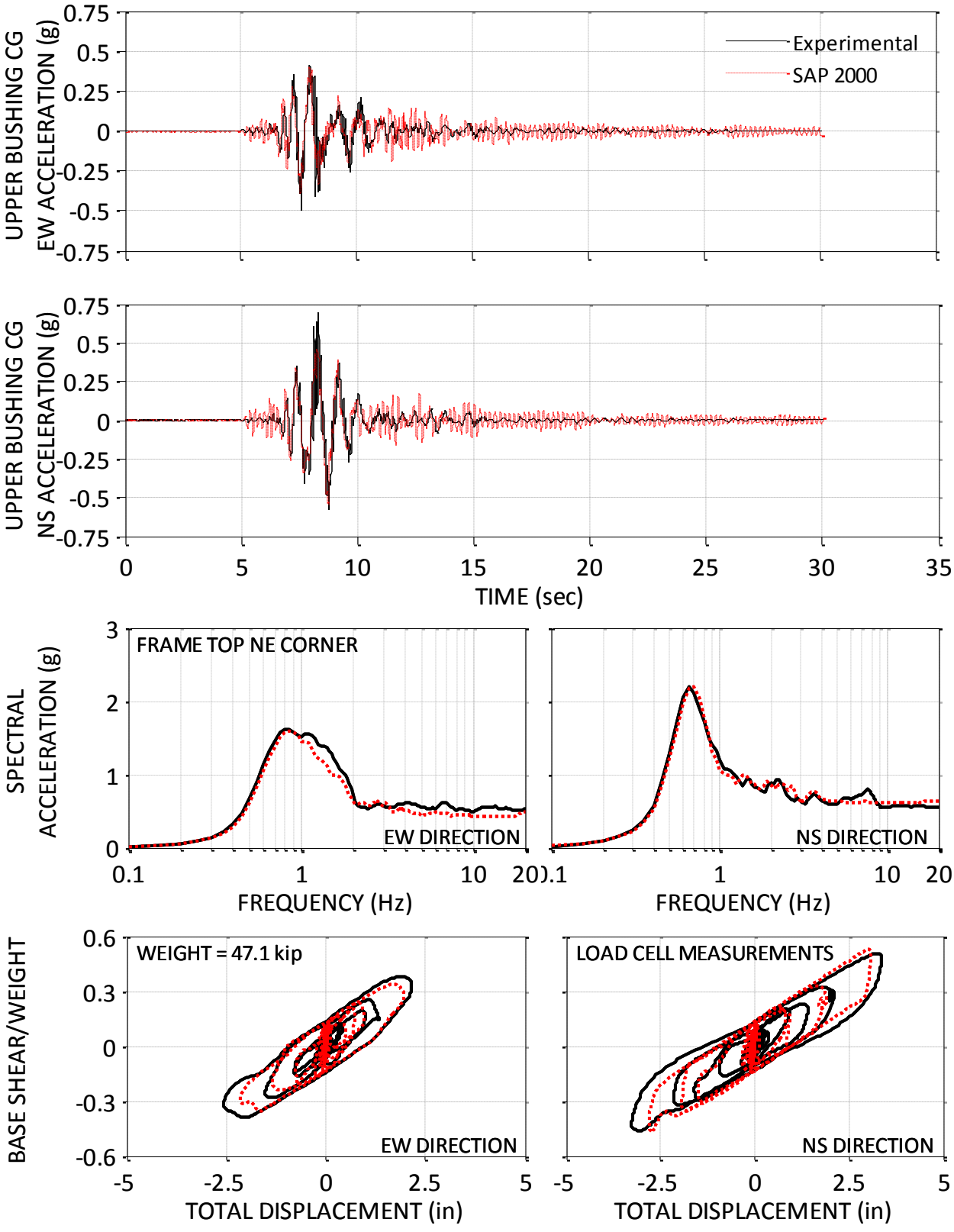
LRB SYSTEM (Bolted-Bolted Configuration)
SYLMAR 90% BI-AXIAL (FN in EW direction)
LENGTH SCALE=3 SYMMETRIC BUSHING CONFIGURATION



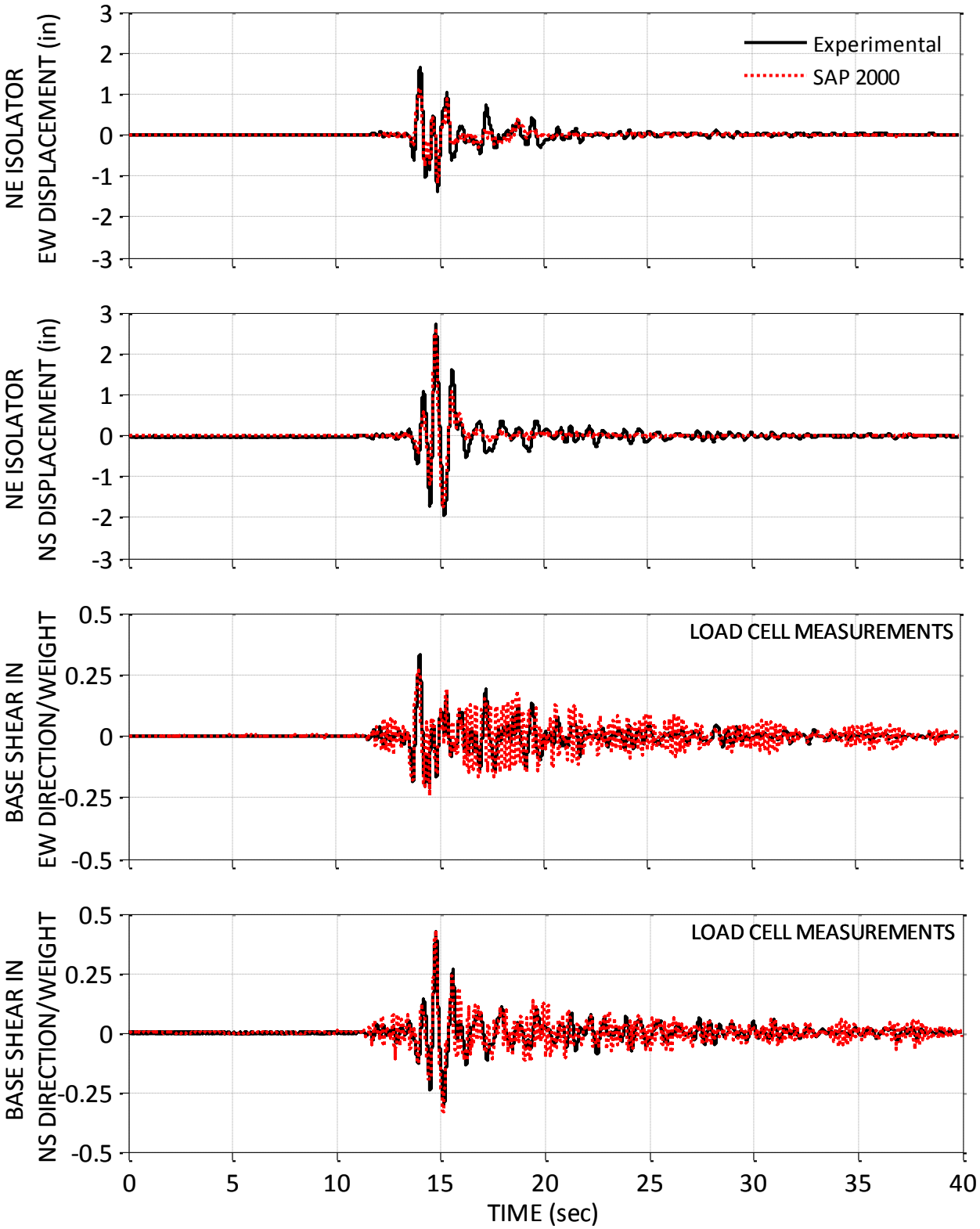

UPPER BUSHING CG
EW ACCELERATION (g)
0.75
0.5
0.25
0
-0.25
-0.5
-0.75
Experimental
SAP 2000
UPPER BUSHING CG
NS ACCELERATION (g)
0
5
10
15
20
25
30
35
TIME (sec)
SPECTRAL
ACCELERATION (g)
FRAME TOP NE CORNER
EW DIRECTION
NS DIRECTION
2
1.5
1
0.5
0
0.1
1
10
20
FREQUENCY (Hz)
BASE SHEAR/WEIGHT
WEIGHT = 47.1 kip
LOAD CELL MEASUREMENTS
0.6
0.3
0
-0.3
-0.6
-4
-2
0
2
4
TOTAL DISPLACEMENT (in)

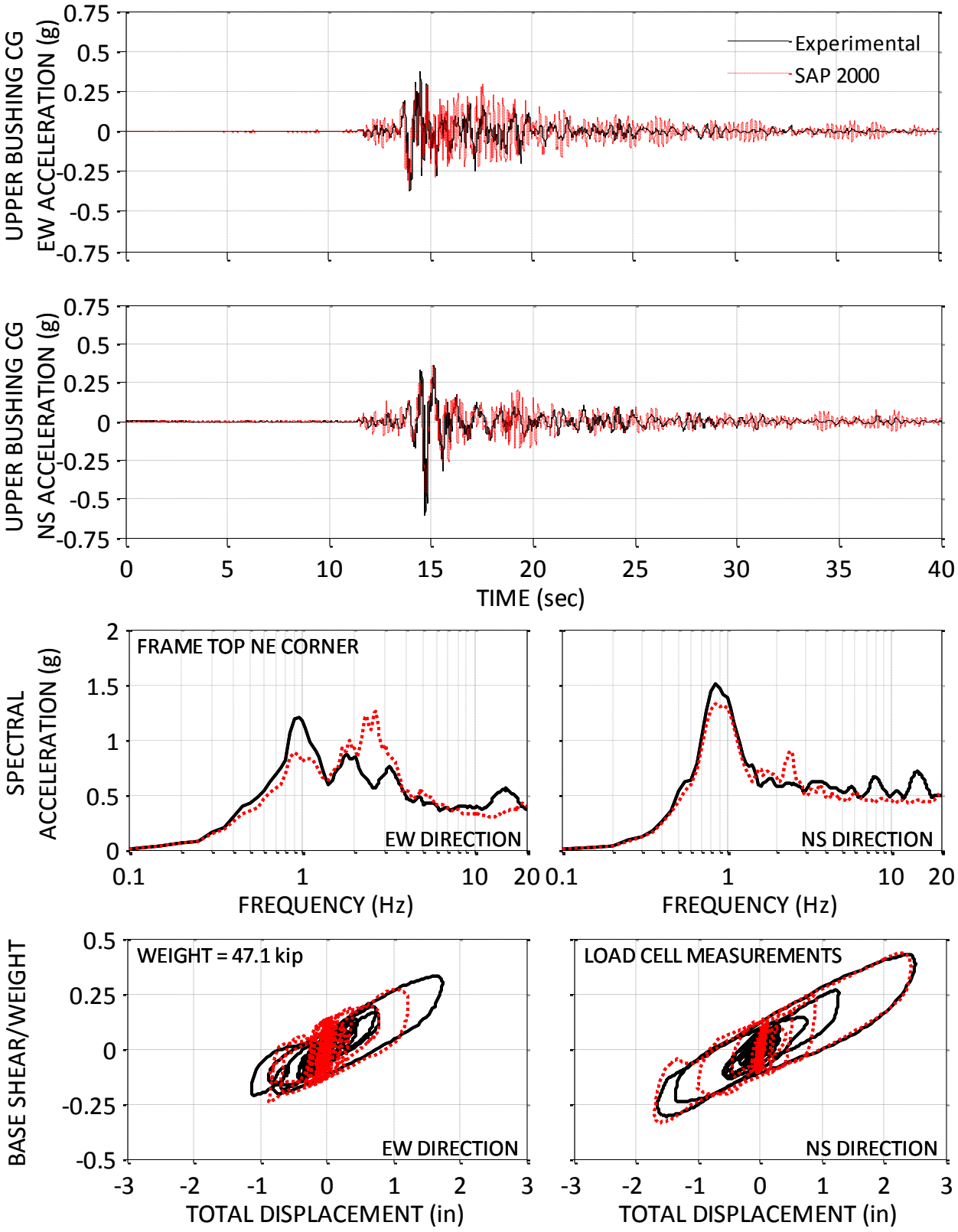
LRB SYSTEM (Bolted-Bolted Configuration)
TAKARAZUKA 97% BI-AXIAL (FN in EW direction)
LENGTH SCALE=3 SYMMETRIC BUSHING CONFIGURATION




UPPER BUSHING CG
EW ACCELERATION (g)
0.75
0.5
0.25
0
-0.25
-0.5
-0.75
Experimental
SAP 2000
UPPER BUSHING CG
NS ACCELERATION (g)
0
5
10
15
20
25
30
35
TIME (sec)
SPECTRAL
ACCELERATION (g)
FRAME TOP NE CORNER
EW DIRECTION
NS DIRECTION
3
2
1
0
0.1
1
10
20
FREQUENCY (Hz)
BASE SHEAR/WEIGHT
WEIGHT = 47.1 kip
LOAD CELL MEASUREMENTS
0.6
0.3
0
-0.3
-0.6
-5
-2.5
0
2.5
5
TOTAL DISPLACEMENT (in)

LRB SYSTEM (Bolted-Bolted Configuration)
BOLU 104% BI-AXIAL (FN in EW direction)
LENGTH SCALE=3 SYMMETRIC BUSHING CONFIGURATION



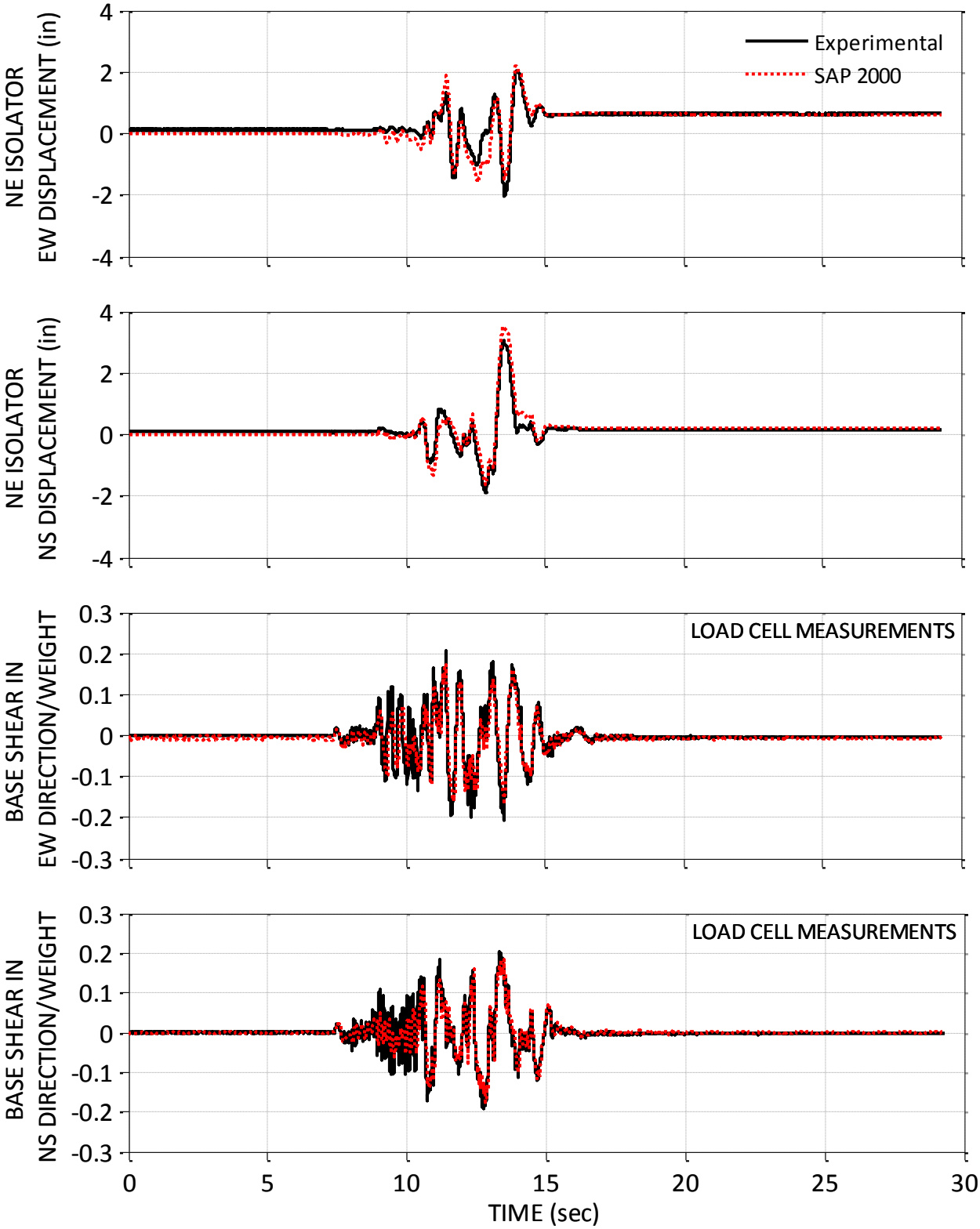

UPPER BUSHING CG
EW ACCELERATION (g)
0.75
0.5
0.25
0
-0.25
-0.5
-0.75
Experimental
SAP 2000
UPPER BUSHING CG
NS ACCELERATION (g)
0
5
10
15
20
25
30
35
40
TIME (sec)
SPECTRAL
ACCELERATION (g)
FRAME TOP NE CORNER
EW DIRECTION
NS DIRECTION
2
1.5
1
0.5
0
0.1
1
10
20
FREQUENCY (Hz)
BASE SHEAR/WEIGHT
WEIGHT = 47.1 kip
LOAD CELL MEASUREMENTS
-3
-2
-1
0
1
2
3
TOTAL DISPLACEMENT (in)

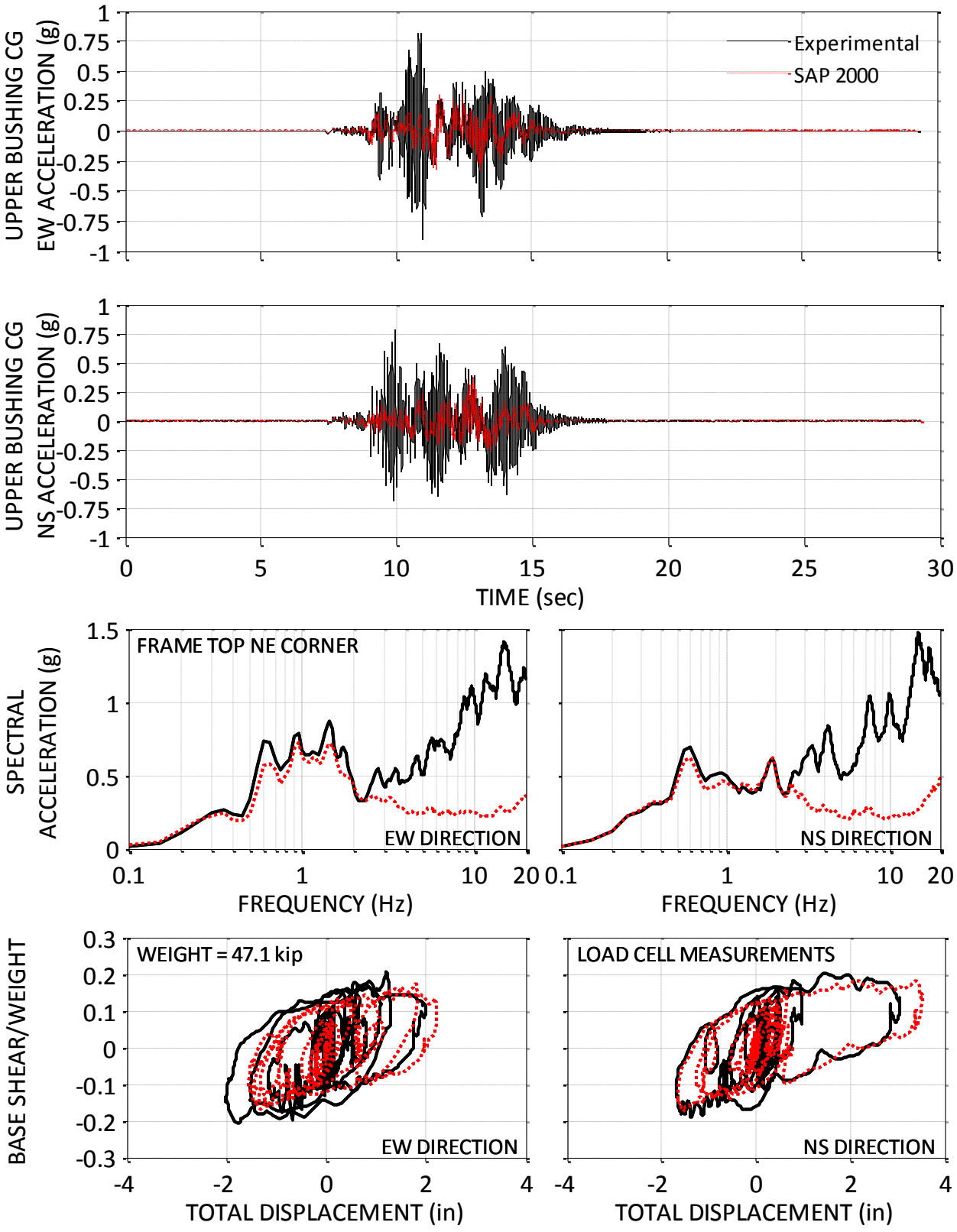
This Page is Intentionally Left Blank

PART C-2
SUMMARY OF EXPERIMENTAL AND ANALYTICAL COMPARISONS FOR THE TRIPLE FRICTION PENDULUM SYSTEM AT LENGTH SCALE OF 3 AND MODELING USING THE PARALLEL MODEL

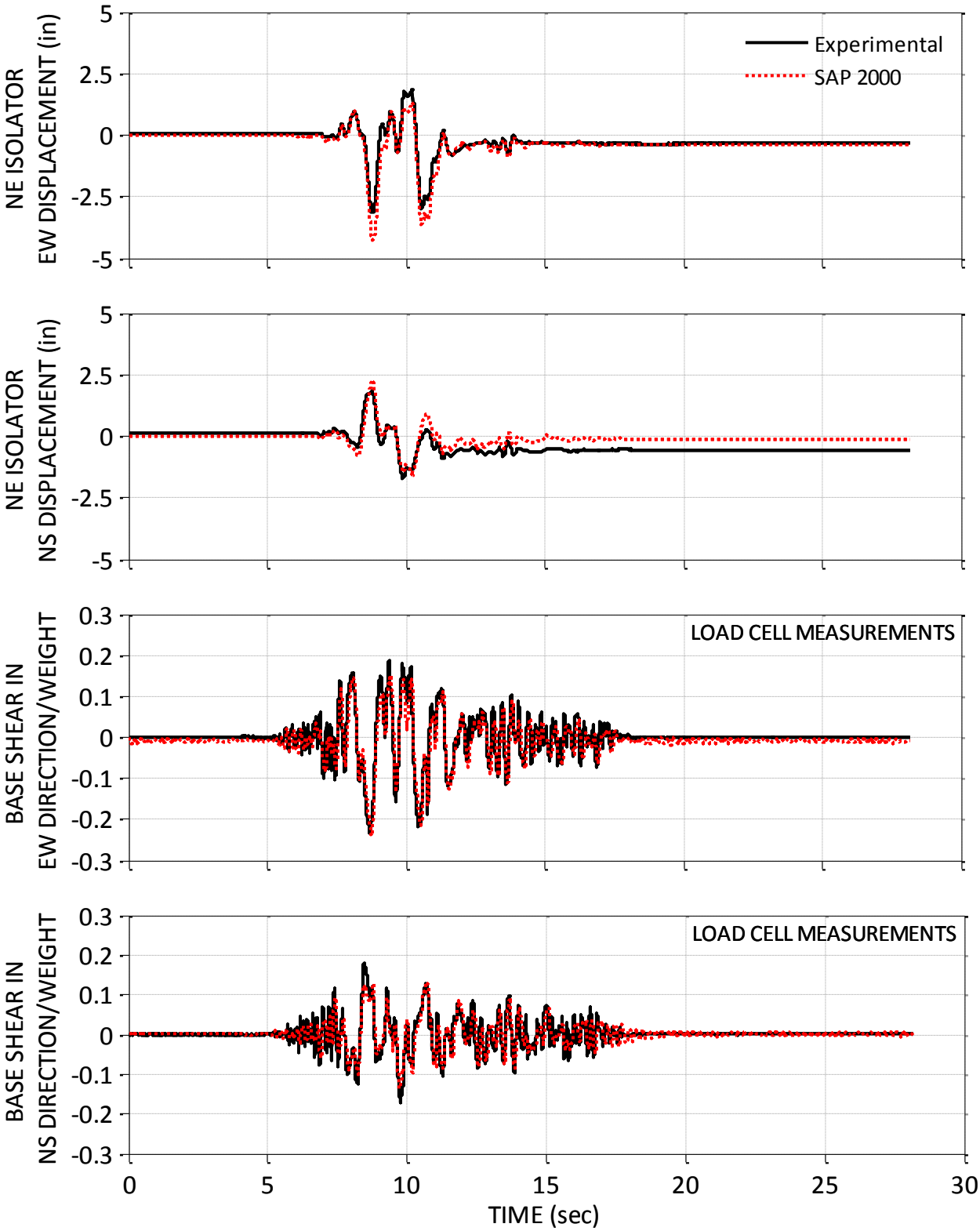
(PERCENTAGE AMOUNT IS SCALE FACTOR APPLIED TO ACCELERATION OF ACTUAL MOTION. FOR EXAMPLE, 100% DENOTES MOTION AS RECORDED, 200% DENOTES THAT ACCELERATION WAS SCALED UP BY FACTOR OF 2)

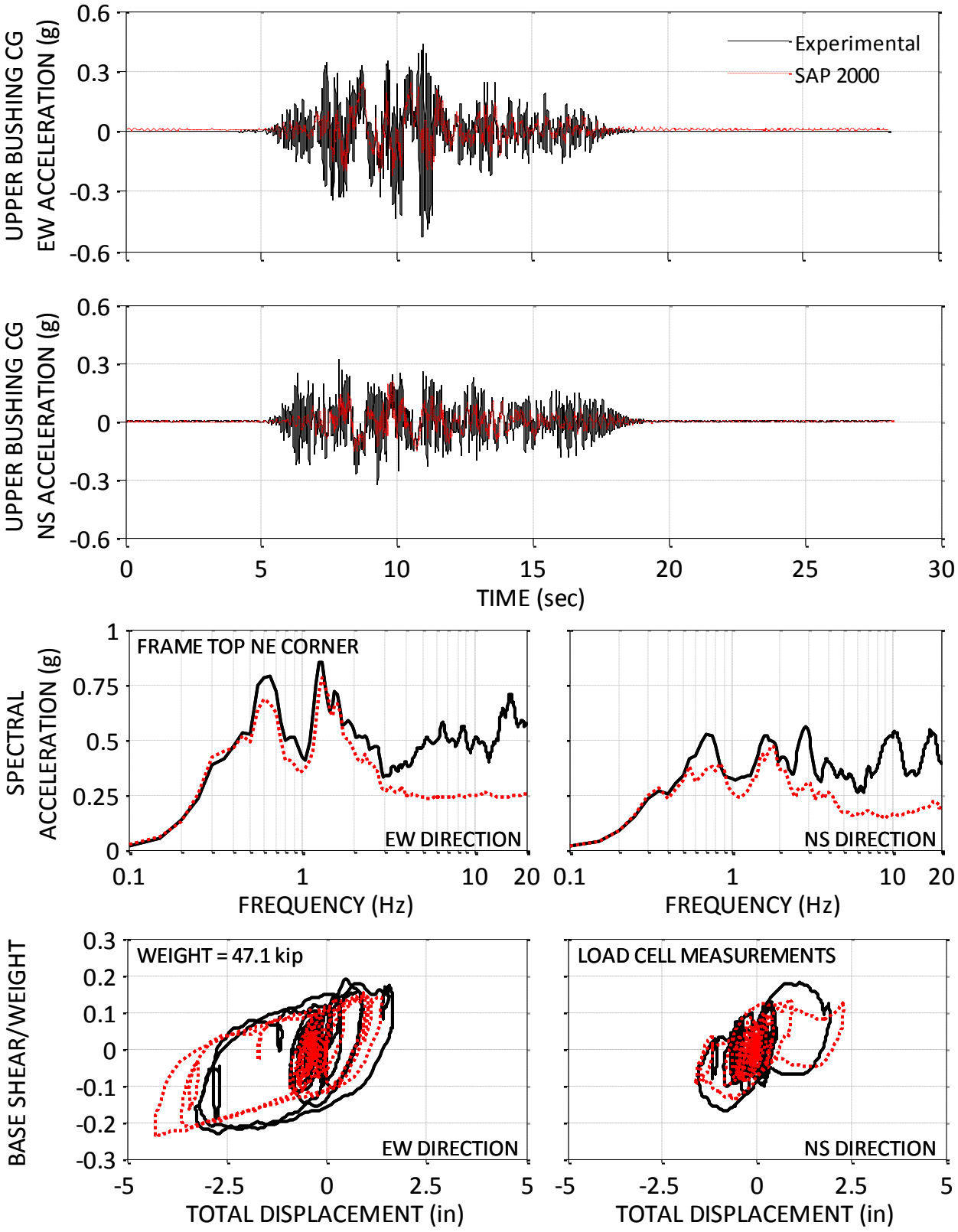
TRIPLE FP SYSTEM (Friction-Bolted Configuration)
KARAKYR 137% BI-AXIAL (FN in EW direction)
LENGTH SCALE=3 SYMMETRIC BUSHING CONFIGURATION



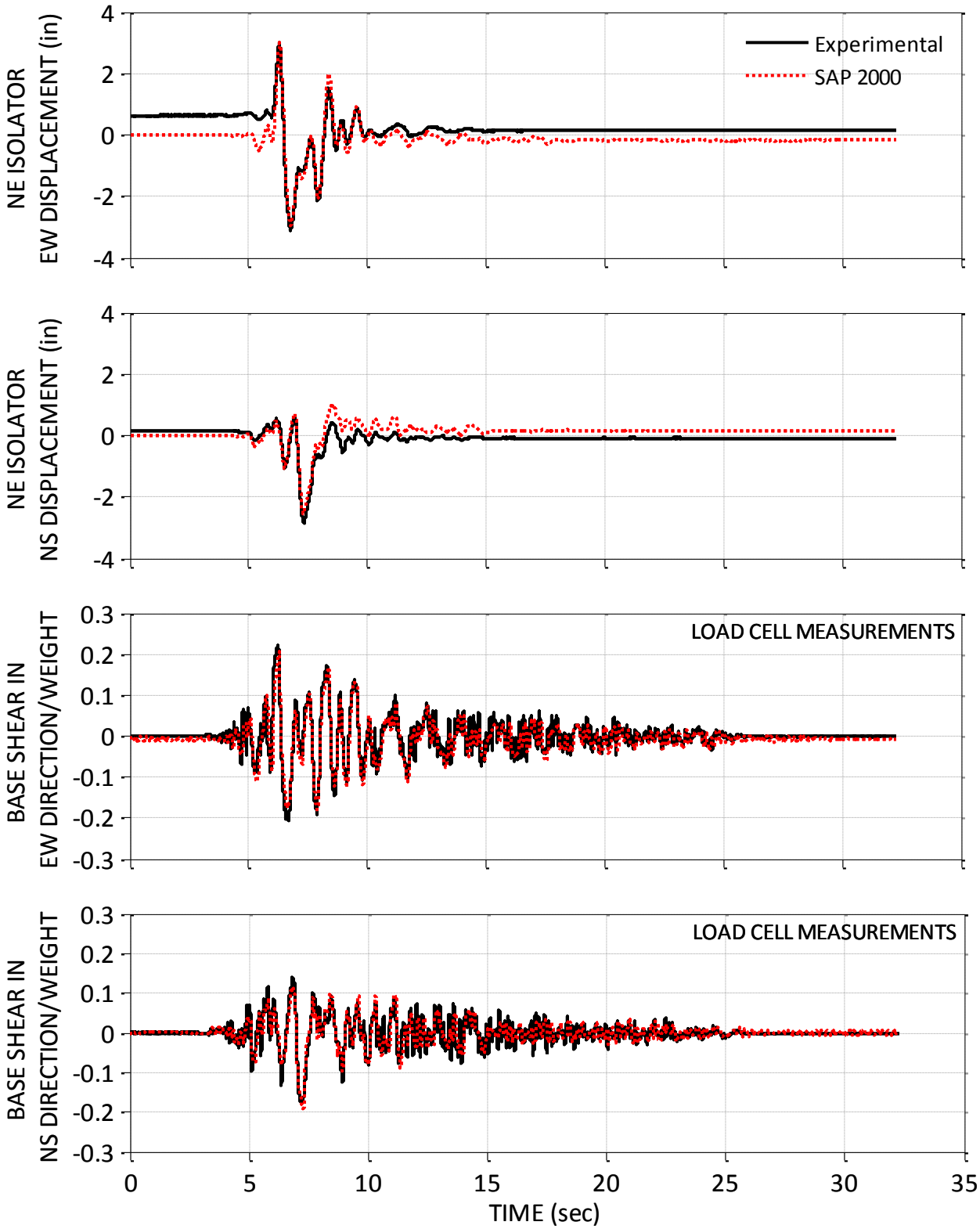

UPPER BUSHING CG
EW ACCELERATION (g)
Experimental
SAP 2000
UPPER BUSHING CG
NS ACCELERATION (g)
TIME (sec)
SPECTRAL
ACCELERATION (g)
FRAME TOP NE CORNER
EW DIRECTION
NS DIRECTION
FREQUENCY (Hz)
BASE SHEAR/WEIGHT
WEIGHT = 47.1 kip
LOAD CELL MEASUREMENTS
TOTAL DISPLACEMENT (in)

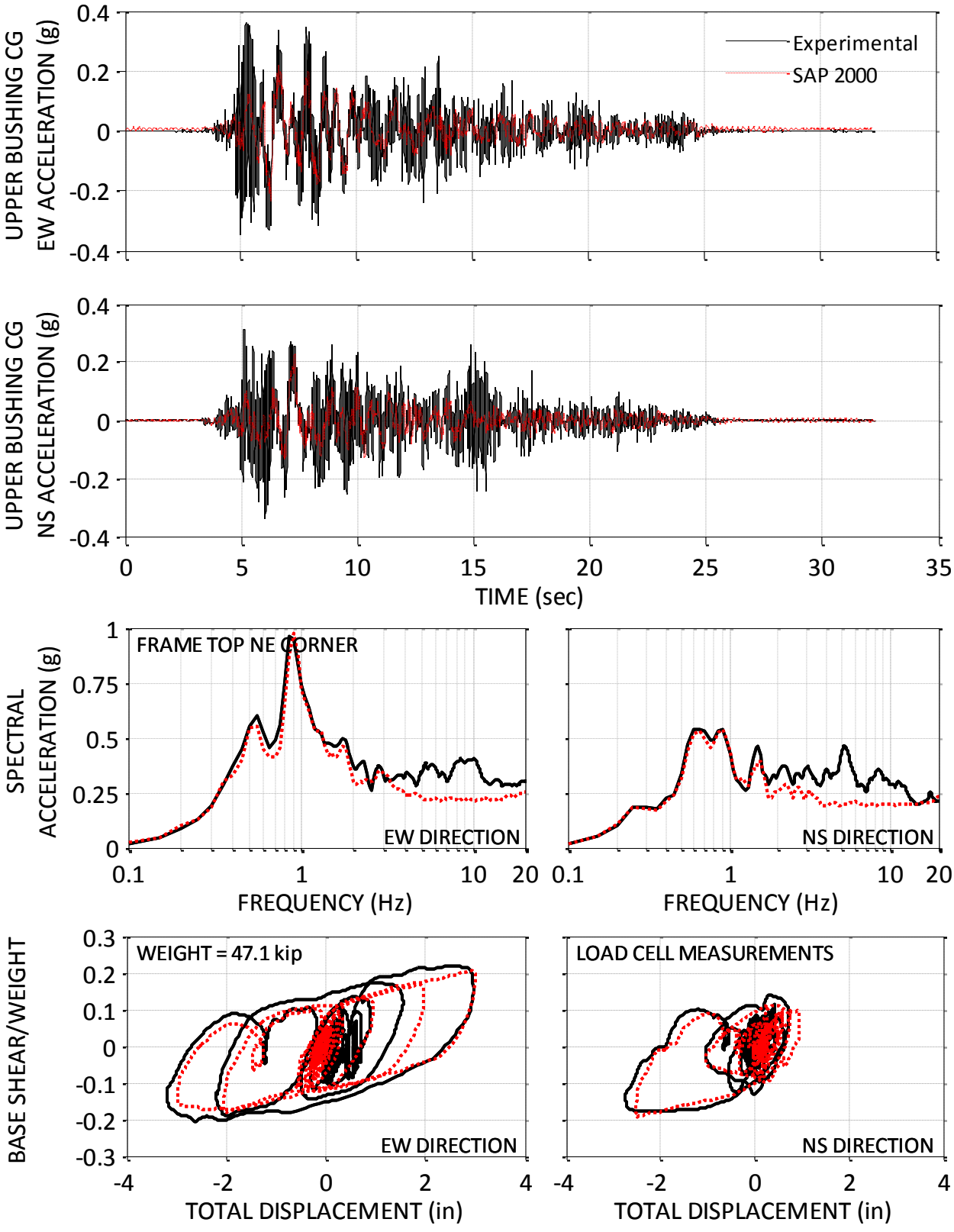
TRIPLE FP SYSTEM (Friction-Bolted Configuration)
LGPC 94% BI-AXIAL (FN in EW direction)
LENGTH SCALE=3 SYMMETRIC BUSHING CONFIGURATION



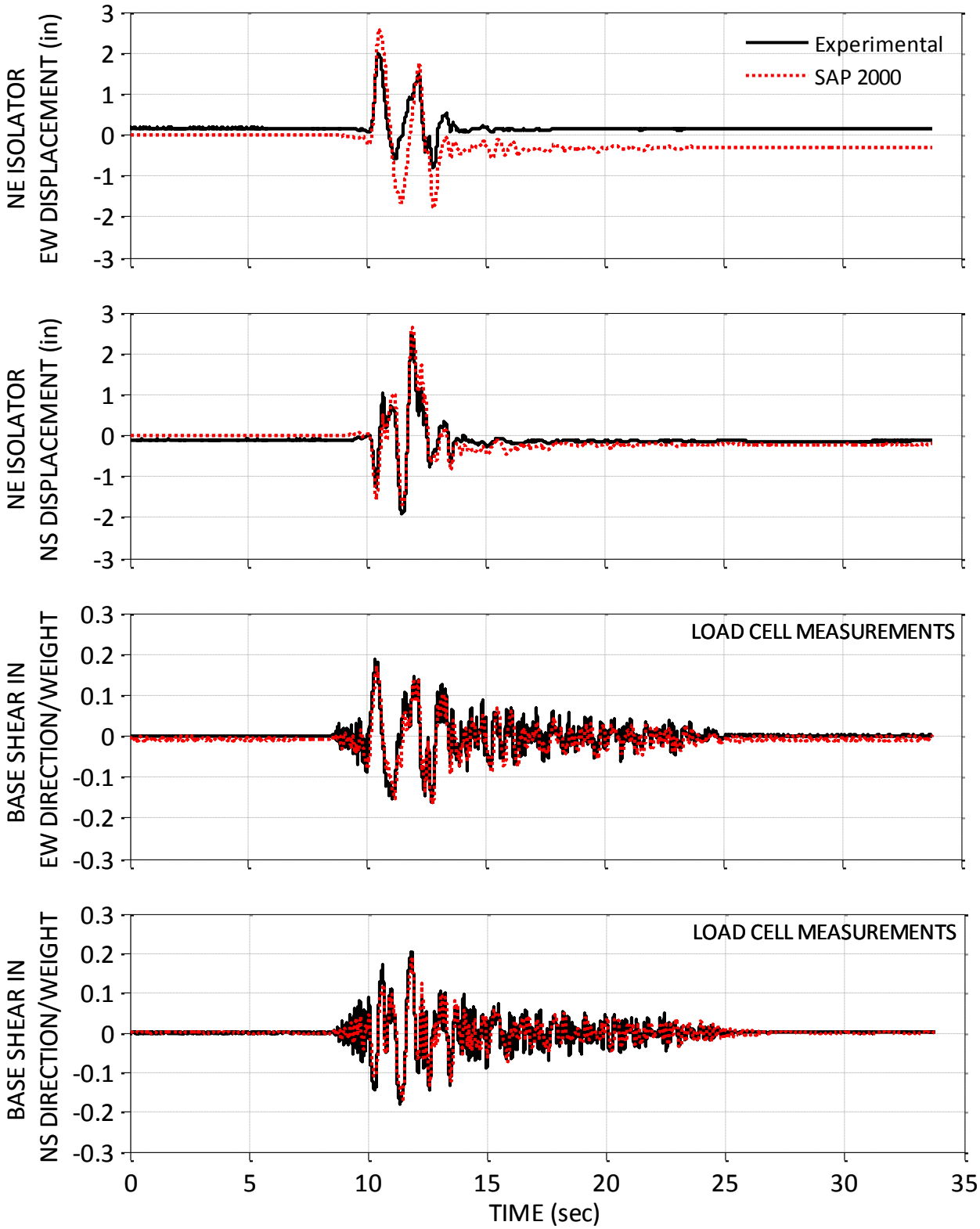

UPPER BUSHING CG
EW ACCELERATION (g)
0.6
0.3
0
-0.3
-0.6
Experimental
SAP 2000
UPPER BUSHING CG
NS ACCELERATION (g)
0.6
0.3
0
-0.3
-0.6
0
5
10
15
20
25
30
TIME (sec)
SPECTRAL
ACCELERATION (g)
1
0.75
0.5
0.25
0
FRAME TOP NE CORNER
EW DIRECTION
0.1
1
10
20
FREQUENCY (Hz)
NS DIRECTION
0.1
1
10
20
FREQUENCY (Hz)
BASE SHEAR/WEIGHT
0.3
0.2
0.1
0
-0.1
-0.2
-0.3
WEIGHT = 47.1 kip
EW DIRECTION
-5
-2.5
0
2.5
5
TOTAL DISPLACEMENT (in)
LOAD CELL MEASUREMENTS
NS DIRECTION
-5
-2.5
0
2.5
5
TOTAL DISPLACEMENT (in)

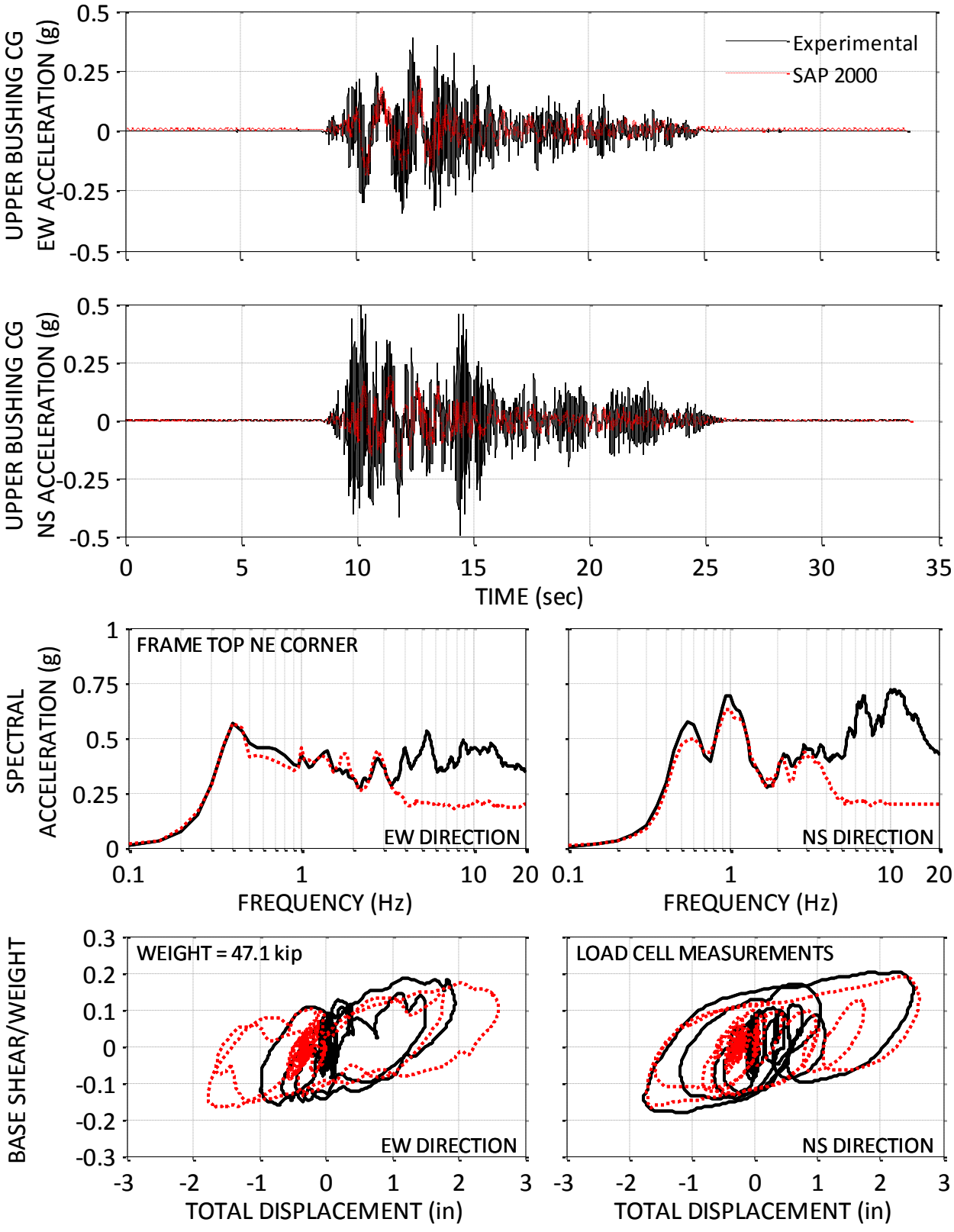
TRIPLE FP SYSTEM (Friction-Bolted Configuration)
SARATOGA 157% BI-AXIAL (FN in EW direction)
LENGTH SCALE=3 SYMMETRIC BUSHING CONFIGURATION



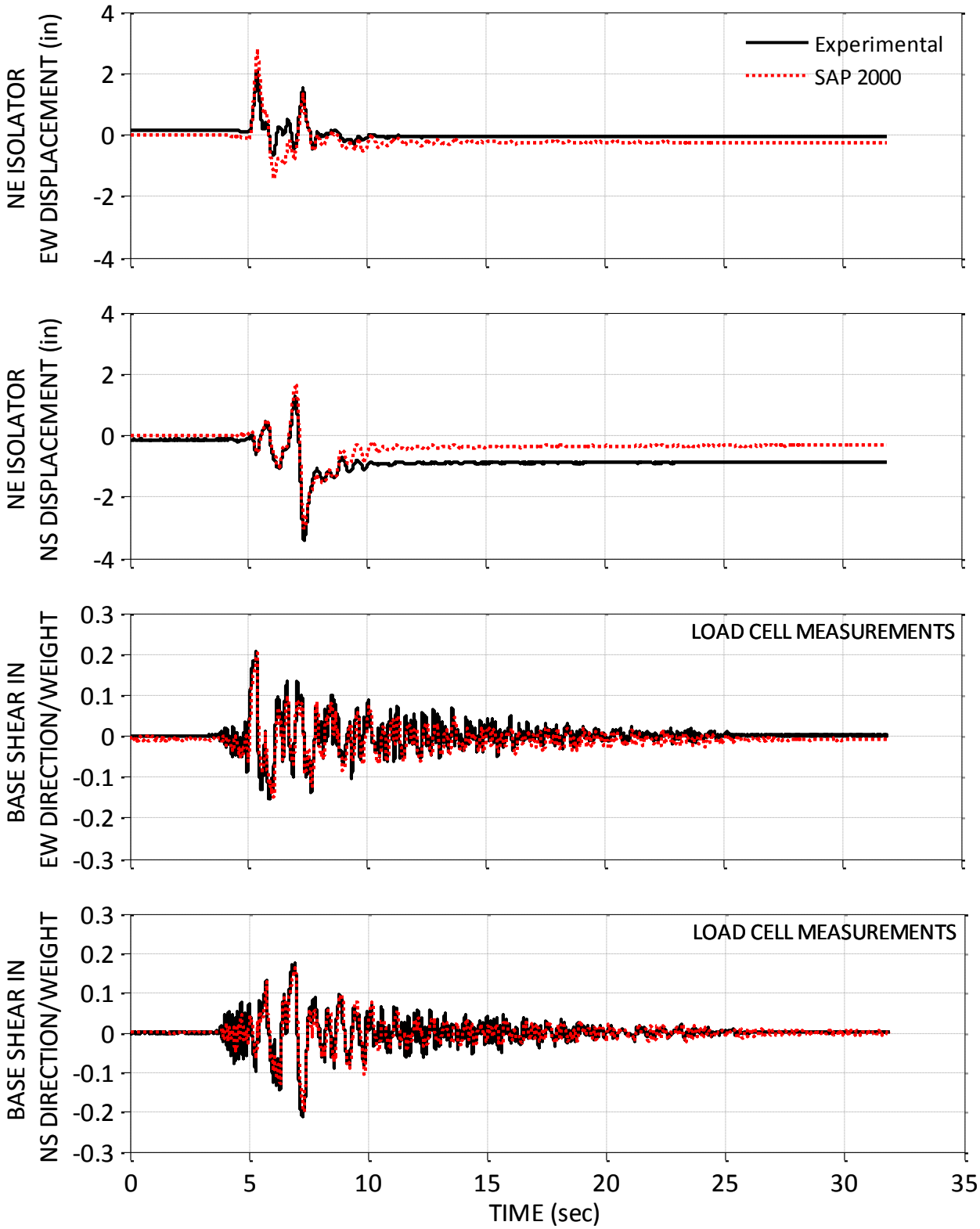

UPPER BUSHING CG
EW ACCELERATION (g)
Experimental
SAP 2000
UPPER BUSHING CG
NS ACCELERATION (g)
TIME (sec)
SPECTRAL
ACCELERATION (g)
FRAME TOP NE CORNER
EW DIRECTION
NS DIRECTION
FREQUENCY (Hz)
BASE SHEAR/WEIGHT
WEIGHT = 47.1 kip
LOAD CELL MEASUREMENTS
TOTAL DISPLACEMENT (in)

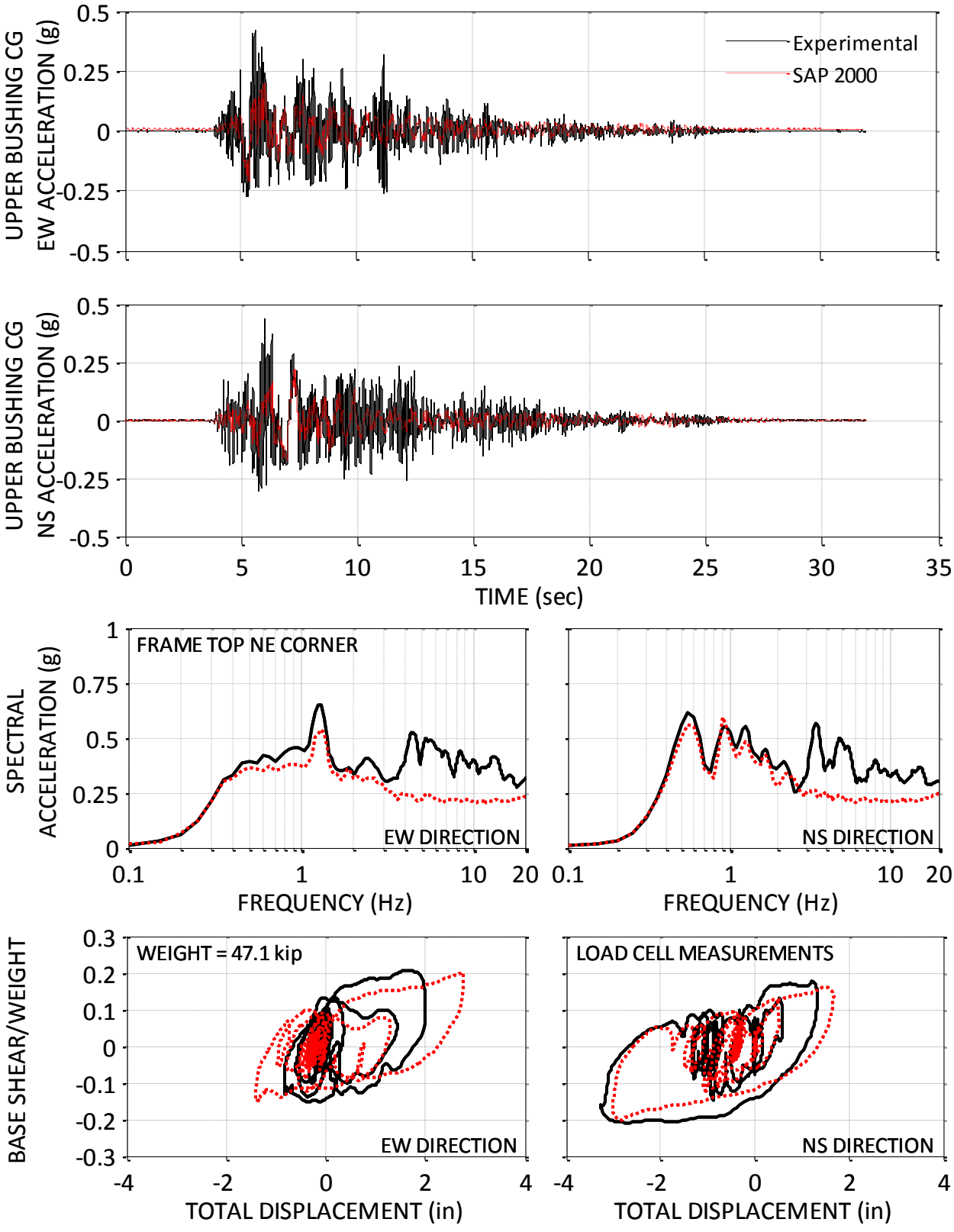
TRIPLE FP SYSTEM (Friction-Bolted Configuration)
JENSEN FILTER 97% BI-AXIAL (FN in EW direction)
LENGTH SCALE=3 SYMMETRIC BUSHING CONFIGURATION



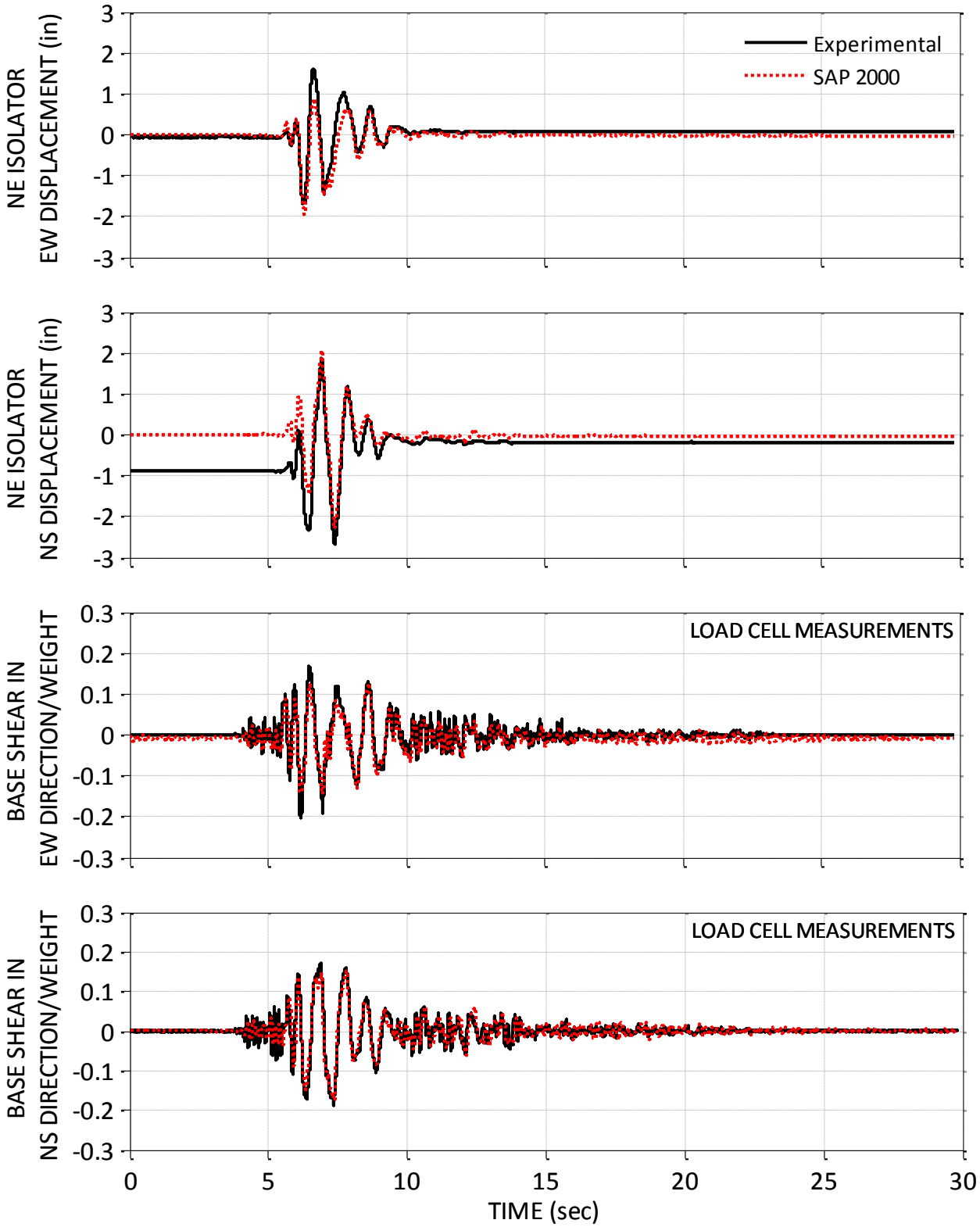

UPPER BUSHING CG
EW ACCELERATION (g)
Experimental
SAP 2000
UPPER BUSHING CG
NS ACCELERATION (g)
TIME (sec)
SPECTRAL
ACCELERATION (g)
FRAME TOP NE CORNER
EW DIRECTION
NS DIRECTION
FREQUENCY (Hz)
BASE SHEAR/WEIGHT
WEIGHT = 47.1 kip
LOAD CELL MEASUREMENTS
TOTAL DISPLACEMENT (in)

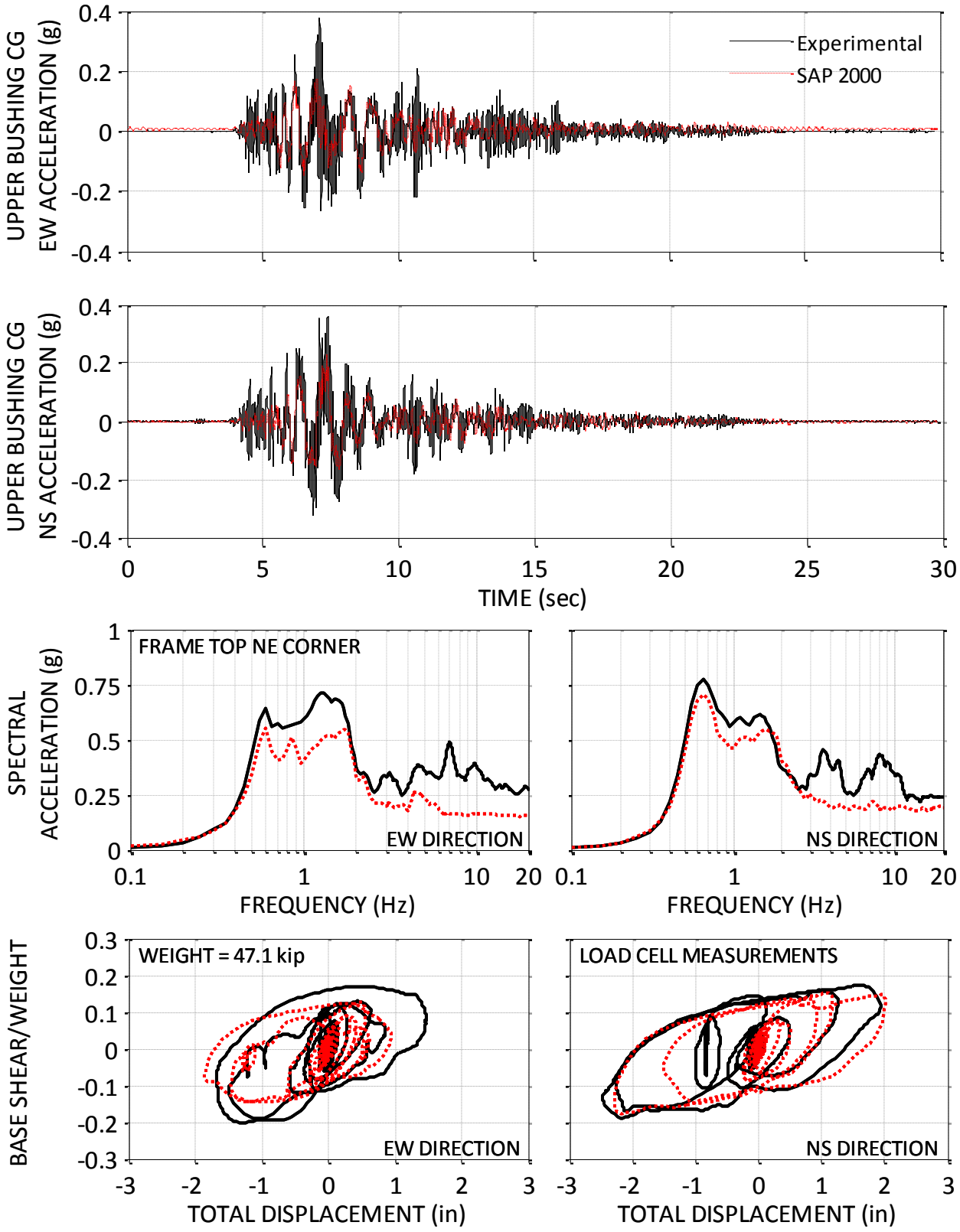
TRIPLE FP SYSTEM (Friction-Bolted Configuration)
SYLMAR 90% BI-AXIAL (FN in EW direction)
LENGTH SCALE=3 SYMMETRIC BUSHING CONFIGURATION



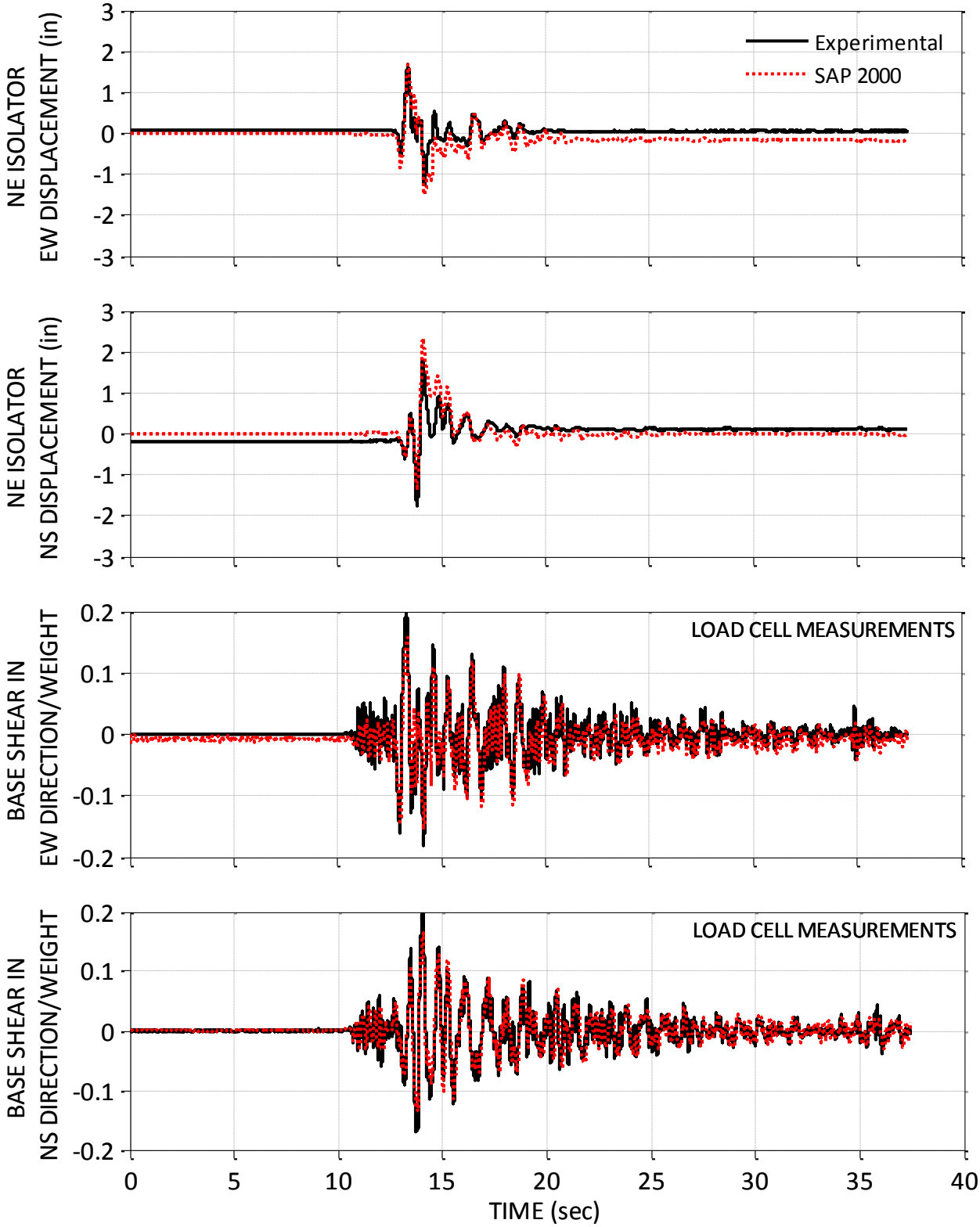

UPPER BUSHING CG
EW ACCELERATION (g)
Experimental
SAP 2000
UPPER BUSHING CG
NS ACCELERATION (g)
TIME (sec)
SPECTRAL
ACCELERATION (g)
FRAME TOP NE CORNER
EW DIRECTION
NS DIRECTION
FREQUENCY (Hz)
BASE SHEAR/WEIGHT
WEIGHT = 47.1 kip
LOAD CELL MEASUREMENTS
TOTAL DISPLACEMENT (in)

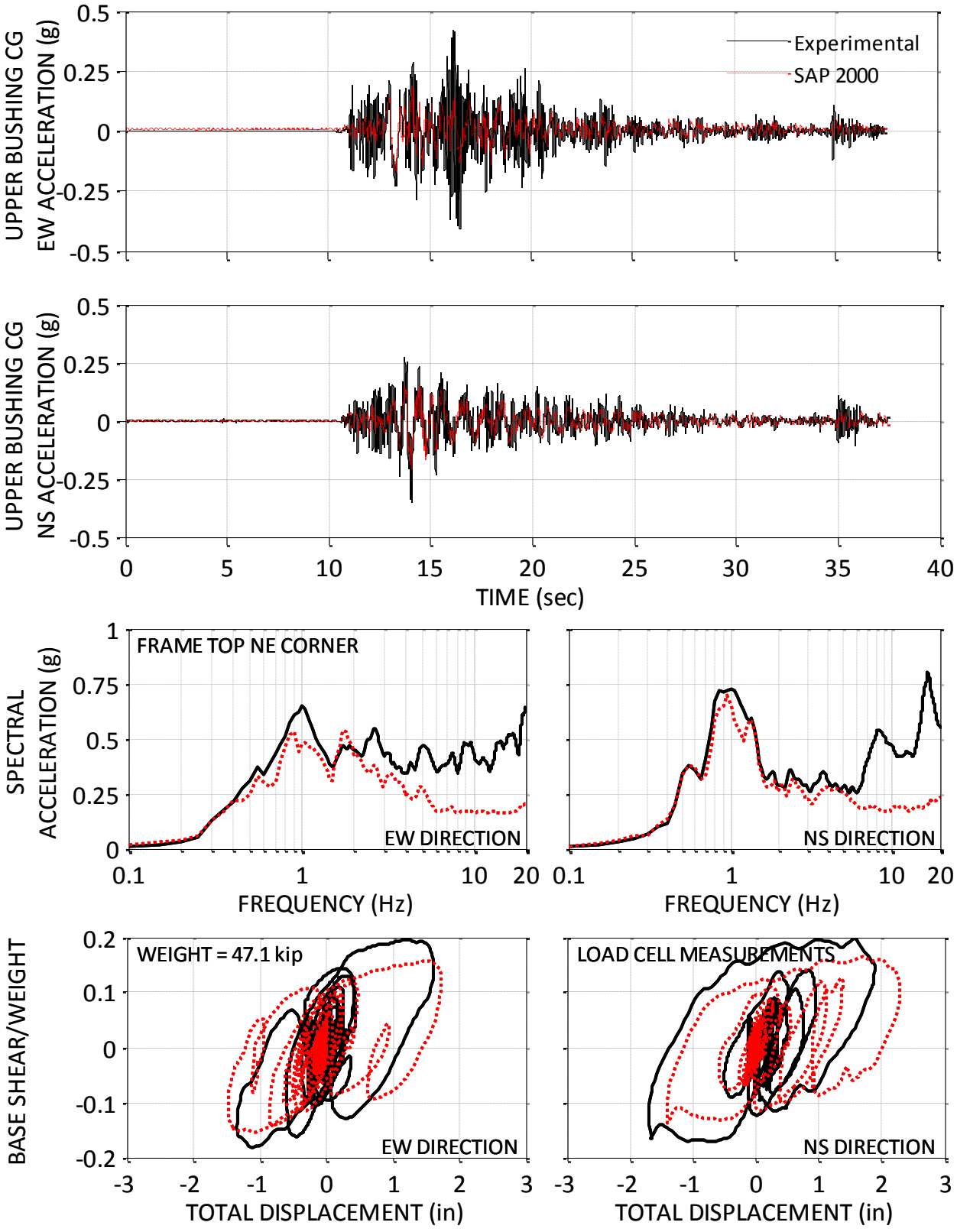
TRIPLE FP SYSTEM (Friction-Bolted Configuration)
TAKARAZUKA 97% BI-AXIAL (FN in EW direction)
LENGTH SCALE=3 SYMMETRIC BUSHING CONFIGURATION



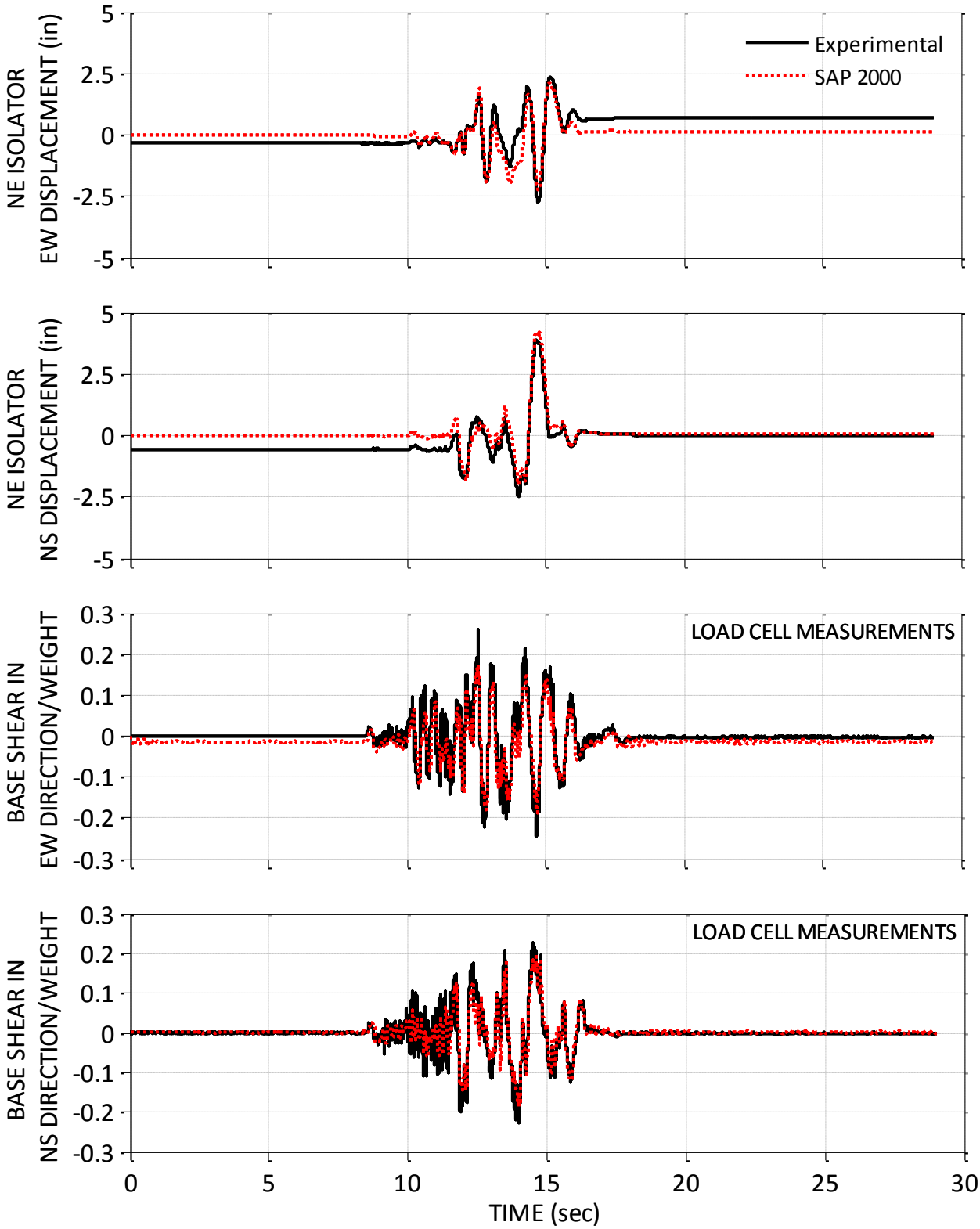

UPPER BUSHING CG
EW ACCELERATION (g)
Experimental
SAP 2000
UPPER BUSHING CG
NS ACCELERATION (g)
TIME (sec)
SPECTRAL
ACCELERATION (g)
FRAME TOP NE CORNER
EW DIRECTION
NS DIRECTION
FREQUENCY (Hz)
BASE SHEAR/WEIGHT
WEIGHT = 47.1 kip
LOAD CELL MEASUREMENTS
TOTAL DISPLACEMENT (in)

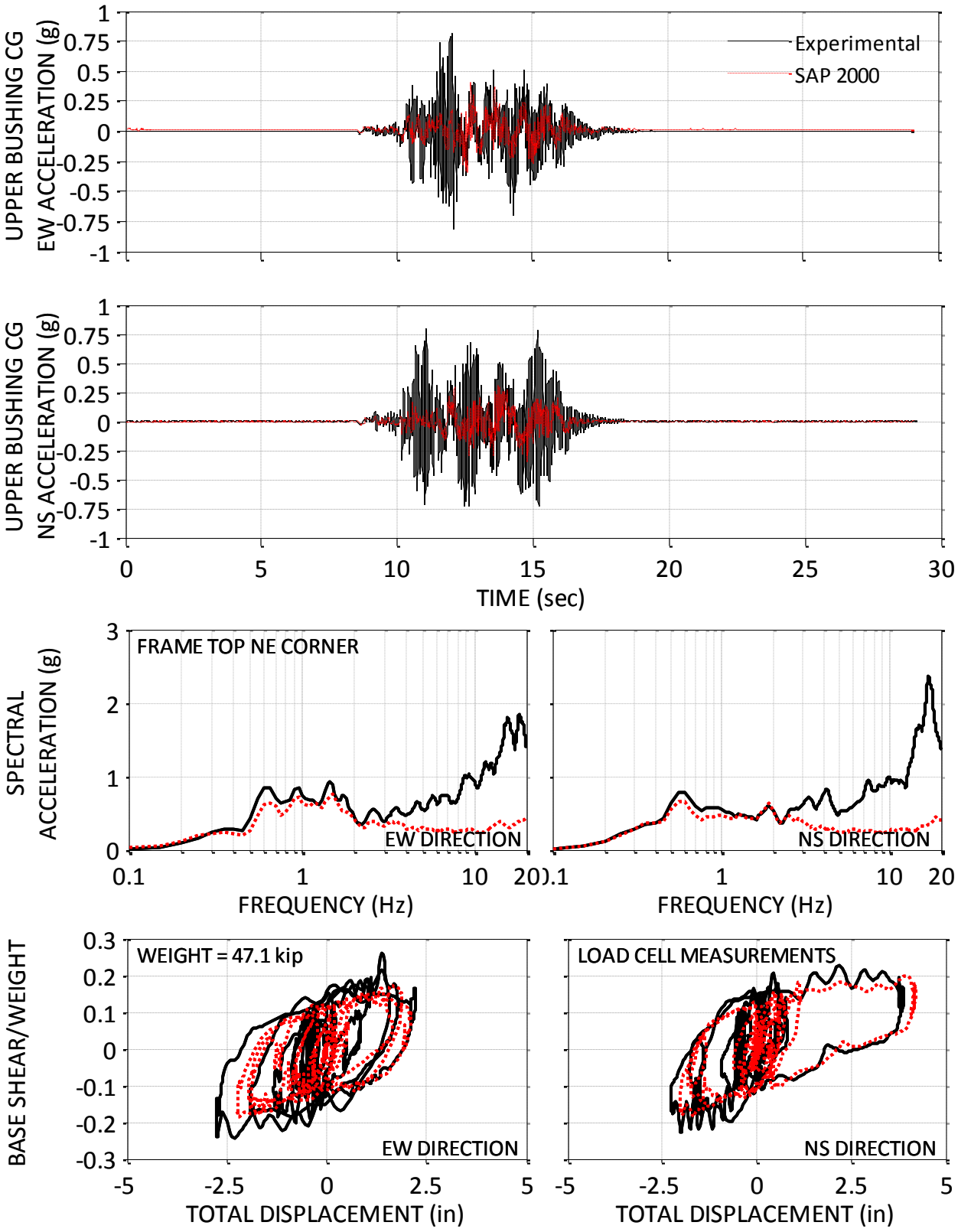
TRIPLE FP SYSTEM (Friction-Bolted Configuration)
BOLU 104% BI-AXIAL (FN in EW direction)
LENGTH SCALE=3 SYMMETRIC BUSHING CONFIGURATION



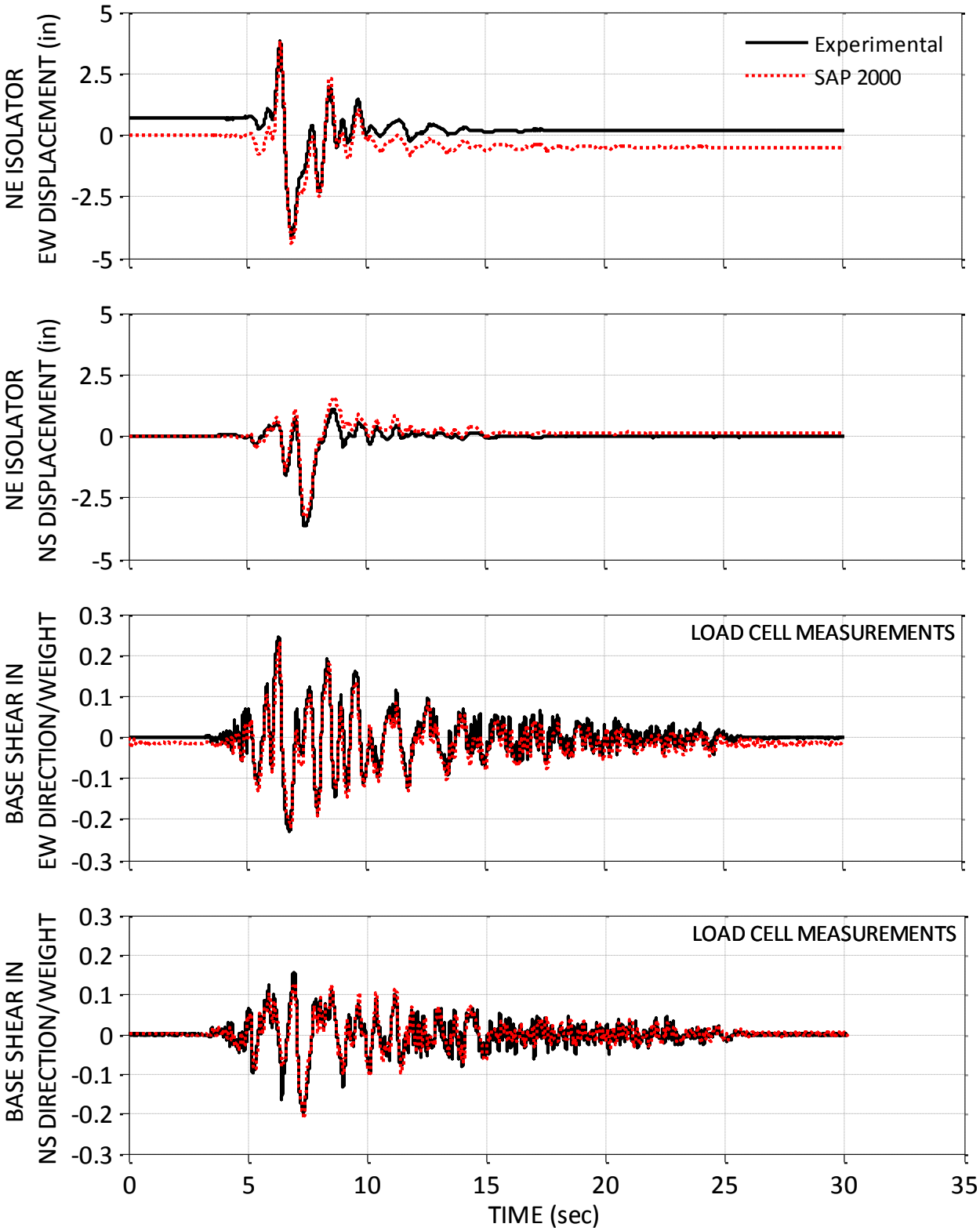

UPPER BUSHING CG
EW ACCELERATION (g)
Experimental
SAP 2000
UPPER BUSHING CG
NS ACCELERATION (g)
TIME (sec)
SPECTRAL
ACCELERATION (g)
FRAME TOP NE CORNER
EW DIRECTION
NS DIRECTION
FREQUENCY (Hz)
BASE SHEAR/WEIGHT
WEIGHT = 47.1 kip
LOAD CELL MEASUREMENTS
TOTAL DISPLACEMENT (in)

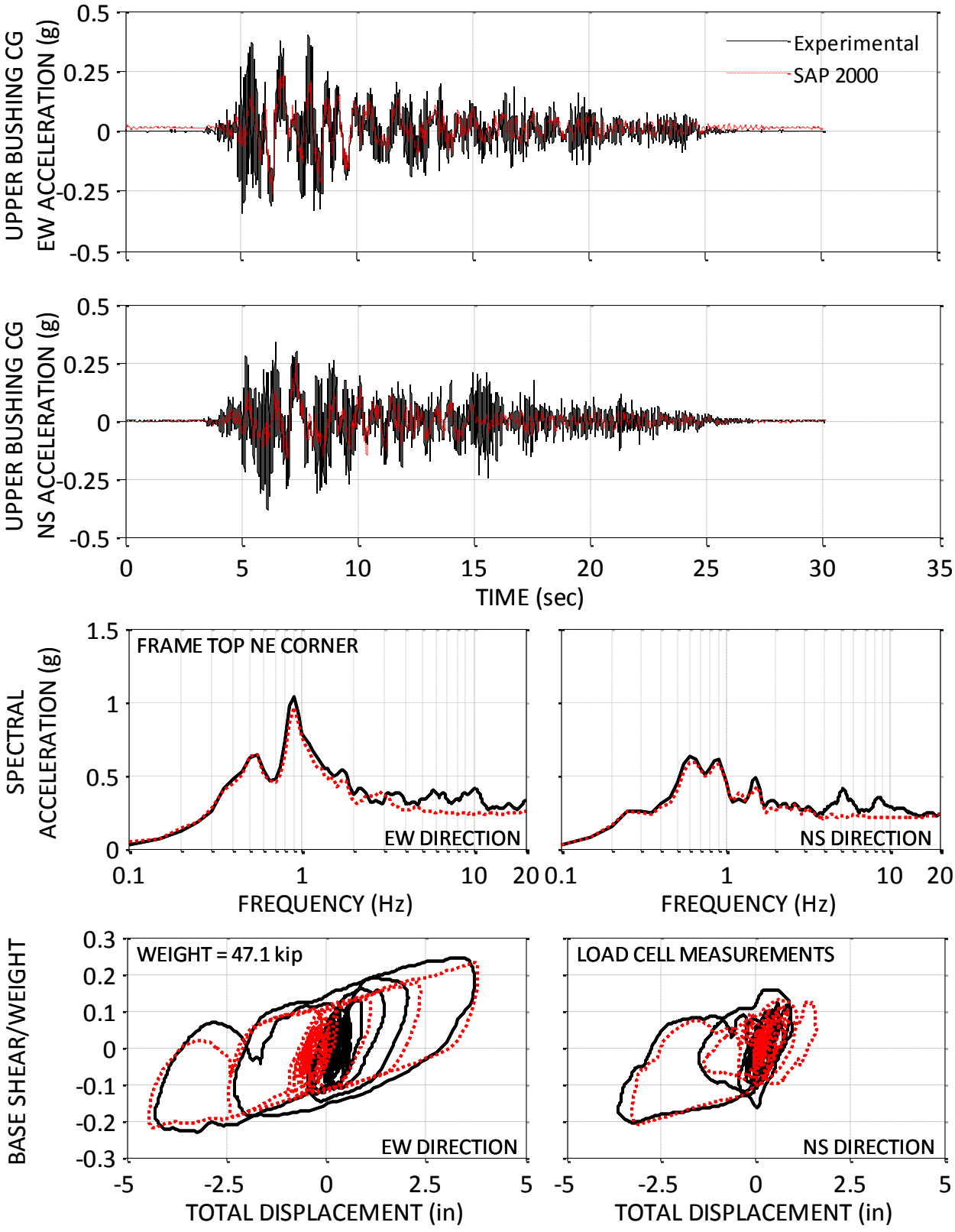
TRIPLE FP SYSTEM (Friction-Bolted Configuration)
KARAKYR 171% BI-AXIAL (FN in EW direction)
LENGTH SCALE=3 SYMMETRIC BUSHING CONFIGURATION



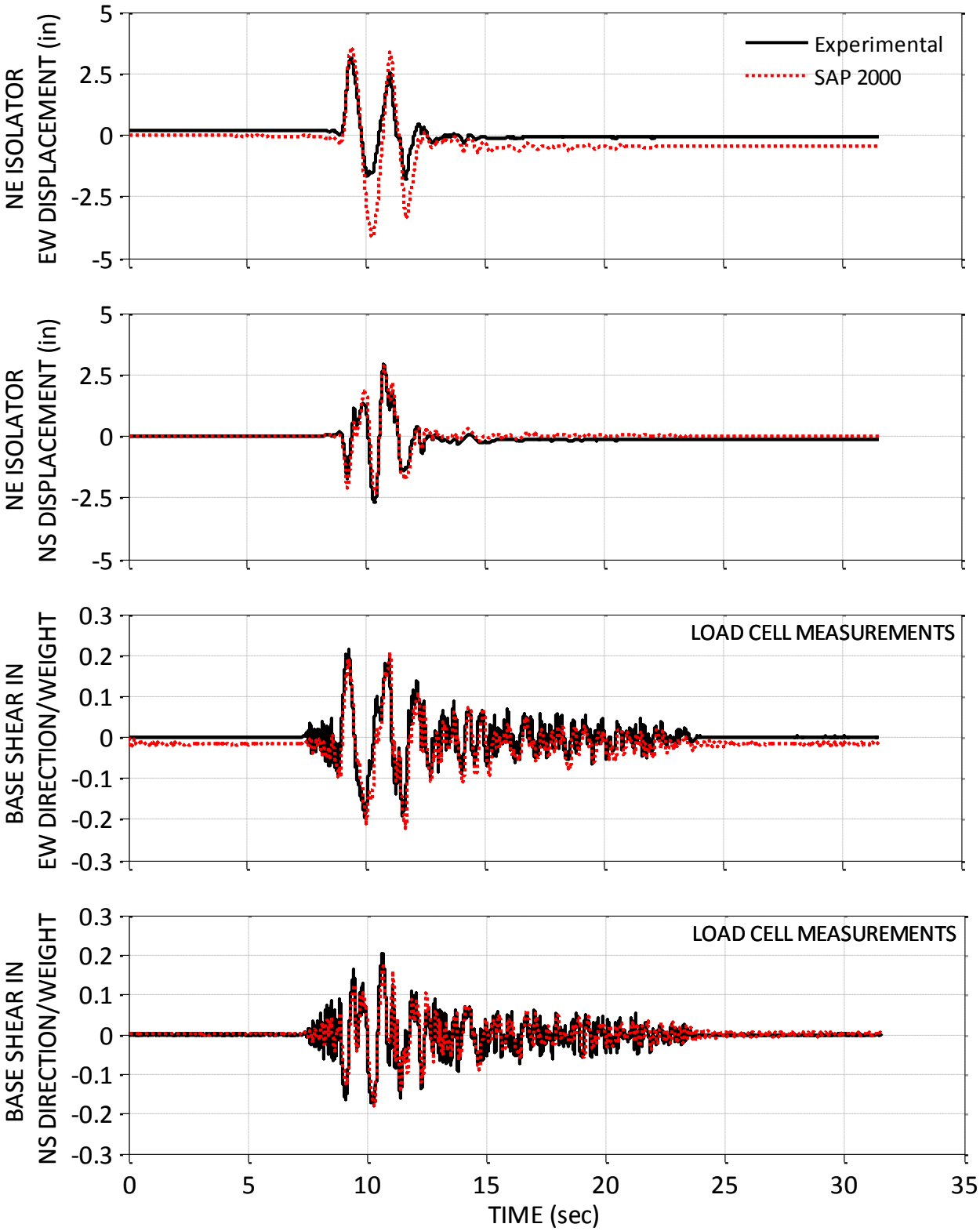

UPPER BUSHING CG
EW ACCELERATION (g)
Experimental
SAP 2000
UPPER BUSHING CG
NS ACCELERATION (g)
TIME (sec)
SPECTRAL
ACCELERATION (g)
FRAME TOP NE CORNER
EW DIRECTION
NS DIRECTION
FREQUENCY (Hz)
BASE SHEAR/WEIGHT
WEIGHT = 47.1 kip
LOAD CELL MEASUREMENTS
TOTAL DISPLACEMENT (in)

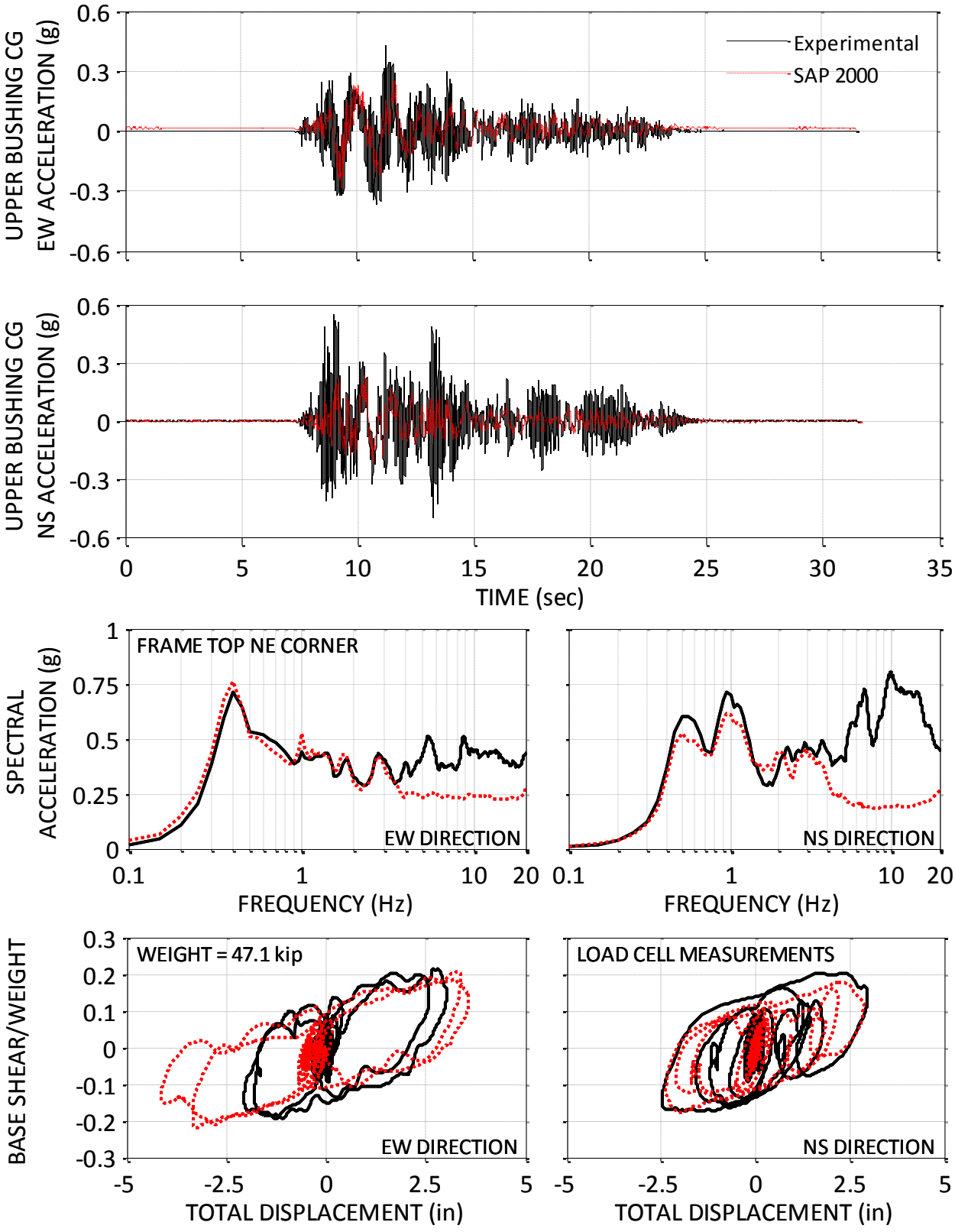
TRIPLE FP SYSTEM (Friction-Bolted Configuration)
SARATOGA 196% BI-AXIAL (FN in EW direction)
LENGTH SCALE=3 SYMMETRIC BUSHING CONFIGURATION



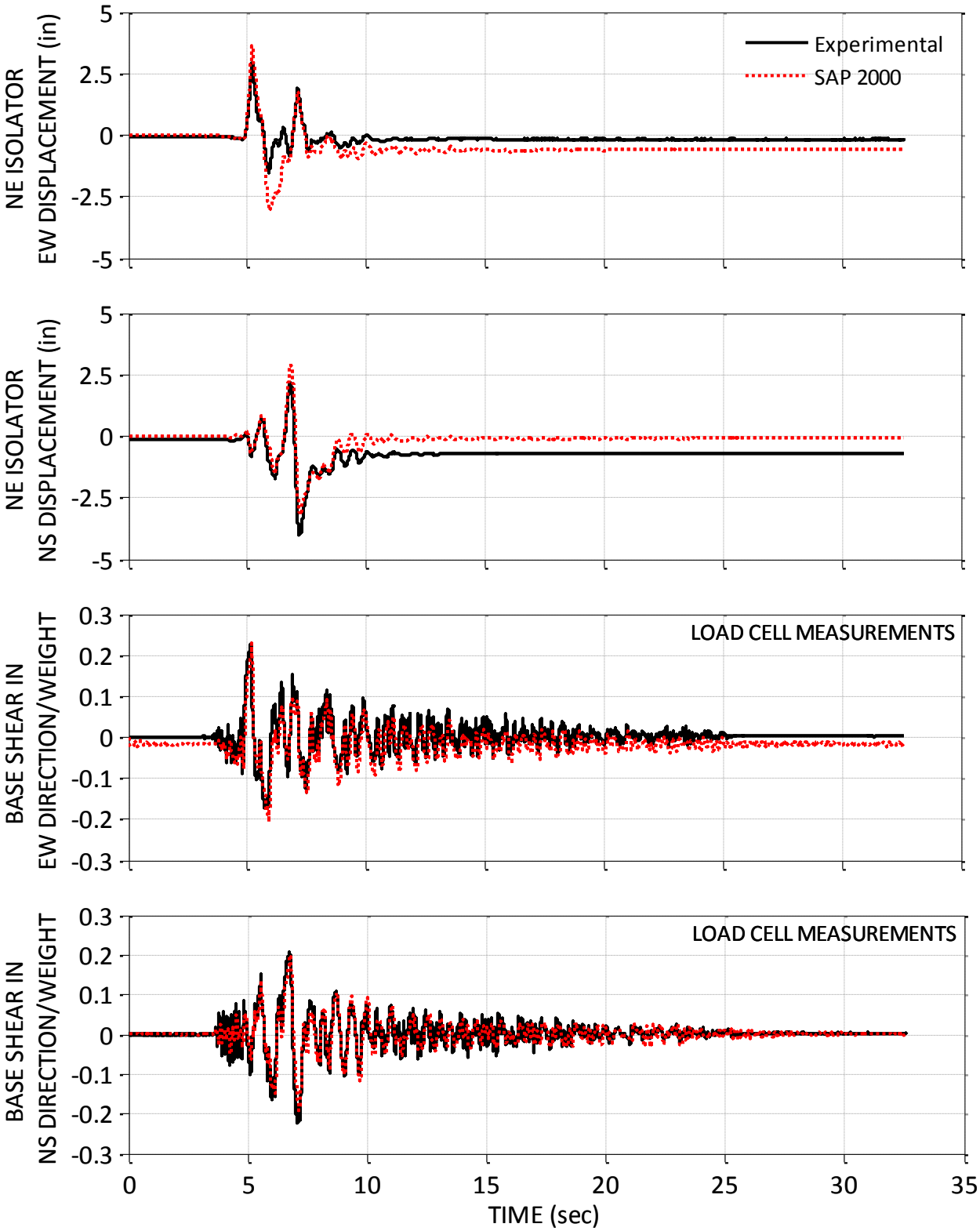

UPPER BUSHING CG
EW ACCELERATION (g)
Experimental
SAP 2000
UPPER BUSHING CG
NS ACCELERATION (g)
TIME (sec)
SPECTRAL
ACCELERATION (g)
FRAME TOP NE CORNER
EW DIRECTION
NS DIRECTION
FREQUENCY (Hz)
BASE SHEAR/WEIGHT
WEIGHT = 47.1 kip
LOAD CELL MEASUREMENTS
TOTAL DISPLACEMENT (in)

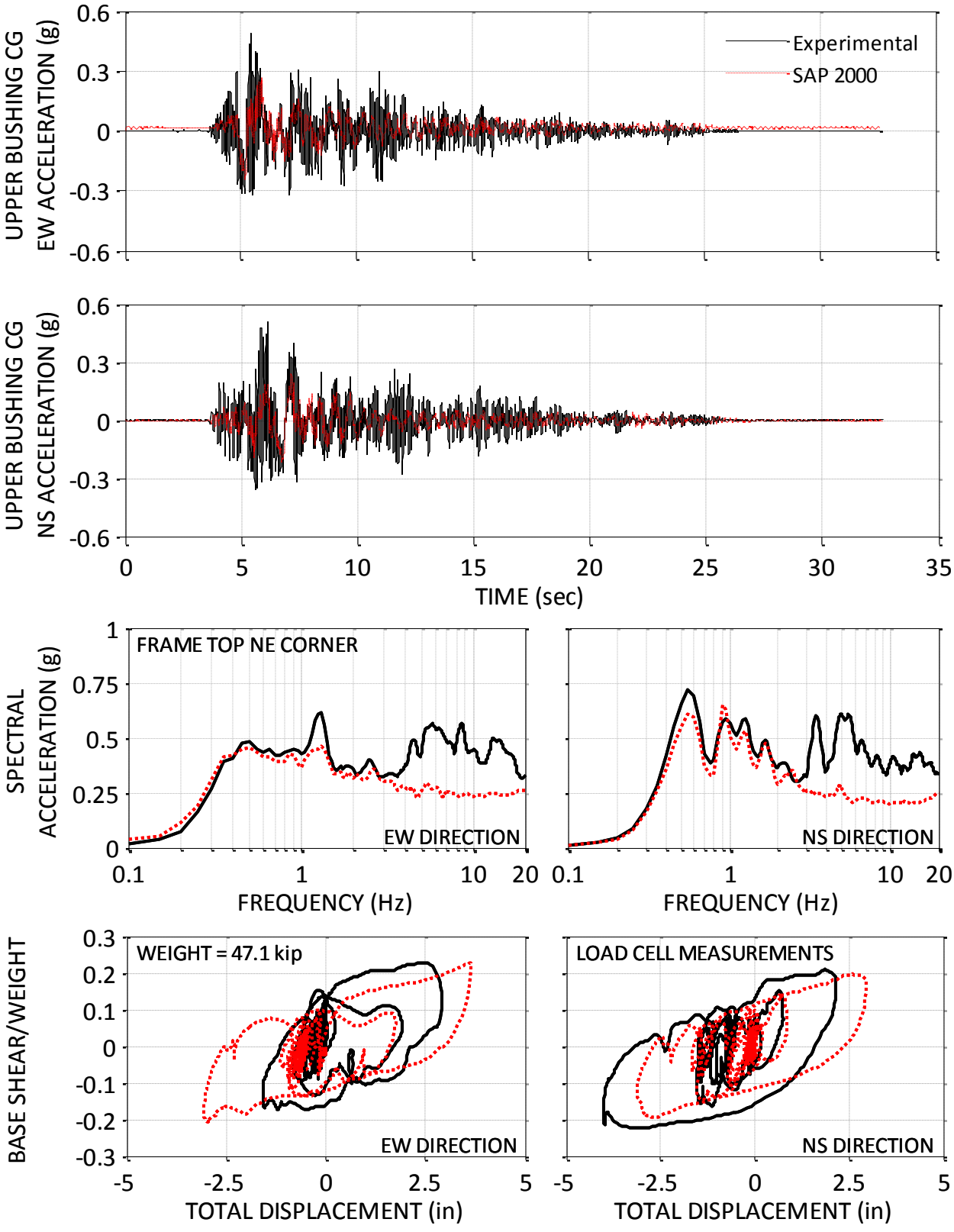
TRIPLE FP SYSTEM (Friction-Bolted Configuration)
JENSEN FILTER 121% BI-AXIAL (FN in EW direction)
LENGTH SCALE=3 SYMMETRIC BUSHING CONFIGURATION



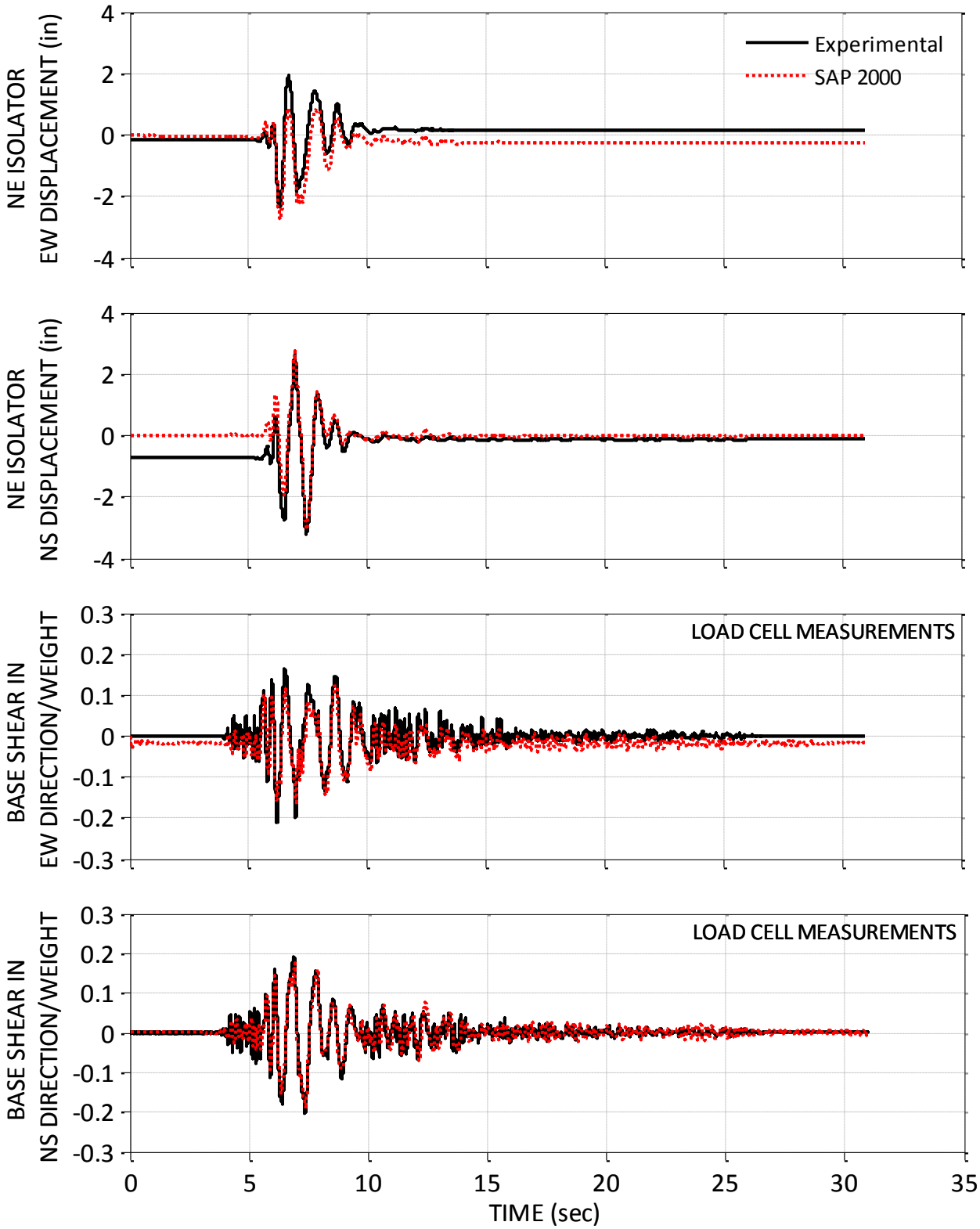

UPPER BUSHING CG
EW ACCELERATION (g)
Experimental
SAP 2000
UPPER BUSHING CG
NS ACCELERATION (g)
TIME (sec)
SPECTRAL
ACCELERATION (g)
FRAME TOP NE CORNER
EW DIRECTION
NS DIRECTION
FREQUENCY (Hz)
BASE SHEAR/WEIGHT
WEIGHT = 47.1 kip
LOAD CELL MEASUREMENTS
TOTAL DISPLACEMENT (in)

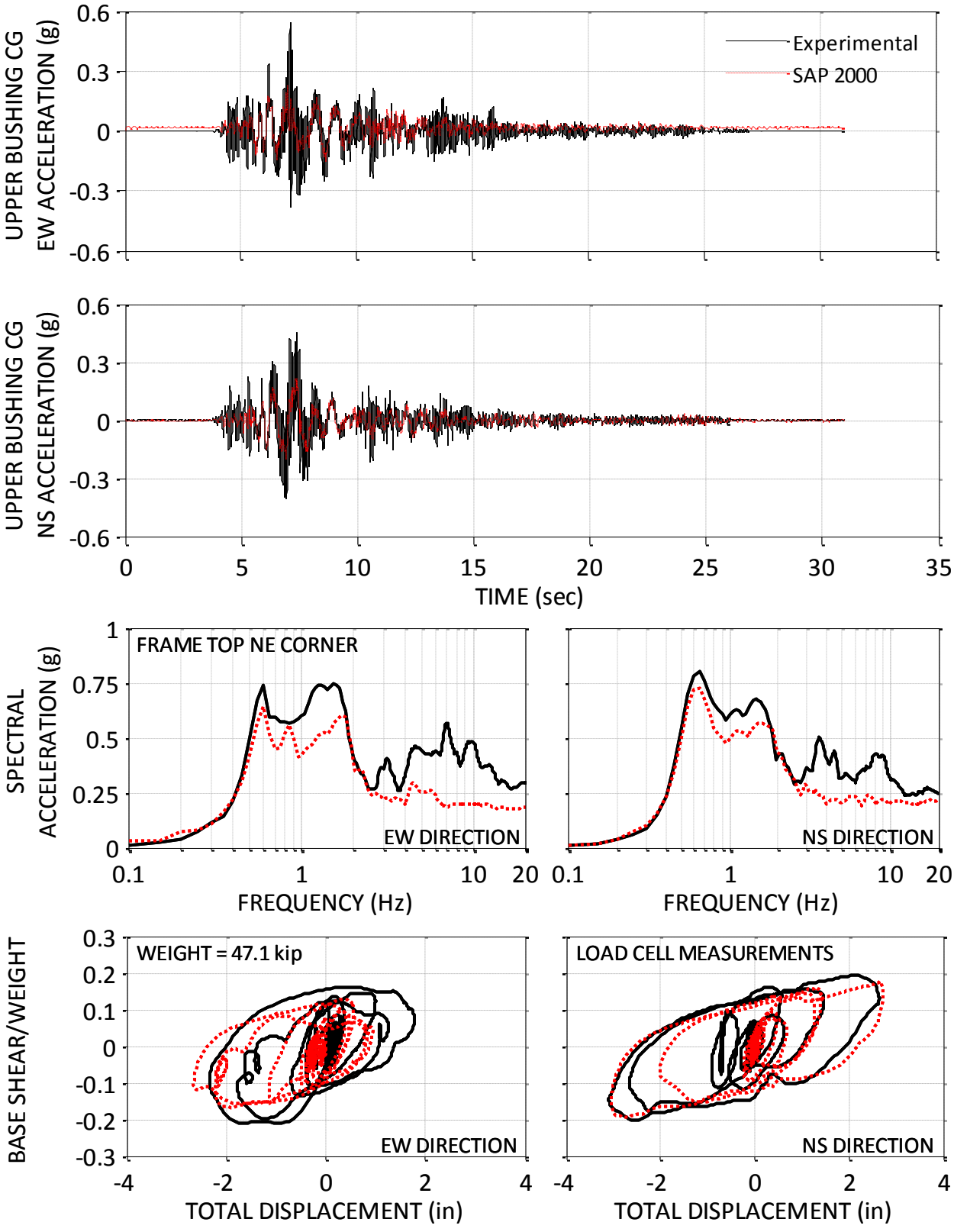
TRIPLE FP SYSTEM (Friction-Bolted Configuration)
SYLMAR 113% BI-AXIAL (FN in EW direction)
LENGTH SCALE=3 SYMMETRIC BUSHING CONFIGURATION



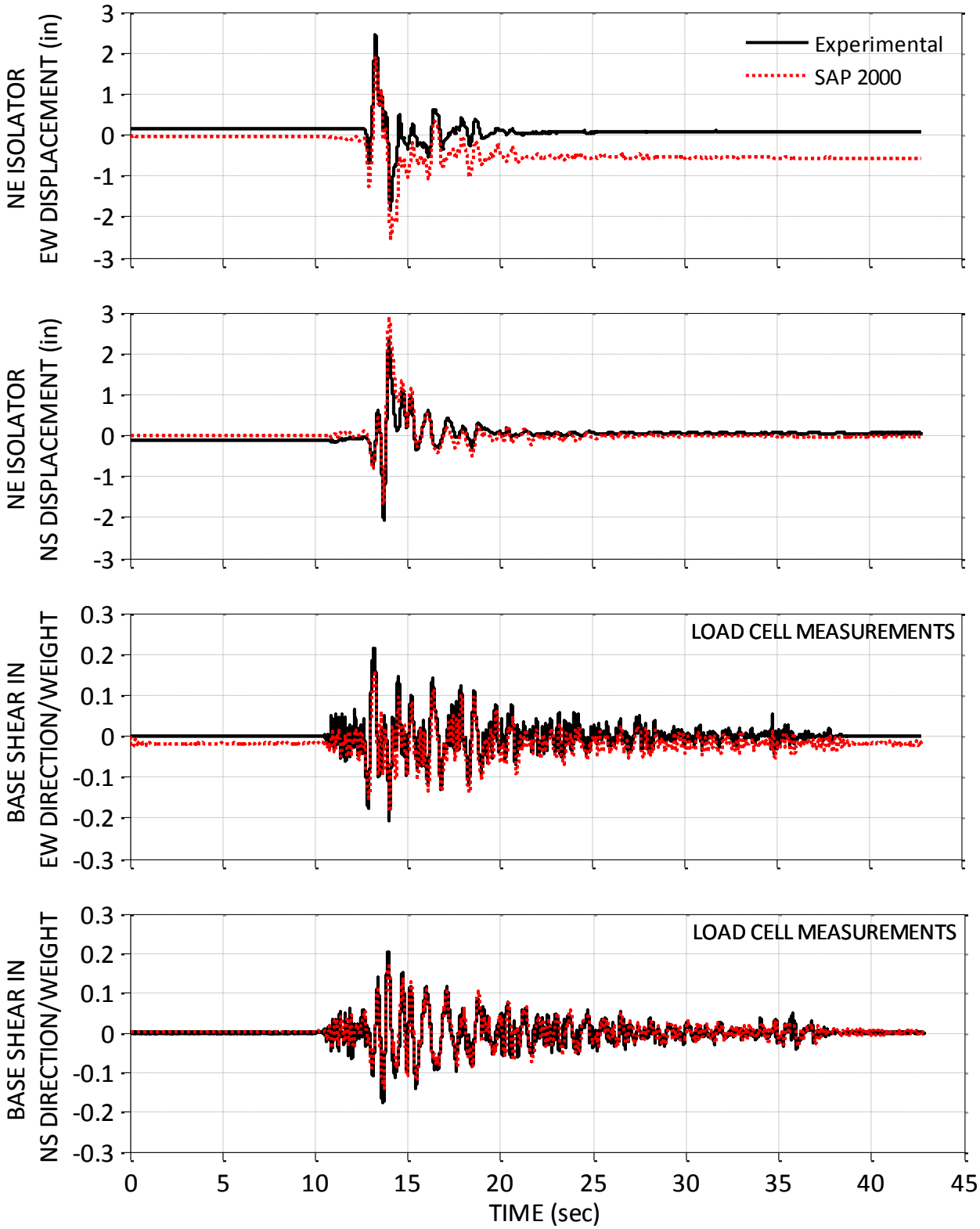

UPPER BUSHING CG
EW ACCELERATION (g)
Experimental
SAP 2000
UPPER BUSHING CG
NS ACCELERATION (g)
TIME (sec)
SPECTRAL
ACCELERATION (g)
FRAME TOP NE CORNER
EW DIRECTION
NS DIRECTION
FREQUENCY (Hz)
BASE SHEAR/WEIGHT
WEIGHT = 47.1 kip
LOAD CELL MEASUREMENTS
TOTAL DISPLACEMENT (in)

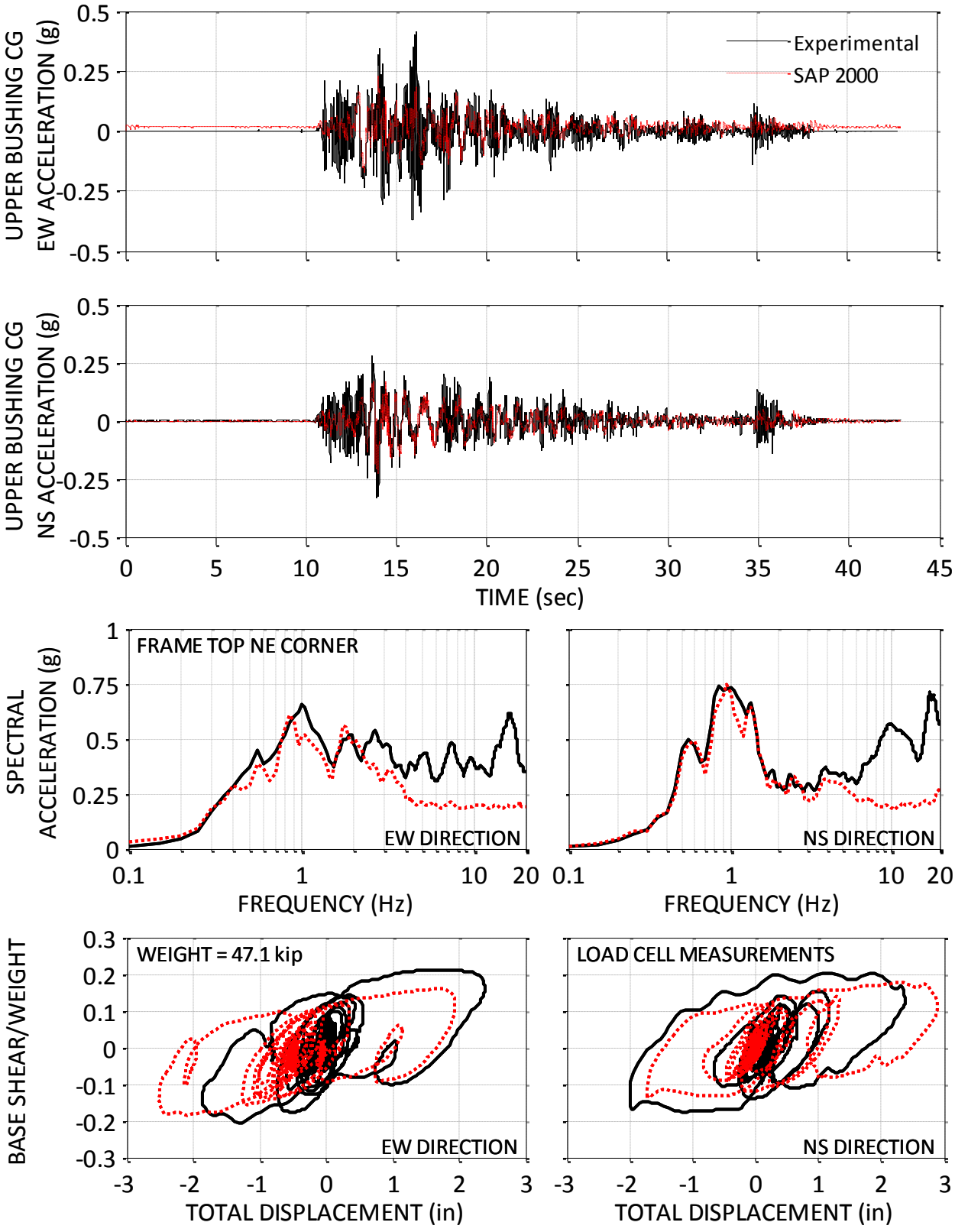
TRIPLE FP SYSTEM (Friction-Bolted Configuration)
TAKARAZUKA 121% BI-AXIAL (FN in EW direction)
LENGTH SCALE=3 SYMMETRIC BUSHING CONFIGURATION



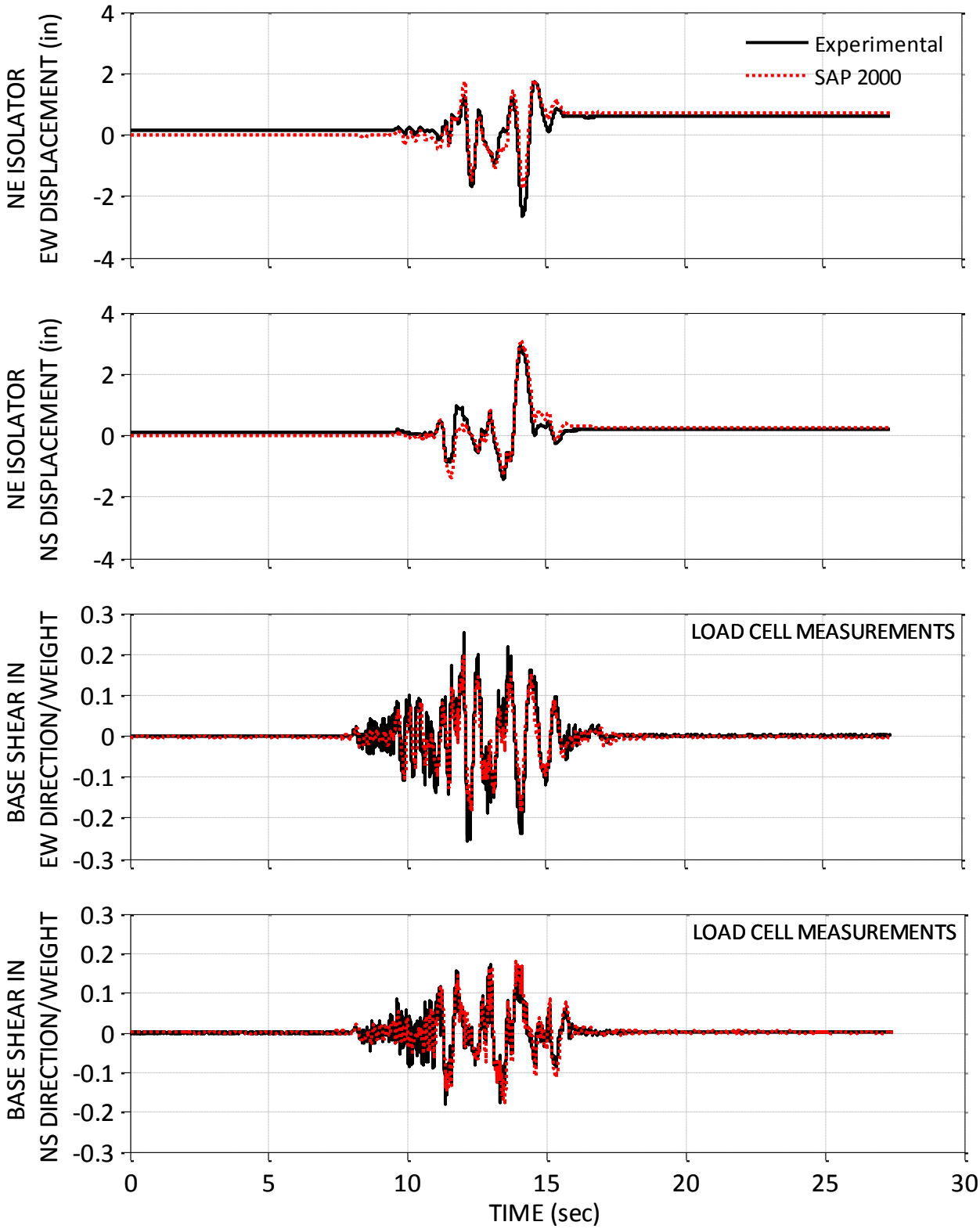

UPPER BUSHING CG
EW ACCELERATION (g)
Experimental
SAP 2000
UPPER BUSHING CG
NS ACCELERATION (g)
TIME (sec)
SPECTRAL
ACCELERATION (g)
FRAME TOP NE CORNER
EW DIRECTION
NS DIRECTION
FREQUENCY (Hz)
BASE SHEAR/WEIGHT
WEIGHT = 47.1 kip
LOAD CELL MEASUREMENTS
TOTAL DISPLACEMENT (in)

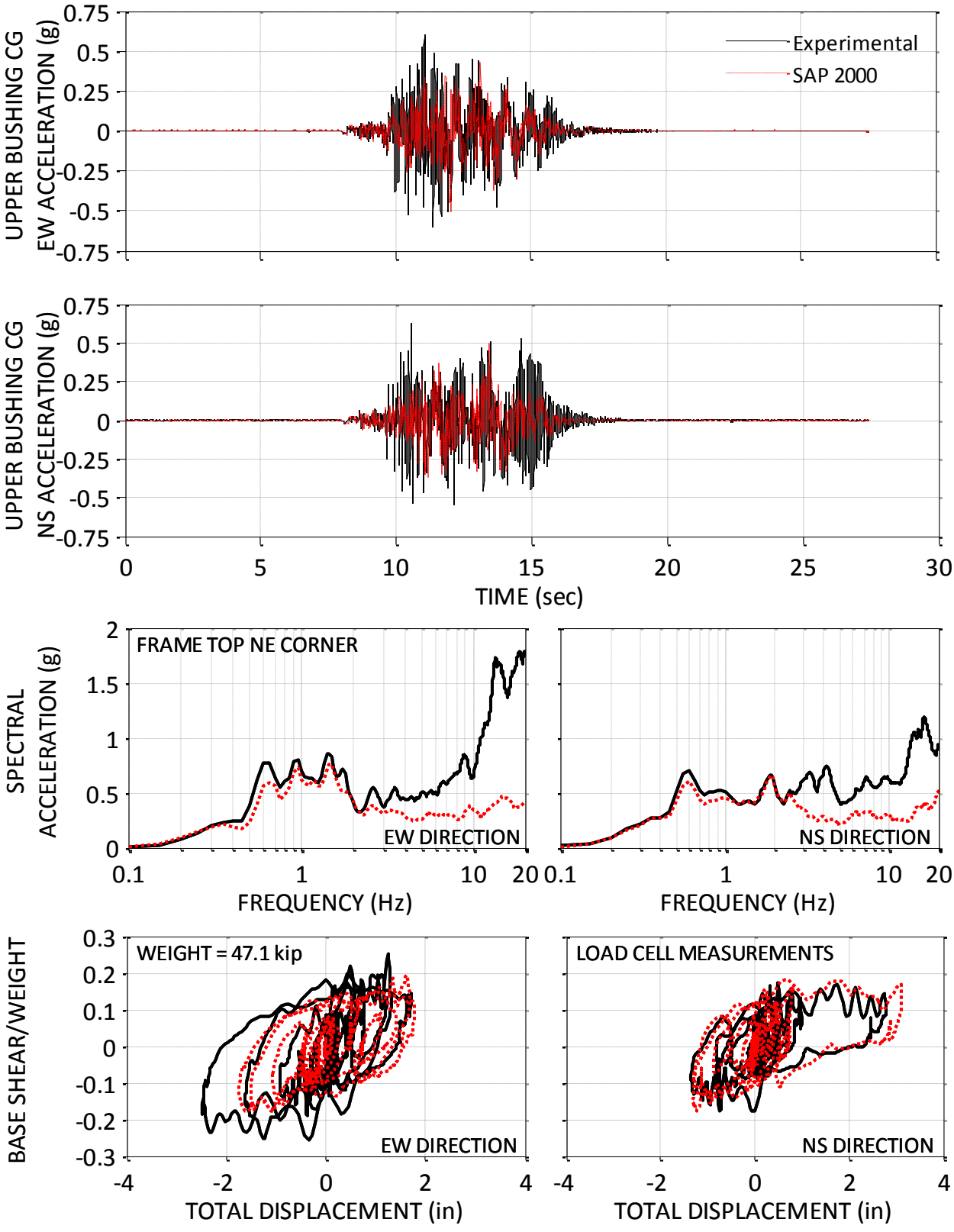
TRIPLE FP SYSTEM (Friction-Bolted Configuration)
BOLU 130% BI-AXIAL (FN in EW direction)
LENGTH SCALE=3 SYMMETRIC BUSHING CONFIGURATION



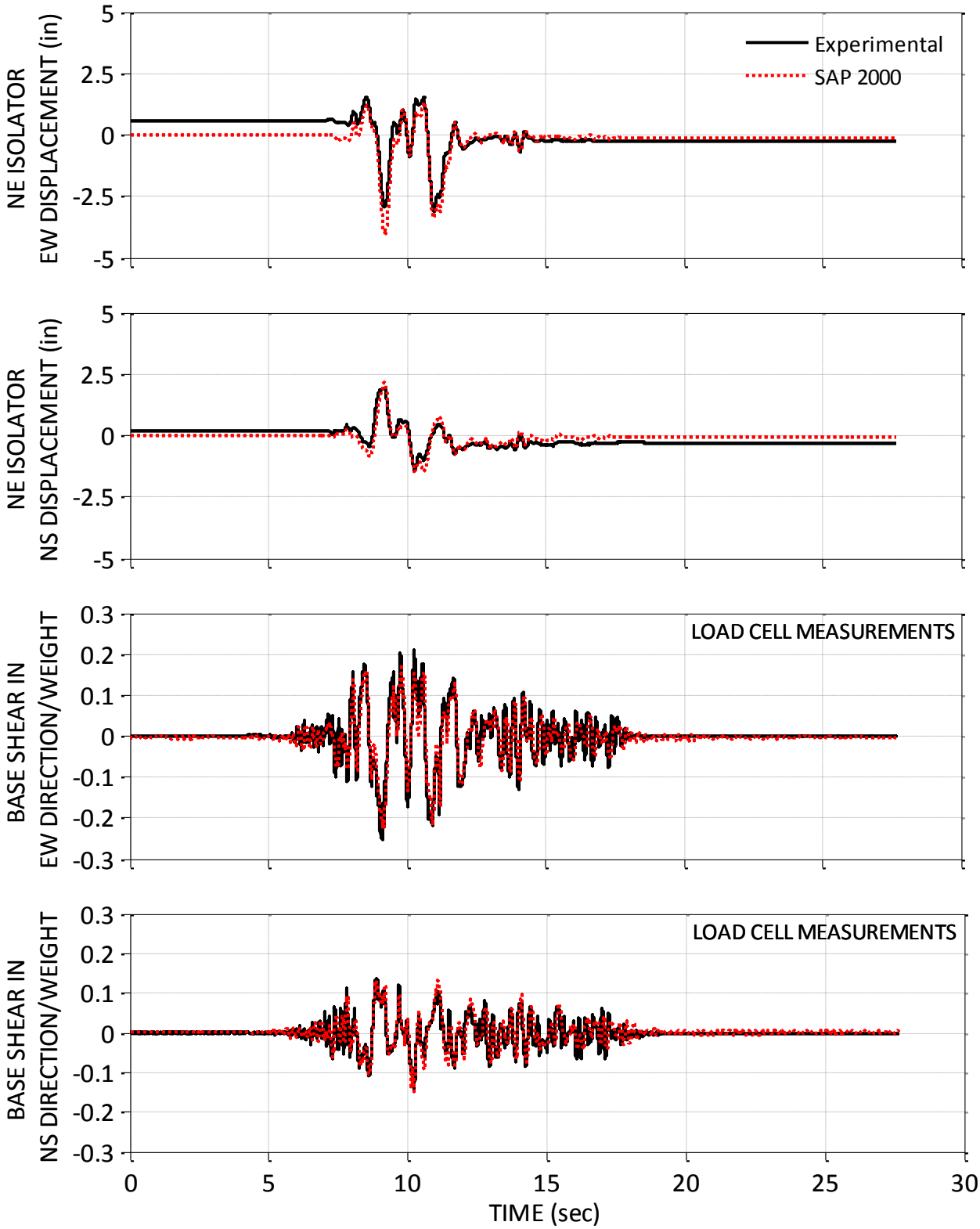

UPPER BUSHING CG
EW ACCELERATION (g)
Experimental
SAP 2000
UPPER BUSHING CG
NS ACCELERATION (g)
TIME (sec)
SPECTRAL
ACCELERATION (g)
FRAME TOP NE CORNER
EW DIRECTION
NS DIRECTION
FREQUENCY (Hz)
BASE SHEAR/WEIGHT
WEIGHT = 47.1 kip
LOAD CELL MEASUREMENTS
TOTAL DISPLACEMENT (in)

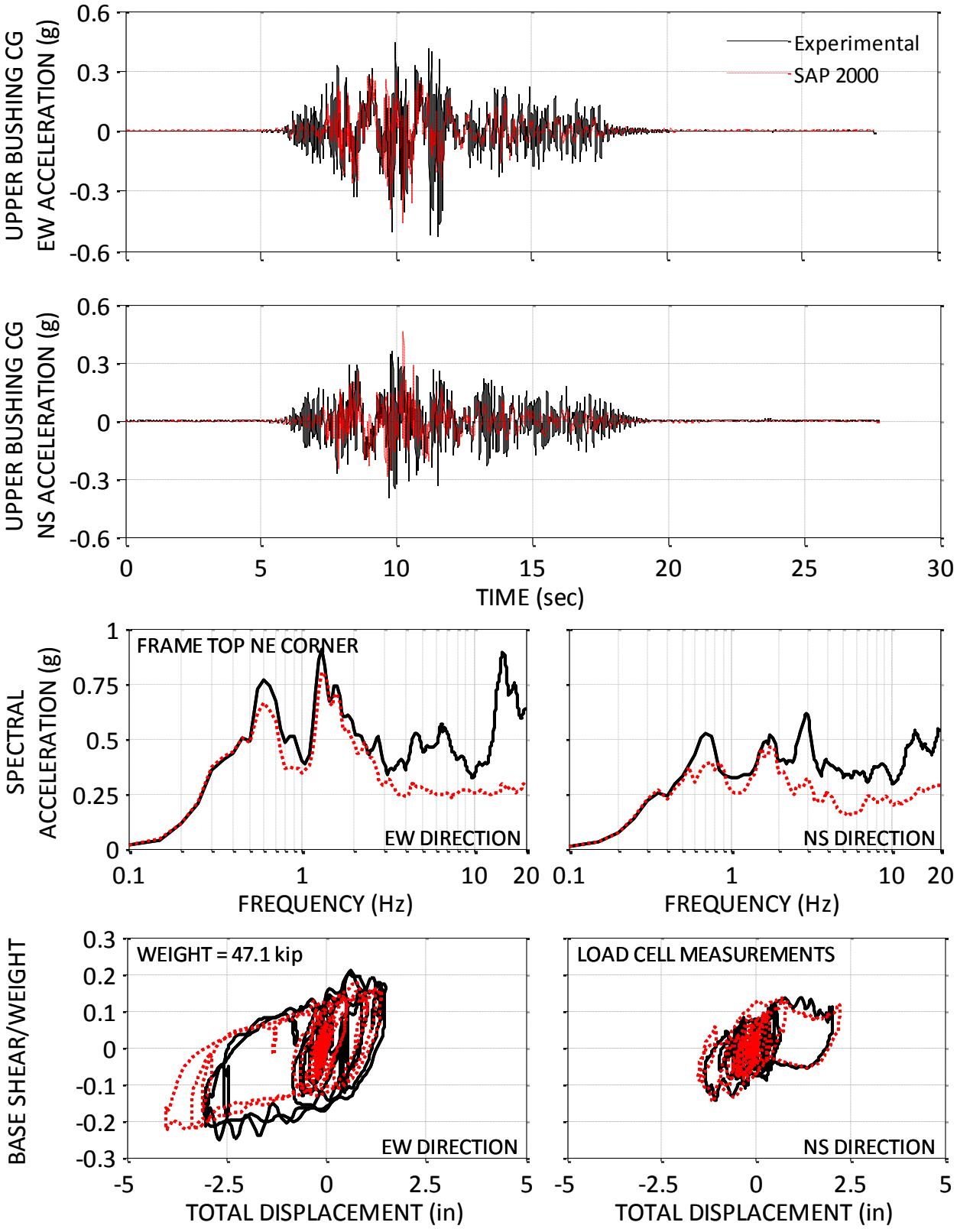
TRIPLE FP SYSTEM (Friction-Bolted Configuration)
KARAKYR 137% TRI-AXIAL (FN in EW direction)
LENGTH SCALE=3 SYMMETRIC BUSHING CONFIGURATION



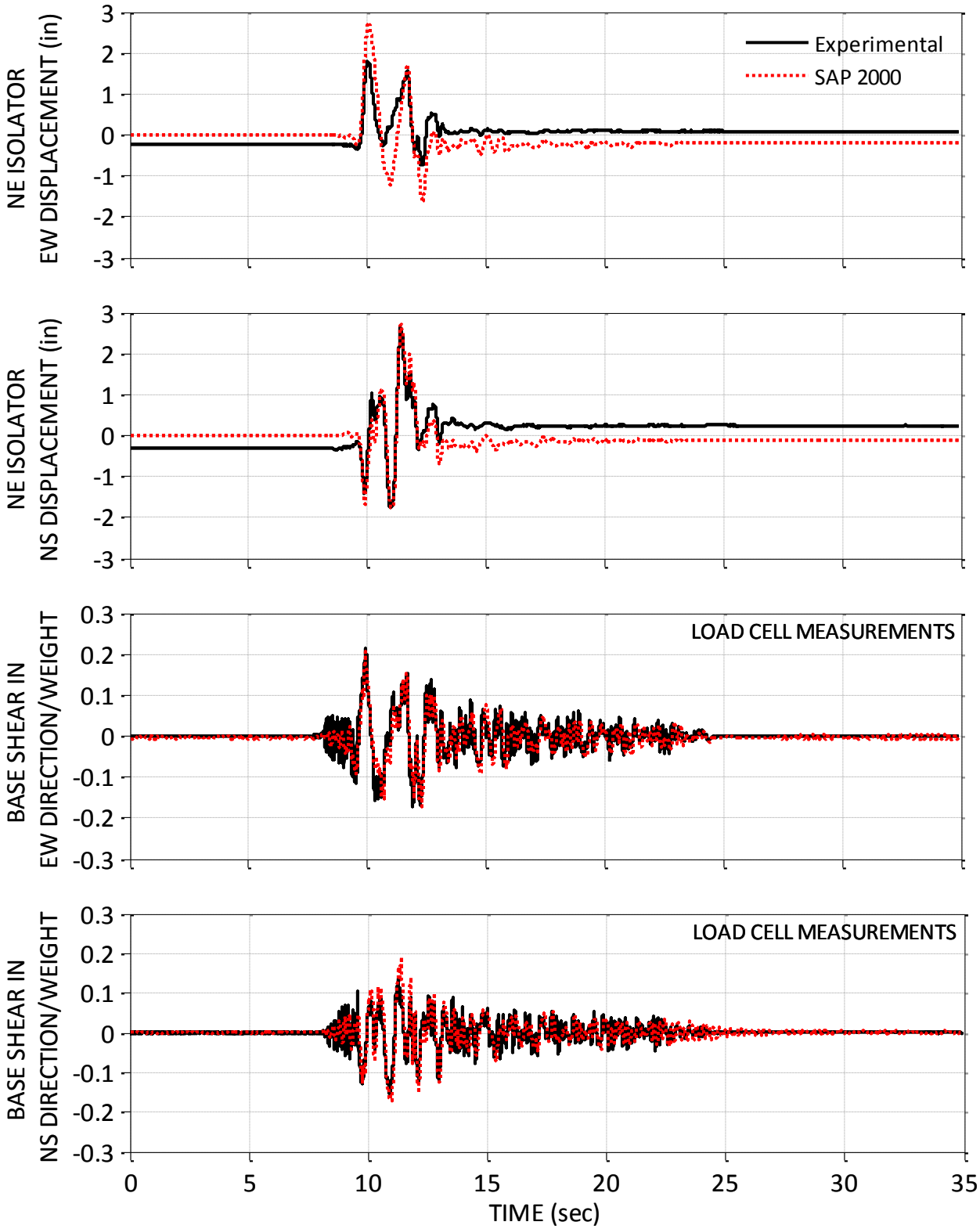

UPPER BUSHING CG
EW ACCELERATION (g)
0.75
0.5
0.25
0
-0.25
-0.5
-0.75
Experimental
SAP 2000
UPPER BUSHING CG
NS ACCELERATION (g)
0
5
10
15
20
25
30
TIME (sec)
SPECTRAL
ACCELERATION (g)
FRAME TOP NE CORNER
EW DIRECTION
NS DIRECTION
2
1.5
1
0.5
0
0.1
1
10
20
FREQUENCY (Hz)
BASE SHEAR/WEIGHT
WEIGHT = 47.1 kip
LOAD CELL MEASUREMENTS
0.3
0.2
0.1
-0.1
-0.2
-0.3
-4
-2
2
4
TOTAL DISPLACEMENT (in)

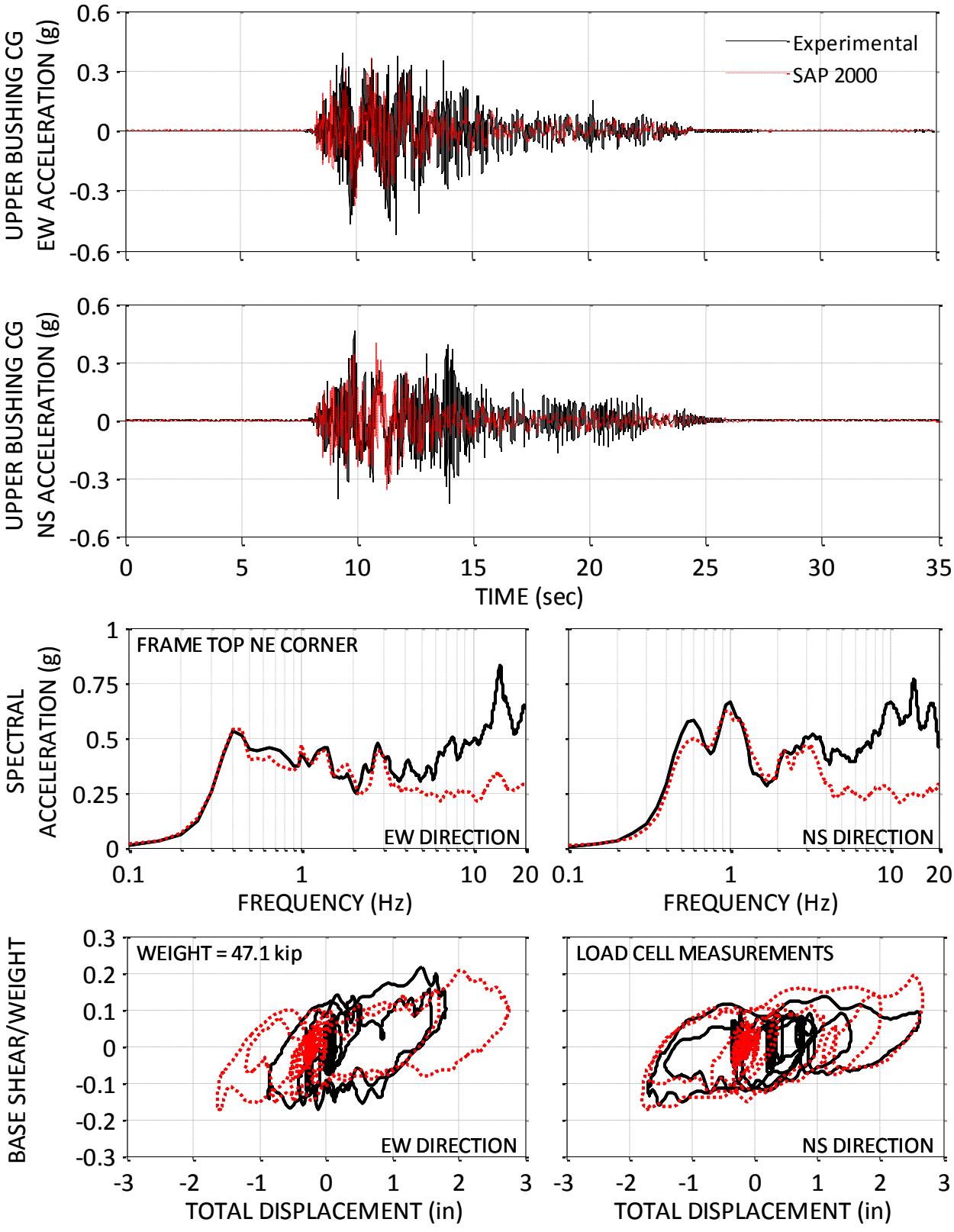
TRIPLE FP SYSTEM (Friction-Bolted Configuration)
LGPC 94% TRI-AXIAL (FN in EW direction)
LENGTH SCALE=3 SYMMETRIC BUSHING CONFIGURATION



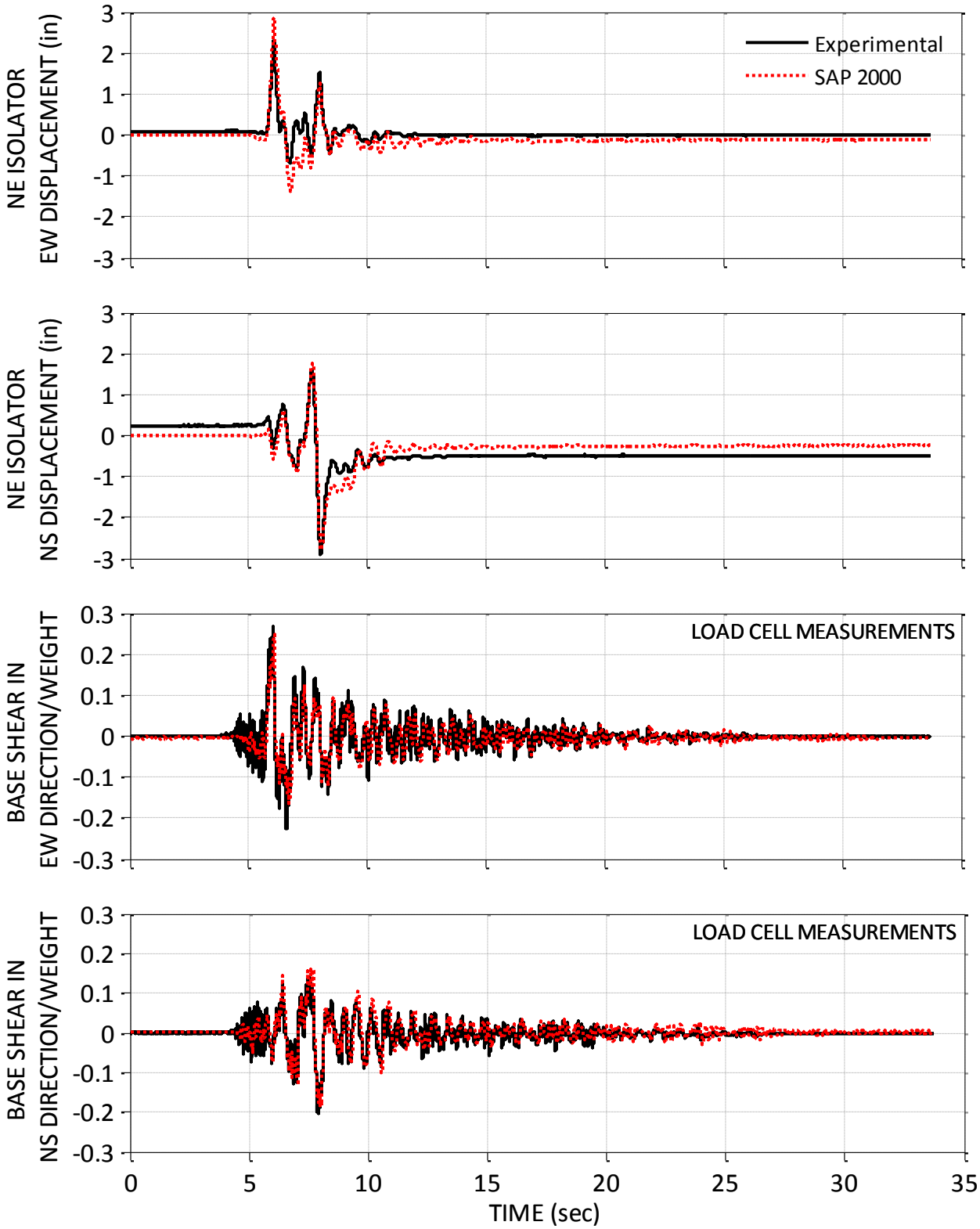

UPPER BUSHING CG
EW ACCELERATION (g)
Experimental
SAP 2000
UPPER BUSHING CG
NS ACCELERATION (g)
TIME (sec)
SPECTRAL
ACCELERATION (g)
FRAME TOP NE CORNER
EW DIRECTION
NS DIRECTION
FREQUENCY (Hz)
BASE SHEAR/WEIGHT
WEIGHT = 47.1 kip
LOAD CELL MEASUREMENTS
TOTAL DISPLACEMENT (in)

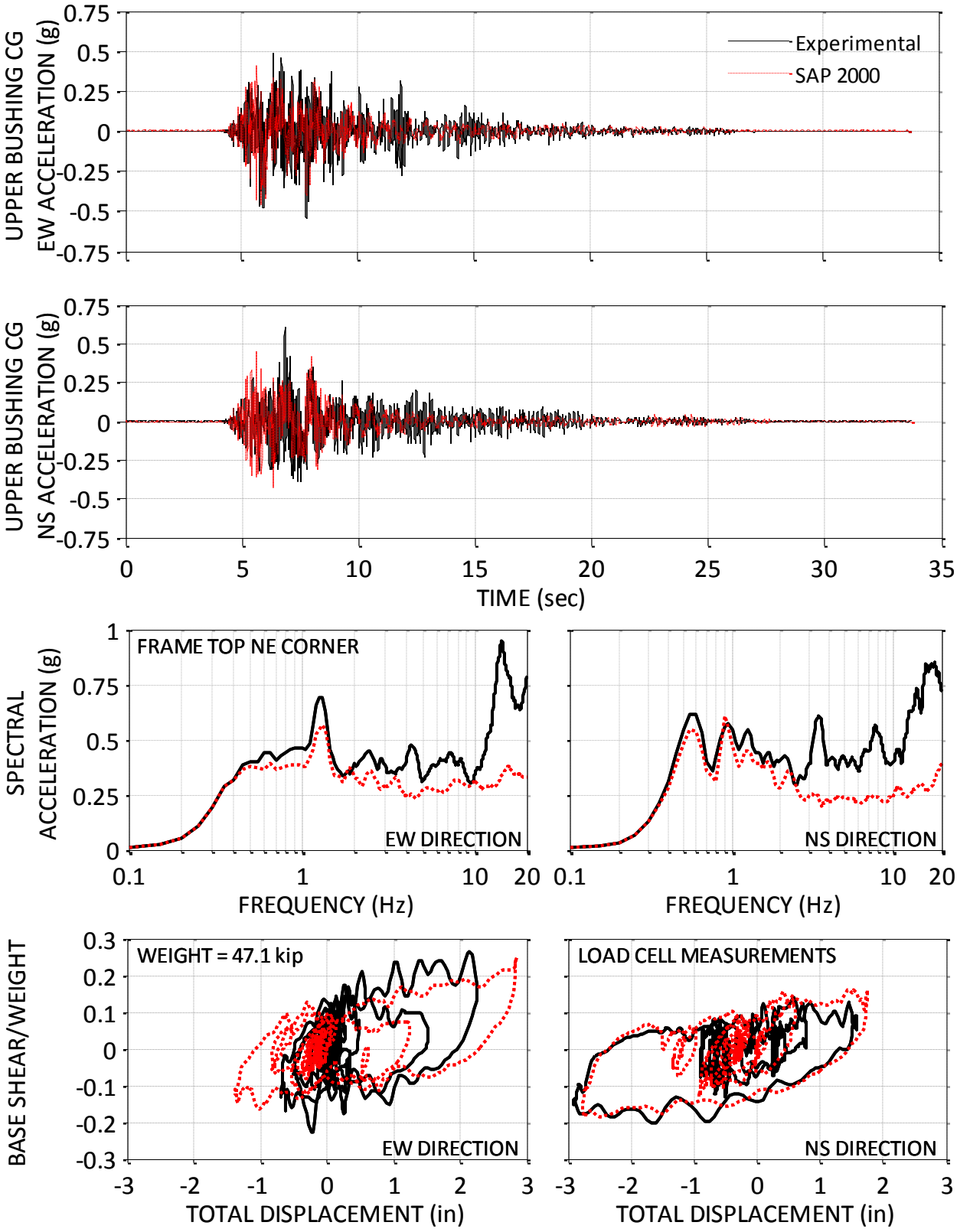
TRIPLE FP SYSTEM (Friction-Bolted Configuration)
JENSEN FILTER 97% TRI-AXIAL (FN in EW direction)
LENGTH SCALE=3 SYMMETRIC BUSHING CONFIGURATION



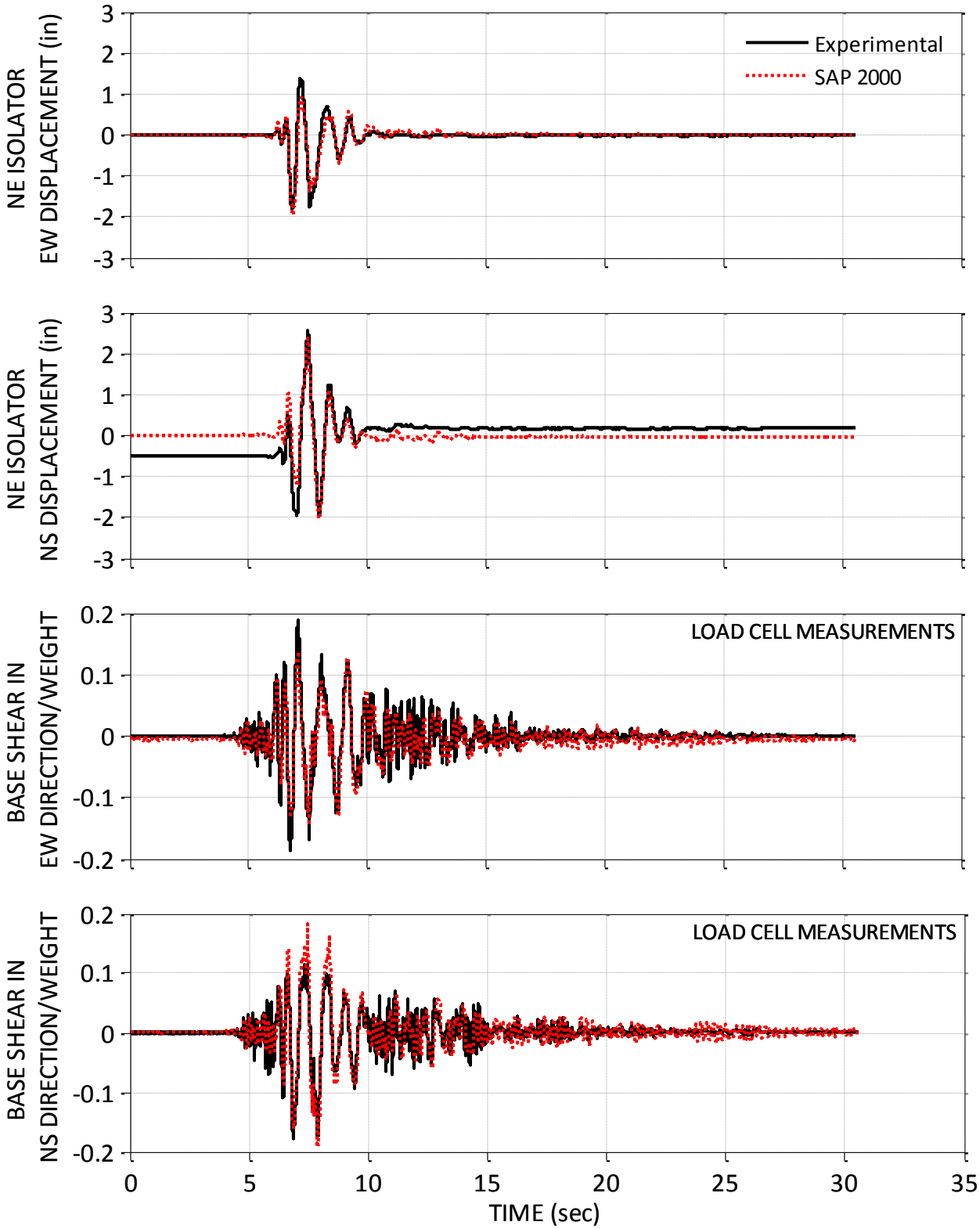

UPPER BUSHING CG
EW ACCELERATION (g)
0.6
0.3
0
-0.3
-0.6
Experimental
SAP 2000
UPPER BUSHING CG
NS ACCELERATION (g)
0
5
10
15
20
25
30
35
TIME (sec)
SPECTRAL
ACCELERATION (g)
FRAME TOP NE CORNER
1
0.75
0.5
0.25
EW DIRECTION
NS DIRECTION
0.1
20
FREQUENCY (Hz)
BASE SHEAR/WEIGHT
WEIGHT = 47.1 kip
LOAD CELL MEASUREMENTS
-3
-2
3
TOTAL DISPLACEMENT (in)

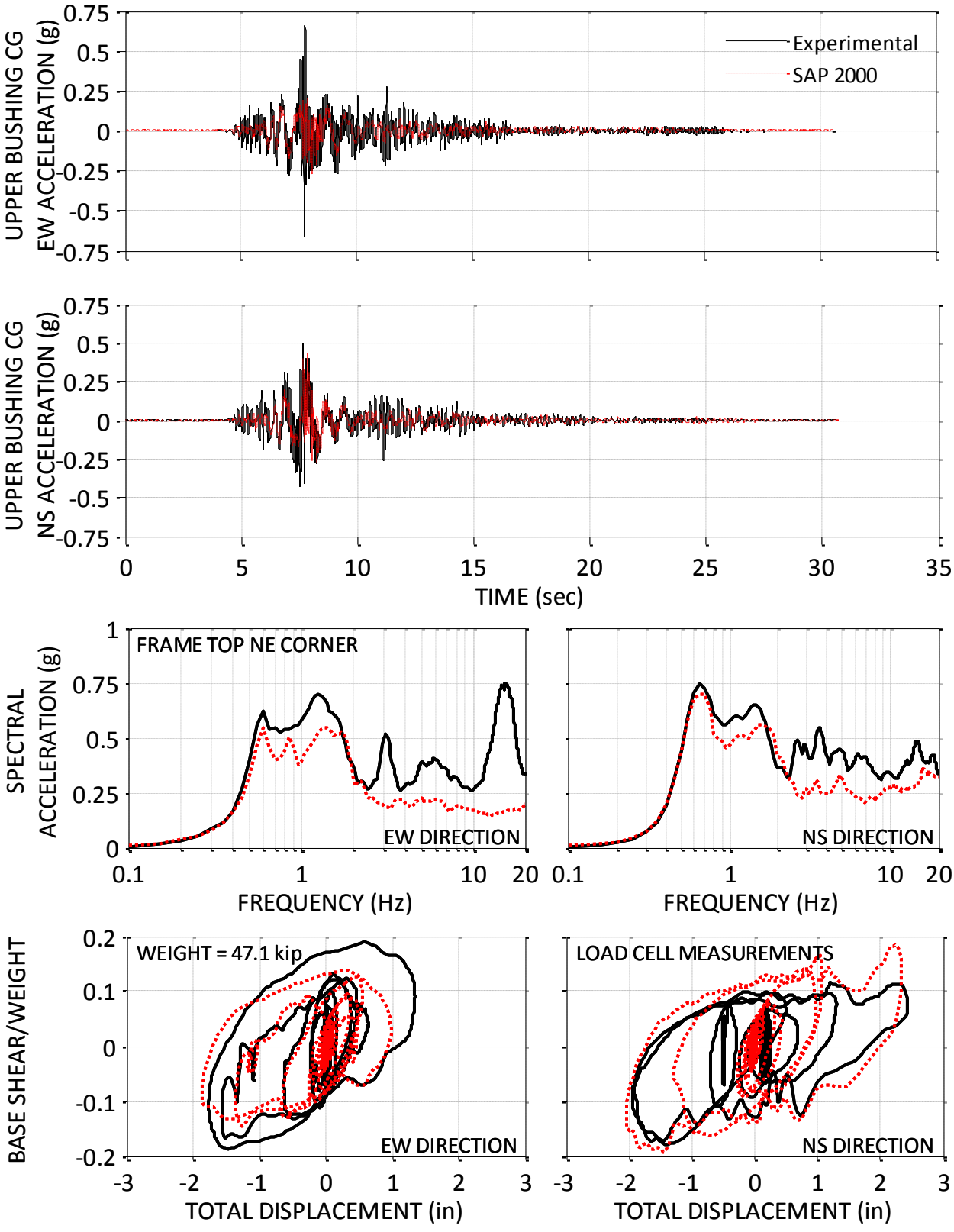
TRIPLE FP SYSTEM (Friction-Bolted Configuration)
SYLMAR 90% TRI-AXIAL (FN in EW direction)
LENGTH SCALE=3 SYMMETRIC BUSHING CONFIGURATION



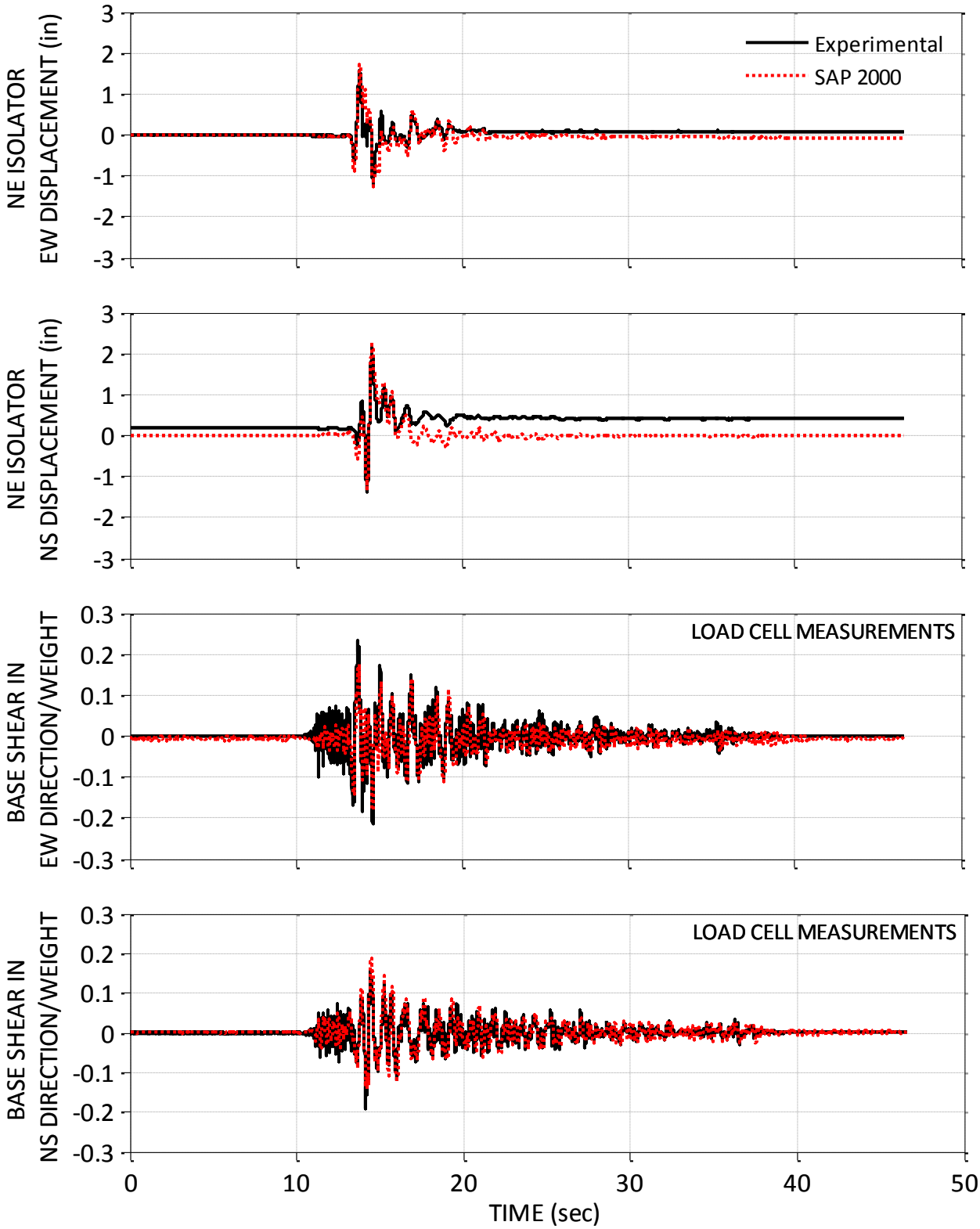

UPPER BUSHING CG
EW ACCELERATION (g)
0.75
0.5
0.25
0
-0.25
-0.5
-0.75
Experimental
SAP 2000
UPPER BUSHING CG
NS ACCELERATION (g)
0
5
10
15
20
25
30
35
TIME (sec)
SPECTRAL
ACCELERATION (g)
1
0.75
0.5
0.25
0
FRAME TOP NE CORNER
EW DIRECTION
NS DIRECTION
0.1
1
10
20
FREQUENCY (Hz)
BASE SHEAR/WEIGHT
0.3
0.2
0.1
-0.1
-0.2
-0.3
WEIGHT = 47.1 kip
LOAD CELL MEASUREMENTS
-3
-2
-1
0
1
2
3
TOTAL DISPLACEMENT (in)

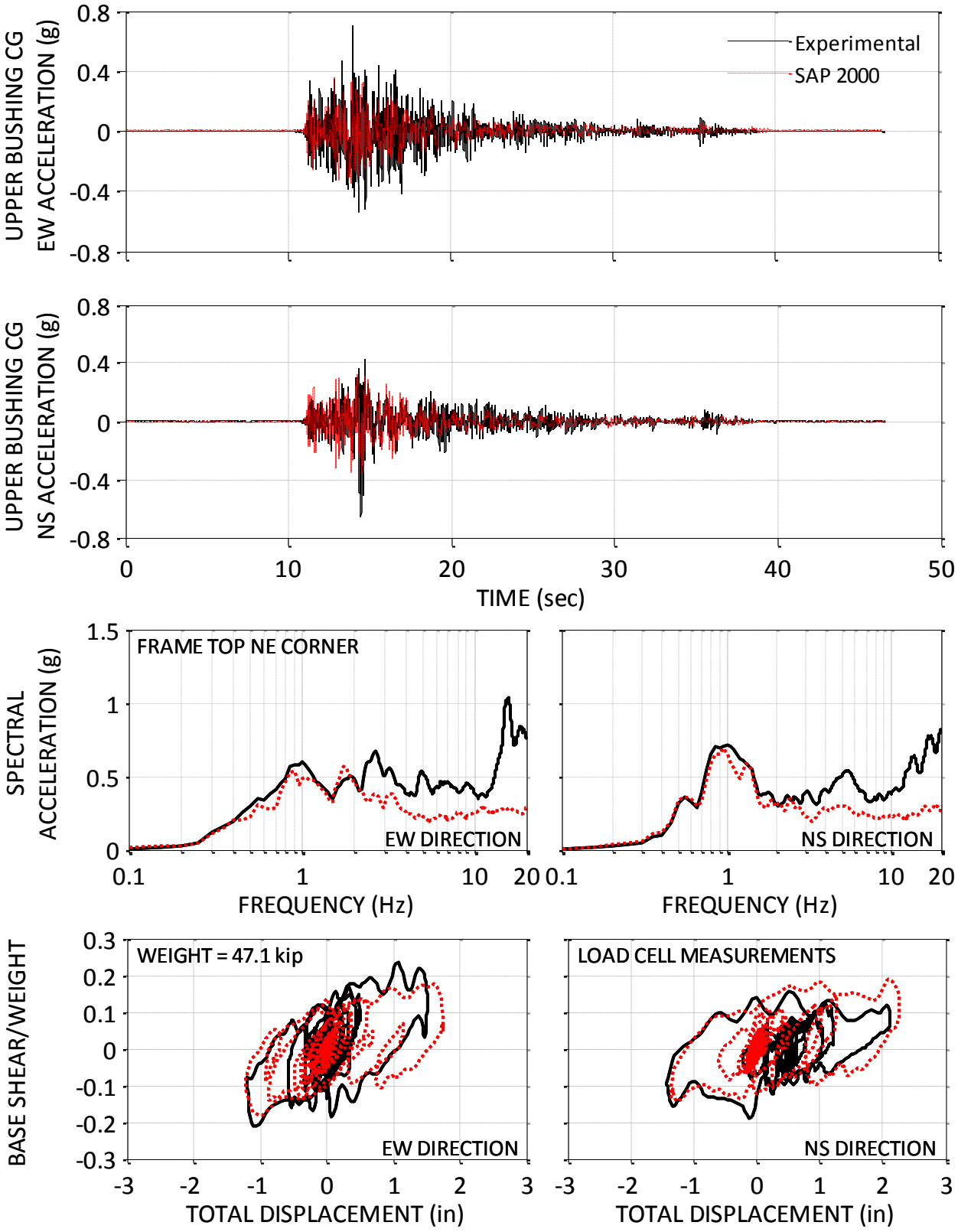
TRIPLE FP SYSTEM (Friction-Bolted Configuration)
TAKARAZUKA 97% TRI-AXIAL (FN in EW direction)
LENGTH SCALE=3 SYMMETRIC BUSHING CONFIGURATION



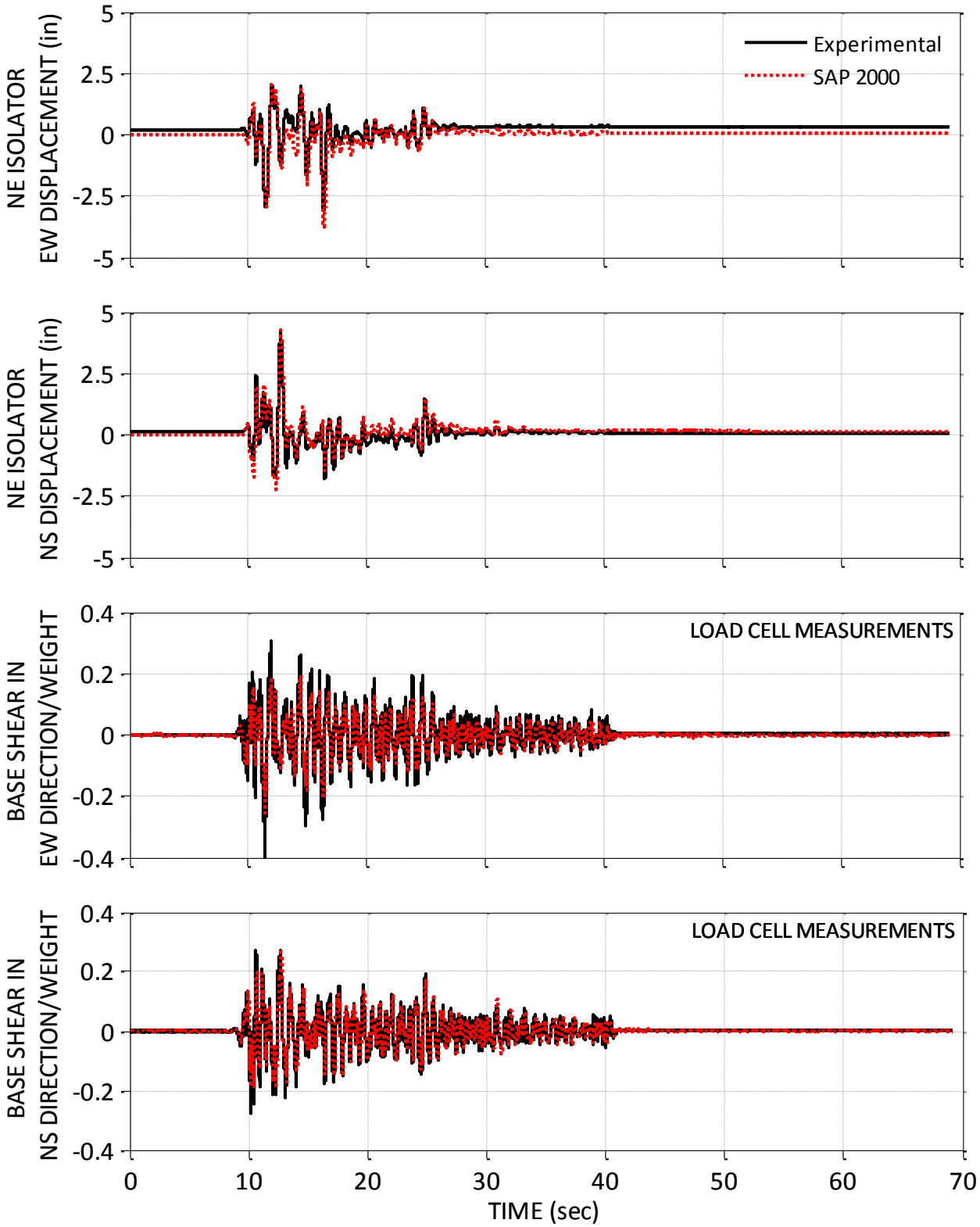

UPPER BUSHING CG
EW ACCELERATION (g)
0.75
0.5
0.25
0
-0.25
-0.5
-0.75
Experimental
SAP 2000
UPPER BUSHING CG
NS ACCELERATION (g)
0
5
10
15
20
25
30
35
TIME (sec)
SPECTRAL
ACCELERATION (g)
1
FRAME TOP NE CORNER
EW DIRECTION
NS DIRECTION
0.1
1
10
20
FREQUENCY (Hz)
BASE SHEAR/WEIGHT
0.2
0.1
-0.1
-0.2
WEIGHT = 47.1 kip
LOAD CELL MEASUREMENTS
-3
-2
-1
2
3
TOTAL DISPLACEMENT (in)

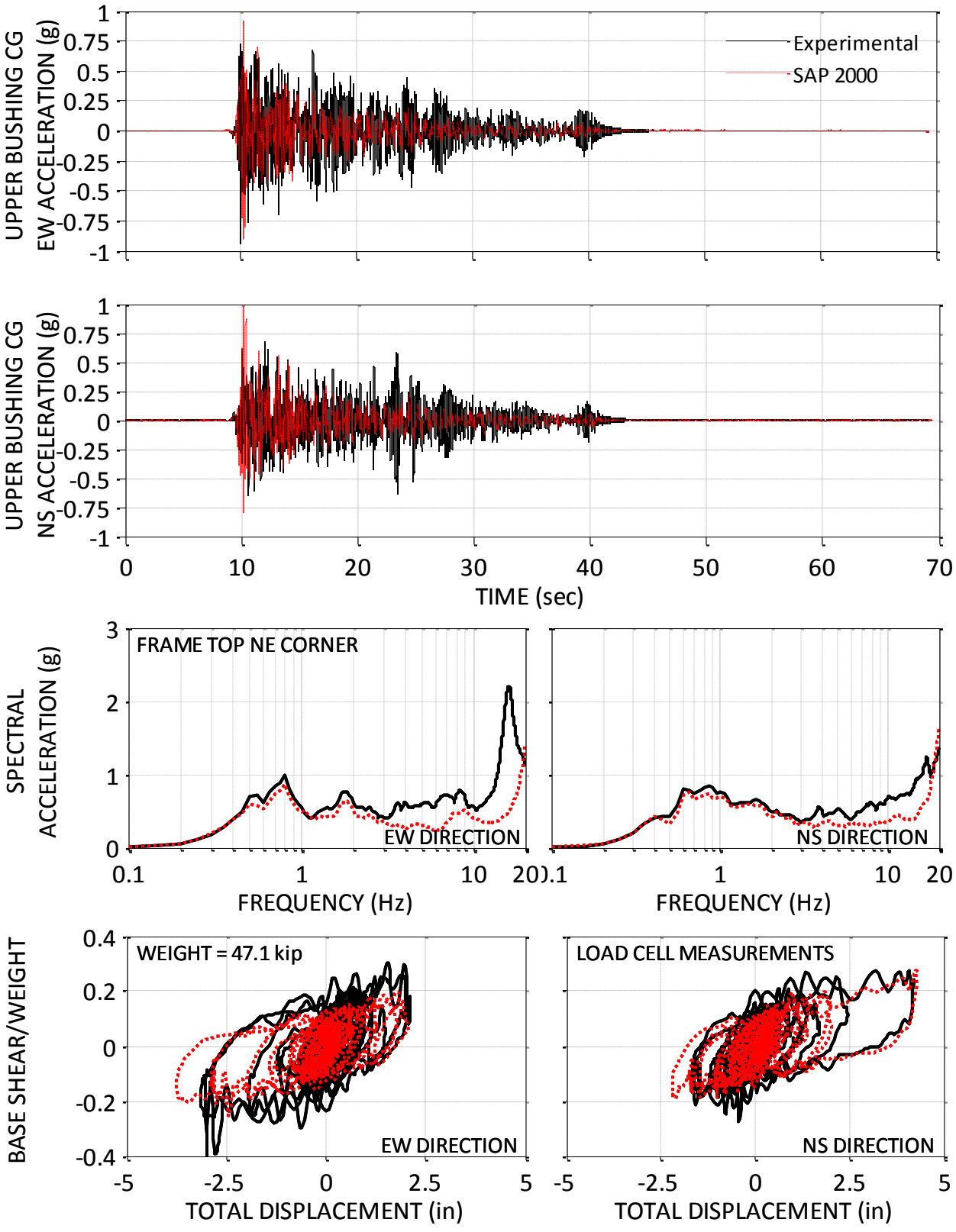
TRIPLE FP SYSTEM (Friction-Bolted Configuration)
BOLU 104% TRI-AXIAL (FN in EW direction)
LENGTH SCALE=3 SYMMETRIC BUSHING CONFIGURATION



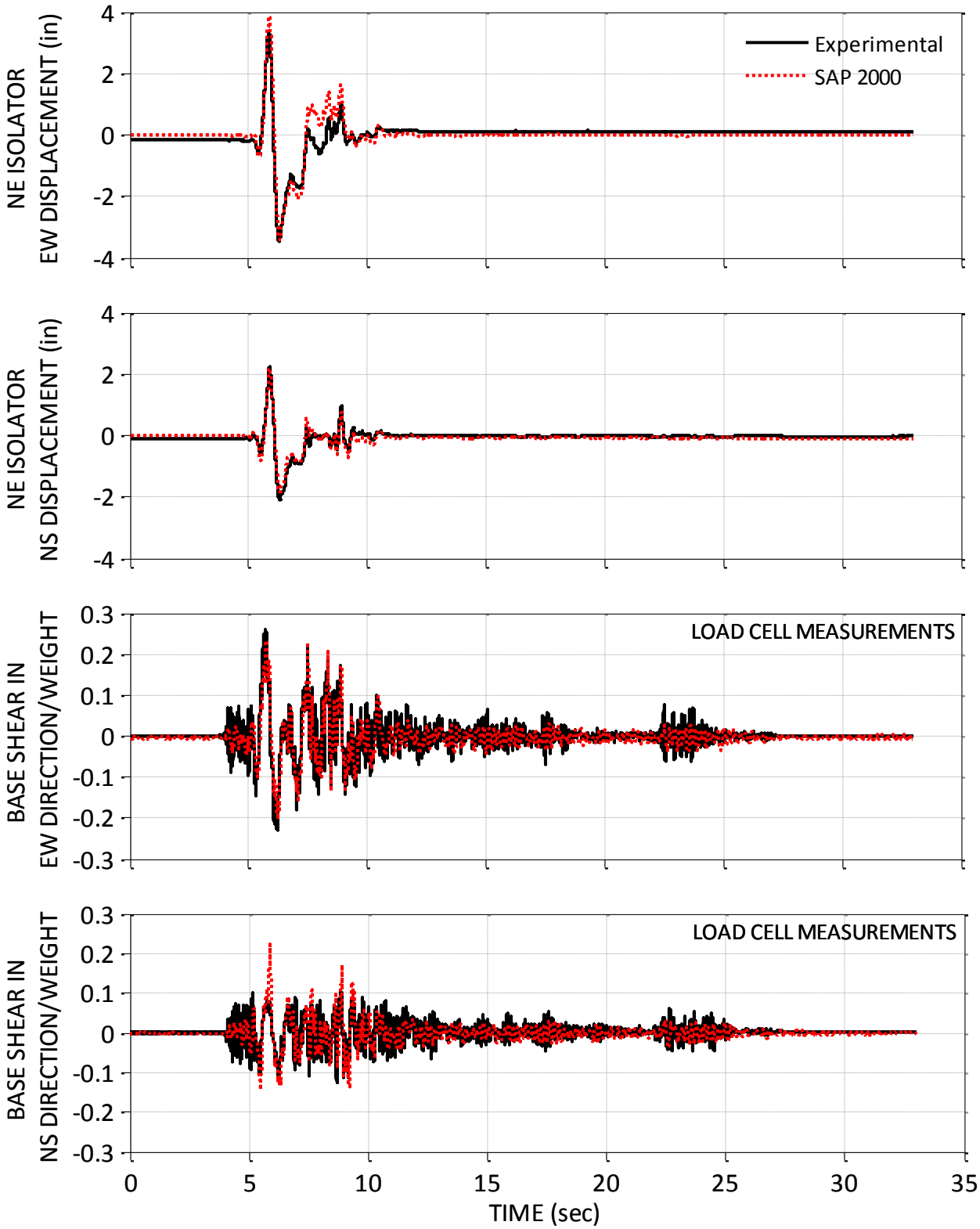

UPPER BUSHING CG
EW ACCELERATION (g)
0.8
0.4
0
-0.4
-0.8
Experimental
SAP 2000
UPPER BUSHING CG
NS ACCELERATION (g)
0.8
0.4
0
-0.4
-0.8
0
10
20
30
40
50
TIME (sec)
SPECTRAL
ACCELERATION (g)
1.5
1
0.5
0
FRAME TOP NE CORNER
EW DIRECTION
NS DIRECTION
0.1
1
10
20
FREQUENCY (Hz)
BASE SHEAR/WEIGHT
0.3
0.2
0.1
0
-0.1
-0.2
-0.3
WEIGHT = 47.1 kip
LOAD CELL MEASUREMENTS
EW DIRECTION
NS DIRECTION
-3
-2
-1
0
1
2
3
TOTAL DISPLACEMENT (in)

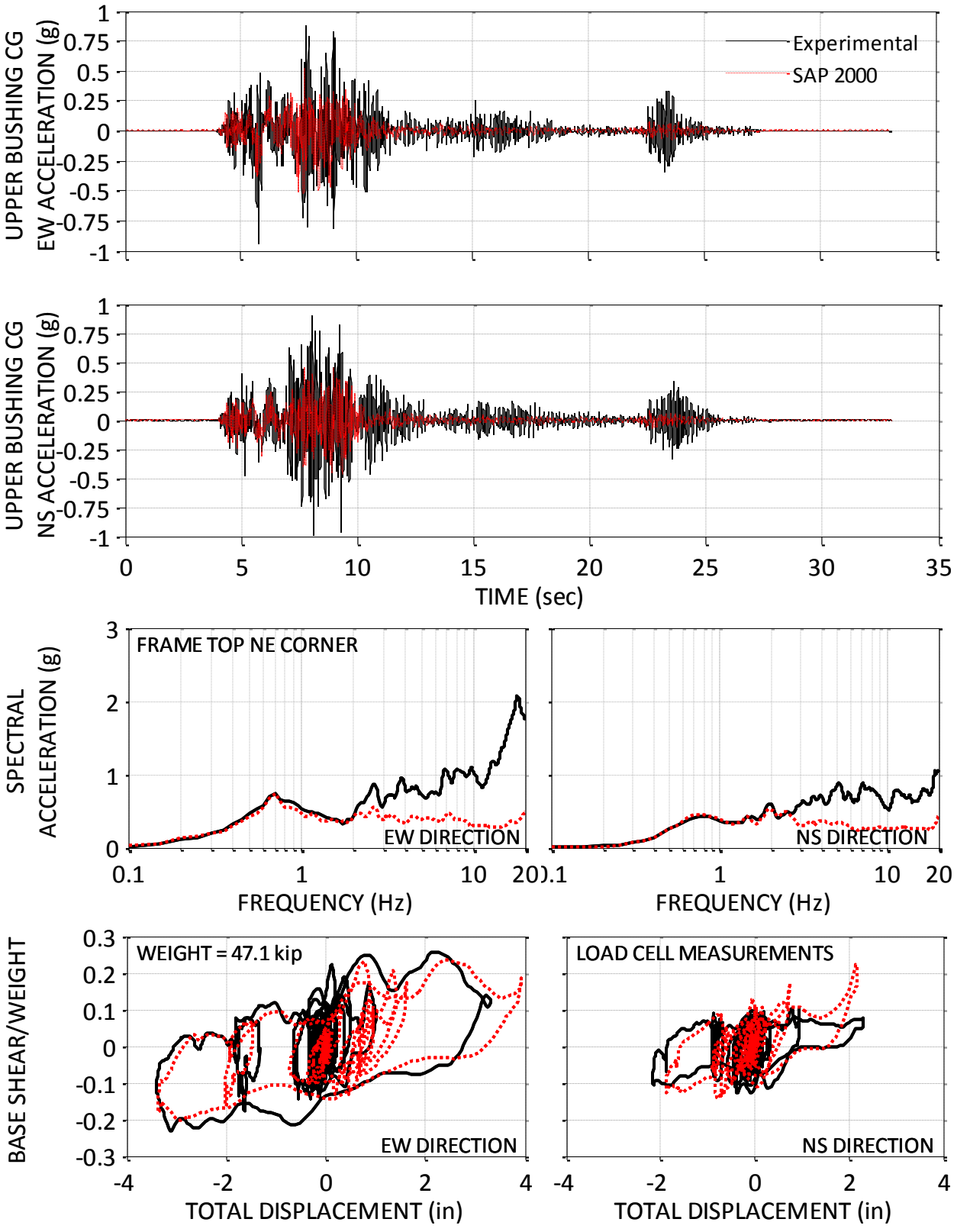
TRIPLE FP SYSTEM (Friction-Bolted Configuration)
EL CENTRO 300% TRI-AXIAL (FN in EW direction)
LENGTH SCALE=3 SYMMETRIC BUSHING CONFIGURATION



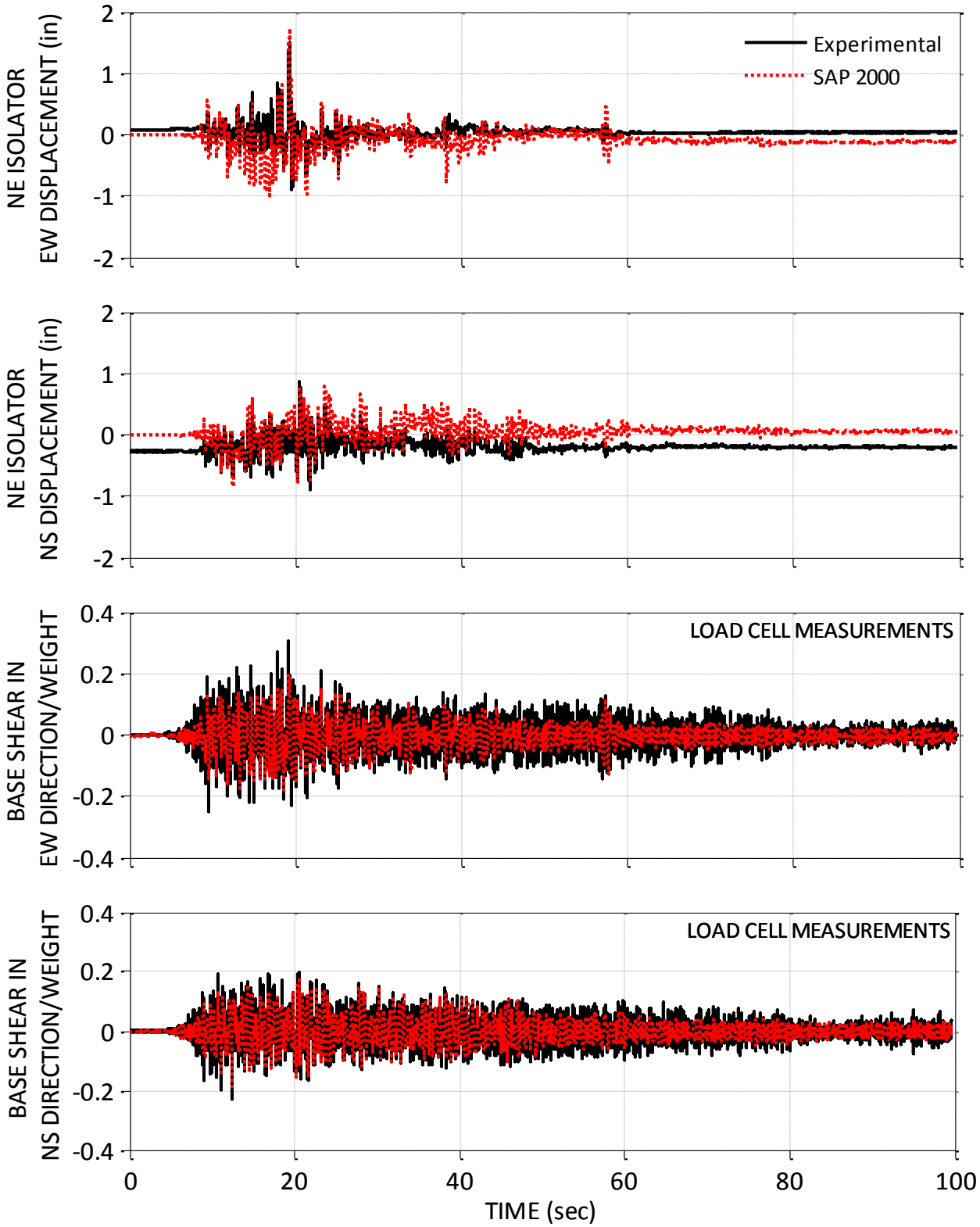

UPPER BUSHING CG
EW ACCELERATION (g)
Experimental
SAP 2000
UPPER BUSHING CG
NS ACCELERATION (g)
TIME (sec)
SPECTRAL
ACCELERATION (g)
FRAME TOP NE CORNER
EW DIRECTION
NS DIRECTION
FREQUENCY (Hz)
FREQUENCY (Hz)
BASE SHEAR/WEIGHT
WEIGHT = 47.1 kip
LOAD CELL MEASUREMENTS
EW DIRECTION
NS DIRECTION
TOTAL DISPLACEMENT (in)
TOTAL DISPLACEMENT (in)

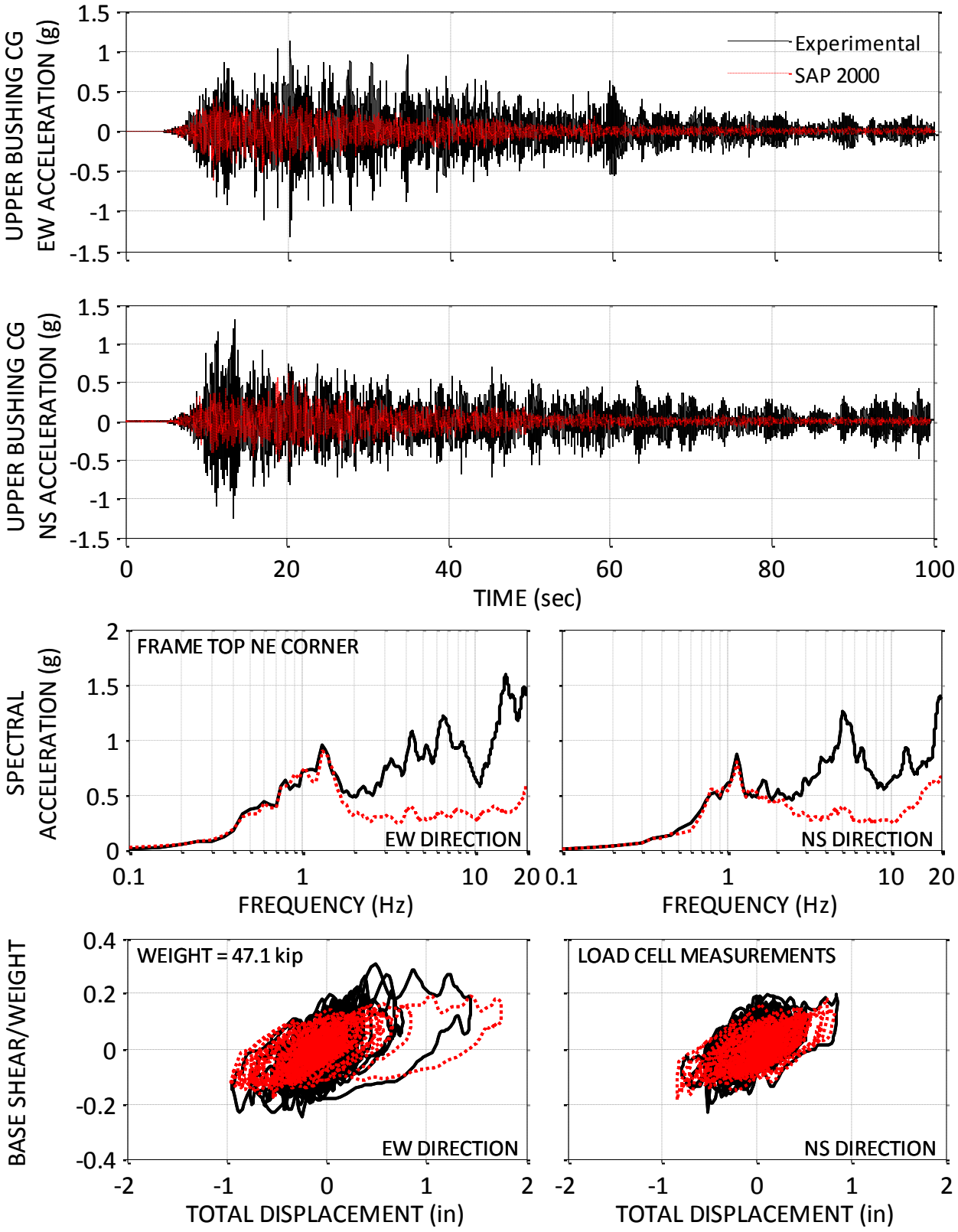
TRIPLE FP SYSTEM (Friction-Bolted Configuration)
PACOIMA DAM 100% TRI-AXIAL (FN in EW direction)
LENGTH SCALE=3 SYMMETRIC BUSHING CONFIGURATION



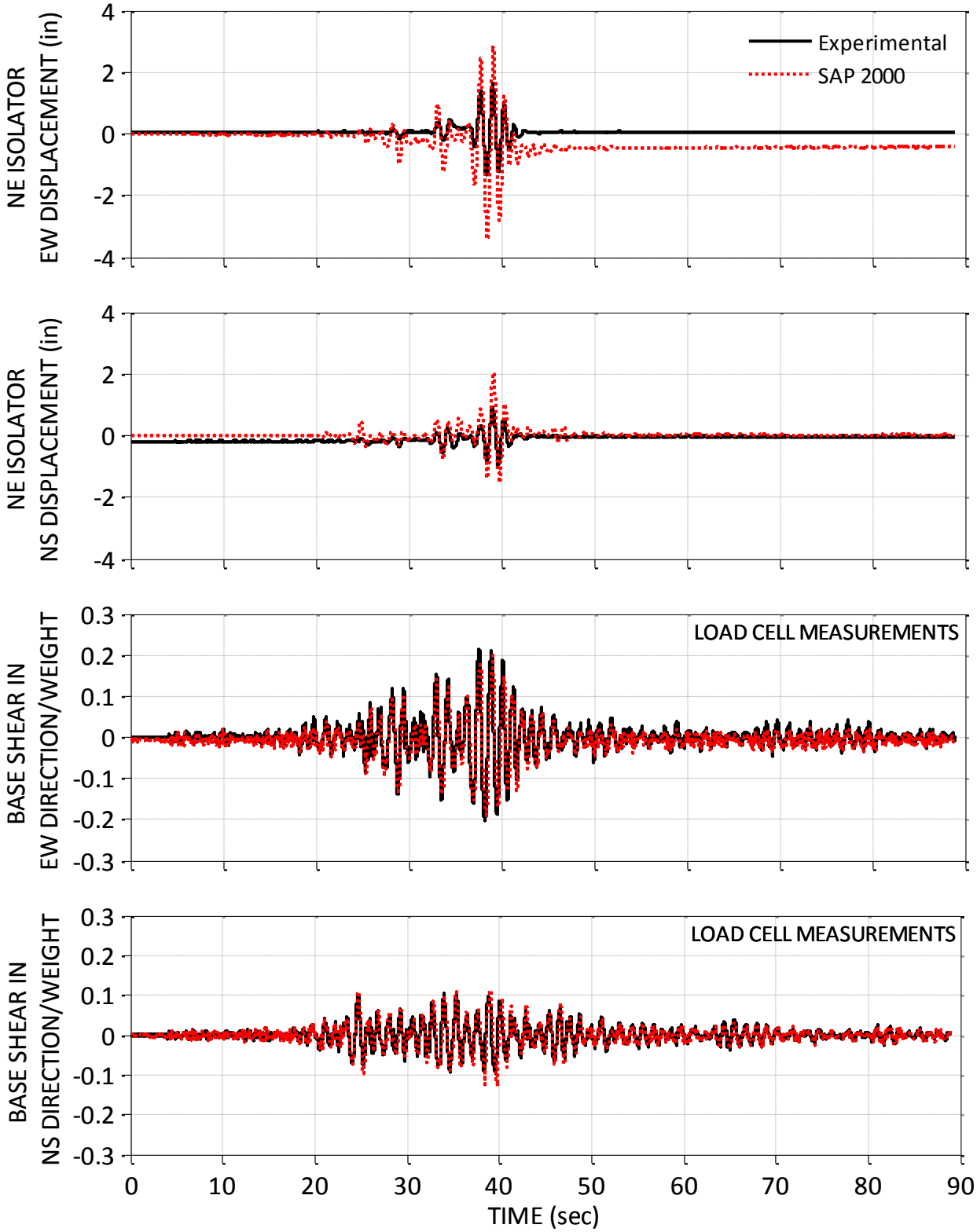

UPPER BUSHING CG
EW ACCELERATION (g)
Experimental
SAP 2000
UPPER BUSHING CG
NS ACCELERATION (g)
TIME (sec)
SPECTRAL
ACCELERATION (g)
FRAME TOP NE CORNER
EW DIRECTION
NS DIRECTION
FREQUENCY (Hz)
FREQUENCY (Hz)
BASE SHEAR/WEIGHT
WEIGHT = 47.1 kip
LOAD CELL MEASUREMENTS
EW DIRECTION
NS DIRECTION
TOTAL DISPLACEMENT (in)
TOTAL DISPLACEMENT (in)

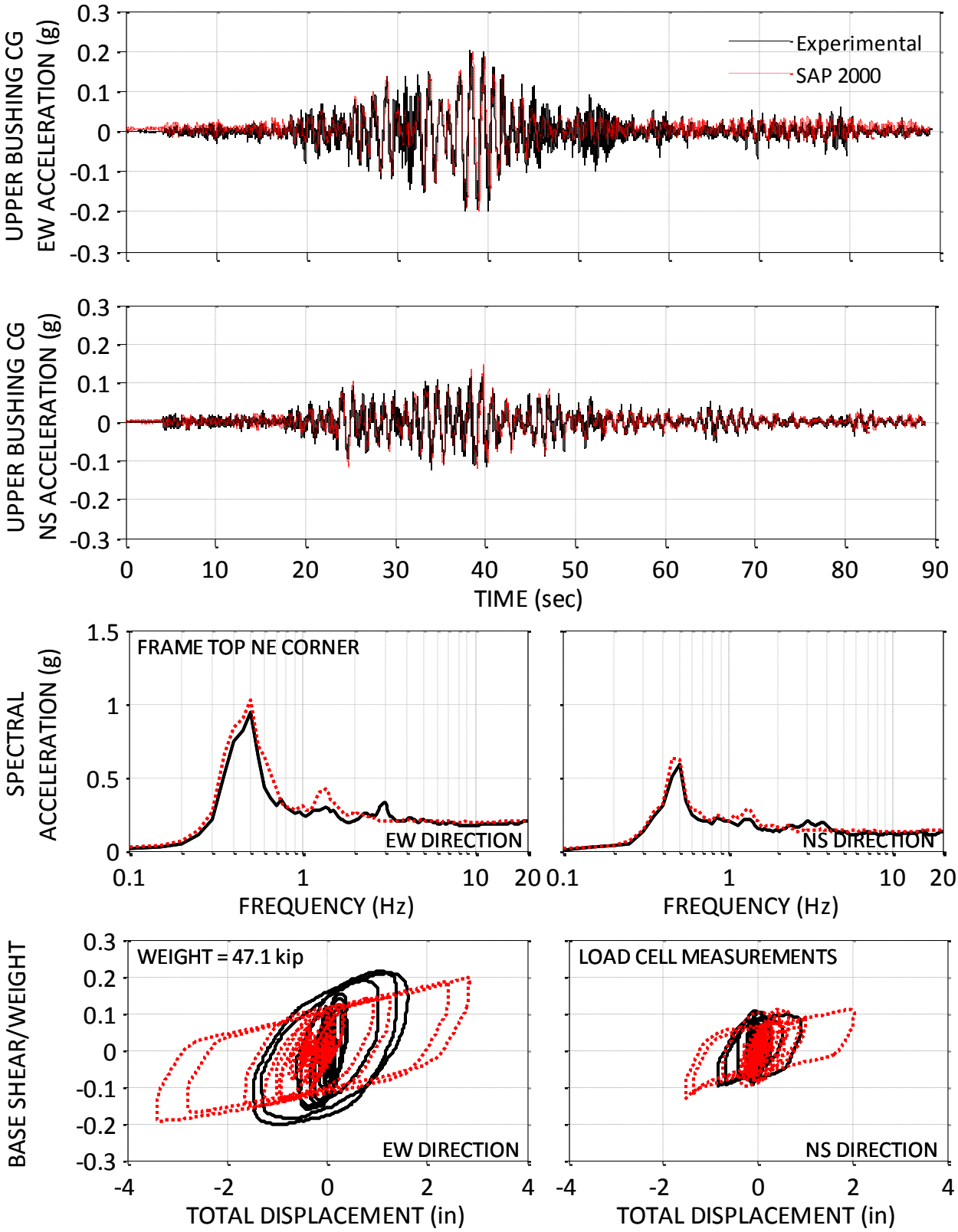
TRIPLE FP SYSTEM (Friction-Bolted Configuration)
CHILE 100% TRI-AXIAL (FN in EW direction)
LENGTH SCALE=3 SYMMETRIC BUSHING CONFIGURATION



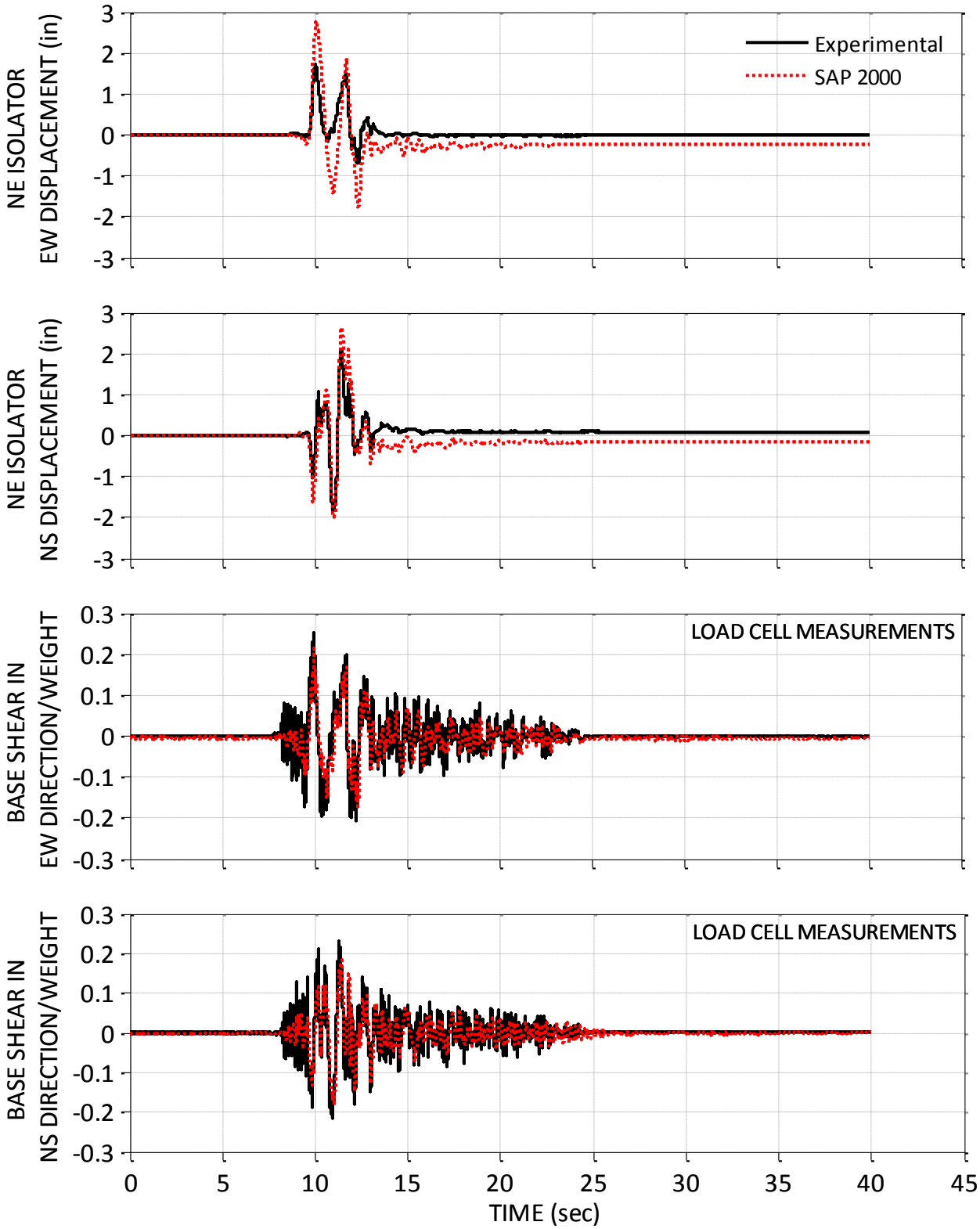

UPPER BUSHING CG
EW ACCELERATION (g)
Experimental
SAP 2000
UPPER BUSHING CG
NS ACCELERATION (g)
TIME (sec)
SPECTRAL
ACCELERATION (g)
FRAME TOP NE CORNER
EW DIRECTION
NS DIRECTION
FREQUENCY (Hz)
BASE SHEAR/WEIGHT
WEIGHT = 47.1 kip
LOAD CELL MEASUREMENTS
TOTAL DISPLACEMENT (in)

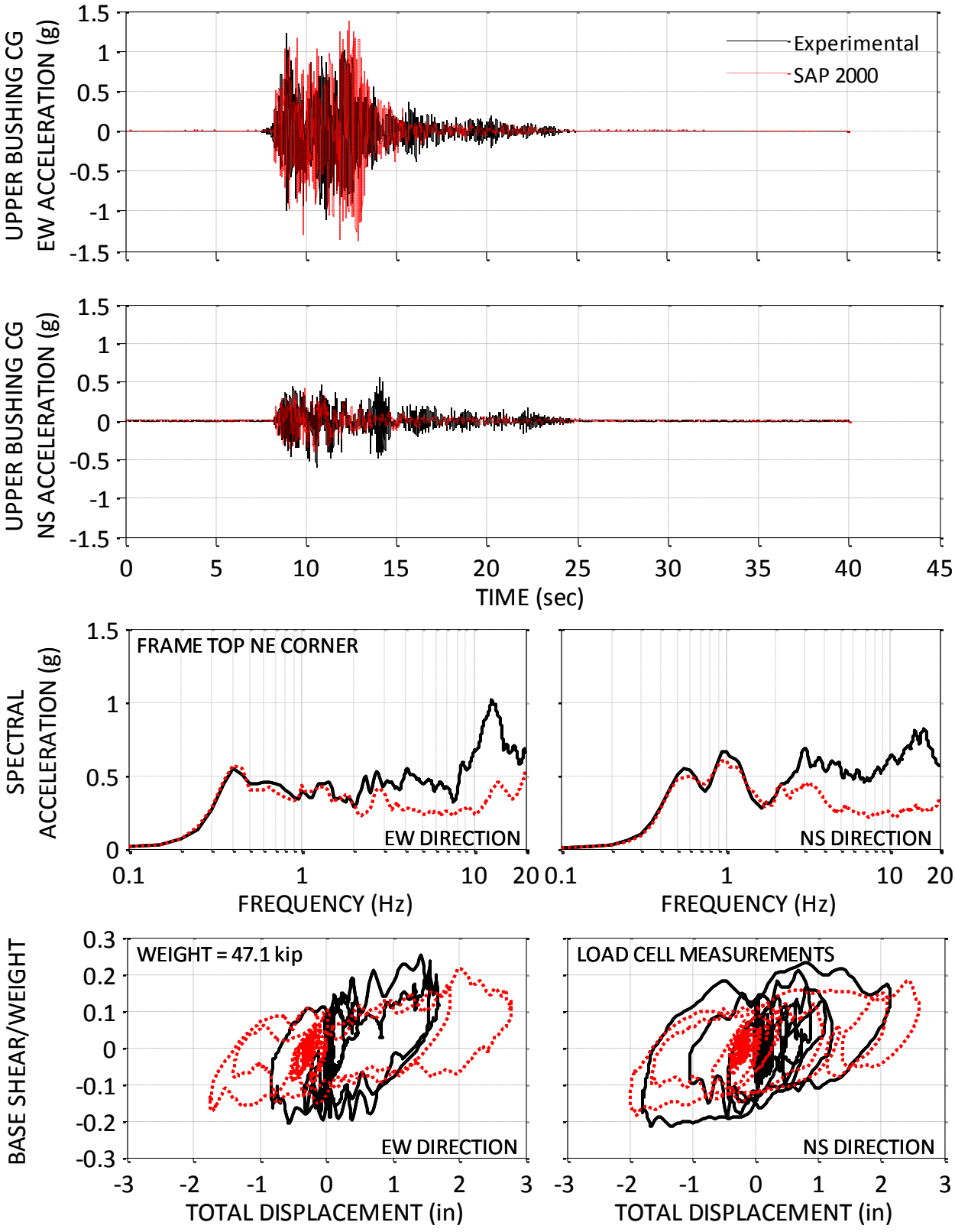
TRIPLE FP SYSTEM (Friction-Bolted Configuration)
MEXICO CITY 100% TRI-AXIAL (FN in EW direction)
LENGTH SCALE=3 SYMMETRIC BUSHING CONFIGURATION



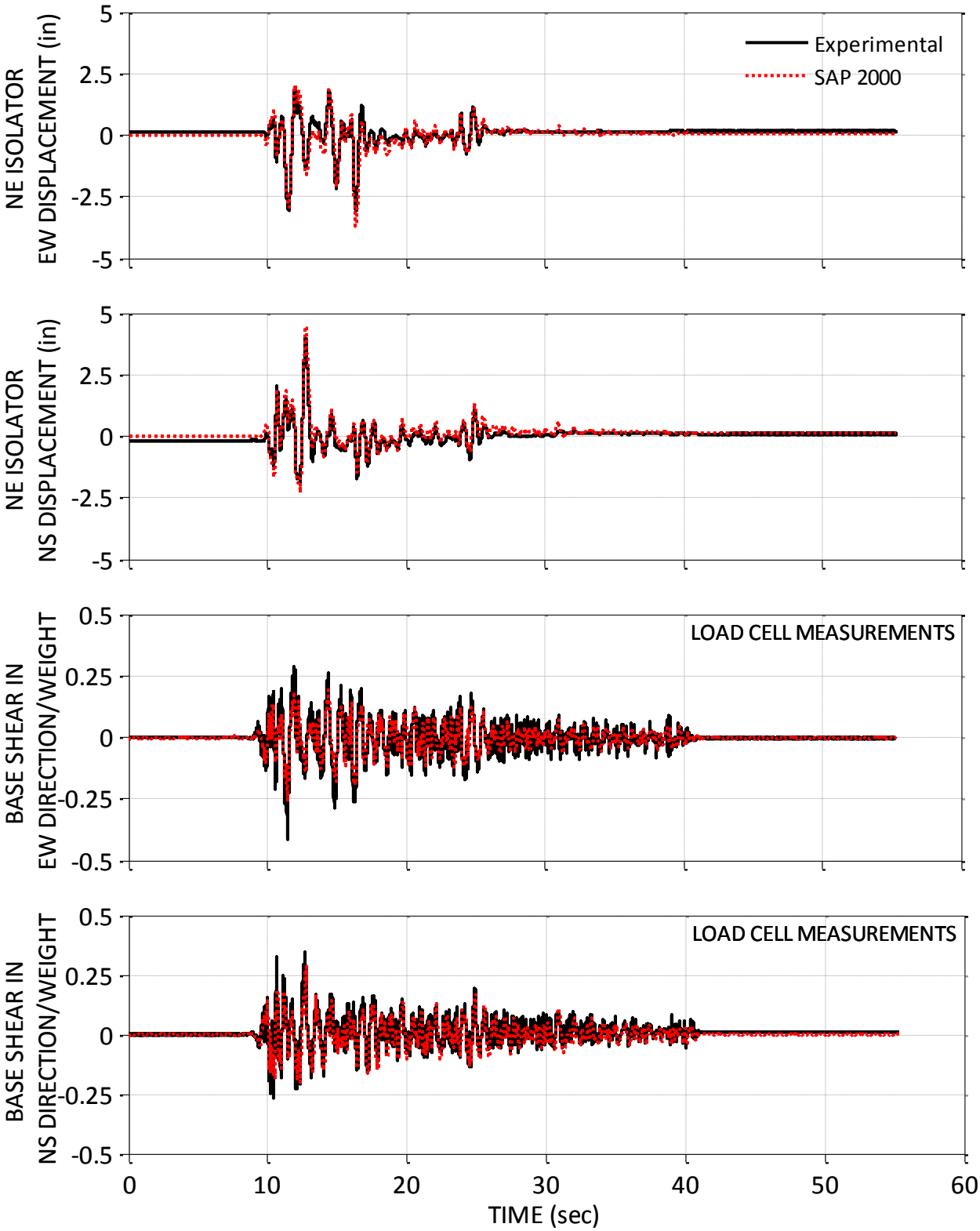

UPPER BUSHING CG
EW ACCELERATION (g)
Experimental
SAP 2000
UPPER BUSHING CG
NS ACCELERATION (g)
TIME (sec)
SPECTRAL
ACCELERATION (g)
FRAME TOP NE CORNER
EW DIRECTION
NS DIRECTION
FREQUENCY (Hz)
BASE SHEAR/WEIGHT
WEIGHT = 47.1 kip
LOAD CELL MEASUREMENTS
TOTAL DISPLACEMENT (in)

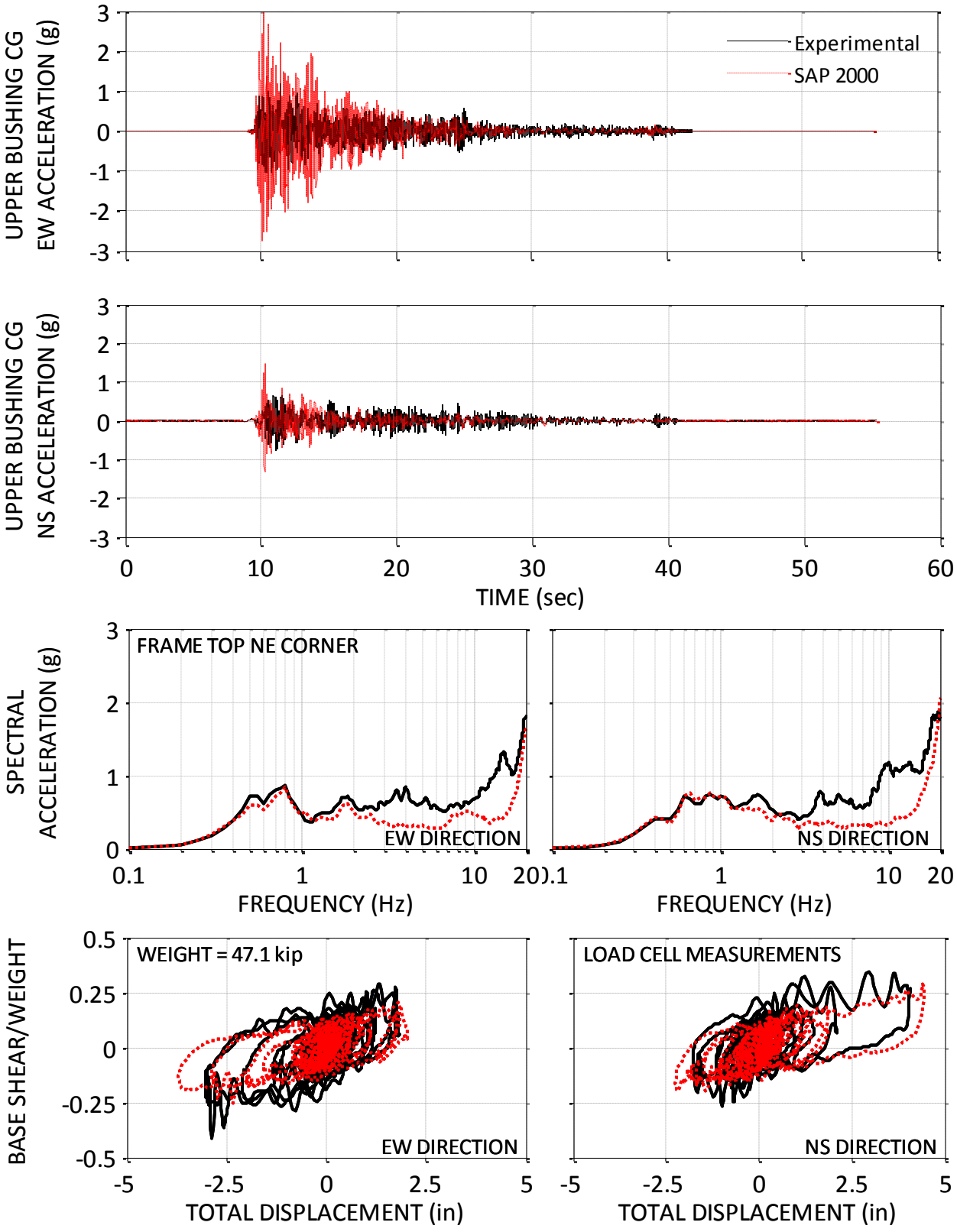
TRIPLE FP SYSTEM (Friction-Bolted Configuration)
JENSEN FILTER 97% TRI-AXIAL (FN in EW direction)
LENGTH SCALE=3 NON-SYMMETRIC BUSHING CONFIGURATION



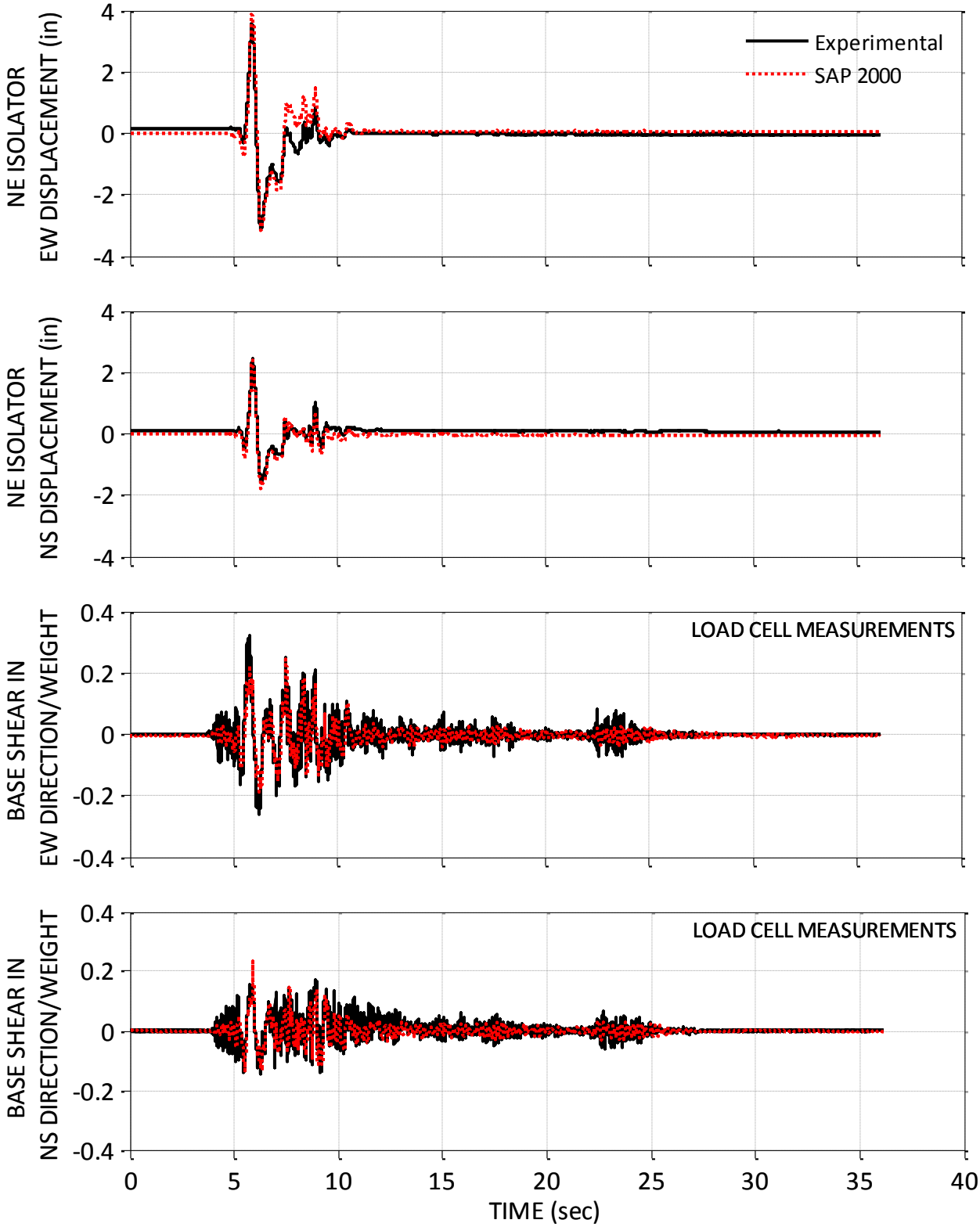

UPPER BUSHING CG
EW ACCELERATION (g)
Experimental
SAP 2000
UPPER BUSHING CG
NS ACCELERATION (g)
TIME (sec)
SPECTRAL
ACCELERATION (g)
FRAME TOP NE CORNER
EW DIRECTION
NS DIRECTION
FREQUENCY (Hz)
BASE SHEAR/WEIGHT
WEIGHT = 47.1 kip
LOAD CELL MEASUREMENTS
TOTAL DISPLACEMENT (in)

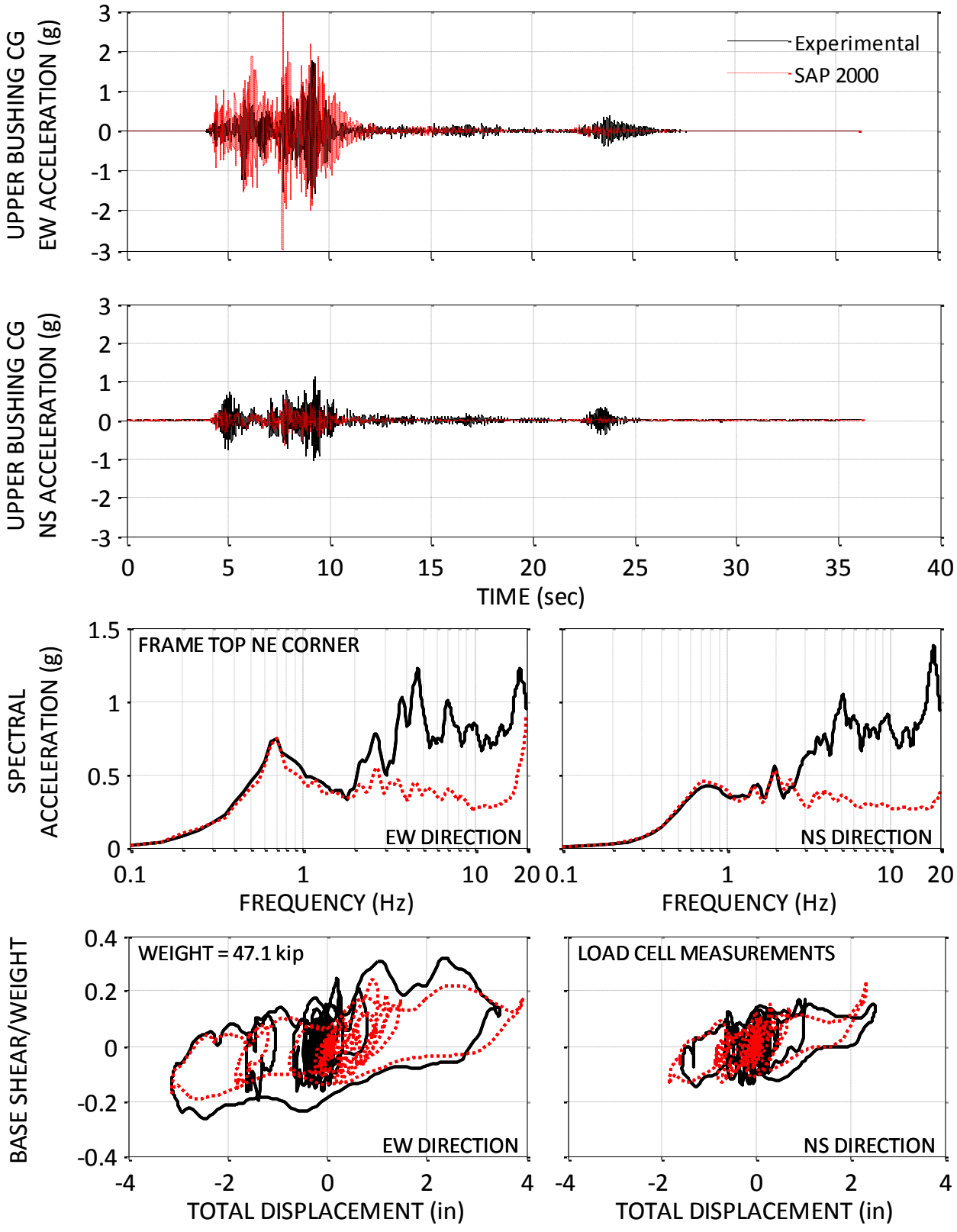
TRIPLE FP SYSTEM (Friction-Bolted Configuration)
EL CENTRO 300% TRI-AXIAL (N90W in EW direction)
LENGTH SCALE=3 NON-SYMMETRIC BUSHING CONFIGURATION



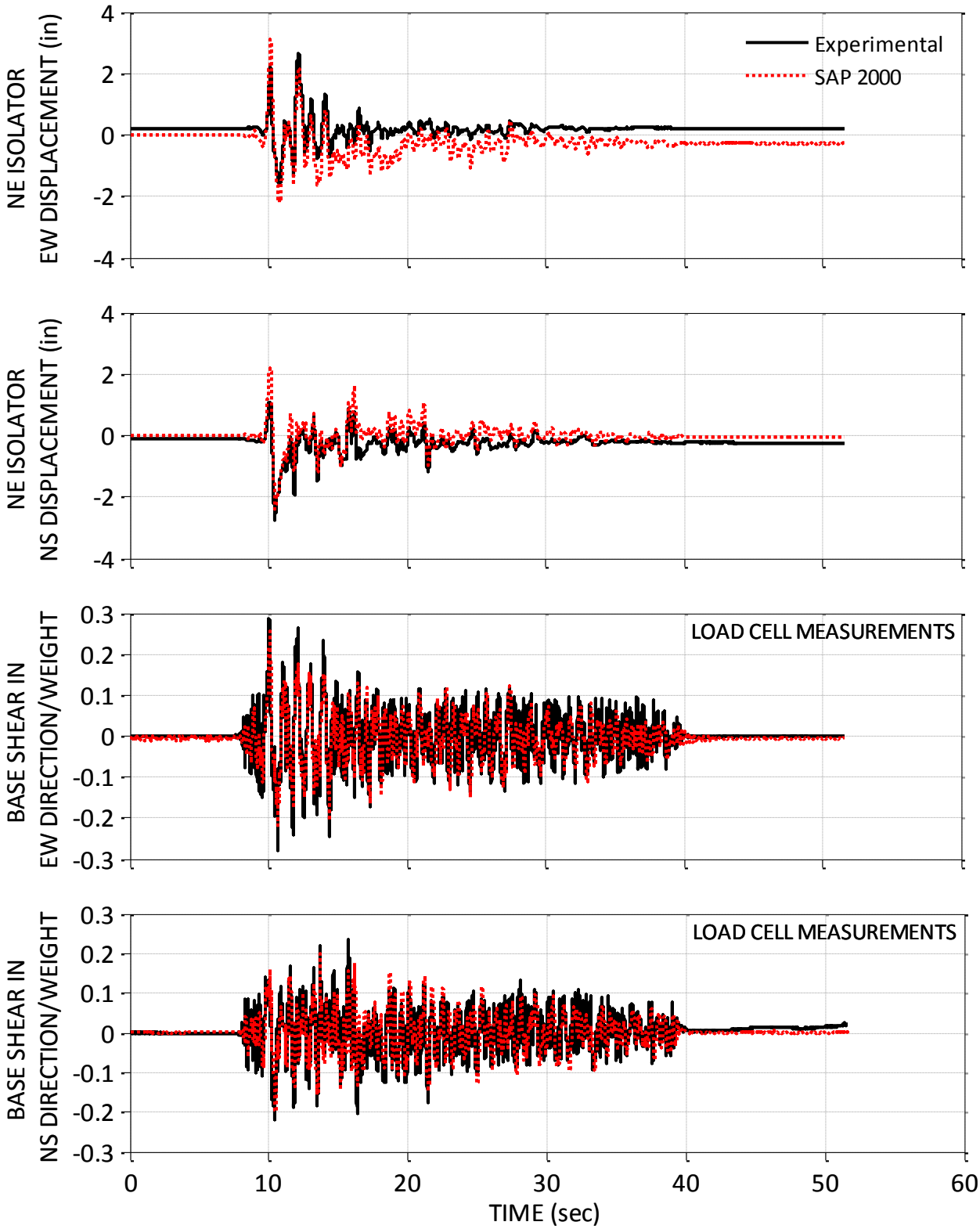

UPPER BUSHING CG
EW ACCELERATION (g)
Experimental
SAP 2000
UPPER BUSHING CG
NS ACCELERATION (g)
TIME (sec)
SPECTRAL
ACCELERATION (g)
FRAME TOP NE CORNER
EW DIRECTION
NS DIRECTION
FREQUENCY (Hz)
FREQUENCY (Hz)
BASE SHEAR/WEIGHT
WEIGHT = 47.1 kip
LOAD CELL MEASUREMENTS
EW DIRECTION
NS DIRECTION
TOTAL DISPLACEMENT (in)
TOTAL DISPLACEMENT (in)

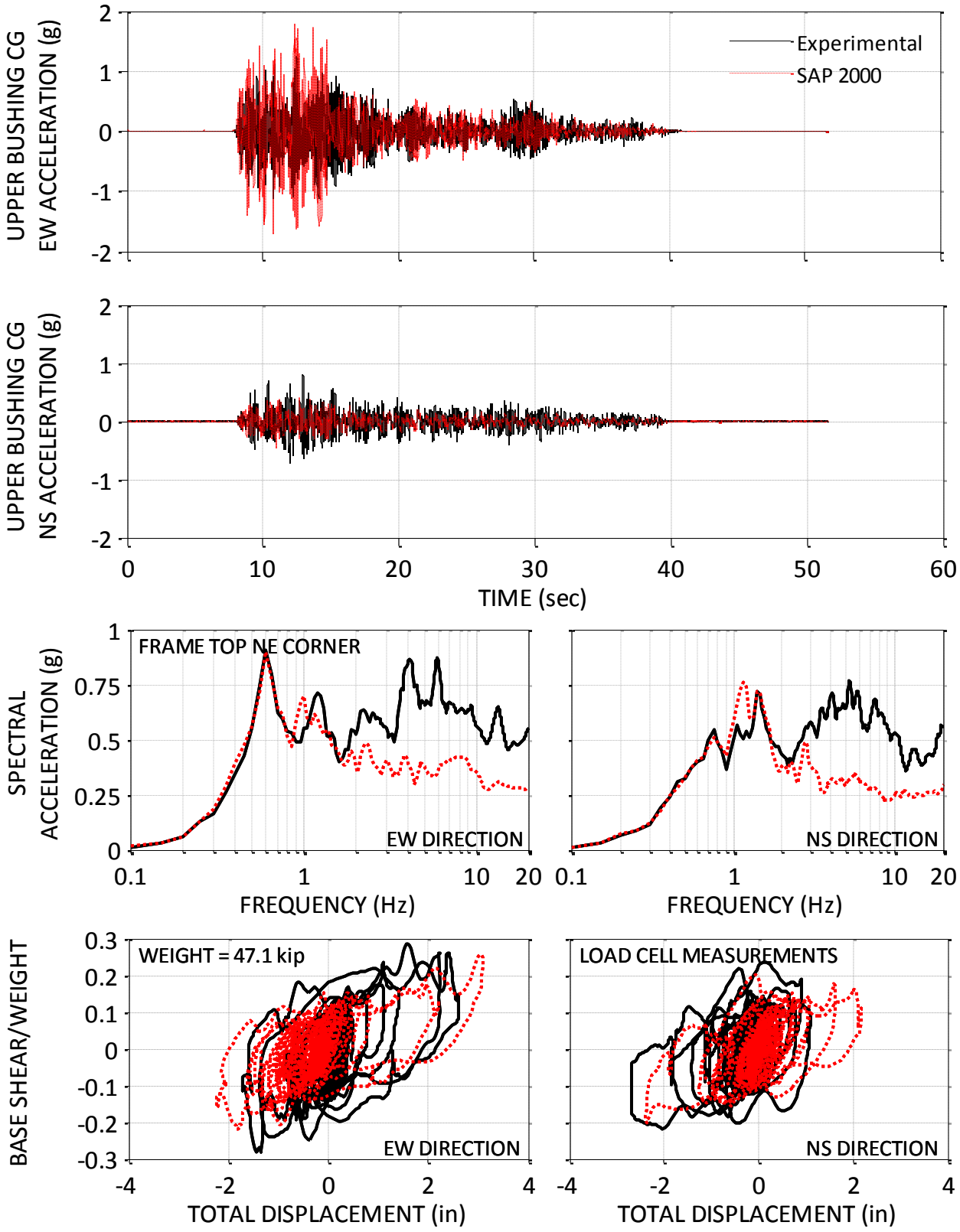
TRIPLE FP SYSTEM (Friction-Bolted Configuration)
PACOIMA DAM 100% TRI-AXIAL (S16E in EW direction)
LENGTH SCALE=3 NON-SYMMETRIC BUSHING CONFIGURATION



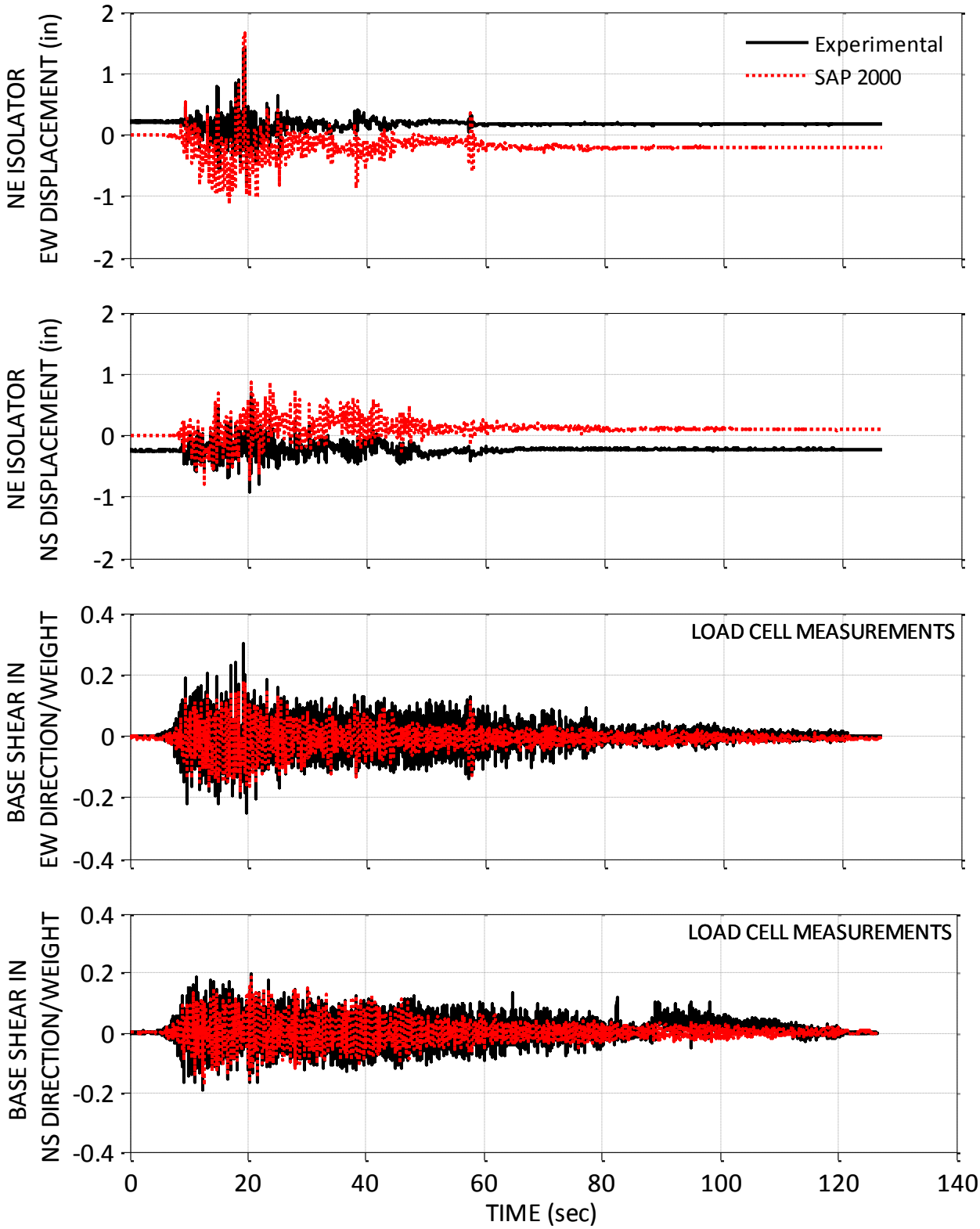

UPPER BUSHING CG
EW ACCELERATION (g)
Experimental
SAP 2000
UPPER BUSHING CG
NS ACCELERATION (g)
TIME (sec)
SPECTRAL
ACCELERATION (g)
FRAME TOP NE CORNER
EW DIRECTION
NS DIRECTION
FREQUENCY (Hz)
BASE SHEAR/WEIGHT
WEIGHT = 47.1 kip
LOAD CELL MEASUREMENTS
TOTAL DISPLACEMENT (in)

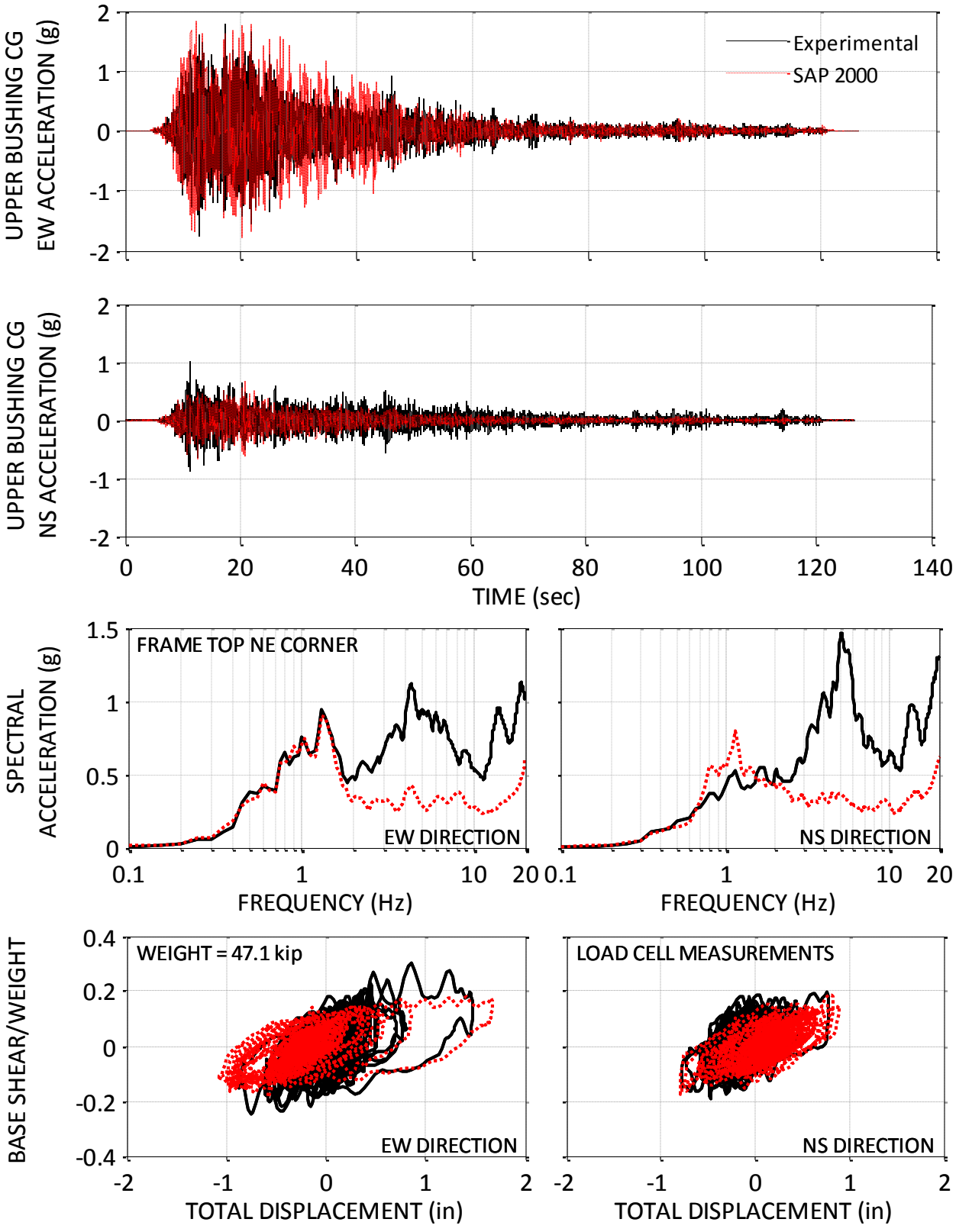
TRIPLE FP SYSTEM (Friction-Bolted Configuration)
TAFT 500% TRI-AXIAL (S69E in EW direction)
LENGTH SCALE=3 NON-SYMMETRIC BUSHING CONFIGURATION



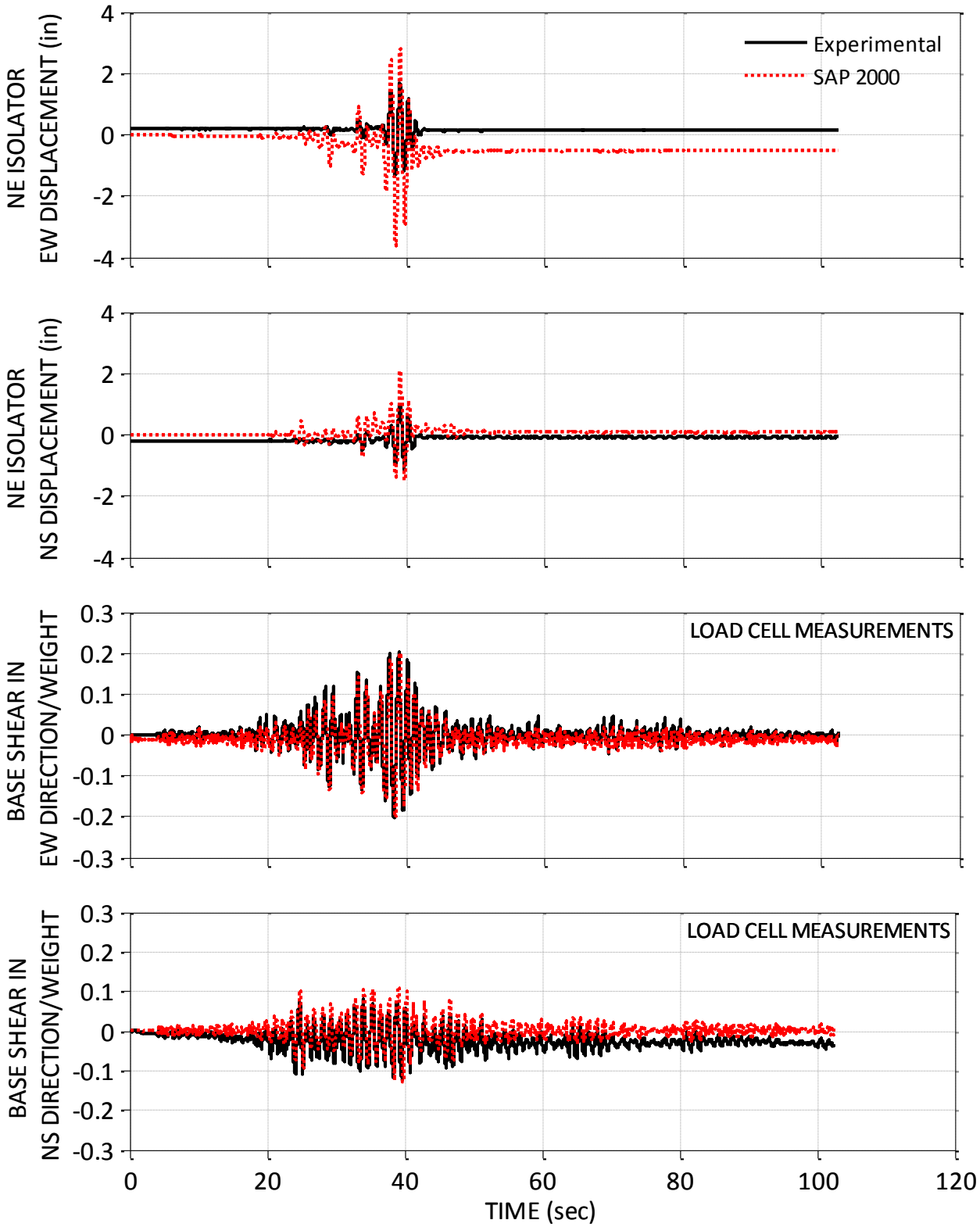

UPPER BUSHING CG
EW ACCELERATION (g)
Experimental
SAP 2000
UPPER BUSHING CG
NS ACCELERATION (g)
TIME (sec)
SPECTRAL
ACCELERATION (g)
FRAME TOP NE CORNER
EW DIRECTION
NS DIRECTION
FREQUENCY (Hz)
BASE SHEAR/WEIGHT
WEIGHT = 47.1 kip
LOAD CELL MEASUREMENTS
TOTAL DISPLACEMENT (in)

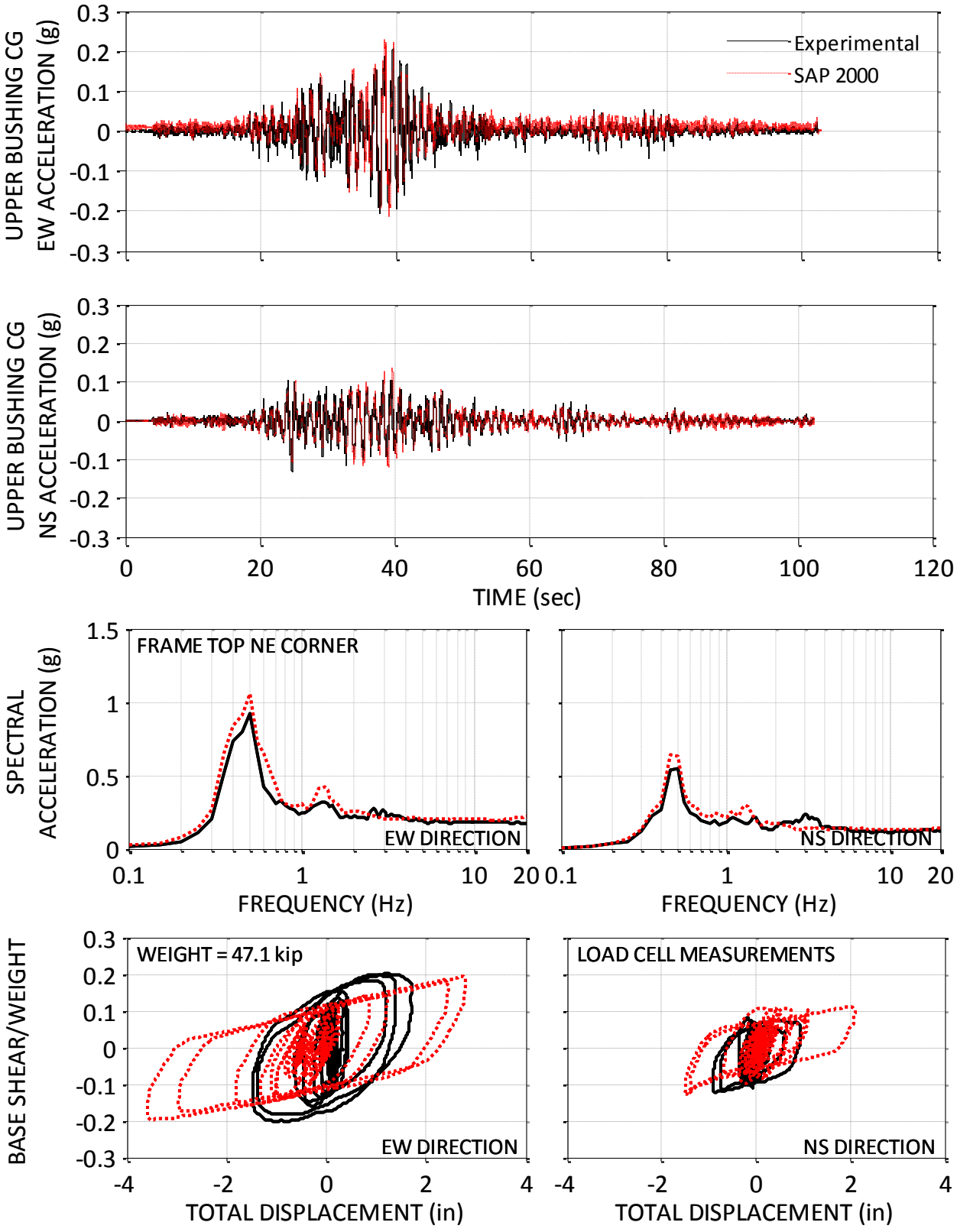
TRIPLE FP SYSTEM (Friction-Bolted Configuration)
CHILE 100% TRI-AXIAL (EW in EW direction)
LENGTH SCALE=3 NON-SYMMETRIC BUSHING CONFIGURATION



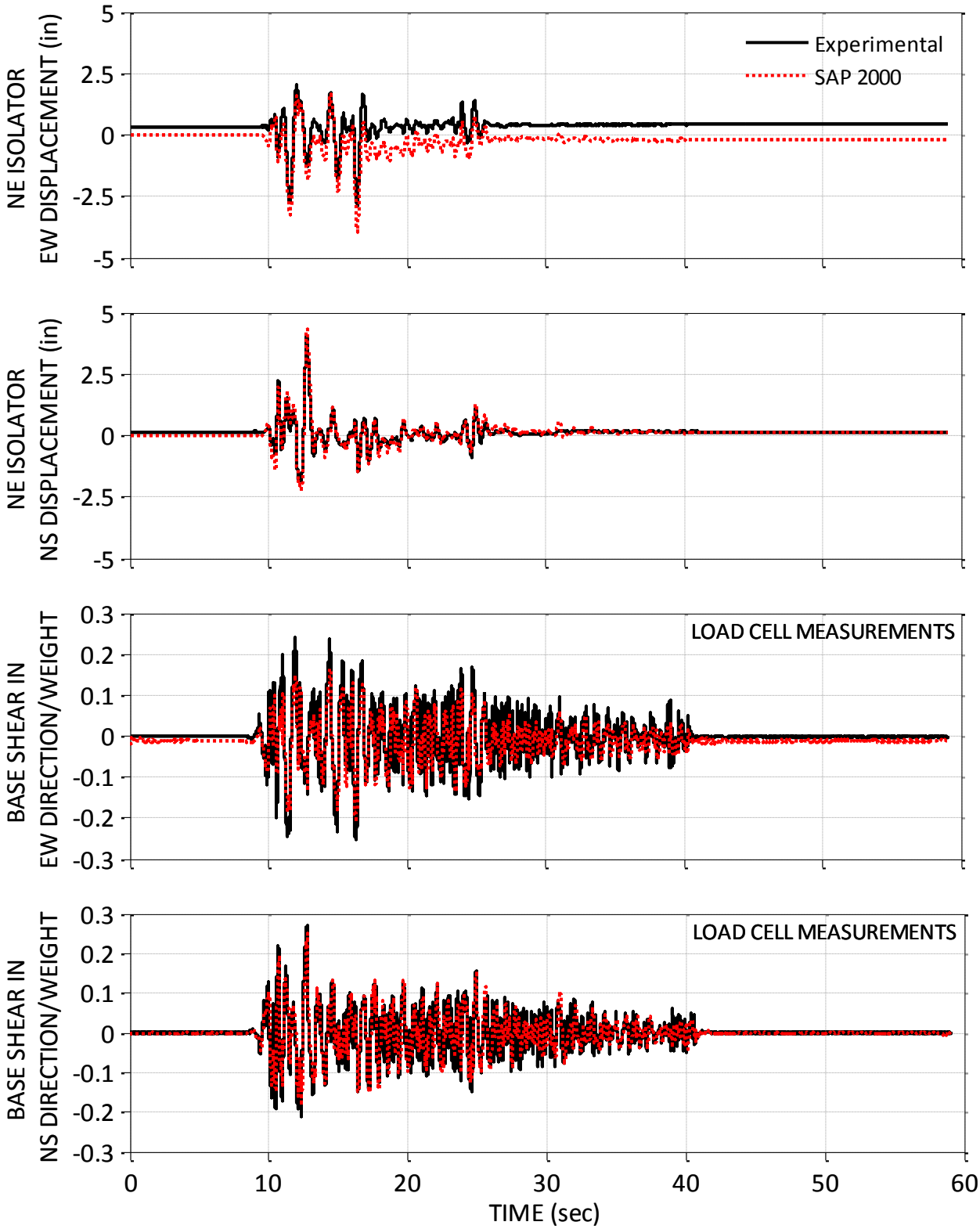

UPPER BUSHING CG
EW ACCELERATION (g)
Experimental
SAP 2000
UPPER BUSHING CG
NS ACCELERATION (g)
TIME (sec)
SPECTRAL
ACCELERATION (g)
FRAME TOP NE CORNER
EW DIRECTION
NS DIRECTION
FREQUENCY (Hz)
BASE SHEAR/WEIGHT
WEIGHT = 47.1 kip
LOAD CELL MEASUREMENTS
TOTAL DISPLACEMENT (in)

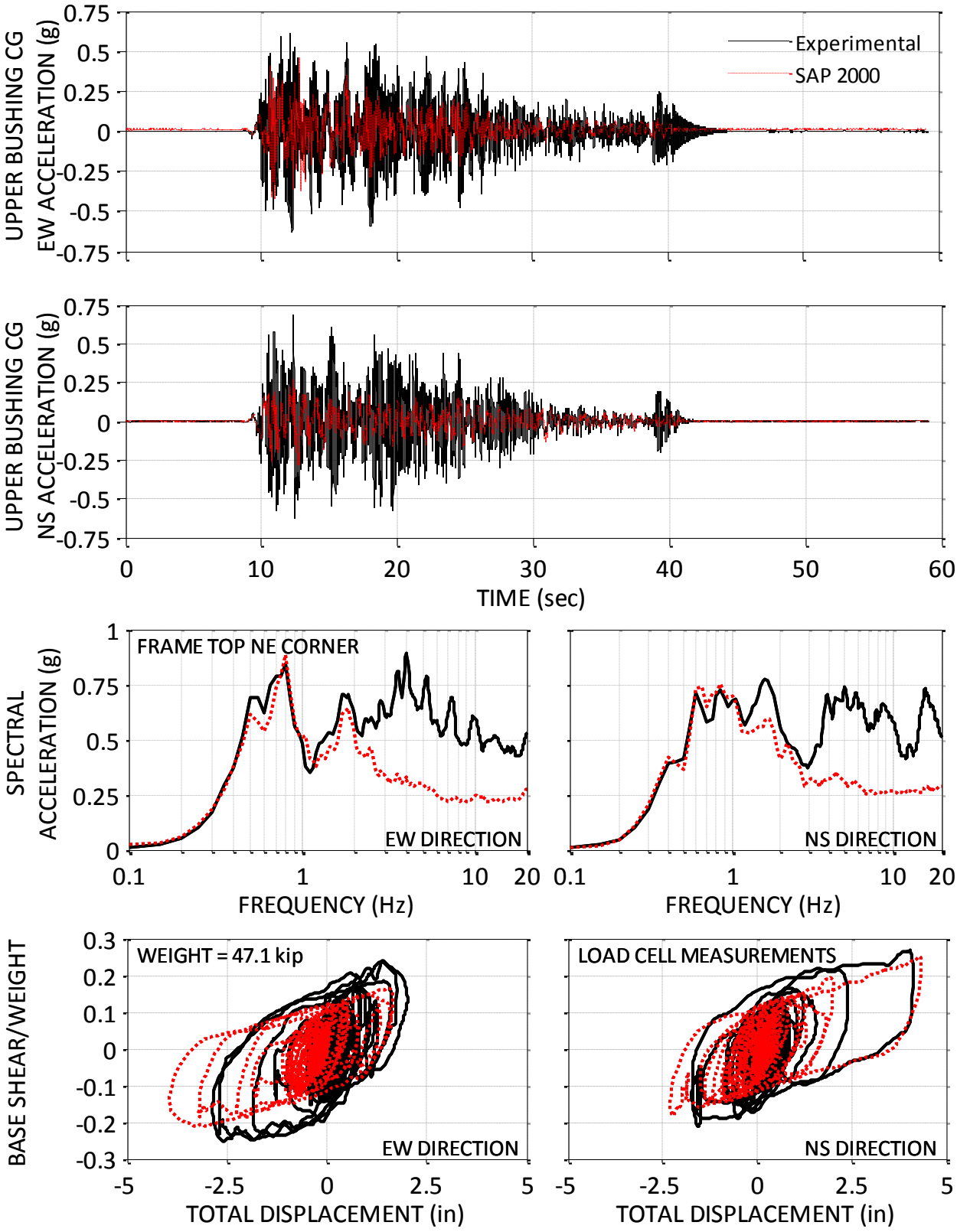
TRIPLE FP SYSTEM (Friction-Bolted Configuration)
MEXICO CITY 100% TRI-AXIAL (N90W in EW direction)
LENGTH SCALE=3 NON-SYMMETRIC BUSHING CONFIGURATION



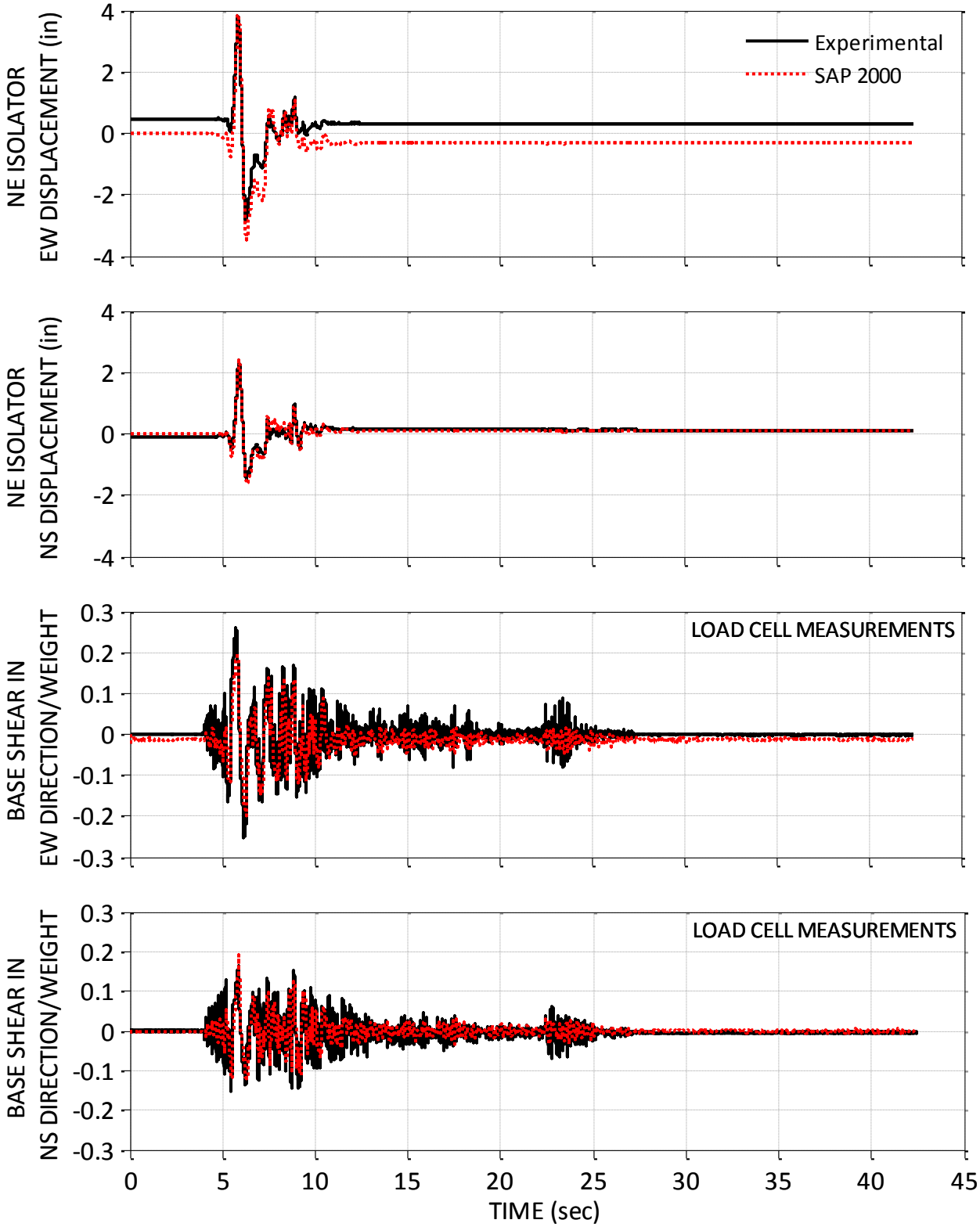

UPPER BUSHING CG
EW ACCELERATION (g)
Experimental
SAP 2000
UPPER BUSHING CG
NS ACCELERATION (g)
TIME (sec)
SPECTRAL
ACCELERATION (g)
FRAME TOP NE CORNER
EW DIRECTION
NS DIRECTION
FREQUENCY (Hz)
BASE SHEAR/WEIGHT
WEIGHT = 47.1 kip
LOAD CELL MEASUREMENTS
TOTAL DISPLACEMENT (in)

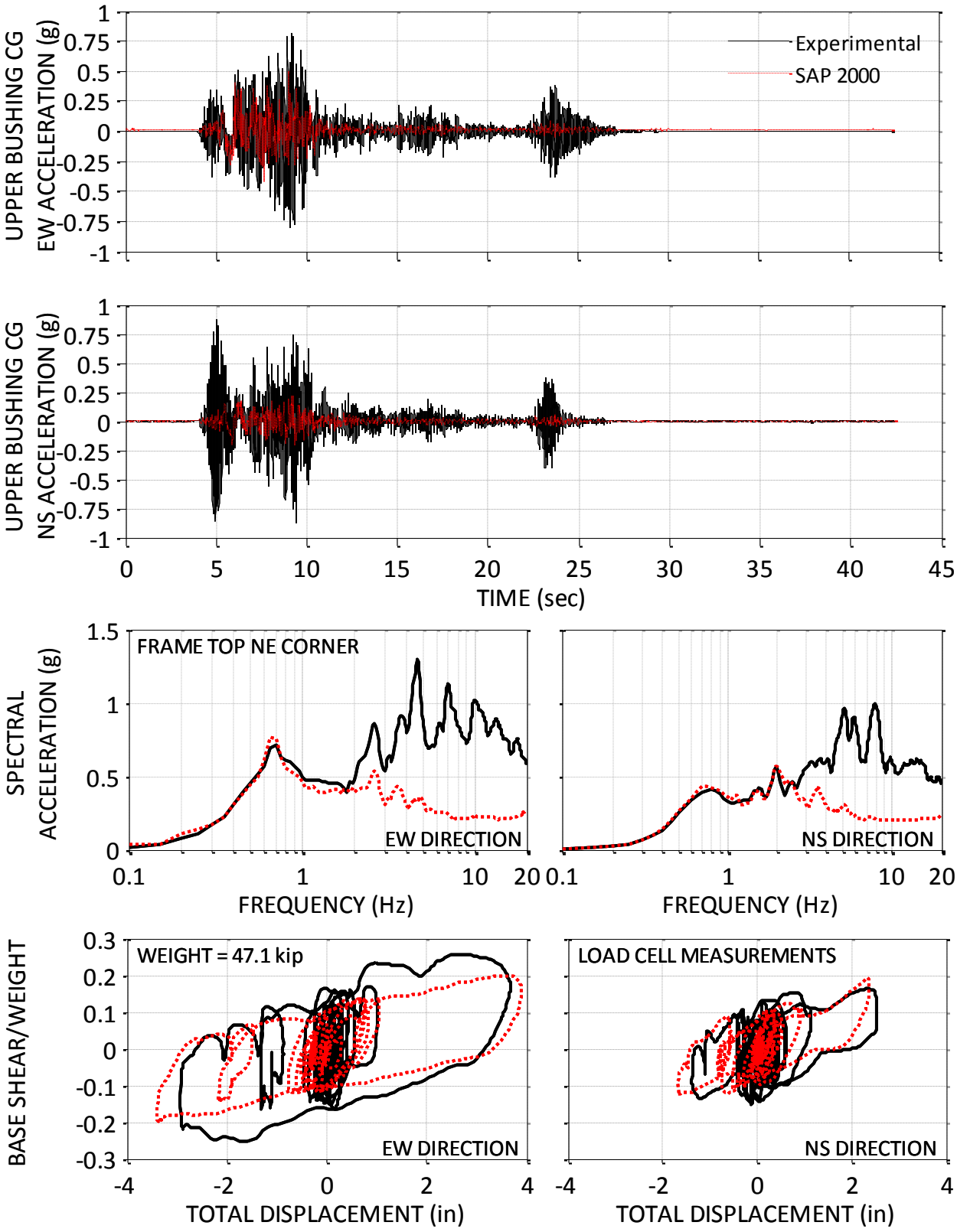
TRIPLE FP SYSTEM (Friction-Bolted Configuration)
EL CENTRO 300% BI-AXIAL (N90W in EW direction)
LENGTH SCALE=3 NON-SYMMETRIC BUSHING CONFIGURATION



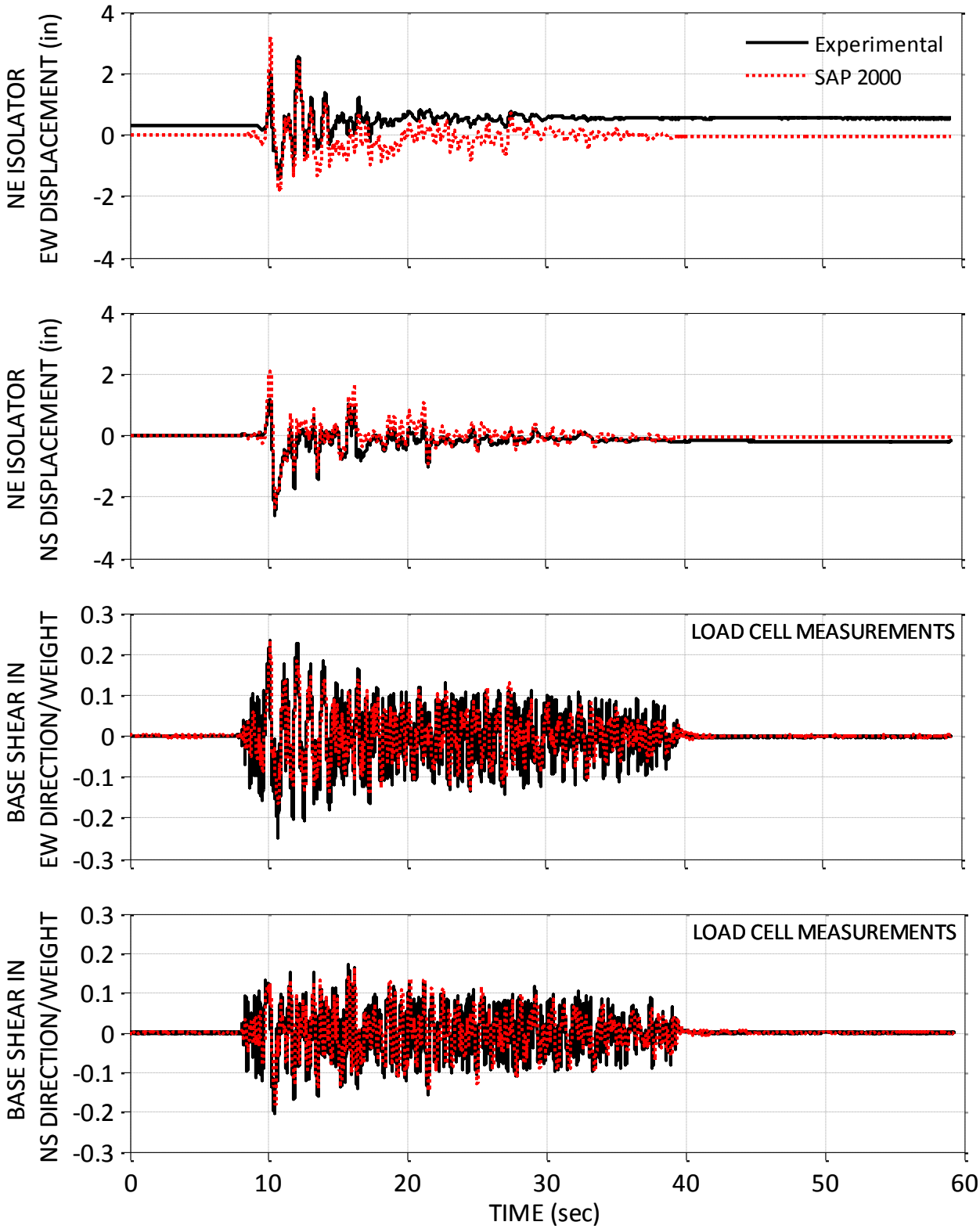

UPPER BUSHING CG
EW ACCELERATION (g)
0.75
0.5
0.25
0
-0.25
-0.5
-0.75
Experimental
SAP 2000
UPPER BUSHING CG
NS ACCELERATION (g)
0
10
20
30
40
50
60
TIME (sec)
SPECTRAL
ACCELERATION (g)
1
0.75
0.5
0.25
0
FRAME TOP NE CORNER
EW DIRECTION
NS DIRECTION
0.1
1
10
20
FREQUENCY (Hz)
BASE SHEAR/WEIGHT
0.3
0.2
0.1
-0.1
-0.2
-0.3
WEIGHT = 47.1 kip
LOAD CELL MEASUREMENTS
-5
-2.5
2.5
5
TOTAL DISPLACEMENT (in)

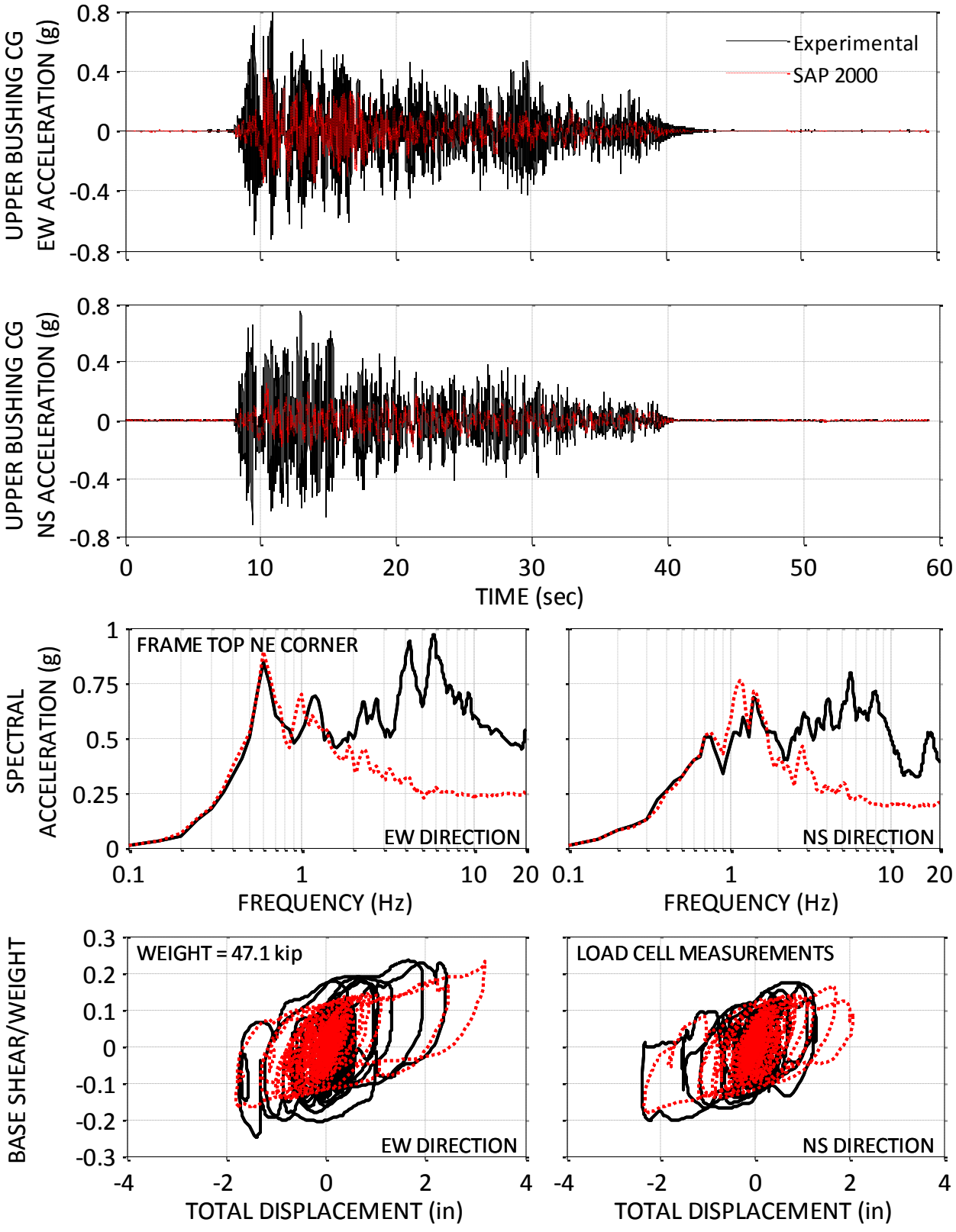
TRIPLE FP SYSTEM (Friction-Bolted Configuration)
PACOIMA DAM 100% BI-AXIAL (S16E in EW direction)
LENGTH SCALE=3 NON-SYMMETRIC BUSHING CONFIGURATION



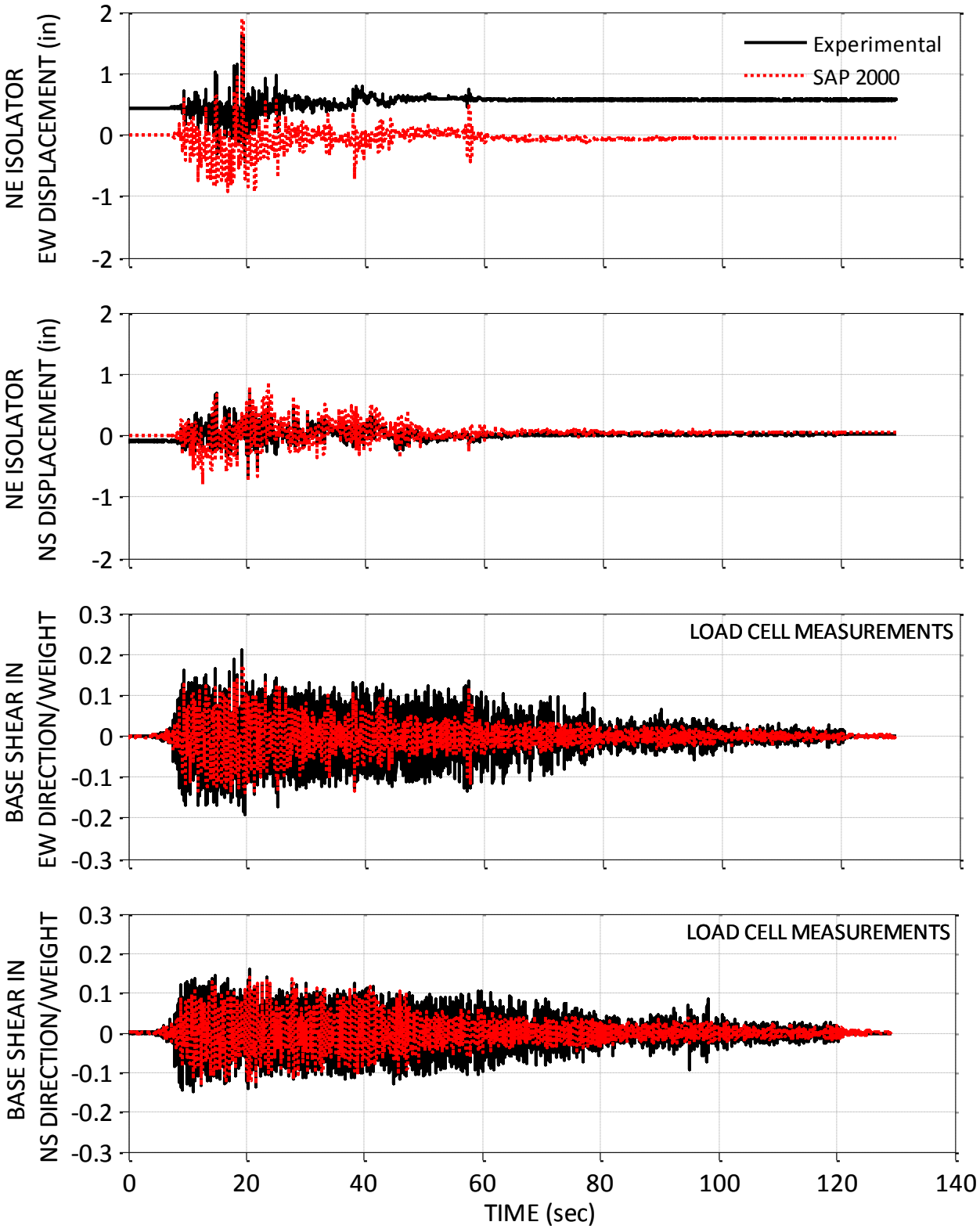

UPPER BUSHING CG
EW ACCELERATION (g)
Experimental
SAP 2000
UPPER BUSHING CG
NS ACCELERATION (g)
TIME (sec)
SPECTRAL
ACCELERATION (g)
FRAME TOP NE CORNER
EW DIRECTION
NS DIRECTION
FREQUENCY (Hz)
BASE SHEAR/WEIGHT
WEIGHT = 47.1 kip
LOAD CELL MEASUREMENTS
TOTAL DISPLACEMENT (in)

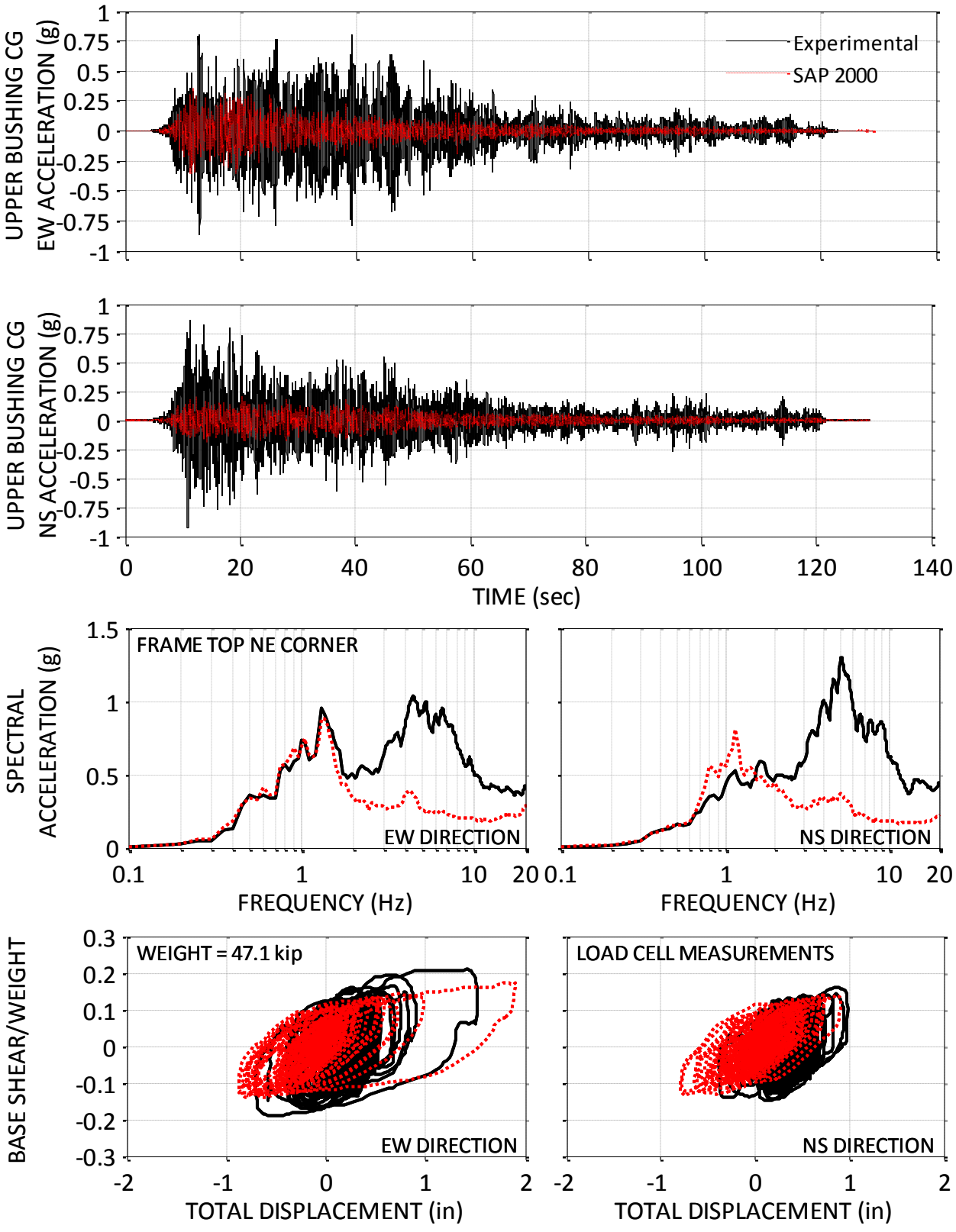
TRIPLE FP SYSTEM (Friction-Bolted Configuration)
TAFT 500% BI-AXIAL (S69E in EW direction)
LENGTH SCALE=3 NON-SYMMETRIC BUSHING CONFIGURATION




UPPER BUSHING CG
EW ACCELERATION (g)
0.8
0.4
0
-0.4
-0.8
Experimental
SAP 2000
UPPER BUSHING CG
NS ACCELERATION (g)
0
10
20
30
40
50
60
TIME (sec)
SPECTRAL
ACCELERATION (g)
FRAME TOP NE CORNER
EW DIRECTION
NS DIRECTION
1
0.75
0.5
0.25
0
0.1
1
10
20
FREQUENCY (Hz)
BASE SHEAR/WEIGHT
WEIGHT = 47.1 kip
LOAD CELL MEASUREMENTS
0.3
0.2
0.1
-0.1
-0.2
-0.3
-4
-2
2
4
TOTAL DISPLACEMENT (in)

TRIPLE FP SYSTEM (Friction-Bolted Configuration)
CHILE 100% BI-AXIAL (EW in EW direction)
LENGTH SCALE=3 NON-SYMMETRIC BUSHING CONFIGURATION

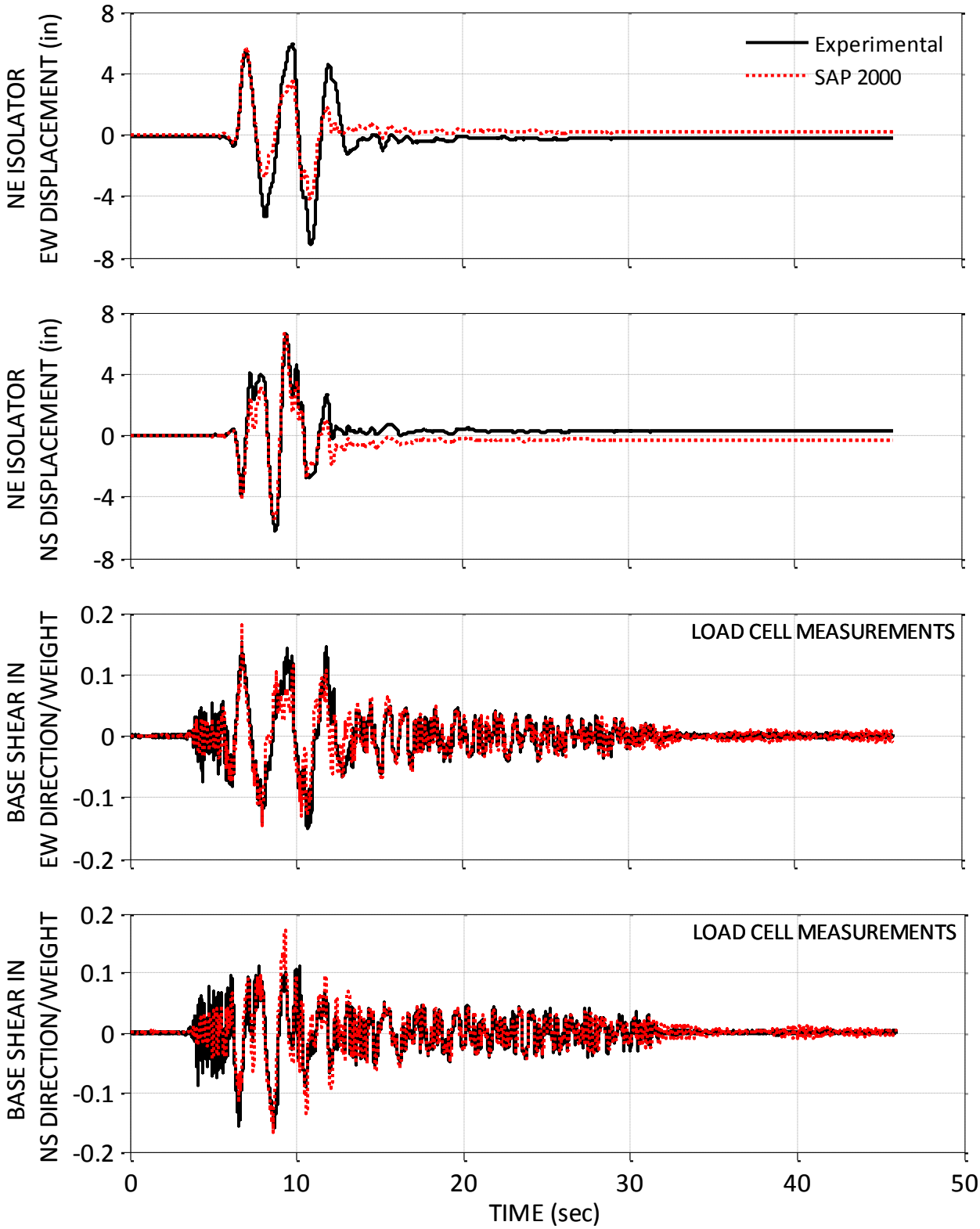


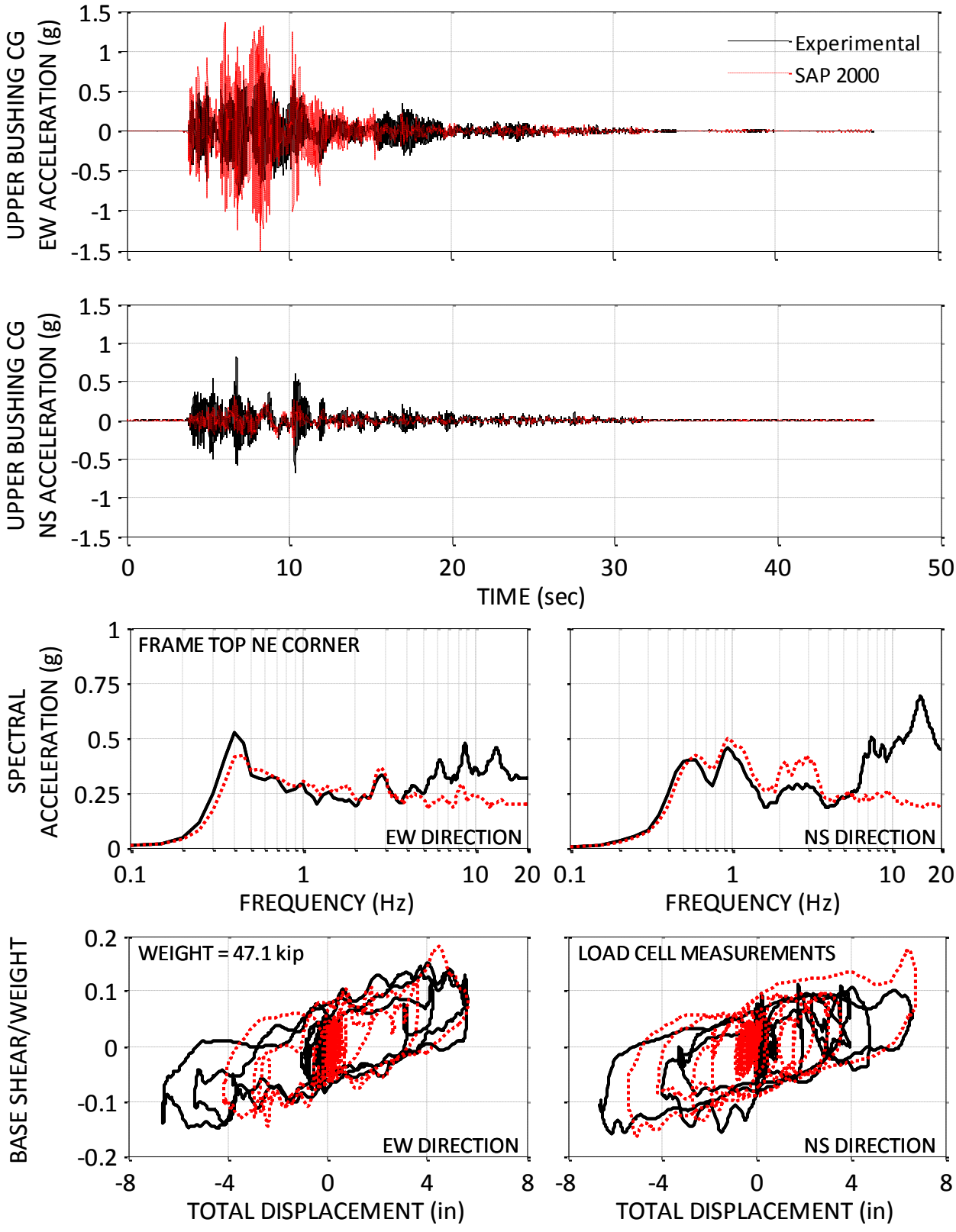

UPPER BUSHING CG
EW ACCELERATION (g)
Experimental
SAP 2000
UPPER BUSHING CG
NS ACCELERATION (g)
TIME (sec)
SPECTRAL
ACCELERATION (g)
FRAME TOP NE CORNER
EW DIRECTION
NS DIRECTION
FREQUENCY (Hz)
BASE SHEAR/WEIGHT
WEIGHT = 47.1 kip
LOAD CELL MEASUREMENTS
TOTAL DISPLACEMENT (in)

PART C-3
SUMMARY OF EXPERIMENTAL AND ANALYTICAL COMPARISONS FOR THE TRIPLE FRICTION PENDULUM SYSTEM AT LENGTH SCALE OF 1 AND MODELING USING THE PARALLEL MODEL

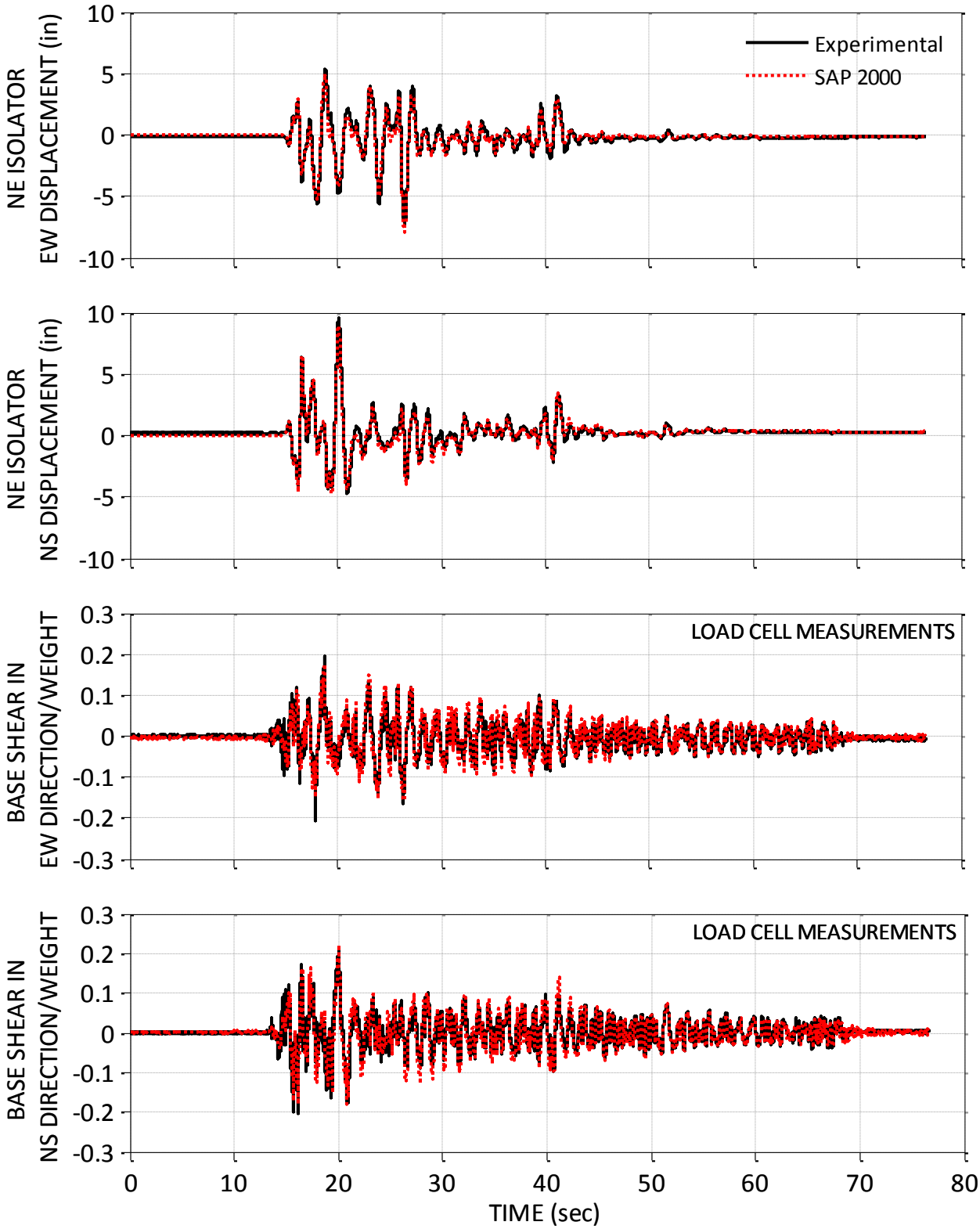
(PERCENTAGE AMOUNT IS SCALE FACTOR APPLIED TO ACCELERATION OF ACTUAL MOTION. FOR EXAMPLE, 100% DENOTES MOTION AS RECORDED, 200% DENOTES THAT ACCELERATION WAS SCALED UP BY FACTOR OF 2)

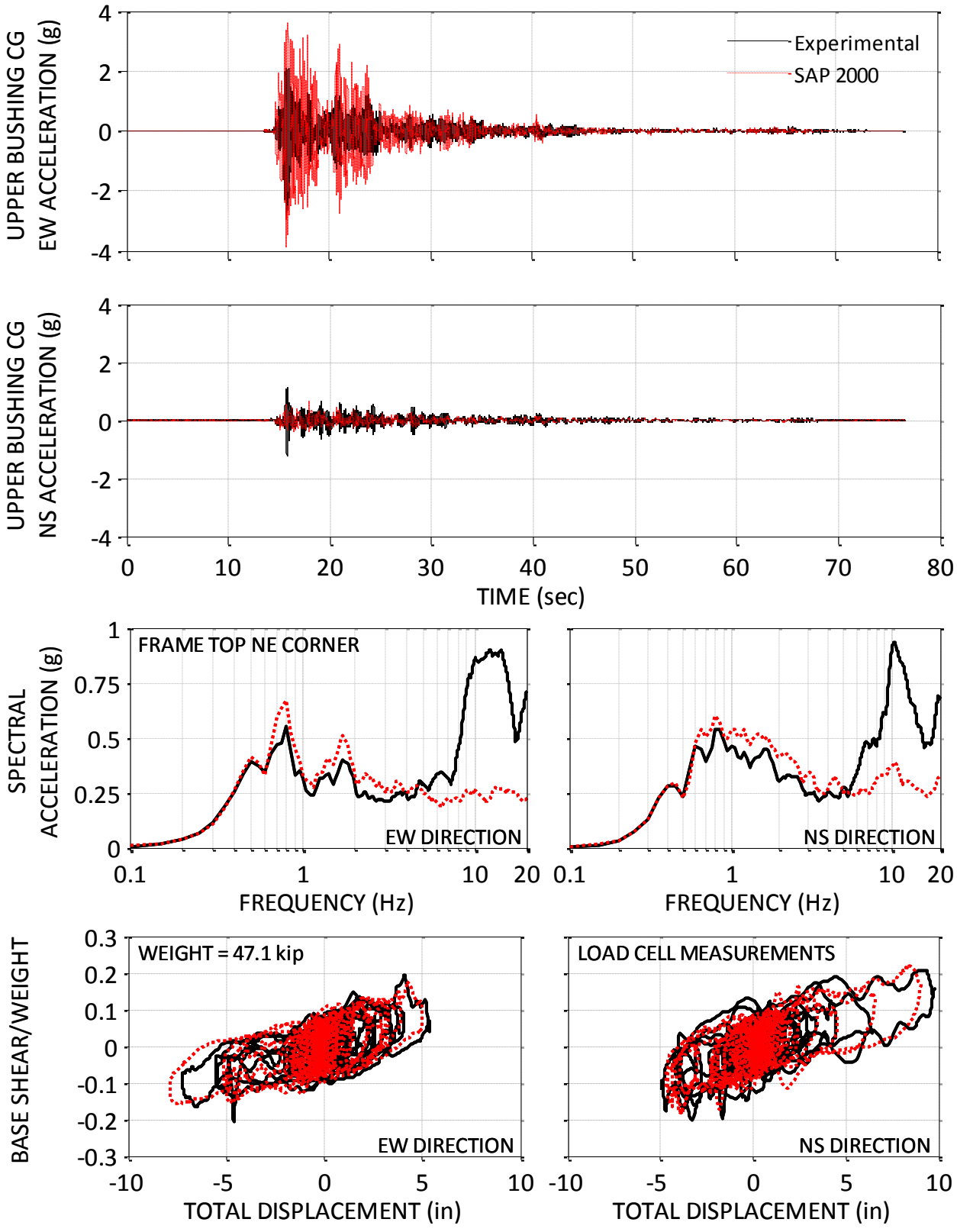
TRIPLE FP SYSTEM (Friction-Bolted Configuration)
JENSEN FILTER 97% TRI-AXIAL (FN in EW direction)
LENGTH SCALE=1 NON-SYMMETRIC BUSHING CONFIGURATION



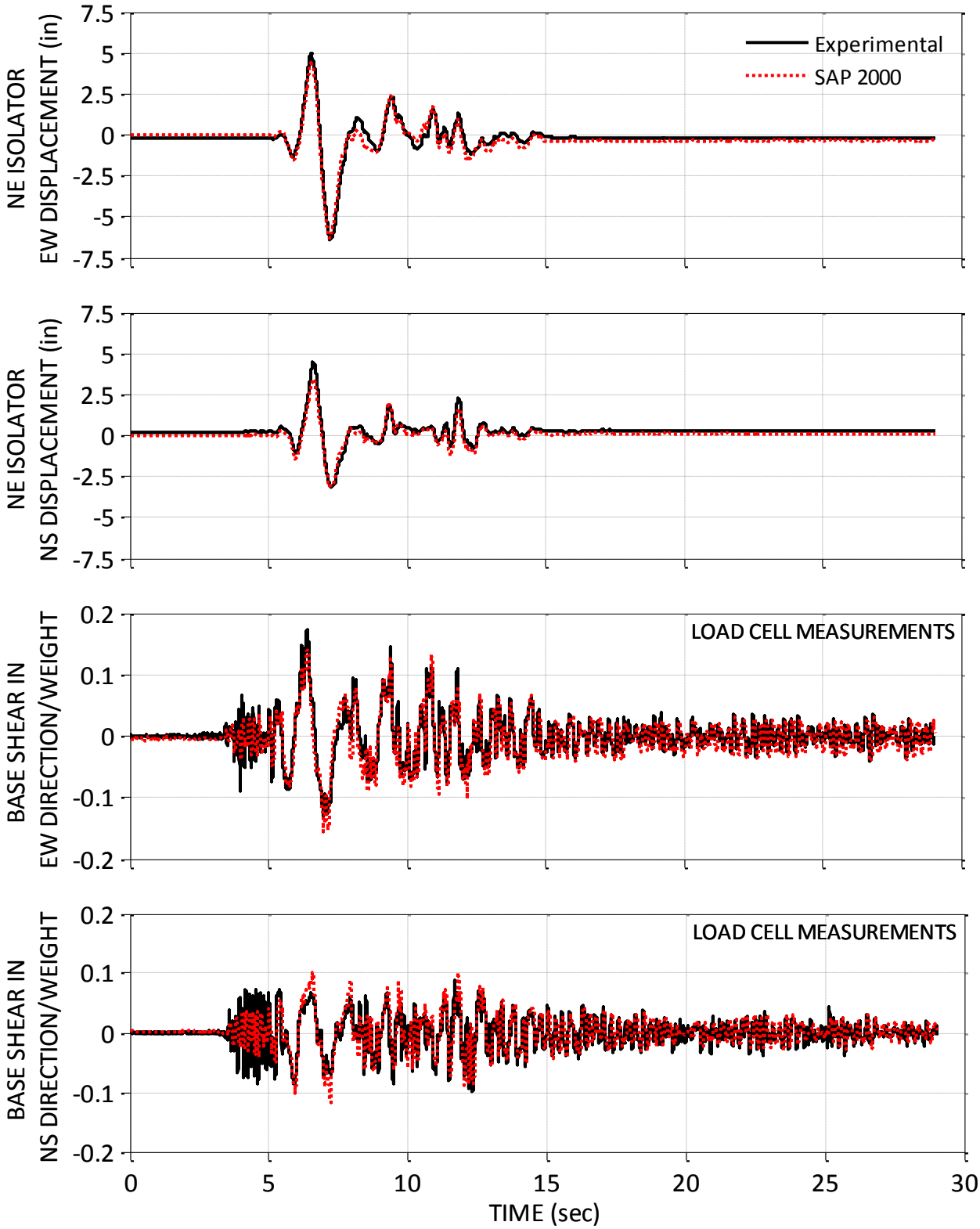

UPPER BUSHING CG
EW ACCELERATION (g)
Experimental
SAP 2000
UPPER BUSHING CG
NS ACCELERATION (g)
TIME (sec)
SPECTRAL
ACCELERATION (g)
FRAME TOP NE CORNER
EW DIRECTION
NS DIRECTION
FREQUENCY (Hz)
BASE SHEAR/WEIGHT
WEIGHT = 47.1 kip
LOAD CELL MEASUREMENTS
TOTAL DISPLACEMENT (in)

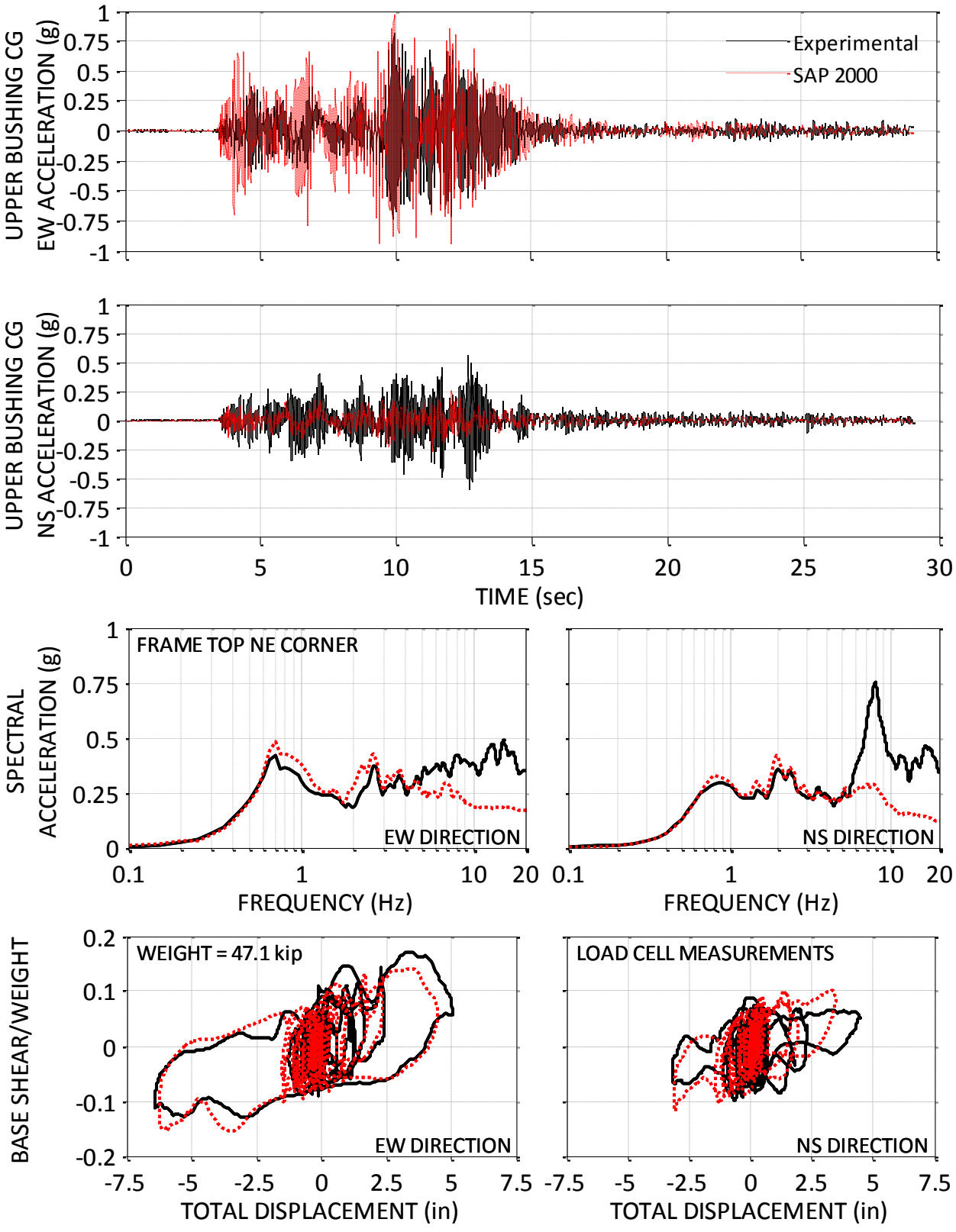
TRIPLE FP SYSTEM (Friction-Bolted Configuration)
EL CENTRO 300% TRI-AXIAL (N90W in EW direction)
LENGTH SCALE=1 NON-SYMMETRIC BUSHING CONFIGURATION



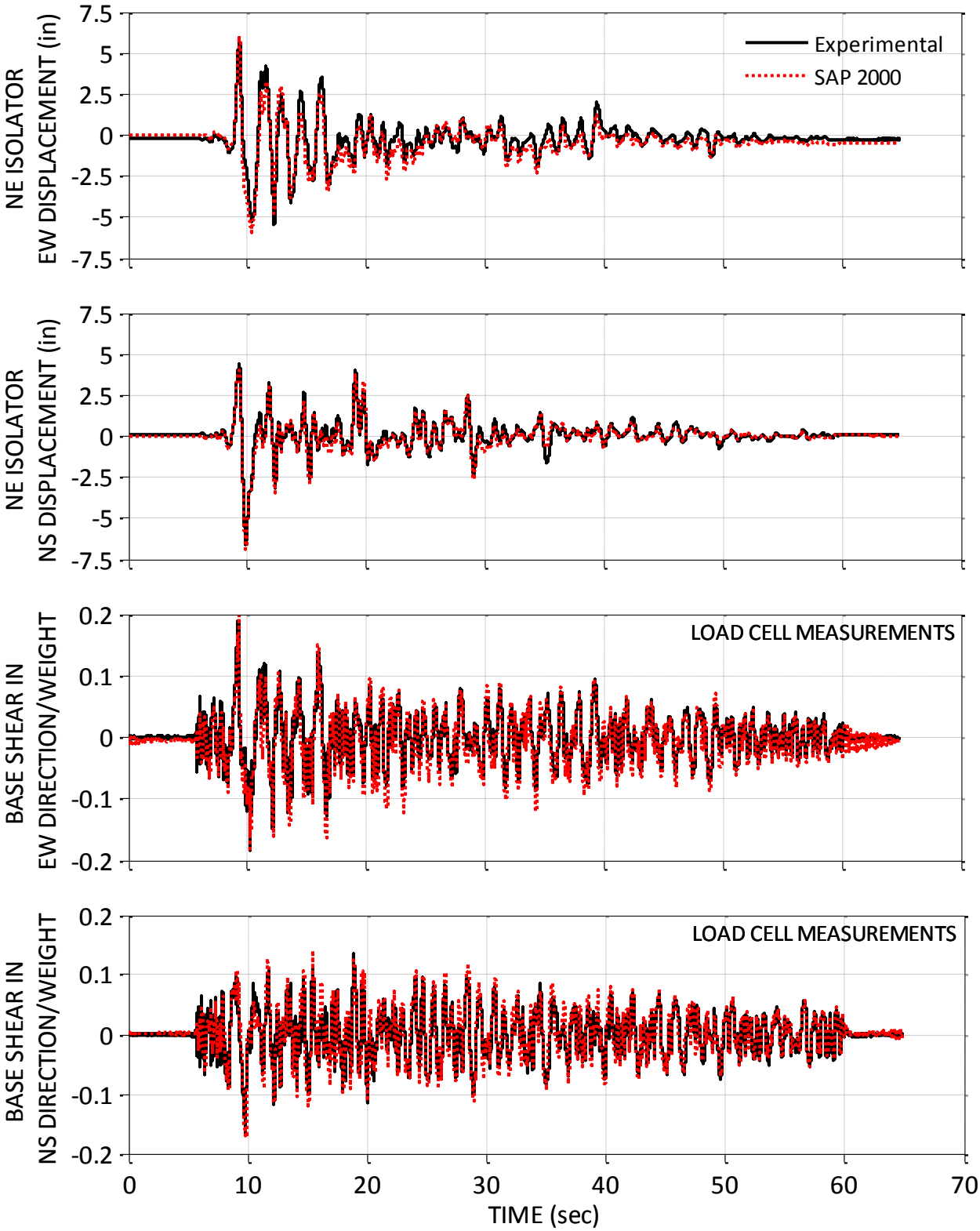

UPPER BUSHING CG
EW ACCELERATION (g)
Experimental
SAP 2000
UPPER BUSHING CG
NS ACCELERATION (g)
TIME (sec)
SPECTRAL
ACCELERATION (g)
FRAME TOP NE CORNER
EW DIRECTION
NS DIRECTION
FREQUENCY (Hz)
BASE SHEAR/WEIGHT
WEIGHT = 47.1 kip
LOAD CELL MEASUREMENTS
TOTAL DISPLACEMENT (in)

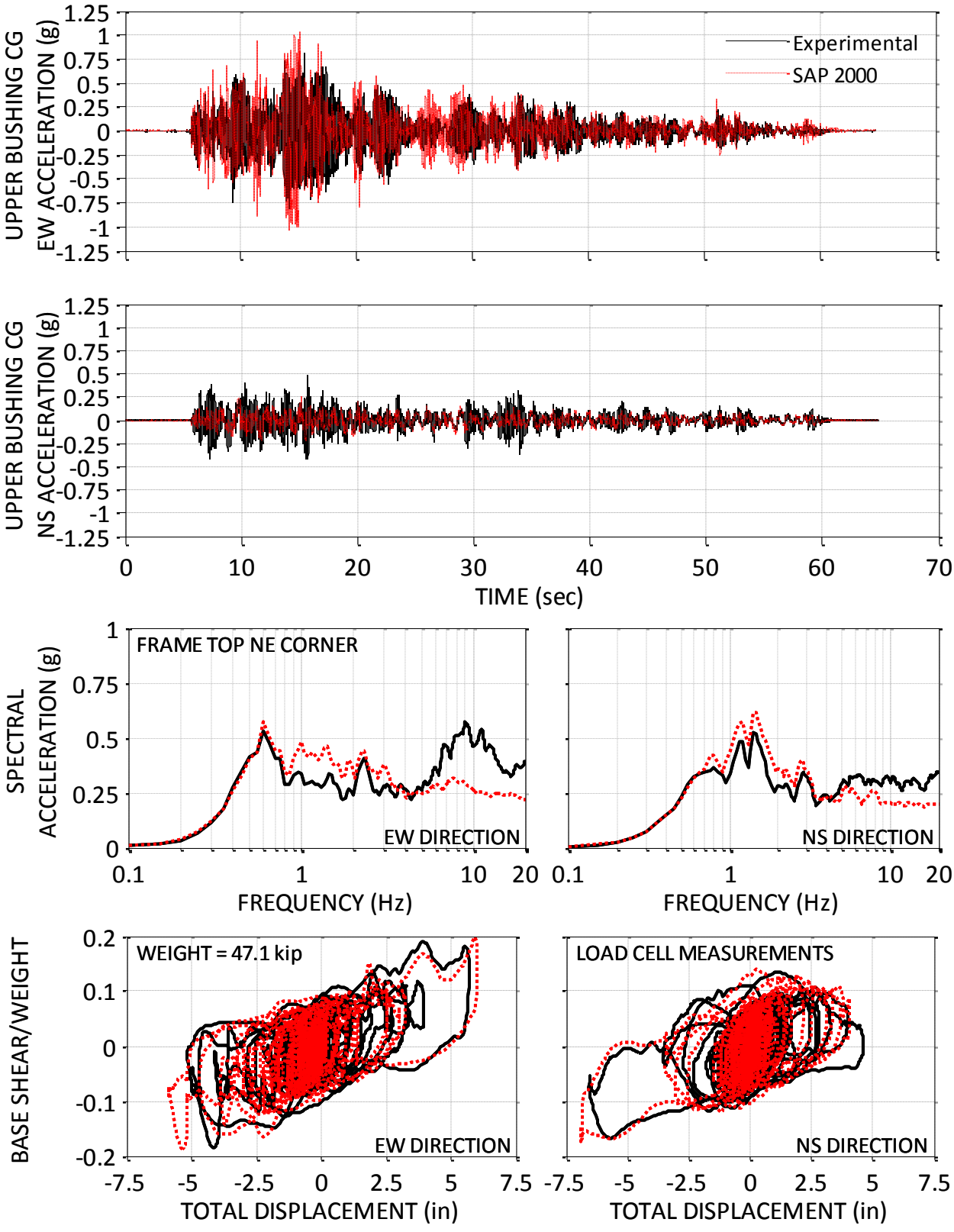
TRIPLE FP SYSTEM (Friction-Bolted Configuration)
PACOIMA DAM 75% TRI-AXIAL (S16E in EW direction)
LENGTH SCALE=1 NON-SYMMETRIC BUSHING CONFIGURATION



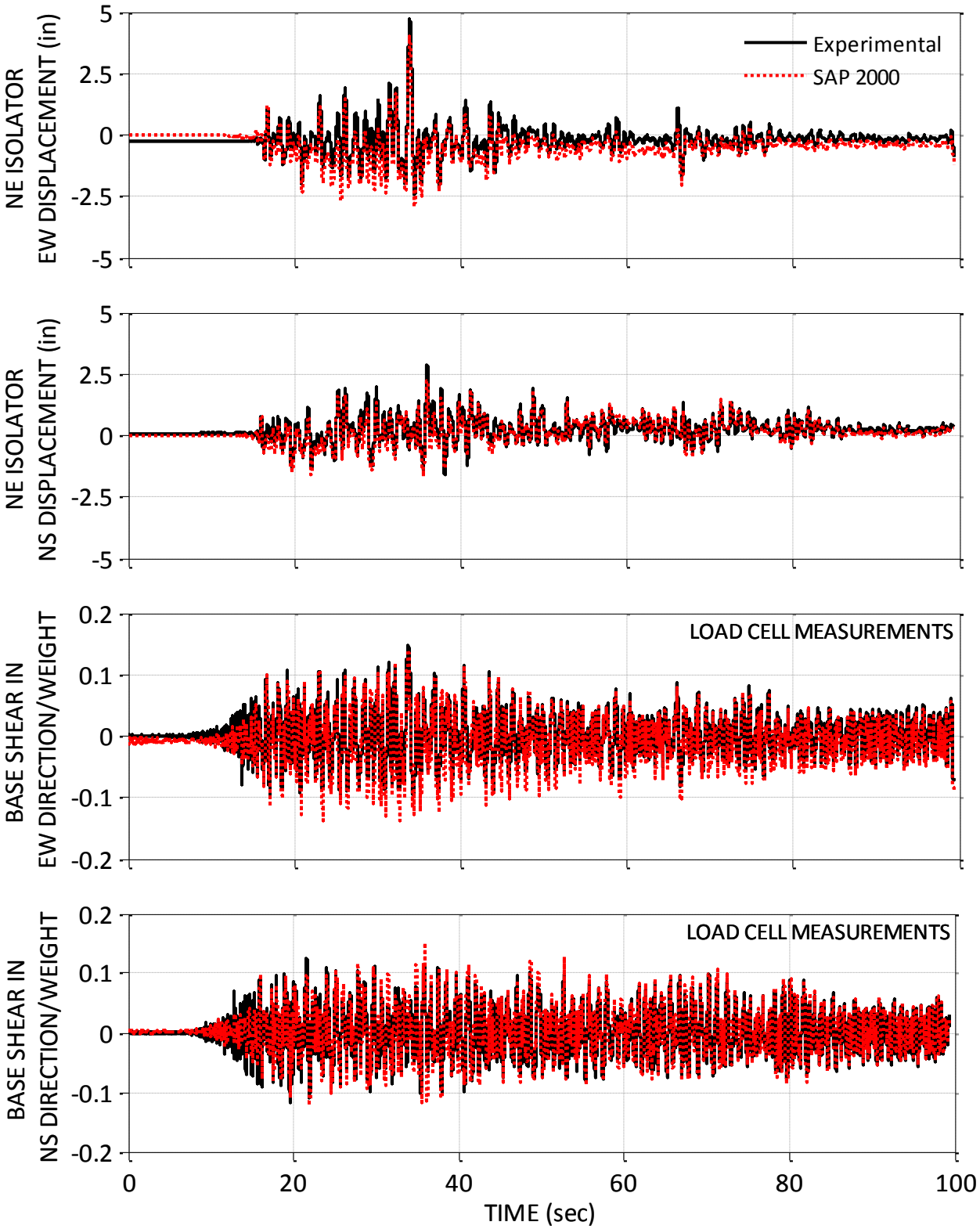

UPPER BUSHING CG
EW ACCELERATION (g)
Experimental
SAP 2000
UPPER BUSHING CG
NS ACCELERATION (g)
TIME (sec)
SPECTRAL
ACCELERATION (g)
FRAME TOP NE CORNER
EW DIRECTION
NS DIRECTION
FREQUENCY (Hz)
BASE SHEAR/WEIGHT
WEIGHT = 47.1 kip
LOAD CELL MEASUREMENTS
TOTAL DISPLACEMENT (in)

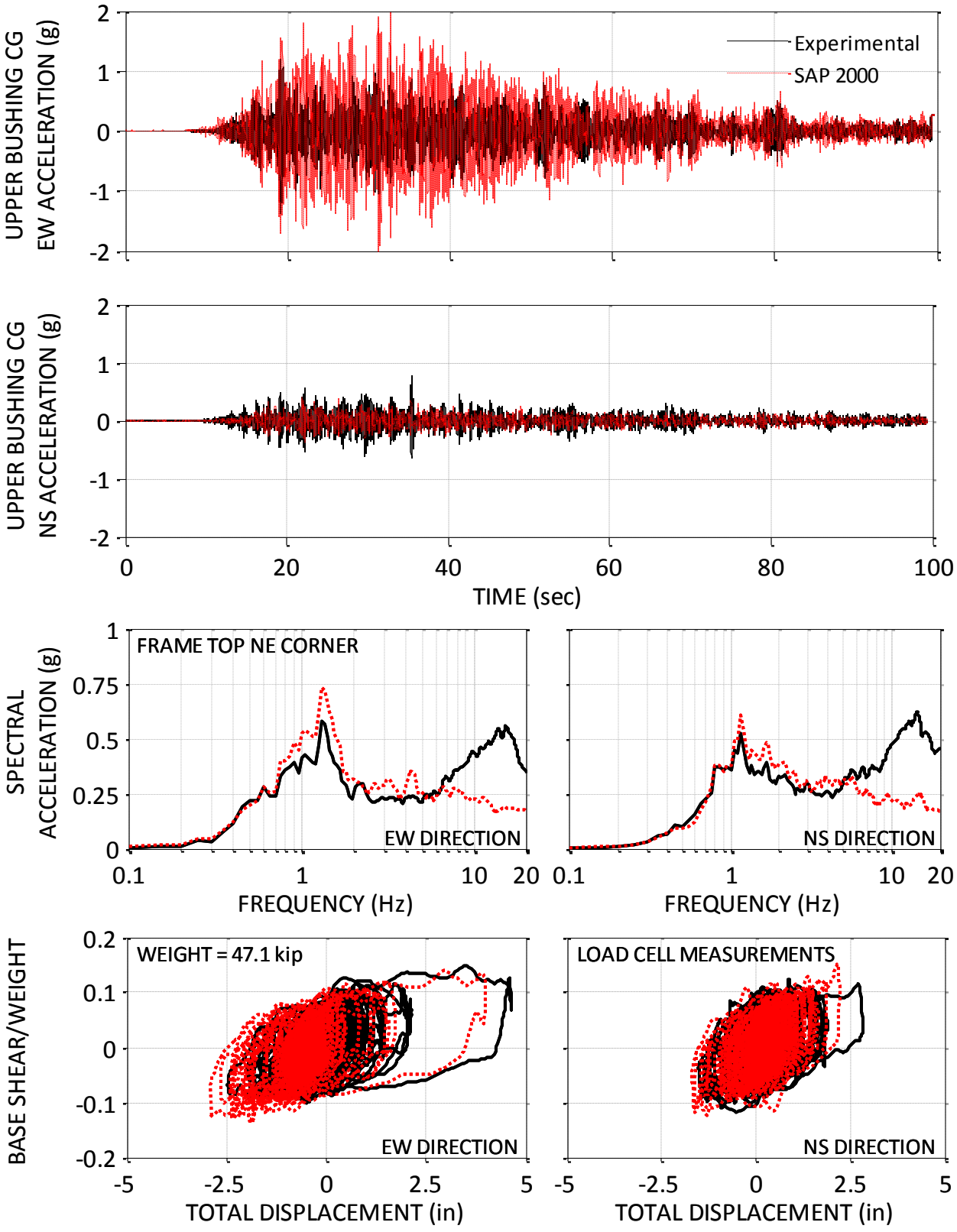
TRIPLE FP SYSTEM (Friction-Bolted Configuration)
TAFT 500% TRI-AXIAL (S69E in EW direction)
LENGTH SCALE=1 NON-SYMMETRIC BUSHING CONFIGURATION



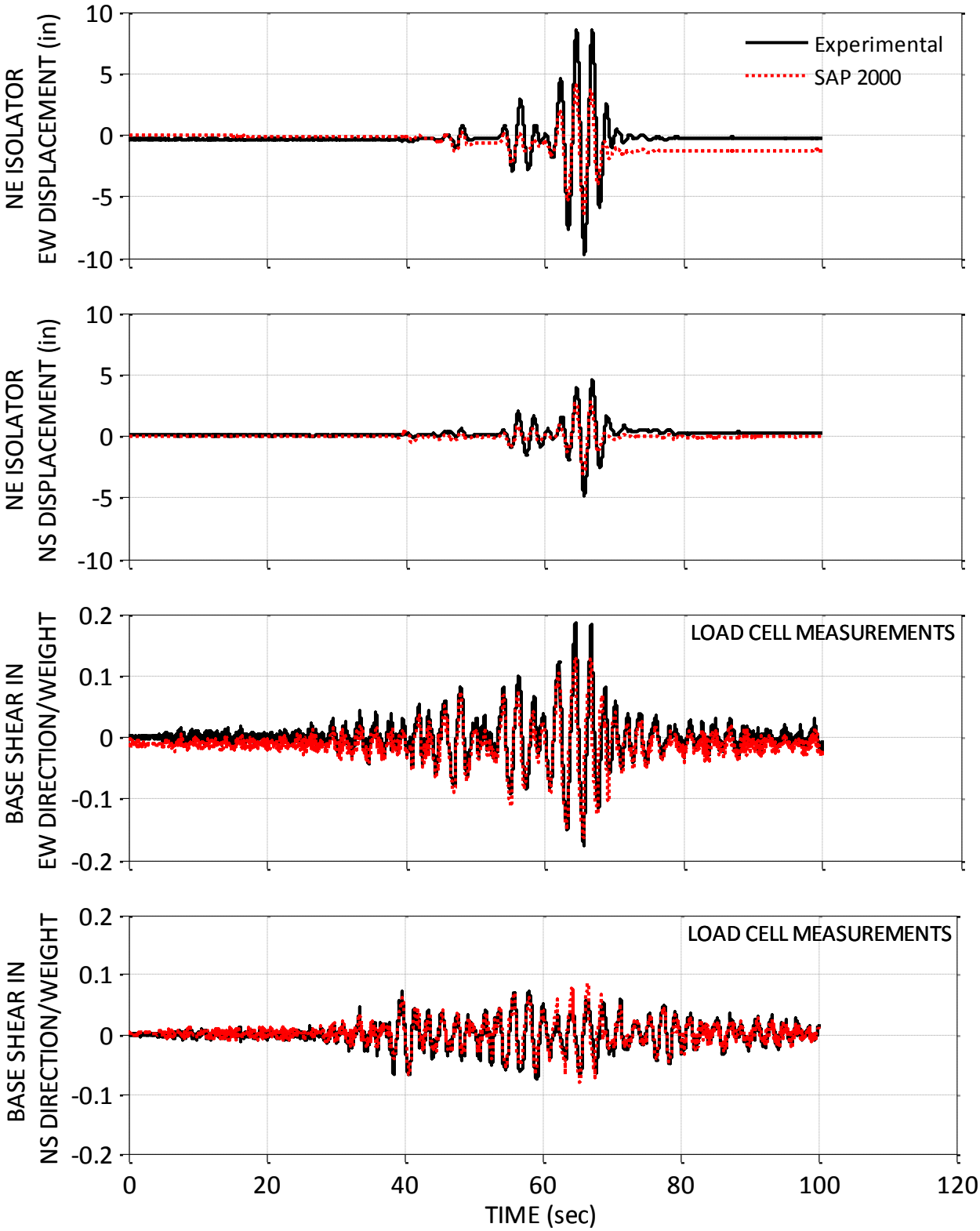

UPPER BUSHING CG
EW ACCELERATION (g)
Experimental
SAP 2000
UPPER BUSHING CG
NS ACCELERATION (g)
TIME (sec)
SPECTRAL
ACCELERATION (g)
FRAME TOP NE CORNER
EW DIRECTION
NS DIRECTION
FREQUENCY (Hz)
BASE SHEAR/WEIGHT
WEIGHT = 47.1 kip
LOAD CELL MEASUREMENTS
TOTAL DISPLACEMENT (in)

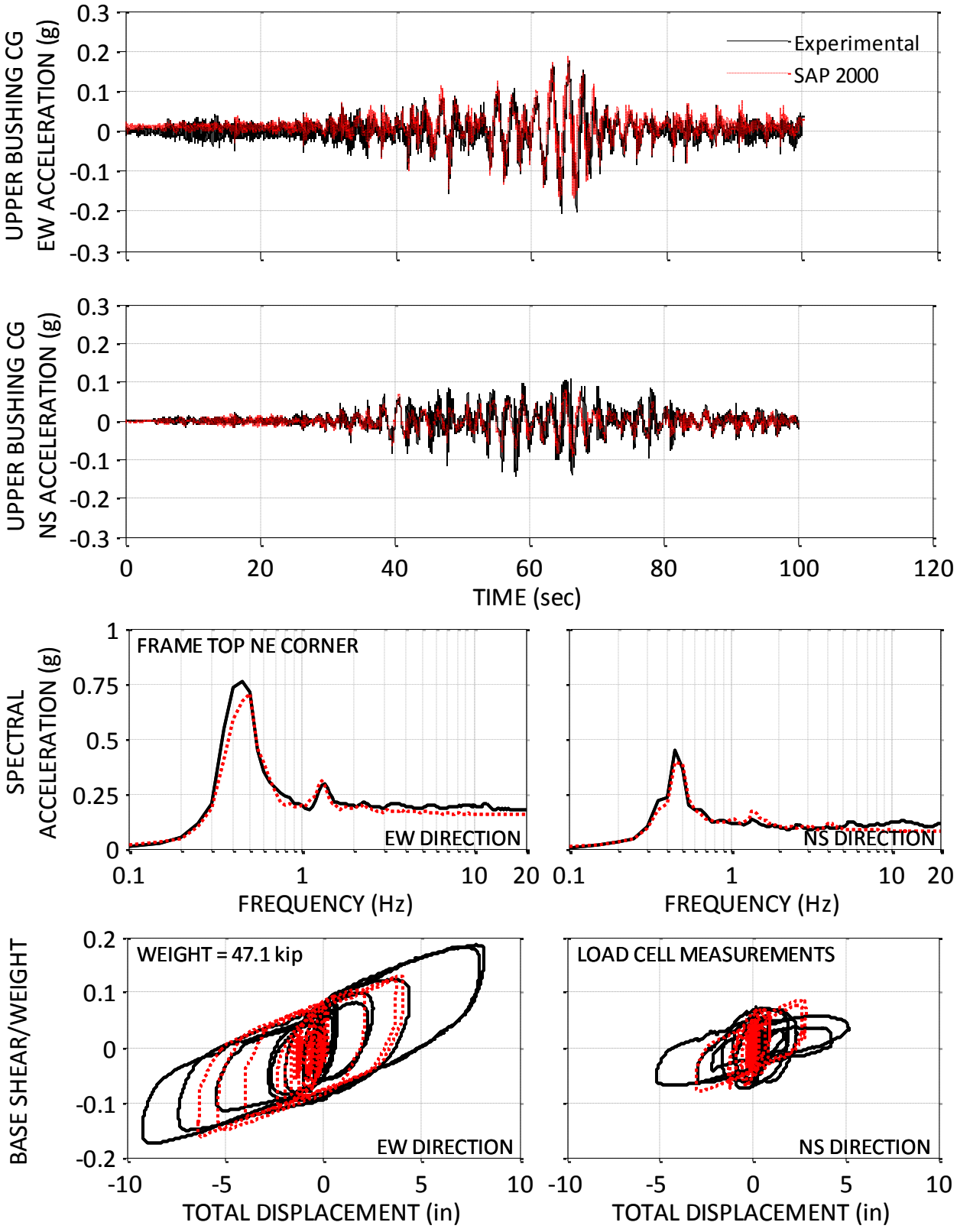
TRIPLE FP SYSTEM (Friction-Bolted Configuration)
CHILE 100% TRI-AXIAL (EW in EW direction)
LENGTH SCALE=1 NON-SYMMETRIC BUSHING CONFIGURATION



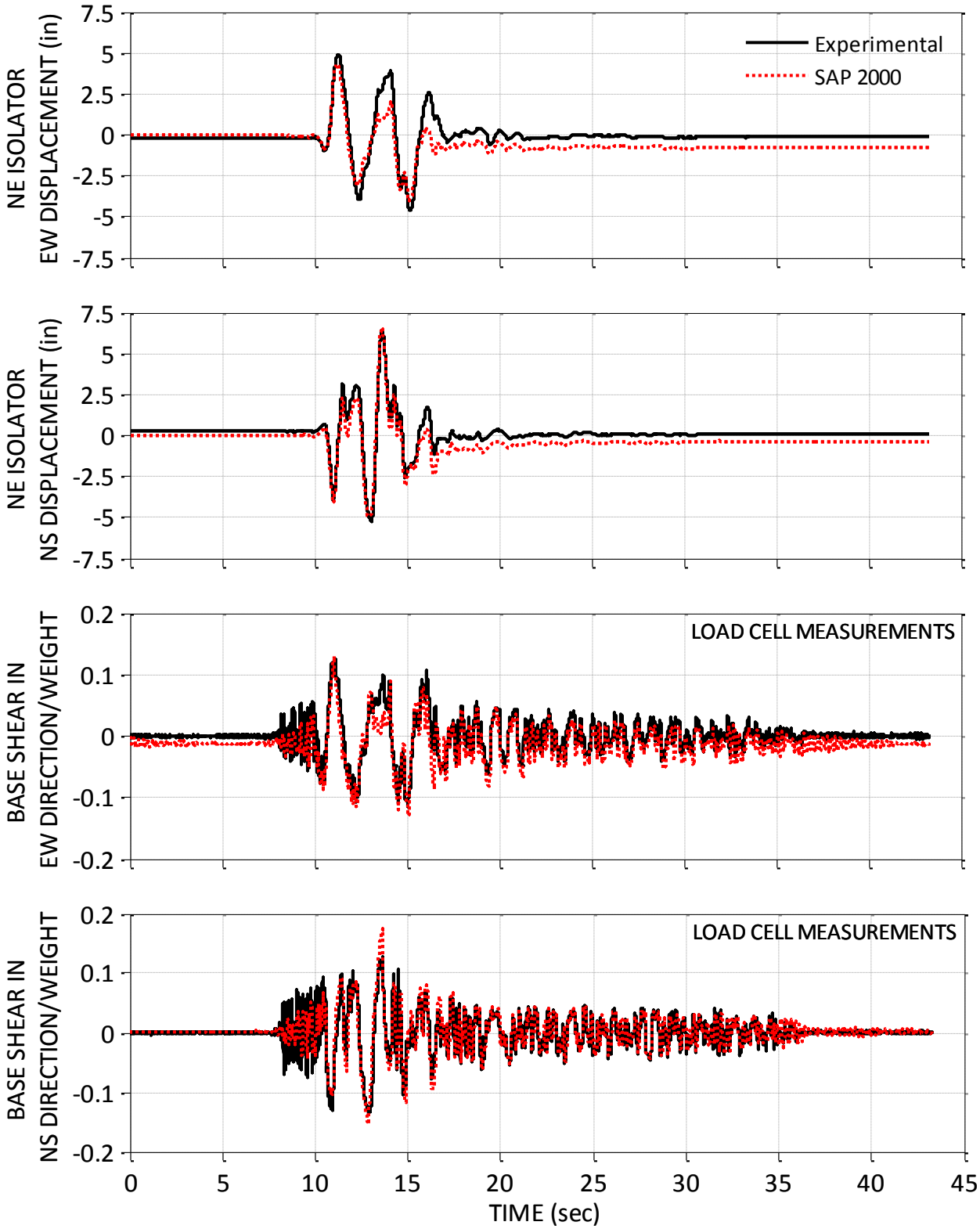

UPPER BUSHING CG
EW ACCELERATION (g)
Experimental
SAP 2000
UPPER BUSHING CG
NS ACCELERATION (g)
TIME (sec)
SPECTRAL
ACCELERATION (g)
FRAME TOP NE CORNER
EW DIRECTION
NS DIRECTION
FREQUENCY (Hz)
BASE SHEAR/WEIGHT
WEIGHT = 47.1 kip
LOAD CELL MEASUREMENTS
TOTAL DISPLACEMENT (in)

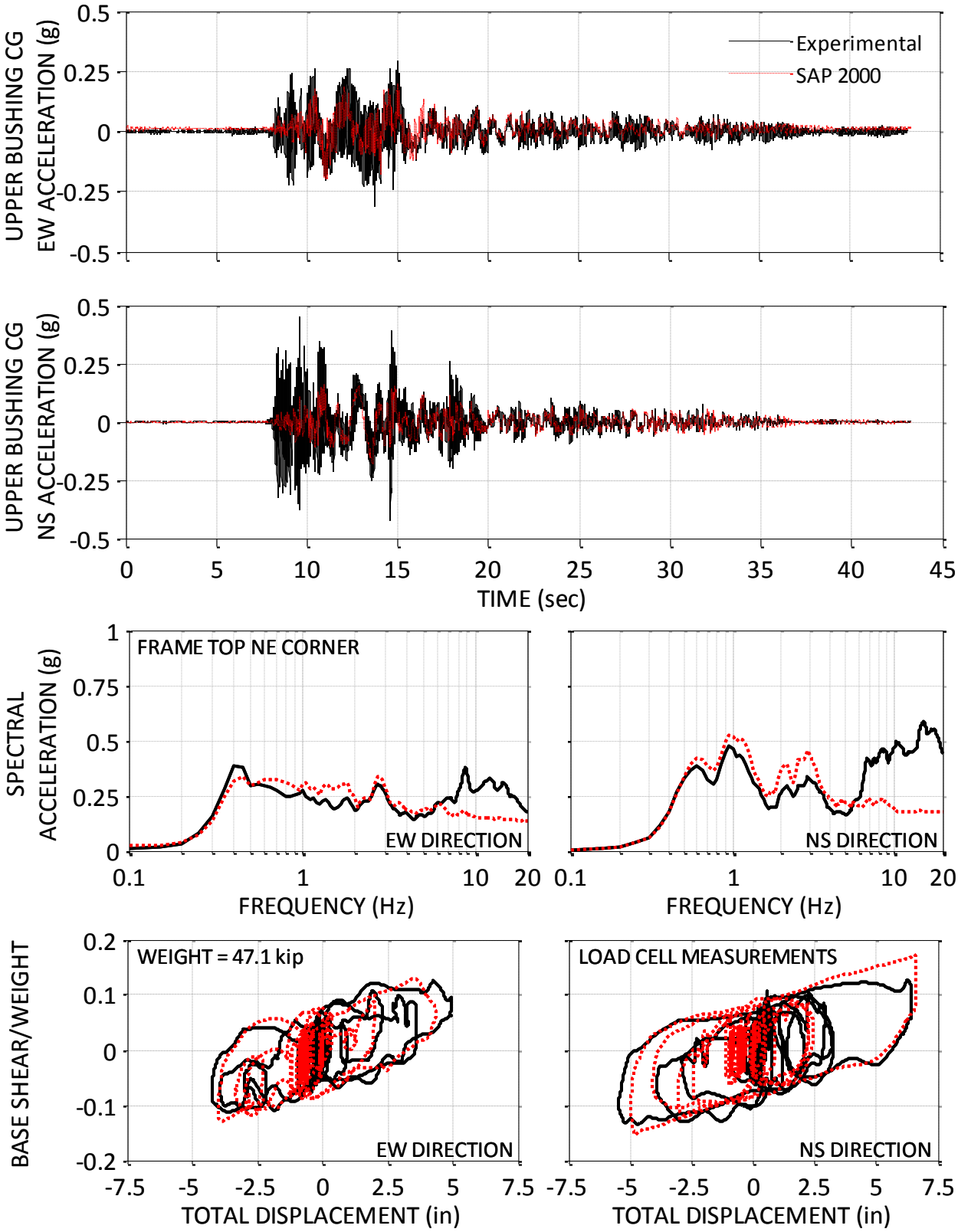
TRIPLE FP SYSTEM (Friction-Bolted Configuration)
MEXICO 70% TRI-AXIAL (N90W in EW direction)
LENGTH SCALE=1 NON-SYMMETRIC BUSHING CONFIGURATION



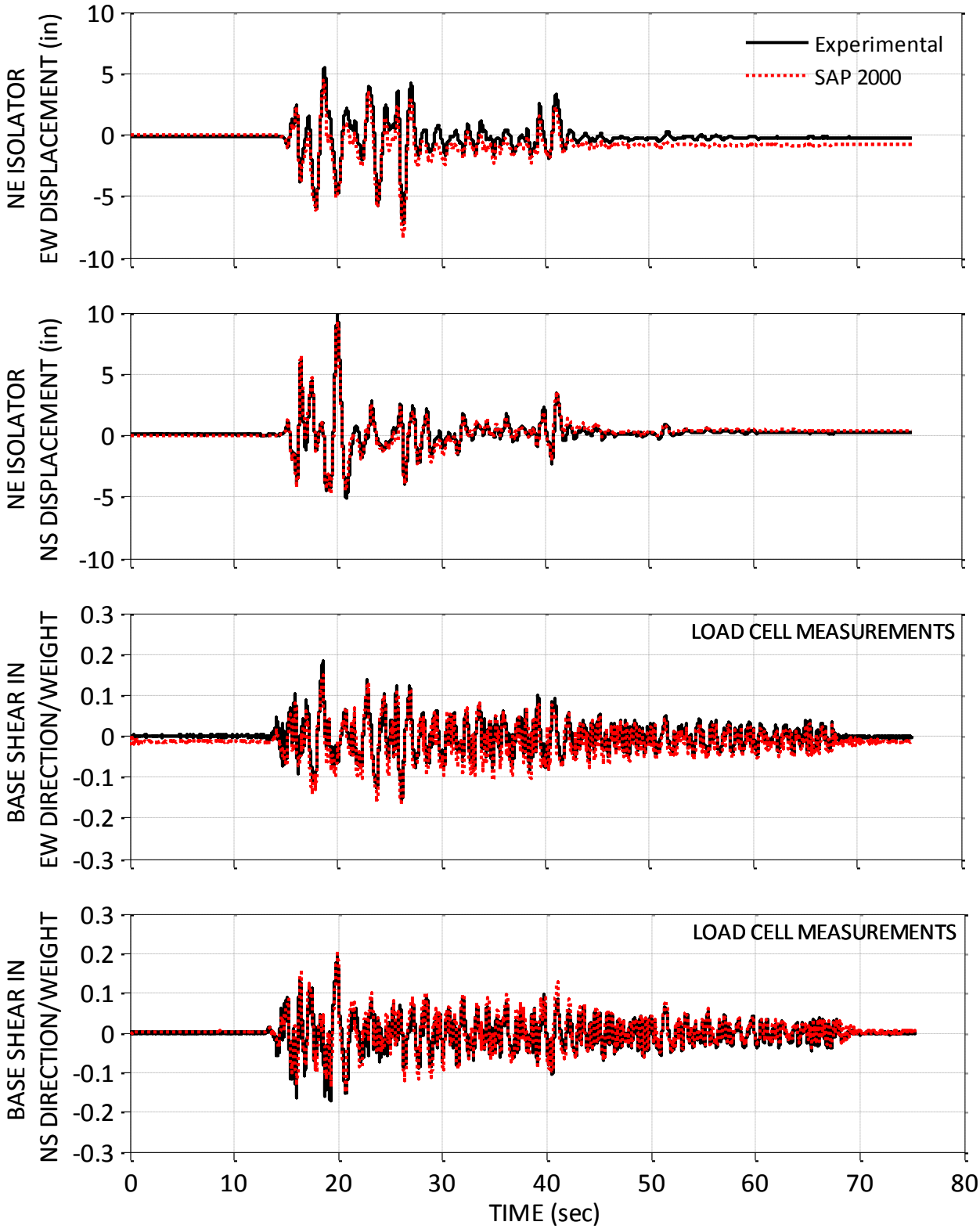

UPPER BUSHING CG
EW ACCELERATION (g)
Experimental
SAP 2000
UPPER BUSHING CG
NS ACCELERATION (g)
TIME (sec)
SPECTRAL
ACCELERATION (g)
FRAME TOP NE CORNER
EW DIRECTION
NS DIRECTION
FREQUENCY (Hz)
BASE SHEAR/WEIGHT
WEIGHT = 47.1 kip
LOAD CELL MEASUREMENTS
TOTAL DISPLACEMENT (in)

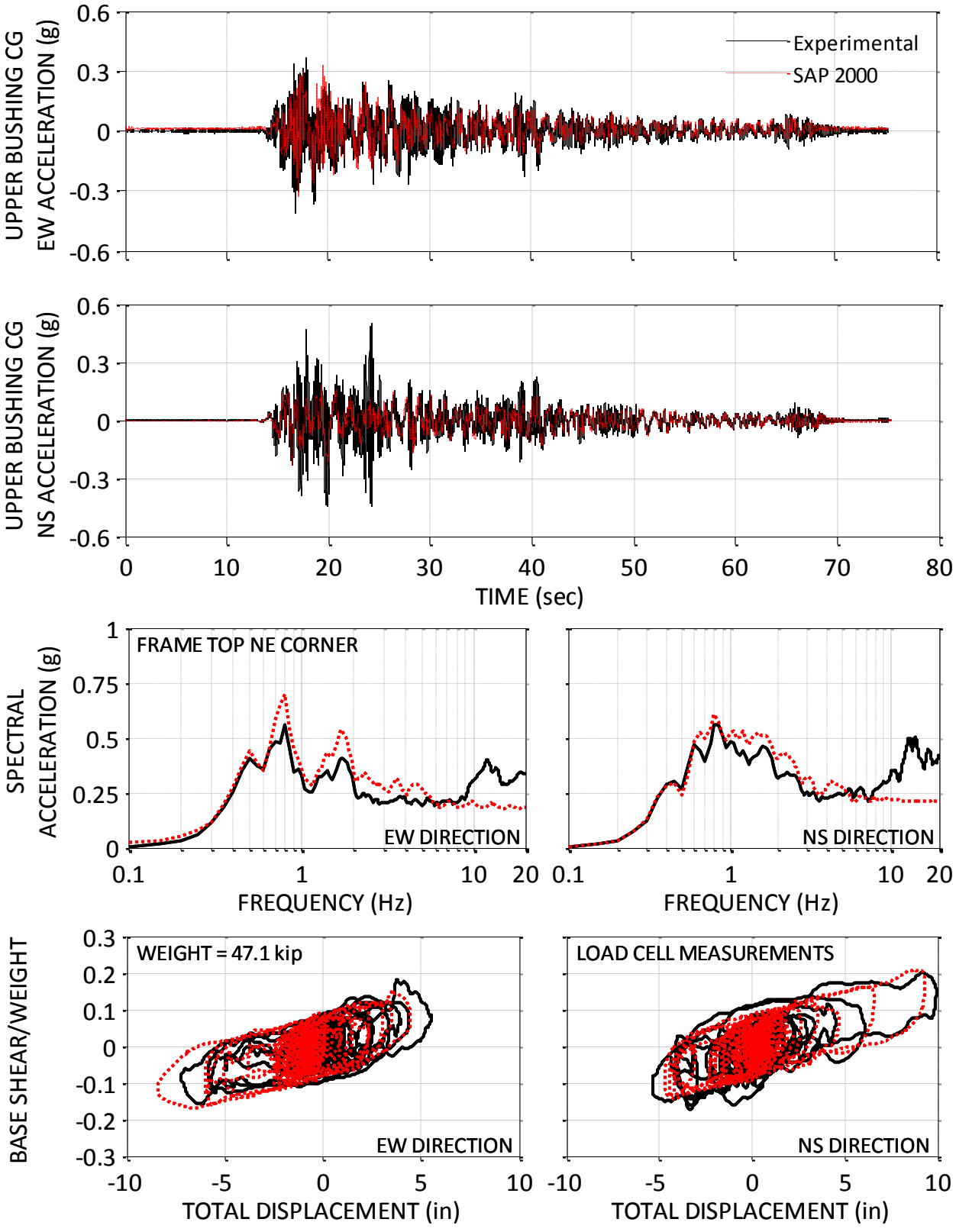
TRIPLE FP SYSTEM (Friction-Bolted Configuration)
JENSEN FILTER 97% BI-AXIAL (FN in EW direction)
LENGTH SCALE=1 NON-SYMMETRIC BUSHING CONFIGURATION



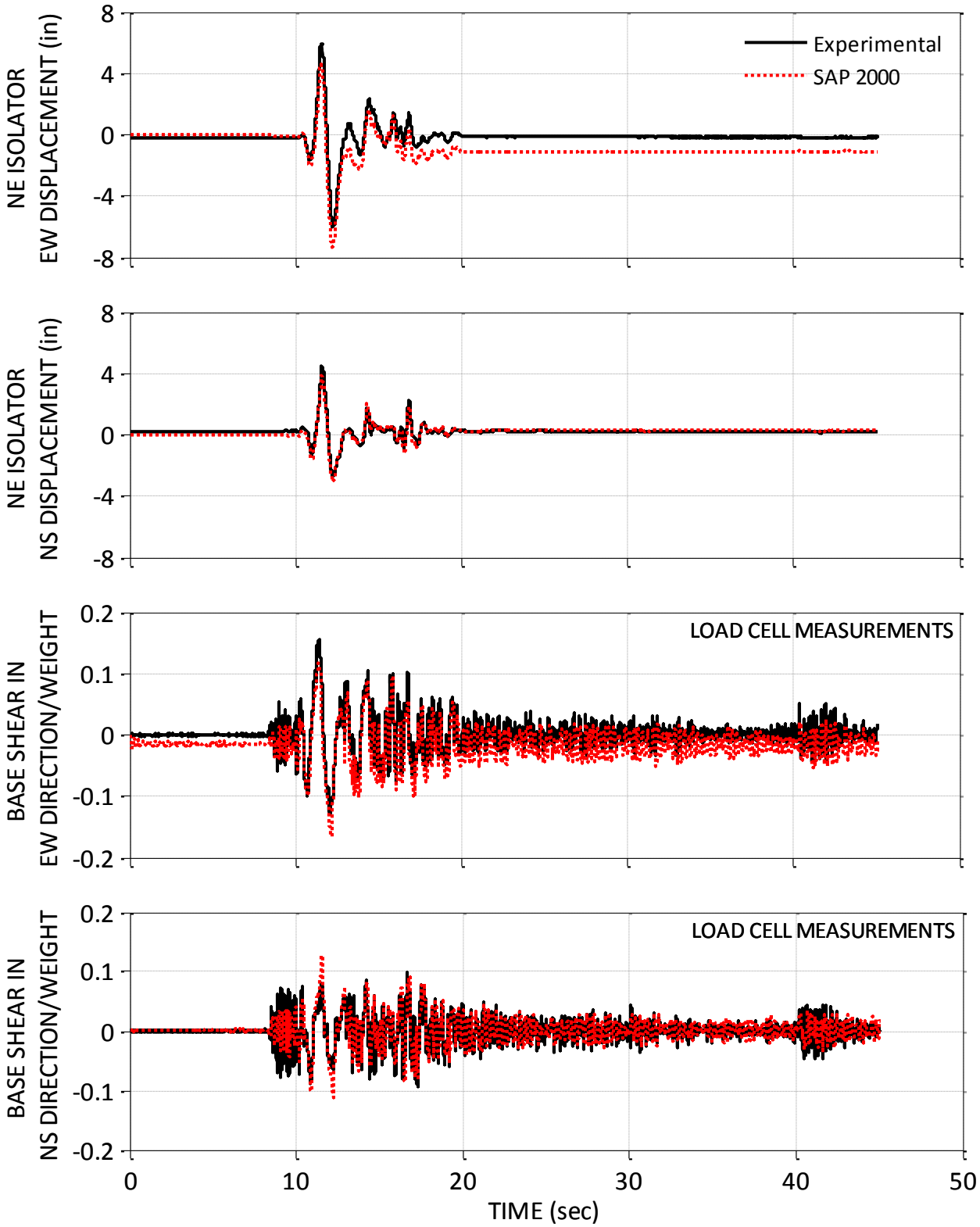

UPPER BUSHING CG
EW ACCELERATION (g)
Experimental
SAP 2000
UPPER BUSHING CG
NS ACCELERATION (g)
TIME (sec)
SPECTRAL
ACCELERATION (g)
FRAME TOP NE CORNER
EW DIRECTION
NS DIRECTION
FREQUENCY (Hz)
BASE SHEAR/WEIGHT
WEIGHT = 47.1 kip
LOAD CELL MEASUREMENTS
TOTAL DISPLACEMENT (in)

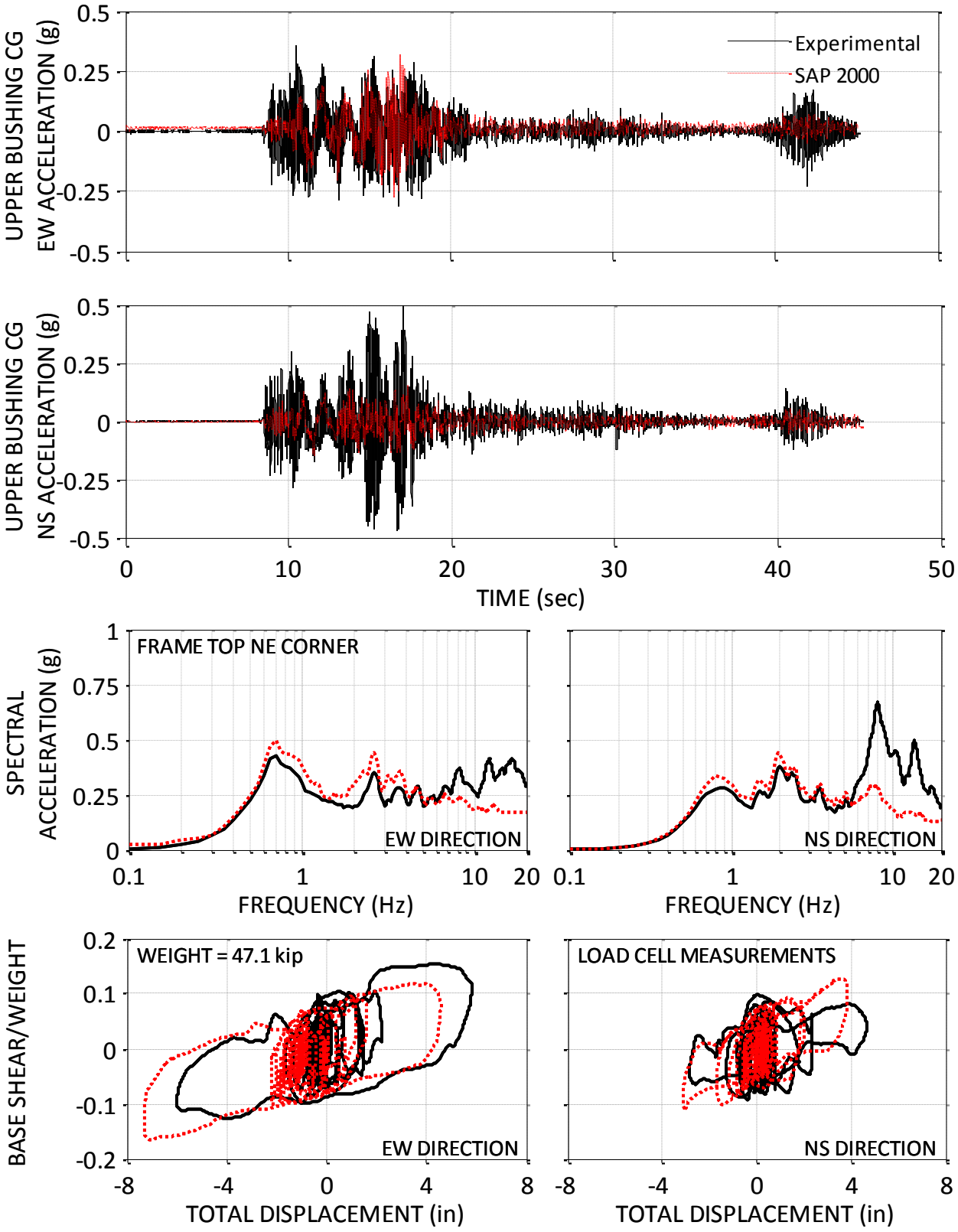
TRIPLE FP SYSTEM (Friction-Bolted Configuration)
EL CENTRO 300% BI-AXIAL (N90W in EW direction)
LENGTH SCALE=1 NON-SYMMETRIC BUSHING CONFIGURATION



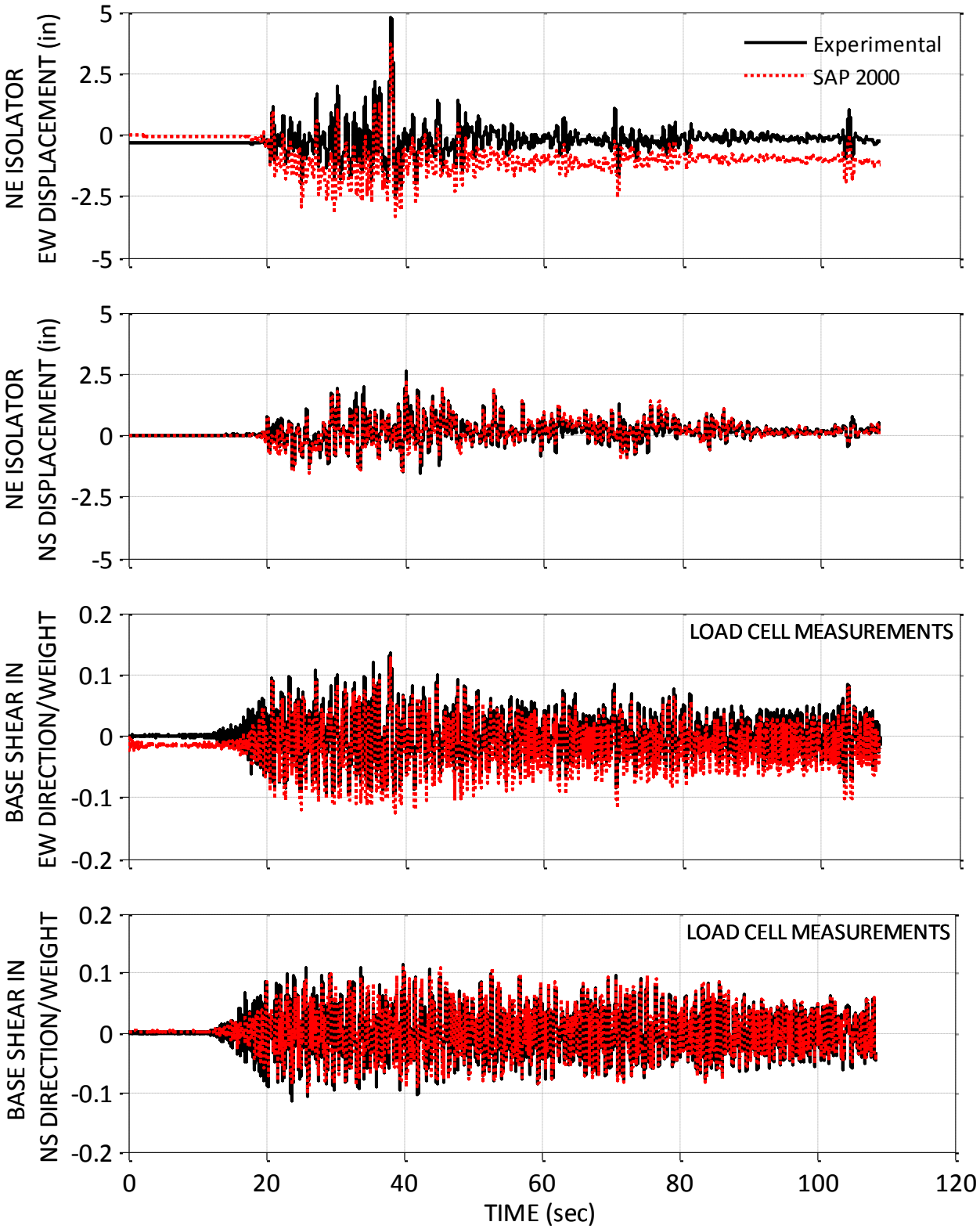

UPPER BUSHING CG
EW ACCELERATION (g)
Experimental
SAP 2000
UPPER BUSHING CG
NS ACCELERATION (g)
TIME (sec)
SPECTRAL
ACCELERATION (g)
FRAME TOP NE CORNER
EW DIRECTION
NS DIRECTION
FREQUENCY (Hz)
BASE SHEAR/WEIGHT
WEIGHT = 47.1 kip
LOAD CELL MEASUREMENTS
TOTAL DISPLACEMENT (in)

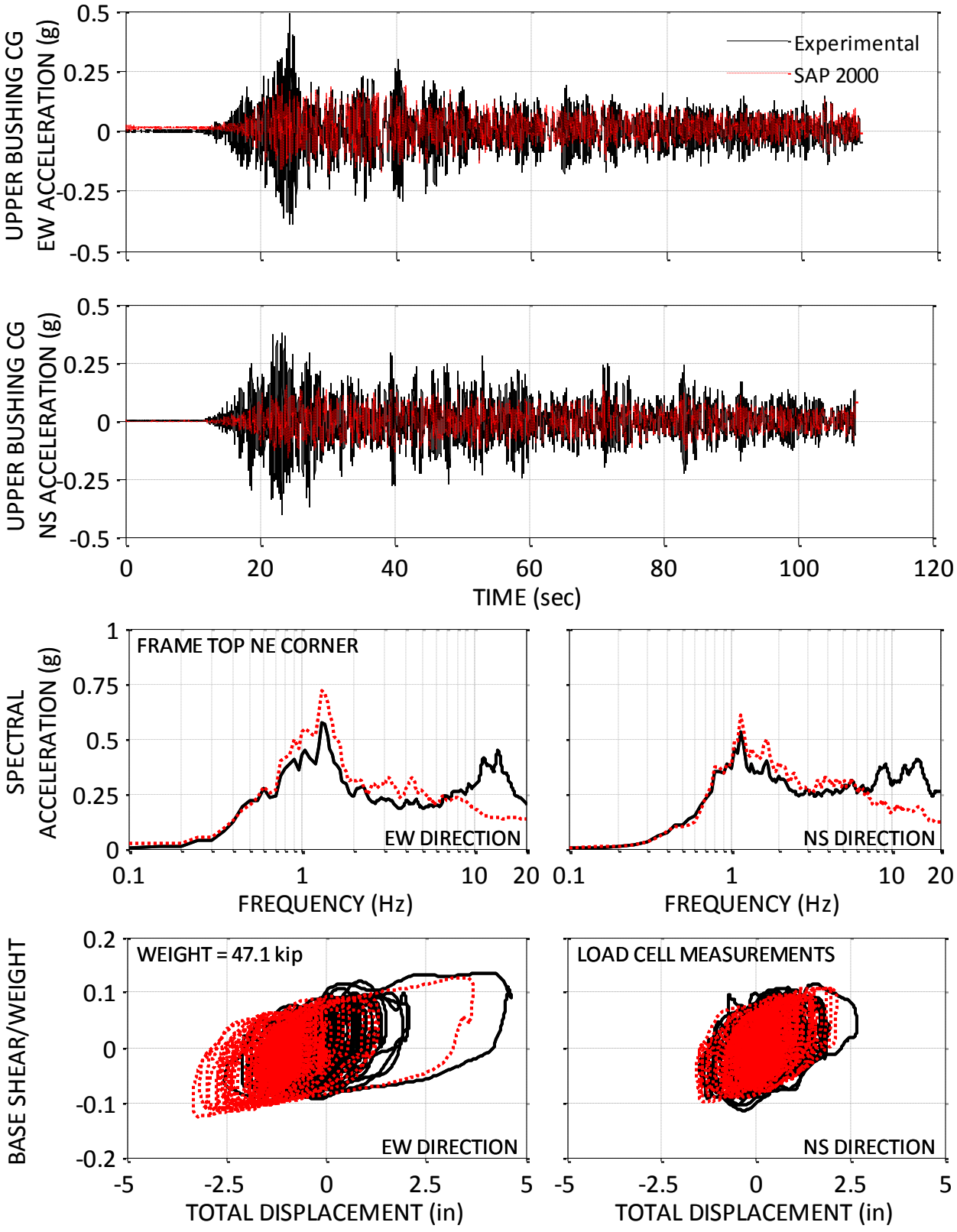
TRIPLE FP SYSTEM (Friction-Bolted Configuration)
PACOIMA DAM 75% BI-AXIAL (S16E in EW direction)
LENGTH SCALE=1 NON-SYMMETRIC BUSHING CONFIGURATION



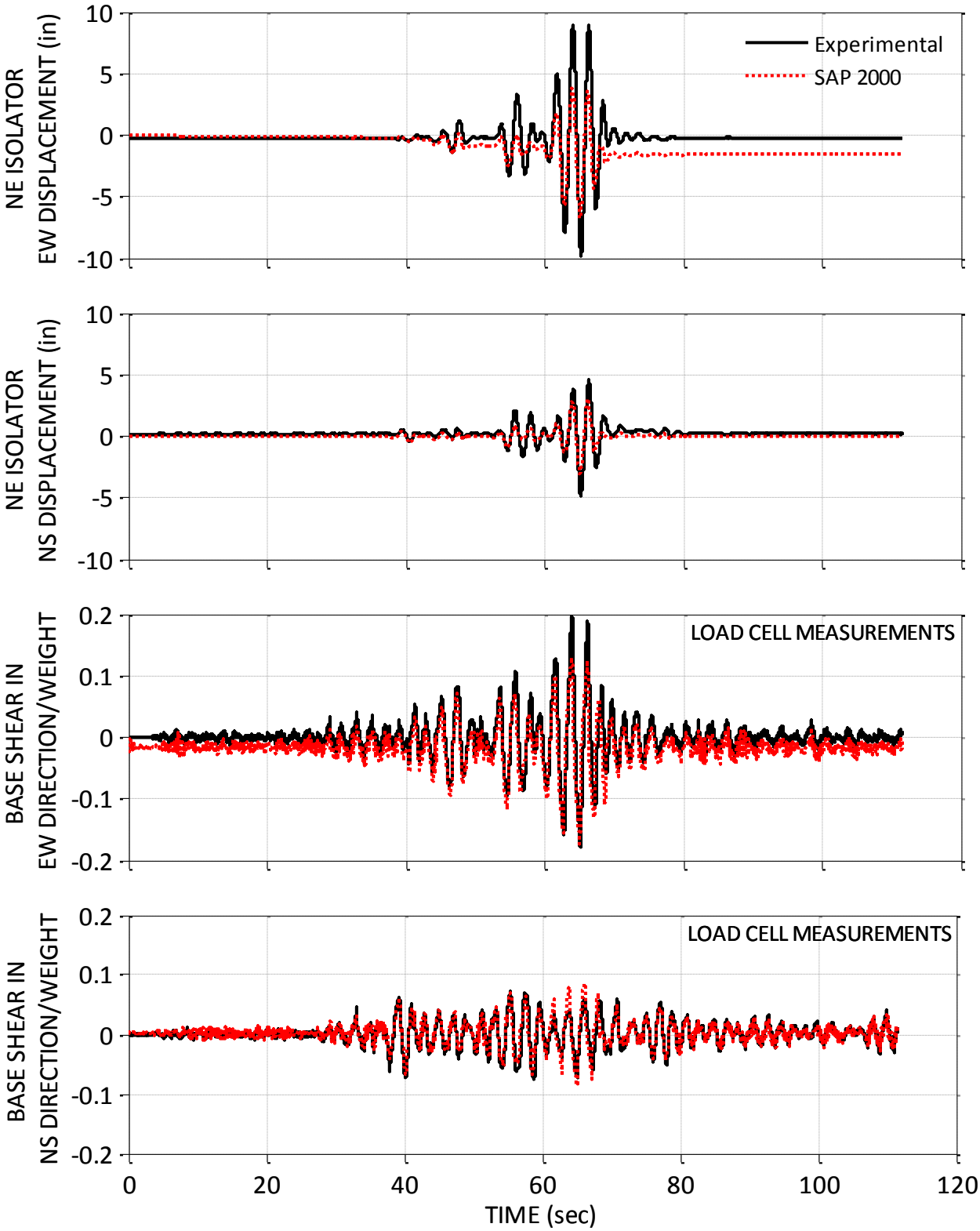

UPPER BUSHING CG
EW ACCELERATION (g)
0.5
0.25
0
-0.25
-0.5
Experimental
SAP 2000
UPPER BUSHING CG
NS ACCELERATION (g)
0
10
20
30
40
50
TIME (sec)
SPECTRAL
ACCELERATION (g)
1
0.75
0.5
0.25
FRAME TOP NE CORNER
EW DIRECTION
NS DIRECTION
0.1
1
10
20
FREQUENCY (Hz)
BASE SHEAR/WEIGHT
0.2
0.1
-0.1
-0.2
WEIGHT = 47.1 kip
LOAD CELL MEASUREMENTS
-8
-4
4
8
TOTAL DISPLACEMENT (in)

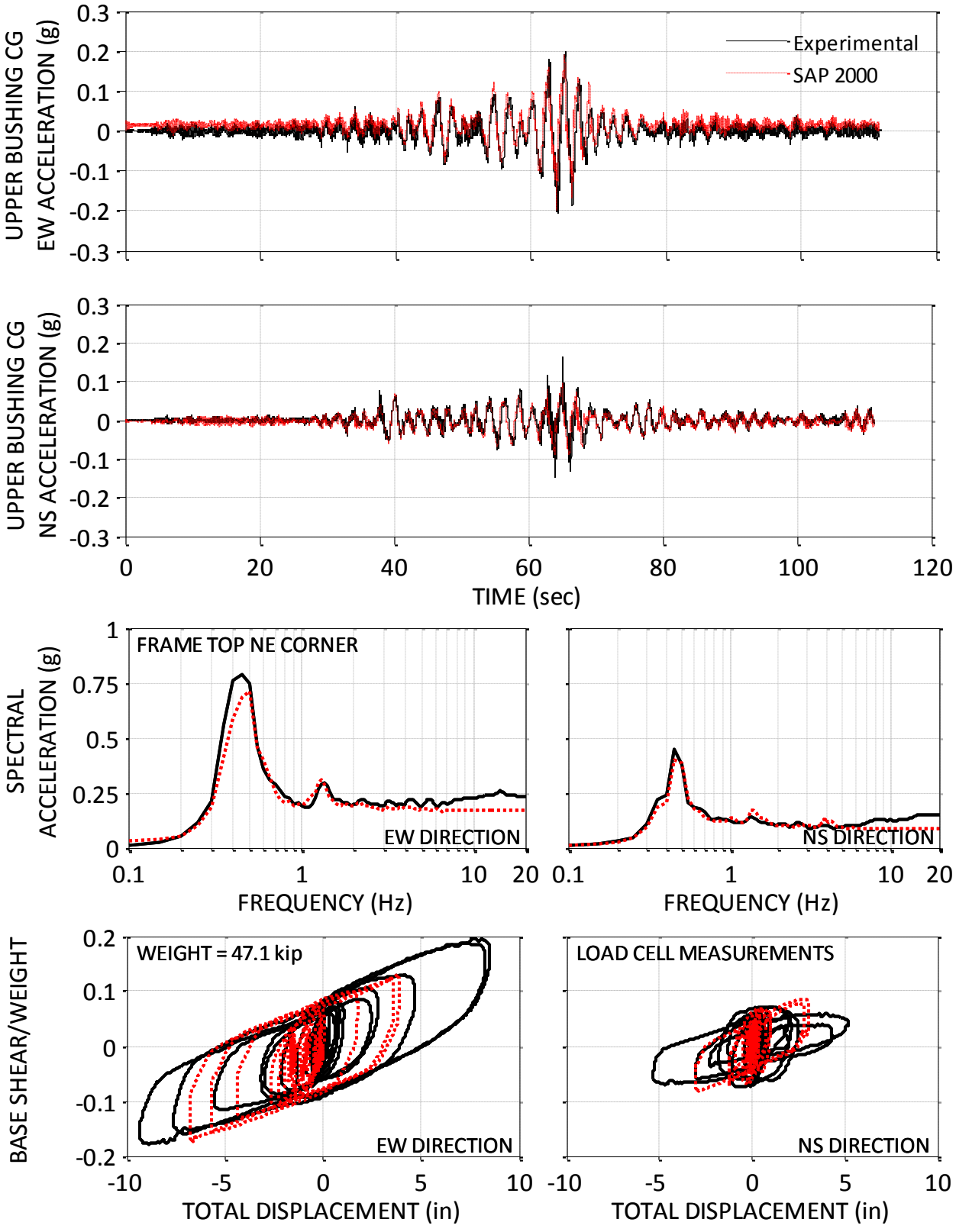
TRIPLE FP SYSTEM (Friction-Bolted Configuration)
CHILE 100% BI-AXIAL (EW in EW direction)
LENGTH SCALE=1 NON-SYMMETRIC BUSHING CONFIGURATION

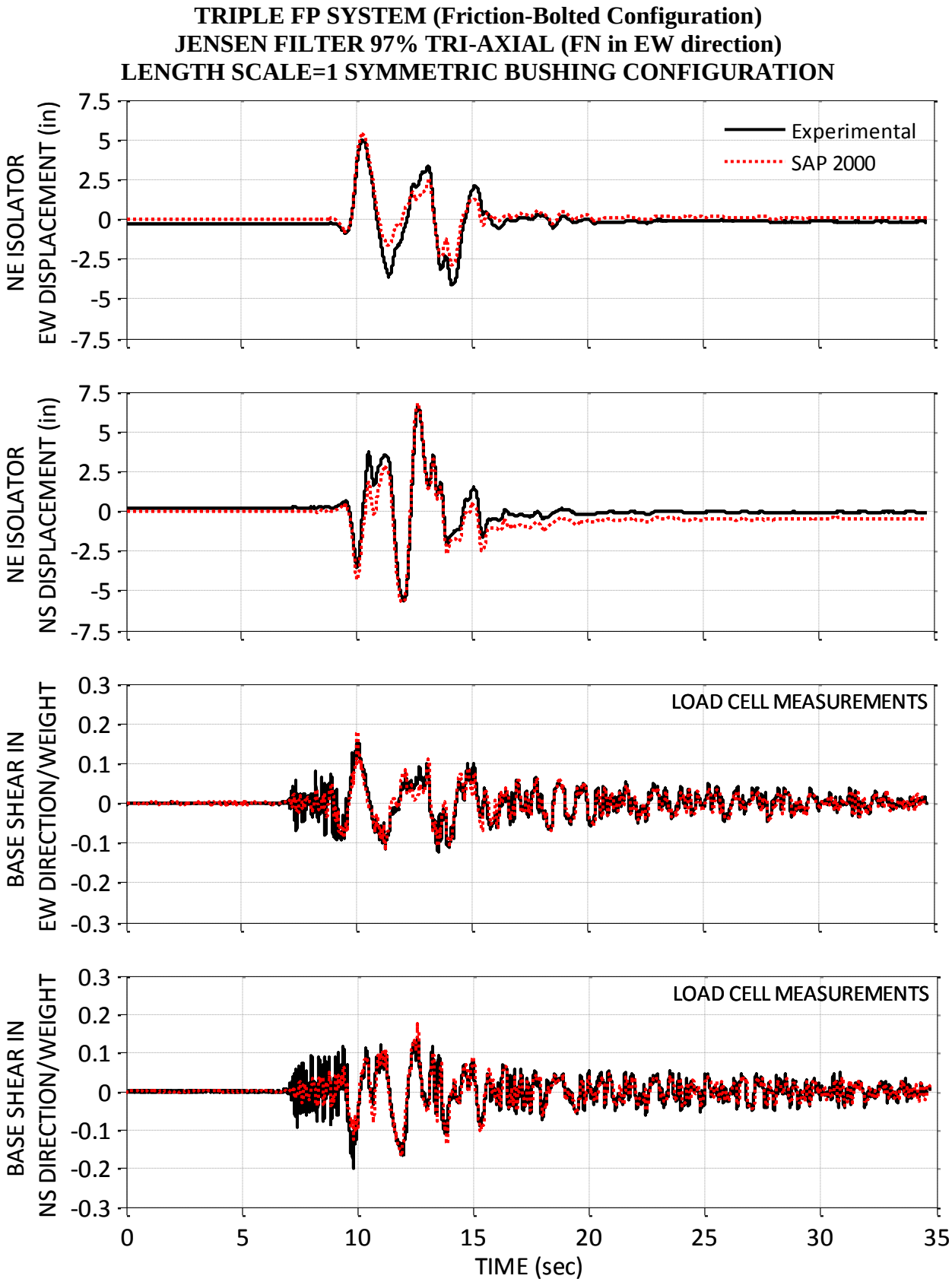


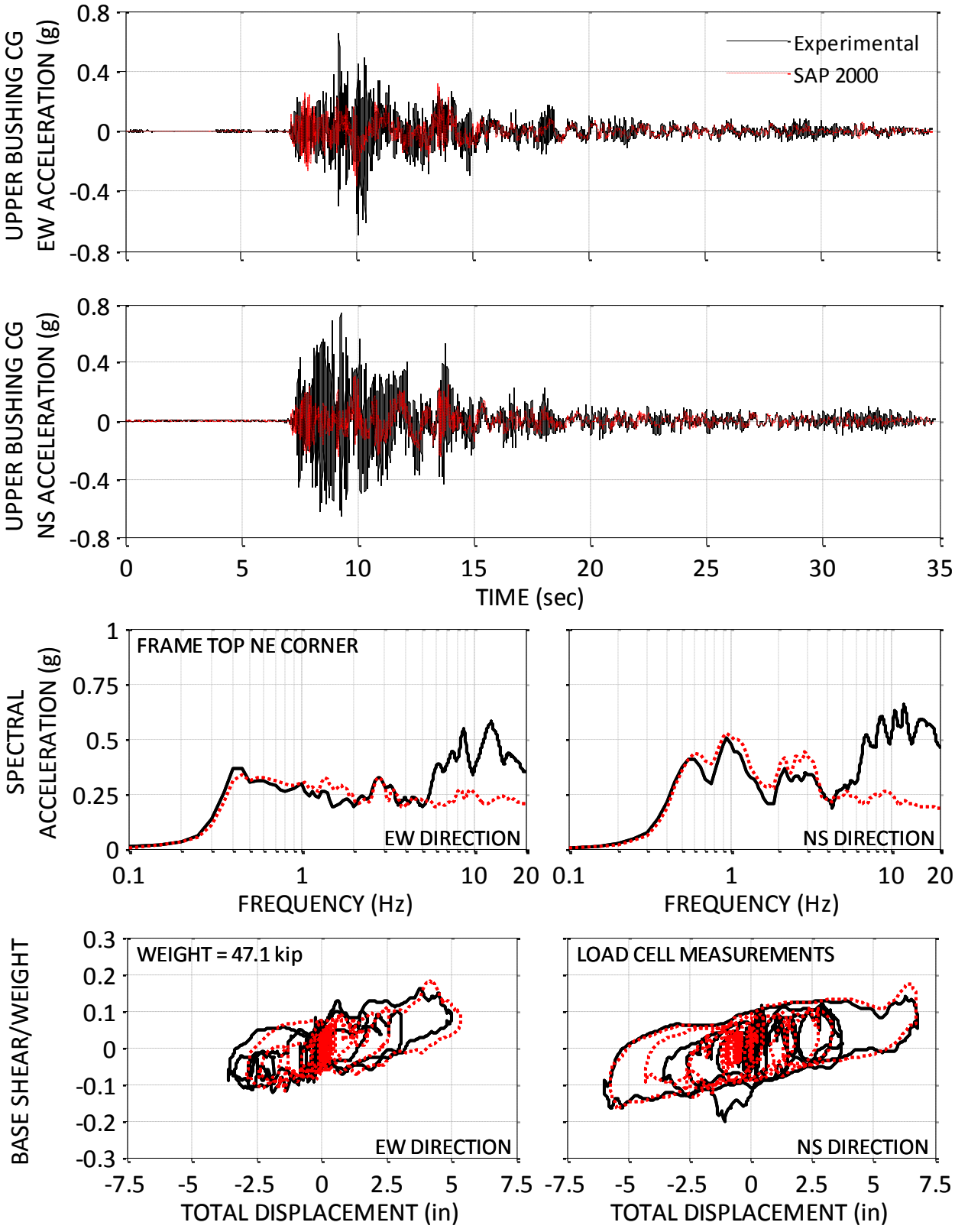

UPPER BUSHING CG
EW ACCELERATION (g)
0.5
0.25
0
-0.25
-0.5
Experimental
SAP 2000
UPPER BUSHING CG
NS ACCELERATION (g)
0
20
40
60
80
100
120
TIME (sec)
SPECTRAL
ACCELERATION (g)
FRAME TOP NE CORNER
EW DIRECTION
NS DIRECTION
1
0.75
0.5
0.25
0
0.1
1
10
20
FREQUENCY (Hz)
BASE SHEAR/WEIGHT
WEIGHT = 47.1 kip
LOAD CELL MEASUREMENTS
0.2
0.1
-0.1
-0.2
-5
-2.5
2.5
5
TOTAL DISPLACEMENT (in)

TRIPLE FP SYSTEM (Friction-Bolted Configuration)
MEXICO 70% BI-AXIAL (N90W in EW direction)
LENGTH SCALE=1 NON-SYMMETRIC BUSHING CONFIGURATION

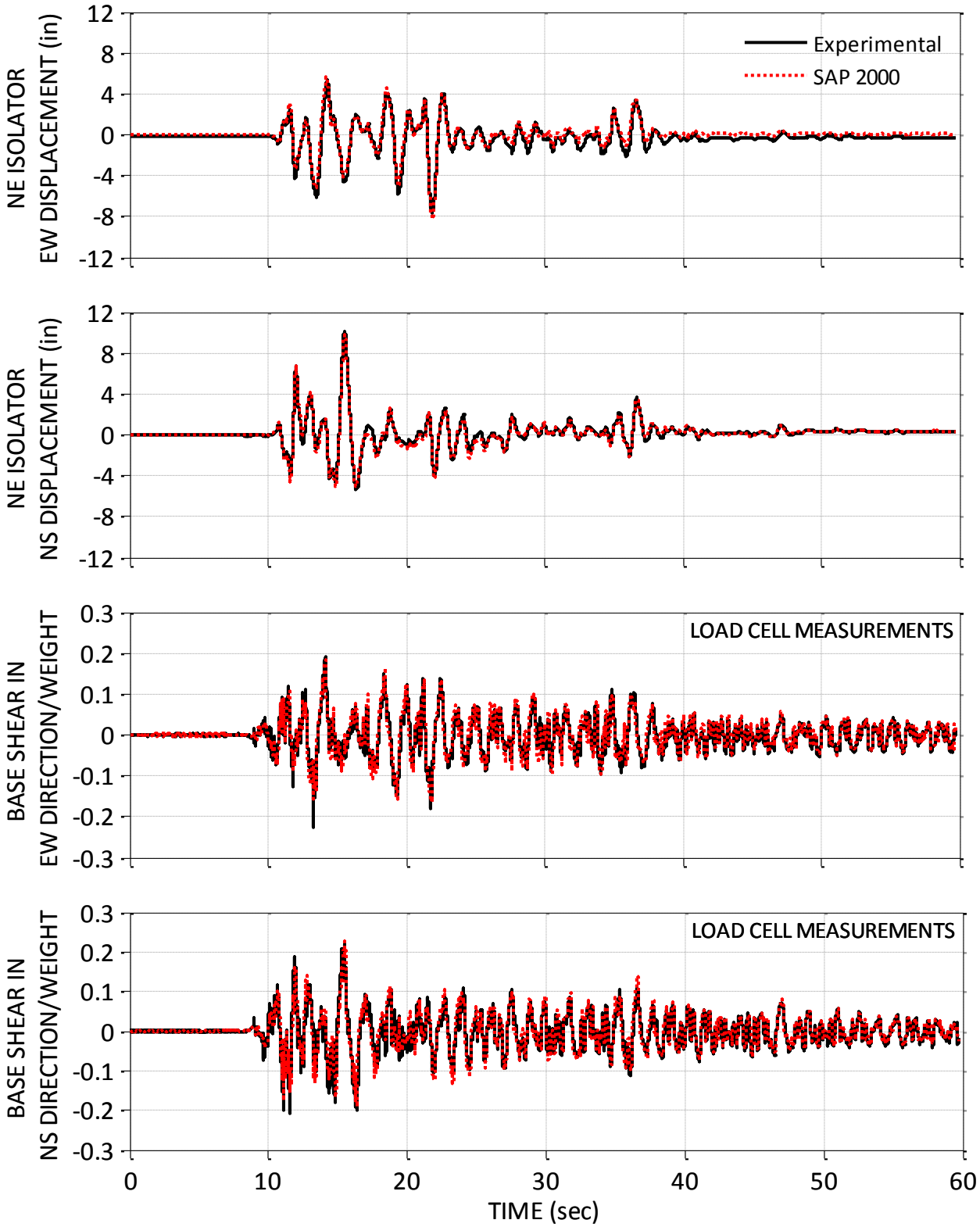


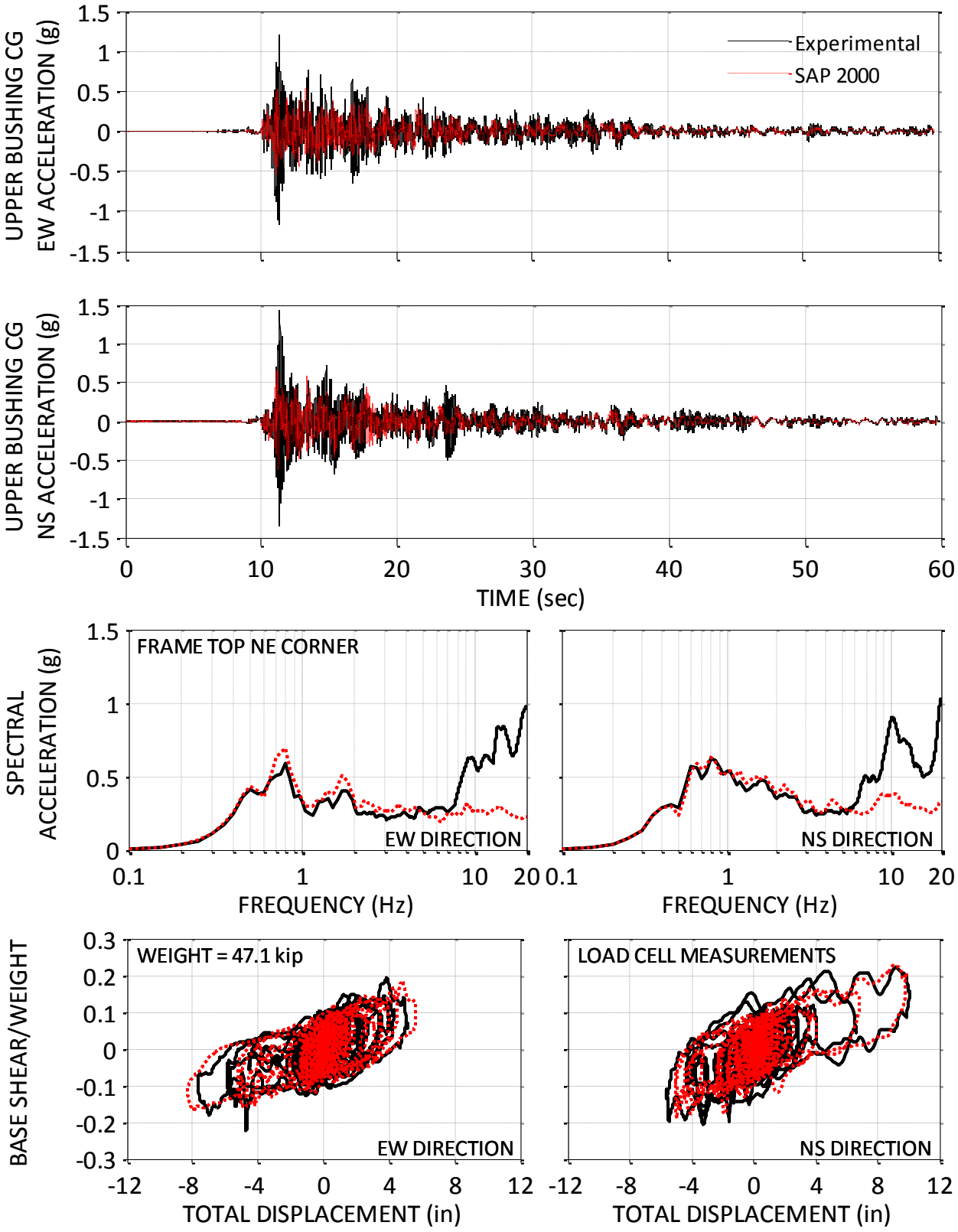

UPPER BUSHING CG
EW ACCELERATION (g)
Experimental
SAP 2000
UPPER BUSHING CG
NS ACCELERATION (g)
TIME (sec)
SPECTRAL
ACCELERATION (g)
FRAME TOP NE CORNER
EW DIRECTION
NS DIRECTION
FREQUENCY (Hz)
BASE SHEAR/WEIGHT
WEIGHT = 47.1 kip
LOAD CELL MEASUREMENTS
TOTAL DISPLACEMENT (in)


TRIPLE FP SYSTEM (Friction-Bolted Configuration)
JENSEN FILTER 97% TRI-AXIAL (FN in EW direction)
LENGTH SCALE=1 SYMMETRIC BUSHING CONFIGURATION
NE ISOLATOR EW DISPLACEMENT (in)
Experimental
SAP 2000
NE ISOLATOR NS DISPLACEMENT (in)
BASE SHEAR IN EW DIRECTION/WEIGHT
LOAD CELL MEASUREMENTS
BASE SHEAR IN NS DIRECTION/WEIGHT
LOAD CELL MEASUREMENTS
TIME (sec)

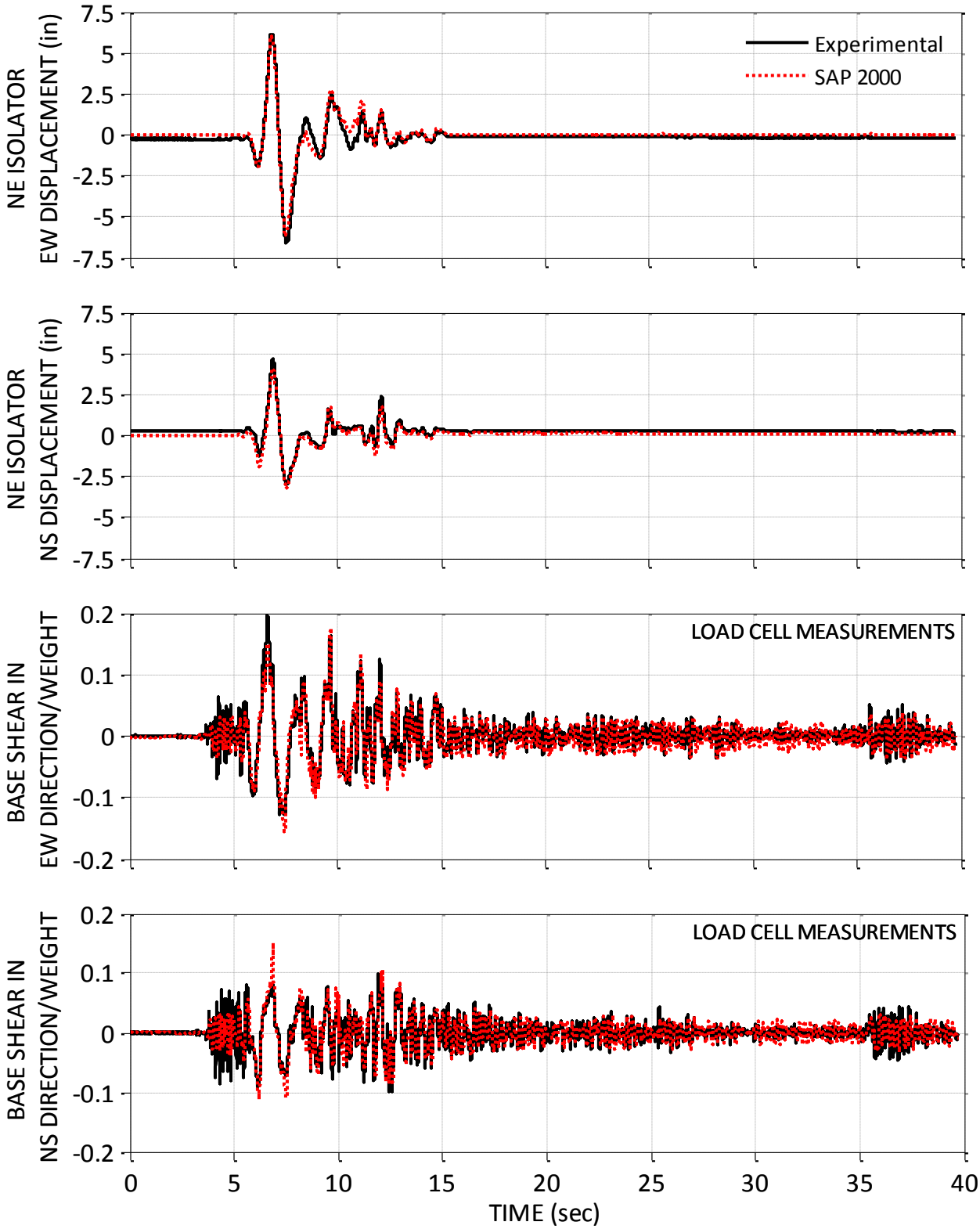

UPPER BUSHING CG
EW ACCELERATION (g)
0.8
0.4
0
-0.4
-0.8
Experimental
SAP 2000
UPPER BUSHING CG
NS ACCELERATION (g)
0.8
0.4
0
-0.4
-0.8
0
5
10
15
20
25
30
35
TIME (sec)
SPECTRAL
ACCELERATION (g)
1
0.75
0.5
0.25
0
FRAME TOP NE CORNER
EW DIRECTION
NS DIRECTION
0.1
1
10
20
FREQUENCY (Hz)
FREQUENCY (Hz)
BASE SHEAR/WEIGHT
0.3
0.2
0.1
0
-0.1
-0.2
-0.3
WEIGHT = 47.1 kip
LOAD CELL MEASUREMENTS
EW DIRECTION
NS DIRECTION
-7.5
-5
-2.5
0
2.5
5
7.5
TOTAL DISPLACEMENT (in)
TOTAL DISPLACEMENT (in)

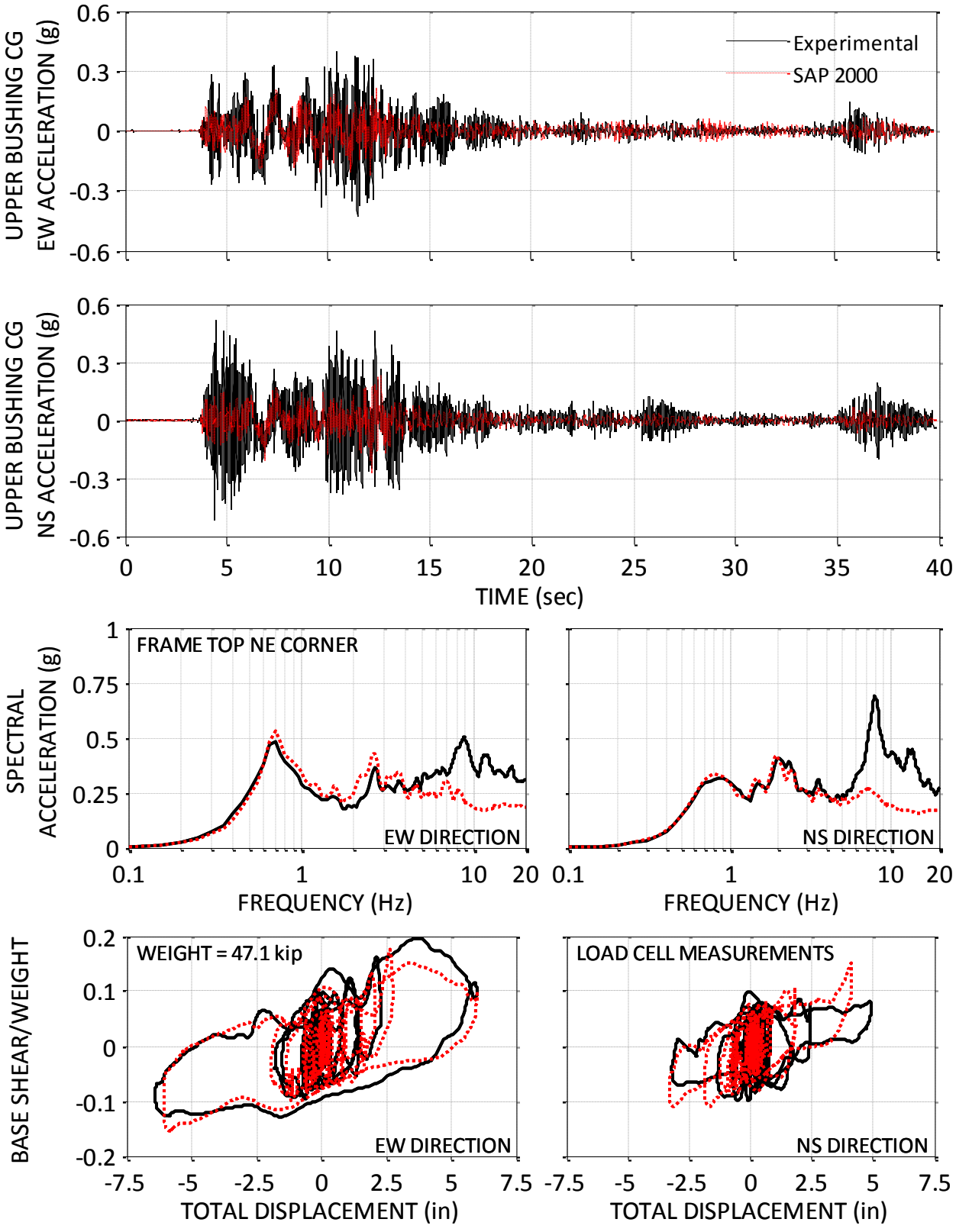
TRIPLE FP SYSTEM (Friction-Bolted Configuration)
EL CENTRO 300% TRI-AXIAL (N90W in EW direction)
LENGTH SCALE=1 SYMMETRIC BUSHING CONFIGURATION



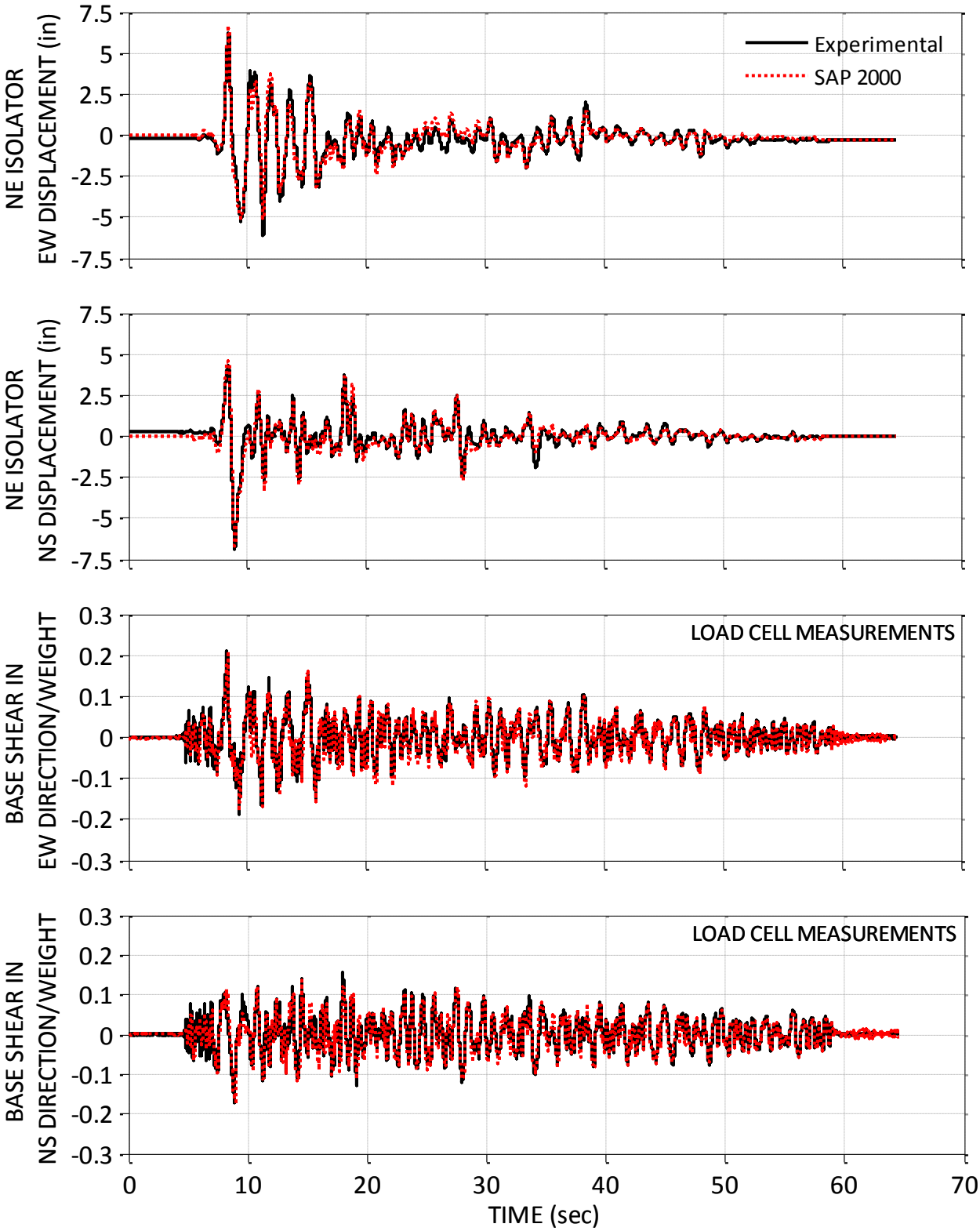

UPPER BUSHING CG
EW ACCELERATION (g)
Experimental
SAP 2000
UPPER BUSHING CG
NS ACCELERATION (g)
TIME (sec)
SPECTRAL
ACCELERATION (g)
FRAME TOP NE CORNER
EW DIRECTION
NS DIRECTION
FREQUENCY (Hz)
BASE SHEAR/WEIGHT
WEIGHT = 47.1 kip
LOAD CELL MEASUREMENTS
TOTAL DISPLACEMENT (in)

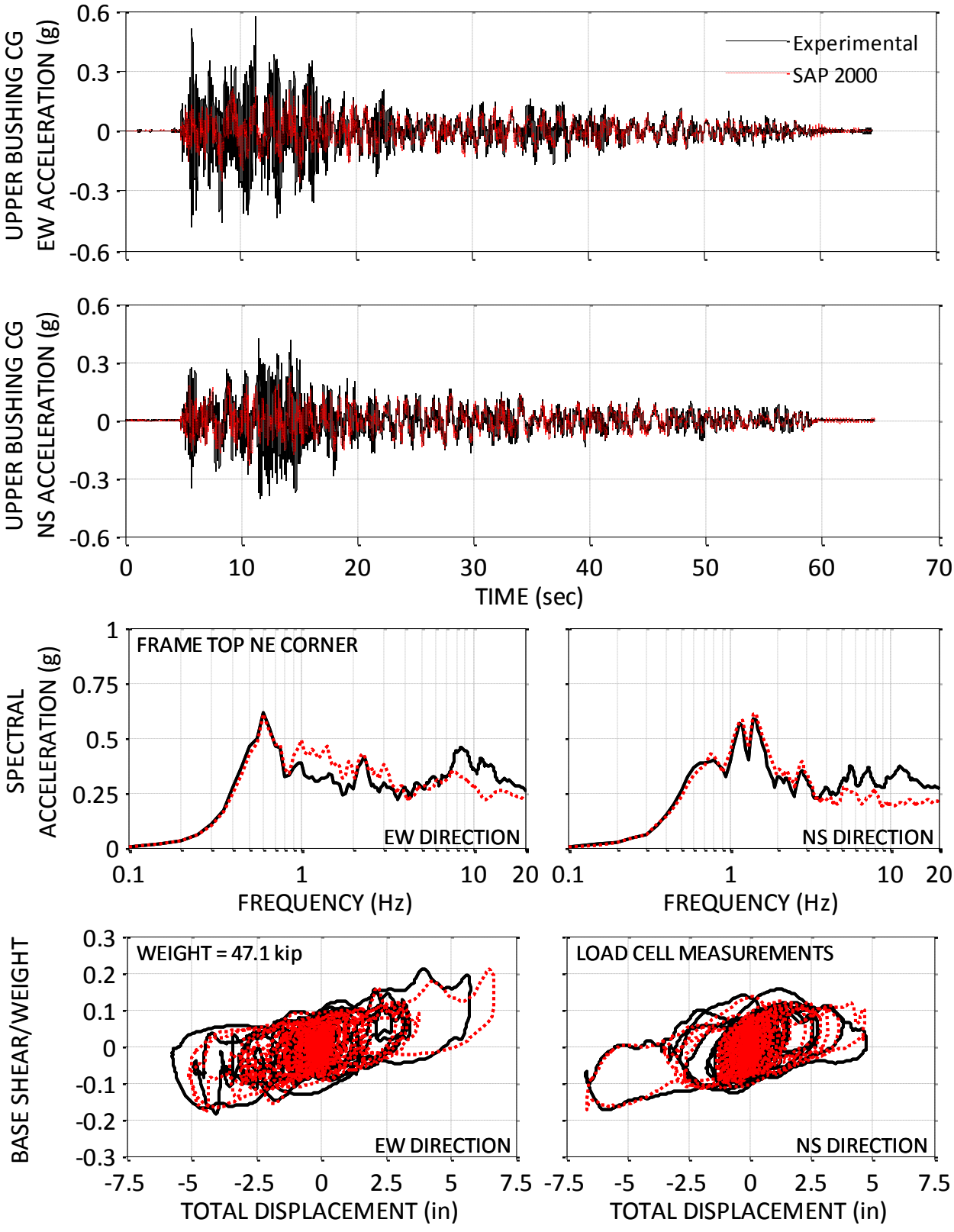
TRIPLE FP SYSTEM (Friction-Bolted Configuration)
PACOIMA DAM 75% TRI-AXIAL (S16E in EW direction)
LENGTH SCALE=1 SYMMETRIC BUSHING CONFIGURATION



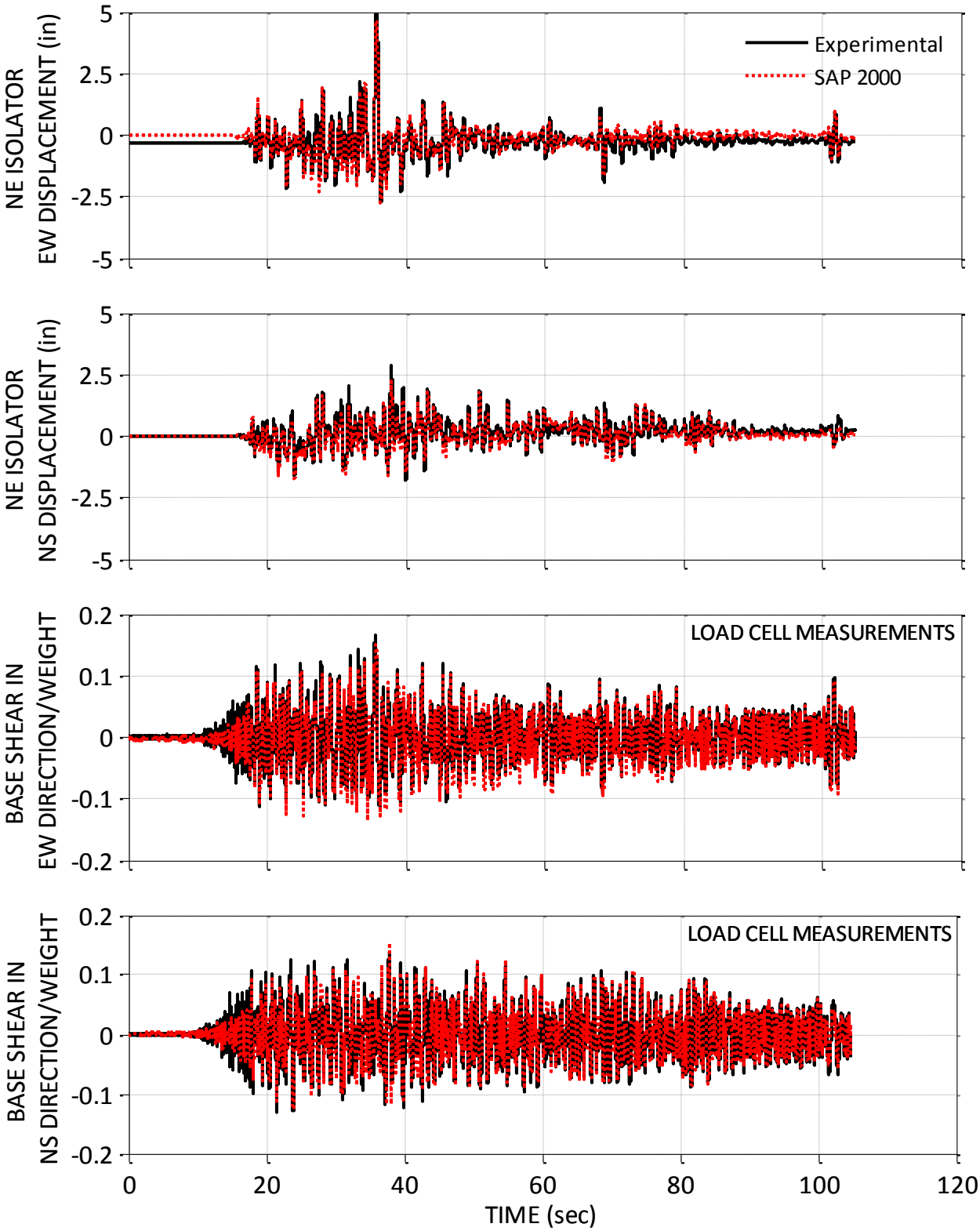

UPPER BUSHING CG
EW ACCELERATION (g)
Experimental
SAP 2000
UPPER BUSHING CG
NS ACCELERATION (g)
TIME (sec)
SPECTRAL
ACCELERATION (g)
FRAME TOP NE CORNER
EW DIRECTION
NS DIRECTION
FREQUENCY (Hz)
BASE SHEAR/WEIGHT
WEIGHT = 47.1 kip
LOAD CELL MEASUREMENTS
TOTAL DISPLACEMENT (in)

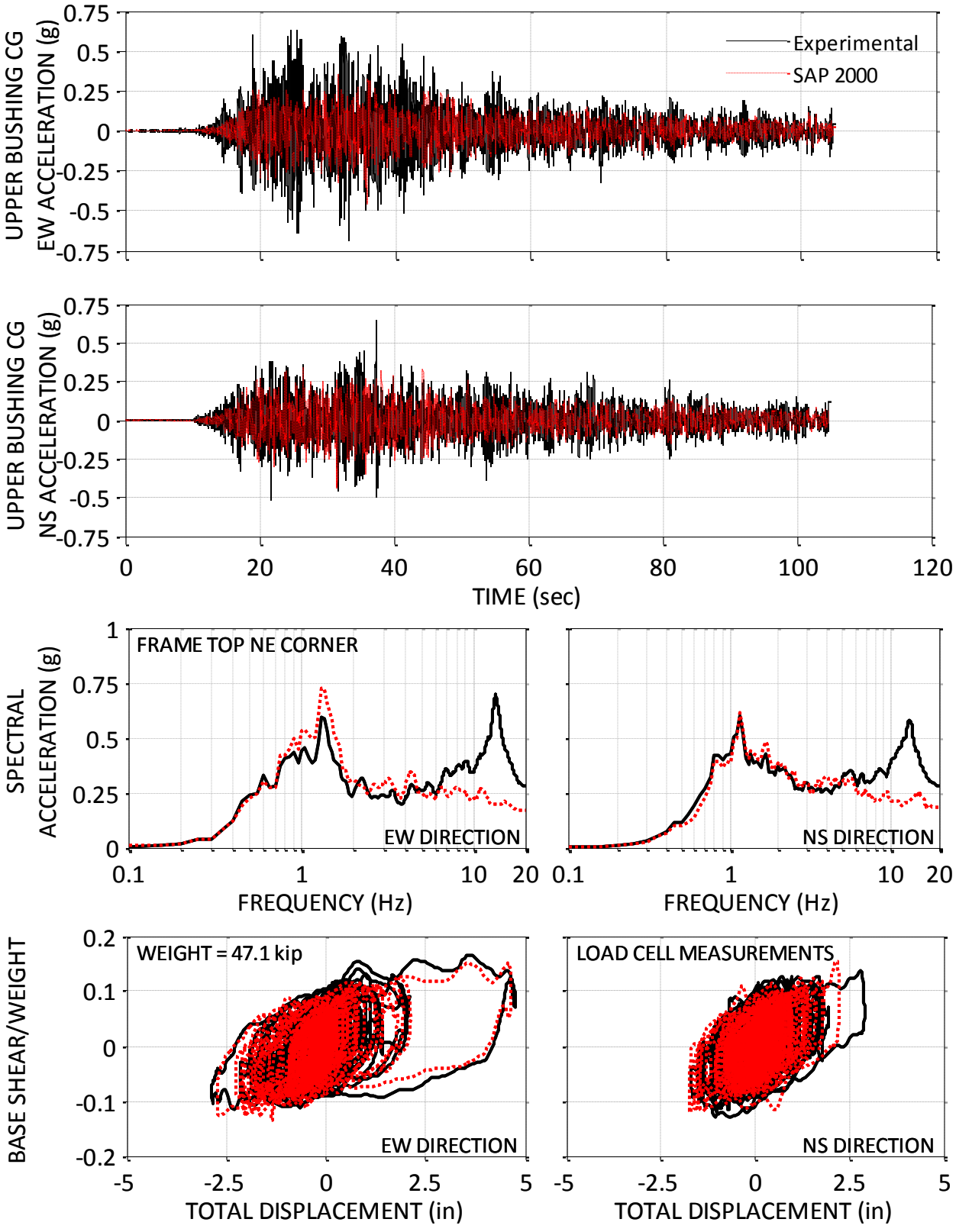
TRIPLE FP SYSTEM (Friction-Bolted Configuration)
TAFT 500% TRI-AXIAL (S69E in EW direction)
LENGTH SCALE=1 SYMMETRIC BUSHING CONFIGURATION



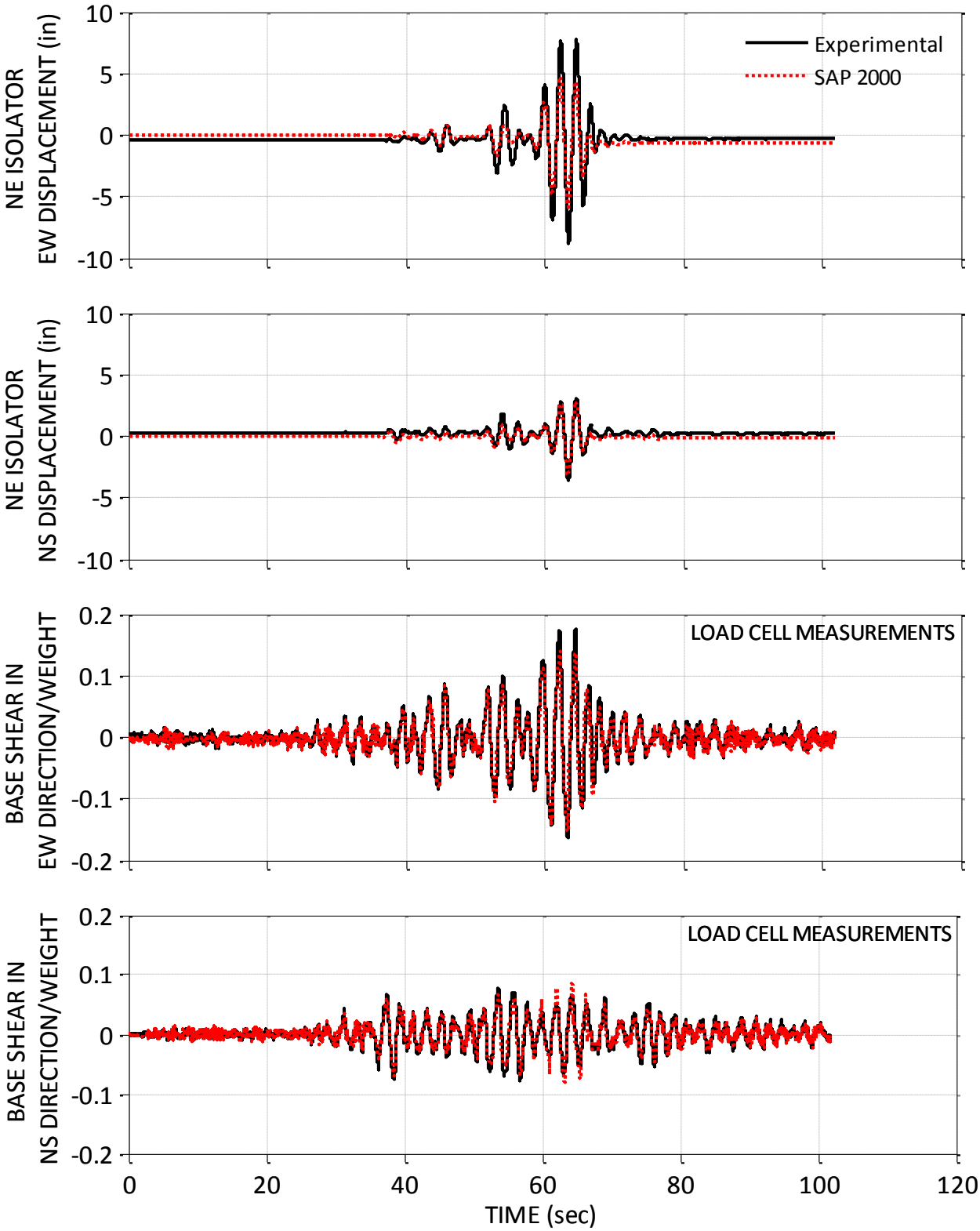

UPPER BUSHING CG
EW ACCELERATION (g)
Experimental
SAP 2000
UPPER BUSHING CG
NS ACCELERATION (g)
TIME (sec)
SPECTRAL
ACCELERATION (g)
FRAME TOP NE CORNER
EW DIRECTION
NS DIRECTION
FREQUENCY (Hz)
BASE SHEAR/WEIGHT
WEIGHT = 47.1 kip
LOAD CELL MEASUREMENTS
TOTAL DISPLACEMENT (in)

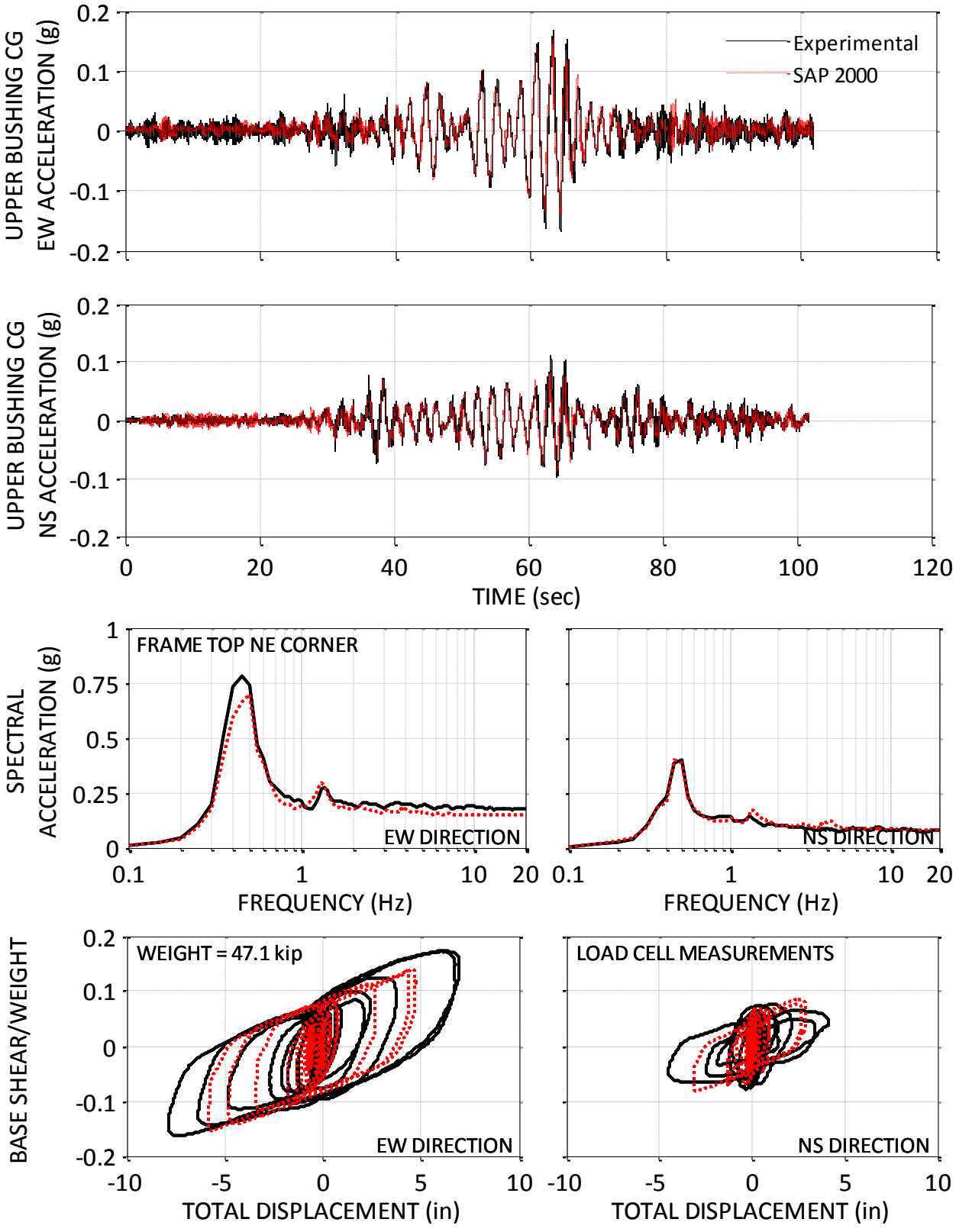
TRIPLE FP SYSTEM (Friction-Bolted Configuration)
CHILE 100% TRI-AXIAL (EW in EW direction)
LENGTH SCALE=1 SYMMETRIC BUSHING CONFIGURATION



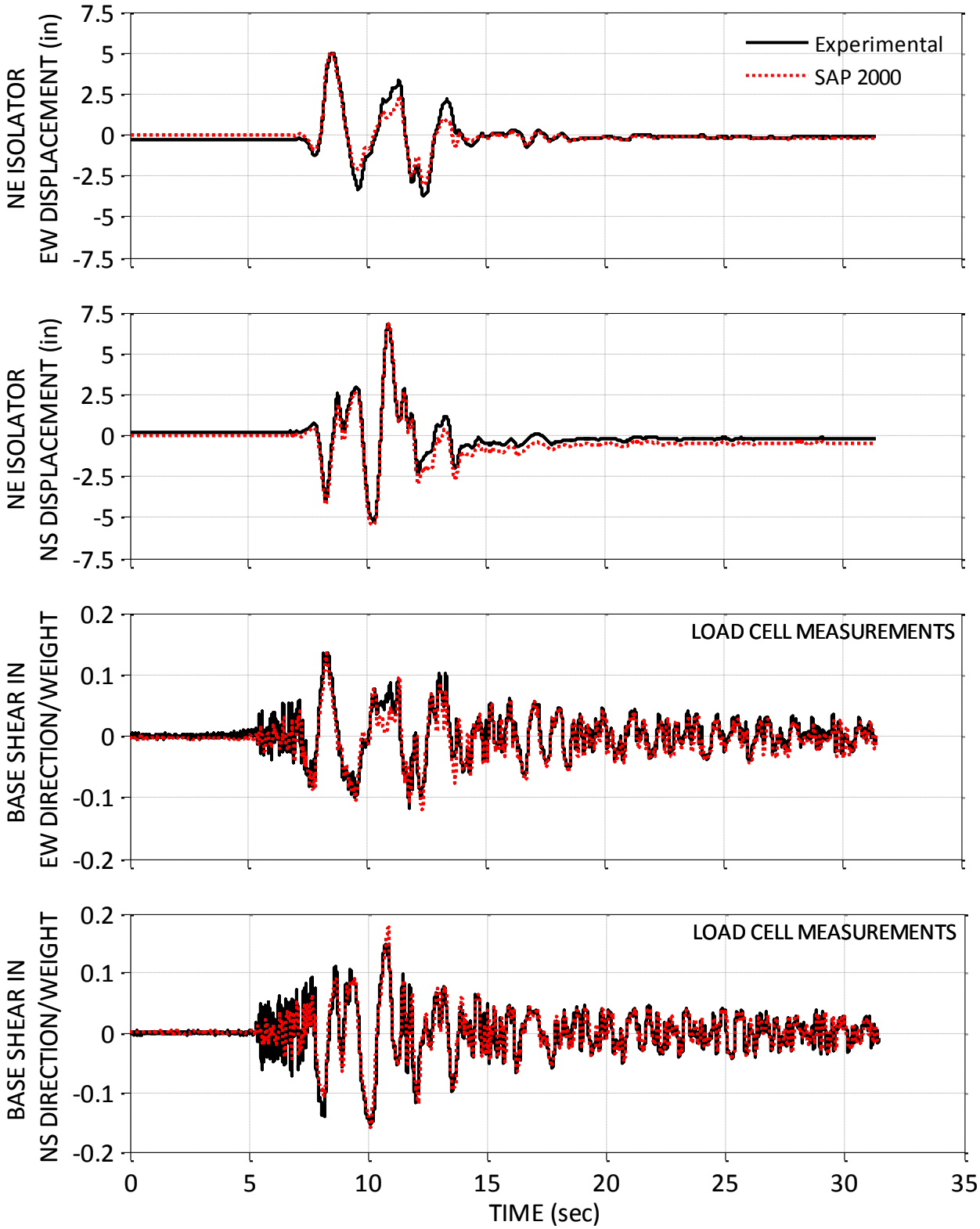

UPPER BUSHING CG
EW ACCELERATION (g)
0.75
0.5
0.25
0
-0.25
-0.5
-0.75
Experimental
SAP 2000
UPPER BUSHING CG
NS ACCELERATION (g)
0
20
40
60
80
100
120
TIME (sec)
SPECTRAL
ACCELERATION (g)
1
FRAME TOP NE CORNER
EW DIRECTION
NS DIRECTION
0.1
10
20
FREQUENCY (Hz)
BASE SHEAR/WEIGHT
0.2
0.1
-0.1
-0.2
WEIGHT = 47.1 kip
LOAD CELL MEASUREMENTS
-5
-2.5
2.5
5
TOTAL DISPLACEMENT (in)

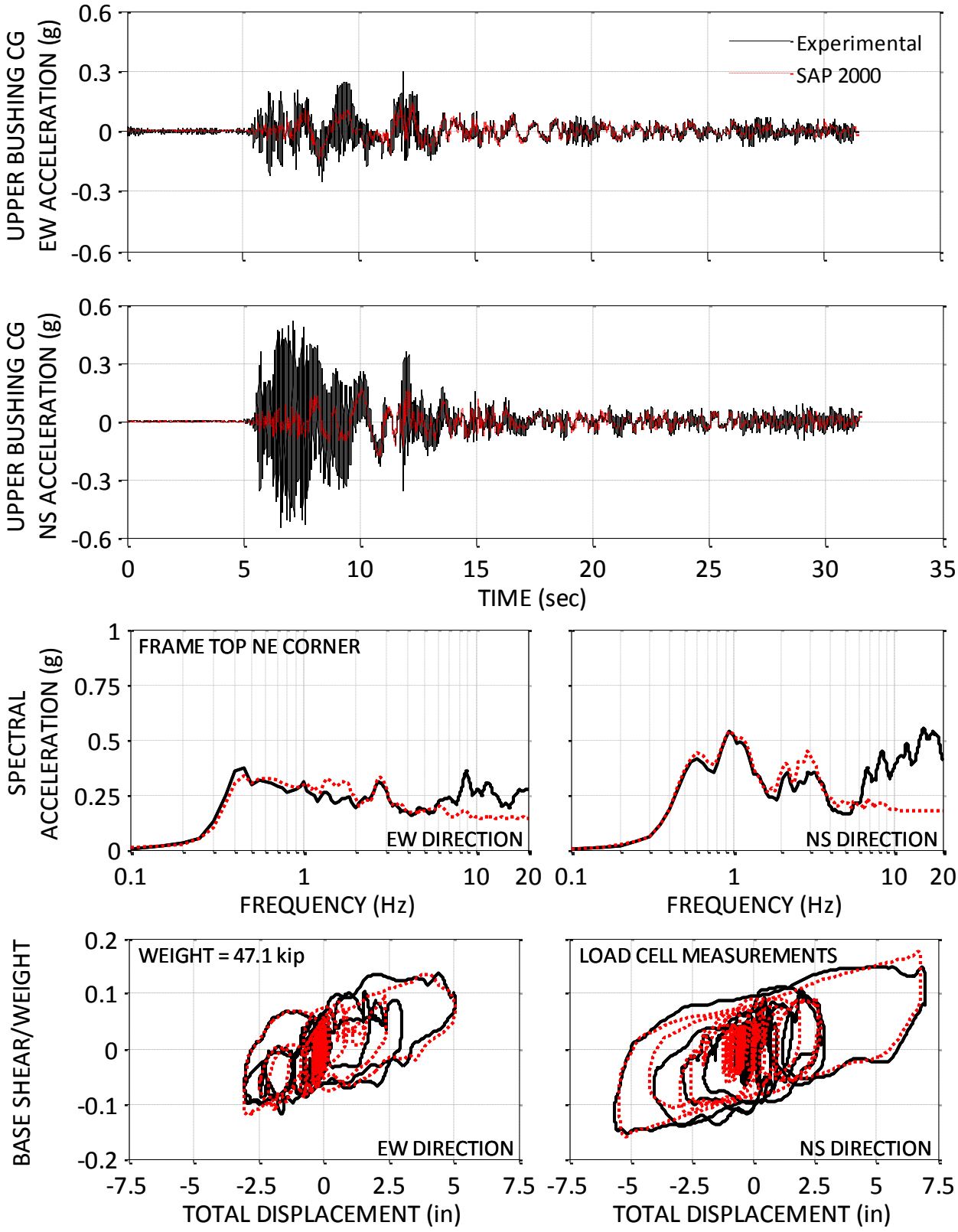
TRIPLE FP SYSTEM (Friction-Bolted Configuration)
MEXICO 70% TRI-AXIAL (N90W in EW direction)
LENGTH SCALE=1 SYMMETRIC BUSHING CONFIGURATION



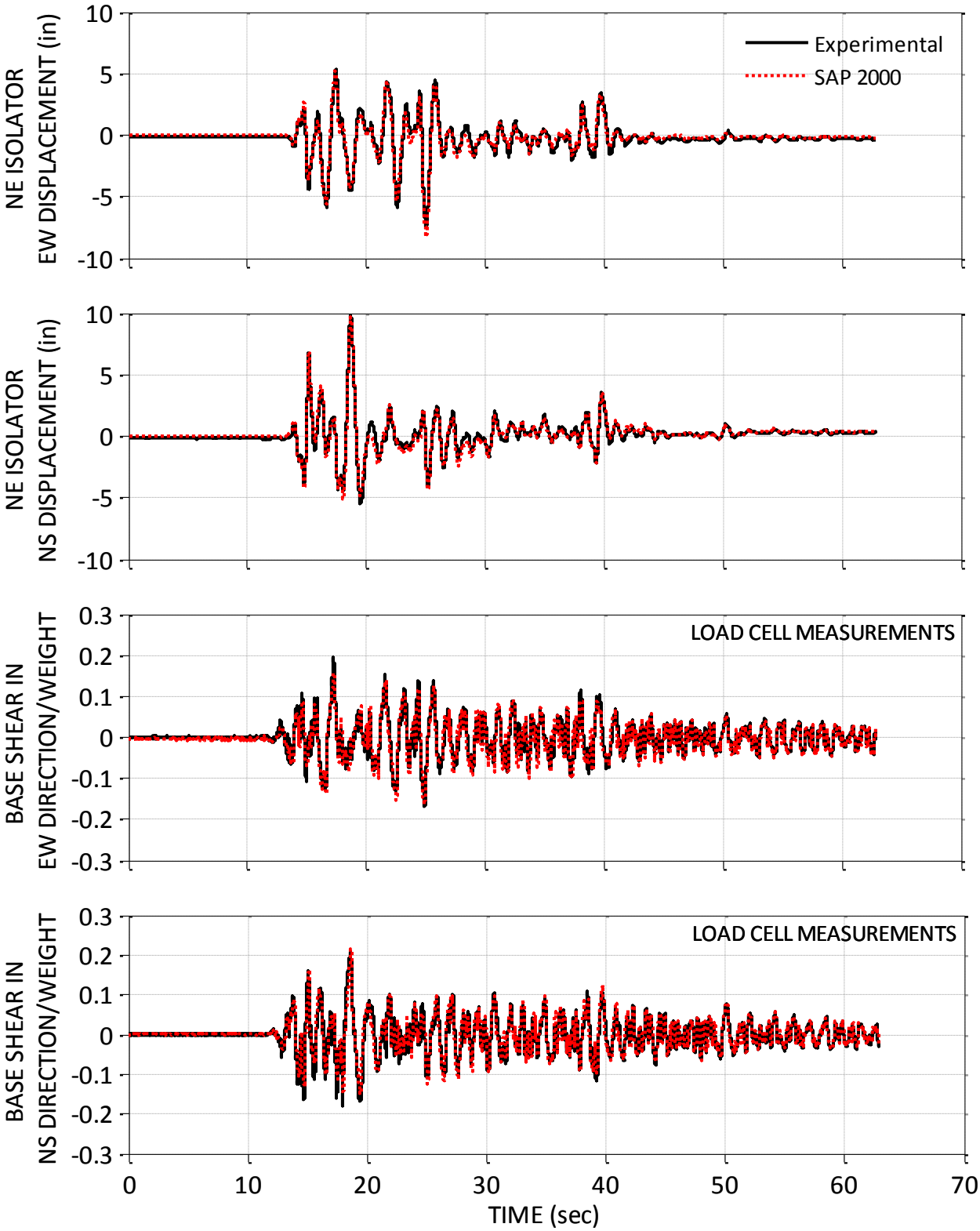

UPPER BUSHING CG
EW ACCELERATION (g)
Experimental
SAP 2000
UPPER BUSHING CG
NS ACCELERATION (g)
TIME (sec)
SPECTRAL
ACCELERATION (g)
FRAME TOP NE CORNER
EW DIRECTION
NS DIRECTION
FREQUENCY (Hz)
BASE SHEAR/WEIGHT
WEIGHT = 47.1 kip
LOAD CELL MEASUREMENTS
TOTAL DISPLACEMENT (in)

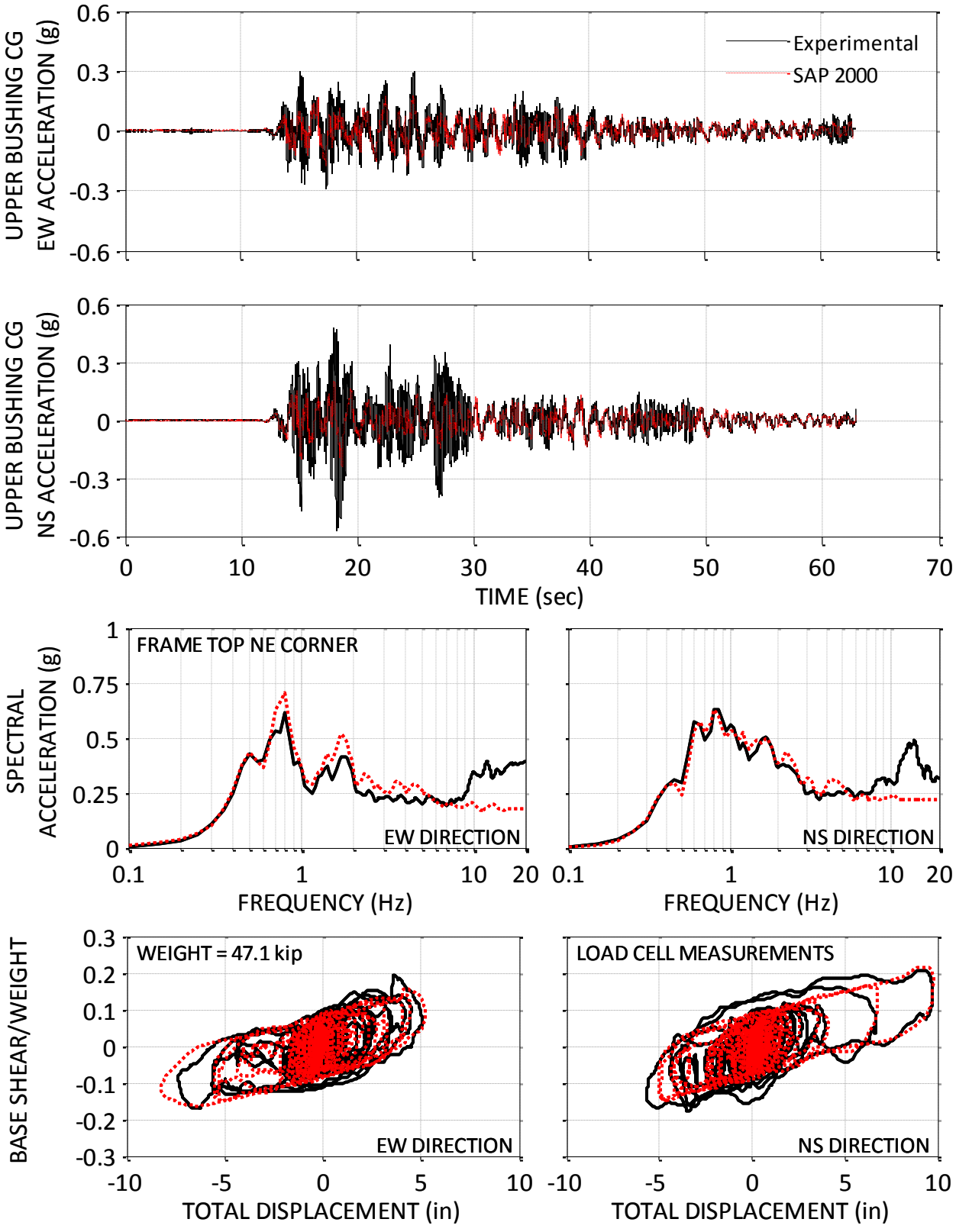
TRIPLE FP SYSTEM (Friction-Bolted Configuration)
JENSEN FILTER 97% BI-AXIAL (FN in EW direction)
LENGTH SCALE=1 SYMMETRIC BUSHING CONFIGURATION



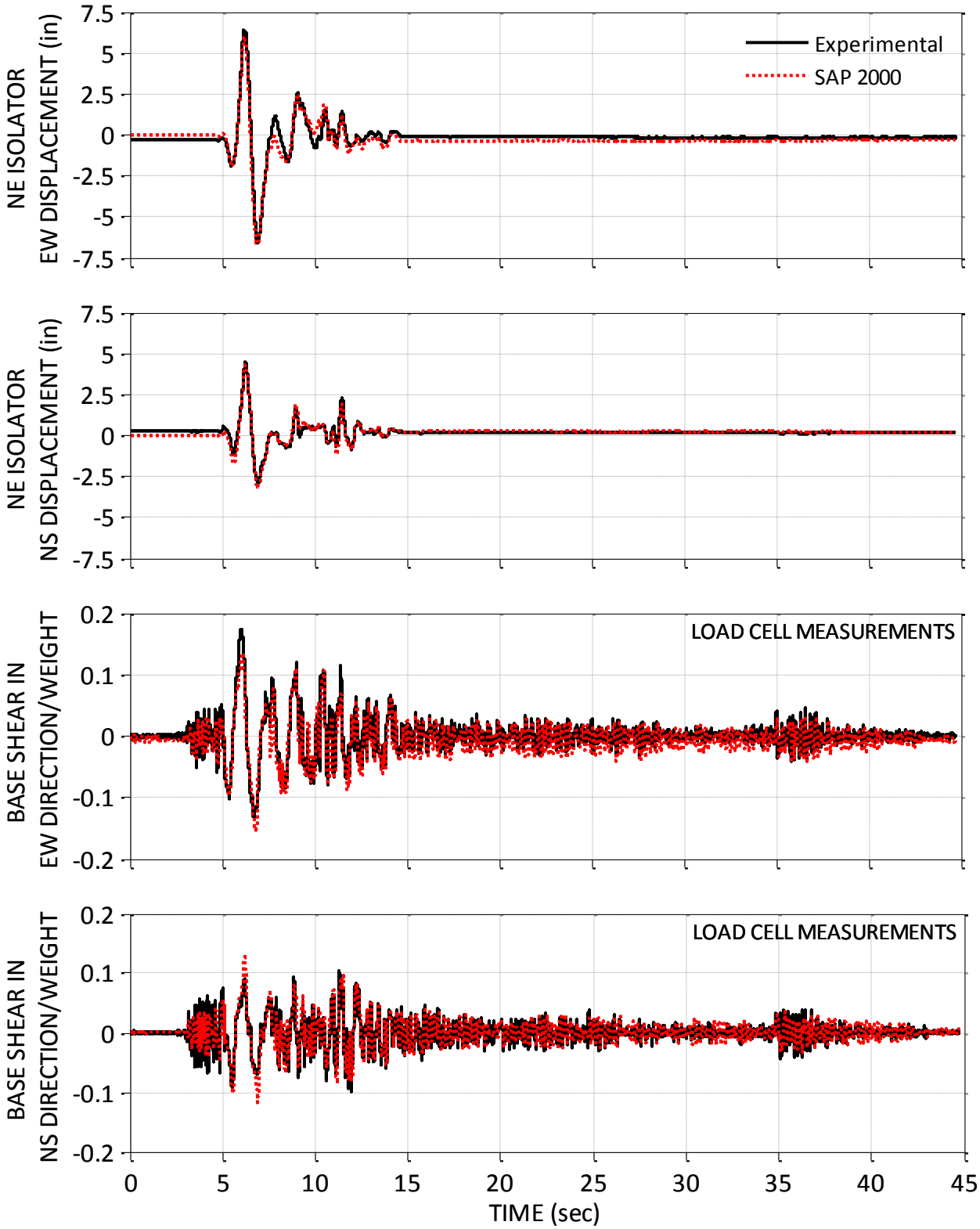

UPPER BUSHING CG
EW ACCELERATION (g)
0.6
0.3
0
-0.3
-0.6
Experimental
SAP 2000
UPPER BUSHING CG
NS ACCELERATION (g)
0
5
10
15
20
25
30
35
TIME (sec)
SPECTRAL
ACCELERATION (g)
1
0.75
0.5
0.25
FRAME TOP NE CORNER
EW DIRECTION
NS DIRECTION
0.1
FREQUENCY (Hz)
BASE SHEAR/WEIGHT
0.2
0.1
-0.1
-0.2
WEIGHT = 47.1 kip
LOAD CELL MEASUREMENTS
-7.5
-5
-2.5
2.5
5
7.5
TOTAL DISPLACEMENT (in)

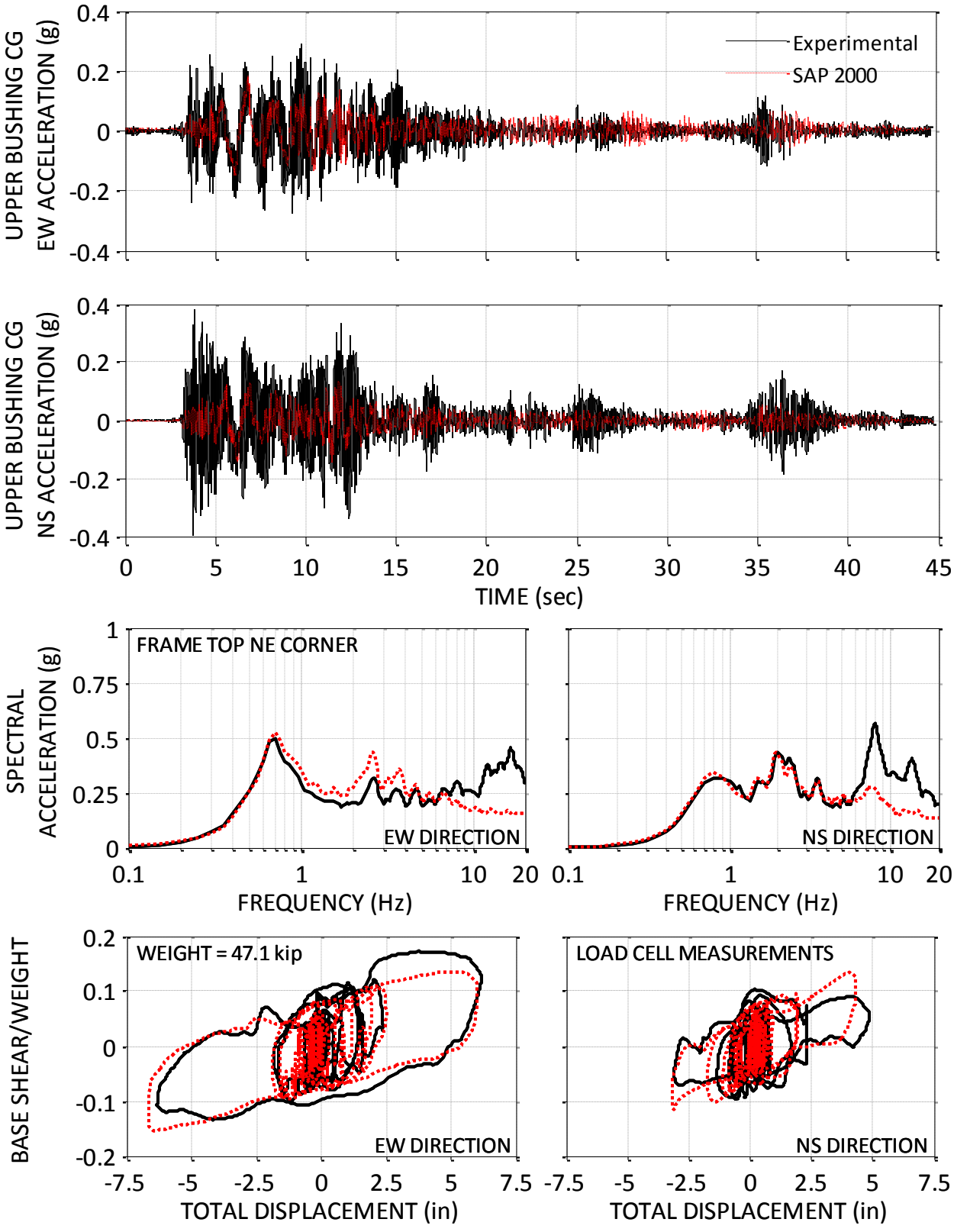
TRIPLE FP SYSTEM (Friction-Bolted Configuration)
EL CENTRO 300% BI-AXIAL (N90W in EW direction)
LENGTH SCALE=1 SYMMETRIC BUSHING CONFIGURATION



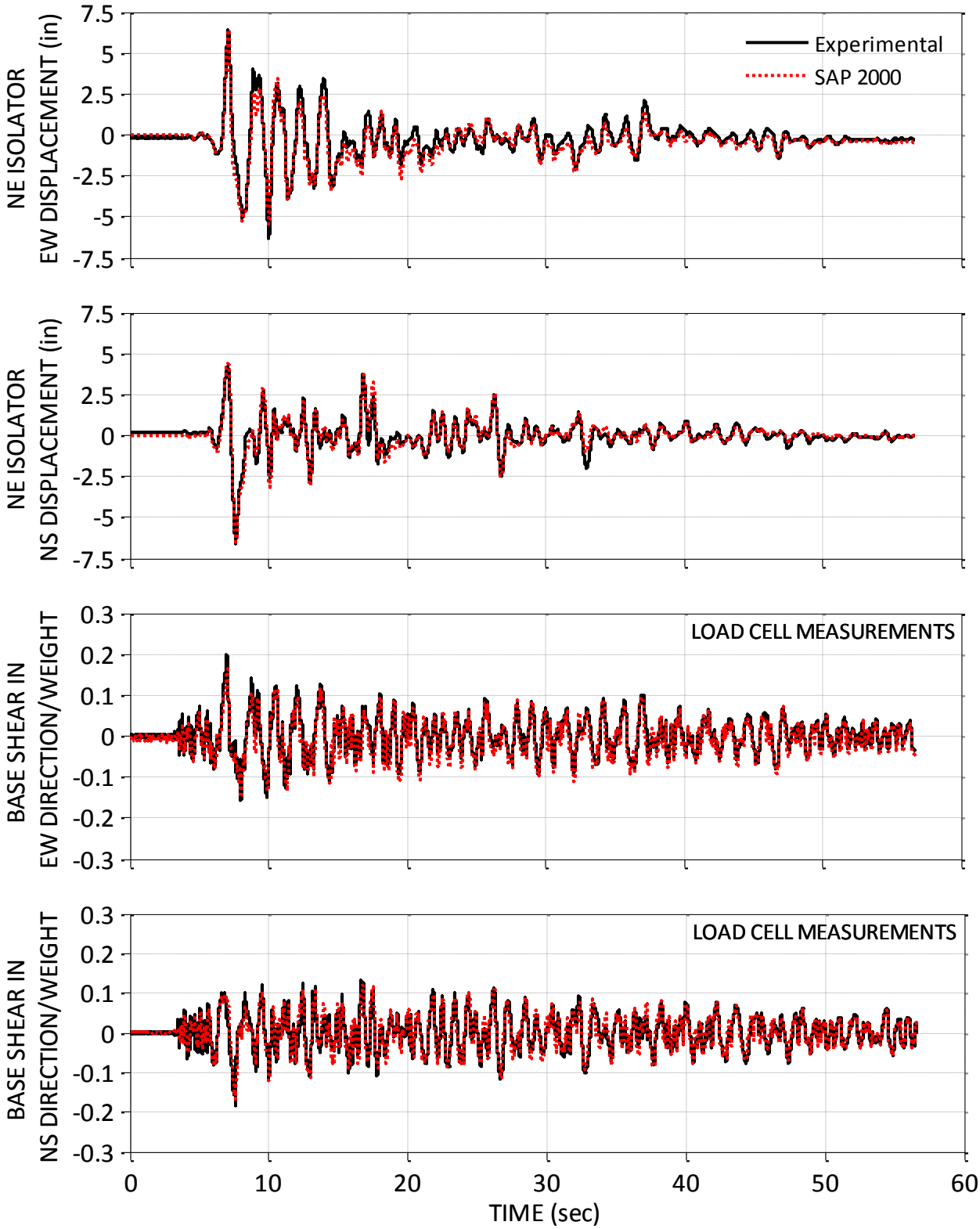

UPPER BUSHING CG
EW ACCELERATION (g)
Experimental
SAP 2000
UPPER BUSHING CG
NS ACCELERATION (g)
TIME (sec)
SPECTRAL
ACCELERATION (g)
FRAME TOP NE CORNER
EW DIRECTION
NS DIRECTION
FREQUENCY (Hz)
BASE SHEAR/WEIGHT
WEIGHT = 47.1 kip
LOAD CELL MEASUREMENTS
TOTAL DISPLACEMENT (in)

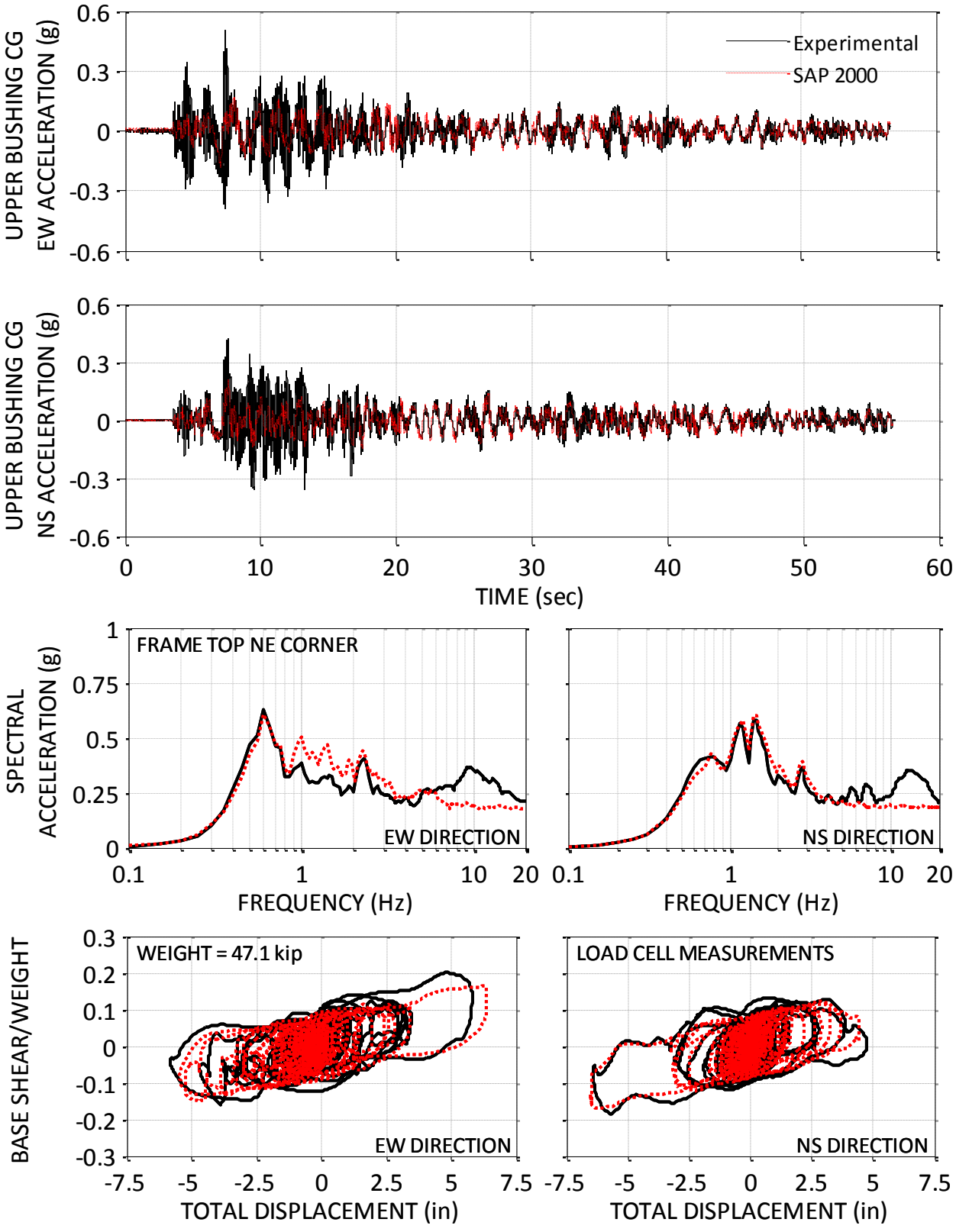
TRIPLE FP SYSTEM (Friction-Bolted Configuration)
PACOIMA DAM 75% BI-AXIAL (S16E in EW direction)
LENGTH SCALE=1 SYMMETRIC BUSHING CONFIGURATION



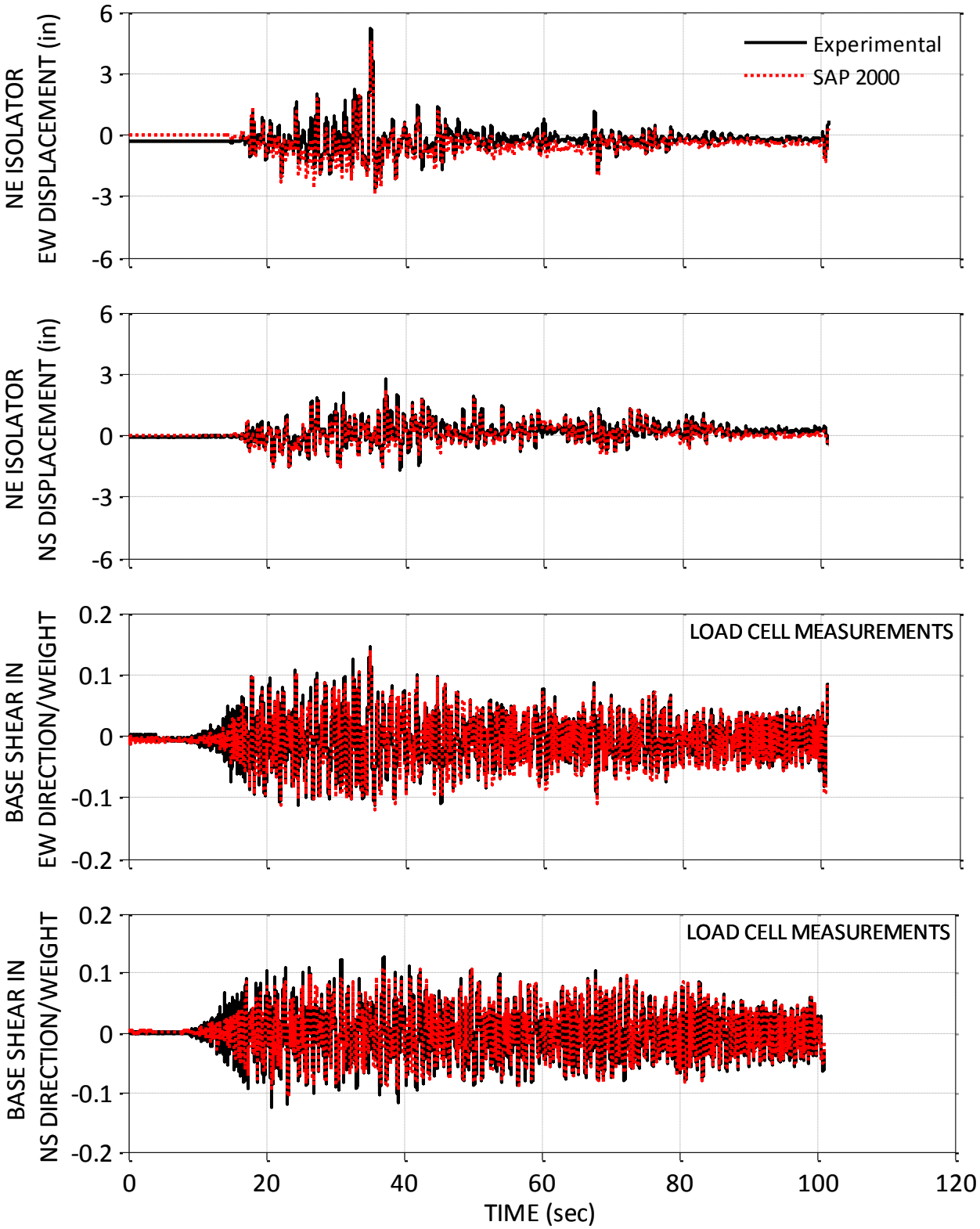

UPPER BUSHING CG
EW ACCELERATION (g)
Experimental
SAP 2000
UPPER BUSHING CG
NS ACCELERATION (g)
TIME (sec)
SPECTRAL
ACCELERATION (g)
FRAME TOP NE CORNER
EW DIRECTION
NS DIRECTION
FREQUENCY (Hz)
BASE SHEAR/WEIGHT
WEIGHT = 47.1 kip
LOAD CELL MEASUREMENTS
TOTAL DISPLACEMENT (in)

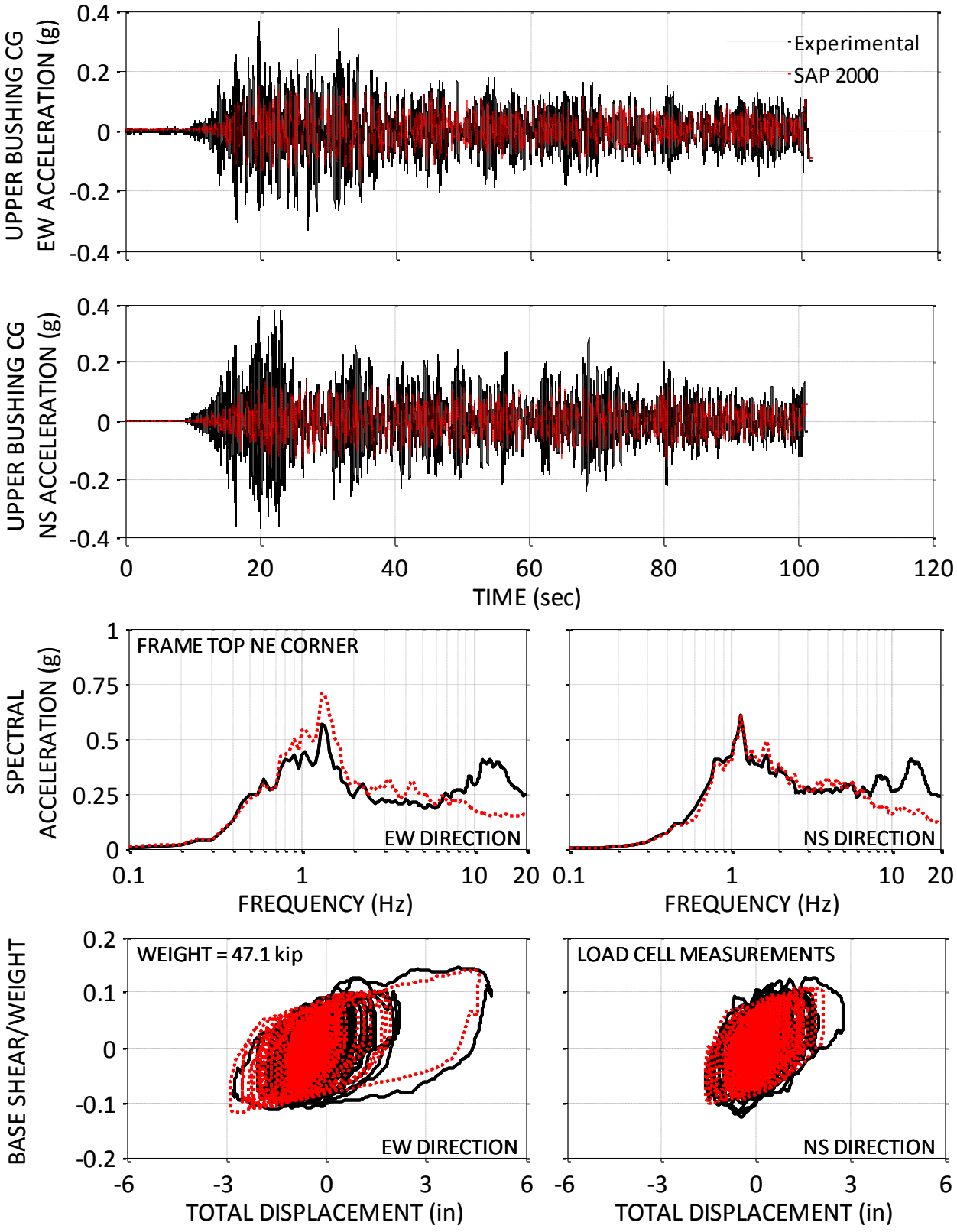
TRIPLE FP SYSTEM (Friction-Bolted Configuration)
TAFT 500% BI-AXIAL (S69E in EW direction)
LENGTH SCALE=1 SYMMETRIC BUSHING CONFIGURATION



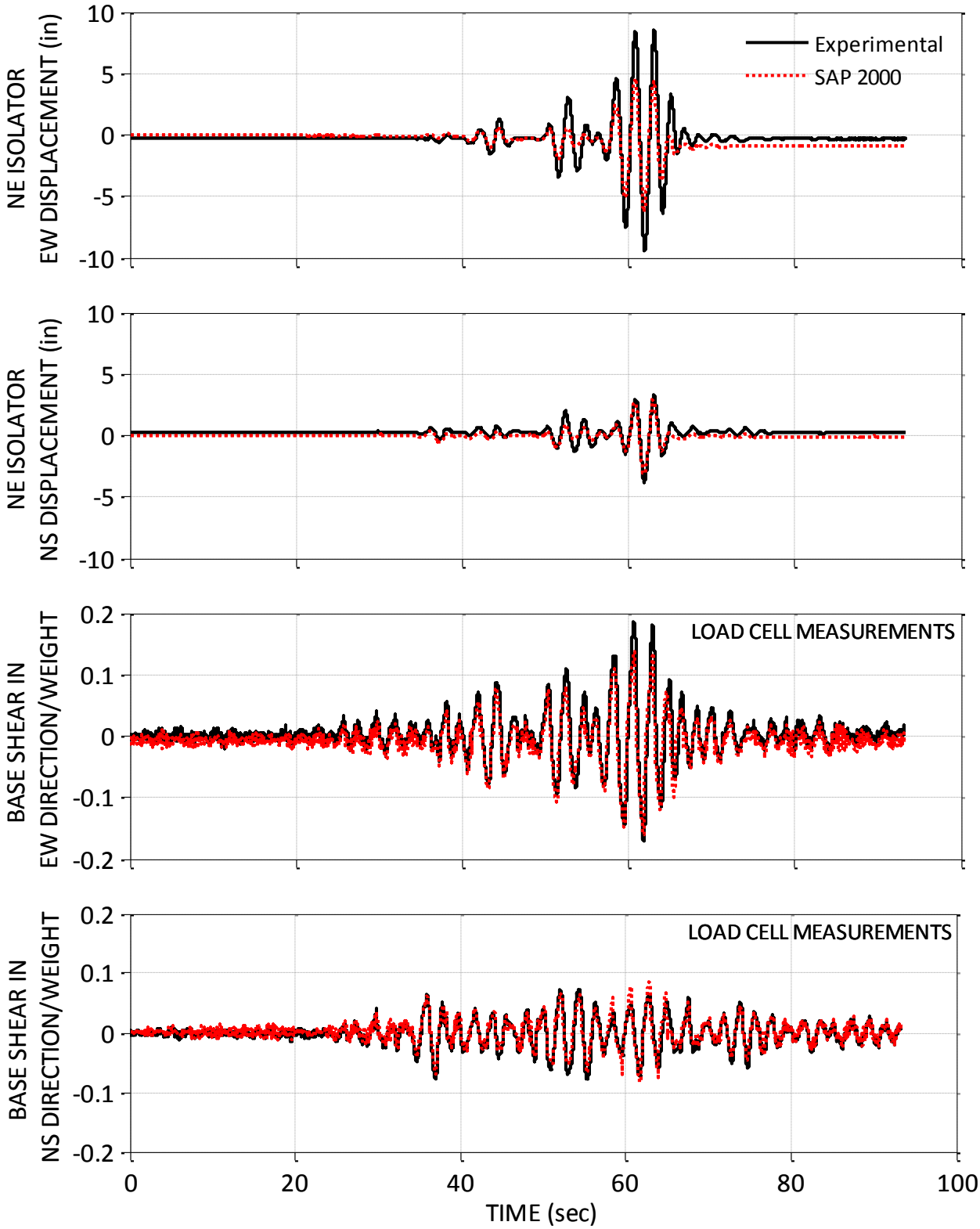

UPPER BUSHING CG
EW ACCELERATION (g)
Experimental
SAP 2000
UPPER BUSHING CG
NS ACCELERATION (g)
TIME (sec)
SPECTRAL
ACCELERATION (g)
FRAME TOP NE CORNER
EW DIRECTION
NS DIRECTION
FREQUENCY (Hz)
BASE SHEAR/WEIGHT
WEIGHT = 47.1 kip
LOAD CELL MEASUREMENTS
TOTAL DISPLACEMENT (in)

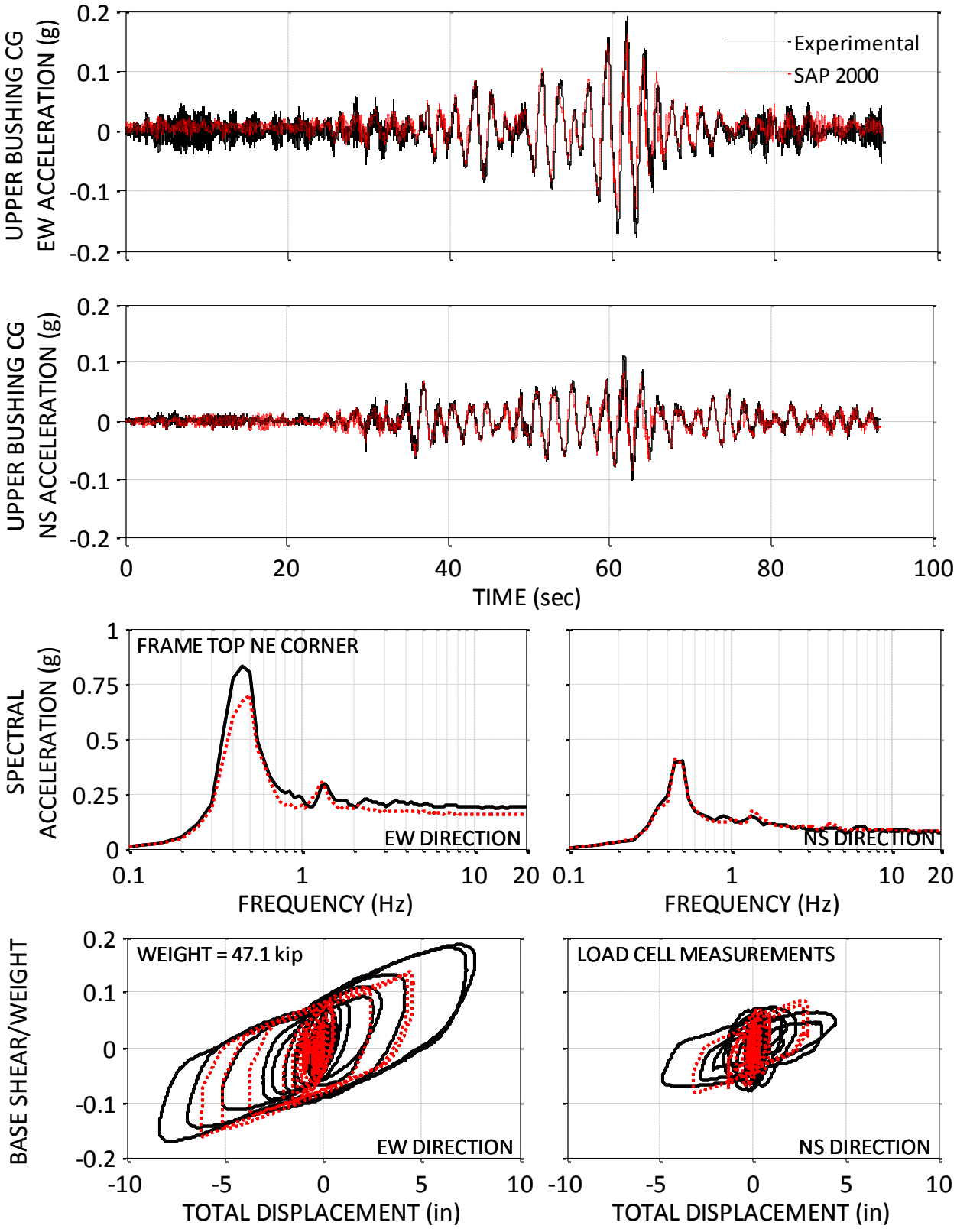
TRIPLE FP SYSTEM (Friction-Bolted Configuration)
CHILE 100% BI-AXIAL (EW in EW direction)
LENGTH SCALE=1 SYMMETRIC BUSHING CONFIGURATION




UPPER BUSHING CG
EW ACCELERATION (g)
Experimental
SAP 2000
UPPER BUSHING CG
NS ACCELERATION (g)
TIME (sec)
SPECTRAL
ACCELERATION (g)
FRAME TOP NE CORNER
EW DIRECTION
NS DIRECTION
FREQUENCY (Hz)
BASE SHEAR/WEIGHT
WEIGHT = 47.1 kip
LOAD CELL MEASUREMENTS
TOTAL DISPLACEMENT (in)

TRIPLE FP SYSTEM (Friction-Bolted Configuration)
MEXICO 70% BI-AXIAL (N90W in EW direction)
LENGTH SCALE=1 SYMMETRIC BUSHING CONFIGURATION



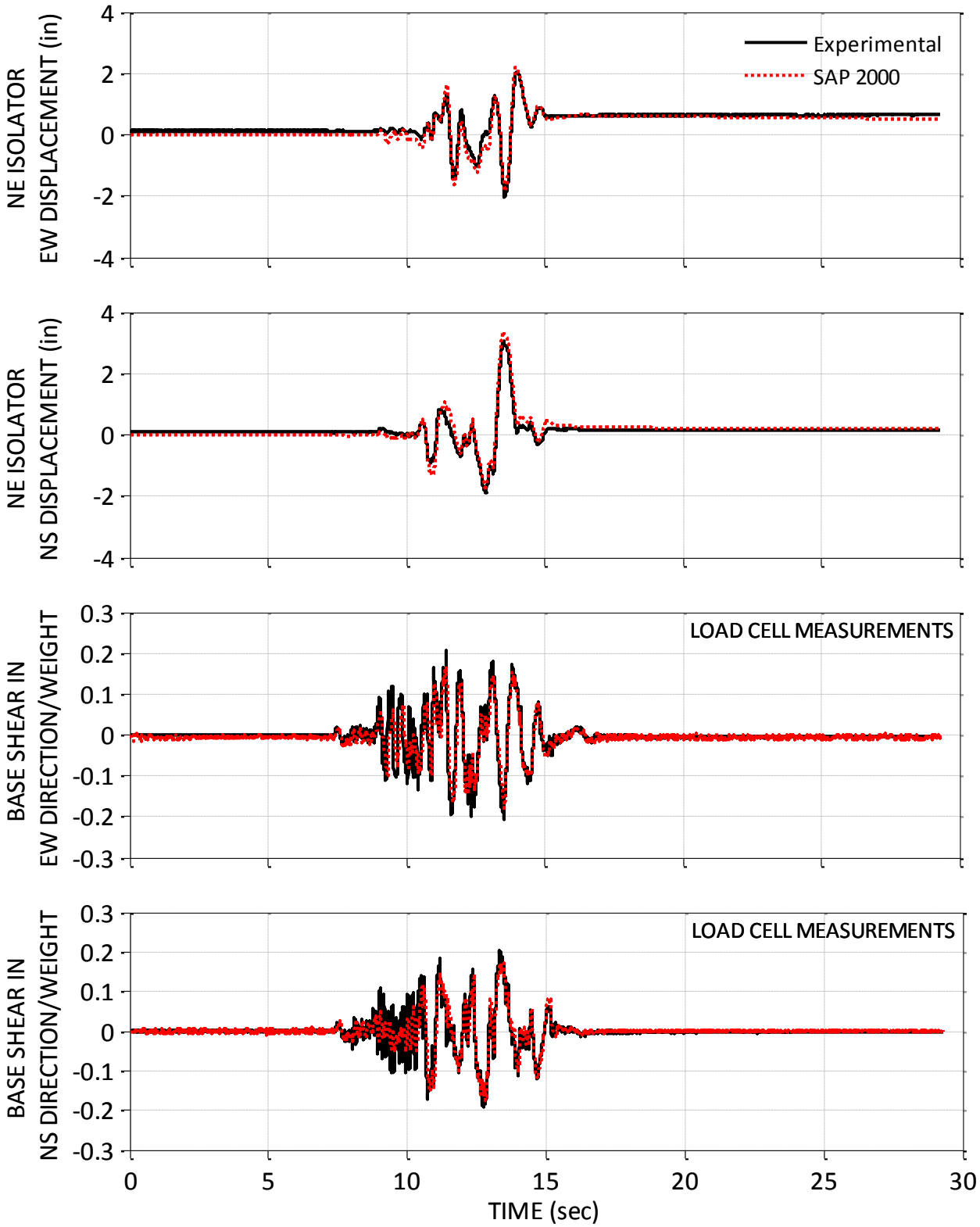

UPPER BUSHING CG
EW ACCELERATION (g)
Experimental
SAP 2000
UPPER BUSHING CG
NS ACCELERATION (g)
TIME (sec)
SPECTRAL
ACCELERATION (g)
FRAME TOP NE CORNER
EW DIRECTION
NS DIRECTION
FREQUENCY (Hz)
BASE SHEAR/WEIGHT
WEIGHT = 47.1 kip
LOAD CELL MEASUREMENTS
TOTAL DISPLACEMENT (in)

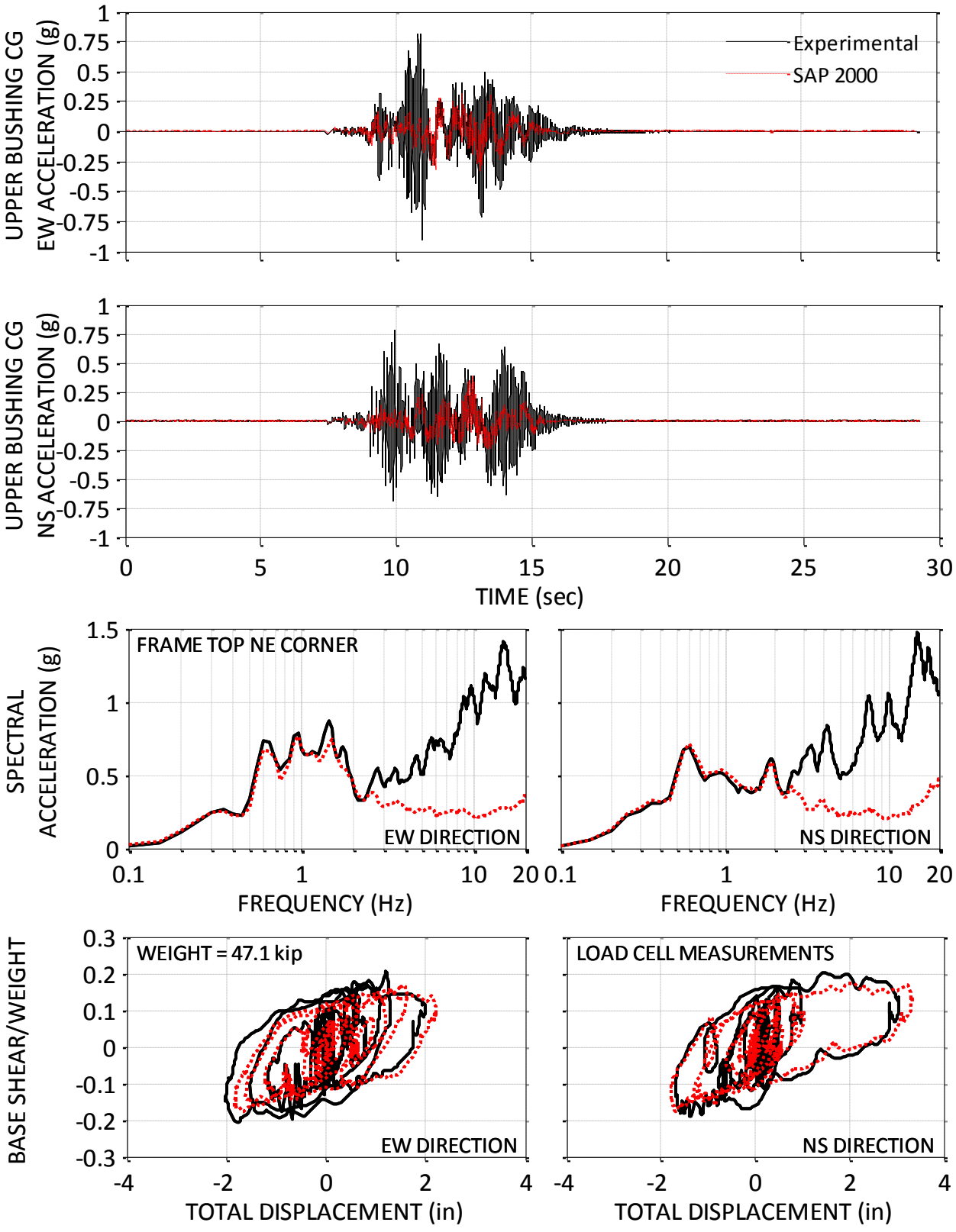
APPENDIX D
SUMMARY OF EXPERIMENTAL AND ANALYTICAL COMPARISONS FOR THE TRIPLE FRICTION PENDULUM SYSTEM MODELLED USING THE SERIES MODEL

PART D-1
SUMMARY OF EXPERIMENTAL AND ANALYTICAL COMPARISONS FOR THE TRIPLE FRICTION PENDULUM SYSTEM AT LENGTH SCALE OF 3 AND MODELING USING THE SERIES MODEL

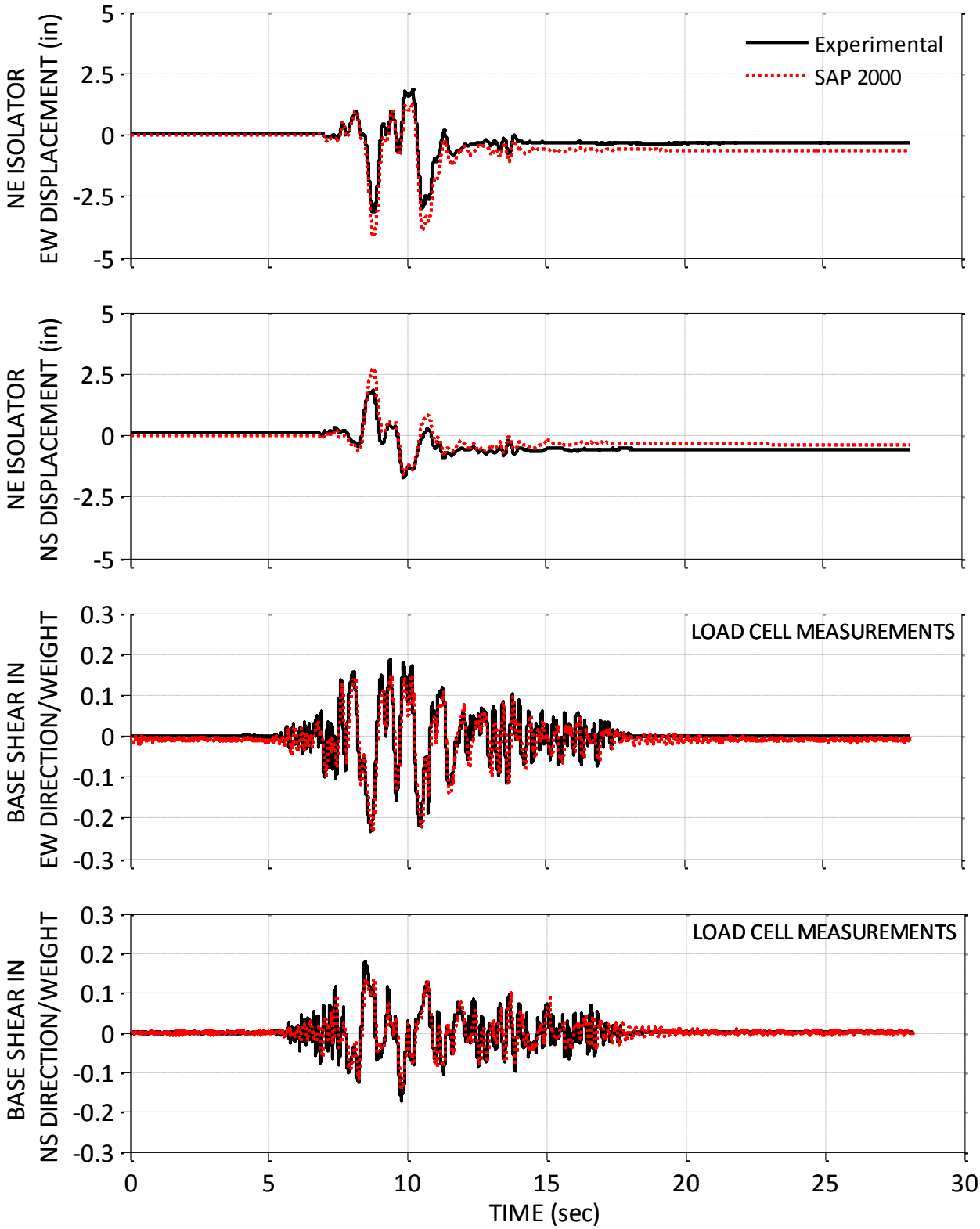
(PERCENTAGE AMOUNT IS SCALE FACTOR APPLIED TO ACCELERATION OF ACTUAL MOTION. FOR EXAMPLE, 100% DENOTES MOTION AS RECORDED, 200% DENOTES THAT ACCELERATION WAS SCALED UP BY FACTOR OF 2)

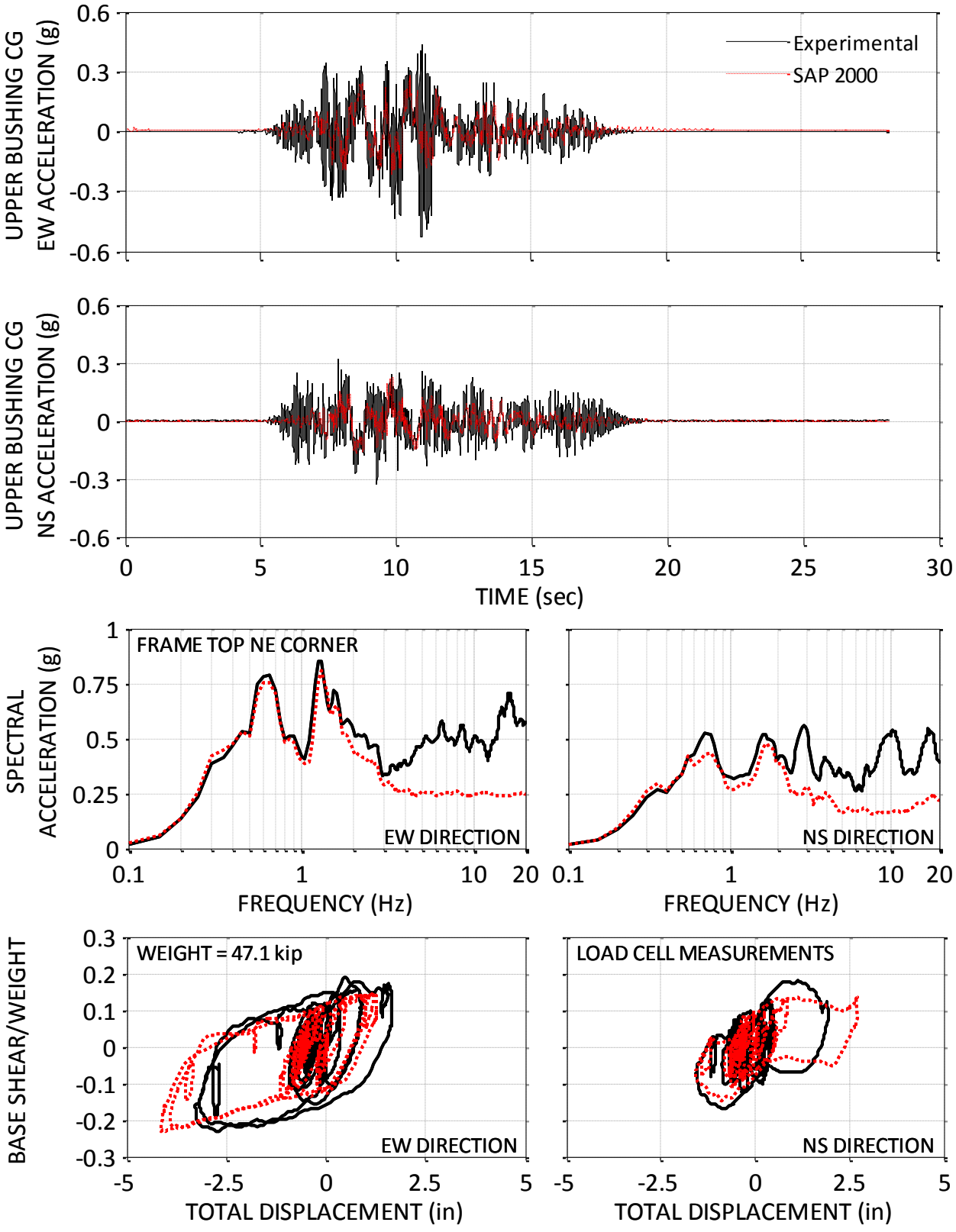
TRIPLE FP SYSTEM (Friction-Bolted Configuration – Series Model)
KARAKYR 137% BI-AXIAL (FN in EW direction)
LENGTH SCALE=3 SYMMETRIC BUSHING CONFIGURATION



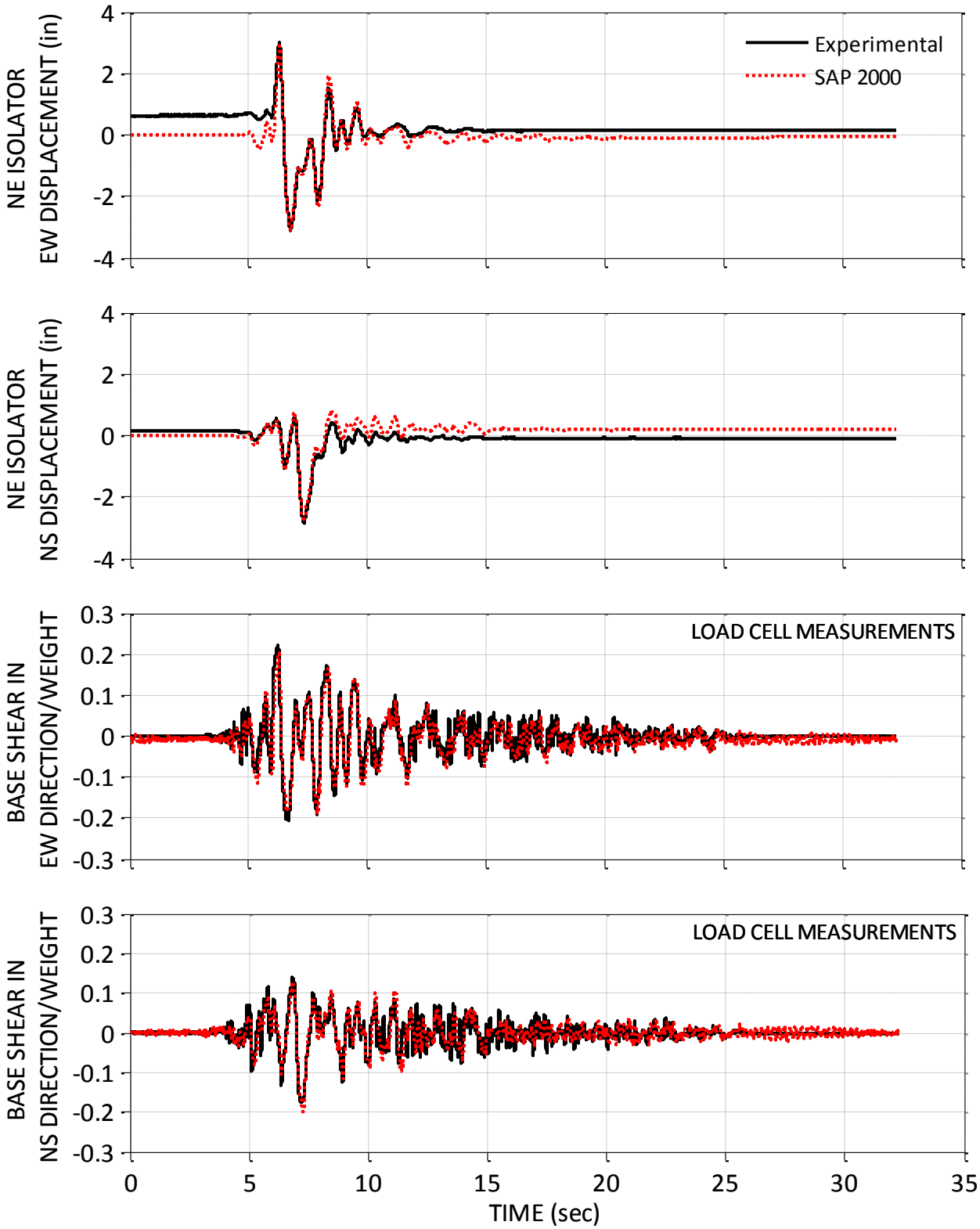

UPPER BUSHING CG
EW ACCELERATION (g)
Experimental
SAP 2000
UPPER BUSHING CG
NS ACCELERATION (g)
TIME (sec)
SPECTRAL
ACCELERATION (g)
FRAME TOP NE CORNER
EW DIRECTION
NS DIRECTION
FREQUENCY (Hz)
BASE SHEAR/WEIGHT
WEIGHT = 47.1 kip
LOAD CELL MEASUREMENTS
TOTAL DISPLACEMENT (in)

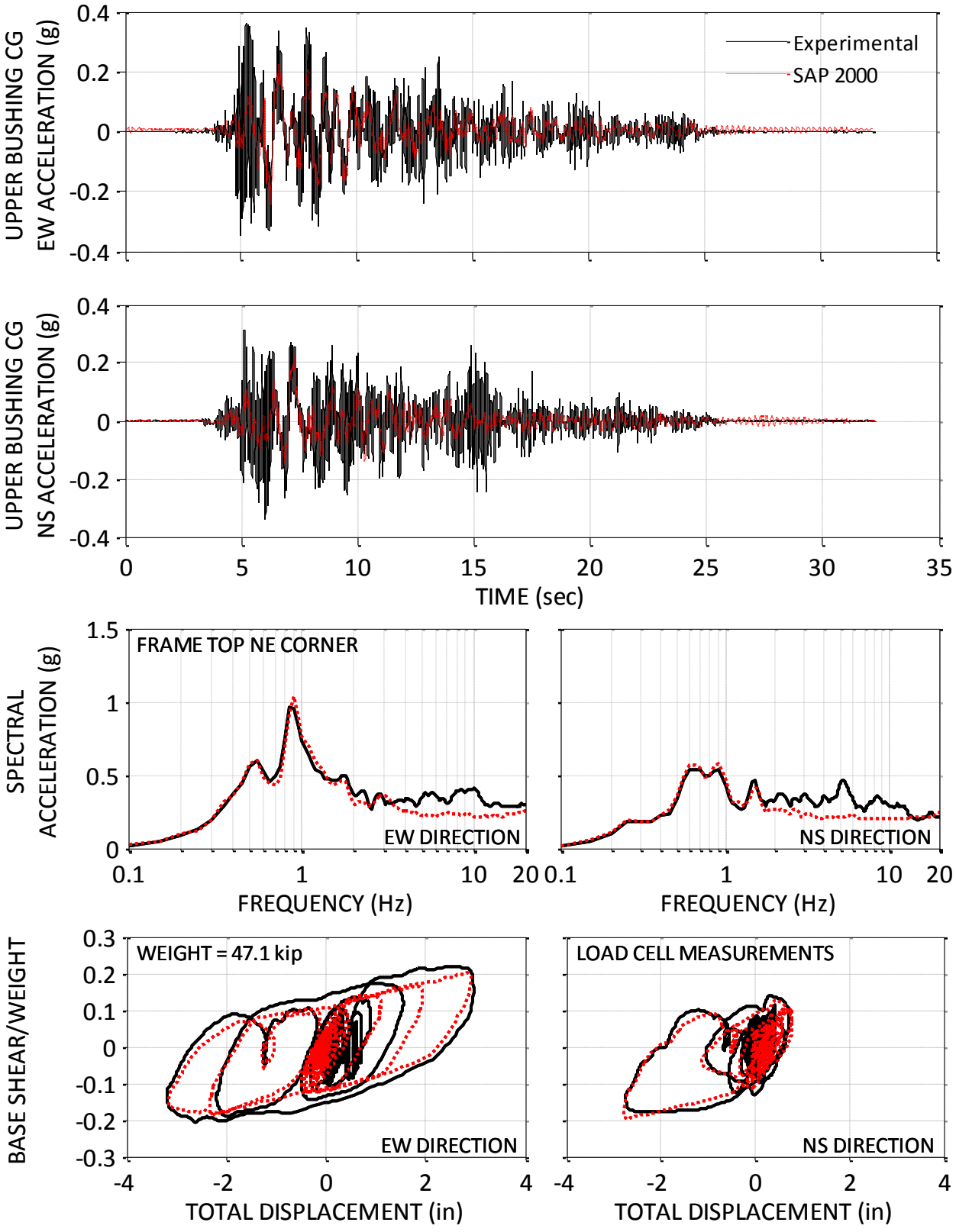
TRIPLE FP SYSTEM (Friction-Bolted Configuration – Series Model)
LGPC 94% BI-AXIAL (FN in EW direction)
LENGTH SCALE=3 SYMMETRIC BUSHING CONFIGURATION



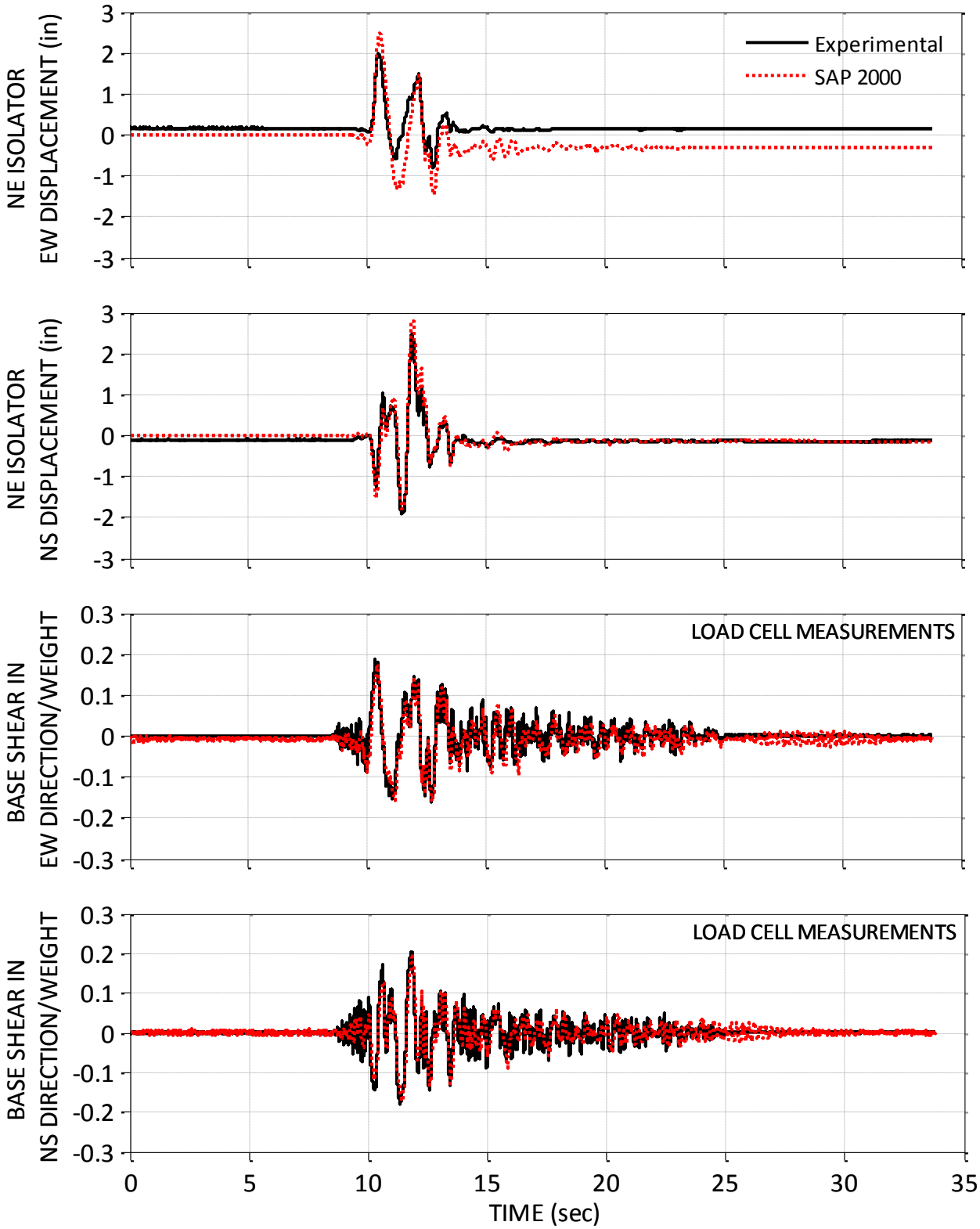

UPPER BUSHING CG
EW ACCELERATION (g)
Experimental
SAP 2000
UPPER BUSHING CG
NS ACCELERATION (g)
TIME (sec)
SPECTRAL
ACCELERATION (g)
FRAME TOP NE CORNER
EW DIRECTION
NS DIRECTION
FREQUENCY (Hz)
BASE SHEAR/WEIGHT
WEIGHT = 47.1 kip
LOAD CELL MEASUREMENTS
TOTAL DISPLACEMENT (in)

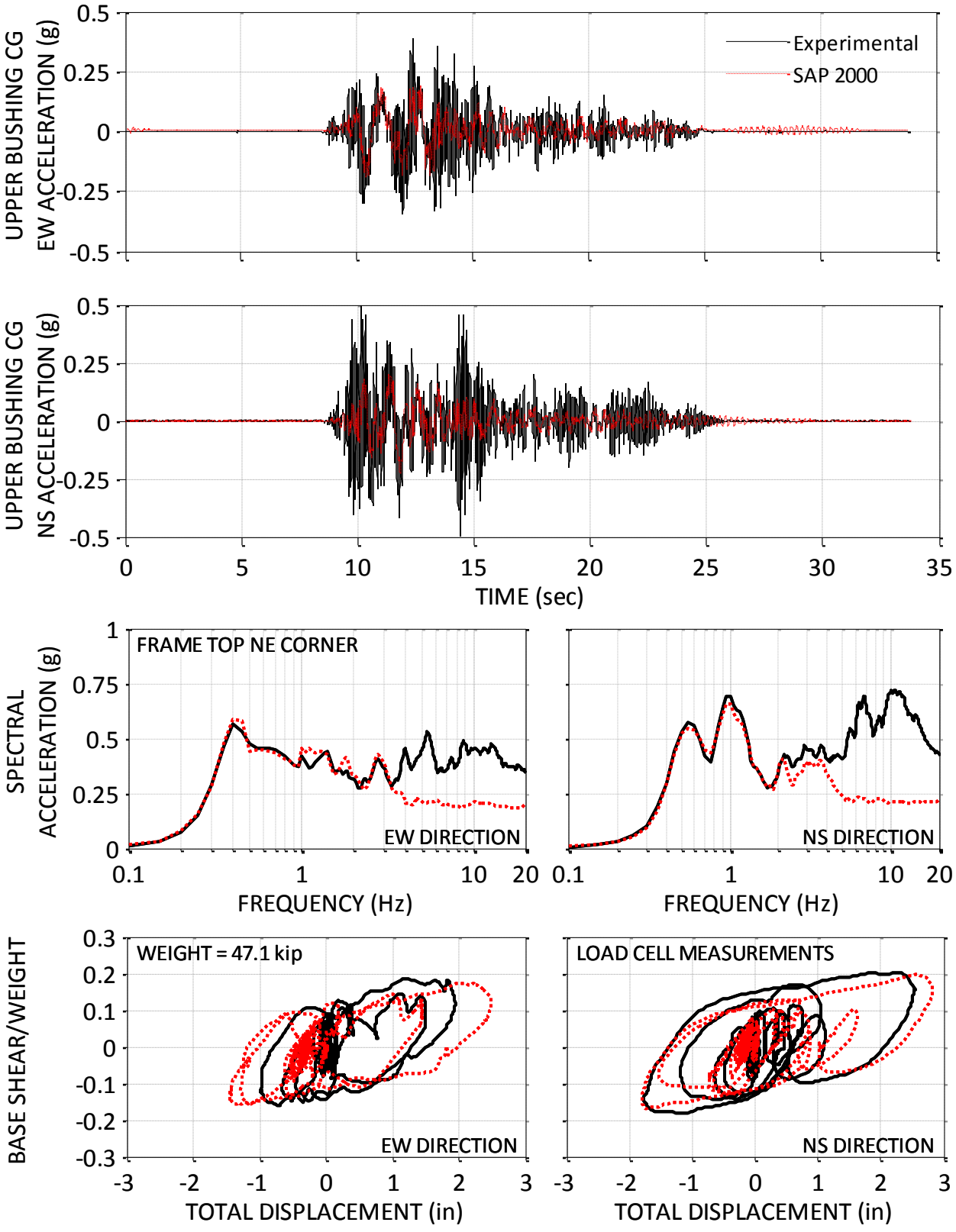
TRIPLE FP SYSTEM (Friction-Bolted Configuration – Series Model)
SARATOGA 157% BI-AXIAL (FN in EW direction)
LENGTH SCALE=3 SYMMETRIC BUSHING CONFIGURATION



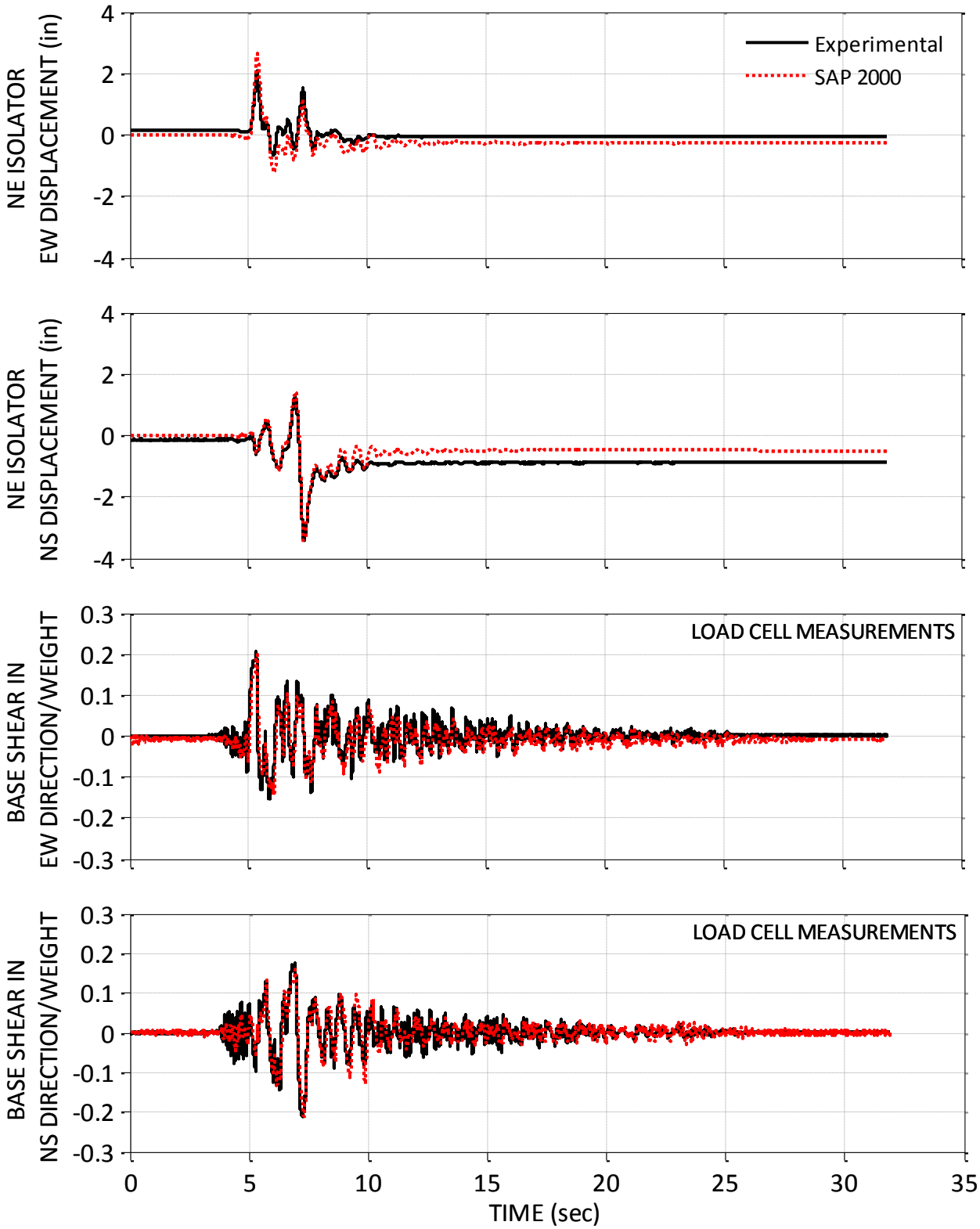

UPPER BUSHING CG
EW ACCELERATION (g)
Experimental
SAP 2000
UPPER BUSHING CG
NS ACCELERATION (g)
TIME (sec)
SPECTRAL
ACCELERATION (g)
FRAME TOP NE CORNER
EW DIRECTION
NS DIRECTION
FREQUENCY (Hz)
BASE SHEAR/WEIGHT
WEIGHT = 47.1 kip
LOAD CELL MEASUREMENTS
TOTAL DISPLACEMENT (in)

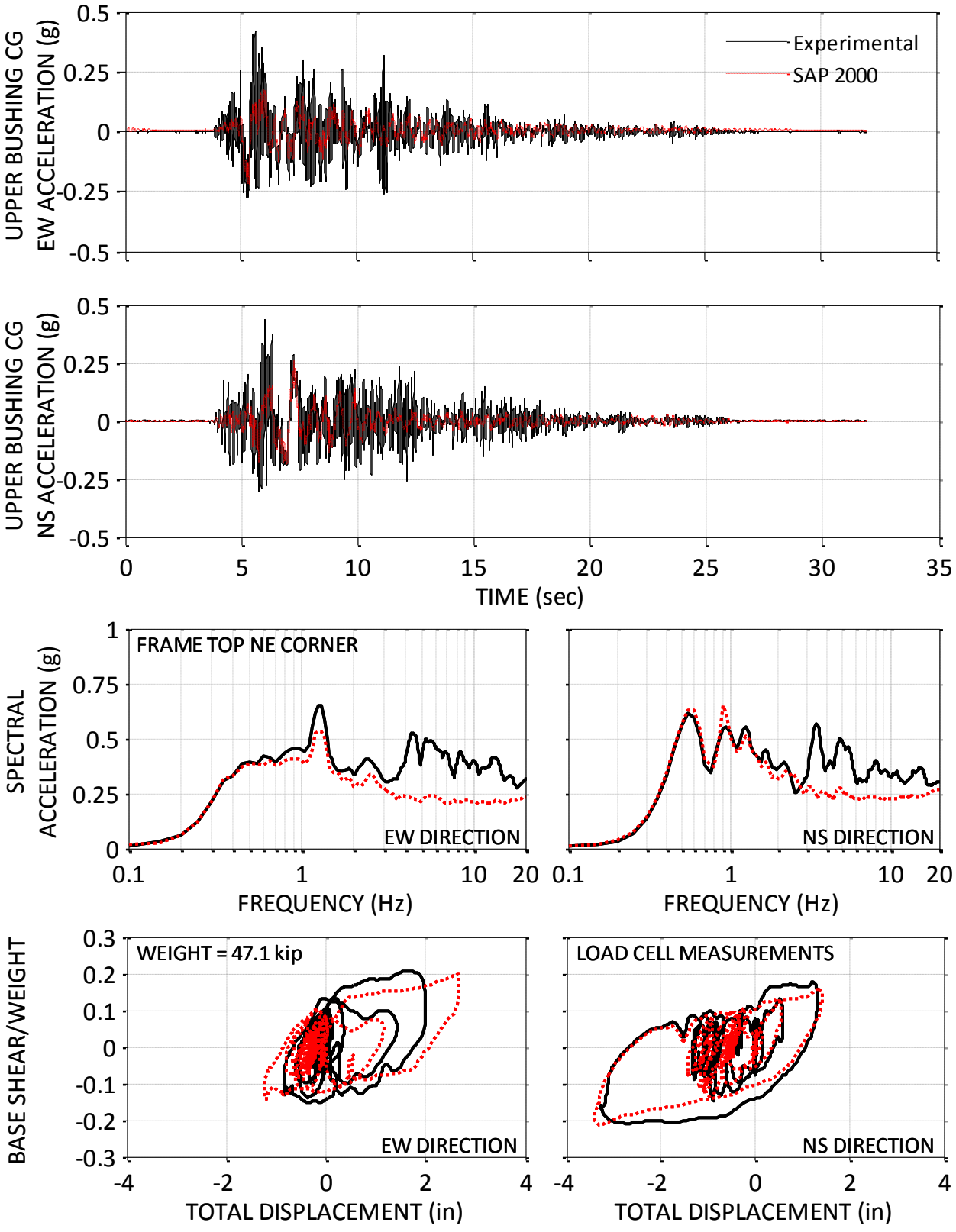
TRIPLE FP SYSTEM (Friction-Bolted Configuration – Series Model)
JENSEN FILTER 97% BI-AXIAL (FN in EW direction)
LENGTH SCALE=3 SYMMETRIC BUSHING CONFIGURATION



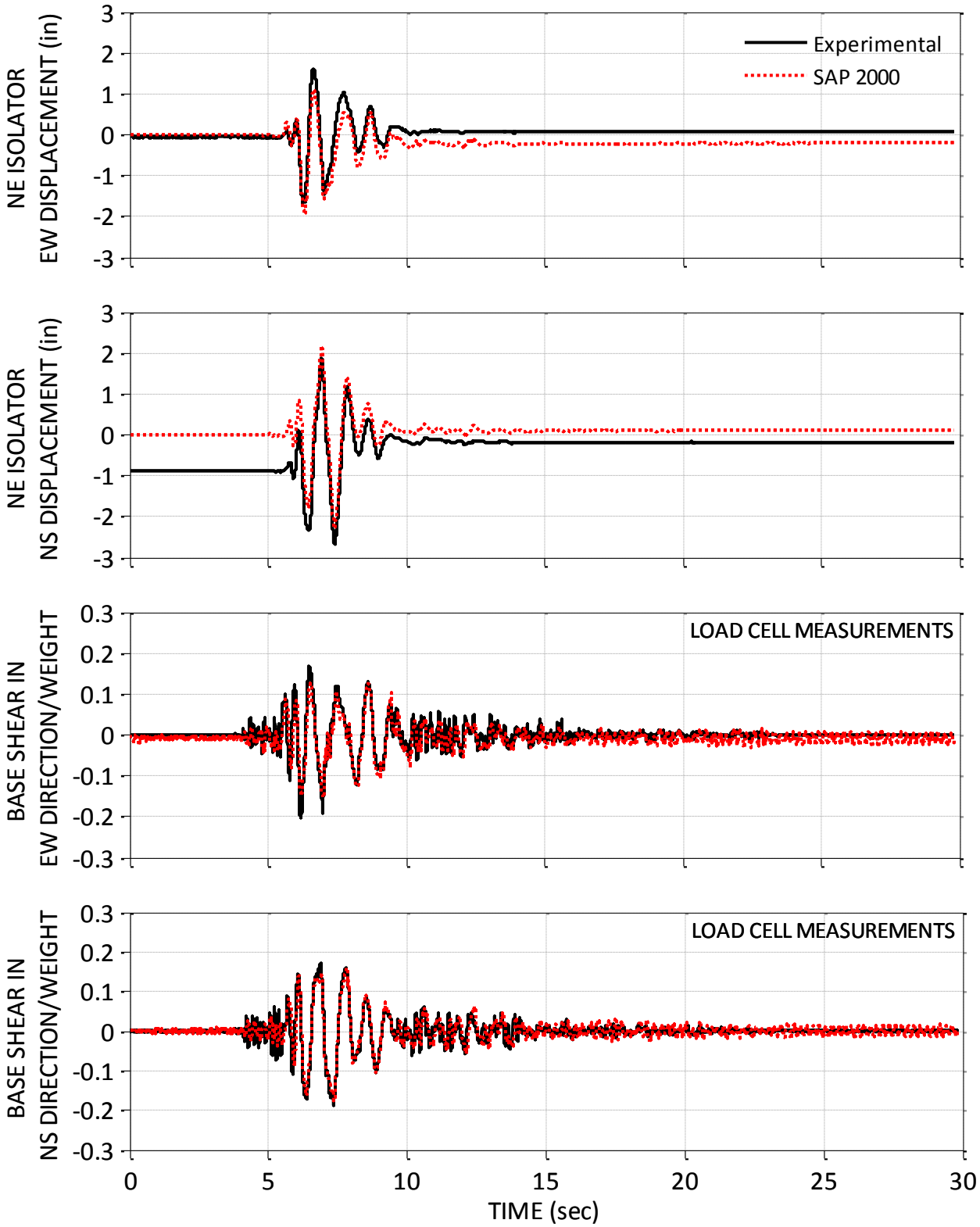

UPPER BUSHING CG
EW ACCELERATION (g)
Experimental
SAP 2000
UPPER BUSHING CG
NS ACCELERATION (g)
TIME (sec)
SPECTRAL
ACCELERATION (g)
FRAME TOP NE CORNER
EW DIRECTION
NS DIRECTION
FREQUENCY (Hz)
BASE SHEAR/WEIGHT
WEIGHT = 47.1 kip
LOAD CELL MEASUREMENTS
TOTAL DISPLACEMENT (in)

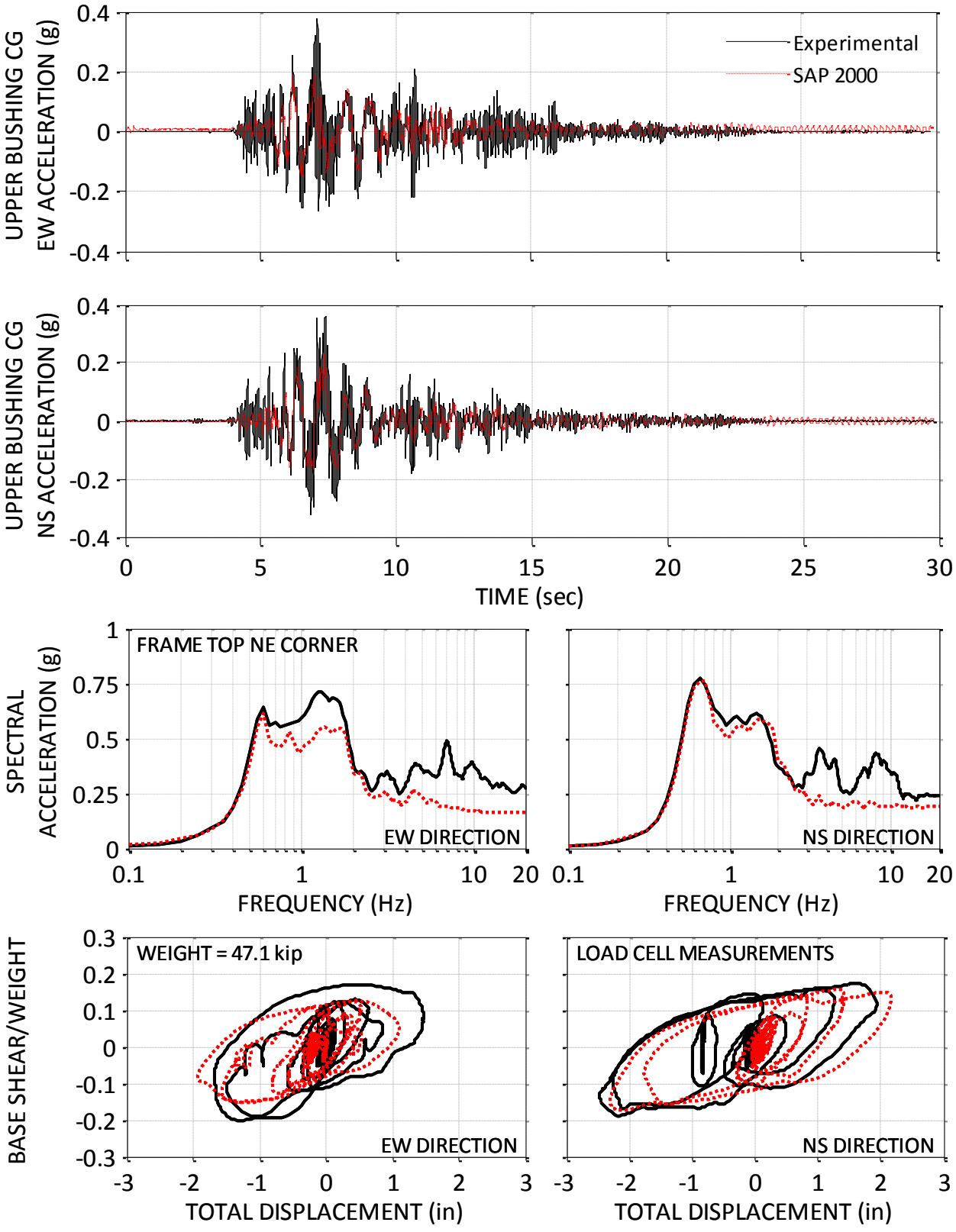
TRIPLE FP SYSTEM (Friction-Bolted Configuration – Series Model)
SYLMAR 90% BI-AXIAL (FN in EW direction)
LENGTH SCALE=3 SYMMETRIC BUSHING CONFIGURATION



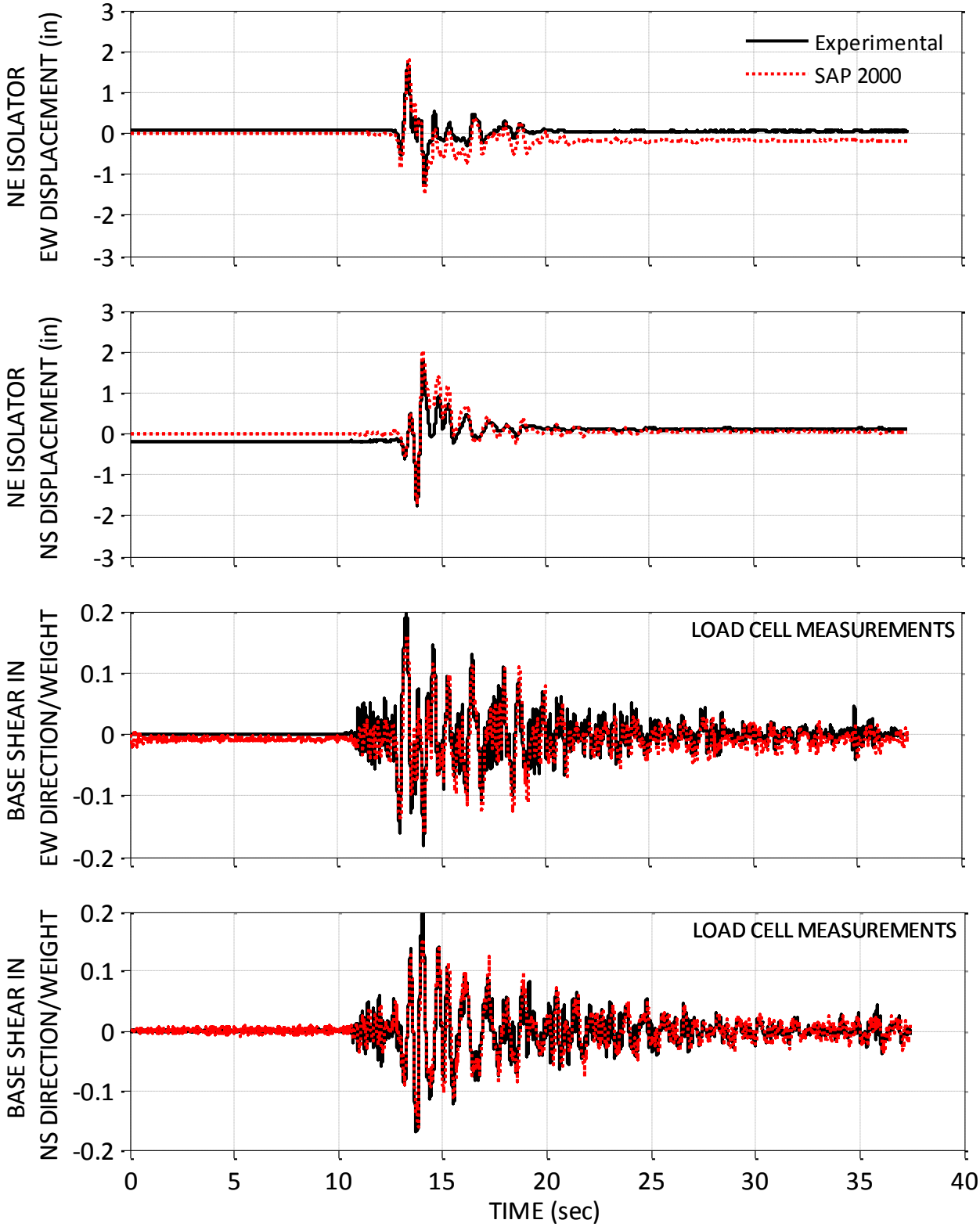

UPPER BUSHING CG
EW ACCELERATION (g)
Experimental
SAP 2000
UPPER BUSHING CG
NS ACCELERATION (g)
TIME (sec)
SPECTRAL
ACCELERATION (g)
FRAME TOP NE CORNER
EW DIRECTION
NS DIRECTION
FREQUENCY (Hz)
BASE SHEAR/WEIGHT
WEIGHT = 47.1 kip
LOAD CELL MEASUREMENTS
TOTAL DISPLACEMENT (in)

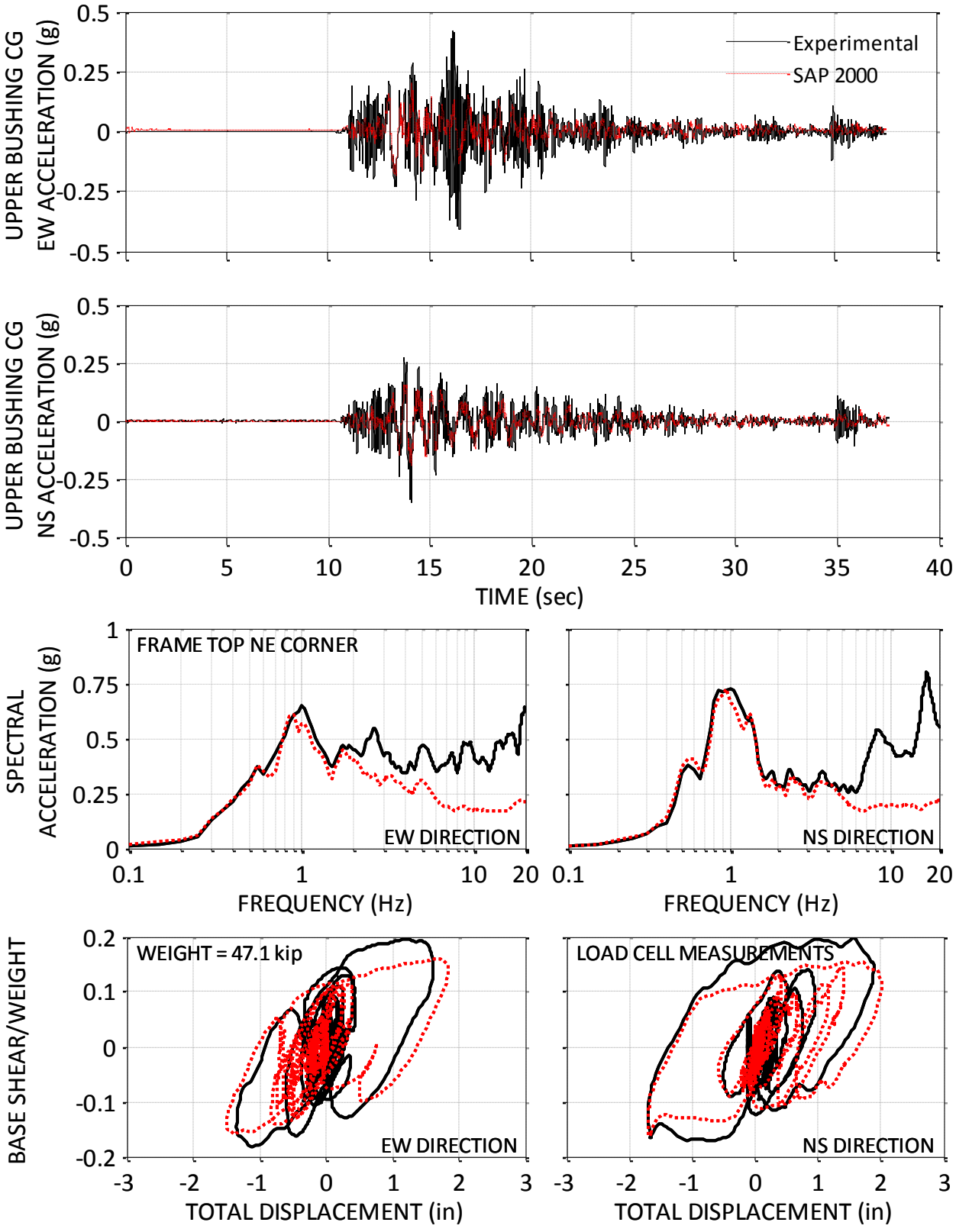
TRIPLE FP SYSTEM (Friction-Bolted Configuration – Series Model)
TAKARAZUKA 97% BI-AXIAL (FN in EW direction)
LENGTH SCALE=3 SYMMETRIC BUSHING CONFIGURATION



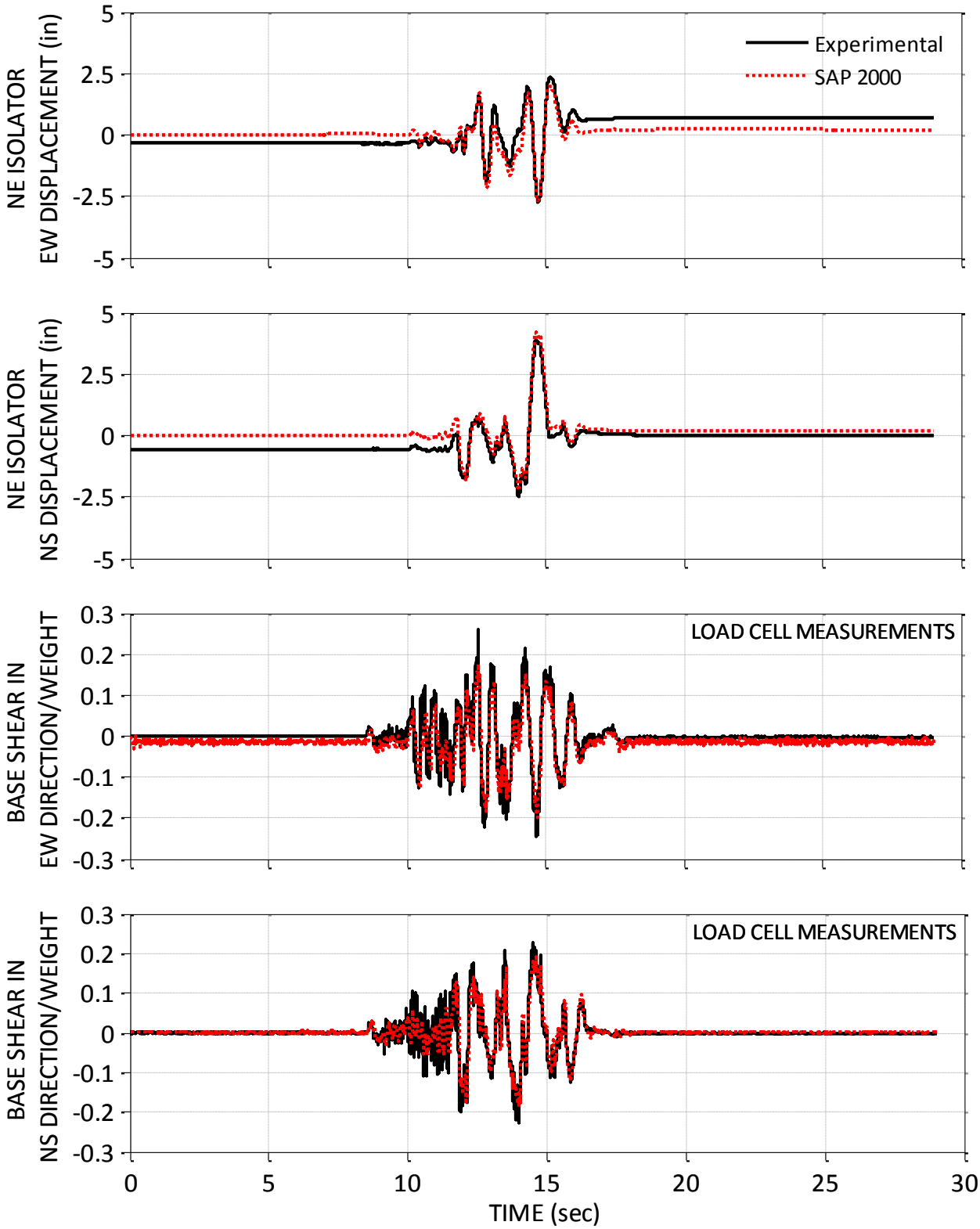

UPPER BUSHING CG
EW ACCELERATION (g)
Experimental
SAP 2000
UPPER BUSHING CG
NS ACCELERATION (g)
TIME (sec)
SPECTRAL
ACCELERATION (g)
FRAME TOP NE CORNER
EW DIRECTION
NS DIRECTION
FREQUENCY (Hz)
BASE SHEAR/WEIGHT
WEIGHT = 47.1 kip
LOAD CELL MEASUREMENTS
TOTAL DISPLACEMENT (in)

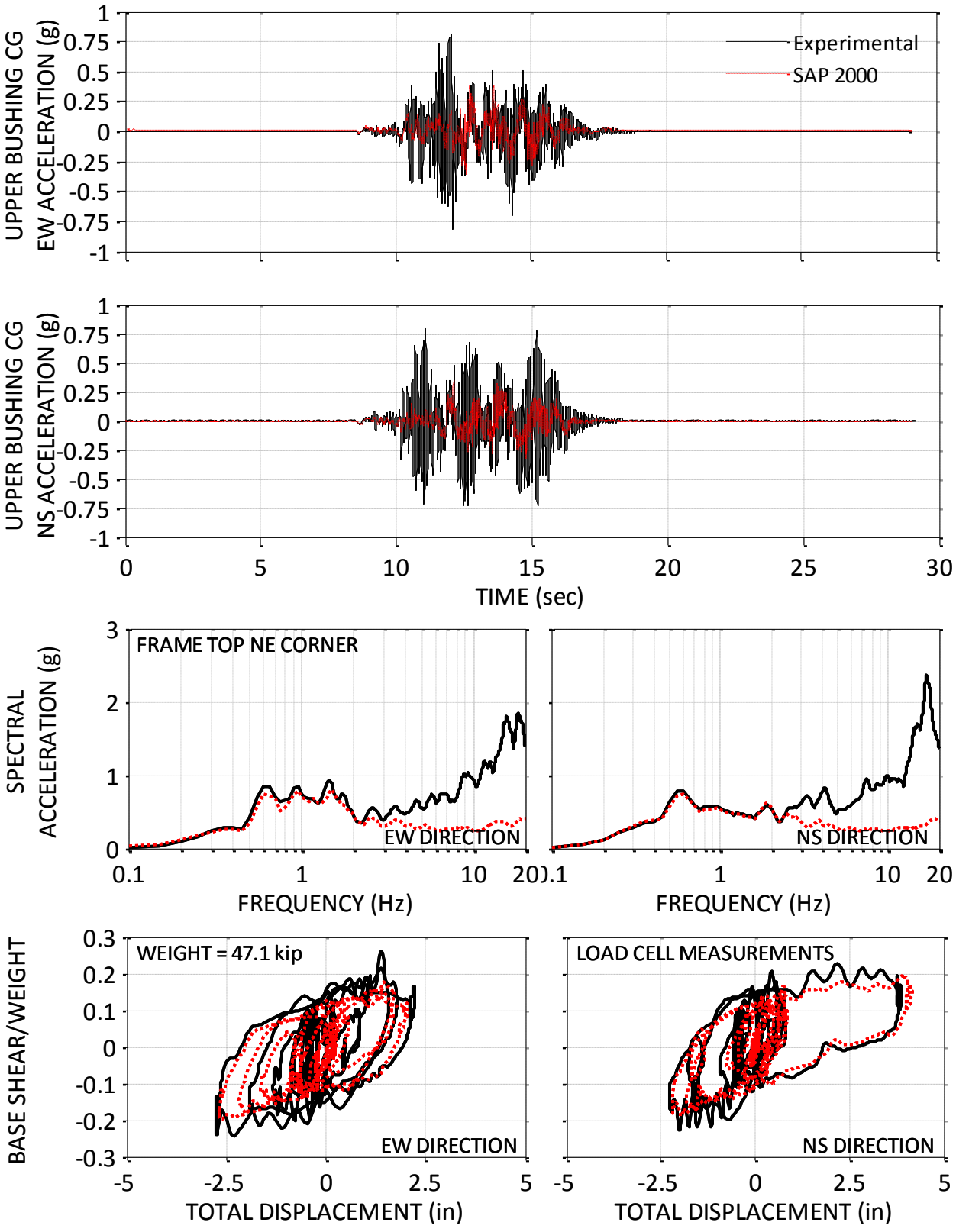
TRIPLE FP SYSTEM (Friction-Bolted Configuration – Series Model)
BOLU 104% BI-AXIAL (FN in EW direction)
LENGTH SCALE=3 SYMMETRIC BUSHING CONFIGURATION



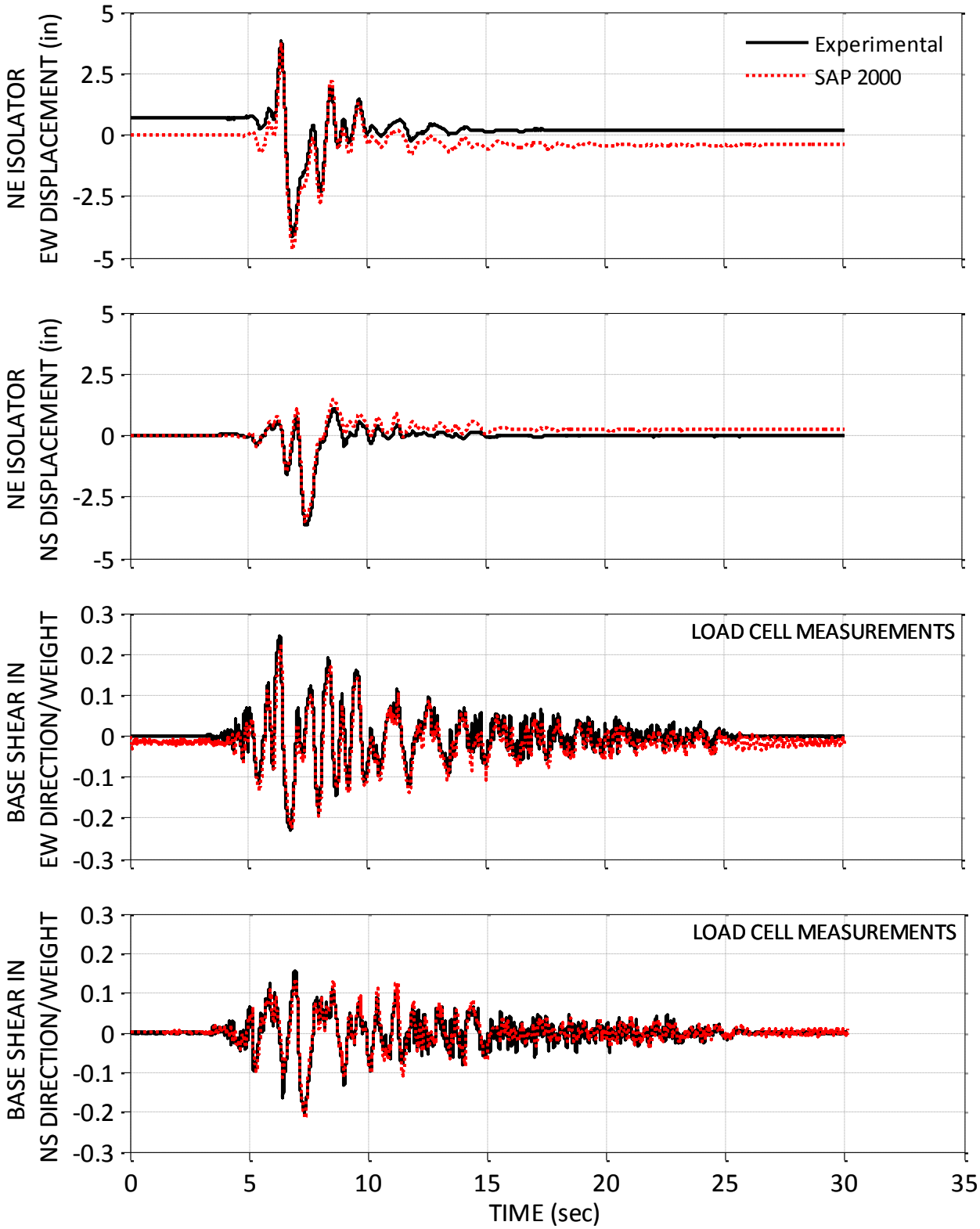

UPPER BUSHING CG
EW ACCELERATION (g)
Experimental
SAP 2000
UPPER BUSHING CG
NS ACCELERATION (g)
TIME (sec)
SPECTRAL
ACCELERATION (g)
FRAME TOP NE CORNER
EW DIRECTION
NS DIRECTION
FREQUENCY (Hz)
BASE SHEAR/WEIGHT
WEIGHT = 47.1 kip
LOAD CELL MEASUREMENTS
TOTAL DISPLACEMENT (in)

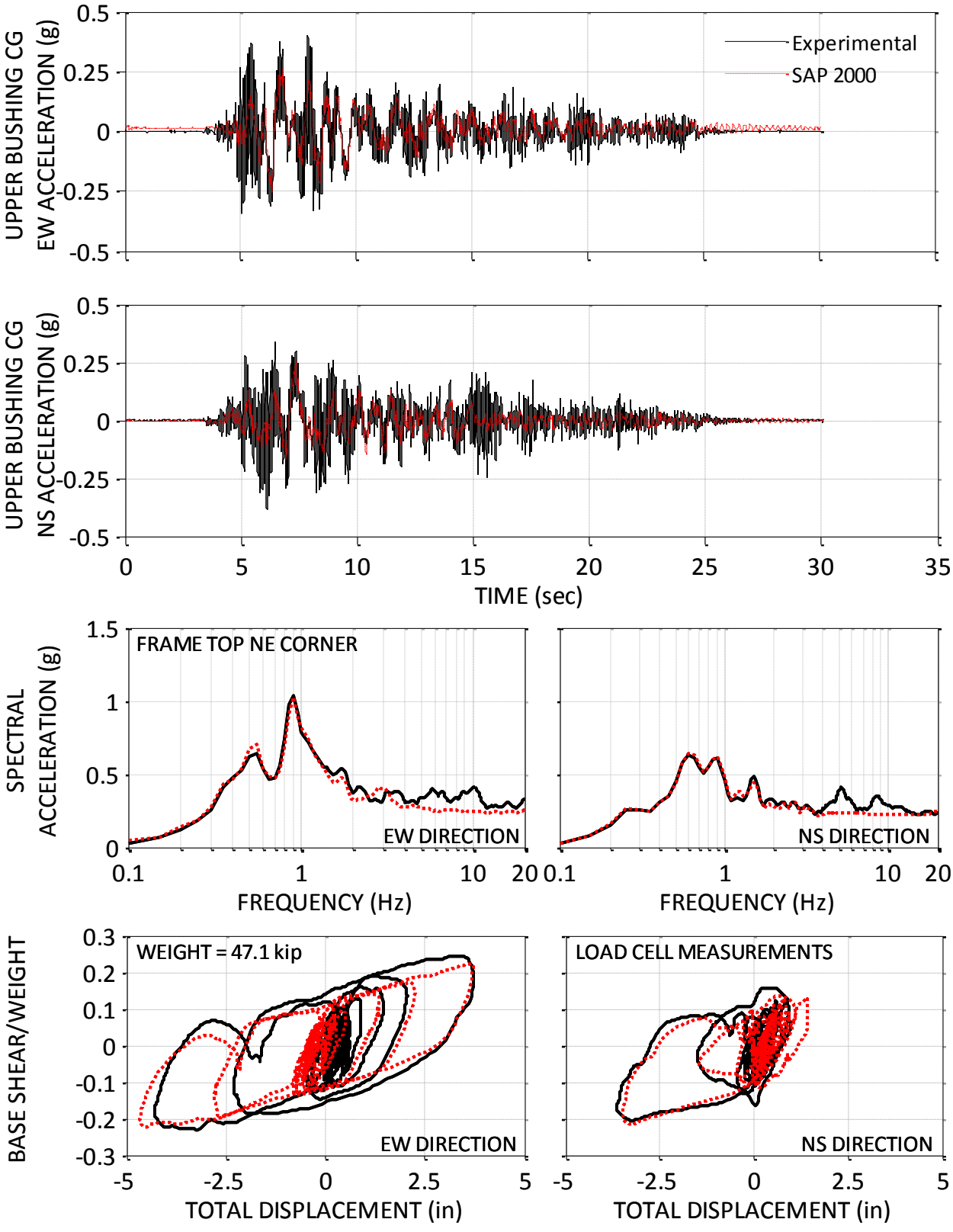
TRIPLE FP SYSTEM (Friction-Bolted Configuration – Series Model)
KARAKYR 171% BI-AXIAL (FN in EW direction)
LENGTH SCALE=3 SYMMETRIC BUSHING CONFIGURATION



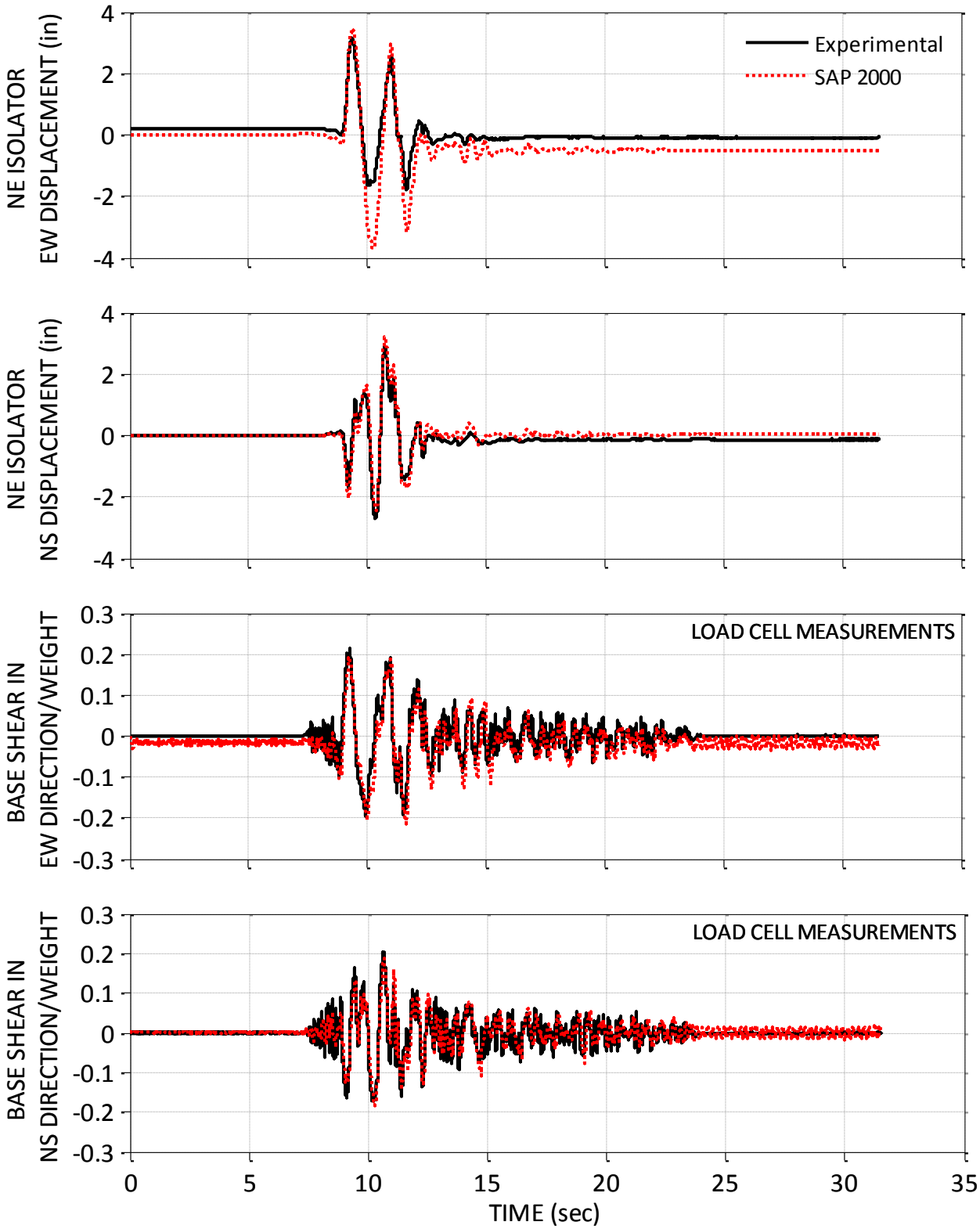

UPPER BUSHING CG
EW ACCELERATION (g)
Experimental
SAP 2000
UPPER BUSHING CG
NS ACCELERATION (g)
TIME (sec)
SPECTRAL
ACCELERATION (g)
FRAME TOP NE CORNER
EW DIRECTION
NS DIRECTION
FREQUENCY (Hz)
FREQUENCY (Hz)
BASE SHEAR/WEIGHT
WEIGHT = 47.1 kip
LOAD CELL MEASUREMENTS
EW DIRECTION
NS DIRECTION
TOTAL DISPLACEMENT (in)
TOTAL DISPLACEMENT (in)

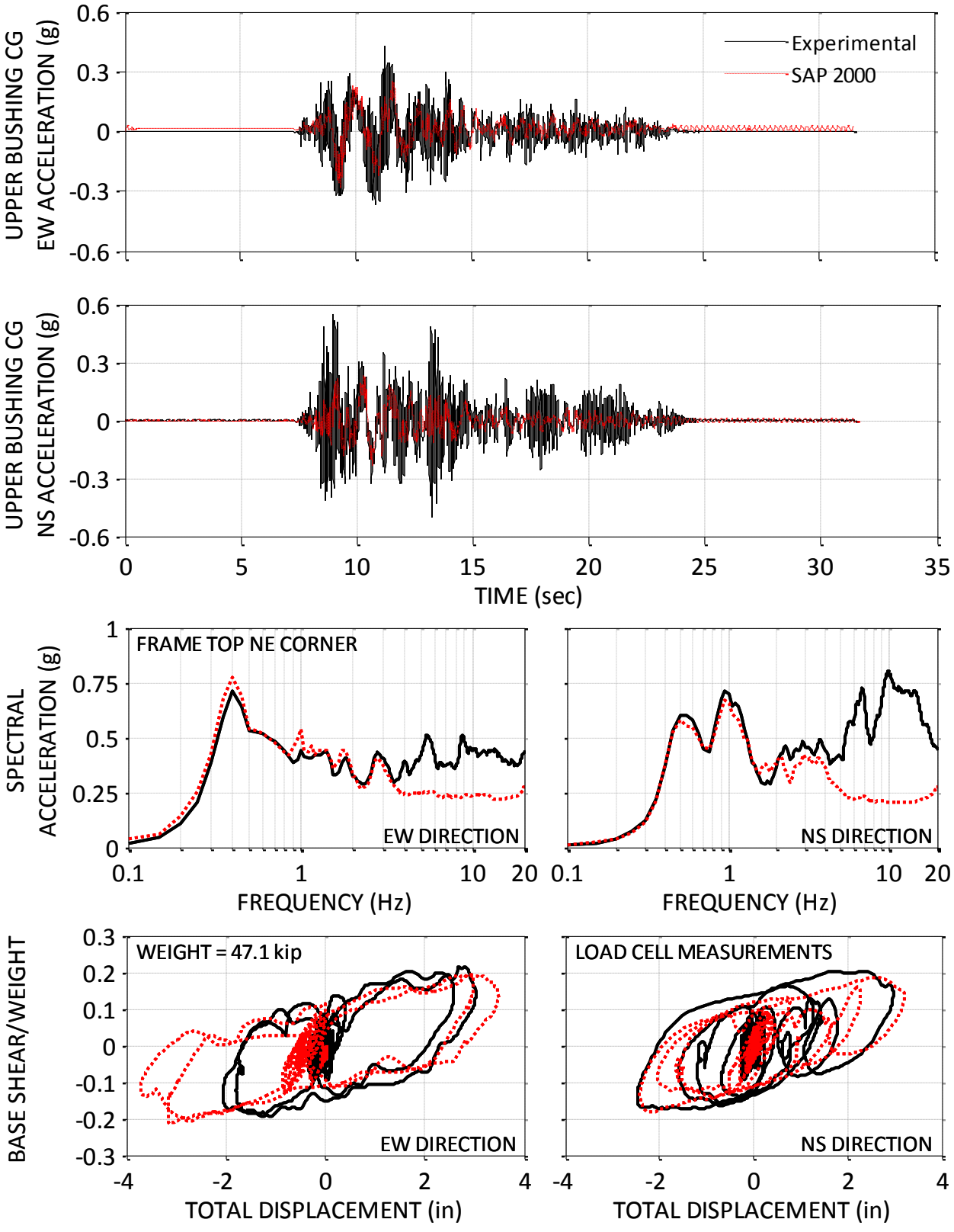
TRIPLE FP SYSTEM (Friction-Bolted Configuration – Series Model)
SARATOGA 196% BI-AXIAL (FN in EW direction)
LENGTH SCALE=3 SYMMETRIC BUSHING CONFIGURATION



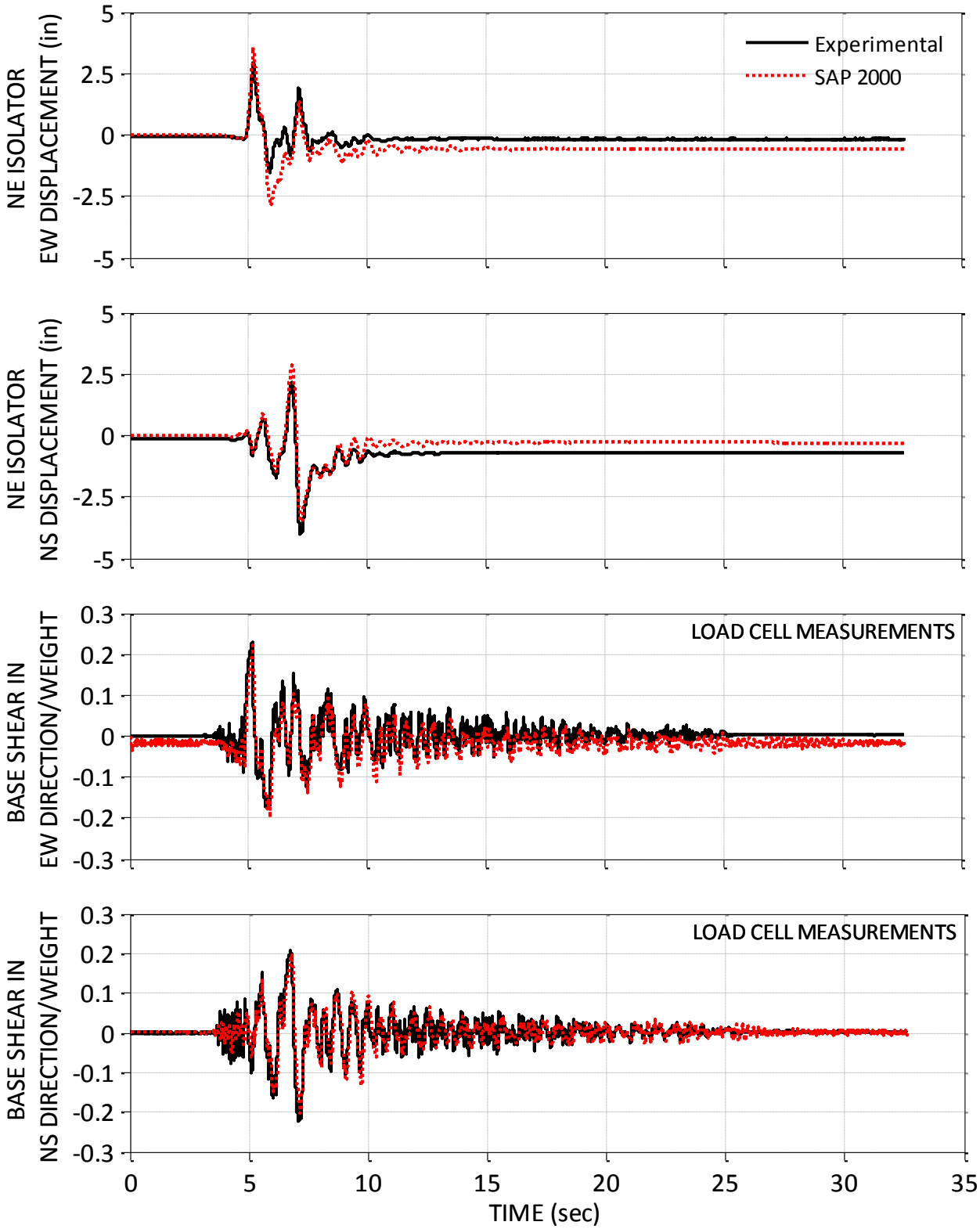

UPPER BUSHING CG
EW ACCELERATION (g)
Experimental
SAP 2000
UPPER BUSHING CG
NS ACCELERATION (g)
TIME (sec)
SPECTRAL
ACCELERATION (g)
FRAME TOP NE CORNER
EW DIRECTION
NS DIRECTION
FREQUENCY (Hz)
BASE SHEAR/WEIGHT
WEIGHT = 47.1 kip
LOAD CELL MEASUREMENTS
TOTAL DISPLACEMENT (in)

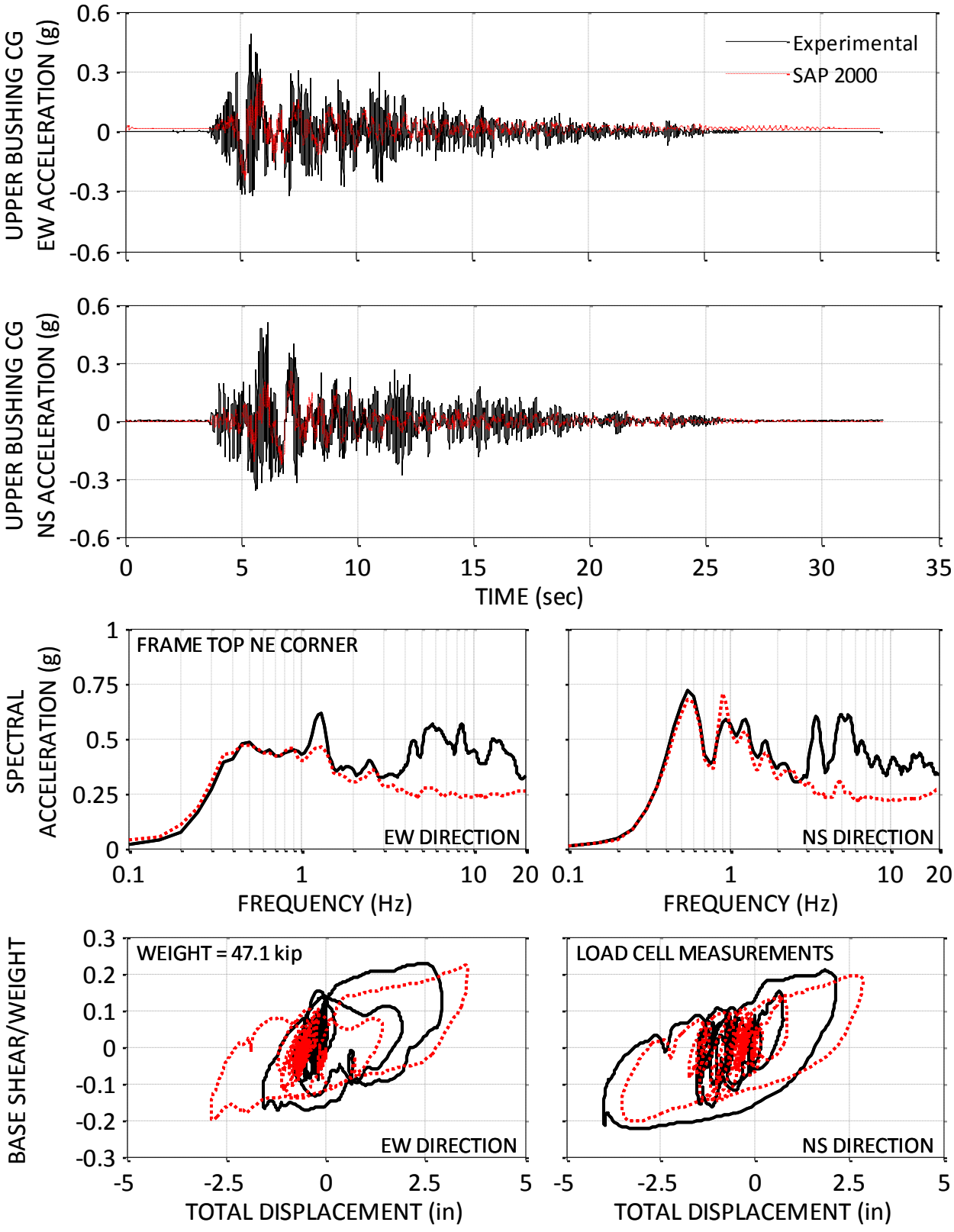
TRIPLE FP SYSTEM (Friction-Bolted Configuration – Series Model)
JENSEN FILTER 121% BI-AXIAL (FN in EW direction)
LENGTH SCALE=3 SYMMETRIC BUSHING CONFIGURATION



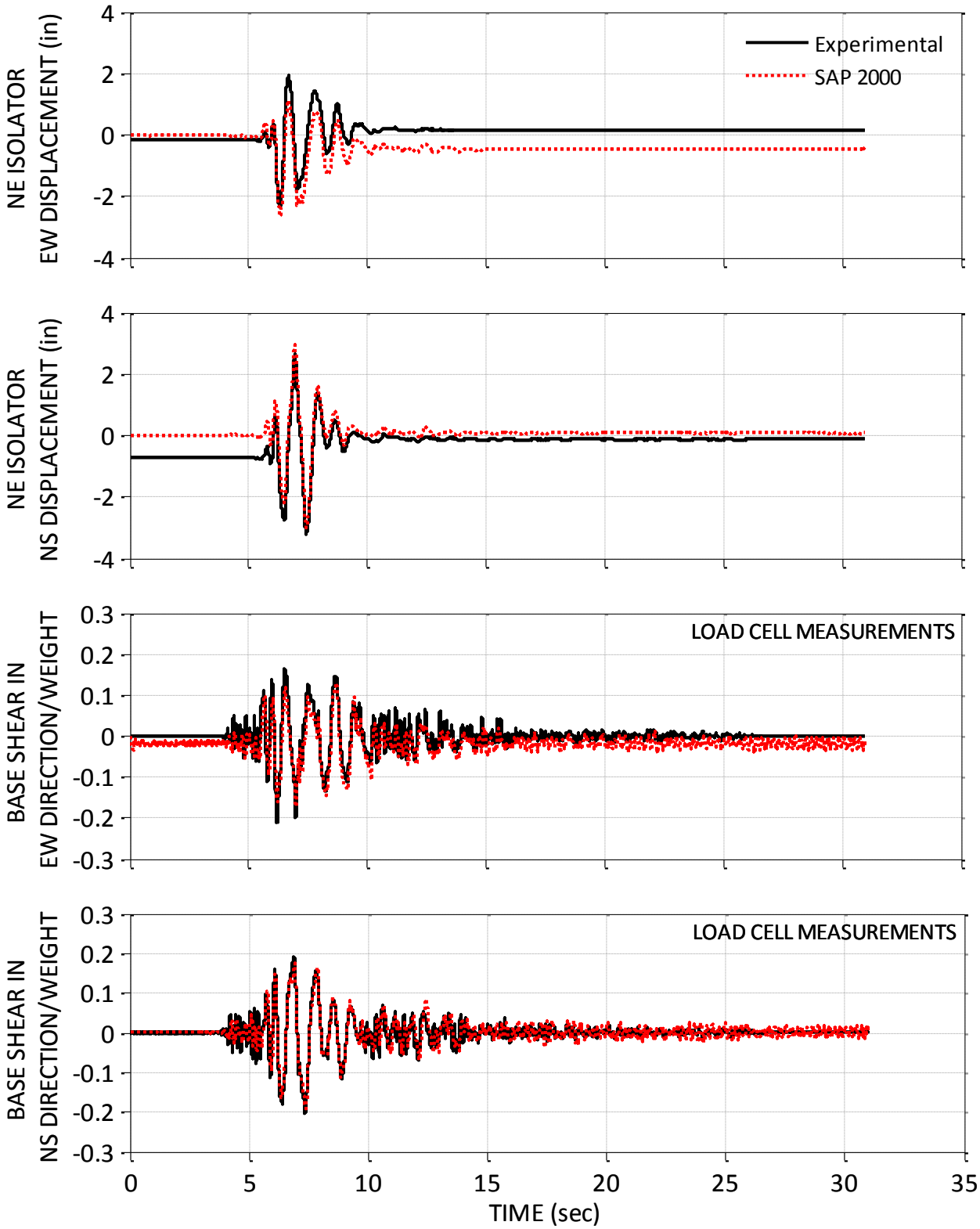

UPPER BUSHING CG
EW ACCELERATION (g)
Experimental
SAP 2000
UPPER BUSHING CG
NS ACCELERATION (g)
TIME (sec)
SPECTRAL
ACCELERATION (g)
FRAME TOP NE CORNER
EW DIRECTION
NS DIRECTION
FREQUENCY (Hz)
BASE SHEAR/WEIGHT
WEIGHT = 47.1 kip
LOAD CELL MEASUREMENTS
TOTAL DISPLACEMENT (in)

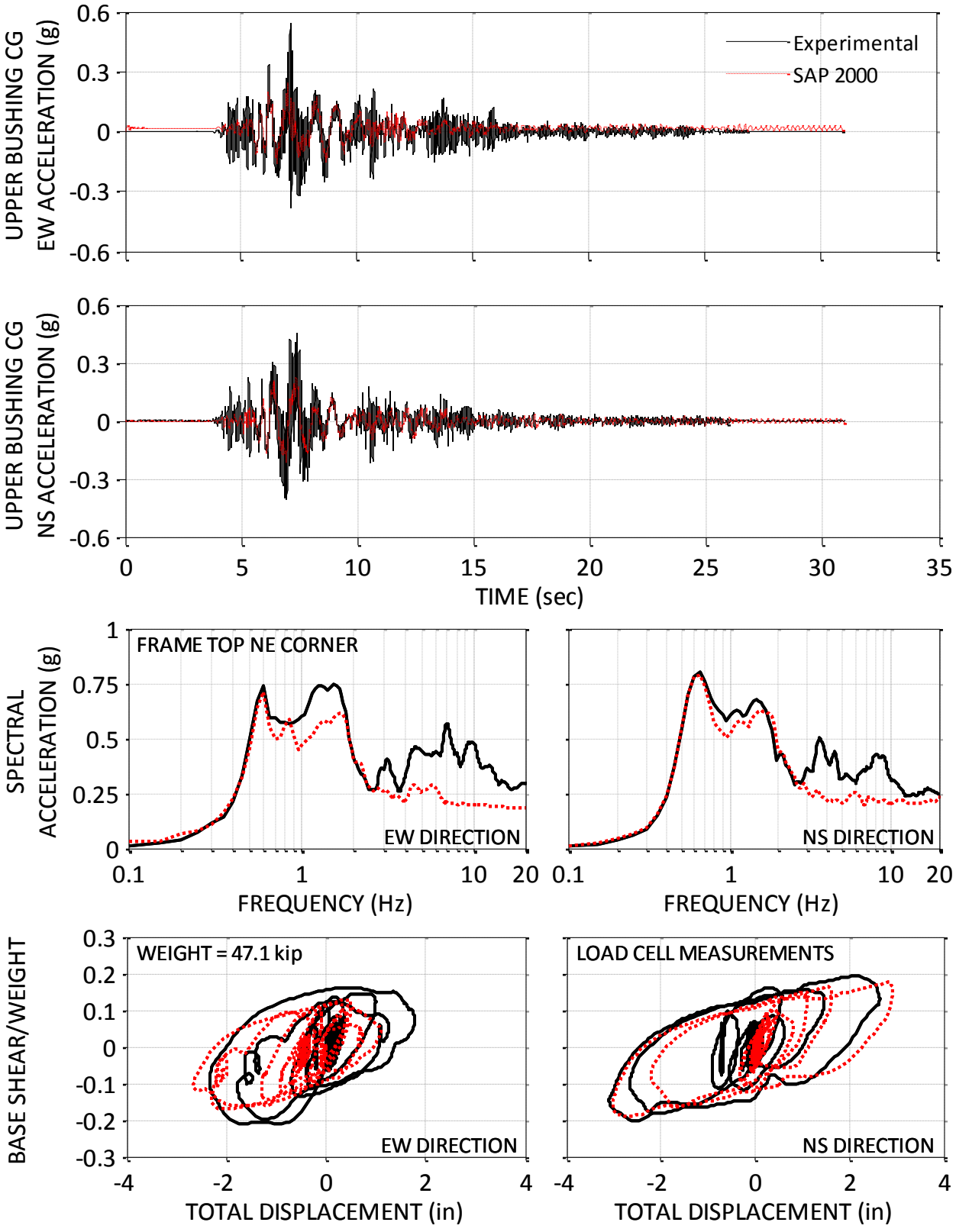
TRIPLE FP SYSTEM (Friction-Bolted Configuration – Series Model)
SYLMAR 113% BI-AXIAL (FN in EW direction)
LENGTH SCALE=3 SYMMETRIC BUSHING CONFIGURATION



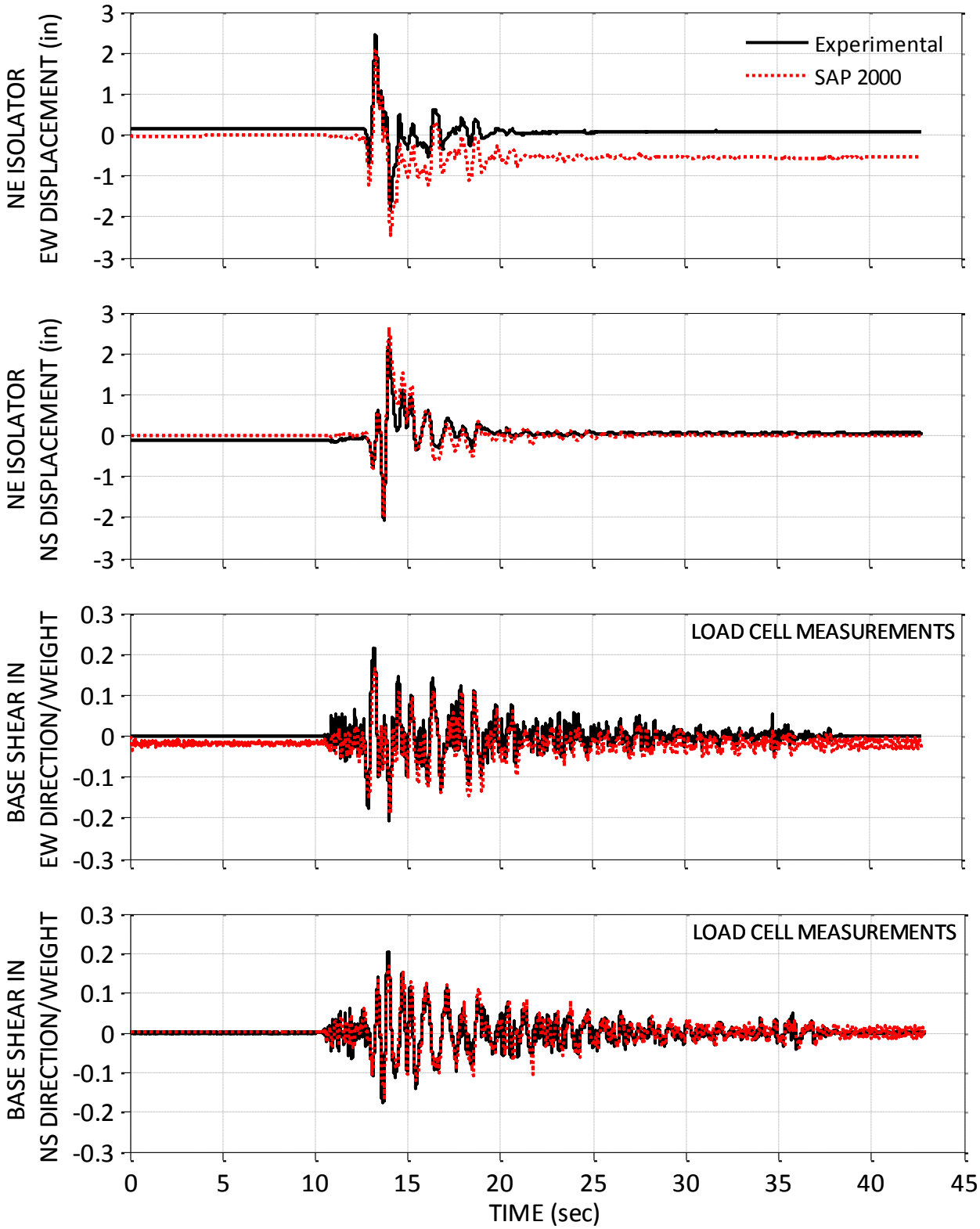

UPPER BUSHING CG
EW ACCELERATION (g)
Experimental
SAP 2000
UPPER BUSHING CG
NS ACCELERATION (g)
TIME (sec)
SPECTRAL
ACCELERATION (g)
FRAME TOP NE CORNER
EW DIRECTION
NS DIRECTION
FREQUENCY (Hz)
BASE SHEAR/WEIGHT
WEIGHT = 47.1 kip
LOAD CELL MEASUREMENTS
TOTAL DISPLACEMENT (in)

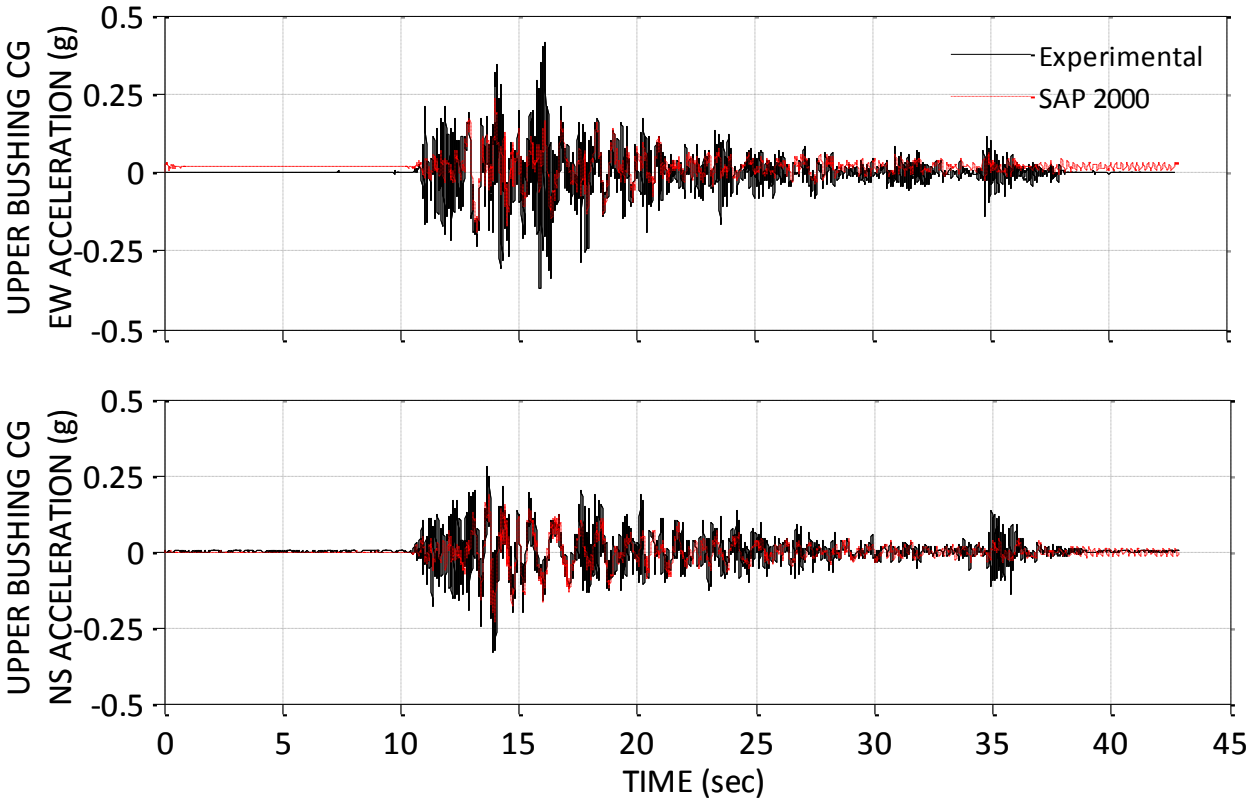
TRIPLE FP SYSTEM (Friction-Bolted Configuration – Series Model)
TAKARAZUKA 121% BI-AXIAL (FN in EW direction)
LENGTH SCALE=3 SYMMETRIC BUSHING CONFIGURATION

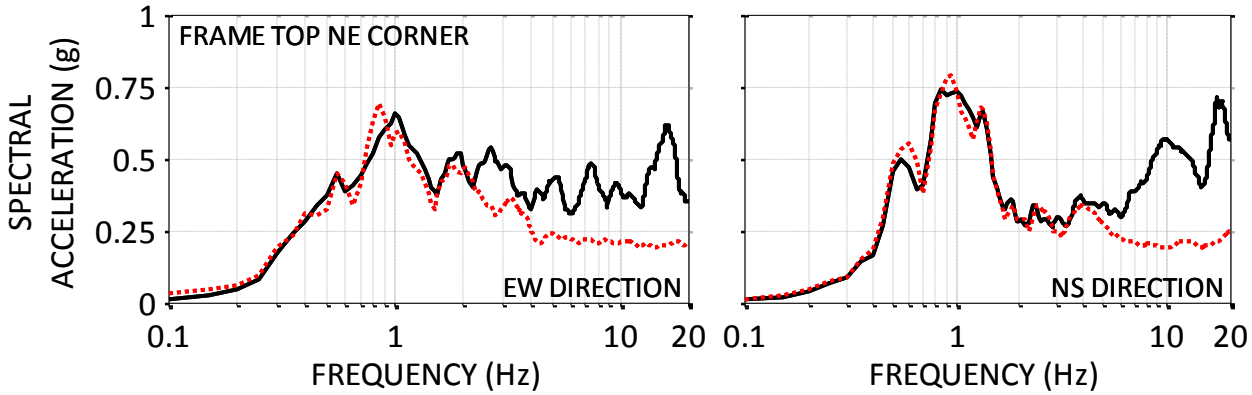


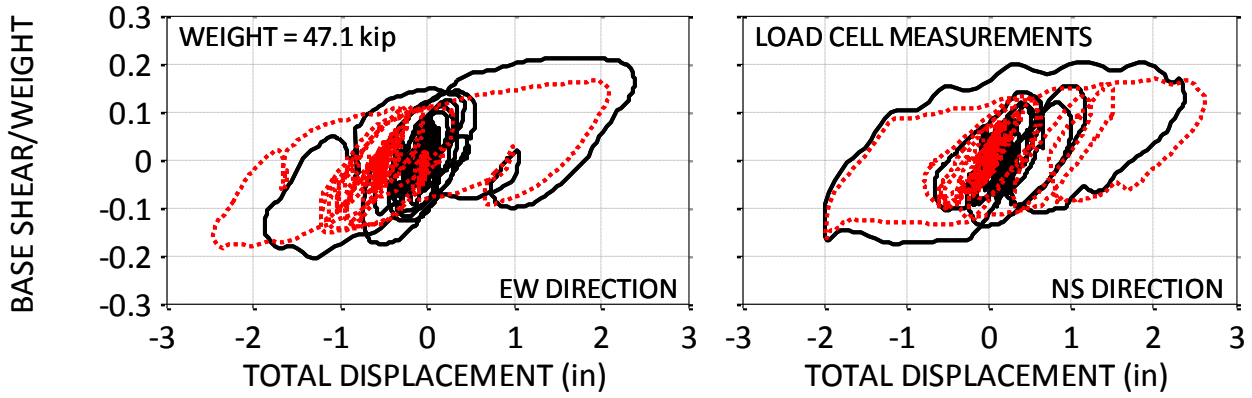

UPPER BUSHING CG
EW ACCELERATION (g)
Experimental
SAP 2000
UPPER BUSHING CG
NS ACCELERATION (g)
TIME (sec)
SPECTRAL
ACCELERATION (g)
FRAME TOP NE CORNER
EW DIRECTION
NS DIRECTION
FREQUENCY (Hz)
BASE SHEAR/WEIGHT
WEIGHT = 47.1 kip
LOAD CELL MEASUREMENTS
TOTAL DISPLACEMENT (in)

TRIPLE FP SYSTEM (Friction-Bolted Configuration – Series Model)
BOLU 130% BI-AXIAL (FN in EW direction)
LENGTH SCALE=3 SYMMETRIC BUSHING CONFIGURATION

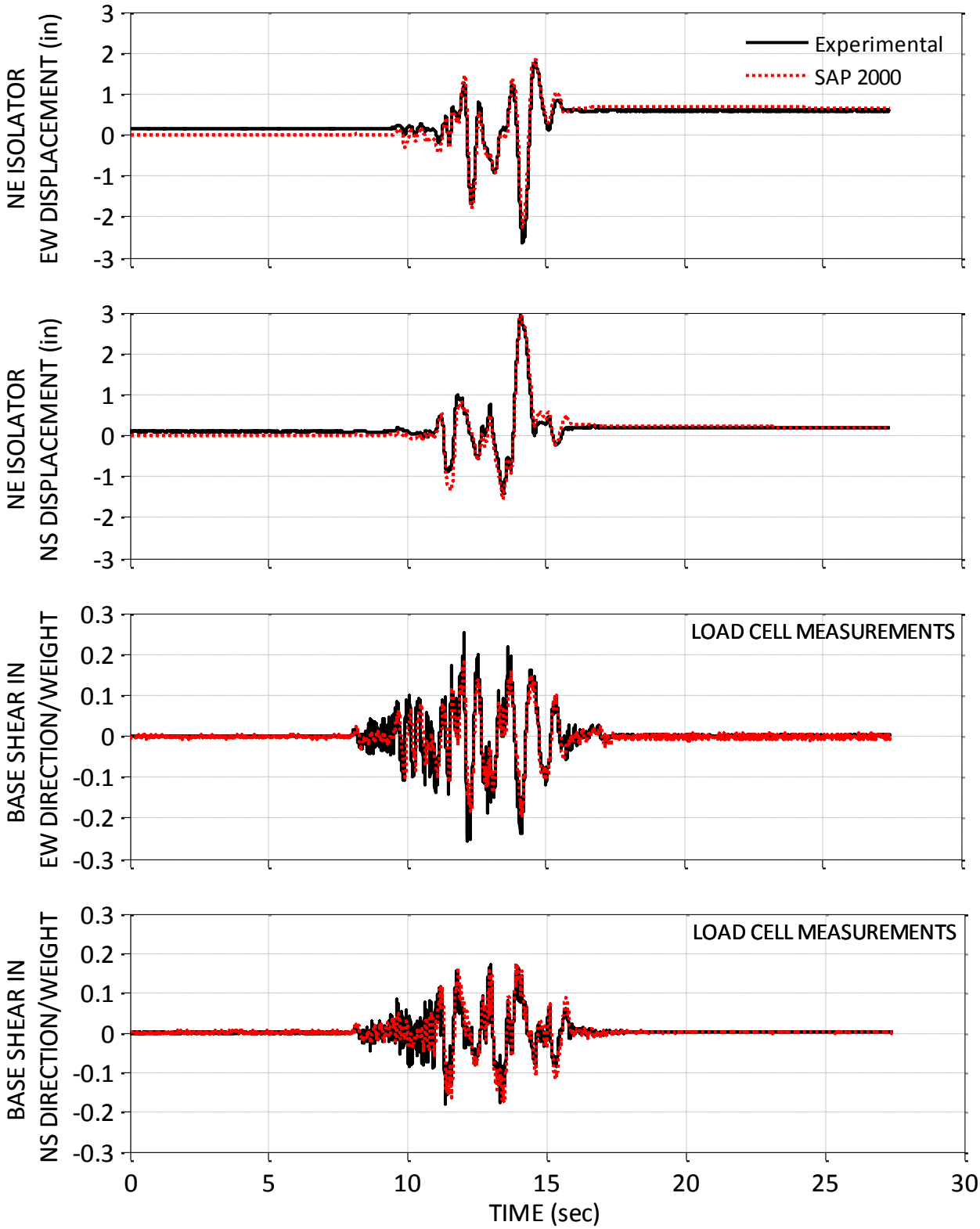


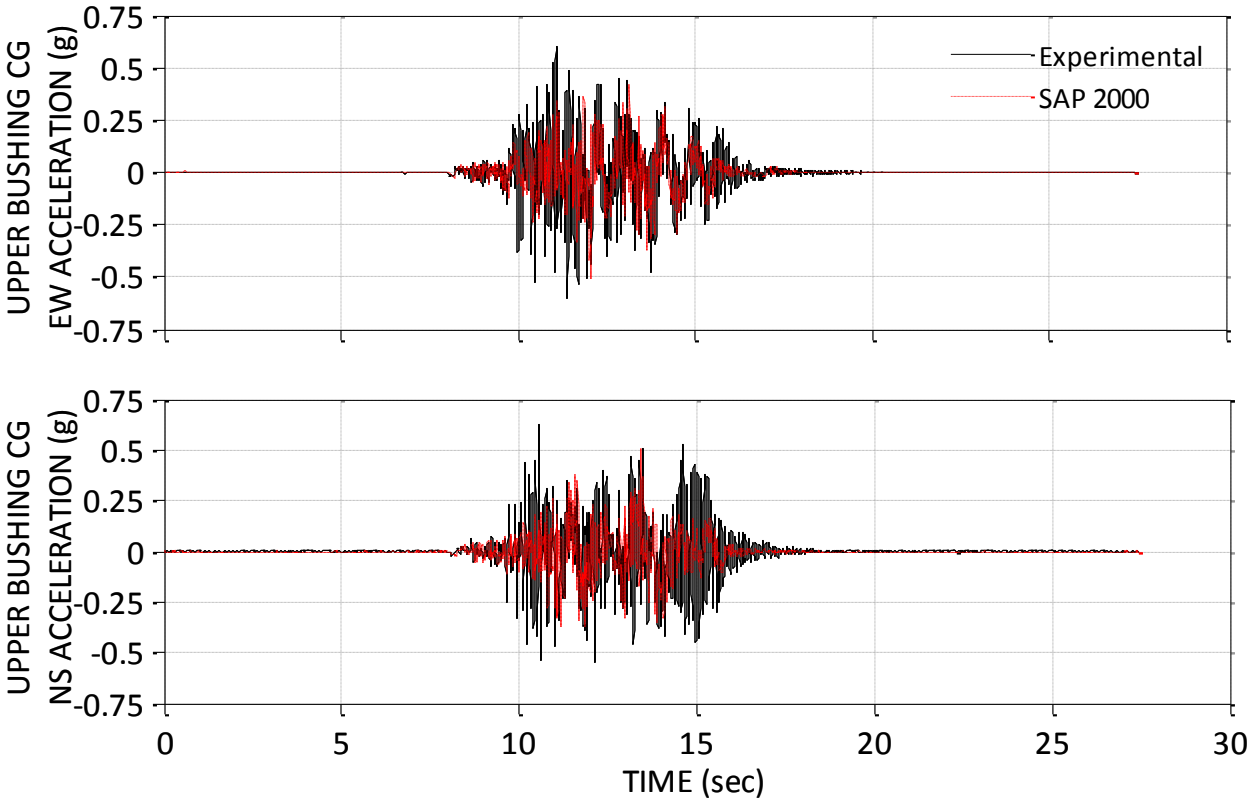

UPPER BUSHING CG
EW ACCELERATION (g)
Experimental
SAP 2000
UPPER BUSHING CG
NS ACCELERATION (g)
TIME (sec)

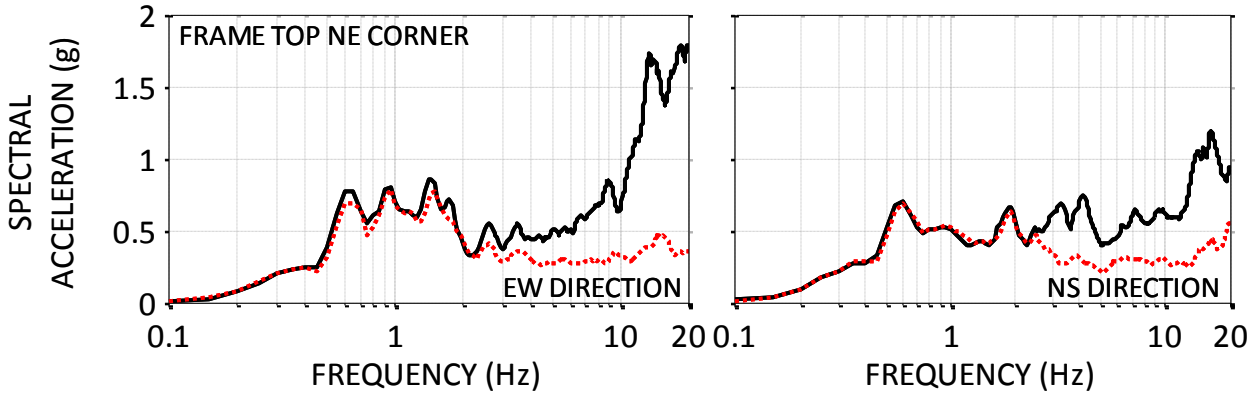

SPECTRAL
ACCELERATION (g)
FRAME TOP NE CORNER
EW DIRECTION
NS DIRECTION
FREQUENCY (Hz)
FREQUENCY (Hz)

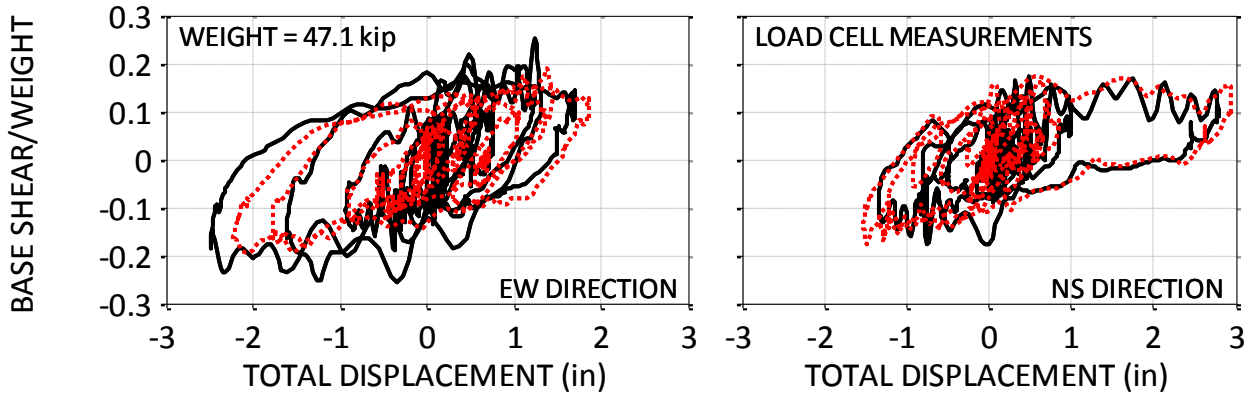

BASE SHEAR/WEIGHT
WEIGHT = 47.1 kip
LOAD CELL MEASUREMENTS
EW DIRECTION
NS DIRECTION
TOTAL DISPLACEMENT (in)
TOTAL DISPLACEMENT (in)

TRIPLE FP SYSTEM (Friction-Bolted Configuration – Series Model)
KARAKYR 137% TRI-AXIAL (FN in EW direction)
LENGTH SCALE=3 SYMMETRIC BUSHING CONFIGURATION

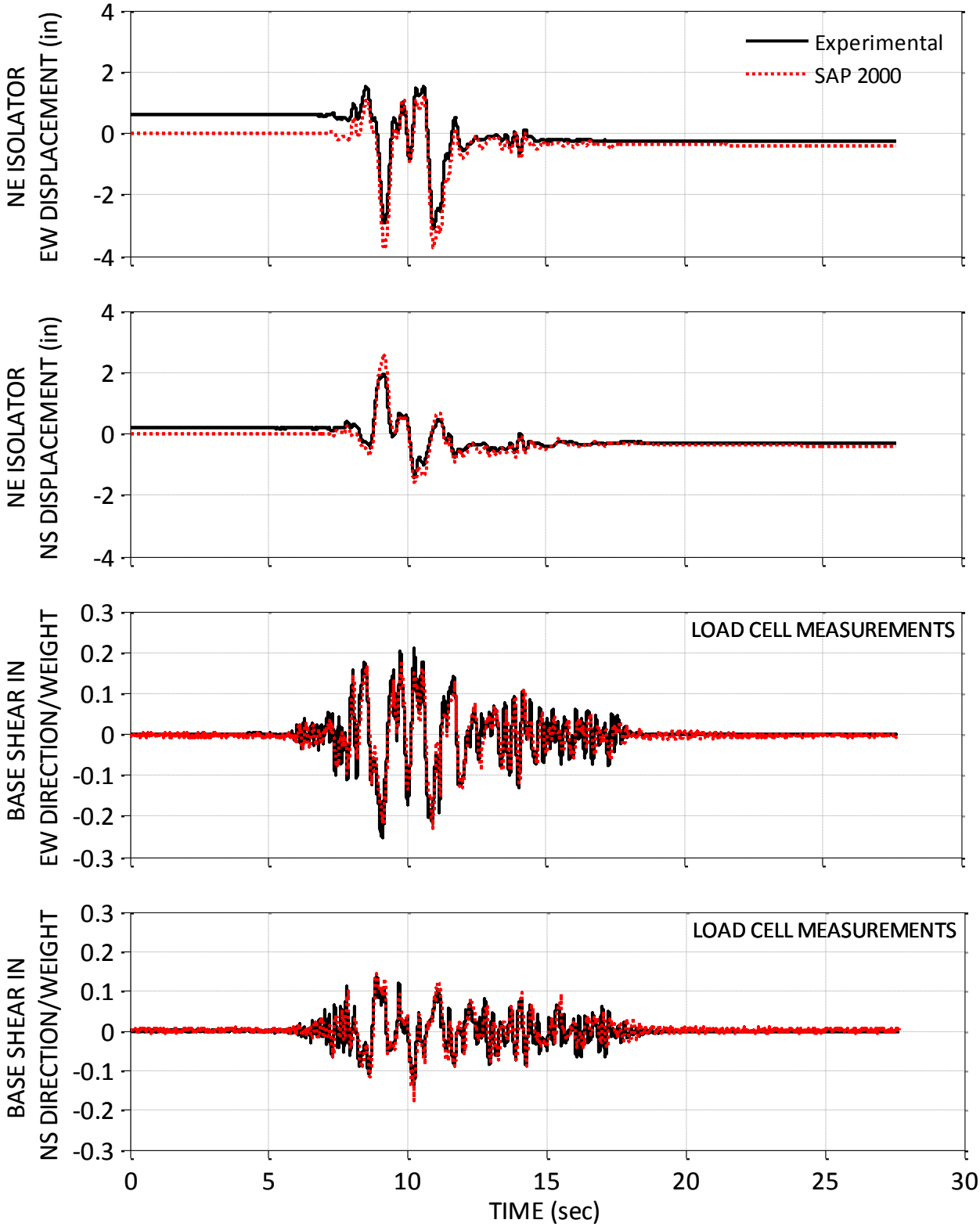


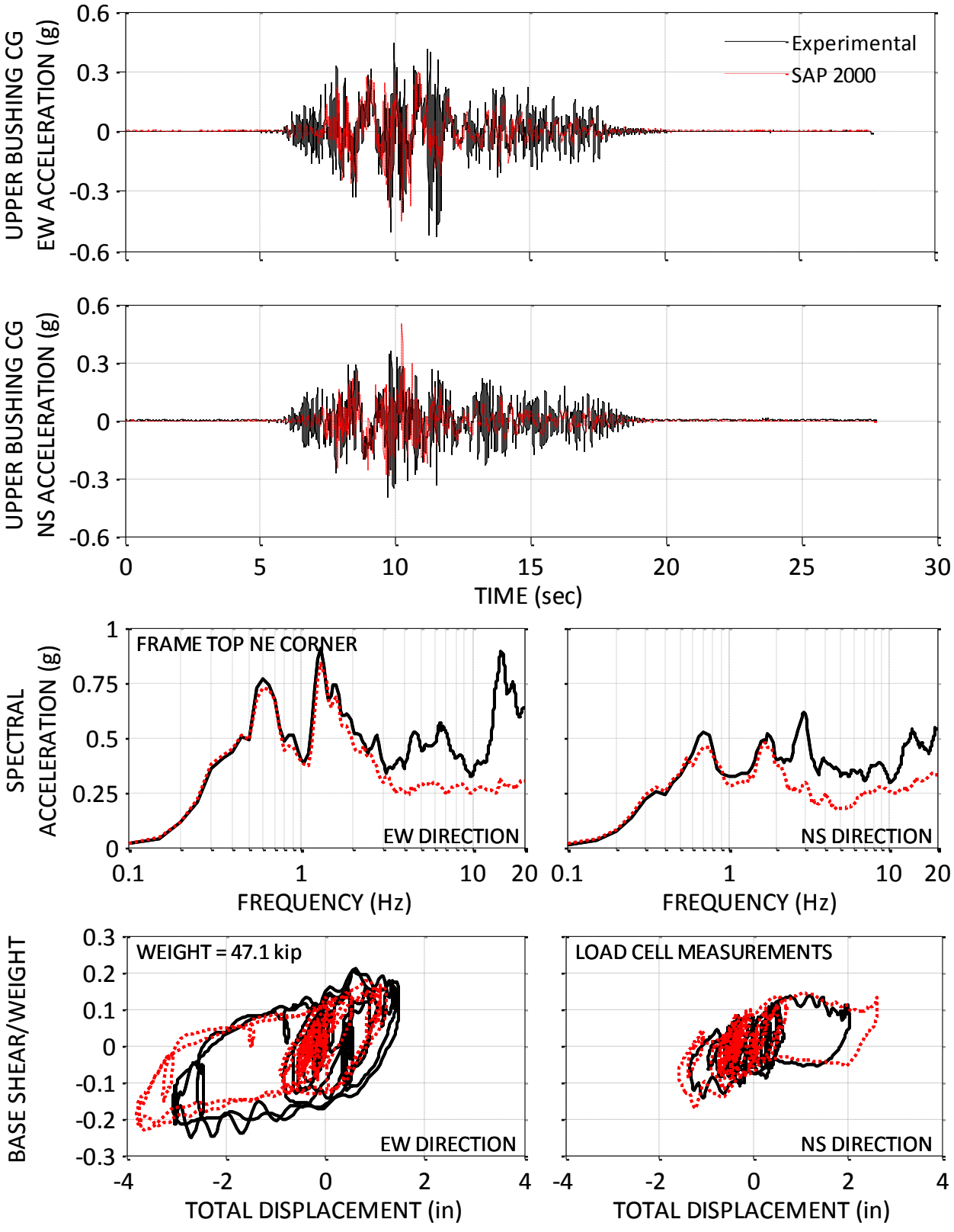

UPPER BUSHING CG
EW ACCELERATION (g)
0.75
0.5
0.25
0
-0.25
-0.5
-0.75
Experimental
SAP 2000
UPPER BUSHING CG
NS ACCELERATION (g)
0
5
10
15
20
25
30
TIME (sec)


SPECTRAL
ACCELERATION (g)
FRAME TOP NE CORNER
2
1.5
1
0.5
0
EW DIRECTION
NS DIRECTION
0.1
1
10
20
FREQUENCY (Hz)

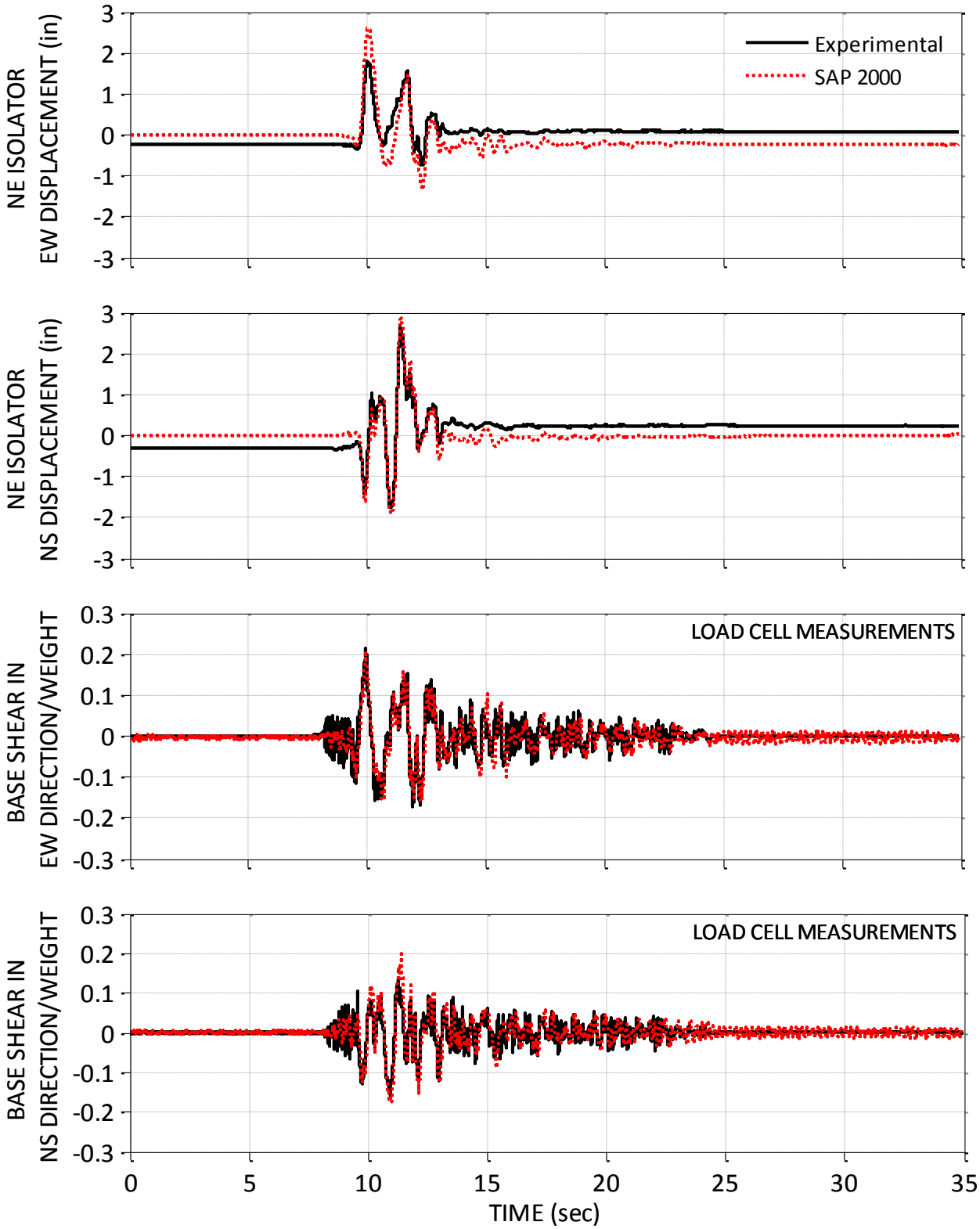

BASE SHEAR/WEIGHT
WEIGHT = 47.1 kip
LOAD CELL MEASUREMENTS
0.3
0.2
0.1
0
-0.1
-0.2
-0.3
EW DIRECTION
NS DIRECTION
-3
-2
-1
0
1
2
3
TOTAL DISPLACEMENT (in)

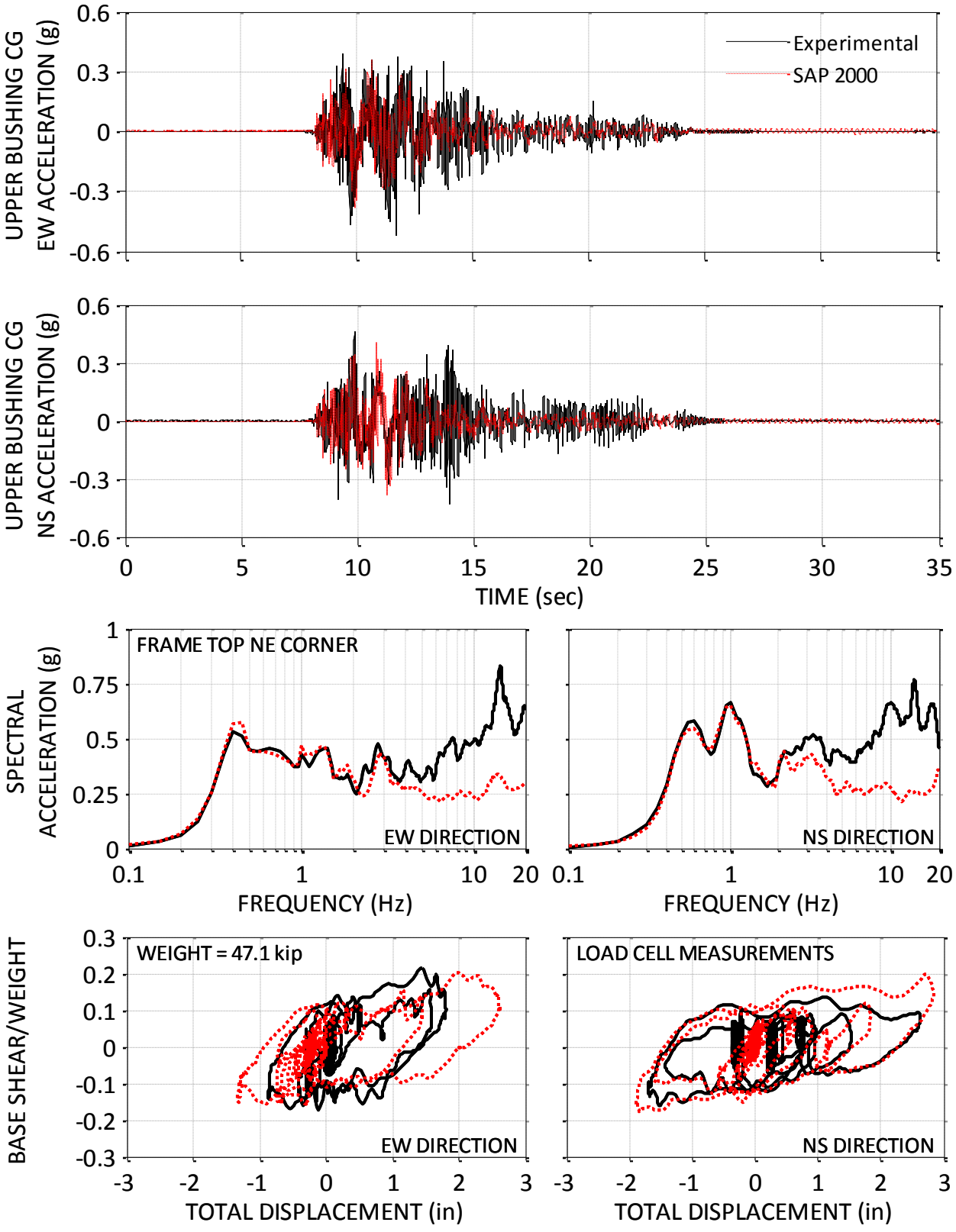
TRIPLE FP SYSTEM (Friction-Bolted Configuration – Series Model)
LGPC 94% TRI-AXIAL (FN in EW direction)
LENGTH SCALE=3 SYMMETRIC BUSHING CONFIGURATION



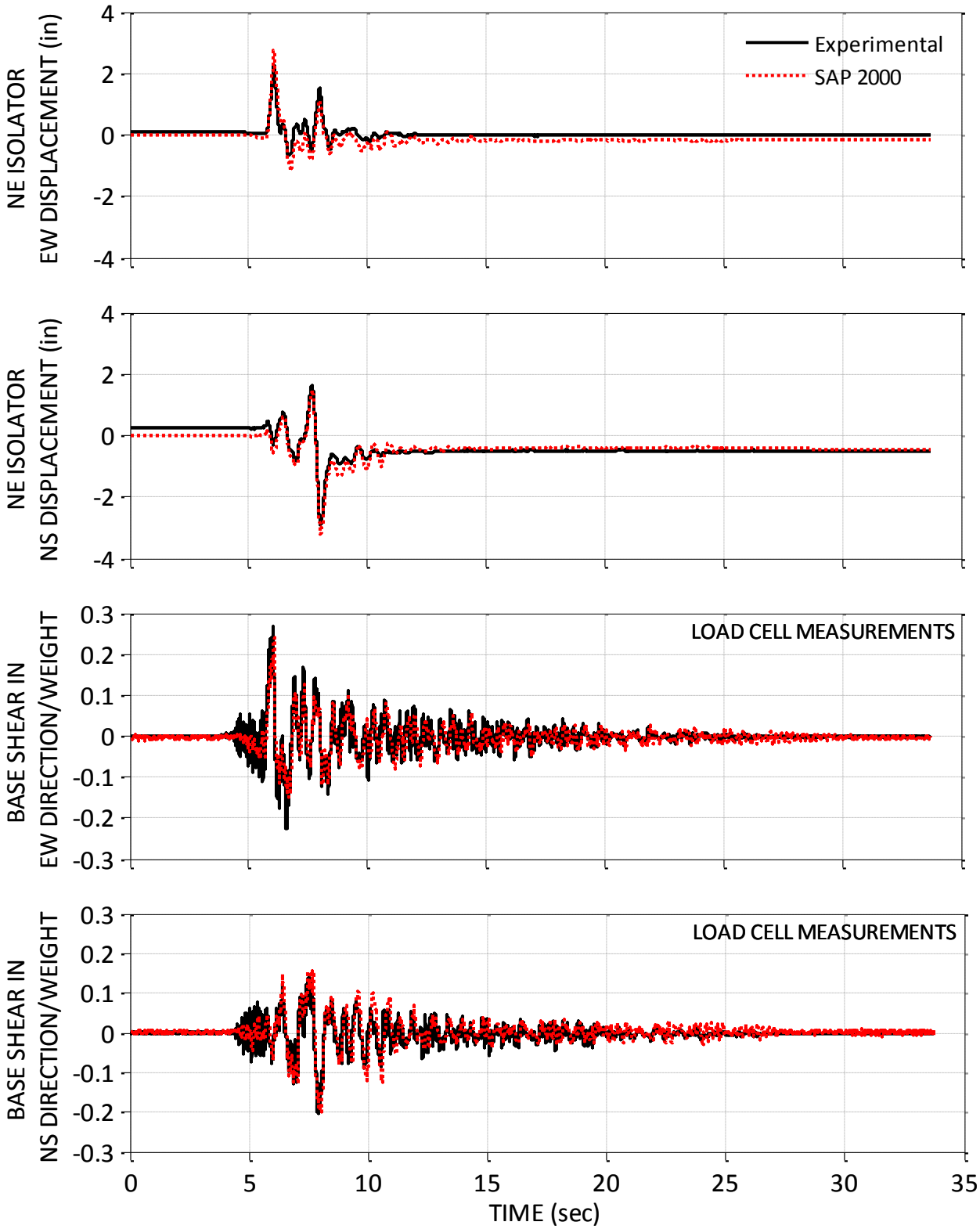

UPPER BUSHING CG
EW ACCELERATION (g)
Experimental
SAP 2000
UPPER BUSHING CG
NS ACCELERATION (g)
TIME (sec)
SPECTRAL
ACCELERATION (g)
FRAME TOP NE CORNER
EW DIRECTION
NS DIRECTION
FREQUENCY (Hz)
BASE SHEAR/WEIGHT
WEIGHT = 47.1 kip
LOAD CELL MEASUREMENTS
TOTAL DISPLACEMENT (in)

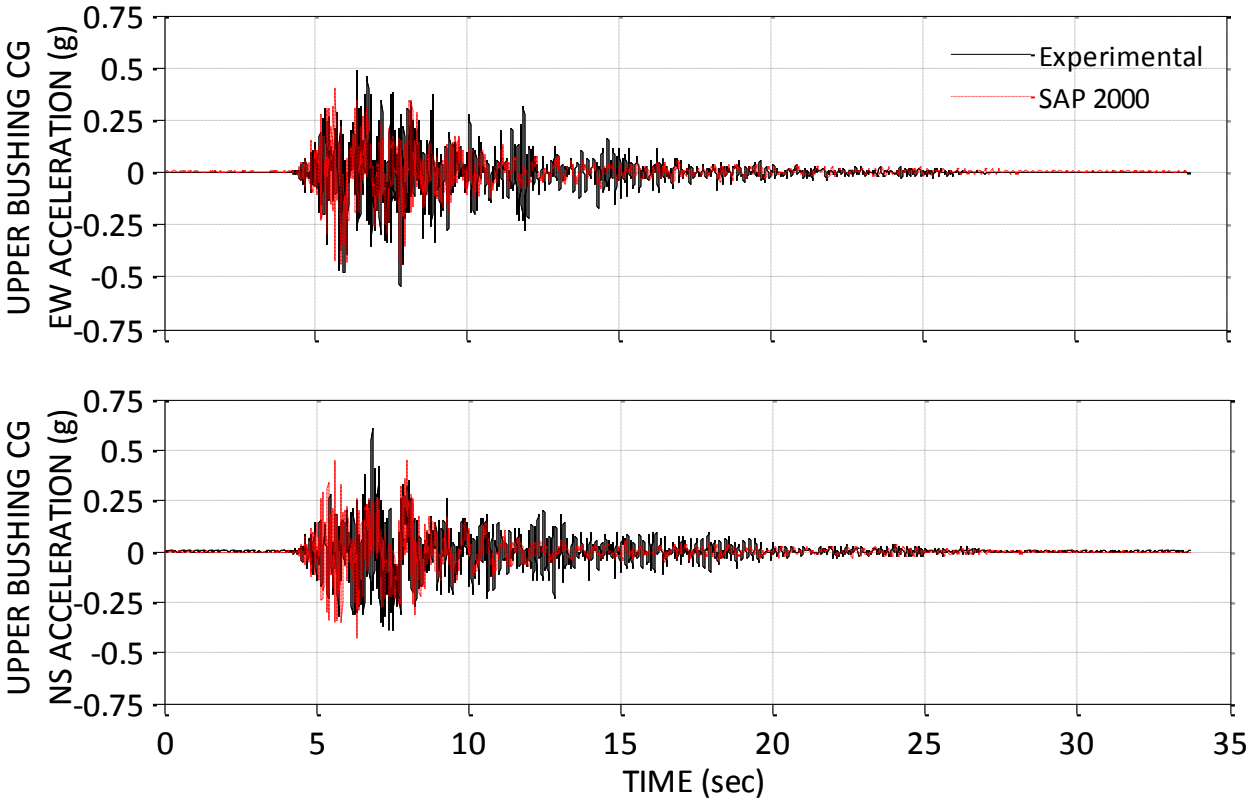
TRIPLE FP SYSTEM (Friction-Bolted Configuration – Series Model)
JENSEN FILTER 97% TRI-AXIAL (FN in EW direction)
LENGTH SCALE=3 SYMMETRIC BUSHING CONFIGURATION

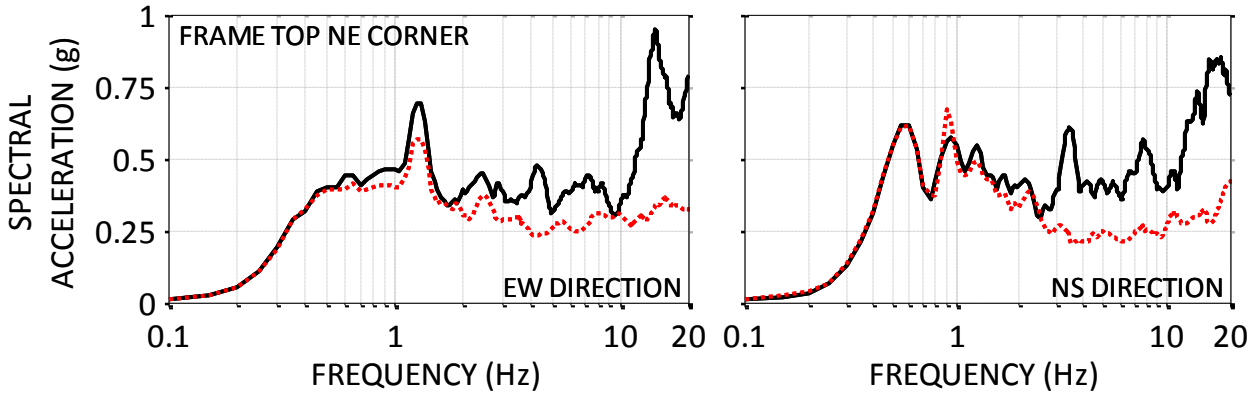


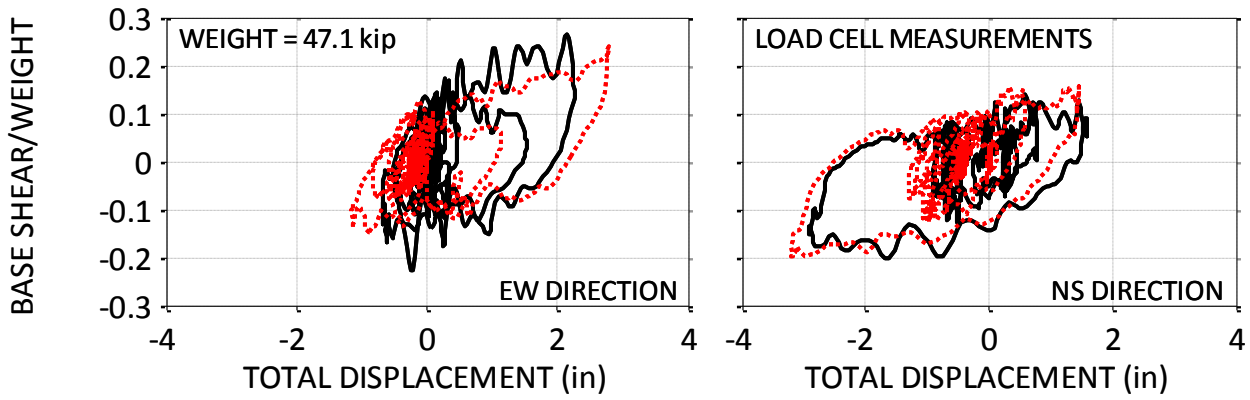

UPPER BUSHING CG
EW ACCELERATION (g)
Experimental
SAP 2000
UPPER BUSHING CG
NS ACCELERATION (g)
TIME (sec)
SPECTRAL
ACCELERATION (g)
FRAME TOP NE CORNER
EW DIRECTION
NS DIRECTION
FREQUENCY (Hz)
BASE SHEAR/WEIGHT
WEIGHT = 47.1 kip
LOAD CELL MEASUREMENTS
TOTAL DISPLACEMENT (in)

TRIPLE FP SYSTEM (Friction-Bolted Configuration – Series Model)
SYLMAR 90% TRI-AXIAL (FN in EW direction)
LENGTH SCALE=3 SYMMETRIC BUSHING CONFIGURATION

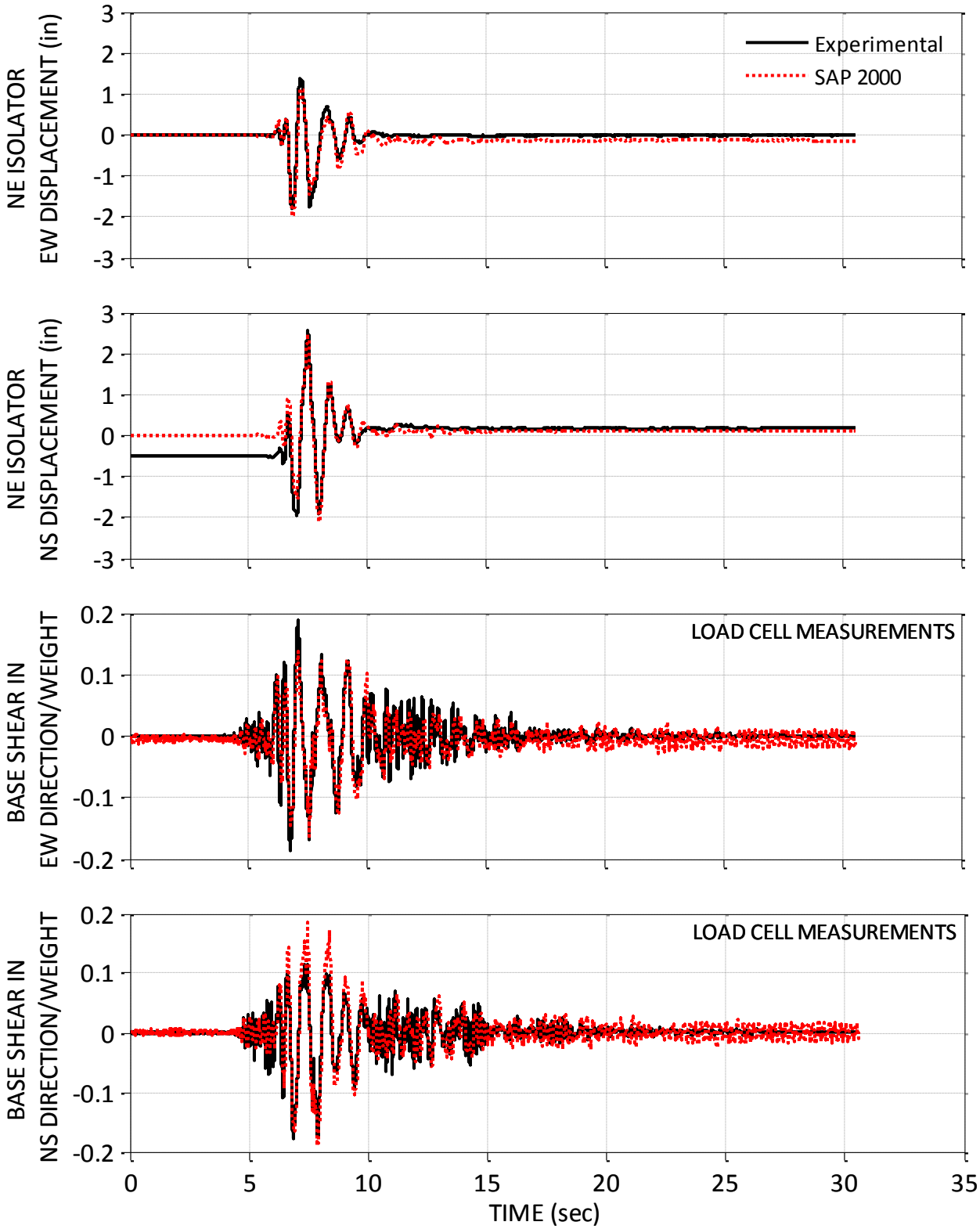


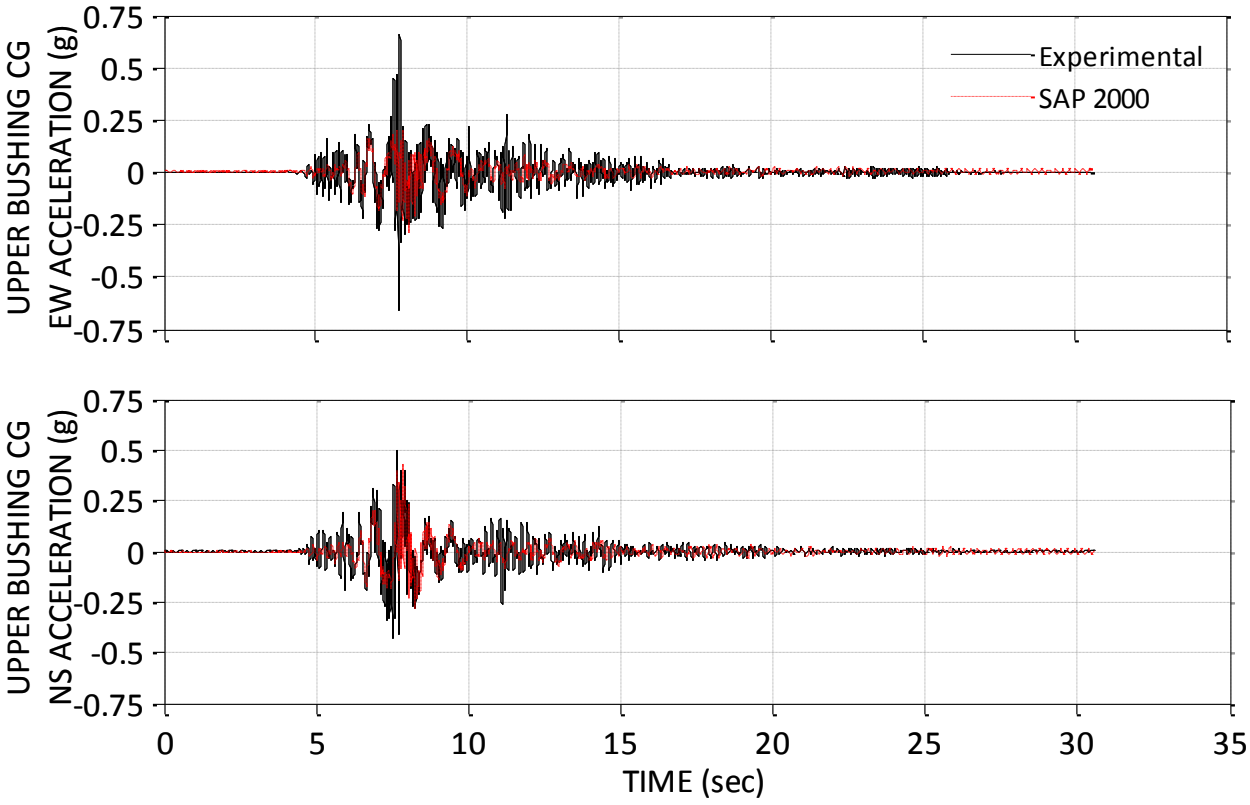

UPPER BUSHING CG
EW ACCELERATION (g)
Experimental
SAP 2000
UPPER BUSHING CG
NS ACCELERATION (g)
TIME (sec)

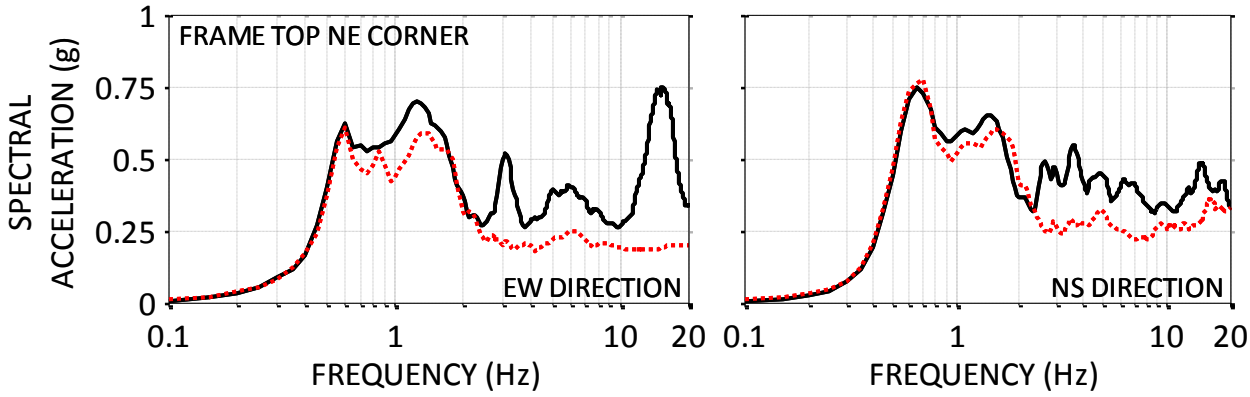

SPECTRAL
ACCELERATION (g)
FRAME TOP NE CORNER
EW DIRECTION
NS DIRECTION
FREQUENCY (Hz)
FREQUENCY (Hz)

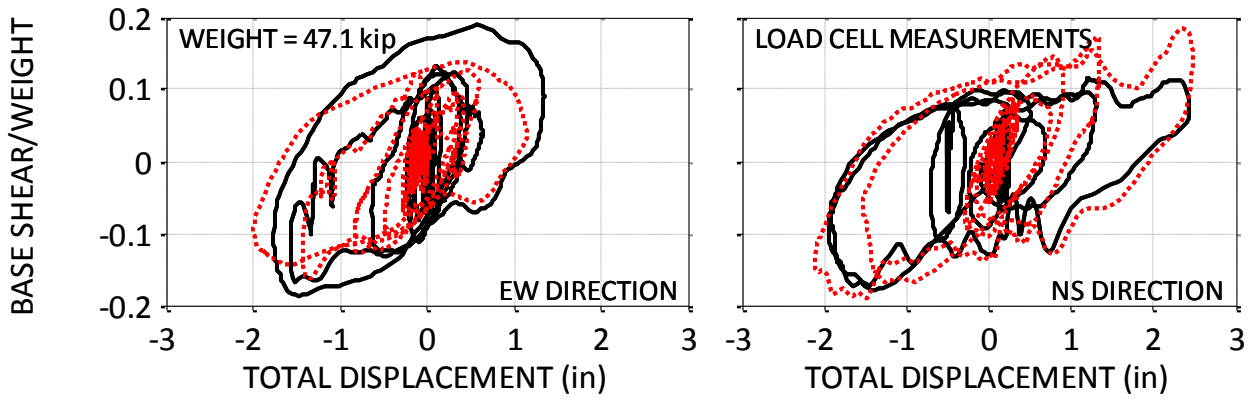

BASE SHEAR/WEIGHT
WEIGHT = 47.1 kip
LOAD CELL MEASUREMENTS
EW DIRECTION
NS DIRECTION
TOTAL DISPLACEMENT (in)
TOTAL DISPLACEMENT (in)

TRIPLE FP SYSTEM (Friction-Bolted Configuration – Series Model)
TAKARAZUKA 97% TRI-AXIAL (FN in EW direction)
LENGTH SCALE=3 SYMMETRIC BUSHING CONFIGURATION

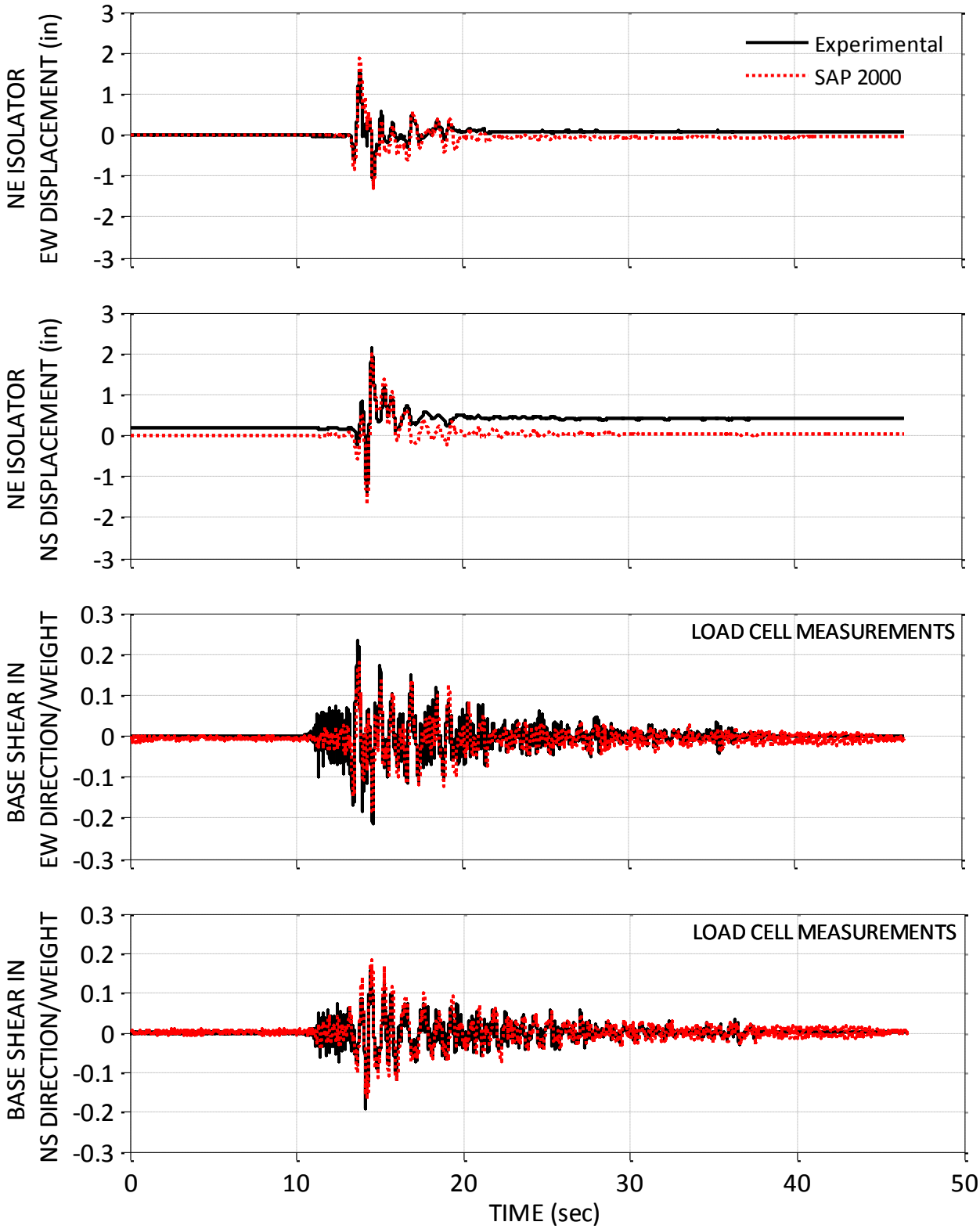


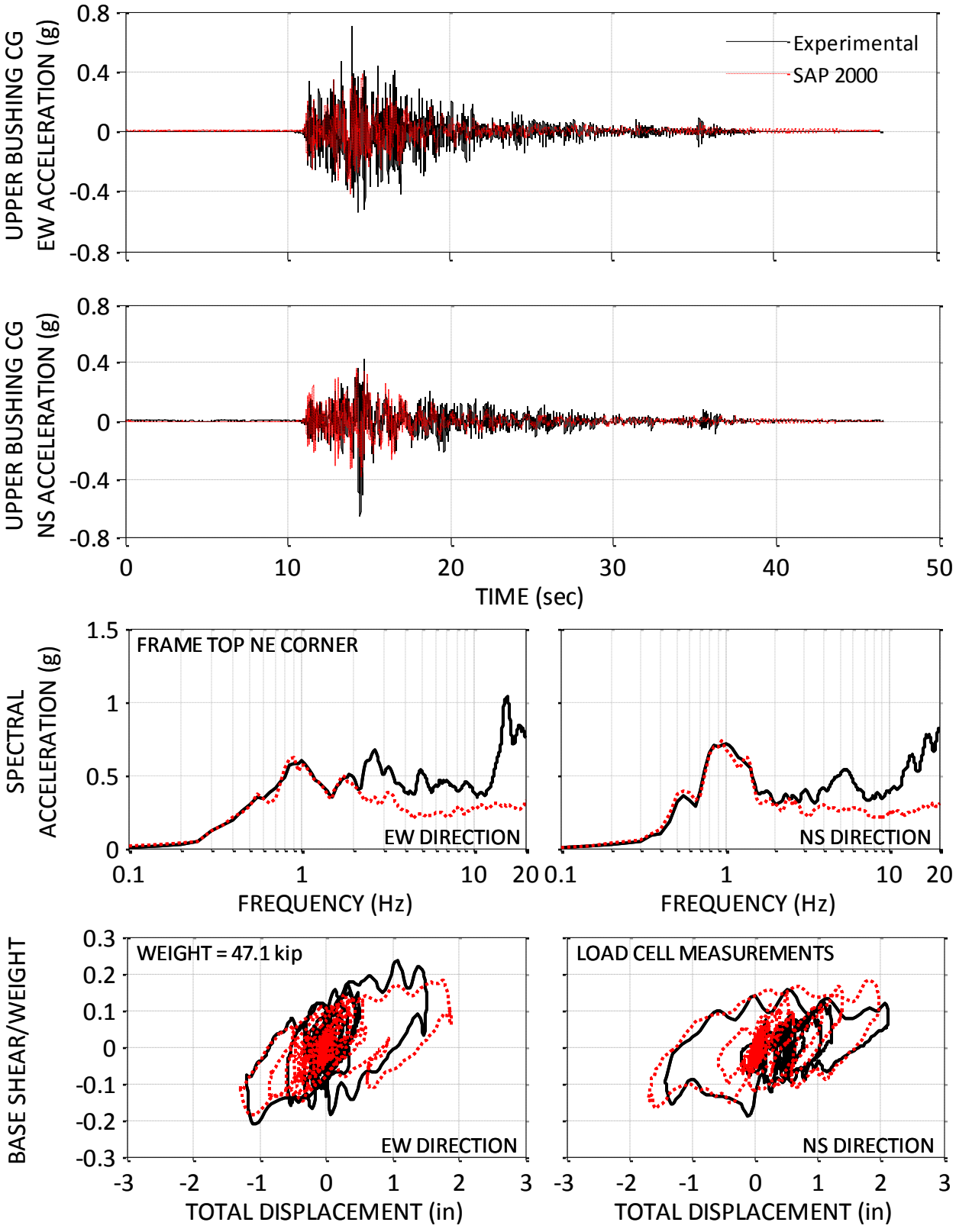

UPPER BUSHING CG
EW ACCELERATION (g)
0.75
0.5
0.25
0
-0.25
-0.5
-0.75
Experimental
SAP 2000
UPPER BUSHING CG
NS ACCELERATION (g)
0
5
10
15
20
25
30
35
TIME (sec)


SPECTRAL
ACCELERATION (g)
1
0.75
0.5
0.25
0
FRAME TOP NE CORNER
EW DIRECTION
NS DIRECTION
0.1
1
10
20
FREQUENCY (Hz)
FREQUENCY (Hz)

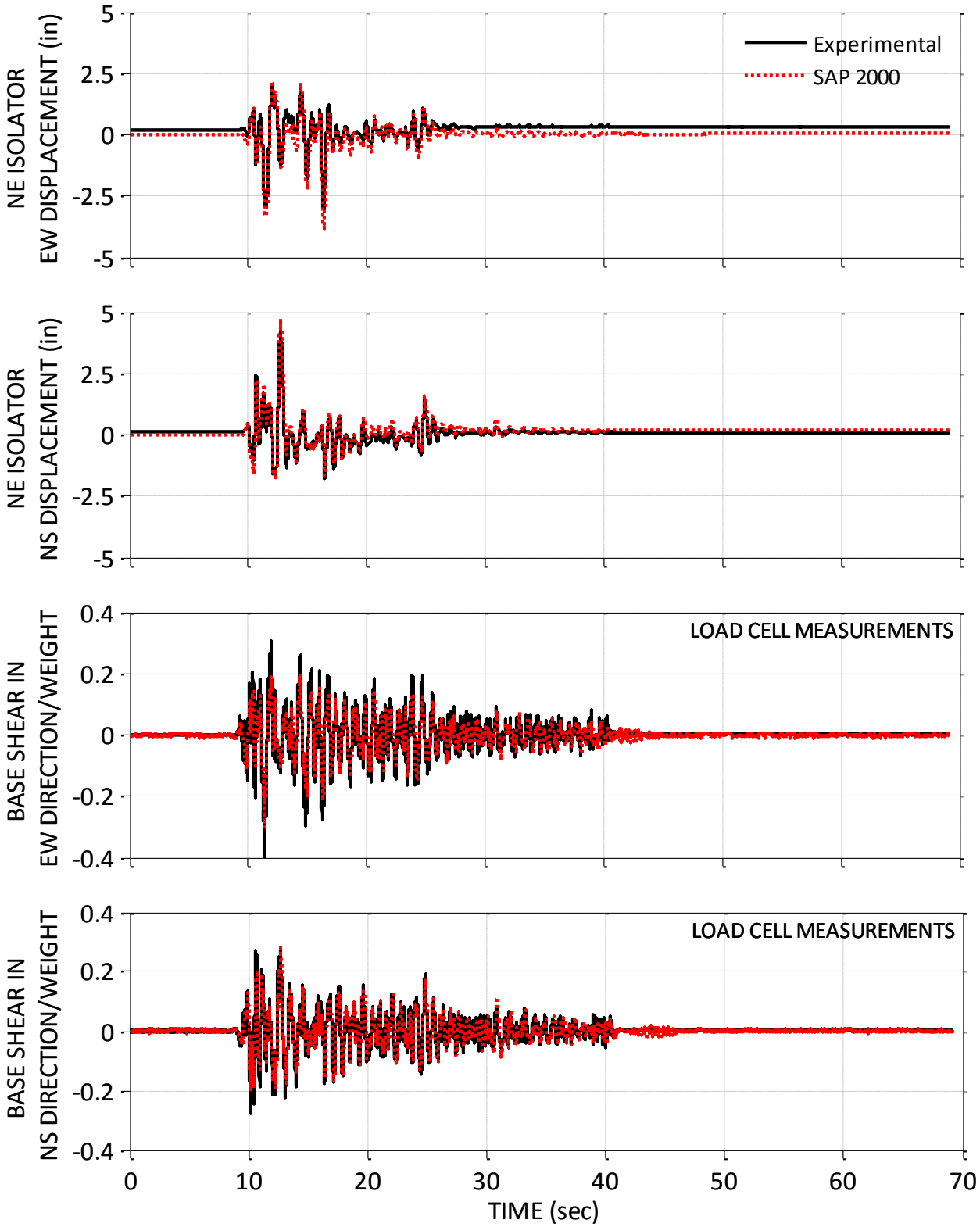

BASE SHEAR/WEIGHT
0.2
0.1
0
-0.1
-0.2
WEIGHT = 47.1 kip
LOAD CELL MEASUREMENTS
EW DIRECTION
NS DIRECTION
-3
-2
-1
0
1
2
3
TOTAL DISPLACEMENT (in)
TOTAL DISPLACEMENT (in)

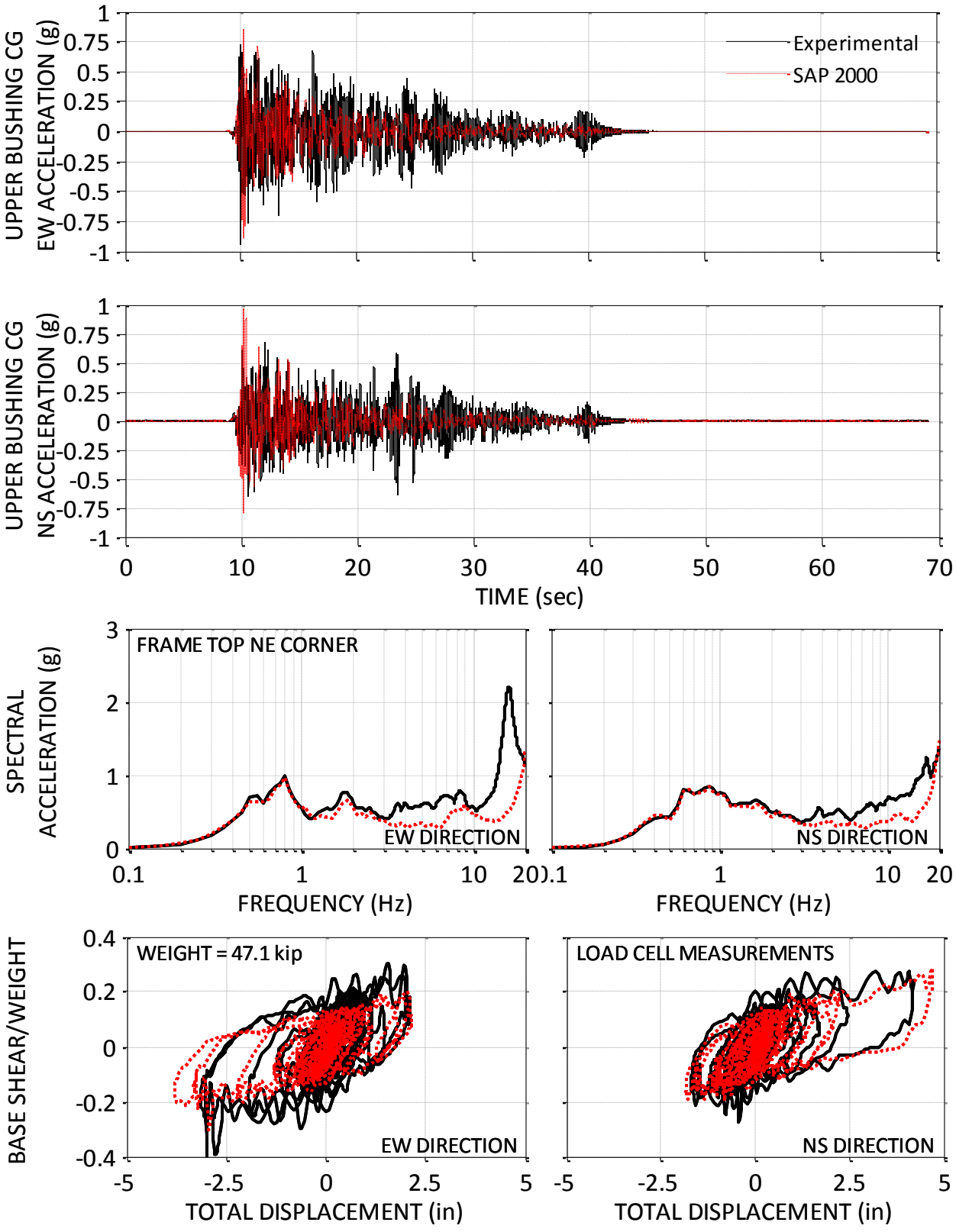
TRIPLE FP SYSTEM (Friction-Bolted Configuration – Series Model)
BOLU 104% TRI-AXIAL (FN in EW direction)
LENGTH SCALE=3 SYMMETRIC BUSHING CONFIGURATION



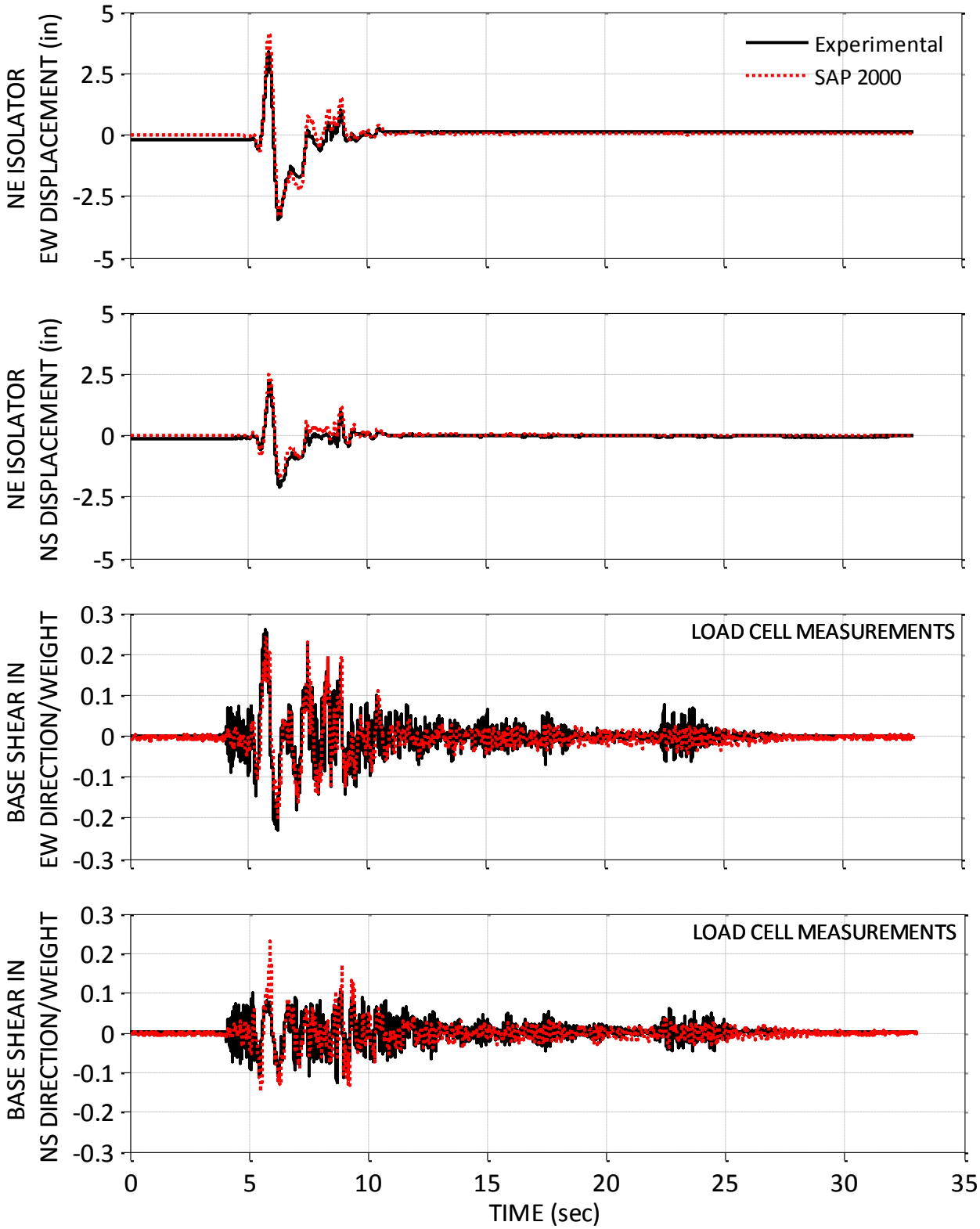

UPPER BUSHING CG
EW ACCELERATION (g)
Experimental
SAP 2000
UPPER BUSHING CG
NS ACCELERATION (g)
TIME (sec)
SPECTRAL
ACCELERATION (g)
FRAME TOP NE CORNER
EW DIRECTION
NS DIRECTION
FREQUENCY (Hz)
BASE SHEAR/WEIGHT
WEIGHT = 47.1 kip
LOAD CELL MEASUREMENTS
TOTAL DISPLACEMENT (in)

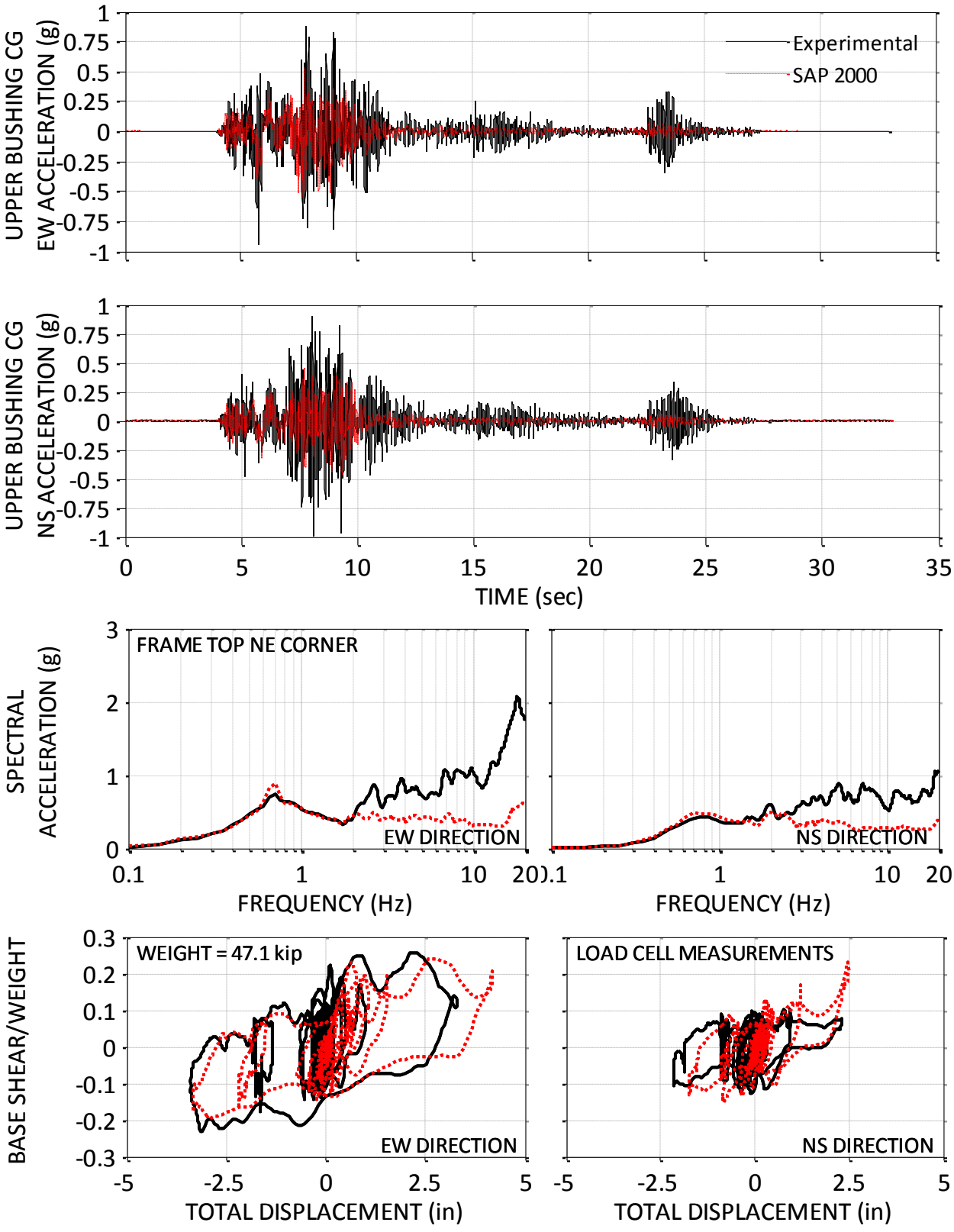
TRIPLE FP SYSTEM (Friction-Bolted Configuration – Series Model)
EL CENTRO 300% TRI-AXIAL (FN in EW direction)
LENGTH SCALE=3 SYMMETRIC BUSHING CONFIGURATION



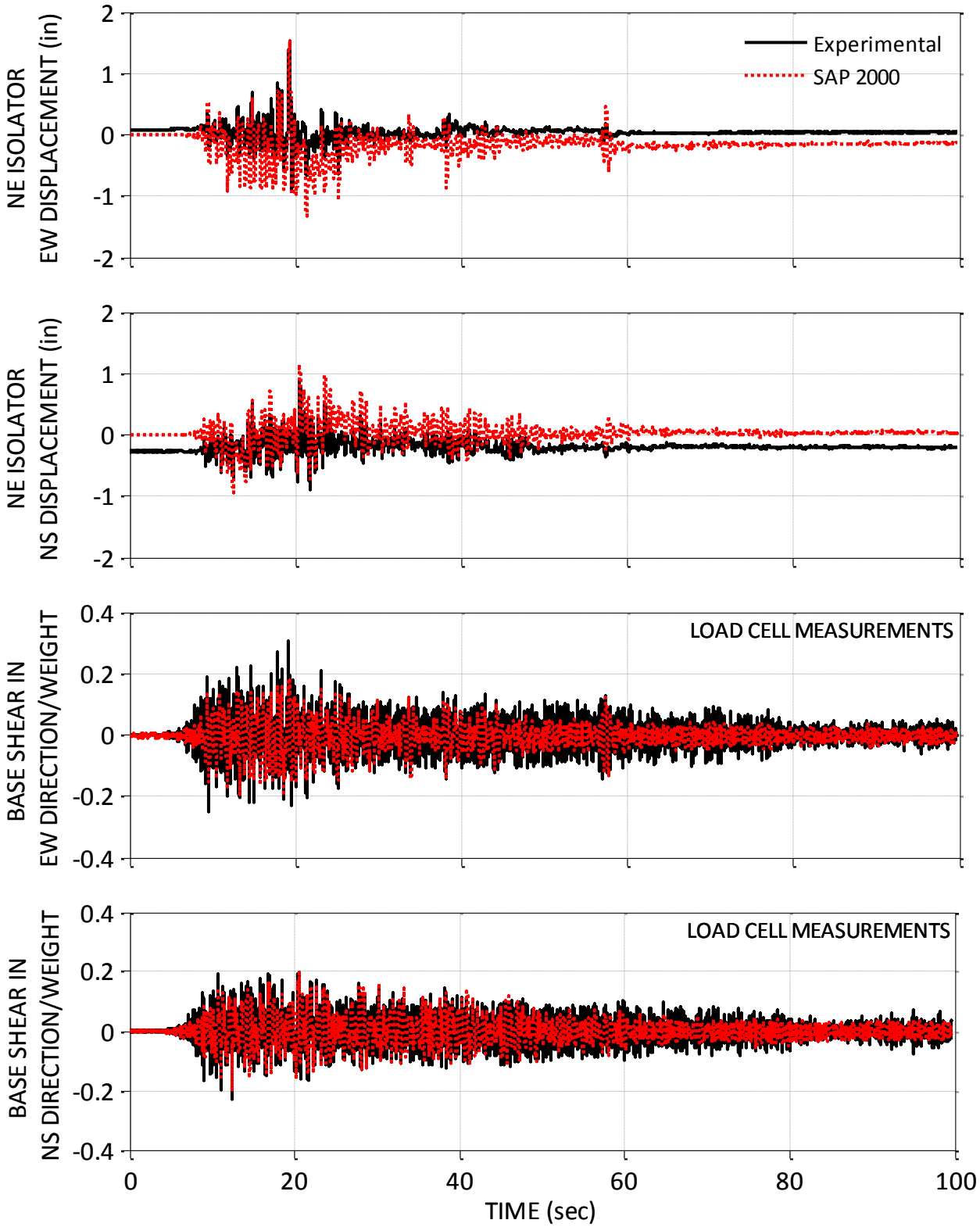

UPPER BUSHING CG
EW ACCELERATION (g)
Experimental
SAP 2000
UPPER BUSHING CG
NS ACCELERATION (g)
TIME (sec)
SPECTRAL
ACCELERATION (g)
FRAME TOP NE CORNER
EW DIRECTION
NS DIRECTION
FREQUENCY (Hz)
FREQUENCY (Hz)
BASE SHEAR/WEIGHT
WEIGHT = 47.1 kip
LOAD CELL MEASUREMENTS
EW DIRECTION
NS DIRECTION
TOTAL DISPLACEMENT (in)
TOTAL DISPLACEMENT (in)

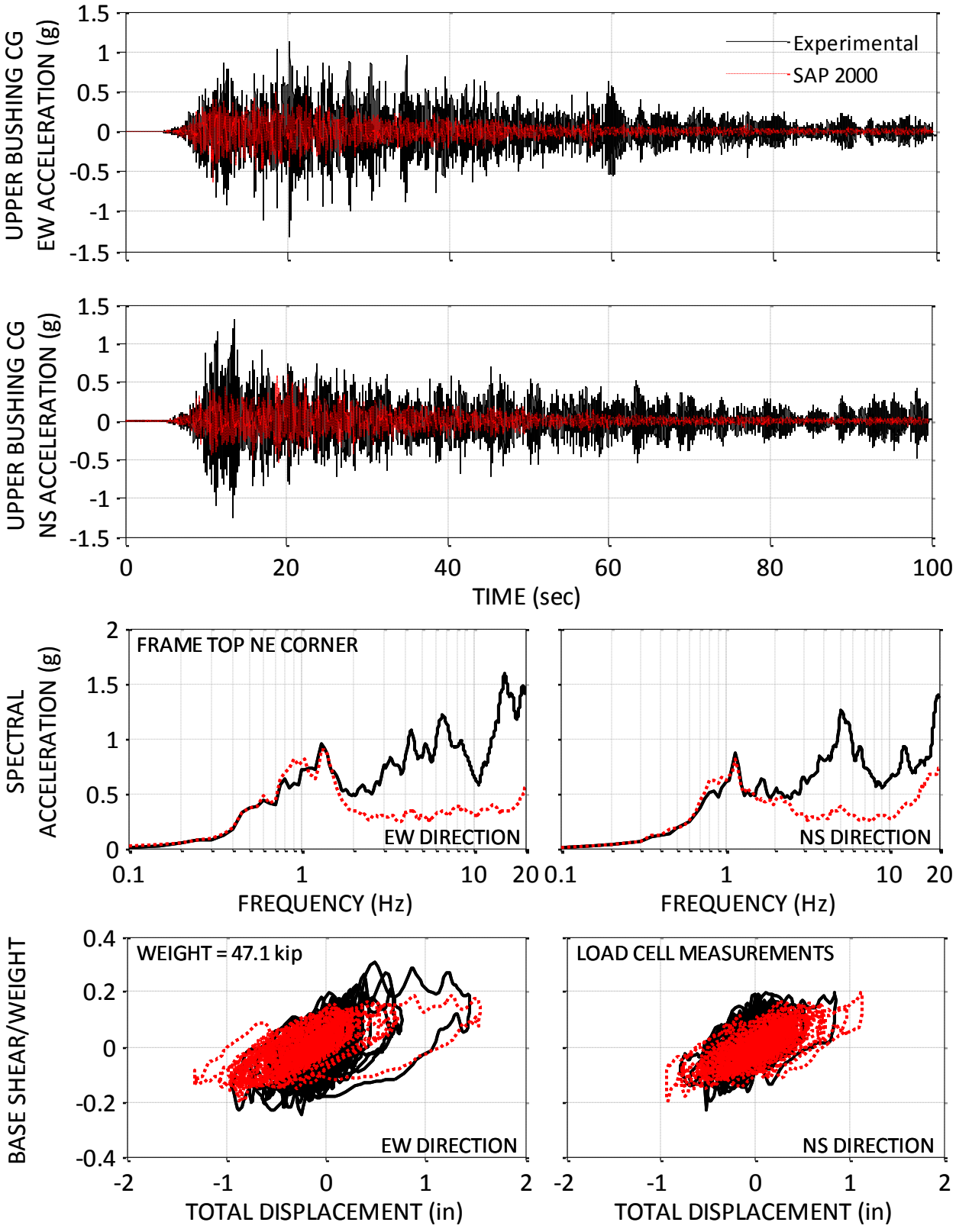
TRIPLE FP SYSTEM (Friction-Bolted Configuration – Series Model)
PACOIMA DAM 100% TRI-AXIAL (FN in EW direction)
LENGTH SCALE=3 SYMMETRIC BUSHING CONFIGURATION



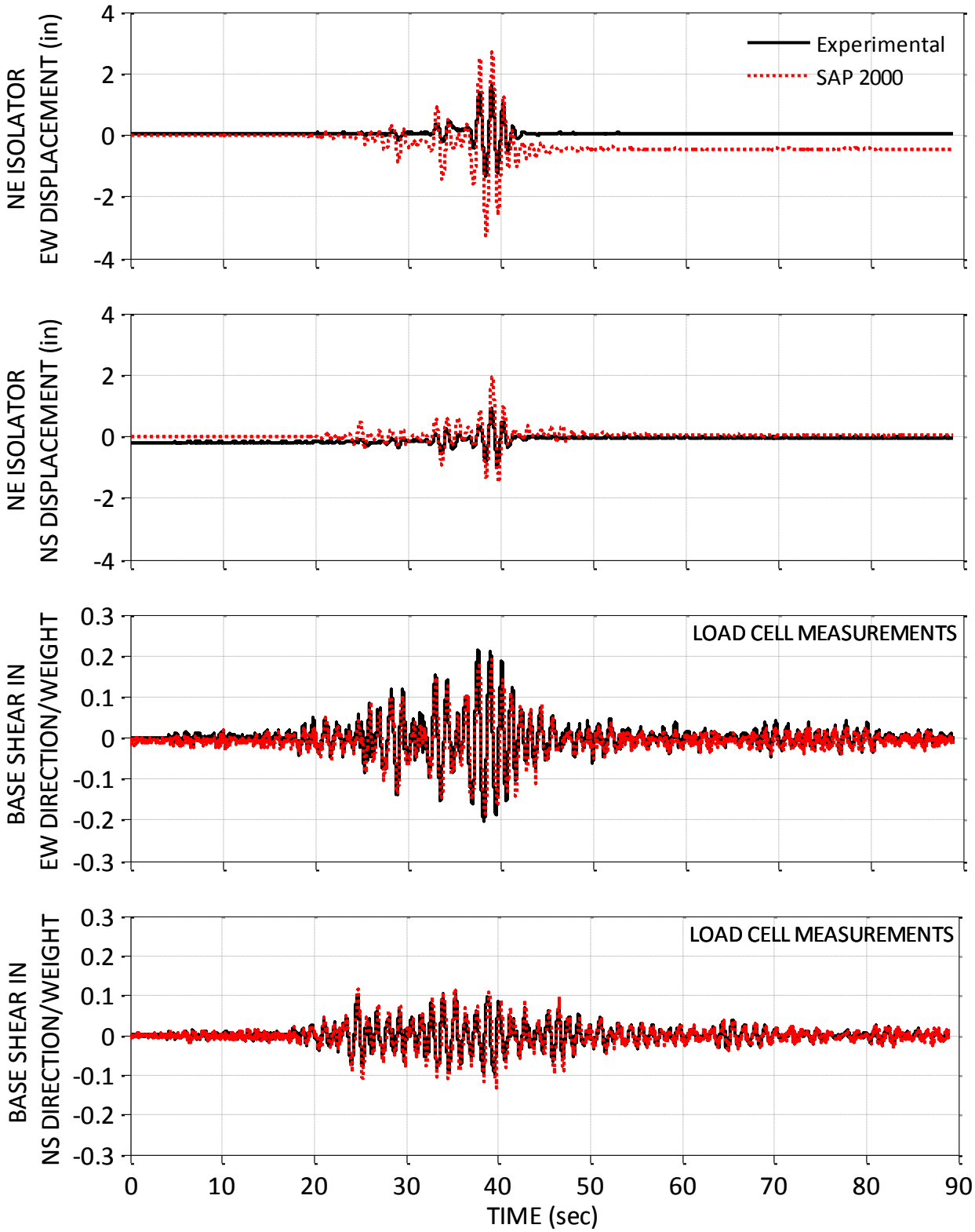

UPPER BUSHING CG
EW ACCELERATION (g)
Experimental
SAP 2000
UPPER BUSHING CG
NS ACCELERATION (g)
TIME (sec)
SPECTRAL
ACCELERATION (g)
FRAME TOP NE CORNER
EW DIRECTION
NS DIRECTION
FREQUENCY (Hz)
FREQUENCY (Hz)
BASE SHEAR/WEIGHT
WEIGHT = 47.1 kip
LOAD CELL MEASUREMENTS
EW DIRECTION
NS DIRECTION
TOTAL DISPLACEMENT (in)
TOTAL DISPLACEMENT (in)

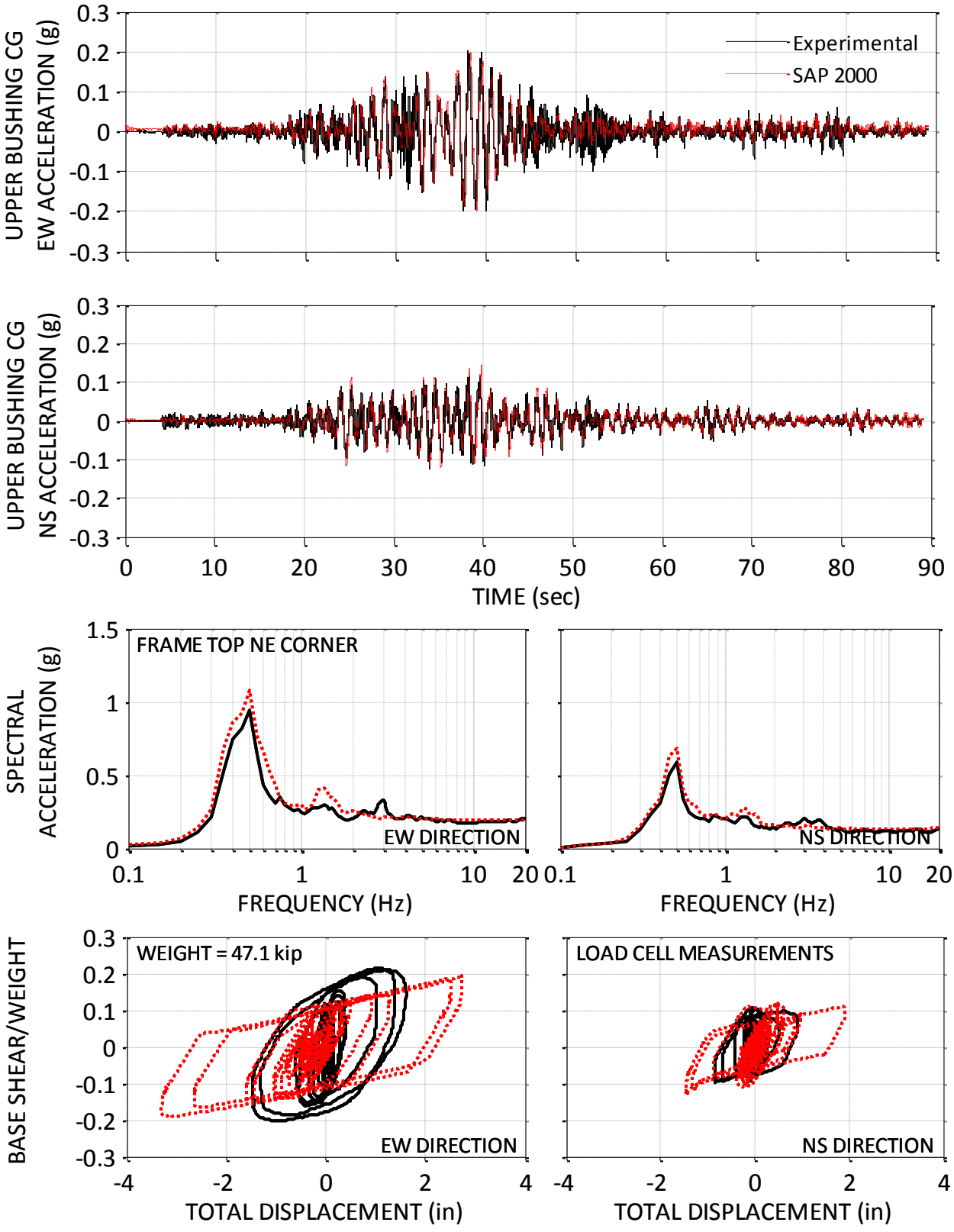
TRIPLE FP SYSTEM (Friction-Bolted Configuration – Series Model)
CHILE 100% TRI-AXIAL (FN in EW direction)
LENGTH SCALE=3 SYMMETRIC BUSHING CONFIGURATION



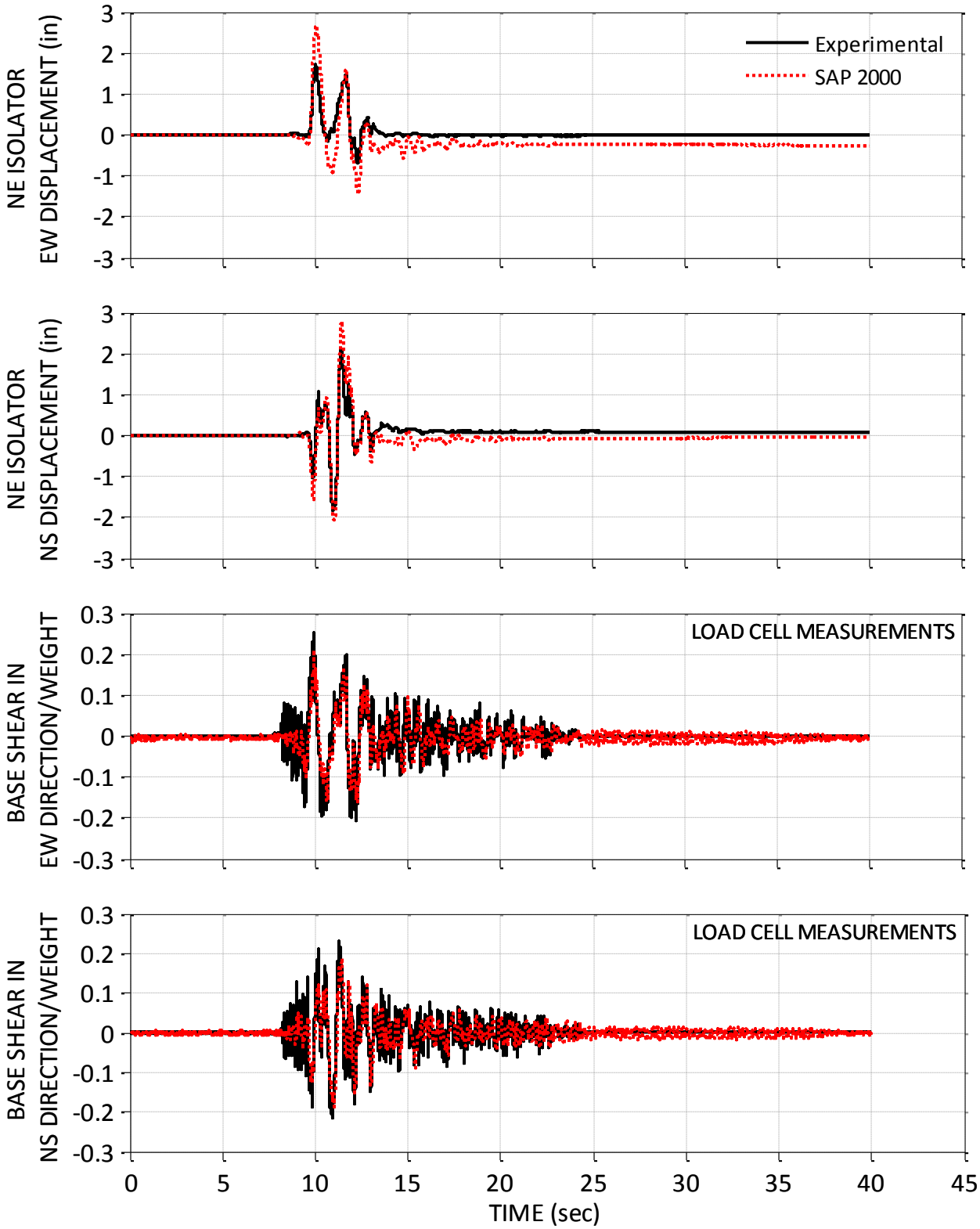

UPPER BUSHING CG
EW ACCELERATION (g)
Experimental
SAP 2000
UPPER BUSHING CG
NS ACCELERATION (g)
TIME (sec)
SPECTRAL
ACCELERATION (g)
FRAME TOP NE CORNER
EW DIRECTION
NS DIRECTION
FREQUENCY (Hz)
BASE SHEAR/WEIGHT
WEIGHT = 47.1 kip
LOAD CELL MEASUREMENTS
TOTAL DISPLACEMENT (in)

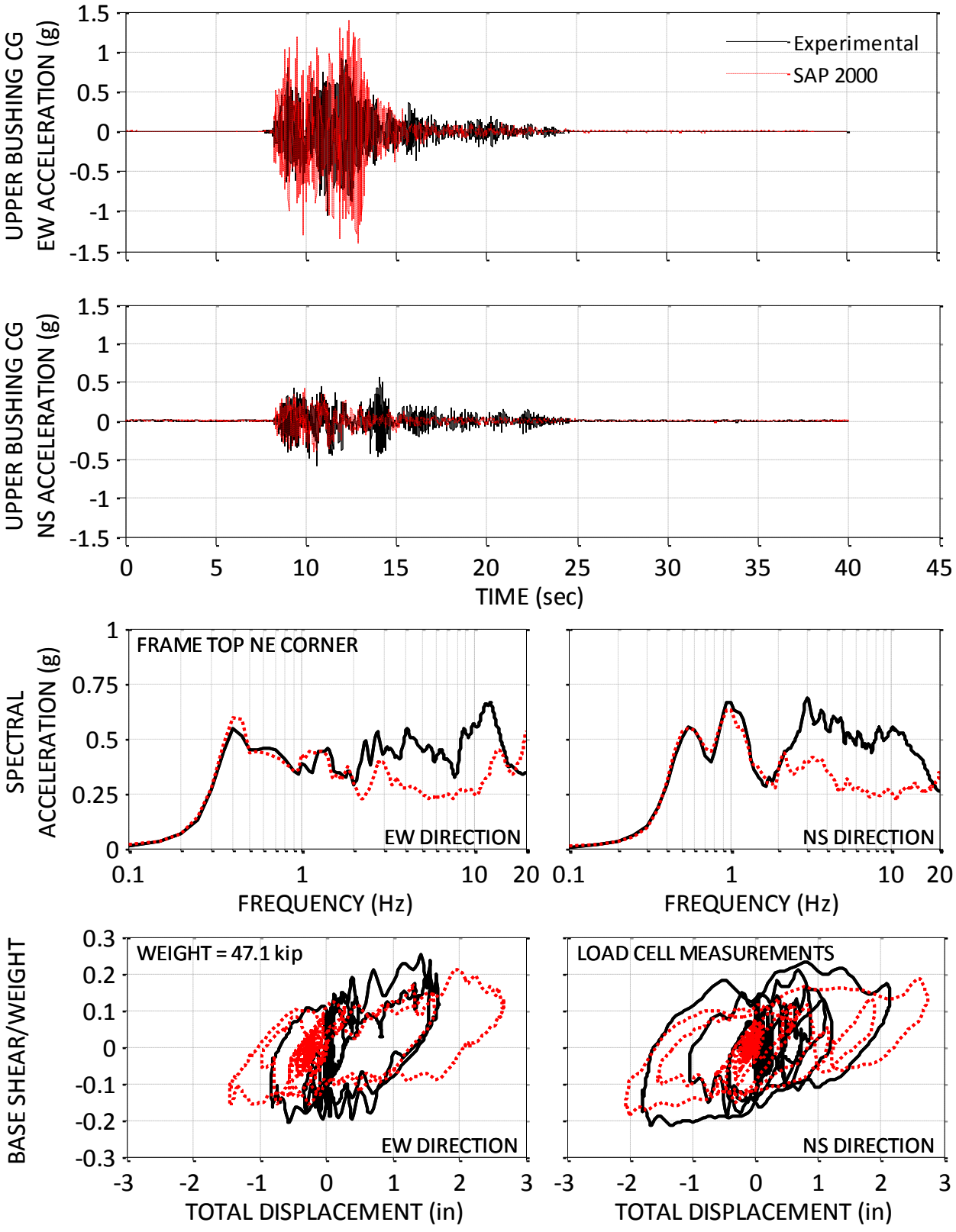
TRIPLE FP SYSTEM (Friction-Bolted Configuration – Series Model)
MEXICO CITY 100% TRI-AXIAL (FN in EW direction)
LENGTH SCALE=3 SYMMETRIC BUSHING CONFIGURATION



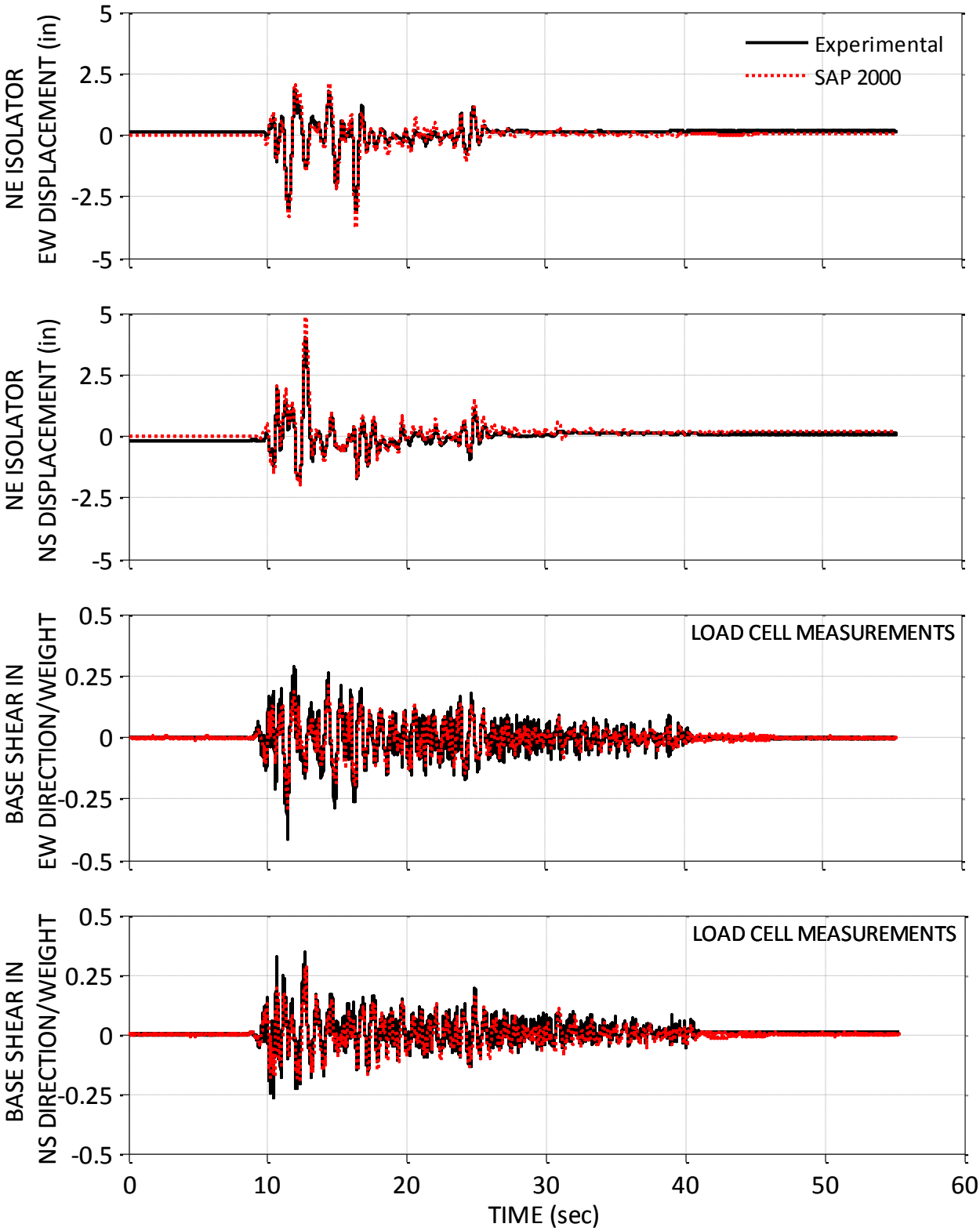

UPPER BUSHING CG
EW ACCELERATION (g)
Experimental
SAP 2000
UPPER BUSHING CG
NS ACCELERATION (g)
TIME (sec)
SPECTRAL
ACCELERATION (g)
FRAME TOP NE CORNER
EW DIRECTION
NS DIRECTION
FREQUENCY (Hz)
BASE SHEAR/WEIGHT
WEIGHT = 47.1 kip
LOAD CELL MEASUREMENTS
TOTAL DISPLACEMENT (in)

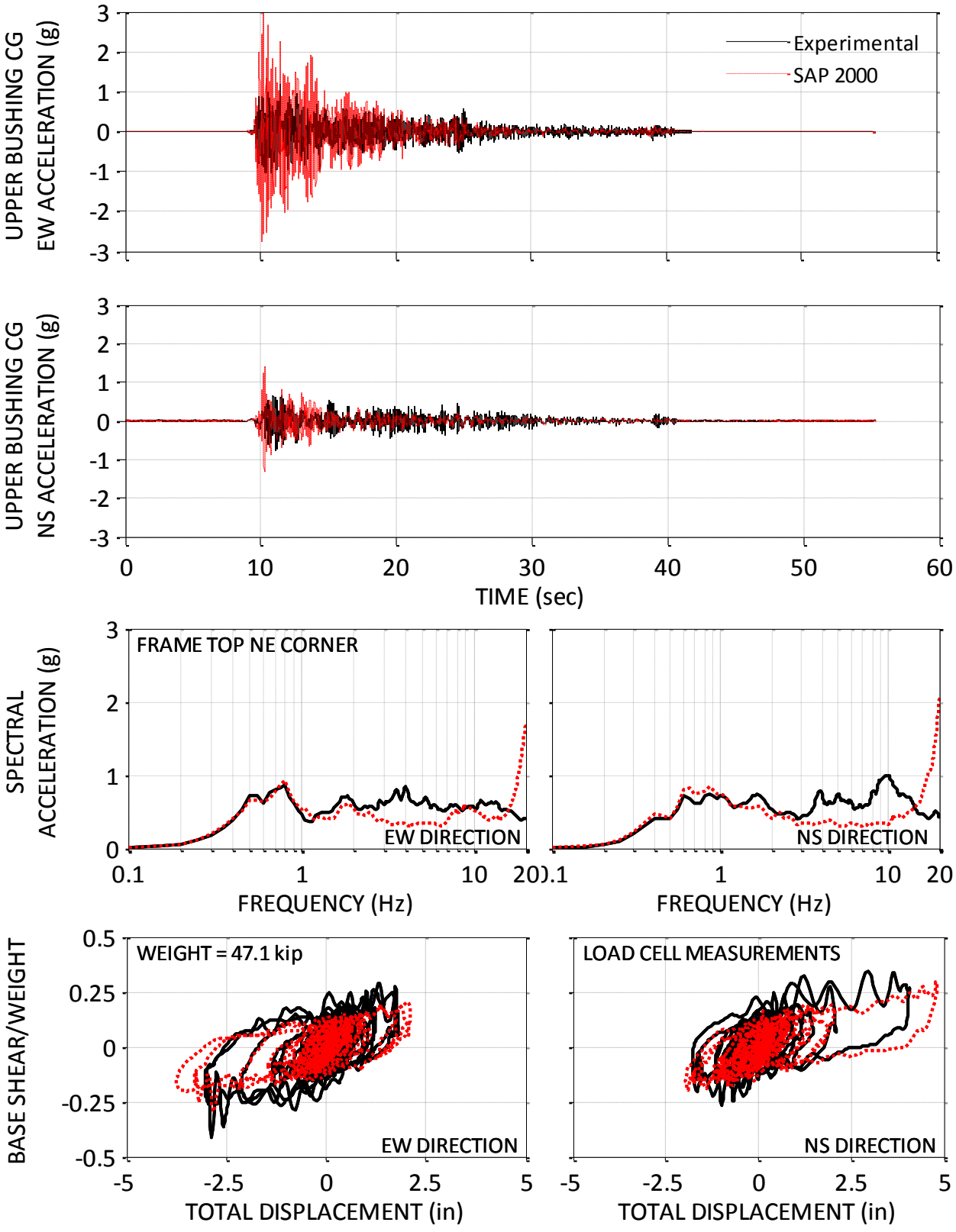
TRIPLE FP SYSTEM (Friction-Bolted Configuration – Series Model)
JENSEN FILTER 97% TRI-AXIAL (FN in EW direction)
LENGTH SCALE=3 NON-SYMMETRIC BUSHING CONFIGURATION



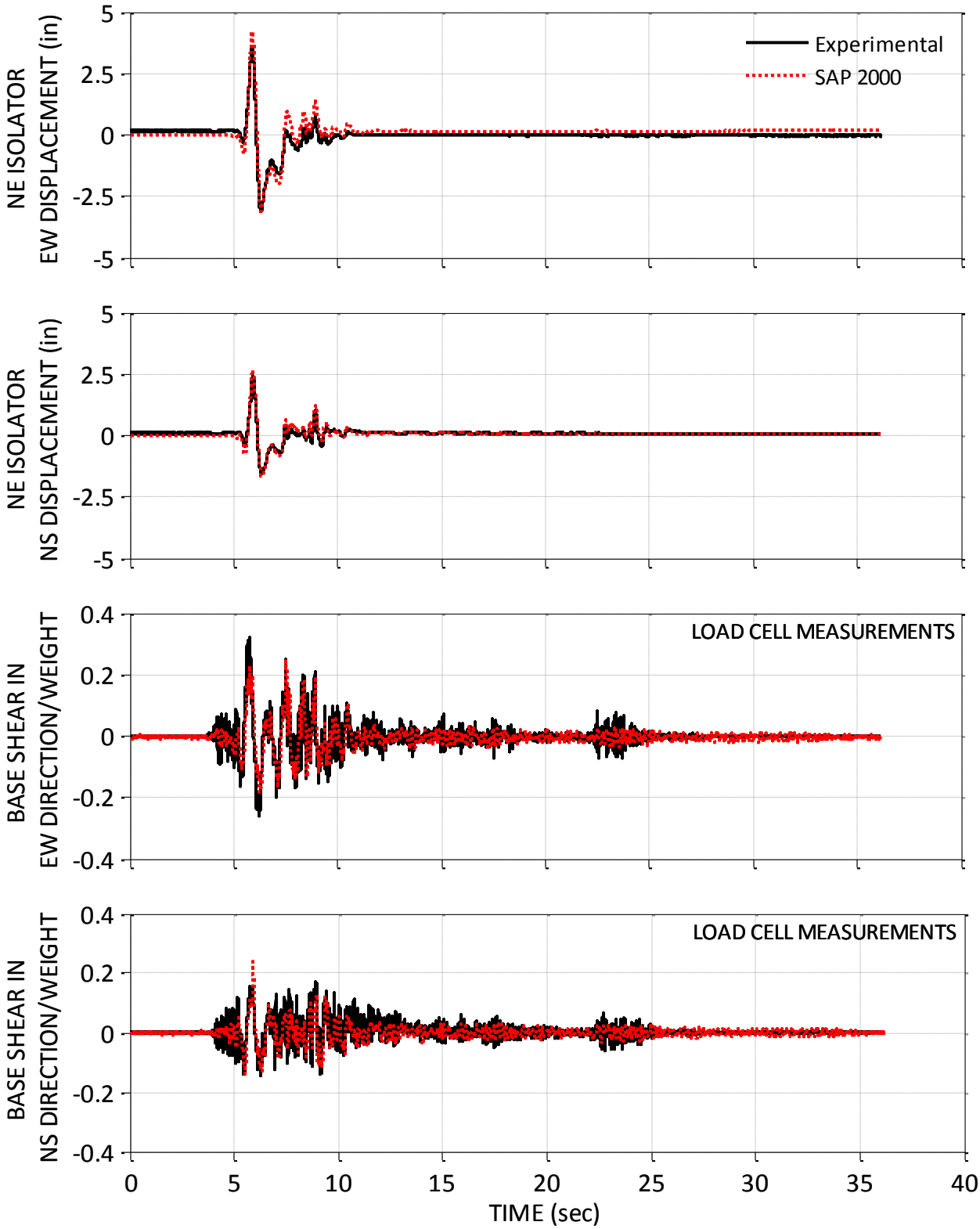

UPPER BUSHING CG
EW ACCELERATION (g)
Experimental
SAP 2000
UPPER BUSHING CG
NS ACCELERATION (g)
TIME (sec)
SPECTRAL
ACCELERATION (g)
FRAME TOP NE CORNER
EW DIRECTION
NS DIRECTION
FREQUENCY (Hz)
BASE SHEAR/WEIGHT
WEIGHT = 47.1 kip
LOAD CELL MEASUREMENTS
TOTAL DISPLACEMENT (in)

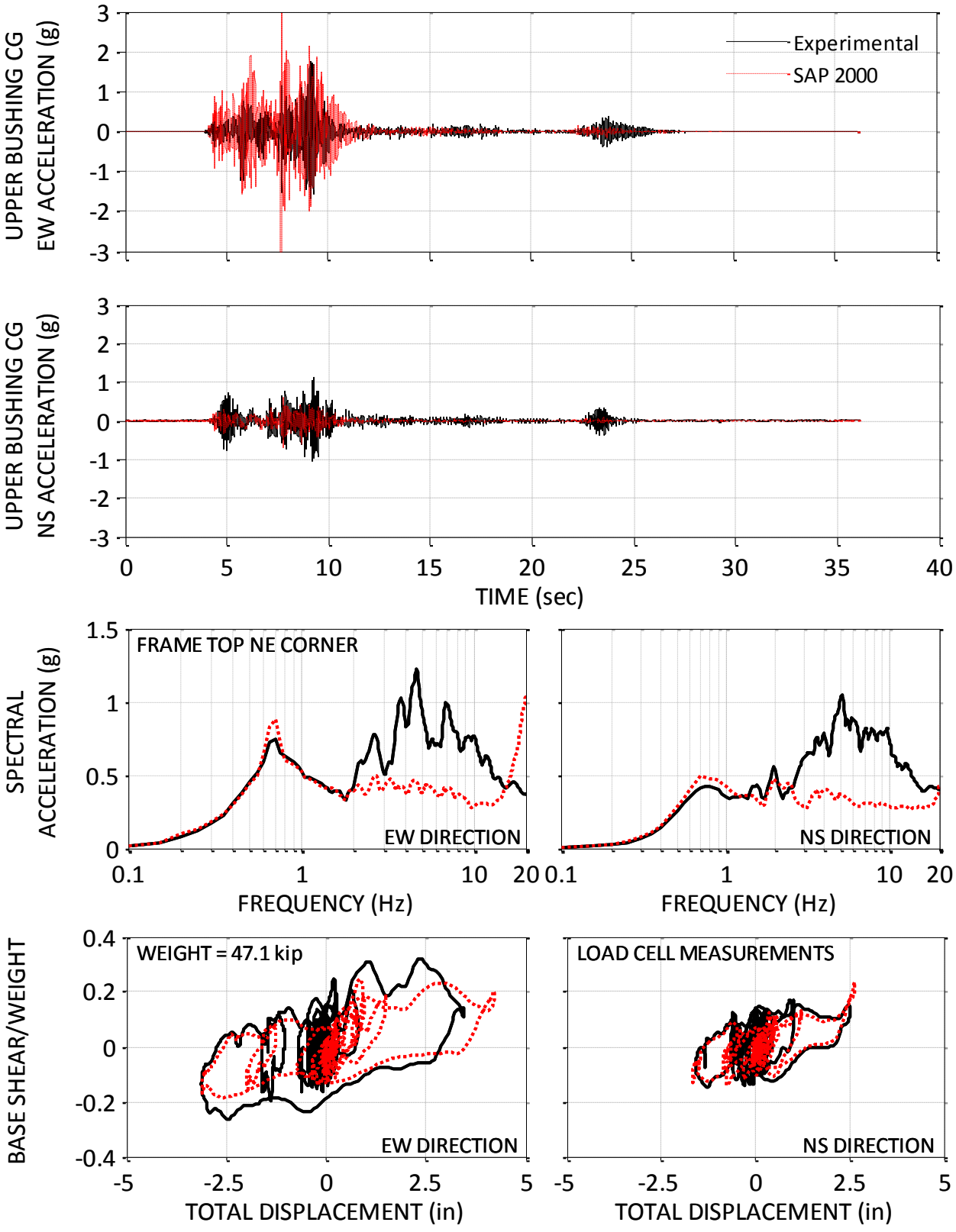
TRIPLE FP SYSTEM (Friction-Bolted Configuration – Series Model)
EL CENTRO 300% TRI-AXIAL (N90W in EW direction)
LENGTH SCALE=3 NON-SYMMETRIC BUSHING CONFIGURATION



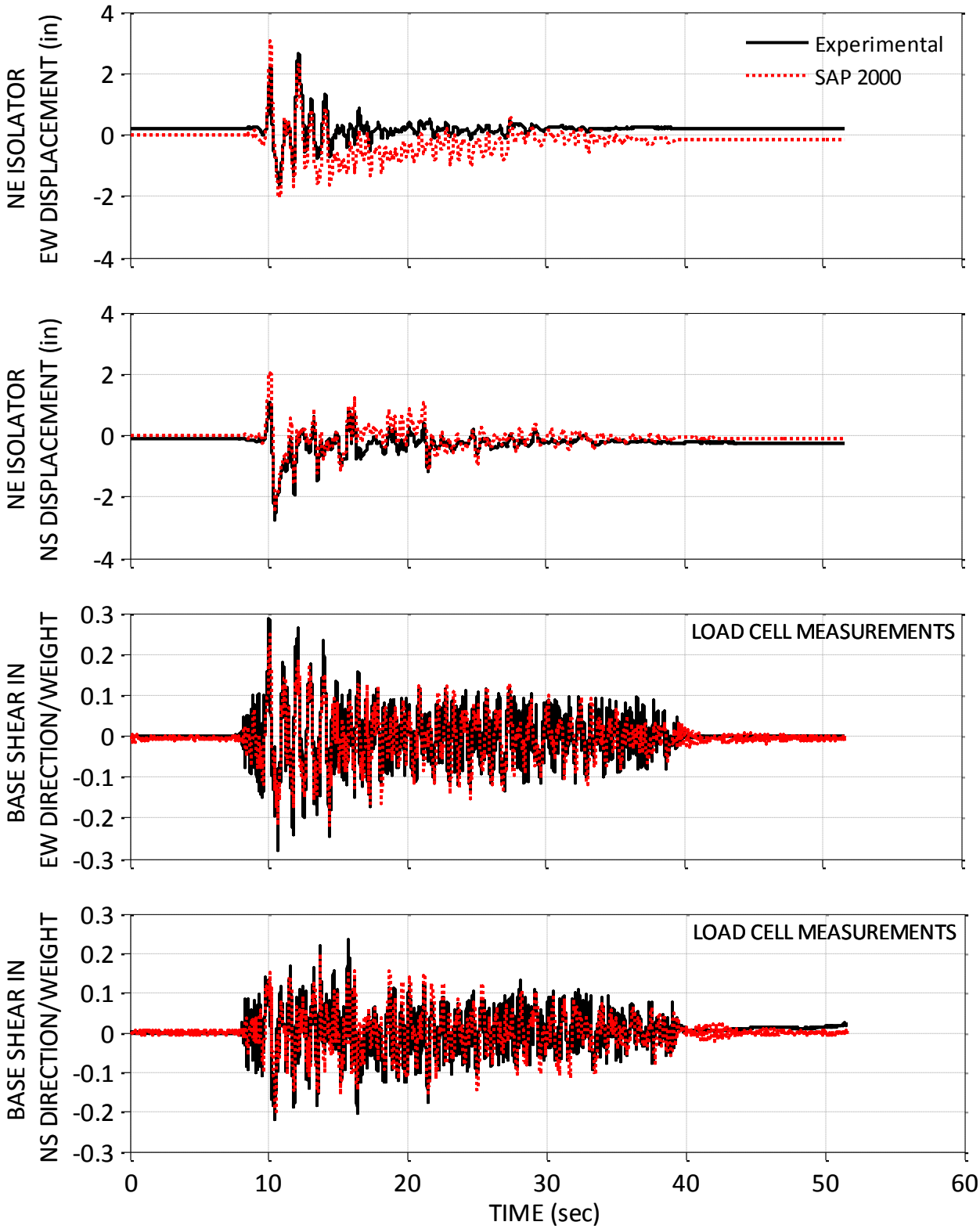

UPPER BUSHING CG
EW ACCELERATION (g)
Experimental
SAP 2000
UPPER BUSHING CG
NS ACCELERATION (g)
TIME (sec)
SPECTRAL
ACCELERATION (g)
FRAME TOP NE CORNER
EW DIRECTION
NS DIRECTION
FREQUENCY (Hz)
FREQUENCY (Hz)
BASE SHEAR/WEIGHT
WEIGHT = 47.1 kip
LOAD CELL MEASUREMENTS
EW DIRECTION
NS DIRECTION
TOTAL DISPLACEMENT (in)
TOTAL DISPLACEMENT (in)

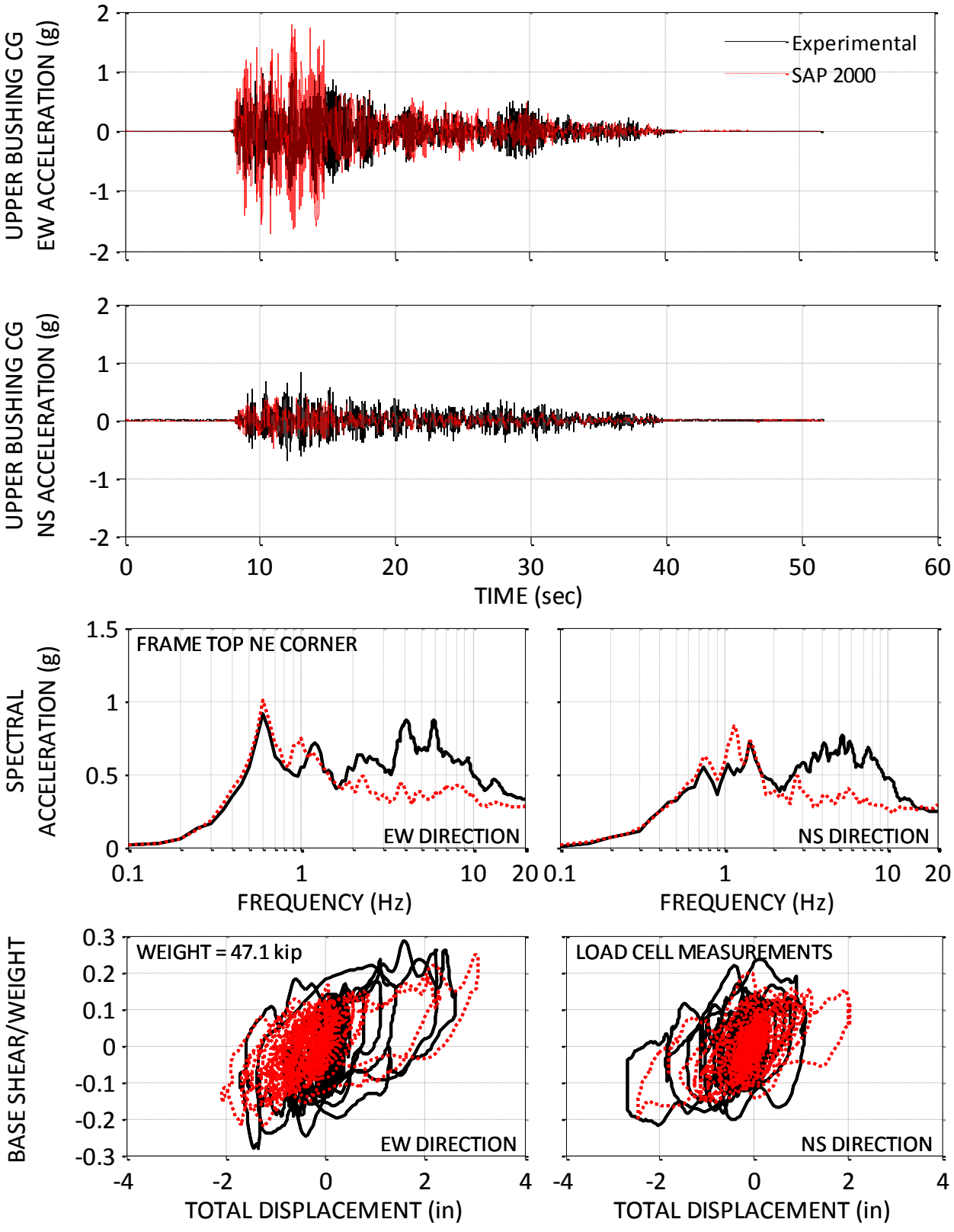
TRIPLE FP SYSTEM (Friction-Bolted Configuration – Series Model)
PACOIMA DAM 100% TRI-AXIAL (S16E in EW direction)
LENGTH SCALE=3 NON-SYMMETRIC BUSHING CONFIGURATION



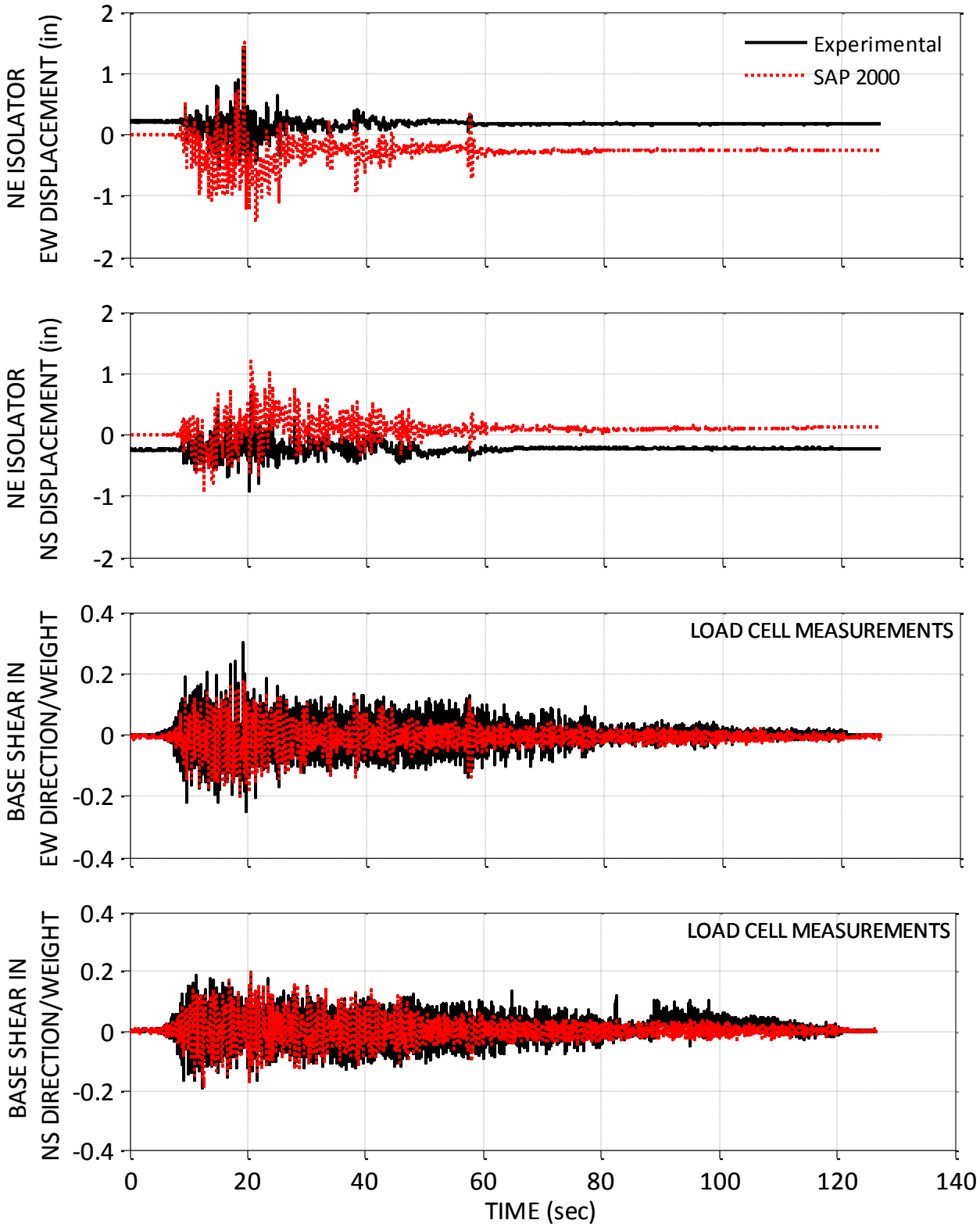

UPPER BUSHING CG
EW ACCELERATION (g)
Experimental
SAP 2000
UPPER BUSHING CG
NS ACCELERATION (g)
TIME (sec)
SPECTRAL
ACCELERATION (g)
FRAME TOP NE CORNER
EW DIRECTION
NS DIRECTION
FREQUENCY (Hz)
BASE SHEAR/WEIGHT
WEIGHT = 47.1 kip
LOAD CELL MEASUREMENTS
TOTAL DISPLACEMENT (in)

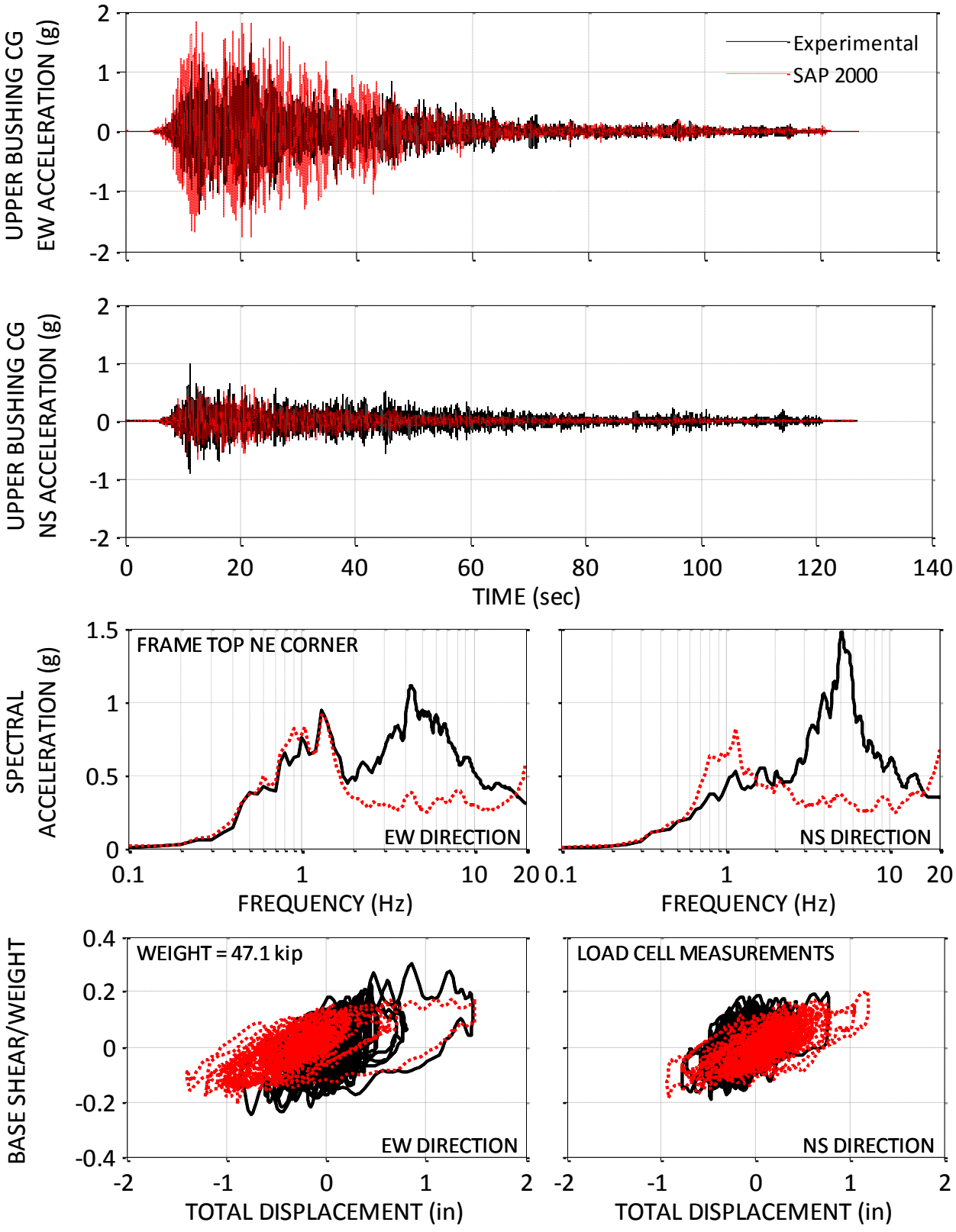
TRIPLE FP SYSTEM (Friction-Bolted Configuration – Series Model)
TAFT 500% TRI-AXIAL (S69E in EW direction)
LENGTH SCALE=3 NON-SYMMETRIC BUSHING CONFIGURATION



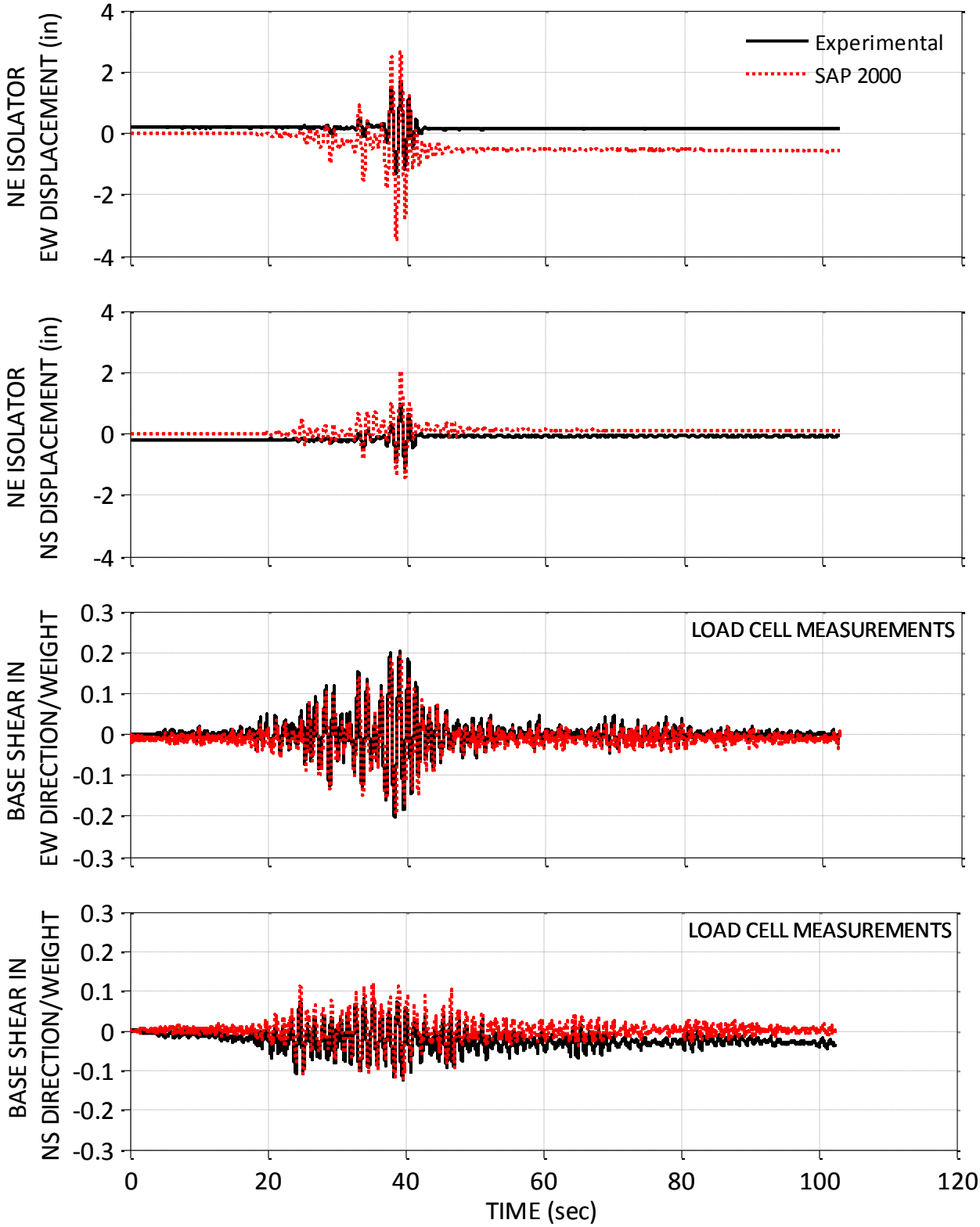

UPPER BUSHING CG
EW ACCELERATION (g)
Experimental
SAP 2000
UPPER BUSHING CG
NS ACCELERATION (g)
TIME (sec)
SPECTRAL
ACCELERATION (g)
FRAME TOP NE CORNER
EW DIRECTION
NS DIRECTION
FREQUENCY (Hz)
BASE SHEAR/WEIGHT
WEIGHT = 47.1 kip
LOAD CELL MEASUREMENTS
TOTAL DISPLACEMENT (in)

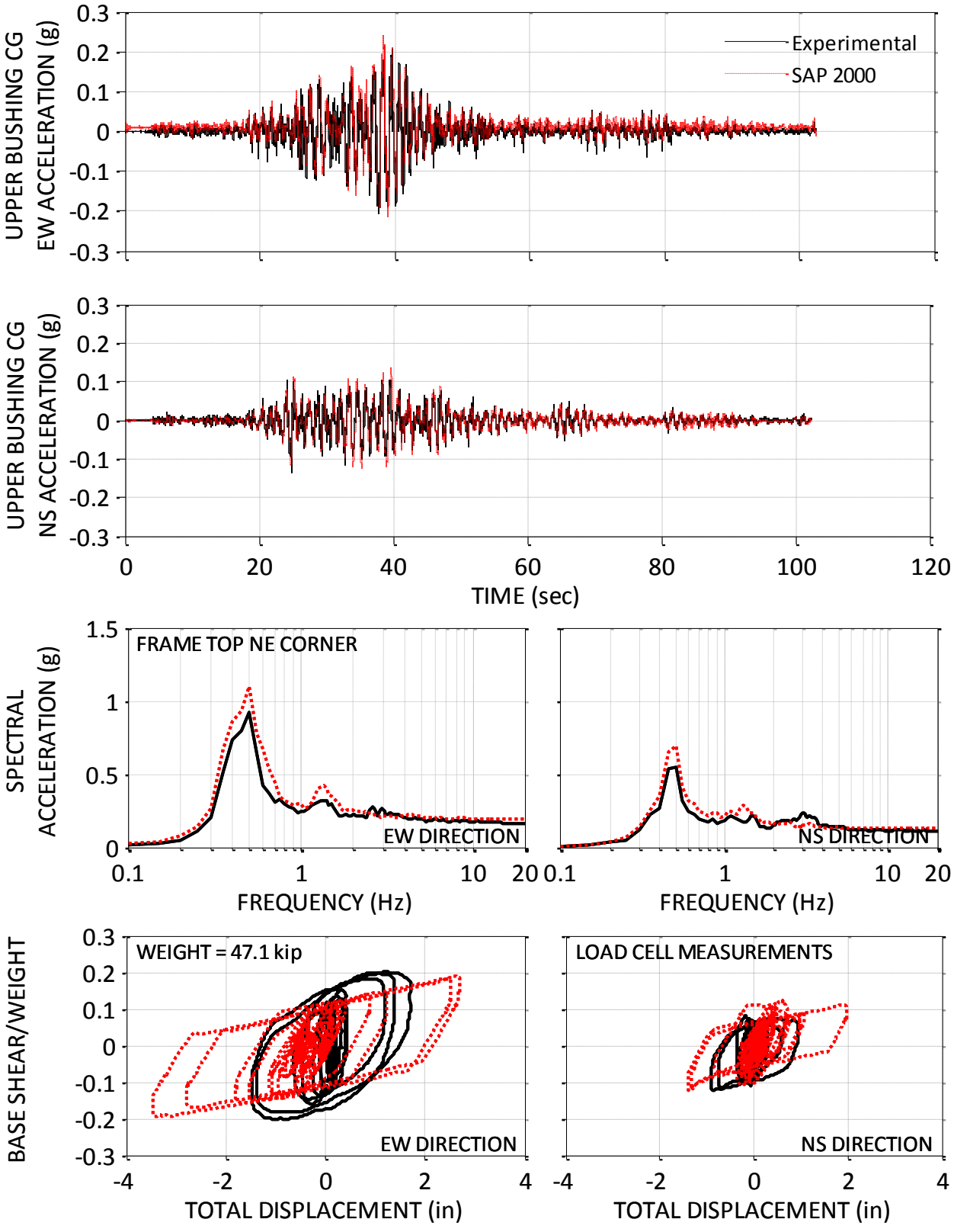
TRIPLE FP SYSTEM (Friction-Bolted Configuration – Series Model)
CHILE 100% TRI-AXIAL (EW in EW direction)
LENGTH SCALE=3 NON-SYMMETRIC BUSHING CONFIGURATION



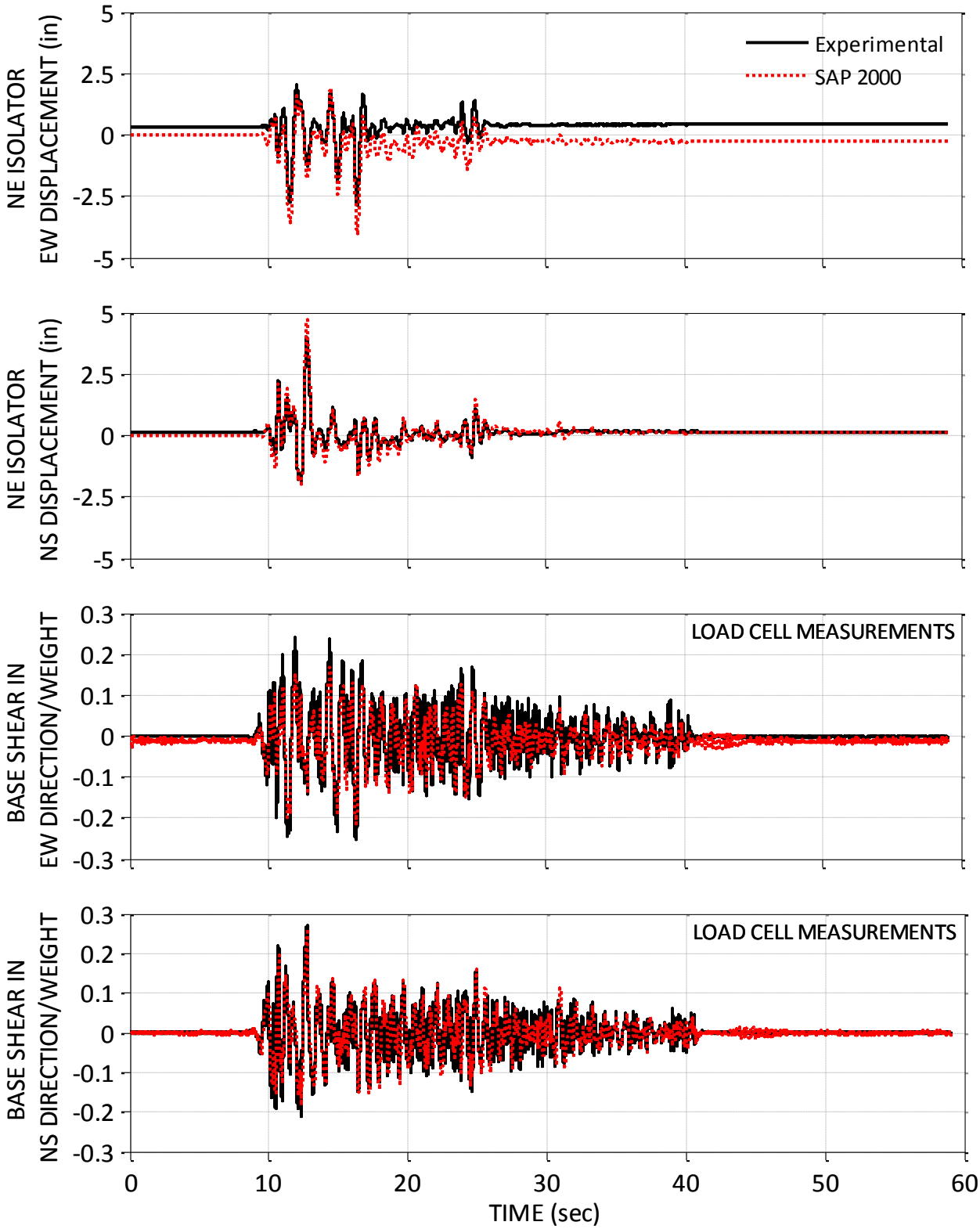

UPPER BUSHING CG
EW ACCELERATION (g)
Experimental
SAP 2000
UPPER BUSHING CG
NS ACCELERATION (g)
TIME (sec)
SPECTRAL
ACCELERATION (g)
FRAME TOP NE CORNER
EW DIRECTION
NS DIRECTION
FREQUENCY (Hz)
BASE SHEAR/WEIGHT
WEIGHT = 47.1 kip
LOAD CELL MEASUREMENTS
TOTAL DISPLACEMENT (in)

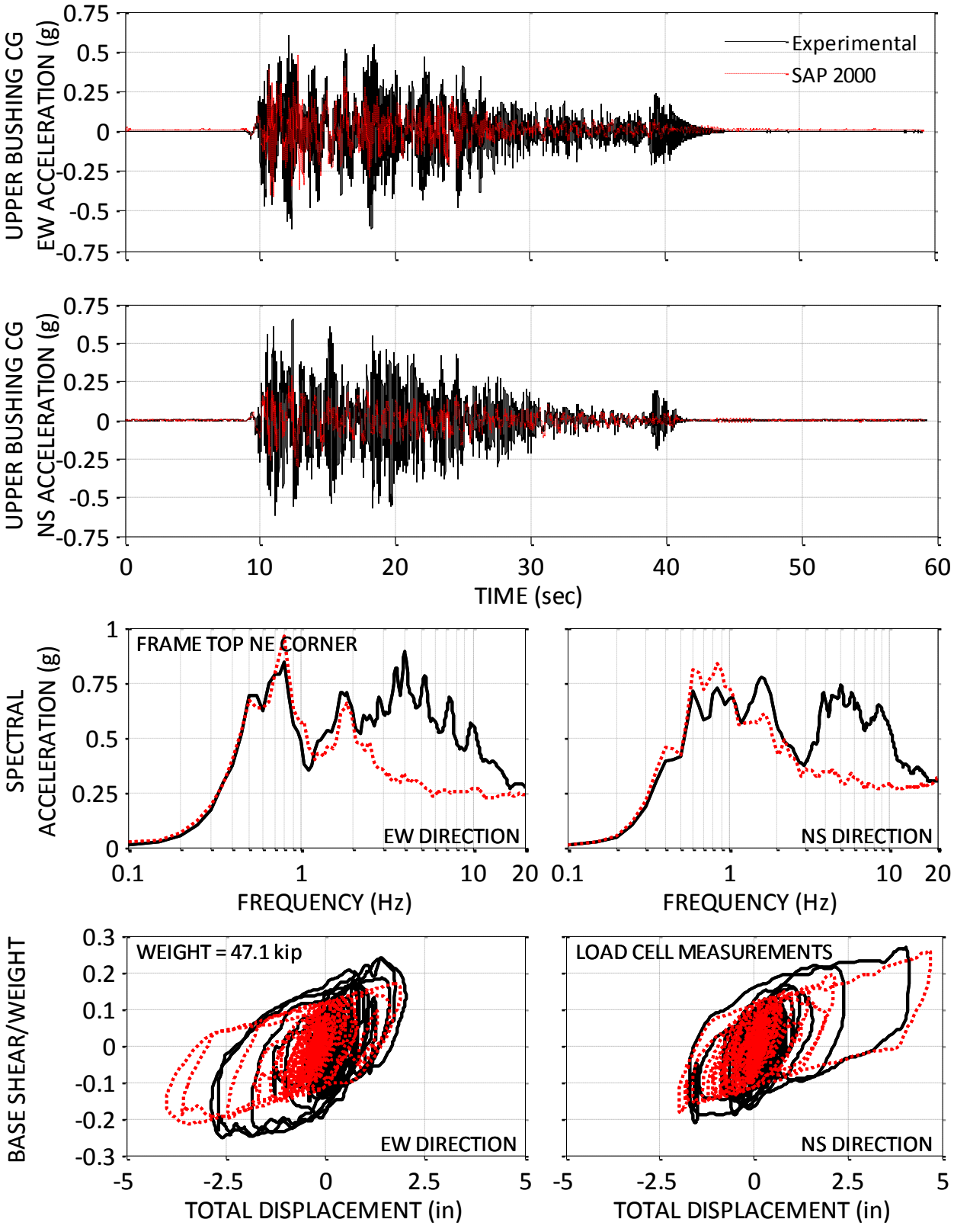
TRIPLE FP SYSTEM (Friction-Bolted Configuration – Series Model)
MEXICO CITY 100% TRI-AXIAL (N90W in EW direction)
LENGTH SCALE=3 NON-SYMMETRIC BUSHING CONFIGURATION



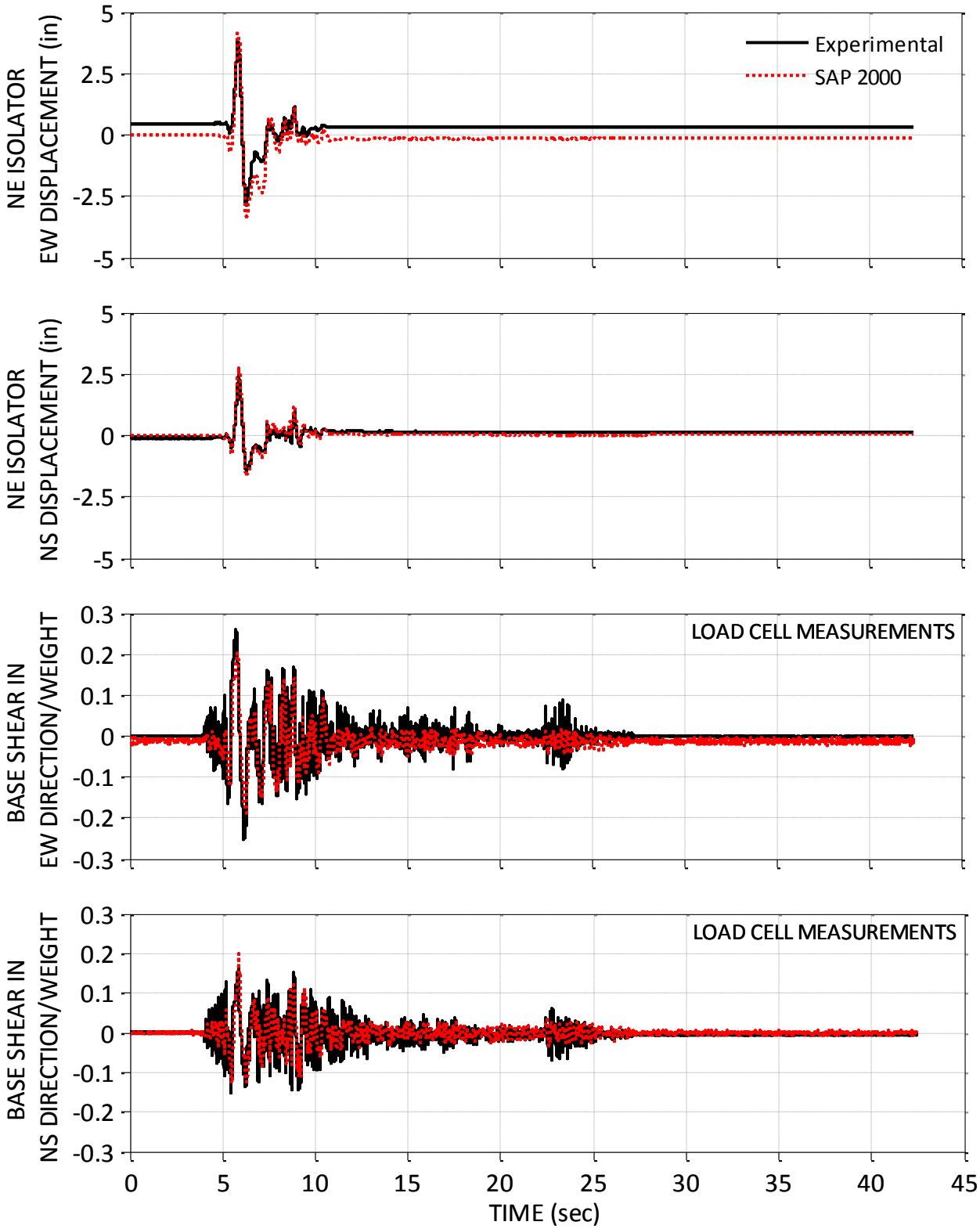

UPPER BUSHING CG
EW ACCELERATION (g)
Experimental
SAP 2000
UPPER BUSHING CG
NS ACCELERATION (g)
TIME (sec)
SPECTRAL
ACCELERATION (g)
FRAME TOP NE CORNER
EW DIRECTION
NS DIRECTION
FREQUENCY (Hz)
BASE SHEAR/WEIGHT
WEIGHT = 47.1 kip
LOAD CELL MEASUREMENTS
TOTAL DISPLACEMENT (in)

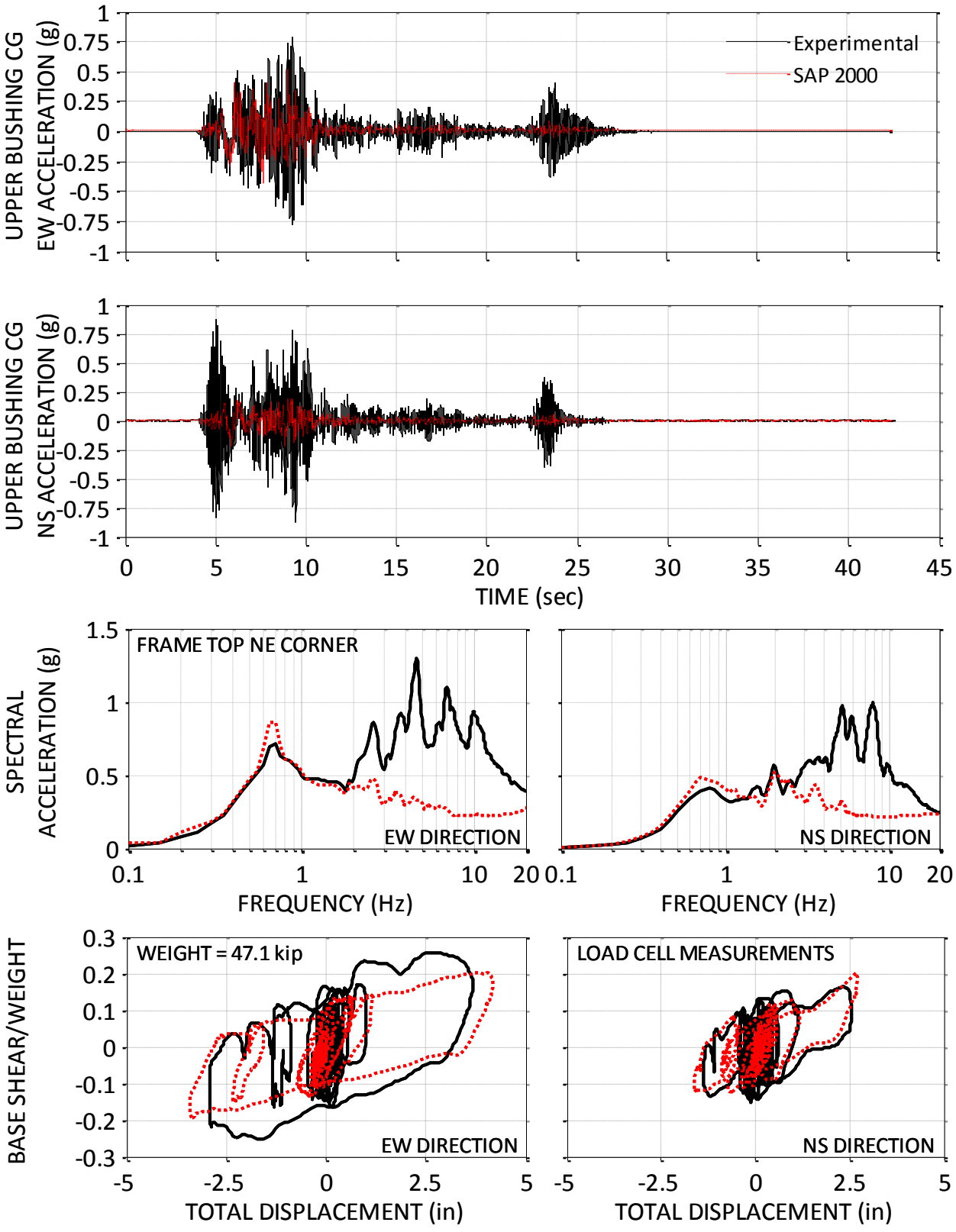
TRIPLE FP SYSTEM (Friction-Bolted Configuration – Series Model)
EL CENTRO 300% BI-AXIAL (N90W in EW direction)
LENGTH SCALE=3 NON-SYMMETRIC BUSHING CONFIGURATION



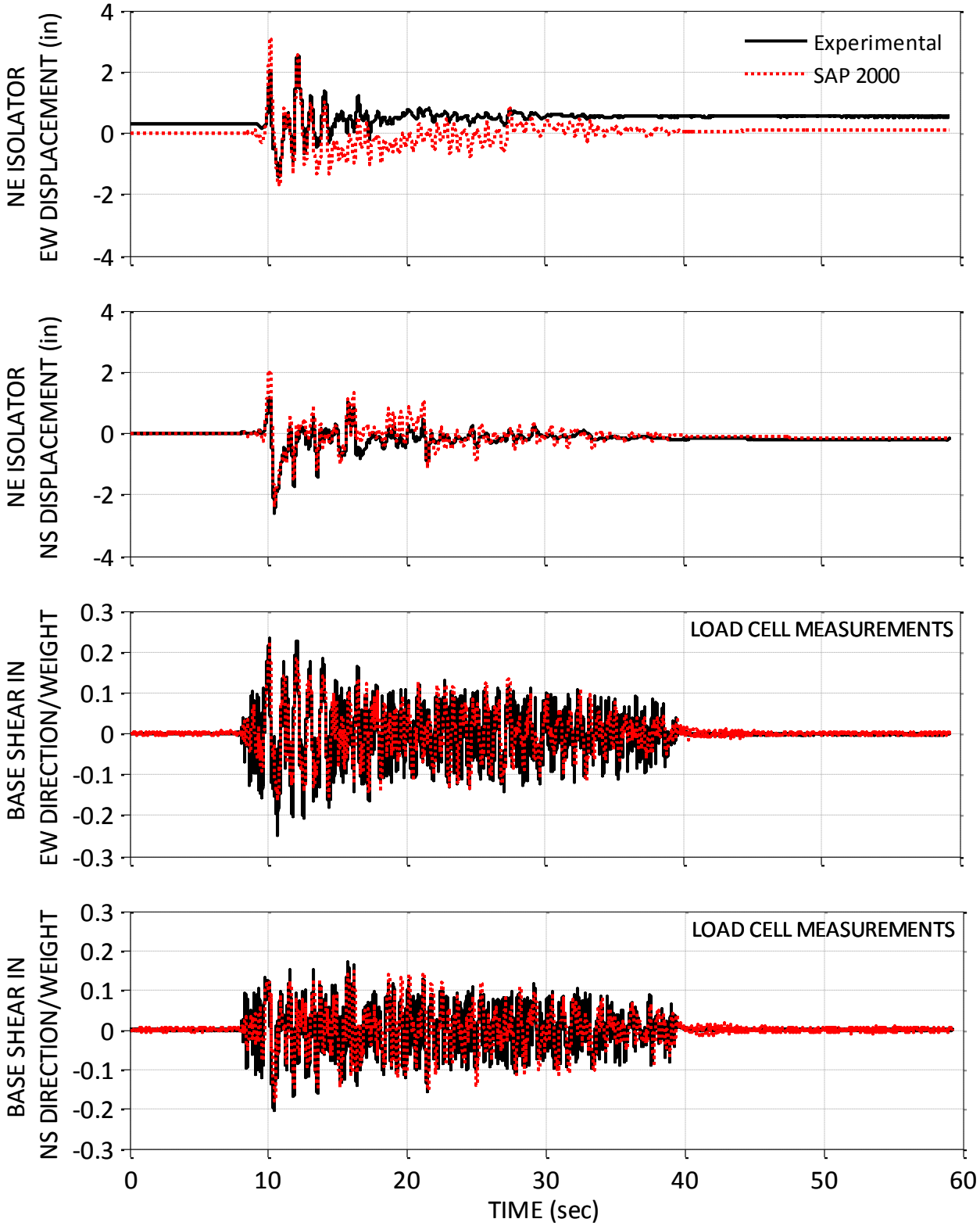

UPPER BUSHING CG
EW ACCELERATION (g)
Experimental
SAP 2000
UPPER BUSHING CG
NS ACCELERATION (g)
TIME (sec)
SPECTRAL
ACCELERATION (g)
FRAME TOP NE CORNER
EW DIRECTION
NS DIRECTION
FREQUENCY (Hz)
BASE SHEAR/WEIGHT
WEIGHT = 47.1 kip
LOAD CELL MEASUREMENTS
TOTAL DISPLACEMENT (in)

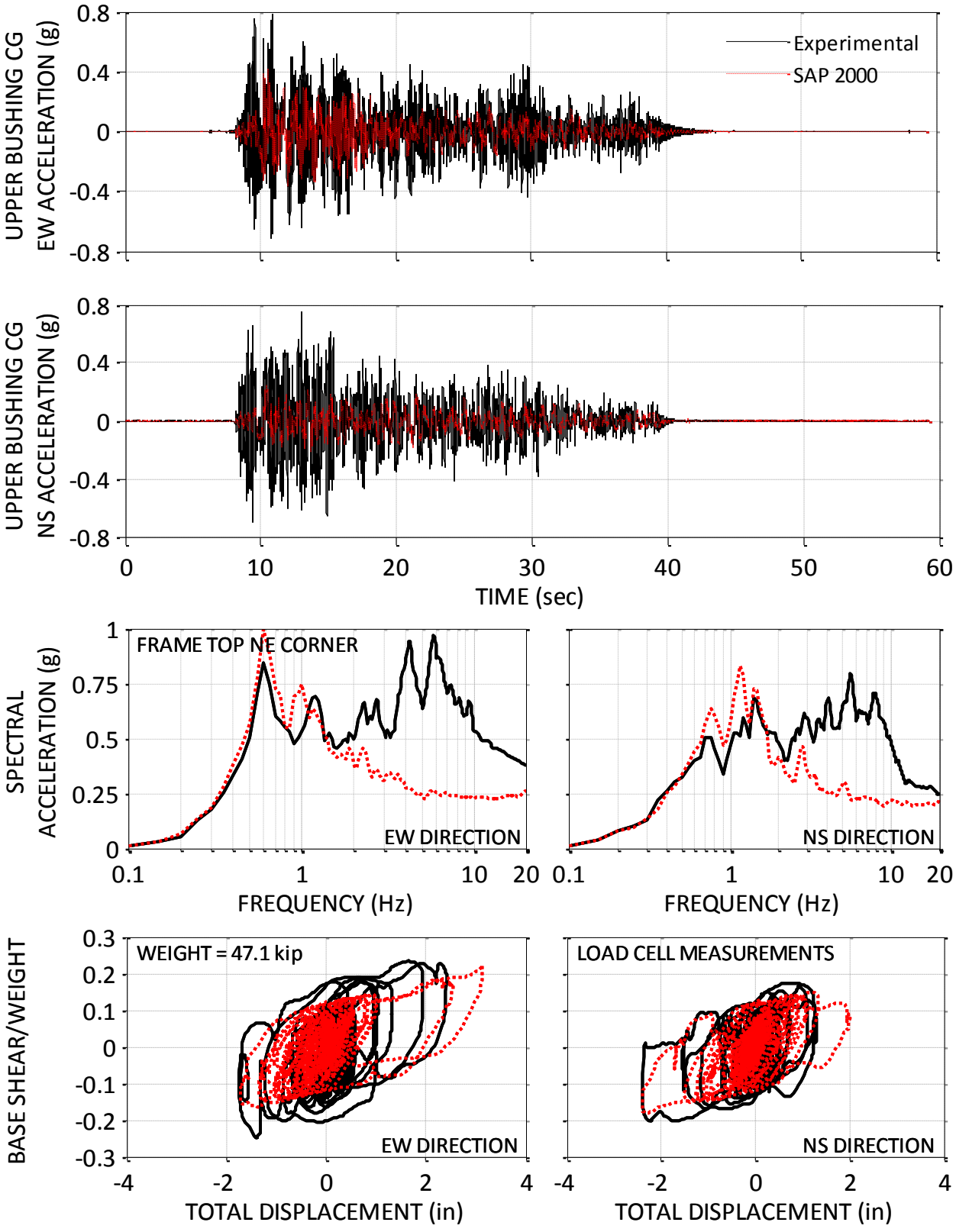
TRIPLE FP SYSTEM (Friction-Bolted Configuration – Series Model)
PACOIMA DAM 100% BI-AXIAL (S16E in EW direction)
LENGTH SCALE=3 NON-SYMMETRIC BUSHING CONFIGURATION



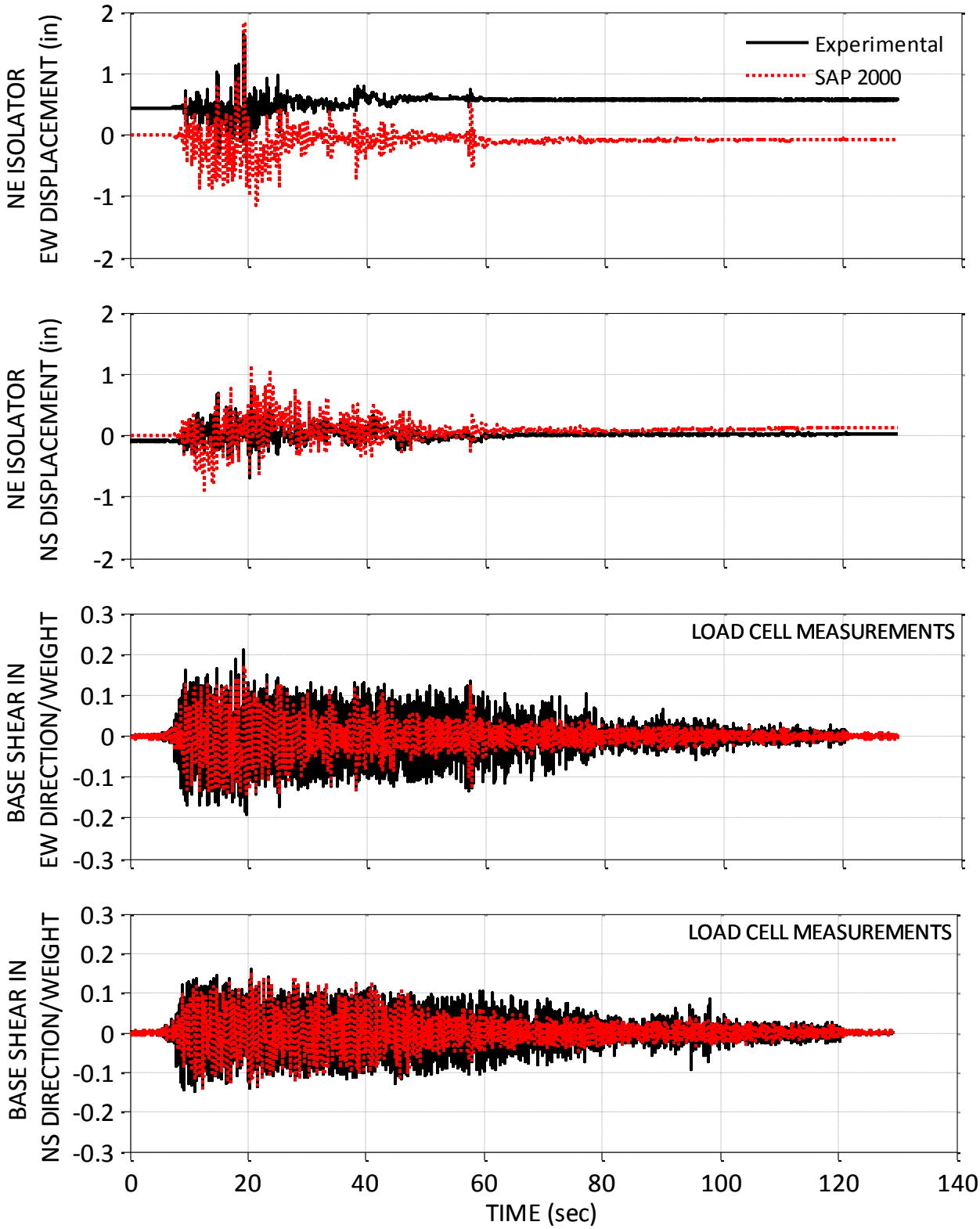

UPPER BUSHING CG
EW ACCELERATION (g)
Experimental
SAP 2000
UPPER BUSHING CG
NS ACCELERATION (g)
TIME (sec)
SPECTRAL
ACCELERATION (g)
FRAME TOP NE CORNER
EW DIRECTION
NS DIRECTION
FREQUENCY (Hz)
BASE SHEAR/WEIGHT
WEIGHT = 47.1 kip
LOAD CELL MEASUREMENTS
TOTAL DISPLACEMENT (in)

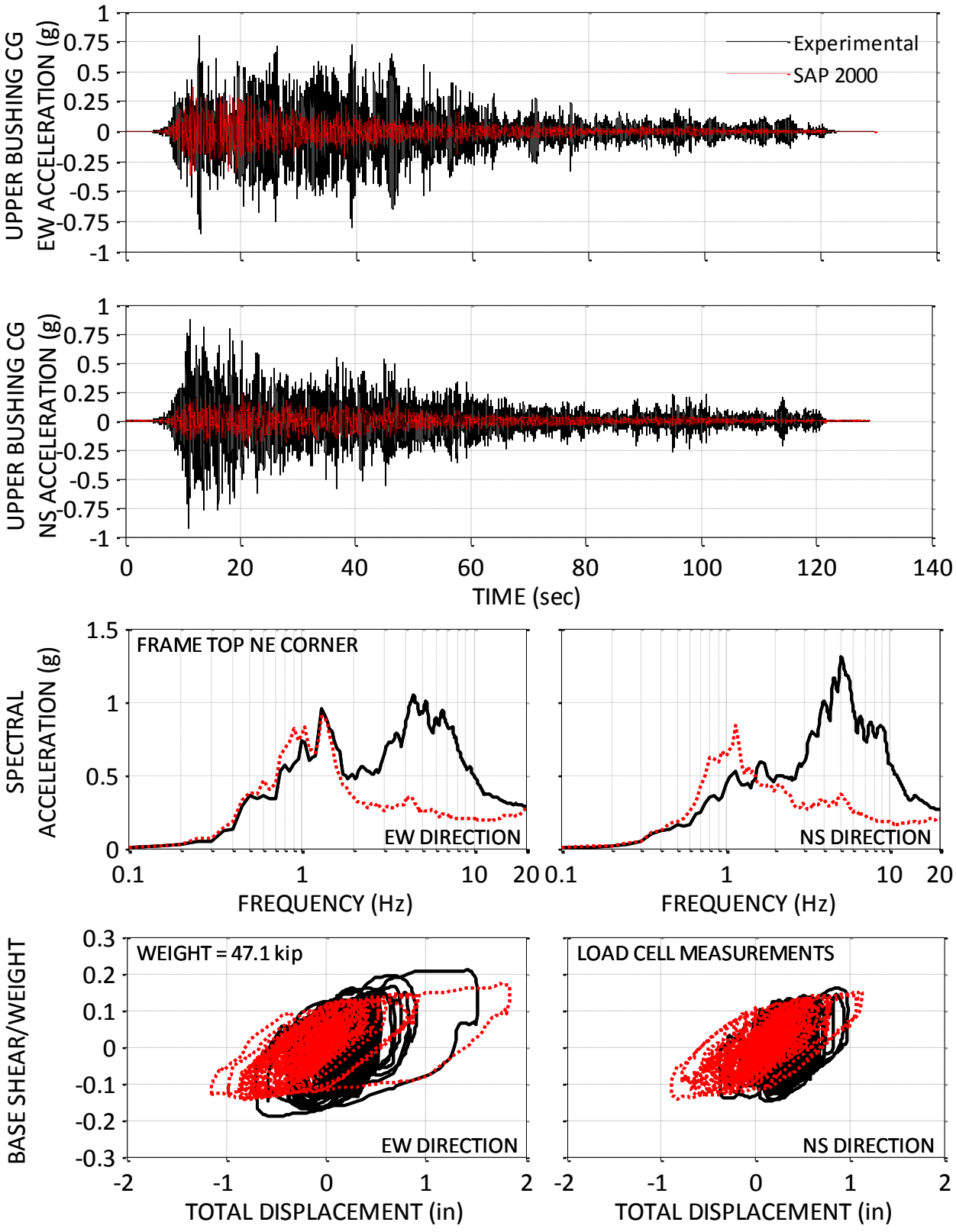
TRIPLE FP SYSTEM (Friction-Bolted Configuration – Series Model)
TAFT 500% BI-AXIAL (S69E in EW direction)
LENGTH SCALE=3 NON-SYMMETRIC BUSHING CONFIGURATION




UPPER BUSHING CG
EW ACCELERATION (g)
0.8
0.4
0
-0.4
-0.8
Experimental
SAP 2000
UPPER BUSHING CG
NS ACCELERATION (g)
0
10
20
30
40
50
60
TIME (sec)
SPECTRAL
ACCELERATION (g)
1
0.75
0.5
0.25
0
FRAME TOP NE CORNER
EW DIRECTION
NS DIRECTION
0.1
1
10
20
FREQUENCY (Hz)
BASE SHEAR/WEIGHT
0.3
0.2
0.1
-0.1
-0.2
-0.3
WEIGHT = 47.1 kip
LOAD CELL MEASUREMENTS
-4
-2
2
4
TOTAL DISPLACEMENT (in)

TRIPLE FP SYSTEM (Friction-Bolted Configuration – Series Model)
CHILE 100% BI-AXIAL (EW in EW direction)
LENGTH SCALE=3 NON-SYMMETRIC BUSHING CONFIGURATION

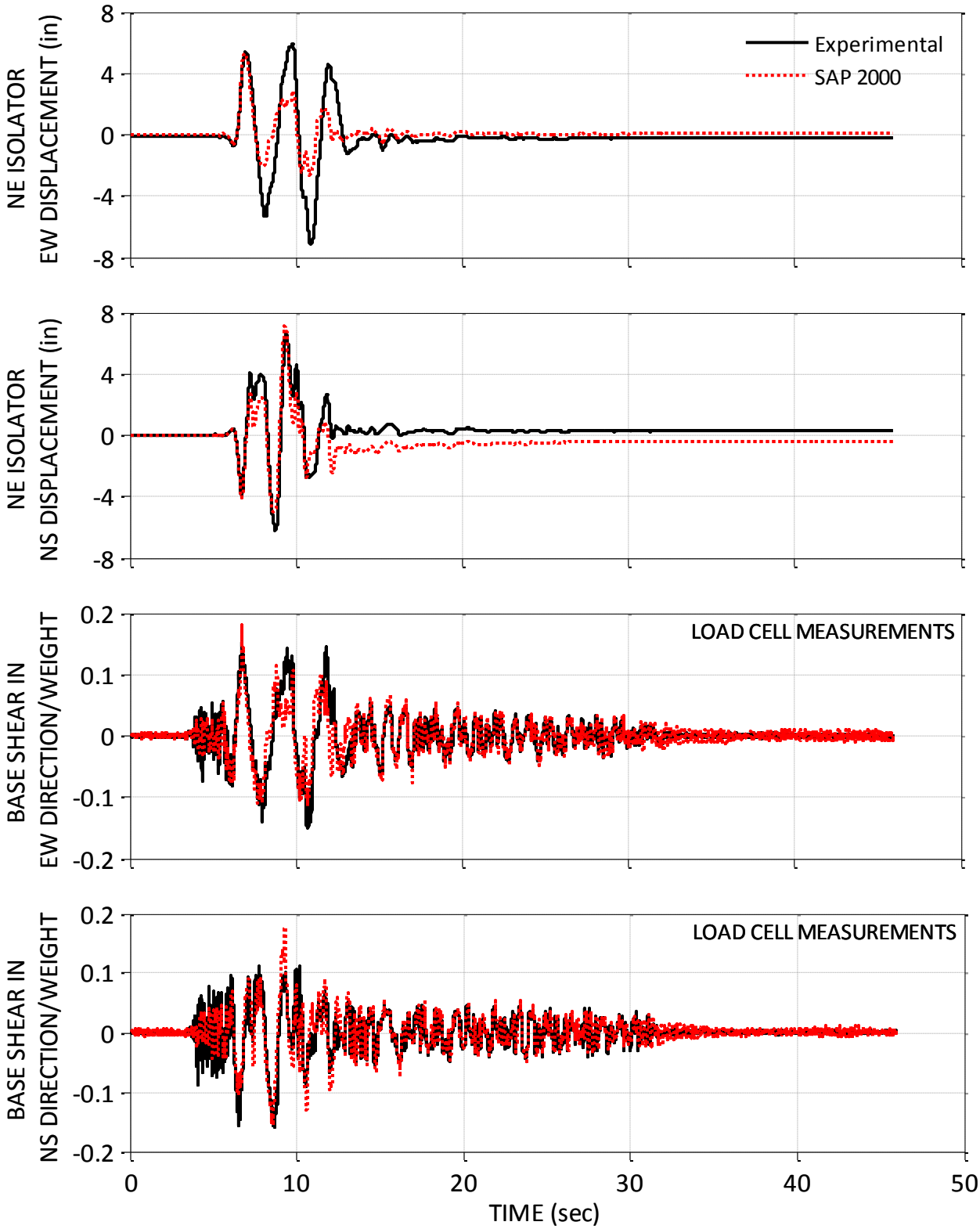


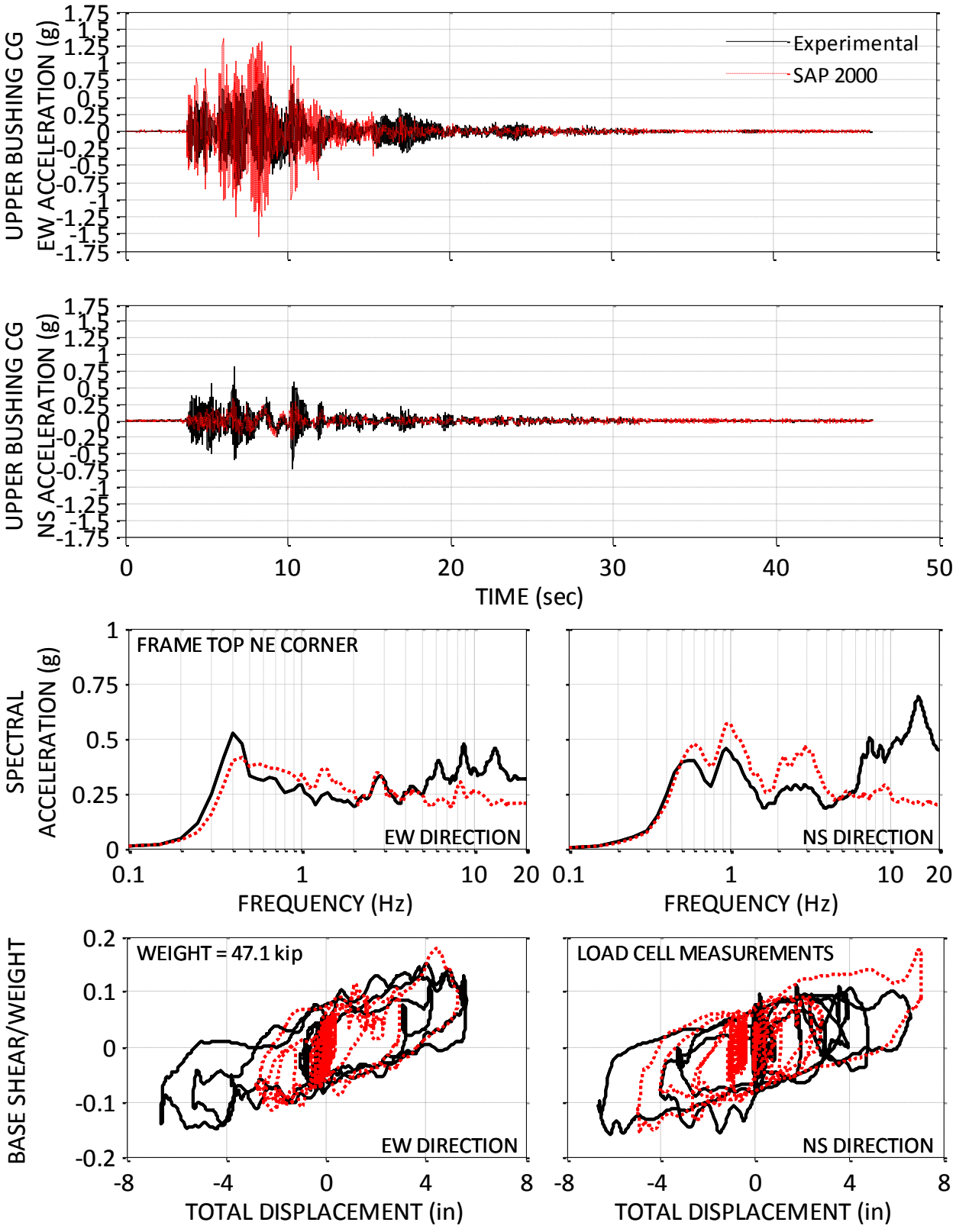

UPPER BUSHING CG
EW ACCELERATION (g)
Experimental
SAP 2000
UPPER BUSHING CG
NS ACCELERATION (g)
TIME (sec)
SPECTRAL
ACCELERATION (g)
FRAME TOP NE CORNER
EW DIRECTION
NS DIRECTION
FREQUENCY (Hz)
BASE SHEAR/WEIGHT
WEIGHT = 47.1 kip
LOAD CELL MEASUREMENTS
TOTAL DISPLACEMENT (in)

PART D-2
SUMMARY OF EXPERIMENTAL AND ANALYTICAL COMPARISONS FOR THE TRIPLE FRICTION PENDULUM SYSTEM AT LENGTH SCALE OF 1 AND MODELING USING THE SERIES MODEL

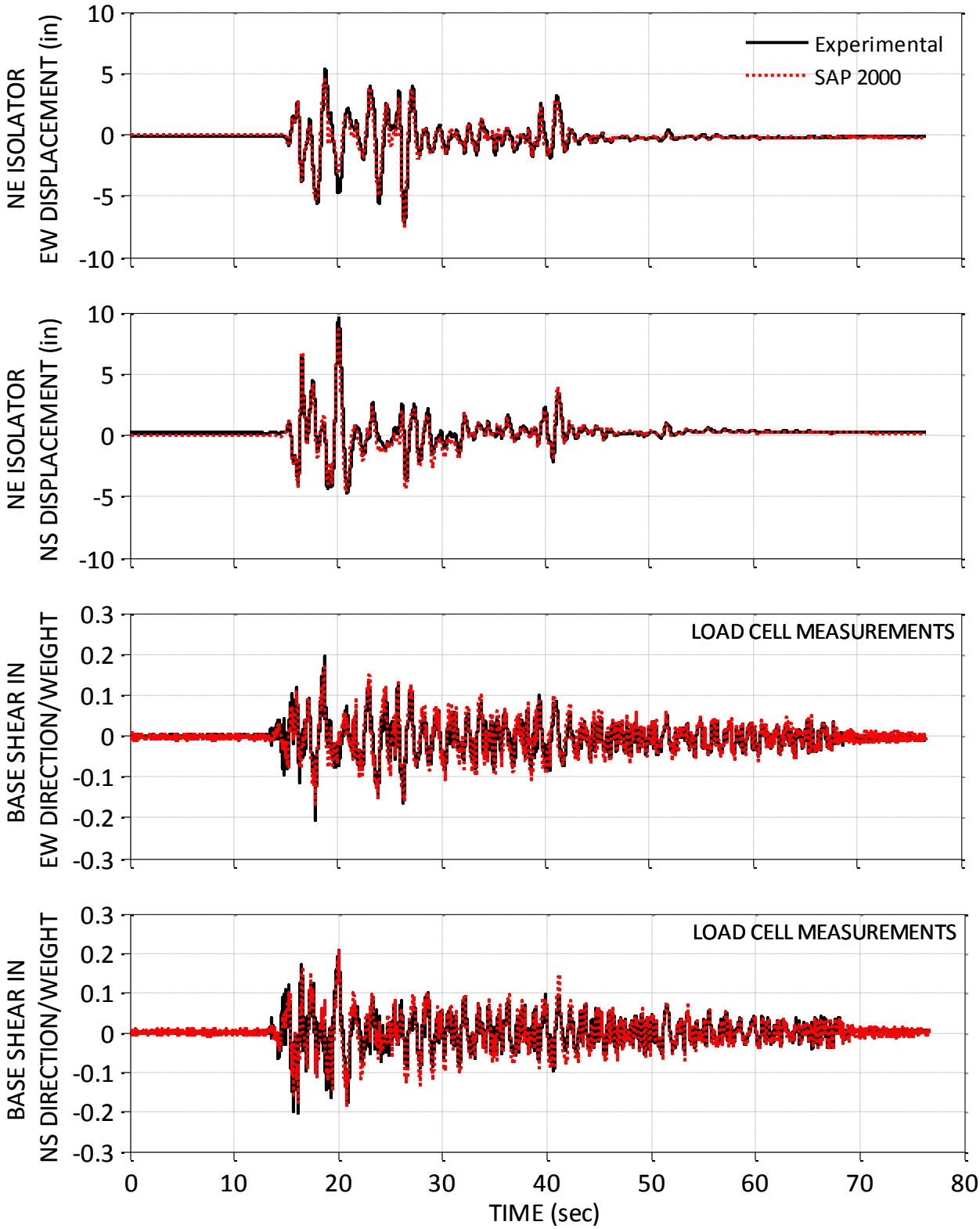
(PERCENTAGE AMOUNT IS SCALE FACTOR APPLIED TO ACCELERATION OF ACTUAL MOTION. FOR EXAMPLE, 100% DENOTES MOTION AS RECORDED, 200% DENOTES THAT ACCELERATION WAS SCALED UP BY FACTOR OF 2)

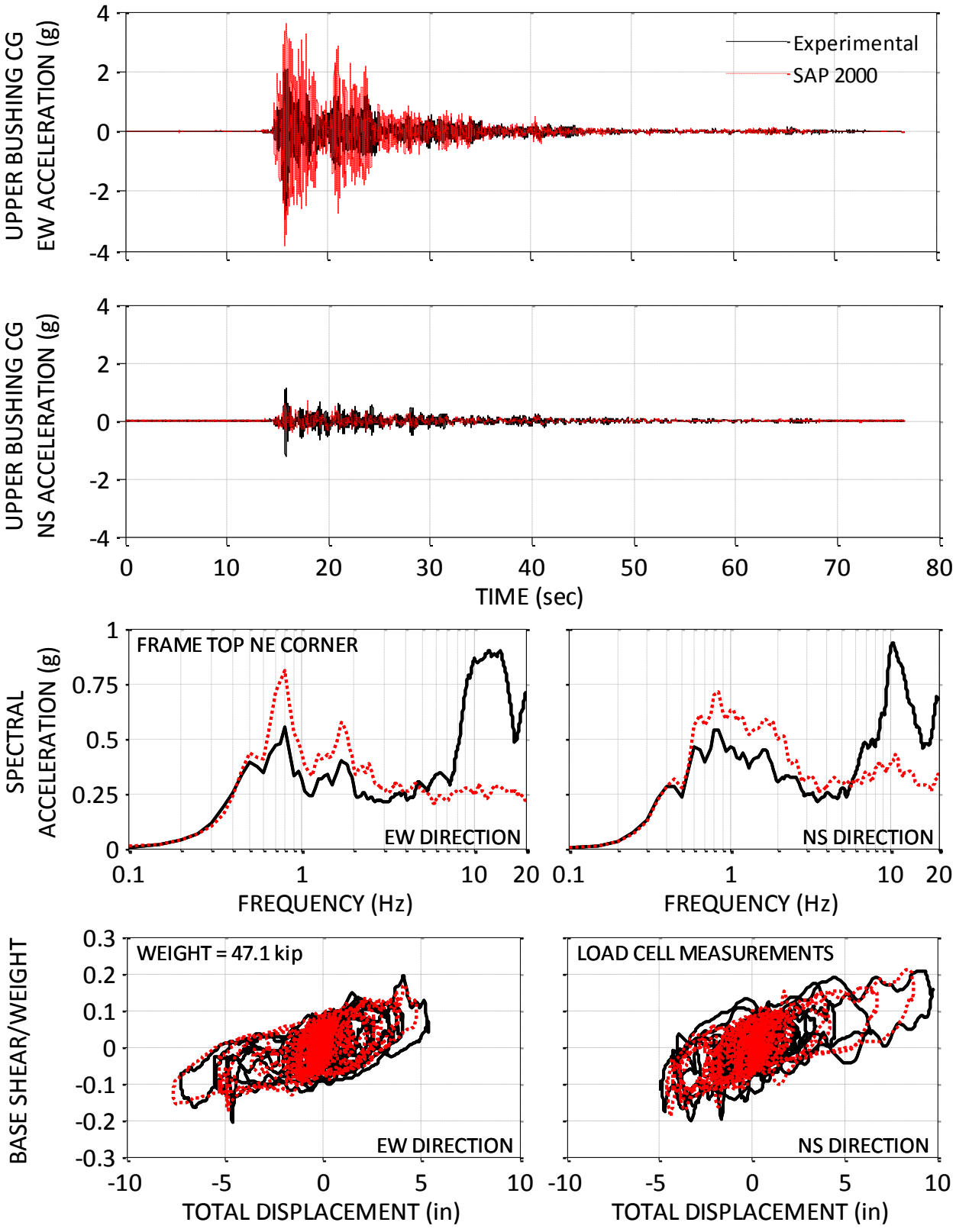
TRIPLE FP SYSTEM (Friction-Bolted Configuration – Series Model)
JENSEN FILTER 97% TRI-AXIAL (FN in EW direction)
LENGTH SCALE=1 NON-SYMMETRIC BUSHING CONFIGURATION



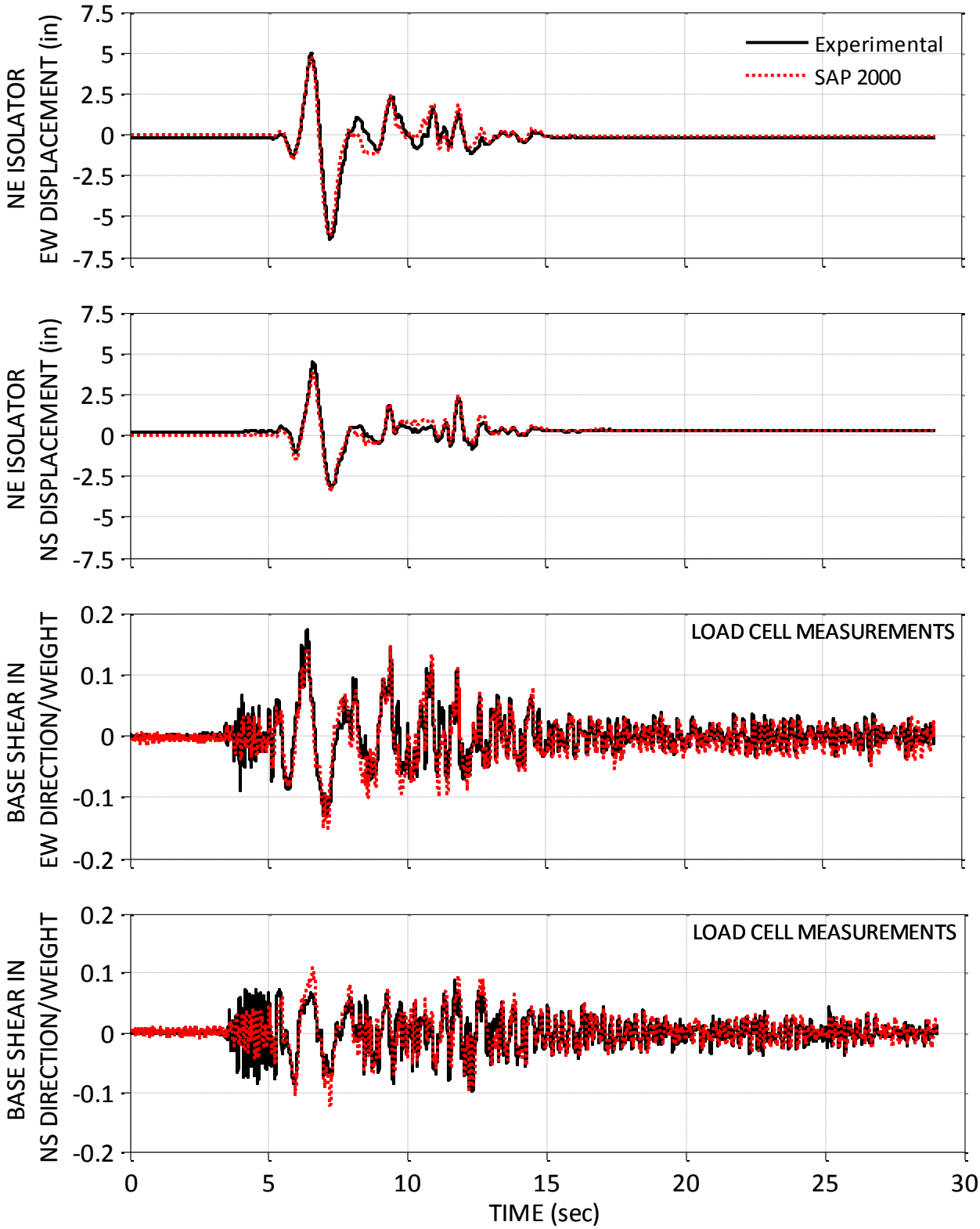

UPPER BUSHING CG
EW ACCELERATION (g)
Experimental
SAP 2000
UPPER BUSHING CG
NS ACCELERATION (g)
TIME (sec)
SPECTRAL
ACCELERATION (g)
FRAME TOP NE CORNER
EW DIRECTION
NS DIRECTION
FREQUENCY (Hz)
BASE SHEAR/WEIGHT
WEIGHT = 47.1 kip
LOAD CELL MEASUREMENTS
TOTAL DISPLACEMENT (in)

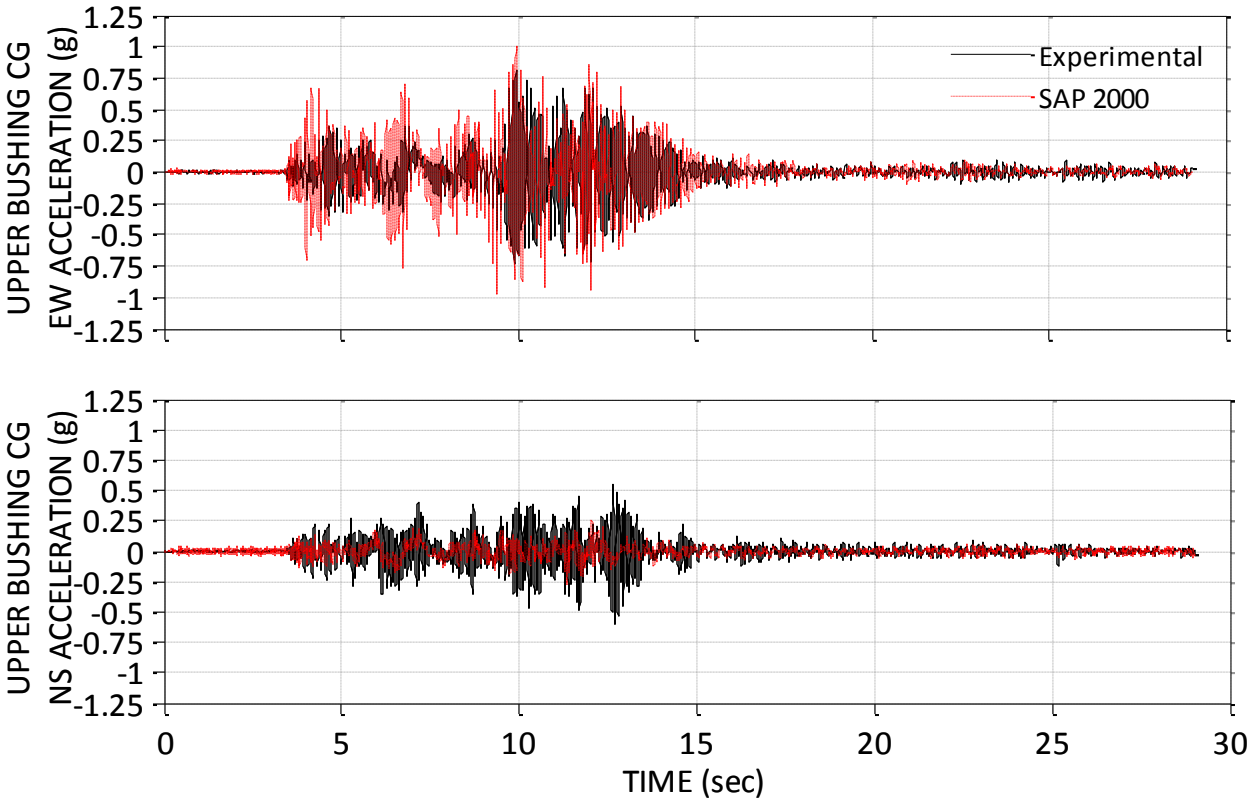
TRIPLE FP SYSTEM (Friction-Bolted Configuration – Series Model)
EL CENTRO 300% TRI-AXIAL (N90W in EW direction)
LENGTH SCALE=1 NON-SYMMETRIC BUSHING CONFIGURATION

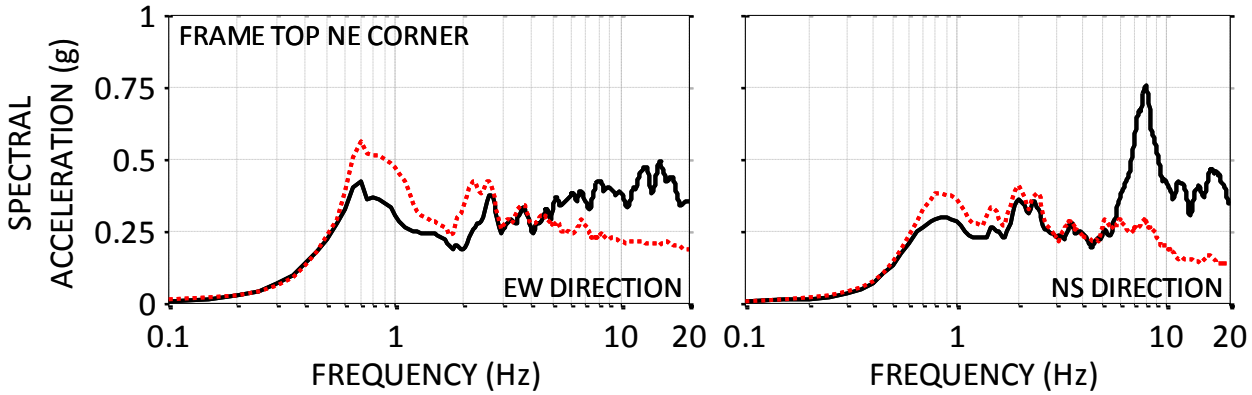


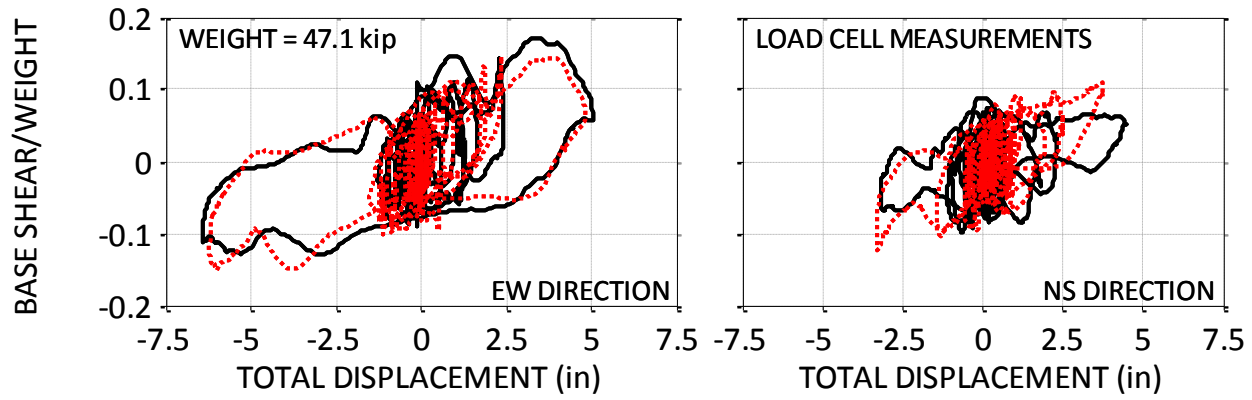

UPPER BUSHING CG
EW ACCELERATION (g)
Experimental
SAP 2000
UPPER BUSHING CG
NS ACCELERATION (g)
TIME (sec)
SPECTRAL
ACCELERATION (g)
FRAME TOP NE CORNER
EW DIRECTION
NS DIRECTION
FREQUENCY (Hz)
BASE SHEAR/WEIGHT
WEIGHT = 47.1 kip
LOAD CELL MEASUREMENTS
TOTAL DISPLACEMENT (in)

TRIPLE FP SYSTEM (Friction-Bolted Configuration – Series Model)
PACOIMA DAM 75% TRI-AXIAL (S16E in EW direction)
LENGTH SCALE=1 NON-SYMMETRIC BUSHING CONFIGURATION

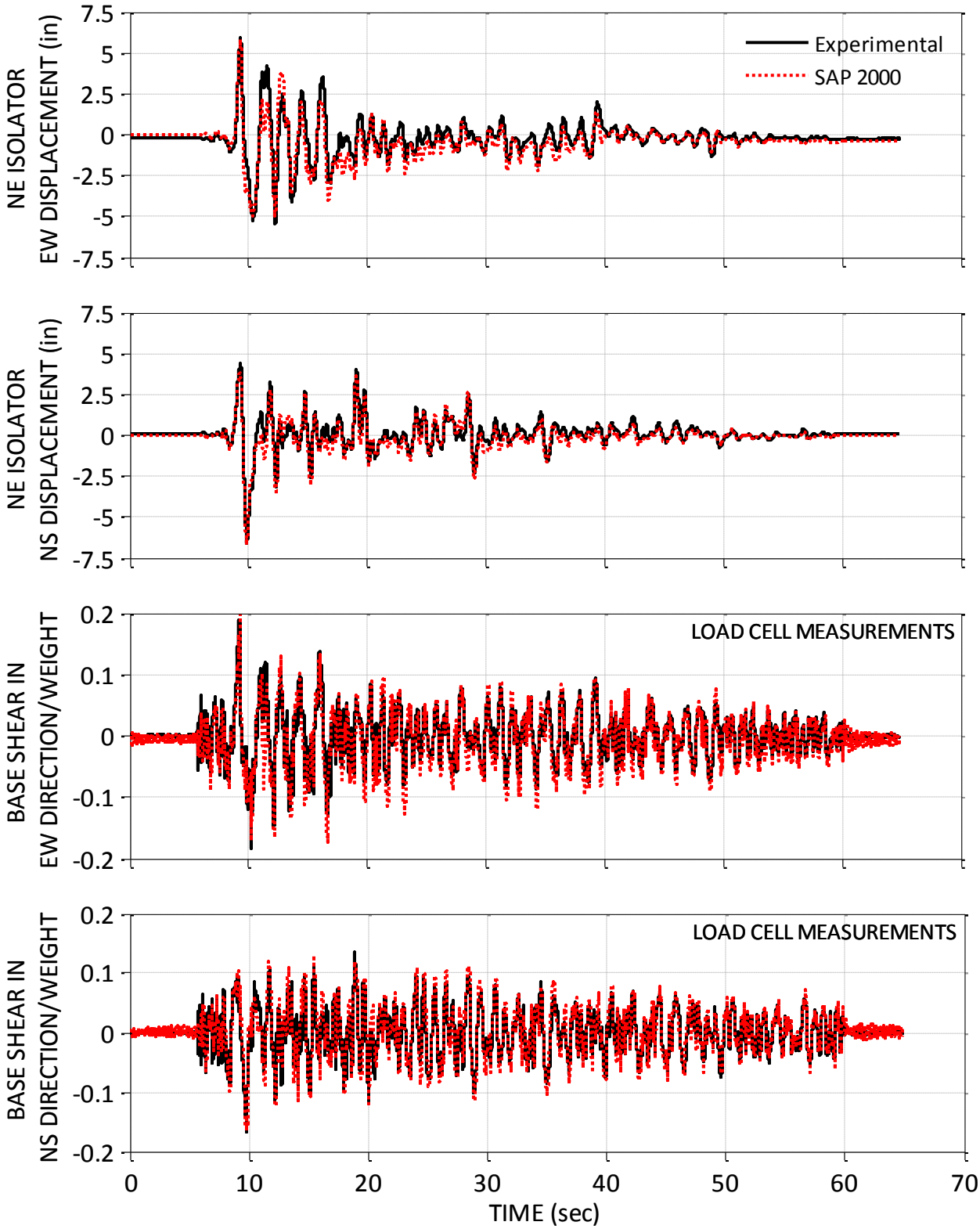


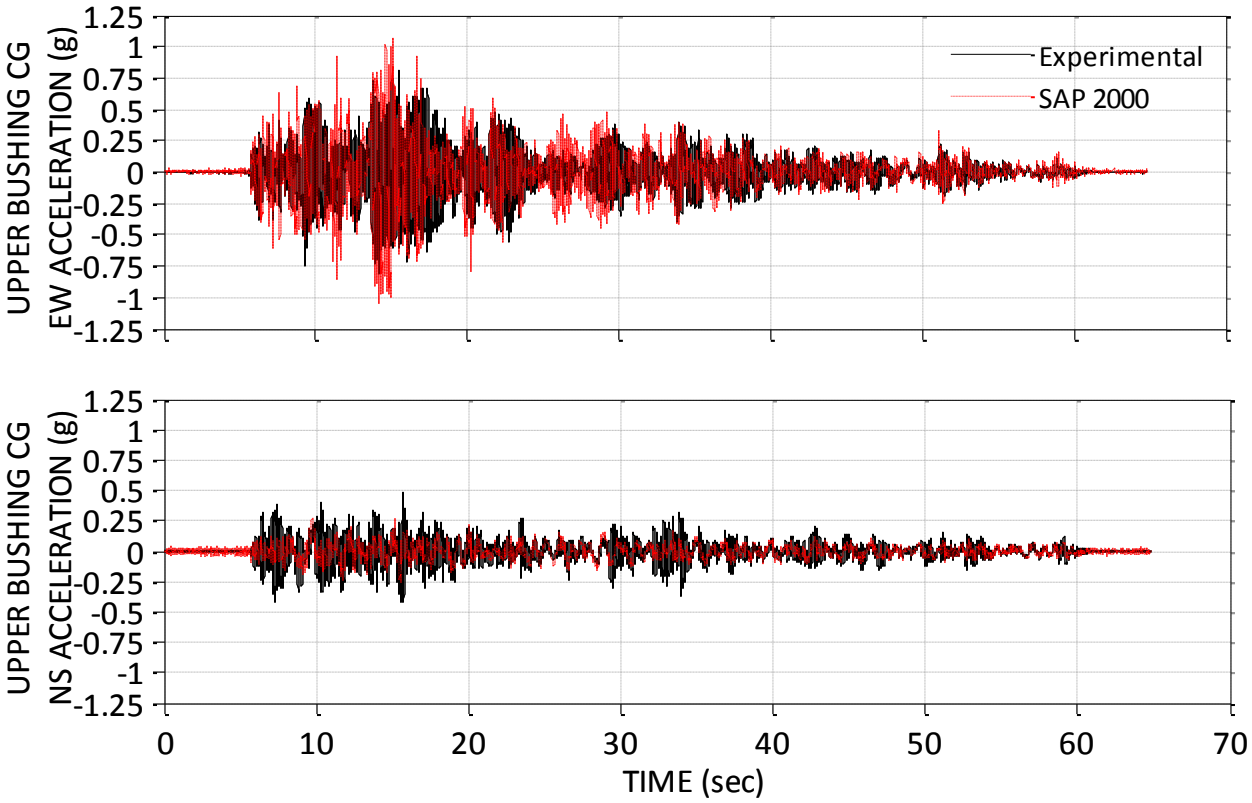

UPPER BUSHING CG
EW ACCELERATION (g)
Experimental
SAP 2000
UPPER BUSHING CG
NS ACCELERATION (g)
TIME (sec)

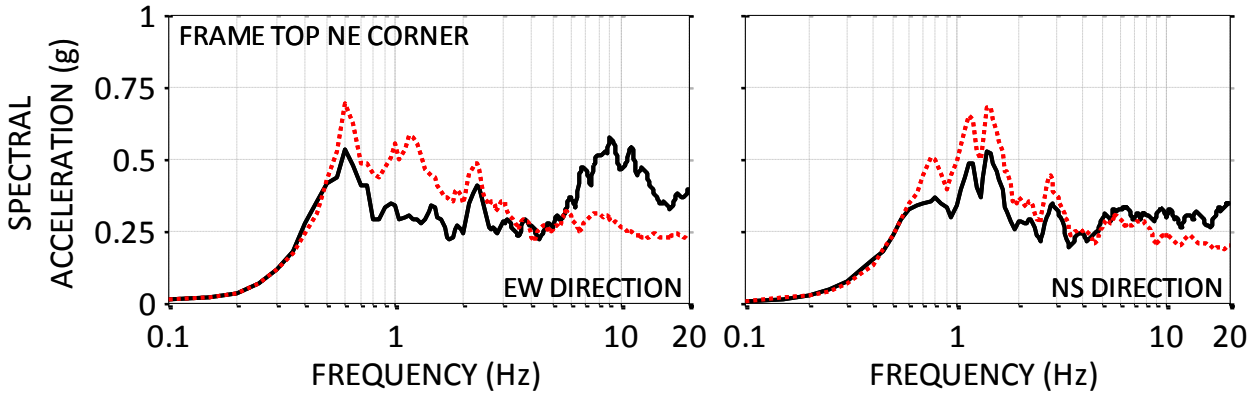

SPECTRAL
ACCELERATION (g)
FRAME TOP NE CORNER
EW DIRECTION
NS DIRECTION
FREQUENCY (Hz)
FREQUENCY (Hz)

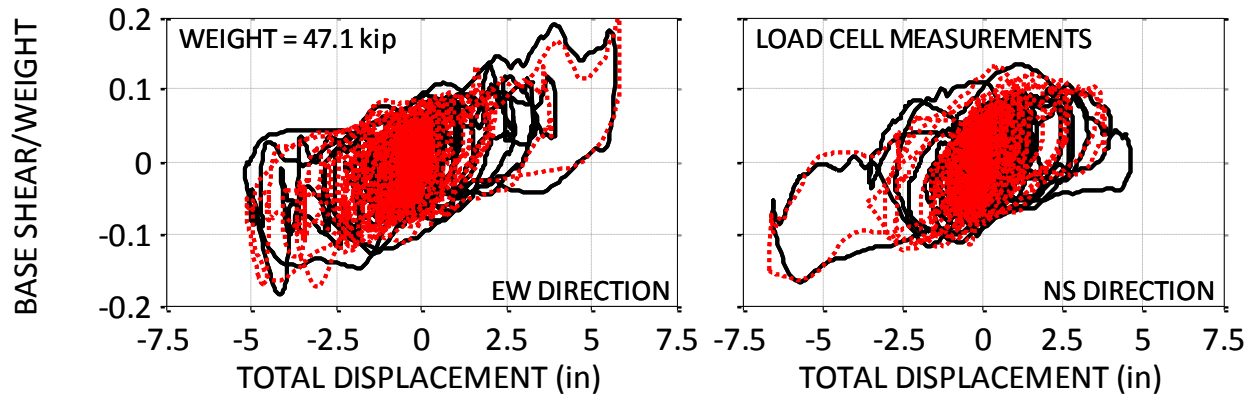

BASE SHEAR/WEIGHT
WEIGHT = 47.1 kip
LOAD CELL MEASUREMENTS
EW DIRECTION
NS DIRECTION
TOTAL DISPLACEMENT (in)
TOTAL DISPLACEMENT (in)

TRIPLE FP SYSTEM (Friction-Bolted Configuration – Series Model)
TAFT 500% TRI-AXIAL (S69E in EW direction)
LENGTH SCALE=1 NON-SYMMETRIC BUSHING CONFIGURATION

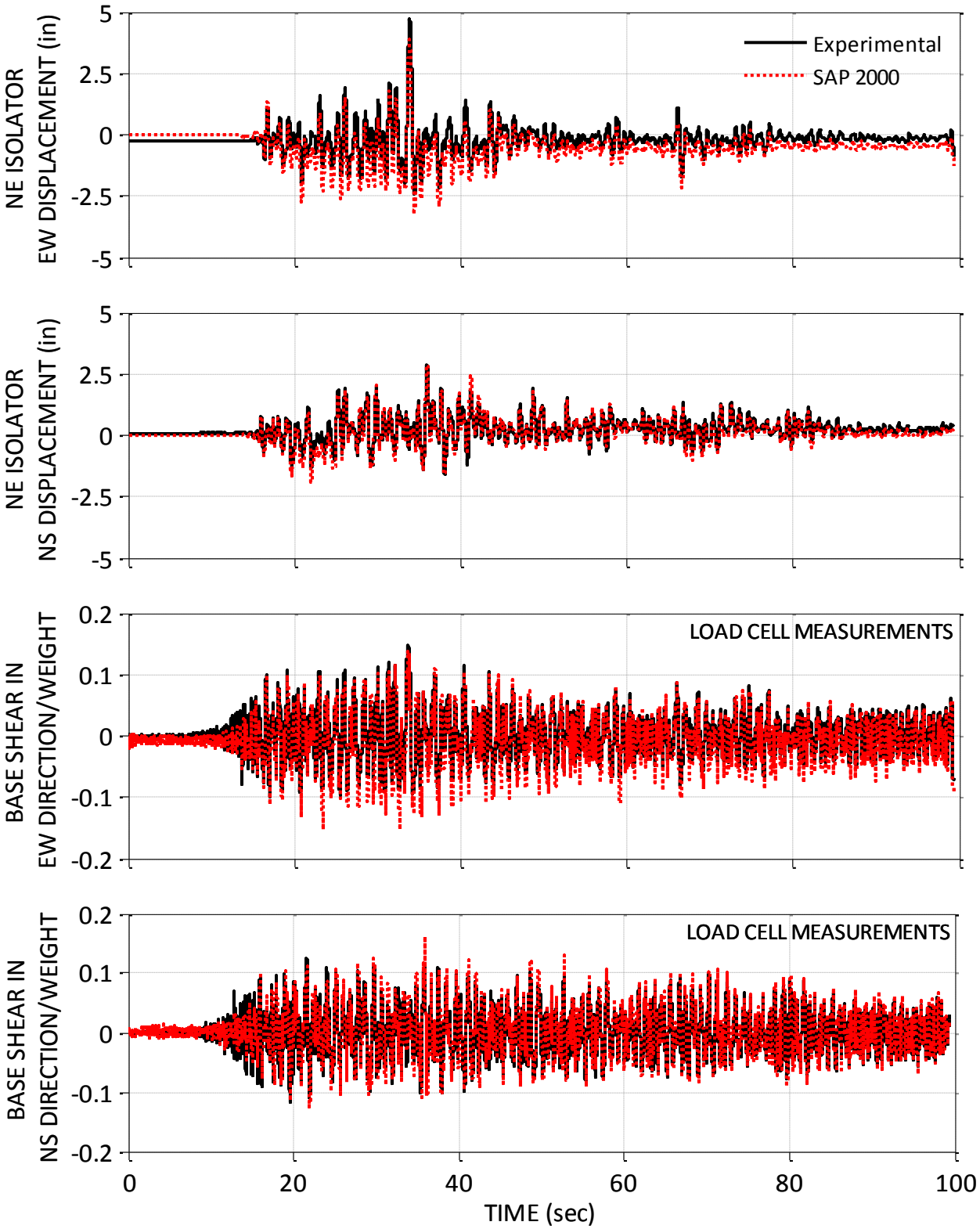


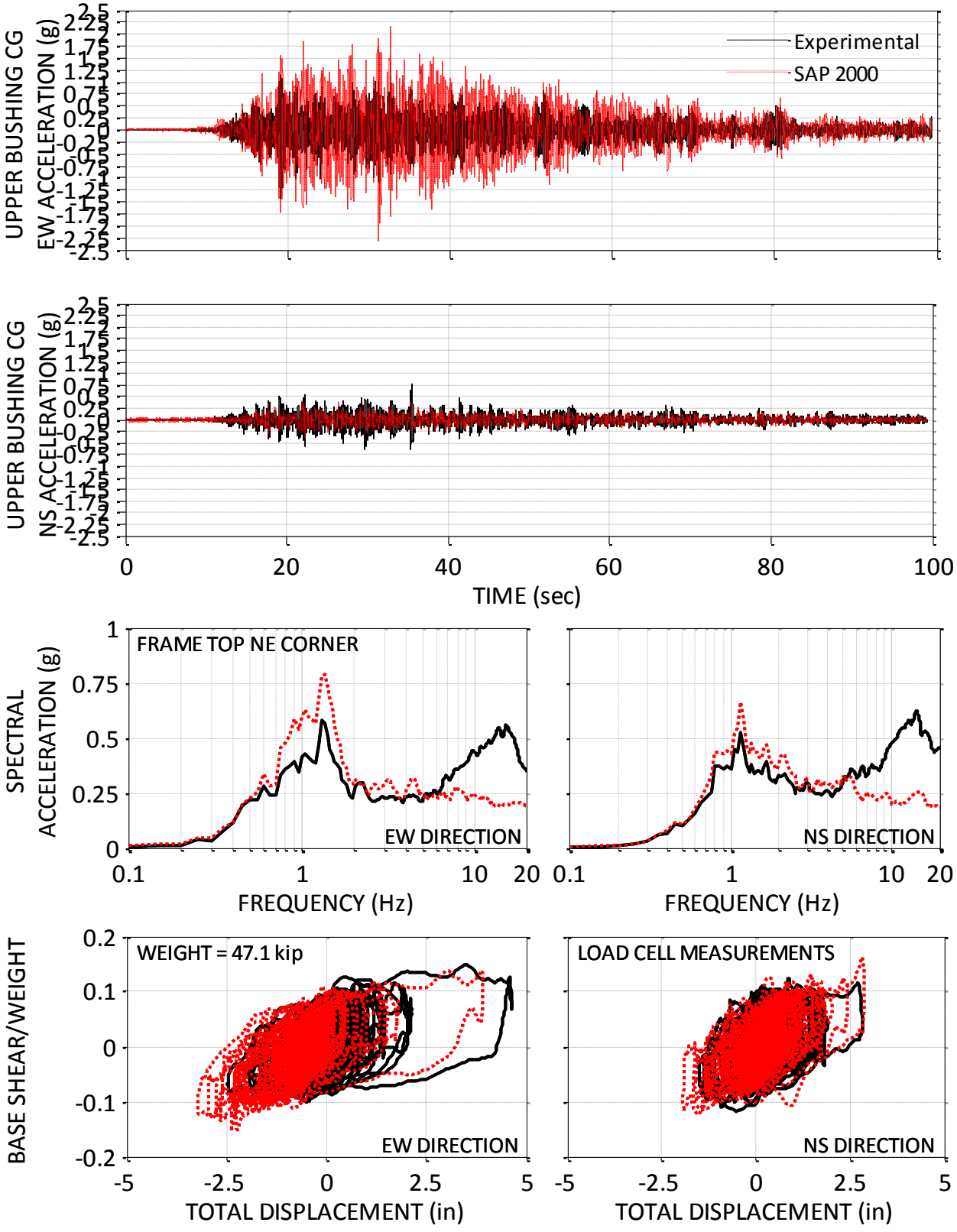

UPPER BUSHING CG
EW ACCELERATION (g)
Experimental
SAP 2000
UPPER BUSHING CG
NS ACCELERATION (g)
TIME (sec)


SPECTRAL
ACCELERATION (g)
FRAME TOP NE CORNER
EW DIRECTION
NS DIRECTION
FREQUENCY (Hz)
FREQUENCY (Hz)

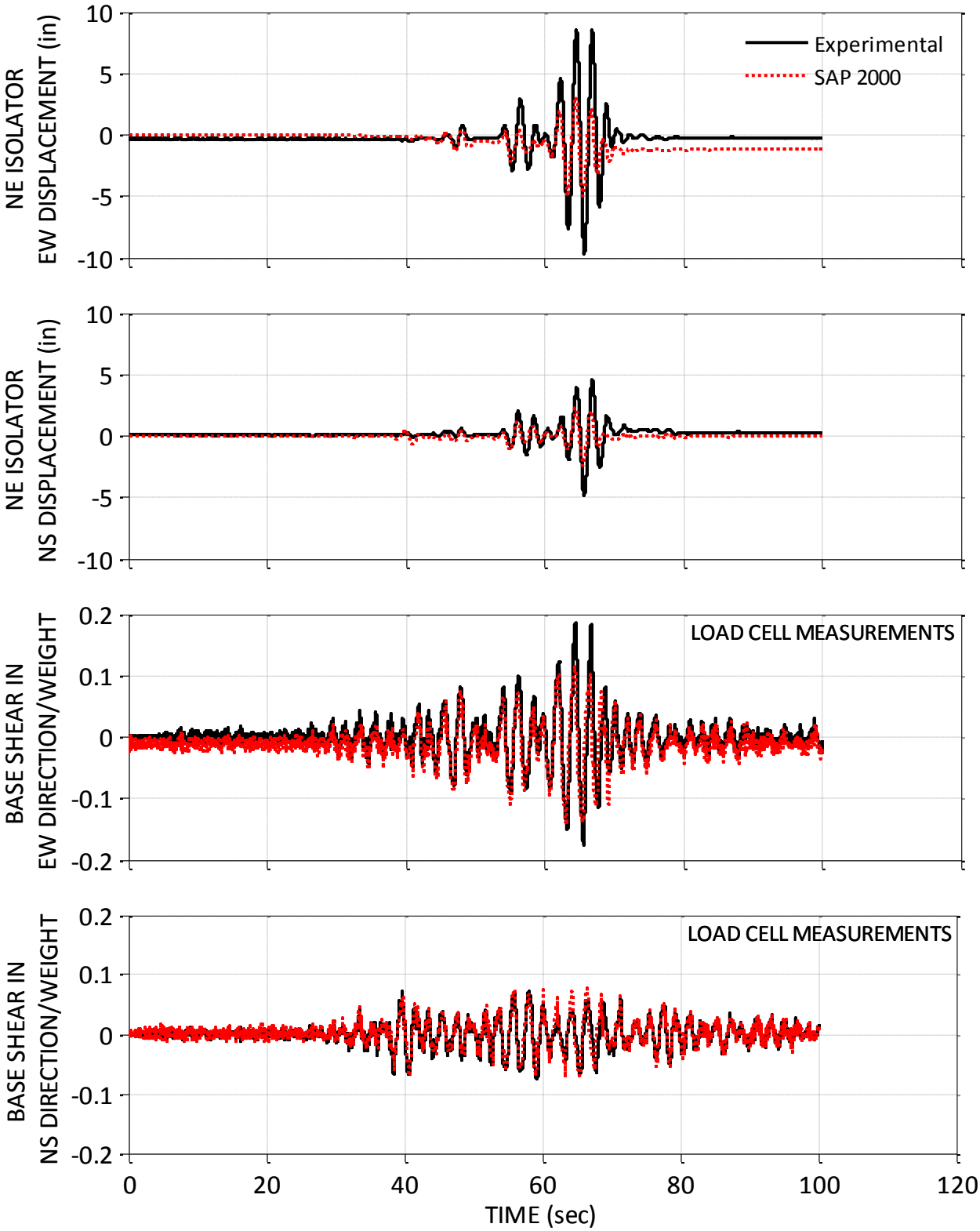

BASE SHEAR/WEIGHT
WEIGHT = 47.1 kip
LOAD CELL MEASUREMENTS
EW DIRECTION
NS DIRECTION
TOTAL DISPLACEMENT (in)
TOTAL DISPLACEMENT (in)

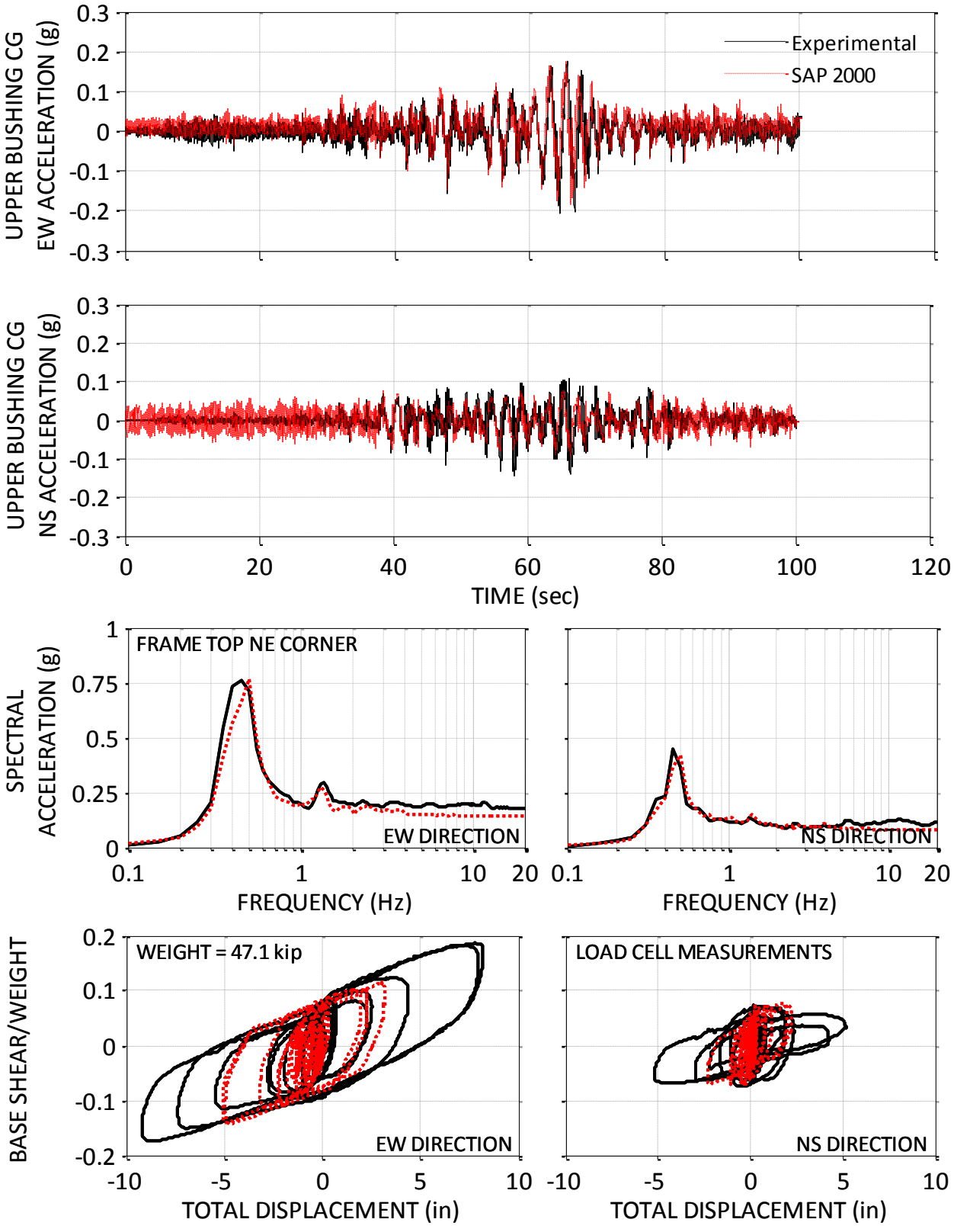
TRIPLE FP SYSTEM (Friction-Bolted Configuration – Series Model)
CHILE 100% TRI-AXIAL (EW in EW direction)
LENGTH SCALE=1 NON-SYMMETRIC BUSHING CONFIGURATION



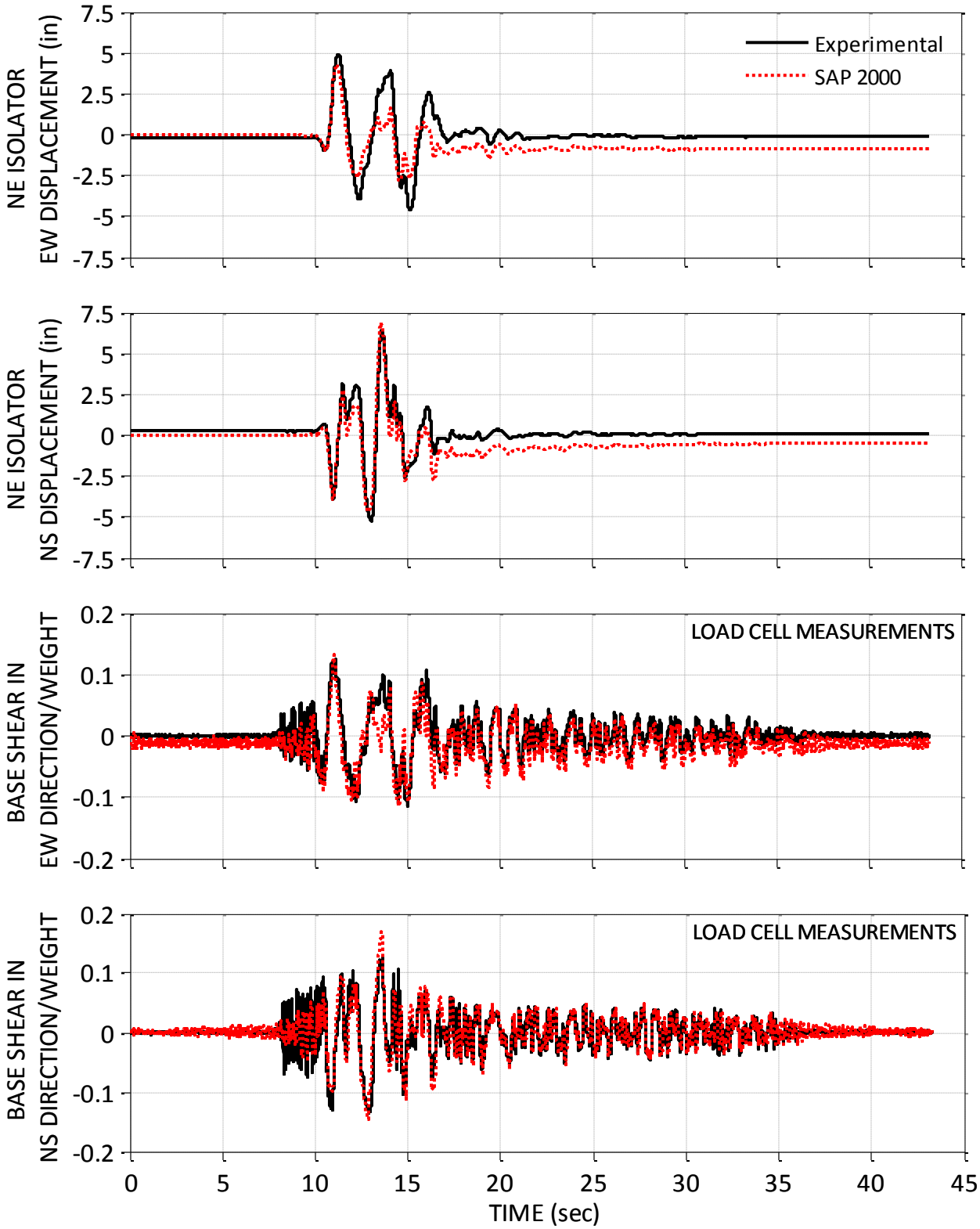

UPPER BUSHING CG
EW ACCELERATION (g)
Experimental
SAP 2000
UPPER BUSHING CG
NS ACCELERATION (g)
TIME (sec)
SPECTRAL
ACCELERATION (g)
FRAME TOP NE CORNER
EW DIRECTION
NS DIRECTION
FREQUENCY (Hz)
BASE SHEAR/WEIGHT
WEIGHT = 47.1 kip
LOAD CELL MEASUREMENTS
TOTAL DISPLACEMENT (in)

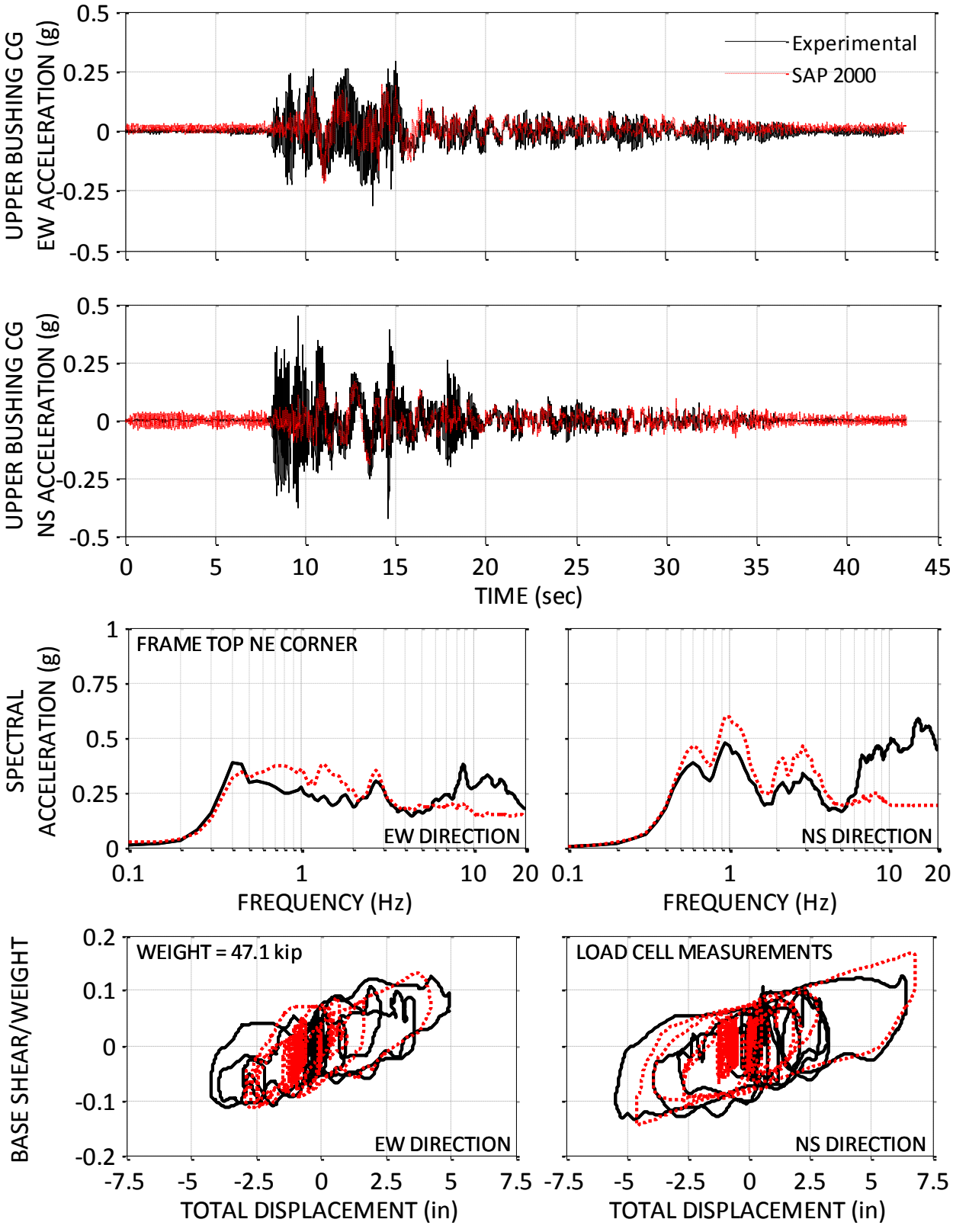
TRIPLE FP SYSTEM (Friction-Bolted Configuration – Series Model)
MEXICO 70% TRI-AXIAL (N90W in EW direction)
LENGTH SCALE=1 NON-SYMMETRIC BUSHING CONFIGURATION



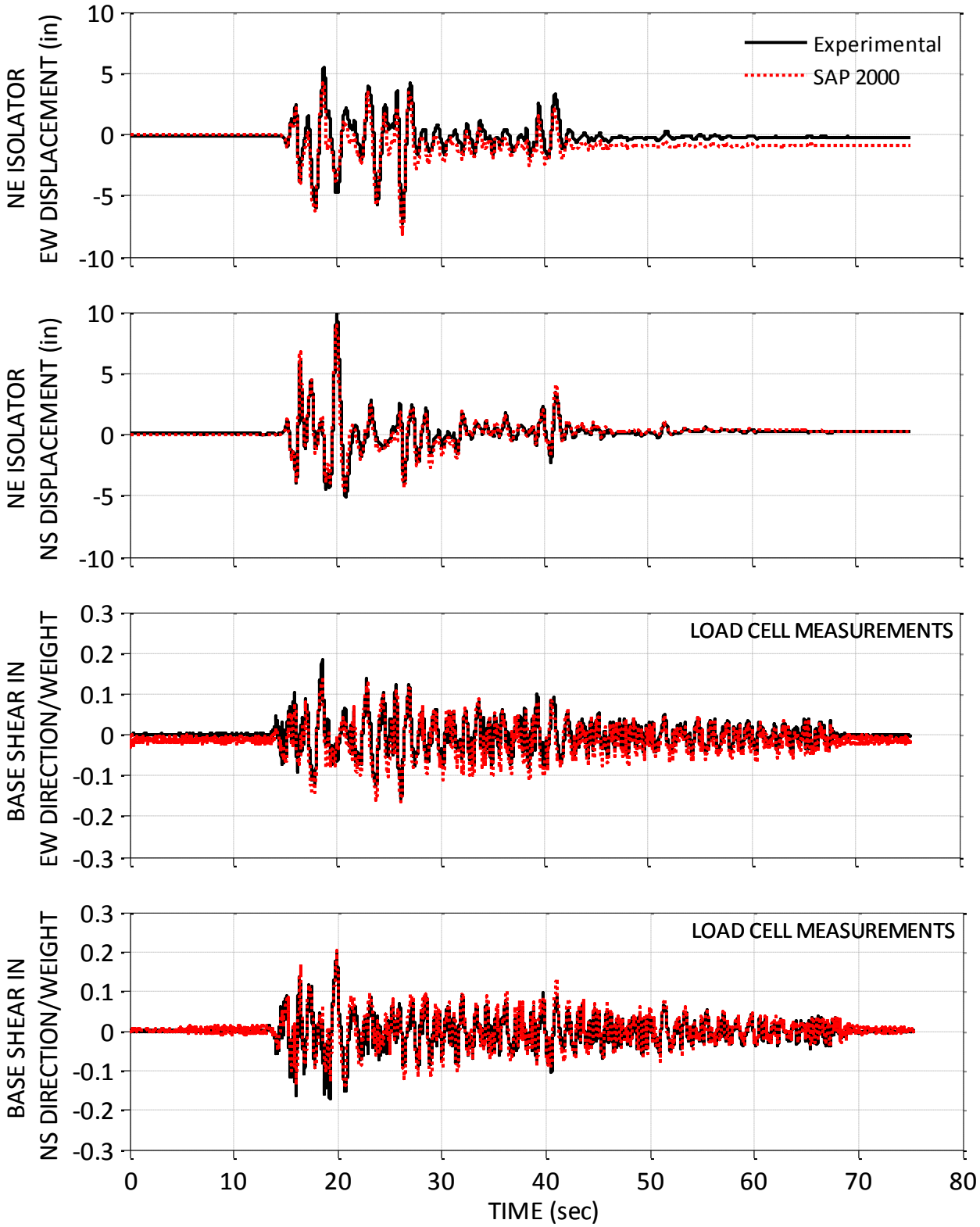

UPPER BUSHING CG
EW ACCELERATION (g)
Experimental
SAP 2000
UPPER BUSHING CG
NS ACCELERATION (g)
TIME (sec)
SPECTRAL
ACCELERATION (g)
FRAME TOP NE CORNER
EW DIRECTION
NS DIRECTION
FREQUENCY (Hz)
BASE SHEAR/WEIGHT
WEIGHT = 47.1 kip
LOAD CELL MEASUREMENTS
TOTAL DISPLACEMENT (in)

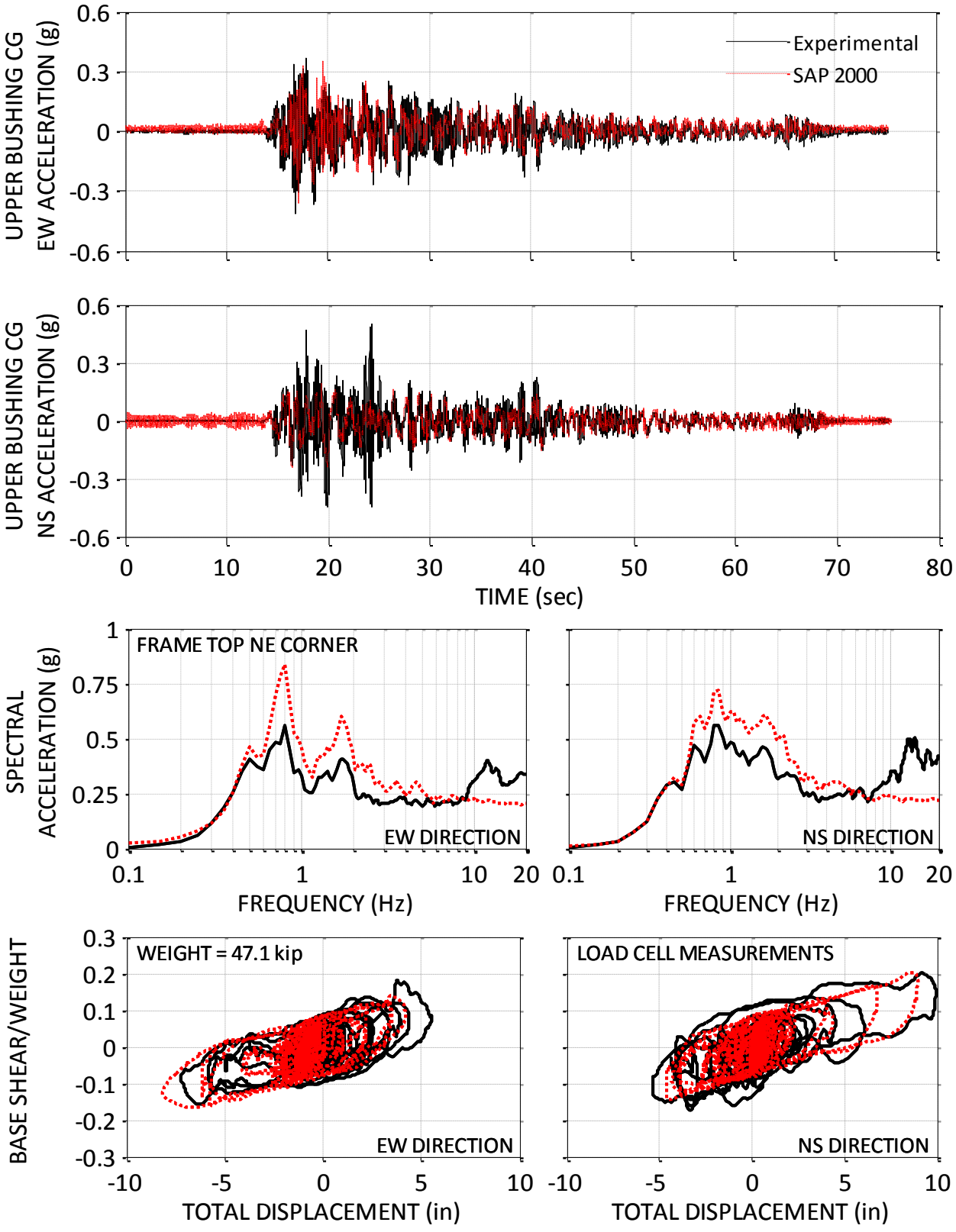
TRIPLE FP SYSTEM (Friction-Bolted Configuration – Series Model)
JENSEN FILTER 97% BI-AXIAL (FN in EW direction)
LENGTH SCALE=1 NON-SYMMETRIC BUSHING CONFIGURATION



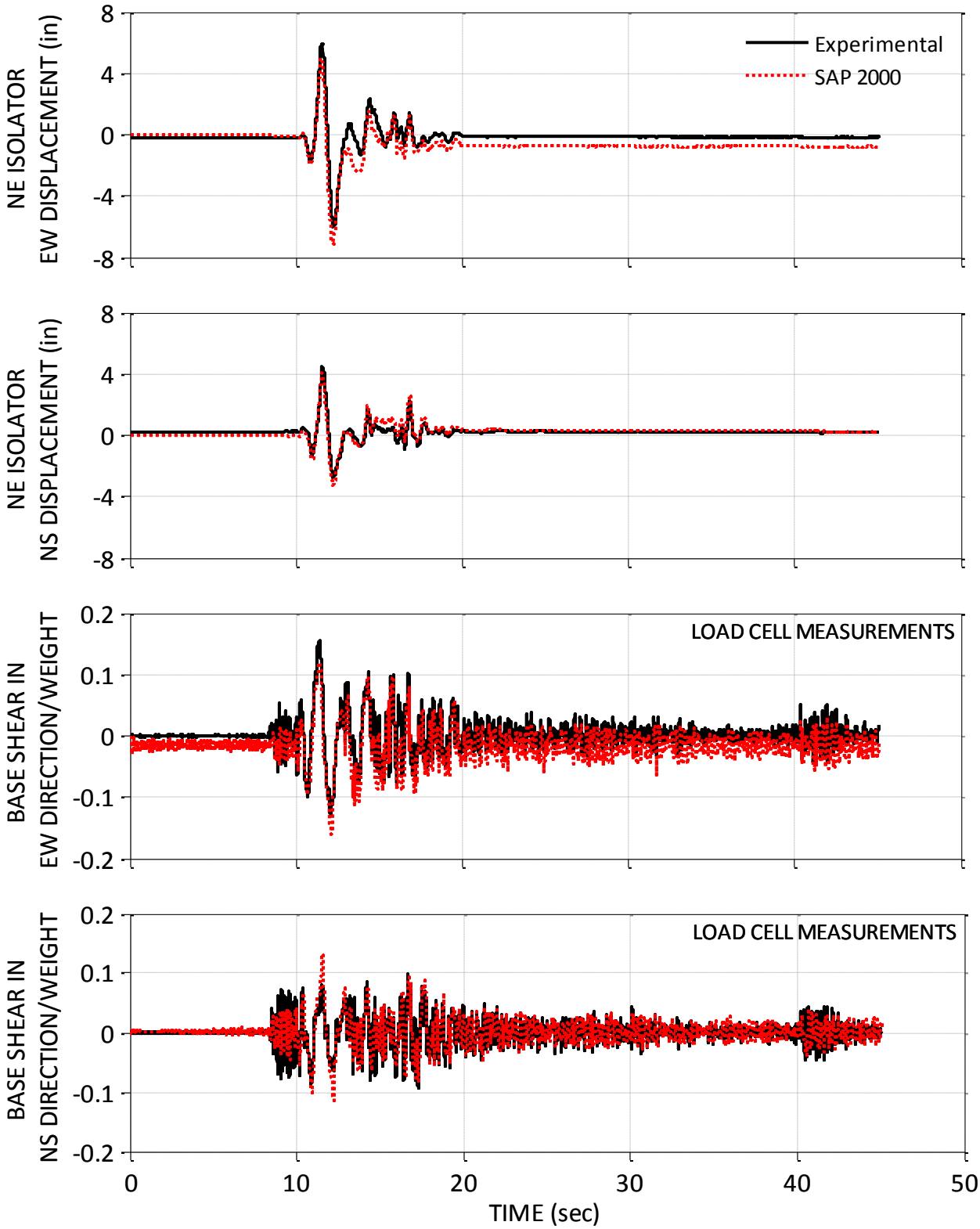

UPPER BUSHING CG
EW ACCELERATION (g)
Experimental
SAP 2000
UPPER BUSHING CG
NS ACCELERATION (g)
TIME (sec)
SPECTRAL
ACCELERATION (g)
FRAME TOP NE CORNER
EW DIRECTION
NS DIRECTION
FREQUENCY (Hz)
BASE SHEAR/WEIGHT
WEIGHT = 47.1 kip
LOAD CELL MEASUREMENTS
TOTAL DISPLACEMENT (in)

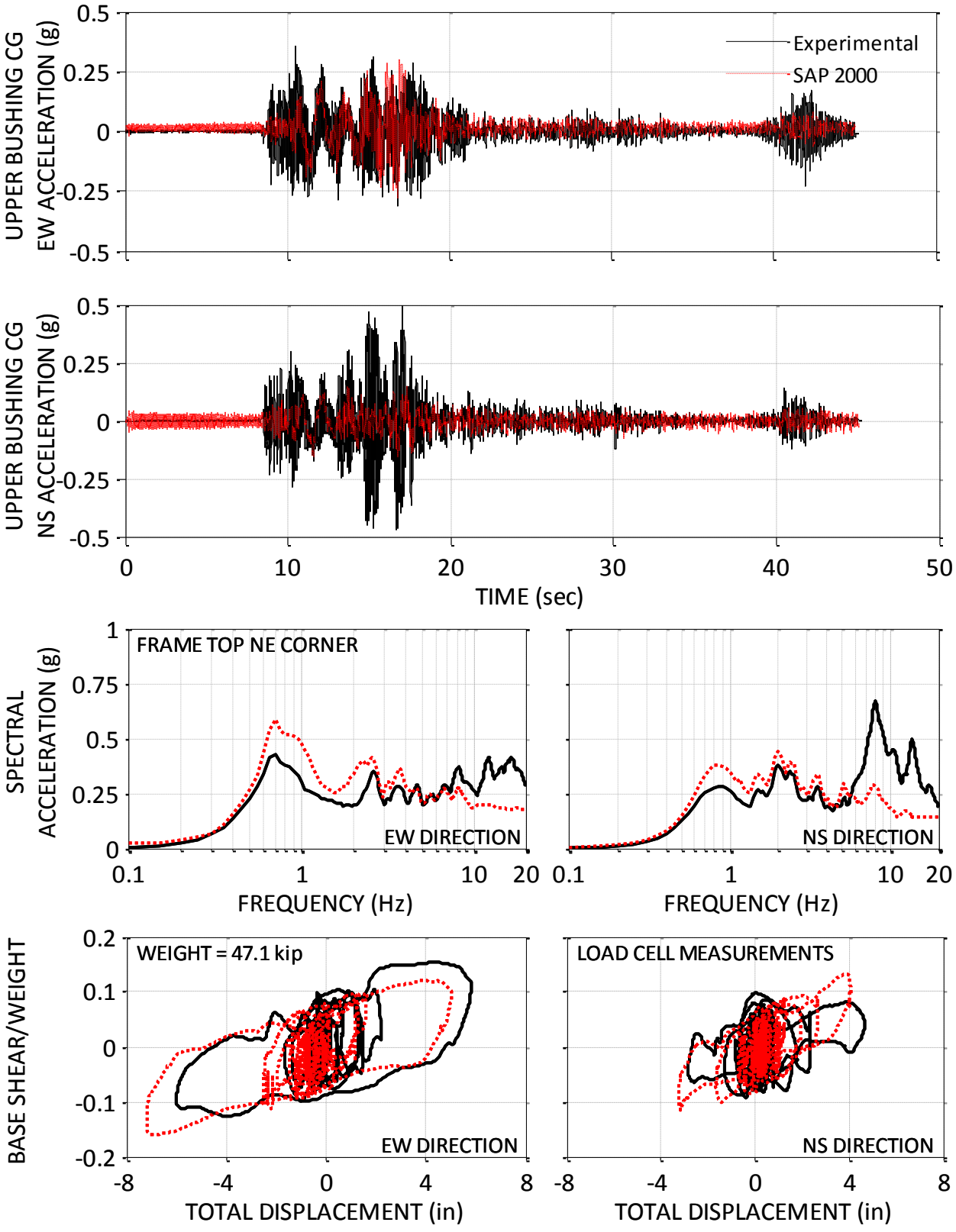
TRIPLE FP SYSTEM (Friction-Bolted Configuration – Series Model)
EL CENTRO 300% BI-AXIAL (N90W in EW direction)
LENGTH SCALE=1 NON-SYMMETRIC BUSHING CONFIGURATION



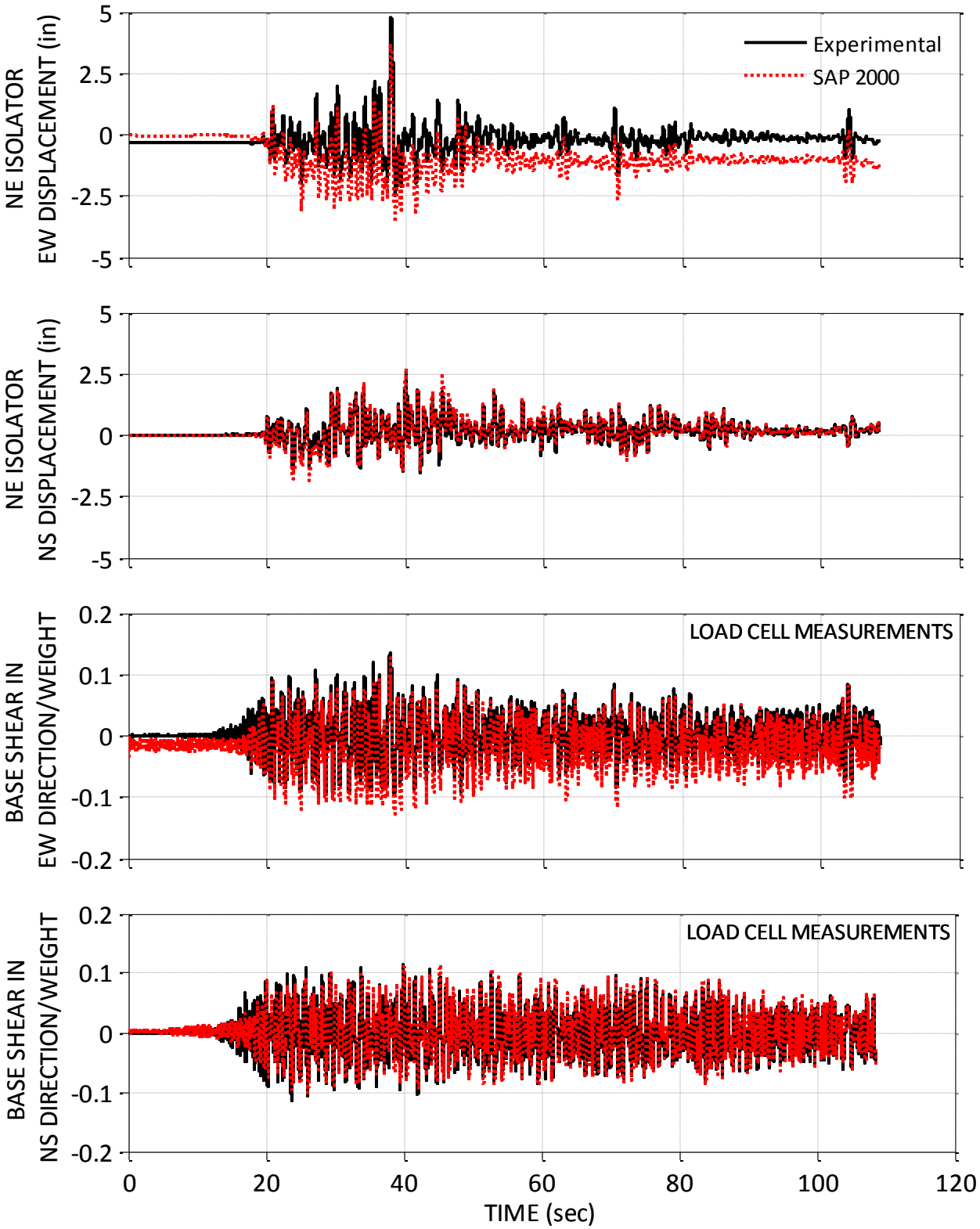

UPPER BUSHING CG
EW ACCELERATION (g)
Experimental
SAP 2000
UPPER BUSHING CG
NS ACCELERATION (g)
TIME (sec)
SPECTRAL
ACCELERATION (g)
FRAME TOP NE CORNER
EW DIRECTION
NS DIRECTION
FREQUENCY (Hz)
BASE SHEAR/WEIGHT
WEIGHT = 47.1 kip
LOAD CELL MEASUREMENTS
TOTAL DISPLACEMENT (in)

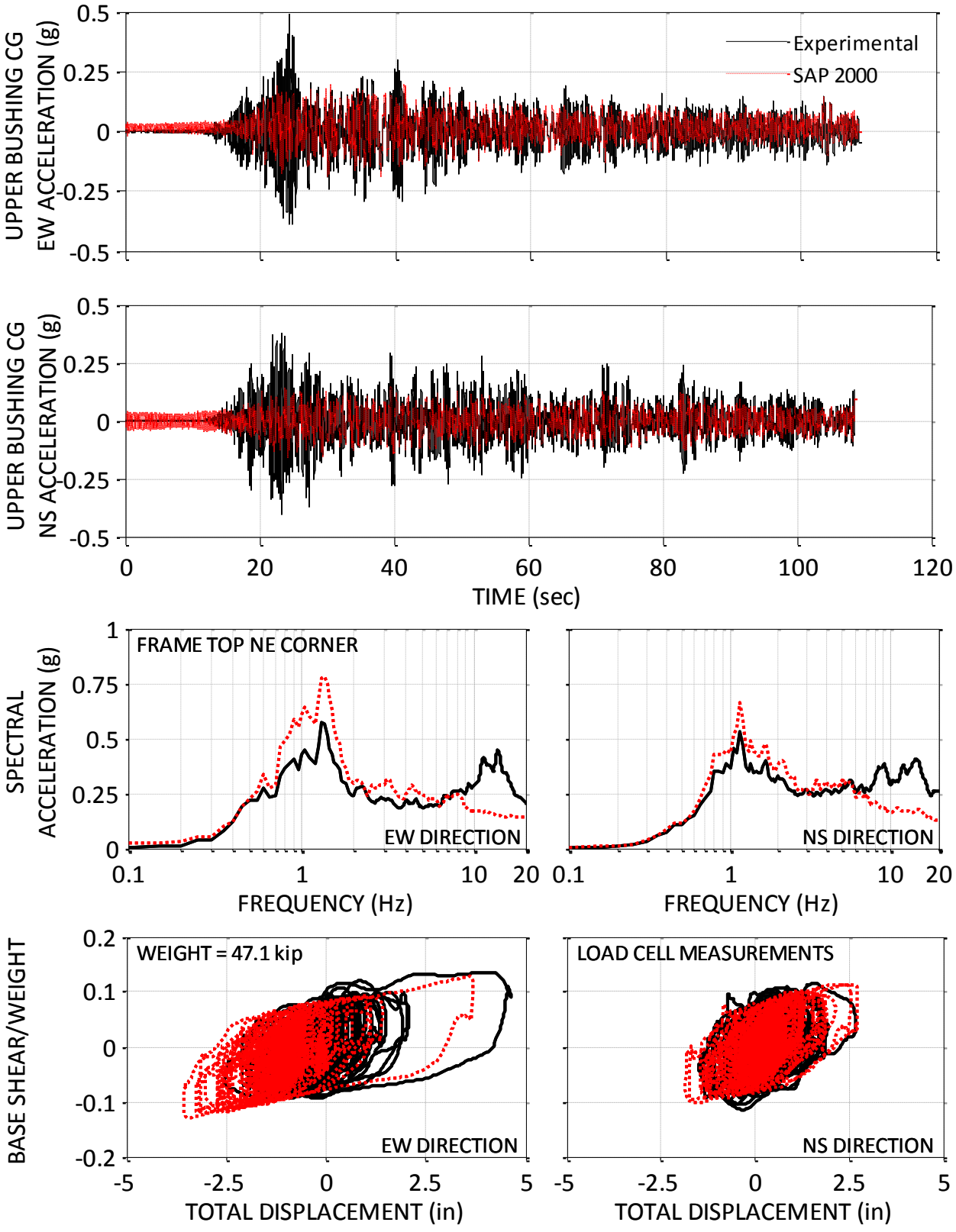
TRIPLE FP SYSTEM (Friction-Bolted Configuration – Series Model)
PACOIMA DAM 75% BI-AXIAL (S16E in EW direction)
LENGTH SCALE=1 NON-SYMMETRIC BUSHING CONFIGURATION



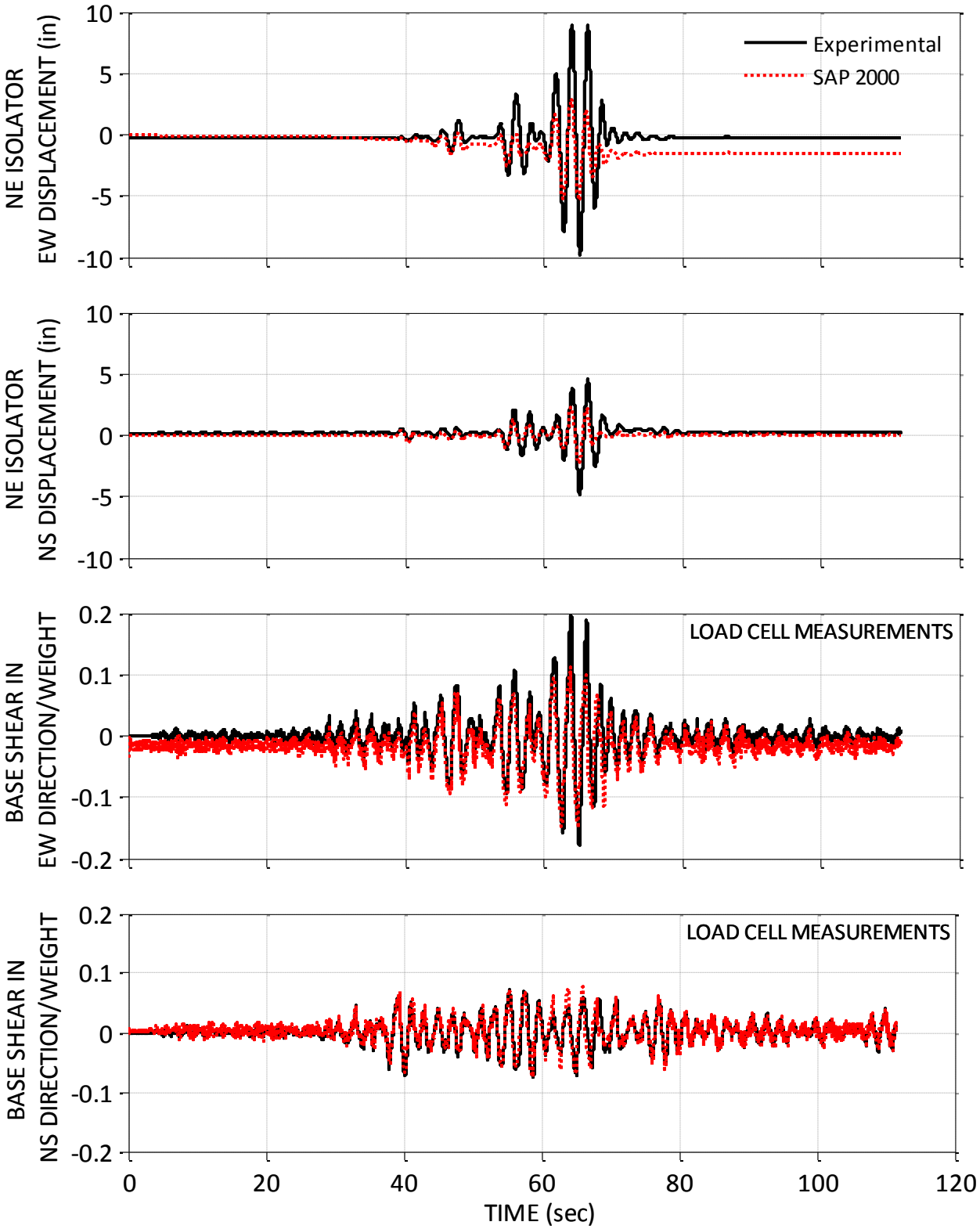

UPPER BUSHING CG
EW ACCELERATION (g)
Experimental
SAP 2000
UPPER BUSHING CG
NS ACCELERATION (g)
TIME (sec)
SPECTRAL
ACCELERATION (g)
FRAME TOP NE CORNER
EW DIRECTION
NS DIRECTION
FREQUENCY (Hz)
BASE SHEAR/WEIGHT
WEIGHT = 47.1 kip
LOAD CELL MEASUREMENTS
TOTAL DISPLACEMENT (in)

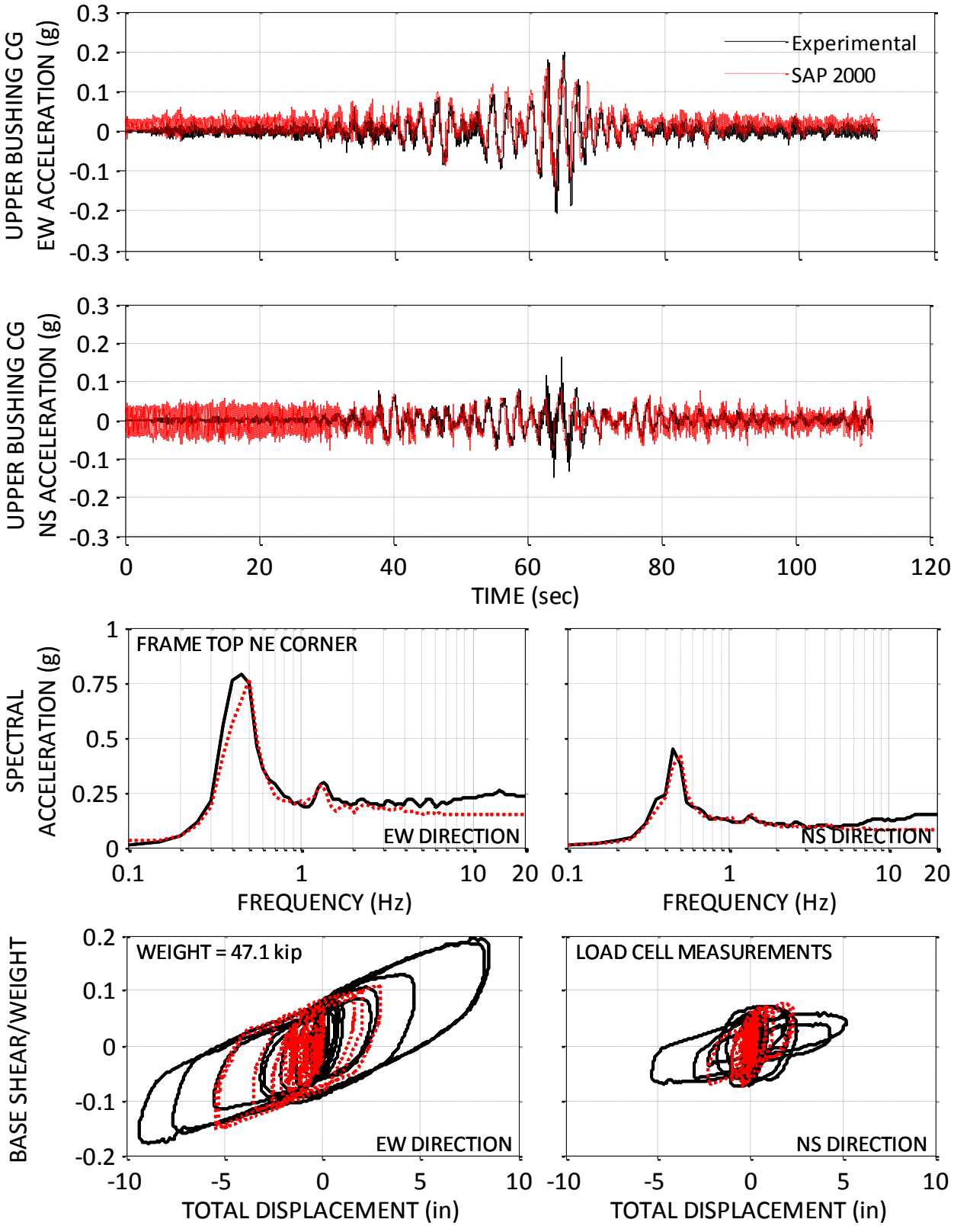
TRIPLE FP SYSTEM (Friction-Bolted Configuration – Series Model)
CHILE 100% BI-AXIAL (EW in EW direction)
LENGTH SCALE=1 NON-SYMMETRIC BUSHING CONFIGURATION



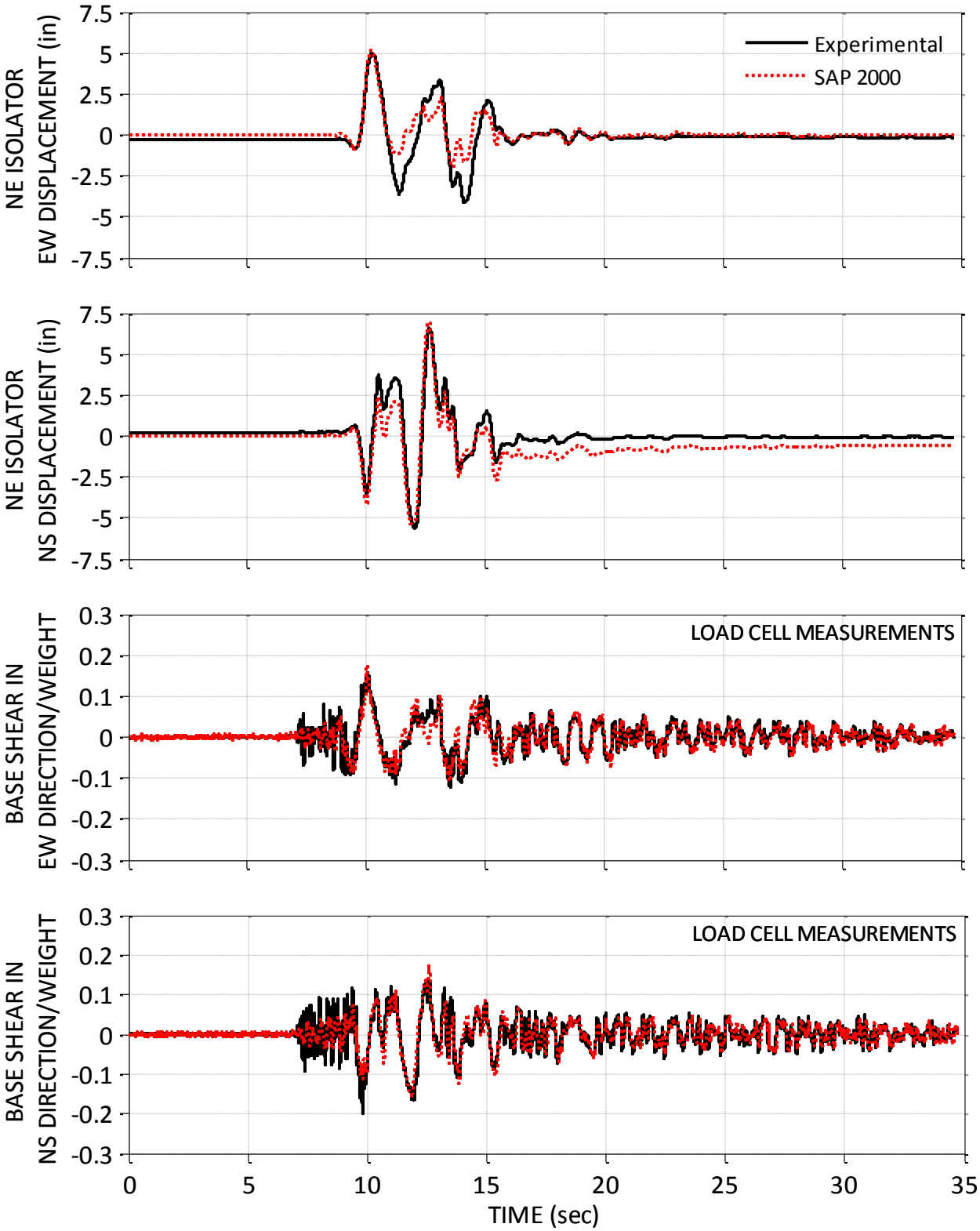

UPPER BUSHING CG
EW ACCELERATION (g)
Experimental
SAP 2000
UPPER BUSHING CG
NS ACCELERATION (g)
TIME (sec)
SPECTRAL
ACCELERATION (g)
FRAME TOP NE CORNER
EW DIRECTION
NS DIRECTION
FREQUENCY (Hz)
BASE SHEAR/WEIGHT
WEIGHT = 47.1 kip
LOAD CELL MEASUREMENTS
TOTAL DISPLACEMENT (in)

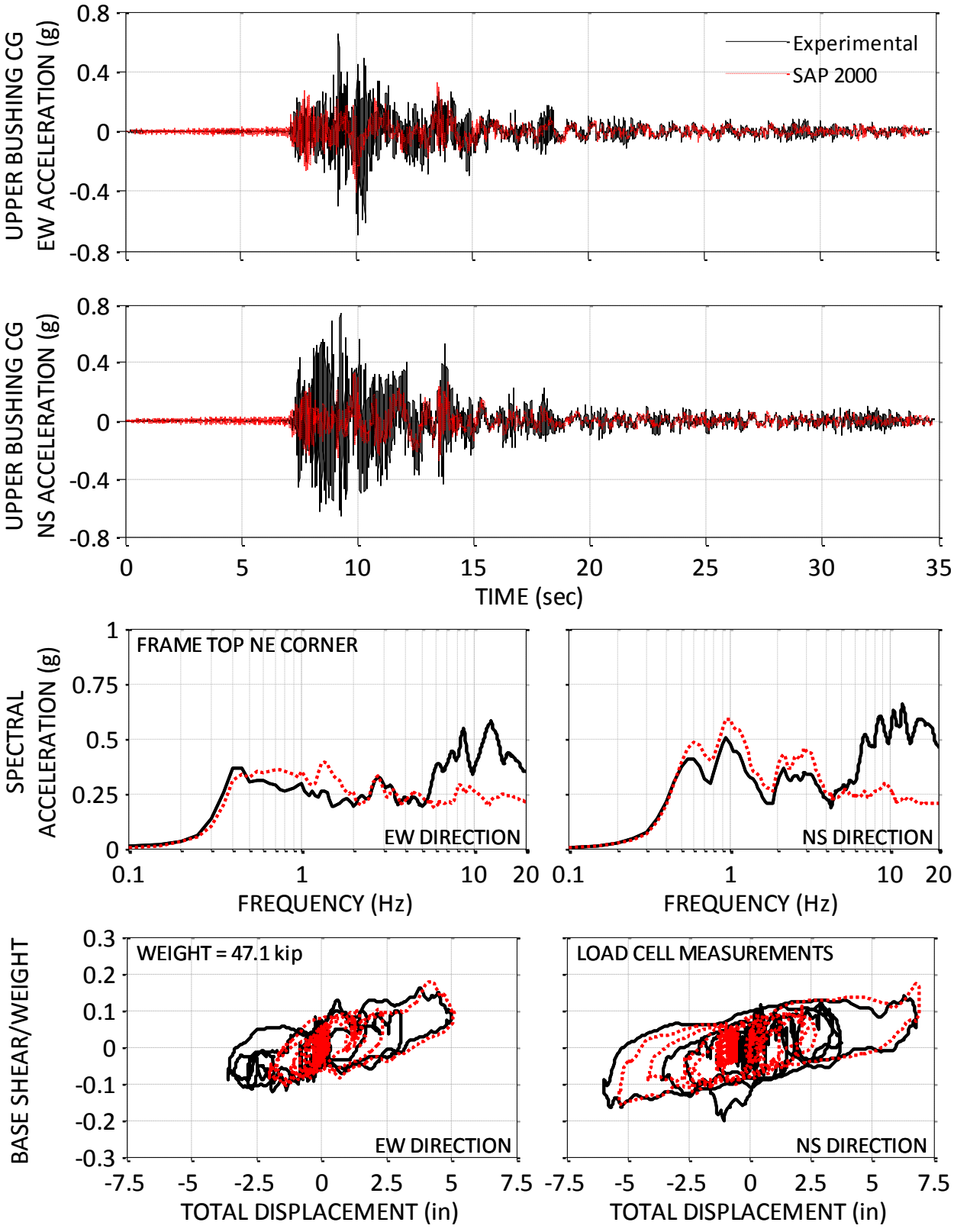
TRIPLE FP SYSTEM (Friction-Bolted Configuration – Series Model)
MEXICO 70% BI-AXIAL (N90W in EW direction)
LENGTH SCALE=1 NON-SYMMETRIC BUSHING CONFIGURATION



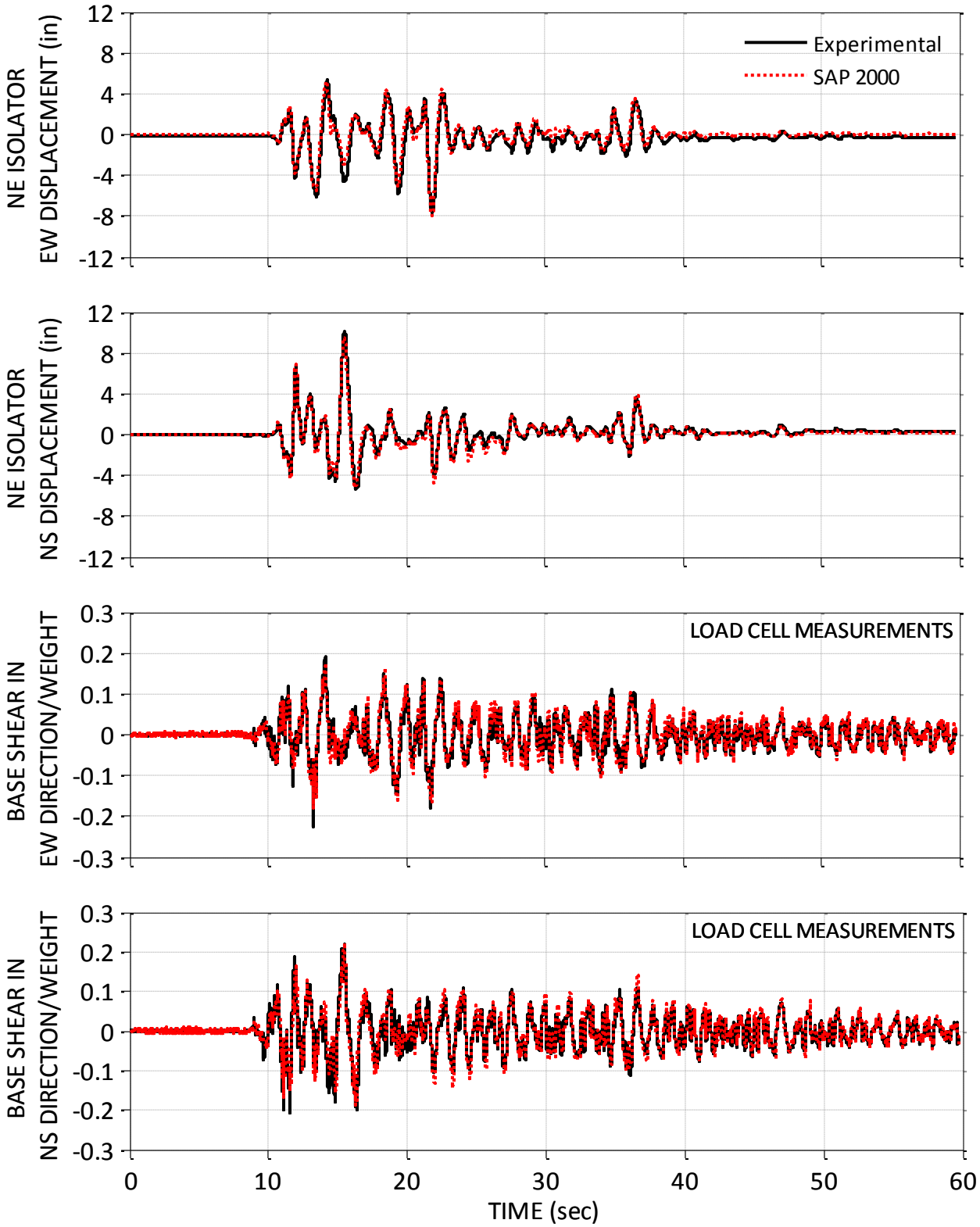

UPPER BUSHING CG
EW ACCELERATION (g)
Experimental
SAP 2000
UPPER BUSHING CG
NS ACCELERATION (g)
TIME (sec)
SPECTRAL
ACCELERATION (g)
FRAME TOP NE CORNER
EW DIRECTION
NS DIRECTION
FREQUENCY (Hz)
BASE SHEAR/WEIGHT
WEIGHT = 47.1 kip
LOAD CELL MEASUREMENTS
TOTAL DISPLACEMENT (in)

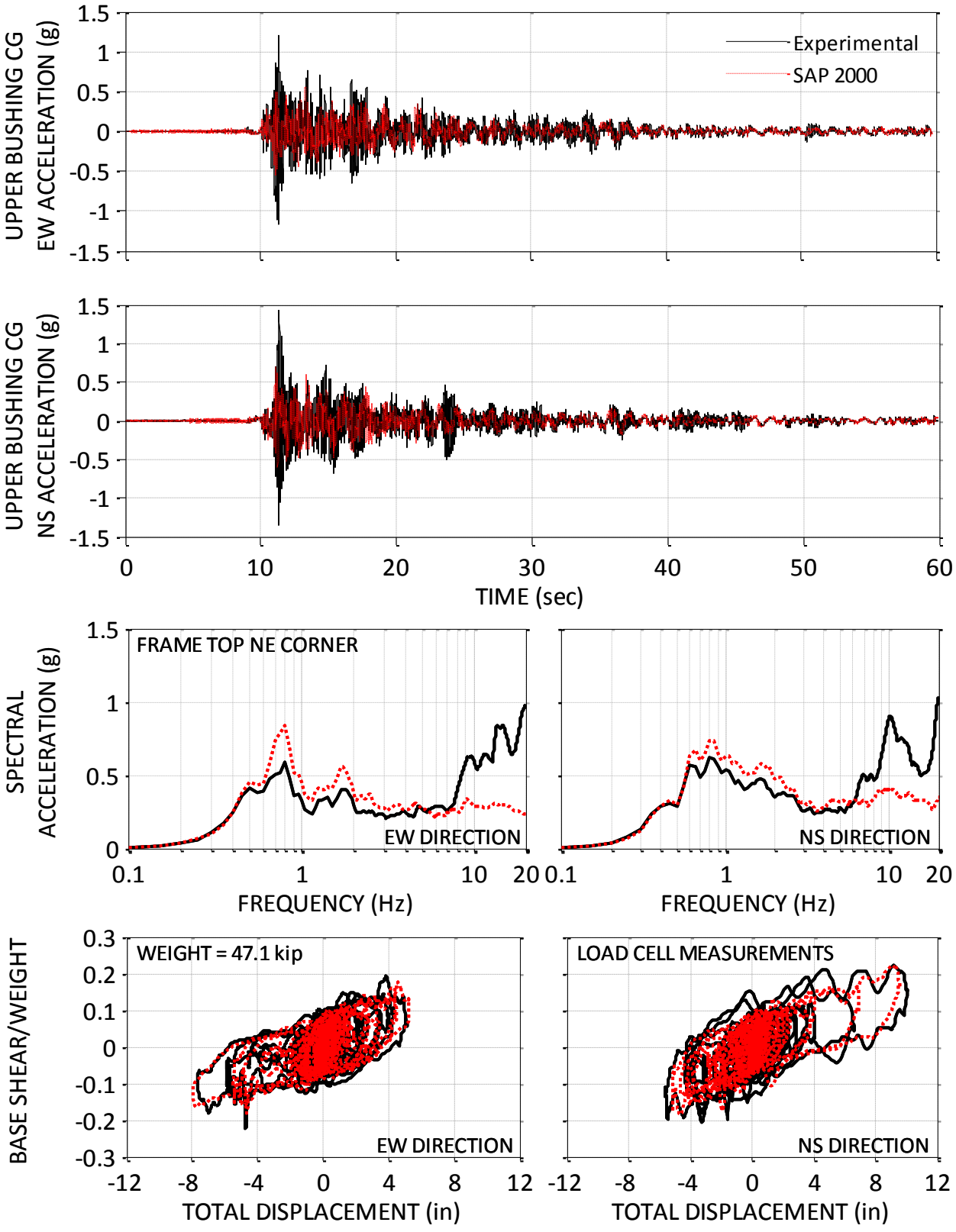
TRIPLE FP SYSTEM (Friction-Bolted Configuration – Series Model)
JENSEN FILTER 97% TRI-AXIAL (FN in EW direction)
LENGTH SCALE=1 SYMMETRIC BUSHING CONFIGURATION



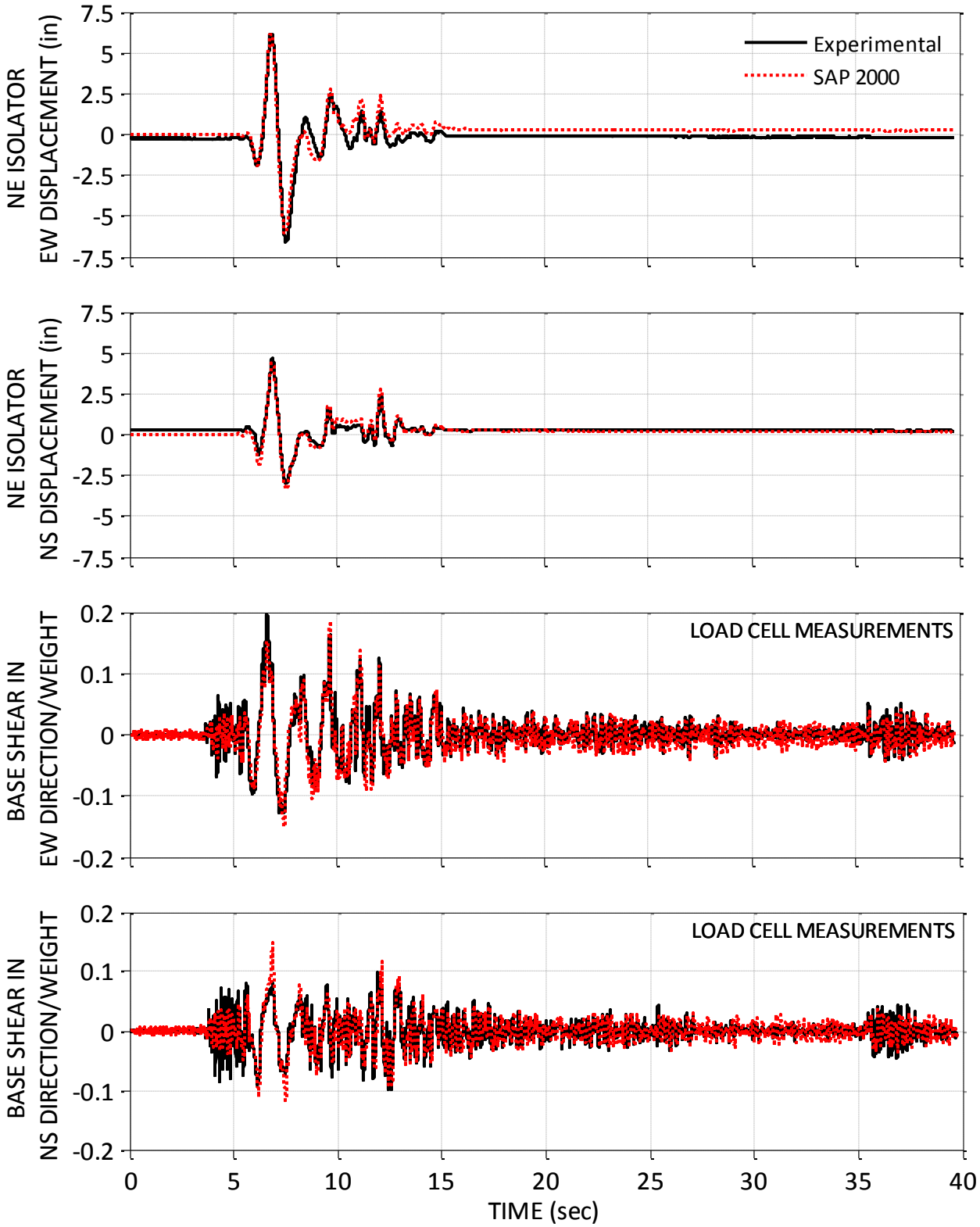

UPPER BUSHING CG
EW ACCELERATION (g)
Experimental
SAP 2000
UPPER BUSHING CG
NS ACCELERATION (g)
TIME (sec)
SPECTRAL
ACCELERATION (g)
FRAME TOP NE CORNER
EW DIRECTION
NS DIRECTION
FREQUENCY (Hz)
BASE SHEAR/WEIGHT
WEIGHT = 47.1 kip
LOAD CELL MEASUREMENTS
TOTAL DISPLACEMENT (in)

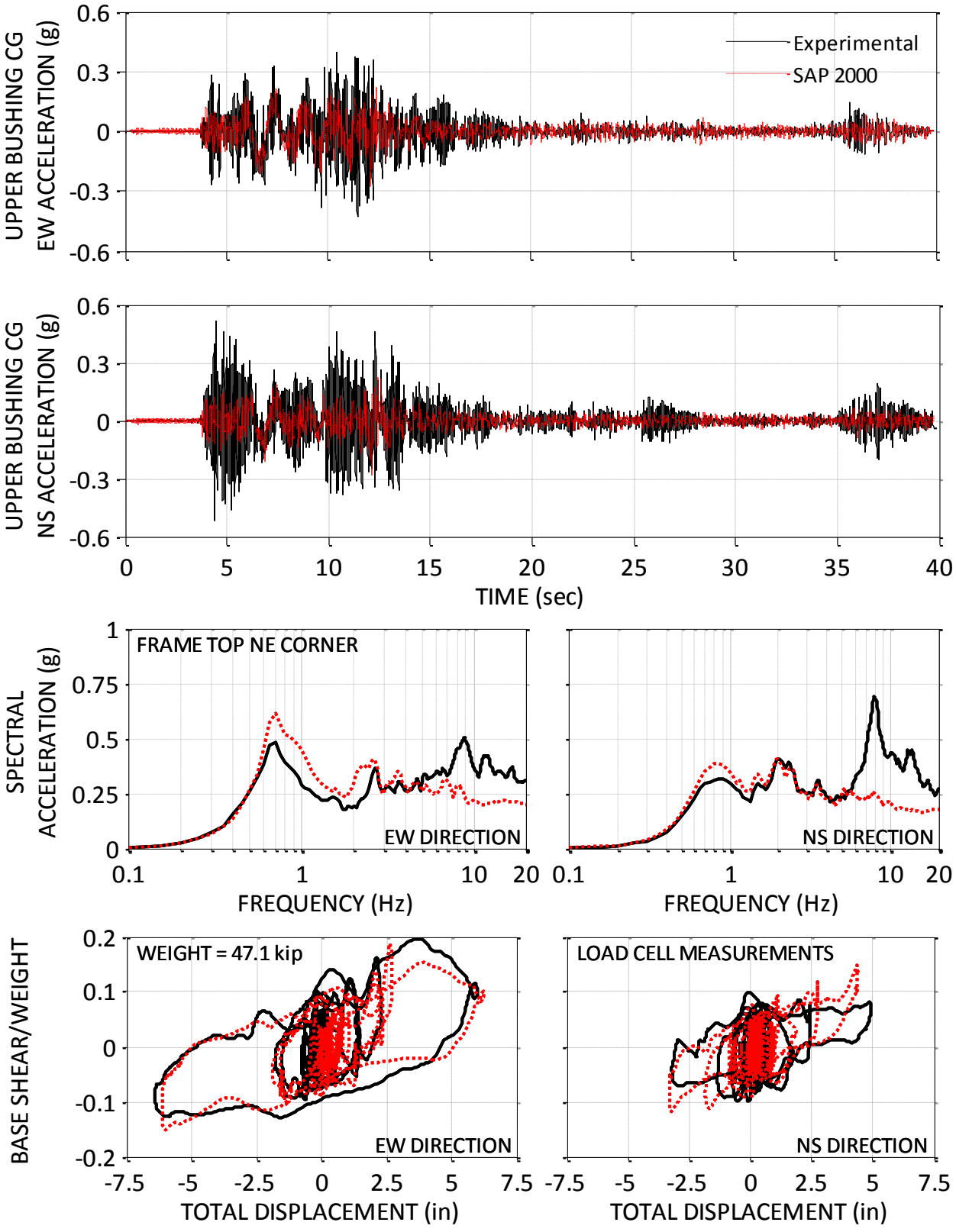
TRIPLE FP SYSTEM (Friction-Bolted Configuration – Series Model)
EL CENTRO 300% TRI-AXIAL (N90W in EW direction)
LENGTH SCALE=1 SYMMETRIC BUSHING CONFIGURATION



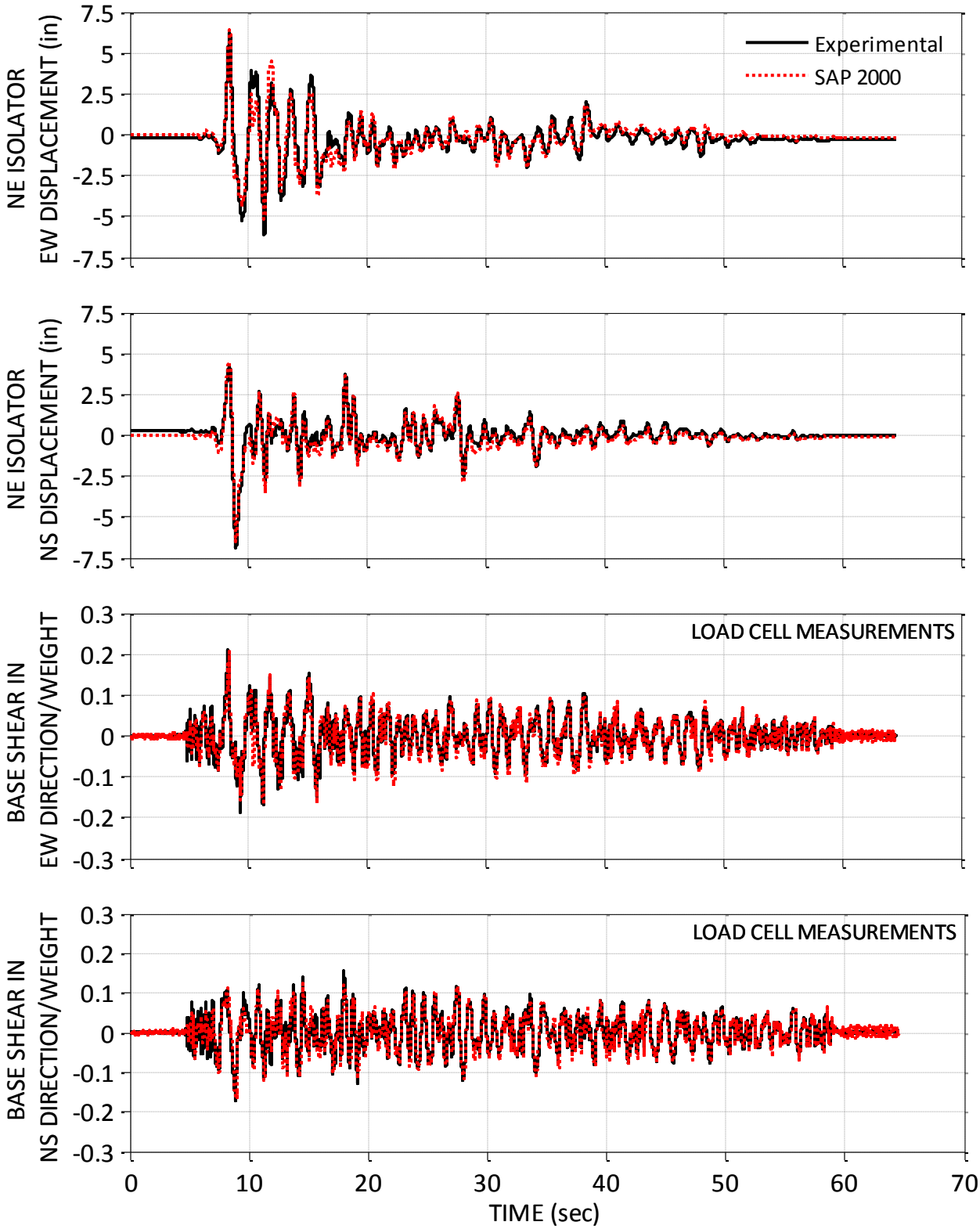

UPPER BUSHING CG
EW ACCELERATION (g)
Experimental
SAP 2000
UPPER BUSHING CG
NS ACCELERATION (g)
TIME (sec)
SPECTRAL
ACCELERATION (g)
FRAME TOP NE CORNER
EW DIRECTION
NS DIRECTION
FREQUENCY (Hz)
BASE SHEAR/WEIGHT
WEIGHT = 47.1 kip
LOAD CELL MEASUREMENTS
TOTAL DISPLACEMENT (in)

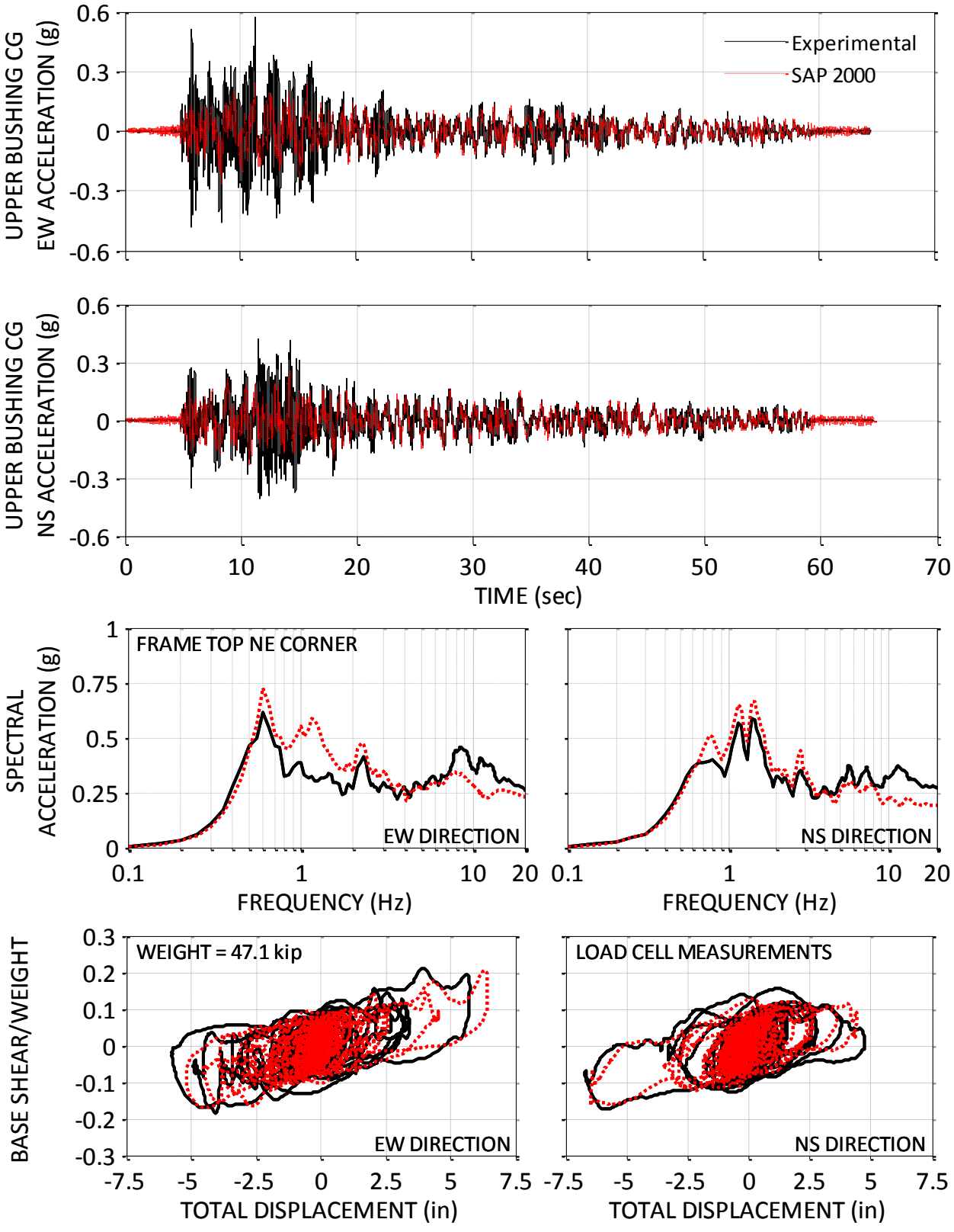
TRIPLE FP SYSTEM (Friction-Bolted Configuration – Series Model)
PACOIMA DAM 75% TRI-AXIAL (S16E in EW direction)
LENGTH SCALE=1 SYMMETRIC BUSHING CONFIGURATION



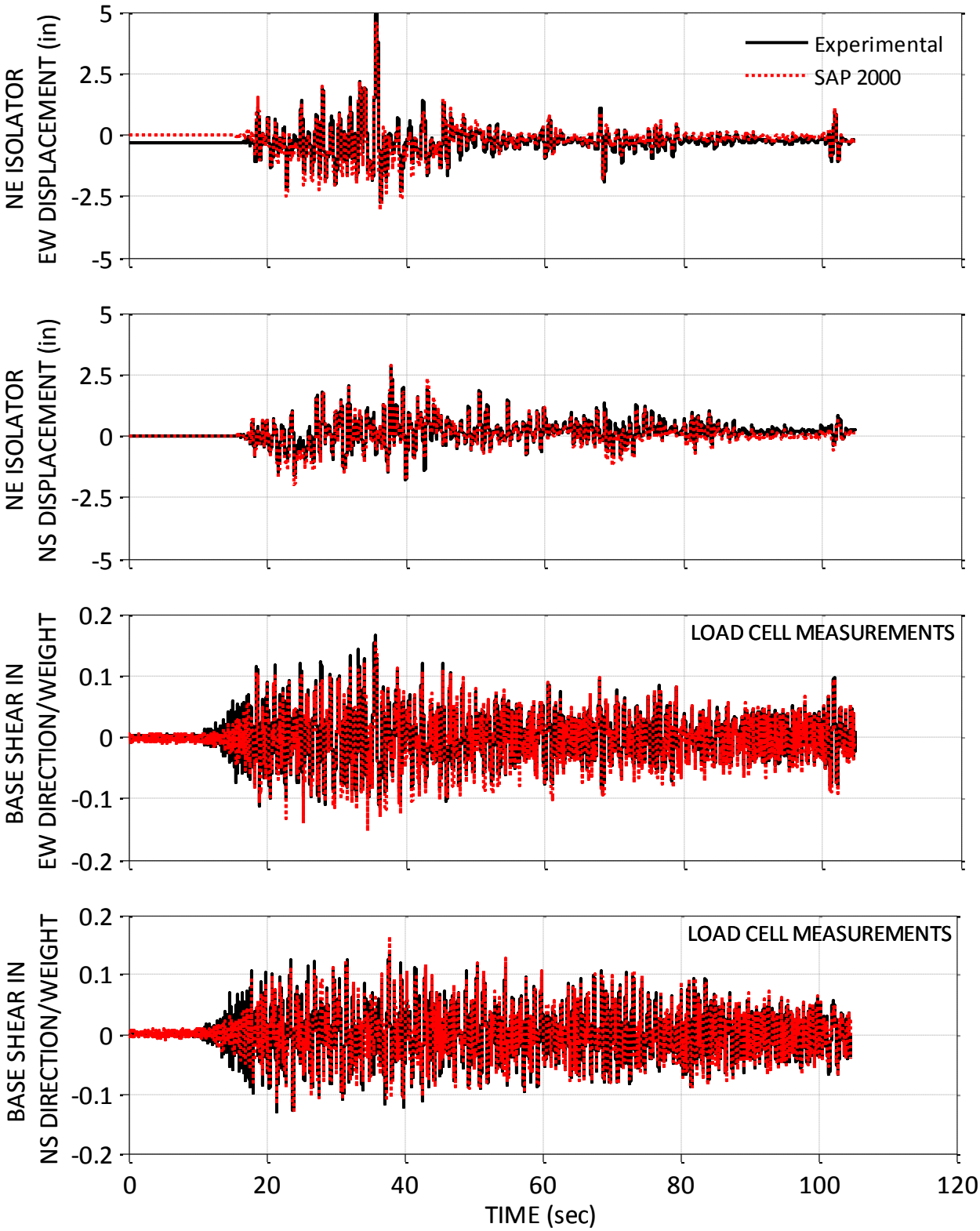

UPPER BUSHING CG
EW ACCELERATION (g)
Experimental
SAP 2000
UPPER BUSHING CG
NS ACCELERATION (g)
TIME (sec)
SPECTRAL
ACCELERATION (g)
FRAME TOP NE CORNER
EW DIRECTION
NS DIRECTION
FREQUENCY (Hz)
BASE SHEAR/WEIGHT
WEIGHT = 47.1 kip
LOAD CELL MEASUREMENTS
TOTAL DISPLACEMENT (in)

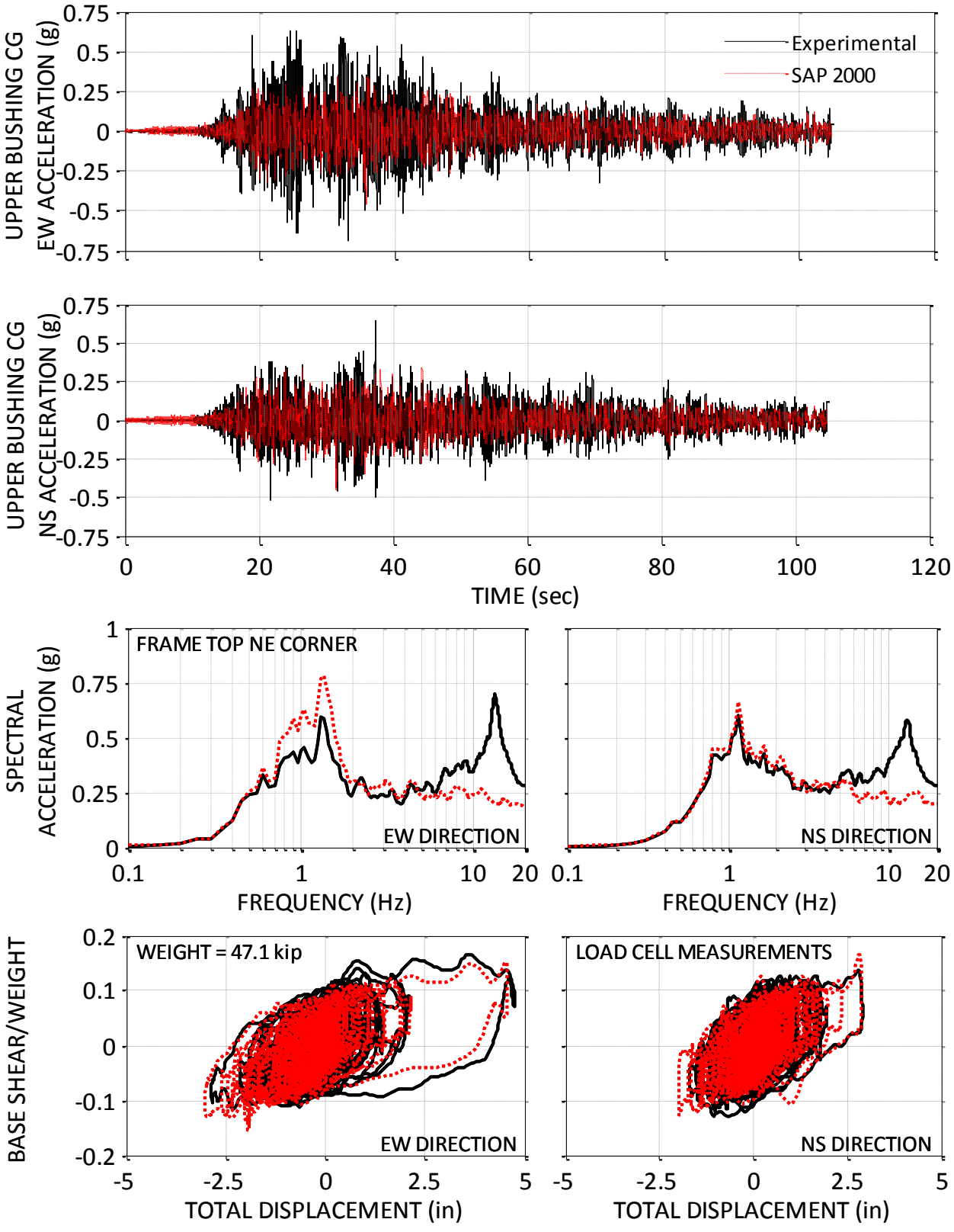
TRIPLE FP SYSTEM (Friction-Bolted Configuration – Series Model)
TAFT 500% TRI-AXIAL (S69E in EW direction)
LENGTH SCALE=1 SYMMETRIC BUSHING CONFIGURATION



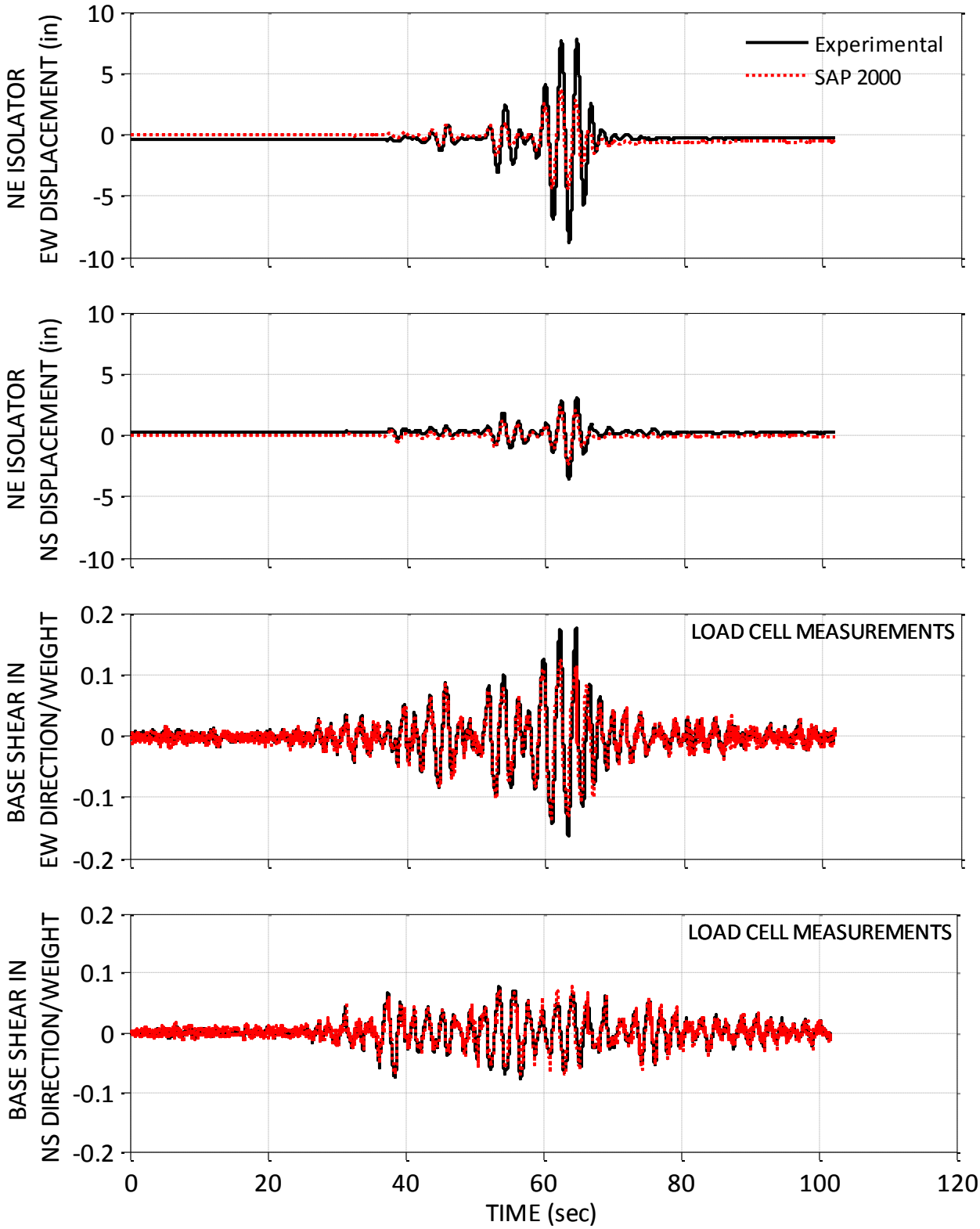

UPPER BUSHING CG
EW ACCELERATION (g)
Experimental
SAP 2000
UPPER BUSHING CG
NS ACCELERATION (g)
TIME (sec)
SPECTRAL
ACCELERATION (g)
FRAME TOP NE CORNER
EW DIRECTION
NS DIRECTION
FREQUENCY (Hz)
BASE SHEAR/WEIGHT
WEIGHT = 47.1 kip
LOAD CELL MEASUREMENTS
TOTAL DISPLACEMENT (in)

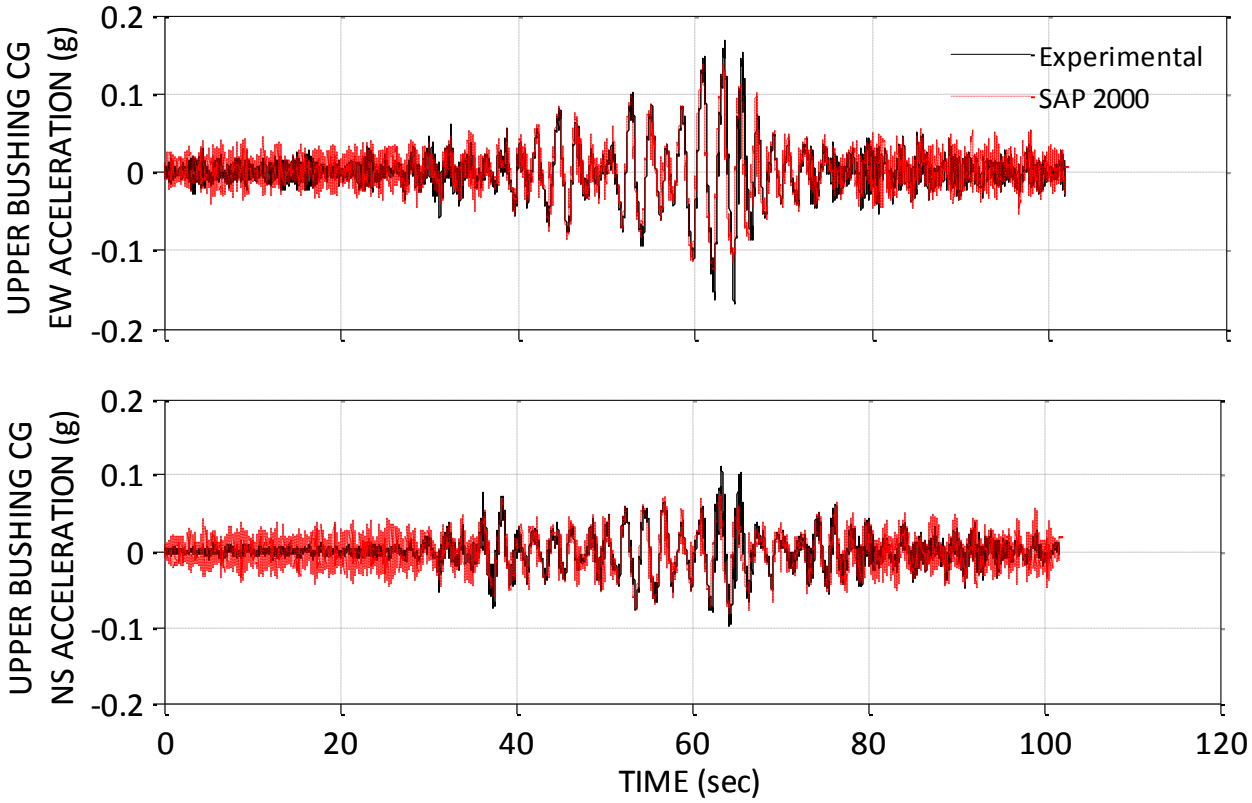
TRIPLE FP SYSTEM (Friction-Bolted Configuration – Series Model)
CHILE 100% TRI-AXIAL (EW in EW direction)
LENGTH SCALE=1 SYMMETRIC BUSHING CONFIGURATION

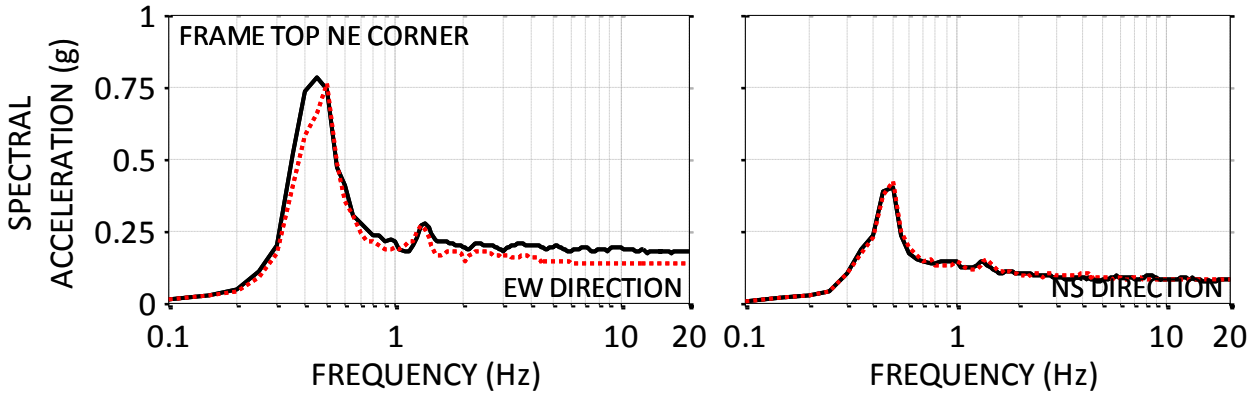


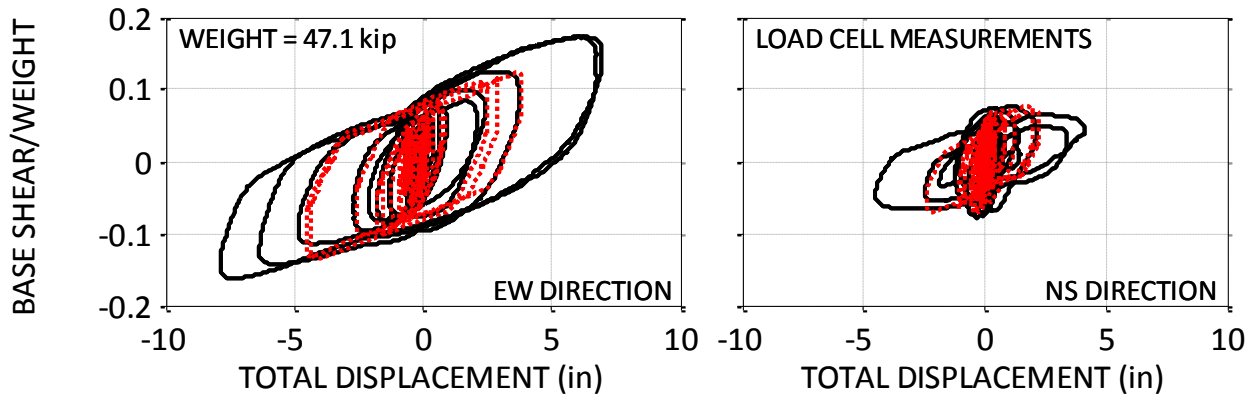

UPPER BUSHING CG
EW ACCELERATION (g)
0.75
0.5
0.25
0
-0.25
-0.5
-0.75
Experimental
SAP 2000
UPPER BUSHING CG
NS ACCELERATION (g)
0
20
40
60
80
100
120
TIME (sec)
SPECTRAL
ACCELERATION (g)
1
FRAME TOP NE CORNER
EW DIRECTION
NS DIRECTION
0.1
10
20
FREQUENCY (Hz)
BASE SHEAR/WEIGHT
0.2
0.1
-0.1
-0.2
WEIGHT = 47.1 kip
LOAD CELL MEASUREMENTS
-5
-2.5
2.5
5
TOTAL DISPLACEMENT (in)

TRIPLE FP SYSTEM (Friction-Bolted Configuration – Series Model)
MEXICO 70% TRI-AXIAL (N90W in EW direction)
LENGTH SCALE=1 SYMMETRIC BUSHING CONFIGURATION

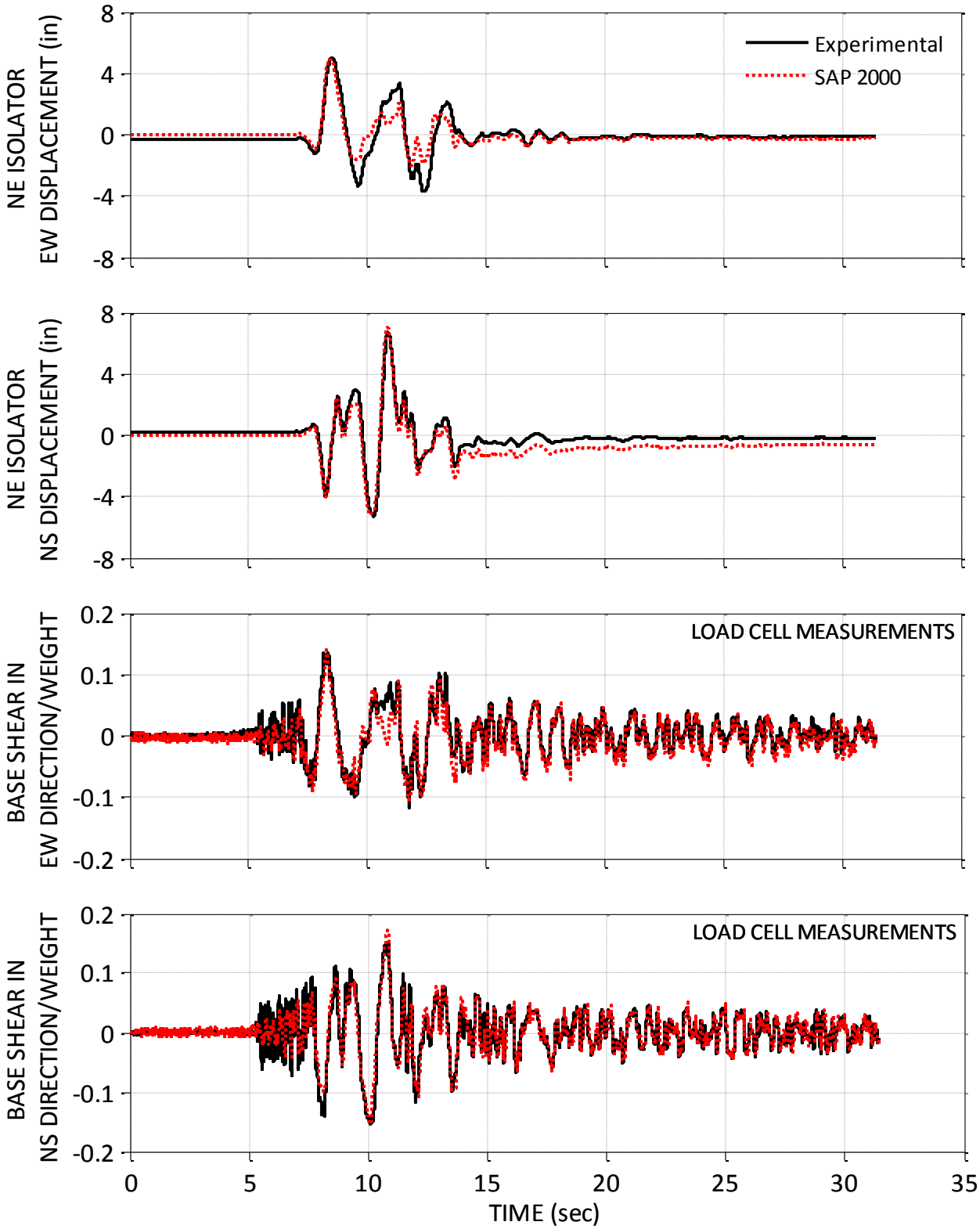


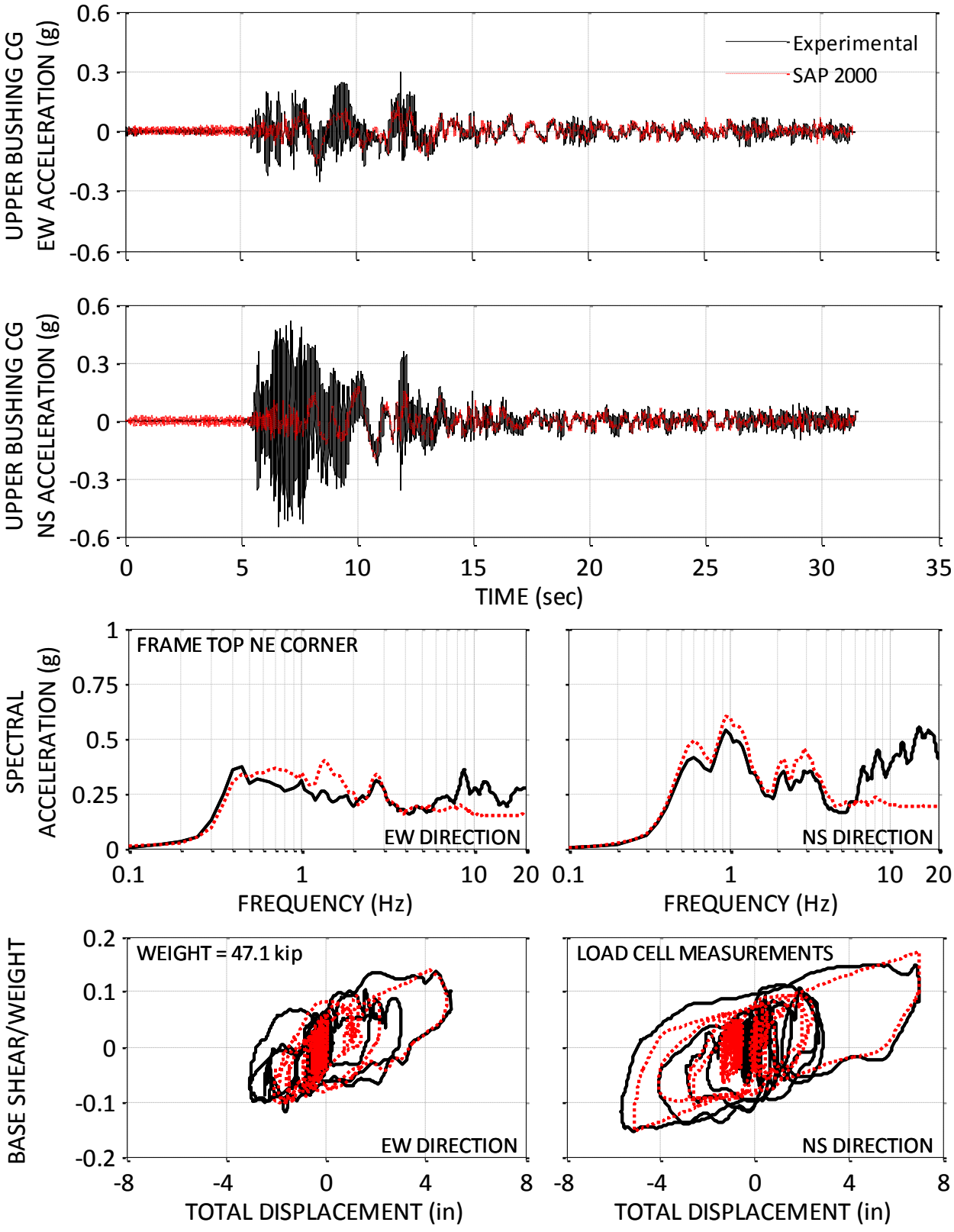

UPPER BUSHING CG
EW ACCELERATION (g)
Experimental
SAP 2000
UPPER BUSHING CG
NS ACCELERATION (g)
TIME (sec)


SPECTRAL
ACCELERATION (g)
FRAME TOP NE CORNER
EW DIRECTION
NS DIRECTION
FREQUENCY (Hz)
FREQUENCY (Hz)

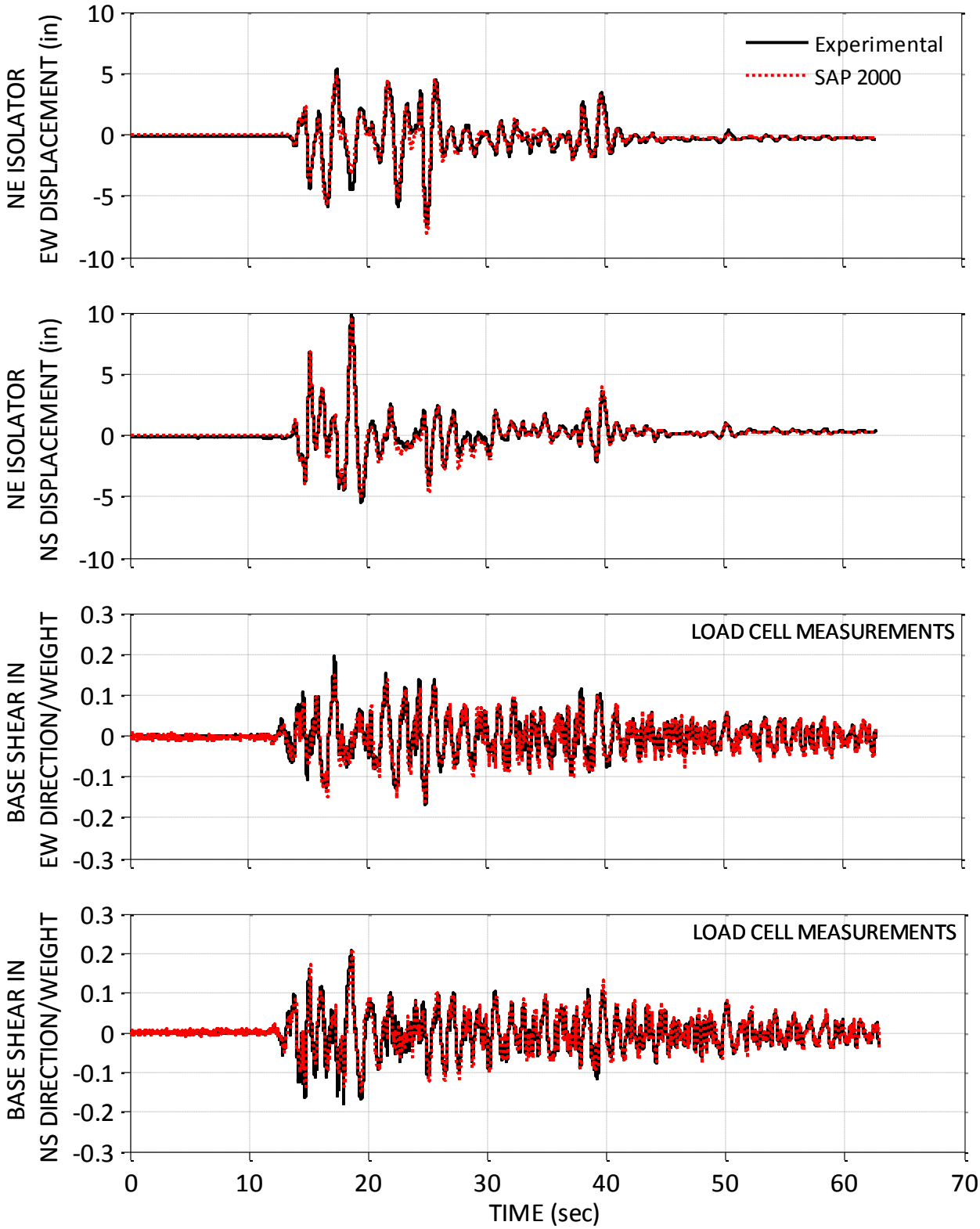

BASE SHEAR/WEIGHT
WEIGHT = 47.1 kip
LOAD CELL MEASUREMENTS
EW DIRECTION
NS DIRECTION
TOTAL DISPLACEMENT (in)
TOTAL DISPLACEMENT (in)

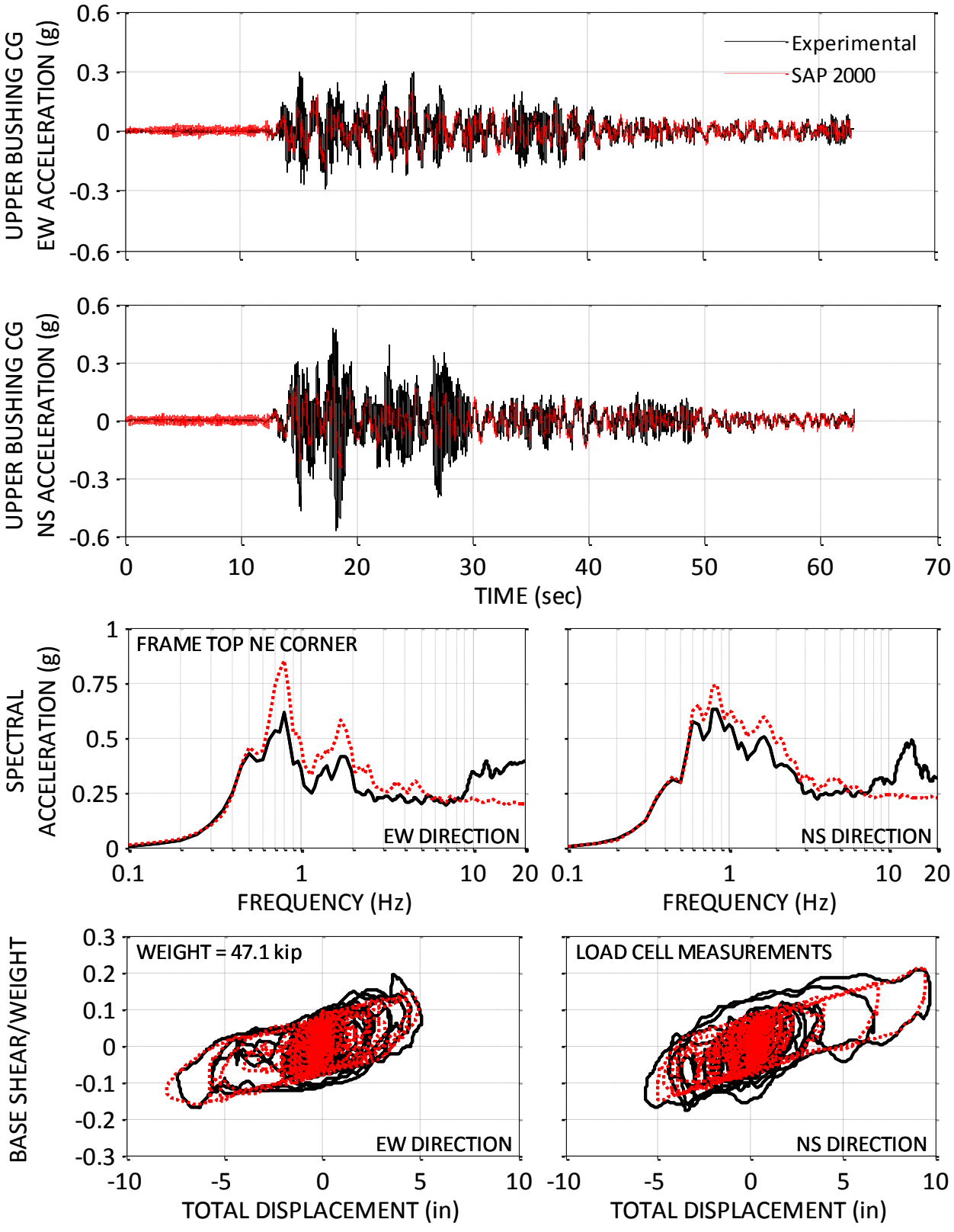
TRIPLE FP SYSTEM (Friction-Bolted Configuration – Series Model)
JENSEN FILTER 97% BI-AXIAL (FN in EW direction)
LENGTH SCALE=1 SYMMETRIC BUSHING CONFIGURATION



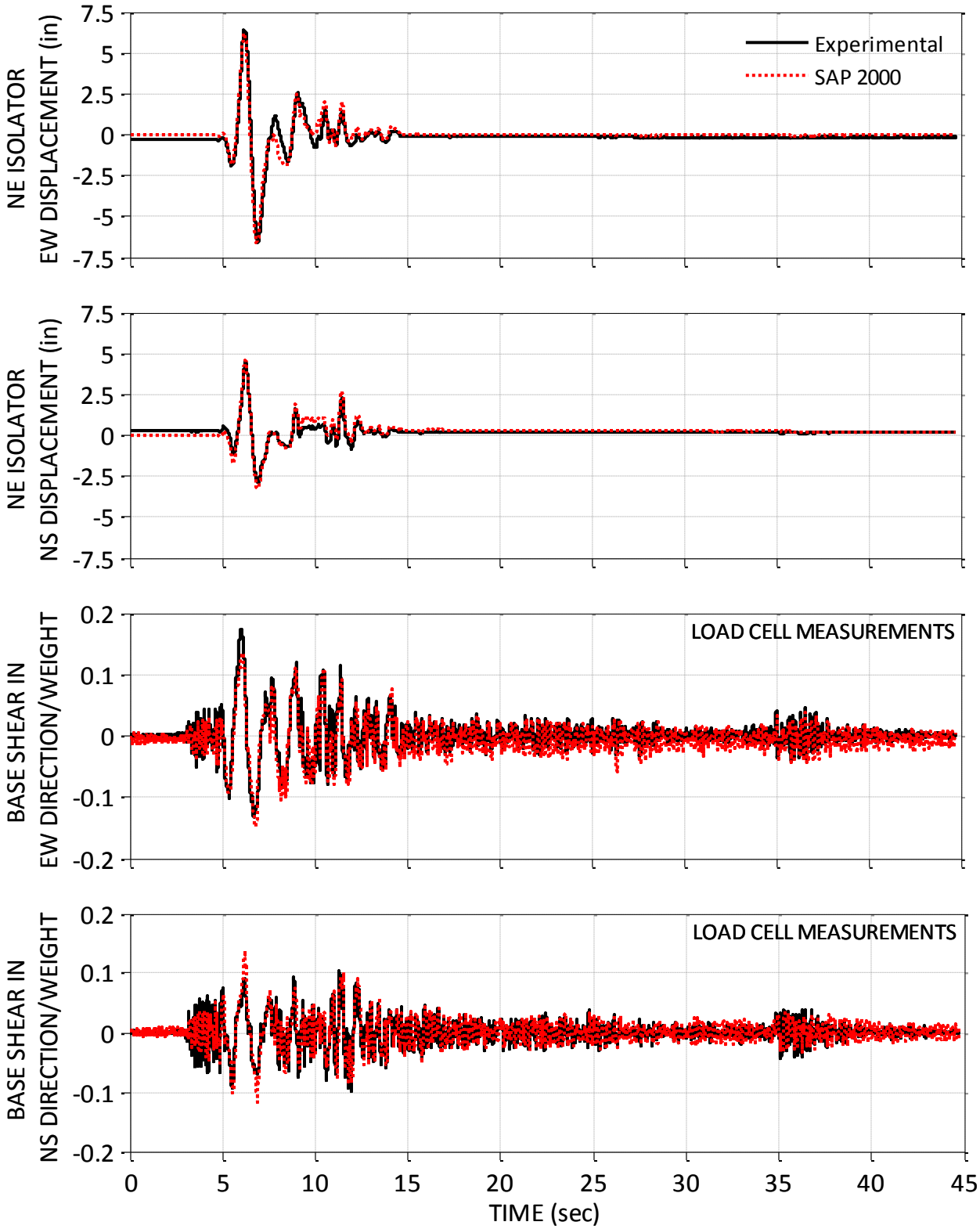

UPPER BUSHING CG
EW ACCELERATION (g)
Experimental
SAP 2000
UPPER BUSHING CG
NS ACCELERATION (g)
TIME (sec)
SPECTRAL
ACCELERATION (g)
FRAME TOP NE CORNER
EW DIRECTION
NS DIRECTION
FREQUENCY (Hz)
BASE SHEAR/WEIGHT
WEIGHT = 47.1 kip
LOAD CELL MEASUREMENTS
TOTAL DISPLACEMENT (in)

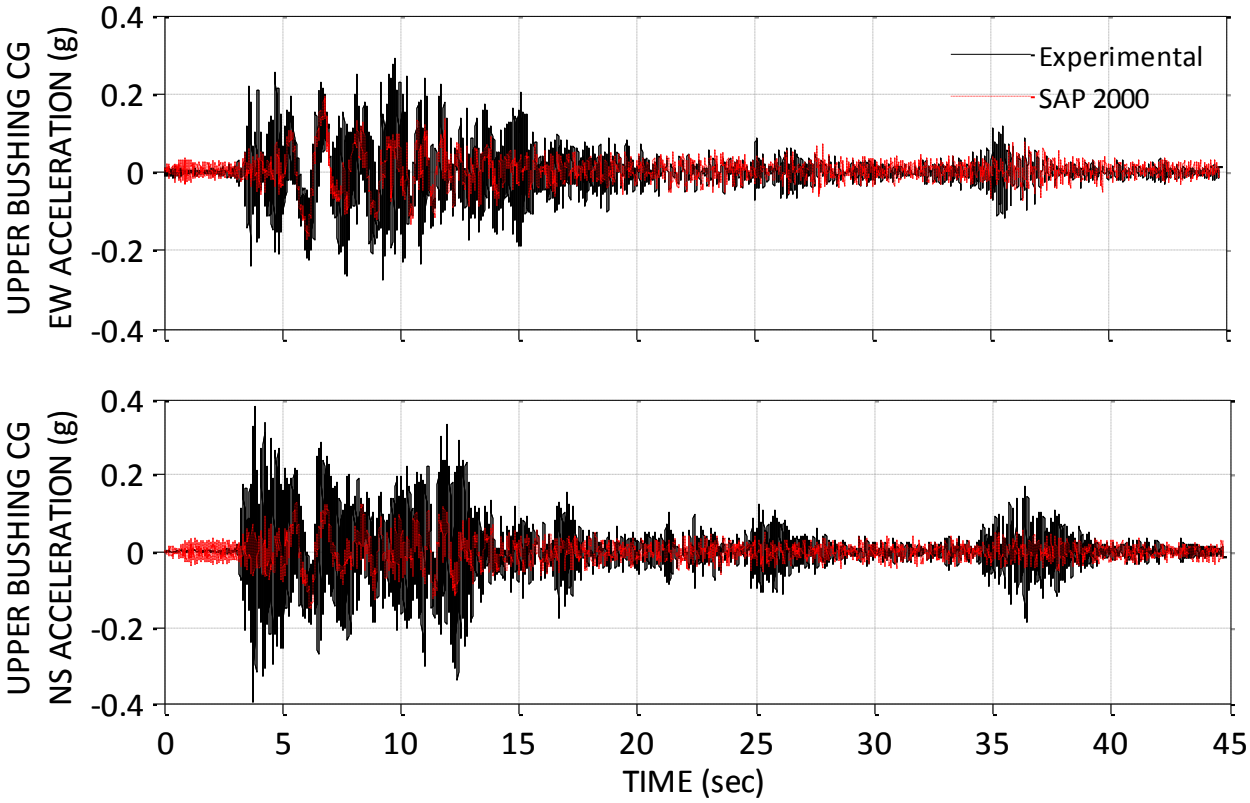
TRIPLE FP SYSTEM (Friction-Bolted Configuration – Series Model)
EL CENTRO 300% BI-AXIAL (N90W in EW direction)
LENGTH SCALE=1 SYMMETRIC BUSHING CONFIGURATION

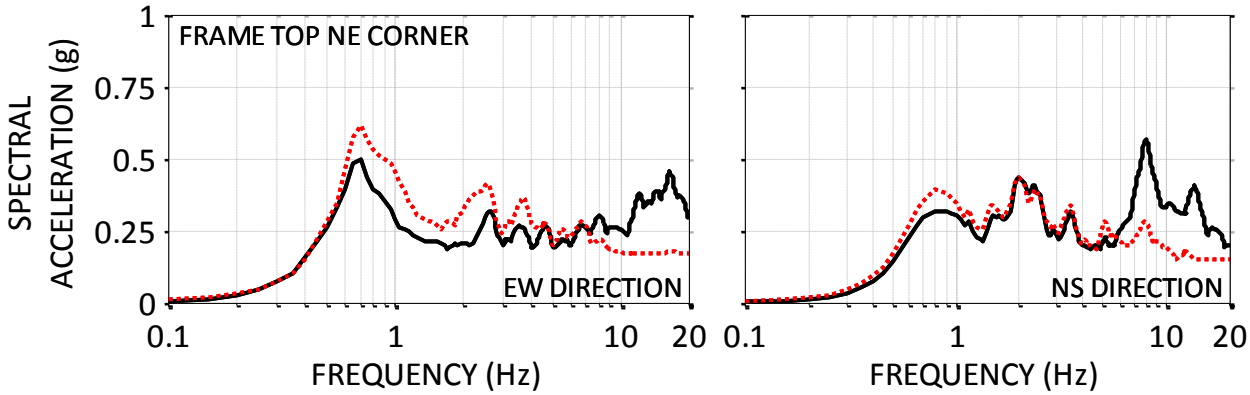


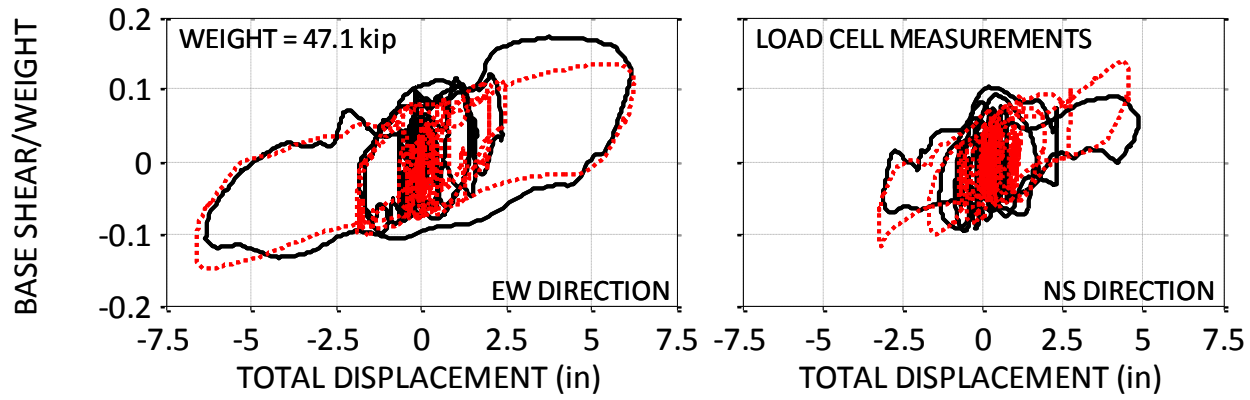

UPPER BUSHING CG
EW ACCELERATION (g)
Experimental
SAP 2000
UPPER BUSHING CG
NS ACCELERATION (g)
TIME (sec)
SPECTRAL
ACCELERATION (g)
FRAME TOP NE CORNER
EW DIRECTION
NS DIRECTION
FREQUENCY (Hz)
BASE SHEAR/WEIGHT
WEIGHT = 47.1 kip
LOAD CELL MEASUREMENTS
TOTAL DISPLACEMENT (in)

TRIPLE FP SYSTEM (Friction-Bolted Configuration – Series Model)
PACOIMA DAM 75% BI-AXIAL (S16E in EW direction)
LENGTH SCALE=1 SYMMETRIC BUSHING CONFIGURATION

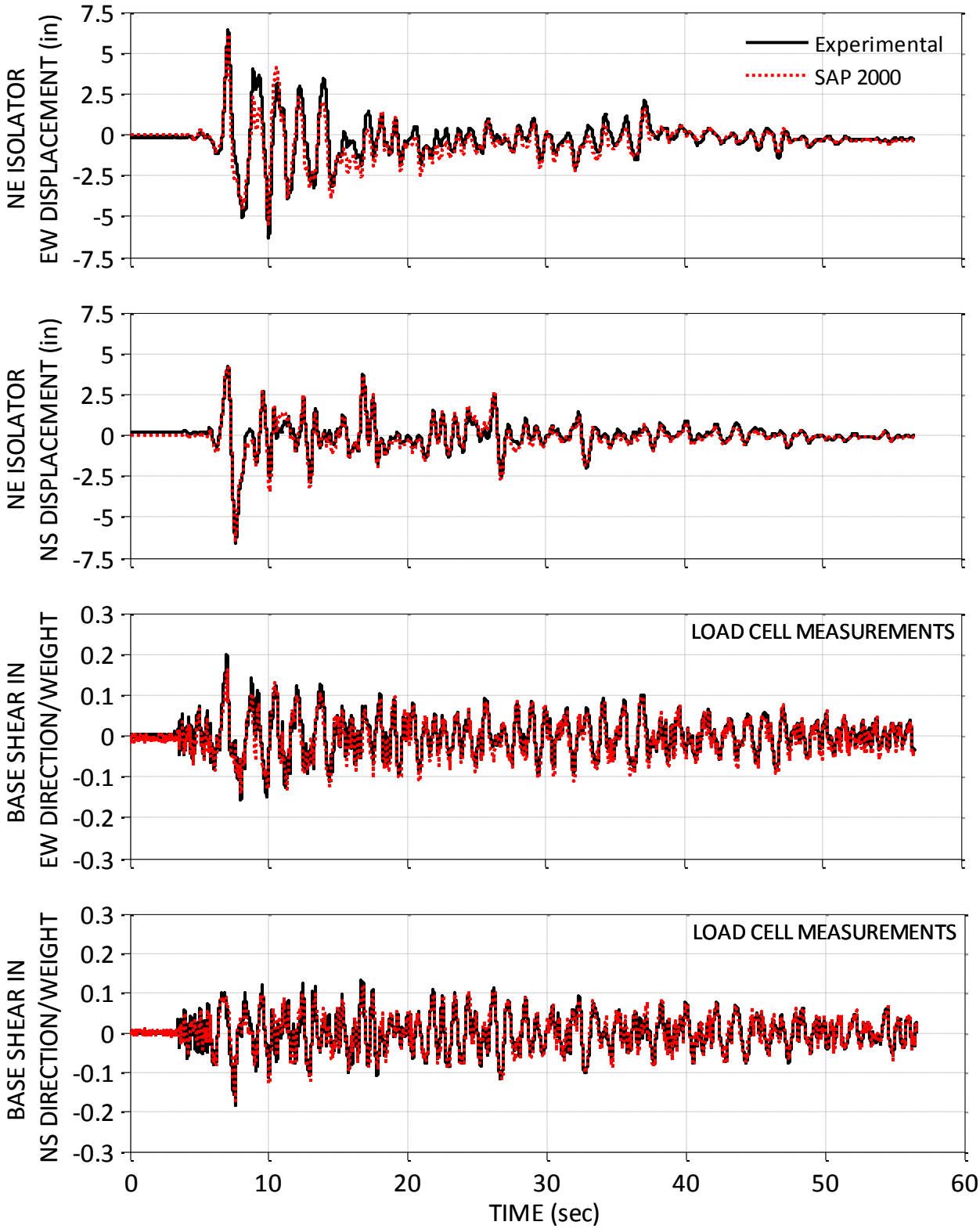


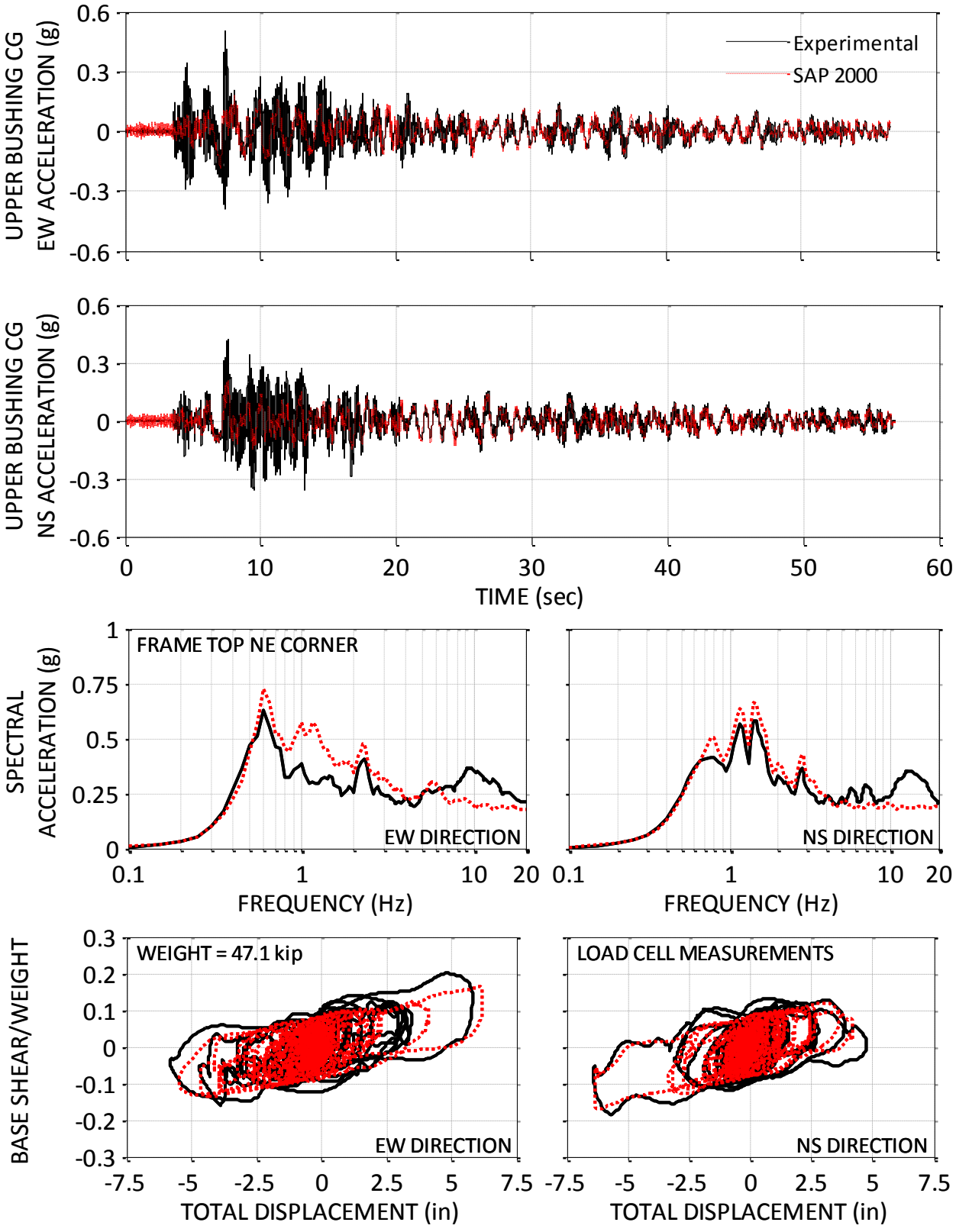

UPPER BUSHING CG
EW ACCELERATION (g)
Experimental
SAP 2000
UPPER BUSHING CG
NS ACCELERATION (g)
TIME (sec)


SPECTRAL
ACCELERATION (g)
FRAME TOP NE CORNER
EW DIRECTION
NS DIRECTION
FREQUENCY (Hz)
FREQUENCY (Hz)

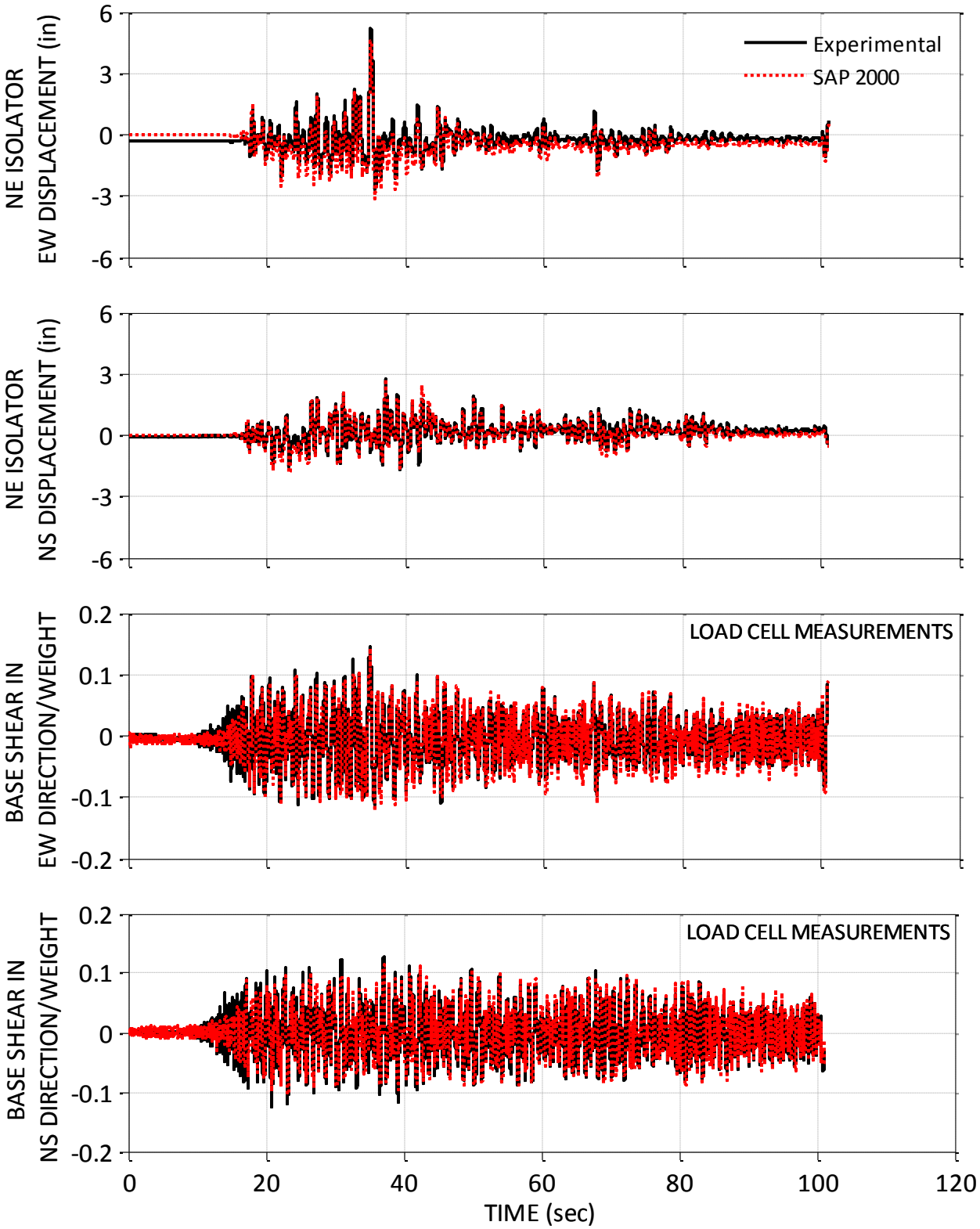

BASE SHEAR/WEIGHT
WEIGHT = 47.1 kip
LOAD CELL MEASUREMENTS
EW DIRECTION
NS DIRECTION
TOTAL DISPLACEMENT (in)
TOTAL DISPLACEMENT (in)

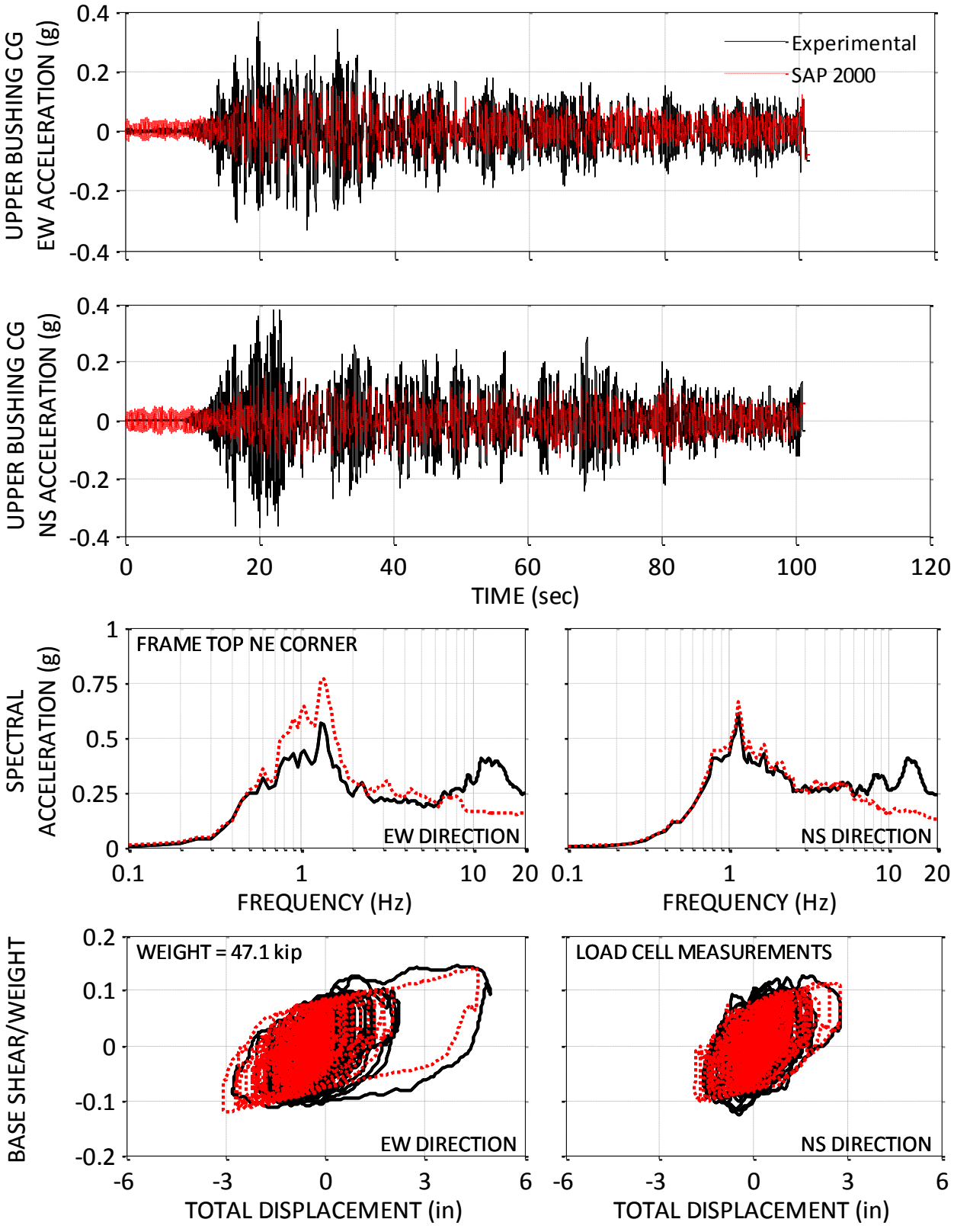
TRIPLE FP SYSTEM (Friction-Bolted Configuration – Series Model)
TAFT 500% BI-AXIAL (S69E in EW direction)
LENGTH SCALE=1 SYMMETRIC BUSHING CONFIGURATION



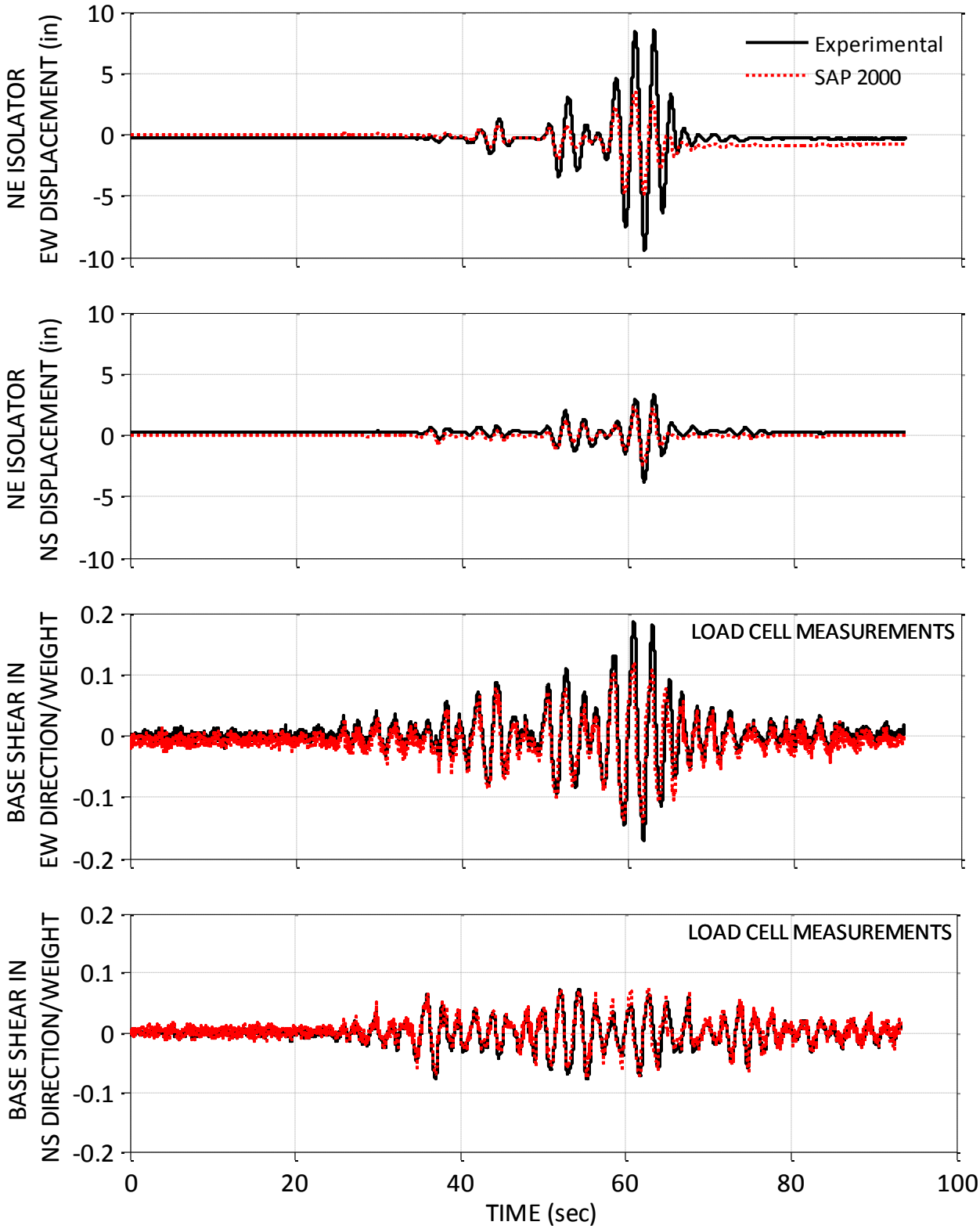

UPPER BUSHING CG
EW ACCELERATION (g)
Experimental
SAP 2000
UPPER BUSHING CG
NS ACCELERATION (g)
TIME (sec)
SPECTRAL
ACCELERATION (g)
FRAME TOP NE CORNER
EW DIRECTION
NS DIRECTION
FREQUENCY (Hz)
BASE SHEAR/WEIGHT
WEIGHT = 47.1 kip
LOAD CELL MEASUREMENTS
TOTAL DISPLACEMENT (in)

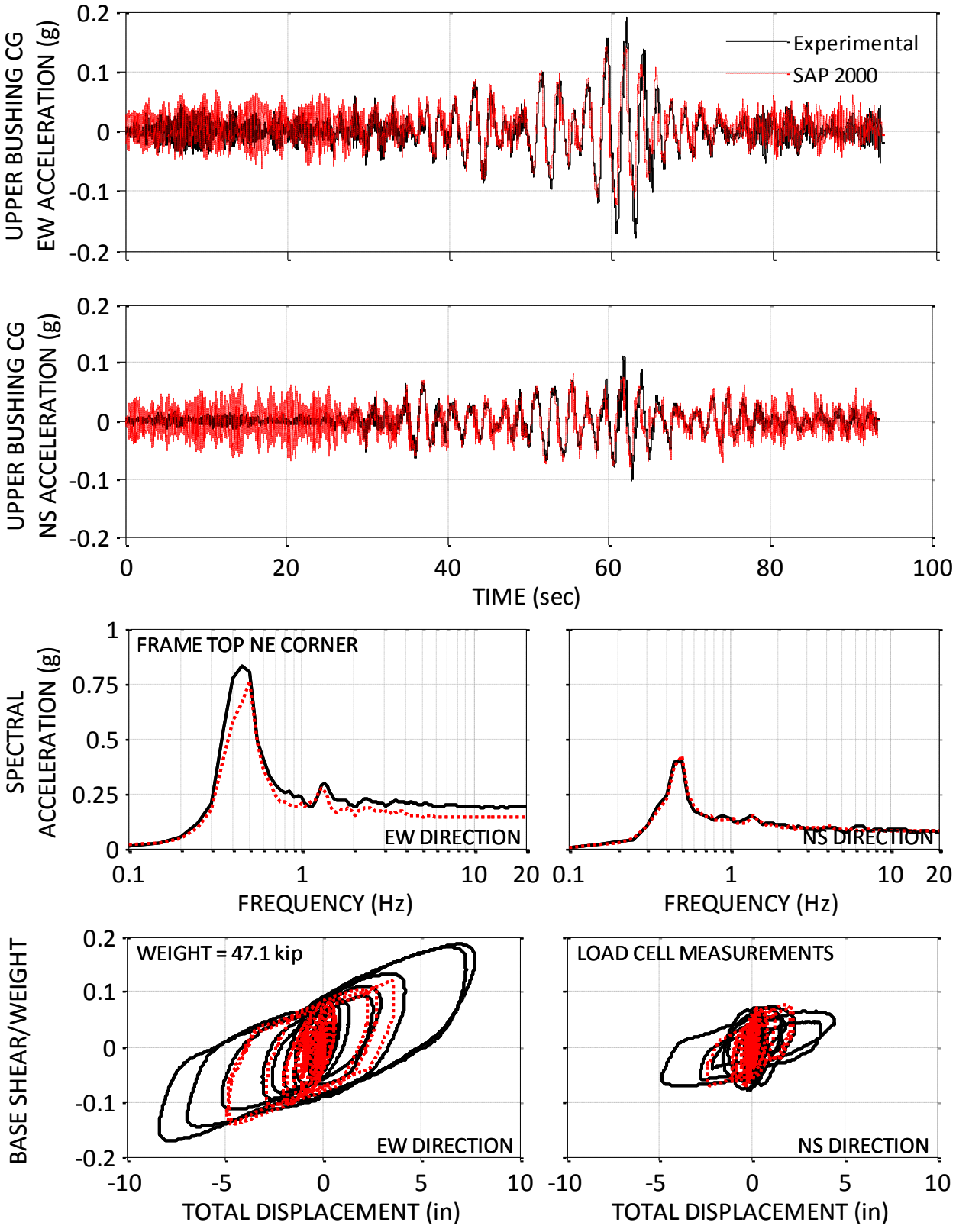
TRIPLE FP SYSTEM (Friction-Bolted Configuration – Series Model)
CHILE 100% BI-AXIAL (EW in EW direction)
LENGTH SCALE=1 SYMMETRIC BUSHING CONFIGURATION




UPPER BUSHING CG
EW ACCELERATION (g)
Experimental
SAP 2000
UPPER BUSHING CG
NS ACCELERATION (g)
TIME (sec)
SPECTRAL
ACCELERATION (g)
FRAME TOP NE CORNER
EW DIRECTION
NS DIRECTION
FREQUENCY (Hz)
BASE SHEAR/WEIGHT
WEIGHT = 47.1 kip
LOAD CELL MEASUREMENTS
TOTAL DISPLACEMENT (in)

TRIPLE FP SYSTEM (Friction-Bolted Configuration – Series Model)
MEXICO 70% BI-AXIAL (N90W in EW direction)
LENGTH SCALE=1 SYMMETRIC BUSHING CONFIGURATION




UPPER BUSHING CG
EW ACCELERATION (g)
Experimental
SAP 2000
UPPER BUSHING CG
NS ACCELERATION (g)
TIME (sec)
SPECTRAL
ACCELERATION (g)
FRAME TOP NE CORNER
EW DIRECTION
NS DIRECTION
FREQUENCY (Hz)
BASE SHEAR/WEIGHT
WEIGHT = 47.1 kip
LOAD CELL MEASUREMENTS
TOTAL DISPLACEMENT (in)

APPENDIX E
GROUND MOTION SCALING PROCEDURE

This Appendix describes the weighted scaling procedure followed as described in Pant et al (2013) for the scaling of the seed motions used in the design example of Section 6.

Scaling of the seed motions was performed as per the requirements of ASCE 7-2010 (Section 16.1.3.2) for a site at a distance greater than 5km from active faults. More specifically, for each motion selected, the 5% damped square root of sum of squares (SRSS) spectrum of the horizontal components was constructed and a factor F_J minimizing the error between the SRSS spectrum and the target MCE_R spectrum was subsequently determined. Note that per ASCE 7-2010 for the case of distance to faults larger than 5km the seed motions need not be rotated to fault-normal (FN) and fault-parallel (FP) directions. Rotation to fault-normal and fault-parallel directions was performed in this case, however, it does not affect the scaling process given that for any orthogonal directions X and Y: $S_X^2(T_i)+S_Y^2(T_i)=S_{FN}^2(T_i)+S_{FP}^2(T_i)$.

The steps of the procedure followed are (note that X and Y are FN and FP directions):

1. First each motion J (J=1 to 7) was scaled in amplitude only by factor F_J in order to minimize the error between the SRSS spectrum of the scaled motion and the target MCE_R spectrum. The error is defined as:

$$E_J=\sum_{i=1}^{4} w_i\left[S_{MCE_R}(T_i)-F_J\sqrt{S_X^2(T_i)+S_Y^2(T_i)}\right]^2$$

That is, the error is the weighted sum of the square of the difference between the target MCE_R spectra acceleration and the SRSS spectral acceleration of the scaled motion X

and Y components at four periods. This equation results in the following direct expression for the scale factor F_J:

$$F_J = \frac{\sum_{i=1}^{4} w_i S_{MCE_R}(T_i)\sqrt{S_X^2(T_i) + S_Y^2(T_i)}}{\sum_{i=1}^{4} w_i \left\{S_X^2(T_i) + S_Y^2(T_i)\right\}}$$

The periods and weight factors used are:

Period T_i(sec)	1.0	2.0	3.0	4.0
Weight factor w_i	0.1	0.3	0.3	0.3

2. The scaled components of the motions resulting from step 1 above do not meet the ASCE 7 criteria. To meet the ASCE 7 criteria, the SRSS spectra of the fault-normal and fault-parallel components of the motions as scaled in step 1 were constructed and then the average of the seven SRSS spectra was calculated. This average spectrum was then compared to the MCE_R spectrum in the range of periods $0.5T_{eff}$ to $1.25T_{eff}$. Per ASCE 7, the average spectrum should not be less than the MCE_R spectrum in the period range of interest. To meet this criterion, a scale factor F_1 that applies to all motions was determined. The final scale factor for each motion is the product $F_J F_1$.
3. The final scale factor $F_J F_1$ applies to both components of the motions, fault-normal and fault-parallel.
4. As a final check, the geometric mean spectra of the scaled motions were constructed and used to obtain the maximum direction spectrum by multiplying by a factor of 1.3. The so calculated average maximum direction spectrum of the scaled motions was then compared to the target MCE_R spectrum for the period range of interest. The two spectra should be reasonably close. Otherwise adjustments to the scale factor should be made.

MCEER Technical Reports

MCEER publishes technical reports on a variety of subjects written by authors funded through MCEER. These reports are available from both MCEER Publications and the National Technical Information Service (NTIS). Requests for reports should be directed to MCEER Publications, MCEER, University at Buffalo, State University of New York, 133A Ketter Hall, Buffalo, New York 14260. Reports can also be requested through NTIS, P.O. Box 1425, Springfield, Virginia 22151. NTIS accession numbers are shown in parenthesis, if available.

NCEER-87-0001 "First-Year Program in Research, Education and Technology Transfer," 3/5/87, (PB88-134275, A04, MF-A01).

NCEER-87-0002 "Experimental Evaluation of Instantaneous Optimal Algorithms for Structural Control," by R.C. Lin, T.T. Soong and A.M. Reinhorn, 4/20/87, (PB88-134341, A04, MF-A01).

NCEER-87-0003 "Experimentation Using the Earthquake Simulation Facilities at University at Buffalo," by A.M. Reinhorn and R.L. Ketter, not available.

NCEER-87-0004 "The System Characteristics and Performance of a Shaking Table," by J.S. Hwang, K.C. Chang and G.C. Lee, 6/1/87, (PB88-134259, A03, MF-A01). This report is available only through NTIS (see address given above).

NCEER-87-0005 "A Finite Element Formulation for Nonlinear Viscoplastic Material Using a Q Model," by O. Gyebi and G. Dasgupta, 11/2/87, (PB88-213764, A08, MF-A01).

NCEER-87-0006 "Symbolic Manipulation Program (SMP) - Algebraic Codes for Two and Three Dimensional Finite Element Formulations," by X. Lee and G. Dasgupta, 11/9/87, (PB88-218522, A05, MF-A01).

NCEER-87-0007 "Instantaneous Optimal Control Laws for Tall Buildings Under Seismic Excitations," by J.N. Yang, A. Akbarpour and P. Ghaemmaghami, 6/10/87, (PB88-134333, A06, MF-A01). This report is only available through NTIS (see address given above).

NCEER-87-0008 "IDARC: Inelastic Damage Analysis of Reinforced Concrete Frame - Shear-Wall Structures," by Y.J. Park, A.M. Reinhorn and S.K. Kunnath, 7/20/87, (PB88-134325, A09, MF-A01). This report is only available through NTIS (see address given above).

NCEER-87-0009 "Liquefaction Potential for New York State: A Preliminary Report on Sites in Manhattan and Buffalo," by M. Budhu, V. Vijayakumar, R.F. Giese and L. Baumgras, 8/31/87, (PB88-163704, A03, MF-A01). This report is available only through NTIS (see address given above).

NCEER-87-0010 "Vertical and Torsional Vibration of Foundations in Inhomogeneous Media," by A.S. Veletsos and K.W. Dotson, 6/1/87, (PB88-134291, A03, MF-A01). This report is only available through NTIS (see address given above).

NCEER-87-0011 "Seismic Probabilistic Risk Assessment and Seismic Margins Studies for Nuclear Power Plants," by Howard H.M. Hwang, 6/15/87, (PB88-134267, A03, MF-A01). This report is only available through NTIS (see address given above).

NCEER-87-0012 "Parametric Studies of Frequency Response of Secondary Systems Under Ground-Acceleration Excitations," by Y. Yong and Y.K. Lin, 6/10/87, (PB88-134309, A03, MF-A01). This report is only available through NTIS (see address given above).

NCEER-87-0013 "Frequency Response of Secondary Systems Under Seismic Excitation," by J.A. HoLung, J. Cai and Y.K. Lin, 7/31/87, (PB88-134317, A05, MF-A01). This report is only available through NTIS (see address given above).

NCEER-87-0014 "Modelling Earthquake Ground Motions in Seismically Active Regions Using Parametric Time Series Methods," by G.W. Ellis and A.S. Cakmak, 8/25/87, (PB88-134283, A08, MF-A01). This report is only available through NTIS (see address given above).

NCEER-87-0015 "Detection and Assessment of Seismic Structural Damage," by E. DiPasquale and A.S. Cakmak, 8/25/87, (PB88-163712, A05, MF-A01). This report is only available through NTIS (see address given above).

NCEER-87-0016 "Pipeline Experiment at Parkfield, California," by J. Isenberg and E. Richardson, 9/15/87, (PB88-163720, A03, MF-A01). This report is available only through NTIS (see address given above).

NCEER-87-0017 "Digital Simulation of Seismic Ground Motion," by M. Shinozuka, G. Deodatis and T. Harada, 8/31/87, (PB88-155197, A04, MF-A01). This report is available only through NTIS (see address given above).

NCEER-87-0018 "Practical Considerations for Structural Control: System Uncertainty, System Time Delay and Truncation of Small Control Forces," J.N. Yang and A. Akbarpour, 8/10/87, (PB88-163738, A08, MF-A01). This report is only available through NTIS (see address given above).

NCEER-87-0019 "Modal Analysis of Nonclassically Damped Structural Systems Using Canonical Transformation," by J.N. Yang, S. Sarkani and F.X. Long, 9/27/87, (PB88-187851, A04, MF-A01).

NCEER-87-0020 "A Nonstationary Solution in Random Vibration Theory," by J.R. Red-Horse and P.D. Spanos, 11/3/87, (PB88-163746, A03, MF-A01).

NCEER-87-0021 "Horizontal Impedances for Radially Inhomogeneous Viscoelastic Soil Layers," by A.S. Veletsos and K.W. Dotson, 10/15/87, (PB88-150859, A04, MF-A01).

NCEER-87-0022 "Seismic Damage Assessment of Reinforced Concrete Members," by Y.S. Chung, C. Meyer and M. Shinozuka, 10/9/87, (PB88-150867, A05, MF-A01). This report is available only through NTIS (see address given above).

NCEER-87-0023 "Active Structural Control in Civil Engineering," by T.T. Soong, 11/11/87, (PB88-187778, A03, MF-A01).

NCEER-87-0024 "Vertical and Torsional Impedances for Radially Inhomogeneous Viscoelastic Soil Layers," by K.W. Dotson and A.S. Veletsos, 12/87, (PB88-187786, A03, MF-A01).

NCEER-87-0025 "Proceedings from the Symposium on Seismic Hazards, Ground Motions, Soil-Liquefaction and Engineering Practice in Eastern North America," October 20-22, 1987, edited by K.H. Jacob, 12/87, (PB88-188115, A23, MF-A01). This report is available only through NTIS (see address given above).

NCEER-87-0026 "Report on the Whittier-Narrows, California, Earthquake of October 1, 1987," by J. Pantelic and A. Reinhorn, 11/87, (PB88-187752, A03, MF-A01). This report is available only through NTIS (see address given above).

NCEER-87-0027 "Design of a Modular Program for Transient Nonlinear Analysis of Large 3-D Building Structures," by S. Srivastav and J.F. Abel, 12/30/87, (PB88-187950, A05, MF-A01). This report is only available through NTIS (see address given above).

NCEER-87-0028 "Second-Year Program in Research, Education and Technology Transfer," 3/8/88, (PB88-219480, A04, MF-A01).

NCEER-88-0001 "Workshop on Seismic Computer Analysis and Design of Buildings With Interactive Graphics," by W. McGuire, J.F. Abel and C.H. Conley, 1/18/88, (PB88-187760, A03, MF-A01). This report is only available through NTIS (see address given above).

NCEER-88-0002 "Optimal Control of Nonlinear Flexible Structures," by J.N. Yang, F.X. Long and D. Wong, 1/22/88, (PB88-213772, A06, MF-A01).

NCEER-88-0003 "Substructuring Techniques in the Time Domain for Primary-Secondary Structural Systems," by G.D. Manolis and G. Juhn, 2/10/88, (PB88-213780, A04, MF-A01).

NCEER-88-0004 "Iterative Seismic Analysis of Primary-Secondary Systems," by A. Singhal, L.D. Lutes and P.D. Spanos, 2/23/88, (PB88-213798, A04, MF-A01).

NCEER-88-0005 "Stochastic Finite Element Expansion for Random Media," by P.D. Spanos and R. Ghanem, 3/14/88, (PB88-213806, A03, MF-A01).

NCEER-88-0006 "Combining Structural Optimization and Structural Control," by F.Y. Cheng and C.P. Pantelides, 1/10/88, (PB88-213814, A05, MF-A01).

NCEER-88-0007 "Seismic Performance Assessment of Code-Designed Structures," by H.H-M. Hwang, J-W. Jaw and H-J. Shau, 3/20/88, (PB88-219423, A04, MF-A01). This report is only available through NTIS (see address given above).

NCEER-88-0008 "Reliability Analysis of Code-Designed Structures Under Natural Hazards," by H.H-M. Hwang, H. Ushiba and M. Shinozuka, 2/29/88, (PB88-229471, A07, MF-A01). This report is only available through NTIS (see address given above).

NCEER-88-0009 "Seismic Fragility Analysis of Shear Wall Structures," by J-W Jaw and H.H-M. Hwang, 4/30/88, (PB89-102867, A04, MF-A01).

NCEER-88-0010 "Base Isolation of a Multi-Story Building Under a Harmonic Ground Motion - A Comparison of Performances of Various Systems," by F-G Fan, G. Ahmadi and I.G. Tadjbakhsh, 5/18/88, (PB89-122238, A06, MF-A01). This report is only available through NTIS (see address given above).

NCEER-88-0011 "Seismic Floor Response Spectra for a Combined System by Green's Functions," by F.M. Lavelle, L.A. Bergman and P.D. Spanos, 5/1/88, (PB89-102875, A03, MF-A01).

NCEER-88-0012 "A New Solution Technique for Randomly Excited Hysteretic Structures," by G.Q. Cai and Y.K. Lin, 5/16/88, (PB89-102883, A03, MF-A01).

NCEER-88-0013 "A Study of Radiation Damping and Soil-Structure Interaction Effects in the Centrifuge," by K. Weissman, supervised by J.H. Prevost, 5/24/88, (PB89-144703, A06, MF-A01).

NCEER-88-0014 "Parameter Identification and Implementation of a Kinematic Plasticity Model for Frictional Soils," by J.H. Prevost and D.V. Griffiths, not available.

NCEER-88-0015 "Two- and Three- Dimensional Dynamic Finite Element Analyses of the Long Valley Dam," by D.V. Griffiths and J.H. Prevost, 6/17/88, (PB89-144711, A04, MF-A01).

NCEER-88-0016 "Damage Assessment of Reinforced Concrete Structures in Eastern United States," by A.M. Reinhorn, M.J. Seidel, S.K. Kunnath and Y.J. Park, 6/15/88, (PB89-122220, A04, MF-A01). This report is only available through NTIS (see address given above).

NCEER-88-0017 "Dynamic Compliance of Vertically Loaded Strip Foundations in Multilayered Viscoelastic Soils," by S. Ahmad and A.S.M. Israil, 6/17/88, (PB89-102891, A04, MF-A01).

NCEER-88-0018 "An Experimental Study of Seismic Structural Response With Added Viscoelastic Dampers," by R.C. Lin, Z. Liang, T.T. Soong and R.H. Zhang, 6/30/88, (PB89-122212, A05, MF-A01). This report is available only through NTIS (see address given above).

NCEER-88-0019 "Experimental Investigation of Primary - Secondary System Interaction," by G.D. Manolis, G. Juhn and A.M. Reinhorn, 5/27/88, (PB89-122204, A04, MF-A01).

NCEER-88-0020 "A Response Spectrum Approach For Analysis of Nonclassically Damped Structures," by J.N. Yang, S. Sarkani and F.X. Long, 4/22/88, (PB89-102909, A04, MF-A01).

NCEER-88-0021 "Seismic Interaction of Structures and Soils: Stochastic Approach," by A.S. Veletsos and A.M. Prasad, 7/21/88, (PB89-122196, A04, MF-A01). This report is only available through NTIS (see address given above).

NCEER-88-0022 "Identification of the Serviceability Limit State and Detection of Seismic Structural Damage," by E. DiPasquale and A.S. Cakmak, 6/15/88, (PB89-122188, A05, MF-A01). This report is available only through NTIS (see address given above).

NCEER-88-0023 "Multi-Hazard Risk Analysis: Case of a Simple Offshore Structure," by B.K. Bhartia and E.H. Vanmarcke, 7/21/88, (PB89-145213, A05, MF-A01).

NCEER-88-0024 "Automated Seismic Design of Reinforced Concrete Buildings," by Y.S. Chung, C. Meyer and M. Shinozuka, 7/5/88, (PB89-122170, A06, MF-A01). This report is available only through NTIS (see address given above).

NCEER-88-0025 "Experimental Study of Active Control of MDOF Structures Under Seismic Excitations," by L.L. Chung, R.C. Lin, T.T. Soong and A.M. Reinhorn, 7/10/88, (PB89-122600, A04, MF-A01).

NCEER-88-0026 "Earthquake Simulation Tests of a Low-Rise Metal Structure," by J.S. Hwang, K.C. Chang, G.C. Lee and R.L. Ketter, 8/1/88, (PB89-102917, A04, MF-A01).

NCEER-88-0027 "Systems Study of Urban Response and Reconstruction Due to Catastrophic Earthquakes," by F. Kozin and H.K. Zhou, 9/22/88, (PB90-162348, A04, MF-A01).

NCEER-88-0028 "Seismic Fragility Analysis of Plane Frame Structures," by H.H-M. Hwang and Y.K. Low, 7/31/88, (PB89-131445, A06, MF-A01).

NCEER-88-0029 "Response Analysis of Stochastic Structures," by A. Kardara, C. Bucher and M. Shinozuka, 9/22/88, (PB89-174429, A04, MF-A01).

NCEER-88-0030 "Nonnormal Accelerations Due to Yielding in a Primary Structure," by D.C.K. Chen and L.D. Lutes, 9/19/88, (PB89-131437, A04, MF-A01).

NCEER-88-0031 "Design Approaches for Soil-Structure Interaction," by A.S. Veletsos, A.M. Prasad and Y. Tang, 12/30/88, (PB89-174437, A03, MF-A01). This report is available only through NTIS (see address given above).

NCEER-88-0032 "A Re-evaluation of Design Spectra for Seismic Damage Control," by C.J. Turkstra and A.G. Tallin, 11/7/88, (PB89-145221, A05, MF-A01).

NCEER-88-0033 "The Behavior and Design of Noncontact Lap Splices Subjected to Repeated Inelastic Tensile Loading," by V.E. Sagan, P. Gergely and R.N. White, 12/8/88, (PB89-163737, A08, MF-A01).

NCEER-88-0034 "Seismic Response of Pile Foundations," by S.M. Mamoon, P.K. Banerjee and S. Ahmad, 11/1/88, (PB89-145239, A04, MF-A01).

NCEER-88-0035 "Modeling of R/C Building Structures With Flexible Floor Diaphragms (IDARC2)," by A.M. Reinhorn, S.K. Kunnath and N. Panahshahi, 9/7/88, (PB89-207153, A07, MF-A01).

NCEER-88-0036 "Solution of the Dam-Reservoir Interaction Problem Using a Combination of FEM, BEM with Particular Integrals, Modal Analysis, and Substructuring," by C-S. Tsai, G.C. Lee and R.L. Ketter, 12/31/88, (PB89-207146, A04, MF-A01).

NCEER-88-0037 "Optimal Placement of Actuators for Structural Control," by F.Y. Cheng and C.P. Pantelides, 8/15/88, (PB89-162846, A05, MF-A01).

NCEER-88-0038 "Teflon Bearings in Aseismic Base Isolation: Experimental Studies and Mathematical Modeling," by A. Mokha, M.C. Constantinou and A.M. Reinhorn, 12/5/88, (PB89-218457, A10, MF-A01). This report is available only through NTIS (see address given above).

NCEER-88-0039 "Seismic Behavior of Flat Slab High-Rise Buildings in the New York City Area," by P. Weidlinger and M. Ettouney, 10/15/88, (PB90-145681, A04, MF-A01).

NCEER-88-0040 "Evaluation of the Earthquake Resistance of Existing Buildings in New York City," by P. Weidlinger and M. Ettouney, 10/15/88, not available.

NCEER-88-0041 "Small-Scale Modeling Techniques for Reinforced Concrete Structures Subjected to Seismic Loads," by W. Kim, A. El-Attar and R.N. White, 11/22/88, (PB89-189625, A05, MF-A01).

NCEER-88-0042 "Modeling Strong Ground Motion from Multiple Event Earthquakes," by G.W. Ellis and A.S. Cakmak, 10/15/88, (PB89-174445, A03, MF-A01).

NCEER-88-0043 "Nonstationary Models of Seismic Ground Acceleration," by M. Grigoriu, S.E. Ruiz and E. Rosenblueth, 7/15/88, (PB89-189617, A04, MF-A01).

NCEER-88-0044 "SARCF User's Guide: Seismic Analysis of Reinforced Concrete Frames," by Y.S. Chung, C. Meyer and M. Shinozuka, 11/9/88, (PB89-174452, A08, MF-A01).

NCEER-88-0045 "First Expert Panel Meeting on Disaster Research and Planning," edited by J. Pantelic and J. Stoyle, 9/15/88, (PB89-174460, A05, MF-A01).

NCEER-88-0046 "Preliminary Studies of the Effect of Degrading Infill Walls on the Nonlinear Seismic Response of Steel Frames," by C.Z. Chrysostomou, P. Gergely and J.F. Abel, 12/19/88, (PB89-208383, A05, MF-A01).

NCEER-88-0047 "Reinforced Concrete Frame Component Testing Facility - Design, Construction, Instrumentation and Operation," by S.P. Pessiki, C. Conley, T. Bond, P. Gergely and R.N. White, 12/16/88, (PB89-174478, A04, MF-A01).

NCEER-89-0001 "Effects of Protective Cushion and Soil Compliancy on the Response of Equipment Within a Seismically Excited Building," by J.A. HoLung, 2/16/89, (PB89-207179, A04, MF-A01).

NCEER-89-0002 "Statistical Evaluation of Response Modification Factors for Reinforced Concrete Structures," by H.H-M. Hwang and J-W. Jaw, 2/17/89, (PB89-207187, A05, MF-A01).

NCEER-89-0003 "Hysteretic Columns Under Random Excitation," by G-Q. Cai and Y.K. Lin, 1/9/89, (PB89-196513, A03, MF-A01).

NCEER-89-0004 "Experimental Study of `Elephant Foot Bulge' Instability of Thin-Walled Metal Tanks," by Z-H. Jia and R.L. Ketter, 2/22/89, (PB89-207195, A03, MF-A01).

NCEER-89-0005 "Experiment on Performance of Buried Pipelines Across San Andreas Fault," by J. Isenberg, E. Richardson and T.D. O'Rourke, 3/10/89, (PB89-218440, A04, MF-A01). This report is available only through NTIS (see address given above).

NCEER-89-0006 "A Knowledge-Based Approach to Structural Design of Earthquake-Resistant Buildings," by M. Subramani, P. Gergely, C.H. Conley, J.F. Abel and A.H. Zaghw, 1/15/89, (PB89-218465, A06, MF-A01).

NCEER-89-0007 "Liquefaction Hazards and Their Effects on Buried Pipelines," by T.D. O'Rourke and P.A. Lane, 2/1/89, (PB89-218481, A09, MF-A01).

NCEER-89-0008 "Fundamentals of System Identification in Structural Dynamics," by H. Imai, C-B. Yun, O. Maruyama and M. Shinozuka, 1/26/89, (PB89-207211, A04, MF-A01).

NCEER-89-0009 "Effects of the 1985 Michoacan Earthquake on Water Systems and Other Buried Lifelines in Mexico," by A.G. Ayala and M.J. O'Rourke, 3/8/89, (PB89-207229, A06, MF-A01).

NCEER-89-R010 "NCEER Bibliography of Earthquake Education Materials," by K.E.K. Ross, Second Revision, 9/1/89, (PB90-125352, A05, MF-A01). This report is replaced by NCEER-92-0018.

NCEER-89-0011 "Inelastic Three-Dimensional Response Analysis of Reinforced Concrete Building Structures (IDARC-3D), Part I - Modeling," by S.K. Kunnath and A.M. Reinhorn, 4/17/89, (PB90-114612, A07, MF-A01). This report is available only through NTIS (see address given above).

NCEER-89-0012 "Recommended Modifications to ATC-14," by C.D. Poland and J.O. Malley, 4/12/89, (PB90-108648, A15, MF-A01).

NCEER-89-0013 "Repair and Strengthening of Beam-to-Column Connections Subjected to Earthquake Loading," by M. Corazao and A.J. Durrani, 2/28/89, (PB90-109885, A06, MF-A01).

NCEER-89-0014 "Program EXKAL2 for Identification of Structural Dynamic Systems," by O. Maruyama, C-B. Yun, M. Hoshiya and M. Shinozuka, 5/19/89, (PB90-109877, A09, MF-A01).

NCEER-89-0015 "Response of Frames With Bolted Semi-Rigid Connections, Part I - Experimental Study and Analytical Predictions," by P.J. DiCorso, A.M. Reinhorn, J.R. Dickerson, J.B. Radziminski and W.L. Harper, 6/1/89, not available.

NCEER-89-0016 "ARMA Monte Carlo Simulation in Probabilistic Structural Analysis," by P.D. Spanos and M.P. Mignolet, 7/10/89, (PB90-109893, A03, MF-A01).

NCEER-89-P017 "Preliminary Proceedings from the Conference on Disaster Preparedness - The Place of Earthquake Education in Our Schools," Edited by K.E.K. Ross, 6/23/89, (PB90-108606, A03, MF-A01).

NCEER-89-0017 "Proceedings from the Conference on Disaster Preparedness - The Place of Earthquake Education in Our Schools," Edited by K.E.K. Ross, 12/31/89, (PB90-207895, A012, MF-A02). This report is available only through NTIS (see address given above).

NCEER-89-0018 "Multidimensional Models of Hysteretic Material Behavior for Vibration Analysis of Shape Memory Energy Absorbing Devices, by E.J. Graesser and F.A. Cozzarelli, 6/7/89, (PB90-164146, A04, MF-A01).

NCEER-89-0019 "Nonlinear Dynamic Analysis of Three-Dimensional Base Isolated Structures (3D-BASIS)," by S. Nagarajaiah, A.M. Reinhorn and M.C. Constantinou, 8/3/89, (PB90-161936, A06, MF-A01). This report has been replaced by NCEER-93-0011.

NCEER-89-0020 "Structural Control Considering Time-Rate of Control Forces and Control Rate Constraints," by F.Y. Cheng and C.P. Pantelides, 8/3/89, (PB90-120445, A04, MF-A01).

NCEER-89-0021 "Subsurface Conditions of Memphis and Shelby County," by K.W. Ng, T-S. Chang and H-H.M. Hwang, 7/26/89, (PB90-120437, A03, MF-A01).

NCEER-89-0022 "Seismic Wave Propagation Effects on Straight Jointed Buried Pipelines," by K. Elhmadi and M.J. O'Rourke, 8/24/89, (PB90-162322, A10, MF-A02).

NCEER-89-0023 "Workshop on Serviceability Analysis of Water Delivery Systems," edited by M. Grigoriu, 3/6/89, (PB90-127424, A03, MF-A01).

NCEER-89-0024 "Shaking Table Study of a 1/5 Scale Steel Frame Composed of Tapered Members," by K.C. Chang, J.S. Hwang and G.C. Lee, 9/18/89, (PB90-160169, A04, MF-A01).

NCEER-89-0025 "DYNA1D: A Computer Program for Nonlinear Seismic Site Response Analysis - Technical Documentation," by Jean H. Prevost, 9/14/89, (PB90-161944, A07, MF-A01). This report is available only through NTIS (see address given above).

NCEER-89-0026 "1:4 Scale Model Studies of Active Tendon Systems and Active Mass Dampers for Aseismic Protection," by A.M. Reinhorn, T.T. Soong, R.C. Lin, Y.P. Yang, Y. Fukao, H. Abe and M. Nakai, 9/15/89, (PB90-173246, A10, MF-A02). This report is available only through NTIS (see address given above).

NCEER-89-0027 "Scattering of Waves by Inclusions in a Nonhomogeneous Elastic Half Space Solved by Boundary Element Methods," by P.K. Hadley, A. Askar and A.S. Cakmak, 6/15/89, (PB90-145699, A07, MF-A01).

NCEER-89-0028 "Statistical Evaluation of Deflection Amplification Factors for Reinforced Concrete Structures," by H.H.M. Hwang, J-W. Jaw and A.L. Ch'ng, 8/31/89, (PB90-164633, A05, MF-A01).

NCEER-89-0029 "Bedrock Accelerations in Memphis Area Due to Large New Madrid Earthquakes," by H.H.M. Hwang, C.H.S. Chen and G. Yu, 11/7/89, (PB90-162330, A04, MF-A01).

NCEER-89-0030 "Seismic Behavior and Response Sensitivity of Secondary Structural Systems," by Y.Q. Chen and T.T. Soong, 10/23/89, (PB90-164658, A08, MF-A01).

NCEER-89-0031 "Random Vibration and Reliability Analysis of Primary-Secondary Structural Systems," by Y. Ibrahim, M. Grigoriu and T.T. Soong, 11/10/89, (PB90-161951, A04, MF-A01).

NCEER-89-0032 "Proceedings from the Second U.S. - Japan Workshop on Liquefaction, Large Ground Deformation and Their Effects on Lifelines, September 26-29, 1989," Edited by T.D. O'Rourke and M. Hamada, 12/1/89, (PB90-209388, A22, MF-A03).

NCEER-89-0033 "Deterministic Model for Seismic Damage Evaluation of Reinforced Concrete Structures," by J.M. Bracci, A.M. Reinhorn, J.B. Mander and S.K. Kunnath, 9/27/89, (PB91-108803, A06, MF-A01).

NCEER-89-0034 "On the Relation Between Local and Global Damage Indices," by E. DiPasquale and A.S. Cakmak, 8/15/89, (PB90-173865, A05, MF-A01).

NCEER-89-0035 "Cyclic Undrained Behavior of Nonplastic and Low Plasticity Silts," by A.J. Walker and H.E. Stewart, 7/26/89, (PB90-183518, A10, MF-A01).

NCEER-89-0036 "Liquefaction Potential of Surficial Deposits in the City of Buffalo, New York," by M. Budhu, R. Giese and L. Baumgrass, 1/17/89, (PB90-208455, A04, MF-A01).

NCEER-89-0037 "A Deterministic Assessment of Effects of Ground Motion Incoherence," by A.S. Veletsos and Y. Tang, 7/15/89, (PB90-164294, A03, MF-A01).

NCEER-89-0038 "Workshop on Ground Motion Parameters for Seismic Hazard Mapping," July 17-18, 1989, edited by R.V. Whitman, 12/1/89, (PB90-173923, A04, MF-A01).

NCEER-89-0039 "Seismic Effects on Elevated Transit Lines of the New York City Transit Authority," by C.J. Costantino, C.A. Miller and E. Heymsfield, 12/26/89, (PB90-207887, A06, MF-A01).

NCEER-89-0040 "Centrifugal Modeling of Dynamic Soil-Structure Interaction," by K. Weissman, Supervised by J.H. Prevost, 5/10/89, (PB90-207879, A07, MF-A01).

NCEER-89-0041 "Linearized Identification of Buildings With Cores for Seismic Vulnerability Assessment," by I-K. Ho and A.E. Aktan, 11/1/89, (PB90-251943, A07, MF-A01).

NCEER-90-0001 "Geotechnical and Lifeline Aspects of the October 17, 1989 Loma Prieta Earthquake in San Francisco," by T.D. O'Rourke, H.E. Stewart, F.T. Blackburn and T.S. Dickerman, 1/90, (PB90-208596, A05, MF-A01).

NCEER-90-0002 "Nonnormal Secondary Response Due to Yielding in a Primary Structure," by D.C.K. Chen and L.D. Lutes, 2/28/90, (PB90-251976, A07, MF-A01).

NCEER-90-0003 "Earthquake Education Materials for Grades K-12," by K.E.K. Ross, 4/16/90, (PB91-251984, A05, MF-A05). This report has been replaced by NCEER-92-0018.

NCEER-90-0004 "Catalog of Strong Motion Stations in Eastern North America," by R.W. Busby, 4/3/90, (PB90-251984, A05, MF-A01).

NCEER-90-0005 "NCEER Strong-Motion Data Base: A User Manual for the GeoBase Release (Version 1.0 for the Sun3)," by P. Friberg and K. Jacob, 3/31/90 (PB90-258062, A04, MF-A01).

NCEER-90-0006 "Seismic Hazard Along a Crude Oil Pipeline in the Event of an 1811-1812 Type New Madrid Earthquake," by H.H.M. Hwang and C-H.S. Chen, 4/16/90, (PB90-258054, A04, MF-A01).

NCEER-90-0007 "Site-Specific Response Spectra for Memphis Sheahan Pumping Station," by H.H.M. Hwang and C.S. Lee, 5/15/90, (PB91-108811, A05, MF-A01).

NCEER-90-0008 "Pilot Study on Seismic Vulnerability of Crude Oil Transmission Systems," by T. Ariman, R. Dobry, M. Grigoriu, F. Kozin, M. O'Rourke, T. O'Rourke and M. Shinozuka, 5/25/90, (PB91-108837, A06, MF-A01).

NCEER-90-0009 "A Program to Generate Site Dependent Time Histories: EQGEN," by G.W. Ellis, M. Srinivasan and A.S. Cakmak, 1/30/90, (PB91-108829, A04, MF-A01).

NCEER-90-0010 "Active Isolation for Seismic Protection of Operating Rooms," by M.E. Talbott, Supervised by M. Shinozuka, 6/8/9, (PB91-110205, A05, MF-A01).

NCEER-90-0011 "Program LINEARID for Identification of Linear Structural Dynamic Systems," by C-B. Yun and M. Shinozuka, 6/25/90, (PB91-110312, A08, MF-A01).

NCEER-90-0012 "Two-Dimensional Two-Phase Elasto-Plastic Seismic Response of Earth Dams," by A.N. Yiagos, Supervised by J.H. Prevost, 6/20/90, (PB91-110197, A13, MF-A02).

NCEER-90-0013 "Secondary Systems in Base-Isolated Structures: Experimental Investigation, Stochastic Response and Stochastic Sensitivity," by G.D. Manolis, G. Juhn, M.C. Constantinou and A.M. Reinhorn, 7/1/90, (PB91-110320, A08, MF-A01).

NCEER-90-0014 "Seismic Behavior of Lightly-Reinforced Concrete Column and Beam-Column Joint Details," by S.P. Pessiki, C.H. Conley, P. Gergely and R.N. White, 8/22/90, (PB91-108795, A11, MF-A02).

NCEER-90-0015 "Two Hybrid Control Systems for Building Structures Under Strong Earthquakes," by J.N. Yang and A. Danielians, 6/29/90, (PB91-125393, A04, MF-A01).

NCEER-90-0016 "Instantaneous Optimal Control with Acceleration and Velocity Feedback," by J.N. Yang and Z. Li, 6/29/90, (PB91-125401, A03, MF-A01).

NCEER-90-0017 "Reconnaissance Report on the Northern Iran Earthquake of June 21, 1990," by M. Mehrain, 10/4/90, (PB91-125377, A03, MF-A01).

NCEER-90-0018 "Evaluation of Liquefaction Potential in Memphis and Shelby County," by T.S. Chang, P.S. Tang, C.S. Lee and H. Hwang, 8/10/90, (PB91-125427, A09, MF-A01).

NCEER-90-0019 "Experimental and Analytical Study of a Combined Sliding Disc Bearing and Helical Steel Spring Isolation System," by M.C. Constantinou, A.S. Mokha and A.M. Reinhorn, 10/4/90, (PB91-125385, A06, MF-A01). This report is available only through NTIS (see address given above).

NCEER-90-0020 "Experimental Study and Analytical Prediction of Earthquake Response of a Sliding Isolation System with a Spherical Surface," by A.S. Mokha, M.C. Constantinou and A.M. Reinhorn, 10/11/90, (PB91-125419, A05, MF-A01).

NCEER-90-0021 "Dynamic Interaction Factors for Floating Pile Groups," by G. Gazetas, K. Fan, A. Kaynia and E. Kausel, 9/10/90, (PB91-170381, A05, MF-A01).

NCEER-90-0022 "Evaluation of Seismic Damage Indices for Reinforced Concrete Structures," by S. Rodriguez-Gomez and A.S. Cakmak, 9/30/90, PB91-171322, A06, MF-A01).

NCEER-90-0023 "Study of Site Response at a Selected Memphis Site," by H. Desai, S. Ahmad, E.S. Gazetas and M.R. Oh, 10/11/90, (PB91-196857, A03, MF-A01).

NCEER-90-0024 "A User's Guide to Strongmo: Version 1.0 of NCEER's Strong-Motion Data Access Tool for PCs and Terminals," by P.A. Friberg and C.A.T. Susch, 11/15/90, (PB91-171272, A03, MF-A01).

NCEER-90-0025 "A Three-Dimensional Analytical Study of Spatial Variability of Seismic Ground Motions," by L-L. Hong and A.H.-S. Ang, 10/30/90, (PB91-170399, A09, MF-A01).

NCEER-90-0026 "MUMOID User's Guide - A Program for the Identification of Modal Parameters," by S. Rodriguez-Gomez and E. DiPasquale, 9/30/90, (PB91-171298, A04, MF-A01).

NCEER-90-0027 "SARCF-II User's Guide - Seismic Analysis of Reinforced Concrete Frames," by S. Rodriguez-Gomez, Y.S. Chung and C. Meyer, 9/30/90, (PB91-171280, A05, MF-A01).

NCEER-90-0028 "Viscous Dampers: Testing, Modeling and Application in Vibration and Seismic Isolation," by N. Makris and M.C. Constantinou, 12/20/90 (PB91-190561, A06, MF-A01).

NCEER-90-0029 "Soil Effects on Earthquake Ground Motions in the Memphis Area," by H. Hwang, C.S. Lee, K.W. Ng and T.S. Chang, 8/2/90, (PB91-190751, A05, MF-A01).

NCEER-91-0001 "Proceedings from the Third Japan-U.S. Workshop on Earthquake Resistant Design of Lifeline Facilities and Countermeasures for Soil Liquefaction, December 17-19, 1990," edited by T.D. O'Rourke and M. Hamada, 2/1/91, (PB91-179259, A99, MF-A04).

NCEER-91-0002 "Physical Space Solutions of Non-Proportionally Damped Systems," by M. Tong, Z. Liang and G.C. Lee, 1/15/91, (PB91-179242, A04, MF-A01).

NCEER-91-0003 "Seismic Response of Single Piles and Pile Groups," by K. Fan and G. Gazetas, 1/10/91, (PB92-174994, A04, MF-A01).

NCEER-91-0004 "Damping of Structures: Part 1 - Theory of Complex Damping," by Z. Liang and G. Lee, 10/10/91, (PB92-197235, A12, MF-A03).

NCEER-91-0005 "3D-BASIS - Nonlinear Dynamic Analysis of Three Dimensional Base Isolated Structures: Part II," by S. Nagarajaiah, A.M. Reinhorn and M.C. Constantinou, 2/28/91, (PB91-190553, A07, MF-A01). This report has been replaced by NCEER-93-0011.

NCEER-91-0006 "A Multidimensional Hysteretic Model for Plasticity Deforming Metals in Energy Absorbing Devices," by E.J. Graesser and F.A. Cozzarelli, 4/9/91, (PB92-108364, A04, MF-A01).

NCEER-91-0007 "A Framework for Customizable Knowledge-Based Expert Systems with an Application to a KBES for Evaluating the Seismic Resistance of Existing Buildings," by E.G. Ibarra-Anaya and S.J. Fenves, 4/9/91, (PB91-210930, A08, MF-A01).

NCEER-91-0008 "Nonlinear Analysis of Steel Frames with Semi-Rigid Connections Using the Capacity Spectrum Method," by G.G. Deierlein, S-H. Hsieh, Y-J. Shen and J.F. Abel, 7/2/91, (PB92-113828, A05, MF-A01).

NCEER-91-0009 "Earthquake Education Materials for Grades K-12," by K.E.K. Ross, 4/30/91, (PB91-212142, A06, MF-A01). This report has been replaced by NCEER-92-0018.

NCEER-91-0010 "Phase Wave Velocities and Displacement Phase Differences in a Harmonically Oscillating Pile," by N. Makris and G. Gazetas, 7/8/91, (PB92-108356, A04, MF-A01).

NCEER-91-0011 "Dynamic Characteristics of a Full-Size Five-Story Steel Structure and a 2/5 Scale Model," by K.C. Chang, G.C. Yao, G.C. Lee, D.S. Hao and Y.C. Yeh," 7/2/91, (PB93-116648, A06, MF-A02).

NCEER-91-0012 "Seismic Response of a 2/5 Scale Steel Structure with Added Viscoelastic Dampers," by K.C. Chang, T.T. Soong, S-T. Oh and M.L. Lai, 5/17/91, (PB92-110816, A05, MF-A01).

NCEER-91-0013 "Earthquake Response of Retaining Walls; Full-Scale Testing and Computational Modeling," by S. Alampalli and A-W.M. Elgamal, 6/20/91, not available.

NCEER-91-0014 "3D-BASIS-M: Nonlinear Dynamic Analysis of Multiple Building Base Isolated Structures," by P.C. Tsopelas, S. Nagarajaiah, M.C. Constantinou and A.M. Reinhorn, 5/28/91, (PB92-113885, A09, MF-A02).

NCEER-91-0015 "Evaluation of SEAOC Design Requirements for Sliding Isolated Structures," by D. Theodossiou and M.C. Constantinou, 6/10/91, (PB92-114602, A11, MF-A03).

NCEER-91-0016 "Closed-Loop Modal Testing of a 27-Story Reinforced Concrete Flat Plate-Core Building," by H.R. Somaprasad, T. Toksoy, H. Yoshiyuki and A.E. Aktan, 7/15/91, (PB92-129980, A07, MF-A02).

NCEER-91-0017 "Shake Table Test of a 1/6 Scale Two-Story Lightly Reinforced Concrete Building," by A.G. El-Attar, R.N. White and P. Gergely, 2/28/91, (PB92-222447, A06, MF-A02).

NCEER-91-0018 "Shake Table Test of a 1/8 Scale Three-Story Lightly Reinforced Concrete Building," by A.G. El-Attar, R.N. White and P. Gergely, 2/28/91, (PB93-116630, A08, MF-A02).

NCEER-91-0019 "Transfer Functions for Rigid Rectangular Foundations," by A.S. Veletsos, A.M. Prasad and W.H. Wu, 7/31/91, not available.

NCEER-91-0020 "Hybrid Control of Seismic-Excited Nonlinear and Inelastic Structural Systems," by J.N. Yang, Z. Li and A. Danielians, 8/1/91, (PB92-143171, A06, MF-A02).

NCEER-91-0021 "The NCEER-91 Earthquake Catalog: Improved Intensity-Based Magnitudes and Recurrence Relations for U.S. Earthquakes East of New Madrid," by L. Seeber and J.G. Armbruster, 8/28/91, (PB92-176742, A06, MF-A02).

NCEER-91-0022 "Proceedings from the Implementation of Earthquake Planning and Education in Schools: The Need for Change - The Roles of the Changemakers," by K.E.K. Ross and F. Winslow, 7/23/91, (PB92-129998, A12, MF-A03).

NCEER-91-0023 "A Study of Reliability-Based Criteria for Seismic Design of Reinforced Concrete Frame Buildings," by H.H.M. Hwang and H-M. Hsu, 8/10/91, (PB92-140235, A09, MF-A02).

NCEER-91-0024 "Experimental Verification of a Number of Structural System Identification Algorithms," by R.G. Ghanem, H. Gavin and M. Shinozuka, 9/18/91, (PB92-176577, A18, MF-A04).

NCEER-91-0025 "Probabilistic Evaluation of Liquefaction Potential," by H.H.M. Hwang and C.S. Lee," 11/25/91, (PB92-143429, A05, MF-A01).

NCEER-91-0026 "Instantaneous Optimal Control for Linear, Nonlinear and Hysteretic Structures - Stable Controllers," by J.N. Yang and Z. Li, 11/15/91, (PB92-163807, A04, MF-A01).

NCEER-91-0027 "Experimental and Theoretical Study of a Sliding Isolation System for Bridges," by M.C. Constantinou, A. Kartoum, A.M. Reinhorn and P. Bradford, 11/15/91, (PB92-176973, A10, MF-A03).

NCEER-92-0001 "Case Studies of Liquefaction and Lifeline Performance During Past Earthquakes, Volume 1: Japanese Case Studies," Edited by M. Hamada and T. O'Rourke, 2/17/92, (PB92-197243, A18, MF-A04).

NCEER-92-0002 "Case Studies of Liquefaction and Lifeline Performance During Past Earthquakes, Volume 2: United States Case Studies," Edited by T. O'Rourke and M. Hamada, 2/17/92, (PB92-197250, A20, MF-A04).

NCEER-92-0003 "Issues in Earthquake Education," Edited by K. Ross, 2/3/92, (PB92-222389, A07, MF-A02).

NCEER-92-0004 "Proceedings from the First U.S. - Japan Workshop on Earthquake Protective Systems for Bridges," Edited by I.G. Buckle, 2/4/92, (PB94-142239, A99, MF-A06).

NCEER-92-0005 "Seismic Ground Motion from a Haskell-Type Source in a Multiple-Layered Half-Space," A.P. Theoharis, G. Deodatis and M. Shinozuka, 1/2/92, not available.

NCEER-92-0006 "Proceedings from the Site Effects Workshop," Edited by R. Whitman, 2/29/92, (PB92-197201, A04, MF-A01).

NCEER-92-0007 "Engineering Evaluation of Permanent Ground Deformations Due to Seismically-Induced Liquefaction," by M.H. Baziar, R. Dobry and A-W.M. Elgamal, 3/24/92, (PB92-222421, A13, MF-A03).

NCEER-92-0008 "A Procedure for the Seismic Evaluation of Buildings in the Central and Eastern United States," by C.D. Poland and J.O. Malley, 4/2/92, (PB92-222439, A20, MF-A04).

NCEER-92-0009 "Experimental and Analytical Study of a Hybrid Isolation System Using Friction Controllable Sliding Bearings," by M.Q. Feng, S. Fujii and M. Shinozuka, 5/15/92, (PB93-150282, A06, MF-A02).

NCEER-92-0010 "Seismic Resistance of Slab-Column Connections in Existing Non-Ductile Flat-Plate Buildings," by A.J. Durrani and Y. Du, 5/18/92, (PB93-116812, A06, MF-A02).

NCEER-92-0011 "The Hysteretic and Dynamic Behavior of Brick Masonry Walls Upgraded by Ferrocement Coatings Under Cyclic Loading and Strong Simulated Ground Motion," by H. Lee and S.P. Prawel, 5/11/92, not available.

NCEER-92-0012 "Study of Wire Rope Systems for Seismic Protection of Equipment in Buildings," by G.F. Demetriades, M.C. Constantinou and A.M. Reinhorn, 5/20/92, (PB93-116655, A08, MF-A02).

NCEER-92-0013 "Shape Memory Structural Dampers: Material Properties, Design and Seismic Testing," by P.R. Witting and F.A. Cozzarelli, 5/26/92, (PB93-116663, A05, MF-A01).

NCEER-92-0014 "Longitudinal Permanent Ground Deformation Effects on Buried Continuous Pipelines," by M.J. O'Rourke, and C. Nordberg, 6/15/92, (PB93-116671, A08, MF-A02).

NCEER-92-0015 "A Simulation Method for Stationary Gaussian Random Functions Based on the Sampling Theorem," by M. Grigoriu and S. Balopoulou, 6/11/92, (PB93-127496, A05, MF-A01).

NCEER-92-0016 "Gravity-Load-Designed Reinforced Concrete Buildings: Seismic Evaluation of Existing Construction and Detailing Strategies for Improved Seismic Resistance," by G.W. Hoffmann, S.K. Kunnath, A.M. Reinhorn and J.B. Mander, 7/15/92, (PB94-142007, A08, MF-A02).

NCEER-92-0017 "Observations on Water System and Pipeline Performance in the Limón Area of Costa Rica Due to the April 22, 1991 Earthquake," by M. O'Rourke and D. Ballantyne, 6/30/92, (PB93-126811, A06, MF-A02).

NCEER-92-0018 "Fourth Edition of Earthquake Education Materials for Grades K-12," Edited by K.E.K. Ross, 8/10/92, (PB93-114023, A07, MF-A02).

NCEER-92-0019 "Proceedings from the Fourth Japan-U.S. Workshop on Earthquake Resistant Design of Lifeline Facilities and Countermeasures for Soil Liquefaction," Edited by M. Hamada and T.D. O'Rourke, 8/12/92, (PB93-163939, A99, MF-E11).

NCEER-92-0020 "Active Bracing System: A Full Scale Implementation of Active Control," by A.M. Reinhorn, T.T. Soong, R.C. Lin, M.A. Riley, Y.P. Wang, S. Aizawa and M. Higashino, 8/14/92, (PB93-127512, A06, MF-A02).

NCEER-92-0021 "Empirical Analysis of Horizontal Ground Displacement Generated by Liquefaction-Induced Lateral Spreads," by S.F. Bartlett and T.L. Youd, 8/17/92, (PB93-188241, A06, MF-A02).

NCEER-92-0022 "IDARC Version 3.0: Inelastic Damage Analysis of Reinforced Concrete Structures," by S.K. Kunnath, A.M. Reinhorn and R.F. Lobo, 8/31/92, (PB93-227502, A07, MF-A02).

NCEER-92-0023 "A Semi-Empirical Analysis of Strong-Motion Peaks in Terms of Seismic Source, Propagation Path and Local Site Conditions, by M. Kamiyama, M.J. O'Rourke and R. Flores-Berrones, 9/9/92, (PB93-150266, A08, MF-A02).

NCEER-92-0024 "Seismic Behavior of Reinforced Concrete Frame Structures with Nonductile Details, Part I: Summary of Experimental Findings of Full Scale Beam-Column Joint Tests," by A. Beres, R.N. White and P. Gergely, 9/30/92, (PB93-227783, A05, MF-A01).

NCEER-92-0025 "Experimental Results of Repaired and Retrofitted Beam-Column Joint Tests in Lightly Reinforced Concrete Frame Buildings," by A. Beres, S. El-Borgi, R.N. White and P. Gergely, 10/29/92, (PB93-227791, A05, MF-A01).

NCEER-92-0026 "A Generalization of Optimal Control Theory: Linear and Nonlinear Structures," by J.N. Yang, Z. Li and S. Vongchavalitkul, 11/2/92, (PB93-188621, A05, MF-A01).

NCEER-92-0027 "Seismic Resistance of Reinforced Concrete Frame Structures Designed Only for Gravity Loads: Part I - Design and Properties of a One-Third Scale Model Structure," by J.M. Bracci, A.M. Reinhorn and J.B. Mander, 12/1/92, (PB94-104502, A08, MF-A02).

NCEER-92-0028 "Seismic Resistance of Reinforced Concrete Frame Structures Designed Only for Gravity Loads: Part II - Experimental Performance of Subassemblages," by L.E. Aycardi, J.B. Mander and A.M. Reinhorn, 12/1/92, (PB94-104510, A08, MF-A02).

NCEER-92-0029 "Seismic Resistance of Reinforced Concrete Frame Structures Designed Only for Gravity Loads: Part III - Experimental Performance and Analytical Study of a Structural Model," by J.M. Bracci, A.M. Reinhorn and J.B. Mander, 12/1/92, (PB93-227528, A09, MF-A01).

NCEER-92-0030 "Evaluation of Seismic Retrofit of Reinforced Concrete Frame Structures: Part I - Experimental Performance of Retrofitted Subassemblages," by D. Choudhuri, J.B. Mander and A.M. Reinhorn, 12/8/92, (PB93-198307, A07, MF-A02).

NCEER-92-0031 "Evaluation of Seismic Retrofit of Reinforced Concrete Frame Structures: Part II - Experimental Performance and Analytical Study of a Retrofitted Structural Model," by J.M. Bracci, A.M. Reinhorn and J.B. Mander, 12/8/92, (PB93-198315, A09, MF-A03).

NCEER-92-0032 "Experimental and Analytical Investigation of Seismic Response of Structures with Supplemental Fluid Viscous Dampers," by M.C. Constantinou and M.D. Symans, 12/21/92, (PB93-191435, A10, MF-A03). This report is available only through NTIS (see address given above).

NCEER-92-0033 "Reconnaissance Report on the Cairo, Egypt Earthquake of October 12, 1992," by M. Khater, 12/23/92, (PB93-188621, A03, MF-A01).

NCEER-92-0034 "Low-Level Dynamic Characteristics of Four Tall Flat-Plate Buildings in New York City," by H. Gavin, S. Yuan, J. Grossman, E. Pekelis and K. Jacob, 12/28/92, (PB93-188217, A07, MF-A02).

NCEER-93-0001 "An Experimental Study on the Seismic Performance of Brick-Infilled Steel Frames With and Without Retrofit," by J.B. Mander, B. Nair, K. Wojtkowski and J. Ma, 1/29/93, (PB93-227510, A07, MF-A02).

NCEER-93-0002 "Social Accounting for Disaster Preparedness and Recovery Planning," by S. Cole, E. Pantoja and V. Razak, 2/22/93, (PB94-142114, A12, MF-A03).

NCEER-93-0003 "Assessment of 1991 NEHRP Provisions for Nonstructural Components and Recommended Revisions," by T.T. Soong, G. Chen, Z. Wu, R-H. Zhang and M. Grigoriu, 3/1/93, (PB93-188639, A06, MF-A02).

NCEER-93-0004 "Evaluation of Static and Response Spectrum Analysis Procedures of SEAOC/UBC for Seismic Isolated Structures," by C.W. Winters and M.C. Constantinou, 3/23/93, (PB93-198299, A10, MF-A03).

NCEER-93-0005 "Earthquakes in the Northeast - Are We Ignoring the Hazard? A Workshop on Earthquake Science and Safety for Educators," edited by K.E.K. Ross, 4/2/93, (PB94-103066, A09, MF-A02).

NCEER-93-0006 "Inelastic Response of Reinforced Concrete Structures with Viscoelastic Braces," by R.F. Lobo, J.M. Bracci, K.L. Shen, A.M. Reinhorn and T.T. Soong, 4/5/93, (PB93-227486, A05, MF-A02).

NCEER-93-0007 "Seismic Testing of Installation Methods for Computers and Data Processing Equipment," by K. Kosar, T.T. Soong, K.L. Shen, J.A. HoLung and Y.K. Lin, 4/12/93, (PB93-198299, A07, MF-A02).

NCEER-93-0008 "Retrofit of Reinforced Concrete Frames Using Added Dampers," by A. Reinhorn, M. Constantinou and C. Li, not available.

NCEER-93-0009 "Seismic Behavior and Design Guidelines for Steel Frame Structures with Added Viscoelastic Dampers," by K.C. Chang, M.L. Lai, T.T. Soong, D.S. Hao and Y.C. Yeh, 5/1/93, (PB94-141959, A07, MF-A02).

NCEER-93-0010 "Seismic Performance of Shear-Critical Reinforced Concrete Bridge Piers," by J.B. Mander, S.M. Waheed, M.T.A. Chaudhary and S.S. Chen, 5/12/93, (PB93-227494, A08, MF-A02).

NCEER-93-0011 "3D-BASIS-TABS: Computer Program for Nonlinear Dynamic Analysis of Three Dimensional Base Isolated Structures," by S. Nagarajaiah, C. Li, A.M. Reinhorn and M.C. Constantinou, 8/2/93, (PB94-141819, A09, MF-A02).

NCEER-93-0012 "Effects of Hydrocarbon Spills from an Oil Pipeline Break on Ground Water," by O.J. Helweg and H.H.M. Hwang, 8/3/93, (PB94-141942, A06, MF-A02).

NCEER-93-0013 "Simplified Procedures for Seismic Design of Nonstructural Components and Assessment of Current Code Provisions," by M.P. Singh, L.E. Suarez, E.E. Matheu and G.O. Maldonado, 8/4/93, (PB94-141827, A09, MF-A02).

NCEER-93-0014 "An Energy Approach to Seismic Analysis and Design of Secondary Systems," by G. Chen and T.T. Soong, 8/6/93, (PB94-142767, A11, MF-A03).

NCEER-93-0015 "Proceedings from School Sites: Becoming Prepared for Earthquakes - Commemorating the Third Anniversary of the Loma Prieta Earthquake," Edited by F.E. Winslow and K.E.K. Ross, 8/16/93, (PB94-154275, A16, MF-A02).

NCEER-93-0016 "Reconnaissance Report of Damage to Historic Monuments in Cairo, Egypt Following the October 12, 1992 Dahshur Earthquake," by D. Sykora, D. Look, G. Croci, E. Karaesmen and E. Karaesmen, 8/19/93, (PB94-142221, A08, MF-A02).

NCEER-93-0017 "The Island of Guam Earthquake of August 8, 1993," by S.W. Swan and S.K. Harris, 9/30/93, (PB94-141843, A04, MF-A01).

NCEER-93-0018 "Engineering Aspects of the October 12, 1992 Egyptian Earthquake," by A.W. Elgamal, M. Amer, K. Adalier and A. Abul-Fadl, 10/7/93, (PB94-141983, A05, MF-A01).

NCEER-93-0019 "Development of an Earthquake Motion Simulator and its Application in Dynamic Centrifuge Testing," by I. Krstelj, Supervised by J.H. Prevost, 10/23/93, (PB94-181773, A-10, MF-A03).

NCEER-93-0020 "NCEER-Taisei Corporation Research Program on Sliding Seismic Isolation Systems for Bridges: Experimental and Analytical Study of a Friction Pendulum System (FPS)," by M.C. Constantinou, P. Tsopelas, Y-S. Kim and S. Okamoto, 11/1/93, (PB94-142775, A08, MF-A02).

NCEER-93-0021 "Finite Element Modeling of Elastomeric Seismic Isolation Bearings," by L.J. Billings, Supervised by R. Shepherd, 11/8/93, not available.

NCEER-93-0022 "Seismic Vulnerability of Equipment in Critical Facilities: Life-Safety and Operational Consequences," by K. Porter, G.S. Johnson, M.M. Zadeh, C. Scawthorn and S. Eder, 11/24/93, (PB94-181765, A16, MF-A03).

NCEER-93-0023 "Hokkaido Nansei-oki, Japan Earthquake of July 12, 1993, by P.I. Yanev and C.R. Scawthorn, 12/23/93, (PB94-181500, A07, MF-A01).

NCEER-94-0001 "An Evaluation of Seismic Serviceability of Water Supply Networks with Application to the San Francisco Auxiliary Water Supply System," by I. Markov, Supervised by M. Grigoriu and T. O'Rourke, 1/21/94, (PB94-204013, A07, MF-A02).

NCEER-94-0002 "NCEER-Taisei Corporation Research Program on Sliding Seismic Isolation Systems for Bridges: Experimental and Analytical Study of Systems Consisting of Sliding Bearings, Rubber Restoring Force Devices and Fluid Dampers," Volumes I and II, by P. Tsopelas, S. Okamoto, M.C. Constantinou, D. Ozaki and S. Fujii, 2/4/94, (PB94-181740, A09, MF-A02 and PB94-181757, A12, MF-A03).

NCEER-94-0003 "A Markov Model for Local and Global Damage Indices in Seismic Analysis," by S. Rahman and M. Grigoriu, 2/18/94, (PB94-206000, A12, MF-A03).

NCEER-94-0004 "Proceedings from the NCEER Workshop on Seismic Response of Masonry Infills," edited by D.P. Abrams, 3/1/94, (PB94-180783, A07, MF-A02).

NCEER-94-0005 "The Northridge, California Earthquake of January 17, 1994: General Reconnaissance Report," edited by J.D. Goltz, 3/11/94, (PB94-193943, A10, MF-A03).

NCEER-94-0006 "Seismic Energy Based Fatigue Damage Analysis of Bridge Columns: Part I - Evaluation of Seismic Capacity," by G.A. Chang and J.B. Mander, 3/14/94, (PB94-219185, A11, MF-A03).

NCEER-94-0007 "Seismic Isolation of Multi-Story Frame Structures Using Spherical Sliding Isolation Systems," by T.M. Al-Hussaini, V.A. Zayas and M.C. Constantinou, 3/17/94, (PB94-193745, A09, MF-A02).

NCEER-94-0008 "The Northridge, California Earthquake of January 17, 1994: Performance of Highway Bridges," edited by I.G. Buckle, 3/24/94, (PB94-193851, A06, MF-A02).

NCEER-94-0009 "Proceedings of the Third U.S.-Japan Workshop on Earthquake Protective Systems for Bridges," edited by I.G. Buckle and I. Friedland, 3/31/94, (PB94-195815, A99, MF-A06).

NCEER-94-0010 "3D-BASIS-ME: Computer Program for Nonlinear Dynamic Analysis of Seismically Isolated Single and Multiple Structures and Liquid Storage Tanks," by P.C. Tsopelas, M.C. Constantinou and A.M. Reinhorn, 4/12/94, (PB94-204922, A09, MF-A02).

NCEER-94-0011 "The Northridge, California Earthquake of January 17, 1994: Performance of Gas Transmission Pipelines," by T.D. O'Rourke and M.C. Palmer, 5/16/94, (PB94-204989, A05, MF-A01).

NCEER-94-0012 "Feasibility Study of Replacement Procedures and Earthquake Performance Related to Gas Transmission Pipelines," by T.D. O'Rourke and M.C. Palmer, 5/25/94, (PB94-206638, A09, MF-A02).

NCEER-94-0013 "Seismic Energy Based Fatigue Damage Analysis of Bridge Columns: Part II - Evaluation of Seismic Demand," by G.A. Chang and J.B. Mander, 6/1/94, (PB95-18106, A08, MF-A02).

NCEER-94-0014 "NCEER-Taisei Corporation Research Program on Sliding Seismic Isolation Systems for Bridges: Experimental and Analytical Study of a System Consisting of Sliding Bearings and Fluid Restoring Force/Damping Devices," by P. Tsopelas and M.C. Constantinou, 6/13/94, (PB94-219144, A10, MF-A03).

NCEER-94-0015 "Generation of Hazard-Consistent Fragility Curves for Seismic Loss Estimation Studies," by H. Hwang and J-R. Huo, 6/14/94, (PB95-181996, A09, MF-A02).

NCEER-94-0016 "Seismic Study of Building Frames with Added Energy-Absorbing Devices," by W.S. Pong, C.S. Tsai and G.C. Lee, 6/20/94, (PB94-219136, A10, A03).

NCEER-94-0017 "Sliding Mode Control for Seismic-Excited Linear and Nonlinear Civil Engineering Structures," by J. Yang, J. Wu, A. Agrawal and Z. Li, 6/21/94, (PB95-138483, A06, MF-A02).

NCEER-94-0018 "3D-BASIS-TABS Version 2.0: Computer Program for Nonlinear Dynamic Analysis of Three Dimensional Base Isolated Structures," by A.M. Reinhorn, S. Nagarajaiah, M.C. Constantinou, P. Tsopelas and R. Li, 6/22/94, (PB95-182176, A08, MF-A02).

NCEER-94-0019 "Proceedings of the International Workshop on Civil Infrastructure Systems: Application of Intelligent Systems and Advanced Materials on Bridge Systems," Edited by G.C. Lee and K.C. Chang, 7/18/94, (PB95-252474, A20, MF-A04).

NCEER-94-0020 "Study of Seismic Isolation Systems for Computer Floors," by V. Lambrou and M.C. Constantinou, 7/19/94, (PB95-138533, A10, MF-A03).

NCEER-94-0021 "Proceedings of the U.S.-Italian Workshop on Guidelines for Seismic Evaluation and Rehabilitation of Unreinforced Masonry Buildings," Edited by D.P. Abrams and G.M. Calvi, 7/20/94, (PB95-138749, A13, MF-A03).

NCEER-94-0022 "NCEER-Taisei Corporation Research Program on Sliding Seismic Isolation Systems for Bridges: Experimental and Analytical Study of a System Consisting of Lubricated PTFE Sliding Bearings and Mild Steel Dampers," by P. Tsopelas and M.C. Constantinou, 7/22/94, (PB95-182184, A08, MF-A02).

NCEER-94-0023 “Development of Reliability-Based Design Criteria for Buildings Under Seismic Load,” by Y.K. Wen, H. Hwang and M. Shinozuka, 8/1/94, (PB95-211934, A08, MF-A02).

NCEER-94-0024 “Experimental Verification of Acceleration Feedback Control Strategies for an Active Tendon System,” by S.J. Dyke, B.F. Spencer, Jr., P. Quast, M.K. Sain, D.C. Kaspari, Jr. and T.T. Soong, 8/29/94, (PB95-212320, A05, MF-A01).

NCEER-94-0025 “Seismic Retrofitting Manual for Highway Bridges,” Edited by I.G. Buckle and I.F. Friedland, published by the Federal Highway Administration (PB95-212676, A15, MF-A03).

NCEER-94-0026 “Proceedings from the Fifth U.S.-Japan Workshop on Earthquake Resistant Design of Lifeline Facilities and Countermeasures Against Soil Liquefaction,” Edited by T.D. O’Rourke and M. Hamada, 11/7/94, (PB95-220802, A99, MF-E08).

NCEER-95-0001 “Experimental and Analytical Investigation of Seismic Retrofit of Structures with Supplemental Damping: Part 1 - Fluid Viscous Damping Devices,” by A.M. Reinhorn, C. Li and M.C. Constantinou, 1/3/95, (PB95-266599, A09, MF-A02).

NCEER-95-0002 “Experimental and Analytical Study of Low-Cycle Fatigue Behavior of Semi-Rigid Top-And-Seat Angle Connections,” by G. Pekcan, J.B. Mander and S.S. Chen, 1/5/95, (PB95-220042, A07, MF-A02).

NCEER-95-0003 “NCEER-ATC Joint Study on Fragility of Buildings,” by T. Anagnos, C. Rojahn and A.S. Kiremidjian, 1/20/95, (PB95-220026, A06, MF-A02).

NCEER-95-0004 “Nonlinear Control Algorithms for Peak Response Reduction,” by Z. Wu, T.T. Soong, V. Gattulli and R.C. Lin, 2/16/95, (PB95-220349, A05, MF-A01).

NCEER-95-0005 “Pipeline Replacement Feasibility Study: A Methodology for Minimizing Seismic and Corrosion Risks to Underground Natural Gas Pipelines,” by R.T. Eguchi, H.A. Seligson and D.G. Honegger, 3/2/95, (PB95-252326, A06, MF-A02).

NCEER-95-0006 “Evaluation of Seismic Performance of an 11-Story Frame Building During the 1994 Northridge Earthquake,” by F. Naeim, R. DiSulio, K. Benuska, A. Reinhorn and C. Li, not available.

NCEER-95-0007 “Prioritization of Bridges for Seismic Retrofitting,” by N. Basöz and A.S. Kiremidjian, 4/24/95, (PB95-252300, A08, MF-A02).

NCEER-95-0008 “Method for Developing Motion Damage Relationships for Reinforced Concrete Frames,” by A. Singhal and A.S. Kiremidjian, 5/11/95, (PB95-266607, A06, MF-A02).

NCEER-95-0009 “Experimental and Analytical Investigation of Seismic Retrofit of Structures with Supplemental Damping: Part II - Friction Devices,” by C. Li and A.M. Reinhorn, 7/6/95, (PB96-128087, A11, MF-A03).

NCEER-95-0010 “Experimental Performance and Analytical Study of a Non-Ductile Reinforced Concrete Frame Structure Retrofitted with Elastomeric Spring Dampers,” by G. Pekcan, J.B. Mander and S.S. Chen, 7/14/95, (PB96-137161, A08, MF-A02).

NCEER-95-0011 “Development and Experimental Study of Semi-Active Fluid Damping Devices for Seismic Protection of Structures,” by M.D. Symans and M.C. Constantinou, 8/3/95, (PB96-136940, A23, MF-A04).

NCEER-95-0012 “Real-Time Structural Parameter Modification (RSPM): Development of Innervated Structures,” by Z. Liang, M. Tong and G.C. Lee, 4/11/95, (PB96-137153, A06, MF-A01).

NCEER-95-0013 “Experimental and Analytical Investigation of Seismic Retrofit of Structures with Supplemental Damping: Part III - Viscous Damping Walls,” by A.M. Reinhorn and C. Li, 10/1/95, (PB96-176409, A11, MF-A03).

NCEER-95-0014 “Seismic Fragility Analysis of Equipment and Structures in a Memphis Electric Substation,” by J-R. Huo and H.H.M. Hwang, 8/10/95, (PB96-128087, A09, MF-A02).

NCEER-95-0015 “The Hanshin-Awaji Earthquake of January 17, 1995: Performance of Lifelines,” Edited by M. Shinozuka, 11/3/95, (PB96-176383, A15, MF-A03).

NCEER-95-0016 “Highway Culvert Performance During Earthquakes,” by T.L. Youd and C.J. Beckman, available as NCEER-96-0015.

NCEER-95-0017 “The Hanshin-Awaji Earthquake of January 17, 1995: Performance of Highway Bridges,” Edited by I.G. Buckle, 12/1/95, not available.

NCEER-95-0018 “Modeling of Masonry Infill Panels for Structural Analysis,” by A.M. Reinhorn, A. Madan, R.E. Valles, Y. Reichmann and J.B. Mander, 12/8/95, (PB97-110886, MF-A01, A06).

NCEER-95-0019 “Optimal Polynomial Control for Linear and Nonlinear Structures,” by A.K. Agrawal and J.N. Yang, 12/11/95, (PB96-168737, A07, MF-A02).

NCEER-95-0020 "Retrofit of Non-Ductile Reinforced Concrete Frames Using Friction Dampers," by R.S. Rao, P. Gergely and R.N. White, 12/22/95, (PB97-133508, A10, MF-A02).

NCEER-95-0021 "Parametric Results for Seismic Response of Pile-Supported Bridge Bents," by G. Mylonakis, A. Nikolaou and G. Gazetas, 12/22/95, (PB97-100242, A12, MF-A03).

NCEER-95-0022 "Kinematic Bending Moments in Seismically Stressed Piles," by A. Nikolaou, G. Mylonakis and G. Gazetas, 12/23/95, (PB97-113914, MF-A03, A13).

NCEER-96-0001 "Dynamic Response of Unreinforced Masonry Buildings with Flexible Diaphragms," by A.C. Costley and D.P. Abrams," 10/10/96, (PB97-133573, MF-A03, A15).

NCEER-96-0002 "State of the Art Review: Foundations and Retaining Structures," by I. Po Lam, not available.

NCEER-96-0003 "Ductility of Rectangular Reinforced Concrete Bridge Columns with Moderate Confinement," by N. Wehbe, M. Saiidi, D. Sanders and B. Douglas, 11/7/96, (PB97-133557, A06, MF-A02).

NCEER-96-0004 "Proceedings of the Long-Span Bridge Seismic Research Workshop," edited by I.G. Buckle and I.M. Friedland, not available.

NCEER-96-0005 "Establish Representative Pier Types for Comprehensive Study: Eastern United States," by J. Kulicki and Z. Prucz, 5/28/96, (PB98-119217, A07, MF-A02).

NCEER-96-0006 "Establish Representative Pier Types for Comprehensive Study: Western United States," by R. Imbsen, R.A. Schamber and T.A. Osterkamp, 5/28/96, (PB98-118607, A07, MF-A02).

NCEER-96-0007 "Nonlinear Control Techniques for Dynamical Systems with Uncertain Parameters," by R.G. Ghanem and M.I. Bujakov, 5/27/96, (PB97-100259, A17, MF-A03).

NCEER-96-0008 "Seismic Evaluation of a 30-Year Old Non-Ductile Highway Bridge Pier and Its Retrofit," by J.B. Mander, B. Mahmoodzadegan, S. Bhadra and S.S. Chen, 5/31/96, (PB97-110902, MF-A03, A10).

NCEER-96-0009 "Seismic Performance of a Model Reinforced Concrete Bridge Pier Before and After Retrofit," by J.B. Mander, J.H. Kim and C.A. Ligozio, 5/31/96, (PB97-110910, MF-A02, A10).

NCEER-96-0010 "IDARC2D Version 4.0: A Computer Program for the Inelastic Damage Analysis of Buildings," by R.E. Valles, A.M. Reinhorn, S.K. Kunnath, C. Li and A. Madan, 6/3/96, (PB97-100234, A17, MF-A03).

NCEER-96-0011 "Estimation of the Economic Impact of Multiple Lifeline Disruption: Memphis Light, Gas and Water Division Case Study," by S.E. Chang, H.A. Seligson and R.T. Eguchi, 8/16/96, (PB97-133490, A11, MF-A03).

NCEER-96-0012 "Proceedings from the Sixth Japan-U.S. Workshop on Earthquake Resistant Design of Lifeline Facilities and Countermeasures Against Soil Liquefaction, Edited by M. Hamada and T. O'Rourke, 9/11/96, (PB97-133581, A99, MF-A06).

NCEER-96-0013 "Chemical Hazards, Mitigation and Preparedness in Areas of High Seismic Risk: A Methodology for Estimating the Risk of Post-Earthquake Hazardous Materials Release," by H.A. Seligson, R.T. Eguchi, K.J. Tierney and K. Richmond, 11/7/96, (PB97-133565, MF-A02, A08).

NCEER-96-0014 "Response of Steel Bridge Bearings to Reversed Cyclic Loading," by J.B. Mander, D-K. Kim, S.S. Chen and G.J. Premus, 11/13/96, (PB97-140735, A12, MF-A03).

NCEER-96-0015 "Highway Culvert Performance During Past Earthquakes," by T.L. Youd and C.J. Beckman, 11/25/96, (PB97-133532, A06, MF-A01).

NCEER-97-0001 "Evaluation, Prevention and Mitigation of Pounding Effects in Building Structures," by R.E. Valles and A.M. Reinhorn, 2/20/97, (PB97-159552, A14, MF-A03).

NCEER-97-0002 "Seismic Design Criteria for Bridges and Other Highway Structures," by C. Rojahn, R. Mayes, D.G. Anderson, J. Clark, J.H. Hom, R.V. Nutt and M.J. O'Rourke, 4/30/97, (PB97-194658, A06, MF-A03).

NCEER-97-0003 “Proceedings of the U.S.-Italian Workshop on Seismic Evaluation and Retrofit,” Edited by D.P. Abrams and G.M. Calvi, 3/19/97, (PB97-194666, A13, MF-A03).

NCEER-97-0004 "Investigation of Seismic Response of Buildings with Linear and Nonlinear Fluid Viscous Dampers," by A.A. Seleemah and M.C. Constantinou, 5/21/97, (PB98-109002, A15, MF-A03).

NCEER-97-0005 "Proceedings of the Workshop on Earthquake Engineering Frontiers in Transportation Facilities," edited by G.C. Lee and I.M. Friedland, 8/29/97, (PB98-128911, A25, MR-A04).

NCEER-97-0006 "Cumulative Seismic Damage of Reinforced Concrete Bridge Piers," by S.K. Kunnath, A. El-Bahy, A. Taylor and W. Stone, 9/2/97, (PB98-108814, A11, MF-A03).

NCEER-97-0007 "Structural Details to Accommodate Seismic Movements of Highway Bridges and Retaining Walls," by R.A. Imbsen, R.A. Schamber, E. Thorkildsen, A. Kartoum, B.T. Martin, T.N. Rosser and J.M. Kulicki, 9/3/97, (PB98-108996, A09, MF-A02).

NCEER-97-0008 "A Method for Earthquake Motion-Damage Relationships with Application to Reinforced Concrete Frames," by A. Singhal and A.S. Kiremidjian, 9/10/97, (PB98-108988, A13, MF-A03).

NCEER-97-0009 "Seismic Analysis and Design of Bridge Abutments Considering Sliding and Rotation," by K. Fishman and R. Richards, Jr., 9/15/97, (PB98-108897, A06, MF-A02).

NCEER-97-0010 "Proceedings of the FHWA/NCEER Workshop on the National Representation of Seismic Ground Motion for New and Existing Highway Facilities," edited by I.M. Friedland, M.S. Power and R.L. Mayes, 9/22/97, (PB98-128903, A21, MF-A04).

NCEER-97-0011 "Seismic Analysis for Design or Retrofit of Gravity Bridge Abutments," by K.L. Fishman, R. Richards, Jr. and R.C. Divito, 10/2/97, (PB98-128937, A08, MF-A02).

NCEER-97-0012 "Evaluation of Simplified Methods of Analysis for Yielding Structures," by P. Tsopelas, M.C. Constantinou, C.A. Kircher and A.S. Whittaker, 10/31/97, (PB98-128929, A10, MF-A03).

NCEER-97-0013 "Seismic Design of Bridge Columns Based on Control and Repairability of Damage," by C-T. Cheng and J.B. Mander, 12/8/97, (PB98-144249, A11, MF-A03).

NCEER-97-0014 "Seismic Resistance of Bridge Piers Based on Damage Avoidance Design," by J.B. Mander and C-T. Cheng, 12/10/97, (PB98-144223, A09, MF-A02).

NCEER-97-0015 “Seismic Response of Nominally Symmetric Systems with Strength Uncertainty,” by S. Balopoulou and M. Grigoriu, 12/23/97, (PB98-153422, A11, MF-A03).

NCEER-97-0016 “Evaluation of Seismic Retrofit Methods for Reinforced Concrete Bridge Columns,” by T.J. Wipf, F.W. Klaiber and F.M. Russo, 12/28/97, (PB98-144215, A12, MF-A03).

NCEER-97-0017 “Seismic Fragility of Existing Conventional Reinforced Concrete Highway Bridges,” by C.L. Mullen and A.S. Cakmak, 12/30/97, (PB98-153406, A08, MF-A02).

NCEER-97-0018 “Loss Asssessment of Memphis Buildings,” edited by D.P. Abrams and M. Shinozuka, 12/31/97, (PB98-144231, A13, MF-A03).

NCEER-97-0019 “Seismic Evaluation of Frames with Infill Walls Using Quasi-static Experiments,” by K.M. Mosalam, R.N. White and P. Gergely, 12/31/97, (PB98-153455, A07, MF-A02).

NCEER-97-0020 “Seismic Evaluation of Frames with Infill Walls Using Pseudo-dynamic Experiments,” by K.M. Mosalam, R.N. White and P. Gergely, 12/31/97, (PB98-153430, A07, MF-A02).

NCEER-97-0021 “Computational Strategies for Frames with Infill Walls: Discrete and Smeared Crack Analyses and Seismic Fragility,” by K.M. Mosalam, R.N. White and P. Gergely, 12/31/97, (PB98-153414, A10, MF-A02).

NCEER-97-0022 "Proceedings of the NCEER Workshop on Evaluation of Liquefaction Resistance of Soils," edited by T.L. Youd and I.M. Idriss, 12/31/97, (PB98-155617, A15, MF-A03).

MCEER-98-0001 "Extraction of Nonlinear Hysteretic Properties of Seismically Isolated Bridges from Quick-Release Field Tests," by Q. Chen, B.M. Douglas, E.M. Maragakis and I.G. Buckle, 5/26/98, (PB99-118838, A06, MF-A01).

MCEER-98-0002 "Methodologies for Evaluating the Importance of Highway Bridges," by A. Thomas, S. Eshenaur and J. Kulicki, 5/29/98, (PB99-118846, A10, MF-A02).

MCEER-98-0003 "Capacity Design of Bridge Piers and the Analysis of Overstrength," by J.B. Mander, A. Dutta and P. Goel, 6/1/98, (PB99-118853, A09, MF-A02).

MCEER-98-0004 "Evaluation of Bridge Damage Data from the Loma Prieta and Northridge, California Earthquakes," by N. Basoz and A. Kiremidjian, 6/2/98, (PB99-118861, A15, MF-A03).

MCEER-98-0005 "Screening Guide for Rapid Assessment of Liquefaction Hazard at Highway Bridge Sites," by T. L. Youd, 6/16/98, (PB99-118879, A06, not available on microfiche).

MCEER-98-0006 "Structural Steel and Steel/Concrete Interface Details for Bridges," by P. Ritchie, N. Kauhl and J. Kulicki, 7/13/98, (PB99-118945, A06, MF-A01).

MCEER-98-0007 "Capacity Design and Fatigue Analysis of Confined Concrete Columns," by A. Dutta and J.B. Mander, 7/14/98, (PB99-118960, A14, MF-A03).

MCEER-98-0008 "Proceedings of the Workshop on Performance Criteria for Telecommunication Services Under Earthquake Conditions," edited by A.J. Schiff, 7/15/98, (PB99-118952, A08, MF-A02).

MCEER-98-0009 "Fatigue Analysis of Unconfined Concrete Columns," by J.B. Mander, A. Dutta and J.H. Kim, 9/12/98, (PB99-123655, A10, MF-A02).

MCEER-98-0010 "Centrifuge Modeling of Cyclic Lateral Response of Pile-Cap Systems and Seat-Type Abutments in Dry Sands," by A.D. Gadre and R. Dobry, 10/2/98, (PB99-123606, A13, MF-A03).

MCEER-98-0011 "IDARC-BRIDGE: A Computational Platform for Seismic Damage Assessment of Bridge Structures," by A.M. Reinhorn, V. Simeonov, G. Mylonakis and Y. Reichman, 10/2/98, (PB99-162919, A15, MF-A03).

MCEER-98-0012 "Experimental Investigation of the Dynamic Response of Two Bridges Before and After Retrofitting with Elastomeric Bearings," by D.A. Wendichansky, S.S. Chen and J.B. Mander, 10/2/98, (PB99-162927, A15, MF-A03).

MCEER-98-0013 "Design Procedures for Hinge Restrainers and Hinge Sear Width for Multiple-Frame Bridges," by R. Des Roches and G.L. Fenves, 11/3/98, (PB99-140477, A13, MF-A03).

MCEER-98-0014 "Response Modification Factors for Seismically Isolated Bridges," by M.C. Constantinou and J.K. Quarshie, 11/3/98, (PB99-140485, A14, MF-A03).

MCEER-98-0015 "Proceedings of the U.S.-Italy Workshop on Seismic Protective Systems for Bridges," edited by I.M. Friedland and M.C. Constantinou, 11/3/98, (PB2000-101711, A22, MF-A04).

MCEER-98-0016 "Appropriate Seismic Reliability for Critical Equipment Systems: Recommendations Based on Regional Analysis of Financial and Life Loss," by K. Porter, C. Scawthorn, C. Taylor and N. Blais, 11/10/98, (PB99-157265, A08, MF-A02).

MCEER-98-0017 "Proceedings of the U.S. Japan Joint Seminar on Civil Infrastructure Systems Research," edited by M. Shinozuka and A. Rose, 11/12/98, (PB99-156713, A16, MF-A03).

MCEER-98-0018 "Modeling of Pile Footings and Drilled Shafts for Seismic Design," by I. PoLam, M. Kapuskar and D. Chaudhuri, 12/21/98, (PB99-157257, A09, MF-A02).

MCEER-99-0001 "Seismic Evaluation of a Masonry Infilled Reinforced Concrete Frame by Pseudodynamic Testing," by S.G. Buonopane and R.N. White, 2/16/99, (PB99-162851, A09, MF-A02).

MCEER-99-0002 "Response History Analysis of Structures with Seismic Isolation and Energy Dissipation Systems: Verification Examples for Program SAP2000," by J. Scheller and M.C. Constantinou, 2/22/99, (PB99-162869, A08, MF-A02).

MCEER-99-0003 "Experimental Study on the Seismic Design and Retrofit of Bridge Columns Including Axial Load Effects," by A. Dutta, T. Kokorina and J.B. Mander, 2/22/99, (PB99-162877, A09, MF-A02).

MCEER-99-0004 "Experimental Study of Bridge Elastomeric and Other Isolation and Energy Dissipation Systems with Emphasis on Uplift Prevention and High Velocity Near-source Seismic Excitation," by A. Kasalanati and M. C. Constantinou, 2/26/99, (PB99-162885, A12, MF-A03).

MCEER-99-0005 "Truss Modeling of Reinforced Concrete Shear-flexure Behavior," by J.H. Kim and J.B. Mander, 3/8/99, (PB99-163693, A12, MF-A03).

MCEER-99-0006 "Experimental Investigation and Computational Modeling of Seismic Response of a 1:4 Scale Model Steel Structure with a Load Balancing Supplemental Damping System," by G. Pekcan, J.B. Mander and S.S. Chen, 4/2/99, (PB99-162893, A11, MF-A03).

MCEER-99-0007 "Effect of Vertical Ground Motions on the Structural Response of Highway Bridges," by M.R. Button, C.J. Cronin and R.L. Mayes, 4/10/99, (PB2000-101411, A10, MF-A03).

MCEER-99-0008 "Seismic Reliability Assessment of Critical Facilities: A Handbook, Supporting Documentation, and Model Code Provisions," by G.S. Johnson, R.E. Sheppard, M.D. Quilici, S.J. Eder and C.R. Scawthorn, 4/12/99, (PB2000-101701, A18, MF-A04).

MCEER-99-0009 "Impact Assessment of Selected MCEER Highway Project Research on the Seismic Design of Highway Structures," by C. Rojahn, R. Mayes, D.G. Anderson, J.H. Clark, D'Appolonia Engineering, S. Gloyd and R.V. Nutt, 4/14/99, (PB99-162901, A10, MF-A02).

MCEER-99-0010 "Site Factors and Site Categories in Seismic Codes," by R. Dobry, R. Ramos and M.S. Power, 7/19/99, (PB2000-101705, A08, MF-A02).

MCEER-99-0011 "Restrainer Design Procedures for Multi-Span Simply-Supported Bridges," by M.J. Randall, M. Saiidi, E. Maragakis and T. Isakovic, 7/20/99, (PB2000-101702, A10, MF-A02).

MCEER-99-0012 "Property Modification Factors for Seismic Isolation Bearings," by M.C. Constantinou, P. Tsopelas, A. Kasalanati and E. Wolff, 7/20/99, (PB2000-103387, A11, MF-A03).

MCEER-99-0013 "Critical Seismic Issues for Existing Steel Bridges," by P. Ritchie, N. Kauhl and J. Kulicki, 7/20/99, (PB2000-101697, A09, MF-A02).

MCEER-99-0014 "Nonstructural Damage Database," by A. Kao, T.T. Soong and A. Vender, 7/24/99, (PB2000-101407, A06, MF-A01).

MCEER-99-0015 "Guide to Remedial Measures for Liquefaction Mitigation at Existing Highway Bridge Sites," by H.G. Cooke and J. K. Mitchell, 7/26/99, (PB2000-101703, A11, MF-A03).

MCEER-99-0016 "Proceedings of the MCEER Workshop on Ground Motion Methodologies for the Eastern United States," edited by N. Abrahamson and A. Becker, 8/11/99, (PB2000-103385, A07, MF-A02).

MCEER-99-0017 "Quindío, Colombia Earthquake of January 25, 1999: Reconnaissance Report," by A.P. Asfura and P.J. Flores, 10/4/99, (PB2000-106893, A06, MF-A01).

MCEER-99-0018 "Hysteretic Models for Cyclic Behavior of Deteriorating Inelastic Structures," by M.V. Sivaselvan and A.M. Reinhorn, 11/5/99, (PB2000-103386, A08, MF-A02).

MCEER-99-0019 "Proceedings of the 7th U.S.- Japan Workshop on Earthquake Resistant Design of Lifeline Facilities and Countermeasures Against Soil Liquefaction," edited by T.D. O'Rourke, J.P. Bardet and M. Hamada, 11/19/99, (PB2000-103354, A99, MF-A06).

MCEER-99-0020 "Development of Measurement Capability for Micro-Vibration Evaluations with Application to Chip Fabrication Facilities," by G.C. Lee, Z. Liang, J.W. Song, J.D. Shen and W.C. Liu, 12/1/99, (PB2000-105993, A08, MF-A02).

MCEER-99-0021 "Design and Retrofit Methodology for Building Structures with Supplemental Energy Dissipating Systems," by G. Pekcan, J.B. Mander and S.S. Chen, 12/31/99, (PB2000-105994, A11, MF-A03).

MCEER-00-0001 "The Marmara, Turkey Earthquake of August 17, 1999: Reconnaissance Report," edited by C. Scawthorn; with major contributions by M. Bruneau, R. Eguchi, T. Holzer, G. Johnson, J. Mander, J. Mitchell, W. Mitchell, A. Papageorgiou, C. Scaethorn, and G. Webb, 3/23/00, (PB2000-106200, A11, MF-A03).

MCEER-00-0002 "Proceedings of the MCEER Workshop for Seismic Hazard Mitigation of Health Care Facilities," edited by G.C. Lee, M. Ettouney, M. Grigoriu, J. Hauer and J. Nigg, 3/29/00, (PB2000-106892, A08, MF-A02).

MCEER-00-0003 "The Chi-Chi, Taiwan Earthquake of September 21, 1999: Reconnaissance Report," edited by G.C. Lee and C.H. Loh, with major contributions by G.C. Lee, M. Bruneau, I.G. Buckle, S.E. Chang, P.J. Flores, T.D. O'Rourke, M. Shinozuka, T.T. Soong, C-H. Loh, K-C. Chang, Z-J. Chen, J-S. Hwang, M-L. Lin, G-Y. Liu, K-C. Tsai, G.C. Yao and C-L. Yen, 4/30/00, (PB2001-100980, A10, MF-A02).

MCEER-00-0004 "Seismic Retrofit of End-Sway Frames of Steel Deck-Truss Bridges with a Supplemental Tendon System: Experimental and Analytical Investigation," by G. Pekcan, J.B. Mander and S.S. Chen, 7/1/00, (PB2001-100982, A10, MF-A02).

MCEER-00-0005 "Sliding Fragility of Unrestrained Equipment in Critical Facilities," by W.H. Chong and T.T. Soong, 7/5/00, (PB2001-100983, A08, MF-A02).

MCEER-00-0006 "Seismic Response of Reinforced Concrete Bridge Pier Walls in the Weak Direction," by N. Abo-Shadi, M. Saiidi and D. Sanders, 7/17/00, (PB2001-100981, A17, MF-A03).

MCEER-00-0007 "Low-Cycle Fatigue Behavior of Longitudinal Reinforcement in Reinforced Concrete Bridge Columns," by J. Brown and S.K. Kunnath, 7/23/00, (PB2001-104392, A08, MF-A02).

MCEER-00-0008 "Soil Structure Interaction of Bridges for Seismic Analysis," I. PoLam and H. Law, 9/25/00, (PB2001-105397, A08, MF-A02).

MCEER-00-0009 "Proceedings of the First MCEER Workshop on Mitigation of Earthquake Disaster by Advanced Technologies (MEDAT-1), edited by M. Shinozuka, D.J. Inman and T.D. O'Rourke, 11/10/00, (PB2001-105399, A14, MF-A03).

MCEER-00-0010 "Development and Evaluation of Simplified Procedures for Analysis and Design of Buildings with Passive Energy Dissipation Systems, Revision 01," by O.M. Ramirez, M.C. Constantinou, C.A. Kircher, A.S. Whittaker, M.W. Johnson, J.D. Gomez and C. Chrysostomou, 11/16/01, (PB2001-105523, A23, MF-A04).

MCEER-00-0011 "Dynamic Soil-Foundation-Structure Interaction Analyses of Large Caissons," by C-Y. Chang, C-M. Mok, Z-L. Wang, R. Settgast, F. Waggoner, M.A. Ketchum, H.M. Gonnermann and C-C. Chin, 12/30/00, (PB2001-104373, A07, MF-A02).

MCEER-00-0012 "Experimental Evaluation of Seismic Performance of Bridge Restrainers," by A.G. Vlassis, E.M. Maragakis and M. Saiid Saiidi, 12/30/00, (PB2001-104354, A09, MF-A02).

MCEER-00-0013 "Effect of Spatial Variation of Ground Motion on Highway Structures," by M. Shinozuka, V. Saxena and G. Deodatis, 12/31/00, (PB2001-108755, A13, MF-A03).

MCEER-00-0014 "A Risk-Based Methodology for Assessing the Seismic Performance of Highway Systems," by S.D. Werner, C.E. Taylor, J.E. Moore, II, J.S. Walton and S. Cho, 12/31/00, (PB2001-108756, A14, MF-A03).

MCEER-01-0001 "Experimental Investigation of P-Delta Effects to Collapse During Earthquakes," by D. Vian and M. Bruneau, 6/25/01, (PB2002-100534, A17, MF-A03).

MCEER-01-0002 "Proceedings of the Second MCEER Workshop on Mitigation of Earthquake Disaster by Advanced Technologies (MEDAT-2)," edited by M. Bruneau and D.J. Inman, 7/23/01, (PB2002-100434, A16, MF-A03).

MCEER-01-0003 "Sensitivity Analysis of Dynamic Systems Subjected to Seismic Loads," by C. Roth and M. Grigoriu, 9/18/01, (PB2003-100884, A12, MF-A03).

MCEER-01-0004 "Overcoming Obstacles to Implementing Earthquake Hazard Mitigation Policies: Stage 1 Report," by D.J. Alesch and W.J. Petak, 12/17/01, (PB2002-107949, A07, MF-A02).

MCEER-01-0005 "Updating Real-Time Earthquake Loss Estimates: Methods, Problems and Insights," by C.E. Taylor, S.E. Chang and R.T. Eguchi, 12/17/01, (PB2002-107948, A05, MF-A01).

MCEER-01-0006 "Experimental Investigation and Retrofit of Steel Pile Foundations and Pile Bents Under Cyclic Lateral Loadings," by A. Shama, J. Mander, B. Blabac and S. Chen, 12/31/01, (PB2002-107950, A13, MF-A03).

MCEER-02-0001 "Assessment of Performance of Bolu Viaduct in the 1999 Duzce Earthquake in Turkey" by P.C. Roussis, M.C. Constantinou, M. Erdik, E. Durukal and M. Dicleli, 5/8/02, (PB2003-100883, A08, MF-A02).

MCEER-02-0002 "Seismic Behavior of Rail Counterweight Systems of Elevators in Buildings," by M.P. Singh, Rildova and L.E. Suarez, 5/27/02. (PB2003-100882, A11, MF-A03).

MCEER-02-0003 "Development of Analysis and Design Procedures for Spread Footings," by G. Mylonakis, G. Gazetas, S. Nikolaou and A. Chauncey, 10/02/02, (PB2004-101636, A13, MF-A03, CD-A13).

MCEER-02-0004 "Bare-Earth Algorithms for Use with SAR and LIDAR Digital Elevation Models," by C.K. Huyck, R.T. Eguchi and B. Houshmand, 10/16/02, (PB2004-101637, A07, CD-A07).

MCEER-02-0005 "Review of Energy Dissipation of Compression Members in Concentrically Braced Frames," by K.Lee and M. Bruneau, 10/18/02, (PB2004-101638, A10, CD-A10).

MCEER-03-0001 "Experimental Investigation of Light-Gauge Steel Plate Shear Walls for the Seismic Retrofit of Buildings" by J. Berman and M. Bruneau, 5/2/03, (PB2004-101622, A10, MF-A03, CD-A10).

MCEER-03-0002 "Statistical Analysis of Fragility Curves," by M. Shinozuka, M.Q. Feng, H. Kim, T. Uzawa and T. Ueda, 6/16/03, (PB2004-101849, A09, CD-A09).

MCEER-03-0003 "Proceedings of the Eighth U.S.-Japan Workshop on Earthquake Resistant Design f Lifeline Facilities and Countermeasures Against Liquefaction," edited by M. Hamada, J.P. Bardet and T.D. O'Rourke, 6/30/03, (PB2004-104386, A99, CD-A99).

MCEER-03-0004 "Proceedings of the PRC-US Workshop on Seismic Analysis and Design of Special Bridges," edited by L.C. Fan and G.C. Lee, 7/15/03, (PB2004-104387, A14, CD-A14).

MCEER-03-0005 "Urban Disaster Recovery: A Framework and Simulation Model," by S.B. Miles and S.E. Chang, 7/25/03, (PB2004-104388, A07, CD-A07).

MCEER-03-0006 "Behavior of Underground Piping Joints Due to Static and Dynamic Loading," by R.D. Meis, M. Maragakis and R. Siddharthan, 11/17/03, (PB2005-102194, A13, MF-A03, CD-A00).

MCEER-04-0001 "Experimental Study of Seismic Isolation Systems with Emphasis on Secondary System Response and Verification of Accuracy of Dynamic Response History Analysis Methods," by E. Wolff and M. Constantinou, 1/16/04 (PB2005-102195, A99, MF-E08, CD-A00).

MCEER-04-0002 "Tension, Compression and Cyclic Testing of Engineered Cementitious Composite Materials," by K. Kesner and S.L. Billington, 3/1/04, (PB2005-102196, A08, CD-A08).

MCEER-04-0003 "Cyclic Testing of Braces Laterally Restrained by Steel Studs to Enhance Performance During Earthquakes," by O.C. Celik, J.W. Berman and M. Bruneau, 3/16/04, (PB2005-102197, A13, MF-A03, CD-A00).

MCEER-04-0004 "Methodologies for Post Earthquake Building Damage Detection Using SAR and Optical Remote Sensing: Application to the August 17, 1999 Marmara, Turkey Earthquake," by C.K. Huyck, B.J. Adams, S. Cho, R.T. Eguchi, B. Mansouri and B. Houshmand, 6/15/04, (PB2005-104888, A10, CD-A00).

MCEER-04-0005 "Nonlinear Structural Analysis Towards Collapse Simulation: A Dynamical Systems Approach," by M.V. Sivaselvan and A.M. Reinhorn, 6/16/04, (PB2005-104889, A11, MF-A03, CD-A00).

MCEER-04-0006 "Proceedings of the Second PRC-US Workshop on Seismic Analysis and Design of Special Bridges," edited by G.C. Lee and L.C. Fan, 6/25/04, (PB2005-104890, A16, CD-A00).

MCEER-04-0007 "Seismic Vulnerability Evaluation of Axially Loaded Steel Built-up Laced Members," by K. Lee and M. Bruneau, 6/30/04, (PB2005-104891, A16, CD-A00).

MCEER-04-0008 "Evaluation of Accuracy of Simplified Methods of Analysis and Design of Buildings with Damping Systems for Near-Fault and for Soft-Soil Seismic Motions," by E.A. Pavlou and M.C. Constantinou, 8/16/04, (PB2005-104892, A08, MF-A02, CD-A00).

MCEER-04-0009 "Assessment of Geotechnical Issues in Acute Care Facilities in California," by M. Lew, T.D. O'Rourke, R. Dobry and M. Koch, 9/15/04, (PB2005-104893, A08, CD-A00).

MCEER-04-0010 "Scissor-Jack-Damper Energy Dissipation System," by A.N. Sigaher-Boyle and M.C. Constantinou, 12/1/04 (PB2005-108221).

MCEER-04-0011 "Seismic Retrofit of Bridge Steel Truss Piers Using a Controlled Rocking Approach," by M. Pollino and M. Bruneau, 12/20/04 (PB2006-105795).

MCEER-05-0001 "Experimental and Analytical Studies of Structures Seismically Isolated with an Uplift-Restraint Isolation System," by P.C. Roussis and M.C. Constantinou, 1/10/05 (PB2005-108222).

MCEER-05-0002 "A Versatile Experimentation Model for Study of Structures Near Collapse Applied to Seismic Evaluation of Irregular Structures," by D. Kusumastuti, A.M. Reinhorn and A. Rutenberg, 3/31/05 (PB2006-101523).

MCEER-05-0003 "Proceedings of the Third PRC-US Workshop on Seismic Analysis and Design of Special Bridges," edited by L.C. Fan and G.C. Lee, 4/20/05, (PB2006-105796).

MCEER-05-0004 "Approaches for the Seismic Retrofit of Braced Steel Bridge Piers and Proof-of-Concept Testing of an Eccentrically Braced Frame with Tubular Link," by J.W. Berman and M. Bruneau, 4/21/05 (PB2006-101524).

MCEER-05-0005 "Simulation of Strong Ground Motions for Seismic Fragility Evaluation of Nonstructural Components in Hospitals," by A. Wanitkorkul and A. Filiatrault, 5/26/05 (PB2006-500027).

MCEER-05-0006 "Seismic Safety in California Hospitals: Assessing an Attempt to Accelerate the Replacement or Seismic Retrofit of Older Hospital Facilities," by D.J. Alesch, L.A. Arendt and W.J. Petak, 6/6/05 (PB2006-105794).

MCEER-05-0007 "Development of Seismic Strengthening and Retrofit Strategies for Critical Facilities Using Engineered Cementitious Composite Materials," by K. Kesner and S.L. Billington, 8/29/05 (PB2006-111701).

MCEER-05-0008 "Experimental and Analytical Studies of Base Isolation Systems for Seismic Protection of Power Transformers," by N. Murota, M.Q. Feng and G-Y. Liu, 9/30/05 (PB2006-111702).

MCEER-05-0009 "3D-BASIS-ME-MB: Computer Program for Nonlinear Dynamic Analysis of Seismically Isolated Structures," by P.C. Tsopelas, P.C. Roussis, M.C. Constantinou, R. Buchanan and A.M. Reinhorn, 10/3/05 (PB2006-111703).

MCEER-05-0010 "Steel Plate Shear Walls for Seismic Design and Retrofit of Building Structures," by D. Vian and M. Bruneau, 12/15/05 (PB2006-111704).

MCEER-05-0011 "The Performance-Based Design Paradigm," by M.J. Astrella and A. Whittaker, 12/15/05 (PB2006-111705).

MCEER-06-0001 "Seismic Fragility of Suspended Ceiling Systems," H. Badillo-Almaraz, A.S. Whittaker, A.M. Reinhorn and G.P. Cimellaro, 2/4/06 (PB2006-111706).

MCEER-06-0002 "Multi-Dimensional Fragility of Structures," by G.P. Cimellaro, A.M. Reinhorn and M. Bruneau, 3/1/06 (PB2007-106974, A09, MF-A02, CD A00).

MCEER-06-0003 "Built-Up Shear Links as Energy Dissipators for Seismic Protection of Bridges," by P. Dusicka, A.M. Itani and I.G. Buckle, 3/15/06 (PB2006-111708).

MCEER-06-0004 "Analytical Investigation of the Structural Fuse Concept," by R.E. Vargas and M. Bruneau, 3/16/06 (PB2006-111709).

MCEER-06-0005 "Experimental Investigation of the Structural Fuse Concept," by R.E. Vargas and M. Bruneau, 3/17/06 (PB2006-111710).

MCEER-06-0006 "Further Development of Tubular Eccentrically Braced Frame Links for the Seismic Retrofit of Braced Steel Truss Bridge Piers," by J.W. Berman and M. Bruneau, 3/27/06 (PB2007-105147).

MCEER-06-0007 "REDARS Validation Report," by S. Cho, C.K. Huyck, S. Ghosh and R.T. Eguchi, 8/8/06 (PB2007-106983).

MCEER-06-0008 "Review of Current NDE Technologies for Post-Earthquake Assessment of Retrofitted Bridge Columns," by J.W. Song, Z. Liang and G.C. Lee, 8/21/06 (PB2007-106984).

MCEER-06-0009 "Liquefaction Remediation in Silty Soils Using Dynamic Compaction and Stone Columns," by S. Thevanayagam, G.R. Martin, R. Nashed, T. Shenthan, T. Kanagalingam and N. Ecemis, 8/28/06 (PB2007-106985).

MCEER-06-0010 "Conceptual Design and Experimental Investigation of Polymer Matrix Composite Infill Panels for Seismic Retrofitting," by W. Jung, M. Chiewanichakorn and A.J. Aref, 9/21/06 (PB2007-106986).

MCEER-06-0011 "A Study of the Coupled Horizontal-Vertical Behavior of Elastomeric and Lead-Rubber Seismic Isolation Bearings," by G.P. Warn and A.S. Whittaker, 9/22/06 (PB2007-108679).

MCEER-06-0012 "Proceedings of the Fourth PRC-US Workshop on Seismic Analysis and Design of Special Bridges: Advancing Bridge Technologies in Research, Design, Construction and Preservation," Edited by L.C. Fan, G.C. Lee and L. Ziang, 10/12/06 (PB2007-109042).

MCEER-06-0013 "Cyclic Response and Low Cycle Fatigue Characteristics of Plate Steels," by P. Dusicka, A.M. Itani and I.G. Buckle, 11/1/06 06 (PB2007-106987).

MCEER-06-0014 "Proceedings of the Second US-Taiwan Bridge Engineering Workshop," edited by W.P. Yen, J. Shen, J-Y. Chen and M. Wang, 11/15/06 (PB2008-500041).

MCEER-06-0015 "User Manual and Technical Documentation for the REDARS^{TM} Import Wizard," by S. Cho, S. Ghosh, C.K. Huyck and S.D. Werner, 11/30/06 (PB2007-114766).

MCEER-06-0016 "Hazard Mitigation Strategy and Monitoring Technologies for Urban and Infrastructure Public Buildings: Proceedings of the China-US Workshops," edited by X.Y. Zhou, A.L. Zhang, G.C. Lee and M. Tong, 12/12/06 (PB2008-500018).

MCEER-07-0001 "Static and Kinetic Coefficients of Friction for Rigid Blocks," by C. Kafali, S. Fathali, M. Grigoriu and A.S. Whittaker, 3/20/07 (PB2007-114767).

MCEER-07-0002 "Hazard Mitigation Investment Decision Making: Organizational Response to Legislative Mandate," by L.A. Arendt, D.J. Alesch and W.J. Petak, 4/9/07 (PB2007-114768).

MCEER-07-0003 "Seismic Behavior of Bidirectional-Resistant Ductile End Diaphragms with Unbonded Braces in Straight or Skewed Steel Bridges," by O. Celik and M. Bruneau, 4/11/07 (PB2008-105141).

MCEER-07-0004 "Modeling Pile Behavior in Large Pile Groups Under Lateral Loading," by A.M. Dodds and G.R. Martin, 4/16/07(PB2008-105142).

MCEER-07-0005 "Experimental Investigation of Blast Performance of Seismically Resistant Concrete-Filled Steel Tube Bridge Piers," by S. Fujikura, M. Bruneau and D. Lopez-Garcia, 4/20/07 (PB2008-105143).

MCEER-07-0006 "Seismic Analysis of Conventional and Isolated Liquefied Natural Gas Tanks Using Mechanical Analogs," by I.P. Christovasilis and A.S. Whittaker, 5/1/07, not available.

MCEER-07-0007 "Experimental Seismic Performance Evaluation of Isolation/Restraint Systems for Mechanical Equipment – Part 1: Heavy Equipment Study," by S. Fathali and A. Filiatrault, 6/6/07 (PB2008-105144).

MCEER-07-0008 "Seismic Vulnerability of Timber Bridges and Timber Substructures," by A.A. Sharma, J.B. Mander, I.M. Friedland and D.R. Allicock, 6/7/07 (PB2008-105145).

MCEER-07-0009 "Experimental and Analytical Study of the XY-Friction Pendulum (XY-FP) Bearing for Bridge Applications," by C.C. Marin-Artieda, A.S. Whittaker and M.C. Constantinou, 6/7/07 (PB2008-105191).

MCEER-07-0010 "Proceedings of the PRC-US Earthquake Engineering Forum for Young Researchers," Edited by G.C. Lee and X.Z. Qi, 6/8/07 (PB2008-500058).

MCEER-07-0011 "Design Recommendations for Perforated Steel Plate Shear Walls," by R. Purba and M. Bruneau, 6/18/07, (PB2008-105192).

MCEER-07-0012 "Performance of Seismic Isolation Hardware Under Service and Seismic Loading," by M.C. Constantinou, A.S. Whittaker, Y. Kalpakidis, D.M. Fenz and G.P. Warn, 8/27/07, (PB2008-105193).

MCEER-07-0013 "Experimental Evaluation of the Seismic Performance of Hospital Piping Subassemblies," by E.R. Goodwin, E. Maragakis and A.M. Itani, 9/4/07, (PB2008-105194).

MCEER-07-0014 "A Simulation Model of Urban Disaster Recovery and Resilience: Implementation for the 1994 Northridge Earthquake," by S. Miles and S.E. Chang, 9/7/07, (PB2008-106426).

MCEER-07-0015 "Statistical and Mechanistic Fragility Analysis of Concrete Bridges," by M. Shinozuka, S. Banerjee and S-H. Kim, 9/10/07, (PB2008-106427).

MCEER-07-0016 "Three-Dimensional Modeling of Inelastic Buckling in Frame Structures," by M. Schachter and AM. Reinhorn, 9/13/07, (PB2008-108125).

MCEER-07-0017 "Modeling of Seismic Wave Scattering on Pile Groups and Caissons," by I. Po Lam, H. Law and C.T. Yang, 9/17/07 (PB2008-108150).

MCEER-07-0018 "Bridge Foundations: Modeling Large Pile Groups and Caissons for Seismic Design," by I. Po Lam, H. Law and G.R. Martin (Coordinating Author), 12/1/07 (PB2008-111190).

MCEER-07-0019 "Principles and Performance of Roller Seismic Isolation Bearings for Highway Bridges," by G.C. Lee, Y.C. Ou, Z. Liang, T.C. Niu and J. Song, 12/10/07 (PB2009-110466).

MCEER-07-0020 "Centrifuge Modeling of Permeability and Pinning Reinforcement Effects on Pile Response to Lateral Spreading," by L.L Gonzalez-Lagos, T. Abdoun and R. Dobry, 12/10/07 (PB2008-111191).

MCEER-07-0021 "Damage to the Highway System from the Pisco, Perú Earthquake of August 15, 2007," by J.S. O'Connor, L. Mesa and M. Nykamp, 12/10/07, (PB2008-108126).

MCEER-07-0022 "Experimental Seismic Performance Evaluation of Isolation/Restraint Systems for Mechanical Equipment – Part 2: Light Equipment Study," by S. Fathali and A. Filiatrault, 12/13/07 (PB2008-111192).

MCEER-07-0023 "Fragility Considerations in Highway Bridge Design," by M. Shinozuka, S. Banerjee and S.H. Kim, 12/14/07 (PB2008-111193).

MCEER-07-0024 "Performance Estimates for Seismically Isolated Bridges," by G.P. Warn and A.S. Whittaker, 12/30/07 (PB2008-112230).

MCEER-08-0001 "Seismic Performance of Steel Girder Bridge Superstructures with Conventional Cross Frames," by L.P. Carden, A.M. Itani and I.G. Buckle, 1/7/08, (PB2008-112231).

MCEER-08-0002 "Seismic Performance of Steel Girder Bridge Superstructures with Ductile End Cross Frames with Seismic Isolators," by L.P. Carden, A.M. Itani and I.G. Buckle, 1/7/08 (PB2008-112232).

MCEER-08-0003 "Analytical and Experimental Investigation of a Controlled Rocking Approach for Seismic Protection of Bridge Steel Truss Piers," by M. Pollino and M. Bruneau, 1/21/08 (PB2008-112233).

MCEER-08-0004 "Linking Lifeline Infrastructure Performance and Community Disaster Resilience: Models and Multi-Stakeholder Processes," by S.E. Chang, C. Pasion, K. Tatebe and R. Ahmad, 3/3/08 (PB2008-112234).

MCEER-08-0005 "Modal Analysis of Generally Damped Linear Structures Subjected to Seismic Excitations," by J. Song, Y-L. Chu, Z. Liang and G.C. Lee, 3/4/08 (PB2009-102311).

MCEER-08-0006 "System Performance Under Multi-Hazard Environments," by C. Kafali and M. Grigoriu, 3/4/08 (PB2008-112235).

MCEER-08-0007 "Mechanical Behavior of Multi-Spherical Sliding Bearings," by D.M. Fenz and M.C. Constantinou, 3/6/08 (PB2008-112236).

MCEER-08-0008 "Post-Earthquake Restoration of the Los Angeles Water Supply System," by T.H.P. Tabucchi and R.A. Davidson, 3/7/08 (PB2008-112237).

MCEER-08-0009 "Fragility Analysis of Water Supply Systems," by A. Jacobson and M. Grigoriu, 3/10/08 (PB2009-105545).

MCEER-08-0010 "Experimental Investigation of Full-Scale Two-Story Steel Plate Shear Walls with Reduced Beam Section Connections," by B. Qu, M. Bruneau, C-H. Lin and K-C. Tsai, 3/17/08 (PB2009-106368).

MCEER-08-0011 "Seismic Evaluation and Rehabilitation of Critical Components of Electrical Power Systems," S. Ersoy, B. Feizi, A. Ashrafi and M. Ala Saadeghvaziri, 3/17/08 (PB2009-105546).

MCEER-08-0012 "Seismic Behavior and Design of Boundary Frame Members of Steel Plate Shear Walls," by B. Qu and M. Bruneau, 4/26/08 . (PB2009-106744).

MCEER-08-0013 "Development and Appraisal of a Numerical Cyclic Loading Protocol for Quantifying Building System Performance," by A. Filiatrault, A. Wanitkorkul and M. Constantinou, 4/27/08 (PB2009-107906).

MCEER-08-0014 "Structural and Nonstructural Earthquake Design: The Challenge of Integrating Specialty Areas in Designing Complex, Critical Facilities," by W.J. Petak and D.J. Alesch, 4/30/08 (PB2009-107907).

MCEER-08-0015 "Seismic Performance Evaluation of Water Systems," by Y. Wang and T.D. O'Rourke, 5/5/08 (PB2009-107908).

MCEER-08-0016 "Seismic Response Modeling of Water Supply Systems," by P. Shi and T.D. O'Rourke, 5/5/08 (PB2009-107910).

MCEER-08-0017 "Numerical and Experimental Studies of Self-Centering Post-Tensioned Steel Frames," by D. Wang and A. Filiatrault, 5/12/08 (PB2009-110479).

MCEER-08-0018 "Development, Implementation and Verification of Dynamic Analysis Models for Multi-Spherical Sliding Bearings," by D.M. Fenz and M.C. Constantinou, 8/15/08 (PB2009-107911).

MCEER-08-0019 "Performance Assessment of Conventional and Base Isolated Nuclear Power Plants for Earthquake Blast Loadings," by Y.N. Huang, A.S. Whittaker and N. Luco, 10/28/08 (PB2009-107912).

MCEER-08-0020 "Remote Sensing for Resilient Multi-Hazard Disaster Response – Volume I: Introduction to Damage Assessment Methodologies," by B.J. Adams and R.T. Eguchi, 11/17/08 (PB2010-102695).

MCEER-08-0021 "Remote Sensing for Resilient Multi-Hazard Disaster Response – Volume II: Counting the Number of Collapsed Buildings Using an Object-Oriented Analysis: Case Study of the 2003 Bam Earthquake," by L. Gusella, C.K. Huyck and B.J. Adams, 11/17/08 (PB2010-100925).

MCEER-08-0022 "Remote Sensing for Resilient Multi-Hazard Disaster Response – Volume III: Multi-Sensor Image Fusion Techniques for Robust Neighborhood-Scale Urban Damage Assessment," by B.J. Adams and A. McMillan, 11/17/08 (PB2010-100926).

MCEER-08-0023 "Remote Sensing for Resilient Multi-Hazard Disaster Response – Volume IV: A Study of Multi-Temporal and Multi-Resolution SAR Imagery for Post-Katrina Flood Monitoring in New Orleans," by A. McMillan, J.G. Morley, B.J. Adams and S. Chesworth, 11/17/08 (PB2010-100927).

MCEER-08-0024 "Remote Sensing for Resilient Multi-Hazard Disaster Response – Volume V: Integration of Remote Sensing Imagery and VIEWS^{TM} Field Data for Post-Hurricane Charley Building Damage Assessment," by J.A. Womble, K. Mehta and B.J. Adams, 11/17/08 (PB2009-115532).

MCEER-08-0025 "Building Inventory Compilation for Disaster Management: Application of Remote Sensing and Statistical Modeling," by P. Sarabandi, A.S. Kiremidjian, R.T. Eguchi and B. J. Adams, 11/20/08 (PB2009-110484).

MCEER-08-0026 "New Experimental Capabilities and Loading Protocols for Seismic Qualification and Fragility Assessment of Nonstructural Systems," by R. Retamales, G. Mosqueda, A. Filiatrault and A. Reinhorn, 11/24/08 (PB2009-110485).

MCEER-08-0027 "Effects of Heating and Load History on the Behavior of Lead-Rubber Bearings," by I.V. Kalpakidis and M.C. Constantinou, 12/1/08 (PB2009-115533).

MCEER-08-0028 "Experimental and Analytical Investigation of Blast Performance of Seismically Resistant Bridge Piers," by S.Fujikura and M. Bruneau, 12/8/08 (PB2009-115534).

MCEER-08-0029 "Evolutionary Methodology for Aseismic Decision Support," by Y. Hu and G. Dargush, 12/15/08.

MCEER-08-0030 "Development of a Steel Plate Shear Wall Bridge Pier System Conceived from a Multi-Hazard Perspective," by D. Keller and M. Bruneau, 12/19/08 (PB2010-102696).

MCEER-09-0001 "Modal Analysis of Arbitrarily Damped Three-Dimensional Linear Structures Subjected to Seismic Excitations," by Y.L. Chu, J. Song and G.C. Lee, 1/31/09 (PB2010-100922).

MCEER-09-0002 "Air-Blast Effects on Structural Shapes," by G. Ballantyne, A.S. Whittaker, A.J. Aref and G.F. Dargush, 2/2/09 (PB2010-102697).

MCEER-09-0003 "Water Supply Performance During Earthquakes and Extreme Events," by A.L. Bonneau and T.D. O'Rourke, 2/16/09 (PB2010-100923).

MCEER-09-0004 "Generalized Linear (Mixed) Models of Post-Earthquake Ignitions," by R.A. Davidson, 7/20/09 (PB2010-102698).

MCEER-09-0005 "Seismic Testing of a Full-Scale Two-Story Light-Frame Wood Building: NEESWood Benchmark Test," by I.P. Christovasilis, A. Filiatrault and A. Wanitkorkul, 7/22/09 (PB2012-102401).

MCEER-09-0006 "IDARC2D Version 7.0: A Program for the Inelastic Damage Analysis of Structures," by A.M. Reinhorn, H. Roh, M. Sivaselvan, S.K. Kunnath, R.E. Valles, A. Madan, C. Li, R. Lobo and Y.J. Park, 7/28/09 (PB2010-103199).

MCEER-09-0007 "Enhancements to Hospital Resiliency: Improving Emergency Planning for and Response to Hurricanes," by D.B. Hess and L.A. Arendt, 7/30/09 (PB2010-100924).

MCEER-09-0008 "Assessment of Base-Isolated Nuclear Structures for Design and Beyond-Design Basis Earthquake Shaking," by Y.N. Huang, A.S. Whittaker, R.P. Kennedy and R.L. Mayes, 8/20/09 (PB2010-102699).

MCEER-09-0009 "Quantification of Disaster Resilience of Health Care Facilities," by G.P. Cimellaro, C. Fumo, A.M Reinhorn and M. Bruneau, 9/14/09 (PB2010-105384).

MCEER-09-0010 "Performance-Based Assessment and Design of Squat Reinforced Concrete Shear Walls," by C.K. Gulec and A.S. Whittaker, 9/15/09 (PB2010-102700).

MCEER-09-0011 "Proceedings of the Fourth US-Taiwan Bridge Engineering Workshop," edited by W.P. Yen, J.J. Shen, T.M. Lee and R.B. Zheng, 10/27/09 (PB2010-500009).

MCEER-09-0012 "Proceedings of the Special International Workshop on Seismic Connection Details for Segmental Bridge Construction," edited by W. Phillip Yen and George C. Lee, 12/21/09 (PB2012-102402).

MCEER-10-0001 "Direct Displacement Procedure for Performance-Based Seismic Design of Multistory Woodframe Structures," by W. Pang and D. Rosowsky, 4/26/10 (PB2012-102403).

MCEER-10-0002 "Simplified Direct Displacement Design of Six-Story NEESWood Capstone Building and Pre-Test Seismic Performance Assessment," by W. Pang, D. Rosowsky, J. van de Lindt and S. Pei, 5/28/10 (PB2012-102404).

MCEER-10-0003 "Integration of Seismic Protection Systems in Performance-Based Seismic Design of Woodframed Structures," by J.K. Shinde and M.D. Symans, 6/18/10 (PB2012-102405).

MCEER-10-0004 "Modeling and Seismic Evaluation of Nonstructural Components: Testing Frame for Experimental Evaluation of Suspended Ceiling Systems," by A.M. Reinhorn, K.P. Ryu and G. Maddaloni, 6/30/10 (PB2012-102406).

MCEER-10-0005 "Analytical Development and Experimental Validation of a Structural-Fuse Bridge Pier Concept," by S. El-Bahey and M. Bruneau, 10/1/10 (PB2012-102407).

MCEER-10-0006 "A Framework for Defining and Measuring Resilience at the Community Scale: The PEOPLES Resilience Framework," by C.S. Renschler, A.E. Frazier, L.A. Arendt, G.P. Cimellaro, A.M. Reinhorn and M. Bruneau, 10/8/10 (PB2012-102408).

MCEER-10-0007 "Impact of Horizontal Boundary Elements Design on Seismic Behavior of Steel Plate Shear Walls," by R. Purba and M. Bruneau, 11/14/10 (PB2012-102409).

MCEER-10-0008 "Seismic Testing of a Full-Scale Mid-Rise Building: The NEESWood Capstone Test," by S. Pei, J.W. van de Lindt, S.E. Pryor, H. Shimizu, H. Isoda and D.R. Rammer, 12/1/10 (PB2012-102410).

MCEER-10-0009 "Modeling the Effects of Detonations of High Explosives to Inform Blast-Resistant Design," by P. Sherkar, A.S. Whittaker and A.J. Aref, 12/1/10 (PB2012-102411).

MCEER-10-0010 "L'Aquila Earthquake of April 6, 2009 in Italy: Rebuilding a Resilient City to Withstand Multiple Hazards," by G.P. Cimellaro, I.P. Christovasilis, A.M. Reinhorn, A. De Stefano and T. Kirova, 12/29/10.

MCEER-11-0001 "Numerical and Experimental Investigation of the Seismic Response of Light-Frame Wood Structures," by I.P. Christovasilis and A. Filiatrault, 8/8/11 (PB2012-102412).

MCEER-11-0002 "Seismic Design and Analysis of a Precast Segmental Concrete Bridge Model," by M. Anagnostopoulou, A. Filiatrault and A. Aref, 9/15/11.

MCEER-11-0003 'Proceedings of the Workshop on Improving Earthquake Response of Substation Equipment," Edited by A.M. Reinhorn, 9/19/11 (PB2012-102413).

MCEER-11-0004 "LRFD-Based Analysis and Design Procedures for Bridge Bearings and Seismic Isolators," by M.C. Constantinou, I. Kalpakidis, A. Filiatrault and R.A. Ecker Lay, 9/26/11.

MCEER-11-0005 "Experimental Seismic Evaluation, Model Parameterization, and Effects of Cold-Formed Steel-Framed Gypsum Partition Walls on the Seismic Performance of an Essential Facility," by R. Davies, R. Retamales, G. Mosqueda and A. Filiatrault, 10/12/11.

MCEER-11-0006 "Modeling and Seismic Performance Evaluation of High Voltage Transformers and Bushings," by A.M. Reinhorn, K. Oikonomou, H. Roh, A. Schiff and L. Kempner, Jr., 10/3/11.

MCEER-11-0007 "Extreme Load Combinations: A Survey of State Bridge Engineers," by G.C. Lee, Z. Liang, J.J. Shen and J.S. O'Connor, 10/14/11.

MCEER-12-0001 "Simplified Analysis Procedures in Support of Performance Based Seismic Design," by Y.N. Huang and A.S. Whittaker.

MCEER-12-0002 "Seismic Protection of Electrical Transformer Bushing Systems by Stiffening Techniques," by M. Koliou, A. Filiatrault, A.M. Reinhorn and N. Oliveto, 6/1/12.

MCEER-12-0003 "Post-Earthquake Bridge Inspection Guidelines," by J.S. O'Connor and S. Alampalli, 6/8/12.

MCEER-12-0004 "Integrated Design Methodology for Isolated Floor Systems in Single-Degree-of-Freedom Structural Fuse Systems," by S. Cui, M. Bruneau and M.C. Constantinou, 6/13/12.

MCEER-12-0005 "Characterizing the Rotational Components of Earthquake Ground Motion," by D. Basu, A.S. Whittaker and M.C. Constantinou, 6/15/12.

MCEER-12-0006 "Bayesian Fragility for Nonstructural Systems," by C.H. Lee and M.D. Grigoriu, 9/12/12.

MCEER-12-0007 "A Numerical Model for Capturing the In-Plane Seismic Response of Interior Metal Stud Partition Walls," by R.L. Wood and T.C. Hutchinson, 9/12/12.

MCEER-12-0008 "Assessment of Floor Accelerations in Yielding Buildings," by J.D. Wieser, G. Pekcan, A.E. Zaghi, A.M. Itani and E. Maragakis, 10/5/12.

MCEER-13-0001 "Experimental Seismic Study of Pressurized Fire Sprinkler Piping Systems," by Y. Tian, A. Filiatrault and G. Mosqueda, 4/8/13.

MCEER-13-0002 "Enhancing Resource Coordination for Multi-Modal Evacuation Planning," by D.B. Hess, B.W. Conley and C.M. Farrell, 2/8/13.

MCEER-13-0003 "Seismic Response of Base Isolated Buildings Considering Pounding to Moat Walls," by A. Masroor and G. Mosqueda, 2/26/13.

MCEER-13-0004 "Seismic Response Control of Structures Using a Novel Adaptive Passive Negative Stiffness Device," by D.T.R. Pasala, A.A. Sarlis, S. Nagarajaiah, A.M. Reinhorn, M.C. Constantinou and D.P. Taylor, 6/10/13.

MCEER-13-0005 "Negative Stiffness Device for Seismic Protection of Structures," by A.A. Sarlis, D.T.R. Pasala, M.C. Constantinou, A.M. Reinhorn, S. Nagarajaiah and D.P. Taylor, 6/12/13.

MCEER-13-0006 "Emilia Earthquake of May 20, 2012 in Northern Italy: Rebuilding a Resilient Community to Withstand Multiple Hazards," by G.P. Cimellaro, M. Chiriatti, A.M. Reinhorn and L. Tirca, June 30, 2013.

MCEER-13-0007 "Precast Concrete Segmental Components and Systems for Accelerated Bridge Construction in Seismic Regions," by A.J. Aref, G.C. Lee, Y.C. Ou and P. Sideris, with contributions from K.C. Chang, S. Chen, A. Filiatrault and Y. Zhou, June 13, 2013.

MCEER-13-0008 "A Study of U.S. Bridge Failures (1980-2012)," by G.C. Lee, S.B. Mohan, C. Huang and B.N. Fard, June 15, 2013.

MCEER-13-0009 "Development of a Database Framework for Modeling Damaged Bridges," by G.C. Lee, J.C. Qi and C. Huang, June 16, 2013.

MCEER-13-0010 "Model of Triple Friction Pendulum Bearing for General Geometric and Frictional Parameters and for Uplift Conditions," by A.A. Sarlis and M.C. Constantinou, July 1, 2013.

MCEER-13-0011 "Shake Table Testing of Triple Friction Pendulum Isolators under Extreme Conditions," by A.A. Sarlis, M.C. Constantinou and A.M. Reinhorn, July 2, 2013.

MCEER-13-0012 "Theoretical Framework for the Development of MH-LRFD," by G.C. Lee (coordinating author), H.A Capers, Jr., C. Huang, J.M. Kulicki, Z. Liang, T. Murphy, J.J.D. Shen, M. Shinozuka and P.W.H. Yen, July 31, 2013.

MCEER-13-0013 "Seismic Protection of Highway Bridges with Negative Stiffness Devices," by N.K.A. Attary, M.D. Symans, S. Nagarajaiah, A.M. Reinhorn, M.C. Constantinou, A.A. Sarlis, D.T.R. Pasala, and D.P. Taylor, September 3, 2014.

MCEER-14-0001 "Simplified Seismic Collapse Capacity-Based Evaluation and Design of Frame Buildings with and without Supplemental Damping Systems," by M. Hamidia, A. Filiatrault, and A. Aref, May 19, 2014.

MCEER-14-0002 "Comprehensive Analytical Seismic Fragility of Fire Sprinkler Piping Systems," by Siavash Soroushian, Emmanuel "Manos" Maragakis, Arash E. Zaghi, Alicia Echevarria, Yuan Tian and Andre Filiatrault, August 26, 2014.

MCEER-14-0003 "Hybrid Simulation of the Seismic Response of a Steel Moment Frame Building Structure through Collapse," by M. Del Carpio Ramos, G. Mosqueda and D.G. Lignos, October 30, 2014.

MCEER-14-0004 "Blast and Seismic Resistant Concrete-Filled Double Skin Tubes and Modified Steel Jacketed Bridge Columns," by P.P. Fouche and M. Bruneau, June 30, 2015.

MCEER-14-0005 "Seismic Performance of Steel Plate Shear Walls Considering Various Design Approaches," by R. Purba and M. Bruneau, October 31, 2014.

MCEER-14-0006 "Air-Blast Effects on Civil Structures," by Jinwon Shin, Andrew S. Whittaker, Amjad J. Aref and David Cormie, October 30, 2014.

MCEER-14-0007 "Seismic Performance Evaluation of Precast Girders with Field-Cast Ultra High Performance Concrete (UHPC) Connections," by G.C. Lee, C. Huang, J. Song, and J. S. O'Connor, July 31, 2014.

MCEER-14-0008 "Post-Earthquake Fire Resistance of Ductile Concrete-Filled Double-Skin Tube Columns," by Reza Imani, Gilberto Mosqueda and Michel Bruneau, December 1, 2014.

MCEER-14-0009 "Cyclic Inelastic Behavior of Concrete Filled Sandwich Panel Walls Subjected to In-Plane Flexure," by Y. Alzeni and M. Bruneau, December 19, 2014.

MCEER-14-0010 "Analytical and Experimental Investigation of Self-Centering Steel Plate Shear Walls," by D.M. Dowden and M. Bruneau, December 19, 2014.

MCEER-15-0001 "Seismic Analysis of Multi-story Unreinforced Masonry Buildings with Flexible Diaphragms," by J. Aleman, G. Mosqueda and A.S. Whittaker, June 12, 2015.

MCEER-15-0002 "Site Response, Soil-Structure Interaction and Structure-Soil-Structure Interaction for Performance Assessment of Buildings and Nuclear Structures," by C. Bolisetti and A.S. Whittaker, June 15, 2015.

MCEER-15-0003 "Stress Wave Attenuation in Solids for Mitigating Impulsive Loadings," by R. Rafiee-Dehkharghani, A.J. Aref and G. Dargush, August 15, 2015.

MCEER-15-0004 "Computational, Analytical, and Experimental Modeling of Masonry Structures," by K.M. Dolatshahi and A.J. Aref, November 16, 2015.

MCEER-15-0005 "Property Modification Factors for Seismic Isolators: Design Guidance for Buildings," by W.J. McVitty and M.C. Constantinou, June 30, 2015.

MCEER-15-0006 "Seismic Isolation of Nuclear Power Plants using Sliding Bearings," by Manish Kumar, Andrew S. Whittaker and Michael C. Constantinou, December 27, 2015.

MCEER-15-0007 "Quintuple Friction Pendulum Isolator Behavior, Modeling and Validation," by Donghun Lee and Michael C. Constantinou, December 28, 2015.

MCEER-15-0008 "Seismic Isolation of Nuclear Power Plants using Elastomeric Bearings," by Manish Kumar, Andrew S. Whittaker and Michael C. Constantinou, December 29, 2015.

MCEER-16-0001 "Experimental, Numerical and Analytical Studies on the Seismic Response of Steel-Plate Concrete (SC) Composite Shear Walls," by Siamak Epackachi and Andrew S. Whittaker, June 15, 2016.

MCEER-16-0002 "Seismic Demand in Columns of Steel Frames," by Lisa Shrestha and Michel Bruneau, June 17, 2016.

MCEER-16-0003 "Development and Evaluation of Procedures for Analysis and Design of Buildings with Fluidic Self-Centering Systems" by Shoma Kitayama and Michael C. Constantinou, July 21, 2016.

MCEER-16-0004 "Real Time Control of Shake Tables for Nonlinear Hysteretic Systems," by Ki Pung Ryu and Andrei M. Reinhorn, October 22, 2016.

MCEER-16-0006 "Seismic Isolation of High Voltage Electrical Power Transformers," by Kostis Oikonomou, Michael C. Constantinou, Andrei M. Reinhorn and Leon Kemper, Jr., November 2, 2016.



ISSN 1520-295X